Wuhong Wang · Klaus Bengler
Xiaobei Jiang   *Editors*

# Green Intelligent Transportation Systems

Proceedings of the 8th International Conference on Green Intelligent Transportation Systems and Safety

Springer

# Lecture Notes in Electrical Engineering

## Volume 503

*Lecture Notes in Electrical Engineering (LNEE)* is a book series which reports the latest research and developments in Electrical Engineering, namely:

- Communication, Networks, and Information Theory
- Computer Engineering
- Signal, Image, Speech and Information Processing
- Circuits and Systems
- Bioengineering
- Engineering

The audience for the books in LNEE consists of advanced level students, researchers, and industry professionals working at the forefront of their fields. Much like Springer's other Lecture Notes series, LNEE will be distributed through Springer's print and electronic publishing channels.

For general information about this series, comments or suggestions, please use the contact address under "service for this series".

To submit a proposal or request further information, please contact the appropriate Springer Publishing Editors:

More information about this series at http://www.springer.com/series/7818

Wuhong Wang · Klaus Bengler
Xiaobei Jiang

Editors

# Green Intelligent Transportation Systems

Proceedings of the 8th International Conference on Green Intelligent Transportation Systems and Safety

Springer

*Editors*
Wuhong Wang
Beijing Institute of Technology
Beijing, China

Xiaobei Jiang
Beijing Institute of Technology
Beijing, China

Klaus Bengler
Technical University of Munich
Munich, Germany

# Contents

# Thought About Parking Charge on Campus

Ting Zhao, Zai-tao Wang and Xue Liu

**Abstract** To explore the influence of the parking charge on campus in China, the paper, viewing from the perspective of purposes, targets and effects, tries to make it clear whether a university is suitable or not for the policy. It is discovered that the location of the campus is the first factor considered, and the problems of fairness, overflow effects, the utilization efficiency of resources, and transparent of the fees will happen. Therefore, advices are given to solve the university campus parking problems.

**Keywords** Parking charge · On campus · Charge fees · In China

The car is becoming more and more popular in contemporary society and has become an important means of transportation in the people's daily travel [1]. With the increase in the number of cars, the number of motor vehicles on and off campus is increasing. Therefore, the university campus is faced with traffic congestion and car parking problem. To reduce the car impact on the university campus, many Chinese colleges and universities begin to collect import passing and parking fees for foreign vehicles. At the end of 2007, Xujiahui Campus of Shanghai Jiaotong University take the lead in launching foreign vehicle parking management, then most colleges and universities in Beijing, Shanghai, Guangzhou, Tianjin, Wuhan, and other cities also began to charge access fee towards foreign vehicles. After adopting those measures, the campus traffic congestion, and parking problems have been alleviated, but there was a lack of further understanding of the consequences generated by the implementation of

T. Zhao
Library, Shandong Women's University, Jinan, Shandong, China

Z. Wang
School of Business Administration, Shandong Women's University, Jinan, Shandong, China

X. Liu (✉)
Department of Public Administration and Policy, Tianjin Administrative Institute, Tianjin 300072, China
e-mail: chinaliuxue@qq.com

the measures. This paper will analyze Chinese university campus location, as well as purpose, object, and effect of levying parking fees, to explore the consequences arising from the Chinese universities charge parking fee, and how to play better the role of the measures in the management of the campus traffic problem.

# 1 The Definition About the Scope of the Problem

On university campus located on the outskirts, it is inappropriate to charge vehicles parking fees. From the perspective of demand, population density in the outskirts is relatively low; economic development level is lower than that in the cities. Population and the number of vehicles are not too much in communities around the school, so the influence on the campus traffic is low. The main campus vehicles are commuting ones for teachers and students. From the perspective of supply, school area is relatively large, the campus road network planning is comparatively perfect, and because of the relatively low cost of parking spaces, the building with parking spaces may thus provide a large number of parking spaces. In this case, the number of campus parking supply is larger than demand. The purpose of charging fees for foreign vehicles going in and out of campus is to balance traffic demand and supply when the former is larger than the latter through economic means, so university in the outskirt does not need to charge vehicles.

Located in the city center area, charging motor vehicles in campus is one possible way for the university to solve the traffic problem. From the perspective of demand, located in the city center area, it contacts more with the outside world. Its surrounding is of a higher level of economic development, a dense population, and a large number of vehicles, which has a significant impact on campus traffic. In addition to commuter vehicles for teachers and students, vehicles on campus include ones from outside. From the perspective of supply, the university campus is located in the urban land; the parking cost is relatively high. Land use on campus is rather compact, with high accessibility, and perfect traffic system around, so there are various traffic ways to replace. In this case, it can be considered to charge motor vehicle passing the campus.

Therefore considering whether levy fees of a vehicle passing the campus, the answer depends on, it should be analyzed according to the condition of the campus itself. The research object of this paper is mainly the university campuses located in the city center area.

## 2  The Problems Caused by Charging Fee to the Cars Outside

### 2.1  Campus Traffic Problem Can not Be Solved Fundamentally

Before the discussion of the parking fee on campus, we should first know the possible effects of it. As the number of the students and staff increasing, the scale of the universities are growing, and the much bigger universities are much similar to small cities. They have athletic facilities, libraries, museums, offices, restaurants, parking lots, so on and so forth. Therefore, the transportation problems are being one of the challenge faced by the universities. Some of the universities have pioneered some pricing reforms—such as offering fare-free public transit and charging market prices for parking. After parking fee charged in some cities, the dynamic transportation, residents' willingness to buy cars and the trip mode are all influenced seriously. Therefore, the promising results imply that many universities can adopt similar reforms to reduce congestion, and the effects of parking fee are focused here on how market-priced parking can benefit universities. The main purpose of charging foreign vehicle on campus is to reduce safety and the environmental problem caused by the increasing number of motor vehicles, benefits, and other issues, to protect guarantee teachers' and students' normal life and learning. Daggett and Gutkowski [2] pointed out that motor vehicle is the cause of campus traffic problems. Motor vehicles on campus can be divided into two categories, vehicles outside and inside campus. Vehicles outside campus include traveling vehicles, vehicles on business, and vehicle for recreation. Traveling vehicles refer to vehicles that travel through the campus because of the shortcut on campus or congestion on roads around a school, which generally do not take up the school parking field; vehicle for business or recreation needs to stay in school for a certain period of time, which is generally not too long, and they need to occupy the school parking lot and even park on roadside; campus vehicle is mainly the commuter vehicle for school staff and students go into and leave school, whose parking time is relatively long and need to take up the school parking field even park on roadside. Compared with social vehicle, the campus vehicle occupies more campus traffic resources, and their number is far larger than that of the social vehicles. Therefore, the main cause of campus traffic problem is due to the campus vehicle if levying fees are taken as a way to reduce the use of vehicles and therefore to control campus traffic problems, then charging campus vehicle should be considered [3, 4].

## 2.2   The Spillover Effect on the Community Surrounding College Campus

After charging vehicle passing campus, campus traffic conditions have improved. Taking the Renmin University of China as an example, after the school parking lot, fees were adjusted to 5 yuan per hour in 2011, the car parking on campus road reduced by about 50%. Some vehicles which intended to pass through the campus beforehand changed their route to the near campus bypass, only during the peak periods in the morning and evening. Yu [5] found that vehicles parked on campus belonged to neighboring communities and workplaces. When universities charged motor vehicles on campus, surrounding communities did not implement that at the same time, or fees were lower than those on campus, so part of the vehicles parking on campus transferred to the roads around the campuses and communities. Vehicles changing the running route or parking locations would generate huge traffic pressure on roads and communities around the university campus, so charging did not solve the traffic congestion problem but transferred it from universities to the surrounding areas. After implementation of the policy in Beijing Normal University, Beijing University of Technology, and other ten colleges and universities in Beijing, illegal parking phenomenon around the campus or on sidewalks tended to grow [6].

## 2.3   Waste of Campus Parking Lot Resources in Universities

The university campus charging vehicle has caused the waste of resources of the parking lot. On the one hand, the vehicles on campus are mainly for students and staffs to commute, whose use of parking lot shows an obvious rule according to time. After 10 p.m. and before 7 a.m. from Monday to Friday on working days, as well as on Saturday and Sunday, the usage of the parking lot is small and there will be some parking lots left. On the other hand, with the implementation of vehicle charging policy in Colleges and universities, although there are signs forbidden parking on the roads near universities, there are still a lot of illegal parking at night. The original intention of charging motor vehicle on campus is to alleviate traffic problems in the universities through economic levers, but because the fee is too high, the campus parking lot is wasted.

## 2.4   Question to the Use of Fee

The amount of fees collected by different colleges are different, but generally include passing fee and parking fee. Public vehicles are required to pay the passing fee according to the number of travel through the campus and parking fee according to the time. University campus is a public place, whether its purpose being to control

the campus traffic problem or others, the public enjoy the right to be informed of the amount and usage of the fee.

## 3 Proposals for University Charging Parking Fee

### 3.1 Vigorously Develop Alternative Modes of Transportation on Campus, Charge on Campus Motor Vehicles

The staff is the main contributor of motor vehicles on campus, if the main goal of charging on-campus vehicle is to solve the campus traffic problem, then charging certain parking fees for school vehicles should be considered. Campus vehicles are primarily commuting tools used by school staff and students, so after levying a fee, some traveler would shift commuting mode, and select an alternative mode of transportation. At this point, it should be ensured that the alternative transportation can undertake the traffic pressure of these travelers. Also, a high level of service is the key to the alternative mode of transportation to keep the part of the traveler's vehicle conversion. There are a lot of traffic points and attraction points on the university campus, and there will be a lot of traffic demand. After teachers and students arrived at school, they still bring considerable pressure to campus traffic system, and if there is no suitable replace mode of transportation, it will also intensify the campus traffic problems. So before levying fees towards campus vehicles, it should be ensured that there is fast and comfortable replaceable transportation around school. Otherwise, the policy could not only restrain the use of cars by teachers and students but also lead to dissatisfaction of teachers and students.

### 3.2 The University and Surrounding Communities Cooperate Closely to Solve the Traffic Problems

There are close relationships between the university campus and its surrounding communities [7]. The spillover effects on the surrounding communities after university charging vehicles show that to resolve the problem of campus traffic, the universities should fully communicate with surrounding communities and implement effective management measures together.

When charging social vehicles different prices can be used. Parking rates can differ according to different parking areas, lowest in the remote part of campus while highest in the center area [8]. The charging rates can also differ according to the time. The daytime rush hour fee should be higher to strengthen the control of traffic demand; at night, traffic charges should be lower to guide parking demand in residential areas to miss the parking peak. Parking fee can be taken on ladder

structure according to parking time, the longer the parking time is, the higher the parking charges will be, thus speeding up the turnover rate of parking spaces.

Effectively integrate resources and guide staggered parking. Roads and parking lot within the university campus have no obligation to open to the society. But under the premise of not affecting the normal campus learning life, considering from the point of view of social resources' effective configuration, if the resources' reasonable use has a positive role to alleviate traffic congestion throughout the city, in order to fully realize the parking lot resources on campus and in the surrounding communities, they can implement staggered parking. University and the surrounding community can reach such a parking agreement: in the daytime, when community residents go to work or travel, there will appear free parking space, this free parking space is available to nearby enterprises, institutions, and schools to use; at night, residents can park their vehicles in the workplace near their community, both sides can exchange certain number of parking spaces according to the need.

### 3.3 The Fees Collected Are Used for Special Purpose to Solve Campus Traffic Problems

Only operated in an open and transparent system, the allocation of public resources can really be optimized. The university should open the specific amount, details, and usage of motor vehicles to accept public supervision and improve the social recognition of parking policy. In foreign cities, parking fees are usually used for specific purpose. Parking fee is mainly used for maintenance and building new parking spaces, or put into control traffic congestion related matters, and the range of use cannot be enlarged, let along used for another purpose. It is a general trend to reduce the rate of vehicle travel by regulation of the market, but the service level should be improved at the same time. Otherwise, it will be difficult to get public recognition [9]. The university campus revenue should also be used to improve the campus transportation system, providing a high level of parking service and a higher level of replaceable traffic mode. Attract more travel staff to use environmental-friendly transportation mode, such as bus, bike, walk to realize the sustainable development of campus transportation system.

## 4 Conclusion

Too much motor vehicles on the university campus lead to the development of colleges and universities trapped in traffic problems. To solve this problem, many colleges and universities begin to charge foreign vehicles. This paper defines the university which is suitable for levying fee and pointed out that the one located in the city center area can consider charging a passing fee, and if the university campus

is located in the suburbs then it is not suitable for the policy. A series of problems will appear after the universities charging foreign vehicles, if these problems are not solved, they will cast a negative influence on the measure. To ensure the effectiveness, effective replaceable transportation modes should be vigorously developed around universities and on campus, and the internal motor vehicles should also be charged; university campus and surrounding communities are an organic whole to solve the traffic problems, and should work closely together to solve the traffic problems; university needs to obtain understanding and support of the public on this issue, the public access the information of the charge amount clearly, flow and usage of fee, and ensure that it is an effective way to devote the money to the management of the campus traffic problems.

# References

1. Barata E, Cruz L et al (2011) Parking at the UC campus: problems and solutions. Cities 28(5):406–413
2. Daggett J, Gutkowski R (2003) University transportation survey: transportation in university communities. Transp Res Rec: J Transp Res Board 1835(1):42–49
3. Attard M, Ison S et al (2014) The effects of road user charges in the context of weak parking policies: The case of Malta. Case Stud Trans Policy 3(1):37–43
4. Caicedo F (2012) Charging parking by the minute: what to expect from this parking pricing policy? Transp Policy 19(1):63–68
5. Yu L (2013) Road parking should be heard. Oriental Morning Post, 2013-01-26004
6. Tan H, Chen S et al (2014) Development of green campus in China. J Clean Prod 64(2):646–653
7. Roemmich JN, Balantekin KN et al (2015) Park-like campus settings and physical activity. J Am Coll Heal 63(1)
8. Shoup D (2008) The politics and economics of parking on campus. In: The implementation and effectiveness of transport demand management measures: an international perspective, p 121
9. Zhao R, Guo Y, Yang Y, Hao M (2013) Expanding parking fees, don't make regulating congestion into accumulating wealth. Xinhua Daily Telegraph. 2013-09-08003

# International Development History and Experience of Bicycle Transportation and Its Inspiration

**Zai-tao Wang and Ting Zhao**

**Abstract** In order to sum up the experience of bicycle transportation and mirror for its development in China, the paper compares its development history in the UK and the USA with that in several European countries, and mainly discusses the successful experience of the bicycle transportation in the European countries. The paper argues that understanding the unique contexts of Chinese cities is necessary for the success of the bicycle transportation, therefore some suggestions are given based on the analysis of the characteristics of the Chinese cities.

**Keywords** Engineering of communication and transportation system · Bicycle transportation · Development history · The characteristics of the Chinese cities

## 1 Introduction

After the founding of new China, the proportion of bicycle travel in the traffic system has first increased and then decreased. Bicycle ownership of urban and rural residents, respectively, in 1993 and 1995 reached the highest value, respectively, 197/100 households and 147/100 households, then bicycle travel proportion and possession amount declined rapidly [1]. With the rapid development of the economy and car-centered development model of transportation, urban car trip proportion continues to increase; therefore giving rise to a series of the problem in urban areas, such as traffic congestion, increasing traffic accidents, deterioration of the environment, fuel consumption, land occupation, etc. Governments all over the country are becoming gradually aware of the problems caused by the widespread use of cars, and begin to implement the concept of sustainable development in the development of urban transport system [2]. Compared with the other motorized modes of transport, bicycle

Z. Wang (✉)
School of Business Administration, Shandong Women's University, Jinan, Shandong, China
e-mail: wzt0813@163.com

T. Zhao
Library, Shandong Women's University, Jinan, Shandong, China

travel has advantages like flexibility, less pollution to the environment, high space and resources utilization rate, which are key factors to solve the urban traffic problem, and to realize the sustainable development of urban traffic [3]. Since 2005, many cities began to attach importance to the development of bicycle traffic [4]. On September 5, 2012, Ministry of Housing and Urban-Rural Development, National Development and Reform Commission, and Ministry of Finance jointly issued Guidance on the Strengthening of Urban Pedestrian and Bicycle Transportation System Construction, requiring the strengthening of urban pedestrian and bicycle traffic system construction. And it puts forward a clear goal which is, in 2015, in the urban district with a population of more than 10 million, walking and bicycle travel should take more than 45% of its transportation.

Developed countries such as UK, USA, Germany, the Netherlands, etc., earlier suffered more serious traffic problems in the cities. In the process of solving urban traffic problems in these countries, different measures of adopting bicycle traffic had different effects [5]. Bicycle travel in the United Kingdom has first increased and then declined in recent years. Its government has taken positive remedial measures, but the effect is not significant. Relative to the British, in America and European countries, bicycles have experienced the process of rise, fall, and rise again. Therefore, the study of the historical evolution and successful experience of the bicycles in these countries will cast practical reference and direction to the contemporary development of urban bicycle traffic of China. This article will analyze development course of bicycles in Britain, the United States and typical European countries, compare their national policies, measures and results, and combine them with the Chinese cities' own characteristics to provide suggestions for the development of China's bicycles.

## 2  Development Process of Bicycle Worldwide

As a whole, after World War II in the United States and European countries, usage of bicycles experienced rise, fall, and rise again. The author will divide bicycles use history into three stages: rapid development, rapid decline, and recovery period.

Rapid development period (1948–1952). After World War II, due to restrictions such as automobile manufacturing technology, price, fuel shortage, road construction level, etc., the car did not become the main means of transport quickly in the United Kingdom, the United States, and European countries. Bicycle is the most important means of transport, the possession amount and use of it reached its peak in 1950, in the United States and some countries in Europe, such as Denmark, Holland, and Germany, the proportions bicycle travel were up to 50–80%.

Rapid decline period (1953–1975). During 1950s–1960s, the expansion of the city speeded up; the car possession rate increases rapidly. Cars usage expansion deteriorated the condition of bicycle travel from environmental and safety aspects, therefore the proportion of bicycle travel declined rapidly. From 1950–1975, in 25 years time, the European bicycle travel reduced by about 40%, to 14–35%. The average travel distance per day of British bicycle was only one-fifth of the peak.

Recovery period (1976 to date). The extensive use of cars in these countries has brought adverse effects on land, energy, environment, and safety. To ease and solve these problems, after 1975, the European countries significantly increased the support of public transport and slow traffic in the development of urban transport policy. Implementation of "carrot and stick policy"—inhibiting car travel as well as encouraging bicycle travel, has achieved remarkable results. By 1995, the proportion of bicycle travel in these European countries rose by about 25%; the proportion of bicycle travel in Berlin, Germany, even peaked up to the highest level of 45%. Measures taken by the United States also achieved results—in 1977 the proportion of its bicycle travel was 0.6%; in 1995, it increased to 0.9%; and in 2011, it reached 1.7%. Although it was much lower than that of European countries, we should pay attention to that with the steady increase of its city size, average income, and vehicle demand in the same period, the proportion of bike travel can continue to improve, which was more valuable. And it provides more reference significance to Chinese cities which are similarly in the process of rapid urbanization and motorization.

In Britain, the rapid increase in cars has also brought above problems, but these countries have adopted different policies to solve urban problems, while British government implemented the car-dominated policy. It increases demand for cars through increasing the supply of traffic such as building new roads, expanding capacity of original roads, and increasing motor vehicle parking spaces; pedestrians and bicycle travelers' needs are largely ignored, so the amount of British bike trips continues to drop. In 2012, 20% of the trip was less than a mile, and 66% of the trip was within 5 miles. But even if there is such a high proportion of short trips suitable for bicycles, bicycle travel in the UK accounted for only 2%.

# 3 Analyses of Bicycle Development Experiences in European Countries

Safe and convenient are the most important two factors that affect the selection of the bicycle rider. When promoting cycling, Denmark, the Netherlands and Germany and other European countries give full play to the role of government for bicycle travel to create a good and safe riding condition, as well as provide convenient and secure parking facilities to increase the attractiveness of bicycles.

## 3.1 Positive Role of Governments at All Levels

European countries have maintained a higher rate of bicycle travel, which is inseparable with the governments' policies of promoting, guiding and supporting the bicycle. Governments devote financial investment and policy innovation into the development of bicycle traffic, so that it can maintain a high rate of bicycle travel. Countries give

full play to macro-control and policy guidance of government at all levels, governments at all levels are responsible for bicycle planning and project construction.

The EU, similar to the role of the central government of China, is the highest administrative unit to promote bicycle traffic. Major activities include the overall EU bicycle network planning, strengthen bicycle network connections in different countries and the construction, funding bicycle infrastructure construction in backward countries and regions, actively carrying out the bicycle traffic related research, summarize, and share national experiences of bicycle traffic development.

Central governments from the overall grasp the future development direction of their own bicycle policies, determine the overall development objectives, and accordingly prepare bicycle development plan, provide necessary financial support to the related project, and actively coordinate with relevant parties.

The states, counties, and regional level of government, which are on the intermediate level of the domestic administrative system, are mainly responsible for the planning and construction of bicycle traffic related facilities within the administrative areas, bicycle facilities connections among administrative regions, guidance and related policies to the development of bicycle traffic, and necessary funding.

Municipal administrative units, having the most detailed data on bicycle traffic, according to local conditions and needs, carry out bicycle planning, promotion, infrastructure construction and other activities.

## 3.2   Riders' Rights Are Guaranteed by Strict Laws and Regulations

In the Netherlands, Denmark and other countries, pedestrians and cyclists successively enjoy the highest right of passage and are protected by relevant laws. In mixed or relatively narrow road, cyclists enjoy absolute priority, which is strictly protected by law enforcement agencies; if there is no evidence that the rider deliberately run into the vehicle, collision is attributed entirely to the driver of the car. Especially when the riders are kids or the elderly, collision is attributed entirely to the driver of the car. Law enforcement supervision to the rider is also very strict, in the rider has illegal behavior, he is also very likely to be punished.

## 3.3   Good Riding Environment

Improve bicycle road network planning on a strategic level. In order to reduce the mutual interference between the bicycle flow and the motor vehicle flow and increase the safety of the bicycle riding, construction of bicycle lane was accelerated. Road intersection and signal lamp were reformed. During the recovery period of bicycle travel, the typical European countries carried out the expanded to the bicycle network

**Fig. 1** The improvement of bicycle safety at the intersection of intersection. *Source* Dijkstra Lewis

in large scale, for example, the 1996 German bicycle lane network was 31,236 km long, 18,352 km longer than that in 1976; meanwhile, bicycle lane network in Holland was 18,948 km, twice of that in 1978. Bicycle lanes can completely eliminate the mutual influence between motor vehicles and bicycles, while on the road cross conflict cannot be completely avoided, but European road designers have done a large amount of effective work in improving bicycle safety and spread at the road intersection. Figure 1 shows the improvements made by the designers of Holland in improving the safety of bicycles at the intersection of roads. After passing through the intersection, the bicycle immediately enters the bicycle lanes, and separated from motor vehicle lanes, the bike lanes ensure the riders' safety. The distance between the motor vehicle lane and the bicycle road improves the visibility of the operators of the two kinds of traffic tools, and reduces the possibility of accidents. A two door pillar of safe island not only forces the motor vehicle to slow down when turning right, and two sets of traffic signals ensure that the riders have the priority to pass, improving the intersection safety and speed.

In the streets of residential area where traffic volume is small, traffic purification is implemented. On the one hand, motor vehicles are inconvenient to travel in residential area, and the speed is limited to below 30 km/h; on the other hand, create convenient conditions for bicycle in the residential area, such as expanding regional bicycle network, the establishment of bicycle or preferential street, strengthen the regional bike lane link, and to create a more comfortable and safe riding environment for the rider. Figure 2 shows the streets of Germany in the traffic purification area.

**Fig. 2** The streets of Germany in the traffic purification area. *Source* John Pucher

## 4 Characteristics of Chinese Cities

### 4.1 Long History and Solid Foundations of Bikes in Chinese Cities

The bicycle's development in China can be divided into four stages, namely introduction and slow development stage (1900–1978), rapid growth stage (1978–1995), rapid decrease stage (from 1995 to 2002), and diversified development stage (since 2002). At present, both China's bicycle production and export amount accounted for more than 60% of the world's total amount; the domestic consumption of the bicycle is also the world's first [6]. In China, the bicycle is of the largest number of people's livelihood transportation, and the proportion of bicycle travel in the city has been as high as more than 65%. Although experienced a substantial decline from the mid-1990s, now the proportion of bicycle travel in a lot of cities is still higher than that in Germany, Holland, and other countries which have carried out good bike program. Besides, in most Chinese cities, bicycle-related roads and parking facilities are also completely reserved.

### 4.2 Structural Difference Between New and Old Urban Areas in China

Because of the historical development and the strictly control of urban planning by the government, Chinese old cities are compactly laid out, with land mixed used, and therefore are relatively highly accessible, so travel distance is relatively short, and

the vast majority of travels are within bicycle travel range. Compared with that, in the new city area, there is a better planning and more perfect road network, and land use intensity and population density are lower than that in the old city area.

## 4.3  Chinese Cities' Scale Continues to Expand

In 1990, the built-up area of China's urban area was 12,200 km$^2$, which increased by 78.3% to 21,800  km$^2$ in ten years. After another 10 years of development, in 2010 China's urban built-up area further increased to 40,500 km$^2$, an increase of 85.5%. From a multiple perspective, in 2010, China's urban built-up area is 3.3 times the size of that in 1990. With the expansion of the scale of urban space, people's travel distance increases, and the demand for suitable mobile traffic mode of medium and long distance travel is increased.

# 5  Policy Recommendations

According to the British, American and European countries' bicycle traffic development experience, combined with the characteristics of Chinese Cities, following suggestions on the further development of bicycle traffic in China's cities are put forward.

## 5.1  Clear Support for the Development of Bicycle Should Be Provided

The development of bicycle traffic in Europe and other developed countries has proved that the bicycle traffic does not necessarily decline with the development of economy and the improvement of people's living standard. Its development course in the British shows that role of bicycle traffic being neglected long in the perspective of policy is an important reason, leading to a sharp decline in the proportion of bicycle travel; and bicycle traffic development depends on the attitude of the central government and the corresponding transport policy. Different levels of governments of EU countries play very important roles in promoting the bicycle travel and inhibiting car use. It is through a series of policies and measures that the bicycle revives under the background of motorization, and keeps at high rate. Bicycle development in Chinese cities is at the crossroad, compared with western countries in urban traffic system, transport means in Chinese cities is mixed and have not yet been finalized, and urban traffic system is strongly plastic, therefore the recent 5 to 10 years is golden period of guiding bicycle traffic development. The central government's attitude and policy

towards the bicycle traffic will determine whether Chinese city will maintain a high rate of bicycle use, or continues to decline and become the edge of the city traffic.

Low-income groups still accounted for a higher proportion in the city, being the highest economic way, walking, bicycle traffic and public transportation are the main ways of group travel. If bicycle travel is reduced, this part of travel will turn to public transportation, and considering that China's urban public transport still cannot meet travelers' need, therefore it is determined that in China urban bicycle traffic will still be one of the most important ways to travel for quite a long period in the future. Therefore to realize the further development of bicycle traffic in China, the central government of must provide clear support.

## 5.2 Different Bicycle Development Strategies Should Be Adopted in Old City and the New One

The old city should solve middle and short distance travel, as well as bicycle and public transport interchange. Road network in old city is overall of low density, with poor road network system, and there is a contradiction between limited traffic facility supply and traffic and need high demand, so efficiency traffic mode which does not affect the environment is needed. Compared with other ways, public transport has the highest efficiency of road usage. Road utilization efficiency of the bicycle is just second to that of public transport, but it has a less negative impact on the environment and can make full use of the old city road network, giving full play to the advantages of flexibility in a suitable range of bicycles. Taking into account that the old urban area is of high population density, high proportion of bicycle travel, intensive urban land and space resources and other characteristics, can consider to develop public bicycle in the old city, making use to bicycle traffic's short distance travel advantage and its connecting role to the public transportation system.

Give full play to bicycles' feeder and transfer function to public transport in the new city area. Road network and construction level in new city area can better adapt to the public transportation operation, so public transport should be vigorously developed there, ensuring that the public transport is the main part of passenger transport structure, and considering bicycle as a useful supplement, while suppressing bicycle in long distance transportation. So we can consider setting up perfect bicycle parking facilities in the vicinity of the new city bus station, realizing the integration of bicycle and public transport, and reducing demand for car travel.

## 5.3  The Cyclists' Right Should Be Protected

For a long time, although the number and travel proportion of bicycles are high, the traffic construction has not received due attention. In 1995, the central government pointed out that the large number of bicycle on highway is the main cause of conflict between motor vehicle and non-motor vehicle, to improve traffic safety and efficiency bicycle number should be reduced. Subsequently, Beijing, Shanghai, Nanjing, Shenzhen, Dalian and other cities introduced legislation to restrict the development of bicycle. Although the government of different cities were conscious to bicycle's importance to sustainable urban transport development, Beijing, Hangzhou, and other cities mentioned the will to develop bicycles in the overall urban planning, but lack effective laws and regulations to protect the rider's right to passage. Guidance on the Strengthening Urban Pedestrian and Bicycle Transportation System Construction clearly puts forward to protect the pedestrian and bicycle's basic right of way, and strengthens the governance towards illegal occupation of the walkway and phenomenon. But the premise of strictly enforcing the law is that there must be laws to go by, at present China lacks laws and regulations to protect the rights of way of bicycle traffic from central to local. Therefore, it is the pressing matter of the moment to introduce relevant laws and regulations in accordance with the traffic situation in China, to protect the rider's right of passage. Meanwhile, learn from the experience of European countries, increase strength of law enforcement and punishment towards motor vehicle drivers and riders, therefore provide security for riders from the laws and regulations and enforcement process; provide good bicycle safety education and training for the rider; increase publicity to driver of the vehicle of abiding the traffic rules and road traffic safety management measures, and improve citizen law-abiding consciousness so that they can consciously safeguard the traffic order.

## 6  Conclusion

Through comparison and analysis of the history of the development of bicycle traffic of the United Kingdom, the United States and European countries, it is shown that the direction of bicycle traffic development depends on the attitude of central government and the corresponding traffic policy. The central government must demonstrate clear support attitude in the bicycle traffic problem in the city, giving due attention and status to the bicycle traffic in the city traffic system.

Compared with cities of the developed countries, Chinese cities have their own characteristics. The priority of urban bicycle traffic development in China is the introduction of relevant laws and regulations to protect the bicycle's right of passage and take measures to ensure the safety and convenience of bicycles, ensure interchange between middle and short distance bicycle travel and public transport in old city area, as well as play bicycle's role of supplementary and cohesive to public transport in new city area.

# References

1. Zhang H, Shaheen SA, Chen X (2014) Bicycle evolution in China: from the 1900s to the present. Int J Sustain Transp 8(5):317–335
2. Jindong HU, Qunqi WU (2013) International comparison of integrative development of multiple traffic and its inspiration. Urb Dev Stud 04:99–105
3. Heinen E, van Wee B, Maat K (2010) Commuting by bicycle: an overview of the literature. Transp Rev 30(1):59–96
4. Haixiao Pan (2011) The evolving cycle transport policy in china and urban sustainable development. Urb Plan Forum 04:82–86
5. Pucher J, Buehler R (2008) Making cycling irresistible: lessons from the Netherlands, Denmark and Germany. Transp Rev 28(4):495–528
6. Pucher J, Buehler R (2007) At the frontiers of cycling: policy innovations in the Netherlands, Denmark, and Germany. World Transp Policy Pract 13(3):8–57

# Time Series Piecewise Linear Representation Based on Trend Feature Points

**Dong-Lin Ma and Yu-Li Zhang**

**Abstract** As local maximum and minimum can reflect the trend feature of subsequence, an approach of time series piecewise linear representation based on trend feature point is proposed. The points with large fluctuation can be extracted by judging the variation amplitude of slope. The results of the experiment show that the LMMS algorithm can meet the requirements of different compression ratios, and ensure small fitting error, stable performance, and good adaptability in time series datasets with low volatility. It has nice fitting effect in the volatile datasets under the low compression ratio condition. The relationship between the fitting error of piecewise linear representation algorithm with the whole fluctuation ratio of data and compression ratio is discussed. It can provide a certain reference for time series data mining effectively.

**Keywords** Time series · Local maximum and minimum · Variation amplitude of slope · Trend feature point · Piecewise linear representation

Massive time series datasets are commonplace in a variety of online monitoring applications in mechanical engineering, space exploration, and so forth. Data mining on time series can discover useful information which contains and realizes the knowledge acquisition [1–3]. Time series data in practical application is massive, multi-dimensional, dynamic, and complicated. So data mining in the original sequence data directly will not only cost highly in the storage and computation but also probably affect the accuracy and reliability of the data mining algorithms. As with these problems, representation of the data is the key to efficient and effective solutions.

D.-L. Ma · Y.-L. Zhang
School of Computer and Communication, Lanzhou University of Technology, Lanzhou 730050, China

D.-L. Ma (✉)
Information Center, Lanzhou University of Technology, Lanzhou 730050, China
e-mail: 592004890@qq.com

# 1 Introduction

In recent years, many high-level representations of time series have been proposed for data mining. Keogh et al. [4] introduced the algorithm of PLR into the field of time series data mining, and proposed a dimensionality reduction technique which is called Piecewise Aggregate Approximation (PAA). Therefore, Perng et al. [5] proposed a representation method in time series based on landmarks which consist of extremum and inflection points. The method is based on the feature points of the original time series to achieve an approximate representation. Xiao et al. [6] divided time series into several line segments based on some Feature Points (FPS). The time of keeping extremum of these feature points must surpass a threshold value $C$. The value of $C$ will influence the compression ratio and the fitting result. However, this method may result in neglecting non-extremum points with high fluctuation ratio. Zhan et al. [7] proposed a new piecewise linear representation of time series based on Slope Extract Edge Point (SEEP). The result of segment is very good when the slope change range is concentrated. Jia et al. [8] put forward an adaptive piecewise linear representation of time series based on error restricted. It can give the number of fitting lines automatically according to a given error on the special points of time series. Guerrero et al. [9] presents an approach based on the formalization of the segmentation process as a multi-object optimization problem and the resolution of that problem with an evolutionary algorithm. Charbonnier et al. [10] presents a trend extraction method which is robust to the presence of artefacts and step-like variations and does not require a priori tuning of the parameters of the method. Hu et al. [11] uses the minimum description length to discover the intrinsic cardinality and dimensionality of time series.

In this chapter, we present a piecewise linear representation of time series which is based on Local Maximum Minimum and Slope (LMMS) to extract trend feature points. This algorithm with low computational complexity and high quality of approximating lines. It can improve the quality of data fitting, effectively inhibiting the interference of noise, accurately extract trend feature with better adaptability and practicality.

# 2 Related Definitions

**Definition 1** [12] (*Time series*) Time series is an ordered set of elements which consists of sample value and sample time. There is a time series $X$, $X = \{x(t_1), x(t_2), \ldots x(t_n)\}$, where $x(t_i)$ is the sample value at the sample time $t_i$, $t_i$ increasing strictly, i.e., $t_1 < t_2 < \cdots t_n$. Suppose each sample value includes the occurrence time of objective target and $m$ species attribute, i.e., $x(t_i) = \{t_i, x_1(t_i), x_2(t_i), \ldots x_j(t_i), \ldots x_m(t_i)\}$, where $x_j(t_i)$ is the sample value of attribute $j$ at the sample time $t_i$.

**Definition 2** [7] (*Piecewise linear representation of time series*) Given a time series $X = (x_1, x_2, \ldots, x_n)$, the set of segment points is $x_t = (x_{t_1}, x_{t_2}, \ldots, x_{t_n})$, $(x_{t_1} = x_1, x_{t_n} = x_n, x_{t_j} = x_i, \ 1 \le i \le n$ and $1 \le t_j \le n)$, there is a PLR of $X$ such that $X_L = \{ f_1(x_{t_1}, x_{t_2}), f_2(x_{t_2}, x_{t_3}), \ldots, f_{m-1}(x_{t_{m-1}}, x_{t_m}) \}$, the function $f_{m-1}(x_{t_{m-1}}, x_{t_m})$ represents the linear fitting function at the interval $\left[ x_{t_{m-1}}, x_{t_m} \right]$.

**Definition 3** (*Fitting error of PLR*) Given a time series $X = (x_1, x_2, \ldots x_n)$, the PLR of time series $X_L$ would be represented by a sequence by linear interpolation. The fitting sequence is expressed as $X' = (x'_1, x'_2, \ldots, x'_n)$. The fitting error of this algorithm can be calculated by Eq. (1).

$$E = \sqrt{\sum_{i=1}^{n} \left( x_i - x'_i \right)^2} \tag{1}$$

**Definition 4** (*Compression Ratio of PLR*) Given a time series $X = (x_1, x_2, \ldots, x_n)$, the PLR of time series is $X' = (x'_1, x'_2, \ldots, x'_m)$, $(x_1 = x'_1$ and $x_n = x'_m)$, the Compression Ratio (CR) of algorithm is calculated by Eq. (2).

$$C = \left( 1 - \frac{m}{n} \right) \times 100\%, \tag{2}$$

where $n$ is the length of original time series and $m$ is the length of linear fitting sequence.

**Definition 5** [13] (*Local maximum and minimum*) Given a subsequence $X''_i = (x''_{i_1}, \ldots, x''_{i_j}, \ldots, x''_{i_k})$, if $x''_{i_m} \ge \forall x''_{i_j}$, the point $x''_{i_m}$ is a local maximum point. If $x''_{i_n} \le \forall x''_{i_j}$, the point $x''_{i_n}$ is a local minimum point, where $1 \le m \le k, 1 \le n \le k$. So the sequence of local maximum points and minimum points is expressed as $X'' = (X''_1, \ldots, X''_l)$.

## 3 Algorithm Description

### 3.1 Extraction Local Maximum and Minimum of Subsequence

The experimental data is selected partially from the public electroencephalogram dataset which is provided by the department of epileptology in the university hospital of Bonn. It contains 80 points from the 730th to 809th. As shown in Fig. 1, B, C, E, and F are the local maximum and minimum point extracted from sequence. By connecting the local maximum and minimum points of subsequences, it is able to reflect the trend of increasing, decreasing or stability level and effectively inhibit the interference of noise.

**Fig. 1** Extraction trend feature points of time series
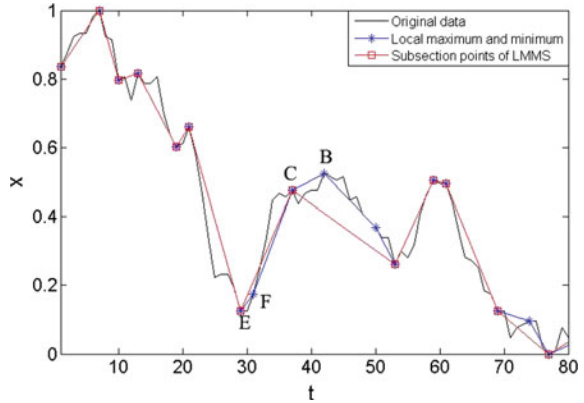


## 3.2 Judgement Variation Amplitude of Slope

Though judging the variation amplitude of the slope, the trend feature point is extracted from the datasets of local maximum and minimum. As shown in Fig. 1, B, C, E, and F are the set of extracting local maximum and minimum points. The slope $\tan(\overrightarrow{AB})$ of the line which is connecting B and its neighbor point A is calculated $\left(\overrightarrow{AB}\right.$ represents tilt angle of the line). The slope $\tan(\overrightarrow{BC})$ of the line which is connecting $B$ and its neighbor point C also is calculated. When the variation amplitude of slope $\left|\tan(\overrightarrow{AB}) - \tan(\overrightarrow{BC})\right|$ is bigger than or equal to threshold D, this point is the trend feature point, otherwise, the point is not the trend feature point (D is an input parameter of the algorithm, which is the minimum of the variation amplitude of slope).

## 4 Experiment Results and Discussions

## 4.1 Experimental Data

In order to verify the performance of the proposed algorithm, random samples from different areas of time series data are selected with different length. The dataset of leleccum comes from Matlab software. The bearing vibration dataset is the public roller bearing vibration signals which is from the University of Brunel. The EEG dataset is one of the public electroencephalogram datasets which is provided by the department of epileptology in the university hospital of Bonn. The Jokulsa river dataset is about the mean daily flow of Jokulsa Eystri river from 1972 to 1974. The Rotor Rub dataset is from Vibration and Noise Signal Sample Analyze of Rotor. The
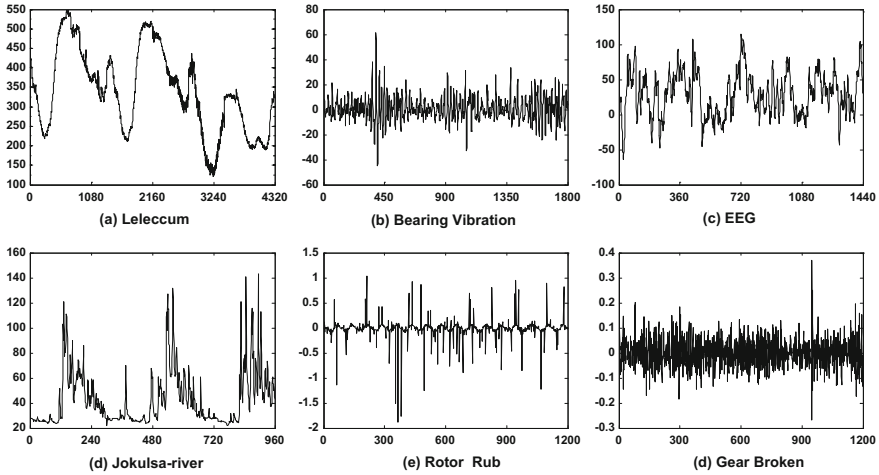
**Fig. 2** Experiment datasets

**Table 1** ADFR of six datasets

| Data | Leleccum | Bearing vibration | EEG | Jokulsa river | Rotor rub | Gear broken |
|------|----------|-------------------|-----|---------------|-----------|-------------|
| AFDR | 0.000164 | 0.0014 | 0.0013 | 0.0039 | 0.0061 | 0.0186 |

Gear Broken dataset is from Vibration and Noise Signal Sample Analyze System Version2.1. All of them are shown in Figs. 2a and 3f.

In order to reflect the global fluctuation feature of the data directly, the fluctuation of adjacent data is evaluated using the Adjacent Data Fluctuation Ratio (ADFR), which is defined by Eq. (3) [13].

$$ADFR = \frac{1}{n-1} \sum_{i=1}^{n-1} (x_{i+1} - x_i)^2, \tag{3}$$

where $x_i$ is the value of a point of time series and $n$ is the length of time series. The ADFR of six datasets is shown in Table 1.

## 4.2 Experimental Method

In order to analyze the characteristic of PLR, which is based on Local Maximum Minimum and slope to extract trend feature point, the six datasets in Fig. 2 are used to compare their performance by the representative methods PAA, FPS, SEEP, and LMMS. Under the same compression ratios, the fitting error is chosen as the evaluation index of algorithm. The six datasets in the experiment are sampled from

(a) Fitting error of algorithms in
Leleccum

(b) Fitting error of algorithms in
Bearing Vibration

(c) Fitting error of algorithms in EEG

(d) Fitting error of algorithms in
Jokulsa_river

(e) Fitting error of algorithms in
Rotor Rub

(f) Fitting error of algorithms in
Gear Broken
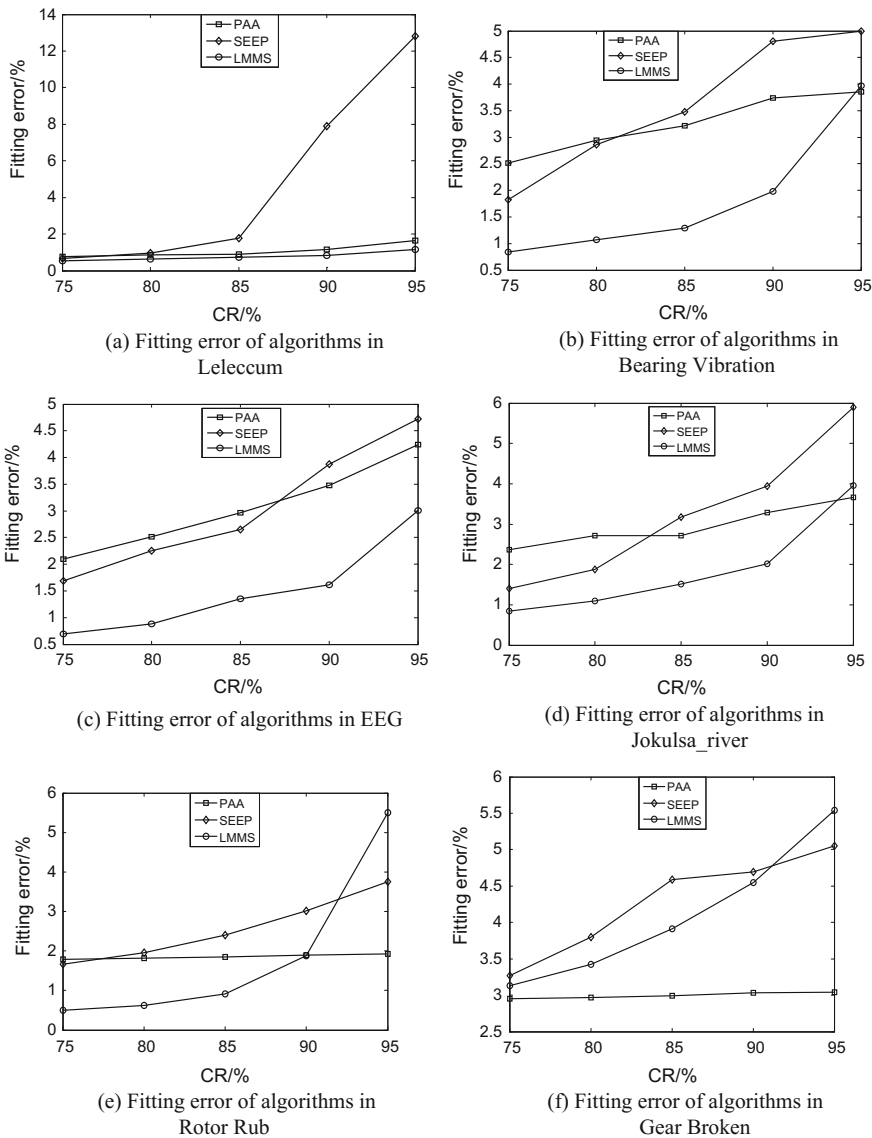
**Fig. 3** Fitting error of algorithms in different areas of time series data

different fields and the difference of numerical value is very large. In the data, values
are normalized within range [0, 1] according to the Eq. (4).

$$\text{norm}(x_i) = \frac{x_i - \min(x)}{\max(x) - \min(x)} \tag{4}$$

**Table 2** Fitting errors of algorithms in CR of 80%

| CR | 80% | | | |
|---|---|---|---|---|
| Algorithm Datasets | PAA | FPS | SEEP | LMMS |
| Leleccum | 0.85 | 0.74 | 0.96 | 0.63 |
| Bearing vibration | 2.94 | 1.65 | 2.86 | 1.07 |
| EEG | 2.51 | 1.65 | 2.25 | 0.88 |
| Jokulsa_river | 2.71 | 2.63 | 1.87 | 1.09 |
| Rotor rub | 1.82 | 2.2 | 1.95 | 0.62 |
| Gear broken | 2.97 | [a] | 3.80 | 3.42 |

[a]Means this algorithm on the dataset does not exist corresponding CR

## 4.3 Results and Discussions

### 4.3.1 A Comparison of Four PLR Algorithms Under Same Compression Ratios

In the experiment, the compression ratio of the PLR is 80%. The results of different algorithms on different datasets are shown in Table 2.

The results show that the fitting error of LMMS algorithm at the first five time series is least when the compression ratio is 80%. The whole fitting error of PAA algorithm is relatively stable but weakens local trends feature. The ability of FPS algorithm cannot meet the needs of compression ratio. The SEEP algorithm has a very good effect when the variation amplitude of slope of the time series is focused. By extracting trend feature points, piecewise linear representation LMMS reflects the feature of the time series accurately and ensures a high fitting quality.

### 4.3.2 A Comparison of PLR Algorithm Under Different Compression Ratios

Under different compression ratios, the fitting error of three algorithm of PLR is compared at each dataset. The value of the compression ratios are 75, 80, 85, 90, and 95%, the experimental results are shown in Fig. 3.

As can be seen from Fig. 3, the LMMS algorithm proposed in this chapter has obvious advantages in terms of time series datasets Leleccum, Bearing Vibration, EEG, Jokulsa river, and Rotor Rub. The fitting error is less than the other two algorithms when the compression ratio is less than or equal to 90%. The fitting error is large with a high compression ratio using the three algorithms. The fitting error of PAA algorithm showed relatively stable. The fitting error increases as the compression ratio increases. The fitting error is relatively slow and steady growth under the low compression ratio. If the compression ratio is more than 85%, there is a significant growth trend.

**Fig. 4** C336rmx_50353
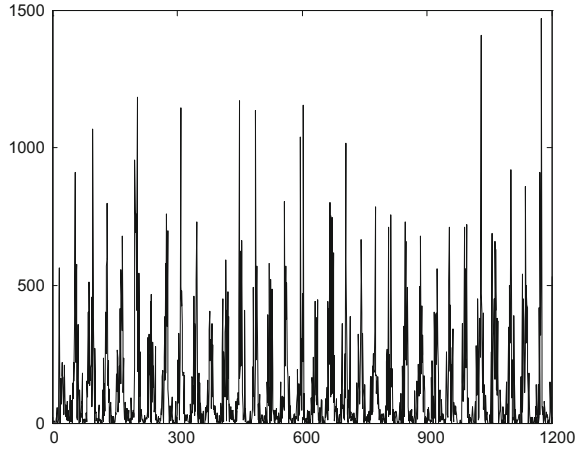


**Fig. 5** Fitting errors of algorithms
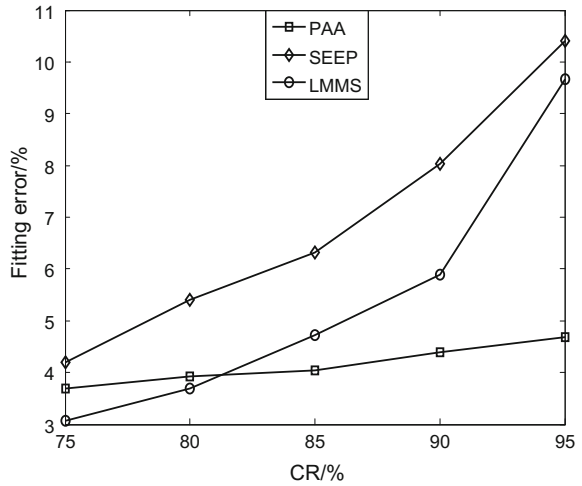


### 4.3.3 Discussions

The C336rmx_50353 dataset is about ten-day average rainfall of the 50353 station in China from 1954 to 1987. It is shown in Fig. 4. Its ADFR is 0.0216 more than other datasets. On comparing the performance of algorithm of PLR under different compression ratios on this dataset, the result of experiment is shown in Fig. 5.

In this section, we compare the experimental results of the Rotor Rub dataset and the C336rmx_50353 dataset. There is a close relationship between the fitting error of piecewise linear representation and the whole volatility characteristic of time series datasets itself. The LMMS algorithm of PLR can meet the requirement of different compression ratios of low volatility time series, which has little fitting error, stable performance, and good adaptability. When the whole volatility of the data is

relatively large, the LMMS algorithm is suitable for piecewise linear representation at a low compression ratio. The fitting error of algorithm PAA is less at a high compression ratio. Especially for datasets C336rmx_50353, its volatility value is large, and piecewise linear representation does not fit very well. Piecewise linear representation of time series is usually difficult to adapt to different time series data characteristics, and it needs to use appropriate algorithms for piecewise linear representation according to the different characteristics of the data. Accordingly, it can help improve the efficiency and accuracy of the data mining algorithms, which will provide policy support for data analysis.

## 5 Conclusion

In this chapter, the LMMS algorithm of piecewise linear representation based on the trend feature points was proposed, which integrated the ideas of local optimum value and the variation amplitude of slope. The primary trend feature of time series was accurately extracted with trend feature points as the segment points.

The results of experiment showed that the LMMS algorithm met the requirements of different compression ratios, and ensured small fitting error, stable performance and good adaptability in time series datasets with low volatility. The high volatility of the time series datasets required lower compression ratio for the fitting effect to be ideal. We compared the performance of the upper four algorithms using same compression ratio and different compression ratios and discovered that the fitting error of piecewise linear representation was influenced by the compression ratio of requirement and the whole volatility of the time series data. The fitting error increased when the whole volatility of datasets and the compression ratios increased. According to the whole characteristics of the data and the requirement of compression ratio choosing a suitable algorithm will improve the accuracy and reliability of data mining. The efficiency and effectiveness of time series data mining with this algorithm will improve using the LMMS algorithm.

## References

1. Keogh E, Smyth P (1997) A probabilistic approach to fast pattern matching in time series databases. Knowl Disc Databases 1997:24–30
2. Keogh E, Chu S, Hart D et al (2001) An online algorithm for segmenting time series, In: Proceedings of IEEE 13th international conference on data mining (ICDM), San Jose, CA, USA, pp 289–296

3. Lin J, Keogh E, Wei L et al (2007) Experiencing SAX: a novel symbolic representation of time series. Data Min Knowl Disc 15(2):107–144
4. Keogh E, Chakrabarti K, Pazzani M et al (2001) Dimensionality reduction for fast similarity search in large time series databases. Knowl Inf Syst 3(3):263–286
5. Perng CS, Wang H, Zhang SR et al (2000) Landmarks: a new model for similarity-based pattern querying in time series databases. In: Proceedings IEEE 16th international conference on data engineering, San Diego, CA, USA, pp 33–42
6. Xiao H, Hu Y (2005) Data mining based on segmented time warping distance in time series database. J Comput Res Dev 42(1):72–78
7. Zhan Y, Xu R, Chen X (2006) Time series piecewise linear representation based on slop extract edge point. Comput Sci 33(11):139–142
8. Jia PT, LIN W, He HC (2008) Adaptive piecewise linear representation of time series based on error restricted. Comput Eng Appl 44(5):10–13
9. Guerrero JL, Berlanga A, García J et al (2010) Piecewise linear representation segmentation as a multiobjective optimization problem, distributed computing and artificial intelligence. Springer, Berlin, pp 267–274
10. Charbonnier S, Damour D (2008) A robust auto-tuning on-line trend extraction method. Proc 17th IFAC World Congr 17(1):7288–7293
11. Hu B, Rakthanmanon T, Hao Y et al (2014) Using the minimum description length to discover the intrinsic cardinality and dimensionality of time series. Data Min Knowl Discov 2014:1–42
12. Zhou Q, Wu TJ (2007) Trend feature extraction method based on important points in time series. J Zhejiang Univ (Eng Sci) 41(11):1782–1787
13. Yan CF, Fang JF, Wu LX et al (2013) An approach of time series piecewise linear representation based on local maximum minimum and extremum. J Inf Comput Sci 2013:2747–2756
14. Dash S, Maurya MR, Venkatasubramanian V et al (2004) A novel interval-halving framework for automated identification of process trends. AIChE J 50(1):149–162
15. Zhao H, Guo L-L, Zeng X-Y (2016) Evaluation of bus vibration comfort based on passenger crowdsourcing mode. Math Probl Eng 2016(2132454):10p

# Passenger Presence and Injury Severity of Single-Vehicle Crashes and Rear-End Crashes with Trucks

**Quan Yuan, Shuai Jing, Yibing Li and Wei Hao**

**Abstract** Single-vehicle crashes and rear-end crashes with trucks are two major types of serious crashes in the roads of China, especially in expressways. In order to identify the influences of passenger presence on the injury severity of these crashes, 200 crash samples from Beijing were used to carry out the statistical analysis and comparative study. Chi-squared test was applied to analyze the significance of the main contributing factors related to the passenger presence in vehicles. The results revealed that driving with passengers had lower mortality than driving solo, especially for the drivers older than 25 years. Two passengers in vehicles appeared to have the lowest mortality in crashes. Male drivers with male passenger(s) had more risk to be involved in a crash than other gender groups. Compared with driving solo, when passengers existing in vehicles, speeding and low visibility increased the likelihood of rear-end crash; younger driver, speeding, suburban area increased the likelihood of single-vehicle crash. Speeding was a typical significant factor to influence the two types of crashes, which suggested that drivers with passengers were more liable to drive with over speed. These research findings are hopeful to contribute to crash prevention and injury reduction in future.

**Keywords** Passenger presence · Driver · Single-vehicle crash · Rear-end crash Severity

Q. Yuan (✉) · S. Jing · Y. Li
State Key Laboratory of Automotive Safety and Energy, Tsinghua University, Beijing 100084, China
e-mail: yuanq@tsinghua.edu.cn

W. Hao
School of Traffic and Transportation Engineering, Changsha University of Science and Technology, Changsha 410114, China
e-mail: weihaocsust@sina.com

# 1  Introduction

China is a developing country with a growing number of vehicles and very high frequency of traffic crashes. Rear-end crashes (REC) and single-vehicle crashes (SVC) make up a large proportion of traffic crashes and are usually associated with heavy casualties and property losses. Meanwhile, these two crash types represent main accidents in expressways. In China, the frequency of rear-end crashes is the third highest among various types of vehicle crashes [1]. A variety of human, vehicle, road, and environmental factors have different impacts on the occurrence of crashes. As an important factor related to traffic safety, passenger presence in vehicles may increase or decrease the risk and severity of crashes. To date, there have been some studies on how the presence of passengers in vehicles affects crashes, which provide insights on the relevant human factors in traffic events.

Many studies have revealed that the impact of passenger presence on severity and crash risk for young drivers [2–6]. There are different results, in some cases advantageous and some disadvantageous.

Passenger presence increases crash risk for teenage drivers, and the crash risk is even higher when the passengers are all male teenagers [5]. Teenagers are more likely to peer influences compared with adults. Distractions were more likely to be reported for girls and students [6]. Conversation between driver and passengers was the most typical type of distraction.

The crash risk will increase for young drivers, during darkness condition, and in slow traffic volume roadway [7]. The presence of two or more passengers will significantly increase the risk of car crash injury for younger drivers [8].

For accidents that happened at night, driving with a single passenger was safer compared with driving either solo or with two or more passengers [9]. Furthermore, significant differences are likely to exist between night and day. This may be as a result of different passenger effects on driver behavior. Drivers are used to having safer driving behavior if they are accompanied by other passengers and strong correlations are found between passengers and crash characteristics [10, 11].

In China, few studies examined the influence of passengers in vehicles on the frequency and severity of crashes. The big data of traffic accidents in China lack of information related to passengers in vehicles involved in crashes. This chapter tries to employ crash data to explore the situations of passengers in typical accidents. Using 200 serious rear-end crashes and single-vehicle crashes in Beijing, the analysis aimed to identify the factors that are related to the presence of passengers for the two main types of crashes. The results indicated how the passenger factors impact on the injury severity of crashes and provided useful insight into the severity reduction of traffic crashes.

## 2  Data and Method

### 2.1  Crash Data

100 REC crashes and 100 SVC crashes were extracted from the real-world crash cases analyzed by the Crash Reconstruction Lab of Tsinghua University for the Bureau of Beijing Traffic Security Administration. The SVC mainly refers to the collisions between vehicles and road facilities (e.g., trees, poles, barriers, and guardrails). All the vehicles involved in SVC were passenger vehicles. Every REC case contained two vehicles and all the front vehicles are trucks. The main data were obtained from the police records on the crashes, and researchers' detections on the vehicles involved in crashes.

### 2.2  Candidate Variables

The in-depth data of crashes included the information of time, driver, passenger, vehicle, road, and environment, and was described by 19 variables for each crash (Table 1). The severity levels for occupants involving in crashes were defined as not injured, injured, and fatal.

### 2.3  Statistical Methods

Based on the crash data, the characteristics of the crashes and the correlation between these factors and injury severity of crashes were examined under the consideration of how many passengers there were in vehicles. The descriptive statistics were carried out to find the relationship between the number, gender, and age of passengers in vehicle and the frequency and injury severity of crashes. And chi-square test was used to find out significant variables related to the status of passenger presence in vehicles.

## 3  Results

### 3.1  Descriptive Statistics

Overall, Table 2 shows that the frequency of driving solo (without other passengers) was much lower than that of driving with passenger(s), 73 versus 127. On the other hand, the mortality of driving solo exceeded that of driving with passengers, 56% versus 32%.

**Table 1** List of main variables related to crashes

| Type | Variables | Categories |
|------|-----------|-----------|
| Time | Time of day | Day (7:00–19:00), night |
| | Day of week | Weekday, weekend |
| Drivers | Residence | Beijing (local), other province/city |
| | Age | $\leq$25 years, >25 years |
| | Gender | Male, female |
| | Injury | Fatal, injured, not injured |
| Passengers | Presence | Yes, no |
| | Age | $\leq$25 years, >25 years |
| | Gender | Male, female |
| | Injury | Fatal, injured, not injured |
| Vehicles | Vehicle type | Commercial vehicle, passenger vehicle |
| | Crash position | Full frontal crash, offset crash |
| | Speed | Speeding, not speeding (from crash report) |
| Environment | Weather | Good (Clear), adverse (cloudy, rain, snow, haze, others) |
| | Visibility | Day, night(lighting or not) |
| | Area | Urban, suburban |
| Road | Road surface | Dry, wet |
| | Line type | Straight, crossing/exit/entrance |
| | Road type | Expressway, others |
| | Lanes in the same direction | <3 lanes, $\geq$3 lanes |

**Table 2** Driver's injury severity versus passenger number

| | Passenger number in vehicles | | | | | | | | | | | | | | | | | |
|--|--|--|--|--|--|--|--|--|--|--|--|--|--|--|--|--|--|--|
| | 0 | | | 1 | | | 2 | | | 3 | | | 4 | | | >4 | | |
| | F | I | N | F | I | N | F | I | N | F | I | N | F | I | N | F | I | N |
| REC | 17 | 16 | 3 | 11 | 30 | 5 | 1 | 7 | 1 | 1 | 2 | 0 | 0 | 1 | 0 | 2 | 1 | 2 |
| SVC | 24 | 11 | 2 | 15 | 15 | 2 | 2 | 7 | 3 | 2 | 3 | 0 | 5 | 5 | 1 | 2 | 1 | 0 |
| Total | 41 | 27 | 5 | 26 | 45 | 7 | 3 | 14 | 4 | 3 | 5 | 0 | 5 | 6 | 1 | 4 | 2 | 2 |

Note: *F* fatal; *I* injured; *N* not injured

Figure 1 shows the Mortality by passenger number for total 200 cases. It can be seen that the mortality is reduced with the increase of passenger number; it gets the lowest point at two passenger number, and then inversely turns to increase gradually. Therefore, two passengers in vehicle present the best situation.

Table 3 illustrates the driver's injury severity when compared driving solo with driving with passenger(s). For the total cases, when crashes occurred, the mortality of driving solo was higher than that of driving with passengers. For the REC, the

**Fig. 1** Mortality by passenger number for 200 cases
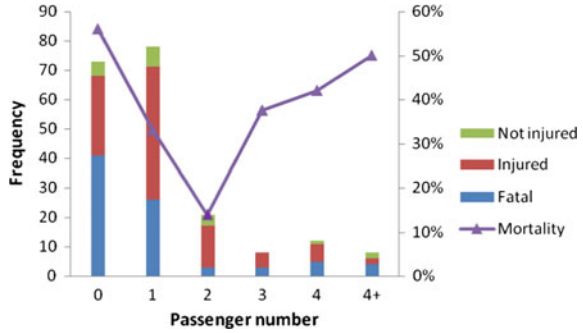


**Table 3** Driver's injury severity compared driving solo with driving with passenger(s)

| | Driving solo | | | | | Driving with passenger(s) | | | | |
|---|---|---|---|---|---|---|---|---|---|---|
| | F | I | N | Total | Mortality (%) | F | I | N | Total | Mortality (%) |
| REC | 17 | 16 | 3 | 36 | 47.2 | 15 | 41 | 8 | 64 | 23.4 |
| SVC | 24 | 11 | 2 | 37 | 64.9 | 26 | 31 | 6 | 63 | 41.3 |
| Total | 41 | 27 | 5 | 73 | 56.2 | 41 | 72 | 14 | 127 | 32.3 |

**Table 4** Occupants' gender group by two types of crashes

| Gender group type | REC N (%) | SVC N (%) | Total |
|---|---|---|---|
| Male driver/no passenger | 35 | 35 | 70 |
| Male driver/male passenger(s) | 27 | 33 | 60 |
| Male driver/female passenger(s) | 18 | 10 | 28 |
| Male driver/mixed gender | 8 | 14 | 22 |
| Male driver/unknown passenger(s) | 9 | 4 | 13 |
| Female driver/male passenger(s) | 1 | 1 | 2 |
| Female driver/mixed passenger(s) | 0 | 1 | 1 |
| Female driver/no passenger | 1 | 2 | 3 |
| Female driver/unknown passenger(s) | 1 | 0 | 1 |
| Total | 100 | 100 | 200 |

mortality of driving solo was about twice of driving with passengers (47.2% vs. 23.4%). And for the SVC, the difference of mortality was about 1.6 times higher.

Table 4 shows the different gender of passengers in vehicles, which was divided into nine different gender groups.

For the two crash types, solo driving of male driver accounted for 35% and ranked first. Male driver with male passengers accounted for 27 and 33%, respectively, which ranked second. Male drivers with male passengers had more proportions than male drivers with female passengers or mixed gender passengers, especially for the SVC.

**Table 5** Male driver and passengers with different gender versus injury severity in fatal crashes

|  | Rear crash | | Single crash | | Total | |
|---|---|---|---|---|---|---|
|  | Fatal (%) | Injured | Fatal (%) | Injured | Fatal (%) | Injured |
| Male driver/male passenger(s) | 17 (63) | 10 | 14 | 18 | 31 | 28 |
| Male driver/female passenger(s) | 14 (74) | 4 | 4 | 6 | 18 | 10 |
| Male driver/mixed gender | 6 (75) | 2 | 6 | 8 | 12 | 10 |
| Male driver/no passenger | 16 (46) | 19 | 23 | 12 | 39 | 31 |
| Total | 53 | 35 | 47 | 44 | 100 | 79 |

Table 5 presents the driver's injury severity with different gender group of passengers for male drivers in fatal crashes. Totally, driving solo ranked first and male driver–male passengers appeared second. The two types of crashes had quite different results. Solo driving of male driver accounted for 33% for REC and 49% for SVC. From this result, it can be concluded that driving solo is apt to involve in single-vehicle crash. Male driver with male passengers had a larger share than the group involving mixed gender.

Table 6 shows the different injury severity with different driver's age and number of passengers in vehicles. In REC, for the younger driver ($\leq 25$ years), driving with passengers had higher mortality than driving solo (54% vs. 29%). However, for the older driver (>25 years), the contrary situation appeared; driving with passengers possessed of lower mortality than driving solo (16% vs. 52%). In SVC, whether younger or older drivers, driving solo resulted in higher mortality than driving with passengers and the differences are close. Totally, for younger drivers, these two situations of passenger presence had similar mortality (46% vs. 44%), while for older drivers, driving solo had higher mortality than driving with passengers (58% vs. 27%).

## 3.2 Chi-Square Test

Based on the data above, descriptive statistics was summarized in Tables 7 and 8. Further, Chi-square tests were performed on individual pairs to evaluate the relationship of typical variables with the status of passenger existence. Results showed that for the REC, vehicle speed, vehicle type, visibility, and road surface status were significant factors related to having passenger(s) and no passengers in vehicles. For SVC, driver's age, speeding, and crash area were significant factors associated with the passenger carriage situation. For these two types of crashes, speeding was the overlapped significant factor, which revealed that drivers with other passenger(s) were more likely to drive with over speed.

**Table 6** Driver's age versus injury severity

| | | Driving solo | | | | Driving with passenger(s) | | | |
|---|---|---|---|---|---|---|---|---|---|
| | | F | I | N | Mortality (%) | F | I | N | Mortality (%) |
| REC | ≤25 years | 2 | 5 | 0 | 29 | 7 | 5 | 1 | 54 |
| | >25 years | 15 | 11 | 3 | 52 | 8 | 36 | 7 | 16 |
| | Subtotal | 17 | 16 | 3 | 47 | 15 | 41 | 8 | 23 |
| SVC | ≤25 years | 4 | 1 | 1 | 67 | 9 | 12 | 2 | 39 |
| | >25 years | 20 | 10 | 1 | 65 | 17 | 19 | 4 | 43 |
| | Subtotal | 24 | 11 | 2 | 65 | 26 | 31 | 6 | 41 |
| Total | ≤25 years | 6 | 6 | 1 | 46 | 16 | 17 | 3 | 44 |
| | >25 years | 35 | 21 | 4 | 58 | 25 | 55 | 11 | 27 |
| | Total | 41 | 27 | 5 | 56 | 41 | 72 | 14 | 32 |

Note: *F* fatal; *I* injured; *N* not injured

**Table 7** Data summary of REC

| Variables | Categories | Having passenger(s) (%) | No passenger(s) (%) | Chi-squared | *p*-Value |
|---|---|---|---|---|---|
| Time of day | Night (19:00–7:00) | 47 | 25 | 0.18 | 0.67 |
| Residence | Other province/city | 50 | 28 | 0.002 | 0.97 |
| Drivers' age | Younger driver (<26 years) | 13 | 7 | 0.01 | 0.92 |
| Speed | Speeding | 42 | 33 | 8.33 | 0.004[***] |
| Crash area | Suburban | 42 | 24 | 0.01 | 0.92 |
| Crash position | Full frontal | 42 | 19 | 1.6 | 0.2 |
| Rear vehicle type | Passenger vehicle | 29 | 18 | 3.39 | 0.07[**] |
| Weather | Adverse weather | 11 | 8 | 038 | 0.54 |
| Visibility | Adverse visibility | 27 | 7 | 5.31 | 0.02[***] |
| Road line | Crossing/entrance | 6 | 6 | 1.16 | 0.28 |
| Road surface | Wet | 1 | 4 | 4.42 | 0.04[***] |
| Road type | Express way | 29 | 12 | 1.37 | 0.24 |
| Day of week | Weekday | 51 | 25 | 1.33 | 0.25 |
| Lanes in the same direction | ≥3 lanes | 31 | 19 | 0.17 | 0.68 |

[***]Statistical significant for 95%, [**]Statistical significant for 90%

**Table 8** Data summary of SVC

| Variables | Categories | Having passenger(s) (%) | No passenger(s) (%) | Chi-squared | p-Value |
|---|---|---|---|---|---|
| Time of day | Night (19:00–7:00) | 37 | 21 | 0.037 | 0.847 |
| Residence | Other province/city | 25 | 11 | 0.717 | 0.397 |
| Drivers' age | Younger driver (<26 years) | 24 | 6 | 5.31 | 0.02[***] |
| Speed | Speeding | 50 | 22 | 4.58 | 0.03[***] |
| Crash area | Suburban | 53 | 24 | 4.88 | 0.027[***] |
| Crash position | Full frontal | 29 | 52 | 0.26 | 0.609 |
| vehicle type | Passenger vehicle | 51 | 32 | 0.506 | 0.477 |
| Weather | Adverse weather | 3 | 11 | 1.69 | 0.19 |
| Visibility | Adverse visibility | 20 | 31 | 0.22 | 0.64 |
| Road line | Crossing/entrance | 5 | 8 | 0.01 | 0.907 |
| Road surface | Wet | 10 | 3 | 1.24 | 0.265 |
| Road type | Express way | 6 | 9 | 0.07 | 0.794 |
| Day of week | Weekday | 37 | 23 | 0.114 | 0.735 |
| Lanes in the same direction | ≥3 lanes | 8 | 17 | 0.3575 | 0.55 |

[***]Statistical significant for 95%

## 4 Discussion

The statistical results revealed the characteristics of passengers in these selected crashes, such as gender, age, number, and their corresponding influence on the injury severity of crashes, as well as their relationship with other factors of crashes.

In the cases, the frequency of driving with passengers was much higher than that of driving solo, which is similar to the findings of Lam et al. [8]. However, the mortality of driving solo exceeded that of driving with passenger. This means that drivers are less likely to be involved in a fatal crash when accompanied by other passengers, which are in common with the research results of Rueda-Domingo et al. [10]. Furthermore, crash data showed that two passengers except for drivers in vehicles constitute the safest situation with lowest mortality when crashes happened.

For the two types of crashes, solo driving of male drivers accounted for 35% and ranked the first. Male drivers with male passengers had the proportions of 27 and 33%, respectively. Male drivers and male passengers in vehicles were involved in more crashes than male drivers with female passengers or passengers with mixed gender. In other words, male drivers with male passengers had higher crash risk, which is consistent with the previous research findings [5].

The analysis of these selected two types of crashes revealed quite different results. Male drivers driving solo accounted for 33% for REC and 49% for SVC. From this result, it can be concluded that solo drivers without passengers' company are likely to be involved in single-vehicle crashes, which is inconsistent with other similar studies [11]. Passengers' influence on driving safety is quite different with different countries and traffic culture.

Concerning driver's age, in REC, the older driver (>25 years) driving with passengers caused much lower mortality than driving solo (16% vs. 52%), while the younger driver (≤25 years) appeared a contrary situation. In SVC, for all drivers, whether younger or older, driving with passengers had lower mortality than driving solo. Totally, for younger drivers (≤25 years), these two situations of passenger presence had similar mortality and for older drivers (>25 years), driving solo had higher mortality than driving with passengers. Therefore, in general, it can be seen that driving with passengers is safer than driving solo, especially for the older drivers (>25 years). Although more passengers in vehicles may cause distraction of drivers, we found a different result that more passengers are safer. Perhaps people drive more carefully when they are accompanied by other related passengers (e.g., family members, important colleagues, etc.).

Chi-square tests showed that for REC, a significantly larger proportion of having passenger(s) and no passengers in vehicles were related to speeding, vehicle type, visibility, and road surface status. When there were passengers in vehicles, speeding and bad visibility increased the likelihood of rear-end crash. On the other hand, for SVC driver's age, speeding and crash area were significant factors associated with the passenger carriage status. When there were other passengers in vehicles, younger driver (≤25 years), speeding, location (suburban area) increased the likelihood of single-vehicle crash. Moreover, speeding was a common factor for the two types of crashes, which revealed that drivers with other passengers were more liable to drive with over speed. Younger drivers with younger passengers were more likely to be involved in SVC in high-speed conditions, which is consistent with Lee and Abdel-Aty [11].

In China, there have been some new related policy and law for the passenger presence in vehicles, such as if trainee drivers will drive cars into the expressway, they should be companied by a skilled driver with at least three years driving experience. Like that, the influence of passengers will be further studied and applied in the improvement of traffic safety.

## 5 Conclusion

To sum up, this chapter demonstrated the influences of passenger presence on injury severity based on the related data of 200 serious rear-end crashes and single-vehicle crashes in Beijing, China. In general, for the selected crash cases, driving with passengers are safer than driving solo. Two passengers with the driver in vehicles appeared to have the lowest mortality in crashes. For the two crash types, solo drivers are more

likely to be involved in single-vehicle crashes. Compared with other gender groups, male drivers with male passengers had higher crash risk. And older drivers are likely to be involved in fatal rear-end crashes when driving solo at night. Compared with driving solo, when there were other occupants in vehicles, speeding and low visibility increased the likelihood of rear-end crash; younger driver, and speeding, suburban area increased the likelihood of single-vehicle crash. These conclusions may provide useful reference for the research of automotive safety and crash prevention. In future, more in-depth data analysis and statistics will be carried out, and more insightful results could contribute to the relevant research of traffic safety and injury reduction of occupants.

# References

1. Traffic Management Bureau of the Ministry of Public Security of China. Annual Statistical Report of China Road Traffic Collisions (2012), Beijing, 2013
2. Engström I, Gregersen NP, Granström K et al (2008) Young drivers–reduced crash risk with passengers in the vehicle. Accid Anal Prev 40(1):341–348
3. Simons-Morton B, Lerner N, Singer J (2005) The observed effects of teenage passengers on the risky driving behavior of teenage drivers. Accid Anal Prev 37(6):973–982
4. Simons-Morton BG, Ouimet MC, Zhang Z et al (2011) The effect of passengers and risk-taking friends on risky driving and crashes/near crashes among novice teenagers. J Adolesc Health Official Publ Soc Adolesc Med 49(6):587–593
5. Williams AF, Ferguson SA, McCartt AT (2007) Passenger effects on teenage driving and opportunities for reducing the risks of such travel. J Saf Res 38:381–390
6. Heck KE, Carlo RM (2008) Passenger distractions among adolescent drivers. J Saf Res 39:437–443
7. Vollrath M, Meilinger T, Kruger H (2002) How the presence of passengers influences the risk of a collision with another vehicle. Accid Anal Prev 34:649–654
8. Lam LT, Norton R, Woodward M et al (2003) Passenger carriage and car crash injury: a comparison between younger and older drivers. Accid Anal Prev 35:861–867
9. Keall MD, Frith WJ, Patterson TL (2004) The influence of alcohol, age and number of passengers on the night-time risk of driver fatal injury in New Zealand. Accid Anal Prev 36:49–61
10. Rueda-Domingo T, Lardelli-Claret P, Luna-del-Castillo JD et al (2004) The influence of passengers on the risk of the driver causing a car collision in Spain analysis of collisions from 1990 to 1999. Accid Anal Prev 36:481–489
11. Lee C, Abdel-Aty M (2008) Presence of passengers: does it increase or reduce driver's crash potential? Accid Anal Prev 40:1703–1712

# Study on the Electric Vehicle Adaptive Cruise Control Based on the Model Predictive Control Algorithm

**Zhenhai Gao and Hai Song**

**Abstract** In this chapter, according to the characteristics of the electric vehicle regenerative braking, considering safety, economy, and comfort in adaptive cruise control, a kind of electric vehicle adaptive cruise control algorithm has been built, which has two layers, the decision layer calculates the optimal acceleration based on the model predictive control algorithm and vehicle longitudinal control layer tracks the optimal acceleration with fuzzy algorithm. Then, using the software Amesim and Simulink to simulate the typical working condition simulations, the results show that the control algorithm can effectively realize electric vehicle adaptive cruise, and capture braking energy.

**Keywords** Electric cars · Adaptive cruise control · Model predictive control

## 1 Introduction

The adaptive cruise system is a kind of advanced driving assistant systems, through the sensor such as millimeter wave radar obtaining the velocity and distance from ahead vehicle, and by controlling the host vehicle speed it can keep the safe distance from the other vehicles to implement adaptive cruise [1, 2]. The adaptive cruise technology was developing rapidly, many scholars did deep research in it, Gennaro Nicola Bifulco et al. analysed the driving characteristics using the learning feature of human to achieve adaptive cruise [3], Seungwuk Moon et al. used the collision time index and data of drivers without collision based on the confusion matrix method to design the whole speed range of adaptive cruise, and tested in real vehicles [4].

Z. Gao · H. Song (✉)
State Key Laboratory of Automotive Simulation and Control, Jilin University, Changchun 130022, China
e-mail: songhai1985@sina.com

39

With the increasing number of car in recent years, automobile exhaust pollution was more and more serious. The electric vehicles with low emissions, environmental protection began to get more and more application. In the field of new energy, vehicle's advanced driver assistance technologies, Behnam Ganji, Abbas z. Kouzani et al. used sliding mode control with hybrid vehicle as research object to achieve the technology of adaptive cruise [5], Sebastien Glaser et al. proposed the green intelligent adaptive cruise system, using the pure electric vehicle as the research platform, introduced how to use the electric car energy recovery characteristics to design the adaptive cruise system.

From above, it can be seen that there are the similarities and differences between the electric vehicle adaptive cruise system and the traditional vehicle adaptive cruise system. For the comprehensive solution of the electric vehicle safety, energy saving and comfort in the adaptive cruise, with the characteristics of regenerative braking of electric vehicle, we proposed an electric vehicle adaptive cruise control system to realize adaptive cruise considering electric motor properties, the giving control system consists of the decision layer and the vehicle longitudinal control layer. The decision layer computes the optimal vehicle acceleration by the information from outside sensors. Through calculating the vehicle longitudinal control layer to calculate the motor and the braking system control quantity, then it implements tracking the vehicle acceleration accurately and maximizes the recovery of braking energy.

## 2  The Decision Algorithm Design

Model predictive control is a method of optimization control, which solves the sampling process of a limited open-loop optimal problem in each control action to obtain the optimal control effect [7]. In control process, the initial state of the optimal control problem is the current state, and the solution of optimal control sequence only implemented on the first control action.

### 2.1  Prediction Model

We use the pure electric vehicle as the research object for analysis. The movement of vehicles relations and the host vehicle dynamic states are used as a predictive model. As shown in Fig. 1, according to Newton's motion laws, we get the electric vehicle longitudinal dynamics Formula (1); in Formula (1), D is the distance between the host vehicle and ahead vehicle; $v_{rel}$ is relative speed of two vehicles; $T_s$ is the time step; $a_h$ is the acceleration of the host vehicle; $v_h$ is the host vehicle velocity; $j$ is the jerk of the host vehicle; $u(k)$ is the incremental acceleration of the input system. In the real scenario, D and $v_{rel}$ are measuring by sensors such as millimeter wave radar, and other information measuring by electric car sensors, reading on the can bus.

**Fig. 1** The prediction model
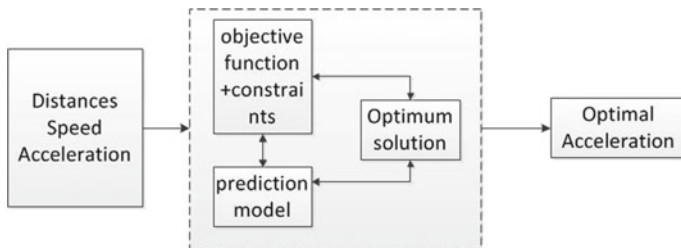


**Fig. 2** The decision controller frame

$$\begin{cases} D(k+1) = D(k) + v_{\text{rel}}(k)T_s - \frac{1}{2}a_h(k)T_s^2 \\ v_{\text{rel}}(k+1) = v_{\text{rel}}(k) - a_h(k)T_s \\ v_h(k+1) = v_h(k) + a_h(k)T_s \\ a_h(k+1) = (1 - \frac{T_s}{\tau})a_h(k) + \frac{T_s}{\tau}u(k) \\ j(k+1) = -\frac{1}{\tau}a_h(k) - \frac{1}{\tau}u(k) \end{cases} \tag{1}$$

## 2.2 Model Predictive Controller Design

According to the mathematical vehicle model, which was established in Formula (1), we can establish a framework for decision controller shown in Fig. 2.

According to the given vehicle, following movement Formula (1), it can define the model state: $x(k)$, which is $x(k) = [D(k), v_{\text{rel}}(k), v_h(k), a_h(k), j(k)]$. Then, it can be written as matrix form

$$x(k+1) = Ax(k) + Bu(k) \tag{2}$$

In which

$$A = \begin{bmatrix} 1 & 0 & T_{\mathrm{s}} & -\frac{1}{2}T_{\mathrm{s}}^2 & 0 \\ 0 & 1 & 0 & -\frac{1}{2}T_{\mathrm{s}}^2 & 0 \\ 0 & 0 & 0 & -T_{\mathrm{s}} & 0 \\ 0 & 0 & 0 & 1-\frac{T_{\mathrm{s}}}{\tau} & 0 \\ 0 & 0 & 0 & -\frac{1}{\tau} & 0 \end{bmatrix} \quad B = \begin{bmatrix} 0 \\ 0 \\ 0 \\ \frac{T_{\mathrm{s}}}{\tau} \\ \frac{1}{\tau} \end{bmatrix}$$

### 2.2.1 The Objective Function

The objective function is the cost function to achieve electric vehicle optimal performance on the road. The performance of the electric vehicle mainly evaluating the safety, energy consumption, and convenience [8]. Generally, using distance to evaluate safety, with the variable time headway model [9], the optimization goal is to minimize the real and desired distance between the host vehicle and ahead vehicle.

Electric vehicles use motor to drive, its energy consumption evaluation characterization through battery charged state, also can be described by motor power change. So it can be used for the change of the output torque of the motor to measure the energy consumption. The electric vehicle acceleration is proportional to the motor torque so that we can use the electric vehicle acceleration to describe the status of energy consumption, the optimization goal of energy consumption is to minimize the electric vehicle acceleration.

In vehicle dynamics, the vehicle acceleration and jerk commonly are described as the vehicles driving smooth while adding speed or subtracting speed. The cost function J can be used to evaluate the electric vehicles comfort. The vehicle comfortable optimization goal is to minimize the jerk and acceleration.

According to the above optimization goal, the cost function J of model predictive controller is designed. The cost function J is used to predict the optimal control in each control iteration step. The controller predictive time domain is $N_{\mathrm{P}}$, control item domain is $N_{\mathrm{C}}$. From above the cost function, J needs safety, comfortable, and energy consumption goal to minimize, Formula (2) shows the matrix form of the vehicle state. We put the cost function in the prediction of deviation value domain and control domain as shown in (3), in which the first part calculates the predicted field deviation value, the second part calculates the control domain system accumulated value of input amount. On each control cycle through solving the minimizing the cost function J, it can be calculated the optimal acceleration value of the decision layer.

$$J = \sum_{i=1}^{Np} \|x(k+i|t) - x_{\mathrm{ref}}(k+i|t)\|_Q^2 + \sum_{i=1}^{Nc} \|u(k+i|t)\|_R^2 \tag{3}$$

### 2.2.2 The Constraint

Vehicle adaptive cruise system is usually working in a safe range, the system runs in a fixed range generally, the control quantity and control increment quantity need to limit, so system required the constraints

$$u_{\min} = -5.5 \text{ m/s}^2, \quad u_{\max} = 2.5 \text{ m/s}^2, \quad \Delta u_{\min} = -2 \text{ m/s}^3, \quad \Delta u_{\max} = 2 \text{ m/s}^3$$

The controller need to control every step of constraints that

$$u_{\min}(t+k) \leq u(t+k) \leq u_{\max}(t+k) \qquad k = 0, 1, \ldots, N_c - 1$$
$$\Delta u_{\min}(t+k) \leq \Delta u(t+k) \leq \Delta u_{\max}(t+k) \quad k = 0, 1, \ldots, N_c - 1$$

## 3 The Vehicle Longitudinal Control Algorithm Design

From above, the optimal acceleration is calculated by decision layer, we need to change the optimal acceleration to the input of motor and braking system, it needs to calculate the control quantity. So the vehicle longitudinal control layer is established as a control block diagram shown in Fig. 3, which uses the optimal acceleration to control quantity for the motor and braking system.

The electric vehicle can recover energy while the vehicle is braking, so we establish a fuzzy decision module in the controller to calculate the regenerative braking and traditional braking rate. The input of decision module is the vehicle speed and acceleration, the output is the motor regenerative braking percentage in total braking so that the controller is able to use the acceleration error to calculate the control quantity the motor and the braking system of electric vehicle.
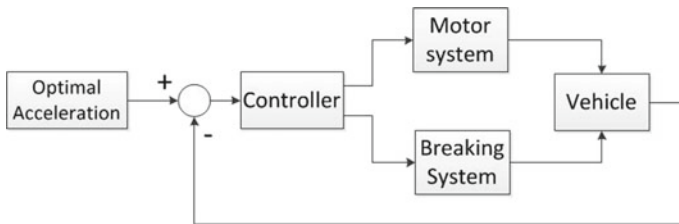


**Fig. 3** The framework of control layer

# 4 Simulation

## 4.1 Model Building

In the field of multidisciplinary complex system modeling and simulating platform software Amesim, a kind of electric vehicle physical model has been structured, shown in Fig. 4.

Reference controller algorithm which given in the second quarter, with the visualization simulation tool simulink, the upper model predictive controller model is built, as shown in Fig. 5. The top decision-making unit, which uses model predictive control algorithm in the second quarter, is encapsulated to the S function module of simulink to achieve calculating the optimum acceleration. Lower level executive level controller uses fuzzy algorithm, through rules designed to calculate the braking force distribution coefficient, and then the input optimal acceleration of the control layer is changed into actual control quantity of motor and the braking system, then the control quantity is sending to the Amesim electric vehicle model. By the method of Amesim, turning its model into S function of simulink, then implementation to simulink as the main body of the joint simulation.
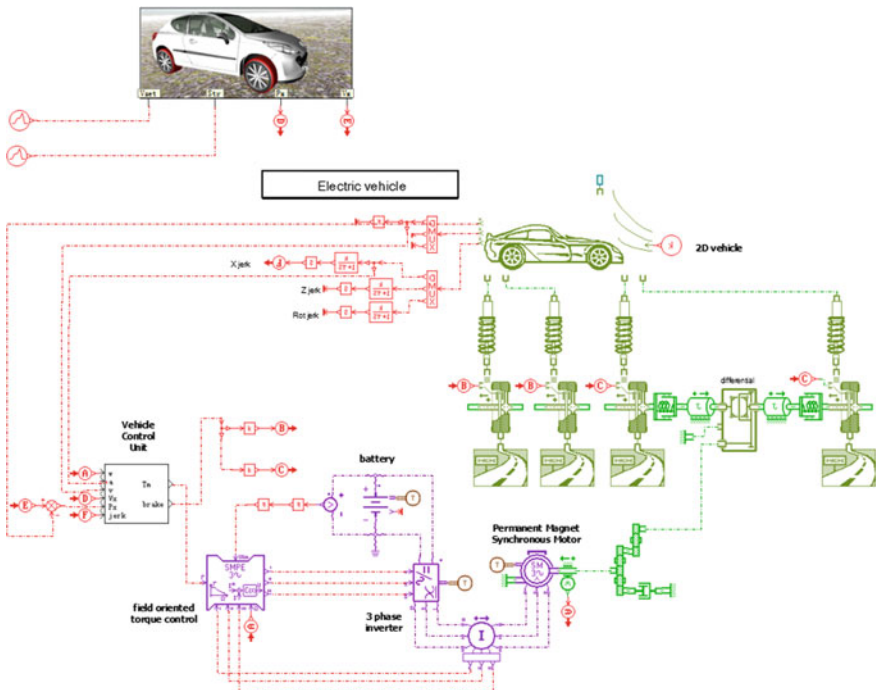


**Fig. 4** The host vehicles and ahead vehicle model
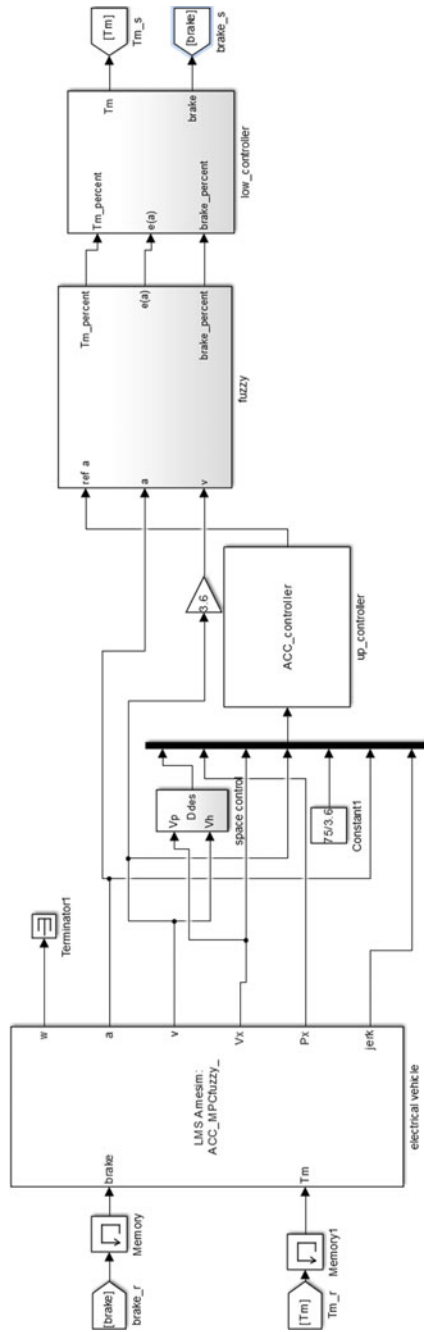
**Fig. 5** The electric vehicle controller model in simulink in Amesim

## *4.2   The Simulation Results*

We select three typical working conditions of adaptive cruise for electric vehicle adaptive cruise simulation experiments, respectively is linear variable speed cruise condition, following condition, cut in following condition.

### 4.2.1   Linear Variable Set Speed Cruise Condition

As shown in Fig. 6, dotted line in the figure represents the target speed, and the solid line shows the actual speed. First, the vehicle speed stability to 30 km/h, at $T = 50$ s when the target speed is set to 40 km/h, at $T = 100$ s when the target speed is set to 55 km/h, at $T = 150$ s when the target speed is set to 40 km/h, at $T = 200$ s when the target speed is set to 35 km/h. As you can see by the picture, the target speed change, speed on the local immediately follow the target speed, smooth change can be stable after 10 s to the target speed.

The cruise condition decision-making target acceleration and the actual vehicle acceleration as shown in Fig. 7, can be seen from the figure in the actual vehicle acceleration and speed of a target price it is better to follow, to ensure the adaptive cruise control system, the realization of the function of cruise control.

### 4.2.2   The Following Condition

As shown in Fig. 8, the host vehicle is driving with speed of 55 km/h, the ahead vehicle in the same lane driving at 40 km/h, at start two vehicles are far away (100 m); with the gap between two vehicles shrinking, the host vehicle switches to the following pattern, keeps the distance in 20 m, and makes the speed as same as the ahead vehicle.
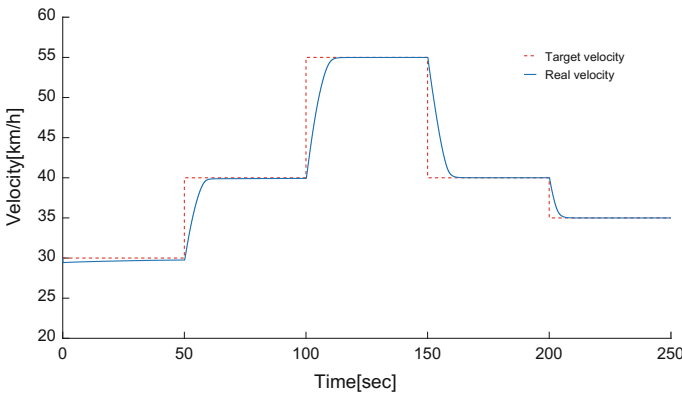


**Fig. 6**  The velocity of cruise condition time history curve
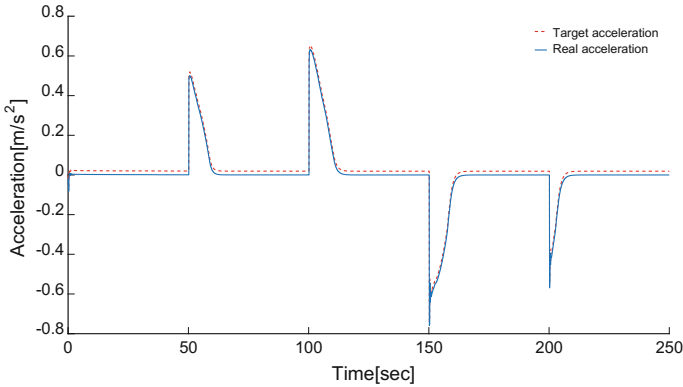
**Fig. 7** The acceleration of cruise condition time history curve
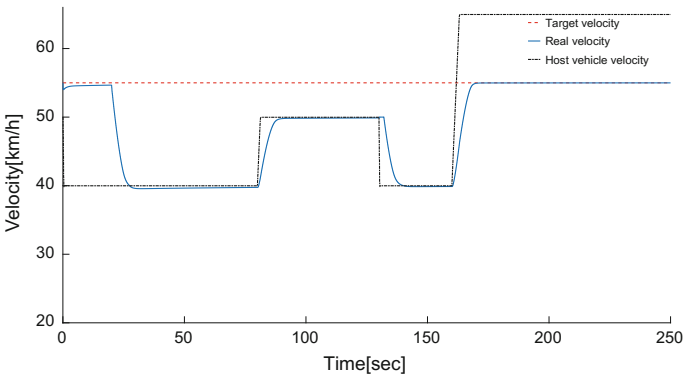


**Fig. 8** The velocity of following condition time history curve

Finally, the ahead vehicle accelerates to 65 km/h, with the distance increasing, when the distance large than a certain value, adaptive cruise control system keeps the set speed of 55 km/h. It can be seen from Fig. 8, when the host vehicle closes to the ahead vehicle, the speed of the host vehicle reducing gradually, then it reaches to the same speed as the ahead vehicle. In the process of following, no matter the ahead vehicle accelerating or decelerating, the host vehicle can follow the velocity of the ahead vehicle quickly and smoothly. When the ahead vehicle is driving away, the host vehicle can restore the cruise control, and keep the speed to the set value.

The acceleration of decision by cruise condition and the actual vehicle acceleration are shown in Fig. 9, it can be seen from the figure that the vehicle's actual acceleration and speed of target following target acceleration and speed well, shown that the host vehicle's actual acceleration can follow the target acceleration quickly and accurately. In this condition, the distances between the two vehicles are shown in Fig. 10, you can see when closing to the ahead vehicle, the adaptive cruise system can control the distance of the ahead vehicle and host vehicle effectively, then keep a safe distance.
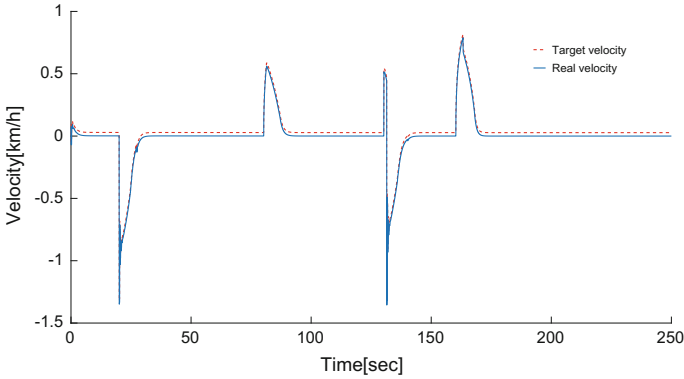
**Fig. 9** The acceleration of following condition time history curve
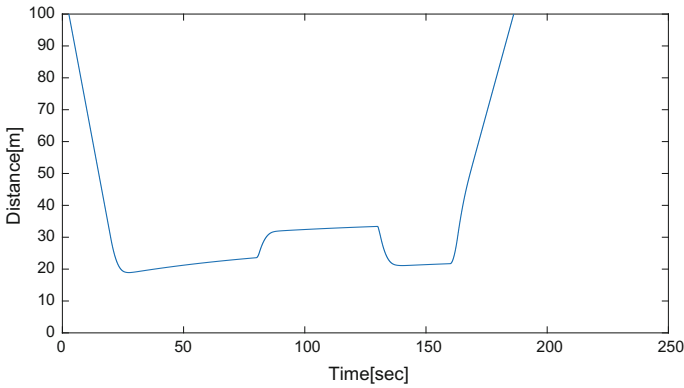


**Fig. 10** The distance of following condition time history curve

### 4.2.3 The Cut in Following Conditions

As shown in Fig. 11, the host vehicle is driving with speed of 75 km/h. The ahead vehicle with speed of 80 km/h cut in 30 m place away in the front lane, and to slow down to 55 km/h, again after uniform speed to 40 km/h, and then accelerate to 70 km/h and switch lanes. Can be seen from Fig. 12 vehicle ahead after cut into the lane on the local deceleration, began to slow to follow on the local vehicle ahead, in the process of vehicle ahead change the speed still can follow the change of the velocity.

It can be seen from the Fig. 13, adaptive cruise system effectively control the distance between the host vehicle and ahead vehicle, in the case of sharp slowdown of ahead vehicle the system can ensure the safe distance.
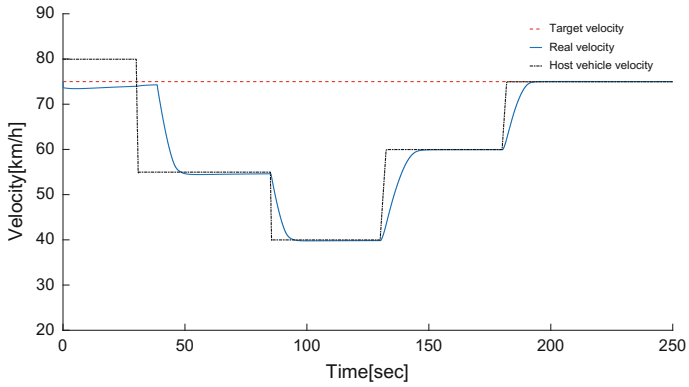
**Fig. 11** The velocity of cut in condition time history curve
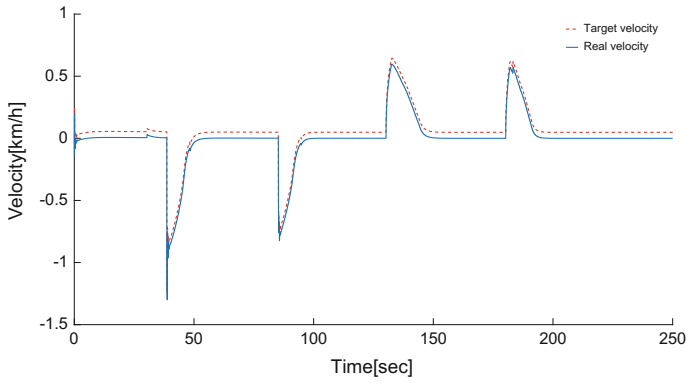


**Fig. 12** The acceleration of cut in condition time history curve
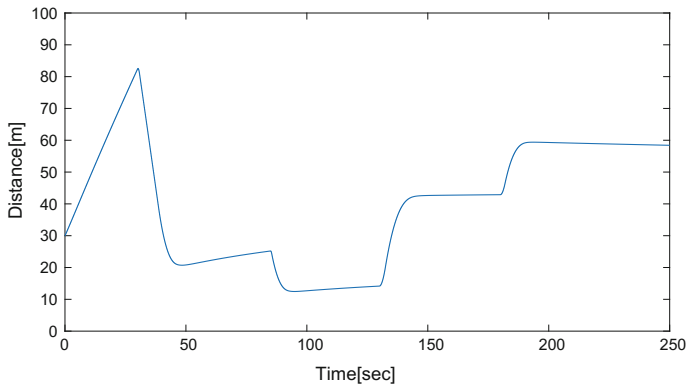


**Fig. 13** The distance of following condition time history curve

## 5  Analysis

From above, the electric vehicle adaptive cruise control system did well work in the three typical working conditions. The torque of electric vehicle motor drive system and the master cylinder pressure of the braking system are plotted as shown in Fig. 14, in the following conditions, the electric vehicle can achieve adaptive cruise control just by regenerative braking, shows that the lower fuzzy decision is able to calculate the distribution ratio of regenerative braking correctly, achieve the goal of reducing energy consumption. It can be seen in Fig. 15, due to the sharp slowdown of the ahead vehicle speed, motor, and brake system provide braking at the same time to achieve the demand of deceleration. The simulation results show that the proposed
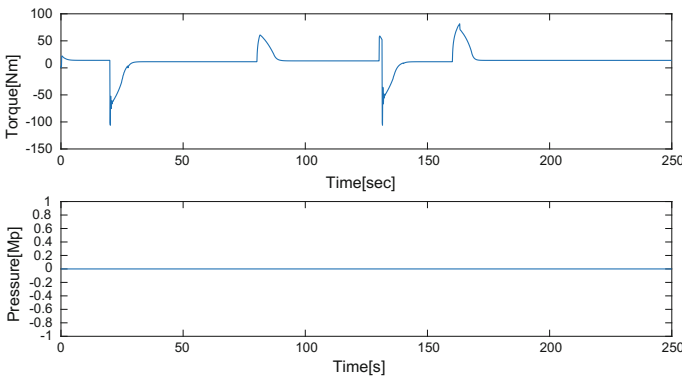


**Fig. 14** Motor torque and brake system master cylinder pressure value of following condition time history curve
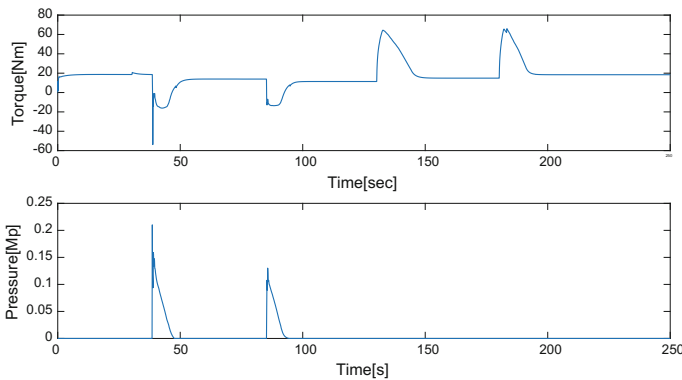


**Fig. 15** Motor torque and brake system master cylinder pressure value of cut in condition time history curve

algorithm in the cut in and cut out working conditions of can effectively implement the following control, and can realize the cruise and according to the actual situation of switching.

# 6 Conclusion

In this chapter, considering adaptive cruise system the safety, energy consumption, comfort requirements, with the characteristics of the regenerative braking of electric vehicle, we proposed decision algorithm based on model predictive control algorithm and the vehicle longitudinal control algorithm, then the simulation experiments are taken. The conclusion is as follows:

(1) Thought three typical working conditions of adaptive cruise simulation, verify the algorithm designed realize the adaptive cruise control.
(2) Under different working conditions, the algorithm can adjust output to realize braking energy as design.

# References

1. Fancher P, Bareket Z, Ervin R (2001) Human-centered design of an acc-with-braking and forward-crash-warning system. Veh Syst Dyn 36(2–3):203–223
2. Moon S, Yi K, Moon I (2008) Design, tuning and evaluation of integrated ACC/CA systems. IFAC Proc Volumes 41(2):8546–8551
3. Bifulco GN, Pariota L, Simonelli F et al (2013) Development and testing of a fully adaptive cruise control system. Transp Res Part C Emerg Technol 29(29):156–170
4. Moon S, Moon I, Yi K (2009) Design, tuning, and evaluation of a full-range adaptive cruise control system with collision avoidance. Control Eng Pract 17(4):442–455
5. Ganji B, Kouzani AZ, Sui YK et al (2014) Adaptive cruise control of a HEV using sliding mode control. Expert Syst Appl 41(2):607–615
6. Glaser S, Orfila O, Nouveliere L et al (2013) Smart and green ACC, adaptation of the ACC strategy for electric vehicle with regenerative capacity. Intelligent Vehicles Symposium. IEEE, pp 970–975
7. Nikolaou M (2001) Model predictive controllers: a critical synthesis of theory and industrial needs. Adv Chem Eng 01:131–204
8. Li SE (2013) Economy-oriented vehicle adaptive cruise control with coordinating multiple objectives function. Veh Syst Dyn 51(1):1–17
9. Vogel KA (2003) Comparison of headway and time to collision as safety indicators. Accid Anal Prev 35(3):427

# Study on Parking Mechanism Based on Parking Spaces Time Series

**Xing-pei Wei, Yong-gang Wang, Yan-qiu Cheng and Gao-xiang Zhu**

**Abstract** In order to further improve the accuracy of the parking lot scale and solve the traffic organization problem of the large-scale integrated underground parking lot, this paper analyzes the shortcomings of the traditional parking demand forecasting model which lacks the description of the dynamic change mechanism of the parking process, resulting in the poor accuracy of the prediction result. The time-varying law of the cumulative product/attract of each parking lot is obtained through the data fitting, and the correction coefficient is introduced according to the comparison between the reference land and the project land—The time—varying law model of the project land is obtained, and the net time—varying curve is drawn by the image method to obtain the parking scale of the project land.

**Keywords** Parking demand forecast · Time series · Parking spaces · Resource sharing

## 1 Introduction

With the growing contradiction of the rapid growth of motor vehicles, a serious impediment to the development of the city, and quickly became a hot spot for the transport academia.

At the macro level, Zhou Zhi-yong determine the six evaluation indexes of urban parking facilities planning scheme [1]; Qi Jing, Guo Si-zhen analyzed the reasons for the parking problem from the planning, management, policies regulations and investment environment [2]; In parking scale calculation, Guan Hong-zhi proposed

X. Wei (✉) · Y. Cheng
Transportation Planning and Management, Highway College, Chang'an University, Xi'an, Shaanxi 710064, China
e-mail: 328436143@qq.com

Y. Wang · G. Zhu
Transportation Engineering, Highway College, Chang'an University, Xi'an, Shaanxi 710064, China

a parking demand forecasting model [3]; Cheng Feng established the model of the balance between the parking facilities supply and the road network capacity [4]. Wang Feng-yuan used the traffic influence function to analyze the impact of road network traffic growth rate and parking rate on parking demand [5]; Wang Wen-bo, Chen Hong and others established the traffic accident sequence prediction model based on the correlation vector machine (RVM) [6]; Li Lin-bo established the parking construction method based on the berth function and the location condition [7].

In this paper, "Xi Xian New District" Energy Finance and Trade Zone start area large underground car park (under construction) as an example, the model of parking occurrence attracting model and the parking spaces forecasting model are constructed.

## 2  Parking Spaces Time Series Prediction Model and Parameter Calibration

There is a certain degree of dynamic complementary relationship between the parking occurred and attract the process.

### 2.1  The Forecast of the Reference Parking Lot's Parking Spaces Time Series

First, with an hour interval, making a traffic survey for the reference parking lot. The mathematic software is used to fit the research data, and the time-varying equation with high goodness is selected:

$$Q_i(t) = (at^3 + bt^2 + ct + d) \tag{1}$$

In the formula: $Q_i(t)$ stands for class $i$ land accumulation product/attract function value.

Drawing the time-varying images, so as to obtain reference to the parking lot parking spaces time series image, as shown in Fig. 1.

Assuming that a land has only two types of land for office and commercial, the corresponding parking attraction/occurrence (entry/exit) changes over time as shown below:
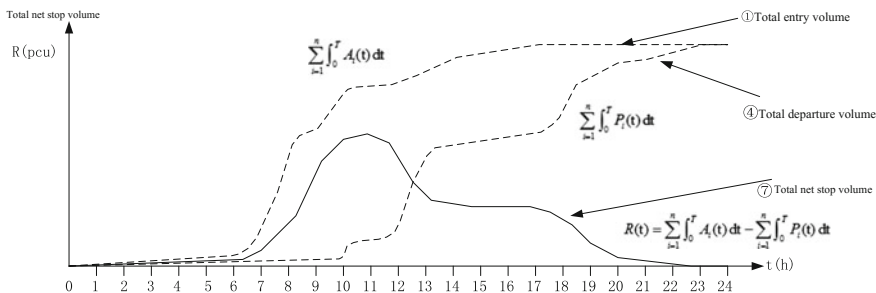
**Fig. 1** Net time-varying curve

**Table 1** Land use property correction coefficient table

| $\tau_j$ | Commercial | Office | Apartment | Hotel | Meeting |
|---|---|---|---|---|---|
| $\leq 0.25$ | 0.74 | 0.72 | 0.80 | 0.83 | 0.86 |
| 0.25–0.35 | 0.76 | 0.74 | 0.81 | 0.83 | 0.88 |
| 0.35–0.55 | 0.80 | 0.76 | 0.82 | 0.84 | 0.89 |
| 0.55–0.75 | 0.82 | 0.79 | 0.88 | 0.89 | 0.91 |
| 0.75–0.95 | 0.89 | 0.86 | 0.91 | 0.95 | 0.98 |
| 1 | 1.00 | 1.00 | 1.00 | 1.00 | 1.00 |

## 2.2 The Forecast of the Case Parking Lot's Parking Spaces Time Series

Consider the difference between the reference parking lot and the case parking lot in area and the intensity of the surrounding land development, the correction coefficient $\varphi_{ij}$ ($i =$ A, B, C, D; $j =$ 1, 2, 3, 4, 5) is introduced to modify the fitting equation.

$$Q_i(t) = (at^3 + bt^2 + ct + d) \times \varphi_i \tag{2}$$

$$\varphi_{ij} = \frac{S'_{ij}}{S_{ij}} \times \tau_j \tag{3}$$

In the formula: $\varphi_{ij}$ stands for "$I$" area "$j$" class land amendment factor; $S$ represents the area, $\tau_j$ represents the land development intensity correction factor.

$\varphi_{ij}$ calibration method:

According to Formula (2) of the steps, the case of parking lots and reference to the parking area ratio is easy to determine. That is, the calibration of $\varphi_{ij}$, the quantitative calibration of these factors, combined with the development and utilization of various types of land use intensity and parking product/attract of the corresponding relationship between the empirical data, developed a land use nature correction coefficient table, as shown in Table 1.

Through the investigation to determine the case car park and the reference parking lot around the land development situation, determine the proportion of various types of land size, according to the table to determine $\tau_j$, and then calibration $\varphi_{ij}$.

# 3 "Xi Xian" Energy Trade Starting Area Parking Lot Planning

## 3.1 Parking Demand—Supply Model Prediction and Analysis

Underground parking lot planning total parking 5061, Using the parking demand forecasting model, combined with the development and utilization of land around the Feng Jing Avenue in Xi Xian New District, the local traffic policy makes the following coefficient calibration:

The price factor $\mu$ is 0.8, the facility reduction factor $\delta$ is 0.95, the traffic policy reduction factor $\theta$ is 0.9, the peak turnover rate $\rho$ is set to 9.12, and the peak period utilization rate $\gamma$ is 0.9. According to the "Xi Xian New Area Integrated Transportation System Planning" (2015), "Xi Xian New District, Shaanxi Province Urban Planning Management Technical Regulations (Trial)" (2014), develop a land use property parking rate table, using the parking demand—supply model to predict, the results are as follows (Table 2).

## 3.2 Research on the Law of Net Limit Change

### 3.2.1 Data Acquisition and Fitting

Collecting the similar nature and considerable size of the parking lot parking product/attract time-varying data, drawing and fitting, as shown below (Fig. 2).

The results of the parking product/attract polynomial equation are as follows (Table 3).

Five properties of the land to improve the degree of goodness $R^2 > 0.97$, so accept the above fitting results.

**Table 2** Forecast results of parking demand—supply model

| Project | Partition 1 | Partition 2 | Partition 3 | Partition 4 | Total |
|---|---|---|---|---|---|
| Plan number | 1314 | 849 | 1157 | 1741 | 5061 |
| Calculation number | 1784 | 1532 | 1385 | 1573 | 6274 |
| Shortage number | 470 | 683 | 228 | −168 | 1213 |
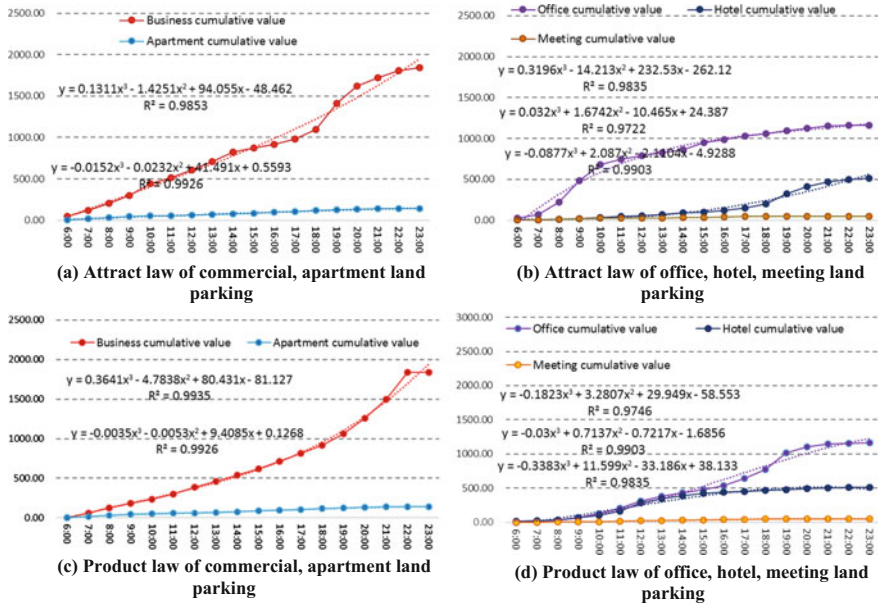
Fig. 2  The time—varying curve of the occurrence/attracting time of each type of land

**Table 3**  Polynomial equation fitting result

|  | Parking product law | Parking attract law | $R^2$ |
|---|---|---|---|
| Commercial | $y = 0.1311x^3 - 1.4251x^2$ $+ 94.055x - 48.462$ | $y = 0.3372x^3 - 4.4294x^2$ $+ 74.473x - 75.118$ | 0.9853/0.9935 |
| Office | $y = 0.3196x^3 - 14.213x^2$ $+ 232.53x - 262.12$ | $y = -0.1823x^3 + 3.2807x^2$ $+ 29.949x - 58.553$ | 0.9835/0.9746 |
| Apartment | $y = -0.0152x^3 - 0.0232x^2$ $+ 41.491x + 0.5593$ | $y = -0.0035x^3 - 0.0053x^2$ $+ 9.4085x + 0.1268$ | 0.9926/0.9926 |
| Hotel | $y = 0.032x^3 + 1.6742x^2$ $- 10.465x + 24.387$ | $y = -0.03x^3 + 0.7137x^2$ $- 0.7217x - 1.6856$ | 0.9722/0.9903 |
| Meeting | $y = -0.0877x^3 + 2.087x^2$ $- 2.1104x - 4.9288$ | $y = -0.3383x^3 + 11.599x^2$ $- 33.186x + 38.133$ | 0.9903/0.9835 |

### 3.2.2  Model Application

According to the energy starting area A, B, C, D four plots of different properties of the composition of the proportion of land to determine the correction factor $\varphi_{ij}$.

**Table 4** Results comparison list

| Project | Area 1 | Area 2 | Area 3 | Area 4 | Total |
|---|---|---|---|---|---|
| Planning Number | 1314 | 849 | 1157 | 1741 | 5061 |
| Traditional | 1784 | 1532 | 1385 | 1573 | 6274 |
| Case | 1459 | 1157 | 871 | 1671 | 5158 |

$$\varphi_{ij} = \begin{bmatrix} 2.38 & 1.80 & 1.70 & 4.21 \\ 0.93 & 1.97 & 0.16 & 0 \\ 0.74 & 0 & 0 & 0 \\ 0 & 0 & 0.59 & 0 \\ 0 & 0 & 0 & 1.71 \end{bmatrix}$$

According to Formula (2), the fitting equation is modified to obtain the cumulative time-dependent change function of the parking product/attract of the four plots of the energy starting area. Adjust some time points is carried out within the acceptable range, and then the time limit The curve is as follows:



(a) Change of parking spaces time in zone A



(b) Change of parking spaces time in zone B



(c) Change of parking spaces time in zone C



(d) Change of parking spaces time in zone D
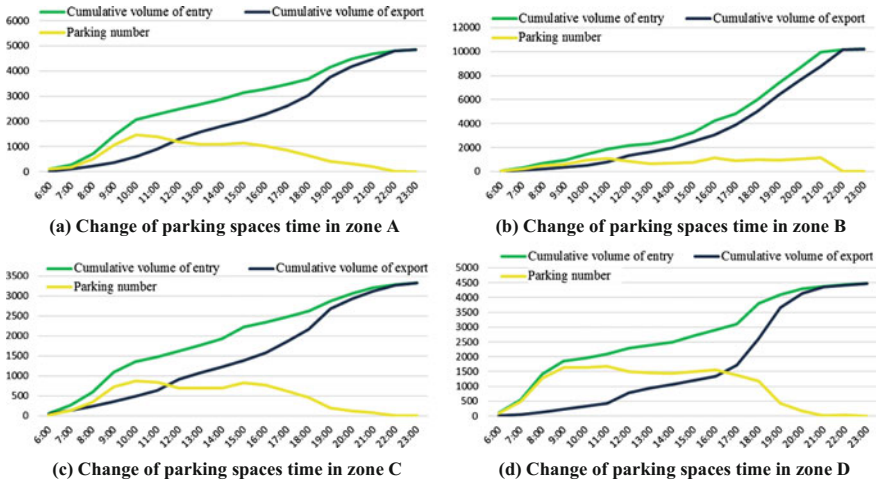
By the above four parking areas of the parking spaces time curve can be further accurate grasp of the underground parking lot vehicle real-time distribution.

### 3.2.3 Compare Results

The parking spaces time series prediction results are as follows (Table 4).

We can see that the traditional algorithm of supply-supply model is too large from the table above, because the method of predicting the law of parking numbers of the

zone is based on the change of the parking numbers, and then to predict the number of parking spaces in each district, further improved the accuracy of parking demand forecast.

# 4 Conclusion

The idea of parking demand forecast provided by the paper is based on the independence characteristics of the vehicle parking process, and the real-time dynamic thinking of the intermittent influence of the large-scale integrated parking lot, compared with the traditional parking product/attract rate prediction method is more accurate and reasonable, and more generally adaptable. This method explores the mechanism of vehicle parking process, based on the characteristics of time and space distribution, improved the parking turnover rate, and it contributes for making full use of land resources. The parking spaces curve of each zone and the result of its derivative, which is of practical significance for the formulation and implementation of the traffic organization scheme of the super-large comprehensive parking lot.

# References

1. Zhou Z, Chen J, Wang W (2004) Urban parking facilities planning self-evaluation simplified decision-making method. J Traffic Transp Eng 4(4):53–57
2. Qi J, Guo S, Zhang Y (2012) The solution of traffic in commercial center—taking Guanyinqiao business circle as an Example. J Chongqing Jiao tong Univ (Nat Sci), 31(s1):52–54, 184
3. Guan H, Wang X, Wang X (2006) Research on forecasting method of parking demand. J Beijing Univ Technol 32(7):600–604
4. Cheng F, Yan K, Wen Y (2006) Study on the supply of parking facilities in urban central area. Highw Eng 31(5):99–103
5. Wang F, Zhou X, Yan Y (2007) Parking demand forecasting model based on land use and traffic characteristics. J Traffic Transp Eng 7(2):84–88
6. Wang W, Chen H, Wei L (2016) Research on forecasting model of traffic accident time series. China Saf Sci J 26(6):52–56
7. Li L, Wang M, Dong Z (2010) Parking method based on berth function and location condition. China J Highw Transp 23(1):111–115

# Tensile Stiffness of Elastomeric Isolation Bearings Under Shear Deformation

Y. Dang, Q. Xu and L. L. Xu

**Abstract** The compression–shear behavior of rubber bearings is investigated by theoretical analysis and confirmed by extensive experimental work. Nevertheless, whether theoretical analysis predicts the tension–shear behavior of isolators is unclear. To clarify the variation rule of the tensile stiffness of the bearing under shear deformation, Haringx's theory is extended and the tensile stiffness is presented considering shear deformation. The variation of the stiffness of the bearing in the shear deformation is analyzed based on the derived expressions. Results show that the magnitude of the shear strain does not affect the vertical tensile stiffness and the vertical tensile stiffness is equal to the pure tensile stiffness when the tension is equal to the critical value, which is the product of the shear modulus and the shear area of the bearing. When the tension is not equal to the critical value, the vertical tensile stiffness is less than the pure tensile stiffness, decreasing with increasing shear strain. The change rule of vertical tensile stiffness is different in the different tensile forces. When tensile force is less than the critical value, tensile stiffness increases with the increasing tensile force. When tensile force is more than critical value, tensile stiffness decreases with the increase of tensile force, and the mechanics of isolators in tension are not exactly the mirror image of those for the isolators in compression. In the tension–shear state, the tensile component perpendicular to the rubber layer is smaller than that in the pure tension state. Therefore, compared with pure tension, tensile failure does not easily occur in bearings experiencing a large horizontal displacement. This phenomenon is consistent with the shaking table test.

**Keywords** Elastomeric isolation bearings · Shear deformation · Tensile stiffness Rotation vertical displacement

Y. Dang (✉) · Q. Xu · L. L. Xu
School of Civil Engineering, Lanzhou University of Technology, Lanzhou 730050, China
e-mail: 601363791@qq.com

# 1   Introduction

Rubber bearings are widely used in buildings and bridges because of their high compressive capacity and low horizontal stiffness. Bearings need to withstand the gravity of the structure vertically and produces a large horizontal displacement, which can reduce the horizontal seismic energy input to the upper structure to achieve the effect of an isolated horizontal earthquake. Therefore, research on the horizontal performance of the support is more thorough. However, in the case of high-rise and high-aspect ratio isolated buildings, certain bearings are subjected to a certain amount of tension. This tension accompanied with lateral displacement is caused by global overturning of building during strong earthquakes. However, whether theoretical analysis predicts tension–shear behavior of isolators remains unclear. Given that a negative pressure induces cavitation in the elastomer and the tension stress to produce cavitation is relative low, the tensile strain is also extremely small. Thus, the behavior of bearings in tension–shear states is not exactly predicted by experiment. Therefore, design engineers are concerned that an isolator does not experience tension. All current seismic isolated codes require that the tensile stress does not exceed the stain at cavitation, for example, the tensile stress of isolators is less than 1 MPa in the Chinese seismic design code [1], and the tensile strain of isolators is less than 5% of total elastomer thickness in Japan [2]. However, several shaking table tests show that isolators will experience large vertical deformation when the earthquake ground is extremely strong, and the tensile strain of isolators reaches 20–40%. The test isolators did not fail in both case, but clearly, the tensile strain markedly exceeds the strain at cavitation, and the change in the vertical stiffness of the isolation bearing affects the seismic isolation effects. This outcome indicates that the performance of bearing in tension–shear state is different from that in tension state. This chapter aims to demonstrate whether the isolator in tension and shear is damaged. The essential point is the tensile stiffness of the isolator in tension–shear states, which is of considerable significance for further applications of seismic isolation technology in high-rise buildings.

# 2   State of the Art

For calculating the vertical stiffness of bearings, Uryu [3] proposed the tensile stiffness formula: $K_t = E_t A / t_r$, where $E_t$ is the vertical tensile modulus of the bearings, $A$ is the section area, and $t_r$ is the total thickness of rubber. Yan et al. [4] developed and extended the model of Koh and Kelly, suggested a theoretical formula for tensile stiffness, and verified the formula using experimental results. Yang et al. [5] proposed the double stiffness and the origin tensile stiffness models of rubber bearing based on the tensile stress–strain relationship, and the calculated results were in agreement with the experimental value.

In the study of tension–shear properties of rubber bearings, numerous experiments were conducted abroad. Kelly and Takhirov investigated tension buckling and related this occurrence to compression buckling in elastomeric bearings [6]. Liu Qin completed the ultimate tensile failure test of bearings under shear deformation and found that the ultimate tensile stress decreases with the increase in shear deformation [7]. Takayama et al. [8] presented the experimental results of the tensile test with the offset shear strain by using 16 rubber bearings of seven types. They found that tension hysteresis curve shows the elastic tensile strain of approximately 5–10%. As the tensile strain increases, the hysteresis curve shows a bilinear type. Even with 100% tensile strain given with an offset shear strain of 200%, the rubber bearings did not rupture. Although the internal voids associated with three axial tensions could logically occur in rubber layers, obvious differences in compression and shear characteristics were not observed. Miyama and Masuda [9] completed a shaking table test with a steel frame isolated structure. The maximum tensile strain of the bearing was 17%. Fu [10] also completed the test with a steel frame isolated structure and obtained the maximum tensile strain of 30%. Nimura [11] completed a shaking table test to simulate seismic response of a slender isolated structure, and the tensile strain was 41.8%. The test isolators did not fail in all cases, but tensile strain evidently exceeds the strain at cavitation markedly.

In the above studies, the mechanics of bearings in tension–shear states were considered similar to that in pure states. Thus, the tensile stiffness of bearings was obtained by modifying the pure tension stiffness. Alternatively, the characteristics of bearings in tension–shear states were considered similar to those in compression–shear states, and the tensile stiffness of the bearings were obtained using the compression–shear theory. In fact, according to the results of tension–shear performance bearing experiments conducted by Takayama, as well as other shaking table tests, the behavior of the bearing in tension–shear states is not similar to that in pure tension states from the results of shaking table tests and not the mirror image of those in the compression–shear states. In this chapter, the tensile stiffness of rubber bearings with lateral displacement is studied, and the theoretical formulas of tensile stiffness are given for different tension load stages. The rule of tensile stiffness in tension–shear state is also discussed.

## 3   Methodology

### 3.1   Calculation Model of Rubber Isolator in the Tension–Shear State

The rubber bearing used to be considered as a homogeneous and isotropic column with an equivalent height that includes rubber layers and steel shims. The bottom end is fixed, and the top end is allowed to move horizontally and vertically but not

**Fig. 1  a** Calculation model of the rubber isolator; **b** Internal force diagram of the bearing
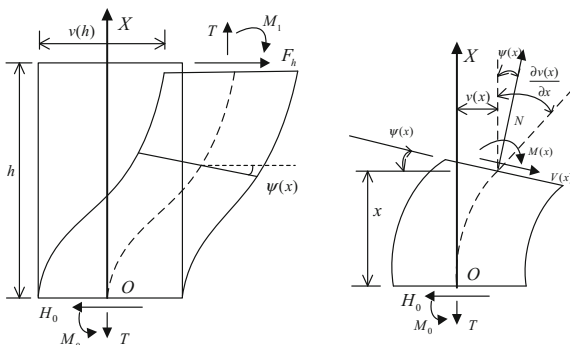


rotate. The top end of the column is subjected to a tensile force $T$, a horizontal force $F_h$, and a bending moment $M_1$, as shown in Fig. 1a.

We consider that each cross-section deformation satisfies plane section assumption; the horizontal displacement and the rotation angle at any cross-section of the bearing are expressed as $v$ and $\psi$, respectively. The shear deformation $\gamma_1$ at the cross-section can be expressed as

$$\gamma_1 = v' - \psi \tag{1}$$

According to the general principle of material mechanics, shear force $V$ and bending moment $M$ are given by

$$V = GA_s \cdot \gamma_1 = GA_s(v' - \psi) \tag{2}$$

$$M = EI_s \psi' \tag{3}$$

The shear stiffness $GA_s$ and bending stiffness $EI_s$ of the bearing can be obtained as follows [12, 13]:

$$GA_s = GA \frac{h}{t_r} \tag{4}$$

$$EI_s = 0.6G \cdot I \cdot \left(1 + \frac{2}{3}S_1^2\right) \cdot \frac{h}{t_r}, \tag{5}$$

where $A$ = effective cross-section area of bearing; $G$ = shear modulus; $h$ = height of bearing(rubber plus steel); $t_r$ = the total thickness of rubber; $E$ = Yang's modulus; $I$ = moment of inertia of cross-section; and $S_1$ = the first shape factor of bearing.

When rotation $\psi$ is small, the equations of equilibrium for bending moment and shear force, shown in Fig. 1b, are

$$M - T \cdot v - M_0 + H_0 \cdot x = 0 \tag{6a}$$

$$V - H_0 + T \cdot \psi = 0 \tag{6b}$$

**Fig. 2** Geometry of the axial
displacement of a bearing
due to lateral deformation
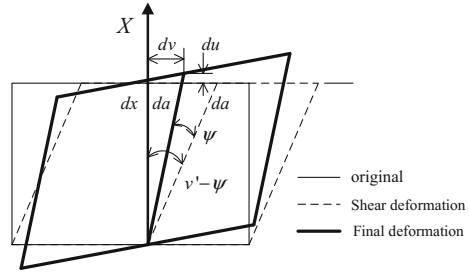


Substitution of Eqs. (2) and (3) into Eq. (6a, b) yields

$$EI_s \frac{GA_s}{GA_s - T} v'' - T \cdot v = M_0 - H_0 \cdot x \tag{7a}$$

$$EI_s \frac{GA_s}{GA_s - T} \psi'' - T \cdot \psi = -H_0 \tag{7b}$$

$$v' = \frac{-T + GA_s}{GA_s} \psi + \frac{H_0}{GA_s} \tag{7c}$$

## 3.2 Vertical Displacement of the Top of a Bearing

The vertical displacement of the top of a bearing due to a lateral deformation can be obtained geometrically, as shown in Fig. 2.

We visualize a displacement of the center line of element through an angle, $v' - \psi$ with no downward displacement; then, an opposite rotation of the entire element through an angle $\psi$. The vertical displacement of the element, shown as $du$ in Fig. 2, is given by

$$du = da(\cos v' - \cos(v' - \psi)), \tag{8}$$

where

$$da = \frac{dx}{\cos(v' - \psi)} \tag{9}$$

Using small-angle approximations for sine and cosine, we obtain

$$\cos v' - \cos(v' - \psi) = -2 \sin\left[\frac{1}{2}(v' - \psi + v')\right] \sin\left[\frac{1}{2}(v' - v' + \psi)\right]$$

$$\approx -\frac{1}{2}(2v' - \psi)\psi \tag{10}$$

and

$$\cos(v' - \psi) \approx 1 - \frac{1}{2}(v' - \psi)^2 \tag{11}$$

leading to

$$\begin{aligned} \mathrm{d}u &= -\frac{\mathrm{d}x}{\left(1 - \frac{1}{2}(v' - \psi)^2\right)} \cdot \frac{1}{2}(2v' - \psi)\psi \\ &= -\mathrm{d}x\left(1 + \frac{1}{2}(v' - \psi)^2\right) \cdot \frac{1}{2}(2v' - \psi)\psi \approx -\frac{1}{2}(2v' - \psi)\psi\,\mathrm{d}x \end{aligned} \tag{12}$$

Then, the vertical displacement of the bearing in the whole height is obtained as follows:

$$\delta_v = -\frac{1}{2}\int_0^h (2v' - \psi)\psi\,\mathrm{d}x \tag{13}$$

The displacement $\delta_v$ caused by the geometric deformation of the bearing is referred to as rotational vertical displacement in this chapter.

### 3.3   Vertical Tensile Stiffness of Bearing in Shear State

From Eqs. (7a, b, c), we can see that $T = GA_s$ is a critical state in which the equations are ill-conditioned. Taking $T = GA_s$ as the cutoff point, the vertical tensile stiffness of bearing is discussed in three cases.

(1)   $0 < T < GA_s$

Equations (7a, b, c) can be written as

$$\frac{1}{\alpha^2}v'' - v = \frac{M_0}{T} + \frac{H_0}{T} \cdot x \tag{14a}$$

$$\frac{1}{\alpha^2}\psi'' - \psi = -\frac{H_0}{T} \tag{14b}$$

$$v' = \frac{1}{\beta}\psi + \frac{H_0}{GA_s}, \tag{14c}$$

where

$$\alpha^2 = \frac{T(GA_s - T)}{EI_s \cdot GA_s} \tag{15a}$$

$$\beta = \frac{GA_s}{(GA_s - T)} \tag{15b}$$

Using boundary condition as shown in Fig. 1(a)

$$v(0) = 0, \ \psi(0) = 0, \ \psi(h) = 0, \ H_0 = F_h \tag{16}$$

The solution for Eqs. (14a, b, c) is

$$v(x) = \frac{F_h}{\alpha\beta T}\left[(N + 1)\left(1 - e^{\alpha x}\right) + N\left(1 - e^{-\alpha x}\right) + \alpha\beta x\right] \tag{17a}$$

$$\psi(x) = \frac{F_h}{T}\left[1 - (N + 1)e^{\alpha x} + Ne^{-\alpha x}\right], \tag{17b}$$

where

$$N = \frac{1 - e^{\alpha h}}{e^{\alpha h} - e^{-\alpha h}} \tag{18}$$

From Eq. (17a), the horizontal displacement of the top of bearing can be obtained as follows:

$$v(h) = \delta_h = \frac{F_h}{\alpha\beta T}[2(2N + 1) + \alpha\beta h] \tag{19}$$

The substitution of Eqs. (17a, b) into Eq. (13) gives

$$\delta_v = -\frac{F_h^2}{2\alpha\beta T^2}Q, \tag{20}$$

where

$$Q = \alpha\beta h - 2\alpha(2 - \beta)N(N + 1)h + (2N + 1)(2 + \beta) \tag{21}$$

The terms $F_h$ and $T$ can be eliminated by $\delta_h$ from Eq. (19), giving

$$\delta_v = -\frac{\alpha\beta Q h^2}{2(2(2N + 1) + \alpha\beta h)^2} \cdot \gamma^2, \tag{22}$$

where $\gamma =$ the total shear strain of bearing, which is defined as follows:

$$\gamma = \frac{\delta_h}{h} \tag{23}$$

Thus, the total vertical displacement of the bearing in the tension–shear state can be expressed as superposition of the pure tensile vertical displacement and the rotational vertical displacement [14]

$$\delta_{sv} = \delta_{tv} + \delta_v, \tag{24}$$

where $\delta_{tv}$ = pure tensile vertical displacement, which can be obtained as follows:

$$\delta_{tv} = \frac{T}{K_{vt0}} \tag{25}$$

Pure tensile stiffness, $K_{vt0}$, is defined as [7]

$$K_{vt0} = \frac{E_{tb}A_s}{h} \tag{26}$$

and [5]

$$E_{tb} = \frac{E_t \cdot E_{b0}}{E_t + E_{b0}}, \tag{27}$$

where the rubber's bulk elastic module is $E_{b0} = 200$ N/mm$^2$ and the elastomer's vertical tensile modulus is $E_t = 0.6G(1 + 2kS_1^2)$. Given that the influence of rubber hardness change is not considered, the rubber hardness correction factor $k = 1$ [4].

The vertical stiffness is obtained by inverting the result of differentiating Eq. (24) with respect to the vertical load but the form of solution is very complex, therefore, the tensile stiffness of bearing in this load stage can be calculated by the difference method as follows:

$$K_{vt} = \frac{T^+ - T^-}{\delta_{sv}^+ - \delta_{sv}^-}, \tag{28}$$

where $T^+$ = tensile force $T$ plus a small amount $\Delta T$, $T^-$ = tensile force minus a small amount $\Delta T$, with $\Delta T$ considered as 0.01 MPa, $\delta_{sv}^+$ = vertical displacement coincidental with $T^+$, and $\delta_{sv}^-$ = vertical displacement coincidental with $T^-$.

(2) $T = GA_s$

Using the boundary condition in Eq. (16), the solutions for Eqs. (6a, b) are as

$$v(x) = \frac{F_h}{GA_s} \cdot x \tag{29a}$$

$$\psi(x) = 0 \tag{29b}$$

Substituting Eqs. (29a, b) into Eq. (13), the rotational vertical displacement $\delta_v$ is zero, which indicates that bearing does not rotate and the total vertical displacement of bearing is pure tension vertical displacement. Thus, the bearing experiences pure tension deformation in the vertical direction, and shear deformation exerts no influence on the bearing tensile stiffness.

(3) $T > GA_s$

The solutions for Eqs. (7a, b, c) are

$$v(x) = -\frac{F_h}{\alpha_1 \beta T} * \left\{ \frac{1 - \cos(\alpha_1 h)}{\sin(\alpha_1 h)}(1 - \cos(\alpha_1 x)) + \sin(\alpha_1 x) - \alpha_1 \beta x \right\} \quad (30a)$$

$$\psi(x) = -\frac{F_h}{T} \left\{ \frac{1 - \cos(\alpha_1 h)}{\sin(\alpha_1 h)} \sin(\alpha x) - (1 - \cos(\alpha_1 x)) \right\}, \quad (30b)$$

where

$$\alpha_1^2 = \frac{T(T - GA_s)}{EI_s \cdot GA_s} \quad (31)$$

The parameter $\beta$ is calculated using Eq. (15b).

By substituting Eqs. (30a, b) into Eq. (13), the rotational vertical displacement of bearing can be obtained as follows:

$$\delta_v = -\frac{\alpha_1 \beta h^2}{2} \left\{ \frac{\alpha_1 \beta h \, \cos(\alpha_1 h) - 2\sin(\alpha_1 h) + 2\alpha_1 h - \beta \, \sin(\alpha_1 h)}{-4\cos(\alpha_1 h) + \alpha_1^2 \beta^2 h^2 \cos(\alpha_1 h) + 4 + \alpha_1^2 \beta^2 h^2 - 4\alpha_1 \beta h \, \sin(\alpha_1 h)} \right\} \gamma^2 \quad (32)$$

In this load stage, the total vertical displacement of bearing in the tension–shear state can also be expressed as superposition of the pure tensile vertical displacement and the rotational vertical displacement, and calculated using Eq. (24). However, the bearing will yield and produce nonlinear tensile deformation, the pure tensile stiffness $K_{vt0}$ is modified by a correct factor $\mu_\sigma$ proposed by conference [8]. Therefore, the pure tensile stiffness $K_{vt0,s}$ in this load stage is obtained as follows:

$$K_{vt0,s} = \mu_\sigma \cdot K_{vt0}, \quad (33)$$

where

$$\mu_\sigma = -0.65 \ln\left(\frac{T}{GA_s}\right) + 1.1 \quad (GA_s < T < 5GA_s) \quad (34)$$

Thus, the equivalent vertical tensile stiffness of bearing can be calculated as follows:

$$K_{vt} = \frac{T}{\delta_{sv}} \quad (35)$$

## 4 Result Analysis and Discussion

According to the formulas for calculating the vertical tensile stiffness above, the mechanical properties of an actual rubber bearing under different load conditions are discussed. For the bearing, the following dimension is considered as shown in Table 1.

**Table 1** Internal parameters of bearing

| Parameters | Value | Parameters | Value |
|---|---|---|---|
| Shear modulus of the rubber $G$ (MPa) | 0.61 | Diameter of bearing (mm) | 280 |
| Number of steel shim | 19 | Thickness of the steel shim (mm) | 2 |
| Number of rubber layer | 20 | Thickness of the rubber layer (mm) | 10 |
| The thickness of top and bottom end steel plate (mm) | 21 | Total height of bearing $h$ (mm) | 238 |
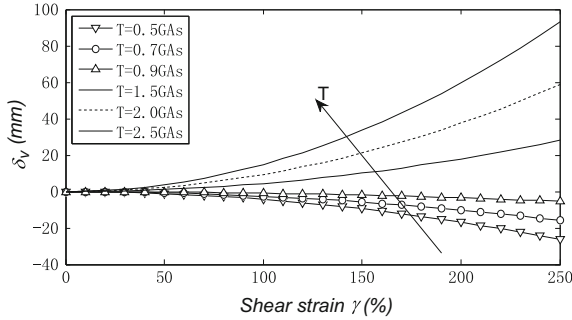


**Fig. 3** Curve of rotational vertical displacement–shear strain for different tensile force

## 4.1 Effect of Tensile Force and Shear Strain on the Rotation Vertical Displacement of the Bearing

The key factor affecting vertical tensile stiffness of the bearing is the rotational vertical displacement $\delta_v$, which is caused by the rotation of the rubber layer. This factor reflects the influence of the shear strain on the bearing tensile stiffness.

By substituting the above values into Eqs. (22) and (32), the curve of rotational vertical displacement–shear strain can be drawn as shown in Fig. 3 for different tensile forces, including $0.5GA_s$, $0.7GA_s$, $0.9GA_s$, $1.5GA_s$, $2.0GA_s$, and $2.5GA_s$, in which the shear strain varies from 0 to 250%.

As seen in Fig. 3, when the tensile force $T < GA_s$, the value $\delta_v$ is negative, decreasing with the increase in tensile force. The rotation angle of each section as calculated using Eq. (17b) is positive, indicating that the rubber layers produce a downward inclination. When the tensile force $T > GA_s$, the rotation angle of each section calculated by Eq. (30b) is negative, indicating that the rubber layers produce an upward inclination.

**Fig. 4** Relationship of ratio value of $K_{vt}/K_{vt0}$ and $\gamma$ for different tensile forces if $T < GA_s$
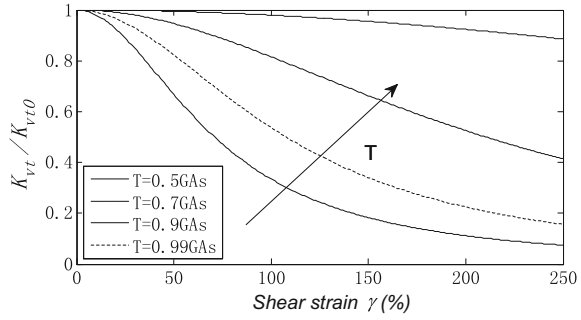


**Fig. 5** Relationship of ratio value of $K_{vt}/K_{vt0}$ and $\gamma$ relation for different tensile forces if $T > GA_s$
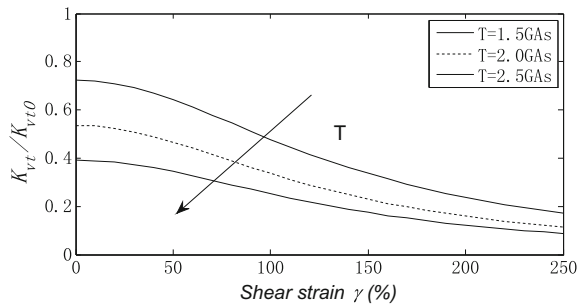


## 4.2 Influence of Tensile Force and Shear Strain on Vertical Tensile Stiffness

The load stage of tensile force $T < GA_s$ is first discussed. As plotted using Eq. (28), Fig. 4 presents the ratio value of $K_{vt}/K_{vt0}$ versus shear strain for different tensile forces, including $0.5GA_s$, $0.7GA_s$, $0.9GA_s$, and $0.99GA_s$.

Figure 4 shows the relationship between the ratio value of $K_{vt}/K_{vt0}$ and shear strain. The ratio value increases with the increase in tensile force and tends toward 1, meaning that tensile stiffness is smaller than pure tensile stiffness in the tension–shear state. Meanwhile, the ratio value decreases with the increase in shear strain, indicating that the smaller the shear strain is, the closer the tensile stiffness is to the pure tensile stiffness. This outcome is consistent with the variation in deformation and vertical stiffness of the actual bearing, meaning that the correction proposed in this chapter is in line with the actual situation.

In the load stage of tensile force $T > GA_s$, Fig. 5, which is plotted using Eq. (35), shows the relationship between the ratio value of $K_{vt}/K_{vt0}$ and shear strain for different tensile loads, including $1.5GA_s$, $2.0GA_s$ and $2.5GA_s$.

The stiffness ratio value decreases with the increase in tensile force. These outcomes mean that the tensile stiffness in shear state is less than pure tensile stiffness; meanwhile, the ratio value decreases with shear strain, indicating that the smaller the shear strain is, the closer the tensile stiffness is to pure tensile stiffness.

**Fig. 6** $\psi_{\mathrm{mid}}$ and shear strain relation for different tensile forces: **a** $T < GA_s$; **b** $T > GA_s$
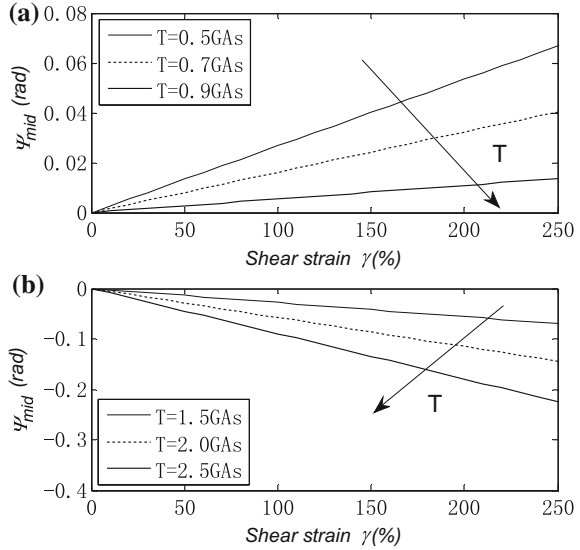


The vertical tensile stiffness of bearing in the tension–shear state is less than the pure tensile stiffness and decreases with shear strain. However, the change processes of vertical tensile stiffness are different in different tension load stages. When the tensile force $T < GA_s$, the vertical tensile stiffness increases with tensile force; in contrast, the vertical tensile stiffness decreases with tensile force when $T > GA_s$.

## 4.3 Comparison of Variation for Vertical Stiffness and Vertical Compression Stiffness

The vertical behavior of the bearing in the tension–shear state is not the exact mirror image of those in the compression–shear state because the changes in vertical rotation displacement caused by shear deformation are different in these two situations.

The rotation angle of the rubber layer at $h/2$ is defined as $\psi_{\mathrm{mid}}$, and the change process of $\psi_{\mathrm{mid}}$ with shear strain is discussed for different tensile forces as shown in Fig. 6.

Figure 6 (a and b, drawn by Eqs. (17b) and (30b), respectively) show the relationship between $\psi_{\mathrm{mid}}$ and shear strain for different tensile forces. The value of $\psi_{\mathrm{mid}}$ increases with shear strain in both figures; however, in Fig. 6a, the value of $\psi_{\mathrm{mid}}$ is positive, meaning that the middle rubber layer experiences clockwise rotation and decreases with the increase in tensile force for the tensile force $T < GA_s$. When the tensile force approaches $GA_s$, the curve tends to level. In Fig. 6(b), when the tensile force $T > GA_s$, the value $\psi_{\mathrm{mid}}$ is negative and increases with the increase of tensile force, meaning that the rubber layer experiences anticlockwise rotation.
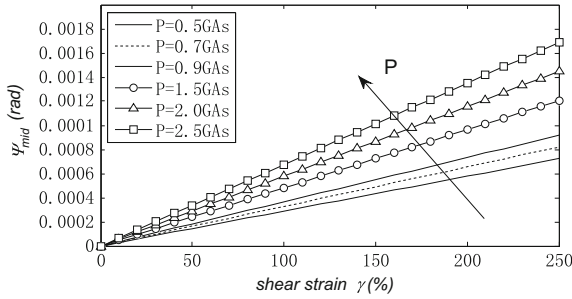
**Fig. 7** $\psi_{\mathrm{mid}}$ and shear strain relation for different compressive forces

When the bearing is under compression, the relationship between $\psi_{\mathrm{mid}}$ and $\gamma$ can be obtained using Eqs. (7a, b, c) by simply replacing $T$ with $-P$, where $P$ is the compressive force; moreover, the bending stiffness is five times that in tension [5]. The change process of $\psi_{\mathrm{mid}}$ with shear strain was analyzed for different tensile forces as shown in Fig. 7. The value of $\psi_{\mathrm{mid}}$ is positive, meaning that the layers experience clockwise rotation; however, the value is markedly less than that in tension and increases with shear strain and compressive force. The change process of $\psi_{\mathrm{mid}}$ with $\gamma$ under compression is a mirror image of those for tensile force $T > GA_s$.

Therefore, from the geometric deformation point of view, if the bearing under the action of compression–shear, the rotational angle of rubber layer is positive, and the layers experience clockwise rotation, thus inducing the top of bearing into a downward displacement. The angle $\theta$ between the compressive force and the tangential direction of the rubber layer is acute, which gives the load a component along the layers and induces further shear deformation in the rubber, leading to the continuous increase in vertical displacement as shown in Fig. 8a. Thus, the vertical compressive stiffness of the bearing is smaller than the pure compressive stiffness and decreases with the increase in shearing strain. In addition, greater compressive force indicates smaller compressive stiffness.

When the bearing is under tension below $GA_s$ with shear deformation as shown in Fig. 8b, the rotational angle of the rubber layer is positive, and the layers experience a clockwise rotation; however, the angle between the force and the tangential direction of the rubber layer is obtuse, thus giving the load a component along the layers, reducing the shear deformation of rubber, and thereby offsetting part of the downward vertical displacement caused by shear deformation. Therefore, in this tensile load stage, the vertical tensile stiffness increases with tension and gradually tends toward pure tensile stiffness. The change processes in vertical tensile stiffness are different from those of vertical compressive stiffness.

The vertical tensile stiffness in the shear state is equal to pure tensile stiffness without shear deformation when tensile force $T = GA_s$. When the tensile force $T > GA_s$, the rotational angle of the rubber layer is negative, and layers experience anticlockwise rotation. The angle between the force and the tangential direction of the rubber layer is acute, thus giving the load a component along the layers and inducing
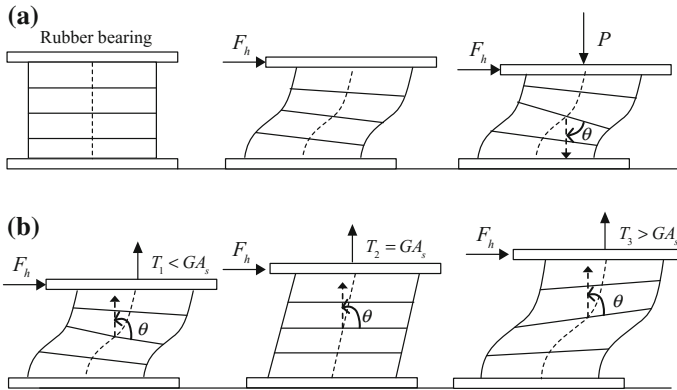
**Fig. 8** Deformation of bearing under different load conditions

further shear deformation in the rubber layers, leading to a continuous increase in vertical displacement as shown in Fig. 8b. Thus, the vertical tensile stiffness of bearing is smaller than the pure tensile stiffness and decreases with the increase of shearing strain; moreover, greater tensile force translates to smaller tensile stiffness, which is identical to the vertical compression stiffness.

Meanwhile, the tensile component along the direction perpendicular to the rubber layer in the tension–shear state is smaller than that of the bearing in the pure tension state owing to inclination of the rubber layer, which improves the tensile damaging performance of the bearing.

## 5 Conclusions

To determine the tensile properties of bearing under shear deformation, we deduced the theoretical formula for calculation of the tensile stiffness of the rubber isolation bearing based on the Haringx's theory. Through numerical analysis, the following conclusions can be drawn:

(1) Under shear deformation, the tensile stiffness of the bearing is less than pure tensile stiffness and decreases with the increase in shear deformation.
(2) In different load stages of tension, the change processes of vertical tensile stiffness are different: $T = GA_s$ is a critical state; at this time, shear deformation does not exert any effect on bearing performance. When the bearing is under tension below $GA_s$ with shear deformation, the vertical tensile stiffness increases with the increasing tensile force and gradually tends toward pure tensile stiffness. The change processes of vertical tensile stiffness are different from those of vertical compressive stiffness; when the tensile force $T > GA_s$, the vertical tensile stiffness decreases with increasing tensile force, and the deformation

characteristics of bearing in tension is a mirror image of those in compression. In addition, the change processes of vertical tensile stiffness are the same as those of vertical compressive stiffness.

(3) Compared with that subjected to pure tension, the bearing under the action of tension and shear can produce larger vertical displacement, which improves the tensile damaging performance of bearing.

The study on vertical tensile stiffness under the shear deformation of isolators can accurately predict whether high-rise base-isolated structure is safe under rare earthquakes. On the basis of the calculation formula of vertical tensile stiffness given in this chapter, further experimental verification is necessary, particularly the hysteretic model of vertical tensile stiffness and the ultimate tensile properties.

# References

1. Ministry of Housing and Urban-Rural Development of China (2001) Code for seismic design of buildings, Beijing, China
2. Architectural Institute of Japan (2001) Recommendation for the design of base isolated building, Marozen Corporation, Miyama, Tokyo, pp 31–41
3. Uryu M, Nishikawa T (1999) Study on stiffness, deformation and ultimate characteristics of base-isolated rubber bearings: horizontal and vertical characteristics under shear deformation. J Struct Constr Eng 479:119–128
4. Yan WM, Zhang ZQ, Chen SC, Ren XX (2014) Modeling and analyzing of tensile stiffness for seismic isolated rubber bearing. J Eng Mech 31(2):184–189 (in Chinese)
5. Yang QR, Liu WG, He WF, Feng DM (2010) Tensile stiffness and deformation model of rubber isolators in tension and tension-shear states. J Eng Mech 136(4):429–437
6. Kelly JM, Takhirov SM (2007) Tension buckling in multilayer elastomeric isolation bearings. J Mech Mater Struct 2(8):1591–1605
7. Liu Q (2015) The type test evaluation and the study on tension-shear behavior of isolated rubber bearings. Guangzhou University, Guangzhou
8. Ivvabe N, Takayama M, Kani N, Wada A (2000) Experimental study on the effect of tension for rubber bearings. In: 12th world conference on earthquake engineering. Auckland, New Zealand, 2000
9. Miyama T, Masuda K (2000) Shaking table tests on base-isolated buildings having high aspect ratios: the tensile force on the rubber bearing and the subsequent setting vibration. J Struct Constr Eng 573:61–68
10. Fu WQ et al (2007) An experimental study on shaking table of isolated structure model with LRB(1). J Harbin Inst Technol 39(2):201–205
11. Nimura A et al (2005) Simulation analysis of shaking table tests for slender base-isolated building. In: Proceedings of Summaries of Technical Papers of Annual Meeting, Architectural Institute of Japan, Kinki, Japan
12. Chang C-H (2002) Modeling of laminated rubber bearings using an analytical stiffness matrix. Int J Solids Struct 39(24):6055–6078

13. Gent AN (2001) Structural engineering with rubber: how to design rubber components. Hanser, Munich, Germany
14. Kelly JM, Konstantinidis DA (2011) Mechanics of rubber bearing for seismic and vibration isolation. Wiley, New York

# The Personalized Multi-criteria Route Planning Problem in Repeated Travel and Its Solution Algorithm

**Ci-yun Lin, Bowen Gong, Zhi-jian Wang, Man-rong Yuan, Kai-jian Hu and Chen-gang Wang**

**Abstract** Existing research on the personalized multi-criteria route planning (PMRP) problem seldom considers drivers' travel characteristics for different types of travel, which significantly affects a driver's performance in reality. In this research, the PMRP problem in repeated travel is presented and defined. The relative differences between route-costs and their respective minimums are considered as the driver's route choice criteria for repeated travel. The range of each criterion value from the driver's experience data is introduced into the problem definition as the constraint. In addition, a travel-law-based route planning (TRP) algorithm is designed, implemented, and evaluated in comparison to the genetic algorithm (GA) for solving the proposed problem. The comparison results show that the TRP algorithm achieved better results in terms of running time, criteria values, and comprehensive objective function values. The experimental results also show that for the given cases, the TRP algorithm effectively avoided impractical solutions and achieved a 0.96-second average run time to reach approximate comprehensive objective function values for the routes chosen by two drivers in practice over a real-road network with 2000 nodes and 7014 edges using a PC with a 2.53-GHz-CoreTM i5-based dual-core processor.

C. Lin · B. Gong (✉)
College of Transportation, Jilin University, Changchun 130022, China
e-mail: gongbowen@jlu.edu.cn

Z. Wang
College of Electrical and Control Engineering, North China University of Technology, Beijing 100144, China

M. Yuan
Traffic Police Squad, Kunming Municipal Public Security Bureau, Kunming 650011, China

K. Hu
Jinan Automobile Test Centre, Jinan 250011, China

C. Wang
Some Troops of North Theater, Shenyang 110011, China

## 1  Introduction

With the development of intelligent navigation and its corresponding applications, the increasingly intensive demand of dynamically determining personalized multi-criteria optimum routes for repeated travel has coincided with the growth in drivers' personalized travel demands and the scale of real-road networks. According to a resident travel survey in many Chinese cities, repeated instances of travel comprise over 70% of residents' daily travel [1]. The personalized multi-criteria route planning (PMRP) problem in repeated travel yet plays a significant role in many transportation and network related analyses, such as service facility layouts, network organization optimization, and traffic guidance strategy determination. It is very meaningful for drivers, service providers, and traffic managers to effectively solve the PMRP problem for repeated travel. However, in most existing studies, little interest is given to drivers' travel characteristics for repeated travel in PMRP problem definition and algorithm design [1, 2].

Moreover, although the traditional definition of the PMRP problem provides an ideal goal for each criterion based on its importance-value from a driver's opinion to reach the global optimum, it has been seldom achieved in real-road networks. Quasi-optimum solutions must be accepted in reality [3–5]. However, rules or constraints considering drivers' travel characteristics for different types of travel for quasi-optimum solutions are seldom included in the problem definition. In addition to these, existing PMRP algorithms also have a number of limitations. They are usually highly sensitive to the criteria. Some criteria do not offer enough parallel optimization for the algorithms to work well. Long-running times and lack of control mechanisms for the degree of optimization for each criterion from a driver's point of view significantly affect the performance in reality. All of these enhance the difficulty associated with solving the PMRP problem for repeated travel [6–8].

The rest of this chapter is organized as follows. Section 2 defines the PMRP problem for repeated travel. Section 3 details the TRP algorithm. In Sect. 4, we evaluate the performance of the TRP algorithm compared to a GA for solving the PMRP problem for repeated travel. Finally, the conclusions are proposed in Sect. 5.

## 2  Definition of the PMRP Problem in Repeated Travel

A road network is a graph $G = (V, E)$ consisting of a set of nodes $V$ with $N = |V|$ and a set of directed edges $E$ with $M = |E|$, in which an intersection is a node, and a driving direction of a road between two adjacent intersections is an edge between two adjacent nodes. Each edge $e \in E$ has an associated vector of edge-costs $t_e = \begin{bmatrix} t_{e,1} & t_{e,2} & \cdots & t_{e,c} & \cdots & t_{e,C} \end{bmatrix}$, in which $t_{e,c}$ is the $c$th edge-cost of edge $e$ that represents the distance or time incurred by traversing edge $e$, etc.

For two fixed $O, D \in E$, set $L_{O,D}$ to be the set of all the routes without any loops or repeated edges between $O$ and $D$. Each route $l \in L_{O,D}$ has an associated vector

of route-costs $h_l = \begin{bmatrix} h_{l,1} & h_{l,2} & \cdots & h_{l,c} & \cdots & h_{l,C} \end{bmatrix}$, in which $h_{l,c}$ is the $c$th route-cost of route $l$ and can be calculated using $h_{l,c} = \sum_{e \in l} t_{e,c}$. In this research, we define the relative differences in the route-costs of route $l$ and their minimums of all the routes between $O$ and $D$ as a driver's route choice criteria for repeat travel between $O$ and $D$. Set $\delta_l = \begin{bmatrix} \delta_{l,1} & \delta_{l,2} & \cdots & \delta_{l,c} & \cdots & \delta_{l,C} \end{bmatrix}$ to be the vector of all the criteria values, in which $\delta_{l,c}$ is the $c$th criterion value and can be calculated using $\delta_{l,c} = \frac{h_{l,c} - r_c}{r_c}$, $r_c$ is the minimum of the $c$th route-cost of all routes in $L_{O,D}$.

The PMRP problem in repeated travel is finding the optimum route $l^*$ from all routes that satisfies the constraint conditions defined in $0 \le \delta_{l^*,c} \le \theta_c$ and $0 \le f(\delta_{l^*}, w) \le \beta$, in which the comprehensive objective function value $f(l^*)$ is minimized by $f(l^*) = \min_{l \in L_{O,D}} f(\delta_l, w)$, $w = \begin{bmatrix} w_1 & w_2 & \cdots & w_c & \cdots & w_C \end{bmatrix}$ is the vector of the important criteria and $\sum_{c=1}^{C} w_c = 1$. $\theta_c$ and $\beta$ are real numbers, which separately represent the accepted ranges of $\delta_{l^*,c}$ and $f(l^*)$ by a driver for repeated travel is between $O$ and $D$. The accepted ranges of the criteria values can be obtained from a statistical analysis on the history of repeated travel data [9, 10].

## 3 The Travel-Law-Based Route Planning Algorithm

### 3.1 Initializing the Candidate Route Set Q

"Experience routes" are usually the predetermined routes used in reality. It may be more realistic to initialize $Q$ using the "experience routes" between $O$ and $D$. An unfixed-length decimal encoding method is used for encoding the routes. This means that a route is a positive integer sequence consisting of IDs of all the nodes from $O$ to $D$ over the route [11].

### 3.2 Determining the Key Nodes of Each Candidate Route in Q

In the TRP algorithm, the starting node of the part with the worst travel condition is a key node in each candidate route. There are $C + 1$ key nodes for each candidate route, in which $C$ is a positive integer. Given a candidate route $l$ ($l \in Q$), the key nodes may be determined as follows.

Set $v_l$ to be the set of nodes except $O$ and $D$ in route $l$ and $m_l = |v_l|$. Each node $i$ ($i \in v_l$) has an associated vector $\rho_{l,i} = \begin{bmatrix} \rho_{l,i,1} & \rho_{l,i,2} & \cdots & \rho_{l,i,c} & \cdots & \rho_{l,i,C} & \rho_{l,i,C+1} \end{bmatrix}$ of size $C + 1$, in which $\rho_{l,i,c}$ is calculated using Eq. (1) and $l_{i,D}$ is the part from node $i$ to node $D$ in route $l$. The variable $x_{O,D}$ is the Euclidean distance between $O$ and $D$, and $x_{i',D}$ is the Euclidean Distance between the vertical projection point $i'$ of node $i$

in the straight connecting line between $O$ and $D$. Based on $\rho_{l,i}(i \in v_l)$, a set of key nodes $n_l = \left\{ n_{l,1}\ n_{l,2}\ \cdots\ n_{l,c}\ \cdots\ n_{l,C}\ n_{l,C+1} \right\}$ of size $C+1$ is determined, in which $\rho_{l,n_{l,c},c}$ of node $n_{l,c}(1 \le c \le C+1)$ is maximized over all the nodes in $v_l$:

$$\rho_{l,i,c} = \begin{cases} \left( \frac{h_{l_i,D,c}}{x_{i',D}} - \frac{r_c}{x_{O,D}} \right) / \frac{r_c}{x_{O,D}}, & 1 \le c \le C \\ f\left( \delta_{l_{i,D}}, w \right), & c = C+1 \end{cases} \tag{1}$$

## 3.3   Determining the Replaced Parts in Each Candidate Route

The new routes are generated by replacing the parts containing the key nodes. Given a key node $n_{l,c}$, the number of nodes in the replaced part, $m_{l,c}$, can be calculated using Eq. (2), in which $K$ is the maximum number of iterations, $\tau_{l,c}$ is the maximum of $\rho_{l,i,c}(i \in v_l)$, and $\Gamma_{k,c}$ is the maximum of $\tau_{l,c}(l \in Q)$ over the $k$th iteration [12]:

$$m_{l,c} = 1 + \frac{m_l \tau_{l,c}}{\Gamma_{k,c}} \left( 1 - \frac{k}{K} \right) \tag{2}$$

Next, we set $u$ and $v$ separately to be the starting and ending nodes of the replaced part in route $l$, respectively. We set $\mu = m_{l,c} + 2$, set $p_1$, and $p_2$ separately to be the number of nodes between nodes $O$ and $n_{l,c}$, and the number of nodes between nodes $n_{l,c}$ and $D$ in route $l$, respectively. Then, nodes $u$ and $v$ can be determined using the rules.

## 3.4   Generating New Routes and Updating the Candidate Route Set

In this section, the Dijkstra algorithm is employed to calculate the replacement routes. To influence the choice and obtain replacement routes with better travel conditions, the edge-costs of all the edges in $E$ are calculated using Eq. (3), in which $\eta_{e,c}$ is the $c$th edge-cost, $f(t_e, w)$ is the comprehensive objective function of all the edge-costs of edge $e$, and $\varepsilon_{e,c}$, and $\varepsilon_{e,C+1}$ are random items. It is clear from this that the key node $n_{l,c}$ and the calculation formula of the edge-cost $\eta_{e,c}$ correspond to each other [13, 14, 15]

$$\eta_{e,c} = \begin{cases} t_{e,c} + \varepsilon_{e,c}, & 1 \le c \le C \\ f(t_e, w) + \varepsilon_{e,C+1} & c = C+1 \end{cases} \tag{3}$$

When the replacement routes are generated, $C+1$ new candidate routes are also generated by replacing the replaced parts with the replacement routes. After all the

new routes are generated, the new routes should be added into $Q$. If the total number of routes in $Q$ is larger than the maximum number allowed, then the routes with larger $f(\delta_l, w)$ values should be deleted from $Q$. Simultaneously, we delete the routes in which any criterion value or comprehensive objective function value is greater than the driver's accepted range.

## 3.5 The Pseudo Code for the Proposed Algorithm

The pseudo code for the TRA is described in Fig. 1.

**Input:** The road network data, important value of each criterion, IDs of the origin node $O$ and the destination node $D$, the encoded experience routes between $O$ and $D$, the maximum number of iteration $K$, and the size of the candidate route set $J$.

**Output:** The optimal route $l_K^*$ calculated by $K$ times iteration and each criterion value $\delta_{l_K^*, c}$, each route-cost $h_{l_K^*, c}$ and the comprehensive objective function value $f(l_K^*)$ of route $l_K^*$.

**Begin**
    Initialize $Q$ with the encoded experience routes and a empty set $R$;
    **For** $k=1$ to $K$;
        **For** each route $l$ in $Q$;
            **For** each node $i$ in route $l$;
                Calculate $\rho_{l,i}$ [Eq. (6)];
            **End;**
            Determine the key nodes in route $l$ based on section 4.2;
            **For** each key node $n_{l,c}$ in route $l$
                Calculate the number of the replaced nodes in route $l$ $m_{l,c}$ [Eq. (7)];
                Determine the start node $u$ and the end node $v$ of the replaced part in route $l$ based on section 4.3;
                Generate the replacing route between $u$ and $v$ based on Dijkstra algorithm and edge-cost $\eta_{e,c}$ for each edge $e$ in $E$ [Eq. (8)];
                Generate a new route $l_c$ by replacing the part between $u$ and $v$ in route $l$ with the replacing route;
                Insert $l_c$ into $R$;
            **End;**
        **End;**
        Insert all routes in $R$ into $Q$;
        Calculate the comprehensive objective function value $f(\delta_l, w)$ for each route $l$ in $Q$;
        **If** $|Q|>J$
            Delete the routes with the maximum $f(\delta_l, w)$ in $Q$ until $|Q|=J$;
        **End;**
        delete the routes in which any criterion value or the comprehensive objective function value is over its accepted range [Eqs. (4)-(5)]
    **End;**
    Calculate each criterion value for each route $l$ in $Q$;
    Determine the optimal route $l_K^*$ according to Eq. (1) and Eqs. (4)-(5).
    **Return** route $l_K^*$, and each criterion value $\delta_{l_K^*, c}$, each route-cost $h_{l_K^*, c}$ and $f(l_K^*)$ of route $l_K^*$
**End.**

**Fig. 1**  The pseudo code for the TRP algorithm

| Table 1 The congestion probability for different ratios of volume to capacity for an intersection entrance lane | Ratio of volume to capacity | Congestion probability |
|---|---|---|
| | 0–0.34 | 0.1 |
| | 34–0.74 | 0.3 |
| | 0.74–0.8 | 0.6 |
| | 0.8–1 | 0.9 |

## 4   Experiments

In this section, we evaluate the performance of the TRP algorithm by comparing it with the GA for the PMRP problem for repeated travel. Raw data provided for this research includes two drivers' repeated travel data in a real-road network with 2000 nodes and 7014 edges. Three criteria are determined from two drivers' points of view, which separately are the relative differences of the sum of the probability of congestion over all the nodes, the sum of the lengths of all the edges in each candidate route and the sum of the travel time over all the edges in each candidate route and their respective minimums. The linear weighted sum of all the criteria values is defined as the comprehensive objective function $f(l)$ [16]:

$$f(l) = \sum_{c=1}^{3} w_c \delta_{l,c} \tag{4}$$

Table 1 shows the congestion probability for different ratios of volume and capacity of an intersection entrance lane. Table 2 shows the values of the corresponding parameters. Time 1 is the period from 7:00 AM to 9:00 AM for a single day, time 2 is the period from 9:00 AM to 11:00 AM for a single day. The variables $w_1$, $w_2$ and $w_3$ are determined according to the history travel data analysis, $r_1$, $r_2$ and $r_3$ are the minimums of three the criteria, and $\theta_1$, $\theta_2$, $\theta_3$, and $\beta$ are the accepted maximums of three criteria and the comprehensive objective function given in Eq. (3). Table 3 shows the values of $\delta_{l',1}$, $\delta_{l',2}$, $\delta_{l',3}$, $h_{l',1}$, $h_{l',2}$, $h_{l',3}$, and $f(l')$ for each route $l'$ chosen in practice by the two drivers under each set of $(w_c)$ s.

The two algorithms are implemented in Matlab and tested 100 times under each set of $(w_c)$s in Table 2. The testing environment is based on a PC with a 64-bit

**Table 2**  The values of the parameters referred

| Driver | Time | $w_1$ | $w_2$ | $w_3$ | $r_1$ | $r_2$ | $r_3$ | $\theta_1$ | $\theta_2$ | $\theta_3$ | $\beta$ |
|---|---|---|---|---|---|---|---|---|---|---|---|
| 1 | 1 | 0.2 | 0.4 | 0.4 | 29.8 | 18,031.14 | 2654 | 0.3012 | 0.0412 | 0.1012 | 0.1145 |
| | 2 | 0.1 | 0.6 | 0.3 | 18.7 | 18,031.14 | 1650 | 0.5178 | 0.0313 | 0.2023 | 0.1307 |
| 2 | 1 | 0.2 | 0.3 | 0.5 | 29.8 | 18,031.14 | 2654 | 0.2435 | 0.0555 | 0.0552 | 0.0915 |
| | 2 | 0.1 | 0.5 | 0.4 | 18.7 | 18,031.14 | 1650 | 0.4416 | 0.0391 | 0.1525 | 0.1237 |

**Table 3** The values of $\delta_{l',1}$, $\delta_{l',2}$, $\delta_{l',3}$, $h_{l',1}$, $h_{l',2}$, $h_{l',3}$, and $f(l')$ for each route $l'$ chosen in practice by the two drivers under each set of $(w_c)$s

| Driver | $w_1$ | $w_2$ | $w_3$ | $h_{l',1}$ | $h_{l',2}$ | $h_{l',3}$ | $\delta_{l',1}$ | $\delta_{l',2}$ | $\delta_{l',3}$ | $f(l')$ |
|---|---|---|---|---|---|---|---|---|---|---|
| 1 | 0.2 | 0.4 | 0.4 | 38 | 18,709.89 | 2912 | 0.2752 | 0.0376 | 0.0972 | 0.1090 |
|  | 0.1 | 0.6 | 0.3 | 27.8 | 18,500.46 | 1958 | 0.4866 | 0.0260 | 0.1867 | 0.1203 |
| 2 | 0.2 | 0.3 | 0.5 | 36.4 | 18,950.37 | 2789 | 0.2215 | 0.0510 | 0.0509 | 0.0850 |
|  | 0.1 | 0.5 | 0.4 | 26.6 | 18,676.31 | 1865 | 0.4225 | 0.0358 | 0.1303 | 0.1123 |

Windows 8 operating system, 4 GB of memory, a 2.53-GHz-Core™ i5-based dual-core processor, and the Matlab R2011b software package.

In order ensure that we are making a valid comparison between the two methods, some processing is needed for the GA to solve the PMRP problem: (1) the encoded "experience routes" from node 1 to node 1259 is used to initialize the population, (2) the linear weighted sum of all the criteria values of a chromosome is defined as the fitness function of the chromosome, (3) the gene with the maximum $\rho_{l,i,C+1}(i \in l)$ in chromosome $l$ is the mutated gene $I$ of chromosome $l$, (4) the replacement route generating method described in Sect. 3.4 [the edge-cost using Eq. (3) $(c = C + 1)$] is used to determine the replacement genes of the mutated gene, and (5) the crossover operation is carried out for any two chromosomes with the same gene in the population. The pseudo code for the GA is described in Fig. 2 [17].

The number of routes in the initial candidate route set for the TRP algorithm or chromosomes in the initial population for the GA is 4. The maximum number of routes in the candidate route set for the TRP algorithm or chromosomes in the population for the GA is 10. The maximum number of iterations is 100 times for the two algorithms. The number of tests under each set of $(w_c)$ s in Table 2 for each algorithm is 100 times [18].

## 5 Results and Discussion

Figure 3 shows the change in $\bar{f}(l_k^*)$ as $k$ increases under each set of $(w_c)$ s, in which $l_k^*$ is the optimal route (or individual) obtained by iterating $k$ times and $\bar{f}(l_k^*)$ is the average of $f(l_k^*)$ over the 100 tests. The TRP algorithm has a rapid reduction in $\bar{f}(l_k^*)$ during the first ten iterations and achieves a smaller $\bar{f}(l_{100}^*)$ than the GA under each set of $(w_c)$s. The criteria values, route-costs values, and the comprehensive objective function values for the optimum routes achieved by the TRP algorithms under each set of $(w_c)$s are given in Table 4. The corresponding parameter values achieved by the GA under each set of $(w_c)$s are given in Table 5.

The runtime for each algorithm to finish 100 iterations and reach the approximate values of $(f(l'))$s under each set of $(w_c)$ s during the 100 tests is given in Table 6. The TRP algorithm takes less time than the GA to finish 100 iterations. Better yet,

**Input:** The road network data, important value of each criterion, IDs of the origin node $O$ and the destination node $D$, the encoded experience routes between $O$ and $D$, the maximum number of iterations $K$, and the size of the population $J$.

**Output:** The optimal chromosome $l_K^*$ calculated by $K$ times iteration and each criterion value $\delta_{l_K^*,c}$, each route-cost $h_{l_K^*,c}$ and the comprehensive objective function value $f\left(l_K^*\right)$ of chromosome $l_K^*$.

**Begin**

    Initialize a population $H$ with the encoded experience routes;

    **For** $i = 1$ to $K$;

        **For** each chromosome $a$ in $H$;

            **For** each gene $i$ in $a$;

                Calculate the value of $\rho_{l,i,C+1}$  [Eq. (6)];

            **End;**

            Determine the gene $I$ with the maximum of $\rho_{l,i,C+1}\left(i \in V_l\right)$ in $a$;

            Determine the replacing genes of $I$ based on the method for generating the replacing nodes in section 4.5 [the edge-impedance using Eq. (8) $\left(c = C+1\right)$ and form a new chromosome $a_i$;

            Insert the new chromosome $a_i$ into $H$;

        **End;**

        **For** any two chromosomes with the same gene in $H$

            Exchange the genes from the same gene to the last gene of each other and form two new chromosomes $a_j, a_{j+1}$;

            Insert the new chromosomes $a_j, a_{j+1}$ into $H$;

        **End;**

        Calculate the value of the fitness function for each chromosome $q$ in $H$;

        Delete the repeated routes;

        **If** $\left|H\right| > J$;

            Delete the chromosomes with the larger value of the fitness function in $H$ until $\left|H\right| = J$;

        **End;**

        Delete the routes in which any criterion value or the comprehensive objective function value is over its accepted range [Eqs. (4)-(5)]

    **End;**

    Determine the optimum chromosome according to Eq. (1) and Eqs. (4)-(5);

    **Return** route $l_K^*$, and each criterion value $\delta_{l_K^*,c}$, each route-cost $h_{l_K^*,c}$ and $f\left(l_K^*\right)$ of route $l_K^*$

**End.**

**Fig. 2** The pseudo code for the GA
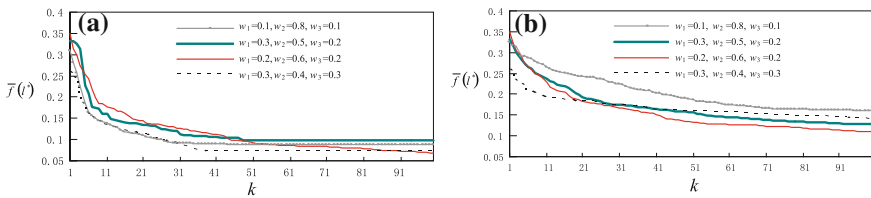


**Fig. 3** The change in $\bar{f}\left(l_k^*\right)$ as $k$ increases under each set of $w_1$, $w_2$ and $w_3$. **a** The change in $\bar{f}\left(l_k^*\right)$ as $k$ increases for the TRA algorithm; **b** The change in $\bar{f}\left(l_k^*\right)$ as $k$ increases for the GA

**Table 4** The values of $\delta_{l^*_{100},1}, \delta_{l^*_{100},2}, \delta_{l^*_{100},3}, h_{l^*_{100},1}, h_{l^*_{100},2}, h_{l^*_{100},3}$, and $f\left(l^*_{100}\right)$ for the optimal route $l^*_{100}$ obtained by the TRA algorithm under each set of $(w_c)$s

| Driver | $w_1$ | $w_2$ | $w_3$ | $h_{l^*_{100},1}$ | $h_{l^*_{100},2}$ | $h_{l^*_{100},1}$ | $\delta_{l^*_{100},1}$ | $\delta_{l^*_{100},2}$ | $\delta_{l^*_{100},3}$ | $f\left(l^*_{100}\right)$ |
|---|---|---|---|---|---|---|---|---|---|---|
| 1 | 0.2 | 0.4 | 0.4 | 37.2 | 18,672.56 | 2815 | 0.2483 | 0.0356 | 0.0607 | 0.0882 |
| | 0.1 | 0.6 | 0.3 | 26.2 | 18,523.87 | 1879 | 0.4011 | 0.0273 | 0.1388 | 0.0981 |
| 2 | 0.2 | 0.3 | 0.5 | 35.4 | 18,976.37 | 2733 | 0.1879 | 0.0524 | 0.0298 | 0.0682 |
| | 0.1 | 0.5 | 0.4 | 24.8 | 18,590.83 | 1749 | 0.3262 | 0.0310 | 0.0600 | 0.0721 |

**Table 5** The values of $\delta_{l^*_{100},1}, \delta_{l^*_{100},2}, \delta_{l^*_{100},3}, h_{l^*_{100},1}, h_{l^*_{100},2}, h_{l^*_{100},3}$, and $f\left(l^*_{100}\right)$ for the optimal chromosome $l^*_{100}$ obtained by the GA under each set of $(w_c)$s

| Driver | $w_1$ | $w_2$ | $w_3$ | $h_{l^*_{100},1}$ | $h_{l^*_{100},2}$ | $h_{l^*_{100},1}$ | $\delta_{l^*_{100},1}$ | $\delta_{l^*_{100},2}$ | $\delta_{l^*_{100},3}$ | $f\left(l^*_{100}\right)$ |
|---|---|---|---|---|---|---|---|---|---|---|
| 1 | 0.2 | 0.4 | 0.4 | 38.2 | 19,090.02 | 3182 | 0.2819 | 0.0587 | 0.1989 | 0.1594 |
| | 0.1 | 0.6 | 0.3 | 26.6 | 18,743.83 | 1988 | 0.4225 | 0.0395 | 0.2048 | 0.1274 |
| 2 | 0.2 | 0.3 | 0.5 | 35.2 | 19,709.65 | 2897 | 0.1812 | 0.0931 | 0.0916 | 0.1099 |
| | 0.1 | 0.5 | 0.4 | 25.4 | 18,964.39 | 1979 | 0.3583 | 0.0518 | 0.1994 | 0.1415 |

**Table 6** The average run time of each algorithm to finish 100 iterations and obtaining the routes with the approximate values of $\left(f(l')\right)$ s under each set of $(w_c)$ s during 100 tests (seconds)

| Algorithm | Average running time for all sets of $(w_c)$s during 100 tests | |
|---|---|---|
| | Finishing 100 times iteration | Obtaining the routes with the approximate values of $\left(f(l')\right)s$ |
| TRP algorithm | 35.44 | 0.96 |
| GA | 42.37 | 4.24 |

the average running time of the TRP algorithm to reach the approximate values of $\left(f(l')\right)$s is 0.961 s, which is less than required to finishing 100 iterations.

# References

1. Gandibleux X, Beugnies F, Randriamasy S (2006) Martins' algorithm revisited for multi-objective shortest path problems with a MaxMin cost function. 4OR: Q J Oper Res 4(1):47–59
2. Mooney P, Winstanley A (2006) An evolutionary algorithm for multicriteria path optimization problems. Int J Geogr Inf Sci 20(4):401–423
3. Pahlavani P, Delavar MR (2014) Multi-criteria route planning based on a driver's preferences in multi-criteria route selection. Transp Res C-Emer 40:14–35
4. Kovacs AA, Parragh SN, Hartl RF (2015) The multi-objective generalized consistent vehicle routing problem. Eur J Oper Res 247(2):441–458

5. Coelho LC, LAPORTE G (2013) A branch-and-cut algorithm for the multi-product multi-vehicle inventory-routing problem. Int J Prod Res 51(23–24):7156–7169
6. Smilowitz K, Nowak M, Jiang TT (2013) Workforce management in periodic delivery operations. Transp Sci 47(2):214–230
7. Liang WY, HUANG CC, Lin YC et al (2013) The multi-objective label correcting algorithm for supply chain modeling. Int J Prod Econ 142(1):172–178
8. Iori M, Martello S, Pretolani D (2010) An aggregate label setting policy for the multi-objective shortest path problem. Eur J Oper Res 207(3):1489–1496
9. Pulido FJ, Mandow L, Perez-De-la-cruz JL (2015) Dimensionality reduction in multiobjective shortest path search. Comput Oper Res 64:60–70
10. Kang TP, Zhang XG, Wang ZF (2011) Algorithm for shortest path of multi-objectives based on k short path algorithm. J Changzhou Inst Technol 24(3):25–28
11. Rajabi-Bahaabadi M, Shariat-Mohaymany A, Babaei M et al (2015) Multi-objective path finding in stochastic time-dependent road networks using non-dominated sorting genetic algorithm. Expert Syst Appl 42(12):5056–5064
12. Ombuki B, Ross BJ, HANSHAR F (2006) Multi-objective genetic algorithms for vehicle routing problem with time windows. Appl Intell 24(1):17–30
13. Osman MS, ABO-SINNA MA, MOUSA AA (2005) An effective genetic algorithm approach to multiobjective routing problems (MORPs). Appl Math Comput 163(2):769–781
14. Guerriero F, Musmanno R (2001) Label correcting methods to solve multicriteria shortest path problems. J Optimiz Theory App 111(3):589–613
15. Ji ZW, Kim YS, Chen A (2011) Multi-objective alpha-reliable path finding in stochastic networks with correlated link costs: a simulation-based multi-objective genetic algorithm approach (SMOGA). Expert Syst Appl 38(3):1515–1528
16. Fang Z, Zong X, Li Q et al (2011) Hierarchical multi-objective evacuation routing in stadium using ant colony optimization approach. J Transp Geogr 19(3):443–451
17. Ghoseiri K, Nadjari B (2010) An ant colony optimization algorithm for the bi-objective shortest path problem. Appl Soft Comput 10(4):1237–1246
18. Bezerra LCT, Goldbarg EFG, Goldbarg MC et al (2013) Analyzing the impact of MOACO components: an algorithmic study on the multi-objective shortest path problem. Expert Syst Appl 40(1):345–355

# A Service-Based Fare Policy for Flex-Route Transit Services

Jin-xing Shen, Yu-han Zhou, Ya-nan Liu and Feng Qiu

**Abstract**  In this chapter, a novel service-based fare strategy is proposed in designing appropriate fare structure when current fixed-route transit turns to flex-route policy, which is now the most popular type of flexible transit services in low-density areas. Service quality offered to each passenger group under two transit policies is assessed and on the premise of pursuing no additional profit in new services, a fare structure is developed based on the variation of service quality as well as cost of provision after implementing flex-route operating policy. In the acquired fare structure, regular riders enjoy discounted fares for imposed delay and curb-to-curb requests pay more money for personal deviation services.

**Keywords**  Flexible transit · Flex-route transit · Fare policy · Service quality
Simulation

## 1  Introduction

There is generally a flat fare policy in conventional fixed-route transit (except some distance-based fare cases) and previous research [1–4] developed fare structures from a macroeconomic perspective combining price elasticity and social costs. Cervero [5, 6] summarized that most studies on transit fare structures suggest that the common practice of flat fares is highly inequitable, penalizing short-distance users, and more differentiated fare practices are expected and necessary in the future, as new transit alternatives to conventional bus continue to emerge.

J. Shen (✉) · Y. Zhou · Y. Liu
Ministry of Education Key Laboratory of Integrated Regulation and Resource Development on
Shallow Lakes, Hohai University, No. 1, Xikang Road, Nanjing 21096, China
e-mail: shenjx03@163.com

F. Qiu
Department of Computer Science, University of Victoria, Victoria, BC V8W3P6, Canada

Flex-route transit (also known as route deviation transit), which is regarded as a combination of conventional flex-route transit and demand responsive service, is by far the most popular form of flexible transit services [7]. As a cost-efficient alternative to satisfy curb-to-curb demand on the basis of serving regular station-to-station passengers, curb-to-curb requests would drive the service vehicle to deviate from the base route and inevitably increase the riding time of in-vehicle riders. In other words, the deviation operation offers high-quality service to curb-to-curb passengers but also has a significant influence on other riders' travel experience.

A recent work by Emele et al. [8] addressed the benefit of design, a more differentiated fare structure than flat fare in flexible transit services, and proposed a pricing mechanism for demand responsive transit by using bid strategy. However, their passenger-based pricing policy in demand responsive transit is effective only at the condition of many available service providers and seems to be unpractical in flex-route transit services, with are generally operated by specific transit divisions.

As a new type of flexible transit services, there are only a few studies related with flex-route transit. Daganzo [9] proved that flex-route services could be possibly more cost-effective than demand responsive systems. Fu [10] determined the optimal slack time allocation in flex-route segments. Quadrifoglio et al. [11] evaluated upper and lower bounds on the maximum longitudinal velocity. Nourbakhsh and Ouyang [12] proved that a flex-route system performs better than other comparable policies under low-to-moderate demand levels. Qiu et al. [13, 14] investigated the choice model between fixed-route and flex-route policies in transit systems and Qiu et al. [15] proposed a two-stage scheduling model for flex-route transit systems. In contrast, some other literatures have been completed for other types of flexible transit services. Most of these works concentrated on the scheduling and deployment of a fleet of demand responsive vehicles, and several reliable copies of scheduling systems have been introduced [16–20].

Existing works mainly deal with the issues of designing and operating flex-route services, and there is yet to be found a comprehensive guideline for designing fare structures in flex-route services. As this new operating policy becomes more and more popular in suburban and rural transit systems, a reasonable fare policy, which could better reflect the transit service values, is necessary for the future development of flex-route services.

In practice, flex-route operating policy is generally considered to make beneficial effect in relatively low-density areas. In some cases, flex-route policy is implemented when the actual demand does not support previous fixed-route service; in other cases, fixed-route and flex-route policies are alternately applied to satisfy varying passenger flow. This chapter intends to propose a general mechanism to assist transit planners in determining the fare structure when the fixed-route transit service turns to flex-route operating policy. We aim to investigate and assess the service values offered to different passenger groups in flex-route services, based on price-performance under fixed-route policy, and this work is considered as a meaningful attempt in constructing appropriate fare structures in emerging flexible transit services.

## 2 System Descriptions

### 2.1 Service Area and Demand

Our analysis is performed mainly based on the MTA Line 646 flex-route service in Los Angeles, which was operated with fixed-route policy in the daytime and flex-route policy at night. It features a rectangular service area and $m$ checkpoints $(C_1, C_2, \ldots, C_m)$ along the base route (see Fig. 1), which are often located at high-density demand sites. Line 646 system has a single service vehicle and $W$ is the maximum allowable deviation width from this base route on either side. Here, we make an assumption that checkpoint demand is uniformly distributed among checkpoints and demand outside checkpoint locations has a uniform distribution in the service area. Similar to Quadrifoglio et al. [11], we assume infinite vehicle capacity and rectilinear movement for they are good approximations of reality.

The fare structure in the flex-route service includes three levels: two-deviation group (type 1 passengers: starting point and destination not at checkpoints), one-deviation group (type 2 passengers: starting point at checkpoints, and destination not at checkpoints; type 3 passengers: starting point not at checkpoints, and destination at checkpoints) and regular passenger group (type 4 passengers: starting point and destination both at checkpoints). The four types of passengers have their respective proportions $\beta_1, \beta_2, \beta_3, \beta_4 (\beta_1 + \beta_2 + \beta_3 + \beta_4 = 1)$.

### 2.2 Two Operating Policies

#### 2.2.1 Fixed-Route Policy

Fixed-route policy provides successive transport service and the vehicle moves back and forth along the base route (see Fig. 1) with $N$ stations including checkpoints. Adjacent stations have the same distance $d$. All passengers can only be served at stations and requests outside stations need to walk to the nearest station for pickup or destination after drop-off.
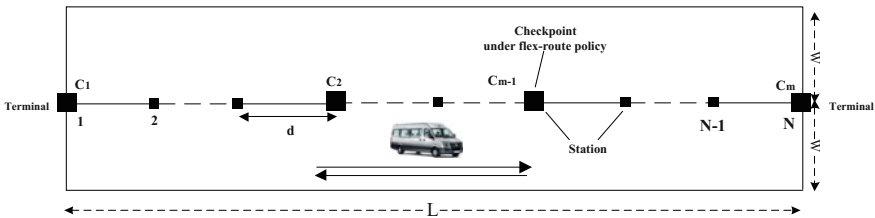


**Fig. 1** Fixed-route transit service

### 2.2.2 Flex-Route Policy

The service vehicle must visit all checkpoints, in turn, every ride and each checkpoint has its predetermined departure time $t_c$. The vehicle cannot arrive at stations later than $t_c$. If deviation services do not use up the allotted slack time of a flex-route segment, there will be idle time at the downstream checkpoint until the scheduled departure time $t_c$.

## 3 Model Description

In the model, we define the speed $V_b$ of the vehicle, the walking speed $V_p$ of passengers, and the dwelling time $T_d$ of each stop.

### 3.1 Measure of Service Value

A reasonable fare policy should reflect transit service values offered. Different from previous studies in fixed-route services where differentiated fare was determined by the in-vehicle performance such as travel distance, in our policy service quality function $S = K + A + R$ is defined to measure service value and constructed as the sum of expected walking time $K$, expected waiting time $A$ and expected riding time $R$. For passengers using curb-to-curb services, their waiting time is defined as the interval between the scheduled pickup time and actual pickup time.

### 3.2 Theoretical Modeling for Fixed-Route Policy

In practical use, planners could develop simulations to make quick assessment of service quality function $S$ under the two transit policies. In this section, we build theoretical models for the fixed-route service to verify the following simulation modeling. For purpose of illustration, we assume that checkpoints are evenly distributed along the base route, as in the Line 646 system. The service quality function of each passenger group can be derived as Qiu et al. [14].

### 3.3 Simulation Modeling

Because theoretical modeling generally overestimates the system performance of flex-route services [21], in our analysis simulation modeling is developed with MAT-LAB 2011b to reproduce flex-route transit operation. In the flex-route service, our

simulation replicates vehicle movement with an insertion algorithm by selecting the minimum additional travel distance at each request insertion step, which is regarded as a classical resolution for scheduling flexible transit services. The insertion algorithm constructs the vehicle routing plans before each ride. Deviation services are provided on a first-come, first-available basis. Curb-to-curb requests are likely to be rejected by deviation services if the allotted slack time is exhausted.

# 4 Result Analyses

## 4.1 Parameter Values

The service area of Line 646 is 10 mile$^2$, with $L = 10$ mile and $W = 5$ mile. There are three checkpoints ($m = 3$) under flex-route policy, two terminal checkpoints and one intermediate checkpoint located in the middle of the base route. Some default parameter values are average walking speed ($V_p = 3$ mile/h), average vehicle speed ($V_b = 25$ mile/h), bus station distance ($d = 0.5$ mile), dwelling time ($T_d = 12$ s), $\alpha = 58\%$ [22]. Based on the real-world operational data, we can set proportions of passengers $\beta_1 = 0.1$, $\beta_2 = 0.4$, $\beta_3 = 0.4$, $\beta_4 = 0.1$.

According to the research by Wardman [23], here, we assume that one unit of walking time and waiting time is respectively 2 times and 1.5 times as costly as in-vehicle riding time. Due to the actual very low curb-to-curb demand, there is only about 6 min slack time per ride in the Line 646 service. Because we intend to study the fare structure at higher demand levels, the default slack time per cycle is assumed to be equal to the actual running time without deviations in order to accommodate more requests.

## 4.2 Experiment Results

In operation, passengers would subscribe to the scheduling system for guaranteed services, and other occasional customers might be rejected by deviation services when the actual demand exceeds the maximum feasible number of curb-to-curb stops in deviation services. Similar to settings of Alshalalfah and Shalaby [24], in our analysis curb-to-curb requests are required to make reservation during the day before, which allows passengers time to manage their trip based on the decision from the scheduling system, and thus rejected passengers are not considered in the calculation of the service quality function.

The theoretical results of each passenger group are displayed in Table 1 [14]. We run the simulation test for the fixed-route service at demand levels 10 passenger/h, 15 passenger/h and 20 passenger/h, respectively and the average cost indicator values are also presented in Table 1. The results show that theoretical and simulation results

**Table 1** Theoretical modeling versus simulation for the fixed-route service

| Test | Indicators (min) | TP 1 | TP 2&3 | TP 4 |
|---|---|---|---|---|
| Theoretical | $K$ | 14.75 | 7.5 | 0 |
| | $A$ | 15.44 | 15.63 | 16.24 |
| | $R$ | 9.2 | 10.5 | 17.5 |
| Simulation | $K$ | 14.78 | 7.49 | 0 |
| | $A$ | 15.44 | 15.58 | 16.29 |
| | $R$ | 9.16 | 10.39 | 17.38 |

match well, which could verify the reliability of our simulation modeling for fixed-route policy, and cost indicators of each passenger group actually maintain stable in the fixed-route service at different demand levels.

## 4.3  Fare Structure Under Flex-Route Policy

The procedure of the service-based fare policy is described as follows: Step 1: assess the service quality value of each passenger group under fixed-route and flex-route policies; Step 2: fix the revenue target after implementing flex-route policy; Step 3: calculate the fare structure in the flex-route service based on price-performance under fixed-route policy.

There are several possible options for transit planners to set up revenue target after implementing flex-route policy. In some real-world differentiated fare cases, the fare of regular passenger group under flex-route policy is the same as the base fare in the fixed-route service, and a higher fare level is set for curb-to-curb passengers. This kind of fare structure absolutely increases the overall transit revenue by providing deviation services. As a nonprofit service, here another possible fare policy is discussed that with sufficient subsidies form government, transit division is not meant to seek additional profit by providing deviation services, and thus the TP 4 fare can expect a discount due to the imposed delay. Because there is still lack of related data and the average fare level almost maintains stable, in our analysis the influence of fare structure on ridership is not considered.

For the Line 646 system, we assumed that revenue under fixed-route policy could cover proportion $\mu$ of total marginal social cost $\text{Cost}_{\text{fixed}}$ of this bus line

$$\mu\text{Cost}_{\text{fixed}} = Q_1 f_{\text{fixed}} + Q_{2\&3} f_{\text{fixed}} + Q_4 f_{\text{fixed}} \tag{1}$$

where $Q_1$, $Q_2$, $Q_3$, $Q_4$ are the quantities of passengers on board in the three passenger groups under fixed-route policy; $f_{\text{fixed}}$ is the flat fare in the fixed-route service. Here, we set $\mu = 0.9$, and the flat fare $f_{\text{fixed}} = 2$ dollars. We further assume $\kappa = 1$, which means that riders are equally sensitive to changes in service quality and in fare levels.
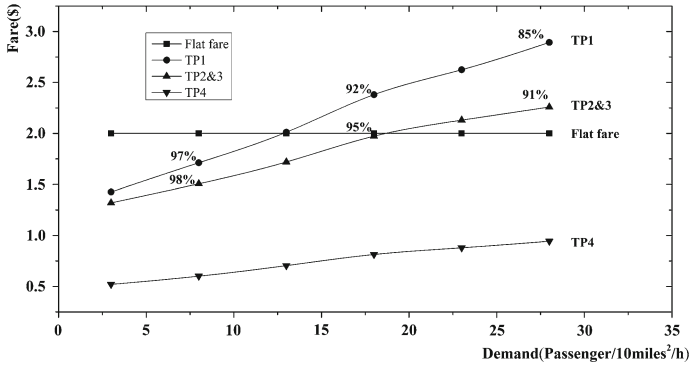
**Fig. 2** The fare structure under two operating policies

The fare structure at different demand levels in the flex-route service is presented in Fig. 2 and it is reasonable to observe the relationship $f_{\text{fixed1}} > f_{\text{fixed2\&3}} > f_{\text{fixed4}}$. At a very low demand level, all three fares are lower than the flat fare $f_{\text{fixed}}$ because of the large idle time at checkpoints, which results in a drop of marginal social costs of the transit system. In reality, in practical use, it is impossible to set such a great slack time for a low actual demand, which would waste lots of useless idle time at checkpoints. Conversely, as the travel demand increases, the acceptance rate of curb-to-curb passengers will undergo a distinct drop (see the percentage in Fig. 2). Thus the slack time should be allotted in coordination with actual demand, which is essential for operating a successful and attractive flex-route service.

## 5 Conclusions

This chapter addresses a problem faced by transit planners in determining efficient fare structures in flex-route services. Different from previous macroeconomic fare policy in conventional fixed-route transit, we propose a micro service-based fare policy which could reflect the transit service value as well as cost of provision. The proposed service-based fare concept is also effective in other emerging innovative transit services, and provides planners a useful tool to design more reasonable and preferred fare structures. In practical use, planners could easily fulfill this service-based fare policy by using simulation modeling for specific flex-route services, which should have already been developed in the planning procedure.

The main purpose of this chapter is to provide a general mechanism to develop the novel service-based fare policy. As a meaningful step in new pricing strategies, there are still some limitations in our research. Some assumptions are made in our analysis because we intend to make the analytic work easier to understand. Vehicle rectilinear movement and uniformly distributed requests may not be realistic in service areas with complex land use plans, so a detailed investigation over the roadway network

and travel demand is necessary before implementing flex-route policy. In practical use, planners could replace above assumptions with real-world data of specific transit services.

# References

1. Borger BD, Mayeres I, Proost S, Wouters S (1996) Optimal pricing of urban passenger transport: a simulation exercise for Belgium. J Transport Econ Policy 30(1):31–54
2. Proost S, Dender KV (2008) Optimal urban transport pricing in the presence of congestion economies of density and costly public funds. Transp Res Part A 42:1220–1230
3. Parry IWH, Small KA (2009) Should urban transit subsidies be reduced? Am Econ Rev 99(3):700–724
4. Mattson J, Ripplinger D (2012) Marginal cost pricing and subsidy of small urban transit. Transp Res Rec 2274:77–83
5. Cervero R (1981) Flat versus differentiated transit pricing: what's a fair fare? Transportation 10:211–232
6. Cervero R (1990) Transit pricing research. Transportation 17:117–139
7. America. TCRP Report 140 (2010) A guide for planning and operating flexible public transportation services. Transportation Research Board of the National Academies, Washington, DC
8. Emele CD, Oren N, Zeng C, Wright S, Velaga N, Nelson J, Norman TJ, Farrington J (2013) Agent-driven variable pricing in flexible rural transport services. Commun Comput Inform Sci 365:24–35
9. Daganzo CF (1984) Checkpoint dial-a-ride systems. Transp Res Part B 18(4–5):315–327
10. Fu L (2002) Planning and design of flex-route transit services. Transp Res Rec 1791:59–66
11. Quadrifoglio L, Hall RW, Dessouky MM (2006) Performance and design of mobility Allowance shuttle transit services: bounds on the maximum longitudinal velocity. Transp Sci 40(3):351–363
12. Nourbakhsh SM, Ouyang Y (2012) A structured flexible transit system for low demand areas. Transp Res Part B 46:204–216
13. Qiu F, Li W, Haghani A (2015) An exploration of the demand limit for flex-route as feeder transit services: a case study in Salt Lake City. Public Transport 7(2):259–276
14. Qiu F, Li W, Haghani A (2015) A methodology for choosing between fixed-route and flex-route policies for transit services. J Adv Transp 49(3):496–509
15. Qiu F, Li W, Shen J (2014) Two-stage model for flex-route transit scheduling. J Southeast Univ (Nat Sci Ed) 44(5):1078–1084 (In Chinese)
16. Fu L (1999) On-line and off-line routing and scheduling of dial-a-ride paratransit vehicles. Comput aided Civ Infrastruct Eng 14:309–319
17. Horn MET (2002) Fleet scheduling and dispatching for demand-responsive passenger services. Transp Res Part C 10:35–63
18. Crainic TG, Malucelli F, Nonato M, Guertin F (2005) Meta-heuristics for a class of demand-responsive transit systems. Informs J Comput 17(1):10–24
19. Cremers MLAG, Haneveld WKK, Vlerk MH (2009) A two-stage model for a day-ahead paratransit planning problem. Math Methods Oper Res 69:323–341

20. Qiu F, Li W, An C (2014) A Google maps-based flex-route transit scheduling system. In: Proceedings of the 14th COTA international conference of transportation professionals, Changsha, China, pp 247–257
21. Qiu F, Li W, Zhang J (2014) A dynamic station strategy to improve the performance of flex-route transit services. Transp Res Part C 48:229–240
22. Hess DB, Brown J, Shoup D (2004) Waiting for the bus. J Public Transp 7(4):67–84
23. Wardman M (2004) Public transport values of time. Transp Policy 11(4):363–377
24. Alshalalfah B, Shalaby A (2012) Feasibility of Flex-Route as a Feeder Transit Service to Rail Stations in the Suburbs: Case Study in Toronto. J Urban Plann Dev 138(1):90–100

# Research on the Key Technology in the Specification for Traffic Impact Analysis

**Xian-tong Jiang, Hui Xiong and Chang Xu**

**Abstract** With the development of urbanization and mobility, traffic issues have increasingly emerged. Due to the large construction scale and the influence of the development, traffic was generated on the network of roads around the project on the whole city, some development plan schemes and development projects would lead to supply–demand imbalance in the traffic of road nets, aggravating the tense situation of urban traffic and triggering a new and chain of traffic issues. Thus, traffic impact analysis is playing a bigger role in the rational development of urban construction and coordinate development between traffic and land exploration and utilization. According to the research on the national and international specification for traffic impact analysis, the article analyzed real issues in the practices, for one thing. For another thing, the author focused on certain key technology, such as traffic impact analysis type, start threshold, research scope, parking demand prediction, etc. The paper aims to provide a basis and technological support for the establishment of the Specification for Traffic Impact Analysis.

## 1 Introduction

When it comes to urbanization rate, it has increased from 36.2%, in 2000, to 57.4%, in 2016, in China. Considering the urbanization rate of 60%, in 2020, and 70%, in 2030, there are 0.24 billion rural Chinese that would shift to the cities, in total. When it comes to mobility development, the total amount of vehicles has grown from 16

X. Jiang (✉) · C. Xu
Modern Logistics Research and Development Center, Academy of Transportation Science China, Beijing 100029, China
e-mail: xiantong86@126.com

H. Xiong
School of Mechanical Engineering, Beijing Institute of Technology, Beijing 100081, China

million, in 2000, to 279 million, in 2015, in China. It is estimated that the number would exceed 300 million in 2020. The traffic jams caused by the rapid growth of vehicle numbers have expanded to the medium-sized and even small cities, and there are more than 100 cities with frequent occurrence of traffic jams.

On one hand, land development would definitely lead to higher traffic demand, resulting in greater traffic pressure on the network of urban roads. On the other hand, developers hope to have a safe and smooth transportation environment around their projects to increase the market competitiveness. Therefore, it is necessary to study the inherent link between the projects and the urban traffic demand, reveal the traffic law influenced by the projects nearby, and explore how to coordinate the relations between the two effectively, thus, to promote the cities to develop in a healthy, orderly, and continuous way. Traffic impact analysis is a powerful tool to coordinate the relation between land utilization and urban traffic.

## 2   Traffic Impact Analysis Type

Traffic impact analysis should run through the whole process of land utilization, whether land use planning stage, or in the construction phase of the program, and will have a different impact on the transportation system because of different planning or design. Therefore, the article integrated some provinces and cities of the traffic impact assessment management regulations, taking into account the control plan and the construction of two stages at the same time, but had different priorities on different cities. Considering that "Specification for traffic impact analysis" (Guobiao standards) is applicable to the whole country, it is suggested that the traffic impact analysis can be divided into two types: Development plan scheme and development project.

## 3   Start Threshold

### 3.1   Purposiveness of Start Threshold

Start threshold is the basis for judging whether the development project needs to carry on the traffic impact analysis, and also determines the necessity of the follow-up work. Different countries or regions have different threshold rules, mainly divided into two categories: one is to divide according to the development project construction scale, that is to say, the traffic impact analysis should be carried out when the scale of the building reaches to a certain extent; the other is the influence degree of road network development projects, that is to say, it is necessary to carry out traffic impact assessment on the degree of traffic impact of different grades of roads.

The first method is simple and easy to control, and it is widely used in the traffic impact analysis of some big cities in China. The second method is to carry out the preliminary traffic assignment for each project, which requires that the basic information is comprehensive and detailed. This method is widely used in foreign countries.

## 3.2 Suggestions of Start Threshold

At present, it is still not mature in China that the threshold method is adopted to produce the influence degree of different grades, because large cities in China have not yet established a complete urban transportation system model to measure the impact of construction projects or planning on the surrounding traffic system. For now, the method to determine the threshold is relatively rough, but the operation is stronger. At the same time, the specified scale of the threshold in a different city is not entirely consistent, therefore, considering similar technical indicators, "Specification for traffic impact analysis" (Guobiao standards) propose requirements only from the perspective of the principle, only from the angle of the principle of the request. More technical parameters and their values will be defined by national or local traffic impact analysis criteria. It is suggested that in the "Specification for traffic impact analysis" (Guobiao standards), the threshold value should be set as follows, to set aside more space for technical standards:

(1) The threshold of traffic impact analysis should be determined based on the plan, the type, scale, and location of the construction project, and the running state of the traffic system.
(2) Traffic impact analysis should be carried out when the scale of the development plan scheme or project reaches the prescribed threshold.

## 4 Research Scope

## 4.1 Quantitative Methods of Research Scope

The scope of the traffic impact analysis should be determined by the scope of the traffic generated by the development project, while this range is mainly determined by the traffic generation intensity of the project, the entry and exit of the projects, as well as the surrounding road network structure. Generally speaking, the larger the amount of traffic generated by the development project, the wider the scope of the traffic impact. On the other hand, for the development projects with similar traffic generation, the more foreign channels they connect with the urban road network, the more traffic flows are generated and attracted, thus, the influence distance is smaller in a single direction. Similarly, the greater the density of the surrounding

road network is, the more parallel the roads are, more traffic will be diverted from development projects, and thus, the smaller the range it can radiate.

At present, national and international quantitative methods on the scope of the traffic impact analysis can be roughly divided into two types. One is used in traffic planning procedures, through the method of trial presumption study traffic impact range; the other one is the application of relevant theoretical model assumptions in particular, direct method of calculus study traffic impact range.

After comparison, although two kinds of methods have definite quantitative indexes, the first type applies a very mature traffic distribution or traffic assignment process, which fully reflects the impact of the actual road network. The second type might identify the project as a homogeneous area, or do not take into account the differences in the actual spatial distribution of traffic. The theoretical model describing the city and traffic travel is too simple to reflect the actual situation. In this regard, the first type of approach is superior to the second one in principle. However, there are obvious defects in the first method. In order to determine the scope of the traffic, the operation process of traffic planning should be repeated.

Therefore, in most cities of our country, in the process of traffic impact analysis, it is necessary to adopt a practical and simple method to determine the scope of traffic impact.

## *4.2   Determining Method*

(1) **The minimum limit of traffic impact analysis**. The minimum limit of any development project that reaches the threshold of traffic impact assessment is a single-layer rectangular network, each side of which are made by the city sub-road (or two highways) surrounded, based on the development project.
(2) **The maximum limit of traffic impact analysis**. In Beijing, for example, in the urban construction projects, the maximum limit is a network, each side of which is composed of two layers of the parallel urban rapid road based on the development project. For the development project located in the outskirts of the construction area, the maximum limit is the entire satellite city or metro road network, as well as all the road network composed of external contacts.
(3) **The scope of the calculation program of the traffic impact analysis**

  (a) The scope of traffic impact is estimated based on the type of traffic impact analysis. For small-scale development projects, the minimum limit range can be selected; for large-scale construction projects, the project can be expanded to the nearest urban trunk road or urban rapid road, with its enclosed area as the initial impact.
  (b) It is necessary to establish a target year (traffic impact analysis perspective years) for the road network model, including the initial centroid effect within the road network, preliminary impact on the road network, and the calibration of the section of the road resistance function. At the same time,
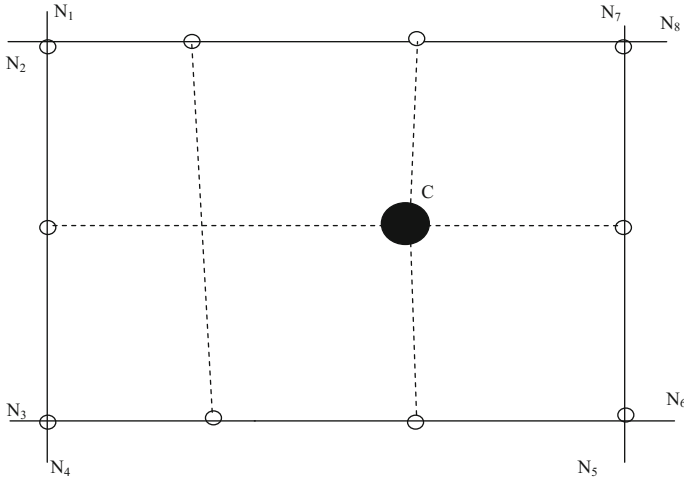
**Fig. 1** Road network model (1)

it is necessary to maintain the openness of the simple road network (in fact, the extension of the road in the model is also extended to the outside of the scope of the original). The scheme is shown in Fig. 1, with C as the centroid of the development project, Ni as road node.

(c) According to the type of development projects, determine the amount of traffic generated based on the relevant standards; determine the proportion of traffic radiation in various directions based on the location.

(d) With the development project as centroid, and endpoint foreign channel network model as a virtual center node, we used the "gravity model" to complete the traffic distribution to obtain the traffic conversion matrix, OD. For Fig. 1, this set of traffic transfer amount is T(C, N1)–T(C, N8), and T(N1, C)–T(N8, C).

(e) Based on this set of traffic OD matrix, traffic assignment is implemented to obtain the traffic volume on each boundary road.

(f) The proportional relation between the traffic generated by the project and the maximum allowable traffic volume at the service level of the road is calculated as follows:

$$R = \frac{V_{\text{P}}}{V_{\text{max}}} = \frac{V_{\text{P}}}{C \cdot r} \tag{1}$$

$V_{\text{p}}$     Project generated traffic;
$V_{\text{max}}$  Maximum allowable traffic volume;
$C$       Traffic capacity of the road;
$r$       Specific service level corresponding to the load, which is the ratio of $V/C$.
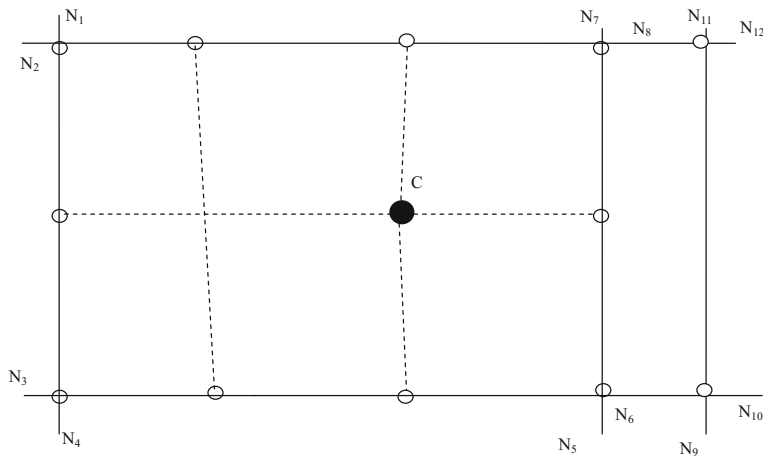
**Fig. 2** Road network model (2)

> In Beijing, for example, the agreed standard value of $r$ agreed is as follows: Located in downtown area, $r = 1.0$; Located in the built-up area of the suburbs, $r = 0.9$; Located in the non-built-up area of the suburbs, $r = 0.8$.
>
> (g) If the results of a certain road $R > 5\%$, the scope of the study was extrapolated to the parallel urban trunk road outside the road (or Urban Expressway). Thus, the expanding road network model is established, as shown in Fig. 2.
>
> (h) In the expanding road network model, we need to repeat steps d–f, until there is no longer any peripheral road to reach the standard in step g, or the expansion of the road network has reached the maximum limit of traffic impact assessment. The cycle will be stopped.

At this point, the scope of the presumption can be used as the scope of the traffic impact analysis of development project. Field traffic survey, traffic demand forecasting, and other work will be carried out within the defined area.

# 5 Parking Demand Forecasting

## 5.1 Prediction Model

Parking demand forecasting has some applications in many big cities in the world. However, the urban development patterns are different in different countries, the social and economic development patterns are different, the parking prediction model is not the same, and there will be a large difference in the calculation. To sum up, there are several kinds of prediction methods:

(1) **Car growth model**. As there is a close relationship between the city's parking demand and the national income and the development of economy and the car ownership rate, so in this model, it is assumed that there is a linear relationship between parking demand and the number of vehicles owned by urban residents. Based on the growth data of cars over the years, a linear regression model is established to calculate the number of cars in the target year. Then, the parking demand of each district is calculated by using the relationship between parking and vehicle ownership. This model can also be used to obtain the nonlinear function relationship between vehicle ownership and parking demand through a large number of statistical data.

$$D_{pi} = D_{bi} \times \frac{C_p}{C_b} \tag{2}$$

$D_{pi}$ Parking demand in zone $i$, in year $p$ (forecast);
$D_{bi}$ Number of parking in base area $I$;
$C_p$ Regional forecast, in year $p$ (forecast);
$C_b$ Number of vehicles in the region.

(2) **Trip attraction model**. The model assumes that the generation of parking demand is related to the social and economic activities in different regions. If the region is able to attract a variety of travel activities, the demand for parking in the region will increase. First, we can get all kinds of travel data for the target year in the region, and then we assign the data to the travel through by the car. Then, the use of the car carrying rate will be converted to the number of vehicles arrived, and finally multiplied by the number of parking peak hours, we can get the peak hours of parking demand. Mathematical models are as follows:

$$D_{pi} = \frac{\left(\sum_{j=1}^{N} \mathrm{TD}_{pij}\right) \times \left(\mathrm{MS}_p\right)}{F_p} \times K \tag{3}$$

$D_{pi}$ Peak hour parking demand in $i$ area, in $p$ year;
$\mathrm{TD}_{pij}$ $i$ area $j$ trip destination number, in $p$ year (There are $n$ kinds of travel purpose);
$\mathrm{MS}_p$ Car traffic distribution coefficient, in $p$ year;
$F_p$ Vehicle carrying capacity, in $p$ year;
$K$ Parking peak value.

(3) **Production rate model**. The production rate model assumes that there is a functional relationship between the parking demand and the land use type and the intensity of each region. The model needs to investigate all kinds of land use and parking rate of the building, and convert them into various types of land unit parking rate. The model is more intuitive and easy to operate, but it needs to be calibrated strictly. Mathematical models are as follows:

$$D_{pi} = \sum_{j=1}^{N} \left(R_{pij}\right)\left(\text{LU}_{pij}\right) \tag{4}$$

$D_{ij}$     Peak hour parking demand in $i$ area, in $p$ year;
$R_{pij}$    Parking demand generation of $j$ land use unit area in $i$ area, in $p$ year;
$\text{LU}_{pij}$   Use area of $j$ land in $i$ area.

(4) **Multiple regression model**. The model assumes that there is a certain rela-tionship between the parking demand in the city and the city's socioeconomic activities and land use, therefore, multiple linear regression analysis is used to build parking demand model. The advantage of this model is that it can reflect most of the factors that affect the parking demand, but the cross relationship between factors is not easy to distinguish. Mathematical models are as follows:

$$D_{pi} = f\left(\text{ER}_{pi}, \text{PO}_{pi}, \text{FA}_{pi}, \text{DU}_{pi}, \text{RS}_{pi}, \text{AO}_{pi}, \ldots\right) \tag{5}$$

$D_{pi}$   Peak hour parking demand in $i$ area, in $p$ year;
$\text{EP}_{pi}$   Number of employed persons in $i$ area, in $p$ year;
$\text{PO}_{pi}$   Population in $i$ area, in $p$ year;
$\text{FA}_{pi}$   Floor area of $i$ area, in $p$ year;
$\text{DU}_{pi}$   Number of households in $i$ area, in $p$ year;
$\text{RS}_{pi}$   Retail floor area in $i$ area, in $p$ year;
$\text{AO}_{pi}$   Car ownership in $i$ area, in $p$ year.

(5) **Traffic volume—parking demand model**. Assuming that there is a functional relationship between the parking demand in each region and the traffic flow through the area, the number of parking demands is assumed to be a function of the number of vehicles passing through the area. Mathematical models are as follows:

$$D_{pi} = f(V_i) \tag{6}$$

$D_{pi}$   Peak hour parking demand in $i$ area, in $p$ year;
$V_i$   Traffic flow in $i$ area, in $p$ year.

(6) **Land use—Parking demand model**. The model assumes that the long-term parking demand is related to the job opportunities, and the short-term parking demand is related to the commercial and retail floor area, while the total parking demand is the sum of long-term demand and short-term demand. Mathematical models are as follows:

$$D_i = A_l\left(e_i \bigg/ \sum^{j} e\right) + A_s\left(F_i \bigg/ \sum^{j} F\right) \tag{7}$$

$D_i$   Peak hour parking demand in $i$ area, in $p$ year;
$A_l$   Cumulative value of long-term parking demand;
$A_s$   Cumulative value of short-time parking demand;
$e_i$   Employment opportunities in $i$ area;
$e$    Total number of jobs in the central business district;
$F_i$   Floor area of commercial and retail buildings in $i$ area;
$F$    Total floor area of commercial and retail buildings in $i$ area;
$j$    Region number.

(7) **Multivariate geometric mean growth model**. The model assumes that there are geometric mean relation in the growth of parking demand, the growth of population, the number of vehicles, the growth of national income, the floor area of buildings, and other variables. Mathematical models are as follows:

$$D_{pi} = D_{bi}(1 + R_{bi})^{p-b} \tag{8}$$

$$R_{bi} = \sum W_{bij} \sqrt[W_{bij}]{\prod_{i=1}^{N} r_{bij}^{W_{bij}}} \tag{9}$$

$D_{pi}$   Parking demand in $i$ area, in $p$ year;
$D_{bi}$   Parking demand in $i$ area, in $b$ year;
$r_{bij}$   Population growth in $i$ area, in $b$ year ($j = 1$); Vehicle growth ($j = 2$); National income growth rate ($j = 3$); Floor area ($j = 4$), etc.;
$W_{bij}$   Weighted values of $i$ area in the year;
$R_{bi}$   Annual growth rate of $i$ area, in $b$ year.

## 5.2  Suggestions of Parking Demand Forecast

To sum up, it is suggested that parking demand forecasting is an important part of traffic impact analysis: In the investigation of the current situation, it is necessary to investigate the situation and operation of the parking system. In the analysis of the new generation of traffic demand, traffic system should be analyzed according to the nature of the use of parking demand, use object, location characteristics, and the supply and demand situation, including the analysis of similar project travel analysis, traffic generation, traffic distribution, mode split and traffic assignment and parking demand forecasting, etc.; In the traffic impact analysis of development project, we should analyze the matching degree between land use and construction scale and the planning of traffic facilities, and analyze the rationality of the arrangement of entrance, internal and external traffic organization and parking facilities.

# 6 Conclusion

As a tool to coordinate land development and urban traffic, traffic impact analysis has been widely used in our country, but there is no national standard to regulate traffic impact analysis. In this chapter, the key technologies of traffic impact analysis, such as traffic impact analysis type, start threshold, research scope, and parking demand prediction. They provide the basis and technical support for "Specification for traffic impact analysis" (Guobiao standards) and the subsequent traffic impact analysis.

# References

1. Wang L (2005) Study on traffic impact evaluation of urban construction project. Municipal Technol 9
2. Wang G, Ye Z (2009) Research methods and application of traffic impact assessment. Transp Syst Eng Inform 6
3. Jing G (2011) Development and consideration of traffic impact assessment in Guangzhou. Traffic Transp
4. Transportation Research Board (2000) High—way capacity manual. TRB, Washington, DC
5. CJJT144 Technical standard for traffic impact assessment of construction projects
6. CJJT141-2010 Technical standard for traffic impact assessment of construction projects
7. DGTJ 08-2165-2015 Technical standards for traffic impact assessment of construction projects in Shanghai

# A Pedestrian Crowd Classification Method Based on the AFC Data in the Urban Rail Transit

**Ji-biao Zhou, Sheng Dong, Peng-fei Zhao and Yong-rui Chen**

**Abstract** Crowds are an important feature of high-dense Mass Rail Transit (MRT), assessing its crowding status is a critical step in crowd management. In this chapter, a pedestrian crowd classification method based on an improved ant colony clustering algorithm (ACCA) is developed for MRT systems. First, survey data from Automatic Fare Collection (AFC) regarding three statuses (check-in/check-out and sum). Second, the PCI-influenced factors were also considered in the method, which included average daily ridership intensity, the duration of crowd, and the scope of crowd influence. Third, to classify the pedestrian crowd, an improved ant colony clustering model and its solving algorithm were presented. The results show that, for the two types of time scale, the passengers' time–space characteristics present a clear image of M, the variation trend of morning and evening peak hour is obvious in the MRT.

J. Zhou · S. Dong (✉)
School of Civil and Transportation Engineering,
Ningbo University of Technology, Ningbo 315211, China
e-mail: 514099665@qq.com

J. Zhou · S. Dong
Key Laboratory for Traffic and Transportation Security of Jiangsu Province,
Huaiyin Institute of Technology, Huaiyin, China

P. Zhao
Beijing Key Laboratory of Traffic Engineering, Beijing University of Technology, Beijing 100124, China

Y. Chen
School of Highway, Chang'an University, Xi'an 710064, China

# 1  Introduction

Crowds are a feature of Mass Rail Transit (MRT) occurring not only at mass gatherings but also at routine events such as daily commute [1]. Hence, assessing its crowding status is a critical step of the MRT systems crowd management. It is well known that MRT has become an effective way to solve the traffic problems [2–4], because of its advantages in safety, comfort, convenience, punctuality, huge carry capacity, and reliability [5–7]. By the end of December 2014, 25 cities have a total of 100 rail transit lines in operation, with a total length of 3055.6 km and 2027 stations in China. Compared with 2014, a new round of construction of urban rail transit has begun by leaps and bounds for China's 13th Five-Year Plan (i.e., 2016–2020). By the end of June 2015, 39 cities are scheduled to build metro by the State Council of China, which will be increased to 50 cities and the total mileage will be over 7300 km by 2020 [8]. With the expansion of the scale of construction and increase of operating lines, China's rail transit operation management will experience single stage of independent operation into multiline network operation phase. Meanwhile, several factors, such as the continued rise of passenger numbers in total and daily, the sustained increasing of average passenger strength, and the time of minimal departure interval is relatively shorter, will put forward higher requirements for the crowd management in the rail transit.

From 2012 to 2014, the annual total ridership (ATR) in 12 worldwide cities has exceeded 1.0 billion [8]. The top three are Beijing, Shanghai, and Seoul, and the followed by nine cities are Moscow, Tokyo, Guangzhou, New York, Mexico City, Hong Kong, Paris, London, and Shenzhen. The ATR was 12.6 billion, which increased to 1.6 billion compared with 2013. ATR in the top three cities, i.e., Beijing, Shanghai, and Guangzhou, exceeded 2.0 billion. Specifically, the ATR of Beijing was 3.39 billion which accounted for 26% Shanghai was 2.83 billion which accounted for 22%, and Guangzhou was 2.22 billion which accounted for 17 percent.

In addition, with the rapid growth of rail transit passenger flow in China, the passenger flow distributions in both space and time are highly concentrated, the contradiction between facilities and transport capacity has become increasingly prominent. It is hard to get into the metro or local commuter trains at peak times [9]. As the crowds of mass transit in particular urban rail transit have become a universal problem in several metropolitan areas not only in developing countries, but also in developed countries, the methods of crowd management and countermeasures need to be proposed urgently.

## 2 Data and Methods

### 2.1 Data Collection

Data collection is based on the ticket record from Automatic Fare Collection (AFC) in Xi'an metro. The analyzed data include two parts, part one is day scale in line 1, and part two is hour scale in line 2. In line 1, the time scale covers the whole range of ridership, from the October 1 to October 31, 2013, the sample in line 1 is 1674 [18 station × 31 days × 3 (check-in/out and sum)]. In line 2, the time scale covers the whole range of ridership, from the 0:00 to 24:00 (24-h clock), March 19, 2013, the sample in line 2 is 1224 [17 station × 24 h × 3 (check-in/out and sum)]. The line 1, line 2 and totally 35 stations in Xi'an metro have been put into operation in 2013, which has a whole mileage of 52.2 km. The average daily ridership (ADR) in Xi'an metro is about 1.05 million in 2015. The operating interval of line 1 is five minutes thirty second as which in line 2 is four minutes thirty-one second. The punctuality rate is above 99% in more than 1200 days of operation. The annual total ridership (ATR) of Xi'an metro network is close to 300 million. With the ridership increases, the average daily ridership intensity (ADRI) in Xi'an metro has reached 17,500 persons per km per day in the fourth quarter of 2014, which reaches the third one in China after Beijing and Guangzhou.

### 2.2 Ant Colony Clustering Algorithm

The degree of crowding (DOC) reflects not only the time characteristic that passengers cluster in pedestrian facilities (e.g., horizontal channel, stair, platform, etc.) in the MRT, but also the level of service (LOS) in the MRT, which provides an important basis for organizing passenger flow in MRT. Classifying the DOC, the pedestrian crowding index (PCI) is proposed, which not only avails crowdedness identification in the MRT, but also helps rail transit managers to predict and organize passenger flow effectively.

#### 2.2.1 Algorithm Description for Pedestrian Crowd

PCI, shorted from pedestrian crowding index, is a measurement that represents the traffic operational quality and the DOC of a single station in the MRT. PCI is a continuous variable ranges from 0 to $+\infty$, which represents the pedestrian operational states and pedestrian crowding status. The larger value indicates a worse operational status and a greater probability of mass accident occurrence during the assessment interval. This is true vice versa. Hence, in this paper, we propose a pedestrian crowd classification method according to three influencing factors, (a) average daily rider-

ship intensity, (b) the duration of crowd, and (c) scope of crowd influence, for the purpose of describing the safety level based on the PCI.

(a) Average daily ridership intensity

The traffic intensity of urban rail ridership, which is defined by the average density of passenger flow in unit time and symbolized by $K_{ij}^{\alpha}$, which can be calculated by Eq. (1).

$$K_{ij}^{\alpha} = Q_{ij}^{\alpha}/S_{ij}^{\alpha} = Q_{ij}^{\alpha}/\sum_{l=1}^{L} \lambda_{ij}^{\alpha,l} s_{ij}^{\alpha,l} \tag{1}$$

where $K_{ij}^{\alpha}$ denotes the DOC in line $i$ and station $j$ according to status $\alpha$, as $\alpha$ could be 1, 2, and 3, which represents check-in status, check-out status, and sum status; $Q_{ij}^{\alpha}$ denotes the total flow in line $i$ and station $j$ according to status $\alpha$, ped/h or ped/d; $S_{ij}^{\alpha}$ denotes the reduced effective area in line $i$ and station $j$ according to status $\alpha$, m$^2$; $\lambda_{ij}^{\alpha,l}$ denotes the convert coefficient for type l facilities available for passengers in line $i$ and station $j$ according to status $\alpha$, of facilities are totally divided into L classes; $s_{ij}^{\alpha,l}$ denotes the actual area of type l facilities available for passengers in line $i$ and station $j$ according to status $\alpha$, m$^2$.

(b) The duration of crowd

The duration of crowd is one of the most significant factors that affect passengers' perception in the MRT, which is described as follows, first through function fitting about the distribution of cumulative frequency corresponded to various densities, the distribution curve about cumulative frequency of passengers' density. Then the change rate is obtained by taking deviation first and then reciprocal against point in the curve. In the end, the duration of crowd is obtained. According to the statistics, the cumulative distribution curve of passenger flow is logarithmic function, as is shown in Eq. (2).

$$y_{\xi} = a_{\xi} \ln(x_{\xi}) - b_{\xi} \tag{2}$$

where $x$ denotes average density of pedestrian in hub, ped/m$^2$; $y$ denotes the cumulative frequency against $x$, non-dimensional; the parameter $a$ and $b$ are constants, $\xi$ represents the different status of PCI, $\xi \in \{1, 2, 3, 4, 5, 6\}$. Equation (3) is obtained from the reciprocal of the deviation from Eq. (2).

$$\frac{dx_{\xi}}{dy_{\xi}} = \frac{x_{\xi}}{a_{\xi}} \tag{3}$$

where the value of $dx/dy$ reflects the change rate of the cumulative frequency of ridership. When the bigger, the density of ridership change faster, and the influence of crowds is more remarkable, this is true vice versa. The time duration under the density $x$, which is represented by $x/a$. $\xi$ here has the same mean to Eq. (2), $\xi \in \{1, 2, 3, 4, 5, 6\}$.

(c)  Scope of crowds influence

The scope of crowds influence is represented by available facilities areas in the MRT. Since the pedestrian characteristics are various at different facilities, the weighting parameter $\lambda_{ij}^{\alpha,l}$ is referenced, in order to reflect the scope of crowds influence, as is shown in Eq. (1). For the purpose of the cumulative effect of the three factors (i.e., average daily ridership intensity, the duration of crowd, and scope of crowds influence), the pedestrian crowding index (PCI) is proposed by the synthesized of the three factors, as is shown in Eq. (4).

$$\mathrm{PCI}_x^{\alpha} = \frac{K^{\alpha} a^{\alpha}}{x} \tag{4}$$

where $x$ denotes average density of pedestrian, ped/m$^2$; $\mathrm{PCI}_x^{\alpha}$ denotes the PCI under status when the pedestrian density is $x$.

### 2.2.2  Algorithm Method for Pedestrian Crowd Classification

(1)  Basic Theory

We treat the data point of PCI as an ant with diverse properties, and we also treat classification center of DOC as food source. Supposing that the total number $M$ of classification is clear and definite, the pedestrian crowding indices $N$ with $n$ properties to be analyzed are defined in Eq. (5).

$$X = \{X_a | X_a = (x_{a1}, x_{a2}, \ldots, x_{an}), a = 1, 2, \ldots, N\} \tag{5}$$

The biased error between pedestrian crowding indices is measured with Euclidean distance, when shorter distance means less biased error. When pedestrian crowding index $a$ is distributed for clustering center $\overline{C_b}(b = 1, 2, \ldots, M)$, ants will release pheromone $\tau_{ab}(c)$ on the path $(a, b)$ from sample $a$ to clustering center $\overline{C_b}$. $\tilde{d}_{ij}$ is the weighted Euclidean distance between the pedestrian crowding indices $X_a$ and $X_b$ in attribute space; $p_{ab}(c)$ is the probability that ants may choose this path $(a, b)$, and they can be calculated by the following equations.

$$\tilde{d}_{ij} = \sqrt{\sum_{v=1}^{n} p_k (x_{iv} - x_{jv})^2} \tag{6}$$

$$\tau_{ij}(k) = \begin{cases} 1, & \tilde{d}_{ij} \leq r \\ 0, & \tilde{d}_{ij} > r \end{cases} \tag{7}$$

$$p_{ab}(c) = \frac{\tau_{ab}(c)\eta_{ab}^{\beta}(c)}{\sum_{d \in D} \tau_{db}(c)\eta_{ab}^{\beta}(c)} \tag{8}$$

where $r$ denotes clustering radius; $D = \left\{ d | \tilde{d}_{ab} \leq r, d = 1, 2, \ldots, N \& d \neq b \right\}$ denotes alternative path for ants $X_b$; Parameter $\beta$ is a expectation inspire factor, which denotes the emphases level of inspire information in the movement of ants; $\eta_{ab}^{\beta}(c)$ is the value of inspire information in iteration $k$, which is distributed from pedestrian crowding index $i$ to the $j$th clustering center $\overline{C_b}$, and its value is defined from the reciprocal of distance between them; when $p_{ab}(c) \geq P_0$, $X_a$ is merged into the neighborhood $X_b$. Once all ants have moved, pedestrian crowding indices in each class may change, so the position of clustering center for each class and the biased error in each class should be updated as well. $C_b$ denotes whole clustering sets merged into domain $X_i$, the updated clustering center $\overline{C_b}$ and biased error $E$ is calculated in Eqs. (9) and (10).

$$\overline{C_b} = \frac{1}{B} \sum_{c=1}^{B} X_c, b = d = 1, 2, \ldots, C \tag{9}$$

$$E = \sum_{b=1}^{C} \sum_{c=1}^{B} \sqrt{\sum_{t=1}^{m} (x_{ca} - c_{ab})^2} \tag{10}$$

where $J$ represents the amount of elements in $C_b$; $C_{ab}$ denotes the $a$th component in $\overline{C_b}$.

Meanwhile, we set the limit of iterations in practice. Once the results meet any one of the two conditions, then stop clustering and display result. That is, (a) when the sum of biased error for all classes is less than $\varepsilon$, (b) when iterations meet the limit otherwise, restart calculation until the conditions are met.

(2) Algorithm Steps

We design the algorithm steps to calculate the ACCA through the MATLAB tools. The purpose of calculation is to find the critical value of PCI classification, the steps can be achieved as follows.

Step 1: Parameter initiation, that is, determine the sample size $N$ of PCI. For the day scale in line 1, clustering under each status of check-in, check-out, and sum, its sample size is 558 (18 station × 31 days). For the hour scale in line 2, clustering under each status of check-in, check-out and sum as well, its sample size is 323 (17 stations × 19 h, because the valid data is only 19 h, not 24 h, and the rest of time the metro is closed for maintenance). The iterations $K$ of three categories of status are limited to 1000.

Step 2: Start iteration based on the matrix of whole information elements, and the ant walking path is determined and marked.

Step 3: Determine the clustering center according to the walking path marked, then calculate the total biased error from sample to clustering center, and obtain the minimum biased error $E_{\min}$.

Step 4: Generate a random number, then on this basis modify the optimal path and calculate the total biased error $E'$ from samples to corresponding clustering center.

**Table 1** The results of PCI classification

| Grade | Check-in | | Check-out | | Sum | |
|---|---|---|---|---|---|---|
| | PCI (hour) | PCI (day) | PCI (hour) | PCI (day) | PCI (hour) | PCI (day) |
| 1 | 0.080 | 3.130 | 0.080 | 2.680 | 0.228 | 11.500 |
| 2 | 0.290 | 10.450 | 0.375 | 8.000 | 0.925 | 35.400 |
| 3 | 0.630 | 21.880 | 0.853 | 16.150 | 2.113 | 72.500 |
| 4 | 1.099 | 37.500 | 1.491 | 27.030 | 3.713 | 122.630 |
| 5 | >1.099 | >37.500 | >1.491 | >27.030 | >3.713 | >122.630 |

Step 5: Judgement, if $E' < E_{min}$, the present is the optimal path, display result and stop iteration; otherwise, run step 6.

Step 6: If iterations meet limit $K$, display result and stop iteration; otherwise, back to step 2 and restart next iteration.

## 3 Results

In the algorithm, pheromone evaporation rate $\rho$ is set as 0.1, while the numbers of ants $n$ is set as 50 and the PCI clustering results are divided into 5 grades. Finally, the computational results are given by Table 1.

In accordance with the idea of pedestrian crowding index (PCI), the color of red, orange, yellow, and green are used for the PCI values and density values. The clustering results are shown in Fig. 1. Meanwhile, the relationship between the pedestrian crowding index and pedestrian crowd density in different time are also presented, as is shown in Fig. 1.

## 4 Conclusion

This paper has presented an improved ACCA to calculate the value of PCI in the MRT, taking into account three influencing factors (average daily ridership intensity, the duration of the crowd, and scope of crowd influence). The proposed model is motivated by the fact that crowds are a feature of MRT, occurring not only at mass gatherings but also at routine events. A pedestrian crowd classification method is proposed to descript the safety level in the MRT, which based on the improved ACCA.

According to the statistics, the cumulative distribution curves of passenger flow are fitted by a logarithmic function, the related parameters are calibrated for different statuses of passengers according to a large data set from ticket records of AFC system in Xi'an, China. A case study about Xi'an MRT is conducted using the PCI to illustrate the advantage of the proposed model compared with a single classification criterion.
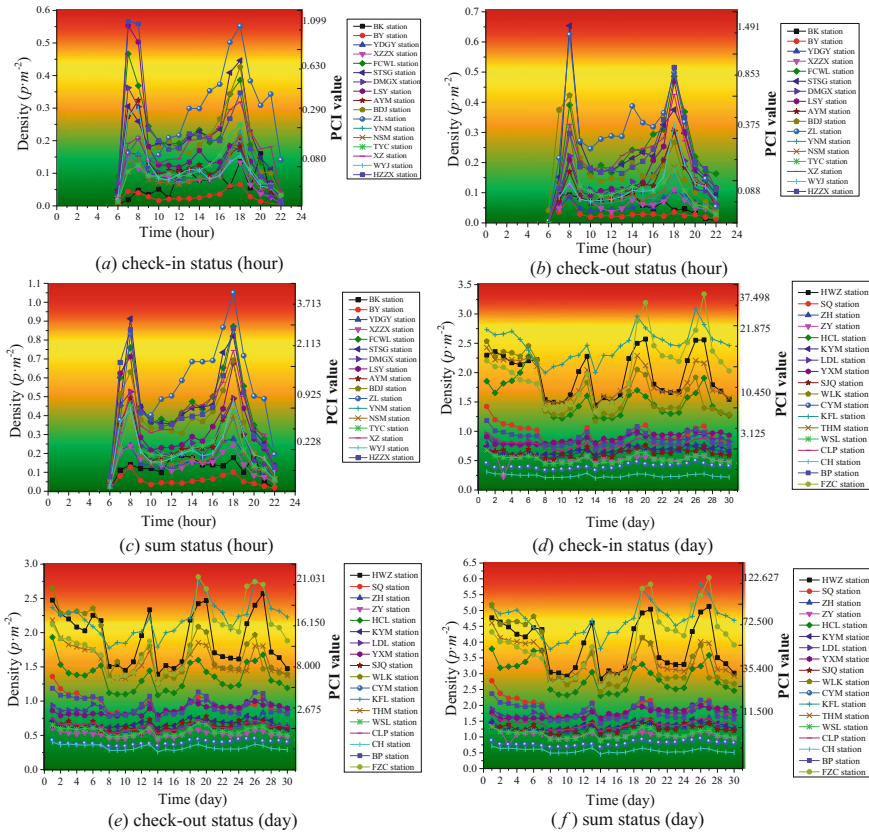
**Fig. 1** The PCI clustering results in Xi'an metro station

The threshold limit of PCI classification is computed by the cluster center depend on the collected data, the maximum value of the threshold for pedestrian crowding index has no upper limit. The results show that the proposed ACCA method is effective and fast to cluster the pedestrian crowding index with objective data. Meanwhile, rational clustering consequence is obtained by altering the evaporation rate and the numbers of ants. Our findings confirm that the improved ACCA is an effective and fast method to cluster pedestrian crowd classification in the MRT.

# References

1. Johansson A, Batty M, Hayashi K, Al Bar O, Marcozzi D, Memish ZA (2012) Crowd and environmental management during mass gatherings. Lancet Infect Dis 12(2):150–156
2. Vuchic VR (2007) Urban transit systems and technology. Wiley, New York
3. Garber N, Hoel L (2014) Traffic and highway engineering. Cengage Learning, Stamford
4. Cascetta E (2013) Transportation systems engineering: theory and methods. Springer Science & Business Media
5. Si B, Fu L, Liu J, Shiravi S, Gao Z (2016) A multi-class transit assignment model for estimating transit passenger flows-a case study of Beijing subway network. J Adv Transp 50(1):50–68
6. Khalid R, Baten M, Nawawi M, Mohd K, Ishak N (2016) Analyzing and optimizing pedestrian flow through a topological network based on M/G/C/C and network flow approaches. J Adv Transp 50(1):96–119
7. Xu X, Li K, Li X (2016) A multi-objective subway timetable optimization approach with minimum passenger time and energy consumption. J Adv Transp 50(1):69–95
8. CAM (2014) Annual report of china urban mass transit in 2014. China Association of Metros, Beijing, China
9. De Palma A, Kilani M, Proost S (2015) Discomfort in mass transit and its implication for scheduling and pricing. Transp Res Part B: Methodol 71(2):1–18

# Impact of Holiday-Free Policy on Traffic Volume of Freeway: An Investigation in Xi'an

**Jianyou Zhao, Jian Cui, Yunjiao Zhang and Tian Luo**

**Abstract**  For the purpose of investigating the influence, brought by the highway-free policy, on the highway traffic volume and traffic safety, traffic prediction of the future, and provide a theoretical basis for the traffic management departments to develop management strategies. The traffic volume from 2012 to 2016 in Xi'an city was forecasted with tolls based on the ARIMA model algorithm, the data of the National Day was selected. And the result of prediction was compared with the actual traffic volume from 2012 to 2016 without the tolls. The results indicated that with the policy implementing, the traffic volume has experienced a dramatic growth: the average annual daily traffic during the National Day from 2012 to 2016 was 386,442 veh., which increased to about 301% compared to with the condition without tolls. On the other hand, the policy also promoted the development of other industries and made distinct social and economic benefit. The above results show that during the holidays the number of cars soared, highlighting the problem of traffic congestion, traffic management departments should formulate corresponding policies to optimize, and play the timeliness of policy, ease traffic congestion, and provide a theoretical basis for promoting the sustainable development of the city.

**Keywords**  Holiday highway · Traffic volume · Toll free · Impact analysis

## 1  Introduction

From 1988 to 2016, after nearly 30 years of development, Chinese highway mileage has reached 130 thousand km, which is ranking the world's first highway mileage [1]. As early as 1984, the 54th executive meeting of the State Council of China put forward to the proposal that raised the funds of highway construction through the multi-channel, namely: Loan roads, charges owing on the loan [2]. Along with the use of highway toll policy throughout China, greatly broaden the investment and

J. Zhao · J. Cui (✉) · Y. Zhang · T. Luo
School of Automobile, Chang'an University, Xi'an ST 710064, Shanxi, China
e-mail: cuijian789145@163.com

financing channels, speed up the construction of high-grade highways, especially highways. In recent years, the government began to cancel the traffic tolls after repaying the loan in a lot of road sections.

In recent years, the majority of developed countries in the construction, management, and maintenance of highway funds, mainly through three channels and methods of rising: general tax, road user tax, and road tolls. Japan tests the policy from June 28, 2010 to the end of the March 2011 [3]. According to the Japanese Ministry of land, the data about some favorable results can be obtained, that the implementing of the policy promoted the development of local tourism industry, reduce the logistics hub of the transportation cost, transfer traffic volume, and the parallel highway public travel time was shortened. However, it also brings some problems.

In July 2012, highway toll-free policy during the holidays in China was performing, free implementation of the time including the Spring Festival, Labor Day, Tomb-sweeping Day, National Day, and other four national holidays. Free access vehicles included 7-seater cars or less than 7 seaters. The National Day in the year 2012 is the first holiday without the tolls according to estimates from the relevant departments, the number of national Day 7-day trip reached the high value: about 740 million with part of the road to supersaturation [4–6].

After reviewing the domestic and foreign research, the author found that Japan has done a lot of research on the impact of expressway toll-free policy [7–9]. Therefore, this paper hopes to do a thorough study on the holidays highway toll-free policy through the comparison of the traffic volume under different condition and policy, in order to analyze the influence of toll-free policy on traffic and transportation volume. Finally, providing the basis for the formulation of the traffic management measures to remiss the traffic congestion and promotes the sustainable development of the city.

## 2   ARIMA Prediction Model

The full name of the ARIMA model is an autoregressive integrated moving average model, abbreviated as ARIMA. The ARIMA $(p, d, q)$ is called the differential autoregressive moving average model, AR is autoregressive, $p$ is autoregressive moving average; MA is moving average, $q$ is the moving average number, $D$ time series is stable as the number of the differential. At the same time, the SA and MA models in ARIMA are used to predict seasonal periodic data.

The basic idea of ARIMA model is as follows: the data sequence formed by the prediction object over time is regarded as a random sequence. Once the model is identified, it can be used to predict the future value from the past and present values of the time series. If a random variable $Y_t$ is assumed to be an observation value in time $t$, the sequence of a group $Y_t$ is called a stochastic process, and the general standard ARIMA $(p, d, q)$ model can be denoted as $Y_t \sim$ ARIMA, which is defined as $\varphi_p(B)W_t = \theta_q(B)a_t$.

In the above formula, $\varphi_p(B) = 1 - \varphi_1 B - \cdots - \varphi_p B^p$, $W_t = (1 - B)^d Y_t$, and $\theta_q(B) = 1 - \theta_1 B - \theta_2 B^2 - \cdots - \theta_q B^q$, $a_t$ is white noise, that is, $a_t \sim N(0, \sigma_a^2)$;

$p, d, q$ is no negative integer; $B$ is the backward shift operator, that is, $BY_t = Y_{t-1}$; $\varphi_1, \varphi_2, \ldots \varphi_p$ is the self-regression parameters, $\theta_1, \theta_2, \ldots, \theta_p$ is the moving average parameters.

The ARIMA model can do the accurate prediction of seasonal index data, the difference between the linear regression model and the ARIMA model is the former cannot reveal the nonlinear characteristics revealed variable linear regression well, and the ARIMA model and the quarterly or monthly model can reveal the nonlinear characteristic of the explained variables; linear regression model directly using the method of least squares estimation of the regression model which is simple, the lag of containing explanatory variables, it is needed to identify the order of itself, and then use the least squares method; regression prediction models using linear time, explain the need to know the predicted variables, and using the ARIMA model does not exist the problem of forecasting.

## 3 Results and Analysis

### 3.1 Data Analysis from 2007 to 2011

The traffic volume of circular highway usually shows an uneven distribution due to the weather, holidays, new roads, or other factors. This paper studies that circular highway of Xi'an city as the study site, the 2007–2011 National Day traffic volume as shown in Fig. 1 and Table 2.

As shown in Table 1, in 2007, the traffic volume was 29,469; the average daily traffic volume in 2008 was 36,926, higher than the same period in 2007 of 7457 vehicles, increased to 25.3%; the average daily traffic volume in 2009 was 47,761, higher than the same period in 2008 10,835, rose to 29.3% in 2010; the average daily traffic volume of 54,668 vehicles, than in 2009, a year-on-year increase of 6907 vehicles, rose to 14.5%; the average daily traffic volume in 2011 was 67,041, higher than the same period in 2010 12,373, rose to 22.6%. Overall, these 5 years growth is steady.
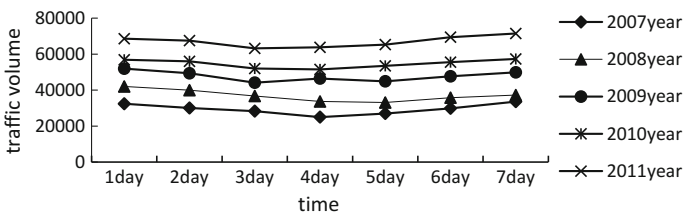


**Fig. 1** The traffic volume trends of the circular highway during the National day from 2007 to 2011

**Table 1** The daily traffic volume during the National Day from 2007 to 2011

| Year | Date | | | | | | |
|------|------|------|------|------|------|------|------|
| | 1 | 2 | 3 | 4 | 5 | 6 | 7 |
| 2007 | 32,409 | 30,065 | 28,324 | 25,005 | 27,009 | 29,874 | 33,592 |
| 2008 | 42,006 | 39,958 | 36,721 | 33,678 | 33,093 | 35,789 | 37,237 |
| 2009 | 51,927 | 49,356 | 44,146 | 46,448 | 44,901 | 47,673 | 49,876 |
| 2010 | 56,860 | 55,999 | 52,006 | 51,506 | 53,466 | 55,534 | 57,305 |
| 2011 | 68,566 | 67,524 | 63,198 | 63,783 | 65,308 | 69,443 | 71,465 |

## *3.2 2012–2016 Traffic Volume in Charges*

The policy was implemented from 2012, so the ARIMA model was established based on the data from 2007 to 2011. Input data into SPSS software. Because the original data is seasonal, seasonal factors should be considered in the modeling process. The results are shown in Fig. 2 (SPSS software screenshot), Table 3 for the specific traffic volume from 2012 to 2016.

Due to the influence factors, such as weather and return traffic highway holidays, the actual traffic volumes usually present the periodic characteristics. The prediction step is same as the modeling process of the ARIMA model, but just adds this condition considering seasonal factors in the process of modeling. This kind of time series model with seasonal circulation, called SARIMA model, can be denoted as $Y_t \sim$ SARIMA$(P, D, Q)$, it defines that $\Phi_P(B) = 1 - \Phi_1 B - \Phi_2 B^2 - \cdots - \Phi_P B^{PS}$, $W_t = (1 - B^S)^D Y_t$, $\Theta_Q(B) = 1 - \Theta_1 B - \Theta_2 B^2 - \cdots - \Theta_Q B^{QS}$, $P, D, Q$ is nonnegative integer, which is defined as "$S$".
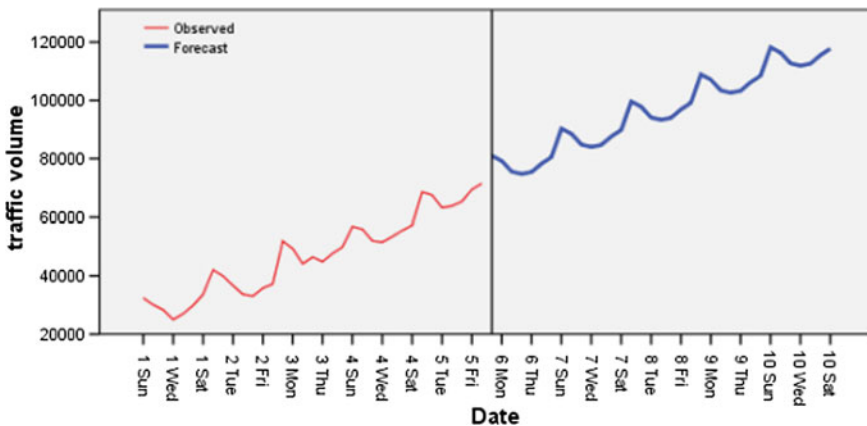


**Fig. 2** The traffic observation and prediction volume during the National Day

**Table 2** 2012–2016 traffic volume per year

| Year | Date | | | | | | |
|------|------|------|------|------|------|------|------|
|      | 1 | 2 | 3 | 4 | 5 | 6 | 7 |
| 2012 | 81,012 | 79,239 | 75,537 | 74,742 | 75,414 | 78,321 | 80,553 |
| 2013 | 90,301 | 88,528 | 84,826 | 84,031 | 84,703 | 87,610 | 89,842 |
| 2014 | 99,590 | 97,816 | 94,115 | 93,320 | 93,991 | 96,899 | 99,131 |
| 2015 | 108,878 | 107,105 | 103,404 | 102,609 | 103,280 | 106,187 | 108,420 |
| 2016 | 118,167 | 116,394 | 112,693 | 111,898 | 112,569 | 115,476 | 117,709 |

As can be seen from Fig. 2, continue to charge the case, the traffic volume showed a gradual growth trend, and the first 3 years of relatively stable. From Table 2 it can be calculated, in 2012 the average daily traffic volume is 77,831 vehicles, which is over 16.1% than 2011, 2013 average daily traffic volume is 87,120 vehicles showed an increase of more than 11.9% in 2012. In 2014 average daily traffic of 96,409 vehicles showed an increase of more than 10.7% in 2013. In 2015, average daily traffic of 105,698 vehicles showed an increase of more than 9.6% in 2014. In 2016, average daily traffic of 114,987 vehicles showed an increase of more than 8.1% in 2015.

## 3.3 Free Traffic from 2012 to 2016

Since the toll-free policy implementation in 2012, the national highway network traffic volume increased. Figure 3 is the circular highway traffic volume in Xi'an City during the National Day, Table 3 is traffic data.

As shown in Fig. 3, after the toll-free policy implementation, the daily traffic volume during the National Day varied between 420 thousand and 350 thousand. The overall trend is 1–4 day traffic volume gradually decreased, 5–7 day traffic volume gradually increased, 1 day and 7 day traffic volume, showing a more obvious, out of the peak. In 2012 average daily traffic of 369,144 vehicles, the average daily traffic
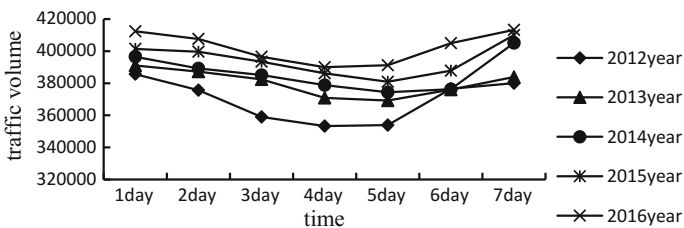


**Fig. 3** 2012–2016 National day free traffic

**Table 3**  2012–2016 free traffic volume

| Year | Date | | | | | | |
|------|---------|---------|---------|---------|---------|---------|---------|
|      | 1 | 2 | 3 | 4 | 5 | 6 | 7 |
| 2012 | 385,671 | 375,654 | 358,976 | 353,256 | 353,876 | 376,549 | 380,023 |
| 2013 | 391,056 | 387,234 | 382,389 | 370,829 | 369,209 | 375,988 | 383,890 |
| 2014 | 396,501 | 389,245 | 385,098 | 378,789 | 374,356 | 376,265 | 405,089 |
| 2015 | 401,423 | 399,671 | 393,454 | 386,209 | 380,912 | 387,820 | 410,012 |
| 2016 | 412,391 | 407,621 | 396,520 | 390,008 | 391,235 | 404,982 | 413,289 |

of 380085 in 2013, the average daily traffic of 386,478 vehicles in 2014, the average daily traffic of 394,214 vehicles in 2015, the average daily traffic of 402,292 in 2016.

## 3.4   Comparison of Toll and Free Traffic Volume

The traffic volumes from 2012 to 2016 with tolls were predicted by the ARIMA model, and the results were compared with the free case. In order to investigate the influence brought by the toll-free policy. Figure 4 is the comparison of toll and free traffic.

As shown in Fig. 4, the traffic volume of highway around Xi'an from 2012 to 2016 free case (without tolls) is far greater than the volume with tolls. Under the circumstances of the case of the daily traffic volume of 96,408 vehicles, the daily traffic free of charge for the case of 386442 vehicles, free of charge compared with the case of an increase of 301%. Small bus has become the main vehicle during the double traffic flow; traffic volume is mainly due to substantial growth during the holidays.
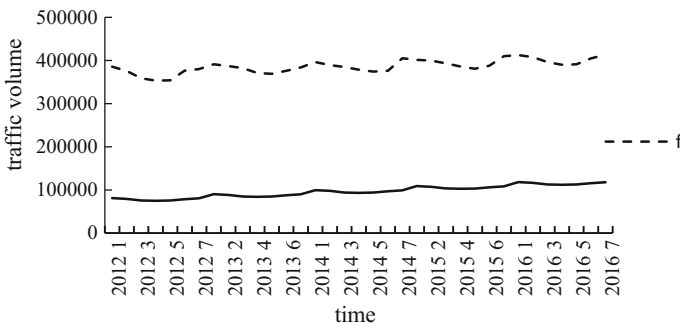


**Fig. 4**  Comparison of toll and free traffic volume

## 4   Discussion and Limitation

### *4.1   Discussion*

The holidays toll-free minibus policy has a wide-ranging effect. From the National Day in 2012, when the free policy was stated to implement, the results indicated that this toll-free policy has a positive influence on the residents travel, economic and social aspects and it can create obvious economic benefits. According to the National Bureau of Statistics data show that in 2016 the National Day golden week, the tourism market made an obvious demand, the country received a total of 593 million tourists, an increase of 12.8%, total tourism revenue of 482 billion 200 million Yuan, an increase of 4.4%.

The traffic volume during the National Day in 2012–2016 increased significantly compared with the condition with the tolls. The travel routes were influenced seriously, most of the minibusses chose the highways instead of the ordinary roads. In the toll-free policy implementation period, more than half the proportion of highway small passenger travel choice. This will further exacerbate the highway congestion degree, on the one hand, causing pressure to pass; on the other hand, it is bad for the optimization of highway network consolidation efficiency and resource allocation.

In addition, the policy also brings some challenges to the toll stations and service areas. It increased the outcome of maintenance and repair during the holidays, which caused the pressure to the companies. To a certain extent, the government owing on the loan and the operation of the toll road.

### *4.2   Limitation*

In the 2012–2016 toll traffic prediction process, this research only considered the effect of time factor on the Beltway highway traffic, without considering the impact of weather, new roads, traffic accident, and other factors, so the model has certain forecast errors, how to investigate the influence caused by the other factors is a problem that is worth studying. In this paper, the circular highway traffic volume of Xi'an city is selected to be the subjects, whether the results is suitable for other city is needed the further study. Due to the lack of the comparison of highway toll objective data, the influence of the implementation of toll-free policy on the highway business needs further analysis.

## 5 Conclusions

This research forecast the traffic volume during the National Day with tolls from 2012 to 2016, and compared the results with the traffic volume which is without tolls; the results can be seen as follows:

1. After the implementation of the policy, the traffic volume increased sharply. The average annual daily traffic during the National Day from 2012 to 2016 was 386,442 veh., which increased to about 301% compared with the condition without tolls.
2. This policy promotes the development of tourism, car rental, accommodation, catering services, and other related industries and creates an obvious economic benefit. According to the National Bureau of Statistics data, in 2016 the National Day Golden Week, the tourism market made the obvious demand.
3. The traffic volume of the ordinary roads decreased, which is bad for optimizing the road network finishing efficiency and resource allocation.

After analyzing the background of the toll-free policy, the contents of the policy and the main effects and the problems brought by the policy, some conclusions were put forward. During the holidays, the number of cars soared, highlighting the problem of traffic congestion, traffic management departments should formulate corresponding policies to optimize, and play the timeliness of policy, ease traffic congestion, provide a theoretical basis for promoting the sustainable development of the city.

## References

1. http://baike.haosou.com/doc/6642138-6855953.html
2. Xuebo D (2011) China thinking institute of highway operation and management of expressway branch on the highway toll problem of the 2011. In: Annual conference and the eighteenth national highway management work conference
3. Atchley P, Shi J, Yamamoto T (2014) Cultural foundations of safety culture: a comparison of traffic safety culture in China, Japan and the United States. Transp Res Part F: Traffic Psychol Behav 26:317–325
4. Ma J, Hu M, Shao J et al Investigation and analysis of the fee. Highway, Toll Free Minibus 2013 Special Holiday (2):150–153
5. Tang Y (2014) Major holidays toll free minibus policy studies. Tianjin Normal University
6. Li Z (2013) 15 major holidays toll free minibus policy implementation of. South China University of Technology
7. 高野,伸栄, 竹内,弓弦 (2011) An analysis of preference for route choice of truck operator in consideration of toll-free highway trial. 日本物流学会誌＝J Jpn Logistics Soc 41–48
8. 樗木,武 (2011) Traffic fluctuation and its interpretation based on one-month data of toll free expressway trials: 2nd report of the study on toll free express trials. Urban Policy Stud 11–24
9. Tsukai M, Inoue S, Kuwano M et al (2013) Statistical analysis on multivariate expressway time series traffic under the different toll policies. Asian Transport Stud 2:411–420

# Safety Risk Assessment Model of Heavy-Haul Transport

**Hua-Lan Wang and Shaochen Qin**

**Abstract** In order to evaluate the safety situation of heavy-haul transport accurately, the model to assess the risk grade of heavy-haul transport is established based on the theory of risk matrix and G1 method. First, the paper constructs the risk assessment index system, which consists of 28 risk factors involved four types of personnel, equipment, environment, and management. Second, the risk factors are sorted by Borda value method, and the key risk factors are found out according to the Borda sequence value, which can help managers to take targeted measures. Finally, the model is employed in the safety assessment of heavy-haul transport of Datong–Baotou railway. The results show that its safety risk grade is in secondary grade. The top three risk factors are the reliability of power system, the damage of water disaster and the rescue equipment. And the result is consistent with the actual. It shows that the risk matrix method is feasible for the safety risk assessment and the proposed model can assess the safety risk of heavy-haul transport objectively.

**Keywords** Heavy-haul transport · Safety risk assessment · Risk matrix · Borda sequence value

## 1 Introduction

Heavy-haul transport can effectively improve the railway transport capacity. It is the focus of the development of China's railway transport industry. But with the increase of traction load and axle-weight,the higher requirements for the organization of train operation, the function of train brake and the quality of fixed equipment on the ground have been put forward. Compared with the general transport, the various risks and insecurities of heavy-haul transport are more prominent, so it is significant to assess the heavy-haul transport safety situation, find out the high-risk factors and control them in advance.

H.-L. Wang (✉) · S. Qin
School of Traffic and Transportation, Lanzhou Jiaotong University, Lanzhou 730070, China
e-mail: wanghualan126@126.com

The safety risk assessment theory has been introduced into the railway transportation in recent years, it has been used for assessment of the security risk of information systems [1], railway tunnels [2, 3], railway natural disasters [4, 5], subgrades with poor geological conditions [6, 7], and train control systems [8]. The research about the heavy-haul transport safety mainly focuses on the safety analysis of single factor, such as the line equipment [9, 10], locomotive and vehicle coupler, and the wheel-rail [11, 12]. Actually, there are many factors influencing the safety of heavy-haul transport, and the influence degree of each factor is different. Only by carrying out the safety risk analysis and comprehensive evaluation under the influence of multiple factors we can accurately grasp the safety situation of heavy transport and find out the key risk factors to provide a theoretical basis for the relevant departments to formulate economic and reasonable risk aversion measures. This paper uses the risk matrix theory to establish the safety risk assessment model of heavy-load transport, and assess the safety risk grade of heavy-haul transport. The safe risk factors are sorted by Borda value method, and the key risk factors are located according to their Borda sequence value. Finally, the example is presented to illustrate the practicality and validity of the proposed method.

The rest of the paper is organized as follows: Sect. 2 analyzes factors affected the safety of heavy-haul transport, lists the indexes of safety risk assessment. In Sect. 3, the risk assessment model of heavy-haul transport is set up, and in Sect. 4, Borda number of the risk factor is calculated, the risk factors are sorted by Borda value method. Section 5 provides the example of assessment for the heavy-haul transport of Datong–Baotou railway. Section 6 summarizes the achieved results and outlines topics for further research.

## 2 Indexes of Safety Risk Assessment

Analyzing the actual situation of safety production and management of railway heavy-haul transport, following the principles of purposiveness, comprehensiveness, operability, and independence as well as combining quantitative and qualitative analysis, referring to the relevant specification [13–15] and research achievements [16–18], the index system of safety risk assessment of heavy-haul transport is established, which is shown in Table 1.

## 3 Risk Matrix of Heavy-Haul Transport

### 3.1 Risk Matrix Design

The risk matrix method is the risk assessment method proposed by the US Air Force Electronic Systems Center (ESC) in 1995. It is an important risk assessment method

**Table 1** Indexes of safety risk assessment of heavy-haul transport

| Risk type | Risk factor | Index description |
|---|---|---|
| Personnel risk | Professional level $u_1$ | The average score of professional test |
| | Safety awareness $u_2$ | The average score of safety knowledge test |
| | Post training $u_3$ | Staff training frequency (person/per year) |
| Equipment risk | Rail $u_4$ | Weight of rail (kg/m) |
| | Subgrade bed $u_5$ | Score based on the stability of subgrade bed and the capacity of subgrade bearing |
| | Curve radius of lines $u_6$ | proportion (%) of over the curves limit which radius is less than 800 m |
| | Longitudinal slope $u_7$ | proportion (%) of over the longitudinal slope limit (heavy-load train direction) |
| | Reserve coefficient of bridges' live load $u_8$ | Reserve coefficient of standard live load |
| | Persistent adhesion coefficient of locomotive $u_9$ | Adhesion coefficient in dry condition |
| | Traction control performance of locomotive $u_{10}$ | Score based on the performance of locomotive adhesion control, advancement of control system, wireless control synchronization performance of coupling locomotives |
| | Performance of coupler and draft gear systems $u_{11}$ | Score based on the center position control performance of couplers and draft gear performance |
| | Tensile strength of coupler $u_{12}$ | (KN) |
| | Axle load of vehicles $u_{13}$ | (t) |
| | Emergency braking distance of trains $u_{14}$ | Emergency braking distance (m) when the initial speed is 90 km/h |
| | Braking performance of trains $u_{15}$ | Both of LOCOTROL and ECP technology adopted, scored 2. LOCOTROL or ECP, scored 1. Else, scored 0 |
| | Running speed of trains $u_{16}$ | (km/h) |
| | Performance of safety monitoring system $u_{17}$ | If the system is vehicle condition monitoring system on the rail side, scored 60. If microcomputer control system then 70. Vehicle signal system, then 80, and vehicle wireless intelligent monitoring system, then 90 |
| | Performance of speed control equipment in marshaling stations $u_{18}$ | Score based on the automation level of speed regulation system |
| | Performance of accident rescue equipment $u_{19}$ | Score based on the standardization level of rescue equipment |

(continued)

**Table 1** (continued)

| Risk type | Risk factor | Index description |
|---|---|---|
| Environment risk | Reliability of power system $u_{20}$ | Score based on mean time between failures |
| | Risk degree of water disaster $u_{21}$ | Determine the value based on the water disaster severity in recent 5 years |
| | Number of debris flow along the railway $u_{22}$ | Mean annual number of debris flows in recent 5 years |
| | Slope stability $u_{23}$ | Evaluate based on the slope form, the geological environment, and slope protection measures |
| | Maximum wind velocity acted on train side $u_{24}$ | Maximum instantaneous speed in 3 s (m/s) |
| Management risk | Advancement of train control systems $u_{25}$ | Evaluate based on data transmission, train tracking, train diagram, operation safety monitoring, and station interlocking mode |
| | Scientificity of rules and regulations $u_{26}$ | Evaluate based on the rationality, systematicness, clearness, and practicability of rules and regulations |
| | Rationality of operation scheme $u_{27}$ | Evaluate based on the train operation mode, the match plan of train weight and density |
| | Completeness of contingency plan $u_{28}$ | Score based on the emergency monitoring, early warning, emergency-response, and after rehabilitative measures |

[19]. For each risk factor of the project, it determined the risk grade by the occurrence probability and the loss of risk factors. Risk matrix design is the core of risk matrix method.

According to the characteristics of heavy-haul transport, the 28 risk factors involved are shown in Table 1, which is denoted by the risk factors set $U = \{u_1, u_2, \ldots, u_{28}\}$. The probability of risk is the probability of occurrence of a risk event, the author defines the risk probability set as $P = \{p_1, \ldots, p_i, \ldots, p_n\}, i = 1, \ldots, n$. The risk loss is the degree of impact on the safety goals after the risk event, and the risk loss set is expressed by $L = \{l_1, \ldots, l_j, \ldots, l_n\}, j = 1, \ldots, m$. The risk matrix $R$ is the function of P and L, which can be described by the function:

$$R = f(P, L) = [R_{ij}], \text{ when } \begin{cases} p_{i1} \leq p \leq p_{i2} \\ l_{j1} \leq l \leq l_{j2} \end{cases}$$

where $R_{ij}$ is the risk grade when the risk probability grade is $i$ and the risk loss grade is $j$. $p_{i1}$ and $l_{j1}$ are the lower limits of risk probability grade $i$ and risk loss grade $j$, respectively, $p_{i2}$ and $l_{j2}$ are the upper limit of risk probability grade $i$ and risk loss grade $j$.

**Table 2** Risk loss grade

| Loss grade | | Boundary value of each loss grade | Description |
|---|---|---|---|
| $l_1$ | Negligible | $l_{11} = 0, l_{12} = 3$ | Once the risk event occurs, it will hardly cause any accident |
| $l_2$ | Small | $l_{21} = 4, l_{22} = 10$ | Once the risk event occurs, it will cause ordinary accidents |
| $l_3$ | Ordinary | $l_{31} = 11, l_{32} = 30$ | Once the risk event occurs, it will cause considerable accidents |
| $l_4$ | Serious | $l_{41} = 31, l_{42} = 60$ | Once the risk event occurs, it will cause serious accidents |
| $l_5$ | Extremely serious | $l_{51} = 61, l_{52} = 100$ | Once the risk event occurs, it will cause extremely serious accidents |

## 3.2 Risk Loss and Risk Probability

The risk loss measures the impact of the risk event on the safety goal of heavy-haul transport. The safety goal of heavy-haul transport is not to cause any rail accident in the process of transport. According to the severity of the loss, railway accidents are classified extremely serious accidents, serious accidents, considerable accidents and ordinary accidents four grades [20]. In accordance with the situation of the railway accident after the occurrence of the risk event, The risk loss is divided into five levels, which are extremely serious, serious, ordinary, small and negligible and denoted by $l_5, l_4, l_5, l_2, l_1$ (at Table 2) respectively, then $L = \{l_1, l_2, l_3, l_4, l_5\}$ expresses the set of risk loss. The classification of railway accidents is based on casualties, economic loss or time loss. The degree of three aspects loss as a basis for dividing quantitative boundary value of the risk loss grade. The risk loss quantitative value takes integer between 0 and 100, the maximum of $l_5$ is 100 and the minimum of $l_1$ is 0.

According to Delphi method, 11 experts are invited to estimate the risk loss grade of each factor based on their experience. The results are shown in Table 3.

By convention, the probability of risk is divided into five grades which are expressed by $P = (p_1, p_2, p_3, p_4, p_5)$, and the risk probability grade and boundary values are shown in Table 4.

Through survey statistics, combined with expert analysis method, it can get the single index risk probability which is shown in Table 5.

## 3.3 Risk Grade

Input the value of $(P, L)$ into the risk matrix function $R = f(P, L) = P \times L$ to get a set of interval values that characterize the risk grades: $\left[ \min(p_i, l_j), \max(p_i \times l_j) \right]$.

**Table 3** Risk loss grade of each factor

| Factors | $l_1$ | $l_2$ | $l_3$ | $l_4$ | $l_5$ |
|---|---|---|---|---|---|
| $u_1$ | | | ✓ | | |
| $u_2$ | | | | | ✓ |
| $u_3$ | | | ✓ | | |
| $u_4$ | | | | ✓ | |
| $u_5$ | | | | ✓ | |
| $u_6$ | | ✓ | | | |
| $u_7$ | | | | ✓ | |
| $u_8$ | | | | ✓ | |
| $u_9$ | | | | | ✓ |
| $u_{10}$ | | | | | ✓ |
| $u_{11}$ | | | ✓ | | |
| $u_{12}$ | | | | ✓ | |
| $u_{13}$ | | | | ✓ | |
| $u_{14}$ | | | | ✓ | |
| $u_{15}$ | | | | | ✓ |
| $u_{16}$ | | | | ✓ | |
| $u_{17}$ | | | | ✓ | |
| $u_{18}$ | | | | ✓ | |
| $u_{19}$ | | | | ✓ | |
| $u_{20}$ | | | | | ✓ |
| $u_{21}$ | | | | ✓ | |
| $u_{22}$ | | | | ✓ | |
| $u_{23}$ | | | ✓ | | |
| $u_{24}$ | | ✓ | | | |
| $u_{25}$ | | | | ✓ | |
| $u_{26}$ | | | ✓ | | |
| $u_{27}$ | | ✓ | | | |
| $u_{28}$ | | | | ✓ | |

**Table 4** Risk probability grade

| Risk probability grade | Boundary value | Description |
|---|---|---|
| $p_1$ | $p_{11} = 0, p_{12} = 0.10$ | The possibility of events is very little, almost impossible |
| $p_2$ | $p_{21} = 0.11, p_{22} = 0.40$ | The probability is less likely, occasional |
| $p_3$ | $p_{31} = 041, p_{32} = 0.60$ | The possibility is likely, occur sometimes |
| $p_4$ | $p_{41} = 0.61, p_{42} = 0.90$ | The possibility is more likely, occur often |
| $p_5$ | $p_{51} = 0.91, p_{52} = 1$ | The possibility is great, occur frequently |

*Note* The risk probability keeps two decimal places

**Table 5** Risk probability grade of each factor

| Factors | $p_1$ | $p_2$ | $p_3$ | $p_4$ | $p_5$ |
|---|---|---|---|---|---|
| $u_1$ | [100, 80] | (80, 70] | (70, 60] | (60, 40] | (40, −∞) |
| $u_2$ | [100, 90] | (90, 80] | (80, 70] | (70, 60] | (60, −∞) |
| $u_3$ | (+∞, 6) | [6, 4) | [4, 2) | [2, 1] | 0 |
| $u_4$ | (+∞, 75] | (75, 60] | (60, 50] | (50, 40] | (40, −∞) |
| $u_5$ | [100, 90] | (90, 80] | (80, 70] | (70, 60] | (60, −∞) |
| $u_6$ | (−∞, 5) | [5, 10) | [10, 20) | [20, 40) | [40, +∞) |
| $u_7$ | (−∞, 2) | [2, 4) | [4, 6) | [6, 8) | [8, +∞) |
| $u_8$ | (+∞, 1.4] | (1.4, 1.2) | (1.2, 1.05] | (1.05, 1.0] | (1.0, −∞) |
| $u_9$ | (+∞, 0.3] | (0.3, 0.2) | (0.2, 0.15) | (0.15, 0.1] | (0.1, −∞) |
| $u_{10}$ | [100, 90] | (90, 80] | (80, 70] | (70, 60] | (60, −∞) |
| $u_{11}$ | [100, 90] | (90, 80] | (80, 70] | (70, 60] | (60, −∞) |
| $u_{12}$ | (+∞, 3500] | [3500, 3000) | [3000, 2500) | [2500, 2000] | (2000, −∞) |
| $u_{13}$ | [35, 30] | (30, 25] | (25, 20] | (35, +∞) | (20, −∞) |
| $u_{14}$ | (−∞, 600) | [600, 800) | (800, 1200) | (1200, 1400] | (1400, +∞) |
| $u_{15}$ | \ | 2 | 1 | 0 | \ |
| $u_{16}$ | (−∞, 80) | [80, 90) | [90, 120) | (120, 140) | [140, +∞) |
| $u_{17}$ | [100, 95] | (95, 80] | (80, 70] | (70, 60] | (60, −∞) |
| $u_{18}$ | [100, 90] | (90, 80] | (80, 70] | (70, 60] | (60, −∞) |
| $u_{19}$ | [100, 90] | (95, 80] | (80, 70] | (70, 60] | (60, −∞) |
| $u_{20}$ | [100, 90] | (90, 80] | (80, 70] | (70, 60] | (60 −∞) |
| $u_{21}$ | [0, 0.1] | (0.1, 0.4] | (0.4, 0.6] | (0.6, 0.8] | (0.8, 1] |
| $u_{22}$ | 0 | 1 | [2, 3] | [4, 5] | (5, +∞) |
| $u_{23}$ | [100, 95] | (95, 80] | (80, 70] | (70, 60] | (60, −∞) |
| $u_{24}$ | (−∞, 15) | [15, 20) | [20, 25) | [30, 35) | [35, +∞) |
| $u_{25}$ | [100, 95] | (95, 80] | (80, 70] | (70, 60] | (60, −∞) |
| $u_{26}$ | [100, 95] | (95, 80] | (80, 70] | (70, 60] | (60, −∞) |
| $u_{27}$ | [100, 90] | (90, 80] | (80, 65] | (65, 60] | (60, −∞) |
| $u_{28}$ | [100, 95] | (95, 80] | (80, 70] | (70, 60] | (60, −∞) |

The evaluation index of the risk grade is expressed by $\eta_i = \max(p_i \times l_j)$, which is shown in Table 6.

The risk grade of a factor can be judged by the value of $\eta_i$.

(1) If $0.3 \le \eta_i \le 10$, the risk grade is $r_1$, which means the risk of heavy-haul transport is acceptable.

(2) If $10 \le \eta_i \le 40$, the risk grade is $r_2$, which means the risk is in a critical state. There is no great risk, no casualties or property damage for the present, but it should be monitored and excluded when the serious trend appears.

**Table 6** Evaluation index of risk grade

|       | $l_1$ | $l_2$ | $l_3$ | $l_4$ | $l_5$ |
|-------|-------|-------|-------|-------|-------|
| $p_1$ | 0.3   | 1     | 3     | 6     | 10    |
| $p_2$ | 1.2   | 4     | 12    | 24    | 40    |
| $p_3$ | 1.8   | 6     | 18    | 36    | 60    |
| $p_4$ | 2.7   | 9     | 27    | 54    | 90    |
| $p_5$ | 3     | 10    | 30    | 60    | 100   |

**Table 7** Risk grade

|       | $l_1$ | $l_2$ | $l_3$ | $l_4$ | $l_5$ |
|-------|-------|-------|-------|-------|-------|
| $p_1$ | $r_1$ | $r_1$ | $r_1$ | $r_1$ | $r_2$ |
| $p_2$ | $r_1$ | $r_1$ | $r_1$ | $r_2$ | $r_2$ |
| $p_3$ | $r_1$ | $r_1$ | $r_2$ | $r_2$ | $r_3$ |
| $p_4$ | $r_1$ | $r_1$ | $r_2$ | $r_3$ | $r_4$ |
| $p_5$ | $r_1$ | $r_2$ | $r_2$ | $r_3$ | $r_4$ |

(3) If $40 \leq \eta_i \leq 60$, the risk grade is $r_3$, it means a higher risk that indicates there are the possibilities of casualties or property damage, which is not expected to exist. And it must take measures.

(4) If $\eta_i \geq 60$, the risk grade is $r_4$, which indicates that the risk is especially high. It cannot be accepted and must be immediately excluded.

For quantitative analysis and calculation, the risk grade $r_1, r_2, r_3, r_4$ is expressed as quantization values 1, 2, 3, and 4, respectively. According to the risk grade evaluation index, the risk grade is divided as shown in Table 7.

## 4  Borda Sequence Value of Risk Factors

With the above risk assessment matrix, it can judge the risk grade of each risk factor in heavy-haul transportation. However, due to there are a number of heavy-haul transport risk factors and often many risk knots gathering at the same risk grade, it is difficult to judge the key factors. In this paper, the Borda value method is used to sort the risk factors according to their importance to screen out the most important risk factors. And the key risk factors can be found out based on the Borda sequence value.

The Borda number of the risk factor is calculated as follows [21]:

$$b_i = \sum_{k=1}^{2} (N - R_{ik})$$

**Table 8** Comprehensive weights of factors

| $u_1$ | $u_2$ | $u_3$ | $u_4$ | $u_5$ | $u_6$ | $u_7$ | $u_8$ | $u_9$ | $u_{10}$ | $u_{11}$ | $u_{12}$ | $u_{13}$ | $u_{14}$ |
|---|---|---|---|---|---|---|---|---|---|---|---|---|---|
| 0.0151 | 0.1758 | 0.0043 | 0.0087 | 0.0087 | 0.0017 | 0.0095 | 0.0219 | 0.1005 | 0.1548 | 0.0024 | 0.0166 | 0.0199 | 0.0314 |
| $u_{15}$ | $u_{16}$ | $u_{17}$ | $u_{18}$ | $u_{19}$ | $u_{20}$ | $u_{21}$ | $u_{22}$ | $u_{23}$ | $u_{24}$ | $u_{25}$ | $u_{26}$ | $u_{27}$ | $u_{28}$ |
| 0.1406 | 0.0285 | 0.0439 | 0.0126 | 0.0114 | 0.0914 | 0.0079 | 0.0079 | 0.0031 | 0.0011 | 0.0571 | 0.0056 | 0.0014 | 0.0166 |

where $N$ is the total number of risk factors; $K$ is the criterion including risk loss and risk probability. $R_{ik}$ is the number of risk factors that are a greater influence than the risk impact or risk probability of risk factor $i$.

$b_i$ is arranged in ascending order, the number of elements in the sequence after $b_i$ is the Borda sequence value which means the number of risk factors that are more crucial than risk $i$ in the same risk knot.

## 5 Determination of the Comprehensive Risk Grade

The key factors affecting the safety of heavy-haul transport can be determined by risk matrix method and Borda sequence value. But the judgment on the comprehensive risk grade of heavy-haul transport should be evaluated on the basis of the risk matrix assessment result and the weight of each risk factor. The paper adopts G1 method to determine the weights of risk factors. G1 method is simple and has no limitation on the number of factors, and it possesses isotonicity, which is suitable to determine index weights of comprehensive assessment problem with multi-factor and multi-index [22]. According to G1 method, 11 experts are invited to give the factors' weights, the comprehensive weight of each risk factor is obtained by weighted average method (see Table 8).

The comprehensive risk grade of heavy-haul transport is described as:

$$\mathrm{RRT} = \sum_{i=1}^{n} \mathrm{RR}_i \times \mathrm{RW}_i$$

where n is the total number of risk factors; $RR_i$ is the risk grade of the risk factor $i$; and $RW_i$ is the weight of the risk factor $i$. $RR_i$ and $RW_i$ are the risk grade and the weight of the risk factor $i$ respectively.

## 6 Case Study

In this section, the proposed methodology is applied to evaluate the safety risk of heavy-haul transport in Datong–Baotou railway, its risk index values are shown in Table 9.

**Table 9** Index values of Datong–Baotou railway

| $u_1$ | $u_2$ | $u_3$ | $u_4$ | $u_5$ | $u_6$ | $u_7$ | $u_8$ | $u_9$ | $u_{10}$ | $u_{11}$ | $u_{12}$ | $u_{13}$ | $u_{14}$ |
|---|---|---|---|---|---|---|---|---|---|---|---|---|---|
| 82 | 87 | 4 | 60 | 80 | 33.48 | 4 | 1.12 | 0.24 | 80 | 90 | 3430 | 25 | 800 |
| $u_{15}$ | $u_{16}$ | $u_{17}$ | $u_{18}$ | $u_{19}$ | $u_{20}$ | $u_{21}$ | $u_{22}$ | $u_{23}$ | $u_{24}$ | $u_{25}$ | $u_{26}$ | $u_{27}$ | $u_{28}$ |
| 2 | 80 | 82 | 85 | 78 | 70 | 0.55 | 0 | 75 | 19 | 80 | 85 | 80 | 78 |

*Note* Quantitative measurable indexes valued based on the actual data of Datong–Baotou railway, qualitative indexes determined by exporter evaluation

Table 10 shows the risk matrix and Borda sequence value of Datong–Baotou railway.

It can be seen from Table 10 that there are risk knots in Borda sequence values of risk factors, namely, the Borda sequence values of several risk factors are the same. For example, there are 3 risk factors which Borda sequence values are 1, and there are 5 risk factors with Borda sequence value 9. For the risk factors of the same Borda sequence values, the paper uses interpolation method to subdivide the probability grade of the original indexes. And by adjusting the Borda sequence value after the subdivided probability grade, it can basically eliminate the risk knot in the Borda order value. For the few risk factors with same probability grade, it can determine their importance order by consulting expert opinion. The adjusted Borda sequence values are shown in Table 10.

The comprehensive risk grade value of the heavy-haul transport of Datong–Baotou railway is $RRT = 0.0296r_1 + 0.8794r_2 + 0.0914r_3 = 2.0626$, which is slightly more than the second-grade risk value. It indicates that the heavy-haul transport system of Datong–Baotou railway is in a critical state of risk, which is no large risk, casualties or property damage in the short run. But it is best to take measures to reduce the risk grade to less than grade 2 monitor the risk state at the same time. And it must be excluded as soon as possible when there is a serious trend of risk.

Reason analysis: There are 6 risk factors at the first risk grade, 21 at the secondary risk grade, 1 at the third risk grade in 28 risk factors involved in the Datong–Baotou railway of the heavy-haul transport. Although most factors are on secondary risk grade, the reliability of the power system is a risk factor of high weight and have a lower point that is 70 which is at the third risk grade, so the risk grade of the heavy-haul transport system of Datong–Baotou railway is slightly higher than the secondary grade.

Solutions: according to the Borda sequence value of risk factors of Datong–Baotou railway heavy-haul transport, the top three risk factors are the reliability of the power system, the water disaster risk, and the rescue equipment. It shows that the security risk mainly exists in these three aspects. The author proposed: the reliability of the power system can be improved through rebuilding aging lines and equipment, enhancing the ability of bearing high load and reducing fault time. Meanwhile, water disaster risk can be reduced by strengthening the maintenance of the subgrade and side slope. The risk of accident rescue can be decreased by purchasing the rollover equipment which meet the rescue demand of the heavy-haul transport.

**Table 10**  Risk matrix and Borda sequence value of Datong–Baotou railway

| Factors | $p$ | $l$ | $R_i$ | $b_i$ | Borda sequence value | Adjusted Borda value |
|---|---|---|---|---|---|---|
| $u_1$ | $p_1$ | $l_4$ | $r_1$ | 26 | 21 | 22 |
| $u_2$ | $p_2$ | $l_5$ | $r_2$ | 48 | 4 | 5 |
| $u_3$ | $p_3$ | $l_3$ | $r_2$ | 34 | 15 | 15 |
| $u_4$ | $p_2$ | $l_4$ | $r_2$ | 23 | 25 | 26 |
| $u_5$ | $p_2$ | $l_4$ | $r_2$ | 23 | 25 | 25 |
| $u_6$ | $p_4$ | $l_2$ | $r_1$ | 31 | 17 | 17 |
| $u_7$ | $p_3$ | $l_4$ | $r_2$ | 30 | 18 | 19 |
| $u_8$ | $p_3$ | $l_4$ | $r_2$ | 30 | 18 | 18 |
| $u_9$ | $p_2$ | $l_5$ | $r_2$ | 48 | 4 | 6 |
| $u_{10}$ | $p_2$ | $l_5$ | $r_2$ | 48 | 4 | 7 |
| $u_{11}$ | $p_1$ | $l_3$ | $r_1$ | 10 | 27 | 27 |
| $u_{12}$ | $p_2$ | $l_4$ | $r_2$ | 43 | 9 | 13 |
| $u_{13}$ | $p_2$ | $l_4$ | $r_2$ | 43 | 9 | 10 |
| $u_{14}$ | $p_2$ | $l_4$ | $r_2$ | 43 | 9 | 9 |
| $u_{15}$ | $p_2$ | $l_5$ | $r_2$ | 49 | 4 | 4 |
| $u_{16}$ | $p_2$ | $l_4$ | $r_2$ | 43 | 9 | 14 |
| $u_{17}$ | $p_2$ | $l_4$ | $r_2$ | 43 | 9 | 11 |
| $u_{18}$ | $p_2$ | $l_4$ | $r_2$ | 43 | 4 | 12 |
| $u_{19}$ | $p_3$ | $l_4$ | $r_2$ | 50 | 1 | 2 |
| $u_{20}$ | $p_3$ | $l_5$ | $r_3$ | 55 | 0 | 0 |
| $u_{21}$ | $p_3$ | $l_4$ | $r_2$ | 50 | 1 | 1 |
| $u_{22}$ | $p_1$ | $l_4$ | $r_1$ | 26 | 21 | 21 |
| $u_{23}$ | $p_2$ | $l_3$ | $r_2$ | 33 | 16 | 16 |
| $u_{24}$ | $p_2$ | $l_4$ | $r_1$ | 23 | 23 | 24 |
| $u_{25}$ | $p_2$ | $l_4$ | $r_2$ | 43 | 8 | 8 |
| $u_{26}$ | $p_2$ | $l_3$ | $r_2$ | 27 | 20 | 20 |
| $u_{27}$ | $p_2$ | $l_2$ | $r_1$ | 23 | 23 | 23 |
| $u_{28}$ | $p_3$ | $l_4$ | $r_2$ | 50 | 1 | 3 |

## 7  Conclusions and Future Research

This paper established the risk grade assessment model and constructed a safety risk assessment index system with 28 heavy risk factors for heavy-haul transport. In the model solutions, using Delphi method to determine the risk probability and the risk loss grade, taking the G1 method to determine the weight of risk factors, and key risk factors can be identified based on the revised Borda sequence value. Finally, the

real case shows that the safety risk grade of heavy-haul transport can be assessed accurately by proposed model and the key risk factors can be found out. It provides the help for the corresponding managers to locate the major risks in heavy-haul transport and adopt cost-effective and feasible measures.

Future research should be dedicated to further improve the quantization method for qualitative indexes, and explore more objective methods to determine the risk loss grade and risk probability of heavy-haul transport.

# References

1. Li H-T, Liu Y, He D-Q (2007) A security risk assessment model for IT system and its application on railway passenger ticket system. China Railway Sci 28(1):127–130
2. Xin S (2012) Research on the methods of rail tunnel risk assessment index. J Railway Eng Soc 168(9):71–74
3. Xu Z-R (2011) Discussion and analysis of underground water risk assessment for railway tunnel. J Railway Eng Soc 153(6):39–43
4. Ma S-H, Ma Y-J, Cheng X-D et al (2011) Determining method and risk assessment of strong wind region along high-speed railway in China. J Railway Eng Soc 150(3):37–45
5. Shen X-M, Liu P-L, Wang J-F (2012) Assessment of water-inrush risks of karst tunnel with analytic hierarchy process. China Railway Sci 147(12):56–63
6. Li H (2011) Risk factor analysis and risk evaluation on railroad bed in landslide district in southwestern mountainous area, Southwest Jiaotong University
7. Wei Y-X, Luo Y-N, Liao S et al (2012) Risk assessment and management of railway subgrade in soft soil area. J Railway Eng Soc 171(12):63–68
8. Zhang Y-D (2013) Study on the safety risk identification and analysis of train control system of high-speed railway, Southwest Jiaotong University
9. González-Nicieza C, Álvarez-Fernández MI, Menéndez-Díaz A, Álvarez-Vigil AE, Ariznavarreta-Fernández F (2008) Failure analysis of concrete sleepers in heavy haul railway tracks. Eng Fail Anal 15(1–2):90–117
10. Esmaeili M, Yousefi Mojir P (2011) Substructure nonlinear effects on sleeper design pressure in heavy haul railway tracks. J Transp Eng 137(9):656–664
11. Wang K-Y, Zhai W-M, Feng Q-B et al (2009) Effect of the coupler free angle on wheel/rail dynamic safety performance of heavy haul locomotive. China Railway Sci 30(6):72–76
12. Xiong J-Y, Deng Y-Q, Cao Y-B et al (2014) Wheel-rai1 wear on heavy haul lines and its influences on running stability of trains. J Southwest Jiaotong University 49(2):302–309
13. PRC Ministry of Railways (2012) Book of railway laws and regulations. Railway Press, Beijing
14. PRC Ministry of Railways (2005) Design specification of railway bridge and culvert. Railway Press, Beijing
15. PRC Ministry of Railways (2008) Management rules of railway technology. Railway Press, Beijing
16. Li W (2008) Analysis & study on transportation safety problems of da-qin heavy-haul railway, Beijing Jiaotong University
17. Yang Y-D, Hu S-J (2004) Study on safety ensuring system for da-qin heavy haul railway. China Saf Sci J 14(9):46–51
18. Zhu Y-B, Wei Q-C (2005) Safety analysis on heavy-loaded train transportation. China Saf Sci J 15(3):6–9

19. Ruan X, Yin Z-Y, Chen A-R (2013) A review on risk matrix method and its engineering application. J Tongji Univ (Nature Science) 41(3):381–385
20. PRC Ministry of Railways (2007) Investigation and handling rules of railway accidents. Railway press, Beijing
21. Li S-Q, Yan Z, Yu D (2010) Application of risk matrix in classification of dangerous and hazardous factors. China Saf Sci J 20(4):83–87
22. Guo Y-J (2002) Theories and methods of comprehensive assessment. J Sci Press, Beijing

# An Optimal Transmission Reliability Enhancement Mechanism for Cooperative Driving System

**Hongzhuan Zhao, Tianlong Gu and Wenyong Li**

**Abstract** Advances in V2X technologies have enabled vehicles to communicate with each other for sharing emergency warning message (EWM) and providing drivers with potential collision warnings in the vicinity of the intersection. In the vicinity of the intersection, vehicular ad hoc networks (VANET) are a long-term solution contributing significantly toward vehicle cyber-physical systems (VCPS) in providing access to cooperative driving system. Thus, the cooperative driving system is a typical VCPS. However, EWM has transmission delay, error, and redundancy due to the inherent characteristics of VANET. For minimizing the transmission delay, and decreasing error and redundancy of EWM, and then achieving reliable EWM in the vicinity of the intersection, we propose an optimal transmission reliability enhancement mechanism (OTREM) for the cooperative driving system. In detail, through analyzing the inherent characteristics of transmission delay, error, and redundancy of EWM, we design transmission delay and error optimal schemes according to the traffic information transmission method and principle, and construct the vehicle roles change strategy using the modified finite automata to propagate EWM to the right roles of the endangered vehicles for decreasing redundancy of EWM.

**Keywords** Vehicular cyber-physical systems (VCPS) · Vehicular ad hoc network (VANET) · Optimal transmission reliability enhancement mechanism (OTREM) Finite automata

H. Zhao (✉) · W. Li
School of Architecture and Transportation Engineering, Guilin University of Electronic Technology, Guilin 541004, China
e-mail: zhz19850108@126.com

H. Zhao · T. Gu
School of Information and Communication, Guilin University of Electronic Technology, Guilin 541004, China

# 1   Introduction

Equipped with V2X technology, vehicles become the best actors to monitor traffic states in a fully distributed and localized way. Instead of propagating traffic states to a central infrastructure system, these smart vehicles locally share and aggregate traffic state information through cooperative V2X (Vehicle-to-Vehicle and Vehicle-to-Infrastructure) communications using vehicular ad hoc networks (VANET) for obtaining sufficient and real-time information in the vehicular cyber system, which can realize effectively cooperative driving in the vehicular physical system. Thus, we name the deep fusion system of the vehicular cyber system and vehicular physical system as a vehicular cyber-physical system (VCPS), which is a typical cyber-physical system (CPS) [1].

In the vicinity of the intersection, VANETs are a long-term solution contributing significantly toward VCPS in providing access to the cooperative driving system. In fact, the cooperative driving system relies on exchanging cooperative driving messages propagated to all or a selected cluster of vehicles [2]. However, some unique characteristics of VANET (i.e., high vehicle mobility, dynamic topology changes with frequent link breakage, and unstable quality of wireless propagation) involve serious challenges. Thus, many unreliable factors, such as transmission delay, error, and redundancy, can prevent emergency warning message (EWM) from being correctly propagated to the right vehicles timely [3–5]. These unreliable factors seriously affect VANET of the cooperative driving system in the vicinity of intersection to propagate EWM to the right endangered vehicles timely, accurately, and with low redundancy [6]. Therefore, the key issue of the message propagation over a VANET is how a vehicle of cooperative driving system in the vicinity of intersections reliably and quickly propagates the message to the target vehicles. Thus, traffic information reliable and fast dissemination with optimal low delay in VANET environment is a challenging task [7].

Traditional methods for obtaining reliable EWM mainly focus on optimizing a single previously mentioned unreliable factor, or use the perspective of the discrete cyber system or the physical components which is one of the key factors behind success; the success of such designs is quickly subverted if resources are limited to a certain level or the target system is complex and huge. Thus, the traditional methods may lead to significant performance degradation. Recent researches on VANET have shown that significant performance improvement is possible by coupling the physical objects with the cyber components, which are responsible for propagating EWM to the surrounding endangered vehicles opportunely and effectively [8].

Thus, to handle the above problems, we propose an OTREM of VANET in the vicinity of intersection for cooperative driving system from the perspective of VCPS. The OTREM is developed in the process of analyzing and handling transmission delay and error of EWM. Meanwhile, vehicles in VANET of cooperative driving system play different roles which depend on their location and the types of EWM, so we design the roles transition mechanism to propagate EWM to the right vehicles timely and accurately for reducing redundancy of VANET.
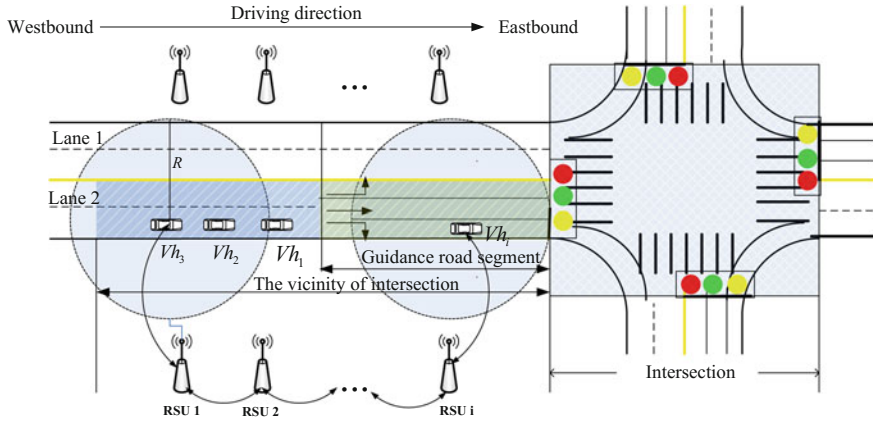
**Fig. 1** A scenario of cooperative driving system in the vicinity of intersection

In order to describe our OTREM, we give the cooperative driving system scenarios in the vicinity of intersection using V2X communication which are shown in Fig. 1. $Vh_1$ or more remote $Vh_i$ can deliver EWM when an emergency event happens. If $Vh_2$ and $Vh_3$ can get EWM in a limited range of delay, the drivers may perceive this situation immediately, and then $Vh_3$ can avoid potential dangers via prompt reactions. $Vh_3$ can benefit from the proposed OTREM in the vicinity of intersection if the driver in the scenarios of driver's visibility is poor, the driver is not paying enough attention and the driver does not have enough time to react in the endangered situations.

## 2 The Mechanism of Error and Transmission Delay Analyzing and Handling

Considering OTREM architecture of VANET in the cooperative driving system, a part of our main work is to design algorithms which control the rate $R$ and range $D$ of propagation based on the observed network feedback, and perceived information error $e(t)$. According to the practical situation, we consider the fact that propagation accuracy, tightly coupled with the physical system process, is largely relevant to the number of packets which is propagated to EWM receivers. Therefore, we need to optimize the rate of propagation $R$ for controlling the information accuracy. According to the above presentation, we give two rates of propagation control functions as follows:

$$q(t) = 1 - \exp(-\alpha |e(t) - e_Y|^2) \tag{1}$$

$$R_{\max}(t) = B . \log_2\left(1 + \frac{S}{N}\right) \tag{2}$$

$$R_{\text{real}}(t) = q(t) . R_{\max}(t) \tag{3}$$

Let $\frac{S}{N}$ present the signal-to-noise ratio and $\alpha$ present the adjustable sensitivity of error and specify how sensitive the controller to the perceived information error [8]; $e(t)$ is the perceived information error at time $t$. $e_Y$ is an adjustable threshold of error; $q(t)$ presents the transmission probability based on information error; $B$ is the bandwidth of VANET; $R_{\max}(t)$ is the maximum value of the propagation rate and $R_{\text{real}}(t)$ is the real value of the propagation rate.

The range control algorithm obeys the theory that the range $D$ should increase when channel occupancy $U$ decreases, and vice versa. Thus, we bring a range control function which is based on heuristics. Meanwhile, we choose a solution which tries to keep the value of information propagation rate (IPR) closing to its peak value. When the controller maintains $U$ between $U_{\min} = 0.4$ and $U_{\max} = 0.8$, perfect IPR performance may be achieved [9]. So, we choose a linear adaptive function which keeps $U$ between these values by adapting $D$:

$$D = F(U) = \begin{cases} D_{\max} & U < U_{\min} \\ D_{\min} + \frac{U_{\max} - U}{U_{\max} - U_{\min}}(D_{\max} - D_{\min}) & U_{\min} \le U < U_{\max} \\ D_{\min} & U \ge U_{\max} \end{cases} \tag{4}$$

The $D$ limits, $D_{\min}$ and $D_{\max}$, come from the safety requirement. The above options of the range controller, maybe not optimal, but is a robust scheme that perfectly tolerates the changes in network density and propagation rate.

Except for decreasing the error of VANET in VCPS, we want to achieve low EWM transmission delay. EWM transmission delay is the duration from the time of emergency event happening at the trigger vehicle ($Vh_T$) to the time of the EWM is successfully received by the following vehicle ($Vh_F$), it often contains response delay, mechanical delay, message queuing delay, channel access delay, retransmission delay, etc. So, we divide the EWM transmission delay into two parts which are the waiting delay and the retransmission delay.

The waiting delay $De_{\text{wait}}$ is defined as the duration from the time of EWM generating to the time of EWM beginning to propagate on the wireless channel. In order to measure $De_{\text{wait}}$, we assume that EWM propagation process from each $Vh_T$ is Poisson distribution and the number of $Vh_T$ set is $Q$. The arrival rate of EWM $\lambda$ is the set of all $Vh_T$ propagation rates. We also assume the channel service process as Poisson distribution and each EWM has the same packet size. $\mu$ presents the channel service rate and only when $\mu > \lambda$, VANET is stable [10]. So $De_{\text{wait}}$ is defined as follows:

$$De_{\text{wait}} = \frac{2\mu - \lambda}{\mu(\mu - \lambda)} \tag{5}$$

In our paper, we use the rule of first come first serve (FCFS) [11]. Assuming that the vehicle No. $i$ propagates EWM from $Vh_T$, which is the first EWM successfully received by $Vh_F$. So the retransmission delay ($De_{\text{forwarding}}$) is defined as the duration from the time that the first EWM is generated by $Vh_T$ to the time that EWM of the vehicle No. $i$ is generated by $Vh_F$. Let $q$ present the probability of EWM being successfully received by $Vh_F$, $\theta_0$ represents the initial EWM propagation rate and $f(\theta_0, i)$ represents the EWM propagation rate after the vehicle No. $i$ propagating the EWM for a $Vh_T$. Thus, the average $De_{\text{forwarding}}$ is described as follows:

$$De_{\text{forwarding}} = \sum_{i=2}^{\infty} (1-q)^{i-1} q \left( \sum_{j=1}^{i-1} \frac{1}{f(\theta_0, i)} \right) \tag{6}$$

So the total delays ($De_{\text{total}}$) of EWM propagation are presented as follows:

$$De_{\text{total}} = De_{\text{wait}} + De_{\text{forwarding}} \tag{7}$$

The initial EWM transmission rate is usually needed to be high so that the EWM transmission delay can be possibly little. However, if the rate keeps high or decrease slowly, the total arrival rate of EWM may increase rapidly due to the occurrence of new $Vh_T$ which leads to a heavily loaded network and long waiting time, so we need to balance $De_{\text{wait}}$ and $De_{\text{forwarding}}$ for optimizing the propagation rate. On the other hand, if the EWM transmission rate decreases too quickly, the retransmission delay may increase sharply.

For an approaching $Vh_T$, its maximum delay in receiving the EWM mainly depends on $\theta_{\min}$. So the value of $\theta_{\min}$ is determined based on the propagation rate, the maximum velocity, the deceleration or acceleration capability and the channel conditions. Let the EWM propagation rate range be $(\theta_{\min}, \theta_0)$. Thus, we improve the multiplicative rate decreasing algorithm to demonstrate the relationship between delay and the number of trigger vehicles [10]. Specifically, beginning with the initial rate $\theta_0$, the EWM propagation rate of $Vh_T$ is decreased by the factor $\alpha$ after every $\sigma$ propagated EWM, until $\theta_{\min}$ is achieved. That is,

$$f(\theta_0, i) = \max\left(\theta_{\min}, \frac{\theta_0}{\alpha^{\lfloor \frac{i}{\sigma} \rfloor}}\right) \tag{8}$$

## 3 The Redundancy Elimination Mechanism of EWM

In this section, we want to ensure every $Vh_T$ can receive EWM according to its requirements and situation, meanwhile eliminating redundancy of EWM.

For describing the IFST-based vehicles' roles change mechanism, four steps need to implement. They are defining the vehicle roles, constructing an alphabet of finite

automata, defining state transition function and constructing finite automata, respectively.

Firstly, define the vehicles' roles. We define the vehicles' roles according to the vehicles' states which are described in the previous part of our paper. On the basis of the four roles, we add $Vh_L$ as the leading vehicle to finite automata states set for the purpose of describing all the main emergency scenarios. Thus, the vehicles' roles are classified as $Vh_T, Vh_F, Vh_A, Vh_N, Vh_L$ and construct the finite automata state set as below:

$$Vh_{state} = \{Vh_T, Vh_F, Vh_A, Vh_N, Vh_L\} \tag{9}$$

Second, construct an alphabet of finite automata. This step is to abstract the real-time states or action information as alphabet transition process of finite automata. We construct them as follow:

$w_1$: $Vh_A$ receive EWM and VSD does not hold; $w_2$: $Vh_A$ receive acknowledgement or overtake $Vh_T$; $w_3$: $Vh_A$ LC or crash; $w_4$: $Vh_L$ SD or crash; $w_5$: $Vh_F$ crash; $w_6$: $Vh_F$ receive acknowledgement or overtake $Vh_T$; $w_7$: $Vh_N$ crash; $w_8$: $Vh_N$ receive EWM and VSD does not hold; $w_9$: $Vh_N$ Received EWM; Broadcast the Capability of Offer Help (COH); Receive forwarding EWM (FEWM); $w_{10}$: $Vh_T$ restart;

The alphabet of finite automata includes the states, the transition conditions, and the vehicles' restraint condition. Thus, the state transition conditions construct the alphabet of finite automata:

$$\Sigma = \{w_1, w_2, \ldots, w_{10}\} \tag{10}$$

Third, define states transition function. The input of the alphabet can lead to finite automata states transition according to the states transition function. We define the vehicle states transition function as follows:

$$f_T(Vh_A, w_1) = Vh_F, \; f_T(Vh_A, w_2) = Vh_N, \; f_T(Vh_A, w_3) = Vh_T$$
$$f_T(Vh_L, w_4) = Vh_T, \; f_T(Vh_F, w_5) = Vh_T, \; f_T(Vh_F, w_5) = Vh_T$$
$$f_T(Vh_F, w_6) = Vh_N, \; f_T(Vh_N, w_7) = Vh_T, \; f_T(Vh_N, w_8) = Vh_F$$
$$f_T(Vh_N, w_9) = Vh_A, \; f_T(Vh_T, w_{10}) = Vh_L, \; f_T(Vh_T, w_{10}) = Vh_A$$
$$f_T(Vh_T, w_{10}) = Vh_F, \; f_T(Vh_T, w_{10}) = Vh_N \tag{11}$$

If vehicles satisfy the states transition condition, through matching the condition parameters of input alphabet table, achieves state transition.

Fourthly, construct finite automata. According to the vehicle roles, the alphabet table, the states transition function, the initial states and the terminal state, a deterministic finite automata $T$ can be constructed as follows:

$$T = \{\{Vh_T, Vh_F, Vh_A, Vh_N, Vh_L\}, \{w_1, w_2, \ldots, w_{10}\},$$
$$\{f_T(Vh_A, w_1) = Vh_F, f_T(Vh_A, w_2) = Vh_N, \ldots, f_T(Vh_T, w_{10}) = Vh_N\}\} \tag{12}$$

**Fig. 2** Finite automata model for the vehicle roles transition
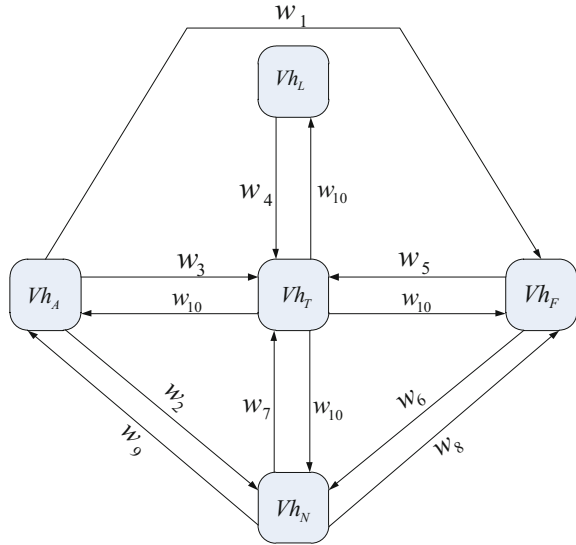
The process of the vehicle roles transition is shown in Fig. 2.

Five vehicle roles $Vh_T$, $Vh_F$, $Vh_A$, $Vh_N$, $Vh_L$ and role transitions are designed to ensure the broadcast consistency of EWM. Meanwhile, the proposed transition mechanism may reduce redundancy messages as much as possible through propagating various EWM to right vehicles.

## 4 Conclusions

In this paper, we analyze and process error, the transmission delay of EWM and propose a scheme of the vehicles' roles change using improved finite automata for propagating EWM to the right vehicles and eliminating redundancy of EWM. The proposed OTREM of VANET in the vicinity of intersection for the cooperative driving system is described from the perspective of VCPS.

# References

1. Jia D, Lu K, Wang J, Zhang X, Shen X (2016) A survey on platoon-based vehicular cyber-physical systems. IEEE Commun Surv Tutorials 18(1):263–284
2. Liu B, El Kamel A (2016) V2x-based decentralized cooperative adaptive cruise control in the vicinity of intersections. IEEE Trans Intell Transp Syst 17(3):644–658
3. Gonzalez S, Ramos V (2016) Preset delay broadcast: a protocol for fast information dissemination in vehicular ad hoc networks (VANETs). Eurasip J Wirel Commun Networking 1:1–13
4. Yadav AK, Tripathi S (2015) DLBMRP: design of load balanced multicast routing protocol for wireless mobile ad-hoc Network. Wirel Pers Commun 85(4):1815–1829
5. Liu J, Yang Z, Stojmenovic I (2013) Receiver consensus: on-time warning delivery for vehicular ad-hoc networks. IEEE Trans Emerg Top Comput 1(1):57–68
6. Fan X, Wang C, Yu J, Xing K, Chen Y, Liang JA (2015) Reliable broadcast protocol in vehicular ad hoc networks. Int J of Distrib Sens Netw 1–14
7. Zemouri S, Djahel S, Murphy J (2014) A fast, reliable and lightweight distributed dissemination protocol for safety messages in urban vehicular networks. Ad Hoc Netw 27:26–43
8. Huang C-L, Fallah YP, Sengupta R, Krishnan H (2010) Adaptive intervehicle communication control for cooperative safety systems. IEEE Netw 24(1):6–13
9. Fallah YP, Huang C, Sengupta R, Krishnan H (2010) Design of cooperative vehicle safety systems based on tight coupling of communication, computing and physical vehicle dynamics. In: Proceedings of the 1st ACM/IEEE international conference on cyber-physical systems, pp 159–167
10. Yang X, Liu J, Vaidya N, Zhao F (2004) A vehicle-to-vehicle communication protocol for cooperative collision warning. In: The first annual international conference on mobile and ubiquitous systems: networking and services, 2004 MOBIQUITOUS, pp 114–123
11. Rogiest W, Laevens K, Walraevens J, Bruneel H (2015) When random-order-of-service outperforms first-come-first-served. Oper Res Lett 43(5):504–516

# Energy Management Strategy for Hybrid Engineering Vehicles with Composite Energy Storage

**Pan Luo, Muyi Lin, Yong Chen, Li Zhao and Bin Ma**

**Abstract** To improve the energy utilization efficiency of hybrid engineering vehicles with composite energy storage, a new energy management strategy based on fuzzy control theory was proposed. The vehicle model of the hybrid loader was established with MATLAB/Simulink and the energy distribution of it in the "V" type working condition was simulated. The fuel consumption of the traditional loader and the hybrid loader with the proposed energy management strategy were simulated and compared in two typical working cycles. A hardware-in-loop simulation platform was built to validate the presented energy management strategy. The simulation and experimental results show that the energy management strategy used in the hybrid loader can make various power devices work in high efficiency, which significantly improves the fuel economy of the vehicle.

**Keywords** Composite energy storage · Energy management · Fuzzy control
Fuel economy

## 1 Introduction

To meet the requirements of high energy density and power density, most of the hybrid engineering vehicles were equipped with engine, battery, and hydraulic accumulator. And at the same time, a reasonable design of energy management strategy was also needed to make full use of the advantages of these devices and to meet the acquirement for energy saving and emission reduction [1, 2]. In literature [3, 4], the advantages and disadvantages of oil–electric hybrid vehicle control strategy and

P. Luo (✉) · M. Lin · Y. Chen · L. Zhao · B. Ma
School of Mechanical and Electronic Engineering, Beijing Information Science and Technology University, Beijing 100192, China
e-mail: 13522262835@139.com

M. Lin
e-mail: lin_muyi@163.com

M. Lin · Y. Chen · L. Zhao · B. Ma
Collaborative Innovation Center of Electric Vehicles in Beijing, Beijing 100192, China

oil–hydraulic hybrid vehicle control strategy were compared and analyzed, while the control strategy of oil–electric–hydraulic hybrid vehicle was ignored. In literature [5], the energy saving principle and working mode of oil–hydraulic hybrid system were studied, but regenerative braking energy was not distributed. In literature [6], oil–electric–hydraulic hybrid power vehicle was designed to effectively reuse the vehicle braking energy and to improve the fuel economy of internal combustion engine, but the effect of vehicle was not optimal because the energy distribution was not carried out on the vehicle working conditions.

In most of the current researches, the energy management strategy of oil–electric–hydraulic hybrid power system was not combined with their working conditions. Thus, in this chapter, we present an energy management strategy for composite energy storage hybrid loader based on fuzzy control logic method and working conditions. The dynamic characteristics of power components and energy storage devices are analyzed by simulation in the "V" type working condition. In order to prove the effectiveness of the presented energy management strategy, the fuel consumption of the traditional loader and the energy management strategy based hybrid loader are simulated on two typical working cycles. To verify the correctness of the simulation results the experiments are carried out on hardware-in-loop simulation platform which is built with dSPACE real-time simulation system.

## 2 Oil–Electric–Hydraulic Hybrid Loader

The oil–electric–hydraulic hybrid loader with parallel structure (Fig. 1) is mainly composed of engine, electric motor, battery, accumulator, hydraulic torque converter, single row planetary coupler, etc. In this system, the high energy density of battery can keep the engine working in high-efficiency range; the high power density of accumulator can satisfy the power requirements in high power output and emergency braking conditions to reduce the damage of the battery. Controlling the output torque of the engine and keeping the motor working in high-speed range will improve the efficiency of the motor, so as to improve the efficiency of the whole hybrid system [7].

## 3 Fuzzy Theory-Based Energy Management Strategies

### 3.1 Working Modes

In the proposed hybrid system, the power of the engine, motor, and hydraulic motor were distributed based on working conditions. When the demand of load torque was satisfied, the charge/discharge capacities of battery will keep balance and the energy utilization ratio will be improved. The specific working modes are as follows:

(1) Starting mode
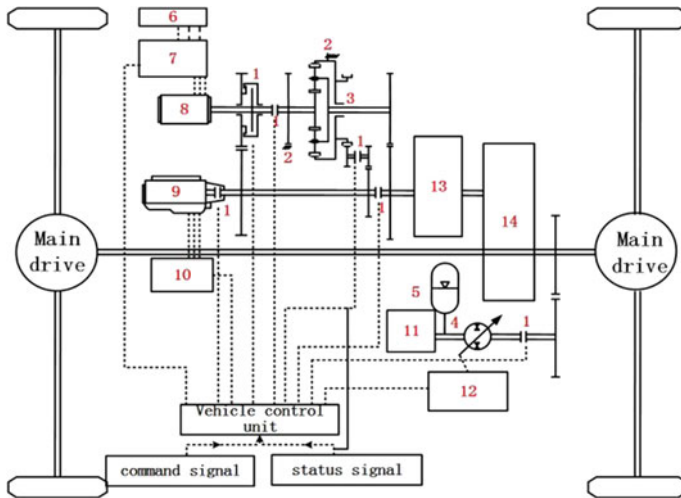
**Fig. 1** Schematic overview of system structure 1. Electromagnetic clutch. 2. Lockup device. 3. Planet gear mechanism. 4. The secondary components. 5. Accumulator. 6. The battery. 7. Motor controller. 8. Electrical motor. 9. Engine. 10. Engine controller. 11. Hydraulic system. 12. Hydraulic pump/motor controller. 13. Hydraulic torque converter. 14. Transmission

The demand power of the loader is relatively large and the emission is poor. With the advantage of high power density of hydraulic accumulator, the loader is driven by hydraulic secondary component instead of engine.

(2) Oil–electric hybrid mode

    (a) When the loader demand torque is less than the lower limit of the engine optimal torque range, the engine will be adjusted to work in the optimal working range. The motor/generator working in the generator state will be coupled with engine and the electrical energy conversed from engine excess output energy will be stored in battery.

    (b) When the loader demand torque is greater than the upper limit of the engine optimal torque range and the battery SOC is larger than its lower working limit value, the engine will be adjusted to work in the optimal working range. The motor/generator working in the motor state will be coupled with engine and the discharged electric energy will be converted into the kinetic energy to meet the load demand of the loader.

(3) Oil–hydraulic hybrid mode

When the loader is in high power output condition, the hydraulic accumulator will be coupled with the engine to output torque to make the engine work in optimal range if the hydraulic accumulator can meet the work requirements, otherwise, the engine will provide torque beyond the optimal torque range.

(4) Engine driving mode

Calculating the values of loader external load torque and engine calibration output torque, when the loader external load torque is in the optimal torque range of engine calibration, the loader will be driven by engine alone.

(5)   Electric mode

Calculating the value of loader external load torque, when the value is in the optimal torque range of engine calibration and the power battery SOC is relatively high, the external load will be driven by motor alone.

(6)   Regenerative braking mode

Taking the advantages of high power density and instantaneous charging-discharging liquid of hydraulic accumulator, the pump can be used to recover the energy and produce the braking torque.

## 3.2   Fuzzy Controller

In fuzzy controller, the load demand torque, battery SOC, and accumulator SOC were selected as the input values, and the engine output torque was taken as the output value. The ratio of load demand torque to engine optimal torque was divided into five subsets: {S1, S2, S3, S4, S5}, the domain scope is [0, 4]; The battery SOC and accumulator SOC were divided into three subsets: {t1, t2, t3} and {V1, V2, V3}, the domain scope is [0, 1]; The ratio of engine output torque to optimal torque was divided into five subsets: {u1, u2, u3, u4, u5}, the scope is [0, 4]. Triangular membership function with fast operation and high precision was selected in fuzzy controller. According to a large number of simulation data, expert opinions and theories, the fuzzy rules were formulated as follows:

1.  If (XQZJ is NB) and (XSOC is NB) and (BSOC is NB) then (SCJZ is NS);
2.  If (XQZJ is NB) and (XSOC is NB) and (BSOC is NS) then (SCJZ is NS);
3.  If (XQZJ is NB) and (XSOC is NB) and (BSOC is 0) then (SCJZ is NS);
     ......
124. If (XQZJ is PB) and (XSOC is PB) and (BSOC is PB) then (SCJZ is 0).

The three-dimensional interface of fuzzy logic input and output can be obtained according to the formulated fuzzy logic control rules and membership function relation of input and output. It is shown in Fig. 2.

## 4   Simulation

The whole simulation model of the traditional loader [8] and the hybrid loader implementing the proposed energy management strategy were established with MATLAB/Simulink in Fig. 3.
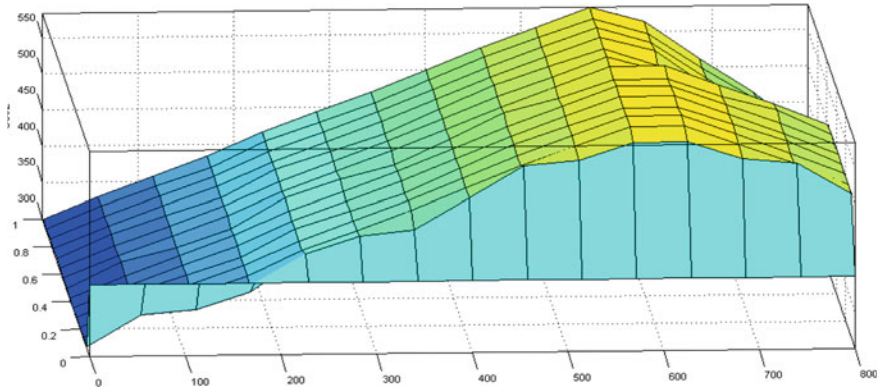
**Fig. 2** Control chart of engine fuzzy controller
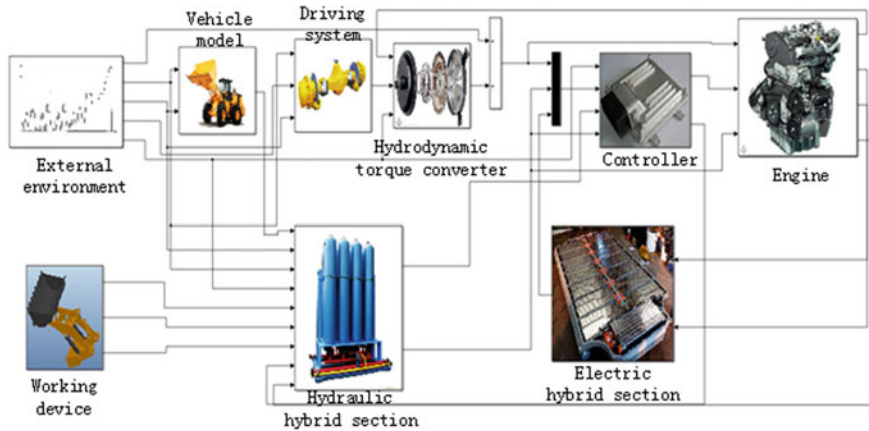


**Fig. 3** The simulation model of hybrid loader

## 4.1 Dynamic Characteristics of Power Components

For a loader, the driving cycles of it are complex and changeable, which can be divided into running cycles and working cycles. For working cycles, the four commonest types of them are I type, T type, V type, and L type [9].

The comparison of engine torque, motor torque, and hydraulic secondary component torque can be obtained under the "V" type working cycle in Fig. 4. The comparison of engine and motor velocity is depicted in Fig. 5.

From Figs. 4 and 5, the following can be concluded: (1) If the demand engine torque is less than the lower limit of the optimal engine torque, the engine increases the output torque to work in high efficiency range, and the excess torque is converted into electrical energy by generator which can be stored in battery; (2) If the demand engine torque beyond the upper limit of the optimal engine torque and is very large,

Fig. 4 Comparison of
torque
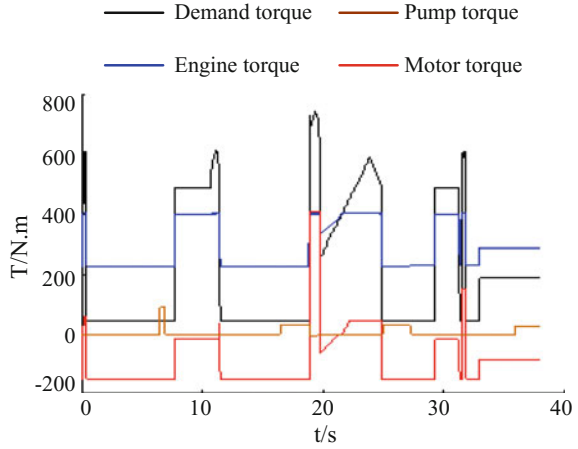


Fig. 5 Comparison of
velocity
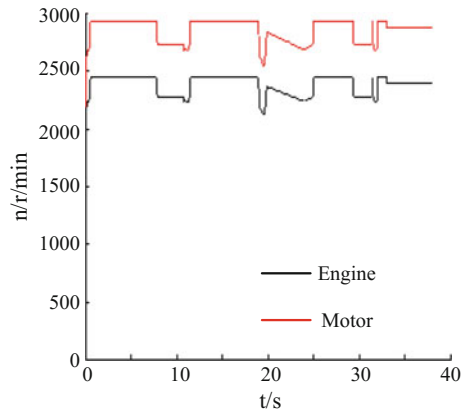


the hydraulic secondary component torque is coupled with engine torque; otherwise, the motor torque is coupled with engine torque.

## 4.2 Dynamic Characteristics of Energy Storage Devices

When the loader worked in "V"-type working cycle, the current and SOC of the battery, the pressure and SOC of the braking accumulator, the pressure and SOC of the potential energy recovery accumulator can be obtained in Figs. 6, 7, and 8.

As can be seen from Figs. 6, 7, and 8, (1) the current and SOC of the battery changed with the working conditions to keep the engine working in high-efficiency range and to maintain the SOC of the battery in a reasonable range; (2) Regenerative braking accumulator can fully recover the braking energy and meet the requirement

**Fig. 6** Current and SOC of the battery
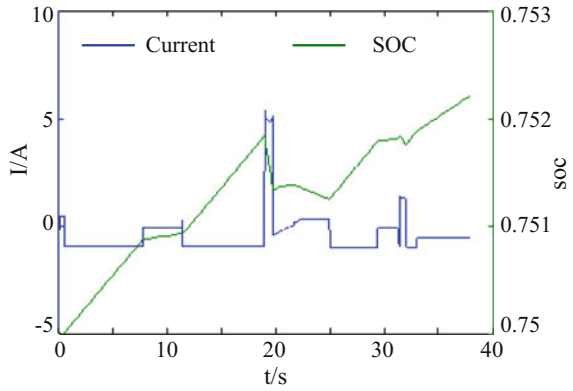


**Fig. 7** Pressure and SOC of the braking accumulator
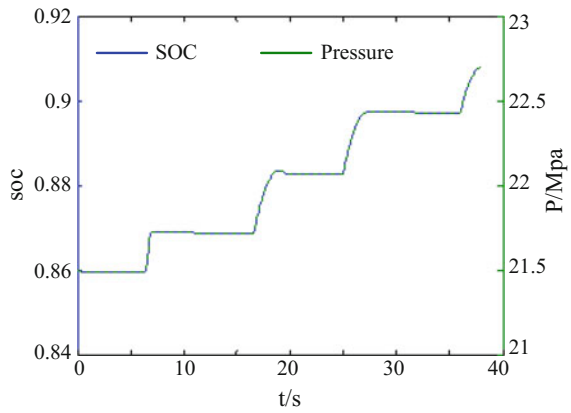


**Fig. 8** Pressure and SOC of the potential energy recovery accumulator
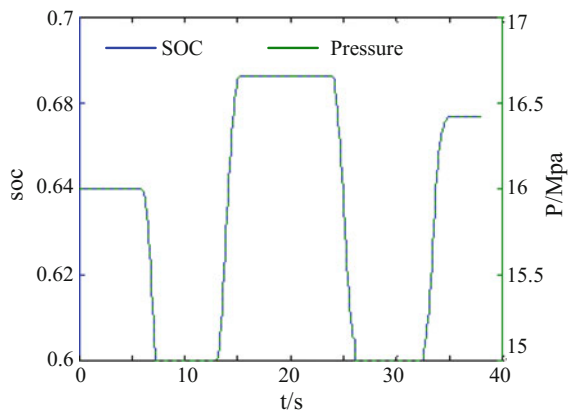


of loader load torque in time when the loader braking and demand torque high; (3) Potential energy recovery accumulator can fully recover the potential energy of the falling loader working device and release energy to assist the working pump to realize the lifting of the loader working device.
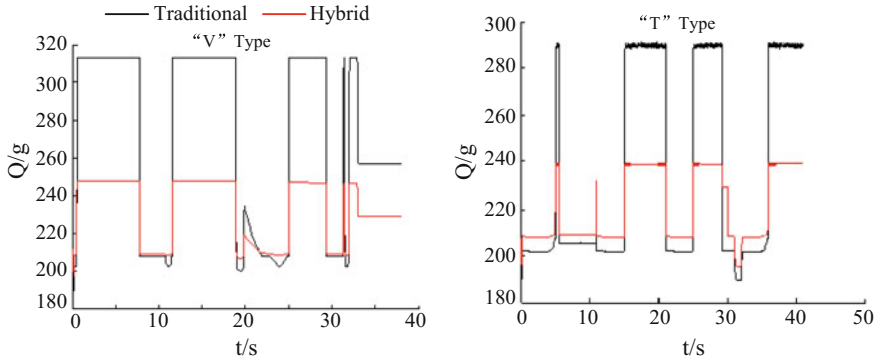
**Fig. 9** The comparison of fuel consumption on two different working cycles

## 4.3 Fuel Consumption

Traditional loader and hybrid loader with the proposed energy management strategy were simulated in two different working cycles, and the comparisons of fuel consumption of them are depicted in Fig. 9.

Figure 9 shows that the hybrid loader with the proposed energy management strategy can obviously achieve load shifting on large torque output and idle condition under two different working cycles. The presented fuzzy rules based energy management strategy can save energy well.

## 5 Experiments

### 5.1 Experimental Setup

As shown in Fig. 10, the hardware-in-loop simulation test platform we used consists of dSPACE real-time simulator, AutoBox, host computer, power supply, hydraulic accumulator, and hydraulic pump station platform.

### 5.2 Experimental Results

The experimental results were obtained when the hydraulic accumulator was at two different initial pressure 21.5, 15.5 MPa. In order to verify the effectiveness of the proposed fuzzy control based energy management strategy, the experimental results were compared with the simulation results in Fig. 11.
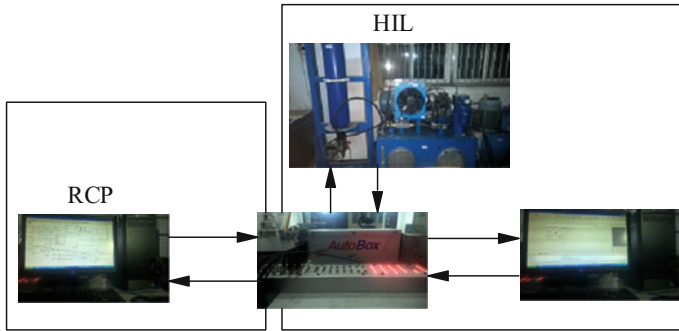
**Fig. 10** Schematic overview of the dSPACE based hardware-in-loop test platform cycles
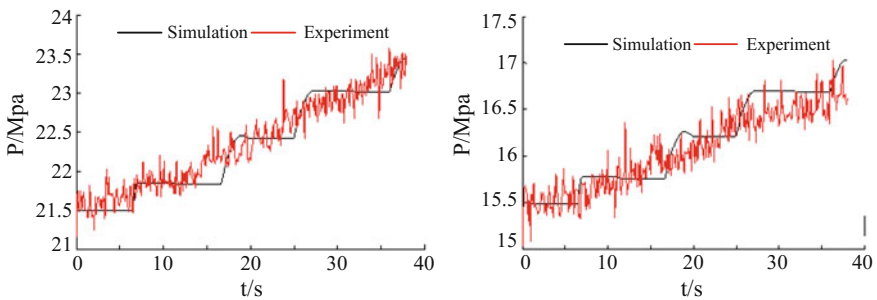


**Fig. 11** Hydraulic accumulator pressure at different initial pressure cycles

We can find that the experimental results are basically consistent with the simulation results. However, due to the influence of the control strategy and the experimental equipment itself, the trend of energy release of accumulator is not particularly obvious. The experimental results verify the reliability of the simulation results and prove the correctness of the fuzzy rules based energy management strategy.

## 6 Conclusions

(1) The proposed fuzzy control-based energy management strategy was simulated in MATLAB/Simulink. The simulation results indicate that the presented energy management strategy is reasonable and it can be used to keep the engine working in the high range, to keep the battery SOC in a reasonable interval, to significantly reduce the fuel consumption of the loader.

(2) The results of Hardware-in-loop tests were also agreement with the simulation results, which show that the simulations are correct and the effectiveness of the presented energy management strategy can be proved.

(3) The proposed energy management strategy can effectively solve the energy management problem of oil–electric–hydraulic hybrid loader and provide reference for the future design of vehicle controller.

# References

1. Zaher MH, Cetinkunt S (2013) Real time energy management strategy for hybrid electric powertrains. SAE Technical Paper 2013-01-2396
2. Salmasi FR (2007) Control strategies for hybrid electric vehicles: evolution, classification, comparison, and future trends. IEE Trans Veh Technol 56(5):2393–2404
3. Karbaschian MA, Söffker D (2014) Review and comparison of power management approaches for hybrid vehicles with focus on hydraulic drives. Energies 7:3512–3536
4. Zhao P, Chen Y, Zhou H (2016) Overview of hydraulic hybrid engineering machinery system and control strategy. J Zhejiang Univ (Eng Sci) 03:449–459
5. Zhang L, Fu M, Wang Y (2015) Simulation and analysis of electro-hydraulic hybrid system based on AMESim. J Mech Electr Eng 4:561–565, 570
6. Hui S, Lifu Y, Junqing J et al (2010) Control strategy of hydraulic/electric synergy system in heavy hybrid vehicles. Energy Convers Manag 52:668–674
7. Matheson P, Stecki J (2003) Modeling and simulation of a fuzzy logic controller for a hydraulic-hybrid powertrain for use in heavy commercial vehicles. SAE Technical Paper 2013-01-3275
8. Xue D, Chen Y (2004) System simulation technology and application based on MATLAB/Simulink. Tsinghua University Press, Beijing
9. Yue Z, Lin M, Chen Y et al (2016) Control strategy of hydraulic hybrid vehicle for multi-system combined braking. Chin Hydraulics Pneumatics 10:18–26

# Pareto-Improving User Equilibrium Model Under Tradable Credit and Link Capacity Constraints

**Juan Shao, Chao Sun, Jian Rong and Lin Cheng**

**Abstract** This chapter presents a user equilibrium model under tradable credit and link capacity constraints (UE-CC) that explicitly considers the characteristics of congested roads in urban traffic network. This model hypothesizes that for each origin-destination (OD) pair no traveler can reduce his/her generalized travel cost by unilaterally changing paths. To obtain the total amount of credits, credit charges on each link and credit cost, this chapter extends the UE-CC model to a Pareto-improving user equilibrium model under tradable credit and link capacity constraints (PUE-CC). This new model uses minimization of system optimal travel time as the objective function and uses the nonlinear complementarity functions of route travel time, route credit cost and route congested delay as the constraints. A relaxation algorithm is developed to solve the PUE-CC model. Numerical examples illustrate the essential ideas of the PUE-CC model and the applicability of the designed solution algorithm.

**Keywords** Traffic congestion · User equilibrium model · Pareto-improving
Tradable credit scheme · Capacity constraints · Relaxation algorithm

## 1 Introduction

Traffic sustainable development has become one of the most severe social problems in almost all large cities worldwide. And the core of this problem is sustainable growth of private cars. Much travel time is wasted on the trips due to traffic congestion, and

J. Shao (✉) · J. Rong
Traffic Engineering Association, Floor 6, Building 3, Area 4, Hanwei International Plaza, Fengtai
District, Beijing 100071, China
e-mail: shaojuan17@163.com

C. Sun · L. Cheng
School of Transportation, Southeast University, Nanjing 210096, China

C. Sun
NEXTRANS Center, Purdue University, West Lafayette 47906, USA

J. Rong
College of Metropolitan Transportation, Beijing University of Technology, Beijing 100124, China

this will make travelers feel stressed and depressed which will bring to the increase in traffic accident rate. The traffic conditions become uncertain, and travelers will depart earlier to avoid the possible delays caused by traffic congestion and travel time variability [1, 2]. Therefore, finding policy measures that can potentially manage the traffic demand in effective and sustainable ways should be provided on the research agenda.

For the development of TCS theory, Yang and Wang presented a tradable credit distribution and charging scheme, they assumed the credits were universal for all links [3], and then they quantitatively analyzed how to describe network mobility with TCS in the user equilibrium network. Through considering travelers' transaction costs and their loss aversion behaviors, Bao et al. made some studies on managing network mobility with TCS [4]. Han and Cheng used a bi-level model to research the efficiency and effectiveness of TCS on enhancing network capacity [5]. In addition, there are also many scholars who did some research on managing bottleneck congestion network with TCS [6, 7]. For comprehensive reviews of TCS, interested readers may refer to Fan and Jiang [8], Grant-Muller and Xu [9] and Dogterom et al. [10]. TCS is used to mitigate the urban traffic congestion, while the above models do not consider the characteristics of congested roads in urban traffic network. In other words, the above models assume the practical link flow can be greater than the road capacity. In addition, the above models assume the total amount of credits and credit charges on each link is known variables, however, these indexes should be determined through traffic network designing (i.e., these indexes are decision variables instead of known parameters).

At present, many scholars apply the Pareto-improving methods to the congestion pricing which are provided in Table 1, which highlights the aspects of trip mode (e.g., car or both car and bus), the type of multi-class, the network size (e.g., large, medium or small), and whether revenue redistribute. Although there are many researches on Pareto-improving method, all these studies are applied to congestion pricing. Hence, the Pareto-improving method corresponding to TCS which is also a price measure to alleviate traffic congestion need to be studied.

Considering the characteristics of congested roads in urban traffic network, this chapter presents a UE-CC model. This new model can avoid the traffic flows exceed the road capacities. Analyzing the properties of the solution of UE-CC model, this chapter also proposes a PUE-CC model. This is the first attempt to integrate the Pareto-improving theory into the network equilibrium framework with tradable credit constraints. The main contributions of this chapter are as follows: (1) Analyze the relationship between traffic flow and link travel time in congested traffic network, UE-CC model is built; (2) Use Karush-Kuhn-Tucker (KKT) conditions to analyze the properties of solutions of UE-CC model, PUE-CC model is presented to obtain the total amount of credits, credit charges on each link and credit cost; and (3) Designed a relaxation algorithm to deal with the nonlinear complementarity problem of PUE-CC model.

**Table 1** Literature review on Pareto-improving method

| Literature | Trip mode | Multi-class | Network size | Revenue redistribution |
|---|---|---|---|---|
| Song et al. [11] | Car | Yes | Large | No |
| Song et al. [12] | Car and bus | No | Small | Yes |
| Lawphongpanich and Yin [13] | Car | No | Large | No |
| Wu et al. [14] | Car and bus | Yes | Medium | No |
| Liu et al. [15] | Car and bus | Yes | Small | Yes |
| Nie and Liu [16] | Car and bus | Yes | Small | Yes |
| Guo and Yang [17] | Car | Yes | Small | Yes |
| Guo [18] | Car | No | Small | Yes |
| Xiao and Zhang [19] | Car | No | Small | Yes |
| Chu et al. [20] | Car and bus | Yes | Small | Yes |

## 2 User Equilibrium Model Under Tradable Credit and Capacity Constraints

### 2.1 Characteristics of Congested Link Flow

Based on traffic flow theory (i.e., flow-speed-density relationship), the traffic flows will first increase with the increase of traffic density, then reach to the maximum traffic flows (i.e., congested state). Therefore, the relationship between link travel time and link flow is described in Fig. 1 where the presence of congestion generates two alternative link travel times for the same flow level. However, existing researches corresponding to TCS assume the relationship between link travel time and link flow is shown in Fig. 2. This limits the usefulness of such models for high-congestion situations. Thus, we need to consider the constraints of road capacity (i.e., $x_a \le c_a$).



**Fig. 1** Realistic representation of the flow-delay relationship on a road link
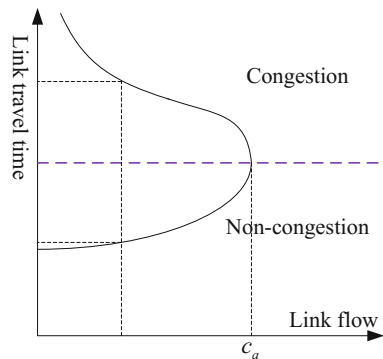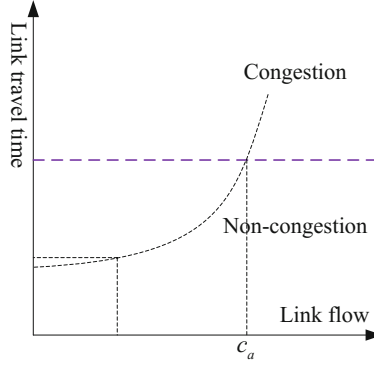
**Fig. 2** Typical assumption for the flow-delay relationship on a road link

## 2.2   Formulation of UE-CC

As described in Sect. 2.1, the link flow should less than or equal to the road capacity
in the congested traffic network. At the same time, the amount of credits should be
conservative. Thus, the UE-CC model is presented as follows:

$$\min_{\mathbf{x}} z(\mathbf{x}) = \sum_a \int_0^{x_a} t_a(x)\mathrm{d}x \tag{1}$$

$$\text{s.t.} \sum_{r \in R_\omega} f_r^\omega = q^\omega, \quad \forall \omega \in W \tag{2}$$

$$x_a = \sum_{\omega \in W} \sum_{r \in R^\omega} f_r^\omega \delta_{a,r}^\omega, \quad \forall a \in A \tag{3}$$

$$x_a \leq c_a, \quad \forall a \in A \tag{4}$$

$$\sum_{a \in A} \kappa_a x_a \leq K, \quad \forall a \in A \tag{5}$$

$$f_r^w \geq 0, \quad \forall r \in R^\omega,\, \omega \in W \tag{6}$$

where $W$ denote the set of OD node; $q^\omega$ is traffic demand generated between OD
pair $\omega \in W$; $f_r^\omega$ denote the traffic flow on route $r \in R^\omega$ between OD pair $\omega \in W$;
$R^\omega$ is the set of routes connecting OD pair $\omega$;$\delta_{a,r}^\omega$ is the route-link incidence matrix;
$x_a$ is the link flow on link $a$; $c_a$ is the capacity on link $a$; $\kappa_a$ denotes the credit charges
on link $a$; $K$ denotes the total amount of credits; and $A$ is the set of links.

## *2.3 Model Properties*

**Proposition 1** *(Existence) The proposed model has at least one solution.*

*Proof* The feasible set [i.e., Eqs. (2)–(6)] is non-empty, closed, and convex due to it is linear constraint. At the same time, the objective function [i.e., Eq. (1)] is positive and continuous with respect to **x**. Thus, the proposed model has at least one solution [21]. This completes the proof. ☐

**Proposition 2** *(Equivalence) At the state of UE-CC traffic flow pattern, for each OD pair, no traveler can reduce his/her generalized travel cost by unilaterally changing paths.*

*Proof* The Karush-Kuhn-Tucker (KKT) conditions of the UE-CC model can be analyzed by using the Lagrangian of the model formulation, incorporating the constraints (2, 4–6) where Eq. (3) is substituted into objective function (1):

$$L(\mathbf{q}, \mathbf{d}, p, \mathbf{v}) = z(\mathbf{x}) + \sum_{\omega} \mu^{\omega} \left( q^{\omega} - \sum_{r \in R_{\omega}} f_r^{\omega} \right)$$

$$+ \sum_{a} d_a(x_a - c_a) + \sum_{a} p \left( \sum_{a \in A} \kappa_a x_a - K \right) - \sum_{\omega} \sum_{r} v_r^{\omega} f_r^{\omega} \quad (7)$$

where $\mu^{\omega}$, $d_a$, $p$, and $v_r^{\omega}$ are the Lagrangian multipliers of demand conservation constraint, road capacity constraint, total amount of credits constraint, and route flow nonnegative constraint, respectively. Since the first-order condition of the Lagrangian with respect to traffic demand is

$$\frac{\partial L(\mathbf{q}, \mathbf{d}, p, \mathbf{v})}{\partial f_r^{\omega}} = \sum_{a \in A} t_a(x_a)\delta_{a,r}^{\omega} - \mu^{\omega} + \sum_{a \in A} d_a\delta_{a,r}^{\omega} + \sum_{a \in A} p\kappa_a\delta_{a,r}^{\omega} - v_r^{\omega},$$

$$\forall r \in R^{\omega}, \omega \in W \quad (8)$$

The optimality conditions of the UE-CC model can be written as

$$\left\{ \sum_{a \in A} [t_a(x_a) + d_a + p\kappa_a]\delta_{a,r}^{\omega} - \mu^{\omega} \right\} \cdot f_r^{\omega} = 0, \ \sum_{a \in A} [t_a(x_a) + d_a + p\kappa_a]\delta_{a,r}^{\omega}$$

$$- \mu^{\omega} \geq 0, \ f_r^{\omega} \geq 0, \quad \forall r \in R^{\omega}, \ \omega \in W \quad (9)$$

$$\left( K - \sum_{a \in A} \kappa_a x_a \right) \cdot p = 0, \ K - \sum_{a \in A} \kappa_a x_a \geq 0, \ p \geq 0, \quad \forall a \in A \quad (10)$$

$$(c_a - x_a) \cdot d_a = 0, \ c_a - x_a \geq 0, d_a \geq 0, \ \forall a \in A \quad (11)$$

and Eq. (2) remains the same. This completes the proof.

**Proposition 3** *(Uniqueness of traffic flow); The traffic flow solution of proposed model is unique.*

*Proof* The Hessian matrix of the objective function with respect to traffic demand is

$$\frac{\partial^2 z(\mathbf{x})}{\partial x_a \partial x_{a'}} = \begin{cases} \frac{\partial t(x_a)}{\partial x_a} & a = a' \\ 0 & \text{otherwise} \end{cases} \tag{12}$$

In addition, as saying in last section, link performance function $t(x_a)$ increases with respect to $\mathbf{x}$ (i.e., the objective function is strict monotonicity). And the feasible set is convex. Thus, the traffic flow solution of proposed model is unique. This completes the proof. $\qquad\qquad\square$

## 2.4 Pareto-Improving User Equilibrium Model Under Tradable Credit and Link Capacity Constraints

There are many solutions of the total amount of credits, credit charges on each link and credit costs. To deal with this situation, the method of searching the maximum Pareto efficiency (i.e., minimum total system delay) of these solutions is used in this chapter. Under certain traffic equilibrium state and network configurations, it is possible to achieve Pareto improvement using TCS. However, no formulation is presented on finding the optimal TCS and its corresponding flow pattern to minimize the total system delay. The Pareto-improving tradable credit rationing problem can be formulated as a mathematical program with following complementarity constraints:

$$\min_{\mathbf{x}, \boldsymbol{\kappa}, K, p} F = \sum_{a \in A} [x_a \cdot t_a(x_a)] \tag{13}$$

s.t. Eqs. (9–11, 2)

## 3 Solution Algorithm

A relaxation algorithm is developed to solve the PUE-CC model in this chapter. The main idea of relaxation algorithm is adding a slack variable to each nonlinear complementarity constraint. Therefore, the Eqs. (9)–(11) are substituted as follows:

$$\left\{ \sum_{a \in A} [t_a(x_a) + d_a + p\kappa_a]\delta_{a,r}^{\omega} - \mu^{\omega} \right\} \cdot f_r^{\omega} \leq \theta^f, \sum_{a \in A} [t_a(x_a) + d_a + p\kappa_a]\delta_{a,r}^{\omega}$$
$$- \mu^{\omega} \geq 0, f_r^{\omega} \geq 0, \quad \forall r \in R^{\omega}, \omega \in W \tag{14}$$

$$\left(K - \sum_{a\in A}\kappa_a x_a\right)\cdot p \le \theta^p, \; K - \sum_{a\in A}\kappa_a x_a \ge 0, \; p \ge 0, \quad \forall a \in A \tag{15}$$

$$(c_a - x_a)\cdot d_a \le \theta^d, \; c_a - x_a \ge 0, \; d_a \ge 0, \quad \forall a \in A \tag{16}$$

The slack variables $\theta = \left(\theta^f, \theta^p, \theta^d\right) > 0$ decrease with predefined scaling factor at each iteration. The relaxation algorithm is provided as follows.

| | |
|---|---|
| Step 1 | (Initialization) Set initial slack variables $\theta^0 > 0$, tolerance error $\varepsilon$, scaling factor $0 < \lambda < 1$, and initial iteration number $n = 0$ |
| Step 2 | (Relaxation problem solving) Solve the relaxation problem [i.e., objective function is Eq. (13), subject to Eqs. (14–16, 2)] using nonlinear solver in GAMS [22] |
| Step 3 | (Check Convergence) If $\theta^n < \varepsilon$, then stop, the last solutions in Step 2 are the optimal solutions. Otherwise, set $\theta^{n+1} = \lambda \cdot \theta^n$; $n = n + 1$, go to Step 2 |

The Step 2 in above algorithm is coded in GAMS 23.8, other steps are coded in Matlab R2015b and the algorithm is tested on a personal computer with Intel(R) Core(TM) i7-5600U CPU 2.60 GHz, 8 GB memory.

## 4   Numerical Examples

In this section, a test network is presented in Fig. 3. The network consists of 7 nodes, 11 links, and 3 OD pairs. The commonly used BPR performance function $(t_a(x_a) = t_a^0(1 + 0.15(x_a/C_a)^4)$, where $t_a$, $t_a^0$, $x_a$, and $C_a$ are the travel time, free-flow travel time, flow, and capacity on link a, respectively.) is adopted. The initial values are $\theta^0 = (1, 1, 1)$, $\varepsilon = 1E - 5$. and $\lambda = 0.2$.

To find out the congested links in the network, the traffic flows are assigned in the user equilibrium model only under link capacity constraints [i.e., objective function is Eq. (1), subject to Eqs. (2)–(4, 6)] in Table 2, where $v/c$ is the saturation of traffic flow. It can be seen that links 3, 4, and 5 reach to the saturation state, and hence cause a queuing delay $d_a$. In this case, the total system delay is $\sum_a x_a(t_a(x_a) + d_a) = 12927$.
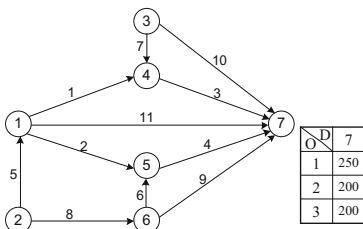


| link | $C_a$ | $t_a^0$ | link | $C_a$ | $t_a^0$ | link | $C_a$ | $t_a^0$ |
|---|---|---|---|---|---|---|---|---|
| 1-4 | 200 | 6 | 2-1 | 100 | 4 | 6-7 | 200 | 16 |
| 1-5 | 200 | 5 | 6-5 | 150 | 3 | 3-7 | 200 | 15 |
| 4-7 | 200 | 6 | 3-4 | 150 | 5 | 1-7 | 100 | 17 |
| 5-7 | 200 | 7 | 2-6 | 150 | 10 | | | |

**Fig. 3** Network topology and ODs and link characteristics

**Table 2** Link equilibrium flows with capacity constraints

| Link | $x_a$ | $t_a(x_a)$ | $d_a$ | $v/c$ | Link | $x_a$ | $t_a(x_a)$ | $d_a$ | $v/c$ |
|------|-------|-----------|-------|-------|------|-------|-----------|-------|-------|
| 1–4 | 174 | 6.519 | 0 | 0.87 | 3–4 | 26 | 5.001 | 0 | 0.17 |
| 1–5 | 101 | 5.048 | 0 | 0.50 | 2–6 | 100 | 10.295 | 0 | 0.67 |
| 4–7 | 200 | 6.906 | 4.382 | 1.00 | 6–7 | 0 | 16.000 | 0 | 0.00 |
| 5–7 | 200 | 8.064 | 4.704 | 1.00 | 3–7 | 174 | 16.288 | 0 | 0.87 |
| 2–1 | 100 | 4.602 | 3.733 | 1.00 | 1–7 | 75 | 17.810 | 0 | 0.75 |
| 6–5 | 100 | 3.089 | 0 | 0.67 | | | | | |

For mitigating the traffic queuing delay, the TCS can be carried out. Since the traffic flows in links 3, 4. and 5 are saturated, the travelers who path through these links should pay some credits. The convergence curve of designed relaxation algorithm is shown in Fig. 4. Meanwhile, the evolution processes of link flows are examined in Fig. 5. The Fig. 4 shows that the designed relaxation algorithm can converge to a high accuracy, after 2 s CPU time, the tolerance error is about 1E-5. The link flows can rapidly converge to equilibrium results as well.

The equilibrium traffic flows of PUE-CC model are shown in Table 3. The links 3, 4, and 5 should be charged 6, 7, and 5 credits, respectively. The travelers will reselect the shortest routes. Based on the principle of the amount of credits conservation, the total amount of credits is $K = \sum_a \kappa_a x_a = 1711$; the credit cost is $p = 0.53$. In this case, the total system delay is $\sum_a x_a(t_a(x_a) + d_a + p\kappa_a) = 11796$. Thus, the PUE-CC model can be used to design the tradable credit system which make the traffic flows reassign. And this model can ensure the traffic flows on the links all less than or equal to the road capacities; reduce the queuing delay effectively; decrease the total system travel time, improve the utilization efficiency of urban traffic roads; and mitigate traffic congestion.

**Fig. 4** Convergence of relaxation algorithm
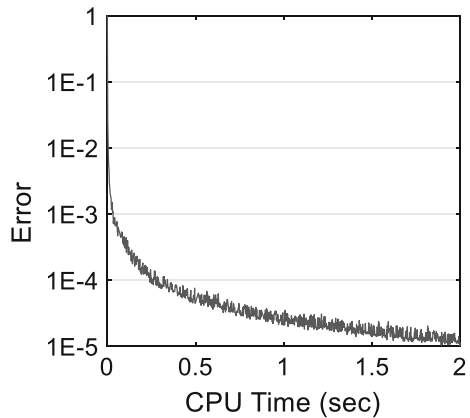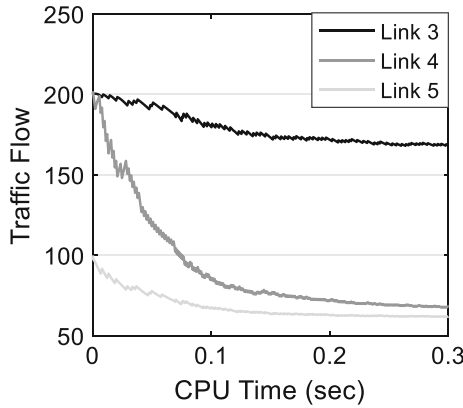
**Fig. 5** Evolution processes of link flows

**Table 3** Link equilibrium flows of PUE-CC model

| Link | $x_a$ | $\kappa_a$ | $t_a + d_a + p\kappa_a$ | $v/c$ | Link | $x_a$ | $\kappa_a$ | $t_a + d_a + p\kappa_a$ | $v/c$ |
|------|-------|------------|-------------------------|-------|------|-------|------------|-------------------------|-------|
| 1–4 | 151 | 0 | 6.292 | 0.75 | 3–4 | 82 | 0 | 5.067 | 0.55 |
| 1–5 | 62 | 0 | 5.007 | 0.31 | 2–6 | 94 | 0 | 10.231 | 0.63 |
| 4–7 | 162 | 6 | 12.185 | 0.81 | 6–7 | 139 | 0 | 16.560 | 0.69 |
| 5–7 | 62 | 7 | 13.552 | 0.31 | 3–7 | 107 | 0 | 15.184 | 0.54 |
| 2–1 | 61 | 5 | 9.081 | 0.61 | 1–7 | 88 | 0 | 18.529 | 0.88 |
| 6–5 | 77 | 0 | 3.031 | 0.51 | | | | | |

## 5 Conclusions

This chapter proposed UE-CC model, a new model that explicitly considers both TCS and capacity constraint in travelers' route choice decision process. Since UE-CC model could not obtain the total amount of credits, credit charges on each link and credit cost which are important planning control indexes in real engineering projects, PUE-CC model was presented. The analysis results indicated that (1) total system delay of PUE-CC model is less than that in traditional user equilibrium model with capacity constraints; (2) the relaxation algorithm is an effective method for solving the proposed PUE-CC model; and (3) the PUE-CC model can be used to design the tradable credit system and PUE-CC model can reduce the queuing delay effectively and mitigate traffic congestion.

# References

1. Xu Z, Jiang H (2016) Evaluation system for the sustainable development of urban traffic and ecological environment based on support vector machine. J Comput Theor Nanosci 13(10):6978–6981
2. Sun C, Cheng L, Zhu S et al (2017) Multi-criteria user equilibrium model considering travel time, travel time reliability and distance. Transp Res Part D: Transp Environ
3. Yang H, Wang X (2011) Managing network mobility with tradable credits. Transp Res Part B: Methodol 45(3):580–594
4. Bao Y, Gao Z, Xu M et al (2014) Tradable credit scheme for mobility management considering travelers' loss aversion. Transp Res Part E: Logistics Transp Rev 68:138–154
5. Han F, Cheng L (2017) Stochastic user equilibrium model with a tradable credit scheme and application in maximizing network reserve capacity. Eng Optim 49(4):549–564
6. Tian LJ, Yang H, Huang HJ (2013) Tradable credit schemes for managing bottleneck congestion and modal split with heterogeneous users. Transp Res Part E: Logistics Transp Rev 54:1–13
7. Nie YM, Yin Y (2013) Managing rush hour travel choices with tradable credit scheme. Transp Res Part B: Methodol 50:1–19
8. Fan W, Jiang X (2013) Tradable mobility permits in roadway capacity allocation: review and appraisal. Transp Policy 30:132–142
9. Grant-Muller S, Xu M (2014) The role of tradable credit schemes in road traffic congestion management. Transport Rev 34(2):128–149
10. Dogterom N, Ettema D, Dijst M (2017) Tradable credits for managing car travel: a review of empirical research and relevant behavioural approaches. Transport Rev 37(3):322–343
11. Song Z, Yin Y, Lawphongpanich S (2009) Nonnegative Pareto-improving tolls with multiclass network equilibria. Transp Res Rec: J Transp Res Board 2091:70–78
12. Song Z, Yin Y, Lawphongpanich S et al (2014) A Pareto-improving hybrid policy for transportation networks. J Adv Transp 48(3):272–286
13. Lawphongpanich S, Yin Y (2010) Solving the Pareto-improving toll problem via manifold suboptimization. Transp Res Part C: Emerg Technol 18(2):234–246
14. Wu D, Yin Y, Lawphongpanich S (2011) Pareto-improving congestion pricing on multimodal transportation networks. Eur J Oper Res 210(3):660–669
15. Liu Y, Guo X, Yang H (2009) Pareto-improving and revenue-neutral congestion pricing schemes in two-mode traffic networks. Netnomics 10(1):123–140
16. Nie YM, Liu Y (2010) Existence of self-financing and Pareto-improving congestion pricing: impact of value of time distribution. Transp Res Part A: Policy Pract 44(1):39–51
17. Guo X, Yang H (2010) Pareto-improving congestion pricing and revenue refunding with multiple user classes. Transp Res Part B: Methodol 44(8):972–982
18. Guo X (2012) Pareto-improving congestion pricing and revenue refunding with elastic demand
19. Xiao F, Zhang HM (2014) Pareto-improving toll and subsidy scheme on transportation networks. EJTIR 14(1):46–65
20. Chu Z, Chen H, Cheng L et al (2016) Pareto-improving hybrid policy with multiclass network equilibria. Transportation Research Board 95th annual meeting
21. Facchinei F, Pang JS (2007) Finite-dimensional variational inequalities and complementarity problems. Springer Science & Business Media
22. Rosenthal E (2008) GAMS-A user's guide. GAMS Development Corporation

# Calculation Model of Urban Rail Transit Share Rate Based on Game Theory

**Guo-zhu Cheng, Jun-feng Ma, Li-hui Qin, Li-xin Wu and Tian-jun Feng**

**Abstract** As a green, safe, fast, large-capacity, and sustainable public transit, urban rail transit can improve traffic congestion, environmental pollution, and other issues. In order to provide theoretical basis for the calculation of urban rail transit network scale, calculation model of urban rail transit (URT) share rate is established based on game theory between managers and travelers. To analyze the costs of managers and travelers, the model considers energy and environment cost for managers, and it selects economy, efficiency, and safety cost for travelers. To analyze the benefits of managers and travelers, it is assumed that managers' benefit is operating income, and travelers' benefit is comfort benefit, which is analyzed by structural equation method. Taking Harbin of China as case, this chapter introduces the specific calculation methods and steps, and the result shows that the reasonable share rate of URT is 18.26% for Harbin city. This method can provide references for transportation planning and it also has a certain application value for traffic operation environment improvement and energy conservation.

**Keywords** Urban rail transit · Energy cost · Environmental cost · Share rate Game theory

G. Cheng (✉)
School of Traffic, Northeast Forestry University, Harbin 150040, China
e-mail: guozhucheng@126.com

J. Ma
School of Transportation Science and Engineering, Harbin Institute of Technology, Harbin 150090, China

L. Qin
School of Water Conservancy and Civil Engineering, Northeast Agricultural University, Harbin 150030, China

L. Wu · T. Feng
School of Transportation Science and Engineering, Jilin Jianzhu University, Changchun 130118, China

People are increasingly concerned about economic benefits, pollution of the environment and service level of transportation. URT is a green, safe, fast, large-capacity, and sustainable public transit. It has been found that the energy consumption of URT is about one-tenth of car, and there are no harmful gases during the operation of URT. In China, the passenger volume of URT is about 13.8 billion in 2015. Regarded as an efficient tool to improve road traffic congestion, the URT system has been popularized in more and more Chinese cities.

At present, China is still in the exploration stage of URT construction, and there is blindness in URT planning, which will restrict the development of the city. In addition, at the first stage of "13th Five-Year" of China, there are 44 cities have got permission to build URT, and a new wave of URT construction is coming. It is necessary to carry out relevant research on URT share rate, and provide theoretical reference for URT planning.

The prediction of URT share rate is equivalent to the problem of travel mode split. Mcfadden presented a Logit model based on random utility from the perspective of disaggregate model [1]. Then, Naveen [2] used Logit model to calculate urban traffic structure from different angles, respectively. After that many scholars improved the LOGIT model and increased the complexity of the model. Liu T. L. used the continuous equilibrium model to describe the choice of commute travel mode [3]. Vij A. summarized the modeling method in the discrete selection model and proposed a hybrid model [4]. In fact, for the sustainable development of urban transport system, energy, and environmental factors should also be considered. So, it is not reasonable to consider from the angle of traveler only.

## 1 Analysis and Modeling of URT Share Rate

In urban transportation system, the competitors of URT are mostly private car, bus and taxi. Therefore, this study mainly focuses on share rate of these four travel modes. In China, traffic system construction is controlled by government. In the relationship between manager and traveler, manager is in a leading position and traveler is in a position to follow. First of all, manager will configure traffic resources preliminary. Then, travelers will choose transport modes according to the service level provided by traffic managers. Finally, the choice of traveler will affect the cost of manager conversely, and manager will optimize the configuration of transport facility based on traveler's feedback. In this chapter, Stackelberg game theory is used to establish bi-level programming model between managers and travelers.

Travel mode choosing is a probability problem. According to the weak law of large numbers, share rate of travel modes equals to travelers' choosing probability. In order to meet the sustainable development of urban transport, this chapter selects energy and environment indicators for manager. The cost of manager can be calculated by Eq. (1).

$$\min_{F_i} \text{RB} = \sum_{i=1}^{4} (\text{EN}_i + \text{WR}_i) - \sum_{i=2}^{4} \text{ET}_i,$$

$$\text{s.t.} \sum_{i=1}^{4} F_i \times H_i \geq O, \, F_i > 0 \tag{1}$$

where RB is manager's cost, CNY/d; $\text{EN}_i$ is energy cost, CNY/d; $\text{WR}_i$ is environmental cost, CNY/d; $\text{ET}_i$ is operating income, CNY/d; $F_i$ is operating frequency, times/d; $H_i$ is average passengers flow volume, p/time; $O$ is total travel demand of URT, bus, taxi and car, p/d; $i$ stands for four travel modes, from 1 to 4 for private car, taxi, bus, and URT.

When choosing travel mode, traveler always tries to select the most effective way. This chapter mainly considers the cost of traveler from three perspectives: economic, efficiency, and safety. The cost of traveler can be calculated by Eq. (2).

$$\min_{F_i, P_i} \text{RC} = \sum_{i=1}^{4} [(\text{EC}_i + \text{TC}_i + \text{CC}_i - \text{FC}_i) \times P_i] \times O,$$

$$\text{s.t.} \sum_{i=1}^{i=4} P_i = 1, \, P_i > 0 \tag{2}$$

where RC is traveler's cost, CNY/p; $\text{EC}_i$ is economic cost, CNY/p; $\text{TC}_i$ is efficiency cost, CNY/p; $\text{CC}_i$ is safety cost, CNY/p; $\text{FC}_i$ is comfort benefit, CNY/p; $P_i$ is share rate of the four travel modes.

## 2 Model Parameters Calibration

### 2.1 Managers' Cost

#### 2.1.1 Energy Cost

Energy refers to the resources consumed by vehicles. Motor vehicles mainly use gasoline, and URT relies on electricity to support. Energy cost can be calculated by Eq. (3). The unit energy consumption of different travel mode is shown in Table 1 [5].

$$\text{EN}_i = F_i \times H_i \times L \times e_i \times k, \tag{3}$$

where $L$ is average travel distance, km; $e_i$ is unit energy consumption, L/p/km; $k$ is unit price of energy, CNY/L.

| **Table 1** Energy consumption standards for all vehicles | Traffic modes | Energy consumption (kJ/p/km) | Corresponding gasoline (L/p/km) |
|---|---|---|---|
| | URT | 209 | 0.006 |
| | Bus | 670 | 0.018 |
| | Car | 2479 | 0.067 |
| | Taxi | 2479 | 0.067 |

### 2.1.2 Environmental Cost

The key to the calculation of air pollution cost is to obtain emission of pollutants and unit management cost. Pollutant management cost can be calculated by Eq. (4) [6]. Referring to previous studies,the cost of treatment for each pollutant and vehicle exhaust emission factor are shown in Table 2 [7] and Table 3 [8].

$$\text{WR}_i = F_i \times \sum_{j=1}^{4} \text{EF}_{ij} \times \text{CF}_j \times l, \tag{4}$$

where $\text{EF}_{ij}$ is emission factors of different pollutants of different travel modes, g/km; $\text{CF}_j$ is pollutant management costs, CNY/g; $l$ is average travel distance per time, km/time; $j$ stands for four main pollutants.

## 2.2 Travelers' Cost

### 2.2.1 Economic Cost

Economic cost has a great impact on the choice of travel mode. The cost of public transport can be regarded as ticket price corresponding to average travel distance. Private car's cost should include fuel cost, depreciation, parking fee, maintenance cost, etc., and it should be calculated according to specific circumstances.

| **Table 2** Treatment cost of each pollutant | Pollutant | NOx | HC | CO | PM |
|---|---|---|---|---|---|
| | Cost (CNY/g) | 16.68 | 3.79 | 13.47 | 1111.00 |

| **Table 3** Vehicle exhaust emission factor (*unit* g/km) | Emission factor | NOx | HC | CO | PM |
|---|---|---|---|---|---|
| | Private car/taxi | 0.408 | 0.149 | 1.027 | 0.024 |
| | Bus | 11.073 | 1.776 | 3.092 | 0.203 |

### 2.2.2 Safety Cost

Travelers' safety cost can be estimated based on the probability of traffic accident and accident loss. It can be calculated by Eq. (5).

$$CC_i = M \times CP_i, \tag{5}$$

where $M$ is average property loss of an accident, CNY; $CP_i$ is accident probability of each travel mode.

Comparing with other travel modes, URT has low traffic accident rate and it is a safer travel mode.

### 2.2.3 Efficiency Cost

Travel time includes both running time and waiting time. The efficiency cost can be obtained by monetization of travel time value. Running time is determined by average travel distance and speed. Waiting time of public transport is determined by its operating frequency. When operating frequency is high, waiting time will be short; conversely, waiting time will be long. The inverse relationship can be used to estimate the relationship between waiting time and operating frequency. Traveler's efficiency-cost can be calculated by Eq. (6)

$$TC_i = \left( \frac{L}{V_i} + \frac{TH}{F_i} \right) \times S_k \tag{6}$$

where, $V_i$ is average travel speed of each travel mode, km/h; TH is operating time of public transit, h/d; $S_k$ is travelers' unit time value, CNY/h.

## 2.3 Benefit Indicators

### 2.3.1 Operating Income of Manager

In the process of public transport operating, the income mainly comes from ticket revenue. Most of the revenues are invested in public transport operations, including power, labor, management, maintenance, and other expenses. According to the research, the net income of a common public transport line is about five percent of the ticket revenue [9]. Therefore, operating income can be calculated by Eq. (7).

$$ET_i = 0.05 \times O \times P_i \times f_i, \tag{7}$$

where $f_i$ is the ticket price of public transport, CNY.

### 2.3.2 Comfort Benefit of Traveler

Comfort is a comprehensive indicator of mental and physical. This study uses structural equation method (SEM) to evaluate travelers' comfort level based on survey data. Then, considering time value of passengers in different comfort conditions, comfort benefits of different travel modes are obtained. It can be calculated by Eq. (8).

$$FC_i = LEV_i \times MF, \tag{8}$$

where $LEV_i$ is traveler comfort level; MF is the benefit corresponding to different traveler comfort level. Based on relevant study, when traveler is in the most comfort level, corresponding comfort benefit is 15.2 CNY/h [10]. The benefit of each trip should be converted according to average travel time of different cities.

Structural equation model includes the measurement model and the structural model, it can be seen as follows:

$$x = A_x\xi + \delta, \ y = A_y\eta + \varepsilon \tag{9}$$

$$\eta = B\eta + \gamma\xi + \zeta, \tag{10}$$

where $x$ and $y$ are observed variables; $\xi$ is external variable; $\eta$ is internal variable; $\delta$ and $\varepsilon$ are error variables; $B$ is path coefficient of external variable to internal variable; $\gamma$ is load factor; and $\zeta$ is residual matrix.

Based on research results of comfort [11], this chapter constructs structural equation model to calculate traveler comfort benefit. The model was categorized into three influential factors as follows: perceived quality, facility level, and accessibility. It is impossible to measure the four latent variables directly. Therefore, a quantitative evaluation was conducted by setting up 12 measurement variables, which could assess these four factors indirectly. Figure 1 shows the structure of model.

Based on survey results, the hypothesis was tested by verifying the causalities among each latent variable and executing confirmatory factor analysis. Some cases were determined to be outliers (68 out of 500 cases). The outliers were removed to improve the reliability and validity of the model as well as to estimate a more correct factor loading value. By analyzing the comfort model using SEM, fitness indexes shown in Table 4 were generated. It can be seen that test indicators meet standard value, so the model is reasonable. Table 5 is load factors of variables.

## 3   Calculation of URT Share Rate

Previous studies show that the solution of bi-level programming is an NP-hard problem. Solutions to the problem of bi-level planning include genetic algorithm, penalty function method, fuzzy function method, and so on. However, most methods can only solve the local optimal solution. This chapter presents an approximate algorithm. The
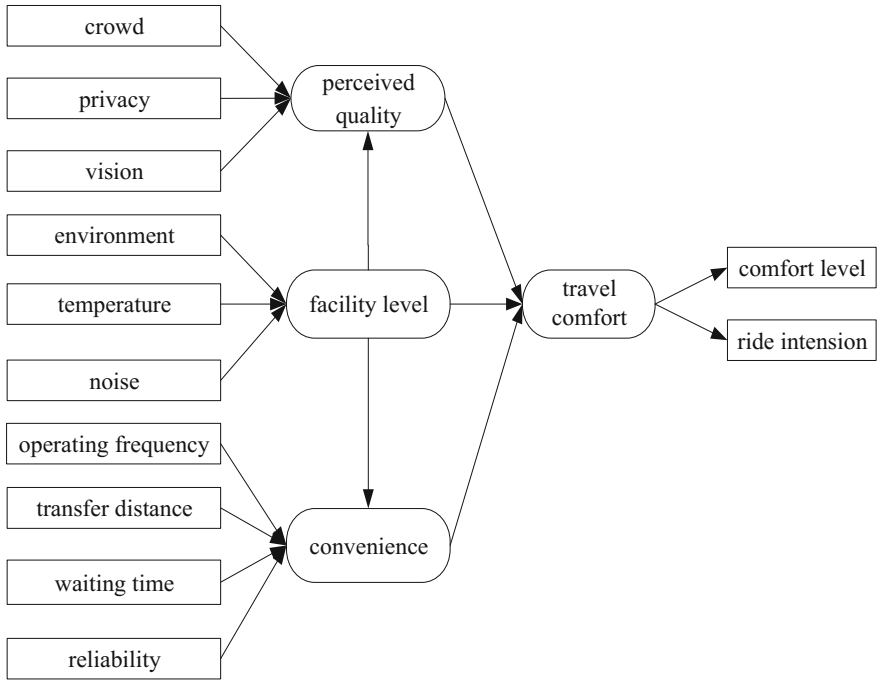
**Fig. 1** Structure of model

**Table 4** Fit statistics for SEM

| Indexes | Fitness indexes | Standard value |
|---|---|---|
| P | 0.056 | >0.05 |
| CMIN/DF | 1.463 | <3.00 |
| RMSEA | 0.046 | <0.08 |
| GFI | 0.944 | >0.90 |
| AGFI | 0.916 | >0.90 |
| CFI | 0.980 | >0.90 |
| NFI | 0.941 | >0.90 |

first step is solving upper layer function. Then, upper-level optimization objective can be regarded as a constraint condition of lower level function. Finally, the relative optimal solution of the lower layer function can be calculated. The result ensures that upper objective function is optimal and lower objective function is suboptimal. The expression is shown as Eq. (12).

**Table 5** Path coefficients of variables

| Relationship | | Path coefficients | | Relationship | | Path coefficients | |
|---|---|---|---|---|---|---|---|
| Convenience | <— | Facility level | 0.965 | Transfer distance | <— | Convenience | 0.834 |
| Perceived quality | <— | Facility level | 0.999 | Waiting time | <— | Convenience | 0.791 |
| Travel comfort | <— | Perceived quality | 0.849 | Reliability | <— | Convenience | 0.882 |
| Travel comfort | <— | Convince | 0.755 | Environment | <— | Facility level | 0.928 |
| Travel comfort | <— | Facility level | 0.625 | Temperature | <— | Facility level | 0.884 |
| Privacy | <— | Perceived quality | 0.729 | Noise | <— | Facility level | 0.726 |
| Crowd | <— | Perceived quality | 0.788 | Comfort level | <— | Travel comfort | 0.878 |
| Vision | <— | Perceived quality | 0.838 | Ride intension | <— | Travel comfort | 0.807 |
| Operating frequency | <— | Convenience | 0.834 | | | | |

$$\min_{P_i,F_i} RC = \sum_{i=1}^{4} [(EC_i + TC_i + CC_i - FC_i) \times P_i]$$

$$s.t. \begin{cases} \sum_{i=1}^{4} (EN_i + WR_i - ET_i) = RB(F_i^*, P_i^*) \\ \sum_{i=1}^{4} F_i \times H_i \geq O; F_i > 0; \sum_{i=1}^{i=4} P_i = 1, P_i > 0 \end{cases} \tag{12}$$

## 4 Case Study

### 4.1 Parameter Calibration

Harbin city, which is the capital of Heilongjiang province of China, is chosen as the case in this chapter. According to the traffic survey in 2015, urban population of Harbin is 4.74 million; travel intensity is 2.03 times/d; average travel distance is 6562 m; average travel time is 34 min; there are 3273 accidents happened per year, and the average loss of property for an accident was 14,400CNY. Calibrated model parameters are listed in Table 6.

According to average travel time of Harbin, the comfort benefit is 8.6 CNY/time. Dividing it into five levels, the benefits of different level can be seen in Table 7.

**Table 6** Calibrated model parameters

| Parameters | Private car | Taxi | Bus | URT |
|---|---|---|---|---|
| Speed (km/h) | 18.0 | 20.0 | 13.5 | 60.0 |
| Average amount of passengers (p/time) | 2.6 | 2.9 | 70.0 | 1000.0 |
| Economic cost (CNY) | 10 | 16 | 1 | 2 |
| Number of accidents | 2377 | 743 | 153 | 0 |
| Accident probability($10^{-5}$) | 2.0 | 2.6 | 2.3 | 0 |

As shown in Table 7, using structural equation can get the comfort level of various travel modes in Harbin, and benefits corresponding to different comfort level can be obtained using interpolation method according to Table 8. It can be seen that the comfort level of private car is the highest because of its convenience; URT also gets a higher comfort level mainly because of the speed and high frequency; the comfort level of taxi and bus are relatively low.

According to specific situation of Harbin, each variable was constrained. The optimal objective function of the manager is expressed as follows:

$$\min_{P_i, F_i} RB = 0.31F_1 + 0.50F_2 + 3.01F_3 + 0.02F_4 + 2400503P_2 + 150031P_3 + 300062P_4$$

$$\text{s.t.} \begin{cases} 2.6F_1 + 2.9F_2 + 70F_3 + 1000F_4 \geq 5001049 \\ 500000 < F_1 < 800000; 100000 < F_2 < 500000; 30000 < F_3 < 60000; 2000 < F_4 < 5000 \end{cases}$$

The traveler's objective function is as follows:

$$\min_{P_i, F_i} RC = 24.98P_1 + 31.72P_2 + 24.68P_3 + 1.55P_4 + 6000P_2/F_2 + 5625P_3/F_3 + 1875P_4/F_4$$

$$\text{s.t.} \begin{cases} P_1 + P_2 + P_3 + P_4 = 1, \ P_2 + P_3 + P_4 > 0.70 \\ 0.10 < P_1 < 0.50; 0.03 < P_2 < 0.15; 0.50 < P_3 < 0.60; 0.15 < P_4 < 0.35 \end{cases}$$

**Table 7** Comfort benefit of different level

| Comfort level | 1 | 2 | 3 | 4 | 5 |
|---|---|---|---|---|---|
| Benefit | 1.7 | 3.4 | 5.1 | 6.8 | 8.6 |

**Table 8** Comfort level and benefit of different kinds of motorized travel modes

| Coefficients | Private car | Taxi | Bus | Rail transit |
|---|---|---|---|---|
| Comfort level | 3.52 | 2.52 | 2.23 | 3.44 |
| Comfort benefit | 6.05 | 4.33 | 3.84 | 5.92 |

**Table 9** The share rate of these four kinds of travel modes

| Share rate (%) | Private car | Taxi | Bus | URT | Total |
|---|---|---|---|---|---|
| Current value | 15.43 | 2.27 | 29.54 | 2.27 | 50.00 |
| Planning value | 16.00 | 7.00 | 26.46 | 15.54 | 65.00 |
| Calculated value | 14.29 | 1.95 | 30.50 | 18.26 | 65.00 |

## 4.2 Calculation Results

LINGO software was used to solve the optimal solution of upper function. The result is shown in Table 9. At present, share rate of these four travel modes is 50%, but it will reach 65% in the forward planning. Therefore, the sum of four travel modes should be converted into 65%. The results of share rate are shown in Table 9. Compared with the calculation values, current and planning share rate of URT and bus are low, the share rate of private car is relatively high; It is suggested that increasing the share rate of URT and bus.

## 5 Conclusion

In this chapter, the game theory is used to describe the competition among private car, taxi, bus, and URT. Calculation model of URT share rate is established, and it takes energy and environment as main target. Finally, taking Harbin as an example, this chapter demonstrates the application of the model and gives the suggestions for the development of URT in Harbin.

## References

1. Mcfadden D (1987) A method of simulated moments for estimation of discrete response models without numerical integration. Econometrica 57(5):995–1026
2. Eluru N, Chakour V, El-Geneidy AM (2012) Travel mode choice and transit route choice behavior in Montreal: insights from McGill University members commute patterns. Public Transp 4(2):129–149
3. Liu TL, Huang HJ, Yang H et al (2009) Continuum modeling of park-and-ride services in a linear monocentric city with deterministic mode choice. Transp Res Part B Methodol 43(6):692–707
4. Vij A, Carrel A, Walker JL (2013) Incorporating the influence of latent modal preferences on travel mode choice behavior. Transp Res Part A Policy & Pract 54(54):164–178
5. Gangtian H (2003) Planning, construction and management of urban rail system—experience from Tokyo. Urban Mass Transit 6(3):1–7 (in Chinese)
6. Shi L, Wang QD, Fu ML (2009) Application of situation of residents travel to estimate vehicles emission of Beijing. J Beijing Technol Bus Univ 27(2):12–15 (in Chinese)

7. Zhou ZH, Cai M (2015) Comprehensive benefit evaluation of pedestrian bridge based on air pollutant cost factors of IPA. J Wuhan Univ Technol 39(1):97–101 (in Chinese)
8. Fan SB, Tian LD, Zhang DX et al (2015) Emission factors of vehicle exhaust in Beijing. Environ Sci 7:2374–2380 (in Chinese)
9. Ge HZ (2013) The administration of public transportation companies based on cost and benefit analysis (7):44–46 (in Chinese) (Shang Ye Jing Ji)
10. Li TY, Shao MH (2011) Comparison of the public transport time for passengers considering congestion. J Transp Sci Eng 27(3):82–86 (in Chinese)
11. Zhou J, Guo Y, Dong S et al (2016) Structural equation modeling for pedestrians' perception in integrated transport hubs. Procedia Eng 137:817–826

# Using Loop Detector Big Data and Artificial Intelligence to Predict Road Network Congestion

**Zhi-wei Guan, Xi-yao Liu, Ling Yang, Hong-lin Zhao, Xiao-feng Liu and Feng Du**

**Abstract** Understanding the temporal-spatial congestion evolution is important to mitigate traffic congestion and improve traffic efficiency. Most studies used floating car data to analyze the urban congestion, however, its market penetrate is low in many cities, thus the data is not enough in terms of quantity and coverage. Loop detector is the most frequently used sensor, its data has the attributes of long-term and large-scale coverage, and utilizing the loop detector big data is helpful to analyze the congestion evolution. Therefore, this study proposes a data-driven congestion analysis approach, which consists of loop detector data processing, traffic simulation, and artificial intelligence to predict the urban temporal-spatial congestion evolution. A case study in Tianjin, China is conducted, and the case study result shows that the evening peak has more serious traffic congestion than the morning peak, the prediction accuracy of feed forward back-propagation neural network (BPNN) increases with the time interval aggregation level increasing, and the prediction accuracy is 85.7% with 30 min interval aggregation.

**Keywords** Traffic congestion · Traffic big data · Artificial intelligence
Traffic simulation

## 1 Introduction

In recent decades, with the rapid development of motorization and the significant increase of urban population, traffic congestion has become a worldwide big-city issue. Traffic congestion causes a series of economic and social problems, such as

Z. Guan · X. Liu · H. Zhao · X. Liu · F. Du
School of Automotive and Transportation, Tianjin University of Technology and Education,
Tianjin 300222, China

L. Yang (✉)
School of Information Technology Engineering, Tianjin University of Technology and Education,
Tianjin 300222, China
e-mail: 335351859@qq.com

travel delay, fuel waste, air pollution, traffic accident, and so on. According to the 2015 Urban Mobility Report [1], drivers in America have suffered from a great loss due to traffic congestion, i.e., more than 3 billion gallons of fuel and nearly 7 billion extra hours in their vehicles. The total nationwide price incurred by traffic congestion is $160 billion, in other words, $960 per commuter. In Beijing, traffic operation is susceptible to holidays and severe weather, which always cause large-scale traffic congestion. On the mid-autumn day of 2015, the road performance index increased to 9.2, the average speed of the whole road network was only 19.6 km/h, and the evening peak hours ended until 10 pm [2]. In 2015, the peak hour congestion delay index of Beijing was 2.06, this means the actual travel time is twice that of free traffic flow, and the average speed was 22.61 km/h [3]. Meanwhile, intelligent transportation systems (ITS) have been constructed widely to mitigate traffic congestion and improve traffic efficiency, lots of traffic detectors have been used in two categories, i.e., fixed detectors (e.g., loop detector, video, infrared detector, and microwave detector) and mobile detectors (e.g., mobile phone, floating car, radio frequency identification, transit card, and unmanned aerial vehicle) [4–6].

In the past years, different methods using the data of different traffic detectors were proposed to predict road network congestion evolution for further traffic control and management. Qiu et al. [7] used the Vehicle Infrastructure Integration (VII) probe vehicle data and loop detector data and proposed a dual loop detector method combining with VII, and then the spatial-temporal speed and density were predicted. Rempe et al. [8] used five months of floating car data in Munich road network, proposed a congestion cluster identification approach to determine which degrees these clusters can represent the traffic congestion level of the road network. Kong et al. [9] estimated the urban traffic congestion based on the floating car trajectory data. Wen et al. [10] used multisource traffic data, such as floating car data, loop detector data, and other data to analyze the traffic congestion, and proposed a dynamic macroscopic index, i.e., traffic performance index, to reflect the spatial-temporal congestion evolution situation in Beijing. However, both the VII data and floating car data are collected by the mobile sensors, if the market penetration of these sensors is low, the data coverage and accuracy will be unacceptable, especially for small-size and medium-size cites because traffic budget is limited and the market penetration of mobile traffic sensors is low in these cities.

Compared with other sensors, loop detector is the most commonly used traffic sensor to collect continuous traffic data at the fixed traffic site, it always works with the traffic signal control system (e.g., SCATS and SCOOT system). Moreover, the loop detector data always covers large-scale urban area and its quantity is massive for a long-term time period, which is crucial for temporal-spatial congestion evaluation and prediction. In addition, big data and artificial intelligence have gained great academic, industrial and governmental attention in recent years. It is said that they will have an immense impact on how people travel and how government manages the traffic flow, and they are a promising option to evaluate the urban traffic congestion and predict the dissemination of traffic congestion. Generally, due to the low market penetration of mobile traffic sensors, the large-scale coverage and long-term data collection of loop detector, it is promising to use loop detector big data

to evaluate the urban temporal-spatial congestion evolution. In addition, traffic congestion is susceptible to road infrastructure, traffic flow, weather, and holiday, and it is a complex and nonlinear problem to predict traffic congestion, which is a tough task for traditional mathematical methods. Therefore, this study aims to propose a data-driven congestion analysis approach, uses loop detector big data and artificial intelligence to predict the urban temporal-spatial congestion evolution.

## 2  Network Speed Acquisition

Loop detectors are always installed at the intersection stop lines and road segments, to collect specific traffic flow parameters, such as volume, occupancy, and speed. Speed is the direct and effective indicator to measure the traffic congestion status. However, the performance of loop detector is susceptible to heavy traffic and pavement distress, which may lead to low-quality traffic detection, such as data inaccuracy and data missing. In this context, it is necessary to check the original detection data of loop detectors and improve the data quality. An example of loop detector data in Tianjin City, China was shown in Fig. 1, and the traffic volume is collected at 5 min interval, the morning peak hour is from 7:50 am to 8:50 am, the afternoon peak hour is from 4:50 pm to 5:50 pm, the total daily volume is 6247 vehicles, and the volume data from 11:55 pm to 12:00 am is missing. Regarding the missing and inaccurate data, the average value of 3 to 5 previous traffic volume data can be used to substitute the missing data.

```
AM Total:   2603    AM peak   465 07:50 - 08:50

          12:   13:   14:   15:   16:   17:   18:   19:   20:   21:   22:   23:
    :05    40    22    18     0    39    48    21    27    22    21    27    12
    :10    21    25    33     0    38    40    38    18    26    30    35    21
    :15    34    22    17     0    46    31    37    22    19    24    11    13
    :20    26    25    40     0    31    24    20    12    35     4    18    17
    :25    24    35    44     2    33    33    23    42    25    33    29    12
    :30    50    34    41    33    31    32    29    46    20    28    16    16
    :35    24    43    45    23    23    41    13    40    30    34    22    11
    :40    21    35    29    40    33    37    40    30    28    18    14    11
    :45    18    21     9    19    35    64    26    29    26    21    16    14
    :50    25    19     0    34    14    31    39    24    23    34    21    11
    :55    31    19     0    46    25    23    31    18    25    30    20    14
    :60    21    23     0    21    27    24    44    35    17    21    10     -
Hourly
Total    335   323   276   218   375   428   361   343   296   298   239   152

PM Total:   3644    PM peak   433 16:50 - 17:50

Daily Total  6247
```

**Fig. 1**  Loop detector data

In addition, only the volume data is recorded due to the insufficient traffic investment and faulty traffic data management. As the absence of other traffic parameters, particularly for speed, it is difficult to evaluate the traffic congestion evolution. In this situation, it is an alternative to convert traffic volume to speed by traffic simulation as the following reasons: (1) traffic simulation has its unique advantages, such as economic efficiency, safety, repeatability, the ease of use, and controllability; (2) traffic simulation is a useful tool to measure and analyze the operation of complex traffic system without utilizing mathematical models; and (3) calibrated traffic simulation model can reach a high accuracy as much as 90% or more. Therefore, VISSIM-based traffic simulation method is proposed to acquire the speed by using the related traffic data, the proposed method is shown in Fig. 2.

As Fig. 2 shows, there are six steps to conduct speed-oriented simulation as follows: (1) draw the links in the VISSIM software and each link represents a road segment, and make the links connected to form some intersections; (2) set the traffic route and volume of entry lanes in the intersection, and deploy traffic detectors at the given distance interval; (3) set the road deceleration zone, especially on the intersection corner, and adjust the default software parameters according to the real-life traffic data, such as desired vehicle speed, deceleration/acceleration velocity, traffic composition, and so on; (4) set the intersection signal time schemes, including cycle length, phase, offset, green time, and so on; (5) establish and calibrate the traffic simulation model; and (6) output the simulated speed data.

**Fig. 2** Speed-oriented simulation flowchart
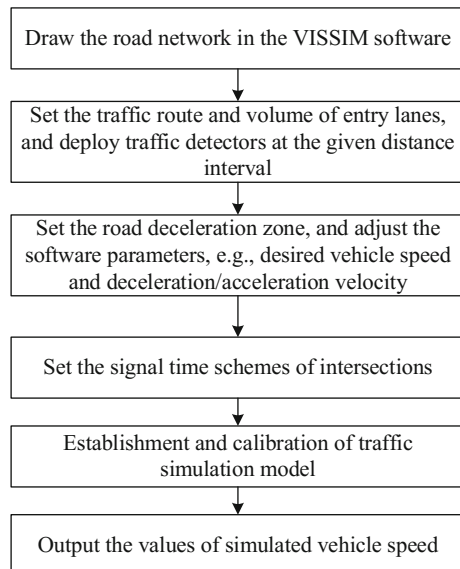
## 3  Network Congestion Representation

Travel speed of each link can be obtained by the aforementioned traffic simulation, and then traffic congestion threshold is set at different speed levels. Once the link speed is lower than the threshold, the link is considered to be congested. As each link faces the congestion evolution, uncongested and congested, a binary variable is introduced to represent the link congestion situation, i.e., 1 represents the status of traffic congestion, and 0 represents the uncongested situation. In addition, link congestion situation is relevant to the different time periods, e.g., morning hours and evening hours, weekdays and weekends, therefore, a time sequence is used to measure the link congestion evolution with a time interval. For example, the time interval is set at 30 min, i.e., each link has 2 congestion status per hour, and 48 congestion status per day. Furthermore, road network consists of different links, each link has its congestion status, thus matrix is adopted, and the matrix rows are used to represent different links. Accordingly, the congestion status of a road network with n links and t time intervals can be represented as follows:

$$
\begin{bmatrix}
x_1^1 & x_1^2 & \ldots & x_1^t \\
x_2^1 & x_2^2 & \ldots & x_2^t \\
\ldots & \ldots & \ldots & \ldots \\
x_n^1 & x_n^2 & \ldots & x_n^t
\end{bmatrix},
\tag{1}
$$

where there are $n$ links, and $x_n^t$ is a binary number and represents the congestion status of the nth link at time $t$. Based on the link congestion matrix in different periods, the congestion status of road network can be predicted.

## 4  Traffic Congestion Evolution Prediction

As the congestion forecasting of road network is a high-dimensional time sequence learning problem, this is hardly solved by traditional computational methods. In recent years, artificial intelligence and machine learning have gained quite a lot of concerns, they can deal with the problems that are most difficult to solve by traditional methods. Feed forward back-propagation neural network (BPNN) is one of the frequently used artificial intelligent methods. Therefore, BPNN is adopted to predict the traffic congestion in this study. BPNN consists of three layers and imitates the human brain's functions. The input layer is the congestion status matrix of road network in a given time period, then these signals of the input layer is multiplied by some weight value and summed, next, signals propagate through the hidden layers to the output layer. The output layer is the congestion status of designated links in a designated time periods. In addition, input signals from previous neurons are

weighted individually and summed, and then the output signals are passed on to the neurons of the next layer.

The procedure of BPNN learning can be described as follows: First, some of the training cases (i.e., the road network traffic congestion matrix in a given time period) are applied to the neural network, and the network generates some output according to the current synaptic weights. Then, the output is compared with the known output and the mean-squared error is calculated, and the error is propagated backward and the synaptic weights make small changes in each layer in order to reduce the error value. The process is repeated again until the total error decreases below the predefined threshold. Next, the neural network is said to be trained well and the data of learning case is applied to the trained-well neural network. Finally, the learning result is obtained (i.e., the predicted traffic congestion matrix in a designated time period). In the above process, the following parameters should be determined: the size of neural network, the transfer functions of input, hidden and output layer, and the error value. As to the traffic congestion evolution prediction, the input is the congestion status matrix of given time period, i.e., formula (1), and the output is the congestion status of designated time period.

## 5   Case Study

A road network with 23 links in Tianjin, China is used to illustrate the proposed data-driven congestion analysis approach. The loop detector data was collected from May 4, 2015 to June 5, 2015, i.e., weekdays in 5 weeks, the data was updated every 5 min, and there were 921, 600 volume records. Data quality improvement method is used to substitute the missing and inaccurate traffic data, and each link corresponds to a road segment. As only the traffic volume and intersection signal time schemes are available in the urban traffic control system, VISSIM-based traffic simulation is conducted to obtain the link speed according to the method in Sect. 2. In order to evaluate the congestion prediction performance, these loop detector data are aggregated at 5, 15, and 30 min, respectively. In addition, the data of the first four weeks is used to train the BPNN, and the remaining data is used for testing neural network.

### 5.1   Simulation Analysis

Traffic simulation is conducted to obtain the link speed by using VISSIM software, and one intersection simulation is shown in Fig. 3, which includes the scenarios of four signal phases. In addition, the link speed can be acquired through the simulation, and the spatial-temporal congestion evolution of one direction of the intersection is depicted in Fig. 4. As Fig. 4 shows, the morning peak hour is approximately from 7:30 am to 8:30 am, and the evening peak hour is approximately from 5:50 pm to

(a) phase 1                                             (b) phase 2

(c) phase 3                                             (d) phase 4
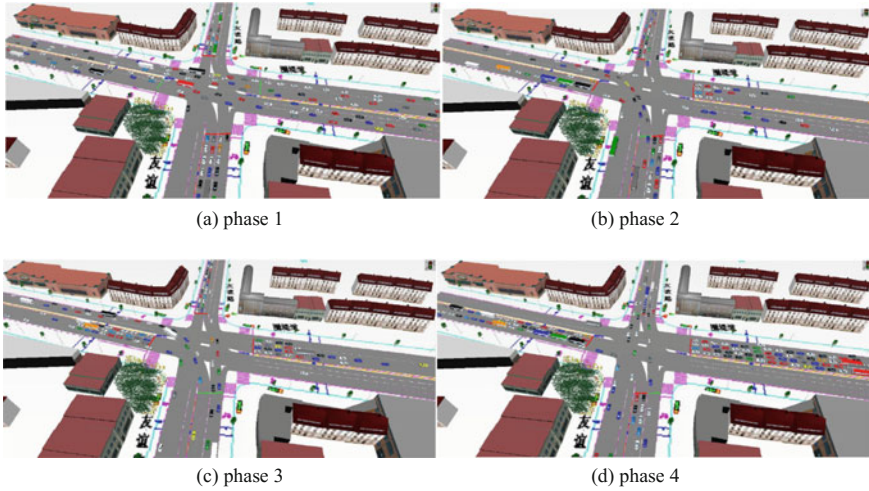
**Fig. 3** Intersection simulation scenarios



(a) morning congestion distribution          (b) evening congestion distribution
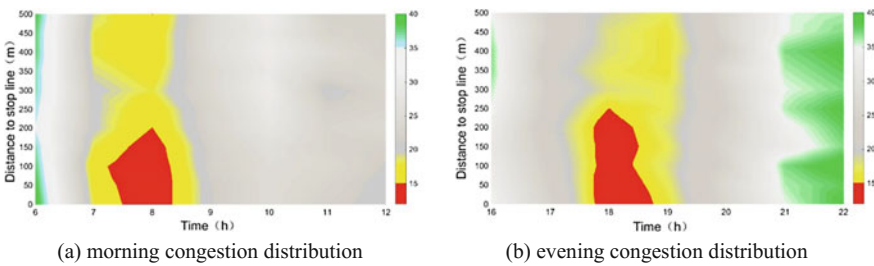
**Fig. 4** Traffic congestion evolution of the intersection

6:50 pm, and the traffic speed is below 15 km/h. Moreover, the maximum queuing length of morning peak and evening peak is about 200 and 250 m, respectively. This indicates that the evening peak has more serious traffic congestion than the morning peak.

## 5.2 Prediction Analysis

Loop detector data with three different aggregation levels are tested using the BPNN model and the trained model is used to predict traffic congestion evolution. The parameters of BPNN model are set as follows: the number of input, hidden and output unit is 1, 20, and 1, respectively; three transfer functions are adopted in the input, hidden and output layer, respectively, i.e., tansig, tansig, and purelin; the number of iterative epochs is 200; the learning rate is 0.05; and the goal error is 0.005. Loop

detector data of the first four weeks is used to train the BPNN model, and the data of the fifth week is used to test the model.

The BPNN model was implemented at the MATLAB platform and executed for 20 times to ensure the model convergence. Then, the actual and predicted data of the fifth week are compared and the comparison result is listed in Table 1. Table 1 shows that the traffic congestion prediction accuracy increases with the aggregation time interval increasing from 5 to 30 min, the reason may be that the time interval becomes longer, the traffic flow fluctuation becomes smaller, and the prediction accuracy is improved. Furthermore, based on the trained BPNN model, the road network congestion evolution situation of the fifth week can be predicted, and each link has a binary congestion status. Then, the temporal-spatial congestion evolution can be displayed on the graphic map. The congestion evolution of June 5, 2015 is depicted in Fig. 5. In Fig. 5, the congestion threshold is 15 km/h, the links with speed lower than 15 km/h are marked in red, and the links with speed greater than 35 km/h are marked in green. Meanwhile, Figure indicates that it is more congested during evening peak hours compared with morning peak hours, and the congestion begins to dissipate after 9:00 pm because less passengers and vehicles engage in traffic activities since then.

## 6  Conclusions

This study proposed a data-driven method to understand the temporal-spatial congestion evolution. The study case shows that the evening peak suffers more serious traffic congestion than the morning peak, in addition, the prediction accuracy of BPNN increases with the time interval aggregation level increasing, and the prediction accuracy is 85.7% when the time interval aggregation level is equal to 30 min. Furthermore, other deep learning algorithms can be adopted to predict the traffic congestion evolution so as to improve the prediction accuracy.

**Table 1** Comparison of traffic congestion prediction with different aggregation levels

| No. | Aggregation level (min) | Prediction accuracy (%) |
|---|---|---|
| 1 | 5 | 75.8 |
| 2 | 15 | 81.4 |
| 3 | 30 | 85.7 |



(a) from 7:30AM to 8:30AM   (b) from 5:50PM to 6:50PM   (c) from 9:00PM to 10:00PM
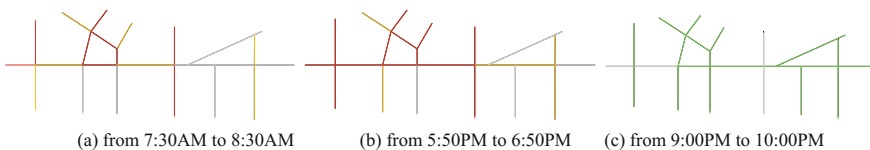
**Fig. 5** Congestion evolution situation using prediction data of June 5, 2015

# References

1. Schrank D, Eisele B, Lomax T (2015) TTI's 2015 urban mobility report. In: Proceedings of the 2015 annual urban mobility report, Texas A&M Transportation Institute, Texas, USA
2. China news net. Road network performance index increased to 9.2 in Beijing City [EB/OL] (2015-09-25). http://news.sina.com.cn/c/2015-09-25/doc-ifxieynu2298438.shtml
3. Amap company (2015) Traffic operation analysis report of Chinese big cities in 2015. Beijing, China
4. Niu XY, Liang D, Song XD (2014) Understanding urban spatial structure of Shanghai Central city based on mobile phone data. Urban Planning Forum 6:61–67 (In Chinese)
5. Chen J, Yang DY (2013) Estimating smart card commuters' origin-destination distribution based on APTS data. J Transp Syst Eng Inf Technol 13(4):47–53 (In Chinese)
6. Liu XF, Guan ZW, Song YQ, Chen DS (2014) An optimization model of UAV route planning for road segment surveillance. J Central South Univ 21(6):2501–2510
7. Qiu TZ, Lu XY, Chow HF (2009) Real-time density estimation on freeways with loop detector and probe data. In: Proceedings of the 12th IFAC symposium on transportation systems, USA, pp 298–303
8. Rempe F, Huber G, Bogenberger K (2016) Spatio-temporal congestion patterns in urban traffic network. Transp Res Procedia 15:513–524
9. Kong XJ, Xu ZZ, Shen GJ, Wang JZ, Yang QY, Zhang BS (2016) Urban traffic congestion estimation and prediction based on floating car trajectory data. Future Gener Comput Syst 61:97–107
10. Wen HM, Sun JP, Zhang X (2014) Study on Traffic congestion patterns of large city in China taking Beijing as an example. Procedia-Soc Behav Sci 138:482–491

# Traffic Performance Comparison of Short-Term and Long-Term Driving Restriction Policy—A Case Study of Tianjin, China



**Xiao-feng Liu, Zhi-wei Guan, Jie Geng, Jin-jian Xiao and Li-mei Gao**

**Abstract** Few research studied the effects of short-term and long-term driving restriction policy. Aiming to this gap, Tianjin City, China was taken as an empirical example to evaluate the effects of the two policies in this study. First, traffic survey of several segments and intersections was conducted to compare their traffic volume before and after the implementation of driving restriction policy. Then, a revealed preference-based survey was conducted to evaluate the policy effects. The case study indicates that the long-term driving restriction policy has transferred massive passenger flow into the public transport system, but it is only effective to reduce traffic volume in short-term; some traffic flow transfers to the weekends and the hour preceding the restriction time; rule-breaking behavior is pervasive for the short-term driving restriction policy; and the short-term earns high marks than the long-term policy. Additionally, some countermeasures were provided to improve the effects of the driving restriction policy.

**Keywords** Driving restriction policy · Policy evaluation · Traffic analysis

## 1 Introduction

Rapid motorization and urbanization have caused worldwide traffic congestion in many countries. Due to traffic congestion, the US economic loss was $160 billion in 2015, with more than 3 billion gallons of fuel consumption and approximately 7 billion extra hours delay [1]. In 2015, the peak hour congestion delay index of Beijing was 2.06, and the average speed was 22.61 km/h [2]. In this situation, different driving restriction policies were proposed to mitigate the traffic congestion and reduce air

X. Liu · Z. Guan (✉) · J. Geng · J. Xiao
School of Automotive and Transportation, Tianjin University of Technology and Education, Tianjin 300222, China
e-mail: zhiwguan@163.com

L. Gao
Traffic Science Research Institution of Tianjin City, Tianjin 300074, China

pollution. In 1975, Singapore began to conduct the licensing scheme in an area with
7.5 km$^2$. During the peak hours, vehicles entering this area need to have a permission
license, except transit bus and emergency vehicles. In 1995, Singapore conducted a
road pricing scheme, and vehicles were charged when they were on the designated
roads. After the implementation of driving restriction policy, the number of private
cars used decreased, and more people transferred to the public transport system [3].
In 2003, London conducted a traffic congestion charging scheme in the downtown
area with 22 km$^2$. In the early months of this policy, the travel speed increased from
8.69 to 10.56 miles/h, the traffic congestion level reduced by 30%, however, in 2006,
the downtown area suffered from traffic congestion as before [4]. In China, Beijing
limits the annual sale number of new cars, i.e., no more than 240,000 vehicles per
year, in addition, a one-day-one-week driving restriction scheme has been conducted,
which expects to take off approximately 20% of cars off the road on every weekday.

As to the performance evaluation of driving restriction policy, some studies ana-
lyzed the benefits/costs of driving restriction policy and discussed the sensitivity
of different factors on policy evaluation [5–7]. On the other hand, some empirical
studies focused on the before and after comparison of the policy implementation.
Song et al. took the 2008 Beijing Olympic Games as an example, conducted a taxi
questionnaire survey before and after the Games, and found that the taxi occupancy
rate increased significantly during the Olympic Games period [8]. Gallego et al.
looked at the driving restriction program in Mexico and the public transport reform
in Santiago, they found that the effects of the policies varied across income groups
widely, and the driving restriction can still be effective in a short time period, in first
several months [9]. Grange and Troncoso quantified the effects of vehicle restriction
on private and public transport flows in Santiago, Chile, they found that the perma-
nent vehicle restriction did not reduce vehicle flow, and the traffic flow increased
about 3.5% during the two hours preceding the driving restriction [10].

In summary, the abovementioned research aimed to the long-term policy and
studied the implementation effects of driving restriction policy. Actually, short-term
driving restriction policy has also been conducted for some great events (e.g., the 2008
Beijing Olympic Games, the 2016 Hangzhou G20 Submit), which has some different
traffic effects. However, the traffic performance difference between the short-term
and long-term driving restriction policy is seldom studied. Therefore, this study
takes Tianjin City, China as an example, conducts traffic survey and questionnaire
survey of short-term and long-term driving restriction policy, and aims to evaluate the
effects of the two policies and provide some suggestions for the traffic management
department.

## 2 Driving Restriction Policy

### 2.1 Short-Term Driving Restriction Policy

In this study, if the driving restriction policy was conducted for less than three months, it was defined as short-term policy; and if the driving restriction policy was conducted for more than one year, it was defined as long-term policy. In 2013 and 2014, a short-term and long-term driving restriction policy were conducted in Tianjin City, respectively. The former was used particularly for the 6th East Asian Games, and the latter was conducted to mitigate traffic congestion and reduce air pollution. In 2013, Tianjin City held the 6th East Asian Games from October 6 to October 15, and more than two thousands of athletes participated in this Game.

In order to make the traffic system operate smoothly, Tianjin conducted a 5-days driving restriction policy for several roads on October 8, 9, 10, 11, and 14 (October 12 and 13 were the weekends, and the policy did not work at weekends). The restriction roads were marked in blue and traffic rules were listed in Fig. 1, i.e., once the tail number of vehicle license plate was the same with the designated regulation number, this vehicle was not permitted to drive on these restriction roads, otherwise, the drivers would be punished. For example, on October 8, vehicles with tail number 8 and 9 were not allowed to run on the restriction roads. Similarly, on October 14, vehicles with tail number 0 and 1 were not allowed to drive on the restriction roads.

### 2.2 Long-Term Driving Restriction Policy

Since March 1, 2014, Tianjin has implemented a long-term driving restriction policy to mitigate the serious traffic congestion and the increasing air pollution. The restric-



**Fig. 1** The restriction roads, and the restriction tail number of license plate for short-term driving restriction policy

**Table 1**  Comparison of segment traffic volume with short-term policy

| No. | Road segment | Pre-policy (pcu) October 8 | Post-policy (pcu) October 15 | Decrease degree (%) |
|---|---|---|---|---|
| 1 | Yingshui road (West–East) | 3163 | 2961 | −6.39 |
| 2 | Fukang road (West–East) | 3422 | 3183 | −6.98 |
| 3 | Weidi road (East–West) | 3496 | 3420 | −2.17 |

tion region covered the urban area inside the outer ring road, which was greater than 300 km². Additionally, during the time period from 7:00 am to 7:00 pm on weekdays, a one-day-a-week driving restriction scheme was conducted, in which 20% of cars were expected to be off the roads. For example, vehicles with tail number 1 and 6, were not allowed to drive inside the outer ring road on Monday.

## 3   Traffic Survey and Comparison

In 2013, the short-term driving restriction policy was implemented on October 8, and the policy expired on October 15. Thus, traffic survey was conducted on October 8 and 16, respectively, to compare the traffic performance of pre- and post-policy. Videos were used to record the traffic volume of road segments from 7:30 am to 8:30 am. The comparison of segment traffic volume was shown in Table 1. As Table 1 shows, during the time period of short-term driving restriction policy, the traffic volume decreased slightly, the maximum decrease degree was 6.98%, and the minimum decrease degree was only 2.17%. Theoretically speaking, traffic volume was supposed to reduce by nearly 20% according to the one-day-a-week restriction scheme. There may be two reasons accounting for this gap. The first reason was that many drivers did not know the policy, so they did not obey the traffic regulation. It was reported that more than five thousands of vehicles broke the driving restriction policy at that time. The second reason was that some regulated vehicle owners did not follow the driving restriction policy because their destinations were far from the city center or public transport stations, thus they "illegally" violated the traffic regulation with an "acceptable" punishment cost. As to the long-term policy, traffic survey was conducted on February 18 and March 13 of the year 2014, and on April 20 of the year 2017, respectively. Videos were used to record the traffic volume of road segments from 5:30 pm to 6:30 pm. The comparison of segment traffic volume was shown in Table 2.

As Table 2 shows, at the early months of long-term driving restriction policy, the maximum decrease degree was 15.99% at Weidi road (East–West), the minimum decrease degree was 2.89% at Nanjing road (North–South). As Weidi road was the urban arterial road connecting the east region with the west region, its flow decreased significantly. While Nanjing road located at the central business district, the commercial traffic flow was high, thus its volume just decreased slightly. However,

**Table 2** Comparison of segment traffic volume with long-term policy

| No. | Road segment | Pre-policy (pcu) Feb 18, 2014 | Post-policy (pcu) March 13, 2014 | Post-policy (pcu) April 20, 2017 |
|---|---|---|---|---|
| 1 | Dagu Nan road (West–East) | 3526 | 3367 (−4.51%) | 4428 (+25.58%) |
| 2 | Dagu Nan road (East–West) | 3636 | 3288 (−9.57%) | 3914 (+7.65%) |
| 3 | Nanjing road (North–South) | 2218 | 2154 (−2.89%) | 2297 (+3.56%) |
| 4 | Nanjing road (South–North) | 2374 | 2261 (−4.76%) | 2302 (−3.03%) |
| 5 | Weidi road (East–West) | 3228 | 2712 (−15.99%) | 2188 (−32.22%) |
| 6 | Weidi road (West–East) | 3374 | 3132 (−7.17%) | 2774 (−17.78%) |
| 7 | Weijin road (North–South) | 3155 | 2950 (−6.50%) | 2574 (−18.42%) |
| 8 | Weijin road (South–North) | 3142 | 2958 (−5.86%) | 3024 (−3.76%) |

*Note* The number in the brackets is the increase/decrease degree of traffic volume

the driving restriction policy seems to be not effective in long-term. The volume of Dagu Nan road (an urban freeway) increased significantly, and its travel speed was more than 40 km/h. In addition, the volume of Weidi road and Weijin road (North–South) decreased greatly with the travel speed decreasing, this indicates that these segments become more congested than before.

## 3.1 Comparison of Intersection Traffic Volume

Nine intersections in different urban districts were surveyed in 2014 and 2015, respectively [11], to compare the traffic performance of pre- and post-policy. The traffic volume comparison of long-term policy was shown in Fig. 2.

On weekdays, as Fig. 2 shows, traffic volume of seven intersections increased, only two decreased from 6:00 am to 7:00 am; at morning peak hours from 7:00 am to 9:00 am, traffic volume decreased at 7 intersections, and increased at two intersections; during the time period from 7:00 am to 7:00 pm, seven intersections had smaller volume, and the remaining had greater volume. On weekends, most intersections had greater volume. In summary, different intersections had different traffic flow characteristics, most intersections had smaller volume during the restriction time period, and the traffic flow of most intersections was brought forward to the hour preceding the restriction, i.e., the average volume of one hour preceding the restriction increased about 7.66%, additionally, the traffic flow of most intersections was postponed to the weekends, thus most intersections became more congested at the weekends, i.e., the average volume of weekends increased about 8.10%.
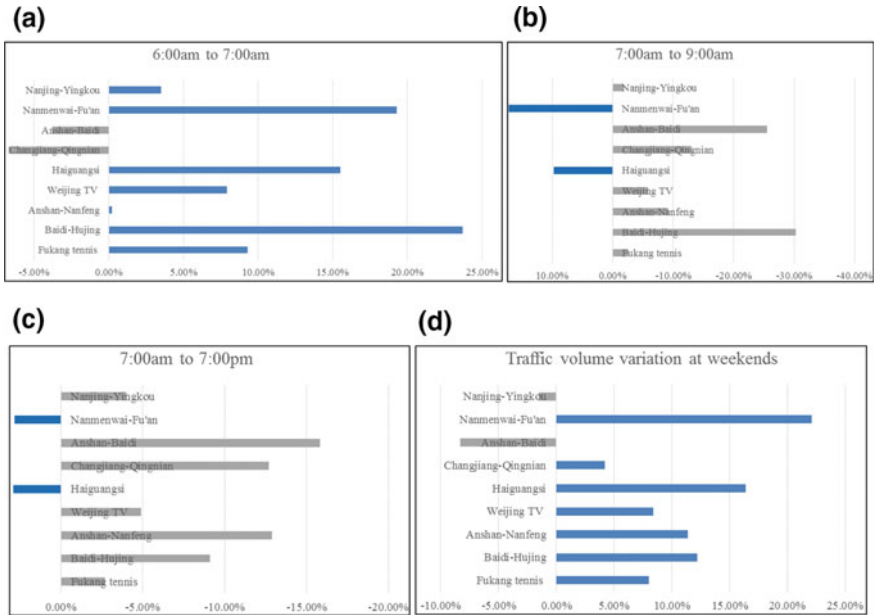
Fig. 2 Traffic volume comparison of long-term policy, **a** comparison at weekdays from 6:00 am to 7:00 am, **b** comparison at weekdays from 7:00 am to 9:00 am, **c** comparison at weekdays from 7:00 am to 7:00 pm, and **d** comparison at weekends

## 3.2 Comparison of Traffic Mode

In order to evaluate the effects of short-term and long-term driving restriction policy, a revealed preference-based survey was conducted in terms of respondents' information, traffic modes, evaluation score and policy suggestions in 2014. Due to the limited budget, 700 questionnaires were sent out and the response rate was 91%. The comparison of traffic mode was shown in Fig. 3. It can be seen from Fig. 3 that the percentage of car use decreased from 25.64 to 17.53%, the percentages of subway, bus, e-bike, carpool, and taxi increased, while the percentages of bike and walk remained almost unchanged. That is to say, long-term driving restriction policy has made great role in transferring massive passenger flow into the public transport mode.

## 4 Evaluation of Driving Restriction Policy

In the abovementioned questionnaire survey, 52% respondents were male, 48% were female; 3% respondents were under 18 years old, 44% aged from 18 to 35, 36% aged from 35 to 45, 15% aged from 45 to 60, and 2% were over 60 years old. As to family
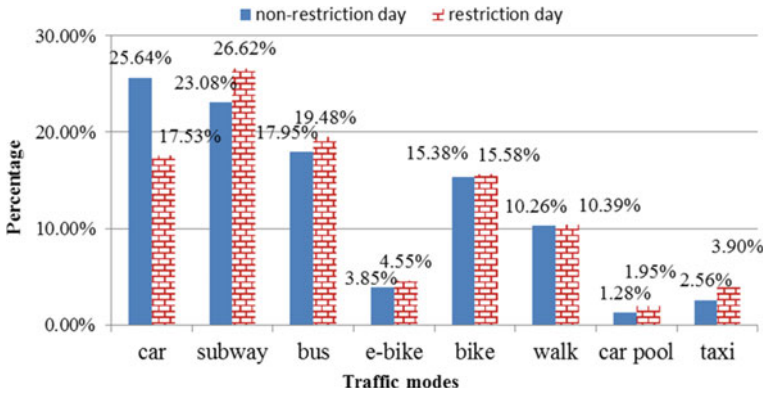
**Fig. 3** Traffic mode comparison with/without long-term policy

annual income, 15% families earned less than 50,000 RMB, 14% earned more than 150,000 RMB; 23%, and more than 90% respondents knew the short-term and long-term driving restriction policy, respectively. In addition, respondents were asked to give their scores to the two driving restriction policies. The scale used in this survey ranged from 0 to 100 scores, 0 represented the worst evaluation and 100 represented the best evaluation. The score result was shown in Fig. 4.

As to the short-term policy, 74% respondents marked scores higher than 80, and 26% respondents marked scores lower than 80. As to the long-term policy, 61% respondents marked scores higher than 80, which was much lower than the short-term policy. 39% respondents marked scores lower than 80, which was much higher than the short-term policy. In other words, with the restriction time extending and restriction region expanding, more respondents gave a low mark for the long-term policy. Furthermore, the increasing travel cost will put down the evaluation scores
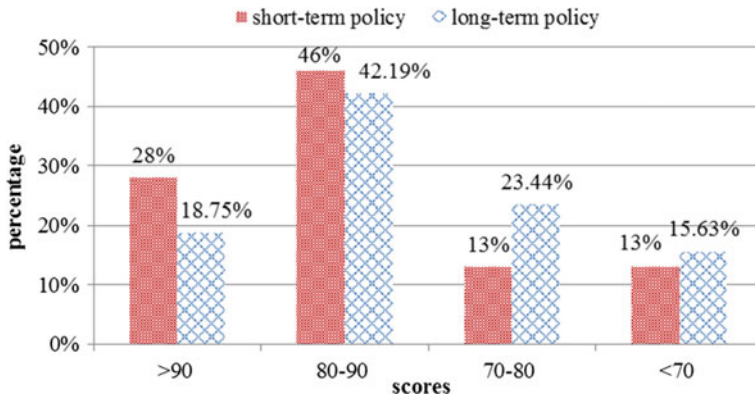


**Fig. 4** Policy evaluation

of commercial respondents. Proponents, especially for respondents without a car, said that it is necessary to conduct long-term driving restriction policy for traffic congestion mitigation and air pollution reduction, most of them hoped that their travel time could be reduced and the crowded situation of public transport system could be improved. However, opponents thought that the driving restriction policy deprived their rights to drive, and increased their purchase and car-use cost.

## 5    Conclusions and Discussions

The comparison and analysis of traffic survey and questionnaire survey demonstrates that: (1) the short-term driving restriction policy is effective to reduce traffic volume, while the long-term driving restriction policy is only effective in the first several months because the amount of civilian vehicles and traffic trip demand will increase rapidly in the forthcoming years; (2) some traffic flow starts earlier in the morning due to the driving restriction, and the traffic volume increased about 7.66% during one hour preceding the restriction time; (3) some traffic flow is postponed to the weekends, and the traffic volume increased about 8.10%; (4) traffic rule-breaking behavior is pervasive for the short-term driving restriction policy because some drivers may not know this "short-term" and "temporary" policy, and the violation cost is "acceptable"; (5) the short-term policy earns more scores than the long-term policy, because the latter will cause more inconveniences in terms of restriction time and area coverage; and (6) the long-term driving restriction policy has transferred massive passenger flow into the public transport system.

Furthermore, some countermeasures can be taken to improve the effects of driving restriction policy as follows: (1) the government should put more money to improve the level of service of public transport system, including increasing the number of buses, optimizing the bus network, and so on; (2) the government could accelerate the construction of rail transit to meet the rapid growth of passenger flow, and improve the transport transfer facilities to attract more passengers to take public transport; and (3) the government could develop the urban intelligent transportation systems further and improve the traffic efficiency.

The result is promising, however, the traffic and questionnaire survey data (such as speed and travel delay) is limited due to the budget, sufficient data could put forward the research further. Moreover, the benefits and costs of the short-term and long-term driving restriction policies could be evaluated further from the point of view of traffic equity, economic development and air pollution reduction, which is helpful for the policymakers to make a more comprehensive and cautious driving restriction policy.

# References

1. Schrank D, Eisele B, Lomax T (2015) TTI's 2015 urban mobility report. In: Proceedings of the 2015 annual urban mobility report Texas A&M Transportation Institute, Texas, USA
2. Amap company (2015) Traffic operation analysis report of Chinese big cities in 2015. Beijing, China
3. Chin ATH (1996) Containing air pollution and traffic congestion: transport policy and the environment in Singapore. Atmos Environ 30(5):787–801
4. Debell C (2003) London's success gives green light to RUC. Traffic Eng Control 44(5):183–186
5. Yoram S, Golani A (2005) Effect of auto restraint policies on travel behavior. Transp Res Rec: J Transp Res Board (1932):156–163 (Transportation Research Board of the National Academies, Washington, D.C.)
6. Choo S, Mokhtarian P (2008) How do people respond to congestion mitigation policies? A multivariate probit model of the individual consideration of three travel-related strategy bundles. Transportation 35:145–163
7. Jose A G, Fauth G R (1980) Downtown auto restraint policies: the costs and benefits for Boston. J Transport Econ Policy 133–153
8. Song LJ, Zhang DX, Chen JC (2008) Analysis of taxi operation characteristics with traffic control. J Transp Syst Eng Inf Technol 8(6):127–131
9. Gallego F, Montero JP, Salas C (2013) The effect of transport policies on car use: evidence from Latin American cities. J Public Econ 107(2):47–62
10. Grange LD, Troncoso R (2011) Impacts of vehicle restrictions on urban transport flows: the case of Santiago, Chile. Transp Policy 18(6):862–869
11. Yang Y, Li G, Wang R, Qiu P, Jia N (2016) A study of the impact of vehicle restriction policies on traffic flow: a case study of Tianjin. Traffic Inf Saf 34(1):116–122 (In Chinese)

# Exploring Elderly People's Activity and Travel Behavior Mechanism: A Case of Harbin, China

**Xiaowei Hu, Yang Wang, Hanlin Zhang and Zeju Xie**

**Abstract** With the increase of the aging of population, the activity-travel issue of elderly people has been getting more and more attention. Based on the survey and statistics results, this chapter study the elderly people's activity-travel behavior, and introduce the structural equation model to analyze the relationship between the elderly people's activities and travel behavior. The exogenous variables include the family structure, education levels, and economic status, while the endogenous variables contain the travel activity purpose, travel mode, and travel intensity; then we explored the regularity of elderly people's activity and traveling features, and quantified the influence of different factors. This study can provide a reference for developing rational elderly people traffic policy.

**Keywords** Structural equation model · Elderly people · Activity and travel behavior · Model evaluation

## 1 Introduction

With the aging of our population intensified, it is expected in 2020 people over the age of 60 in China will reach 250 million, the total population the proportion will be more than 17.5%. Because special physiological, psychological and behavioral characteristics of the elderly people, the existing transport facilities and services should consider the elderly people's travel needs and activities. So how to understand the elderly people's activity and travel behavior mechanism, and propose reasonable and effective travel policy for elderly people' travel, which is a worthy study for researchers.

Researchers have analyzed the relationship between the mobility and travel needs of the elderly people [1], elderly people's travel preferences and choice [2], elderly

X. Hu (✉) · Y. Wang · H. Zhang · Z. Xie
School of Transportation Science and Engineering, Harbin Institute of Technology, Harbin, Heilongjiang 150090, China
e-mail: xiaowei_hu@hit.edu.cn

people's daily travel mode [3], and the relationship between the elderly people's activities and travel behavior [4], and the suggestions of improving public transport's service to facilities elderly people's travel [5]. Recently, researches of China also carried out the analysis of the elderly people's activities space and travel behavior, and the studies mainly focused on the social characteristic's association with the travel behavior [6, 7], elderly people's travel changes [8], and comparative analysis of the elderly people's travel similarities and reasons in different cities [9].

In order to ensure the mobility of the elderly, improve the elderly people's quality of life, it needs to improve the urban transport environment and meet elderly people's travel and activity demand by modern transportation technology. However, there are relatively few studies on the elderly people's activity and travel behavior mechanism analysis in China, and it is unclear on the individual attributes and their activity-travel characteristic of elderly people. So this chapteer based on the investigation of Harbin elderly people's activity and travel behavior, and combined with the with structural equation model to explore the activity and travel behavior mechanism of the elderly people.

## 2 Investigations of Elderly People's Activities and Travel in Harbin

In order to acquire the elderly people's activity and travel pattern, we conducted a survey in Harbin on April 2015. The questionnaire design involved 21 variables, which takes into the activities and travel characteristics of the elder, such as the activity purpose, travel mode, family structure, and so on. A total of 120 questionnaires were issued and 106 questionnaires were collected, including 96 valid questionnaires, while the effective questionnaires ratio is 80%. Table 1 shows the social characteristics of the respondents.

### 2.1 Elderly People's Activity Purpose

There are five options in elderly people's activity purpose survey, including the leisure activity, shopping, go to hospital, work, gathering, and other things. The proportion of these six activity purposes is 50.1, 25.1, 3.6, 6.1, 10.2 and 4.9%, respectively. Compared with the investigation of Changchun [9] and Kunming [10], leisure and entertainment activity and shopping are the two main purposes of elderly people's daily activity.

According to the preliminary findings of the survey, the range of elderly people' shopping is mainly around the commercial facilities near the living community to complete the shopping activities (distance for the walk within 15 min). With the increase of walking distance, the number of elderly people's shopping activity is

**Table 1** Social characteristics of the respondents

| Appellation | Attributes | No. of questionnaire | Percentage (%) |
|---|---|---|---|
| Sex | Male | 44 | 45.8 |
| | Female | 52 | 54.2 |
| Age | 56–59 | 16 | 17.3 |
| | 60–64 | 34 | 35.4 |
| | 65–70 | 21 | 21.9 |
| | 71–75 | 18 | 18.8 |
| | >75 | 7 | 6.6 |
| Family structure | Living alone | 5 | 5.2 |
| | Couple | 3 | 3.1 |
| | Two generations | 20 | 20.8 |
| | Three generations | 68 | 70.9 |
| Cultural level | Primary school | 16 | 16.7 |
| | Junior high school | 28 | 29.1 |
| | High school | 29 | 30.2 |
| | College and above | 23 | 24.0 |

decreasing, which is different from foreign country's private car travel and shopping activity. Meanwhile, with the body function's decline, the incidence of the elderly people is gradually increasing; the survey shows that more than 31% of the elderly people would go to hospital more than once in every month.

## 2.2 Elderly People's Travel Patterns

The mode choice survey of elderly people includes walking, bicycle, public bus, private car, and other mode, while the proportions is 42.2, 5.3, 47.4, 2.5 and 2.6%, respectively. Compared with Changchun [9], Kunming [10], Guangzhou [11], we can find that walking and public bus are the main travel mode choice, and these two modes are the mainstream choice in elderly people's short distance travel.

In the travel time survey, we find that elderly people's shopping activities are more concentrated in the morning and afternoon time; while the morning travel mainly concentrated in shopping malls, food markets, and school, and the evening travel mainly concentrated in schools, parks, and other leisure lot. In the survey also found that elderly people's travel intensity has a great impact on the mode choice. For the long-distance travel, the elderly people prefer to travel by bus, while for the short distance travel, the elderly people prefer to travel by walking. This is similar to the study of Srichuae et al. [12], elderly people's mode choice mainly affected by the travel purpose, residential area, and travel distance.

# 3   Basic Structural Equation Model

The structural equation model is a multivariate statistical analysis method to analyze the relationship among observation variables and latent variables [13–15], which can realize the analysis and research of the complex relationship among multivariable data, and its composition includes measurement equations and structure equation.

## 3.1   Measurement Equation

The measurement equation presents the potential relationship among observation variable $X$, $Y$, and the independent variables $\eta$, $\xi$.

$$X = \Lambda_X \xi + \delta \qquad (1)$$

$$Y = \Lambda_Y \eta + \varepsilon, \qquad (2)$$

where $X$ is the exogenous indicator variables; $Y$ is the Endogenous indicator variables; $\Lambda_X$ and $\Lambda_Y$ are the factor load of the index variable $(X, Y)$; $\delta$ and $\varepsilon$ are the measurement errors of exogenous variables; $\xi$ and $\eta$ are the external potential variables and internal potential variables.

## 3.2   Structural Equation

The structural equation is a set of equations representing the relationship between latent variables and latent variables, which can be expressed by the following equation

$$\eta = B\eta + \Gamma\xi + \zeta, \qquad (3)$$

where $B$ is the structural coefficient matrix, which represents the relationship between endogenous latent variables $\eta$; $\Gamma$ is the structure coefficient matrix, which indicates the relationship between the latent variables $\xi$ and the latent variables $\eta$; $\zeta$ is the residual value of the structural equation, which can be called the disturbance of potential variables.

## 3.3   Model Solution

The structural equation model contains eight parameter matrices $\Lambda_X$, $\Lambda_Y$, $B$, $\Gamma$, $\Phi$, $\Psi$, $\Theta_\varepsilon$, and $\Theta_\delta$. The first four matrices $\Lambda_X$, $\Lambda_Y$, $B$, and $\Gamma$ have been described above, $\Phi$ is the variance–covariance matrix of the external variable $\xi$; $\Psi$ is the covariance

matrix of the residuals of the latent variable $\eta$; $\Theta_\delta$ and $\Theta_\varepsilon$ are the variance–covariance matrices of $\delta$ variables and $\varepsilon$ variables, respectively. Based on the above parameters, we can derive the following covariance matrix:

$$
\sum(\theta) = \begin{bmatrix} \sum_{YY}(\theta) \ \sum_{YX}(\theta) \\ \sum_{XY}(\theta) \ \sum_{XX}(\theta) \end{bmatrix}
$$

$$
= \begin{bmatrix} \Lambda_Y(I-B)^{-1}(\Gamma \, \Phi \, \Gamma' + \Psi)[(I-B)^{-1}]'\Lambda_Y' + \Theta_\varepsilon \ \ \Lambda_Y(I-B)^{-1}\Gamma \, \Phi \, \Lambda_X' \\ \Lambda_X \Phi \, \Gamma'[(I-B)^{-1}]'\Lambda_Y' \qquad\qquad\qquad\qquad \Lambda_X \Phi \, \Lambda_X' + \Theta_\delta \end{bmatrix}
$$

$$(4)$$

Under the premise that the constructed model is true, $\sum(\theta)$ is equal to the overall covariance matrix $\sum$, then the variance and covariance of observed variables(i.e., Internal and external variables) are the functions of the model parameters.

## 4 Elderly People's Activity—Travel Behavior Model Based on Structural Equation Model

### 4.1 Variable Selection of the Model

This chapter focuses on the relationship between elderly people's daily activities and the travel behaviors. First, the correlation analyses of the variables are conducted, and establish the initial model. Then, according to the calculation results of the initial model, excludes the exogenous variables that have little influence on most of the endogenous variables and leaves the variables that have huge influence, or have little but significant implications. The final selections of the exogenous variables are the education levels of the elderly people, their financial situation, and their family structure. The endogenous variables contain the elderly people's activity purpose, traveling modes, and their traveling intensity. The mechanism between elderly people's activity and travel behavior is expressed by the exogenous latent variables (such as individual and family attribute variables) and the endogenous latent variables (includes the activity purpose, travel mode choice, and travel intensity). Table 2 shows the variables settings for the elderly people's activity-travel behavior equation model.

### 4.2 Variable Selection of the Model

According to the above analysis of variables and the model data, the model is established by the structural equation model software LISREL8.7 and ran the path dia-

**Table 2** Variables setting of elderly people's activity—travel behavior

| Variables types | Variables names | Variables symbol | Observation indicator | Indicator symbol |
|---|---|---|---|---|
| Exogenous variables | Education levels | WHCD | Below high school | X1 |
| | | | Above college | X2 |
| | Financial situation | JJZK | Rich | X3 |
| | | | Well-off | X4 |
| | | | Poor | X5 |
| | Family Structure | JTJG | Alone | X6 |
| | | | Couple | X7 |
| | | | Two generations | X8 |
| | | | Three generations | X9 |
| Endogenous variables | Activity Purpose | CXMD | Leisure activity | Y1 |
| | | | Shopping | Y2 |
| | | | Go to hospital | Y3 |
| | | | Gathering | Y4 |
| | | | Work | Y5 |
| | | | Pick up children | Y6 |
| | Traveling Modes | CXFS | Walk | Y7 |
| | | | Bus | Y8 |
| | | | Others | Y9 |
| | Traveling Intensity | CXQD | Number of trips | Y10 |
| | | | Max travel distance | Y11 |
| | | | Maximum duration | Y12 |

grams of the structural relationship between the activity and travel behavior of the elderly people, which is shown in Fig. 1.

## 4.3 Model Results Analysis

(1) The correlation coefficient between exogenous variable culture level and endogenous variable activity purpose, travel mode and travel intensity were 0.43, 0.68, 0.25, respectively, which indicated that with the improvement of the
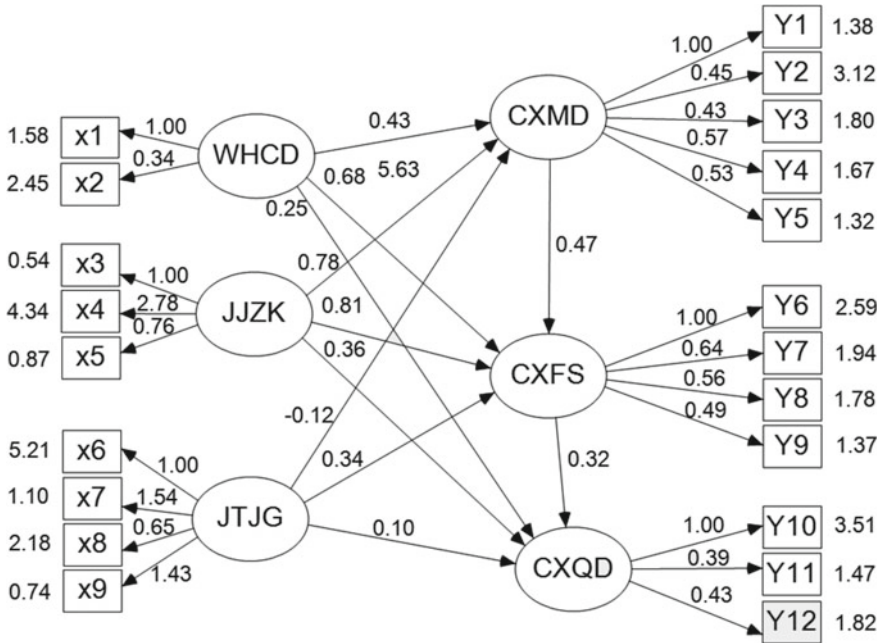
**Fig. 1** Path diagrams of elderly people's activity-travel behavior

educational level of the elderly people, has a larger impact on activity purpose and travel mode choice, while has not too much impact on the travel intensity.

(2)  The correlation coefficient between the economic status of the exogenous variable and the endogenous variable, activity purpose, travel mode and travel intensity were 0.78, 0.81 and 0.36, respectively, which means that with the increase of the income of the elderly people, has a larger impact on activity purpose and travel mode choice, while has not too much impact on the travel intensity.

(3)  The correlation coefficient between the family structure of the exogenous variable and the endogenous variable, activity purpose, travel mode, and travel intensity were −0.12, 0.34, and 0.10, respectively, which means that elderly people's family structure has negative impact on the activity purpose.

(4)  The correlation coefficient between the activity purpose of the endogenous variable and travel mode was 0.47, which indicates that the elderly people's different activity purpose will choose different travel modes; while the correlation coefficient between the travel mode of the endogenous variable and travel intensity was 0.32, which means that the elderly people's mode choice will affect their travel intensity.

## *4.4 Model Evaluation*

In this chapter, the following indicators are used to evaluate the fitting effects of the structural equation model of the elderly people's activity-behavior mechanism. The value of relative fit index (CFI) is 0.85, the value of adjusted good fit index (AGFI) is 0.95, and the approximate root mean square error index (RMSEA) is 0.091.

## 5 Conclusions

Based on the questionnaire survey of the elderly people in Harbin, this chapter explores the relationship between activity purpose and travel patterns of the elderly people. The structural equation model is applied to the behavior analysis and establishes the elderly people's activity-travel behavior analysis model.

Also, it analyzes the influence of different external variables on the decision-making of the elderly people and the interaction between the different activity-travel choices. We can get the basic characteristics and patterns of the elderly people's activities-travel and provide a theoretical basis for making reasonable traffic policy through the study of decision-making mechanism of the elderly people's activities-travel behaviors.

In the future, we will introduce the activity-based theory, and combine the spatial geography method, as well as the IC data to deepen the study of the elderly people's activity-travel behavior.

## References

1. Cole R, Burke M, Leslie E, Donald M, Owene N (2010) Perceptions of representatives of public, private, and community sector institutions of the barriers and enablers for physically active transport. Transp Policy 17:496–504
2. Alsnih R, Hensher DA (2003) The mobility and accessibility expectations of seniors in an aging population. Transp Res Part A 37:903–916
3. Pettersson P, Schmöcker J-D (2010) Active ageing in developing countries?—Trip generation and tour complexity of older people in Metro Manila. J Transp Geogr 18(5):613–623
4. Banister D, Bowling A (2004) Quality of life for the elderly: the transport dimension. Transp Policy 11:105–115
5. van den Berg P, Arentze T, Timmermans H (2011) Estimating social travel demand of senior citizens in the Netherlands. Transp Policy 19:323–331

6. Zhang Z, Mao B, Liu MA (2007) An analysis of travel patterns of the elders in Beijing. J Transp Syst Eng Inf Technol 7(6):11–20 (In Chinese)
7. Chen T, Hen Tuan-sheng, Yue F, Yang L (2007) A study of factors influencing travel choice behavior of older Chinese. J Southwest Jiaotong Univ (Social Sciences) 8(5):17–21 (In Chinese)
8. Han Y, Guan H, Li D (2015) Analysis of trip attitude adjustment of public transit of the elderly based on Heider's balance theory. J Beijing Univ Technol 41(6):906–911 (In Chinese)
9. Hu X, Wang J, Wang L (2013) Understanding the travel behavior of elderly people in the developing country: a case study of Changchun, China. Procedia—Soc Behav Sci 96:873–880
10. Dong R, Li L, Han W, Han G (2016) Study on the travel behavior characteristics of the urban elderly in Kunming. Mod Urban Res 1:102–108 (In Chinese)
11. Jiang H, Zhu X, Sun Z, Wu L (2014) The differentiation of transportation and its effects on transportation equality in Guangzhou. Planners 1:94–100 (In Chinese)
12. Srichuae S, Nitivattananon V, Perera R (2016) Aging society in Bangkok and the factors affecting mobility of elderly in urban public spaces and transportation. IATSS Res 40:26–34
13. Wang J, Sun X, Hu X (2014) Urban passenger transportation prices linkage based on structural equation model. J Wuhan Univ Technol (Transp Sci Eng) 38(5):941–944 (In Chinese)
14. Shiftan Y, Outwater ML, Zhou Y (2008) Transit market research using structural equation modeling and attitudinal market segmentation. Transp Policy 15:186–195
15. Roorda MJ, Ruiz T (2008) Long- and short-term dynamics in activity scheduling: a structural equations approach. Transp Res Part A 42:545–562

# Research on Travel Features of Car Based on RFID Big Data in Chongqing Main City

**Hong Yang, Lei Zhang, Long-chun Cheng and Chao Gao**

**Abstract** In recent years, RFID data acquisition system has been widely used in the field of urban road traffic, in the face of urban traffic congestion situation. In this chapter, the characteristics of car trips are studied by analyzing the data collected by the RFID system in the core area of Chongqing. After the study shows that the main city of Chongqing, the size of a large car trip; Work and home is the main purpose of travel; The number of vehicles per day to reach more than 660,000 vehicles; travel volume reached more than 1,600,000 times; the travel time is more than 30 min; In the travel time distribution, there is a significant difference in vehicle travel time between the working time and nonworking day and so on.

**Keywords** Big data · Car · RFID · Travel characteristics · Path identification
OD segmentation

## 1 Introduction

Chongqing City, with a population of 8.52 million, is one of the central cities in the southwest region of China. In recent years, the city's economy has increased maintain a two-digit rate of growth, improved greatly with the degree of mobility, and raised obviously motor vehicle ownership. As shown in the following illustration: vehicles the average annual increase of 16.7% doubling in 5 years (Fig. 1).

Due to the rapid growth of cars, the urban functional core area, bridge segment presents a long time congestion situation. As a result of which growth speed leads in long time congestion at the core area and the bridge around. During peak hours, vehicles is difficult to increase and dissipate, and the average speed 23.1 km/h of main trunk road, lower 6.2 km/h than 2011, and the decline is more obvious. Con-

H. Yang (✉) · L. Zhang · L. Cheng
Chong Qing Municipal Institute of Design, Chongqing 400020, China
e-mail: 849087452@qq.com

C. Gao
College of Traffic and Transportation, Chongqing Jiaotong University, Chongqing 400074, China
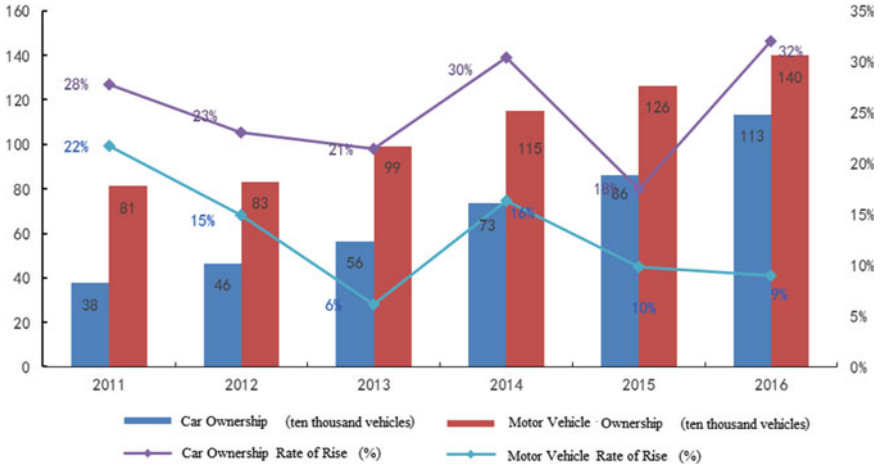
**Fig. 1** In recent years, the trend of vehicle change in Chongqing

gestion area in a total of 79, compared with 2015, it has increased by 12, and the plugging point of 53 distribution in the most important area, accounting for more than 67%. Congestion mileage 180 km, the increase of 45 km compared to 2015, of which the most important area 95 km, accounted for 53%. In the core area of 16 bridges across the river, 10 peak periods are in serious congestion. Five business circle congestion range spread trend. The expansion area of Liangshan, University area tunnel congestion time for a long 6–8 h, is normal congestion. It is necessary to carry out a special study on the characteristics of car trips (Fig. 2).

Car travel features [3] mainly include total travel, number of travel vehicles, travel purposes, distance, traveling time, trip intensity, mode of travel, and travel time consumption. At present, there are two main methods to analyze the characteristics of car trip [4]: One is the use of artificial investigation. Another method is to use external detection equipment (such as video, geomagnetic) monitoring and identification of vehicle identity. The first method requires a lot of man energy and financial resources, and data is collected amount less, or the memory of being the inquirer or field sampling point, there are usually larger deviation, is difficult to accurately describe actual situation [5]. The second method depends on the density of detector layout size and the type of data acquisition, through the automatic data collection system, continuous access to a lot of useful data, and the data is accurate [6].

In recent years, some areas and city start trying to apply RFID technology to urban traffic management at home and abroad. Comprehensive foreign application experience and the situation of domestic trial [4]. RFID technology in the field of road traffic management, which involves many departments, such as transportation, public security, environmental protection, and urban construction and so on. The system is to automatically identify the vehicle mounted on the RFID electronic tags, with the background of the application of the information processing system can
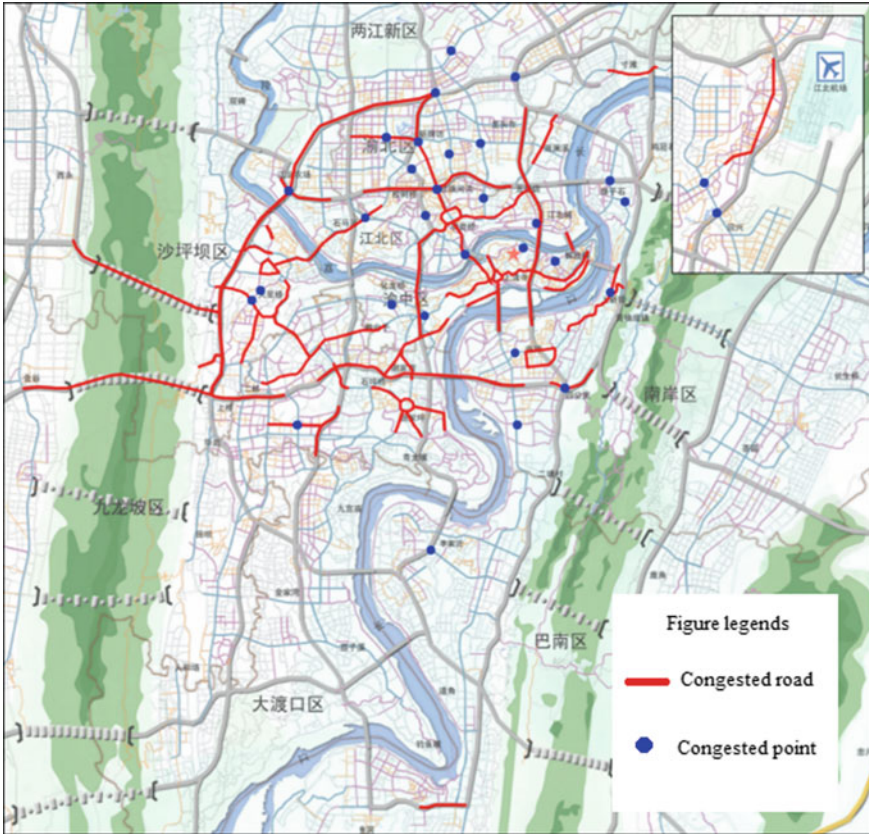
**Fig. 2** The position of congestion and congestion points in Chongqing

record the vehicle running state information. In this chapter, we try to use the data collected by the RFID system which is the first trial in the core area of Chongqing to explore the characteristics of the car trip. It will lay a solid foundation for the future analysis of the road traffic system and the research of travel demand management measures.

## 2 RFID Traffic Information Gathering System in Chongqing

"Chongqing traffic information card (electronic identification plate)" which based on radio frequency identification technology (RFID) is an important application in the field of intelligent transportation, and it is a national informatization pilot project approved by the national development and reform commission. By obtaining the

vehicle dynamic identification information, this system can be an urban public information internet of things system which may be widely used in traffic control, public safety, public travel services, highway rapid transit, logistics, access/exit management of the buildings, residential areas, and car parks.

So far intelligent traffic management and service system based on RFID technology in Chongqing were constructed. Traffic management department has issued about 4 million pieces of electronic cards. The issuance of these cards basically covers all cars in Chongqing. In the core area, it has constructed road gathering point about 860 (as shown below). These points include the city's main roads and key bayonet. Electronic cards solve the problem that "the inability to accurately identify the vehicle identity", which is the new trend of the traffic management, and it can provide strong technical support for the management of urban transportation planning and construction by analyzing the big data collected.

## 3   Technology Path

It is important that we analyze big data through collecting RFID system and look for car travel features in the chapter. Processing of the original data, we should identify two important work, which one is path identification and traffic reduction based on RFID data, the other is OD segmentation.

### 3.1   Path Identification and Traffic Reduction Based on RFID Data

Path recognition is a very complicated process which the basic idea of the following Fig. 3.

### 3.2   OD Segmentation

Through the acquisition of RFID data records and according to the time order by the data records, we should determine each vehicle travel path in all day, and then we need to calculate the adjacent two paths of time intervals, by a large number of sample data, calculate the time difference between two RFID records. According to the time difference identify the existence of residence between two records the points, the basis of the division is according to the acquisition point of the travel between 80% points + 30 min. Identifies whether the vehicle stays between the two collecting points, and the travel OD of the vehicle through the point of stopping (Fig. 4).
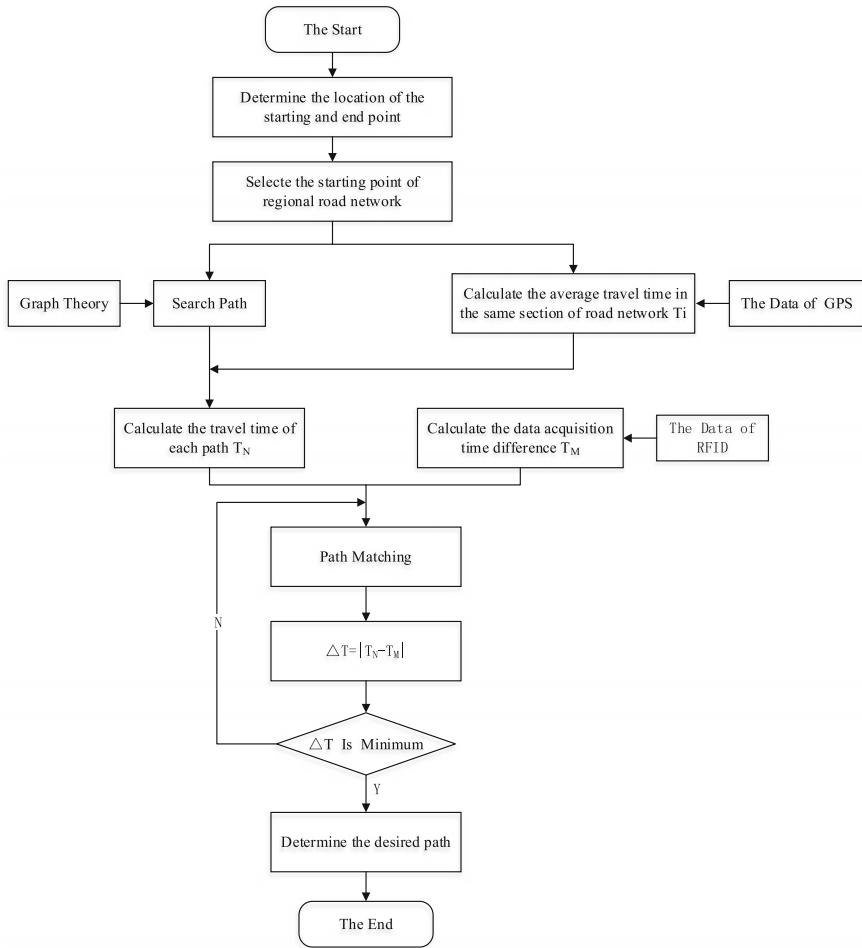
**Fig. 3** Path identification and traffic reduction process based on RFID data

## 4   Analysis of Car Travel Characteristics in Core Urban Area

In order to study the characteristics of car travel, this chapter utilized about 700 million RFID data records which were collected within the inner ring highway of Chongqing, from September to December, 2016. We will obtain many parameters of car travel when we statistically analyze the RFID data by big data technology such as the number of cars travel, the purpose of travel, travel rate, average travel time, average travel distance, travel time distribution, and other characteristics of the parameters. By analyzing the main parameters of car travel, it provides a good basis for traffic management and forecasting model.
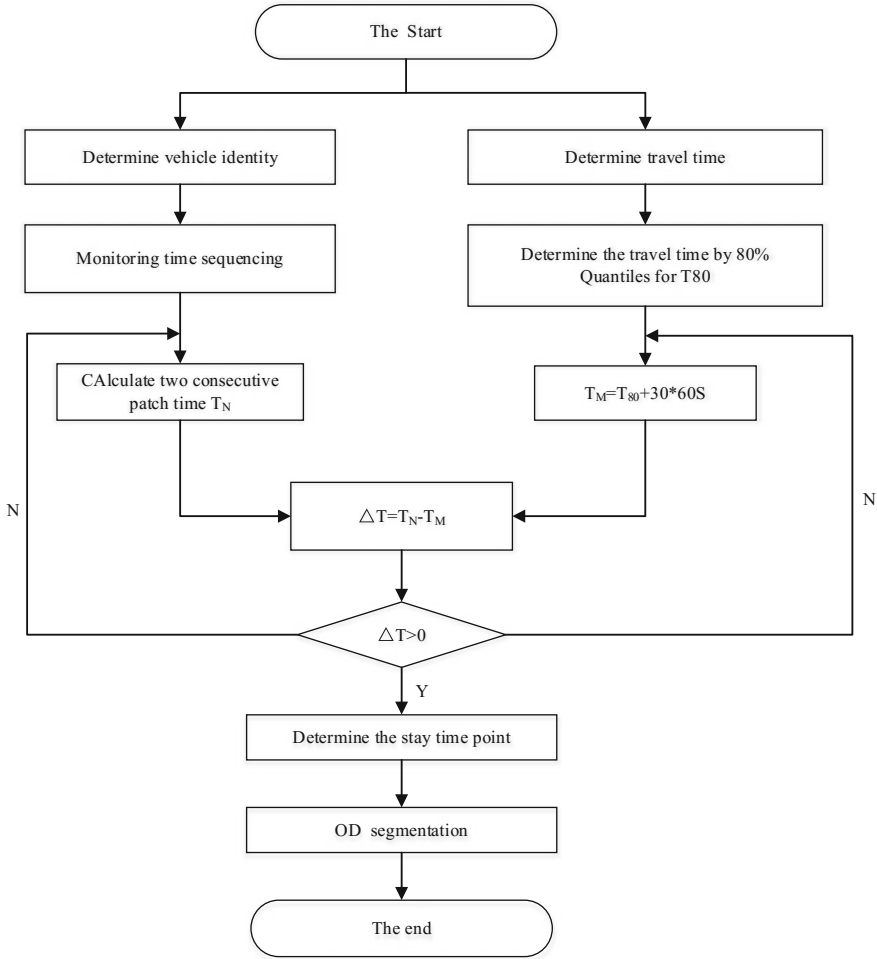
**Fig. 4** OD segmentation flowchart

## 4.1 Number of Vehicles Travel

The number of travel vehicles is the total number of vehicles that describe the city's day in the road network, which is an important parameter reflecting the traffic condition of a city. As the research object of this chapter, Chongqing municipality, according to the statistical analysis of the RFID data collected, the main urban working day average travel vehicles about 661,500 vehicles, but not working day average travel total of about 633,500 vehicles. After comparing the number of travel vehicles on weekdays and nonworking days, it is considered that the number of cars traveling on workdays is significantly higher than that of nonworking day cars. And in the

one-week sunrise line of the number of vehicles, in contrast, can also show Friday is the total car travel is the highest day, reached 683,500 vehicles; next is Monday, about 661,500 vehicles; This can also conform to the general rule of residents travel. Friday after work most residents drive out of the main city, on Monday to work into the main urban characteristics.

## 4.2 Total Travel

Gross travel means the total number of vehicles traveling on the road network on the same day, which can reflect the traffic congestion in a city. According to the analysis of the RFID data in Chongqing core area. The average travel amount of is 1,600,500 times in the working days, which is 1,499,600 times in the nonworking days. Thus, it can be seen that the total amount of car trips on weekdays is higher than on nonworking days. At the same time, there is two are basically consistent, which is the distribution characteristics of total travel and the number of travel vehicles. The biggest day of the one-week trip is Friday, about 1,652,000 times, which is also fully illustrated on Friday is the busiest day of traffic conditions in the core area of Chongqing. And Sunday is a one-week trip to the smallest, about 1,460,900 times, from this data can also indicate that Sunday most residents do not travel. It can be explained that most of the weekend at home to rest and verified that the previous explanation of work is the main city of Chongqing to travel an important purpose.

## 4.3 Trip Intensity

Travel intensity refers to the average number of daily trips, which can be calculated by the number of car trips in one day and the number of cars. It reflects the frequent degree of the resident's car travel, and can also show the residents' demand for the trip. This is a very important indicator to predict the total quantity of car demand in the future urban residents, and also a major indicator of the response frequency.

According to calculations, in Chongqing urban area average 2.4 times/day trip intensity in 2016, compared with 2.2 times/day in 2010, increased 0.2 times/day. In 2016, the average working day trip intensity is 2.42 times/day, nonworking day is about 2.38 times/day in the core area, which can present a weekday car travel times higher than nonworking days. The following illustration shows that the intensity of car travel is basically flat in workdays. The following illustration shows that the car travel intensity is basically flat on weekdays, and stays about 2.42 times/day. Instead of nonworking days, travel intensity varies a bit, Saturday is 2.33 times/day, and Sunday reached 2.43 times/day.

### *4.4 Average Travel Time Consumption*

The average travel time is called a trip time consumption and reflected of a city car travel intensity of the important macro statistics. It also can be used to reflect the residents use car travel time of the statistics. According to a large number of data statistics, Chongqing Urban residents of the average travel about 30.8 min. Residents spend less than 30 min in a 70.9%, less than 1 h in proportion to 93.1%. The percentage of average travel consumption is shown in the following illustration.

### *4.5 The Days Distribution of Car Trips*

The days distribution of car trips means that cars have been traveling for several days in one weeks. This chapter analyzes the regularity of car distribution in the core area of Chongqing in the five days of workday, as shown in the following illustration. The vehicles used each day accounted for about 33%. Average vehicle usage rate of 61.4%.

## 5 Conclusion

In this chapter, we have used the RFID data of the core area of Chongqing from September to December in 2016. Using big data's software comprehensively process and analysis the car travel characteristics. Through the analysis, we can further improve that the size of a large car trip; Work and home is the main purpose of travel; the number of vehicles per day to reach more than 660,000 vehicles; travel volume reached more than 1,600,000 times; the travel time is more than 30 min; In the travel time distribution, there is a significant difference in vehicle travel time between the working time and nonworking day and so on.

## References

1. Chongqing Urban Planning Bureau & Chongqing Transport Planning Institute Chongqing Urban, Traffic Operation Analysis Annual Report, Chongqing (2011)
2. Chongqing Urban Planning Bureau & Chongqing Transport Planning Institute Chongqing Urban, Traffic Operation Analysis Annual Report, Chongqing (2016)
3. Zhang YY, Zhu LY, Wen HM, Zhang X (2016) Analysis on the characteristics of urban car trip behavior based on OBD data. In: The 11th annual meeting of China intelligent transportation, Chongqing, pp 1314–1324
4. Liu LH, Song X (2011) Comparative analysis of vehicle detector performance and development of traffic flow detection technology. Urban Constr Theor Res (30)

5. Zhang HS, Zhang Y, Wen HM, Hu DC (2007) Estimation approaches of average link travel time using GPS data. J Jilin Univ 27(3):533–537
6. Cheng XM. Research on travel features of car based on RFID big data in NanJing the core area. https://sanwen8.cn/p/1fcIQ9m.html
7. Han JW, Micheline K, Pei J (2013) Data ming concepts and techniques, 3rd edn. China Machine Press
8. Lu FQ, Chen XW, Hu XJ (2010) Characteristic research of resident's bus trip based on bus OD data. J Transp Eng Inf 8(2):31–37
9. Lu J, Wang W (2004) Study of resident trip time consumption characteristic. J Highw Transp Res Dev 21(10):102–104

# The Traffic Signal Control Method and Applicable Condition of U-Turn in Urban Arterial Road

**Xian-cai Jiang, Chen Yu and An-ni Wang**

**Abstract** In order to improve the low traffic efficiency at intersection caused by concentrated traffic conflict in Chinese urban road, the traffic signal-coordinated control method between median opening and intersection is proposed from the view of space–time resources optimization, and the road conditions and traffic conditions suitable for the U-turn in urban arterial road are analyzed. The intersection of Yangtze River road and Songshan road in Harbin is taken as an example, VISSIM simulation results show that the cycle, average delay, queue length, and waiting time of pedestrian crossing roads at the intersection decrease significantly after the application of U-turn and traffic signal-coordinated control method, which effectively verify the feasibility of the method. The method is beneficial to the traffic signal-coordinated control among urban arterial road.

**Keywords** Traffic engineering · Traffic signal-coordinated control · U-turn Simulation evaluation

## 1 Introduction

Urban arterial road as the main skeleton of city road network, plays a key role to smooth urban transportation. However, there still exist some problems which are caused by road design and operation, such as traffic bottleneck at the intersection because of concentrated traffic conflict, unbalanced utilization of the space–time resources in intersection and road section, traffic safety, environment pollution, etc. Although scholars have put forward some effective methods to improve the utilization of intersection of space–time resources, such as traffic channelization design, traffic signal optimized control, left-turn vehicles bypass, one-way traffic, application of grid computing technologies [1], information dynamics in transportation systems

X. Jiang (✉) · C. Yu
School of Transportation Science and Engineering, Harbin Institute of Technology, Harbin 150090, China
e-mail: jxc023@126.com

A. Wang
Zhejiang Scientific Research Institute of Transport, Hangzhou 311305, China

with traffic signalized control [2], and so on, the processing of conflict traffic flow at intersection is limited to the time separation, the problems of unbalanced space–time resources utilization and concentrated traffic conflict are still not solved. Unconventional intersection designs have been proposed to decrease intersection delay and travel time, for example, by redirecting left-turns from the minor approach away from the main intersection and replacing them with a right-turn followed by U-turn [3]. U-turn improves the movements at the intersection by separating a part of traffic conflicts to road section, and balances the utilization of space–time resources in intersection and road section by simplifying the complexity of signalized control to increase the capacity of the intersection. So, U-turn is adopted by more and more countries to optimize the traffic operation at the intersection.

Zhao et al. proposed a lane-based optimization model for the integrated design of median U-turn intersection types, lane markings, distances between the median crossovers and the main intersection, and signal timing [4]. Chen et al. selected the raised median to discuss the design method of median width, median opening, and left turn lane [5]. Distefano and Leonardi proposed the guidelines for U-turn lane design, and the safety principles in order to reduce unsafe conditions during inversion maneuvers as much as possible [6]. Zhou et al. developed a working model to guide the location of U-turn median openings by minimizing the average delay for U-turn movements [7]. Those designs are suitable for the condition of low U-turn volume, if the U-turn volume is heavy; no consideration is given to avoid the impact of the traffic flow at the intersection.

Liu and Bie addressed a traffic regulation scheme at a signalized intersection, termed as the Hook-turn (HT) scheme, and compared the performance of HT with the classic U-turn (UT) scheme based on VISSIM simulations [8]. Wang et al. designed a scheme of U-turn lane right set and given the corresponding traffic signalized control mode, which could avoid four kinds of conflict between U-turn traffic and other traffic in time and space, and improve the efficiency and safety of U-turn traffic [9]. Also, those signalized control methods did not take the intersection and the median openings as a whole to optimize the traffic operation; especially the U-turn volume is heavy. This paper will estimate the effects of traffic signal-coordinated control between median opening and intersection, and analyze its suitable road and traffic conditions.

## 2 The Signalized Control Method of U-Turn in Urban Arterial Road

### 2.1 Rout Arrangement of Left-Turn Vehicles

The left-turn vehicles of south and north approach shall turn right, U-turn, and pass through intersection to realize left-turn goal, as shown ① → ① and ④ → ④ in Fig. 1. Similarly, the left-turn vehicles of east and west approach shall be pass through the intersection, U-turn, and turn right in order to complete left-turn, as shown ② → ② and ③ → ③ in Fig. 1. There are some advantages of arranging the U-turn lane out-
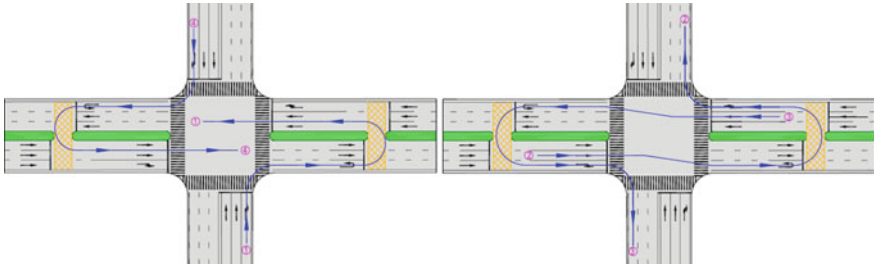
**Fig. 1** Route arrangement of left-turn vehicles

side of the road. First, the U-turn vehicles will have enough turning radius to run smoothly; second, it can reduce the lane changing of U-turn vehicles, and avoid mutual interference between U-turn vehicles and non-U-turn vehicles.

## 2.2 Traffic Signalized Control Method

In order to reduce vehicles' parking times and delays when U-turn vehicles often interrupt the straight vehicles at the median opening, traffic signal-coordinated control method between the median openings and the intersection is proposed to carry out. In order to reduce the bypass distance of left-turn vehicles, the length between the median opening and the intersection is often short, so synchronous coordinated signalized control is a good choice. The traffic signalized control scheme is arranged in Table 1 and Fig. 2.

## 2.3 Road Condition of U-Turn

(1) Road width

In addition to small vehicles, the left-turn flow may be including buses. In order to ensure bus to smoothly pass through the median opening, the one-way width of the arterial road must exceed the bus minimum turning radius, which is more than 12 meters. So, the central strip road or the road of two-way six lanes and more is better.

**Table 1** Traffic signalized control scheme

| The first phase | | | The second phase | | |
|---|---|---|---|---|---|
| West median opening | intersection | East median opening | West median opening | intersection | East median opening |
| ⇄ | ↙⇄↱ | ⇉ | ⇐ | ↓↓↰ | ⇒ |
| Intersection pedestrian signal of east–west direction | | | Intersection pedestrian signal of south–north direction | | |

(a) The first phase                              (b) The second phase
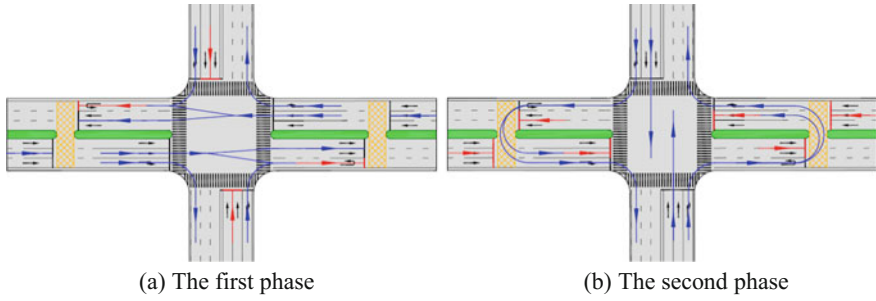
**Fig. 2** Traffic signalized control scheme

(2)  Location of median opening

In order to reduce the bypass distance of left-turn vehicles, the location of median opening in urban arterial road shall met the following conditions at the same time, as shown in Fig. 3.

When the traffic flow of east and west approaches is released in the first signal phase, in order to avoid U-turn vehicle queue to overflow intersection, the distance from the median opening to intersection stop line shall store all the U-turn vehicles which arrive in one signal cycle, i.e.,:

$$L_e \geq \frac{(V_{wl} + V_{sl}) \times t_1 \times d}{3600n}, \; L_w \geq \frac{(V_{nl} + V_{el}) \times t_1 \times d}{3600n} \tag{1}$$

where $L_e$ is the distance from the east median opening to intersection stop line(m), $L_w$ is the distance from the west median opening to intersection stop line (m), $V_{wl}$ is the peak hour left-turn traffic volume of west approach(pcu/h), $V_{sl}$ is the peak hour left-turn traffic volume of south approach(pcu/h), $V_{nl}$ is the peak hour left-turn
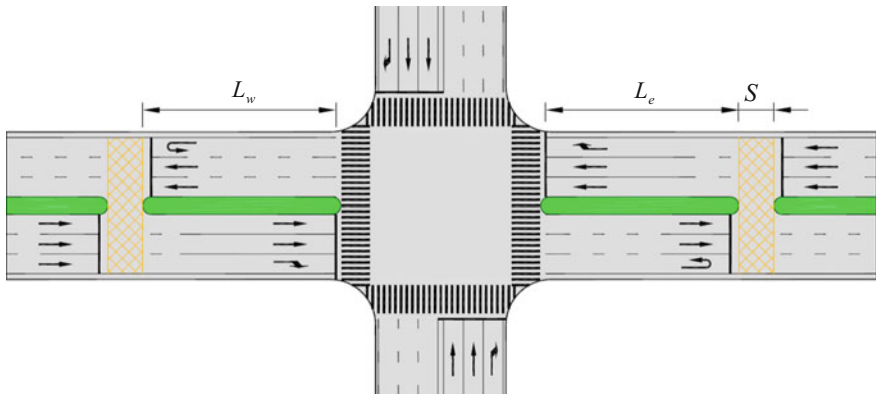


**Fig. 3** The width and location of median opening

traffic volume of north approach(pcu/h), $V_{el}$ is the peak hour left-turn traffic volume of east approach(pcu/h), $t_1$ is the green time of the first phase(s), $d$ is the average space headway in queue, commonly 6.0–6.5 m, $n$ is the lane number of U-turn.

The second signal phase releases the traffic flow of south and north approaches, in order to ensure that the first left-turn vehicle from south or north approach arrives at the stop line of east or west approach at the end of the second phase, the distance from the median opening to intersection stop line shall not be too long, that is

$$L_e \leq \frac{v_{sl} \times t_2}{3.6 \times 2}, \; L_w \leq \frac{v_{nl} \times t_2}{3.6 \times 2} \tag{2}$$

where $v_{sl}$ is the average speed of left-turn vehicles from south approach(km/h), $v_{nl}$ is the average speed of left-turn vehicles from north approach(km/h), $t_2$ is the green time of the second phase(s).

(3)   Width of median opening

When left-turn vehicles pass through the median opening, the width of the median opening at road section must meet the requirement of lateral clearance, as shown in Fig. 4.

When median opening only permits unilateral U-turn, the width of median opening shall not be less than 4.5 m, because the width of a bus is about 2.5 m, extra plus every 1 m lateral clearance on both sides. If median opening permits bilateral U-turn, the width of median opening shall be more than 9 m. Generally, one median opening with bilateral U-turn is adopted between two intersections. But if the intersection spacing is too long, two median openings with unilateral U-turn may be better in order to reduce the bypass distance of left-turn vehicles. The type of median opening between two intersections can be determined by the following method, as shown in Fig. 4.

With the help of Formulas (1) and (2), the maximum value $L_e$ of first intersection and $L_w$ of second intersection can be obtained. When the intersection spacing $L_s$ meets Formula (3), two median openings with unilateral U-turn shall be adopted
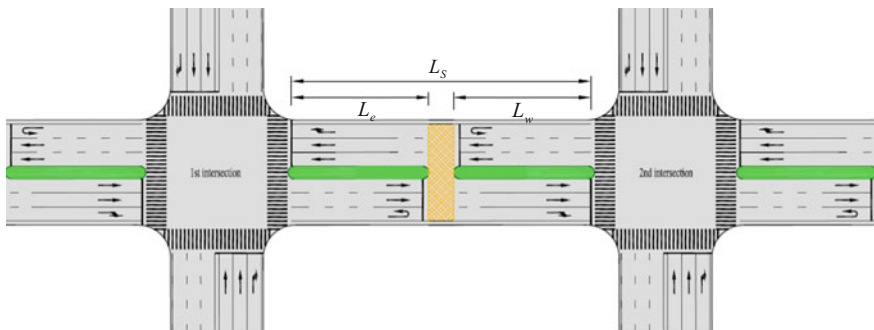


**Fig. 4**   Distance from median opening to intersection

between two intersections. Otherwise, one median opening with bilateral U-turn is the best choice.

$$L_s - (\max L_e + \max L_w) \geq 100\,\text{m} \tag{3}$$

### 2.4  Traffic Conditions

When synchronous coordinated signalized control is adopted between the median opening and intersection, the longest distance between two median openings shall not exceed $vC/4$ according to the suitable condition of synchronous coordinated signalized control. Let $W$ is the sum of intersection width in arterial direction with the width of one median opening, so the lane length from intersection to the median opening is

$$L = (vC/4 - W)/2 \tag{4}$$

Then the maximum capacity of one-way U-turn lane is

$$V_{wl} + V_{sl} \leq (L/d) \times 3600/C = 1800(vC/4 - W)/(dC), \ V_{nl} + V_{el} = V_{wl} + V_{sl} \tag{5}$$

## 3   Case Study

The intersection of Yangtze River road and Songshan road and its adjacent roads in Harbin is taken as an example to carry out case analysis.

### 3.1  Basic Information

(1)  Road conditions

Yangtze River road is an urban arterial road with 10 lanes bidirectional which has three boards. The road runs from east to west, and the eastern section length is 340 m, while western is 220 m. Songshan road is a secondary road with 6 lanes bidirectional which has one board, and it runs from south to north.

(2)  Traffic conditions

The traffic composition is mainly cars and buses, and the peak hour traffic volume of each approach is shown in Table 2. The average speed of road section is 35 km/h, while the approach is 20 km/h.

**Table 2** Peak hour traffic volume of the intersection of Yangtze River road and Songshan road

| Flow direction | East approach/pcu·h$^{-1}$ | West approach/pcu·h$^{-1}$ | South approach/pcu·h$^{-1}$ | North approach/pcu·h$^{-1}$ |
|---|---|---|---|---|
| Left-turn | 0 | 262 | 332 | 286 |
| Straight | 1664 | 1810 | 850 | 756 |
| Right-turn | 302 | 366 | 538 | 184 |

(3) Traffic signalized control scheme

The fixed control is executed at the intersection whose signal timing scheme is shown in Table 3. The east approach is prohibited to turn left, and pedestrians cross the crosswalk.

## 3.2 Optimization Scheme

(1) Route arrangement of left-turn vehicles

The left-turn vehicles in the direction of Songshan road turn left by turning right, U-turn and then going straight after entering the intersection. The left-turn vehicles in the direction of Yangtze Road turn left by going straight, U-turn and then turning right after entering the intersection.

(2) Intersection layout

The intersection layout should be divided again due to the U-turn traffic organization, as shown in Table 4.

The distance from the west U-turn to intersection stop line is 52 m according to the Formulas (1) and (2), and the distance from the east U-turn to intersection stop line is location is 70 m, satisfying the traffic condition constraints of Formula (5). The outer lane is set to U-turn lane, and the width of median opening is 8 m.

**Table 3** Signal timing scheme of the intersection of Yangtze River road and Songshan road

| Phase plan | ↓↓ | ↘↓ | ⇌ | ⇉ |
|---|---|---|---|---|
| Green time/s | 32 | 25 | 28 | 54 |
| Yellow time/s | 3 | 3 | 2 | 6 |
| Red time/s | 126 | 133 | 131 | 101 |
| Pedestrian phase | West discharging | East discharging | South discharging | South and north discharging |
| Cycle/s | 161 | | | |

**Table 4** Intersection layout of Yangtze River road and Songshan road

| Approach | North | | | South | | | West | | | East | | |
|---|---|---|---|---|---|---|---|---|---|---|---|---|
| | Straight | Right | Exit | Straight | Right | Exit | Straight | Right | Exit | Straight | Right | Exit |
| Lane number | 3 | 1 | 3 | 3 | 1 | 3 | 5 | 1 | $5^a$ | 4 | 1 | $6^a$ |

*PS* [a]indicates that the exit has a U-turn lane

(3)  Signal timing scheme

When the U-turn is used in the arterial road, the two groups of signal lights at the U-turn are equipped with the same timing scheme, and should be coordinated with the signal lights at the intersection. The signal timing scheme at the intersection and U-turn is shown in Table 5.

## 3.3  Scheme Evaluation

(1)  VISSIM simulation

The geometric shape of the intersection together with the traffic volume of each approach, traffic composition, average running speed, and current signal timing parameters are input into the VISSIM. The current traffic organization scheme and the optimized organization scheme are respectively subjected to traffic simulation, the simulation results are shown in Table 6.

(2)  Evaluation analysis

As seen in Table 6, the delay is reduced from 63.55 to 39.2 s, and the average queue length decreases from 67 to 44.5 m after the optimization design. The current control scheme has four phases, $V/C$ is 0.882; the new scheme is reduced to two, and the $V/C$ is 0.431, which greatly alleviate the traffic pressure at the intersection. The signal cycle is reduced from 161 to 94 s, which shortens the waiting time of pedestrian crossing, the delay of pedestrian crossing is reduced by 73 s, and the behavior of running through the red light is effectively controlled. All the traffic evaluation indexes have proved that the optimization design is reasonable and feasible.

**Table 5**  Signal timing scheme of the intersection and U-turn



**Table 6**  Comparison of traffic simulation results before and after optimization

| Evaluation period | Saturation | Delay/s·veh$^{-1}$ | Queue length/m | Pedestrian crossing delay/s | Service level |
|---|---|---|---|---|---|
| Current | 0.88 | 63.55 | 67.00 | – | Level 4 |
| Optimized | 0.43 | 39.20 | 44.50 | −73.00 | Level 2 |

# 4 Conclusions

The traffic signal-coordinated control method between the median opening and intersection is proposed from the views of space–time resources optimization, and the road conditions and traffic conditions suitable for the U-turn in the urban arterial road are analyzed. VISSIM simulation results show that the cycle, average delay, queue length and waiting time of pedestrian crossing roads at the intersection decrease significantly after the application of U-turn and traffic signal coordinated control method, which effectively verifies the feasibility of the method.

# References

1. Mukherjee S, Pan I, Dey KN (2009) Traffic organization by utilization of resources through grid computing concept. In: Proceedings of world congress on nature & biologically inspired computing. IEEE Publication, New York, pp 1572–1575
2. Sorina CL, Vaisagh V, Heiko A et al (2016) Information dynamics in transportation systems with traffic lights control. Procedia Comput Sci 80:2019–2029
3. Ali Pirdavani, Tom Brijs, Tom Bellemans, Geert Wets (2011) Travel time evaluation of a U-turn facility: comparison with a conventional signalized intersection. Transp Res Rec 2223:26–33
4. Zhao J, Ma W, Head KL, Yang X (2014) Optimal intersection operation with median U-turn: lane-based approach. Transp Res Rec 2439:71–82
5. Chen K, Zhang N, Qian ZD (2007) Median design analysis in the manner of U-turn followed by right-turn. Int Conf Transp Eng 352–357
6. Distefano N, Leonardi S (2016) U-turn lanes in narrow-width median openings: design criteria for a safe and efficient project. Arch Civ Eng 62(3):33–46
7. Zhou H, Peter H, Lu JJ, Wright JE (2003) Optimal location of U-turn median openings on roadways. Transp Res Rec 1847:36–41
8. Liu ZY, Bie YM (2015) Comparison of hook-turn scheme with U-turn scheme based on actuated traffic control algorithm. Transportmetrica A: Transp Sci 11(6):484–501
9. Wang ZJ, Li L, Ma CF (2015) The design of a U-turn lane right set and its control mode at an intersection. In: Proceedings of the 5th international conference on transportation engineering, ICTE 2015, pp 1402–1408

# Statistical Vehicle Specific Power Profiling of Heavy-Duty Vehicles for Mountainous Highways

**Tao Chen, Meng-xue Li, Hong-jing Feng, Bin Chen and Yan Gao**

**Abstract** Based on the previous studies, the characteristics of VSP distribution of heavy-duty diesel vehicles and their impacts due to varying highway grades, as well as velocity factors measured on a mountainous highway in China were investigated. Data were collected using a CAN Bus adapter and a car video recorder mounted on the test vehicles. Statistical distribution models with a scope of bins are established and identified through a goodness of fit test approach by using the sample data. Finally, the model was verified through a goodness of fit testing approach by using a portion of data collected from the mountainous highway. Relative errors between fuel consumption estimates and actual fuel use were generally under 10%, which verifies the reliability and effectiveness of VSP distribution model for heavy-duty diesel vehicles for the mountainous highway.

**Keywords** Heavy-duty diesel · Mountainous highway · Vehicle-specific power distribution

T. Chen (✉) · M. Li
Key Laboratory of Automotive Transportation Safety Techniques of Ministry of Transport, Chang'an University, Xi'an 710064, People's Republic of China
e-mail: chentao@chd.edu.cn

H. Feng
Beijing New Energy Automobile Co, LTD Cai He Road #1, Beijing 100000, People's Republic of China

B. Chen
Sichuan College Key Laboratory of Road Traffic Safety, Sichuan Vocational and Technical College of Communications, Chengdu, Sichuan, China

Y. Gao
The Institute for Traffic Management of Ministry of Public Security, Wuxi 214151, People's Republic of China

# 1   Introduction

Vehicle Special Power (VSP) has been widely utilized to reveal the impact of vehicle operating conditions on emission and energy consumption estimates that are dependent upon the speed, roadway grade, and acceleration or deceleration on the basis of the second by second cycles [1–4]. There is a surprising consistency of VSP distributions at different mean speed. However, most of the studies assumed road grade to zero and focus on the light-duty vehicles. As mountainous highways have great grade variation and the largest loss is in potential energy when climbing up hills due to the large weight of heavy-duty diesel vehicles (HDDV), it is necessary to use highway grade in the VSP calculation [5, 6]. Besides, unlike light-duty vehicles (LDVs), the payload of HDDVs can vary widely based on different axle number thus to cause a large variation in VSP range [7, 8]. This paper focuses on the HDDVs VSP distribution on mountainous highways by deriving the highway grades to be used in the VSP calculation, then fitting the samples into a specific distribution and verifying it through a goodness of fit testing approach by using a portion of test data.

# 2   Literature Review

Vehicle specific power, a function of vehicle speed, acceleration, and road grade, a surrogate for power demand, has been widely used in emission and fuel consumption modeling field [9, 10]. The United States Environment Protection Agency developed Motor Vehicle Emission Simulator (MOVES) for the estimation of emissions produced by on-road and non-road sources [11]. International Vehicle Emissions (IVE) model funded by U.S. Environmental Protection Agency (USEPA) divided VSP into intervals and use engine stress to calculate the pollutants [12, 13]. Since it has been proved that there are direct physical interpretation and good statistical relations with on-road vehicle emissions and fuel consumption [14]. Song et al. found that use of VSP distribution to calibrate micro-simulation model is reasonable. For a traffic network, the VSP bin distribution is able to reflect fuel consumption per unit of time and the combination of VSP bin distribution and average travel speed is able to reflect the fuel consumption per unit of distance [7, 15]. Frey et al. took the average fuel consumption rate under different VSP Bins to calculate the fuel consumption on diesel engines [15]. Younglove et al. investigated VSP distributions for five driving cycles. VSP distributions were given and emission rates were also calculated and compared with the binned VSP by using the CMEM model [16]. However, the works above neglect the most contributing factor of VSP, grade, which varies widely on mountainous highways and findings of those studies mostly based on LDVs, HDDVs can have an extensive range of VSP due to changes of payload based on different axle number.

## 3 Field Data Collection

The K1133~K1176 section of Xihan Highway was selected as a test route, the route length is 44 km, grade ranges from 1 to 5%. There are two test vehicles, both are GB emission compliant diesel combinations with 6 axles. One is a Delong M3000 with a 9.726L engine in which maximum power is 247 kW. The mass of it ranges from 15$t$ to 40$t$. The other one is Delong X3000 with an 11.596L engine in which maximum power is 276 kW. The mass of the vehicles ranges from 14.5$t$ to 53.1$t$. A CAN Bus adapter and a car video recorder mounted on the test vehicles. Integrate the recorded stake mark and tunnel position with alignment data of design drawings to quantify road grade.

## 4 Statistical Methods

### 4.1 VSP and Binning

VSP takes into account aerodynamic drag, tire rolling resistance, and road grade. VSP is generally defined as power per unit mass of the vehicle and is a function of vehicle speed, acceleration, and road grade. As in Eq. (1)., the type and load of HDDVs affect weight, frontal area, air resistance coefficient, and rolling resistance coefficient to influence the distribution character of VSP. The parameters of test vehicle can be obtained from the references, the simplified VSP model of test vehicles can be given as Eqs. (2) and (3). Equation (2) is used for empty load and Eq. (3) is used for full payload.

$$
\begin{aligned}
\text{VSP} = \frac{P_b}{m} &= \frac{\frac{\text{d(KE+PE)}}{\text{dt}} + F_{\text{rolling}} \times v + F_{\text{aerodynamic}} \times V}{m} \\
&= v \times (a \times (1 + \varepsilon_i) + g \times \text{grade} + g \times C_R) + \frac{1}{2} \times \rho_a \frac{C_D \times A}{m} (v + v_w)^2 \times v \\
&= gv(C_R + \text{grade}) + av(1 + \varepsilon_i) + 0.5 C_D A \rho_a v^3 / m
\end{aligned}
\tag{1}
$$

where m is vehicle mass, $v$ is vehicle speed, $a$ is vehicle acceleration, $\varepsilon_i$ is "Mass factor", which is the equivalent translational mass of the rotating components of the powertrain, grade is vertical rise/slope length, g is acceleration of gravity (9.8 m/s$^2$), $C_R$ is coefficient of rolling resistance, $C_D$ is drag coefficient, $A$ is frontal area of the vehicle, $\rho_a$ is ambient air density, $v_w$ is headwind into the vehicle.

To execute the VSP method, one must have a second by second speed profile and data regarding road grade. Each second by the second estimate of VSP and the corresponding fuel rates were categorized into those VSP bins. VSP distribution rate is the percent of time spent on VSP mode in speed bins. Based on the existing studies, we calculate the VSP according to the instantaneous speed of each data record in this
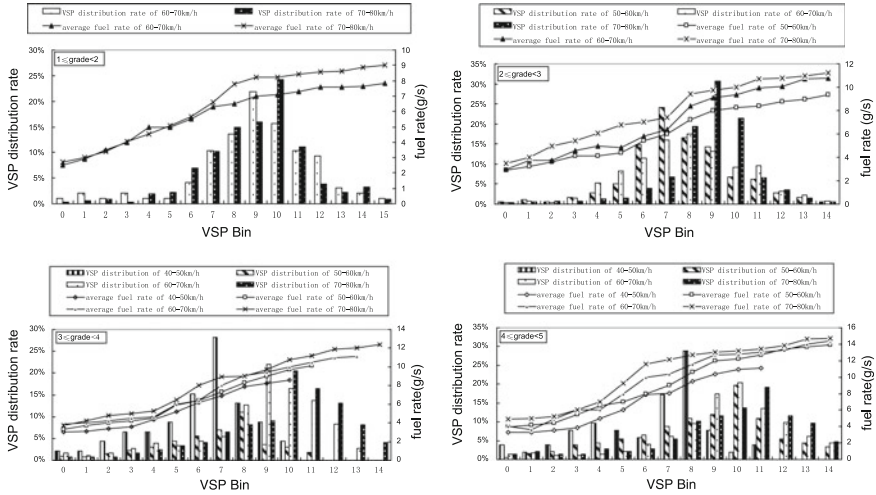
**Fig. 1** VSP distribution versus average fuel rate of empty payload

paper. If the instantaneous speed is located in a speed bin, only the one corresponding record is located in it. The binning and distribution rate is described in Eqs. (4) and (5).

$$VSP = v \times (1.1a + 9.807 \times i + 0.2646) + 0.00029 \times v^3 \tag{2}$$

$$VSP = v \times (1.1a + 9.807 \times i + 0.265) + 0.0000745 \times v^3 \tag{3}$$

$$VSP\ Bin = n, \forall : VSP \in [n, n+1) \tag{4}$$

$$R_{i,j} = \frac{N_{i,j}}{N_j} \tag{5}$$

where $R_{i,j}$ is the percent of time spent of $i$ VSP mode in $j$ speed bin, $N_j$ is a cumulative time of $j$ speed bin, $N_{i,j}$ is a time of $i$ VSP mode in $j$ speed bin.

## 4.2 Average Fuel Rate of Grade-Speed Bin

Using Eqs. (2) and (3) to calculate the VSP of each grade-speed bin, the result is shown in Figs. 1 and 2. Equation (6) shows the average transient rate in VSP bin. Average fuel rate $f_{j\text{ASI,links}}$ of $j$ speed bin under certain grade is calculated in Eq. (7).

$$f_{i\text{VSP}} = \frac{\sum f_{i\text{VSP,transient}}}{n} \tag{6}$$
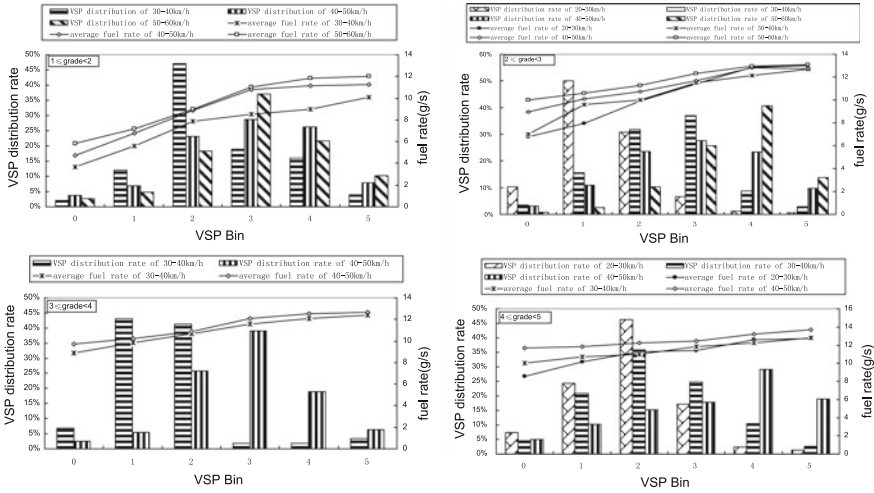
**Fig. 2** VSP distribution versus average fuel rate of full payload

$$f_{j\text{ASI,links}} = \sum_i f_{i\text{VSP}} \times R_{i,j} \tag{7}$$

where $f_{i\text{VSP,transient}}$ is the second by second transient fuel rate in $i$ VSP mode, and n is time spent in $i$ VSP mode.

## 4.3 Data Analysis Results

VSP distribution of grade-speed bin analysis results the VSP data are binned into bins of 1 kW/ton, as shown in Eq. (4), and VSP distribution and average fuel rate are calculated. The grade was divided into 4 parts ($1 \leq$ grade $< 2$, $2 \leq$ grade $< 3$, $3 \leq$ grade $< 4$, $4 \leq$ grade $< 5$) and the speed was separated based on the actual speed range to illustrate the fully loaded and empty load trucks, as shown in Figs. 1 and 2. The figures indicate that VSP distribution rates in each grade-speed bin have their own peak, the corresponding VSP bin of the peak increase as the speed increase, and the shape of VSP distribution is close to normal distribution. In the same grade-speed bin, the corresponding VSP bin of maximum VSP distribution rate with empty payload is greater than full payload. Average fuel rate increases as the VSP bin increase. In the same payload, Average fuel rate increases as the grade increases as well. The maximum VSP bin under empty payload of each grade is much greater than full payload, while average fuel rate of the empty payload is much less than the full payload of the same grade-speed bin.

Since the shape of VSP distribution is close to normal distribution. In order to test its normality, K-S test is used for each grade-speed bins, the result showed that

**Table 1** Normal distribution parameters under empty payload

| Grade (%) | Mean value and variance (km/h) | | | | | | | |
|---|---|---|---|---|---|---|---|---|
| | 40–50 | | 50–60 | | 60–70 | | 60–70 | |
| | $\mu$ | $\sigma$ | $\mu$ | $\sigma$ | $\mu$ | $\sigma$ | $\mu$ | $\sigma$ |
| $1 \leq$ Grade $< 2$ | – | – | – | – | 9.66 | 2.37 | 7.88 | 1.62 |
| $2 \leq$ Grade $< 3$ | – | – | 8.18 | 2.15 | 8.37 | 2.46 | 8.56 | 2.16 |
| $3 \leq$ Grade $< 4$ | 6.33 | 2.35 | 6.42 | 1.88 | – | – | – | – |
| $4 \leq$ Grade $< 5$ | 6.37 | 2.58 | – | – | – | – | – | – |

**Table 2** Normal distribution parameters under full payload

| Grade (%) | Mean value and variance (km/h) | | | | | | | |
|---|---|---|---|---|---|---|---|---|
| | 20–30 | | 30–40 | | 40–50 | | 50–60 | |
| | $\mu$ | $\sigma$ | $\mu$ | $\sigma$ | $\mu$ | $\sigma$ | $\mu$ | $\sigma$ |
| $1 \leq$ Grade $< 2$ | – | – | – | – | 3.56 | 1.33 | 3.72 | 1.23 |
| $2 \leq$ Grade $< 3$ | 1.91 | 0.87 | 2.90 | 1.03 | 3.42 | 1.28 | 4.16 | 1.13 |
| $3 \leq$ Grade $< 4$ | – | – | 1.95 | 0.82 | 3.43 | 1.08 | – | – |
| $4 \leq$ Grade $< 5$ | 2.34 | 0.84 | 2.79 | 1.14 | 3.86 | 1.56 | – | – |

**Table 3** Sample statistics of test route sections

| Payload | No. | Distance (m) | Grade (%) | Speed (km/h) | Sample size |
|---|---|---|---|---|---|
| No-load | 1 | 603 | 3.4 | 70–80 | 62 |
| | 2 | 351 | 2.9 | 50–60 | 46 |
| | 3 | 212 | 4.5 | 40–50 | 25 |
| Full-load | 4 | 334.5 | 3.4 | 40–50 | 56 |
| | 5 | 164.5 | 2.213 | 30–40 | 32 |
| | 6 | 585 | 2.9 | 50–60 | 81 |
| | 7 | 194 | 4.2 | 40–50 | 31 |
| | 8 | 293 | 2.722 | 40–50 | 49 |
| | 9 | 353 | 4.5 | 30–40 | 77 |

there was no evidence to reject most of the null hypothesis regarding the normal distribution of VSP distribution under certain grade and speed. Normal distribution parameters of grade-speed bin of both empty payload and full payload are shown in Tables 1 and 2. The model is verified by measuring the fuel rates using a portion of data collected from the mountainous highway that were not used to calibrate the models. The sample statistics are shown in Table 3. The VSP distribution rate at each speed is obtained based on the VSP distribution model, average transient rate of each grade-speed VSP bin referred from Figs. 1 and 2. Average fuel rate of each grade-speed VSP bin is predicted on Eq. (7). The VSP distribution model is verified by comparing the relative error of the predicted and the collected average fuel rate. The results are shown in Table 4.

**Table 4** Comparison of predicted and collected average fuel rates

| Payload | No. | Predicted average fuel rate (g/s) | Collected average fuel rate (g/s) | Relative error (%) |
|---------|-----|-----------------------------------|-----------------------------------|--------------------|
| Empty   | 1   | 9.15                              | 10.14                             | −9.76              |
|         | 2   | 6.64                              | 7.13                              | −6.87              |
|         | 3   | 6.95                              | 6.89                              | 0.87               |
| Full    | 4   | 9.312                             | 8.82                              | 5.58               |
|         | 5   | 8.488                             | 8.02                              | 5.84               |
|         | 6   | 9.25                              | 8.479                             | 9.09               |
|         | 7   | 9.952                             | 9.124                             | 9.07               |
|         | 8   | 11.51                             | 10                                | 6.90               |
|         | 9   | 11.23                             | 10.51                             | 6.85               |

## 5 Conclusions and Discussions

The study presented in this paper developed the VSP distribution model of HDDVs in the mountainous highway. Incorporate the highway grades into the VSP calculation and binning because of the great variation range. The results show that the distribution of VSP for most sample data followed a normal distribution, and grade was an important influencing factor. The distribution characteristic of VSP varied from different grade. The model was verified by estimating fuel rate using a portion of data collected from the mountainous highway that were not used to calibrate the models. The relative error was less than 10% which shows that this model was suitable for the distribution characteristic prediction and fuel consumption estimation based on VSP approach of HDDVs in the mountainous highway. The proposed approach can help transportation planners and decision-makers to evaluate road traffic fuel economy. There are still limitations of this study. Firstly, different axle types of HDDV will be collected to study the distribution characteristic of VSP. Besides, the data of non-free flow will be collected to study the distribution characteristic of VSP of HDDV to improve the applicability and reduce the error. Finally, we only analyzed the VSP model of loaded trucks and unloaded trucks in this paper.

## References

1. Jiménez-Palacios JL (1999) Understanding and quantifying motor vehicle emissions with vehicle specific power and TILDAS remote sensing. Massachusetts Institute of Technology
2. Zhuo Y, Heng W, Hao L et al. (2013) Statistical vehicle specific power profiling for urban freeways. Soc Behav Sci 98:2927–2938
3. Frey HC, Rouphail NM, Zhai H (2006) Speed and facility-specific emission estimates for on-road light-duty vehicles on the basis of real-world speed profiles. Transp Res Rec J Transp Res Board 1987(1):128–137

4. Song G, Yu L, Tu Z (2015) Distribution characteristics of vehicle-specific power on urban restricted-access roadways. J Transp Eng 138(2):202–209
5. Zang KS, Frey HC (2005) Road grade estimation for on-road vehicle emissions modeling using LIDAR data. In: Proceedings of Annual Meeting of the Air & Waste Management Association
6. Sandberg T (2009) Heavy truck modeling for fuel consumption simulations and measurements. J Linkop Stud Inence Technol Thesis 2002:924
7. Song GH, Yu L (2009) Estimation of fuel efficiency of road traffic by characterization of vehicle-specific power and speed based on floating car data. Transp Res Rec J Transp Res Board 2139(2):11–20
8. Barth M, Younglove T, Scora G (2005) Development of a heavy-duty diesel modal emissions and fuel consumption model. California Partners for Advanced Transportation Technology
9. Frey HC, Unal A, Chen J, Li S, Xuan C (2002) Methodology for developing modal emission rates for EPA's multi-scale motor vehicle and equipment emission system. Publication EPA420-R-02-027
10. Motor vehicle emission simulator (MOVES) (2014) User guide. Environmental Protection Agency, U.S, p 2015
11. IVE Model Users Mannual (Version 2.0) (2008). University of California at Riverside
12. Nam EK, Giannelli R (2005) Fuel consumption modeling of conventional and advanced technology-y vehicles in the physical emission rate estimator (PERE). Draft Report EPA420-P-05-001. U.S. Environmental Protection Agency
13. Song G, Yu L, Zhang Y (2012) Applicability of traffic micro-simulation models in vehicle emission estimations: a case study of VISSIM. The 91st Annual Meeting of the Transportation Research Board, Washington, D.C.
14. Frey HC, Rouphail NM, Zhai H et al (2007) Comparing real-world fuel consumption for diesel- and hydrogen-fueled transit buses and implication for emissions. Transp Res Part D Transp Environ 12(4):281–291
15. Younglove T, Scora G, Barth M (2005) Designing on-road vehicle test programs for the development of effective vehicle emission models. Transp Res Rec 1941:47–56
16. Barth M, Malcolm C, Younglove T et al (2001) Recent validation efforts for a comprehensive modal emissions model. Transp Res Rec: J Transp Res Board 1750:13–23

# Study on Social Network Analysis Method of Bus Network Based on Relation Degree

**Shu-Min Feng, Yi Zhang, Xi-Shuang Han and Xiang-Yang Li**

**Abstract** Conventional bus transportation is of great value in urban transportation network, so it is important to master the regularity between bus lines and explore the optimization method to solve the problem of bus. Divided the degree of relation according to the overlapped stops between the two lines, and the relationship between the routes were divided into three types. The method of measuring the degree of relationship between lines and the modeling steps were given. According to the relationship between bus lines, a bus co-opetition network based on relationship degree was constructed. Using the social network analysis method, the network characteristics were found, the construction steps of the clustering method were given and the network was analyzed. The urban bus co-opetition network of Langfang City was built and the important lines were found by UCINET software. The study of the relationship between the bus lines can cluster the bus lines at the beginning of the bus network planning, which can also provide scientific basis for the operation and management of the buses.

**Keywords** Bus lines · Relation degree · Co-opetition relationship · Social network analysis · UCINET

S.-M. Feng · Y. Zhang (✉)
School of Transportation Science and Engineering, Harbin Institute of Technology, Harbin 150090, China
e-mail: 18722565515@163.com

S.-M. Feng
e-mail: zly@hit.edu.cn

X.-S. Han
Harbin Institute of Technology Shenzhen Graduate School, Shenzhen City 518055, China
e-mail: xshan@hit.edu.cn

X.-Y. Li
School of Management, Harbin Institute of Technology, Harbin 150090, China
e-mail: xiangyangli@hit.edu.cn

# 1 Introduction

Urban residents have been troubled by traffic problems. Conventional bus can ease the pressure of urban public transport, which also plays an important role to decrease traffic congestion. It is of great significance for the optimization and the improvement of the efficiency of bus to explore the internal rules of bus network and find the connection between bus lines. The co-opetition relationship was first used to describe the problem of constructing the market and the allocation of resources between enterprises. Subsequently, the research is applied to the traffic field, most of which were used to describe the relationship between the bus transit and rail transit lines Chien et al. [1, 2] analyzed the transfer of bus lines and rail transit, and proposed a scheme to optimize the cooperation between rail transit and bus lines. Ben-Akiva et al. [3] pointed out that in the case of same travel time and cost, passengers were most likely to choose to take rail transit if the rail traffic can provide higher quality of service and passengers have no preference. Ma et al. [4] analyzed the characteristics of bus and rail transit, and established a competitive model based on Logit model. Fan and Wang [5, 6] constructed a game model to analyze the relationship among the urban traffic. Li [7] pointed out that the competition of bus and rail transit would lead to the evolution of passenger flow of rail transit. In the study of the relationship between bus lines, Ceder et al. [8] proposed a heuristic algorithm to solve the problem of the most common cooperative transfer model; Vicica [9] put forward the method of synchronous transfer to solve the transfer problem of the bus network. Chen [10] proposed a comparative study on the co-opetition statistics and calculation methods based on the passenger traffic volume. Wang [11] proposed a study on the relationship between the bus lines based on the layout, the characteristics of the network were analyzed, and the clustering method of bus line was put forward.

Scholars at home and abroad mainly cared about of the relationship between the bus and rail transit, the methods that solved the co-opetition between bus and rail transit can be used to study the relationship between the bus lines. However, there are few studies on the quantitative analysis of co-opetition relationship in the literature, so there is a need for further research on quantification. Social network analysis method can explore the bus transit network based on the bus lines at the beginning, and improve the operational efficiency is of important significance. The social network analysis method which was based on the relationship degree of bus lines can explore the internal law between bus lines, and it was of great significance to improve operational efficiency and optimize the bus lines.

# 2 Analysis of the Relationship Between Bus Lines

In order to optimize the bus transportation network, usually, the network is divided into a plenty of small parts where the lines closely together. The system may not be able to achieve maximum benefit if the nature of the line is of large difference or

**Fig. 1** Co-opetition of two lines
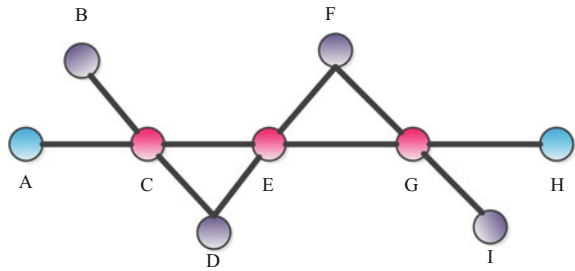
the connection is not close. Therefore, it is very important to study the relationship between the bus lines. Relation degree is used to describe the connection of the bus lines.

The degree of relation is used to represent the physical quantities of two things. The value of relation degree is closer to 1, which shows that the connection is much better [12]. According to the degree of relation between the bus lines, the lines can be divided into two types. Definition the two types as follow.

Uncorrelated lines: There is no overlapped stop between two lines and the relation degree is 0 in defined location; Correlation lines: There are one or more overlapped stops between the lines. The number of the overlapped stops and the location determine the value of the relation degree, the more overlapped stops, the closer the same stops, the larger the degree of relation.

The service area of each stop is generally $0.5 \text{ km}^2$, in order to reduce the amount of calculation that the distance between the two sites is less than 0.5 km is the regarded as the overlapped stops, others are not.

According to the relation degree, the correlation lines can be divided into two types: competition and cooperation lines. Cooperative lines mean there is at least one overlapped stop between the lines and the number of the same stops is less than half of the total. Competitive lines mean the number of overlapped stops more than the half, or the beginning and end stops of two lines are relatively close (less than 0.5 km), the two lines share the passengers in bus network.

Actually, the relationship between bus lines can not only be described by cooperation and competition. Different end stops make the relationship between the two lines different. In Fig. 1, when passengers choose different travel routes, the relationship between the lines are not the same. The lines can be replaced and cooperate with each other, which is known as co-opetition between bus lines.

According to the relation degree, the relationship between bus lines is divided into weak-competition-weak-cooperation type, weak-competition-strong-cooperation type, and strong-competition-weak-cooperation type three types. The weak-competition-weak-cooperation type lines which are of small relation degree can be deleted when optimizing bus network. The lines of strong-competition-weak-cooperation are the key content of route optimization; The goal of optimization bus lines is to make the number weak-competition-strong-cooperation type lines larger.

In line planning, not only taking the passenger travel demand into account, but also the distribution of tourists and the concept of synergy between lines.

## 3 Measurement and Process of Bus Lines Co-opetition Relationship Based on Relation Degree

### 3.1 Calculation Method of Relation Degree

The relation degree can reflect the nature of the relationship between two lines, $\gamma$ means relation degree. The number of stops of line $j$ and line is $k$ is $S_j$ and $S_k$, $S_{jk}$ contains all the stops of line $j$ and line $k$, for $\varphi_{jk}^{i_{jk}}$ measure the associated weights of line $j$ and line $k$, and $\alpha_{jk}^{i_{jk}}$ is the 0–1 variable, when the line $j$ and line $k$ both go through the same stop $i_{jk}$, then the value of $\alpha_{jk}^{i_{jk}}$ is 1, otherwise is 0; $\tau$ means relation weight growth factor, and $\tau > 0$, $i_{id}$ is the order number of overlapped stops, $\varphi_{jk}^{i_{jk}}$ can be obtained by Formula 1.

$$\varphi_{jk}^{i_{jk}} = \alpha_{jk}^{i_{jk}} + \tau(i_{id} - 1) \tag{1}$$

The relation degree of line $j$ and line $k$ is defined as

$$\gamma_{jk} = \frac{\sum_{i_{jk} \in I_{jk}} \varphi_{jk}^{i_{jk}}}{S_{jk}} = \frac{\sum_{i_{jk} \in I_{jk}} \left[\alpha_{jk}^{i_{jk}} + \tau(i_{id} - 1)\right]}{S_{jk}} \tag{2}$$

### 3.2 Example of Calculation of Relation Degree

(1) No adjacent stops in overlapped stops

When there are no adjacent stops in overlapped stops, $i_{id}=0$, in Fig. 2 there are two overlapped stops between line 1 and line 2, thus $S_{jk}=6+6-2=10$, $\gamma_{12}=\frac{2}{10}=0.2$.

(2) Overlapped stops are adjacent

In Fig. 3, there are three overlapped stops between line 1 and line 2, define $\tau = 0.5$, then $\varphi_{jk}^{i_{jk}} = \alpha_{jk}^{i_{jk}} + \tau(i_{id} - 1) = 3+0.5 \times (3-1)=4$, $\gamma_{12}=\frac{4}{8+6-3}=0.37$, there are four overlapped stops between line 1 and line 3, if $\tau = 0.5$, $\varphi_{jk}^{i_{jk}} = \alpha_{jk}^{i_{jk}} + \tau(i_{id} - 1)=4+0.5 \times (2-1 + 2-1)=5$, $\gamma_{13}=\frac{5}{6+8-4}=0.5$.

The two examples show that the degree of relation between two lines is influenced by the number of overlapped stops and their location. As for the value of $\tau$, it reflects the importance of the location of overlapped stops, and the range is 0–1, the location of overlapped stops is more important, the value of $\tau$ is larger.

**Fig. 2** No adjacent stops in overlapped stops



overlapped stops

Line 1

Line 2

**Fig. 3** Adjacent stops in overlapped stops



overlapped stops

Line 1

Line 2

Line 3



Correlated lines

weak-competition-weak-cooperation

weak-competition-strong-cooperation

strong-competition-weak-cooperation

Uncorrelated Lines

$\dfrac{1}{S_{jk}}$
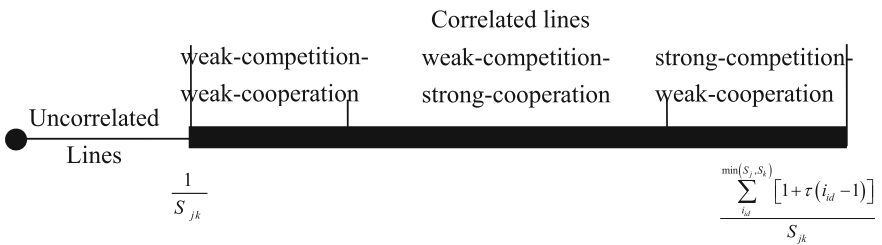
$\dfrac{\sum_{i_{id}}^{\min(s_j,s_k)}\left[1+\tau\left(i_{id}-1\right)\right]}{S_{jk}}$

**Fig. 4** The correspondence between relation value and relation property

The range of the relation degree can be expressed by Fig. 4, the minimum value of the relation degree is 0 value and the maximum value is $\dfrac{\sum_{i_{id}}^{\min(s_j,s_k)}[1+\tau(i_{id}-1)]}{S_{jk}}$. In the closed interval, the relationship between bus lines is divided into three types. The lines of strong-competition-weak-cooperation are important, reasonably control the proportion of completion and cooperation, strengthen the co-opetition between the lines, which can meet the demand for passenger travel, the bus can also enable to improve service quality. However, the three types are not easy to be divided, they can be divided according to the different situation of the urban bus network.

### 3.3 The Steps of Construction of Bus Network Based on the Relation Degree

The steps are as follows:

(1) Region division
    The area that needs to be analyzed is divided into a number of small areas, which roughly divides the connected lines into the same area. Taking the city bus lines into account, so that the division will reduce the workload.
(2) Statistics the number of overlapped stops and calculate the correction value $(i_{id} - 1)$.
(3) Calculation of relation degree
    Take the number that is calculated in the second step into the Formula 2, calculate the relation degree between lines, and draw the cumulative frequency graph, find out the distribution trend, the cumulative frequency of less than 10% line should be removed, and only analysis the lines whose cumulative frequency are more than 90%.
(4) The remaining bus lines using UCINET software for analysis.

## 4 Analysis of Public Transport Network Based on Social Network

### 4.1 Social Network Analysis

Social network analysis, as a part of social science, analyzes the problem from a unique perspective. Social network is based on relational data, and the foundation of social network analysis theory is the relationship between nodes [12]. The main research object is to find out the relationship between the actors and the nodes, the network is established by the relationship, and the relationship is used to explain the behavior of the nodes [11]. Position of the nodes in the network is determined by the relationship between the nodes, the nodes close to constituting a subgroup, their position in the network, the properties and behavior of roughly the same, so it can be divided into the same faction. Social network analysis, which has been widely used in many fields, has been widely used in the study of the relationship between nodes.

## 4.2 The Network Characteristics of Bus Network Based on Social Network Analysis

### 4.2.1 Overall Structure Analysis of Network

The scale, density, and the centrality of the network are the important characters to measure the overall structure of the network.

(1) Scale of network
   The scale is the total number of nodes in the network which is an important index to measure the complexity of the network relationship. The network scale.
(2) Density of network
   The index reflects the close relationship between the actors in the network. There are n actors in undirected networks, the total network overall contains $\frac{n(n-1)}{2}$, in the actual network of m, the network density is the ratio between two, which is $\frac{2m}{n(n-1)}$ [13].
(3) Central potential
   The central potential is the supplement of density, which is the index to measure the degree of centrality of the network. Freeman [14] uses the method of solving the local centrality degree between nodes to obtain the central potential. Center potential can be defined as follows:

$$C_i = \sum_{j=1}^{N} x_{ij} \tag{3}$$

$$x_{ij} = \begin{cases} 1, w_{ij} > 0; i = 1, 2, \ldots, N; j = 1, 2, \ldots, N; i \neq j \\ 0, w_{ij} < 0; i = 1, 2, \ldots, N; j = 1, 2, \ldots, N; i \neq j \end{cases} \tag{4}$$

where $C_i$ is local centrality of node $v_i$; $x_{ij}$ is 0 and 1 variables; $w_{ij}$ is the side weight of node $v_i$ and $v_j$. The central potential of the network can be calculated as follows:

$$C_G = \frac{\sum_{i=1}^{N} (C_0 - C_i)}{\max \sum_{i=1}^{N} (C_0 - C_i)}, \tag{5}$$

where $C_G$ is the central potential of network, $C_0$ is local centrality of core nodes in network. The range of network center potential is a closed interval [0, 1]. The centrality of the network reflects the degree of the centrality of the network, the larger the center potential, the greater the degree of centrality of the network. As for the relationship of public transportation network based on the degree of correlation, the central potential of the network reflects the possibility, and degree of the distribution of the competing relationship between the public transportation lines around a certain or a few lines.

#### 4.2.2 Characteristic Analysis of Nodes

(1)  Centrality

The centrality of nodes includes local centrality and the centrality of the whole network, it needs to consider the indirect relationship between nodes, and the local center is not required. The local center degree of nodes is a measure of the joint local centrality index, by using the Formulas 3–4, we can obtain the local centrality degree of bus network based on the relation degree. The local network degree reflects the closeness between the nodes, the greater the degree of local center node, the more nodes intersected with the nodes in the bus network.

Through the centrality of the bus co-opetition network analysis, we can get the major lines in bus network, the transfer lines are key hubs, so we should pay more attention to the operation management and routes optimization, in order to maximize the benefits of the key lines and ensure the quality of bus services.

(2)  Intermediary

The node which is located between the two nodes and plays a role in the connection the two nodes has intermediary. The bus nodes in the intermediary position assumed transfer large traffic volume, the bus lines connect the different partition, to operate management and optimize the bus network better, we should increase the capacity of lines to ensure the efficient operation of bus.

### 4.3  Subgroup Analysis

#### 4.3.1  The Cliques Analysis of Bus Co-opetition Network

It is important to analysis subgroups in the social network. In short, it means to find out the similar groups in the network, which is represented by cliques. We can obtain the lines whose relationship closely by cliques analysis of bus co-opetition network, the cliques analysis also plays an important role in operation management and route optimization of bus network.

#### 4.3.2  Steps of Subgroup Analysis

①  Set threshold.

The co-opetition network of bus above is a multiple value matrix, so we must set a threshold value, the number which is larger than threshold value set to 1, others are set to 0. The selection of the threshold requires several attempts to find a reasonable value.
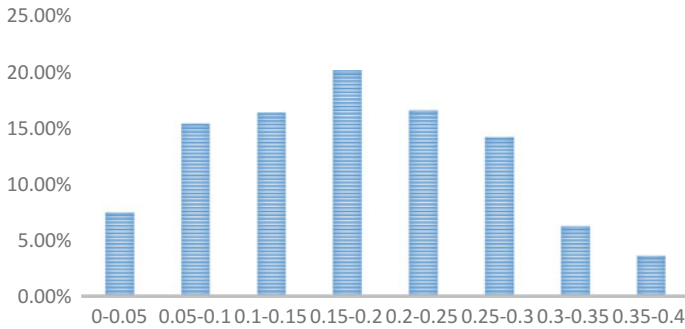
**Fig. 5** Frequency distribution histogram of relation degree between bus lines in Langfang City

② Subgroup analysis.

To find all cliques, if the results are not ideal, you can follow the next steps:

A. There are few cliques in the result: properly reduce the minimum clique size (but not below 3).
B. There are too many cliques in the result: appropriate to increase the minimum clique size.

③ Eliminate shared lines.

In subgroup analysis, we will find that part of the routes belong to multiple cliques, which require the elimination of shared routes, reduce the number of bus lines can achieve the purpose of clustering.

④ Determine the number of classification.

After analysis by UCINET, the key lines of the network can be identified, these key lines, as much as possible, should be clustered in the same cliques, in order to achieve unified management.

## 5 Example Application

Based on the relation degree, the network is established. The bus network of Langfang City includes 29 bus lines. Because the number of bus lines in Langfang City is small, the lines are closely linked, thus the isolated lines not exist, all the lines are considered.

The 29 bus lines of Langfang City contain a total of 406 pairs of combinations, after calculation, the relation degree of bus lines is from 0 to 0.371 and the frequency interval histogram is shown in Fig. 5, the figure suggests that the type of bus network of Langfang City is weak-competition-strong-cooperation type.
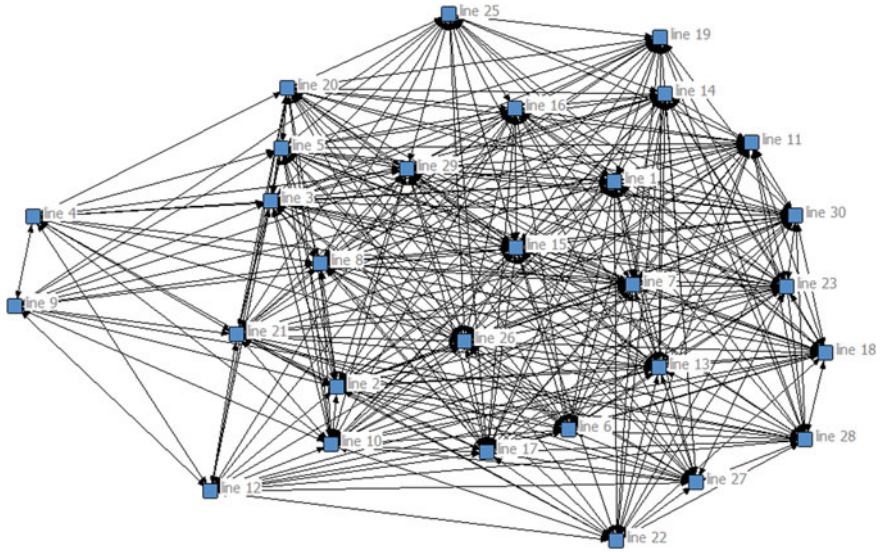
**Fig. 6** Co-opetition bus network of Langfang City

## 5.1 Characteristics Analysis of Bus Network in Langfang City

The bus network of Langfang City is shown in Fig. 6.

### 5.1.1 The Analysis of the Structure of Bus Network in Langfang City

The density calculated of the bus network of Langfang City is 0.0589. According to the Formulas 3 and 4, the local centrality degree of the network nodes of can be obtained, as shown in Table 1. Figure 7 shows local centrality degree of the network, the area of nodes larger, the degree of local centrality is greater. As can be found that the local centrality degrees of line 15 and line 2 are biggest, which indicates that these lines are closely linked to other lines of the network. According to the layout of two bus lines it can be found, the line 2 travels through Langfangbei Railway Station, and line 15 is via Foxconn Station, these stops are the main attraction of passengers flow, which will inevitably lead to cooperation or competition with other bus lines, these two lines should be well considered.

**Table 1**  Centrality degree of nodes in network in Langfang City

| Node | Local centrality | Degree centrality | Closeness centrality | Betweenness centrality |
|------|------------------|-------------------|----------------------|------------------------|
| 1 | 25 | 89.286 | 90.323 | 0.998 |
| 2 | 26 | 92.857 | 93.333 | 1.341 |
| 3 | 25 | 89.286 | 90.323 | 1.096 |
| 4 | 13 | 46.429 | 65.116 | 0.189 |
| 5 | 24 | 89.286 | 90.323 | 1.096 |
| 6 | 24 | 85.714 | 87.500 | 0.558 |
| 7 | 24 | 85.714 | 87.500 | 0.764 |
| 8 | 25 | 89.286 | 90.323 | 1.182 |
| 9 | 13 | 46.429 | 65.116 | 0.356 |
| 10 | 25 | 89.286 | 90.323 | 1.091 |
| 11 | 23 | 82.143 | 84.848 | 0.705 |
| 12 | 18 | 64.286 | 73.684 | 0.726 |
| 13 | 24 | 85.714 | 87.500 | 0.661 |
| 14 | 23 | 82.143 | 84.848 | 0.788 |
| 15 | 26 | 92.857 | 93.333 | 1.016 |
| 16 | 24 | 85.714 | 87.500 | 0.590 |
| 17 | 24 | 85.714 | 87.500 | 0.738 |
| 18 | 21 | 75.000 | 80.000 | 0.446 |
| 19 | 18 | 64.286 | 73.684 | 0.260 |
| 20 | 21 | 78.571 | 82.353 | 0.703 |
| 21 | 25 | 89.286 | 90.323 | 1.322 |
| 22 | 18 | 64.286 | 73.684 | 0.299 |
| 23 | 24 | 85.714 | 87.500 | 0.565 |
| 25 | 19 | 67.857 | 75.676 | 0.530 |
| 26 | 25 | 92.857 | 93.333 | 1.045 |
| 27 | 20 | 71.429 | 77.778 | 0.514 |
| 28 | 20 | 71.429 | 77.778 | 0.747 |
| 29 | 25 | 89.286 | 90.323 | 0.934 |
| 30 | 23 | 82.143 | 84.848 | 0.435 |

## 5.1.2  Analysis on the Characteristics of the Bus Network Nodes in Langfang City

We analyzed the network nodes of the bus network in Langfang City, and the analysis obtains plenty of characteristics of the nodes and they are shown in Table 1.
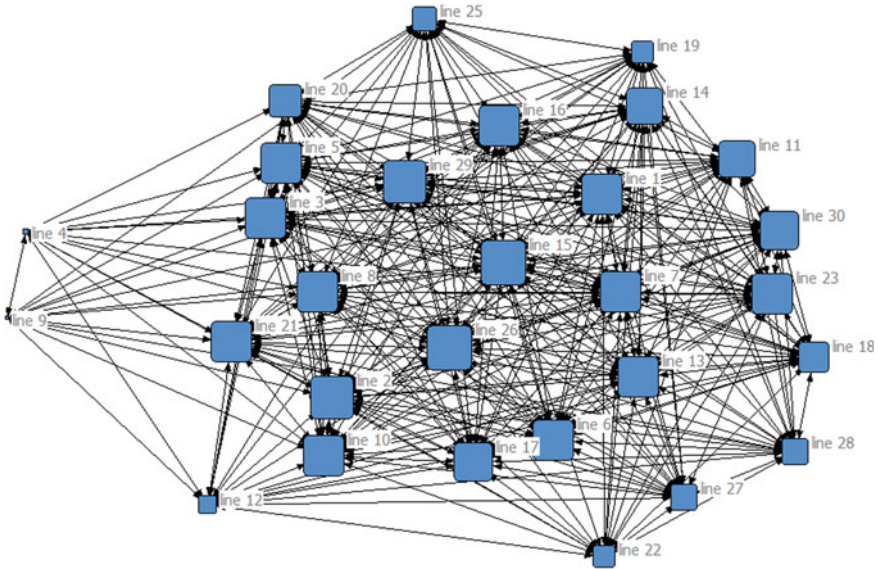
**Fig. 7** The distribution of local centrality degree of bus network in Langfang City
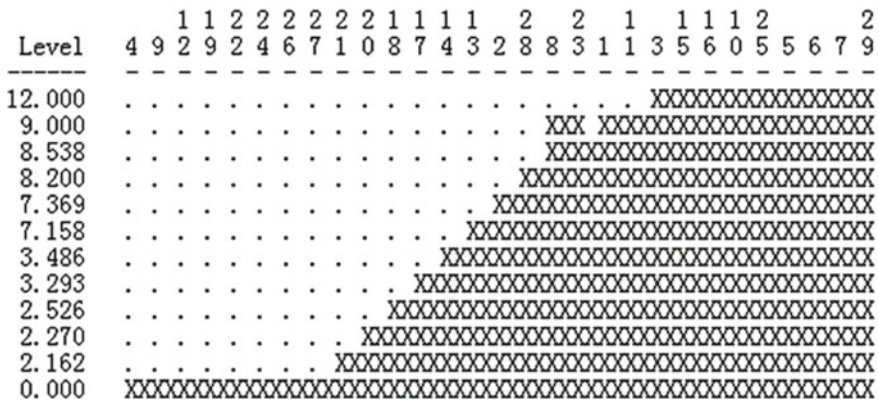


**Fig. 8** Hierarchical clustering graph of shared circuit

## 5.2 Subgroup Analysis of Bus Network in Langfang City

Combined with the establishment steps of subgroup above, UCINET is used to analyze the co-opetition bus network in Langfang City. After several attempts, the threshold value is set to 0.05 which is much suitable, the new matrix is carried out to cluster analysis, finally, we can get the shared hierarchical clustering graph of lines in Fig. 8 and the clustering tree diagram of bus lines in Fig. 9.

**Table 2** Clustering results of bus lines in Langfang City

| Category | Bus lines included | Number of lines |
|---|---|---|
| 1 | 29, 8, 23, 1, 3, 11, 2, 15, 6, 16, 10, 26, 7, 5, 30 | 15 |
| 2 | 18, 17, 14, 13, 20 | 5 |
| 3 | 21, 28, 27 25, 22, 19, 21, 9, 4 | 9 |
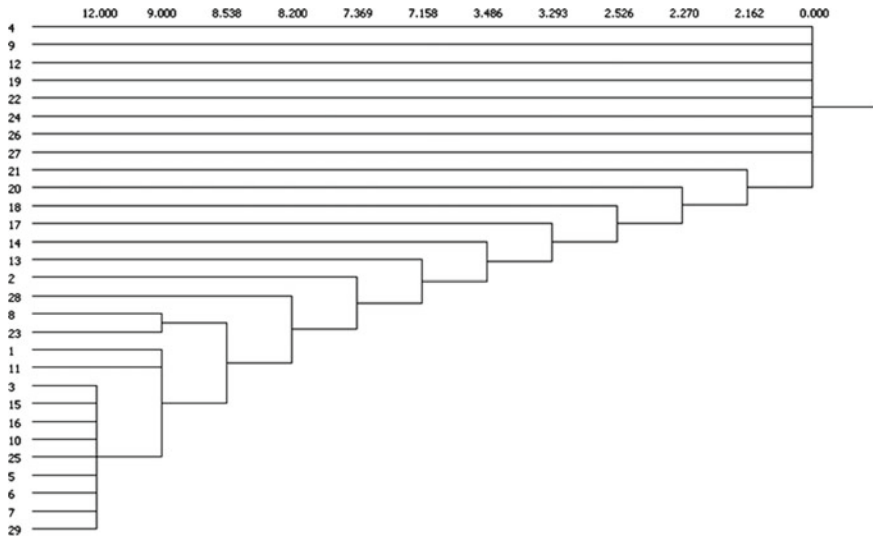


**Fig. 9** Clustering tree diagram of bus lines in Langfang City

Select 7.369 and 2.270 as the cluster threshold values, the lines which level are higher than 7.369 and lower than the number of each are classified as two classes, the others are classified as a class, the results as shown in Table 2. The line 15 and line 2 are of the biggest importance, they are the key lines and belong to the first class, we should consider the relationship between lines in the bus operation management and optimization, in order to achieve the goal of synergy among the lines; The second types of bus lines are of low co-opetition relationship, and the relationship between the lines should be considered as much as possible in traffic planning; Because of the co-opetition relationship is not obvious of the third class, we can ignore the relationship between the lines. However, the lines undertake transfer large traffic volume, we should increase the carrying capacity of these lines to ensure the efficient operation of bus network.

# 6  Conclusions

(1) Define correlation lines, uncorrelation lines of competition and cooperation between lines, according to the degree of relation the correlation lines are divided into weak-competition-weak-cooperation type, weak-competition-strong-cooperation type and strong-competition-weak-cooperation type three types.

(2) The calculation method of relation degree is put forward, and the steps of construction of bus network based on relation are determined.

(3) Taking bus network of Langfang City into account, we analyze the characteristics of the bus network in Langfang City, and find out the line 2 and 15 are the key lines in the network by cluster analysis, the result divides the lines into 3 categories, then we can determine the optimal target of each category.

# References

1. Chien SI, Schonfeld P (1998) Joint optimization of a rail transit line and its feeder bus system. J Adv Transp 32(3):253–284
2. Chowdhury MS, Steven SI (2001) Optimization of transfer coordination for intermodel transit network. In: Transportation Research Board 80th Annual Meeting, Washington, DC, pp 5–25
3. Ben-Akiva M, Morikawa T (2002) Comparing ridership attraction of rail and bus. Transp Policy 9(2):107–116
4. Chaoqun Ma, Yuping Wang et al (2007) Competition model between urban rail and bus transit. Transp Syst Eng Inf 3(7):140–143
5. Fan W (2009) Research of co-opetition mechanism among urban traffic modes. Changsha: Changsha University of Science and Technology, pp 12–38
6. Yi W (2010) Research on Co-opetition Mechanism among Metro and Bus Modes. Changsha: Changsha University of Science and Technology, pp 11–39
7. Li L (2012) Study of competitive theory and method of urban rail transit passenger flow. Zhenjiang: Jiangsu University, pp 66–82
8. Ceder A, Golany B, Tal O (2001) Creating bus timetables with maximal synchronization. Transp Res Part A 35(10):913–928
9. Vicica VR (2012) Urban public transport operation, planning and economy (trans: Song R, He S). Beijing: China Railway Publishing House:223–255
10. Chen Y (2007) Empirical and simulation research on the complex networks of urban bus-transport systems. Nanjing: Nanjing University of Aeronautics & Astronautics, pp 81–89
11. Dixin Wang (2014) Study on the co-opetiton relationship between bus lines based on layout. Harbin Institute of Technology, Heilongjiang
12. Wang Z, Bai J (2007) Application of grey system and fuzzy mathematics in the environmental protection in Harbin: Harbin Institute of Technology press, pp 5–6
13. Liu J (2014) Lectures on whole network approach. Shanghai people's Publishing House pp 19–20
14. Wang Lu (2009) Typical social network analysis software tools and analysis methods. Audio Visual Edu China 4:95–100

# Stabilization Analysis of Mixed Traffic Flow with Electric Vehicles Based on the Modified Multiple Velocity Difference Model

**Chenggang Li, Hongwei Guo, Wuhong Wang and Xiaobei Jiang**

**Abstract**  Electric vehicles have gained popularity in modern society as a solution to both traffic pollution and energy consumption. However, the stabilization of the mixed traffic flow with both electric vehicles (EVs) and fuel electric vehicles (FVs) in the road network has been explored very little. In this study, a modified multiple velocity difference model is developed by taking into account the unique features of EVs. The stability criterion is obtained by the linear analysis, and the coexisting curves are drawn. In addition, the traffic behavior of the modified model is further investigated with numerical simulations. The results show that the characters of different type of vehicles have a great impact on the stability of the mixed traffic flow. Yet, EVs always show better performance in stabilizing the stream than FVs, which indicates that more EVs on the road would help make the traffic much more quickly back to the steady state.

**Keywords**  Stabilization · Electric vehicles · Mixed traffic flow · Modified multiple velocity difference model

## 1  Introduction

Traffic phenomena have been studied in multiple aspects for centuries especially the traffic flow problems. Plenty of physical models are proposed to discuss such issues like traffic accidents [1, 2], traffic flow stability [3–7], and driver behavior [8–10]. Nowadays, due to the severe energy consumption and traffic pollution situations, electric vehicles (EVs) have come into sight as an alternative to replace fuel vehicles (FVs). In fact, the technology of EVs has evolved for decades mainly concentrating

C. Li · H. Guo · W. Wang (✉) · X. Jiang (✉)
Department of Transportation Engineering, Beijing Institute of Technology, Zhongguancun South Street 5, Haidian District, Beijing 100081, People's Republic of China
e-mail: wangwuhong@bit.edu.cn

X. Jiang
e-mail: jiangxiaobei@bit.edu.cn

on two aspects: electricity consumption [11, 12] and the battery life [13, 14]. Rapid development indicates some distinguishing features of EVs compared with FVs such as higher acceleration, lower deceleration, and lower maximum speed which can be used to study the microscopic traffic behavior. However, few works have been conducted to explore the traffic flow stability with both EVs and FVs in the traffic stream. Therefore, we investigate how unique characteristics of electric vehicles affect the stabilization of the mixed traffic flow.

Over the past 60 years, many researchers have attempted to model the traffic behavior to find out the stability condition of traffic flow when disturbances occur. The widely accepted and used model is the optimal velocity (OV) model proposed by Bando et al. [3] in 1995, which described the characteristics of real traffic flow and acquired the kink–antikink density wave when conducting the nonlinear analysis. Helbing and Tilch [4] then proposed the general force (GF) model by considering the negative velocity difference. Based on the GM model, Jiang et al. [5] presented a full velocity difference (FVD) model by taking into account both positive and negative velocity differences. Recently, Wang et al. [6] extended the FVD model into multiple velocity difference (MVD) model. Furthermore, Xie et al. [7] proposed the multiple headway and velocity difference (MHVD) model. Not only microscopic models are presented, several macroscopic models are also put forward. Swaroop et al. [15] introduced a clear definition of traffic flow stability and string stability (car-following stability). Castillo [16] presented a model to evaluate the most important indexes which determine the evolution of disturbance. Yi et al. [17] discussed the second-order macroscopic vehicle traffic flow models in terms of their capability to reproduce stable and unstable traffic flow behaviors and acquired the stability condition by using the wave-front expansion technique. All of the above models have laid solid theoretical foundation for studying the stabilization of traffic flow.

In recent years, mixed traffic phenomena have drawn a lot of attention, and two major types of mixed traffic are being investigated. One is the motorized and non-motorized vehicles mixed traffic, which is widely and intensively discussed especially in developing countries such as China, Vietnam, etc. [18–20]. The other one, which is discussed in this study, is the multi-type vehicles mixed traffic. Quite a few methodologies were applied to model mixed traffic. The cellular automaton model is popularly used to illustrate the multi-type vehicles mixed traffic. Moussa et al. [21] carried out computer simulations using CA model to explore the behaviors of cars and trucks. Zhang et al. [22] used weighted essentially non-oscillatory (WENO) method to solve the multi-class traffic flow model for an inhomogeneous highway. Li et al. [23] pointed out that aggressive lane-changing behavior of fast vehicle can depress the plug formed by slow vehicles and improve traffic flow in mixed traffic. Mu et al. [24] concluded that introduction of micro-cars would alleviate traffic congestion to some extent, and the traffic volume with micro-cars would become bigger than that without micro-cars. Chowdhury et al. [25] and Liu et al. [26] concentrated on the speed difference of vehicles in the traffic flow, which drew a conclusion that larger proportion of large slow vehicle contributing to lower operational capacity. Other than CA model, traffic flow theory is also used to investigate the traffic behavior. Aghabayk et al. [27] compared four types of car–truck combination and pointed

out that the leading vehicle type and the following vehicle type both influence the effect of car–truck mixture on traffic flow. Mason et al. [28] found out that trucks could be more likely to cause traffic jam compared with cars by using both linear and nonlinear stability analysis methods. Jin et al. [29] used a visual angle car-following model to study the stability and concluded that trucks could better stabilize traffic flow than cars, however, the study only considered the change rate of the visual angle. Yang et al. [30] pointed out that the stability of the mixed traffic flow is more determined by the proportions of the different car–truck following scenarios, rather than the numbers of the cars and trucks.

To our knowledge, few studies involve the characteristics of EVs and the car-following theory to investigate the stabilization of the mixed traffic flow. In this study, the multiple velocity difference model is extended to study the EVs and FVs heterogeneous traffic flow and the stability condition of the modified model are explored by conducting both linear stability analysis and nonlinear analysis [13]. Last, numerical simulations are carried out to examine the theoretical analysis.

## 2  The Modified Multiple Velocity Difference Model

Considering the unique features of EVs compared with FVs, four vehicle combinations are discussed in this study: EV following EV (EE), EV following FV (EF), FV following FV (FF), FV following EV (FE). And two major characteristics of EVs are analyzed: higher acceleration rate and lower maximum velocity compared with FV. The difference of acceleration rate between the two types of vehicles is described by the sensitivity $a$ (we assume that the reaction time of all drivers is the same), and the difference of maximum velocity is defined as $V^{\max}$.

In this study, the MVD model [13] is extended to the modified multiple velocity difference model as follows:

$$\ddot{x}_n(t) = a_n[V(\Delta x_n(t)) - v_n(t)] + \sum_{j=1}^{m} k_j \Delta v_{n+j-1}(t),$$

$$(n = 1, 2, \ldots, N),$$

$$(j = 1, \ldots, m, m \ll N),$$

$$V(\Delta x_n(t)) = \frac{V_n^{\max}}{2}[\tanh(\Delta x_n(t) - x_c) + \tanh(x_c)], \tag{2}$$

where $a$ is the sensitivity of a driver, $N$ is the total number of vehicles, $x_n(t)$ is the position of vehicle $n$ at time $t$, $\Delta x_n(t) = x_{n+1}(t) - x_n(t)$ is the headway of vehicle $n$, $v_n(t)$ is the speed of vehicle $n$ at time $t$, $\Delta v_n(t) = v_{n+1}(t) - v_n(t)$ is the speed difference between vehicle $n+j-1$ and vehicle $n+j$, $kj$ are the coefficients of velocity difference, $V(\cdot)$ is the optimal velocity function, $V^{\max}$ is the maximum velocity, $x_c$ is the safety distance. $n$ is the $n$th vehicle that can be either an electric vehicle or a fuel vehicle, the values of $a_n$ and $V_n^{\max}$ depend on the vehicle combinations.

## 3  Linear Stability Analysis

Stabilization of the uniform traffic flow is considered as a situation in which vehicles move with constant velocity and zero acceleration, and headway follows uniform distribution. However, to maintain the steady state requires different headway between different types of vehicle [15].

$$h_e = x_c - \log\sqrt{\frac{V_f^{\max} + V_f^{\max} e^{2x_c}}{v + V_e^{\max} + v e^{2x_c}} - 1},\tag{3}$$

$$h_f = x_c - \log\sqrt{\frac{V_f^{\max} + V_f^{\max} e^{2x_c}}{v + V_f^{\max} + v e^{2x_c}} - 1},\tag{4}$$

where $h_e$ is the uniform headway of EE and EF under the steady state, $h_f$ is the uniform headway of FF and FE under the steady state, $v$ is the uniform velocity.

The stability of the uniform traffic flow with different headways is investigated according to different types of vehicles. To simplify the analysis, we use $h^*$ instead of $h_e$ and $h_f$ below. The solution of the uniform flow is given by

$$x_n^0(t) = h^* n + V(h^*) t,\tag{5}$$

Note that the stability of the uniform traffic flow is determined by the sensitivity $a$, the derivative of the optimal velocity function $V(\cdot)$ at uniform headway $h^*$ and velocity difference. Considering the small disturbance, the uniform flow is stable if

$$V'(h^*) < \frac{a_n}{2} + \sum_{j=1}^{m} k_j,\tag{6}$$

In the mixed traffic flow, two kinds of stability need to be analyzed— the stability of different vehicle combinations and the stability of the whole traffic flow. The stability of the combinations can be defined as follows:

$$S_e = V'(h_e) - \frac{a_e}{2} - \sum_{j=1}^{m} k_j < 0,$$

$$S_f = V'(h_f) - \frac{a_f}{2} - \sum_{j=1}^{m} k_j < 0,\tag{7}$$

The mixed traffic flow reaches stable when the disturbance is suppressed along the entire traffic flow. The solution is given as
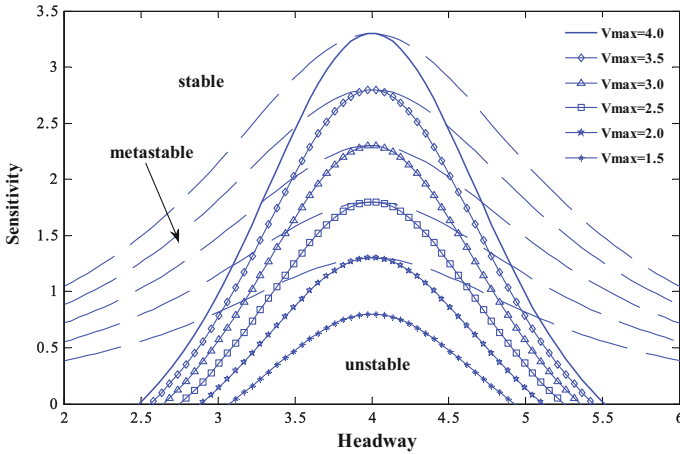
**Fig. 1** Phase diagram in the headway-sensitivity space

$$S_l = \sum_n \left( V'(h^*) - \frac{a_n}{2} - \sum_{j=1}^{m} k_j \right),  \tag{8}$$

Wang et al. [9] pointed out that the stability of the MVD model considering two leading vehicles (set $m = 2$) is better than that of FVD model. In this study, we take $m = 2$, $k_1 = 0.2\ \text{s}^{-1}$, $k_2 = 0.15\ \text{s}^{-1}$. Set safety distance $x_c = 4$. Figure 1 shows the neutral stability curve under the different maximum velocity. With the increase of $V^{\text{max}}$, the stable area is shrinking.

In Fig. 1, for each value of $V^{\text{max}}$, the traffic flow is divided into three regions by solid lines (representing the neutral stability curve) and the dotted lines (representing the coexisting curve): the stable region above the dotted lines, the metastable region between the solid line and the dotted line, and the unstable region below the solid line. With the increase of $V^{\text{max}}$, both the stability curve and the coexisting curve decrease. Consequently, the stable region is enlarged while the unstable region is reduced.

## 4  Simulation

To examine the validity of stability conditions, numerical simulations are carried out for the modified model described by Eq. (1). The boundary is periodic. Assuming that 100 vehicles move around a circle clockwise, and No. 100 vehicle follows No. 1 vehicle. The first 50 vehicles are FVs and the following 50 vehicles are EVs, i.e., 49 EE and FF combinations, 1 EF and FE combination. The initial conditions are given as: $a_e = 2.2$, $a_f = 2.0$, $V_e^{\text{max}} = 2.5$, $V_j^{\text{max}} = 3.0$, $x_c = 4.0\ k_1 = 0.2\ \text{s}^{-1}$,
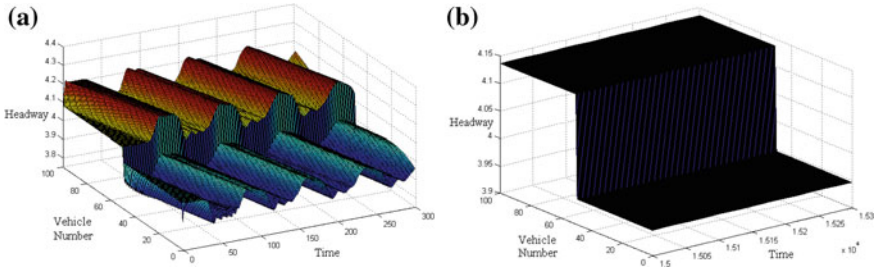
**Fig. 2** Headway variation of all vehicles for the modified model during the time of **a** $0 \leq t \leq 300$, **b** $30{,}000 \leq t \leq 30{,}300$

$k_2 = 0.15 \ \text{s}^{-1}$. The disturbance is added to the first vehicle. Based on the stability conditions above, we have calculations as $S_e = -0.3072$, $S_f = 0.1164$, $S_l = -0.1908$. The numerical analysis shows that EE and EF combinations are stable while FF and FE combinations are unstable. In terms of the whole mixed traffic flow, it comes to the steady state eventually as the fluctuations vanish with time. More specifically, results above indicate that EE and EF combinations could weaken the fluctuations, while FF and FE combinations would amplify the fluctuations.

We further investigate that how mixed traffic flow evolves with time. Two different time ranges are considered, one is $0 \leq t \leq 300$, the reaction of the mixed traffic flow can be obtained when the disturbance added to the first vehicle at the very beginning, the other duration is $30{,}000 \leq t \leq 30{,}300$, we can find out whether the mixed traffic flow goes to steady state or the opposite after 30,000 time steps. Figure 2 shows the headway variation of all vehicles for the modified model. It can be seen that two different headways exist for different vehicle combinations, the headway of EE and EF is smaller than that of FF and FE. Given that the deceleration rate of EVs is lower than that of FVs, larger headway is needed by EVs in the mixed traffic flow. The perturbation conveys from No. 100 vehicle to No. 1 vehicle in this simulation. In Fig. 2a, it can be seen that the fluctuation reaches the peak when perturbation passes to the first vehicle, decreases when passes the last vehicle, and vanishes in the EE combination. Consequently, EE and EF combinations can stabilize the mixed traffic flow while FF and FE combinations perform inversely. It can be seen from Fig. 2b that mixed traffic flow comes to steady state eventually and thus it can be concluded that simulation results correspond to the theoretical results.

It is further being investigated that how the sensitivity $a$ affects the stability of the mixed traffic flow. Table 1 presents the values of $S_e$, $S_f$, $S_l$ as $a_e$ and $a_f$ varies. Compare first two groups of data, the value of $a_e$ is the same, while the value of $a_f$ changes, which leads to a stable situation and an unstable situation, respectively. It can be seen that larger acceleration difference of various vehicles could contribute to unstable condition of the mixed traffic flow more easily. However, the actual acceleration difference between EVs and FVs is observable but not that much. From last three groups of data, we can see that the stability of both vehicle combinations and the mixed traffic flow is dropping with the decrease of $a$. It indicates that the

**Table 1** Values of $S_e$, $S_f$, $S_l$ as $a_e$ and $a_f$ varies

| $a_e$ | $a_f$ | $S_e$ | $S_f$ | $S_l$ |
|-------|-------|-------|-------|-------|
| 2.2 | 2.0 | −0.3072 | 0.1164 | −0.1908 |
| 2.2 | 1.6 | −0.3072 | 0.3164 | 0.0092 |
| 1.8 | 1.6 | −0.1072 | 0.3164 | 0.2092 |
| 1.6 | 1.4 | −0.0072 | 0.4164 | 0.4092 |
| 1.4 | 1.2 | 0.1072 | 0.5164 | 0.6236 |

initial disturbance amplifies as time develops, which leads to the collapse of the whole traffic flow eventually.

Figure 3 illustrates the headway variation of all vehicles between $0 \le t \le 300$, and Fig. 4 describes same situations during the time span $30{,}000 \le t \le 30{,}300$. For the set $(a_e, a_f) = (2.2, 1.6)$, the value of $S_l$ is nearly 0, it seems like that the mixed traffic flow comes to steady at last. It is shows in Fig. 3a that the perturbation increases sharply when passing on in the fuel vehicle combinations and gradually vanishes in electric vehicle combinations. However, as we can see in Fig. 4a, after $t = 30{,}000$, the traffic flow still fluctuates with time. For the set $(a_e, a_f) = (1.8, 1.6)$ and $(a_e, a_f) = (1.6, 1.4)$, numerical analysis shows that the mixed traffic flow is unstable, while it seems in Fig. 3b–c the perturbation can be suppressed at last. However, Fig. 4b–c show that the fluctuations increase after $t = 30{,}000$, that they will never come back to the uniform flow. As for the set $(a_e, a_f) = (1.4, 1.2)$, it is shown in Figs. 3d and 4d that perturbation grows with time and leads to the breakdown of the whole traffic flow. Figures 3 and 4 give the headway variation tendency through time with different values of sensitivity $a$. The simulation results agree with the theoretical analysis.

Based on the numerical analysis and simulations, we come to a conclusion that higher the acceleration, more stable the traffic flow could be achieved. In real traffic stream, the response of each vehicle is vital. With higher acceleration, immediate actions can be taken by EVs facing with the situation that the headway increases suddenly, which implies that the influence of the abrupt change can be suppressed to the minimum by EVs and the subsequent vehicles can also reduce the perturbation each time and finally lead to the steady state of the whole traffic flow. On the contrary, the response of FVs is slow due to the lower acceleration, resulting in the situation that the unexpected change of headway will pass along the stream affecting many more following vehicles, which may give rise to congestion.

Table 1 indicates that the values of $S_e$ and $S_f$ are essential to the stability of the vehicle combinations, and smaller values contribute to better stabilization. It can be further explored whether there is a situation where the stability of FF and FE combinations is better than that of EE and EF combinations. Figure 5 gives the variation tendency of $S_e$ and $S_f$ as the uniform velocity varies. The conditions are given as $V_e^{\max} = 2.5$, $V_j^{\max} = 3.0$, $x_c = 4.0$.

In Fig. 5, three phases are discussed.

- When uniform velocity is lower than 0.5, it can be found that the values of $S_e$ and $S_f$ are less than zero, which means both vehicle combinations are stable. Meanwhile,
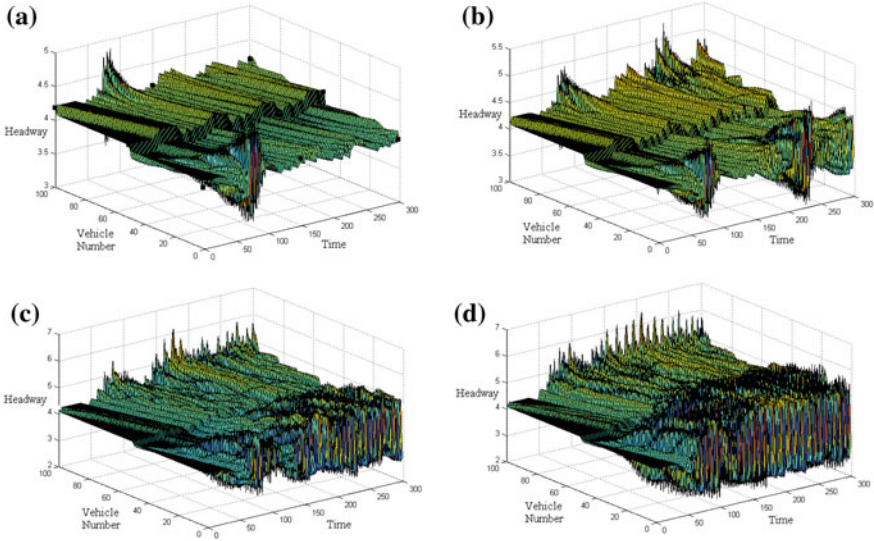
**Fig. 3** Headway variation of all vehicles ($0 \leq t \leq 300$), the patterns **a–d** are assigned with $(a_e, a_f) = (2.2, 1.6), (1.8, 1.6), (1.6, 1.4), (1.4, 1.2)$, respectively
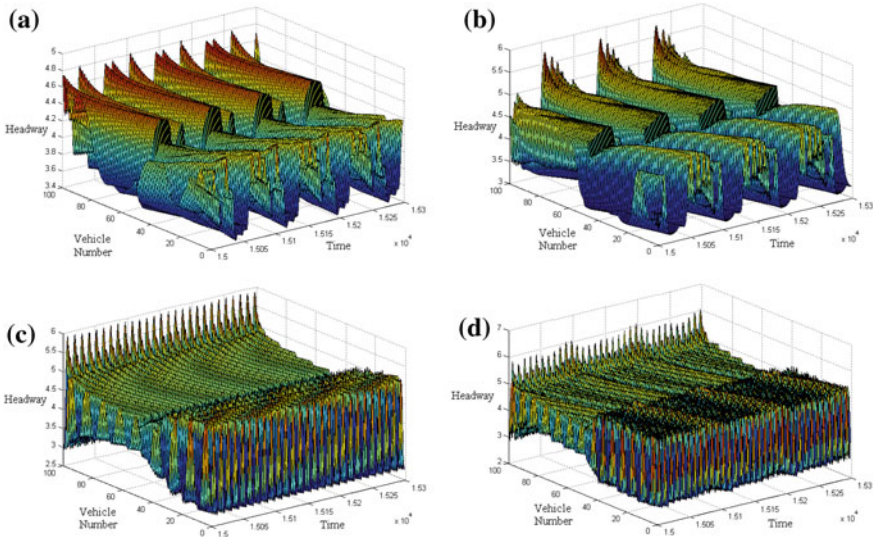


**Fig. 4** Headway variation of all vehicles ($30{,}000 \leq t \leq 30{,}300$), the patterns **a–d** are assigned with $(a_e, a_f) = (2.2, 1.6), (1.8, 1.6), (1.6, 1.4), (1.4, 1.2)$ respectively

EVs can provide better-stabilized effect than FVs. This phenomenon implies that the stability of all vehicle combinations improves with the decreasing velocity.
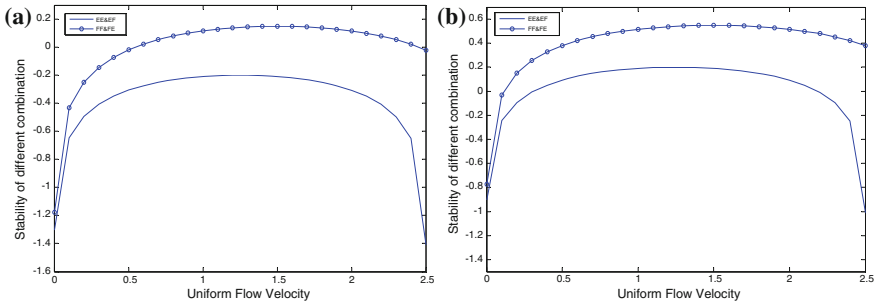
**Fig. 5** Variation tendency of $S_e$ and $S_f$ as the uniform velocity varies, the patterns **a–b** are assigned with $(a_e, a_f) = (2.2, 2.0), (1.4, 1.2)$, respectively

- When the uniform velocity is greater than 0.5 and less than 2.0, $S_f$ grows much faster than $S_e$ and the stability of FF and FE combinations drops much more quickly than that of EE and EF combinations as the uniform velocity increases.
- When the uniform velocity is greater than 2.0. Apparently, EE and EF combinations return to the uniform state much more quickly than FF and FE combinations. The tendency of $S_e$ seems alike to phase (1) while $S_f$ takes much more time to come back to steady state, which indicates that driving EVs on the road network could make the stream more stable than driving FVs under the high-speed situation.

Above all, it can be concluded that both EVs and FVs can stabilize or un-stabilize the mixed traffic flow depending on the acceleration and the uniform velocity, and the stabilization of EE and EF combinations is always better than that of FF and FE combinations. In real traffic flow, EVs would weaken the perturbation caused by the proceeding vehicle regardless of the type, while it takes much more time for FVs to reduce the disturbance, and sometimes FVs even amplify the fluctuation leading to the congestion eventually. Thus, it can be expected that more electric vehicles on the road, more stable the traffic flow would be.

## 5 Conclusions

In this study, the modified multiple velocity difference model is developed to describe the mixed traffic flow considering the unique features of EVs, and four vehicle combinations scenarios are discussed. As for EVs, two particular factors are taken into account, the maximum velocity $V^{\max}$ and acceleration rate described by sensitivity $a$ of the model. The stability condition is derived from the linear and nonlinear analysis, and the criterion is related to the sensitivity $a$, the derivative of the optimal velocity function $V(\cdot)$ at uniform headway $h^{*}$ and velocity difference. Then, numerical simulations are carried out to validate the theoretical results and the headway tendency is depicted by setting different patterns with different $a$ at $0 \leq t \leq 300$ and

30,000 $\leq t \leq$ 30,300. We can conclude that all vehicle combinations can stabilize the mixed traffic flow, however, the EE and EF combinations always show better performance in stabilizing the stream than FF and FE combinations. Hence, we learn that the urban traffic would be more stable with more electric vehicles, and they can reduce not only the traffic pollution but traffic accidents. This study only focuses on the effects of the modified model, however, many other aspects could influence the stabilization of the mixed traffic flow. In our future work, more factors are being considered to study the stability criterion.

# References

1. Quddus MA (2008) Time series count data models: an empirical application to traffic accidents. Accid Anal Prev 40(5):1732–1741
2. Brijs T, Karlis D, Wets G (2008) Studying the effect of weather conditions on daily crash counts using a discrete time-series model. Accid Anal Prev 40(3):1180–1190
3. Bando M, Hasebe K, Nakayama A, Shibta A, Sugiyama Y (1995) Dynamical model of traffic congestion and numerical simulation. Phys Rev E 51(2):1035
4. Helbing D, Tilch B (1998) Generalized force model of traffic dynamics. Phys Rev E 58:133–145
5. Jiang R, Wu QS, Zhu ZJ (2001) Full velocity difference model for a car-following theory. Phys Rev E 64:017101
6. Wang T, Gao ZY, Zhao XM (2006) Multiple velocity difference model and its stability analysis. Acta Phys Sin 55:634–640
7. Xie DF, Gao ZY, Zhao XM (2008) Stabilization of traffic flow based on the multiple information of preceding cars. Commun Comput Phys 3(4):899–912
8. Rosey F, Auberlet JM (2014) Driving simulator configuration impacts drivers' behavior and control performance: An example with studies of a rural intersection. Transp Res Part F 27:99–111
9. Warner HW, Aberg L (2008) Drivers' beliefs about exceeding the speed limits. Transp Res Part F 11(5):376–389
10. Gwyther H, Holland C (2014) Feelings of vulnerability and effects on driving behaviour—a qualitative study. Transp Res Part F 24:50–59
11. Silva C, Ross M, Farias T (2009) Evaluation of energy consumption, emissions and cost of plug-in hybrid vehicles. Energ Convers Manage 50(7):1635–1643
12. Faria R, Maques P, Moura P (2013) Impact of the electricity mix and use profile in the life-cycle assessment of electric vehicles. Renew Sust Energ Rev 24(3):271–287
13. Hawkins TR, Singh B, Majeau BG (2013) Comparative environmental life cycle assessment of conventional and electric vehicles. J Ind Ecol 17(1):53–64
14. Yang SC, Deng C, Tang TQ, Qian YS (2013) Electric vehicle's energy consumption of car-following models. Nonlinear Dynam 71(1–2):323–329
15. Darbha S, Rajagopal KR (1999) Intelligent cruise control systems and traffic flow stability. Transp Res Part C 7(6):329–352
16. Castillo JM (2001) Propagation of perturbations in dense traffic flow: a model and its implications. Transp Res Part B 35(4):367–389
17. Yi JG, Lin H, Alvarez L, Horowitz R (2003) Stability of macroscopic traffic flow modeling through wavefront expansion. Transp Res Part B 37(7):661–679

18. Meng JP, Dai SQ, Dong LY, Zhang JF (2007) Cellular automaton model for mixed traffic flow with motorcycles. Phys A 380(7):470–480
19. Wan LW, Chiou YC, Lin ZS, Hsu CC (2010) Cellular automaton simulations for mixed traffic with erratic motorcycles' behaviors. Phys A 389(10):2077–2089
20. Hu XJ, Wang W, Yang HF (2012) Mixed traffic flow model considering illegal lane-changing behavior: simulations in the framework of Kerner's three-phase theory. Phys A 391(21):5102–5111
21. Moussa N, Daoudia AK (2003) Numerical study of two classes of cellular automaton models for traffic flow on a two-lane roadway. Eur Phys J B 31(3):413–420
22. Zhang P, Wong SC, Shu CW (2006) A weighted essentially non-oscillatory numerical scheme for a multi-class traffic flow model on an inhomogeneous highway. J Comput Phys 212(2):739–756
23. Li, XG, Jia B, Gao ZY, Jiang R (2006) A realistic two-lane cellular automata traffic model considering aggressive lane-changing behavior of fast vehicle. Physica A 367(C):479–486
24. Mu R, Yamamoto T (2012) An analysis on mixed traffic flow of conventional passenger cars and microcars using a cellular automata model. Procedia Soc Behav Sci 43(4):457–465
25. Chowdhury D, Wolf DE, Schreckenberg M (1997) Particle hopping models for two-lane traffic with two kinds of vehicles: effects of lane-changing rules. Phys A 235(3–4):417–439
26. Liu LY, Li XG, Jia B (2014) Traffic dynamics around weaving section with mixed slow and fast vehicles based on cellular automata model. Procedia Soc Behav Sci 138:548–556
27. Aghabayk K, Sarvi M, Young W, Wang Y (2012) Investigating heavy-vehicle interactions during car-following process. Transportation Research Board of the National Academies, Washington, DC
28. Mason AD, Woods AW (1997) Car-following model of multispecies systems of road traffic. Phys Rev E 55(3):2203–2214
29. Jin S, Wang DH, Huang ZY, Tao PF (2011) Visual angle model for car-following theory. Phys A 390(11):1931–1940
30. Yang D, Jin P, Pu Y, Ran B (2014) Stability analysis of the mixed traffic flow of cars and trucks using heterogeneous optimal velocity car-following model. Phys A 395(4):371–383

# Research on Psychological Reaction of Driving Distraction Based on Sample Entropy

Xiao-hua Zhao, Wen-xiang Xu, Ying Yao and Jian Rong

**Abstract** Driving distraction is a task affected by an increasing number of Driving Assistance Systems, which have been a main reason of traffic accident. Understanding the nature of driver distraction and to find a way to analysis the driver distraction we can reduce the traffic accident. This chapter applied the electrocardiography (ECG) for identifying driving situation. ECG data such as heart rate variability (HRV), QRS wave were used to represent driving distraction, the method of sample entropy used to indicate the difference between normal driving and driving distraction. The data have interviewed 34 subjects during two weeks based on driving simulation experiment. The result showed that sample entropy of ECG data on distracted driving is higher than that on normal driving. Especially, the driver who send message during driving has the biggest difference in sample entropy. Driver's QRS waveform showing a greater degree of confusion on the distracted driving.

## 1 Introduction

On the one hand, drivers enjoy facilitate the car's Equipment, on the other hand, they often in dual-task or multi tasks which result in driving distraction. According to the Yerkes–Dodson Law [1] of the human body, people easy to have additional stress and distraction in driving when they are high level of mental stress. Which lends to show error at perception and decision make. Australian Road Safety Committee [2] put forward a definition of the driving distraction: "the driver distraction is diverting driver's attention form driving task consciously or unconsciously (not due to alcohol, drugs, fatigue and other factors). Drivers perform additional tasks and short focus on independent events of driving, objects and people. This change reduces the

X. Zhao (✉) · W. Xu · Y. Yao · J. Rong
College of Metropolitan Transportation, Beijing University of Technology, Beijing 100124, China
e-mail: zhaoxiaohua@bjut.edu.cn

driver's environmental awareness, decision-making level and operational skills". In the 1970s, Sheridan proposed the driving task is composed of three-layer as operation layer, tactics layer, and the strategic layer of the control process, J. A. Michon, T. A. Ranney and other researcher analyses about the control of multilayer driving distraction [3–5]. There are many sources of distraction, a comprehensive comparison is classification to four dimensions as hearing, vision, cognition, and operation. In the research of the NHTSA [6], drivers always use communication equipment, operate wireless vehicle auxiliary device and talk with passengers during driving, etc.

Although there are a large number of studies on driving distraction, most conclusions are focused on distracting behavioral research, which lends to a less of theoretical support for the driving distraction in physiological indicators. However, the response of driving distraction from the physiological level is important. On the one hand, it is conducive to explore the relationship between the physiological indicators and the decision-making response. On the other hand, it can explain the physiological response of behavior indicators when driving distraction. Based on those reasons, the paper compared the HRV indexes of distraction and normal driving under different conditions of driving distraction. The aim of the study is to explore the influence of driving distraction on the driver's psychological index through the calculation of the sample entropy and the trend comparison.

## 2   Methodology

Unlike the traditional method to detect the driving distraction, this study detected the driving distraction by bio-signals, which cause the change of the emotion and body expressions. First, the widely used definition for emotion recognition in computer disciplines was introduced by Picard [7] in the 1990s. Emotion recognition is defined as "measuring observations of motor system behavior that correspond with high probability to an underlying emotion or combination of emotions". This definition is based on the fact that there is importance in finding the way to reflect the change of the emotion.

In order to represent the indicators which can express driving distraction, we use the Electrocardiography (ECG) as measurement index. The ECG records those cardiac electrical currents (voltages, potentials) by means of metal electrodes placed on the body (the recording is visualized by means of an electrocardiographic data) [11]. Normally, we will record the heart rate variability (HRV) which is a promising tool for applications involving medical diagnoses and stress detection. Kim [8] have reported the use of HRV statistics to estimate mental stress which shows the short timescale during the driving distraction. VLF was indicated as unreliable data for short time intervals. The LF/HF ratio is an indicator for autonomic balance [9]. The ECG diagram has been used to show the difference between the normal driving and driving distraction. These graphs illustrate the characteristics of an electrocardiogram in intuitive perspective. The electrocardiogram will give a great deal of insight to researchers who study driving behavior in the future. At begin, this study built the

trends of ECG about the driving distraction, but it is only the first step of the work, but not least.

## 3 Driving Simulator Experiment

### 3.1 Subjects

Thirty-Four healthy subjects (mean age ± SD = 33 ± 12.8 years, range 19–55 years; mean driving experience ± SD = 9.4 ± 8.5 years, range 1–27 years) participated after providing written informed consent. Subjects were recruited by announcement in the university and society.

### 3.2 Apparatus

The fixed-base driving simulator consists of a real car, computers, and video and audio equipment. The road scenario is projected onto three big screens providing a 130° field of view.

AKF2 dynamic multiparameter physiological recorder records the participants' physiological parameters, including electrocardiogram (ECG), heart rate (HR), and respiratory rate. It can be a preliminary analysis of the driver's basic ECG state.

### 3.3 Simulated Scenarios

In China, most of driving distraction produce form urban roads. Because of limited space in urban areas, all of the distracting behavior occurs at a small distance. In order to eliminate the interference of confounding factors on the experimental data, all elements in these scenarios were the same except for driving distraction order. The emergency lane change during the normal driving and distraction, general lane change during the normal driving and distraction, emergency brakes during the normal driving and distraction, general brakes during the normal driving and distraction, normal driving, car calling, send message, tuning radio, and opening the navigation during driving, both of these factors will be reflected in the scene, and all subjects will go through the same experimental scene with random order to ensure the subjects can be compared.

### 3.4 Experimental Designs and Procedures

All participants were given the warning for driving the simulator. Then, the experimenter will check the fatigue level of the pilot before the test and the level of relevant experimental factors. Finally, the experimenter will make the subjects to bring ECG instrument. Before the driving experiment, all participants took 3–5 min for the practice drive depending on their own driving habit, in this scenario, there is no traffic, no driving tasks, it is just to let drivers to familiar with the operation of simulate driving and join themselves to the experiment. The main purpose of the practice drive was to minimize the impact of a participant's unfamiliarity with the driving simulator on the experimental data. After the practice drive, participants were asked to fill out a before-drive questionnaire. This questionnaire mainly inquired the basic information of the driver and the physiological condition before experiment. For the driving experiment, participants were asked to complete driving tasks in scenarios with some task and scenarios without task. Those tasks (calling, sending messages, tuning the radio, and operate navigation) can induce the driving distraction. In order to avoid ordering effects, the sequence of the simulations was counterbalanced across drivers.

After driving scenarios with difference distraction task, participants were asked to fill out post-drive questionnaire that investigate the effects of driving distraction experiment to them.

## 4 Data Collection, Screening, and Processing

### 4.1 Data Collection Procedure

During the experiment, electrocardiograph collects the experimental data. To thoroughly analyze the impact of the task of different distraction during driving and the effect of the ECG, several key points are defined in the core section of the scenarios. Finally, this study compares the data about the ECG and driving situation in different segments of the scenarios.

### 4.2 Data Screening and Processing

Different electrocardiograph (ECG) data could be used to describe different aspects of human stress and record the emotion. Heart rate variability (HRV) is a small increase in the interval between successive heartbeats. In several research, heart rate changes from the autonomic nervous system regulation, there are sympathetic and parasympathetic dual domination, physical load is main influencing factors. Small increase in heart rate variability factors, including high-level neural activity of the

brain, reflecting the heart sympathetic, and parasympathetic nervous activity and balance which can reflect the physical conditions of the experiment better.

The method we used to measure HRV is analysis the curve changes. This method put forward an idea that any form of curve is a combination of a sinusoidal curves. According to a variety of sinusoidal power distribution, we can draw the spectrum curve. The abscissa of the spectral curve is frequency, and the ordinate is the power of density in per unit frequency. The shape of the spectrum has a corresponding relationship with the shape of the instant heart rate curve. The characteristics of the instantaneous heart rate curve change can be estimated from the high-frequency component and the low-frequency component in the spectral curve.

Expect those methods to show the ECG, this study collects the QRS abnormal waveform to show the ECG directly. A QRS wave can be draw by AKF 2 which can draw both of the normal wave and abnormal wave. In this study, the different situation of the driving compared with the QRS wave, then targeted to indicate the difference between the waveforms of driving distraction and normal driving. Those changes may contain most dynamic changes in electrophysiological phenomena which remains to be explored in the further. Above all, we can use those methods to reveal the feature of ECG distracted.

## 5   Results

### 5.1   HRV

The data of the experiment compare the different HRV between the normal driving and driving distraction. Researchers always use the mean and variance to represent the difference between it. In this study, in order to show the difference driving status of drivers, we use the sample entropy method to analyze the source of HRV data.

Sample entropy is an improved time series regularity evaluation algorithm proposed by Richman [10] on the basis of approximate entropy. It is a measure of sequence complexity and a powerful tool for studying nonlinear dynamical time series such as EGC. It only needs shorter data to characterized so that can achieve the purpose of effective analysis, it has a better anti-interference and anti-noise ability, shorter computing time than other analysis method. It is suited for both deterministic signals and random signals.

Very Low Frequency (VLF) can show the low-frequency components of the size which can estimate the characteristics of instantaneous heart rate curve, and the Frequency Domain analyze Methods can show the more detail changes of the ECG in very short time. Everyone's VLF have been transformed to the sample entropy, then the mean and Standard deviation of data has to be computed. The sample entropy under the distracting condition mean $= 0.08 \pm 0.05$SD, and the sample entropy of sending voice message during driving mean $= 0.1 \pm 0.04$SD, sending message during driving is $0.11 \pm 0.06$SD, turning the radio to $0.1 \pm 0.06$SD and opening the
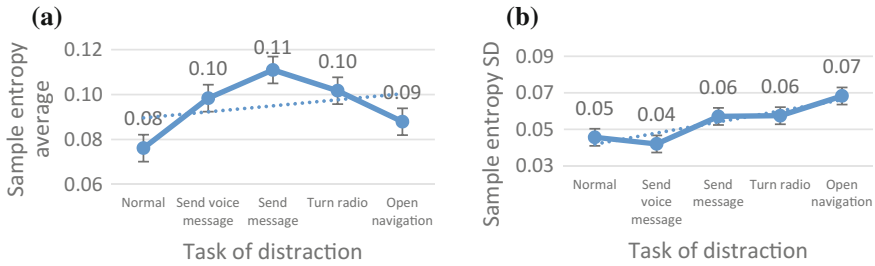
**Fig. 1** The effect of different distraction on sample entropy of VLF. **a** Sample entropy average of different tasks of distraction during driving; **b** Sample entropy SD of different tasks of distraction during driving

navigation $0.09 \pm 0.07$SD. As can been seen from the data, the host of sample entropy increases with the distraction tasks. When we compared with normal driving, drivers who send message during driving had a largest change about sample entropy. And drivers who open the navigation have the same state of sample entropy as normal. Drivers who send voice message and turn the radio have same change which shows the larger mean than the normal driving. Figure 1 shows effect of different distraction tasks on sample entropy average and SD.

The results of test showed that there were significant differences in the sample entropy of the VLF between normal and distraction (Sig = 0.05), And the most significant differences in the sample entropy of the VLF between normal and sending message during driving (Sig = 0.02), the result indicated that the sample entropy of the VLF can response the distraction state of the driver effectively, and it can be used as driving distraction identification criteria.

## 5.2 QRS Waveform

QRS depicts the depolarization of the ventricles, normally between 0.06 and 0.10 s. The graph has maximum width under 0.11 s. Each bloating bounce is accompanied by a QRS waveform, and the QRS abnormal waveform always appears when human does some distraction in daily work. In this study, QRS waveform has been collected and analyzed by the software AKF2 dynamic multiparameter physiological recorder. This software can export both normal and abnormal waveform of QRS, and we select the most significant index of driving distraction which has been proved above as the difference between normal and send message during driving. Figure 2 shows the different count of abnormal waveform between normal driving and driving distraction. It is obvious that the QRS abnormal waveform has appeared in the driving distraction more than the normal driving.
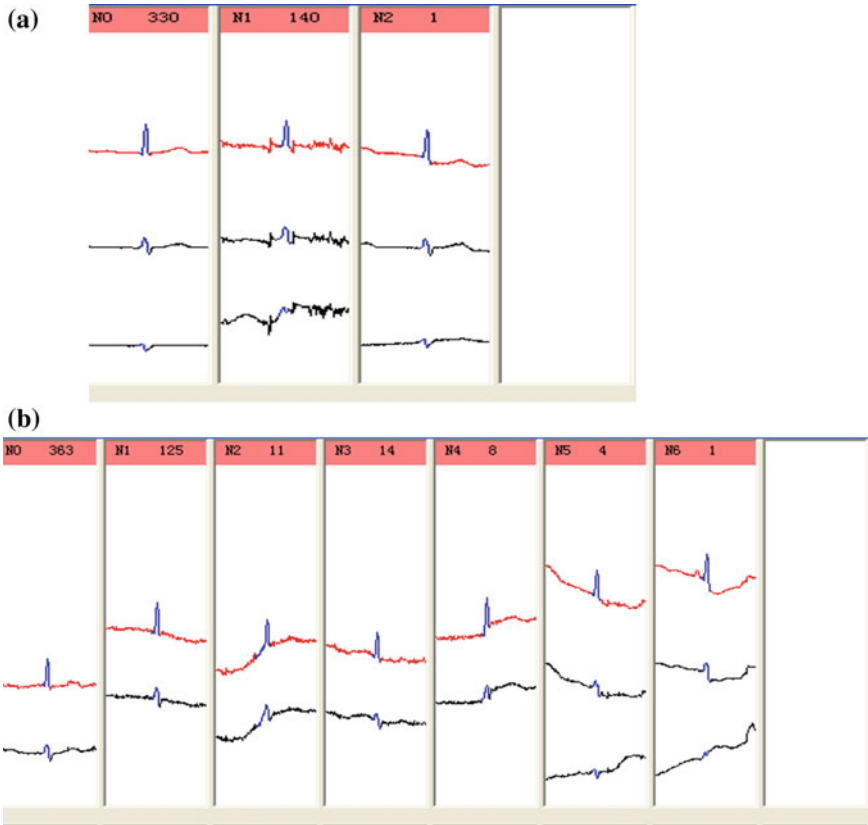
**Fig. 2** Abnormal QRS waveform of driver. **a** Abnormal QRS waveform of driver when does normal driving; **b** Abnormal QRS waveform of driver when driving distraction

From the comparison, we can see that the points of driving distraction are more scattered, and the data of abnormal heart rate of driving distraction are more than normal driving.

## 6 Conclusions and Recommendations

Based on a driving simulator experiment, this chapter analyzed the effects of driving distraction on drivers' ECG, include HRV, QRS waveform when traversing the urban street in daytime. The following findings were obtained in this research.

(1)  HRV

Driving distraction had an impact on drivers' HRV. The sample entropy of VLF and RMSSD are higher when driving distraction than normal driving. And sending message during driving has the highest significance and difference in the distraction tasks compared with the normal driving.

(2)  QRS Waveform

Driving distraction affects the QRS waveform in both of the abnormal and the R-R interval during driving, which influences drivers with more anxiety in driving distraction.

   In conclusion, properly driving distraction do provide the driver more nervous, resulting in rapid heart rate changes, and easily leads to traffic incidents. And the method of sample entropy can be used to analyze the ECG which count by Frequency Domain analysis.

## 7   Discussions

The experiment in this study was conducted under given road conditions, and there were no interactions with other vehicles. To apply the driving distraction more precisely, future research will study the effectiveness of driving distraction in different road and traffic conditions. In particular, the effect of road-change and crossing-waiting are always produce a driving distraction, it is necessary to evaluate the effectiveness of driving distraction at those conditions.

   The analysis of this study just showed the difference of the normal driving and driving distraction, in order to define the driving distraction, it is necessary to find a method to determine a threshold to identify the driving distraction. And the QRS waveform was only export the divergence of driving distraction but not the feature of it. In the study after, finding the feature of this figure can build a map which can be used to define the ECG of driving distracted.

# References

1. Yerkes RM, Dodson JD (1908) The relation of strength of stimulus to rapidity of habit-ormation. J Comp Neurol Psychol 18(5):459–482
2. Wu Q (2009) An overview of driving distraction measure methods. In: Institute of electrical and electronics engineers of distracted driving, vol 53. pp 78–83
3. Sheridan TB (1970) Big research brother as driver: new demands and problems for the man at the wheel. Hum Factors 12(1):95–101
4. Michon JA (1989) Explanatory pitfalls and rule-based driver models. Accid Anal Prev 21(4):341–353
5. Ranney TA (1994) Models of driving behavior-a review of their evolution. Accid Anal Prev 26(6):733–750
6. Dingus TA, Klauer SG, Neale VL et a1 (2006) The 100 car naturalistic driving study phase II of the 100 car field results experiment (Report No. DOTHS810593). Washington, D.C, National Highway Traffic Safety Administration
7. Picard R (1995) Affective Computing. Technical Report 321, Cambridge, Massachusetts, MIT Media Laboratory, Perceptual Computing Section, Cambridge, Massachusetts
8. Riener A, Ferscha A (2009) Heart on the road: HRV analysis for monitoring a driver's affective state. In: Proceedings of the first international conference on automotive user interfaces and interactive vehicular applications
9. Kim D, Seo Y, Kim S, Jung S (2008) Short term analysis of long term patterns of heart rate variability in subjects under mental stress. In: International conference on Bio medical engineering and informatics, 2008. BMEI 2008, vol 2
10. Clifford G, Azuaje F, McSharry P (2006) Advanced methods and tools for ECG data analysis. Artech House
11. Korsakas S et al (2005) Electrocardiosignals and motion signals telemonitoring and analysis system for sportsmen. In: Computers in cardiology. IEEE 2005, pp 363–366.

# Research on Emergency Evacuation Route Choice in the Campus

**Lin Guo, Jibiao Zhou, Sheng Dong, Shuichao Zhang and Feifei Xu**

**Abstract** In order to explore the optimal route choice for emergency evacuation in the campus, we propose a novel route choice method based on brittle characteristics of campus system and improved ant colony algorithm. Both optimal and worst-case emergency evacuation routes are simulated in the campus of Ningbo University of Technology. From the simulation, the length of optimal and worse-case evacuation routes between the starting point and eight exits can be obtained by adjusting the importance value of trip distance and the degree of conformity, under the condition of static relative importance of pheromone concentration to graph *G*. The optimal route of emergency evacuation in the campus can be obtained when the importance of trip distance is above 5 and the degree of conformity is above 0.3; while the worse-case route is obtained with the importance of trip distance above 5 and the degree of conformity below 0.5.

**Keywords** Route choice · Ant colony algorithm · Brittleness · Emergency evacuation

## 1 Introduction

With the increasing socialization of the university campus, the use of the school's site resources for holding large-scale and super large-scale activities has become the trend of social activities. Once accidents occur in large gatherings, the consequences are serious. It is very important to evacuate pedestrians rapidly and safely in emergency situations, strengthen the information management of pedestrian evacuation, prepare all kinds of contingency plans for emergency and improve the competence of emergency management. At the same time, it is a trend to plan the emergency route for pedestrians [1] by solving the optimal path-planning.

L. Guo · J. Zhou (✉) · S. Dong · S. Zhang · F. Xu
School of Civil and Transportation Engineering, Ningbo University of Technology, Ningbo 315211, China
e-mail: zhoubiao666@126.com

In recent years, pedestrian safety emergency evacuation has become one of the hot topics. Four characteristics are vital in the safe evacuation, mainly including psychological and behavioral characteristics of pedestrians in large public places or buildings (Such as cinemas, theaters, stadiums, railway stations, shopping malls, etc.), crowd evacuation behavior, characteristics of crowd evacuation in closed space in emergencies like fire, pedestrian safety evacuation behavior modeling. With the development of computer technology, it is possible to simulate the pedestrian evacuation process [2–4]. In the simulation, the pedestrian trajectory is simulated, pedestrian position at different time point can be recorded and total evacuation time for each pedestrian can be calculated. According to incomplete statistics, about 22 kinds of pedestrian evacuation model and network simulation software are available, of which EVACNET (Evacuation network simulation software), BUILDING EXODUS (Building environment evacuation simulation software), FIRECAM (Fire simulation software), SIMULEX (Evacuation software), etc. [5] are the most prominent ones. With further study of pedestrian safety evacuation behavior and the establishment of simulation platform, the researchers also take the psychological and physiological characteristics of pedestrians into consideration, and build a safe evacuation model; the representative models are social force model, cellular automata model and magnetic force model [6].

The study of safety emergency evacuation covers traffic engineering, evacuation dynamics, statistics, architecture, psychology, safety engineering, image processing, software development, etc., which makes the study a multi-discipline research, but most of the researches done before are only considering a single factor or a single level, and some of the results are not practical. Also, few research results are conducted on the campus and most of them are without complexity theory and system method. To address the problem, we analyze campus safety emergency evacuation route choice based on the brittle characteristics of the university campus, using the improved ant colony algorithm, which is a new exploration of campus safety emergency evacuation theory.

## 2 The Brittle Structure Characteristics of University Campus

### 2.1 Brittleness of Complex System

Brittleness: Under the combined action of internal and external factors, a subsystem of the complex system collapses due to collapses of a neighboring subsystem. The other subsystems collapse like a chain reaction, eventually, the whole complex system crashes down. This property of complex system is called brittleness [8]. The brittleness of complex system reflects the influence on the performance between subsystems, and the influence of subsystem on the performance of the whole system.

System crashes [9]: Set a complex system with input $x_i (i = 1, 2, \ldots, m)$, output as $y_j (j = 1, 2, \ldots, n)$. When $\forall 1 \leq j \leq n$, $y_j = 0$, the corresponding state is a safe state, which shows that the output of the system is normal; when $\exists y_j = 1$, $1 \leq j \leq n$, the corresponding state is a collapsing state, which indicates that the output of the system is abnormal. For $\forall x_i \in [(x_i)_{\min}, (x_i)_{\max}]$, the state of the system is safe, as long as $\exists x_i \notin [(x_i)_{\min}, (x_i)_{\max}]$, the system will collapse.

## 2.2  Brittleness Analysis of University Campus System

University campus system is a complex system. Generally speaking, the university campus system is mainly composed of the pedestrian subsystem, the export subsystem, the transportation subsystem, the channel subsystem and the management and control subsystem, but each subsystem contains a lot of elements, and the relationship between elements is complex. When the external disturbance disturbs a part of the subsystems in the university campus system, because of the correlation between the subsystems, it also affects other subsystems, causing the other subsystems to crash. If the collapse effect reaches a certain extent, the whole system crashes. So brittleness is one of the major characteristics of university campus system.

The collapse of the university campus system is caused by the interaction of its subsystems. The mode of interaction between the subsystems has a great influence on the system crash. The main modes of the subsystems are as follows [7].

Complete brittleness is the collapse of any subsystem, which will affect the other two subsystems; Bilateral brittleness means that there is no brittle connection between two subsystems in a system composed of three subsystems, but the other subsystem has brittle relation with them; Hierarchical brittle relation refers to the crash occurred under the subsystems, will not affect the upper subsystem, while the upper subsystem collapse will affect the lower subsystems.

## 3  Selection of Safety Emergency Evacuation Path Based on Improved Ant Colony Algorithm

The brittle nature of the university campus makes it a collapse tending system. The trend can be delayed through certain technical measures. The brittleness of the system can be represented by a weighted directed graph $G$, whose subsystem is abstracted as the vertex of $G$, a path that connecting all the culminated vertices is the collapse path of the system. The brittleness of the system leads to the inevitability of the existence of the collapse path.

## 3.1 Concept Definition

(1) Hamilton path. Let $G$ be a directed graph, where $V_1$ and $V_2$ are the two vertices of $G$, and if there is a directed edge $H$ starting from $V_1$ to $V_2$ and passing through the other vertices of the directed graph $G$ once and only once. $H$ *is then called* a Hamilton path with directed edge from $V_1$ to $V_2$ in directed graph $G$.

(2) Collapse path $H$. Since the Hamilton path of directed graph $G$ is a starting point from one of its vertices, the collapse effect is transmitted through the directed edge $H$, then, chain reaction and the other subsystem collapses under the influence factor. Finally, the whole system collapses. The Hamilton path $H$ is called a crash path of the directed graph $G$.

(3) Collapse path $H$. If the Hamilton path transmits the collapse effect from a starting vertex in the directed graph $G$ to other subsystems through chain reaction, resulting a whole system collapse, then the Hamilton path $H$ is called a crash path of the directed graph $G$.

(4) The weight of the crash path $H$. The weight of the crash path $H$ is denoted as $W_H$, which is the product of all the edge weights in a path $H = V_{i1}\ V_{i2}...V_{in}$. $W_H$ is the occurrence probability of the path $H$ due to the collapse of the starting point. Let $V_{i1} \rightarrow V_{i2} \rightarrow \cdots \rightarrow V_{in}$ be the direction of the system crash process, assuming that the collapse of the vertices only affects the adjacent vertices. Here,

$$W_H = P(B_{in} B_{in-1} \cdots B_{i1}|B_{i1}), \tag{1}$$

where $B_i$ represents the crash of event $i$.

From (1), it can be derived as follows:

$$
\begin{aligned}
W_H &= P(B_{in} B_{in-1} \cdots B_{i1}|B_{i1}) = \frac{P(B_{in} B_{in-1} \cdots B_{i1})}{P(B_{i1})} \\
&= P(B_{i2}|B_{i1}) P(B_{i3}|B_{i2}) \cdots P(B_{in}|B_{in-1}) \\
&= W_{i1i2} W_{i2i3} \cdots W_{in-1in}
\end{aligned}
\tag{2}
$$

It can be concluded, $W_H$ is the product of all the edge weights in the path.

(5) Maximum crash path and minimum crash path. In all the crash paths $H$ in graph $G$, the maximum weight is called the maximum crash path, is denoted as $H_{\max}$, and the minimum crash path, is denoted as $H_{\min}$. In the case of path choice for university campus emergency evacuation, the maximum crash path is the worst path, which is the most likely to cause the system to be paralyzed. The minimum crash path is the optimal path, which can effectively guide the pedestrian to evacuate safely.

Mathematical Description: The graph $G$ has n vertices, $e = <i, j>$ is any edge, the weight is $w(e) = w_{ij}$, then traverse the path $H$ of all vertices:

$$\max_{H \in E(h)} (\prod_{e \in H} w(e))\text{or} \min_{H \in E(h)} (\prod_{e \in H} w(e)), \tag{3}$$

where $E(H)$ is a collection of all the crash paths in the university campus system.

## 3.2 Improved Ant Colony Algorithm

At the beginning of the algorithm, $m$ ants are placed at the specified starting point $S$. At the same time, each ant can go to the target pixel number stored in the taboo table. At this time, the amount of pheromone on each path is equal, and the pheromone concentration $\tau(i, j) = C$ ($C$ is a smaller constant). Then, each ant selects the next pixel independently according to the amount of residual information on the path and the heuristic information (the reciprocal of the distance between two pixels). The probability $p_k(i, j)$ of the ant whose order number is $m$ moving from pixel $i$ to pixel $j$ is

$$
p_k(i, j) = \begin{cases} \dfrac{[\tau(i,j)]^\alpha \cdot [\eta(i,j)]^\beta}{\sum\limits_{l \in J_k(i)} [\tau(i,j)]^\alpha \cdot [\eta(i,j)]^\beta}, & \text{IF} \quad j \in J_k(i) \\ 0 & \text{otherwise} \end{cases}, \tag{4}
$$

where: $J_k(i)$ is the set of optional vertices selected by the $m$-th ant; $\tau(i, j)$ is the pheromone concentration in $<i, j>$ side, a constant can be chosen as an initial value; the importance of pheromone concentration to G directed graph in the system is reflected by parameter $\alpha$, let $\alpha > 0$; the importance of heuristic information to G directed-graph in the system is reflected by parameter $\beta$, let $\beta > 0$; $\eta(i,j)$ the heuristic information (also referred as heuristic factor), is the expectation from pixel $i$ to pixel $j$. It can be obtained from Formula (5).

$$
\eta(i, j) = 1/d(i, j), \tag{5}
$$

where: $d(i, j)$ is the distance from pixel $i$ to pixel $j$.

A controllable randomly-selected route rule is applied in the process of ant choosing target pixels to ensure the correctness of selection results. That is, set controlled variable $q_0 (0 \le q_0 \le 1)$, before each ant choosing next pixel, a figure $q[0.1]$ will be generated at random, then the route-choosing rule will be forwarded after the comparison between $q$ and parameter $q_0$

$$
j = \begin{cases} \arg \max_{j \in J_k(i)} [\tau(i, j)]^\alpha \cdot \left[w_{ij}\right]^\beta & q < q_0 \\ J & \text{otherwise} \end{cases}, \tag{6}
$$

where $J$ is a constant, selected according to the state transition rules (6).

If the $m$-th ant reaches the set ending point E or goes through all reachable target pixels in the taboo list, it is called the $m$-th ant finishes the first travel, and use the cell array R{$k, m$} to record the travel route and the two dimensional array PL[$k, m$]

to record the travel length. When all m ants finish a travel, this iteration ends. Update the pheromones in all sides at the same time. Thereinto, the pheromones in every side will volatilize and reduce, so let variable $1 - \rho$ ($0 < \rho < 1$) be the volatilization coefficient. When all ants finish a travel, the global update rule (7) is applied into pheromones update in all sides. (The increase of pheromones in side $e = <i, j>$ is controlled by heuristic value):

$$\tau(i, j) = (1 - \rho) \cdot \tau(i, j) + \rho \cdot \prod_{k=1}^{m} \Delta \tau_k(i, j) \tag{7}$$

$$\Delta \tau_k(i, j) = \begin{cases} w_{ij} & \langle i, j \rangle \in H_m \\ 0 & \text{otherwise} \end{cases}, \tag{8}$$

where $\Delta \tau_k(i, j)$ is the pheromone concentration variation. The pheromone concentration variation should be counted after each round of iteration ends; $w_{ij} = Q/L_k$, $L_k$ is the travel distance of the $k$-th ant at this time; $Q$ is intensity coefficient of pheromone increase; $H_m$ is the optimum route of the $m$-th ant at last round.

When all $K$ rounds of iterations end, the optimal (worst) route from start point $S$ to ending point $E$ as well as its length can be obtained through the analysis of ant colony structure array R$\{k, m\}$ and two-dimensional array PL$\{k, m\}$.

The improved algorithm is applied to the process of emergency evacuation route optimization in campus through simulation methods. That is, the obstacles will be generated with certain probability when producing maps in complex brittleness systems, to simulate the contingency in evacuation, which will be more likely to present the real circumstances of emergency evacuation on campus.

## 4  Case Study

We carry out the shortest passenger evacuation route simulation based on improved ant colony algorithm in the scenario of Ningbo University of Technology (NBUT).

According to the algorithm solving process of the improved  ant  colony algorithm in Sect. 3.2, the following results are obtained:

(1)  Optimal and worst route
    According to the simulation results and different parameter settings, the improved Ant Colony Algorithm needs 20 iterations. The best result out of 20 iterations is considered as the optimal path solution for safe evacuation of each exit; the worst result out of 20 iterations is considered as the worst path solution for safe evacuation of each exit. In this model, the physical meaning of the parameters $\alpha$, $\beta$, $\rho$ can be expressed as— the parameter $\alpha$ is used to control the relatively important degree of the pheromone concentration in the system to the directed graph $G$, and the parameter $\beta$ is used to control the relatively important degree of the heuristic information in the system to the directed graph

**Table 1** Parameter selection of optimal and worst route

| Origin-Destination | $\alpha$ | Optimal route | | Worst route | |
|---|---|---|---|---|---|
| | | $\beta$ | $\rho$ | $\beta$ | $\rho$ |
| Logistics Center–Dormitory | 1 | 3 | 0.5 | 3 | 0.1 |
| Logistics Center–Gymnasium | 1 | 1 | 0.3 | 4 | 0.1 |
| Gymnasium–Dormitory | 1 | 2 | 0.5 | 1 | 0.1 |
| Library–Dormitory | 1 | 2 | 0.3 | 1 | 0.3 |
| Library–Logistics Center | 1 | 2 | 0.5 | 3 | 0.3 |
| Library–Gymnasium | 1 | 1 | 0.5 | 2 | 0.3 |

$G$, and the parameter $\rho$ $(0 < \rho < 1)$ is used to control the attenuation parameters of pheromone. Comparing the optimal path and the worst path, we can draw the following:

① The values of the parameters $\beta$ and $\rho$ have great effects on the solution of the maximum crash path problem of the safe evacuation of each exit. According to the analysis, the smaller value of the parameter $\beta$ is, the better solution we can get, and the larger value of the parameter $\rho$ is, the better the solution is. The values of the parameters are shown in Table 1.

(2) Result analysis

① When the parameter $\alpha = 1$ is fixed and the parameter $\beta = 3$ and $\rho = 0.5$, the length of safety emergency evacuation path from library to the building 9 is the best; when the parameter $\beta = 1$ and $\rho = 0.3$, the length of safety emergency evacuation path from logistics center to gymnasium is the best; when the parameter $\beta = 2$ and $\rho = 0.5$, the length of safety emergency evacuation path from gymnasium to the building 9 is the best; when the parameter $\beta = 2$ and $\rho = 0.3$, the length of safety emergency evacuation path from logistics center to the building 9 is the best; when the parameter $\beta = 2$ and $\rho = 0.5$, the length of safety emergency evacuation path from library to gymnasium is the best; When the parameter $\beta = 1$ and $\rho = 0.5$, the length of safety emergency evacuation path from library to logistics center is the best.

② When the parameter $\alpha = 1$ is fixed and the parameter $\beta = 3$ and $\rho = 0.1$, the length of safety emergency evacuation path from library to logistics center is the worst; when the parameter $\beta = 4$ and $\rho = 0.1$, the length of safety emergency evacuation path from logistics center to the building 9 is the worst; when the parameter $\beta = 1$ and $\rho = 0.1$, the length of safety emergency evacuation path from logistics center to gymnasium is the worst; when the parameter $\beta = 1$ and $\rho = 0.3$, the length of safety emergency evacuation path from gymnasium to the building 9 is the worst; when the parameter $\beta = 3$ and $\rho = 0.3$, the length of safety emergency evacuation path from library

to the building 9 is the worst; When the parameter $\beta = 3$ and $\rho = 0.3$, the length of safety emergency evacuation path from library to gymnasium is the worst.

## 5 Conclusion

(1) By comparing the optimal path with the worst path, we can see that in the case where the relatively important degree of the heuristic information to the directed graph $G$ is fixed, the walking distance attention degree and the degree of conformity have a great influence to the path selection. When the walking distance attention degree is less than 5 and the degree of conformity is greater than 0.3, the university campus safety emergency evacuation path is easy to become the optimal path; when the walking distance attention degree is less than 5, and the degree of conformity is less than 0.5, the university campus emergency evacuation path easily mutated into the worst path.

(2) In future studies, the factors that lead to the worst path of the university campus will be identified, clustered and analyzed.

## References

1. Guo R-Y, Huang H-J, Wong SC (2012) Route choice in pedestrian evacuation under conditions of good and zero visibility: Experimental and simulation results. Transp Res Part B: Methodol 46(6):669–686
2. Pan X, Han CS, Dauber K et al (2007) A multi-agent based framework for the simulation of human and social behaviors during emergency evacuations. AI & Soc 22(2):113–132
3. Wang A, Dong B, Yin B et al (2012) Model and simulation on passenger behaviors in comprehensive railway passenger hubs. J Transp Syst Eng Inf Technol 5(1):026–035
4. Zhang Q, Han B, Li D (2008) Modeling and simulation of passenger alighting and boarding movement in Beijing metro stations. Transp Res Part C: Emerg Technol 16(5):635–649
5. Syed AT, Hassanain MA (2013) A simulation model for emergency evacuation time of a library facility using evacnet. Struct Surv 31(2):75–92
6. Helbing D, Molnar P (1995) Social force model for pedestrian dynamics. Phys Rev E 51(5):4282–4297
7. Seyfried A, Steffen B, Lippert T (2006) Basics of modelling the pedestrian flow. Phys A 368(1):232–238
8. Li Q, Jin H, Lin D (2005) The model and analyzing method for complex system's brittleness. Syst Eng 23(1):9–12
9. Wang S, Wang Y (2011) Causation analysis of complex system safety accident based on brittle structure collapse. China Saf Sci J 21(5):138–142

# Engraved Character Recognition of Train Wheelset Based on the Total Least Square Method

**Shuang Zhang, Hua Wang, Jin-gang Gao and Chun-qi Xing**

**Abstract** According to the characteristics of depth information of the engraved characters and the lack of color difference to the background, a line structured light sensor was applied to acquire train wheelset engraved character point cloud information. The total least square method was proposed for a 3D character point cloud processing method, in which the observation vector error and the coefficient matrix error are taken into account. According to the standard deviation of the point cloud data, abnormal points and engraved character points can be eliminated for plane fitting. A high-quality outline of the character information can be extracted from the character point cloud depth data.

**Keywords** Engraved character recognition · Total least square method · Train wheelset · Line structured light

## 1 Introduction

The engraved numbers and letters on wheelset are used to identify important information such as production date, production lot, part name, part number etc. [1]. In comparison to printed characters and paper labels, it can even be applied in various harsh industrial environments [2]. It is an important development direction for industrial information management for the intelligent identification of similar engraved characters or for three-dimensional characters without color difference to the back-

S. Zhang · H. Wang (✉) · J. Gao
School of Mechatronic Engineering, Changchun Institute of Technology, Changchun 130012, China
e-mail: yjsb_wh@ccit.edu.cn

S. Zhang
School of Mechanical Science and Engineering, Jilin University, Changchun 130022, China

C. Xing
School of Mechatronic Engineering, Changchun University of Technology, Changchun 130012, China

**Fig. 1** Wheelset engraved
characters
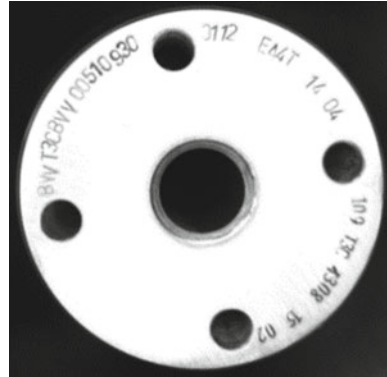


ground [3]. The character information of a wheelset is depicted in Fig. 1. Since there is no color difference between the character and the background, and it cannot be directly recognized via conventional optical character recognition method [4]. This study discusses the method of character information extraction from the image, which collects the depth of the image information via line structured light sensor, combined with total least squares plane fitting.

## 2 Total Least Square Method Applied for the Character Point Cloud Information Process

The plane feature is typically chosen for molded or engraved characters to reduce costs. In this chapter, the characters are fabricated on a relatively flat surface. According to the position between plane and character for point cloud data processing, both the plane and the nearby data can be removed. Only the character data is retained within the point cloud data.

The plane fitting method is one of the basic steps for any contour reconstruction algorithm of 3D point cloud data [5–7]. In the process of 3D point cloud data plane fitting, if the observation vector would only be considered with a random error, the Gaussian–Markov model could be used to fit the plane parameter, using the least squares method. In the classical least squares method, only random errors are assumed to exist in the observed values [8]. However, in the actual data collection process, the influence of the accuracy of the measuring instrument, the actual observation conditions of the environment, the characteristics of the observed objects, and obstacles in the observation process, influence the three-dimensional point cloud data collected by the scanner, which, thus, contains a random error or even an abnormal point. Therefore, a measurement error is inevitable during the fitting process, and an algorithm that assumed only observation vector contained errors would severely affect the accuracy of the fitting plane [9, 10].

With respect to this issue, a point cloud calculating method is introduced in this chapter based on the total least square method, i.e., the character depth information is processed by taking the total least square method, taking the observation vector error and the coefficient matrix error into account to obtain the character image. According to the plane position and character position in depth direction, the plane and other points are deleted with the exception of the character points; then, a complete and clear character image is obtained.

To achieve this, the point cloud processing method based on the total least square method [11, 12] was proposed and the specific steps are as follows:

Step 1: Scanning the three-dimensional character for point cloud data via Line Structure 3D sensor. The line structure light is projected onto the surface of the engraved character area, and a beam of laser light is projected on its surface. Due to the depth difference between engraved character and wheelset plane, the laser light will be severely deformed in the height change area. Both camera and measured object are set at a certain angle to shoot the laser light, three-dimensional coordinate values of the laser light are calculated according to pre-calibration of the laser plane and the camera's geometric position. The projection of these three-dimensional coordinate values on the laser plane provides the character cross-sectional profile. Then, the structured light sensor rotates, and the camera extracts the laser light data after a specific angular rotation. At last, these data are superimposed and combined, and the initial point cloud data is obtained, containing three-dimensional character information.

Step 2: Constructing the plane equation of the initial point cloud data by using the total least square method. Both the machined character and the wheelset end face plane are with a certain distance in the depth direction, which typically ranges at about 0.5 mm. The depth information of the character affects the correct establishment of the wheel face plane when constructing a plane equation; therefore, it should be removed. Elimination of the character points within the point data allows reconstruction of the plane equation.

Step 3: The point cloud data is cut with the plane equation obtained in step 2, and the points below the 0.3 mm of the plane are defined as points with the character information.

Step 4: The remaining point cloud data from the vector direction of the plane are shown, and then the character image is shown.

In this study, the line structured light sensor and the camera were applied for acquiring the 3D data to improve recognition of the three-dimensional characters without color difference to the background. The cutting plane for separating the character data from the point cloud data is fitted via the total least square method. The character information of an image without color difference can be accurately extracted with high efficiency, and the coarse noise interference can also be eliminated.

Compared to the traditional least square method, the advantage of the total least squares method is that it can reduce the influence on the calculated result of both the random error of the coefficient matrix and the observed value [13]. The elements of the coefficient matrix in the data model are not constant; however, in the case of a

composition the observed value or other calculation results of the coefficient matrix must contain a measurement error, and application of the total least squares solution will result in a more accurate result than the least square method [14].

Assuming that both the matrix and the observed values contain errors, the mathematical model of the total least square method Formula (1) is

$$Z - e_z = (A - E_A) \cdot X \tag{1}$$

In Formula (1),

$$Z = \begin{bmatrix} Z_1 \\ \vdots \\ Z_n \end{bmatrix}, \; A = \begin{bmatrix} x_1 & y_1 & 1 \\ \vdots & \vdots & \vdots \\ x_n & y_n & 1 \end{bmatrix}, \; X = \begin{bmatrix} a \\ b \\ c \end{bmatrix}, \; a, b, \text{ and } c \text{ are parameters for the}$$

plane to be fitted. $e_z$ and $E_A$ are measurement error of observed value and measurement error of the coefficient matrix. The total least squares Formula (2) is

$$\min_{[e_z:E_A]} \left\| \begin{bmatrix} E_A : e_z \end{bmatrix} \right\|_F \tag{2}$$

In Formula (2), $\|\|_F$ means norm; $\begin{bmatrix} E_A:e_z \end{bmatrix}$ are $n \times (m+1)$ dimensions of augmented matrix.

Suppose one matrix M with the dimension $n \times m$, then its norm Formula (3) is

$$\|M\|_F = \sqrt{\sum_{i=1}^{n} \sum_{j=1}^{m} m_{ij}^2} = \sqrt{tr\left(M^{\mathrm{T}} M\right)} \tag{3}$$

The total least square Formula (4) for the coefficient matrix and the observed value is as follows

$$\begin{bmatrix} \hat{A}; \hat{Z} \end{bmatrix} = U \overset{\wedge}{\sum} V^{\mathrm{T}} \tag{4}$$

The null space of $\begin{bmatrix} \hat{A}; \hat{Z} \end{bmatrix}$ is the parameter to be estimated via the total least square method, and can be calculated via singular value decomposition method, Formula (5) is shown as follows

$$\hat{X} = -\frac{1}{v_{m+1,m+1}} \begin{bmatrix} v_{1,m+1}, \ldots, v_{m,m+1} \end{bmatrix}^{\mathrm{T}} \tag{5}$$

Set coefficient matrix and observe value correction as $[\Delta A; \Delta Z]$:

$$[\Delta A; \Delta Z] = [A; Z] - \begin{bmatrix} \hat{A}; \hat{Z} \end{bmatrix} = \sigma_{m+1} u_{m+1} v_{m+1}^{\mathrm{T}} \tag{6}$$

Since $\left[\hat{X}, -1\right]^{\mathrm{T}}$ is the vector of $[A; Z]^{\mathrm{T}}[A; Z]$ minimum eigenvalue $\sigma_{m+1}$, Formula (6) can be obtained as follows in Formula (7)

$$\left(A^{\mathrm{T}}A - \sigma_{m+1}^2 I\right)\hat{X} = A^{\mathrm{T}}Z \tag{7}$$

when $\sigma_m > \sigma_{m+1}$ and $v_{m+1,m+1} \neq 0$, $\left(A^{\mathrm{T}}A - \sigma_{m+1}^2 I\right)$ is a positive matrix. Therefore, the parameter to be estimated via the total least square method is shown in Formula (8) as follows:

$$\hat{X} = \left(A^{\mathrm{T}}A - \sigma_{m+1}^2 I\right)^{-1}A^{\mathrm{T}}Z \tag{8}$$

With the three-dimensional point cloud data and the abovementioned total least square fitting plane method, parameter estimation of the fitting plane equation can be obtained.

The first application of the total least square fitting plane method involved a variety of measurement errors, abnormal points, and even engraved character points. Therefore, the measurement abnormal points in the 3D point cloud data and the corresponding engraved character points should be removed to improve the accuracy of plane fitting to obtain the exact fitting plane parameters $a$, $b$, and $c$ estimates. The specific process is as follows:

First, the total least square method is applied to fit the initial plane parameters $a$, $b$, and $c$ estimates.

And then, Formula (9) is applied according to initial $a$, $b$, and $c$ estimates:

$$d_i = \frac{|ax_i + by_i - z_i + c|}{\sqrt{a^2 + b^2 + 1}} \tag{9}$$

This formula enables calculation of the standard deviation of each data point distance $d_i$ in point cloud data, in which $\bar{d} = \frac{1}{n}\sum_{i=1}^{n} d_i$. In case of $d_i > 2\sigma$, the point is considered as an abnormal point and deleted. At last, the plane is re-fitted with retained point cloud data via the total least square method, the parameters $a$, $b$, and $c$ are recalculated, and relatively more accurate plane parameters can be obtained.

# 3 Experimental Results and Analysis

The wheelset engraved character for point cloud data was scanned via line structured light 3D sensor, and the result is shown in Fig. 2.

The total least square method was applied and the point cloud and the abnormal points of the character position were eliminated. The parameters of the fitted plane equation are shown in Table 1 below.

The point cloud data is cut by the plane equation, and only shows point cloud data below 0.5 mm of the plane (see Fig. 3.)

**Fig. 2** The original point
cloud information image
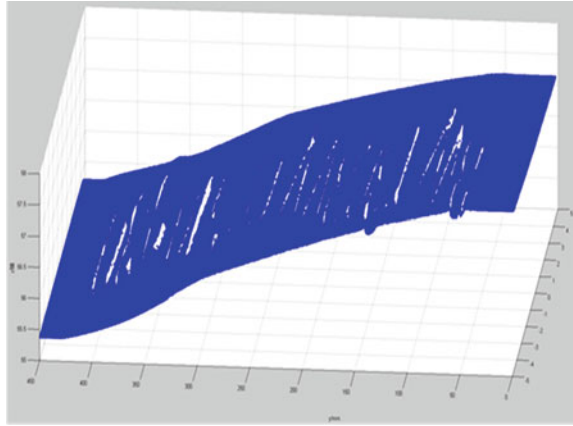


**Table 1** Fitting plane parameters comparison with different methods

| Method | $a$ | $b$ | $c$ | $\sigma_p$ | $\max(D_i)$ |
|---|---|---|---|---|---|
| Least square method | 2.3843 | −0.0088 | 56.8231 | 4.3 | 5.7 |
| Total least square method | 3.4385 | −0.0152 | 55.6517 | 2.8 | 4.9 |



**Fig. 3** Character information image

To effectively compare the least square method and the total least square method
for inferiors and superiors of the fitting plane algorithm, distance $D_i$ from the char-
acter point cloud data to fitting plane and the plane fitting precision were calculated
via Formula (10). In addition, the maximum distance $\max(D_i)$ from the point cloud
to the fitting plane was calculated, in which $n$ is the number of points on the fitting
plane.

$$
\begin{cases}
d_i = \dfrac{|ax_i + by_i - z_i + c|}{\sqrt{a^2+b^2+1}} \\
\sigma_p = \sqrt{\dfrac{\sum_{i=1}^n d_i^2}{n}}, (i = 1, 2, \cdots, n)
\end{cases}
\tag{10}
$$

The results are shown in Table 1 and reveal that the total least square method
is significantly superior to the least squares method, regardless of the maximum
distance from the point to the fitting plane or of the plane fitting accuracy. Two sets
of character images were obtained after the point cloud data cut the point cloud
data at these two fitting planes. Figure 4 is the resulting image from the total least
square method, while Fig. 5 is the resulting image from the least square method.

**Fig. 4** Image cut by the total least squares method
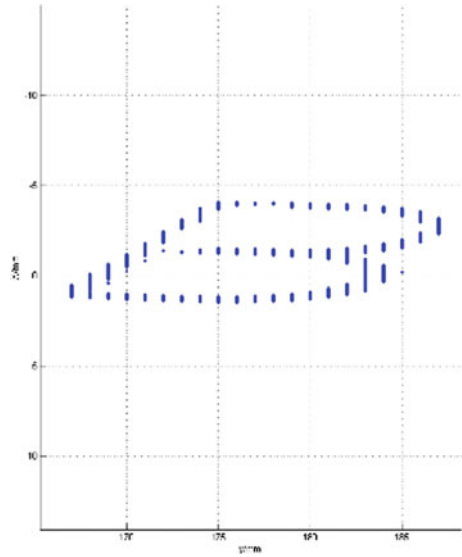


**Fig. 5** Image cut by the least squares method
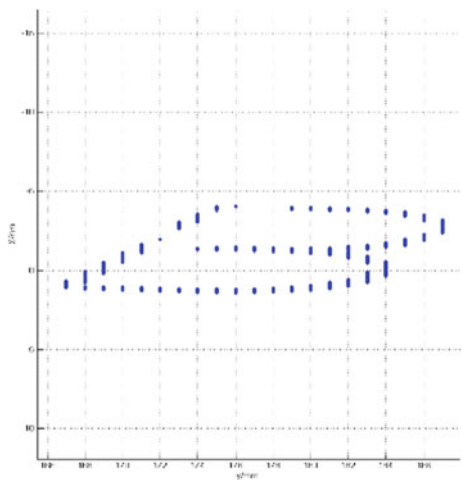


Comparing both images shows that the cutting character image is more complete because the total least square method can fit the plane more accurately for actual plane position and angle, thus providing an improved foundation for the next step character recognition.

# 4   Conclusion

To measure the characteristics of engraved characters on train wheelset and their background without color difference, the character point cloud data was acquired via line structured light sensor. Combined with the method of the total least square plane fitting, the outline of the character information was extracted according to the point cloud depth data. The experimental results indicate that the method is highly executable, with high acquisition efficiency, less required parameters, strong computing integrity, and less susceptibility to local noise. This method can accurately extract the character information within the point cloud information.

# References

1. Berchmans D,Kumar SS (2014) Optical character recognition:an overview and an insight. In: International Conference on Control,Instrumentation,Communication and Computational Technologies (ICCICCT)
2. kaur Amritpal, Arora Madhavi (2013) Neural network based Numerical digits recognization using NNT in Matlab. Int J Comput Sci Eng Surv 4(5):47–59
3. Matei O, Pop PC, Vălean H et al (2013) Optical character recognition in real environments using neural networks and k-nearest neighbor. Appl Intell Int J Artif Intell Neural Netw Comp Prob-Solv Technol 39(4):739–748
4. Vikramdeep Singh R, Randhawa N (2014) Automobile number plate recognition and extraction using optical character recognition. Int J Sci Technol Res 3(10):37–39
5. Lu J, Ye, Z, Zou Y et al (2013) Huber fractal image coding based on a fitting plane. IEEE Trans Image Process 22(1):134–145
6. Men Y, Zhang G, Men C, Li Xiang, Ning MA (2015) A Stereo matching algorithm based on four-moded census and relative confidence plane fitting. Chin J Electron 04:807–812
7. Zlokazov VB, Morozov VA (2014) Robust fitting for the estimation of hidden parameters in experimental distributions on the plane. Phys Part Nucl Lett 11(4):483–485
8. Hulik R, Spanel M, Smrz P et al (2014) Continuous plane detection in point-cloud data based on 3D Hough transform. J Vis Commun Image Represent 25(1):86–97
9. Li X, Li W, Jiang H et al (2013) Automatic evaluation of machining allowance of precision castings based on plane features from 3D point cloud. Comput Ind 64(9):1129–1137
10. Xiao J, Zhang J, Adler B et al (2013) Three-dimensional point cloud plane segmentation in both structured and unstructured environments. Robot Auton Syst 61(12):1641–1652
11. Aydar U, Altan MO (2015) Total least squares registration of 3D surfaces. Int J Environ Geoinf 2(2):27–38
12. Petrášl Ivo, Bednárová D (2010) Total least squares approach to modeling: a matlab toolbox. Acta Montan Slovaca Ročník 15(2):158–170
13. Muñoz LR, Villanueva MG, Suárez CG (2014) A tutorial on the total least squares method for fitting a straight line and a plane. In: International congress on mechanical and electric engineering, 1 al 4 de Diciembre del 2014. Coatzacoalcos, Veracruz, Mexico
14. Markovsky I, Sima DM, Van Huffel S (2009) Total least squares methods, Wiley Inc. WIREs Comp Stat 2010, 2:212–217

# Research on Floating Car Speed Short-Time Prediction with Wavelet–ARIMA Under Data Missing

**Hong Yang, Yi-hua Zhang, Lei Zhang and Tao Xu**

**Abstract** Aiming at the problem of predicting the effect of floating car speed prediction due to missing data and noise disturbance, in this chapter, the accuracy of 5, 10, 20, 30% of the regression filling method, EM method, PMM method to fill the accuracy of the analysis, while using wavelet transform strong time domain and frequency domain resolution characteristics, and the original data is denoised by the translation invariant wavelet transform, combined with the Auto-Regressive Moving Average Model (ARIMA) in terms of time series prediction, a wavelet–ARIMA algorithm for predicting vehicle speed is proposed. The experimental results show that with the increase of the sample data loss rate, the error of the three padding algorithms increases, but the PMM error curve is more gentle. Compared with the un-denoised ARIMA model, the Wavelet–ARIMA model is more accurate for predicting the speed of the floating car.

**Keywords** Floating car speed · Data missing · PMM · Wavelet transform ARIMA

## 1 Introduction

With the continuous improvement of the living standards of urban residents, the growth of car ownership increases rapidly, urban traffic congestion is becoming increasingly serious, traffic congestion from the local, occasional congestion to a large area, frequent congestion changes, it has become a problem which city traffic managers have to solve. A lot of practice at home and abroad show that Intelligent Transportation System (ITS) has a significant effect on alleviating urban traffic congestion, ITS normal and effective operation must be based on real-time, accurate and comprehensive traffic parameters data. Therefore, the urban road traffic parameter acquisition is the basic work of ITS application and research, and it realizes traffic

H. Yang · Y. Zhang (✉) · L. Zhang · T. Xu
Chongqing Municipal Design and Research Institute, Chongqing 400020, China
e-mail: 490422400@qq.com

guidance, control, and management. Because of Floating Car Data (FCD) wide coverage, high-precision, large sample size, real-time, and other characteristics in the field of intelligent transportation at home and abroad to a wide range of applications, the United States [1], Germany [2], Japan [3], and other developed countries have built a lot of traffic information system based on FCD. The normal operation of the floating car data system must base on real-time, dynamic traffic data, one of its core problem is the real-time forecast of the speed of the floating car.

Domestic and foreign scholars in the road speed forecast has made a series of results: In 1993, Greenshields first proposed a speed-density classic model. Ygnace et al. [4] through the floating car data on the average speed of road sections to predict and analyze. At the same time, some of the abnormal data values were processed, and then the road speed regression model is established by using the least squares method and the minimum variance method. In 2007, Weng et al. [5] constructed a floating car dwell time and road length travel speed forecast model based on the collected floating car data. In 2008, De Fabritiis et al. [6] proposed two short-term (1–30 min) travel speed prediction based on the real-time floating car data, two kinds of prediction algorithms based on neural network and pattern matching are proposed, respectively. In 2009, Gong [7] based on the floating vehicle data, combined with historical operation data and real-time data, established the K-Nearest Neighbor Prediction Model, weighted Markov forecasting model, gray Markov forecasting model, respectively, study on the road short-term traffic speed. In 2014, Wang et al. [8] base on the Western Han Dynasty expressway running speed, established speed forecasting model for straight section of mountain expressway based on BP network. However, the above scholars did not consider the floating car data acquisition process vulnerable to driving environment, the data is easy to lose, easy to produce data noise under the road, high-rise buildings and other strong signal interference section which affect the prediction accuracy of the model.

Aiming at the problem such as data loss and noise in floating car data, this chapter considers floating car data as a set of random time series, the error accuracy analysis is carried out under different data loss rate, the data are de-noised by wavelet transform, combined with ARIMA model for short time series characteristics, propose a wavelet–ARIMA car speed forecasting model, draw the conclusion through the example verification.

## 2  Processing Method of Data Missing

The method includes regression grading method, expectation maximization method (EM), forecasting method in multiple packing method (PMM) in this chapter.

## 2.1 Regression Grading Method

Regression grading method is a single fill method, the principle of this method is to establish a regression model by establishing a nonanswer item for the collected observations, the missing values are estimated by the regression model.

## 2.2 EM Method

The E process in EM method is to solve the desired process, That is, the conditional expectation of the missing value is solved under the condition that the data and known parameters have been collected, M process is the maximization process, the conditional expectation of the missing value to be solved in the E process is taken as the missing value, and then calculate the maximum likelihood estimation of the complete data set parameters.

## 2.3 PMM Method

The filling value of the missing data in the PMM method is the closest to the prediction model. Suppose that $X_{\text{miss}}$ is a continuous variable with missing data, the model is

$$X_{\text{miss}} = \beta_0 + \beta_1 X_1 + \beta_2 X_2 + \cdots + \beta_k X_k \tag{1}$$

# 3 Forecasting Model of Floating Car Speed Based on Wavelet–ARIMA

## 3.1 Wavelet Transform of Floating Car Data

Transition invariant discrete wavelet transform (TIDWT) is an improvement to the traditional wavelet domain threshold method [9], the basic principle of the method is to translate the data within a certain range, and the anti-translation of the data obtained by the average, after the translation of the data to the anti-translation.

Suppose there is signal $f(x), 0 \leq x \leq N - 1$, define $S_k$ translational operator for cyclic translational bits

$$S_k(f(x)) = f(x + k) \bmod (N), \tag{2}$$

where $k$ is the amount of translation, the inverse is

$$(S_k)^{-1} = S_{-k} \tag{3}$$

If the signal is subjected to a threshold processing for one analysis operation is $T$. Then, the signal a through the process of eliminating the oscillation can be written as

$$\hat{f}(x) = S_{-k}(T(S_k((x)))) \tag{4}$$

$\hat{f}(x)$ signal for the signal $f(x)$ after the translation of the invariant wavelet transform, transformation based on translation invariant wavelet transform to search for the optimal translational amount $k$, the translation invariant wavelet method of $k$ cyclic shift can be expressed as

$$\hat{T}(f(x), (S_k)_{k \in K}) = \text{AVE}_{k \in K}\{S_{-k}(T(S_k(f(x))))\} \tag{5}$$

$S_k$ represents the translation in the time domain, the displacement is $k(1 \leq k \leq N), k$ is a positive integer. $T$ represents that the signal is subjected to threshold processing. AVE represents the average operation.

### 3.2 ARIMA Model

ARIMA is a stochastic timing model founded by Box et al. [10], also known as the B-J method, the model is too short-term prediction method with high-precision, the modeling idea is: the sample data is treated as a set of random time series, it is modeled directly if the sequence is a stationary time series. If the nonstationary sequence, through the differential conversion to a smooth time series The ARIMA model can be expressed as

$$y_t = \theta_0 + \varphi_1 y_{t-1} + \varphi_2 y_{t-2} + \cdots + \varphi_p y_{t-p} + \varepsilon_t - \theta_1 \varepsilon_{t-1} - \theta_2 \varepsilon_{t-2} \cdots - \theta_q \varepsilon_{t-q} \tag{6}$$

$y_t$ is the original sequence, $\varphi_i (i = 1, 2, 3 \ldots p)$ and $\theta_j (j = 1, 2, 3 \ldots q)$ are model parameters, $\varepsilon_t$ is a set of white noise sequences that obey $N(0, \sigma^2)$.

## 4 Empirical Study

### 4.1 Comparison of Missing Errors in Missing Data at Different Missing Rates

In this chapter, the data of the floating car are 601 bus lines in Chongqing, the data transmission interval is 10 s, every 10 s system will be a bus out of the signal, a total of 180 time series were collected at 8: 00–8: 30 time. Due to the existence of bus and other characteristics of the station, the period of its speed is 0, which is not conducive to the accuracy of missing error statistical analysis, therefore, the

time series with speed of 0 should be excluded. In this chapter, a total of 180-time series were collected, 48 sequences of 0 values were excluded, the effective sample sequence was 132, the specific value of which is shown in Fig. 1 (Fig. 2).

Existing studies have shown that the data missing rate has a significant effect on the accuracy of filling, and the range of missing rates applied by different padding methods is different. This chapter has studied the filling effect of floating car under the condition of 5, 10, 20, and 30% rate.

When the data missing rate was 5%, the average relative error of the regression imputation method was 8.05%, the average relative error of EM method was 9.11%, and the average relative error of PMM method was 8.98%. The following is a further study on the filling error of floating car data missing rate at 10, 20, and 30%, and the error of each filling method is shown in Table 1 (Fig. 3).

From the average error table, it shows that with the increase of the missing rate of the floating vehicle data, the average relative error of each filling method increases, indicating that the missing rate has a significant negative correlation with the filling accuracy. When the missing rate is 5%, the error margin of each filling method is not obvious, however, with the increase of sample data loss rate, the average relative error of EM method increased significantly. When the missing rate is 30%, the average relative error of EM method is 21.36%, the average relative error of regression filling method is 20.65%, the average relative error of PMM method is 18.95%, it shows that the PMM method has a good filling in dealing with the large loss rate.
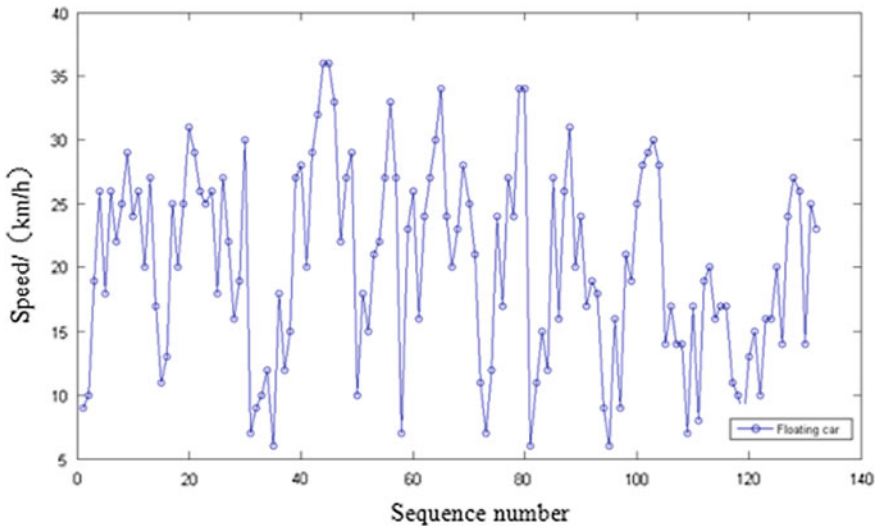


**Fig. 1** Floating car original valid sequence diagram
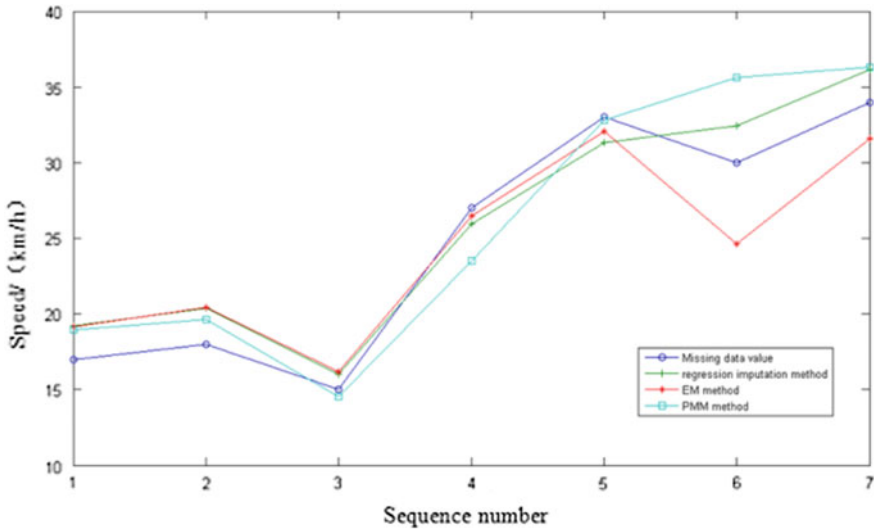
**Fig. 2** Comparison methods of missing rate of 5%

**Table 1** Summary of the errors of different filling methods under different missing rates

| Types | Missing rate of 5% | | Missing rate of 10% | | Missing rate of 20% | | Missing rate of 30% | |
|---|---|---|---|---|---|---|---|---|
| | Average residual | Average relative error (%) | Average residual | Average relative error (%) | Average residual | Average relative error (%) | Average residual | Average relative error (%) |
| Regression imputation method | −1.07 | 8.05 | 1.56 | 12.54 | 1.85 | 15.16 | 2.93 | 20.65 |
| EM method | 0.49 | 9.11 | −1.33 | 11.14 | −2.12 | 17.35 | −3.02 | 21.36 |
| PMM method | −1.06 | 8.98 | −1.29 | 10.66 | −1.72 | 13.28 | −2.55 | 18.95 |

## 4.2 Wavelet—ARIMA Floating Vehicle Speed Forecast

Figure 4 is the Chongqing 601 bus line bus floating car 7: 40–8: 59-time series, the original sequence is decomposed by wavelet and filtered by the invariant wavelet transform to obtain the filtered time series $A(i)$, the isolated noise is shown in Fig. 5.

It can be seen that the autocorrelation function and the partial autocorrelation function are oscillating in the early stage, but gradually attenuated to zero after sequence 11, and the partial autocorrelation function gradually attenuated to zero after sequence 11. Initially, identified that $p = 11, q = 11, d = 1$, model optimization based on goodness of fit $R^2$ and normalized Bayesian Information Criterion (BIC). Finally, ARIMA (3,1,3) is determined as the optimal model. Application of ARIMA (3,1,3) to predict the speed of the floating vehicle.
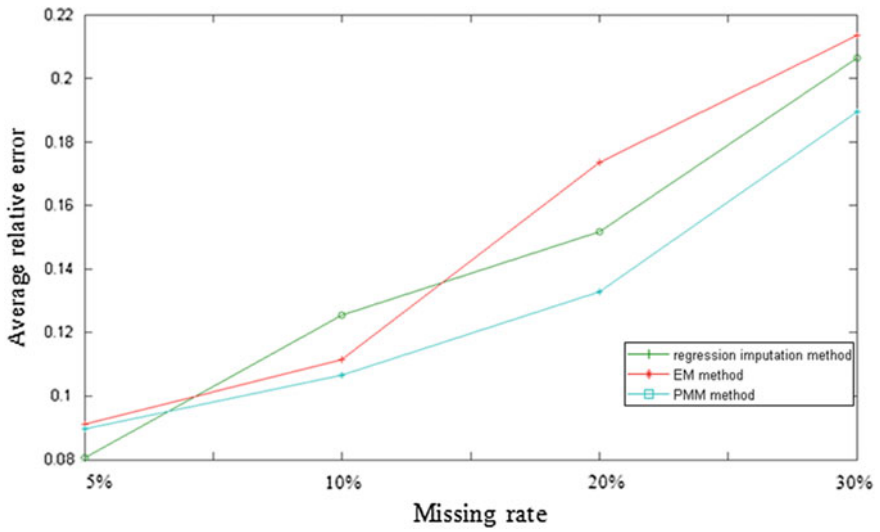
**Fig. 3** Average error distribution for each fill method at different loss rates
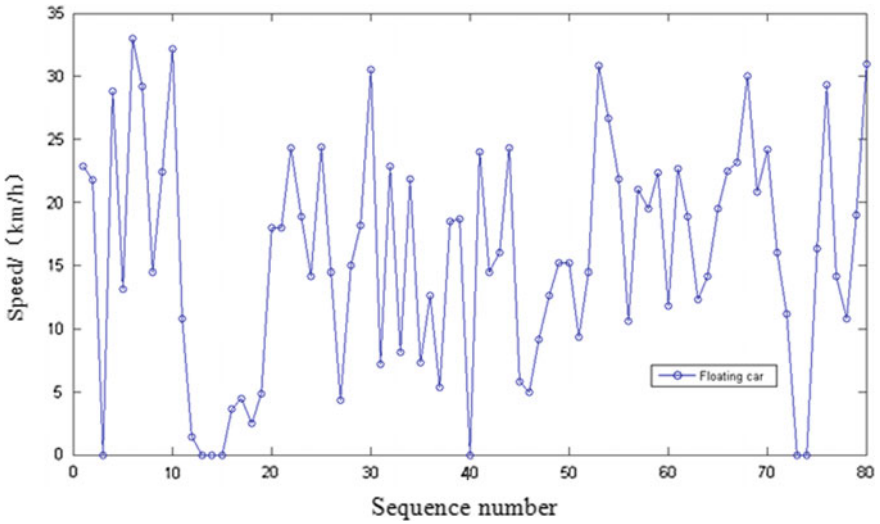


**Fig. 4** Original car speed data time series chart
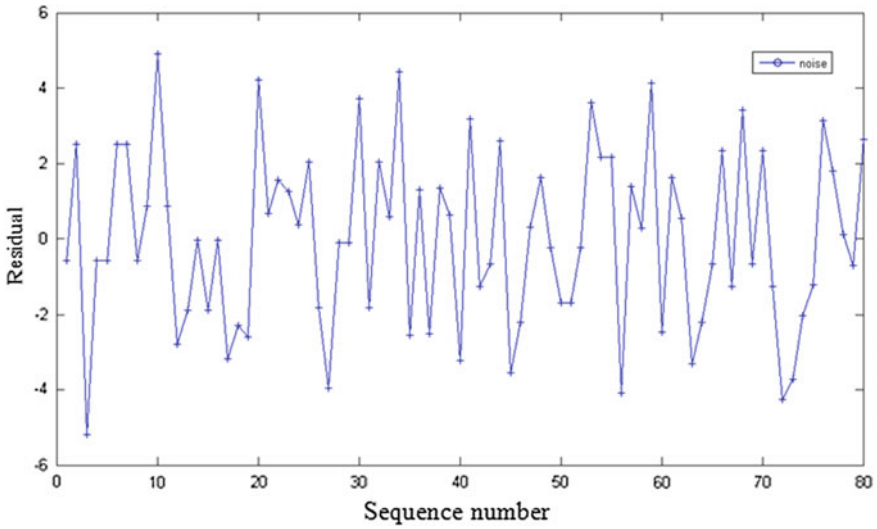
**Fig. 5** After filtering the remaining component chart

## 4.3   *Comparison of Model Prediction Error*

The average error, mean relative error, and root mean square error are used to analyze the error of single ARIMA prediction model and this algorithm (Fig. 6 and Table 2).
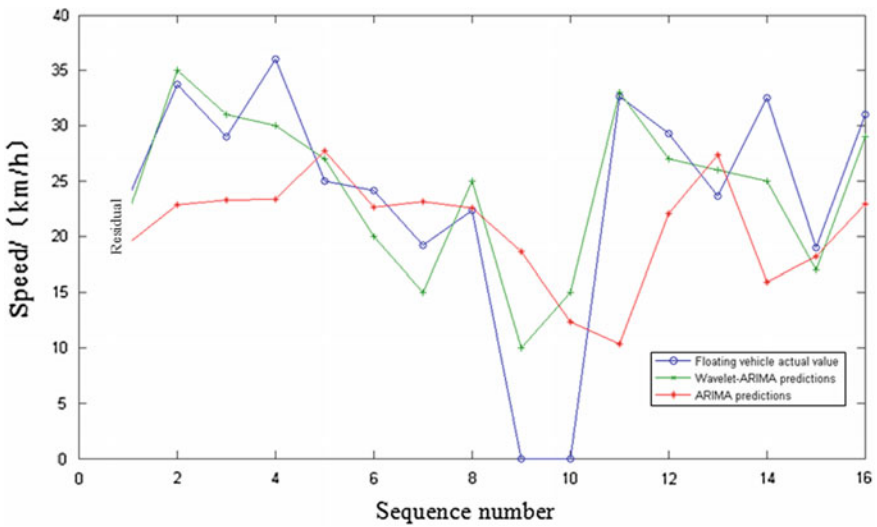


**Fig. 6** Chongqing 601 bus line floating car speed and forecast value

**Table 2** Various types of model error tables

| Types | $R_{ME}$ (%) | $R_{MAE}$ | $R_{MSE}$ |
|---|---|---|---|
| ARIMA | 13.21 | 6.15 | 6.26 |
| Wavelet–ARIMA | 10.81 | 4.07 | 5.53 |

In this chapter, Wavelet–ARIMA model average relative error is 10.81%, the average absolute error is 4.07, the root mean square error is 5.53. Compared with the single ARIMA model without noise reduction, the average relative error of the algorithm is reduced by 18.17%, the average absolute error is 33.82%, the root mean square error is reduced by 11.66%. The essence is the original speed data from noise, by not predicting the de-noised data will lead to reduced accuracy in eliminating the noise, the prediction accuracy of ARIMA model is obviously improved, indicating that this algorithm is applicable in prediction of floating car speed.

## 5 Conclusions and Future Work

In this chapter, we analyze the data filling algorithm of floating car with different missing rate and take the 601 bus line in Chongqing as the sample, the data of floating car data with missing rate of 5, 10, 20, and 30% were filled. With the increase of the missing data of sample data, the error of imputation method, EM method, and PMM method are increased, but the error curve of PMM method is the most slowly, the results show that the PMM method has better stability when dealing with different missing data. Aiming at the noise problem of floating car data collected in this chapter, using the TIDWT de-noised capabilities of the original data, and established ARIMA model, compared with the ARIMA model without de-noised, wavelet–ARIMA model is more accurate for floating car speed prediction.

In this chapter, the method of regression processing, EM method, and PMM method, the study of the remaining padding algorithms would be future work. Although the ARIMA model is accurate for short-term floating car speed forest, the long-term speed prediction accuracy to be further studied, the long-term floating car speed research is one of the next main work.

## References

1. Piao J, McDonald M (2003) Analysis of stop&go driving behavior through a floating vehicle approach. Proceedings of the IEEE intelligent vehicles symposium, pp 9–11
2. Chang AD (2009) Link travel-time collection method based on GPS equipped floating car. Jilin University, Jilin
3. Tang KS, Yao EJ (2006) An example of the development and application of ITS in Japan—brief introduction of P-DRGS based on floating car information in Nagoya. Urban Transp China 4(3):74–76

4. Ygnace JL, Drain C, Yim Y et al (2000) Travel time estimation on the bay area network by using cellular phones as probes. California Path, Berkeley
5. Weng JC, Rong J, Yu Q (2007) Travel speed estimation algorithm and optimization based on floating vehicle data. J Beijing Univ Technol 33(5):459–464
6. De Fabritiis C, Ragona R, Valenti G (2008) Traffic estimation and prediction based on real time floating car. Beijing, China
7. Gong S (2009) Research on forecasting vehicle's velocity based on data from GPS floating cars. Beijing Jiaotong University, Beijing
8. Wang D, Deng BC, Chou JH, Wu YC, Zhang JX (2014) Speed estimation method of straight line section of mountainous expressway. J Transp Sci Eng 30(3):81–86
9. Xie Q, Chen WY, Lin W (2011) Application of translation invariant wavelet transform in eliminating circuit noise. Ship Sci Technol 33(5):74–77
10. Box GEP, Jenkins GM (1970) Time series analysis forecasting and control. Holden-day, San Francisco

# Auto Rack Girders Assembly Holes Measurement Based on Multi-camera Vision

Li-dong Wang, Hua Wang, Zhi-peng Sun, Hang He and Shuang Zhang

**Abstract**  Since single camera's visual field is limited, the measurement method for auto rack girders assembly holes based on multi-group of binocular vision is proposed. The measurement area is divided into several subregions, the measurement data of each subregion is obtained from the binocular vision measurement system, and a larger planar target is used to achieve three-dimensional data registration among adjacent subregion. Since the texture information of truck side-member surface is not abundant, it is difficult to seek the match points on the edge of assembly holes. It is proposed that pasting marked points around the edge of assembly holes for seeking match points. Every two marked points can be connected into one line, and the intersections of the lines and assembly holes' edge are seen as match points. At last, the geometric parameters of spatial circle are fitted according to its geometrical properties. Experimental results show that the matching difficulty will be avoided effectively, the measurement error caused by perspective projection distortion can be reduced, and the method has higher measurement accuracy.

**Keywords**  Feature points · Assembly holes · Planar target

At present, many domestic and foreign scholars have proposed many measurement methods for assembly holes' geometric parameter. An algorithm for obtaining the corresponding center points of spatial circle based on ellipse fitting is proposed by the literature [1–3]. The method can directly measure the spatial coordinates of the center, but if there is a certain angle between the space plane and the image plane of the circle, it would have a greater measurement error. A measurement method for the spatial circle based on structured light is proposed by the literature [4, 5], the method has higher measurement accuracy, but it requires a special light source and more computing.

L. Wang · Z. Sun
Engineering Technology Department, CRRC Changchun Railway Vehicles Co., Ltd., Changchun 130062, China

H. Wang (✉) · H. He · S. Zhang
School of Mechatronic Engineering, Changchun Institute of Technology, Changchun 130012, China
e-mail: yjsb_wh@ccit.edu.cn

Extract the pixel points of the assembly holes' edge, and fit elliptic equations by the least square method. Marked points are pasted around the edge of assembly holes, extract pixel coordinates of marked points' centers, every two markers can be connected into one line, and regard the intersections of the lines and assembly holes' edge as match points, then get the three-dimensional coordinates of assembly holes' edge points by binocular stereo measurement. At last, the geometric parameters of assembly holes are obtained based on its geometrical properties, these parameters mainly include the radius and center coordinates.

# 1 Extract Feature Points

Due to the influence of measurement environment and material, acquired images have a lot of noise. First, the image is preprocessed by the median filter to remove the most of salt and pepper noise. Because Canny operator legitimately balance edge points' precise positioning and noise interference [6], Canny operator is selected to extract edge pixels.

Due to the influence of the camera projection distortion, the projection of the special circle in the image plane often presents as an oval. The least square method is commonly used to fit elliptic equations [7]. Suppose the elliptical general form can be expressed as follows:

$$ax^2 + bxy + cy^2 + dx + ey + g = 0 \tag{1}$$

Since the feature points of assembly holes' edge are not obvious, it is proposed to seek the feature points that the feature points are pasted the marked points around the edge of assembly holes. Every two markers can be connected into one line, and the intersection of the lines and assembly holes' edge are taken as match points (Fig. 1).

Extract each marker's center coordinates. Every two points can determine one line, and the linear equation can be obtained in Eq. (2):

**Fig. 1** Paste markers around the edge of the holes
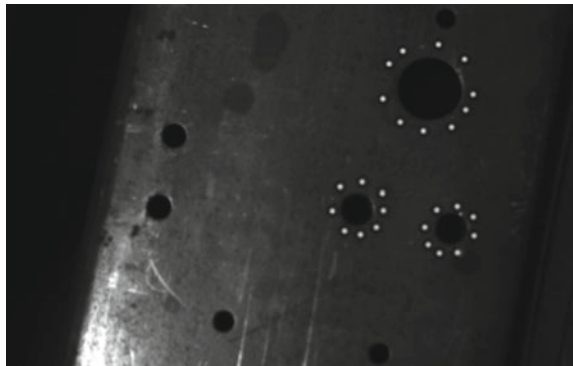
$$y_i = ax_i + b(i = 1, 2, \ldots, n) \tag{2}$$

Two solutions are obtained simultaneously by Eq. (1). The distribution of feature points is shown in Fig. 2.

## 2 Data Registration

As shown in Fig. 3, four cameras are selected as the multi-binocular vision measurement system, and every two cameras make up the binocular vision measurement system. One of the camera coordinates is selected as the local coordinate system $P_{c1}$ and $P_{c2}$. The planar target is placed in the appropriate position between the two binocular vision measurement systems. The center of the calibration plate is selected as the origin of the intermediate coordinate system $P_b$. Its z-axis is perpendicular to the plane of the calibration plate. Its x-axis and y-axis are parallel to the outer side edge of the calibration plate respectively.

The relationship between the local coordinate system and the intermediate coordinate system is determined according to Eq. (3):
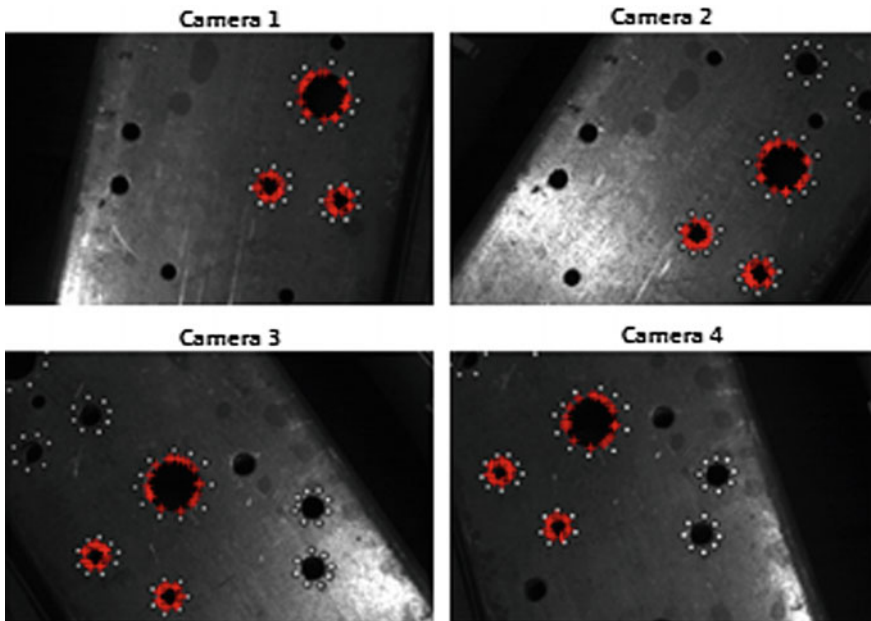


**Fig. 2** Extract feature points of the holes' edge
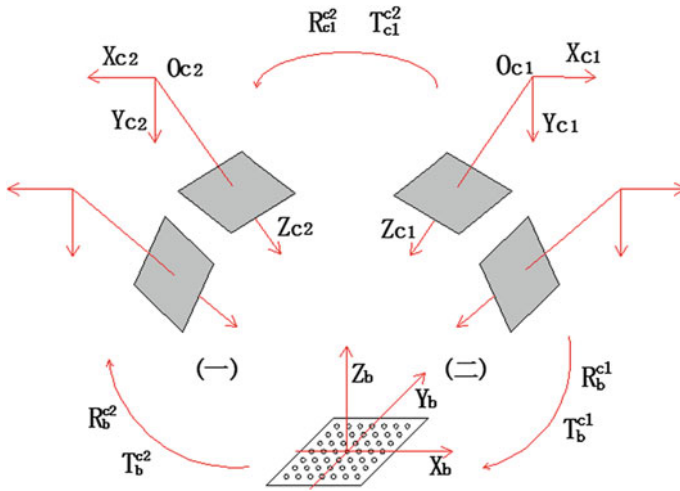
**Fig. 3** Multi-binocular vision sensor structure diagram

$$
\begin{cases}
P_{c2} = H_b^{c2} \cdot P_b \\
P_b = H_{c1}^b \cdot P_{c1} \\
H_{c1}^{c2} = H_b^{c2} \cdot H_{c1}^b
\end{cases}
\tag{3}
$$

The conversion relationship between the local coordinate system $P_{c1}$ and $P_{c2}$ is determined according to Eq. (4).

$$
P_{c2} = H_b^{c2} \cdot H_{c1}^b \cdot P_{c1} = H_{c1}^{c2} \cdot P_{c1}
\tag{4}
$$

The rotation matrix is obtained by Eq. (5).

$$
\begin{cases}
\overrightarrow{P_1 P_2}^b = R_{c1}^b \cdot \overrightarrow{P_1 P_2}^{c1} \\
\overrightarrow{P_2 P_3}^b = R_{c1}^b \cdot \overrightarrow{P_2 P_3}^{c1} \\
\overrightarrow{Q}^b = R_{c1}^b \cdot \overrightarrow{Q}^{c1}
\end{cases}
\tag{5}
$$

Suppose $R_{c1}^b = \begin{bmatrix} r_1 & r_2 & r_3 \\ r_4 & r_5 & r_6 \\ r_7 & r_8 & r_9 \end{bmatrix}$. $r_1, r_2$ and $r_3$ are calculated according to $x$ component of three equations in Eq. (6).

$$
\begin{cases}
\overrightarrow{P_1 P_2}{}_x^b = r_1 \cdot \overrightarrow{P_1 P_2}{}_x^{c1} + r_2 \cdot \overrightarrow{P_1 P_2}{}_y^{c1} + r_3 \cdot \overrightarrow{P_1 P_2}{}_z^{c1} \\
\overrightarrow{P_2 P_3}{}_x^b = r_1 \cdot \overrightarrow{P_2 P_3}{}_x^{c1} + r_2 \cdot \overrightarrow{P_2 P_3}{}_y^{c1} + r_3 \cdot \overrightarrow{P_2 P_3}{}_z^{c1} \\
\overrightarrow{Q}{}_x^{c1} = r_1 \cdot \overrightarrow{Q}{}_x^{c1} + r_2 \cdot \overrightarrow{Q}{}_y^{c1} + r_3 \cdot \overrightarrow{Q}{}_z^{c1}
\end{cases}
\tag{6}
$$

Similarly, the other data of $R_{c1}^b$ is calculated according to $x$ and $y$ component. Once $R_{c1}^b$ is determined, the translation vector can easily be determined according to the average value of these namesake vectors.

$$
T = \left( P_{b1} + P_{b2} + P_{b3} - R_{c1}^b \cdot P_{c11} - R_{c1}^b \cdot P_{c12} - R_{c1}^b \cdot P_{c13} \right)/3
\tag{7}
$$

The same principle can be used to obtain the transformation matrix $H_b^{c2} = \begin{bmatrix} R_b^{c2} & T_b^{c2} \\ 0 & 1 \end{bmatrix}$.

## 3 Fit the Spatial Circle

Since the edge points are in the same space plane, the plane is fitted first [8]. Suppose the spatial plane equation can be expressed as follows:

$$
ax + by + cz - 1 = 0
\tag{8}
$$

The coordinates of edge points can be substituted into Eqs. (8), and (9) can be obtained.

$$
A \times C - W = 0
\tag{9}
$$

The least-squares solution can be obtained according to Eq. (10).

$$
\begin{pmatrix} X \\ K_s \end{pmatrix} = \begin{pmatrix} B^T P B & C^T \\ C & 0 \end{pmatrix}^{-1} \times \begin{pmatrix} B^T P L \\ W \end{pmatrix}
\tag{10}
$$

The center coordinate can be obtained according to Eq. (10). The average distance from the edge points to the center is seen as the radius.

$$
r = \sum_{i=1}^{N} \sqrt{(x_i - x_0)^2 + (y_i - y_0)^2 + (z_i - z_0)^2}/N
\tag{11}
$$

## 4    Implementation and Result

In the experiments four DaHeng MER-040-60UM/UC industrial cameras are adopted, the focal length of the shot is 16 mm. As shown in Fig. 4, multi-group of binocular cameras are installed around the auto rack girder.

Suppose cameras 1 and 2 make up a group and camera 3 and 4 make up the other group, and they together make up multi-binocular vision sensor measurement system. Camera 1 and camera 4 are selected as the group's local coordinate system respectively.

The transformation matrix between the camera 1 and 2 is as follows:

$$M_{12} = \begin{bmatrix} R_{12} & T_{12} \\ 0 & 0 \end{bmatrix} = \begin{bmatrix} 0.9286 & 0.3487 & -0.1269 & 0.1406 \\ -0.3502 & 0.9366 & 0.01097 & -0.04423 \\ 0.1226 & 0.03425 & 0.9918 & 0.01551 \\ 0 & 0 & 0 & 1 \end{bmatrix}$$

The transformation matrix between the camera 3 and 4 is as follows:

$$M_{34} = \begin{bmatrix} R_{34} & T_{34} \\ 0 & 0 \end{bmatrix} = \begin{bmatrix} 0.9667 & 0.2332 & -0.1049 & 0.1523 \\ -0.2289 & 0.9721 & 0.05111 & -0.03184 \\ 0.1139 & -0.02537 & 0.9931 & 0.006509 \\ 0 & 0 & 0 & 1 \end{bmatrix}$$

The transformation matrix among adjacent subregion is calculated according to a larger planar target, this matrix is also seen as a positional relationship between the cameras 1 and 3.
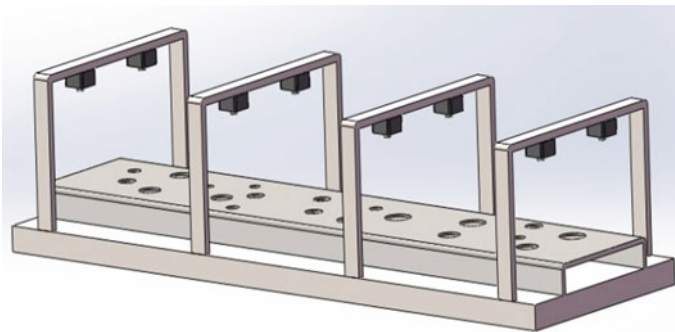


**Fig. 4**  Multi-camera vision measurement structure diagram

$$M_{13} = \begin{bmatrix} R_{13} & T_{13} \\ 0 & 0 \end{bmatrix} = \begin{bmatrix} -0.7378 & 0.6538 & -0.1331 & 0.1617 \\ -0.6517 & -0.6650 & 0.3531 & -0.6586 \\ 0.1431 & 0.3485 & 0.9165 & 0.0812 \\ 0 & 0 & 0 & 1 \end{bmatrix}$$

Extract the pixel coordinates of the holes' edge points, and the three-dimensional coordinates of the points are obtained according to calibration results. The spatial points' distribution in the adjacent two subregions is as shown in Fig. 5.

The positional relationship among adjacent subregion is established according to the transformation matrix $M13$. The measurement data in a subregion is converted into the data in the spatial coordinate system of the other subregion. The spatial points' distribution after coordinate conversion is as shown in Fig. 6.

The center coordinates of each hole are calculated according to its geometric properties, and the average value of the distance to the edge points is seen as the radius of the circle. Fitting effect diagram is shown in Fig. 7.

The measurement data is shown in Table 1, the measurement error comes from the following aspects:

(1) The calibration error from the camera calibration.



(a) Sub-region1                                        (b) Sub-region2
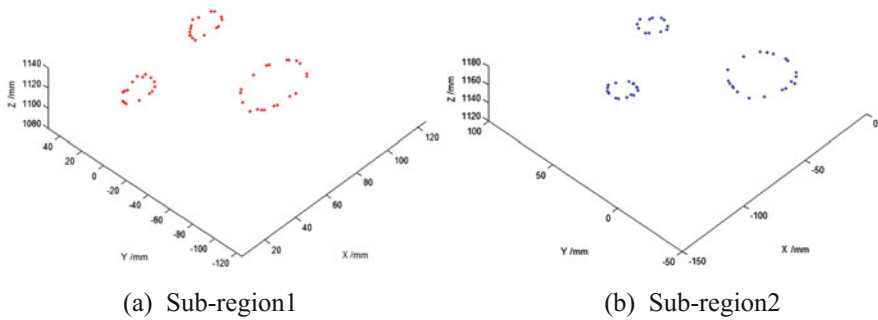
**Fig. 5** Spatial points' distribution in the adjacent two subregions

**Table 1** Center coordinates and radius of each hole

|  | Center coordinate | | | Radius | | |
|---|---|---|---|---|---|---|
|  | X coordinate (mm) | Y coordinate (mm) | Z coordinate (mm) | Measurement value (mm) | Actual value (mm) | Absolute error (mm) |
| Circle 1 | 75.768 | −55.715 | 1121.089 | 17.624 | 17.500 | 0.124 |
| Circle 2 | 35.256 | 10.662 | 1112.744 | 9.123 | 9.000 | 0.123 |
| Circle 3 | 31.963 | −221.796 | 1135.508 | 19.863 | 20.000 | 0.137 |
| Circle 4 | 110.612 | −222.589 | 1137.389 | 8.610 | 8.500 | 0.110 |
| Circle 5 | 86.681 | 21.134 | 1112.464 | 9.119 | 9.000 | 0.119 |
| Circle 6 | 90.767 | −282.557 | 1144.197 | 8.628 | 8.500 | 0.128 |
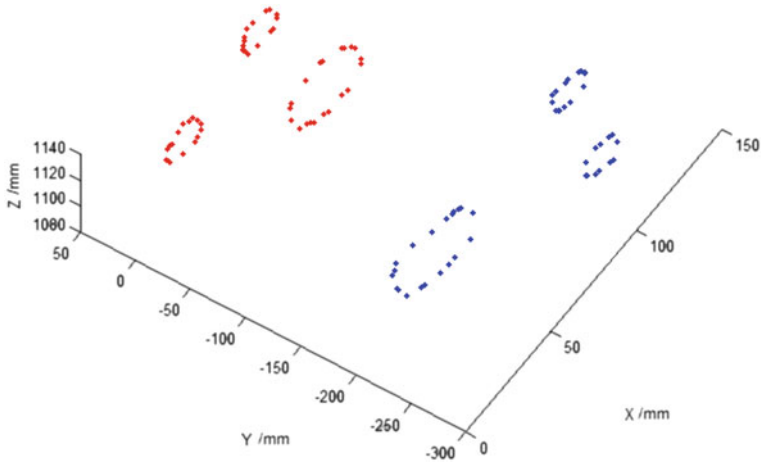
**Fig. 6** Spatial points' distribution after coordinate conversion
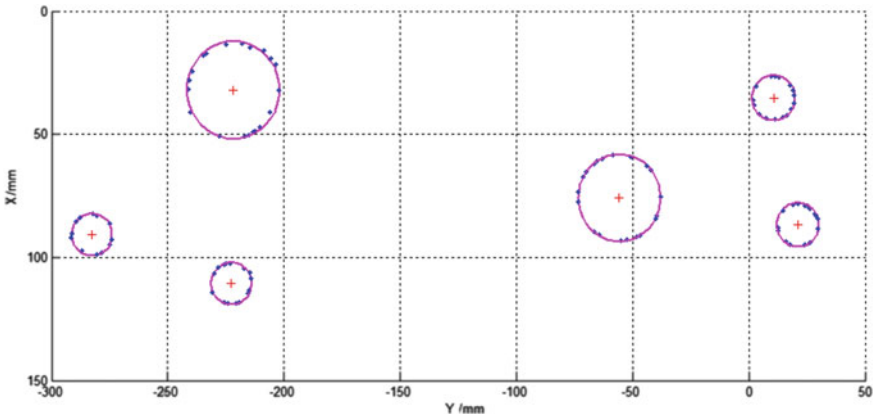


**Fig. 7** Fitting effect diagram of the holes

(2) The edge points' positioning error from edge detection.
(3) The error from extracting marked points' center.
(4) The machining error from the calibration board.

## 5 Conclusion

Since the texture information of truck side-member surface is not abundant, the matching difficulty has been avoided effectively by pasting the marked points around the edge of truck side-member assembly holes. Every two marked points can be

connected into one line, and the intersections of the lines and assembly holes' edge is regarded as match points. The method improves the accuracy of the match. Since the truck side-member has a larger surface and single camera's visual field is limited, multi-group of binocular cameras are used to achieve a wider view of measurement. The problem that data registration often relies on external high-precision auxiliary equipment has been solved by using a larger planar target, only three non-collinear markers of the target are captured in each subregion to calculate the coordinate transformation matrix between each subregion. Experimental results show that the method is easy to implement and it has low cost, its measurement error is about 0.1 mm. In this paper, this method has a meaningful reference for the positioning and assembly of the auto rack girder's holes.

# References

1. D'Amato R, Caja J, Maresca P et al (2014) Use of coordinate measuring machine to measure angles by geometric characterization of perpendicular planes. Estimating uncertainty. Measurement 47(1):598–606
2. Zhang YX, Wang S, Zhang XP et al (2013) Freight train gauge-exceeding detection based on three-dimensional stereo vision measurement. Mach Vis Appl 24(3):461–475
3. Zhang JX et al (1996) Application technology of binocular stereo vision in industrial detection. Tianjin University, Tianjin
4. Wu B, Xue T, Ye SH et al (2010) A two-step method for spatial circle orientation with a structured light vision sensor and error analysis. Measur Sci Technol 21(7):075105-1–075105-7
5. Lins RG, Kurka PRG (2013) Architecture for multi-camera vision system for automated measurement of automotive components. In: 7th annual IEEE international systems conference, pp 520–527
6. Zhang Y, Rockett PI (2006) The Bayesian operating point of the Canny edge detector. IEEE Trans Image Process 15(11):3409–3416
7. Prasad DK, Leung MKH, Quek C et al (2013) ElliFit: an unconstrained, non-iterative, least squares based geometric Ellipse Fitting method. Pattern Recogn: J Pattern Recogn Soc 46(5):1449–1465
8. Li YS, Yang F, Yuan ZK et al (2013) A detection method for 3D circle fitting. Sci Surveying Mapp 38(6):147–148

# An Eco-speed Optimization for Multiple Signalized Intersections Based on V2I

**Hai-lin Kui, Han Wang, Hong-xue Li and Chong-he Tian**

**Abstract** Vehicles driving on urban roads often take a sharp acceleration or braking due to unpredictable status changes of traffic lights at intersections or wait for the green signals. All of these situations cause wastag of fuel and a low of traffic efficiency. This paper describes the detailed scheme of an Eco-Driving Assistance System (EDAS) based on communication on vehicle-to-infrastructure (V2I). Under the condition of ensuring efficiency of transportation, the objective is to formulate an optimized function which minimizes the fuel consumption of vehicles traveling from the start point to their destination. In this paper, the proposal of most economical fuel consumption versus speed is concluded by comparing the fuel consumption in different driving models. The algorithm can effectively reduce the fuel consumption of vehicles driving through the intersections inside cities by using less time of computation in the simulation by using MATLAB.

**Keywords** Eco-driving · Speed optimization · Traffic light intersection · Driving assistance system · Fuel consumption

## 1 Introduction

Due to the superior advantage in achieving a remarkable automobile fuel saving without changing internal engine structure, EDAS has called researchers' extensive attention. Recently, researchers have implemented researches on utilizing Signal Phase and Timing (SPaT) in economical vehicle speed planning and management. De Nunzio et al. [1] provided a total method to the energy consumption minimization while the vehicle driving through a series of signalized intersections and catching green lights all the time in IFP Energies Nouvelles (2016). Wang et al. [2, 3] presented a novel Eco-speed algorithm for vehicles on roads with up-down slopes based on road gradient information in Tsinghua University (2014). However, this can only

H. Kui (✉) · H. Wang · H. Li · C. Tian
College of Transportation, Jilin University, Changchun 130022, China
e-mail: khl69@163.com

realize Eco-driving under the uniform velocity behavior of vehicles passing through intersections, which is a simplified and biased model in transportation planning. In order to solve the aforementioned problem, this research proposes a solution for the minimization of fuel consumption under multi-junction transportation. To be more specific, this model is preferred to prioritize minimum energy consumption in consideration of the traffic efficiency while passing through series of signalized intersections. The assisted management algorithm optimizing the vehicle economical speed can be achieved.

## 2 Model Formulations

EDAS based on V2I mainly includes 4 steps. First, establish a vehicle model which contains the longitudinal dynamical model and the fuel consumption model. Second, according to the real-time speed and the current position of the vehicle which are provided by GPS, the SPaT information [4], the road information, the vehicle dynamic model, the vehicle fuel consumption model, etc., we can build up a vehicle speed optimization computational approach. Third, output the optimized speed. Finally, prompt the driver to drive at an optimal speed. The aforementioned process is shown in Fig. 1.

### 2.1 The Vehicle Dynamical Model

In the process of building vehicle dynamic model, we assumed that: (1) Vehicle traveling in a simplified traffic road with all vehicles in free flow, with no influences, stem from pedestrians or nonmotor vehicles; (2) The process of acceleration and decel-



**Fig. 1** Basic diagram of eco-driving assistance system
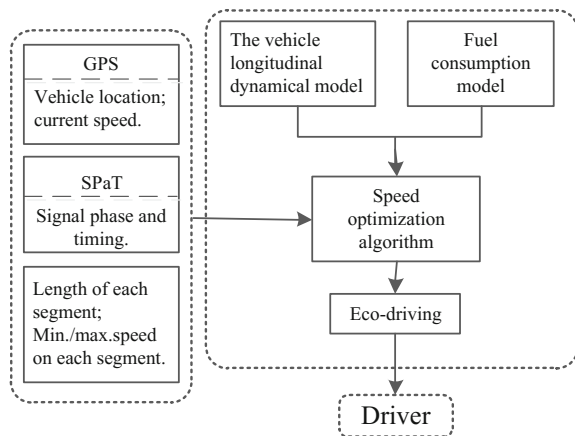
eration are uniform variable linear motion; (3) There are no losses for transmission and no loss in any braking, no slip at the wheels. Therefore, the vehicle kinematic model can be calculated as follows:

$$
\begin{aligned}
\frac{\mathrm{d}v}{\mathrm{d}t} &= \frac{1}{m\delta}\big[F_t - (F_f + F_w + F_i)\big] \\
&= \frac{1}{m\delta}\left(\frac{T_{tq}i_g i_0 \eta_T}{r} - mgfv\cos\alpha + \frac{1}{21.15}C_D A v^3 + mg\sin\alpha\right)
\end{aligned}
\tag{1}
$$

where $F_t$: the vehicle tractive effort (N), $F_f$: the vehicle rolling resistance (N), $F_w$: the air resistance (N), $F_i$: the ramp resistance (N). $T_{tq}$: the motor torque (N m), $i_g$: the transmission gear ratio, $i_0$: the main gear ratio, $\eta_t$: the mechanical efficiency, $r$: the wheel radius (m), $m$: the total vehicle mass (kg), $g$: the gravitational acceleration (m/s$^2$), $f$: the rolling resistance factor, $\alpha$: the traffic road slope. $C_D$: the air resistance coefficient, $A$: the vehicle frontal area (m$^2$), $\delta$: the rotating mass conversion factor.

## 2.2  Fuel Consumption Model

To compare the fuel consumption at each speed model, we establish a fuel consumption mathematical model in which vehicle speed is the only variable and the rest of the basic parameters are known [5]. Using instantaneous fuel consumption based on power polynomial models:

$$
\mathrm{FC}(t) = \begin{cases} \alpha_0 + \alpha_1 p(t) + \alpha_2 p^2(t) & \forall P(t) \geq 0 \\ \alpha_0 & \forall P(t) < 0 \end{cases}
\tag{2}
$$

$$
P(t) = \frac{F_f + F_w + F_i + 1.04m\frac{\mathrm{d}v}{\mathrm{d}t}}{3600\eta_t}v(t)
\tag{3}
$$

where $\mathrm{FC}(t)$ is the rate of fuel consumption at $t$(ml/s), $P(t)$ is the engine power for instantaneous (kW). $\alpha_0$, $\alpha_1$ and $\alpha_2$ are the parameters that can be obtained for a specific vehicle [5]. Vehicle traveling in urban roads that have $n$ intersections $\{S_0, \ldots, S_n\}$, $d_{S_{i-1,i}}$ is the length between the two intersections.

In order to enhance the fuel economy of the overall roads based on multiple intersections, speed is optimized for a single-segment before the vehicle is passing through and recovery later as shown in Fig. 2. The mathematical formulation for optimal fuel consumption $J_i$ problem in the single-segment model consists of an upstream segment and a downstream segment:

$$
J_i = \int_{t_i}^{t_{id}} \mathrm{FC}(t)\mathrm{d}t + \int_{t_{iu}}^{t_i} \mathrm{FC}(t)\mathrm{d}t
\tag{4}
$$

where $t_i$ is the time of arriving at the $S_i$, $t_{iu}$ is the time of arriving at upstream, $t_{id}$ is the time of passed downstream, as shown in Fig. 2. We defined an upstream $S_{id}$, which is the distance of the vehicle have to accelerate or decelerate to recovery after passed the intersection.

## 2.3 The Optimization Problem

In order to ameliorate the vehicle fuel economy of driving in urban traffic networks for the whole journey, the objective of this eco-driving solution based on the given signal lights information is to minimize the value of the energy consumption with economic speed.

We consider the crossing time at each intersection as soon as possible through the intersection and require to trade off the fuel consumption and traffic efficiency. The Optimization objective can be written as follows:

$$
\begin{cases}
\min \sum_{i=1}^{n} \int_{t_{iu}}^{t_{id}} FC(t)\mathrm{d}t \\[2mm]
\min \dfrac{\mathrm{d}v}{\mathrm{d}t} = \dfrac{v_{t+1}^2 - v_t^2}{2(d_{s_i} - x_t)} \\[2mm]
v_{\min} < v(t) \le v_{\lim i} \\[2mm]
t_{0f} = \arg\min_{t_{0f}} \sum_{i=1}^{n} \int_{t_{iu}}^{t_{id}} FC(t)\mathrm{d}t
\end{cases}
\tag{5}
$$

where $d_{si}$ is the position of the $i$ - th intersection for $i \in \{1, \dots, n\}$, $v_{\min}$ is the minimum speed of being adjusted on urban roads. $v_{\lim i}$ is the Speed limit of the $i$ - th road for $i \in \{1, \dots, n\}$, $x_{t0}$ and $d_0$ are the vehicle positions at the initiation of the driving distance, $x_{t_f}$ and $d_{nf}$ are the vehicle positions at the destination of the driving distance.
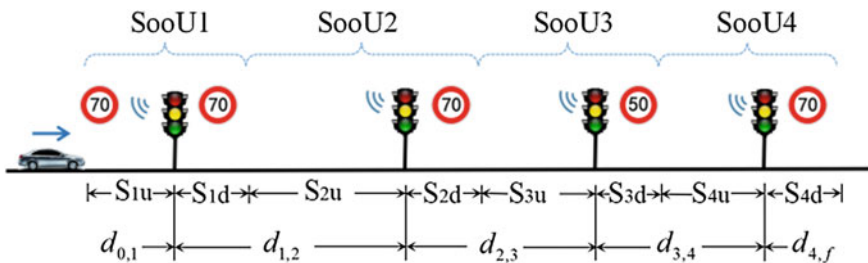


Fig. 2 The schematic diagram of speed optimization of unit i in multi-segment

## 3 The Speed Optimization Algorithm

The speed optimization algorithm of eco-driving assistance system consists of 4 steps:

(1) We estimate the intersection signal phase when vehicle is arriving with the given speed $v_{ECO}$; (2) Remainder timing of the red light is separated into 4 sections are, respectively, citing the different speed models under the different remainder of red light conditions; (3) The fuel consumption of each speed models can be calculated and compared; (4) We output the speed model of which the fuel consumption is least. The flow graph of economical speed algorithm as shown in Fig. 3.

Now running the eco-driving assistance system in the condition of the vehicle starts at any starting time $t_0$. At this moment, the information of the signal phase, timing and vehicle position $x(t)$ are received. When the conditions of the road are determined, the vehicle has a theoretical economic speed which is the best for fuel economy [6]. However, there is an economic speed which is adapted for the conditions of the city road because the vehicle will be affected by traffic flow, nonmotor vehicles, and other factors. Now the vehicle is driving at $v_{ECOi}$ on the $i$ - th road which contains the intersection $S_i . v_{ECOi} = \min\{v_{eco}, v_{\lim i}\}$, Calculate the time $t_v$ for reaching to the intersection:

$$t_v = t_0 + \frac{d_{i-1,i} - x_t}{v_{ECO}} \tag{6}$$

The one unit in the speed optimization model consists of an upstream component and a downstream component. Among them an upstream component is composed of the constant speed and the variable speed, a downstream component contains the
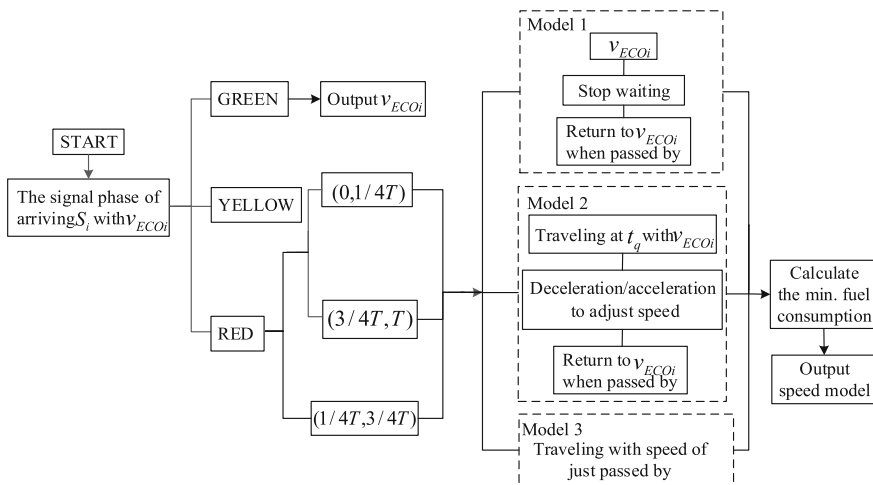


**Fig. 3** The flow graph of algorithm for Eco-speed optimization

recovery speed of passing the intersection $S_i$. We set the period of constant speed is $t_p$, the duration of variable speed is $t_m$, the period of recovery speed is $t_q$.

$$S_u + S_d = v_{\text{ECO}}t_p + v_{\text{ECO}}t_m + \frac{1}{2}a_lt_m^2 + (v_{\text{ECO}} + a_lt_m)t_q \tag{7}$$

$$t_p + t_q + t_m = t_v - t_0 + t_{\text{last}} \tag{8}$$

$$t_p = t_v - t_0 + t_{\text{last}} - t_m - t_q \tag{9}$$

$$t_q = \frac{[v_{\text{ECO}}(t_v - t_0 + t_{\text{last}}) - S_u + S_d]t_m}{a_l} - \frac{t_m}{2} \tag{10}$$

where $a_l$ is the vehicle acceleration (m/s$^2$), $t_m$ is the time of recovery speed after through the intersection.

In this study, the information of traffic lights: cycle time, phase time for known conditions are transferred to the EDAS [7]. It is accessible to formulate the state transformation of the traffic lights as follows:

$$L_i(t) = \begin{cases} 1 & \text{KT} < t \leq \text{KT} + T_{\text{GREEN}} \\ 0 & \text{KT} + T_{\text{GREEN}} < t \leq (K+1)T \end{cases} \tag{11}$$

where $L_i(t)$ is the state of the $i$ - th signal light, $K \in Z$ is the number of the signal cycles, $T$ is the green phase, $T_{\text{REDlast}}$ is remainder of the red light phase.

(1) $L_i(t) = 1$. The speed is directly output. (2) $L_i(t) = 0$. As the speed, distance from the intersection of the location, the signal sequence of traffic light and other factors, the vehicle driving with $v_{\text{ECO}i}$ will be arrived at the intersection in a different period of red light as shown in Fig. 4. Taking into account the different remaining time, then there will be 3 different speed approaches to achieve the purpose of saving fuel and improving the efficiency. It is assumed that the remaining interval time of the red light $t_{\text{REDlast}}$ is divided into three segments now (Fig. 4):

(1) $T_{\text{REDlast}} \in (0, 1/4T)$. The vehicle can decline its velocity before arriving at the intersection, taking into account the factors of efficiency then going through the intersection at the beginning of the next green light as shown in Fig. 5a.

**Fig. 4** The schematic diagram for dividing the remainder of the red light phase
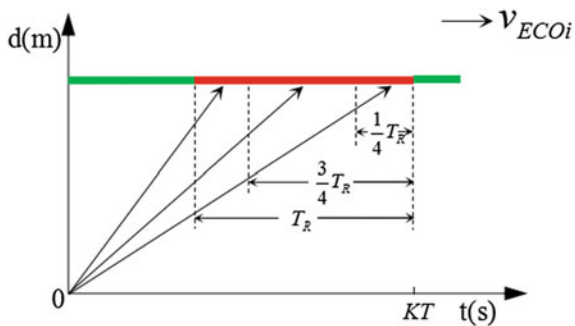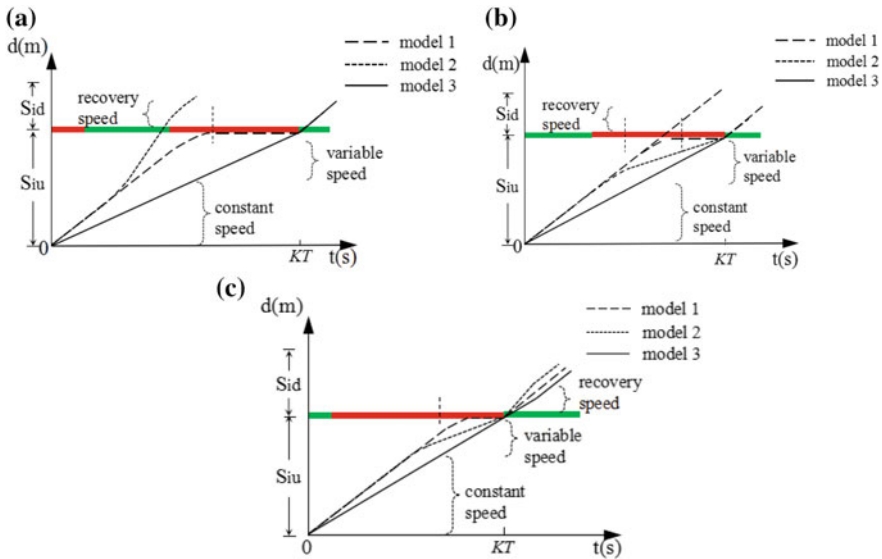
**Fig. 5** The schematic diagram for speed model **a** $T_{\text{Redlast}} \in (0, 1/4T)$ **b** $T_{\text{Redlast}} \in (3/4T, T)$ **c** $T_{\text{Redlast}} \in (1/4T, 3/4T)$

Compare the fuel consumption of the three speed modes as follows. Speed model 1: Traveling at the stop line, and then idling stop to wait. Speed model 2: The vehicle is traveling with $v_{\text{ECO}}$ until the time is $t_p$, and then slow down until the beginning of the green light. Speed model 3: It is possible to travel at the speed of $v_k$ that can through the intersection at the beginning of the green.

$$v_k = \frac{S_{iu} + S_{id}}{t_{iu} + t_{id}} \tag{12}$$

(2) $T_{redlast} \in (3/4T, T)$. The vehicle can increase its velocity before arriving at the intersection, taking into the factors of efficiency account and then going through the intersection at the beginning of the next green light as shown in Fig. 5b. Compare the fuel consumption of the three speed modes as follows: Speed model 1: Traveling at the stop line, and then idling stop to wait. Speed model 2: The vehicle is traveling with $v_{\text{ECO}}$ until the time is $t_p$, and then increase its velocity until the beginning of the green light. Speed model 3: It is possible to travel at the speed of $v_k$ that can through the intersection at the beginning of the green light.

(3) $T_{\text{REDlast}} \in (1/4T, 3/4T)$. The rest can be done in the same manner of condition (2).

## 4   Simulation Results

### 4.1   Simulation Parameter Settings

Using MATLAB for simulation experiments for energy-saving driving assistance system, the parameters of vehicles are shown in Table 1. In order to make the algorithm more suitable for the actual road conditions, choose a city section of Changchun City. The parameters of vehicle, roads and traffic lights are shown in Table 2 [8].

### 4.2   Simulation Results Analysis

The comparison of the time and fuel consumption for the vehicle travel through each section with the different speed model in the simulation by using MATLAB, as shown in Table 2.

Select the economic speed model for fuel optimization. It is necessary to choose the most optimal one in terms of the three vehicle speed models. The optimal eco-driving speed of the vehicle through multiple intersections is revealed in Fig. 6.

The fuel consumption comparison between algorithms based on assisted transportation plan and that of non-assisted operation for the whole route is revealed in the

**Table 1**  The parameters

| The parameters of vehicle | | | | The parameters of roads and traffic lights | | | |
|---|---|---|---|---|---|---|---|
| Parameter | Value | Parameter | Value | Parameter | Value | Parameter | Value |
| $m$ | 1552 kg | $A$ | 2.2 m$^2$ | n | 4 | $v_{\lim 1}$ | 70 km/h |
| $f$ | 0.012 | $i_g$ | 1 | $d_{0,1}$ | 150 m | $v_{\lim 2}$ | 70 km/h |
| $i$ | 0.03 | $i_0$ | 8.28 | $d_{1,2}$ | 1030 m | $v_{\lim 3}$ | 50 km/h |
| $\delta$ | 1.05 | $r$ | 0.31 m | $d_{2,3}$ | 730 m | $v_{\lim 4}$ | 70 km/h |
| $g$ | 9.8 m/s$^2$ | $\alpha_0$ | 32 | $d_{3,4}$ | 690 m | $v_{\min}$ | 30 km/h |
| $\eta_t$ | 0.95 | $\alpha_1$ | 53.4 | $d_{4,f}$ | 150 m | $v_{ECO}$ | 52 km/h |
| $C_D$ | 0.334 | $\alpha_2$ | 2.8 | $T$ | 40 s | $T_{GREEN}$ | 20 s |

**Table 2**  The time and fuel consumption

| | Road1 | | Road2 | | Road3 | | Road4 | |
|---|---|---|---|---|---|---|---|---|
| Model | Fuel (ml) | Time (s) | Fuel (ml) | Time (s) | Fuel (ml) | Time (s) | Fuel (ml) | Time (s) |
| 1 | 10.1 | 10.4 | 75.0 | 78.1 | 77.8 | 85.8 | 55.6 | 62.2 |
| 2 | – | – | 78.6 | 81.7 | 62.9 | 82.5 | 71.1 | 59.1 |
| 3 | – | – | 70.3 | 72.4 | 63.5 | 82.2 | 56.6 | 57.4 |
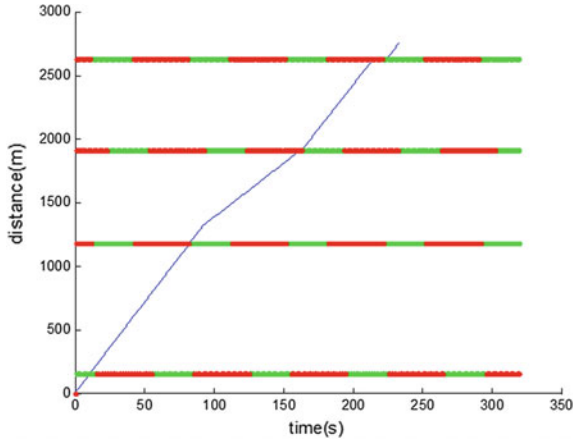
**Fig. 6** The curve of optimal eco-driving speed

Fig. 7. The fuel consumption rate and the cumulate fuel consumption is separately shown in Fig. 7a, b.

## 5 Conclusion

The algorithm used in this paper can effectively reduce the fuel consumption of vehicles driving through the intersections inside cities by using less time of computation in the simulation by using MATLAB. The result of fuel-saving effect is 20% less by comparison with normal fuel consumption in the simulation by using MATLAB.

The speed model which this paper proposed is preferred to prioritize minimum energy consumption in consideration of the traffic efficiency while passing through series of signalized intersections.
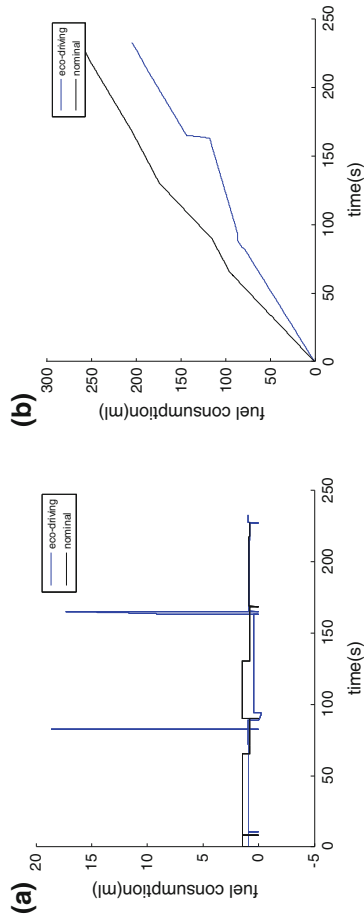
**Fig. 7** Comparison of fuel consumed by an non-assisted vehicle and a test vehicle for eco-driving

# References

1. De Nunzio1 G, de Wit CC et al (2016) Eco-driving in urban traffic networks using traffic signals information. Int J Robust Nonlinear control 26:1307–1324
2. Wang J, Yu Q, Li S et al (2014) Eco speed optimization based on real-time information of road gradient. Automot Saf Energy 5(3):257–262
3. Xu B, Z Fang et al (2016) An assistance system for crossing successive intersections. Automot Eng 38(11):1344–1350
4. Xia H, Boriboonsomsin K, Barth M (2013) Dynamic eco-driving for signalized arterial corridors and its indirect network-wide energy/emissions benefits. J Intel Transp Syst 17(1):31–41
5. Yu Q (2014) Vehicular speed control of eco-driving systems based on connected vehicles. Tsinghua University
6. Dib W, Chasse A, Moulin P, Sciarretta A, Corde G (2014) Optimal energy management for an electric vehicle in eco-driving applications. Control Eng Pract 29:299–307
7. Niu D, Sun J et al (2013) Eco-driving versus green wave speed guidance for signalized highway traffic: a multi-vehicle driving simulator study. Procedia—Soc Behav Sci 96:1079–1090
8. Katsaros K, Kernchen R, Dianati M et al (2011) Application of vehicular communications for improving the efficiency of traffic in urban areas. Wireless Commun Mobile Comput 12(11):1657–1667

# Occupant Restraint System Optimization of Microbus in Front Crash

**Xue-jing Du, Zhan-yu Wang, Huan-huan Guo, Zhen-zhen Wang and Yu-meng Tian**

**Abstract** In order to optimize occupant restraint system and improve the safety of occupant, the effect of occupant restraint system of microbus on head and chest injury is studied. The numerical simulation model is built by MADYMO software according to the frontal crash regulations. The numerical occupant restraint system model of microbus is composed of microbus body, occupant restraint system, and dummy. Based on the calculating results of MADYMO, Head Injury Criterion (HIC), and the amount of chest compression, the safety elongation is 13%, and the limited stress is 4.5 kN. Compared with the occupant restraint system of Microbus before optimization, the WIC, HIC, and chest compression decreased of optimized occupant restraint system decreased by 21.2, 30.8, 1% respectively.

**Keywords** Vehicle collision · Microbus · Occupant restraint system
MADYMO

## 1 Introduction

The performance of the occupant restraint system is directly related to the occupant's injury. A mathematical control model was built by multi-body dynamics analysis method to describe the occupant response and assess occupant's head injury, chest injury, and pelvis during the collision process [1, 2]. Among the occupant restraint system, seat belt has the strongest effect on occupant injury by analyzing the correlation between head injury and each part of occupant restraint system [3]. The performance of seat belt was studied, and the orthogonal experiment was used to optimize the parameters of seat belt [4]. The seat belt with the lowest damage

X. Du (✉) · Z. Wang · Z. Wang · Y. Tian
Department of Vehicle Applied Engineering, School of Transportation College, Northeast
Forestry University, Harbin 150040, China
e-mail: duxuejing99@163.com

H. Guo
Chongqing Changan Automobile Co., Ltd., Chongqing 400000, China

value and optimize parameter configuration interval of the airbag was calculated by numerical model [5, 6]. Then, some methods, theories, and mathematical models were applied to optimize parameters of occupant restraint system [7, 8]. Multi-island genetic algorithm and Kriging model are used to optimize the occupant restraint system [9]. However, researching on the parameters optimization of microbus is limited. Therefore, in order to improve occupant safety and optimize the key parameters of microbus occupant restraint system, the effect of occupant restraint system on occupant injury is studied in this paper.

## 2   Occupant Restraint System Model of Microbus

Taking the microbus with no airbag as an example, the MADYMO simulation model of the occupant restraint system on the front side of the driver is established, which is composed of vehicle body model, restraint system, and dummy model.

### 2.1   Microbus Body Modeling

According to the geometric layout of the microbus, the microbus body model is simplified, and all points of the microbus body in coordinates with X, Z direction are given in Table 1.

The hinge connection is the main way of connecting the components in the microbus body system. In the occupant restraint system simulation model of microbus built by MADYMO, parts connected with different types of hinge, the connection of each part showed in Fig. 1.
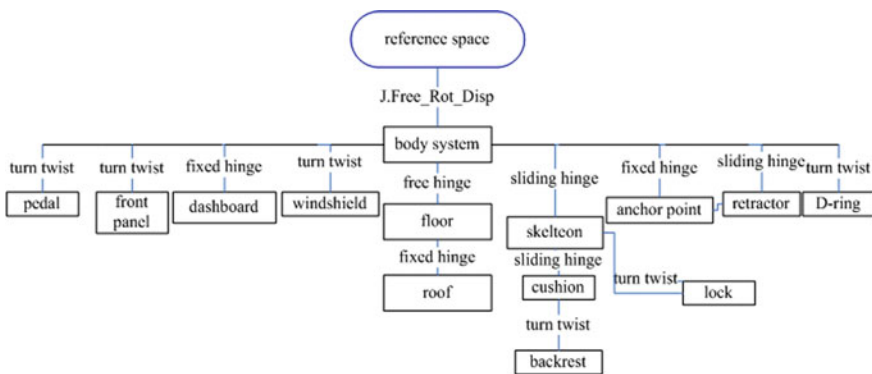


**Fig. 1**   Parts connected of microbus body

**Table 1** Points of microbus body in coordinates (*Unit* meters)

|   | A | B | C | D | E | F | G | H | I | J | K | L | M | N |
|---|---|---|---|---|---|---|---|---|---|---|---|---|---|---|
| X | 1.230 | 1.390 | 2.600 | 1.330 | 1.940 | 2.520 | 1.410 | 1.570 | 1.650 | 1.440 | 1.750 | 2.210 | 2.170 | 2.500 |
| Z | 0.180 | 0.015 | 0.015 | 0.740 | 1.210 | 1.292 | 0.750 | 0.720 | 0.570 | 0.300 | 0.280 | 0.230 | 0.180 | 0.950 |

The microbus body system is connected to the reference space by a free hinge set to a locked state. There is no relative movement of the vehicle roof, which is defined as a consolidation hinge connected to the floor. In the actual assembly, the seat is connected to the front beam of the floor by bolts. The skeleton of seat is defined through the effect of the sliding hinge and the microbus body.

## 2.2 Dummy Positioning

In the microbus model of the frontal crash, Hybrid III 50 Percentile Male oval dome model was used, which composed of 53 different sized ellipsoids attached to the 32 rigid bodies to show the shape of the dummy. The height of the dummy is 175.5 cm and weight is 77.7 kg.

The dummy is positioned on the seat by matching the H point of the dummy with the H point of the seat. The dummy positioning steps are as follows:

(1) The dummy will be adjusted to the top of the seat with visual observation, as close as possible to the seat surface.
(2) Adjust dummy limbs to the measurement values before crash test, and set the INITIAL_JOINT. STATUS of these hinges is LOCK.
(3) The pre-simulation is conducted with the action of the gravity field, then, the dummy close to the surface of seat gradually till static balance.
(4) Copy the final JOINT POSITION data in * .jps file to INITIAL.JOINT_POS, and set the INITIAL.JOINT_STATUS of the limbs is FREE by XMADgic hinge tool.
(5) Dummy positioning work is done as shown as Fig. 2.

**Fig. 2** After visual positioning
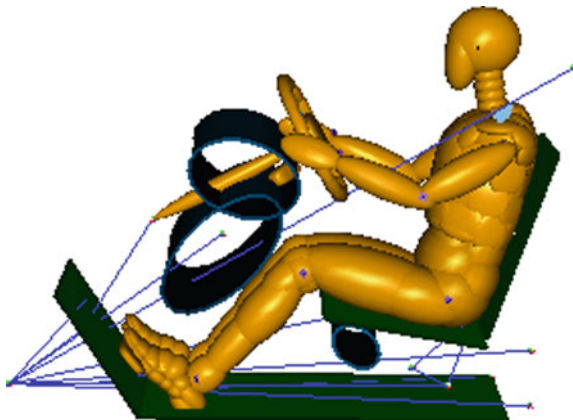
## 2.3 Seat Belt Model

Seat belt model mainly contains fixed point, strap, and retractor. The pre-loader seat belt model is established by hybrid modeling method. In the finite element model, the length, width, and thickness of pectoral girdle of the seat belt are 70 cm, 48 mm, and 1.1 mm respectively. The length, width, and thickness of the belt are 50 cm, 48 mm, and 1.1 mm respectively, and the three-point film mesh is used. Figure 3 is the occupant restraint system model of microbus in MADYMO.

# 3 Parameters Optimization of Occupant Restraint System

## 3.1 Seat Belt Parameters Optimization

### 3.1.1 Stiffness of Seat Belt Strap

The energy absorption of the seat belt is usually determined by the stiffness of seat belt strap. That is elongation, which is generally in the range from 5 to 23%. The relationship between the strap stiffness and chest $C_{3ms}$, head $HIC_{36}$ and chest compression was studied by 10 groups of simulation test. In the simulation test, the strap stiffness is 5, 7, 9, 11, 13, 15, 17, 9, 21, and 23%. The occupant injuries of each part under different strap stiffness are shown in Table 2.

According to Table 2, with the increase of seat belt stiffness, head $HIC_{36}$ is reduced, indicating that the stiffness of strap is positively related to head injury. The correlation between the chest $C_{3ms}$ and the strap stiffness is not significant as the correlation

**Fig. 3** Occupant restraint system model of microbus in MADYMO
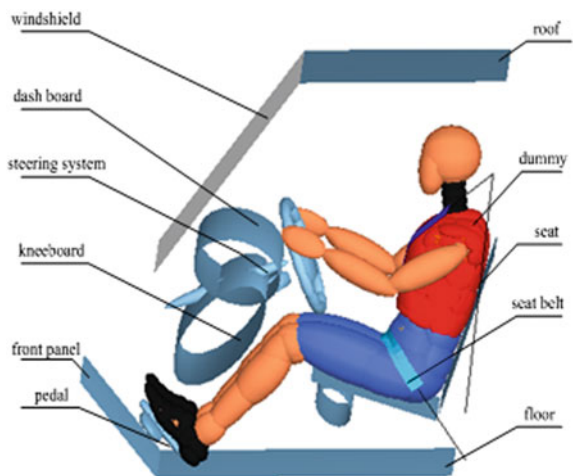
**Table 2** Occupant injury under different strap stiffness

| Ribbon elongation (%) | HIC$_{36}$ | C$_{3ms}$ (m/s$^2$) | Chest compression (mm) |
|---|---|---|---|
| 5 | 1210 | 496.5 | 60.3 |
| 7 | 1123 | 488.2 | 59.2 |
| 9 | 1027 | 475.3 | 58.1 |
| 11 | 978 | 474.3 | 56.1 |
| 13 | 923 | 463.1 | 50.4 |
| 15 | 902 | 471.2 | 56.2 |
| 17 | 877 | 466.3 | 58.7 |
| 19 | 852 | 469.1 | 59.1 |
| 21 | 823 | 462.0 | 66.0 |
| 23 | 796 | 459.8 | 64.0 |

between the head HIC$_{36}$ and the strap stiffness. The relationship between the amount of chest compression and the strap stiffness is not linearly related, which presents a trend of peaking at both sides and lowing in middle. With the head injury as the primary consideration, taking into account the situation of chest compression, the strap stiffness of 13% is selected.

### 3.1.2 Seat Belt Limit

Limitation seat belt can reduce occupant injury. In the MADYMO simulation model, the limit is applied to the seatbelt, and the input value is 4.5 kN. The HIC$_{36}$, C$_{3ms}$, and chest compression values are calculated in the limitation seat belt model. Table 3 shows the occupant injury of the original model and the limitation seat belt model.

It can be seen from Table 3 that the chest C$_{3ms}$ and chest compression output of limitation seat belt are much lower than of original model. Hence, using limitation, seat belt can significantly reduce chest injury.

**Table 3** Occupant injury of original model and limitation seat belt model

| | HIC$_{36}$ | C$_{3ms}$ (m/s$^2$) | Chest compression (mm) |
|---|---|---|---|
| Original model | 1014 | 474.3 | 48.39 |
| Limited seat belt model | 978 | 401.3 | 38.61 |

## 4 Optimization Results

Based on seat belt parameters' optimization analysis, that is the improvement design of microbus safety, optimizing the collision waveform, seat belt stiffness or elongation is 13%, and the seat belt limit value is 4.5 kN. The occupant injury can be calculated by inputting the improved value into the simulation model in MADYMO. Table 4 is occupant injury values of the improved model and original model. Figure 4 is the three-direction synthetic acceleration curve of head. Figure 5 is the three-direction synthetic acceleration curve of chest. Figure 6 is the compression curve of chest. In the figures, the dashed line is the output curve of original basic model, and the solid line is the output curve optimal model.

As can be seen from Table 4, the occupant injury index WIC and HIC of improved model decreased by 21.2 and 30.8%, respectively, compared with that of original model. Chest injury also reduced, and the leg injury was increased in a small range, but it was still far less than the national standard.

It can be seen from Fig. 4, 5, and 6 that the peak of synthetic acceleration of head and chest reduced significantly. The peak of the synthetic acceleration and

**Table 4** Occupant injury values of the improved model and former model

|  | $HIC_{36}$ | $C_{3ms}$ $(m/s^2)$ | Chest compression (mm) | $F_L$ (kN) | $F_R$ (kN) | WIC |
|---|---|---|---|---|---|---|
| GB requirements | ≤1000 | – | ≤75 | ≤10 | ≤10 | – |
| Former | 1014 | 474.3 | 56.1 | 2.817 | 2.752 | 0.910 |
| Improved | 701 | 402.1 | 44.2 | 3.31 | 2.891 | 0.717 |
| Improvement (%) | 30.8 | 15.2 | 21.1 | −17.5 | −5.1 | 21.2 |
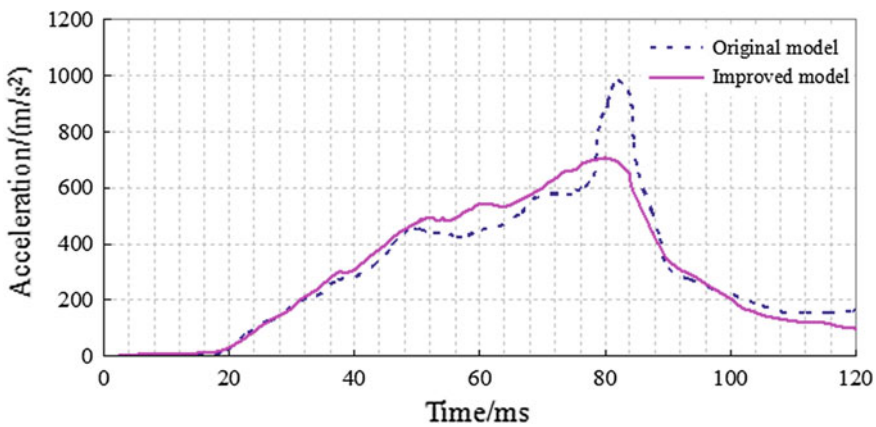


**Fig. 4** Three-direction synthetic acceleration curve of the head
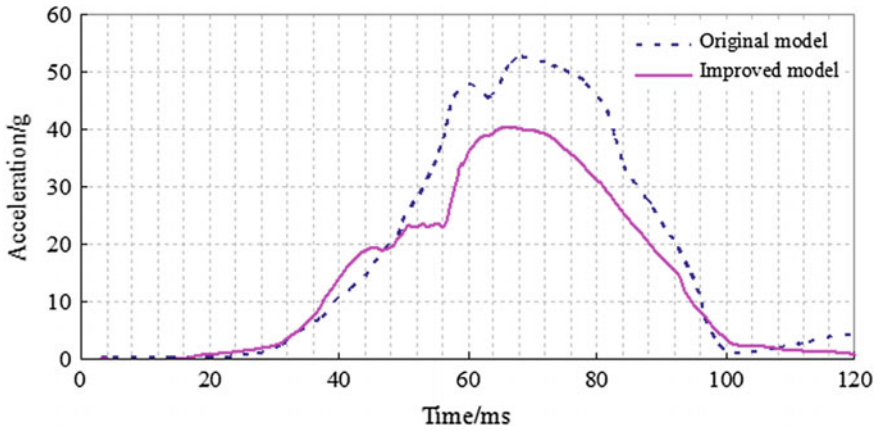
**Fig. 5** Three-way synthetic acceleration curve of the chest
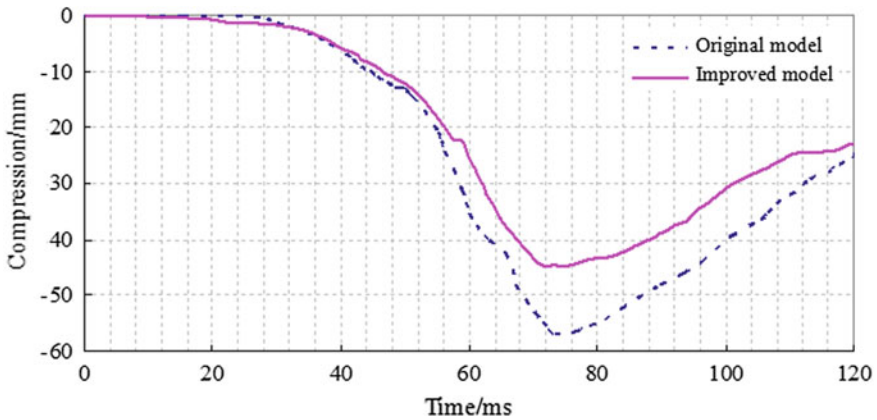


**Fig. 6** Chest compression curve

compression appears earlier than that of the original model, and the model is more relaxed. It is proved that the improved scheme works well.

## 5  Conclusions

Through the simulation of MADYMO, the HIC value of head injury and chest compression were comprehensively analyzed. The elongation of the seat belt was 13%, and the limit value of the seat belt was 4.5 kN. The occupant injury index WIC and HIC of improved model decreased by 21.2 and 30.8% respectively, compared with that of original model. The effect of the improved scheme is obvious.

# References

1. Teng T-L, Chang F-A (2008) Analysis of dynamic response of vehicle occupant in frontal crash. Math Comput Model 48:1724–1736
2. Sheng T (2016) Occupant restraint system simulation and optimization based on TESW. J Trans Nanjing Univ Aeronaut Astronaut 33(22):224–230
3. Martins H, Occupant injury optimization for non-ait bags vehicles. SAE Paper, 2003-01-3752
4. Jian Yuan, Zhengdong Sun, Yongwan Shi (2002) Design optimization and simulation of safety belt. J Automot Eng 24(2):160–163
5. Lin Y, Zhang J, Zhao Y (2003) Performance analysis and improved design on microbus occupant restraint system. J Mech Eng 14(19):1694–1696
6. Ruhai GE, ZHANG Ling, Wang Haotao (2009) Analysis on the influence for the protection on frontal impact by vehicle seat cushion obliquity. J Mech Eng 45(11):230–234
7. Zhang W, Liu H (2008) Occupant restraint system simulation design optimization based on Kriging model and optimization method. J Hunan Univ (Nat Sci) 35(6):23–26
8. Li T, Li G, Gao H, Chen T (2010) Performance improvement of occupant research system. J China Mech Eng 21(8):993–999
9. Tao Ma, Zhang W, Tang T (2014) Study on multi-parameter optimization of occupant restraint system based on global sensitivity analysis and Kriging model. J China Mech Eng 25(13):1813–1816

# Research of Intelligent Car Dual-Navigation System Based on Complex Environment

**Guang-bin Bao, Le Zhang and Hong Zhao**

**Abstract**  The visual path recognition is one of the most important means of intelligent Car navigation. However, it is still faces with many challenges to realize accurate visual navigation in complex environment. As a supplement, manual navigation has the characteristic of high reliability and high flexibility. In this paper, the intelligent car was provided with two navigation modes which can be switched in real time. The first mode adopted the combination between MC9SXS128 Single Chip Micyoco (SCM) as the core controller and a COMS camera to achieve autonomous navigation. The second mode, manual navigation, was brought about by a Play Station 2 (PS2) handle connected to the above SCM mediately. This combination of two navigation mode above is called dual-navigation system. Finally, the experiment results show that the autonomous navigation is competent in navigation task in general complex environment, and it is able to overcome the interference from external environment effectively, such as shadow generated by the backlight and uneven lighting. Besides, manual navigation is quite qualified for navigation tasks in non-general complex environment. And two navigation modes work in with each other well.

**Keywords**  Intelligent car · Complex environment · Recognition · Visual autonomous navigation · Manual navigation

With the instant increase in car parc, urban traffic problems become increasingly prominent, and intelligent transportation system (ITS) has received extensive attention and research [1]. Intelligent car is an important part of ITS, so intelligent traffic cannot be achieved without the intelligent car [2–4]. Navigation system is one of the most important subsystems of intelligent car, and its performance determines the stability and safety of intelligent car directly [5].

In recent years, with the rapid development of intelligent car and the technology of ITS, the trend of car intelligence has been unstoppable, however, because of the complexity and diversity of the road environment, there are still many problems

G. Bao · L. Zhang (✉) · H. Zhao
School of Computer and Communication,
Lanzhou University of Technology, Lanzhou 730050, China
e-mail: 312475689@qq.com

to be solved from intelligent driving to true all-weather unmanned driving. Song and others put forward intelligent cars aided navigation system based on machine vision. In the paper, a new arithmetic of front objective cars area checking based on image entropy was presented. Front objective cars are detected on the considering space-time continuity, the statistical characteristics, and texture character of sequential images. The detection method according to the area information entropy of the image not only improves the accuracy of the goal detection but also reduces system algorithm complexity, and strengthens systematic real-time character and robustness. The intelligent navigate cruise system has significant effect to reduce traffic accident [6]. Li and others proposed a dual-drive dual-control intelligent car bus system so that intelligent car has two driving styles: manual driving and automatic driving, Simultaneously, the style can be switched by voice, touch, and stampede flexibly, but the system has not been implemented concretely [7].

In this paper, 16-bit microcontroller MC9SXS128 was considered as the core controller of intelligent car, and a dual-navigation system which can switch navigation mode in real-time was realized. Then we researched the intelligent car dual-control system by this platform. The visual navigation system and manual navigation system in a complex environment were studied, and some feasible solutions are proposed. Finally, the effectiveness of the navigation system in a complex environment was verified by experiments.

# 1   Hardware System of Intelligent Car

The hardware system of intelligent car is mainly composed of power module, minimum system of microcontrolleru (MCU), motor drive module, and path information acquisition sensor [8, 9]. The power module is responsible for supplying power to the hardware system; MC9SXS128 MCU of Freescale company was chosen as the core controller; L298N was used to the motor drive module, which can drive the four direct-current (DC) motor w1, w2, w3, w4; COMS area-array-camera OV7620 was selected as the path information acquisition sensor; Arduino UNO R3 core board serves as a communication link between the MC9SXS128 core controller and the PS2 remote control handle. The intelligent light compensation module intelligently turns on or off the LEDs by detecting the light intensity of surrounding environment.

The core controller processes the path information which collected from the camera and realizes the four-channel DC motor's control by designed algorithm, then intelligent car achieved visual autonomous navigation. For some special scenarios or tasks, manual navigation can be achieved through the remote control handle.

## 2 Research on Visual Autonomous Navigation System

### 2.1 Intelligent Lights

The camera is the core sensor of intelligent car, and it directly determines whether the intelligent car can track accurately. Because the camera is a photosensitive device and sensitive to light, the shadow generated by backlight of intelligent car's body will cause a large area of noise in its vision (shown in Fig. 8). It is also easy to produce noise in an environment with insufficient exposure and uneven light. Usually, the noise will affect path identification of intelligent car seriously.

Based on the above problems, the basic solution is to adjust the appropriate light threshold according to different light intensities of the environment. Therefore, the determination of the threshold is vital. The threshold method is divided into dynamic threshold method and fixed threshold method. The fixed threshold method cannot adapt well to the change of the ambient light intensity, which is not conducive to extract the black line (path edge). Consequently, general method is to design an algorithm to set the threshold dynamically, which can adapt to different light intensities of the environment and eliminate the interference of noise and pulse effectively to protect edge information of the black line of image. But the dynamic threshold method has its own shortcomings, on the one hand, algorithm of dynamic threshold requires a large number of operations, which increases the operation burden of core controller. Once we want to get more path information and increase the size of the image, it is easy to cause the delay of microcontroller's process and lead to intelligent car unable to track normally; on the other hand, it cannot solve the interference of intelligent car backlight shadow.

In order to solve the defects of dynamic threshold method, this paper proposed a solution which combined hardware and software, that is, under fixed threshold, using the photosensitive resistance of intelligent complement module to detect the surrounding environmental light, then open or close the light (composed of five White light LED lamps) automatically. Once ambient light intensity is lower than illumination intensity which has set in the algorithm, the light will be on; otherwise, the lamps are closed normally.

### 2.2 Path Identification and Control Strategy

#### 2.2.1 Image Preprocessing

First, the image acquired by the camera is binarized, that is, and the pixel in the image is directly compared with the threshold. If the value of the pixel is no less than the threshold, it is judged that the point is white, otherwise, the point is black. Then use a median filter to process the image, which removes the noise caused by system

noise, environmental interference, and other factors, and get a good edge contour image for the late path centerline (path center line) extraction.

### 2.2.2 Path Centerline Extraction and Path Pattern Recognition

In this paper, Fig. 1 was used for a test track to conduct this research, where A and B are the track exit or entrance. Because the path is not both sides of the situation, there are complex path and special path, in order to enable the intelligent car to travel along the track centerline (namely path centerline mentioned above), this paper proposed a horizontal scan and longitudinal scan method to achieve track centerline extraction and path pattern recognition.

The specific ideas for horizontal and vertical scanning are as follows:

(1) Blackline extraction and visualization of general track center

The information collected by the camera is a two-dimensional image (the image pixels collected in this paper are $120 \times 40$), where the coordinates of upper and lower corners of the image are (0,0) and (39,119) respectively, as shown in the Fig. 2 (left figure). A two-dimensional matrix can be constructed according to the size of the captured image to store these image pixels. First, the nearest image of the headlight is given to the MCU to deal with, and the pixels far away from the front can be used as path anticipation and path pattern recognition. So the pixel which is near the front of intelligent car should be scanned by MCU at first, that is, scan the edge of two paths from pixel C (C is the center of the abscissa of the image) to pixel point A and B simultaneously, and record the pixels A and B vertical and horizontal coordinates, which is horizontal scanning, as shown in Fig. 2 (right figure). Accordingly, the actual track centerline abscissa is Center = (A + B).

In order to eliminate interference of random noise, a better solution is to take the abscissa of the n lines near the center of the abscissa as the center of the track abscissa. The specific calculation method as shown in equation

$$\text{Center\_now} = \frac{1}{\text{row} - k} \sum_{i=k}^{\text{row}} \frac{(A_i + B_i)}{2}, k = 0, 1, \ldots 39.$$

**Fig. 1** Test track
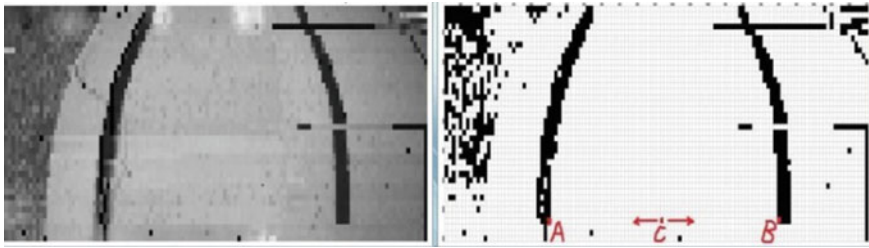
**Fig. 2** Image capture

Among them, the row is the collection of image width, k generally take $k \geq 3$, that is (row-k) generally take 3–6.

In order to facilitate observation, the center line can be visualized through the upper computer, as shown in Fig. 3.

(2)  Pattern recognition on special track paths

For the track path shown on the left in Fig. 4, it is necessary to perform a longitudinal scan on the basis of the lateral scan. Since there is no available value in the longitudinal scanning of the image information in the area which closer to the intelligent car, it is only necessary to scan the one-way pixel D further from the front to identify the path information of the front, as shown in the right figure of Fig 4. When scanning to point D, record the coordinates of the D point pixels.

Horizontal scanning and longitudinal scanning results can be combined to identify any path mode in front of the intelligent car. And then intelligent cat makes the appropriate driving action according to the current path mode. The program flow chart of horizontal-vertical scan is shown in Fig. 5.

Among them, Row_on = 0 means that the point of scanning is black spots; Column_left = 0 or 1, respectively, indicates the left side of the scan points is black or white.

In order to keep the intelligent cat moving along the vicinity of central line of the track, the car needs a reference. Usually choose track centerline as the reference
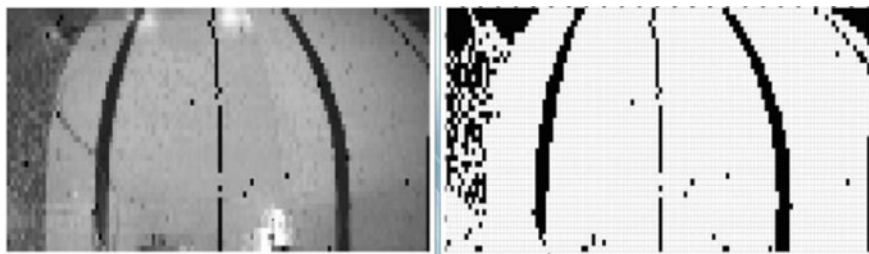


**Fig. 3** Extraction and visualization of track centerline
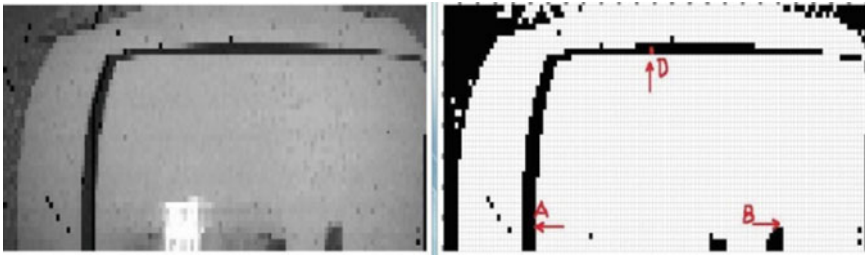
**Fig. 4** The special track (which is more complex than the normal tracks)
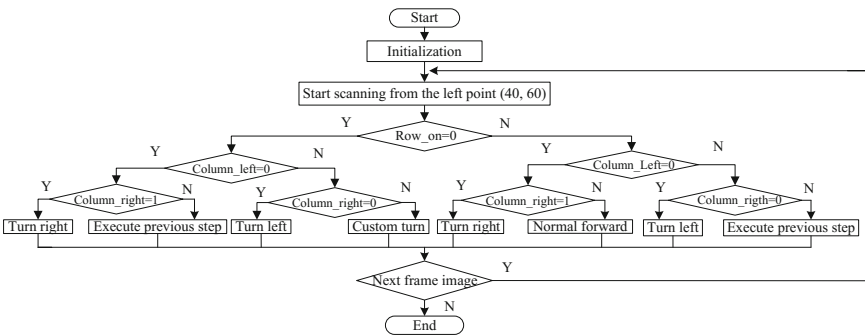


**Fig. 5** Program flow chart of horizontal-vertical scan

line, namely the car axle and the perpendicular bisector of the running state of the track line overlap is the ideal situation, in which the track line Image_center_line is half the width of the track, 60. In fact, however, this ideal situation is usually only a moment, and then there will be a deviation between the two lines, the deviation is defined as Column_center_Dev, that is Column_center_Dev = Image_center_line − Center_now. Obviously, the value of Column_center_Dev is positive or negative.

The deviation value can be used to control the DC motor, and the moving route of intelligent car can be adjusted to the desired state. The method ensures that intelligent car travels near the center line and does not run out of autodrome, however, this method still has a flaw. From the driving trajectory, it is not difficult to find that the swing amplitude of intelligent car is very large when car runs near the center line of the track, which causes the intelligent car to jitter intermittently, further, affects the camera collecting path information, and the probability of noise generated will be increased.

Correction to driving direction of intelligent car varies dynamically through PWM (Pulse Width Modulation). That is, when the Column_center_Dev is small, the car steer slightly, on the contrary, when the Column_center_Dev is large, the car steer greatly. According to the difference of the deviation value, the dynamic selection of
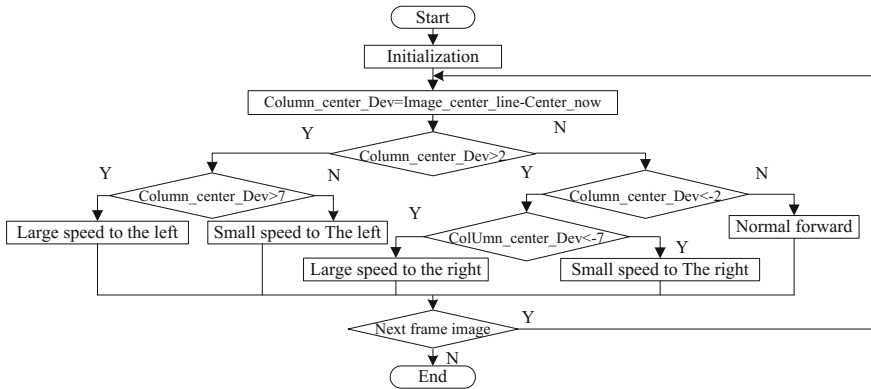
**Fig. 6** Improved algorithm flow chart

the correct correction range can be used to drive the real intelligent car smoothly. The improved algorithm flow chart is shown in Fig. 6.

Likewise, in order to remove the interference from random noise, intelligent car should scan the n points near the black spots which have been detected, where n generally takes 2–5. If these pixels are still determined as black dots, then intelligent car can confirm that the line has been scanned to the front line.

## 3　Research on Manual Navigation System

The moving process of the intelligent car is affected by working environment and its structure. The single drive structure of traditional intelligent car is not flexible enough to meet the real-time control of complex conditions [10]. Handle is a common way of interaction between people and cars, through a handle to control intelligent car can achieve real-time control. Usually, intelligent car and remote control handle need special communication protocol, which is difficult to be transplanted in the cross platform. In this paper, a simple communication method is proposed, through analysis instruction of PS2 by mc9sxs128 core controller, the control of intelligent car is realized easily. The communication block diagram of the handle and the MC9SXS128 core controller is shown in Fig. 7.



**Fig. 7** Communication principle frame diagram
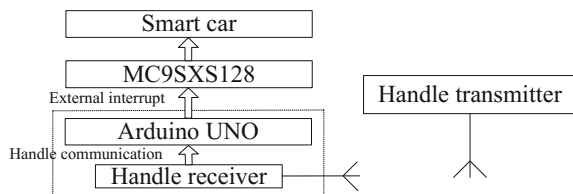
On the premise that the Arduino can communicate with the PS2 handle properly, Arduino UNO R3 controller is considered as a part of the handle receiver (as shown in Fig. 7 dotted box). By modifying the communication codes between Arduino UNO R3 and PS2 handle, the handle instructions are represented by external interrupt I/O, which performance may be high, low, or level transitions, etc. Then this kind of performance is transmitted to the external interrupt of the MC9SXS128 core controller through wires, and the controller analysis the corresponding performance signals, thus manual navigation system realized indirect communication between the MC9SXS128 core controller and the remote control handle, greatly reducing the cross-platform transplant code difficulty.

## 4 Results Analysis and Comparison

Through comparison experiment, as shown in Figs. 8 and 9, the method of using intelligent light compensation is easier to realize, which solved the problem of backlight shadow and underexposure, then less noisy images were obtained, the burden of SCM was reduced. In the overall, the performance is better than the pure fixed threshold method.

Through the comparison experiment, it is not difficult to find that the improved algorithm can make the swing of the intelligent car relative to the center line smaller and make the trajectory more smooth. This algorithm also made the intelligent car run much steadier. Then, intelligent car collected images which included less noise. Comparing the improved algorithm and the previous, the trajectory of the intelligent car which runs on the straight track is shown in Fig. 10.

After comparison, the indirect communication method proposed in this paper can greatly reduce the difficulty of cross-platform code migration, make the operation simpler, and save a lot of workload. Of course, this method also has disadvantage, it needs to occupy the external interrupt resources of MC9SXS128 and Arduino UNO R3, each pair of interrupts can only resolve one PS2 remote control instruction, but the remote control operation for small instruction is fully feasible. It is worth noting
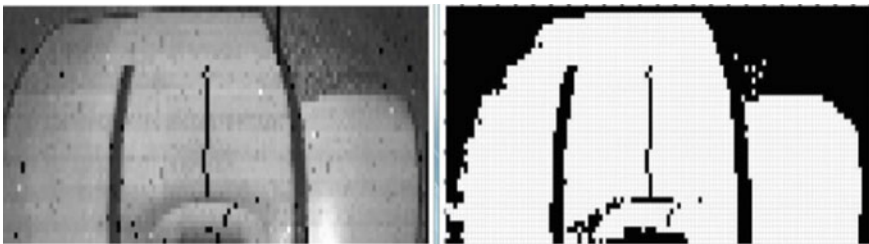


**Fig. 8** Pure fixed threshold method centerline

**Fig. 9** Intelligent light compensation method



Track center line
The lane trajectory before improvement
The lane trajectory after improved algorithm
The black line on the edge of the track
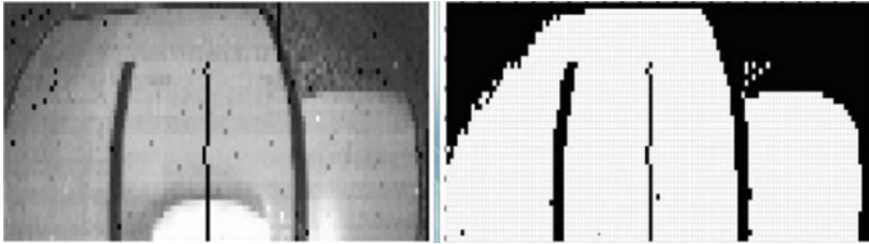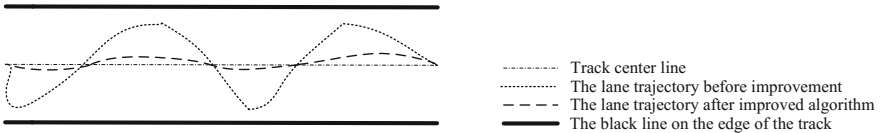
**Fig. 10** Comparison of trajectories

that the ground wire of MC9SXS128 and Arduino UNO R3 must be connected together.

## 5 Conclusions

Taking MC9SXS128 as the core controller, the intelligent car navigation system was designed and implemented. In this paper, an intelligent light compensation method was proposed to solve the problems that light may be uneven and the dynamic threshold algorithm aggravates load of MCU, at last, it obtained an ideal result. Through the improvement of the path recognition algorithm, the accurate identification of the special path mode can be realized. Through the improvement of control strategy, the swing deviated from the track centerline of intelligent car reduced obviously. In addition, this paper also proposed a simple communication method, which realized the communication between the core controller and the remote control handle, and greatly reduced the work difficulty and saved time.

The experiments show that the intelligent car can be switched freely in the automatic tracking mode and remote control handle control mode, and the intelligent car can complete all necessary tasks, and the system has a good anti-interference ability and robustness. How to improve the intelligence, stability, safety, and intelligence of intelligent system will be the focus of the next step.

# References

1. Wang J, Chao Z, Shan Y et al (2010) Research on key technologies for urban unmanned intelligent car. In: Intelligent systems, IEEE, pp 51–54
2. Sun DX, Zhang WB, Liu XY (2012) The intelligent car navigation system based on photoelectric sensor. Adv Mater Res 510:835–841
3. Babu DS, Joseph P et al (2012) Intelligent turning system for a smart car. ICETT 4:45–47
4. Hasan N, Didaralalam SM, Rezwanul Huq S (2011) Intelligent car control for a smart car. Int J Comput Appl 14(3):15–19
5. Zhang YZ, Shi EY, Wu CD et al (2009) On the navigation system based on CCD for smart car. J Northeast Univ 30(2):162–165
6. Song G, Pan Y (2007) The Research of intelligent cars aided navigation system based on machine vision. In: International conference on mechanical engineering and mechanics 2007
7. Li D, Zhang X, Han W et al (2014) Double-drive dual-control smart car bus system. CN: CN104079669A
8. Gao YB, Cong JI, Han PW (2013) Design of smart car system with camera-based path recognition. J Lanzhou Univ Technol 39(06):97–102
9. Zhang HT, Zhao SS, Han JH (2009) Design of intelligent car based on CMOS image sensor. J Henan Univ Sci Technol 30(01):18–21
10. Dai S, Chen B, Fan S (2011) Control and study of wireless control system of intelligent car. Comput Meas Control 19(9):2125–2127

# Research on the Characteristics of Electric Bicycle's Traffic Behavior at the Intersection

Han Do Thi and Yanyan Chen

**Abstract** As a vehicle that stands for the development of new technology, and an effective solution for energy shortage and environmental problems, electric bicycle has not only entered thousands of households but also become the first choice for short-distance travel in many cities in China. Due to its flexibility and convenience, electric bicycle is often involved in unsafe traffic behaviors such as running red light and crossing motor vehicle, therefore disrupt the traffic order at the intersection, which has not only lowered the service level of the intersection and road section but also increased the traffic accident rate. From the perspective of traffic safety, this research first studies the characteristics of the Electric bicycle at the intersection, puts forward the method of calculating the electric bicycle flow at the intersection, and analyzes the delay time of the Electric bicycle after conducting the actual survey, then describes the releasing process of the electric bicycle according to the practical observation, and calculates its dilatation during the releasing process. In the end, the research studies the electric bicycle's queuing process, and the relation between its queuing density and queuing width at the intersection combing with real-life investigation. The research result provides a great reference value in solving the traffic problems with electric bicycle in the urban transport system.

**Keywords** Electric bicycle · Traffic safety · Traffic behavior · Behavior characteristics · Unsafe behavior

H. Do Thi · Y. Chen (✉)
College of Metropolitan Transportation, Beijing University of Technology, No. 100, Pingleyuan, Chaoyang District, Beijing, China
e-mail: cdyan@bjut.edu.cn

H. Do Thi
e-mail: handt84@msn.com

# 1   Introduction

As one of the vehicles powered by new energy resources, electric bicycle (E-Bike) has earned a wide popularity among citizens due to its characteristics of being flexible, convenient, and efficient. In recent years, with the rapid development of E-Bike in many cities in China, not only has it brought along many conveniences to citizens' daily life, many traffic problems have also emerged in the urban transport system, which has become a hot topic of the discussion over traffic problems. The traffic safety of the E-Bike has always been the center of all relevant discussions and controversies. There are many factors that will influence E-Bike's safety, for example, first, the dimension and the weight of the E-Bike influence the geometric and structural design of the road, the park and the designs of other urban transportation facilities, also, the dynamic combination of E-Bike's performances and the riders who utilize these performances determine the specialties of traffic flow and its safety issues. In addition, different from the running characteristic of the motor vehicle, which is moving forward orderly, E-Bike often moves through the gaps among other vehicles, which influences the traffic order and the operation of other transports on the road. At the intersection area, E-Bike riders are often seen running the red light, parking on the motorway or parking over the stop line, these behaviors have not only lowered the efficiency of the intersection but also increased the possibility of traffic accident.

Domestic studies about E-Bike are mostly focused on its behavior in urban transport system and its influence on the safety of urban roads, however, western scholars mainly concentrate on E-Bike market, its market trend and how it is helpful for improving rider's health condition while lacking the emphasis on the characteristics of its traffic behaviors. At present, the study on the characteristics of the E-Bike riders mainly includes the researches carried out by scholars such as MacArthur J, Dill J, Wolf A, and Seebauer S, who had put forward the basic characteristics of E-Bike riders by investigating the riders from Austria and Sacramento [1–3]. The research result is highly replied on riders' feedbacks because the data is collected through questionnaires, in other words, the result is inevitably influenced by individual's subjective feelings. In China, Liu Ying, from the Science Academy of Ministry of Transport, has put forward the travel characteristics of E-Bike after analyzing the questionnaires answered by the E-Bike riders [4]. Recently, she has discussed E-Bike's travel characteristics in urban roads in one of her researches and come up with the dilatation process of E-Bike at the intersection [5]. However, currently, the study on the characteristics of E-Bike's traffic behavior is very rare which has led to the lack of theoretical basis. Therefore, basing on the background described above, this research studies the characteristics of E-Bike's traffic behavior at the intersection from the perspectives, such as when E-Bike enters the intersection, the releasing process of the E-Bike at the intersection, and the characteristics of E-Bike's unsafe behavior. The research achievement is helpful for increasing E-Bike's safety, and further improving the traffic order at the intersection area.

## 2 The Traffic Characteristics of E-Bike at the Intersection Area

E-Bike will join other vehicles when arriving at the intersection area. At the signalized intersection, the characteristics and the speed of the E-Bike while arriving at the intersection will influence rider's next move. Without interference, the arrival of E-Bike is random, however under real-life circumstances, there are many influential factors, such as the difference of the width of the entrance driveway at different intersections will diversify the arrival characteristics of the E-Bike. A group of riders who know each other are more likely to drive in flock on the road and arrive at the intersection on different time gaps. In addition, if the traffic density of E-Bike flow is very big during the green light time at the upper intersection area, there will still be lots of E-Bikes at the intersection area during the red light time at the next phase.

E-Bike's arrival of the intersection reveals an imbalance trend from the perspective of time and space. During the peaks (morning peak and evening peak), the arrival of E-Bike is much higher than normal time or low peak. What's more, E-Bike is more centralized on the cross that leads into the town during the morning peak, yet more on the cross that leads outside the town during the evening peak.

According to Ref. [6], negative binomial distribution is suitable for describing the arrival of huge E-Bike flow at the intersection. This research uses Ref. [6] and the negative binomial distribution to further study the E-Bike flow when arriving at the intersection area. The negative binomial distribution equation is as follows:

$$P(x) = C_{x+\beta-1}^{\beta-1} p^{\beta} (1-p)^x \tag{1}$$

$$p = m/s^2 \tag{2}$$

$$\beta = m^2/(S^2 - M) \tag{3}$$

*In this equation*:
*P(x): The probability for x amount of E-Bikes to arrive during a certain time gap*;
*x: The number of the E-Bikes arrived*;
*p: Model parameter, $0 < p < 1$*;
*$\beta$: Model parameter*;
*m: Sample average*;
*$S^2$: Sample variance*.

# 3   Release and Delay Characteristics of the E-Bike at the Intersection

## 3.1   Analysis on the Releasing Rule of the E-Bike at the Intersection

The intersection area is the place where vehicles join and disperse. E-Bikes stay at the cross till the green light and drive to the intersection area. Many factors will influence the releasing of E-Bike, such as driving speed, conflicts with other vehicles, and the density of the E-Bike. The conflict between pedestrians and motor vehicles can be avoided by setting phases at the intersection area [7], and adding a phase for E-Bike surely can effectively improve the safety situation of the E-Bike, however, the waiting time of other vehicles will also be increased.

The E-Bikes are often released in flock at the intersection area. For riders who have been observing traffic regulations and waiting at the cross, they will drive into the intersection area and pass through it at full speed when the light turns green, therefore causing the dilatation at both sides or the behavior of occupying motorways.

## 3.2   The Dilatation Characteristics of the E-Bike at the Intersection Area

There is a large part of randomness in terms of E-Bike's speed at the intersection area because the riders usually speed up or slow down according to their needs for self-protection. The riders can easily and quickly adjust themselves both on the road and at the intersection area. Therefore, the traffic flow of E-Bike is compressible. The traffic flow density of the E-Bike varies with the changes of the road width, and the flow of E-Bike.

E-Bikes will form a group with big density while queuing at the intersection area and speed out of the parking area once the light turns green. One E-Bike occupies the breadth between 50 cm to 100 cm; so the average breadth occupied is 75 cm, in other words, the transverse pitch among them is quite small when queuing, but it will increase once the E-Bikes start to move, especially when they speed up. After entering the intersection area, the breadth among the queuing E-Bikes has increased significantly, therefore forming the dilatation phenomenon of the queuing E-Bikes [8].

At the signalized intersection, E-Bike is often seen passing the parking line before the green light because it's easy to start and highly mobilized. The traffic dilatation model of the E-Bike can be described with the concept of dilatation, which is the ratio of the transverse density during parking and once the dilatation activates.

$$\kappa_p = \frac{\overline{D}_m}{D_0} \tag{4}$$

*In this equation*:
$\kappa_p$: *Dilatation degree*;
$\overline{D}_m$: *The lateral width of the road occupied by one E-Bike once activating dilatation*;
$D_0$: *The lateral width of the road occupied by one E-Bike under static state, here use*
*0.75 m.*

Choose the entrance driveways with different width; observe the quantity and the transverse driving width of queuing E-Bike flow after entering the intersection area. The analysis finds that the width of the road occupied by one moving E-Bike remains steady, the dilatation figure is as shown in Fig. 1.
Sample Value: $\overline{D}_m = 1.29m$.
In this case, Dilatation Degree: $\kappa_p = \frac{1/0.75}{1/1.29} = 1.72$.

## 3.3 The Delay Characteristics of the E-Bike

In an urban transport system, the intersection area is designed to manage the non-motor vehicle (E-Bike included) according to motor vehicle's traffic capacity. Under the control of signal lights, motor vehicle and non-motor vehicle at the same phase share the same road space [9]. However, the characteristics and the running specifics between E-Bike and motor vehicle are very different, which will easily lead to the reciprocal interference, therefore increasing the delay time to both two types of vehicle. Within the intersection area, E-Bike's delay is caused by two reasons, one is the traffic flow conflicts between E-Bike and other vehicles when passing through the intersection, the other is the time waiting for the right light at the stop line before passing through the intersection [10]. The delay of E-Bike at the intersection is as shown in Fig. 2.

Take the forward-moving E-Bike as an example, Fig 2 suggests that the E-Bike needs to slow down for observing the surroundings or to pull up and wait while getting close to the intersection, which has created the delay. The E-Bike needs to pull up and wait in the stop line if it is red light when arriving at the intersection,



**Fig. 1** The activation of dilatation process by E-Bike at the intersection area
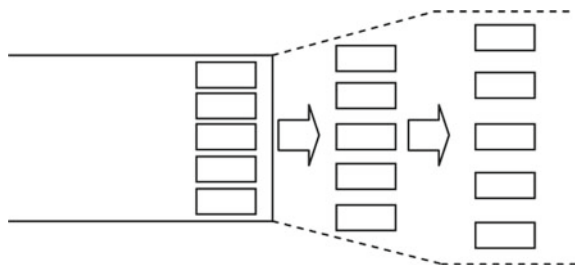
**Fig. 2** E-Bike delay at the intersection area
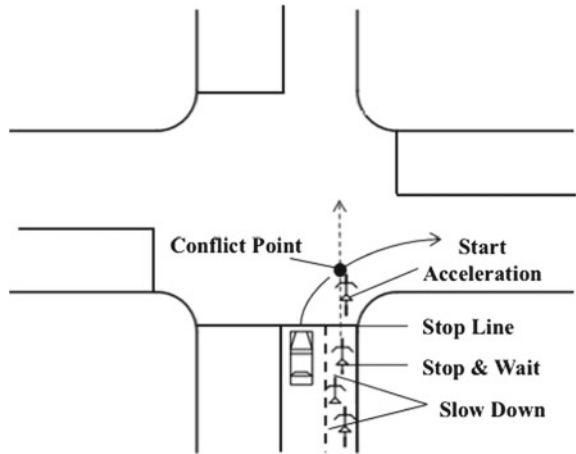
which has created waiting delay. When the light turns green, E-Bike needs to start and
drive into the intersection with accelerated speed, which has created the accelerated
delay [11, 12]. When having conflicts with motor vehicles while passing through
the intersection, E-Bike has to give way to the motor vehicle or slow down to go
around, which has created the avoiding delay. E-Bike is very flexible, but its speed
is relatively slow, which means its acceleration process and moderating process can
be very quick, therefore have very little influence on the delay. The main causes of
delay are parking and conflicts. The factors that influence E-Bike's delay including
the traffic flow at the intersection area, signalized phases and cycle, green light ratio,
stream distribution, etc. [13]. Five typical intersections in Beijing are selected in this
research, after studying the delay of E-Bikes, the research results are as shown in
Table 1.

**Table 1** Vehicle delay time (s)

| Intersection | Direction of the flow | |
|---|---|---|
| | Straight | Left-turning |
| West Da Wang Road Nan Mo Fang (North-South) | 15.63 | 18.73 |
| West Da Wang Road Guang Qu Road (North-South) | 26.34 | 35.95 |
| West Da Wang Road Song Yu South Road (East-West) | 19.45 | 26.49 |
| Nan Mo Fang East-West Ring South Road (North-South) | 30.72 | 41.58 |
| Guang Qu Road East Third Ring Middle Road (South-West) | 29.57 | 34.86 |

Table 1 shows the delay time of E-Bikes at 5 different intersections in Beijing, as suggested in this table that E-Bike has a very severe delay at the intersection, and the left-turning ones have longer delay time than the forward-moving ones.

## 4   The Queuing Characteristics of the E-Bike at the Intersection Area

Density is defined as the intensive degree of vehicles on one driveway. Jam density is defined as the density of the traffic flow at the signalized intersection during the red light when the vehicle's speed is close to zero [14]. At the intersection, the factors that will influence the queuing density of E-Bike including the quantity of queuing vehicles, the width of the driveway, E-Bike rider's behaviors, the width of E-Bike under static state and dynamic state, the dimension of the E-Bike, etc. [15]. Among all the influential factors, this research believes the following three factors have the biggest influence on the queuing density of the E-Bike, queuing length, quantity of queuing vehicles, and the width of motorcycle-only road. The analysis and modeling are based on the three aspects mentioned above.

### 4.1   Queuing Length of the E-Bike

In order to complete the research of this subject, 10 different intersections in Beijing are selected as observing samples. First, conduct the statistical analysis on the queuing length and parking quantity under each width of the driveway, and the result is as shown in Table 2.

According to the analysis results, E-Bike's queuing density stays constant when under same lane-width and different traffic flow situation. The E-Bikes at the rear of the queue will start to fill up the gaps in the front and occupy the whole lane-width only when the queuing length exceeds approximately 10 m.

**Table 2** Correlation analysis on E-Bike's queuing length and parking quantity at the entrance driveway of the intersection area

| Lane-width (m) | Regression equation | Variance | Regression curve figure |
| --- | --- | --- | --- |
| 2.0 | Y = 0.0097x + 0.4861 | 0.708 | Figure 3 |
| 2.5 | Y = 0.9657x + 0.5174 | 0.7514 | Figure 4 |
| 3.0 | Y = 4.441x-3.5312 | 0.897 | Figure 5 |
| 3.5 | Y = 2.9799x-3.1018 | 0.9153 | Figure 6 |
| 4.0 | Y = 1.703x + 4.6061 | 0.8683 | Figure 7 |
| 5.0 | Y = 1.1821 + 1.3193 | 0.7285 | Figure 8 |

**Fig. 3** The regression curve of vehicle queuing length and vehicle quantity when the lane-width is 2 m



$$y = 0.0097x + 0.4861$$
$$R^2 = 0.708$$
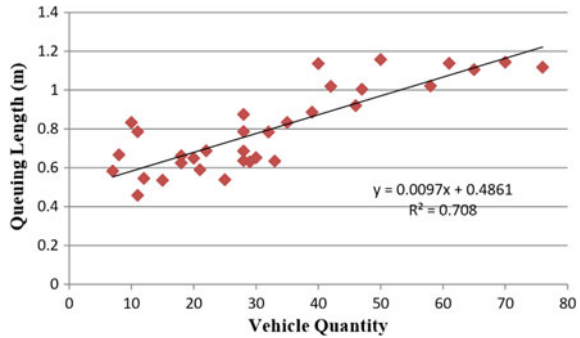
**Fig. 4** The regression curve of vehicle queuing length and vehicle quantity when the lane-width is 2.5 m



$$y = 0.9657x + 0.5174$$
$$R^2 = 0.7514$$
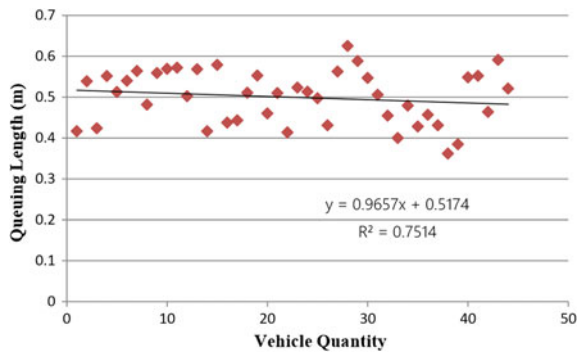
**Fig. 5** The regression curve of vehicle queuing length and vehicle quantity when the lane-width is 3 m



$$y = 4.441x - 3.5312$$
$$R^2 = 0.897$$
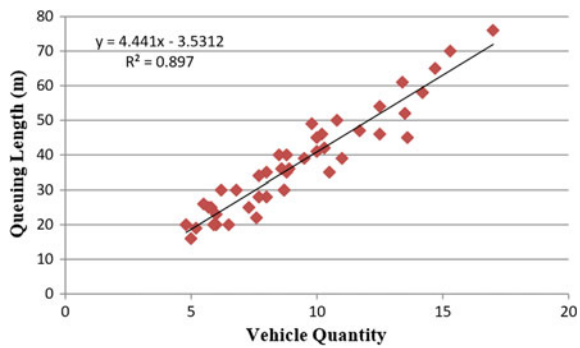
## 4.2 The Relation Between E-Bike's Queuing Density and Queuing Width

After processing the observation data, E-Bike's queuing sections are divided according to its queuing quantity, then calculate the E-Bike's queuing length each section's mid-value stands for, the details are as shown in Table 3 and Fig. 9.

**Fig. 6** The regression curve
of vehicle queuing length
and vehicle quantity when
the lane-width is 3.5 m
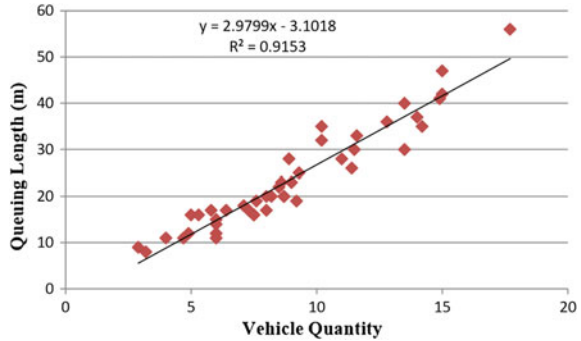


**Fig. 7** The regression curve
of vehicle queuing length
and vehicle quantity when
the lane-width is 4 m
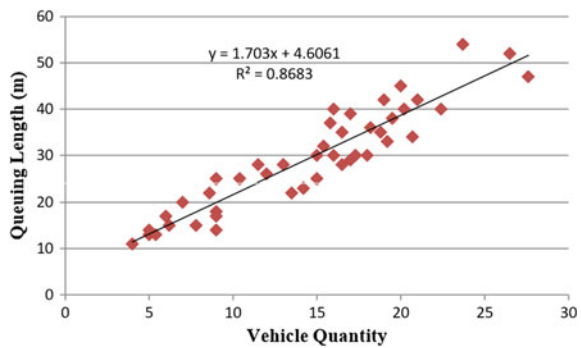


**Fig. 8** The regression curve
of vehicle queuing length
and vehicle quantity when
the lane-width is 5 m
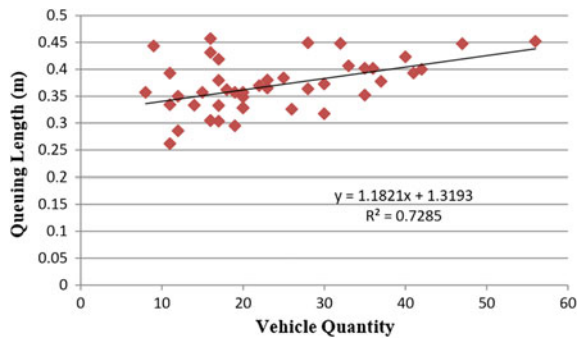


**Table 3** E-Bike queuing density and entrance driveway width

| Entrance driveway width (m) | 2 | 2.5 | 3 | 3.5 | 4 |
|---|---|---|---|---|---|
| Average queuing density (per m$^2$) | 0.3514 | 0.3715 | 0.5033 | 0.5253 | 0.5077 |

As the relation between E-Bike's queuing density and lane-width suggested, E-Bike's queuing density increases linearly with the increase of the entrance driveway width in spite of certain fluctuations.

**Fig. 9** Relation between E-Bike's queuing density and entrance driveway width
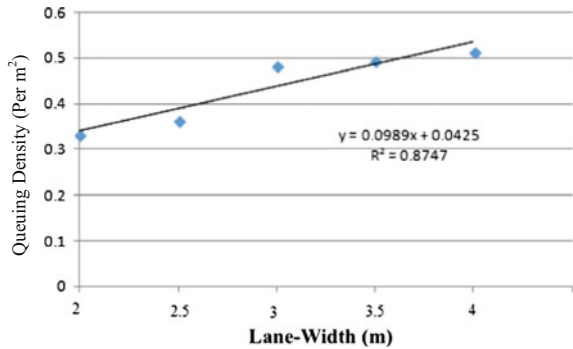
The equation for calculating E-Bike's queuing density when entering the intersection is as shown in Eq. (5), which is also an intuitive relation between E-Bike's queuing density and lane-width.

$$\rho_{EB} = 0.0425 + 0.0989W$$
$$R = 0.8747 \tag{5}$$

*In this equation*:
$\rho_{EB}$: *E-Bike's Queuing Density When Entering the Intersection* (per m$^2$);
$W$: *Entrance Driveway Width at the Intersection* (m).

## 5  Conclusion

By analyzing E-Bike's traffic behaviors, using negative binomial distribution to describe when huge E-Bike flow arrives at the intersection area, this research explains E-Bike's characteristics when arriving at the intersection. Then analyzes its releasing process at the intersection through practical observation and data recording, and calculates E-Bike's dilatation degree during releasing process. In addition, the analysis on E-Bike's delay characteristics is also covered in this research. In the end, the analysis on the recorded data reveals E-Bike's queuing characteristics at the intersection, through studies on the relation between E-Bike's queuing density and lane-width, the research comes up with the model for calculating E-Bike's queuing density when entering the intersection area.

## References

1. Wolf A, Seebauer S (2014) Technology adoption of electric bicycles: a survey among early adopters. Transp Res Part A Policy Pract 69:196–211

2. Popovich N, Gordon E, Shao Z et al (2014) Experiences of electric bicycle users in the Sacramento, California area. Travel Behav Soc 1(2):37–44
3. Johnson M, Rose G (2013) Electric bikes: cycling in the New World City: an investigation of Australian electric bicycle owners and the decision making process for purchase. [2016-10-07]. http://atrf.info/papers/2013/2013_johnson_rose.pdf
4. 刘颖. 城市电动自行车出行交通特性研究. 交通与运输学术版 2011(2):36–39
5. 杜氏欣, 陈艳艳. 城市道路电动自行车交通出行行为特征研究. 黑龙江科技信息 2016(2):256–257
6. 曲昭伟, 周立军, 王殿海. 城市信号交叉口自行车及行人到达与释放规律. 公路交通科技 2004(8):91–94
7. Du W, Yang J, Powis B et al (2013) Understanding on-road practices of electric bike riders: an observational study in a developed city of China. 59C(4):319–326
8. Do Thi H, Yang X (2010) Study of motor bicycle traffic and solutions to improving the Hanoi transport. Transp J 2010(9):48–52
9. 沈维超. 混合交通下平面交叉口通行效率分析. 南京林业大学, 2012
10. Lin S, He M, Tan Y et al (2008) Comparison study on operating speeds of electric bicycles and bicycles experience from field investigation in Kunming, China. Transp Res Rec 2008(2048):52–59
11. Yao L, Wu C (2012) Traffic safety for electric bike riders in China attitudes, risk perception, and aberrant riding behaviors. Transp Res Rec 2314:49–56
12. Wu C, Yao L, Zhang K (2012) The red light running behavior of electric bike riders and cyclists at urban intersections in China: an observational study. Accid Anal Prev 49:186–192
13. 马培建, 袁坤. 基于Synchro的T型交叉口信号配时优化研究. 交通标准化 2008(11):22–27
14. 孙明正, 杨晓光 (2008) 信号控制交叉口自行车流运行特征模型. 城市交通 6(2):92–96
15. Langford BC, Chen J, Cherry CR (2015) Risky riding: naturalistic methods comparing safety behavior from conventional bicycle riders and electric bike riders. Accid Anal Prev 82:220–226

# Establishing Random Forest Model Based on Visual Variables to Detect Driving Fatigue

**Chengxi Ma, Yonggang Wang, Xu Chang, Yanhui Li and Hao Zhu**

**Abstract**  Driving fatigue is a major cause of traffic accidents, and how to detect whether the driver is fatigue has become an urgent issue to be solved, therefore, propose a method of driving fatigue recognition based on visual behavior variables. In order to improve the accuracy of drowsiness detection, 64 professional drivers were recruited to participant in simulated driving experiment, and collect the data of driver's visual variables and the degree of fatigue. Then the random forest algorithm trains 200 samples of 256 samples and tests the 56 samples data remaining, and compares the predictive state and the real state of the driver. The commonly used evaluation index and ROC curves were used to evaluate the forecasting accuracy and performance of random forest algorithm. These two indicators indicate the performance of the model is excellent. At the same time, the random forest algorithm determines the importance of the four groups of indexes in the evaluation model, the blink time was of the highest importance and the pupil diameter was the lowest.

**Keywords**  Driving sleepiness · Visual variables · Random forest algorithm
Driving sleepiness assessment · Simulated driving test

## 1 Introduction

In the process of driving, when the driver engaged in driving activities for a long time, it is easy to enter the fatigue state and lead to traffic accidents in extreme situations [1]. Although the consequences of fatigue driving are serious, however, there is no widespread concern and vigilance [2]. The main reason is the lack of a reliable and accurate equipment or methods to accurately measure the driver's fatigue, and the demand for detecting driving fatigue still faces many challenges [3].

In the past few years, many scholars have researched on driving fatigue detection, research ideas are the following two categories. The first category: the detection

C. Ma (✉) · Y. Wang · X. Chang · Y. Li · H. Zhu
School of Highway, Chang'an University, Xi'an 710064, Shannxi, China
e-mail: 343041747@qq.com

of vehicle status, such as vehicle speed, vehicle lateral position, yaw rate, etc. [4]. However, these parameters may vary depending on the type of vehicle, the experience of the driver, the geometric characteristics of the road, and the state of the road. The second category: the related indicators of detecting the body, such as heart rate, ECG, EEG, physical behavior, physiological changes, etc. [5, 6]. But the data of ECG, EEG, etc. in different vehicle state differ greatly. In addition, this collection of these data has a certain degree of intrusiveness, so it is difficult to be accepted by the driver and application in the actual driving environment [7].

Based on the above considerations, this study uses four groups of highly relevant comprehensive visual variables included blink frequency, blink duration, pupil diameter, and closing duration [8, 9] to build random forest model which can identify driving fatigue quickly, in order to help improve traffic safety.

## 2 Test Methods and Data Collection

### 2.1 Test Participants

A total of 64 experimental subjects (48 males and 16 females) were enrolled in this study. The age of the participants was 20–40 years old. All the experimenters have driver's license, drive for more than 3 years and drive distance of more than 60,000 km, and they are healthy, have good eyesight without any eye diseases. All the experimenters were trained in one day. In order to ensure that all the physical condition of the experimenter is maintained at a good level, alcohol is not allowed for the first week of the experiment. In addition, the experiment obtained the consent of the Ethics Committee, and the research done in this paper has already informed the participants of the experiment in advance.

### 2.2 Test Equipment

Driving simulation experiment of this research used simulated driving equipment for experiments in Chang'an University Road Safety Research Center Laboratory (RSRC) in July 2015. The simulator consists of a real a car placed in front of 3 LCD screens (one in front of a coach driver's seat and two on both sides) with a 135 degree field of view, and can restructure the traffic flow conditions, roadway geometrics infrastructure scenario, vehicle's physical and mechanical characteristics, pavement friction, and natural environment so as to provide a realistic view of driving environment to the driver. During the testing process, the driver's eye movement index is recorded by a professional Smart Eye Pro 6.0 eye tracking system.

**Table 1**  Stanford Sleepiness Scale (SSS)

| Level of sleepiness/fatigue | Scale rating |
|---|---|
| Feeling active, vital, alert, or wide awake | 1 |
| Functioning at high levels, but not at peak; able to concentrate | 2 |
| Awake, but relaxed; responsive but not fully alert | 3 |
| Somewhat foggy, let down | 4 |
| Foggy; losing interest in remaining awake; slowed down | 5 |
| Sleepy, woozy, fighting sleep; prefer to lie down | 6 |
| No longer fighting sleep, sleep onset soon; having dream-like thoughts | 7 |

## 2.3 Data Collection

Before each experiment was conducted, the visual variables were measured as a reference value. Each experimenter drives 4 h in succession, and their visual variables were recorded at end of 2, 3, and 4 h, and asked experimenter about the subjective fatigue. The subjective fatigue standard used in this experiment is the Stanford Sleepiness Scale (SSS), and the level of fatigue is divided into seven categories, see Table 1.

The acquisition of visual variables are: blink frequency (times/min), blink duration(s), closing duration(s), and the pupil diameter (mm). In this test, the value of SSS is in the range of 1–5. In order to facilitate the estimation of the fatigue level, the driver's status can be divided into two categories according to the meaning of each grade. "1–3" represents the awake state, "4–5" represents fatigue state.

According to the result of test, 256 samples data were obtained. This model randomly selects 200 samples of the total samples as the training data set (S) to train the model, and the remaining 56 samples are used for the model test to evaluate the correct rate and accuracy.

## 3 Random Forest Model

### 3.1 Random Forest Algorithm

Random forest is a combination of learning methods, through the subset of data and a subset of variables to create a tree decision tree, the combination of prediction result of multiple decision trees is more precise. The most obvious advantage of this is to overcome the overfitting that the decision tree is likely to produce.

**Fig. 1** Decision tree

## 3.2 Establish Random Forest

Step1: Through the bootstrap resampling technique, a new set of training samples is generated by randomly extracting $N$ samples from the 200 training sample set $S$ collected in the experiment, and the extraction process is repeated to generate $K$ subsample sets. In this paper, 1000 subsample sets are generated.

Step 2: For each subsample set in the previous stage, $v$ variables are randomly selected from the four visual behavior variables $V$ randomly, $v < V$.

Step 3: Constructing a decision tree according to the subsample set selected in the first step and its corresponding sub-feature vector. In this paper, we construct 1000 decision trees. Each of these trees is a decision tree of two categories, starting from its root node according to the principle of the minimum purity of the node, and then the left and right nodes each contain a subset, and then follow the process to continue to split until it meets the branch stop rule. The non-purity of the nodes is measured using the Gini index, and the larger the Gini index, the lower the purity. The set $K_i$ includes the sample records of n classes, the probability of each class is $p_1, p_2 \dots p_n$, then the Gini index is:

$$\text{Gini} = 1 - \sum_{i=1}^{s} p_i^2 \tag{1}$$

Random selection of part of the decision tree as shown in Fig. 1:

Step 4: The 1000 decision trees generated in the third step will form a random forest, and use it to identify the sample of the test set. That is, each decision tree will identify and classify the test samples, and synthesize the classification results of all decision

**Fig. 2** Model test results
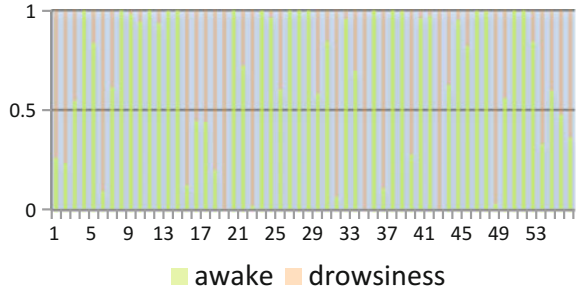


trees. At length, a high probability of voting determines the output of the model. Category "0" voting probability $vp_0$ and category "1" voting probability vp1 are as follows:

$$vp_0 = \frac{v_0}{v_0 + v_1} \quad vp_1 = \frac{v_1}{v_0 + v_1} \tag{2}$$

$v_0$, $v_1$ is the number of votes for "0" and "1". The following is a list of model voting results (voting results in probability form), as shown in Fig. 2.

### 3.3 Evaluation of Training Results

Confusion matrix is a common method for evaluating classification performance. It shows the relationship between the results of model recognition and its real attributes. The 56 samples data are tested, and the results are identified and the true attribute of the samples is used to create confusion matrix, as shown in Fig. 3. In order to evaluate the performance and accuracy of the random forest model to the fatigue state reasonably, the confusion matrix is evaluated from the following two aspects.

1. Commonly used indicators

The accuracy of model identification is usually evaluated using the accuracy rate, recall, and precision.

Accuracy Rate:

$$\text{Accuracy Rate} = \frac{TP + TN}{TP + TN + FP + FN} \tag{3}$$

Recall:

$$\text{Recall} = \frac{TP}{TP + FN} \tag{4}$$

**Fig. 3** Confusion matrix of
test result
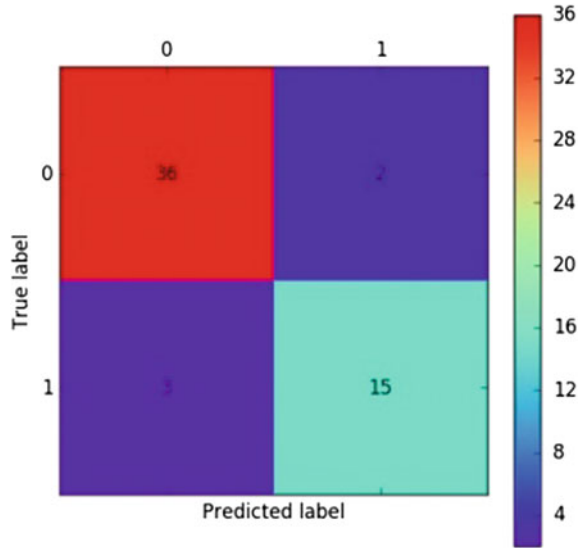


Precision:

$$\text{Precision} = \frac{\text{TP}}{\text{TP} + \text{FP}} \tag{5}$$

The meaning of each parameter is as follows:

TP—True Positive: The positive samples were identified as positive samples;
TN—True Negative: The negative samples were identified as negative samples;
FP—False Positive: The negative samples were identified as positive samples;
FN—False Negative: The positive samples are incorrectly predicted as negative samples.

Because of the great harm caused by fatigue driving in reality, it is more concerned about whether the driver is fatigue, select the state "1" as a positive example.

According to the calculation, the recognition accuracy rate of the model is 0.91, the recall is 0.83, which indicates that the probability of 83% of the real fatigue is predicted to be the fatigue state by the model. The precision is 0.88, which means in the model predicts the fatigue state, 88% of the probability is real fatigue. Through the above calculation, we can see that the accuracy rate is as high as 0.91, the recall and the precision are more than 0. 83, indicating that the accuracy of the model is very high.

2. ROC curve

ROC curve is a very effective model evaluation method as an evaluation index which reflects the sensitivity and specificity. According to the experimental results, draw

**Fig. 4** ROC of random forest
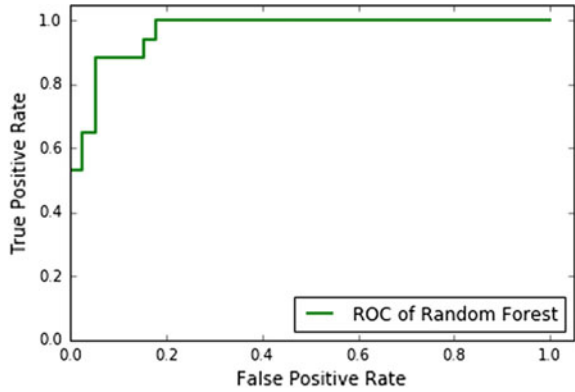


the ROC curve shown in Fig. 4. The ordinate of the ROC curve is defined as the TRR (True Positive Ratio); the abscissa of the ROC curve is defined as the FPR (False Positive Ratio). And TPR and FPR are calculated as follows:

$$\text{TRP} = \frac{\text{TP}}{\text{TP} + \text{FN}} \quad \text{FPR} = \frac{\text{FP}}{\text{TN} + \text{FP}} \tag{6}$$

Intuitively, the TPR represents the probability that the model will correctly predict the positive samples, and the FPR represents the probability that the model will classify negative samples as positive samples. If the ROC curve is biased to the upper left, the larger the area under the curve, the better the performance of the model. AUC (Area Under roc Curve) is a quantitative indicator of the ROC curve, which represents the area enclosed by the ROC curve and the $X$-axis. The performance of the model is measured according to the size of the AUC value. The AUC value is 0.965 in this experiment. Since this value is close to 1, it indicates that the random forest model has excellent performance in predicting the driving fatigue state.

Because in different scenarios, the selection of evaluation indicators is different, the final results are also very different, so we choose two kinds of indicators to evaluate the accuracy of the model. However, the model shows excellent performance under two different evaluation indexes.

## 3.4 Variable Importance

The importance of variables can help to understand which variables affect the driver's mental state, and the importance and ranking of the four visual behavior variables in this study are shown in Fig. 5. The importance of the predictor variables given by the random forest indicates that the blink time has the greatest effect on the model predictions, followed by the closed-eye time, the blinking frequency, and the least affected factor is the pupil diameter.

**Fig. 5** Feature importance
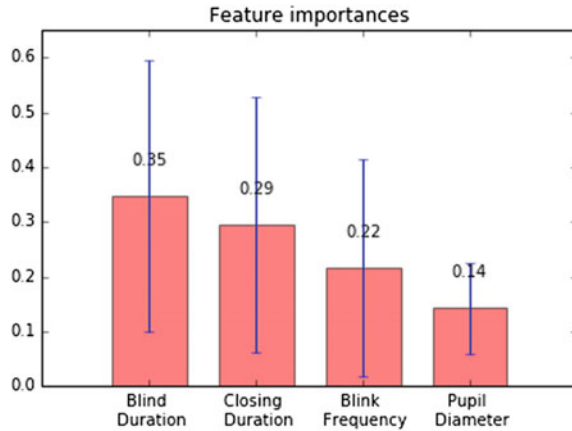


# 4   Conclusion

Aiming at the difficulty of data acquisition and poor recognition effect accuracy in driving fatigue recognition, this paper proposes a method to identify the driving fatigue based on the visual variables to establish the random forest model to detect driving fatigue. A total of 256 samples were collected from simulated driving test, including four groups of visual behavior variables such as blink duration, blink frequency, closing duration, pupil diameter, and corresponding subjective fatigue SSS values. Then, a random forest model was established, and the random forest model was used to identify and judge the results. The results were compared with the experimental records. At length, the confusion matrix and the ROC curve were used to evaluate the results. Concluded as follows:

1. The importance of four groups of visual behavior variables was determined based on random forests. The importance of blink duration is the highest and the pupil diameter is the lowest.
2. The accuracy of the model is as high as 0.91, and the recall rate and accuracy are over 0.8. The ROC curve is excellent and the AUC value is as high as 0.965. These two types of indicators are sufficient to show that the reliability of random forest model for driving fatigue classification prediction is high.

However, there are still some shortcomings in this paper, the test sample is only 256, and the sample size is relatively small, to increase the sample size, further testing is necessary.

**Ethics approval and consent to participate**

This study was approved by the Human and Health Science Ethics Committee at Chang'an University (Reference number: 2014–03–005). Each participant was informed about the purpose of the study, and consented by filling in and returning the questionnaire. All data were recorded and analyzed anonymously.

# References

1. Thiffault P, Bergeron J (2003) Monotony of road environment and driver fatigue: a simulator study. Accid Anal Prev 35(3):381
2. Radun I, Ohisalo J, Radun J et al (2013) Driver fatigue and the law from the perspective of police officers and prosecutors. Transp Res Part F Traffic Psychol Behav 18(5):159–167
3. Yang G, Lin Y, Bhattacharya P (2010) A driver fatigue recognition model based on information fusion and dynamic Bayesian network. Informationces 180(10):1942–1954
4. Mattsson K (2007) In-vehicle prediction of truck driver sleepiness: lane position variables. Luleå Tekniska Universitet
5. Zhao C, Zhao M, Liu J et al (2012) Electroencephalogram and electrocardiograph assessment of mental fatigue in a driving simulator. Accid Anal Prev 45(1):83–90
6. Patel M, Lal SKL, Kavanagh D et al (2011) Applying neural network analysis on heart rate variability data to assess driver fatigue. Expert Syst Appl 38(6):7235–7242
7. Xu C, Wang X, Cheng X et al (2015) Driver drowsiness level analysis and prediction based on decision tree. J Tongji Univ (Nat Sci) 43(1):75–81
8. Horng WB, Chen CY, Chang Y et al (2004) Driver fatigue detection based on eye tracking and dynamk, template matching. In: Danesy D (ed) Proceedings of the Second Workshop on the Atmospheric Chemistry Validation of Envisat, vol 1, pp 7–12
9. Pang X, Li J, Xu X (2011) Threshold value of indices of eye states to monitor drive fatigue. J Tongji Univ (Nat Sci) 39(12):1811–1815

# The Design of Quality Assessment Mode for Public Transit Service—From Rough to Accurate

**Chang Xu, Kun-jie Chen and Xian-tong Jiang**

**Abstract** In order to improve the service level of Qingdao city bus, enhance the management of the transit industry management department, and improve the efficiency of the financial subsidies, this paper concludes the basic principles of service quality assessment, designs the systematic, integral and scientific evaluation index system, and selects the specific indexes of service quality assessment and distributes the weight of the indicators, combining the experience from various assessments of domestic and international public transit system service levels and based on the analysis of service level of the public transit system in Qingdao. Also, the paper combines the evaluation results with the enterprises' financial subsidies and managerial authority, which largely effectively improves the enthusiasm and initiative of public transit enterprises and establishes a solid foundation for the comprehensive upgrade of the service level of Qingdao transit system.

**Keywords** Service quality · Evaluation index system · Results application

## 1 Introduction

In recent years, with the rapid development of urban public transit, urban public transit financial subsidies related to the system were gradually improved. Also, a series of regulations for government procurement of public transit services were released. Among them, the Ministry of Finance, the Ministry of Civil Affairs, and the State Administration for Industry and Commerce jointly issued the "Government Purchases Public Service Management Approach (temporary)" in 2014, which first considered the public transit service as a basic public service and took it into the guide of the government purchase of service; the Ministry of Transport issued the "Urban

C. Xu (✉) · K. Chen · X. Jiang
China Academy of Transportation Science, Beijing 100029, China
e-mail: 51234679@qq.com

Public Transit Development Plan during the 13th Five Year" in 2016 proposed the major task of the government purchase of urban public transit service mechanism and established a government purchase of service system. In 2017, "Regulations for Urban Transit and Tramcar" clearly announced the establishment of operating cost accounting system and compensation subsidies system, and that enterprises shall organize operations in accordance with the route franchise agreement.

Government procurement of public transit service system includes urban public transit financial subsidies, cost regulation, service level assessment methods, the annual plans of operation service, bus fares, dynamic adjustment mechanism, etc. Under this general policy, public transit service level assessment is a closed loop of improving the service level and the efficiency of financial subsidies.

## 2   Overview

At present, there are many urban problems both in China and other countries, such as the imperfection of the assessment system, the lack of examination contents, and the weak effect of the evaluation results. These problems result in the formalism of the transit service quality assessment, lack of monitoring and management from the transportation management department, less effective of the financial subsidies, citizens' unsatisfactory with the service level, etc.

The core of the quality assessment of public transit service is to accurately grasp the three major contents, which are "who will test, how to test and how to use". In other words, first, accurately grasp the assessment of the specific indicators and the weight of indicators. Second, design detailed assessment methods and operation procedures. Last, develop a detailed application methods for assessment results.

Through learning from Singapore, London, Shenzhen, Wuhan, Huzhou, and other cities, this paper compares the assessment organization, assessment methods, assessment indicators selection, assessment results and other aspects, then, standardizes the transit service quality assessment model.

## 3   Analysis and Comparison of Transit Service Level Assessment Cases

### 3.1   Comparison of Assessment Agencies and Methods

In terms of the assessment agencies and methods of the urban public transit service level, this paper mainly focuses on Singapore, Shenzhen, and other cities as cases. The cases are summarized in Table 1.

The comparison table indicates that the assessment organization mainly includes setting up assessment committee by industry management departments, and third-

**Table 1**  Comparison of transit service level assessment agencies and methods

| Cities | Assessment agencies | Assessment methods |
|---|---|---|
| Singapore | Establishment of public transit committee | Periodic review |
| London | The third-party TNS RI | MTS (Bus Mystery Traveler Survey) |
| Shenzhen | Quality assurance management team | Operational + service level indicators |
| Wuhan | City public transit office + intermediary agency | Daily assessment + annual assessment |
| Huzhou | City public transit management team | Daily assessment + annual assessment |

party intermediary agencies; assessment methods include periodic review, daily + annual assessment, random assessment and so on, focusing on the full-time effect of quality assessment.

## 3.2   The Selection of Assessment Indicators

Singapore, Wuhan, and Huzhou are taken into consideration in this section for comparative analysis. Singapore, Wuhan, and Huzhou, respectively, on behalf of the three types of assessment, namely, flexible assessment, moderate assessment, constraint assessment.

Public transit service quality assessment indicators reflect the service level of public transit, playing an important role in guiding the city to enhance the service level. The contents of the assessment indicators should reflect the service quantity and quality in terms of the enterprise operations, safety management, passenger satisfaction, and other aspects. Singapore mainly develops 11 mandatory assessment indicators based on 6 key factors: reliability, passenger capacity, safety, accessibility, integration, and informatization. "Wuhan City Public Transit Service Quality Assessment Method (Trial)" was issued in 2013, clearly indicating that the assessment approach shall combine the daily assessment and the annual assessment of transit enterprises. Huzhou City in 2013 issued "Huzhou Government Purchase of Public Transit Service Assessment Approach", indicating that the comprehensive assessment should be taken to evaluate the service quantity and quality of the urban public transit enterprises. The assessment consists of seasonal assessment and annual comprehensive assessment.

Assessment indicators for different cities are shown in Table 2.

The comparative analysis of three cities indicate:

Through the comparison of the typical cities, the arranged responsibilities of the government and public transit enterprises are the prerequisites for the selection of

**Table 2** Assessment indicators for the public transit service level

| Cities | Indicators |
|---|---|
| Singapore | Reliability: planned completion rate, bus departure punctuality, vehicle failure rate;<br>Capacity: peak passenger load (congestion); Safety: accident rate;<br>Accessibility: the scope of accessibility services (site coverage), track and bus stop convergence rate, bus operation time, bus service plan start interval; Integration: integrated bus and metro services; Information: Latest Information Availability |
| Wuhan | The contents of the daily operation assessment include: vehicle environmental standards, in-vehicle facilities intact rate, service identification complete rate, vehicle cleanliness rate, operation and management (first and last bus time, the number of buses), service pass rate and so on<br>Public transit enterprise management annual assessment contents: basic management, compliance with the law, target completion (trips execution rate, annual operating mileage), safe production (death/millions of kilometers); social reflection, complaints and media exposure |
| Huzhou | Assessment indicators mainly include the implementation of the annual plan, quality of service and the major financial indicators. The implementation of the annual plan includes: routes, vehicles, mileage, information and other indicators; Service level assessment includes: operating routes, vehicles, service standards, safe driving, complaints handling and other indicators |

assessment indicators. When the enterprises are constrained less by the government, the assessment cost increases and enterprises have more flexibility. On the other hand, the enterprises' flexibility and enthusiasm will reduce.

## 3.3 Results Application

This paper compares cases of Paris, Singapore, Shenzhen, and other cities with reference to the results of public transit service quality assessment. The focus is on the links between transit service quality assessment results and the financial subsidies and transit managerial authority.

The urban public transit service quality assessment applications are summarized as follows:

I. Case Analysis of Links of Public Transit Financial Subsidies

The investigation and analysis indicate that generally, there are three ways to link the assessment results to the public transit financial subsidies: First, the government will give different degrees of incentives for the completion of the tasks, bonuses, profits, etc., such as London, Singapore, Copenhagen, etc. Second, either bonus or punishment will be issued based on the quality of the completed tasks, such as Paris, Shenzhen, etc. Third, establishing special funds to subsidize frontline employees, such as Nantong.

**Table 3** The links between transit service level assessment and financial subsidies

| Cities | Methods |
|---|---|
| London | On the basis of the completion of the operating mileage, enterprises providing high-quality service can get dividends up to 15% of the contract price bonus |
| Paris | According to the service completion rate, either bonuses or penalties will be issued up to 700 million euros |
| Singapore | The bus company is self-financing, but the contract regulates that the enterprise can get up to 15% of the profits in accordance with the requirements of the operation tasks, while the government will determine the service level through public feedback and punish those enterprises who did not meet the requirement |
| Copenhagen | The service level links the bonuses, that is, if the actual operating time over the planned operating time is 100, the proportion of bonus is 100%; 99.86 corresponds to 60%; 99.81–99.85 corresponding 30%; 99.76–99.80 corresponding 10%; 99.75 and below corresponding no bonus |
| Shenzhen | 30% of the cost regulatory profits (regulatory costs * 6%) links to the bus service quality. If the service level meets the requirement, the enterprise can get full profit, otherwise, the profit will be deducted accordingly |
| Huzhou | The assessment results are the main basis for reviewing reasonable return on investment (5% of the gross profit margin of the main business income). Among them, the return on investment = the annual comprehensive assessment/100 * the return on investment; no return on investment will be given if the assessment results do not meet the requirement. In 2014, 2 companies have a return on investment of 4.58 million yuan |

The summary of how to link service level assessment and financial subsidies is as follows (Table 3):

II. Case Analysis of Links of Transit Managerial Authority

The investigation and analysis indicate that generally, there are three ways to link the assessment results to the managerial authority: First, extend the authority of those enterprises providing high-quality service, such as London, Copenhagen, Wuhan, etc. Second, either shorten or extend the authority according to the quality of public transit service, such as Chengdu, etc. Third, consider the quality assessment result as an important basis for judging the franchise, such as Xiangtan and so on. The summary of the methods of linking between transit service level assessment and managerial authority is shown in Table 4.

**Table 4** The links between transit service level assessment and managerial authority

| Cities | Methods |
|--------|---------|
| London | Consider the service quality incentive as the core of the contract, the contract period is five years, the quality of service can continue to upgrade for two years |
| Copenhagen | On the basis of the 4-year validity period of the basic contract, the service quality incentive policy will give the operator an additional 8 years of renewed business rewards |
| Wuhan | According to the results of public transport service quality assessment, determine the bus route authorized operating years |
| Chengdu | If listed No. 1 for 2 consecutive years in the service level assessment, the operation authority can increase by 1 year; if listed the worst for 2 consecutive years in the service level assessment, the operation authority will decrease by 1 year |
| Xiangtan | The result of the assessment is a major basis for judging the operation authority, including the bidding and bonus points, suspension of operation authority if fail in assessment in 2 consecutive years |

# 4 The Design of Quality Assessment Mode for Public Transit Service

Through summarizing and analyzing the public transit operation experience in typical cities, this paper is based on the relevant experience and moderately innovate, and establishes a new urban public transit service quality assessment model, which includes design principles, technical process, assessment agencies selection, assessment index system, the application of assessment results, etc.

## 4.1 Design Principles

The following principles are taken into account during the design of the assessment methods:

I. Adhere to the combination of quality and quantity. Operational service quality assessment is generally divided into the quantity indicators and quality indicators.

II. Adhere to the people-oriented principle.

III. Enhance the fine management and further strengthen the intelligent construction, improve operational efficiency.

IV. Adhere to fair, just and open.

## 4.2 Technical Process

The research idea of public transit service quality assessment model is based on the "Government Purchase Service Management Approach", referring to domestic and foreign public transit service quality assessment experience, clarify the assessment organization and assessment methods, establish operational service quality evaluation index system, clarify operational service quality assessment results and other applications.

## 4.3 Assessment Agencies Selection and Assessment Methods

In terms of service quality assessment methods, this paper considers the subjective satisfaction of passengers, urban public transport information development level, etc. The assessment consists of daily assessment, annual assessment, and passenger satisfaction.

After determining the assessment methods, according to the assessment contents and organization functions in different types of service level assessment, appropriate assessment organization is selected. Among them, the key component is the annual comprehensive assessment and result-oriented indicators, which is the comprehensive assessment of public transit service level, involving a number of industry management departments, which needs financial, price, audit, and other departments to cooperate on the assessment. Daily assessment mainly evaluates daily operation service, peak hour situations, and other daily conditions, which is random and flexible in date. It is recommended that the internal organization of the transportation department conducts a number of inspections. The third-party agency assessment takes into account the objectivity and accuracy of the passenger satisfaction, and it is recommended that the Municipal Transportation Commission and the Municipal Finance Bureau jointly commissioned by the investigation of third-party institutions to conduct an objective and impartial investigation and issue the survey results.

## 4.4 Assessment Index System

I.  Establish the Assessment Index System

In this paper, AHP method is used to establish the hierarchical tree structure, and the target hierarchy classification is used as the tool to construct the service level assessment index system of the bus trolley. The index system consists of three layers: target layer, criterion layer, and index layer. Among them, the target layer is through the establishment of public transport trolley service quality assessment index system to achieve the objective target, conduct a comprehensive evaluation on the public transit service level, and set specific evaluation criteria. Criterion layer consists of

**Table 5** Public transit service quality assessment index system

| Classification | | Index |
|---|---|---|
| Quality index | Daily assessment | Completion rate of service facilities |
| | | The vehicle cleanliness rate |
| | | Operating service pass rate |
| | Annual assessment | Public transit accident death rate with responsibilities |
| | | Public transit accident rate |
| | | Vehicle accident rate |
| | | Complaint completion rate |
| | | Number of complaints over operating mileage |
| | | Route first and last time compliance rate |
| | | Real-time forecast rate |
| | | Enterprise basic management |
| | | Intelligent terminal usage rate |
| | | Actual configuration rate of bus driver |
| | | Actual bus driver salary rate |
| | Third-party assessment | Passenger satisfaction rate |
| Quantity index | Daily assessment | Daily checkout rate during peak hours |
| | | Daily punctual departure rate during peak hours |
| | Annual assessment | Planed load mileage completion rate |
| | | Annual checkout rate during peak hours |
| | | Annual punctual departure rate during peak hours |

service quantity and quality levels, which reflects the service quality of a certain level of urban bus trams. The index layer is composed of several evaluation indexes, which is the smallest unit of the index structure of public transit service level, which reflects the service level of a certain part of the criterion layer, describing from the definition of indicators, indicators of calculation formula, and indicators of basic data collection requirements.

This paper collects a number of indicators related to the quality and quantity of service, classifies, and forms the summary table of assessment indicators. Then, the indexes are reclassified and the similar indexes in the same index are compared and analyzed. Based on accessibility, operability and other principles, the necessary indicators in each category are determined. Finally, the formation of public transit service quality assessment index system is finished (Table 5).

II.  Weight Distribution of Assessment Indicators

The weight distribution of service quality assessment indicators is divided into two levels, that is the "quantity" indicators and "quality" indicators of the overall weight distribution. Based on the principle that first to ensure the basic public services,

**Table 6** Service level assessment results application

| No. | Linking methods | Rules |
|---|---|---|
| 1 | Link to transit financial subsidies | "Quantitative" indicators and "quality" indicators of the assessment results were linked with the annual financial subsidies of public transit enterprises. Set the assessment performance for public transit enterprises, and the performance limit should be partial financial subsidies |
| 2 | Link to transit managerial authority | If the route managerial authority expires and the average score of overall service level assessment is over 90, one-time extension will be given as an incentive<br>The comprehensive operation quality assessment over years will be considered as an important reference, when selecting operators for new routes |

and then gradually improve the level of service, the "quantity" indicator is highly emphasized. Therefore, the weights of the "quantity" and "quality" indicators are set to 60 and 40%, respectively.

After a preliminary screening, the "quantity" indicators mainly include operating mileage, morning and evening peak hours checkout rate and punctuality. Considering the accessibility, operability, and importance of factors, the weight is increased if containing both the daily assessment and the annual assessment.

After a preliminary screening, the "quality" indicators mainly include the daily assessment indicators and the annual assessment indicators and passenger satisfaction indicators. Based on the passenger satisfaction comprehensive indicator, the passengers' impression on the overall operation service quality is reflected. Therefore, the weight for this part is increased accordingly. Both daily assessment indicators and annual indicators are distributed based on the number of specific indicators, type, and importance of factors to ensure the rationality.

## *4.5  Results Application*

In terms of the application of public transit service quality assessment results, this paper refers to experience from both domestic and foreign cities, and link the assessment results to the government financial subsidies and route managerial authority.

Among them, a reasonable combination of reward and punishment method is related to the public transit financial subsidies rather than simple punishment or reward. The reward is mainly aimed at the promotion of the service level. For the basic public transit service, punishment will be given to those enterprises failing to meet the requirement, which encourages enterprises to improve their service. In terms of transit route managerial authority, different methods should be applied considering either the routes are previously existed or newly designed. The methods are summarized in Table 6.

## 5   Conclusions

Through the design of systematic public transit service level assessment model, this paper constructs a service level assessment index system. Both the "quantity" indicators and "quality" indicators of the public transit enterprises can be evaluated subjectively, which enhances the management of transportation department. In addition, the financial department can supervise these enterprises in a better way by punishment and reward methods, which largely encourages enterprise to improve their service and increase the efficiency of the financial subsidies usage. Also, through linking the assessment results to both financial subsidies and route managerial authority, a benign operational service quality incentive mechanism is established, which helps the transformation of public transit operation management from rough to accurate.

## References

1. Country Issue (2012) Guidance on giving priority to develop urban public transit issued by the state council (No. 64)
2. Cai Z (2014) Government purchase of services management approach (Temporary) (No. 96)
3. Cai J (2016) Guidance on the promotion of government purchase of services in the field of transportation (No. 34)
4. Ministry of Transport (2017) Management provisions on urban bus and tramways (No. 5)
5. Urban public transit enterprises service level assessment system. GB/T XXX
6. Code for urban public transit operation. GB/T 22484
7. Peng X, Hu Z (2007) An empirical study of quality of urban bus service. J Southw Jiaotong Univ (Social Science edn.)

# Methodology Research on the Integration of Urban Comprehensive Passenger Hub and Nonmotorized Transport

**Jiang-ping Wang and Chang Xu**

**Abstract** With the rapid development of national economy, the passenger car population is increasing continuously and the pressure of urban transport is higher; as one important component of urban transport, urban comprehensive passenger transport hub plays a decisive function in the whole transport system; and in order to guarantee the effective operation of comprehensive passenger transport hub, the research of transport organization is necessary. This article concentrates on the improvement of traffic dispersion function of urban comprehensive passenger transport hub, emphasizes on the deep analysis of integration of nonmotorized transport inside and outside the urban comprehensive passenger transport hub and the study of integration of nonmotorized transport and comprehensive passenger hub, in order to enhance the quick gathering-distribution and transfer functions of urban comprehensive passenger transport hub.

**Keywords** Urban comprehensive passenger transport hub · Nonmotorized transport · The setting method of integration

**Introduction**

## 1 Overview

Urban comprehensive passenger hub is an important part of urban transport, play a decisive role in the entire transportation system, to ensure the efficient operation of the integrated passenger hub and conduct traffic organization research is very necessary. Function level of the comprehensive transportation hub is determined by the traffic organization, with the gradual improvement of the integrated transport system, how to conduct effective comprehensive transportation traffic organization optimized design, thereby shortening the passengers' walking distance to reduce the

J. Wang (✉) · C. Xu
China Academy of Transportation Science, Beijing 100029, China
e-mail: 512346679@qq.com

cross and interfere between the pedestrian flow with traffic flow, to ensure the safe and unimpeded flow of pedestrian flow and traffic flow, and become major study issues of comprehensive transportation.

Nonmotorized transport is an important part of urban transport system, reasonable layout the traffic organization of slow comprehensive transportation and nonmotorized transport system, achieve effective convergence for the internal and external hub, improve the transfer convenience, reduce regional traffic pressure, is the basic premise to play fast distribution and multimode transfer function of the comprehensive passenger hub.

The comprehensive transportation and the nonmotorized transport integration, mainly to guarantee enough space for nonmotorized transport in the internal hub, and rational organize pedestrian flow of the nonmotorized system, protect pedestrians transfer convenience and smooth; complete and perfect pedestrian traffic facilities and reasonable bicycle parking at the external hub to guarantee nonmotorized transport's connection. Therefore, this article analyzes the internal and external nonmotorized transport integration setting in the comprehensive transportation.

## 2 Provide Sufficient Space for Nonmotorized Transport Within the City's Comprehensive Passenger Transport Hub

Urban Comprehensive Passenger Terminal interior space setting need to consider the needs of pedestrian flow and transport organizations sciencely, guarantee to provide sufficient space for nonmotorized transport, in order to provide the user with a good sensation and avoid crowded with people. Therefore, the scale of nonmotorized transport facilities in the hub should be planned by the amount of the passengers during the passenger peaking, and the long-term growth in passenger for the comprehensive traffic hub is considered, then the passenger flow reasonably is forecast, and sufficient space for nonmotorized transport facilities is reserved for long-term expansion (Fig. 1).

## 3 Focus on the Organization of Nonmotorized Transport in the Internal Hub

Consider the features of large crowds gather of short period of time in the integrated transport hub, need reasonable and effective organization and guidance for pedestrian flow line to avoid transfer inconvenience passengers stranded, crowded and dangerous. Therefore, there is a need to do effective pedestrian traffic organization, facilities, and operations management program design and nonmotorized transport infrastructure construction, in order to use the nonmotorized facilities rationally in

**Fig. 1** Hong Kong and Beijing subway nonmotorized transport space
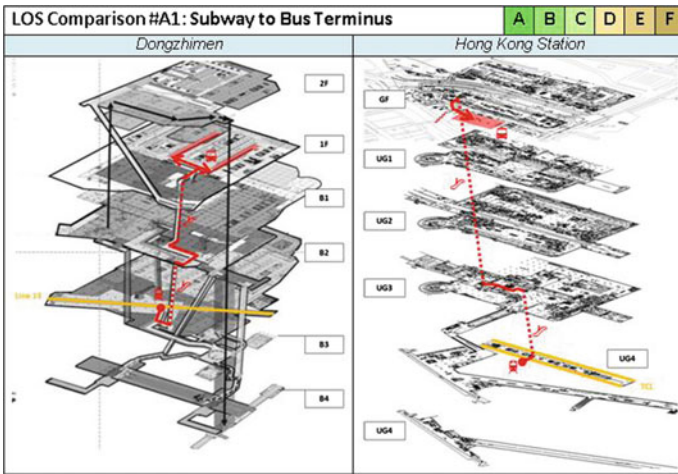


**Fig. 2** Beijing and Hong Kong subway transfer walking track

the limited three-dimensional space of the hub, and do intensive pedestrian organizational guidance and management, protect the large number of passengers safe, fast, comfortable collection, evacuation and transfer.

According to various modes of walking track for transport interchanges within the hub, design the pedestrian flow tissue rationally within the hub, provide convenient nonmotorized transfer channel, and reduce pedestrian detour during transfer (Fig. 2).

Taking full account of the physical and psychological in pedestrian flow line organization, make shortest transfers distance for pedestrians, and by setting up and down escalators and elevators, provide safe and comfortable transfer environment for pedestrians (Fig. 3).

Strengthen information guide settings, by setting clear and precise colorful indication flag and obviously reasonable nonmotorized transport guide signs and markings, laying a continuous guide brick, installing touch-plane Wizard Figure, voice guidance media, continuous handrails, footpaths lights, etc., make pedestrians have a proprietary peer space and paths, and avoid intersecting with other traffic flow,

**Fig. 3** Nonmotorized transport facilities of Beijing and Hong Kong



**Fig. 4** Colorful indication flag and footpaths lights of Tokyo

in order to provide the passengers with safe and convenient transfer environment (Fig. 4).

The traffic language setting should follow the principle of continuity in the transportation hub inside, that is, each spaced a distance there is a corresponding identification indicating the direction of travel, and it is best to mark the distance to the transfer lines (Fig. 5).

## 4   Nonmotorized Transport Should Have Good Accessibility in External Hub

Layout should be reasonable supporting slow traffic facilities, organization of traffic flow lines outside the comprehensive passenger hub, to ensure the safety of pedestrians and smoothly vehicle driving, based on the size of passenger demand in hub

**Fig. 5** Nonmotorized
transport continuous
identification in the
transportation hub





(a) Ground through pattern

(b) Air transit pattern

(c) Underground extension pattern
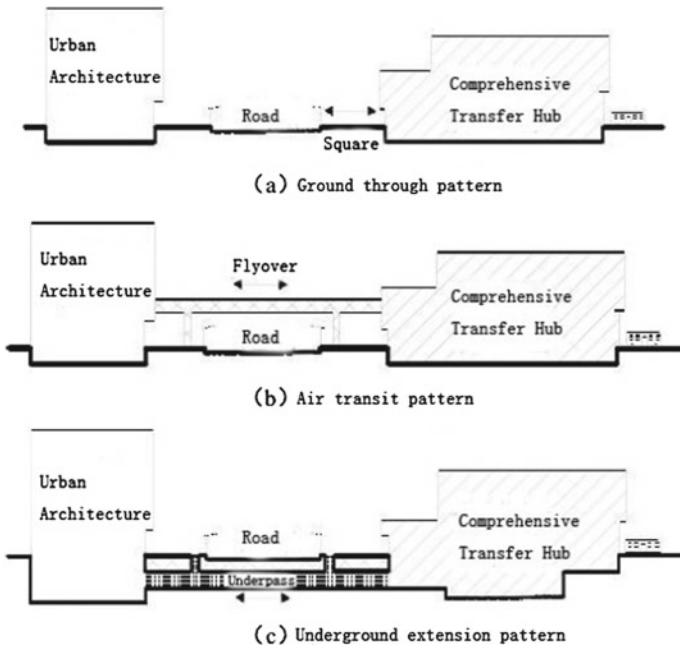
**Fig. 6** Nonmotorized transport convergence form in external hub

station, using diverse nonmotorized transport forms to access comprehensive transportation, and ensure good transport accessibility in external Hub (Fig. 6).

By raise and lower wear the motor vehicle lanes in the external hub, separate the vehicle path and slow path, protect the pedestrians' priorities on areas of conflict with motor vehicles, such as the road and intersections, then, provide adequate transport facilities to protect pedestrians' priority access rights (Fig. 7).

**Fig. 7** Motor vehicle under wear lanes and intersection walkways upgrade

## 5 Bicycle Parking Layout Should Consider the Situation of the Hub Outside the Comprehensive Transportation

The convergence settings of bicycle outside of comprehensive passenger hub should consider comprehensive transportation land use and lay out the bicycle parking reasonably. The travel area of bicycle and vehicle should be separately provided, to ensure each driving safety, reduce the cross-talk between the flow lines, and to provide a good environment for the development of the bicycle trip transportation.

The bike course arrangement in the city comprehensive passenger hub should note the following:

First, according to bicycle parking requirements, hub layout, and the convergence way with the urban roads, consider the location layout of the bicycle parking; Second, the convergence between bicycle parking and city comprehensive transportation should have a clear scope and boundaries, to try fewer bicycle detour; Third, play the small footprint characteristic of the bicycle parking, adapted to local conditions; Fourth, the set location of bicycle parking needs to be eye-catching, and is equipped with a good bicycle parking guidance identification system.

The location of bicycle parking should consider the overall layout of the external hub, converge with the nonmotorized transport network, and make the bicycle transfer more convenient outside the hub (Fig. 8).

## 6 Conclusion

Urban comprehensive passenger hub is an important node in the city's comprehensive transportation system, and integration with the nonmotorized transport can effectively improve the efficiency of public travel and relieve the traffic pressure. This article is based on the organization of urban comprehensive passenger transportation hub, exploreing the setting principles, content, and requirements of nonmotorized
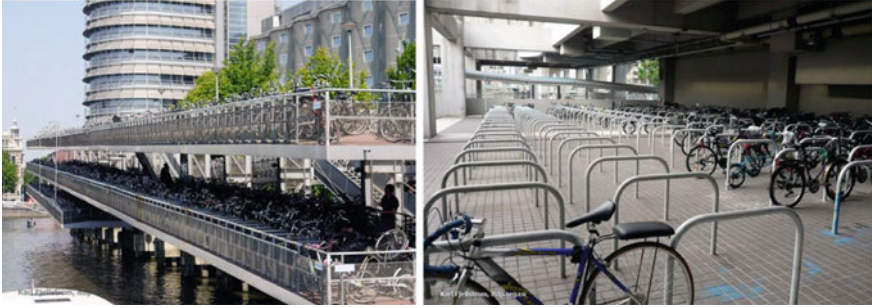
**Fig. 8** Bicycle parking spots setting outside the hub

transport system inside and outside the hub, to provide a reference for the integration settings between urban comprehensive passenger hub and nonmotorized transport system.

# References

1. Zeng H (2006) Zhu strive comprehensive transportation system and planning. Southwest Jiaotong University Press, Chengdu
2. Section Liren, fine wool force by the design and management philosophy of urban transport hub. Integr Transp 2013:76–82
3. Interest integrated passenger terminal transfer organization research. Master thesis, Southwest Jiaotong University (2008)
4. Hu P (2008) Connections of slow traffic integration studies. Master thesis, Huazhong University of Science

# Analysis and Evaluation for B-Double Vehicles Handling Stability

**Hong-guo Xu, Guo-jun Wang, Hong-fei Liu and Yi-hua Zhang**

**Abstract** An analytical method was introduced and used to solve the dynamics equation set which could simplify computational process, and four degrees of freedom (DOF) linear models were developed for B-double vehicles. Under the condition of tractor's steering wheel angle as the step input, motion state variables, steady-state yaw rate gain, and understeer gradient for each vehicle unit were solved with MATLAB. It was analyzed that the correspondence between understeer gradient and steady-state relative yaw angle gain whose impacts on handling stability for vehicle unit were evaluated. With the variation of mass and rear axle tire cornering stiffness, location of mass center and wheelbase, location of articulated point for each vehicle unit, and the effects on the understeer gradient were analyzed. Handling stability was evaluated by the variation of vehicle's operating condition and structural parameters. The results indicate that increasing mass and rear axle tire cornering stiffness properly, moving forward mass center and increasing wheelbase properly, moving backward articulated points, and decreasing mass properly could increase the understeer gradient which lead to the improvement of handling stability. It could provide theoretical basis for B-double vehicles stability tests.

**Keywords** Vehicle dynamics · B-double vehicles · Handling stability
Steady-state yaw rate gain · Understeer gradient · Structural parameters

## 1 Introduction

B-double vehicles possess a more semitrailer than tractor-trailer combinations which could improve about 50% more cargo capacity, cut down a total of fuel consumption for 40% cost-saving, and reduce the pollutant discharge [1]. Now the vehicle combinations were widespread in Europe and America, and *Limits of dimensions, axle load and masses for motor vehicles, trailers and combination vehicles* (GB1589-2016)

H. Xu · G. Wang · H. Liu (✉) · Y. Zhang
School of Transportation, Jilin University, Changchun 130022, China
e-mail: hongfeiliu@jlu.edu.cn

381

was implemented in China in 2016, which added center axle trailer as new type of vehicle [2].

Francer P S gave simulation of directional response to steady-turning maneuver of commercial vehicle for tractor and semitrailer [3]. He also reviewed the effects of steering gains, understeer gradients, effective wheelbases, handling diagrams and critical speeds on heavy trucks with multiple axles and articulated points [4]. Xie L investigated the dynamic behavior of the system about vehicle's combination and motion equations based on Newton's Second Law for computer simulation [5]. Chen W W et al. argued that speed, dimension parameter, load and braking force affect the lateral stability of the tractor-semitrailer combinations with computer simulation results [6]. The study objects of Chen C was about nonlinear and linear model of tractor-semitrailer vehicles in Automated Highway Systems (AHS), which verified the damping was proportional to the longitudinal speed [7]. Pauwelussen J P used phase plane method and handling diagram to study the yaw stability of a single vehicle and tractor-trailer combinations with nonlinear model [8]. Dahlberg E and Wideberg J studied and verified that the fifth wheel was moved further rearwards which results in instability [9]. The handling stability of tractor-semitrailer combination is researched by the separate definition of understeer gradient for tractor and semitrailer, and the effects of structural parameters on the understeer gradients were analyzed [10–12]. Barbieri N et al. considered the lateral stability for the type of Rodo-train and Bi-train with different loads to the evolution/correction of vehicles design, roads design, traffic signs, and vehicle drivers training [13]. Wei C Y believed handling stability of the caravan (car trailer) using root locus method and the effect of yaw rate gain in steady state [14]. Salaani M K introduced the understeer gradient formula and critical speed equations for articulated vehicles [15]. Yang X J used bifurcation and state manifold theory to discuss nonlinear dynamics and used understeer gradient and handling diagram to discuss linear dynamics, which was used to evaluate the handling stability performance [16]. Bao J H et al. presented a linear dynamic model for tractor/full trailer and found that a resistive torque on turntable would improve the stability during obstacle avoidance manoeuvers [17]. Ren Y Y et al. verified that driving speed and loaded mass were more important than fifth wheel lead to affect the stability of tractor-semitrailer using handling diagram with nonlinear model [18]. Tabatabaei S H et al. deemed the effect of tire cornering stiffness variation on directional stability of articulated heavy vehicle and gave suggestions on an appropriate procedure for braking or driving forces distribution [19]. Ou C J et al. regarded that semitrailer's mass, vehicle speed and the distance between tractor front axle and mass center reduced, and the fifth wheel lead and its damping coefficient increased, which could improve the handling stability of tractor-semitrailer based on single lane-change test [20].

The abovementioned investigations lack of understeer gradient equations of B-double vehicles in handling stability analysis. Section 2 describes an analytical method in linear dynamics modeling for B-double vehicles which could simplify the procedures. Section 3 describes the correspondence and analysis of understeer gradient and yaw rate gain in steady state. Section 4 gives the influence of struc-
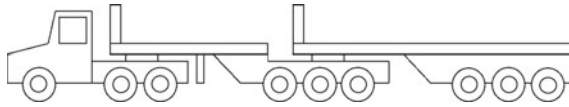
**Fig. 1** B-double vehicles side view

tural parameters on handling stability with understeer gradient. Section 5 draws the conclusions.

## 2 Modeling Using an Analytical Method

B-double vehicles are comprised of tractor, first semitrailer, and second semitrailer as shown in Fig. 1.

Geodetic coordinate system *XOY* and coordinate system *xoy*, $x_1o_1y_1$ and $x_2o_2y_2$ which are consolidated on each vehicle unit's mass center, respectively, were given. Tractor's motion state only contains lateral velocity and yaw rate, and the idealized assumptions are as follows: (a) Road is even, namely unevenness and vertical motion with coupling effect related in riding comfort dynamics is neglected; (b) Roll motion of suspension and relevant effect are neglected; (c) Steering system is taken as a rigid body and steer input is directly acted on the tractor's front wheel; (d) Aerodynamics is neglected; (e) Lateral acceleration of each vehicle unit is limited under the value of 0.4 g (g = 9.8 m/s²), and longitudinal velocity $v_x$ is constant, namely $v_x = v_{x1} = v_{x2}$, which ensure the motion equations are linear.

Roll motion neglected means the load transfer between left and right tire is neglected as well. The width of vehicle body namely wheel track is neglected. The resultant force of left and right tire works on the same axle, and the model contains three mass centers with four DOF which is referred in Fig. 2.

The method is using a whole or an isolation approach to each vehicle unit in different situations. Taking tractor, tractor and first semitrailer, three vehicle units, first and second semitrailer or second semitrailer as one whole for force and motion analysis. With geometrical relationship in Fig. 2, tractor's heading angle and its derivative can be written as:

$$\varphi = \beta + \psi, \ \varphi' = \beta' + \psi' = \beta' + r \tag{1}$$

Then, based on circular motion formula $a_n = v \times \omega$, tractor's lateral acceleration can be expressed as:

$$a_y = v_x\varphi' = v_x\left(\beta' + r\right) \tag{2}$$

Similarly, lateral acceleration of each vehicle unit could be calculated as follows in Table 1.
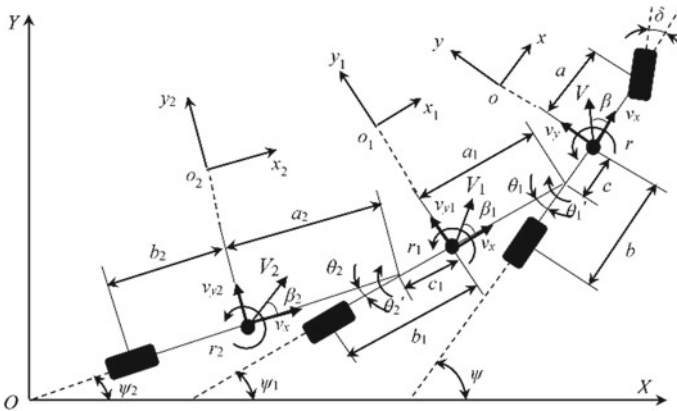
**Fig. 2** Four DOF linear model for B-double vehicles

**Table 1** Expressions for lateral acceleration of each vehicle unit

| Lateral acceleration | Expression |
|---|---|
| Tractor | $a_y = v_x(\beta' + r)$ |
| First semitrailer | $a_{y1} = a_y - (c + a_1)r' + a\theta_1''$ |
| Second semitrailer | $a_{y2} = a_y - (c + a_1 + c_1 + a_2)r' + (a_1 + c_1 + a_2)\theta_1'' + a_2\theta_2''$ |

**Table 2** Expressions for lateral velocity of each axle

| Lateral velocity | Expression |
|---|---|
| Tractor's front and rear axle | $v_y + ar$ and $v_y - br$ |
| First semitrailer's rear axle | $v_x\sin\theta_1 + v_y - (c + a_1 + b_1)r + (a_1 + b_1)\theta_1'$ |
| Second semitrailer's rear axle | $v_x\sin\theta_1 + v_x\sin\theta_2 + v_y - (c + a_1 + c_1 + a_2 + b_2)r + (a_1 + c_1 + a_2 + b_2)\theta_1' + (a_2 + b_2)\theta_2'$ |

Similarly, lateral velocity of each axle could be calculated as follows in Table 2.

Slip angle of each axle tire was calculated approximately as four expressions in Table 2 divided by $v_x$. Lateral force of each axle tire is expressed in the following equation:

$$F_{yf} = k_f\alpha_f, \ F_{yr} = k_r\alpha_r, \ F_{y1} = k_1\alpha_1, \ F_{y2} = k_2\alpha_2 \tag{3}$$

Equation was derived based on lateral force balance theory:

$$ma_y + m_1a_{y1} + m_2a_{y2} = F_{yf} + F_{yr} + F_{y1} + F_{y2} \tag{4}$$

Equation was derived based on yaw moment balance theory of tractor's mass center:

$$I_z r' + I_{z1} r'_1 + I_{z2} r'_2 - (c + a_1) m_1 a_{y1} - (c + a_1 + c_1 + a_2) m_2 a_{y2}$$
$$= a F_{yf} - b F_{yr} - (c + a_1 + b_1) F_{y1} - (c + a_1 + c_1 + a_2 + b_2) F_{y2} \qquad (5)$$

Equation was derived based on yaw moment balance theory for first articulated point with first and second semitrailer:

$$I_{z1} r'_1 + I_{z2} r'_2 - a_1 m_1 a_{y1} - (a_1 + c_1 + a_2) m_2 a_{y2}$$
$$= - (a_1 + b_1) F_{y1} - (a_1 + c_1 + a_2 + b_2) F_{y2} \qquad (6)$$

Equation was derived based on yaw moment balance theory for second articulated point with second semitrailer:

$$I_{z2} r'_2 - a_2 m_2 a_{y2} = -(a_2 + b_2) F_{y2} \qquad (7)$$

To further simplify the equation set, the result of Eqs. (5)–(6) and (6)–(7) was as follows:

$$I_z r' - c m_1 a_{y1} - c m_2 a_{y2} = a F_{yf} - b F_{yr} - c F_{y1} - c F_{y2} \qquad (8)$$
$$I_{z1} r'_1 - a_1 m_1 a_{y1} - (a_1 + c_1) m_2 a_{y2} = -(a_1 + b_1) F_{y1} - (a_1 + c_1) F_{y2} \qquad (9)$$

Constraint conditions of two articulated point are expressed in the following equation:

$$r_1 = r - \theta'_1, r'_1 = r' - \theta''_1, r_2 = r_1 - \theta'_2 = r - \theta'_1 - \theta'_2, r'_2 = r'_1 - \theta''_2 = r' - \theta''_1 - \theta''_2 \qquad (10)$$

Supposing state vector $X = [v_y, r, \theta'_1, \theta_1, \theta'_2, \theta_2]^T$, input vector $U = [\delta]$, and output vector $Y = X = [v_y, r, \theta'_1, \theta_1, \theta'_2, \theta_2]^T$. Then the differential equation set from Eqs. (4) and (7)–(10) could be written in a matrix form as:

$$P X' + Q X = R U \qquad (11)$$

And state-space matrices are obtained as:

$$\begin{cases} X' = -P^{-1} Q X + P^{-1} R U = A X + B U \\ Y = C X + D U \end{cases} \qquad (12)$$

## 3 Analysis on Steady Steering Characteristics

With front steering wheel angle as the step input at an equal speed, the response for vehicle is in uniform circular motion which is evaluated by ratio steady-state

yaw rate gain ($r_s/\delta_f$). Generally, excessive understeer and oversteer make the vehicle out of control. For B-double vehicles, with tractor's front steering wheel angle as the step input at an equal speed, the ratios are used to justify and evaluate the system stability. During steady steering state, it could be derived that: $r = r_1 = r_2 = r_s$, $v_y = v_{y1} = v_{y2} = v_{ys}$, $\beta = \beta_1 = \beta_2 = \beta_s$, $\theta_1 = \theta_2 = \theta_s$, and their derivatives are: $v_y' = r' = r_1' = r_2' = \theta_1' = \theta_1'' = \theta_2' = \theta_2'' = 0$. So Eq. (11) could be written in the following form:

$$X = Q^{-1}RU \tag{13}$$

The ratios steady-state yaw rate gain of tractor, first and second semitrailer could be solved as follows:

$$\left.\frac{r}{\delta}\right)_S = \frac{v_x}{Kv_x^2 + L}, \left.\frac{r_1}{\theta_1}\right)_S = \frac{v_x}{K_1 v_x^2 + L_1 - (b-c)}, \left.\frac{r_2}{\theta_2}\right)_S = \frac{v_x}{K_2 v_x^2 + L_2 - (b_1 - c_1)} \tag{14}$$

Then, the steady-state relative yaw angle gain of tractor and first semitrailer, first and second semitrailer, tractor and second semitrailer could be obtained respectively as follows:

$$\left.\frac{\theta_1}{\delta}\right)_S = \frac{K_1 v_x^2 + L_1 - (b-c)}{Kv_x^2 + L}, \left.\frac{\theta_2}{\theta_1}\right)_S = \frac{K_2 v_x^2 + L_2 - (b_1 - c_1)}{K_1 v_x^2 + L_1 - (b-c)}, \left.\frac{\theta_2}{\delta}\right)_S$$
$$= \frac{K_2 v_x^2 + L_2 - (b_1 - c_1)}{Kv_x^2 + L} \tag{15}$$

where the understeer gradient for each vehicle unit is expressed as follows:

$$K = \frac{1}{k_f}\left(\frac{b}{L}m + \frac{b-c}{L}\frac{b_1}{L_1}m_1 + \frac{b-c}{L}\frac{b_1 - c_1}{L_1}\frac{b_2}{L_2}m_2\right)$$
$$- \frac{1}{k_r}\left(\frac{a}{L}m + \frac{a+c}{L}\frac{b_1}{L_1}m_1 + \frac{a+c}{L}\frac{b_1 - c_1}{L_1}\frac{b_2}{L_2}m_2\right) \tag{16}$$

$$K_1 = \frac{1}{k_r}\left(\frac{a}{L}m + \frac{a+c}{L}\frac{b}{L_1}m_1 + \frac{a+c}{L}\frac{b_1 - c_1}{L_1}\frac{b_2}{L_2}m_2\right) - \frac{1}{k_1}\left(\frac{a_1}{L_1}m_1 + \frac{a_1 + c_1}{L_1}\frac{b_2}{L_2}m_2\right) \tag{17}$$

$$K_2 = \frac{1}{k_1}\left(\frac{a_1}{L_1}m_1 + \frac{a_1 + c_1}{L_1}\frac{b_2}{L_2}m_2\right) - \frac{1}{k_2}\left(\frac{a_2}{L_2}m_2\right) \tag{18}$$

Equation (15) can be expressed in the following form:

$$\left.\frac{\theta_1}{\delta}\right)_S = \frac{K_1}{K} + \frac{K_1}{K}\frac{\frac{L_1 - (b-c)}{K_1} - \frac{L}{K}}{v_x^2 + \frac{L}{K}}, \left.\frac{\theta_2}{\theta_1}\right)_S = \frac{K_2}{K_1} + \frac{K_2}{K_1}\frac{\frac{L_2 - (b_1 - c_1)}{K_2} - \frac{L_1 - (b-c)}{K_1}}{v_x^2 + \frac{L_1 - (b-c)}{K_1}}, \left.\frac{\theta_2}{\delta}\right)_S$$
$$= \frac{K_2}{K} + \frac{K_2}{K}\frac{\frac{L_2 - (b_1 - c_1)}{K_2} - \frac{L}{K}}{v_x^2 + \frac{L}{K}} \tag{19}$$

Conclusions are drawn from Eq. (19): $K$ and $K_1$, $K_1$ and $K_2$, $K$ and $K_2$ affect the steering stability of tractor and first semitrailer, first and second semitrailer, tractor

(a) Convergence lead to stability   (b) Convergence lead to stability   (c) Divergence lead to instability

(d) Convergence lead to stability   (e) Divergence lead to instability   (f) Divergence lead to instability
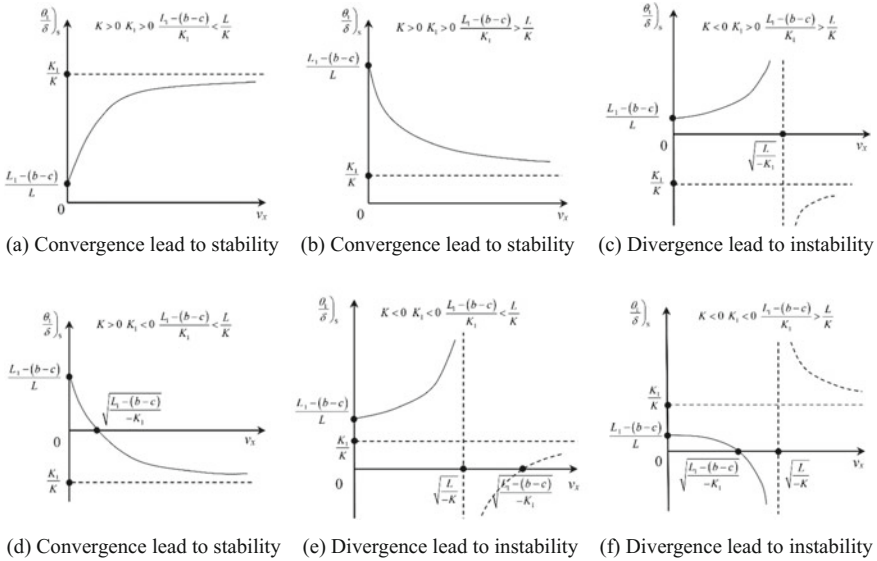
**Fig. 3**  Six situations for first formula in Eq. (19)



(a) Convergence lead to stability   (b) Convergence lead to stability   (c) Divergence lead to instability

(d) Convergence lead to stability   (e) Divergence lead to instability   (f) Divergence lead to instability
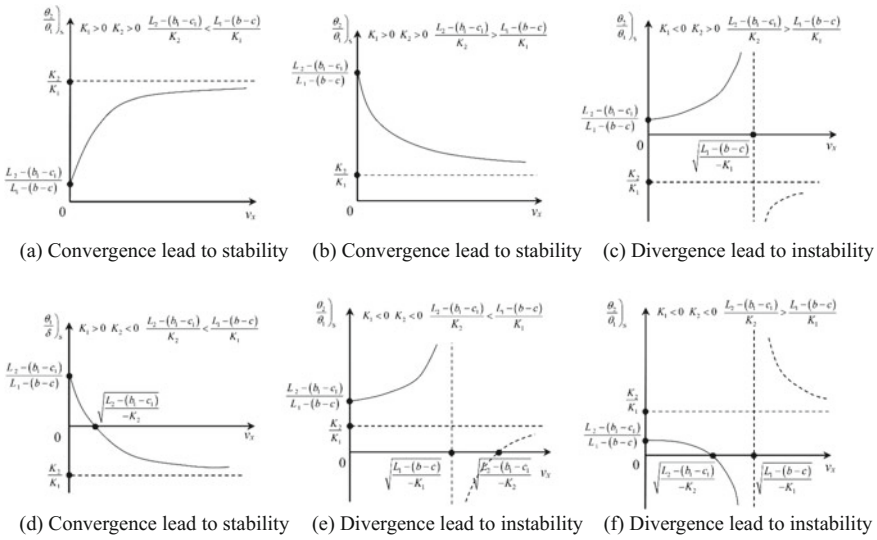
**Fig. 4**  Six situations for second formula in Eq. (19)

and second semitrailer, respectively. Three formulas in Eq. (19) have six situations respectively in Figs. 3, 4, and 5 with quantitative analysis.

(a) Convergence lead to stability  (b) Convergence lead to stability  (c) Divergence lead to instability



(d) Convergence lead to stability  (e) Divergence lead to instability  (f) Divergence lead to instability
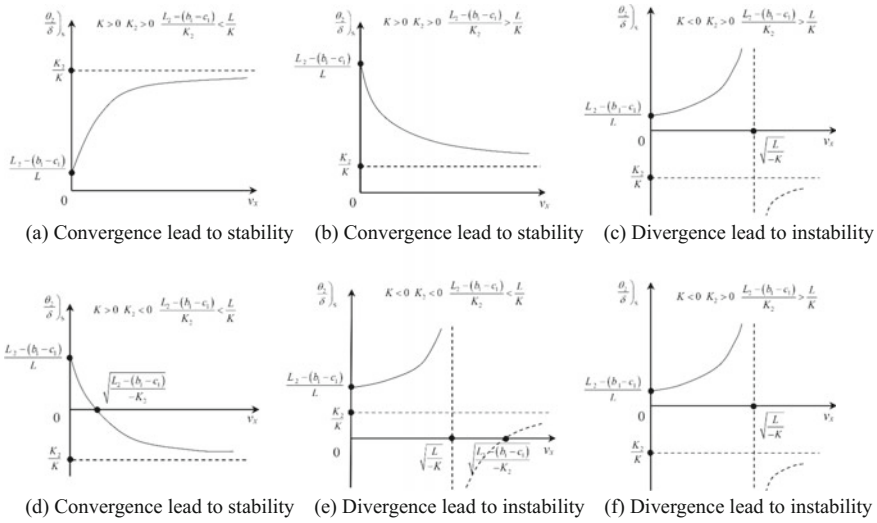
**Fig. 5** Six situations for 3rd formula in Eq. (19)



(a) Curve mesh of $K$ with variation of $m$ and $k_r$

(b) Curve mesh of $K_1$ with variation of $m_1$ and $k_1$

(c) Curve mesh of $K_2$ with variation of $m_2$ and $k_2$
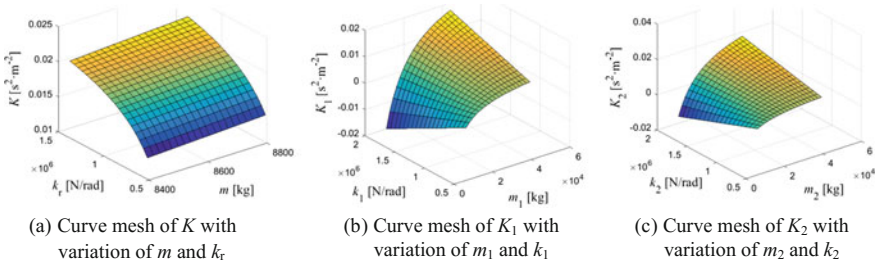
**Fig. 6** Curve mesh of understeer gradient variation with mass and tire cornering stiffness

## 4  The Effect of Structural Parameters on the Stability

The understeer gradient could evaluate the dynamics performance. The variation with structural parameters such as mass, tire cornering stiffness, location of mass center, wheelbase and location of articulated point of each vehicle unit could affect the manoeuver state of B-double vehicles.

Figure 6a shows that $K$ increases with increase in $m$ and $k_r$. In Fig. 6b, $K_1$ increases with $m_1$ increasing. With $k_1$ increasing, $K_1$ decreases when $m_1$ nears empty load; $K_1$ increases when $m_1$ nears to full load. In Fig. 6c, $K_2$ increases with $m_2$ increasing. With $k_2$ increasing, $K_2$ decreases when $m_2$ nears empty load; $K_2$ increases when $m_2$ nears full load.

Figure 7a shows $a$ and $L$ increase (tractor's mass center moved backward) resulting in decrease in $K$. In Fig. 7b, $a_1$ increases (First semitrailer's mass center moved backward) or $L_1$ decreases resulting in decrease in $K_1$. In Fig. 7c, $a_2$ increases (Second

(a) Curve mesh of $K$ with variation of $a$ and $L$

(b) Curve mesh of $K_1$ with variation of $a_1$ and $L_1$

(c) Curve mesh of $K_2$ with variation of $a_2$ and $L_2$
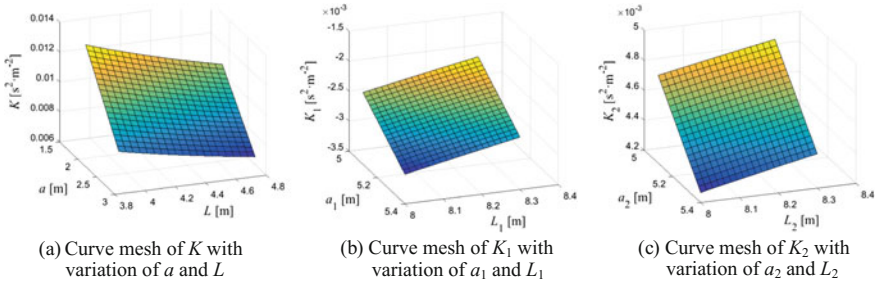
**Fig. 7** Curve mesh of understeer gradient variation with location of mass center and wheelbase



(a) Curve mesh of $K$ with variation of $m$ and $c$

(b) Curve mesh of $K_1$ with variation of $m_1$ and $c$

(c) Curve mesh of $K_2$ with variation of $m_2$ and $c_1$
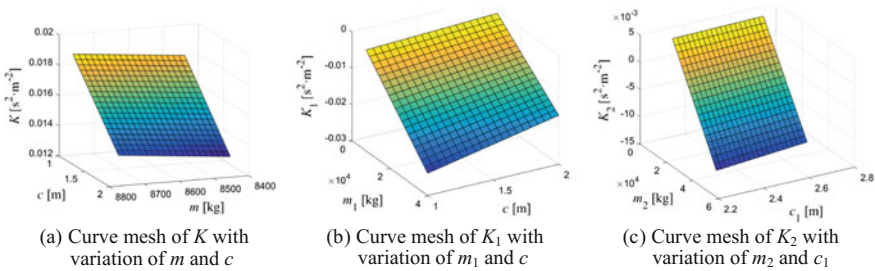
**Fig. 8** Curve mesh of understeer gradient variation with mass and location of articulated point

semitrailer's mass center moved backward) or $L_2$ decreases resulting in decrease in $K_2$.

Figure 8a shows $m$ increasing or $c$ decreasing (First articulated point moved forward) resulting in $K$ increasing. In Fig. 8b, $m_1$ increases or $c$ decreases (First articulated point moved forward) resulting in decrease in $K_1$. In Fig. 8c, $m_2$ increases or $c_1$ decreases (Second articulated point moved forward) resulting in decrease in $K_2$.

# 5 Conclusion

An analytical method was introduced and used in B-double vehicles modeling which contains whole or isolation approach, and it could simplify the procedures for equation set. With tractor's front steering wheel angle as the step input, B-double vehicles were in uniform circular motion in the steady state. In steady state, yaw rate gain and understeer gradient for each vehicle unit were solved directly and relative yaw angle gain could be solved subsequently. There were six situations for relative yaw angle gain respectively which affect handling stability. The understeer gradient increases result in good handling stability otherwise in instability. By changing the structural parameters, conclusions were drawn: (a) With mass (load capacity) increasing,

understeer gradient increases respectively. For two semitrailers, with rear axle tire cornering stiffness increasing, understeer gradient decreases with empty load; otherwise, it increases with full load; (b) For tractor, with mass center moving backward or wheelbase increasing, understeer gradient decreases. For two semitrailers, with mass center moving backward or wheelbase decreasing, understeer gradient decreases; (c) With first articulated point moving forward and tractor's mass increasing, tractor's understeer gradient increases, but first semitrailer's understeer gradient decreases. For second semitrailer, with second articulated point moving forward and mass (load capacity) increasing, its understeer gradient decreases.

Since assumptions were made in deducing the equations, nonlinear factors such as more complex tire model and roll motion were neglected in the analysis of handling stability, which will be investigated in the future.

# References

1. Li J (2013) B-double modular vehicle combinations shown on Logistics Expo. Commercial Veh News 38:4
2. Ying CY (2016) The introduction of national standard Limits of dimensions, axle load and masses for motor vehicles, trailers and combination vehicles revised edition (GB 1589-2016). Auto Saf (08):90–94
3. Fancher PS (1979) Simulation of the directional response characteristics of tractor-semitrailer vehicles. Final report
4. Fancher PS (1985) The static stability of articulated commercial vehicles. Veh Syst Dyn 14(4–6):201–227
5. Xie L (1984) Simulation of tractor-trailer system stability. M.S. thesis, Iowa State University
6. Chen WW, Wang RG, Sun J (1994) Computer simulation of handling stability of tractor-semitrailer. Tractor 3:23–29
7. Chen C, Tomizuka M (1995) Dynamic modeling of tractor-semitrailer vehicles in automated highway systems. California Partners for Advanced Transit and Highways (PATH)
8. Pauwelussen JP (2001) Excessive yaw behaviour of commercial vehicles, a fundamental approach. In: 17th International Technical Conference on the Enhanced Safety of Vehicles (ESV-17), Amsterdam, The Netherlands, 4–7 June 2001
9. Dahlberg E, Wideberg J (2004) Influence of the fifth-wheel location on heavy articulated vehicle handling. In: 8th International Symposium on Heavy Vehicle Weights & Dimensions. Johannesburg, South Africa
10. Liu HF (2005) Study on the simulation and control strategy for yaw motion dynamics of tractor-semi trailer. Jilin University, Changchun
11. Guan ZZ, Liu HF (2006) Study on distinguish method for tractor-semitrailer steady state cornering performance. J Tianjin Univ Technol Educ 16(1):1–3
12. Yang XJ, Li XT (2012) A study on the handling characteristics and lateral stability of tractor-semitrailer combination. Autom Eng 12:1107–1113
13. Barbieri N, de Melo RP, Barbieri R (2005) Analysis of the lateral stability of cargo vehicles combinations-CVCS. In: Proceedings of the COBEM 2005: 18th International Congress of Mechanical Engineering

14. Wei CY (2008) Research on the handling stability of caravans. Jiangsu University, Zhenjiang
15. Salaani MK (2009) The application of understeer gradient in stability analysis of articulated vehicles. Int J Heavy Veh Syst 16(1–2):3–25
16. Yang XJ (2009) Research on the nonlinear dynamics and active control for vehicle cornering destabilization in critical situations. Shandong University, Jinan
17. Ji-hua B, Jin-liang L, Yan Y (2011) Lateral stability analysis of the tractor/full trailer combination vehicle. In: 2011 International Conference on Electric Information and Control Engineering (ICEICE). IEEE, pp 2294–2298
18. Ren YY, Zheng XL, Li XS (2012) Handling stability of tractor semitrailer based on handling diagram. Discrete Dynamics in Nature and Society, vol 2012, Article ID 350360, 16 pp. https://doi.org/10.1155/2012/350360
19. Tabatabaei SH, Zahedi A, Khodayari A (2012) The effects of the cornering stiffness variation on articulated heavy vehicle stability. In: 2012 IEEE International Conference on Vehicular Electronics and Safety (ICVES). IEEE, pp 78–83
20. Ou CJ, Zhou G, Liu XD et al (2015) Simulation and analysis on handling stability of tractor-semitrailer. In: 2015 International Conference on Transportation Information and Safety (ICTIS). IEEE, pp 94–101

# Building and Analyzing the Robustness of Interdependent Transportation Network for Hazmat Transporting Network and the Connected Traffic Network of Hazmat Transport

**Peng Hu, Bin Shuai and Zhenyao Wu**

**Abstract** Hazardous Materials Transportation Network (HMTN) has very tight coupling with Traffic Flow Network of Hazmat Transportation (TFNHT). We build the interdependent system for the two networks. One of them is the HMTN of Zhangjiagang City, another is generated with power-law parameters which is considered as TFNHT. One node from the HMTN is random failed as initial emergency failure. It has an impact on one dependent node from the TFNHT. The dependent node would give traffic pressure on connected nodes from the HMTN. In order to know the stability and robustness of each single network, we propose the Node Failure Rate (NFR) to show the percentage of non-function with iterations going on. The two variables in simulation are different average degrees of the TFNHT and initial failure of one random selecting node which belongs to the set of different degrees. In terms of the basic data and the simulation results, we found that (1) the high average degree of the TFNHT has more impact on the interdependent network than the low average degree of it. It means that high values of average degree can lead interdependent weakness and instability; (2) We suggest that the node of low degree should be considered as the part of hazmat transportation routes, and it reduces as far as possible selecting the nodes of high degree when we design the HMTN for improving the robustness; (3) In the interdependent transportation network, the HMTN is more stability than the connected TFNHT and the two networks have the same NFR rising trend.

## 1 Introduction

Interdependent network has been a hot research area in recent years. Buldyrev et al. [1] propose a basic feature for interdependent network which is that a node from one network failed can lead a dependent node from a dependent network failed. This process is constant change until all dependent relationships cease to function. They found that a very small fraction random failure can lead to the whole interdependent

P. Hu · B. Shuai (✉) · Z. Wu
School of Transportation and Logistics, Southwest Jiaotong University, Chengdu 610031, China
e-mail: shuaibin@home.swjtu.edu.cn

393

network breakdown which means that most of nodes and edges are failed. Vespignani [2] found that the interdependent network has the weakness property with tightly coupling connections based on the North America data of people transferring via different communication media. Gao et al. [3] study the percolation features for the interdependent random network. Kenett et al. [4] mainly review the framework for n interdependent random networks. Veremyev et al. [5] bring a typical and classical problem of minimizing node covered into the interdependent network with cascading failure process [6, 7] for analyzing the robustness of networks. Gong et al. [8] propose a method for designing the resilient interdependent supply chain network. They assume that the solving process is between the model of infrastructure restoration and the model of supply chain restoration. Tang et al. [9] focus on the robustness of the interdependent supply chain network. They consider the node failures as a cascading failure process via failed loads transmission when one node or multiple nodes are failed by emergency situations. The capacity of nodes can determine the current status of it in terms of loads transmission.

Hazardous Materials Transportation Network (HMTN) is also becoming a focus of concern in China because of more emergency accidents occurring with cities developing. At any city, the development of it needs hazmat and the daily life of people require hazmat. Safety transportation is important. But we cannot totally avoid the risk of hazmat transportation. In other words, emergency situations might happen and cause losses to people, property and environment. Generally, we only focus on a single network designing for hazmat transporting. Kara and Verter [10] propose a method to design hazmat transportation network. The method is about a bi-level model. The upper programming is to minimize total risk of people exposed, and the lower programming it to minimize the total cost for choosing different routes. The decision variables of upper model have an impact on the lower model, and also the results of the lower model can give the impact on the upper model. Erkut and Alp [11] consider to design the routes of hazmat transporting with minimum people exposed at first phase. The second phase is to minimize carriage cost for extending the routes selecting and building the network for hazmat transportation. Then, Erkut and Gzara [12] summarize the designing single hazmat network problem as four situations—Unregulated model, which only considers transport cost; Overregulated model, which only considers transport risk; Two-step model first considers risk for hazmat and minimizes cost for carriers at the second step; Bi-level model considers to minimize risk and cost simultaneously. In terms of these methodology, we can design a better network for hazmat shipments. But we cannot know what might happen to the network when one emergency situation occurs at the intersections of the HMTN. The adjacent intersections could get enormous impact from the accident scene. Other hazmat transportation also could be impacted and has an impact on connected intersections. The spread of the emergency situation could be catastrophic, and the traffic pressure transmission of intersections to intersections could lead the HMTN collapse. We need to know about the hazmat network failure process, and the traffic of hazmat shipment failure process. One failure could be depend on one another failure. It is an iteration process.

The aim of this paper is to build the interdependent framework for Hazardous Materials Transportation Network and the Traffic Flow Network of Hazmat Transportation (TFNHT). And we focus on analyzing the robustness of the interdependent transportation network. In Sect. 2, we propose the methodology for researching the failure process on the interdependent network via simulating. In Sect. 3, we apply our simulation model to the HMTN of Zhangjiagang City and generate TFNHT with different average degrees. In terms of the results from Sect. 3, we summarize conclusions in Sect. 4.

## 2 Methodology of Researching Percolation Failure Simulation

### 2.1 Describe a Failure Process in Interdependent Transportation Network

A hazmat shipment network depends on the road network of hazmat transporting. The two networks are coupling. We consider a single node of HMTN randomly failing as an initial failure. It means that one intersection failure might lead to an iterative percolation failure because of the two network falling apart which is a cascading failure process. In order to model the interdependent transportation network, we take into account two networks $G_1$ and $G_2$ for simplicity and without loss of generality as followed (Fig. 1). Both networks have the same number of nodes. Network $G_1$ is physical network to supply the hazmat shipment of network $G_2$. The nodes of $G_1$ is functional. If a node in network $G_1$ is a failure and ceases to function, the correspondence nodes in network $G_2$ should be stopped normal operation and may transfer the traffic flow into others nodes which could give more traffic pressure upon dependent nodes in network $G_1$. Then, these dependent nodes from network $G_1$ would be a failure and give an impact on dependent nodes in network $G_2$ as the same way. We define the dependent connection as the bidirectional edges of the two networks and the whole process as percolation failure in an interdependent transportation network about hazmat transporting.

Figure 1 shows an example for describing the process of percolation failure of the two transportation networks ($G_1$ network and $G_2$ network) and the connections between them, based on the random edges in each network. In network $G_1$, it represents the road transportation network of hazmat. Network $G_2$ shows the flow of hazmat shipments. Every node in network $G_1$ has dependent on one node and only one node in network $G_2$ which means one to one correspondence, and vice versa. Each connection between the two networks $G_1$ and $G_2$ is shown by a vertical straight solid line. If a connection is failure, the vertical straight solid line would be changed into the dotted line. $G_1$-edges and $G_2$-edges are shown by solid lines. Figure 1a, Phase 1: Node 1 (gray color node) in network $G_1$ is failed by traffic accidents of hazmat transportation as emergency situations. Figure 1b, Phase 2: The edges of Node 1 are
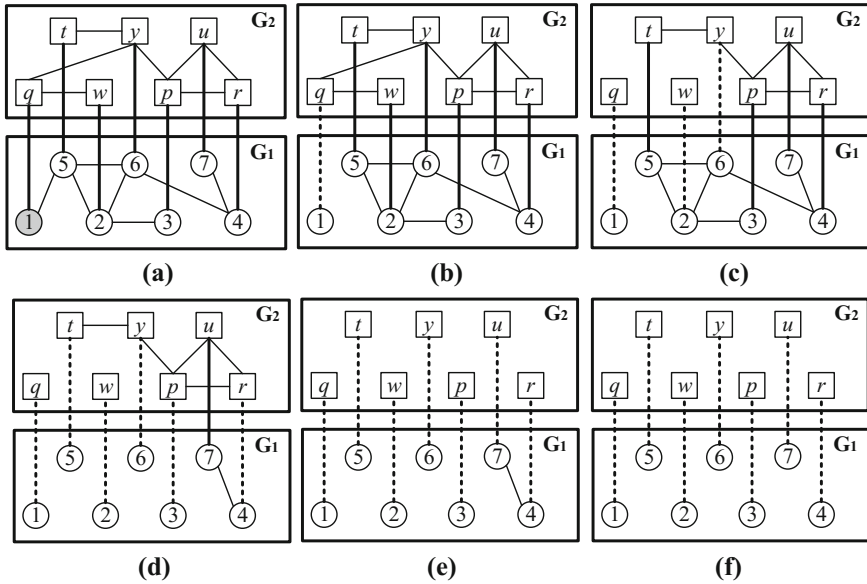
**Fig. 1** Modelling an interdependent transportation network percolation failure as an example

removed. Node $q$ (a dependent node) in network $G_2$ is impacted. Figure 1c, Phase 3: The edges of Node $q$ are also removed. Node $y$ and Node $w$ have an impact on Node 6 and Node 2 through dependent connections. Figure 1d, Phase 4: The edges of Node 2 and Node 6 are removed. The three adjacent nodes, Node 3, Node 4 and Node 5, also have an impact on the dependent nodes, including Node $p$, Node $r$, and Node $t$. Figure 1e, Phase 5: The edges from Node $p$, Node $r$, and Node $t$ are removed. Node $u$ in network $G_2$ has an impacted on Node 7 in network $G_1$. All edges in network $G_2$ have already failed which make network $G_2$ crash. Figure 1f, Phase 6: The only left edge between Node 7 and Node 4 is removed. All edges of network $G_1$ are failed and make it crash. The interdependent network between network $G_1$ and network $G_2$ collapses.

## 2.2　The Cyberspace of HMTN

Building HMTN is for operating hazmat transportation in an urban city. It is a physical road network. In China, we consider the intersections as nodes of HMTN and the road segments as edges of HMTN. Intersections always gather amount of traffic flow and allow a high population density in an urban city. So we focus on nodes percolation failure analysis in this paper and define the HMTN as an undirected network $G_A = (V_A, E_A)$. Let $V_A$ be the set of nodes $V_A = (1, 2, 3, \ldots, n_A)$. Let $E_A$ be the set of edges $E_A = (1, 2, 3, \ldots, m_A)$. Let $k_i$ be the degree of node and $\langle k_A \rangle$ be the average degrees

in network $G_A$, $i \in V_A$. When the percolation failure occurs at nodes of network $G_A$, the degree of nodes $k_i$ would be iterative and dynamic with different phases. If the value of $k_i$ is equal to zero which means that there are no other nodes connecting and all edges are removed, Node $i$ would be failed and cease to function.

## 2.3 The Cyberspace of TFNHT

Constructing the network of hazmat transporting flow is for showing the routes with different shipments. We apply the characteristics of the Dalian HMTN [13] to generate graphs—The network with the flow of hazmat shipments is scale-free network and follows power-law distribution. We define it as a network $G_B = (V_B, E_B)$, where $V_B$ is the set of nodes $V_B = (1, 2, 3, …, n_B)$ and $E_B$ is the set of edges $E_B = (1, 2, 3, …, m_B)$. Nodes in network $G_B$ show the transfer points, origin points or destination points in hazmat shipments. In one period, the flow of hazmat transportation is dynamic and changed. We consider to research on large amount of hazmat traffic flow and treat it as undirected network. Edges in network $G_B$ are to connect different nodes. The degree of nodes is $k_i'$ and the average degree is $\langle k_B \rangle$ in network $G_B$, $i \in V_B$. When the nodes from network $G_A$ has an impact on the nodes of network $G_B$ because of emergency situations, hazmat shipments would be impacted and the degree $k_i'$ could be updated in terms of the traffic flow transferring. If $k_i' = 0$, the flow of hazmat shipments could be broken down in Node $i$.

## 2.4 The Relationship of Interdependent Transportation Network

Let $f_{ij}$ be the dependent connection between Node $i$ from network $G_A$ and Node $j$ from network $G_B$, $i \in V_A$, $j \in V_B$. We consider the interdependence to be one to one correspondence. And let $F$ be the coupling function on both networks, $F(G_A) = F(G_B)$. The HMTN as network $G_A$ can load and support the flow of hazmat transportation from network $G_B$. The normal hazmat transportation from network $G_B$ is important for the interdependent network. If one node in network $G_A$ is failed by emergency situations, the dependent nodes in network $G_B$ fail and have a percolation impact on other nodes in network $G_A$. If there is no nodes or edges failure, the interdependent network gets balance and the giant mutual components are still functional. Specifically, all nodes and edges from both networks are failed, the interdependent network falls apart.

## 2.5    *Methodology on the Simulation of Percolation Failure*

According to the building of a cyberspace of the interdependent transportation network as mentioned before, we propose related definitions and assumptions to set a simulation process for simulating the percolation failure of the interdependent network.

### 2.5.1    Definition

In order to analyze the process of percolation failure in the interdependent network, we propose two related definitions, including the rate of node failure in each network of the interdependent transportation network and the robustness of the HMTN.

**Definition 1** Node Failure Rate (NFR) denotes the percentage of non-function nodes in the network. When NFR=0, it means that all nodes from the network are normal operation. If NFR=1, it shows that the network collapses. The mathematical formulation is as follows:

$$\text{NFR} = \frac{N_{\text{FN}}}{N_{\text{AN}}} \tag{1}$$

where NFR is the rate of node failure in the network. Let $N_{\text{FN}}$ be the number of failed nodes from the network. Let $N_{\text{AN}}$ be the number of all nodes in the network.

**Definition 2** The Robustness of the HMTN is determined by the factor of the Node Failure Rate. The value of the node failure rate is lower, the defense of the HMTN is stronger. And the robustness of the HMTN is better with higher stability. Through simulating the percolation failure process of the emergency situation of hazmat transportation in the interdependent transportation network, we could know the iteration process of the HMTN and the TFNHT. Then, the node failure rate shows the robustness and stability for the HMTN.

### 2.5.2    Assumption

To model the interdependent transportation network, we consider the assumptions as follows:

(1)    Each network in the interdependent network is considered as an undirected network. All interdependence connections are bidirectional. One node's failure leads to one dependent node percolation failure through the interdependence connection.

(2)    When hazmat transportation accident occurs at the HMTN from the interdependent network, we consider only one node failure as percolating simulation starting.

(3) In order to research the percolation failure process of the interdependent transportation network, we do not consider the response facilities to help the interdependent network recover.

(4) According to percolation theory, in the HMTN, fragmental components should stop function because of disconnecting with the giant mutual network, whereas the nodes and edges belonging to the giant components of the network are normal operating. In other words, we focus on the giant components and the fragmental components.

(5) In China, one road (regarded as the edge) from an urban city is normally short and the amount of roads are enormous and have complexity connecting ways. So we only consider the connection of the interdependent transportation network, and do not consider the real distance among nodes.

### 2.5.3 Simulation Model

We do the simulation on the MATLAB R2016b software with the computer which system configuration is 2.40 GHz Intel Processor i7-5500U. And we generate the traffic flow of hazmat transportation on the PAJEK64 4.05 software with the same equipped computer.

*Step* 1: It counts the basic data of the HMTN from interdependent network, including the size of the network, degree of each nodes and average degree. And it generates the TFNHT with different average degrees, the same number of nodes, no constraint on number of lines, the same number of nodes in initial Erdős-Rényi network, and the same probability of preferential attachment. The TFNHT is scale-free network and the generating parameters followed PAJEK software setting [14, 15]. The HMTN and the TFNHT consist of the interdependent transportation network.

*Step* 2: In the HMTN, one node with different node degrees is failed as simulating starting. This initial failure node is randomly generated and impacting nodes of the TFNHT through coupling relationship. Considering the node failed of different node degrees is to analyze the impact of different node degrees on the interdependent transportation network.

*Step* 3: According to assumption (4), if the nodes of the HMTN become fragmental components which are break away from the giant network and should stop function.

*Step* 4: It records the failure nodes in the HMTN, updates the matrix of the HMTN, and recalculates the node degree distribution on the HMTN. It records the impacted nodes in the TFNHT.

*Step* 5: In terms of the interdependent connections between the HMTN and the TFNHT, the impacted nodes from the TFNHT are failure. And it updates the interdependent connections of the two networks.

*Step* 6: It records the failures nodes of the TFNHT, updates the matrix of the TFNHT, and recalculates the node degree distribution on the TFNHT. It records the impacted nodes of the HMTN. Then, the impacted nodes are failure.

**Table 1** The basic data of the network

|              | HMTN | TFNHT |        |        |
| ------------ | ---- | ----- | ------ | ------ |
| Average degree | 2.9114 | 1.7722 | 3.2658 | 7.0127 |
| Number of nodes | 79 | 79 | 79 | 79 |
| Number of edges | 115 | 80 | 167 | 404 |

P.S. "HMTN" means the Hazardous Materials Transportation Network in Zhangjiagang City. "TFN-HT" means the Traffic Flow Network of Hazmat Transportation. The two networks consist of the interdependent network

*Step* 7: We consider the coupling relationship on the interdependent network as the iteration condition—If there are no more nodes failed in the interdependent network, the simulation can stop. Otherwise, it goes to *Step* 3.

## 3   Case Study

We propose the methodology to simulate the percolation failure process for the interdependent transportation network of hazmat shipments. In this section, we apply the method and simulation model to studying the node degree impact when the TFNHT with different average degrees couples with the HMTN of Zhangjiagang City [16].

Figure 2 shows the physical network for hazmat shipping in Zhangjiagang City. It has 79 nodes, 115 edges, and the average degree is 2.9114. One node represents one intersection in the network. And the road segment is denoted by the edge. As shown in Table 1, we also generate the three TFNHT with different average degrees and the same number of nodes. First, the interdependent connections are built between the HMTN and one of the TFNHT. Second, we apply our model to simulating the percolation failure process 100 times on the interdependent network through randomly failing one node as the beginning. Finally, according to the simulation result, we can analyze the robustness of the HMTN in the interdependent network. The simulation results are shown from Figs. 3, 4 and 5. Among these figures, the "$k=1$" means that the initial failure node belongs to the set of node degree 1 in the network which has 1 adjacent node. The "$k=2$" represents that the initial node failed at the set of node degree 2, and the same as the value of $k$ is equal to 1 to 5.

When any node from the HMTN as initial failure, the highest final node failure rate is approximately 50% in Fig. 3a, and in the Fig. 3b, the highest one is about 60%. The interdependent transportation network can defend the random failure, when the average degree of the TFNHT is 1.7722. In Fig. 3a, b, it shows that the initial node failed, which is from the set of degree 3 in the HMTN, and has the highest impact on the HMTN and the TFNHT. And the lowest impact is by the initial failure node which belongs to the set of degree 2 in the HMTN. The impact of the degree 4 set from the HMTN is more than the set of degree 1.
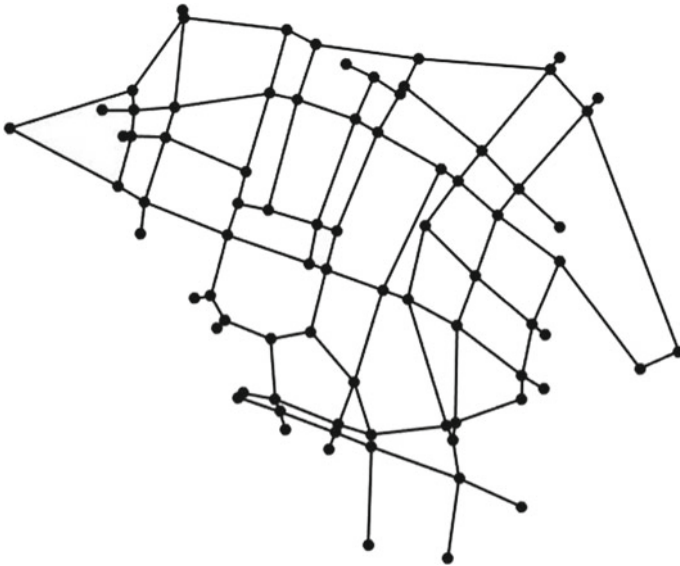
**Fig. 2** The HMTN in Zhangjiagang City



(a) HMTN                                           (b) TFNHT
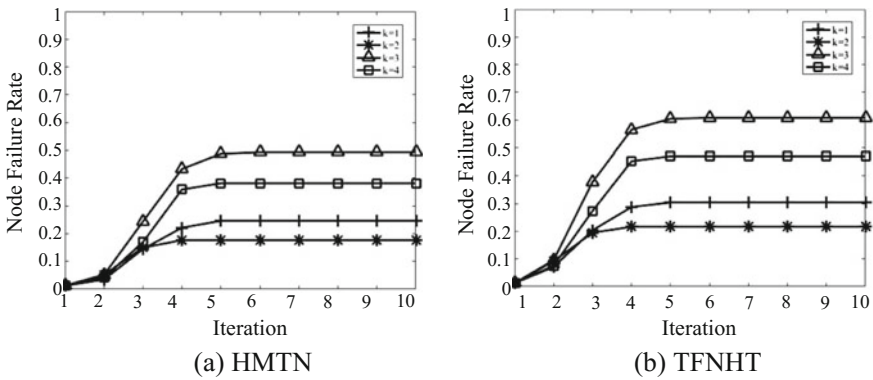
**Fig. 3** When the average degree of the TFNHT is 1.7722, one node of different degree in the HMTN is failed as initial node failure of the interdependent network

According to the ten iterations in the two networks, the highest final rate of node failure reaches approximately 65% in Fig. 4a, and the highest one is near 75% in Fig. 4b. As shown in Fig. 4, if the node as initial failure is randomly selected from the set of degree 3 in the HMTN when the average degree of the TFNHT is 3.2658, it has the strongest impact on the HMTN and the TFNHT. The opposite situation occurs at the set of degree 2, which has the lowest impact on the interdependent network. The fraction in the HMTN, which is from the set of degree 1, has a better defense than the fraction from the set of degree 4.

(a) HMTN  (b) TFNHT
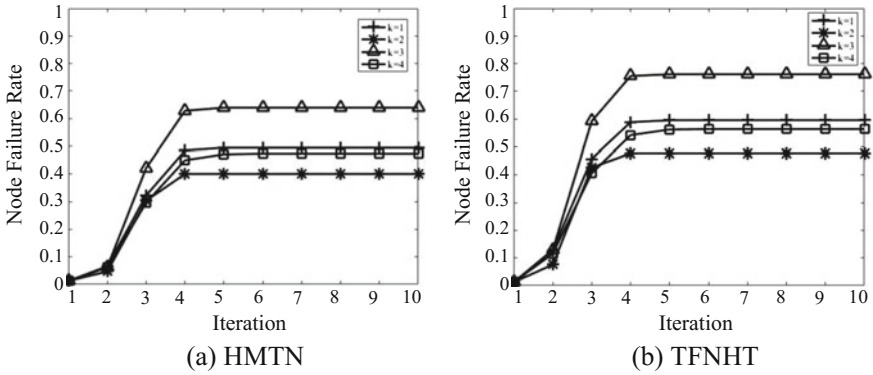
**Fig. 4** When the average degree of the TFNHT is 3.2658, one node of different degree in the HMTN is failed as initial node failure of the interdependent network



(a) HMTN  (b) TFNHT
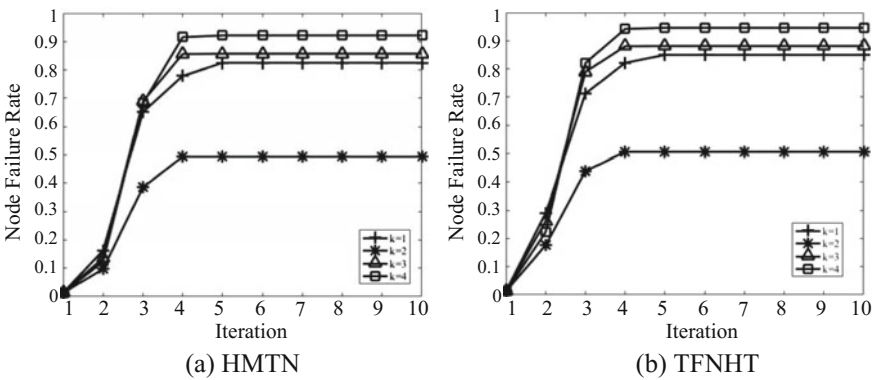
**Fig. 5** When the average degree of the TFNHT is 7.0127, one node of different degree in the HMTN is failed as initial node failure of the interdependent network

In Fig. 5, both of the HMTN and the TFNHT nearly become fragmental components when the initial node failure is from the set of degree 4 in the HMTN. The node failure rate in the HMTN is approximately 90% after the Iteration 4. In the same condition, the node failure rate in the TFNHT can reach 95% which means that only 5% nodes are functional. The set of degree 2 from the HMTN has the lowest impact on the interdependent network. The initial node failed in the HMTN from the set of degree 1 has lower impact than the node from the set of degree 3.

# 4   Conclusions

In this paper, we focus on building the interdependent transportation network between the Hazardous Materials Transportation Network (HMTN) and the Traffic Flow Network of Hazmat Transportation (TFNHT). And we provide a simulation model for simulating one initial node failure as the emergency situation of hazmat shipment to research the percolation failure process in the interdependent transportation network. The selecting process of the initial node is random and from different degree sets in the HMTN, including the set of degree 1 ($k=1$), the set of degree 2 ($k=2$), the set of degree 3 ($k=3$), and the set of degree 4 ($k=4$). By the reason of high density traffic and people at nodes/intersections, we consider only one node belonging different sets of degree as initial emergency accident in HMTN. Through percolation failure simulation, it analyzes the failure process in the interdependent transportation network. The key of the failure process is the relationship between HMTN and TFNHT, which leads the sequence of percolation failure. At the end of the simulation, all coupling relationships will stop function or there is no more nodes failure in the interdependent transportation network. The adjacent matrix in both the two networks and the amount of coupling relationships can decide the robustness of it. In order to research the robustness of both two network, we propose Node Failure Rate to analyze it. With iterations go on, the change of the node failure rate shows the amount of non-function nodes. When there is no more change in node failure rate, the network can get balance or collapse.

We apply the proposed method and simulation model to the HMTN in Zhangjiagang City and analyze its robustness via the simulation result of node failure rate. In summary, according to the simulation results, we found that two factors have an impact on the node failure rate. One factor is average degree of the TFNHT which is generated with the same number of nodes by PAJEK software. Since the average degree of the HMTN is a fixed value which is 2.9114, the value of the average degree of the TFNHT has an impact on each other. From Figs. 3, 4, and 5, the value of the average degree in the TFNHT is growing from 1.7722 to 7.0127. And the final node failure rates of the two network are increasing. The top of the node failure rate in HMTN is rising from 50% to 92%, and in the TFNHT, the rate is rising from 60 to 95%. The bottom of the node failure rate in HMTN is also increasing from 18 to 50%, and the rate of it in the related TFNHT is increasing from 22 to 50%. The decreasing of the average degree of the TFNHT could lead the interdependent transportation network more stability and more robustness. In others words, if the average degree of network has the high value, it means that nodes are connected by lots of links. More adjacent nodes the node has, more impact the node has on the network and leads in collapse. Indeed, if more intersections are frequently used to transport hazmat which means that they have high degree in TFNHT, they could have more impact on lots of intersections in the HMTN via coupling relationships when they cease to function.

Another factor is the degree of the initial failure node in the HMTN which is random chosen process within sets of different node degrees. The initial failure node represents the emergency accident. We consider the average performance through

random failure one node 100 times for each set of different node degrees to analyze the different impacts on HMTN and TFNHT. From Fig. 3, 4 and 5, the lines of "$k=3$" and "$k=4$" have higher node failure rate when the network gets balance. On the contrary, the lines of "$k=1$" and "$k=2$" have the lower node failure rate. The performance of the results shows that the nodes of high degree sets are riskier than the nodes belonging to the low degree sets. It means that we should build emergency rescue stations nearby these nodes from the HMTN which have high degree, and protect it against emergency situations. Especially, the nodes from the set of degree 2 ($k=2$) are the lowest dangerous in the HMTN of Zhangjiagang City. We should avoid choosing it as the part of hazmat transportation routes. Or we could design the HMTN with small amounts of nodes belonging to the set of high degree.

Obviously, in the interdependent network, the HMTN is more robustness than the TFNHT according to the results from Fig. 3, 4 and 5 and comparing each figure a, b. With different average degrees of the TFNHT, the percolation failure process of the two networks has the same rising trend which is reflected in all lines. In future research work, we will research more HMTN of cities and analyze the common features for the interdependent transportation network. Also, the edges failure should be considered. Although we could transfer the edge failure problem into node failure problem, the edge failure needs to consider more parameters, such as the length of edges, the width of the edges, the edges of the radius of turning circle, and the initial failure location on the edge. The key point of the edge failure problem is the coupling relationship between the HMTN and the TFNHT.

# References

1. Buldyrev SV, Parshani R, Paul G, Stanley HE, Havlin S (2010) Catastrophic cascade of failures in interdependent networks. Nature 464(7291):1025–1028
2. Vespignani A (2010) Complex networks: the fragility of interdependency. Nature 464(7291):984–985
3. Gao J, Buldyrev SV, Stanley HE, Havlin S (2012) Networks formed from interdependent networks. Nat Phys 8(1):40–48
4. Kenett DY, Gao J, Huang X, Shao S, Vodenska I, Buldyrev SV et al (2014) Network of interdependent networks: overview of theory and applications. In: Understanding Complex Systems, pp. 3–36
5. Veremyev A, Sorokin A, Boginski V, Pasiliao EL (2014) Minimum vertex cover problem for coupled interdependent networks with cascading failures. Eur J Oper Res 232(232):499–511
6. Hines P, Balasubramaniam K, Sanchez EC (2009) Cascading failures in power grids. IEEE Potentials 28(5):24–30
7. Zhai C, Zhang H, Xiao G, Pan TC (2017) Modeling and identification of worst-case cascading failures in power systems
8. Gong J, Mitchell JE, Krishnamurthy A, Wallace WA (2014) An interdependent layered network model for a resilient supply chain. Omega 46(9):104–116

9. Tang L, Jing K, He J, Stanley HE (2016) Complex interdependent supply chain networks: cascading failure and robustness. Physica A 443:58–69
10. Kara BY, Verter V (2004) Designing a road network for hazardous materials transportation. Transp Sci 38(2):188–196
11. Erkut E, Alp O (2007) Designing a road network for hazardous materials shipments. Comput Oper Res 34(5):1389–1405
12. Erkut E, Gzara F (2008) Solving the hazmat transport network design problem. Comput Oper Res 35(7):2234–2247
13. Chong PY, Shuai B, Deng SW, Yang J, Yin H (2015) Analysis on topological properties of Dalian hazardous materials road transportation network. Math Probl Eng 2015(1):1–11
14. Batagelj V, Mrvar A (2004) Pajek—analysis and visualization of large networks. In: Graph drawing software. Springer, Berlin, Heidelberg, pp. 77–103
15. Pennock DM, Flake GW, Lawrence S, Glover EJ, Giles CL (2002) Winners don't take all: Characterizing the competition for links on the web. Proc Natl Acad Sci USA 99(8):5207–5211
16. Xia Q, Qian Y, Liu MF (2014) Route optimization for hazardous materials transportation based on environmental risk assessment—a case of Zhangjiagang. China Environ Sci 34(1):266–272

# Decision Analysis of Driver's Driving Based on Bayesian Theory

**Yan Xing, Jinling Wang, Shuai Bian, Weidong Liu and Zhu Bai**

**Abstract**  Through the analysis of drivers' psychological decision-making process under different influencees and combined with Bayesian probability theory, the driver's driving decision is studied under the influence of the relative distance between the target vehicle and the leading vehicle, the relative distance between the target vehicle and the lateral object, the acceleration variation between adjacent vehicles, the relative speed between the target vehicle and the leading vehicle, and the relative speed between the target vehicle and the lateral vehicle. The probability of driver's acceleration, deceleration, car following, lane changing, parking, and other behaviors are determined. Finally, based on the above research, the relationship model between the driver's psychological pressure and the motor vehicle running characteristics was established.

**Keywords**  Bayesian theory · Driving decision · Driving behavior
Car following and lane changing

The driver is the decision-maker and operator of motor vehicle operation. Different driving psychologies of the motor vehicle driver can result in different operating characteristics of the motor vehicle. It is helpful to study the operation characteristics of the motor vehicle and improve the traffic safety at the intersection of the vehicle driver under different stimulation.

The research of driving decision originated from human factors engineering. In the early stage, the theory and method of decision science and related disciplines are applied to assist decision-makers to solve the problem of semi-structured and unstructured decision [1]. In the decision-making process, driving behavior is often affected by stimulation and effect of multiple source information such as human,

Y. Xing · J. Wang · S. Bian · W. Liu (✉) · Z. Bai
State Key Laboratory of Automobile Simulation and Control, Jilin University, Changchun 130025, Jilin, China
e-mail: 309474702@qq.com; 359063088@qq.com

Y. Xing
School of Transportation Engineering, Shenyang Jianzhu University,
Liaoning Shenyang 110168, China

vehicle, road, environment, and so on. Due to the limited information processing ability of the drivers, they cannot realize the input and output of multiple source information at the same time, so that sometimes the drivers can not accurately and quickly make driving decisions [2, 3]. Then Wang Xiaoyuan and others based on decision tree driving behavior decision research mechanism constructed the driving decision recognition model [4]. Talaat et al. used decision field theory to describe the psychological decision process of automobile drivers in the dynamic route selection process [5]. Lee Seungho et al. extended the decision field theory and used it to study the decision behavior of people in a changing decision environment [6].

The domestic and foreign scholars have made a lot of research on the suitability and safety of driving behavior, and obtained a series of laws and conclusions, which greatly enriched the theory of driving safety.

# 1 Driver's Psychological Decision Process Description

As a traffic system user and decision maker, after being affected by the surrounding environment, the driver needs to deal with the surrounding environmental information in a timely manner, to analyze the influence of the surrounding objects whether reached its corresponding critical value, and then to form a response driving decision. At the intersection, the driver's driving psychological decision mainly consists of five parts: acceleration, uniform speed, deceleration, parking, and lane changing.

The driver's psychological decision at the intersection of the driver is mainly derived from the influence of the dynamic object and static object on the driver's driving psychology.

The driver's psychological decision at the intersection is mainly derived from the influence of the dynamic object and static object on the driver's driving psychology. According to the driver's perception characteristics, psychological characteristics and the surrounding environment information, combined with the knowledge of kinematics and psychology, this paper gives a decision frame of the driver at the intersection. The first part is about the information of drivers' decision-making. The second part is the driver's perception of traffic information at the intersection. The third part is to process the information of perception. The fourth part is the decision response of the driver.

The driver decision frame of the intersection is shown in Fig. 1.

In the process of driving the vehicle at the intersection, the driver will change the driving decision based on the information of the person, car, road, and environment. Because the driver's psychological decision mainly depends on the subjective judgment and the empirical analysis, the boundary between the decision information is fuzzy. In order to objectively determined the relationship between five kinds of decision and the influence of the object around the motor vehicle, the paper studied the driver's driving decision using the Bayesian probability theory.
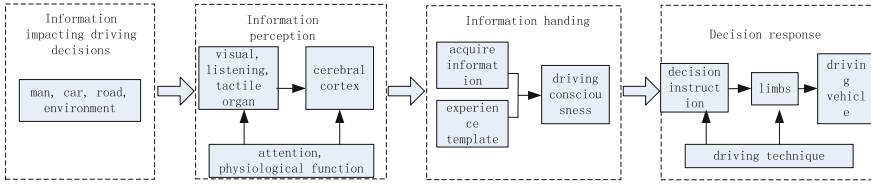
**Fig. 1** Driver's decision frame chart

## 2 The Basic Theory of Bayesian

Assume that $A_1, A_2, \ldots, A_n$ is a complete set of events, and $A_1, A_2, \ldots, A_n$ are n incompatible events. $\sum_{i=1}^{n} A_i = \Omega$, $P(A_i) > 0 \, (i = 1, 2, \ldots, n)$, for any event B, if $P(B) > 0$,

$$P(A_i|B) = \frac{P(A_i)P(B|A_i)}{\sum_{j=1}^{n} P(A_j)P(B|A_j)} \quad i = 1, 2, \ldots n \tag{1}$$

$P(B|A_i)$ and prior probability can be obtained by experiment. Event $A_i|B$ refers to the re-understanding of the phenomenon of A events, after the B event occurs. $P(A_i|B)$ is the posterior probability of random event $A_i$.

Bayesian probability can also be extended to the event probability of random event occurrence under the condition of multiple random events. If the events B and C occur, the probability of occurrence of the event $A_i$:

$$P(A_i|B \cap C) = \frac{P(A_i)P(B \cap C|A_i)}{\sum_{j=1}^{n} P(A_j)P(B \cap C|A_j)} \quad i = 1, 2, \ldots, n \tag{2}$$

## 3 The Establishment of the Decision Model of Driver Behavior Based on Bayesian Probability Theory

At the intersection, the driver's decision events include acceleration $A_1$, uniform speed $A_2$, deceleration $A_3$, parking $A_4$, lane changing $A_5$. The influential information the driver obtained at the intersection is the information event. As shown in Table 1.

According to Table 1 and Bayesian probability formula, the probability of event $A_i$ can be obtained under the conditions of the occurrence of events $B_k, C_l, D_m, E_n, F_s$. As shown in type 3:

$$\begin{aligned}
&P(A_i|B_k \cap C_l \cap D_m \cap E_n \cap F_s) \\
&= \frac{P(A_i)P(B_k \cap C_l \cap D_m \cap E_n \cap F_s|A_i)}{\sum_{j=1}^{5} P(A_j)P(B_k \cap C_l \cap D_m \cap E_n \cap F_s|A_j)} \quad i = 1, 2, 3, 4, 5
\end{aligned} \tag{3}$$

**Table 1** Relationship between Influencing factors and driving decision

| The relative distance from the leading car $B_k(k = 1, 2, 3)$ | The relative distance from the lateral object $C_l(l = 1, 2)$ | Acceleration variation of adjacent vehicles $D_m(m = 1, 2, 3)$ | Relative speed of leading vehicle $E_n(n = 1, 2, 3)$ | Relative speed of lateral vehicle $F_s(s = 1, 2)$ |
|---|---|---|---|---|
| Largen ($B_1$) | Largen ($C_1$) | Largen ($D_1$) | Largen ($E_1$) | Largen ($F_1$) |
| Unchanged ($B_2$) | Reduce ($C_2$) | Unchanged ($D_2$) | Unchanged ($E_2$) | Reduce ($F_2$) |
| Reduce ($B_3$) | – | Reduce ($D_3$) | Reduce ($E_3$) | – |

Because of the events $B_k$, $C_l$, $D_m$, $E_n$, $F_s$ are independent of each other, there is $P(B_k \cap C_l \cap D_m \cap E_n \cap F_s|A_i) = P(B_k|A_i)P(C_l|A_i)P(D_m|A_i)P(E_n|A_i)P(F_s|A_i)$.

Thus, under the conditions of the occurrence of events $B_k$, $C_l$, $D_m$, $E_n$, the probability of driver's driving decision $A_i$ is shown as the formula (4).

$$P(A_i|B_k \cap C_l \cap D_m \cap E_n \cap F_s)$$
$$= \frac{P(A_i)P(B_k|A_i)P(C_l|A_i)P(D_m|A_i)P(E_n|A_i)P(F_s|A_i)}{\sum_{j=1}^{5} P(A_j)P(B_k|A_j)P(C_l|A_j)P(D_m|A_j)P(E_n|A_j)P(F_s|A_j)} \quad i = 1, 2, 3, 4, 5 \tag{4}$$

$P(A_i)$, $P(B_k|A_i)$, $P(C_l|A_i)$, $P(D_m|A_i)$, $P(E_n|A_i)$, $P(F_s|A_i)$ in the above formula can be obtained through the actual traffic investigation.

When the driver gets more information events, the probability of occurrence of various decisions can be obtained by using the above formula. The driver will take the highest probability as the corresponding decision.

Set events: $B_1 : 0 < \Delta x \leq \Delta x_{JRth}$ $B_2 : \Delta x_{JRth} < \Delta x \leq \Delta x_{Gth}$ $B_3 : \Delta x_{Gth} < \Delta x$

Driver's decision events include: accelerate and change lane ($A_1 \cap A_4$), accelerate but not change lane ($A_1 \cap A_5$), follow the former car and change lane ($A_3 \cap A_4$), follow the former car but not change lane ($A_3 \cap A_5$), slow down and change lane ($A_2 \cap A_4$), slow down but not change lane ($A_2 \cap A_5$), braking $A_6$, freedom $A_7$, so the probabilities of decisions making are shown in the formula (12)–(5).

$$P(A_6|B_i) = \frac{P(A_6)P(B_i|A_6)}{P_i} \tag{5}$$

$$P(A_7|B_i) = \frac{P(A_7)P(B_i|A_6)}{P_i} \tag{6}$$

$$P(A_1 \cap A_4|B_i) = \frac{P(A_1 \cap A_4)P(B_i|A_1 \cap A_4)}{P_i} \cdot \eta_{14} \tag{7}$$

$$P(A_1 \cap A_5|B_i) = \frac{P(A_1 \cap A_5)P(B_i|A_1 \cap A_5)}{P_i} \times h_{15} \tag{8}$$

$$P(A_2 \cap A_4|B_i) = \frac{P(A_2 \cap A_4)P(B_i|A_2 \cap A_4)}{P_i} \cdot \eta_{24} \tag{9}$$

$$P(A_2 \cap A_5 | B_i) = \frac{P(A_2 \cap A_5)P(B_i | A_2 \cap A_5)}{P_i} \cdot \eta_{25} \tag{10}$$

$$P(A_3 \cap A_4 | B_i) = \frac{P(A_3 \cap A_4)P(B_i | A_3 \cap A_4)}{P_i} \cdot \eta_{34} \tag{11}$$

$$P(A_3 \cap A_5 | B_i) = \frac{P(A_3 \cap A_5)P(B_i | A_3 \cap A_5)}{P_i} \cdot \eta_{35} \tag{12}$$

where

$$P_i = \sum_{i=1}^{3} \sum_{j=1}^{7} P(A_j)P(B_i | A_j)$$

$$[\sigma_m, \sigma_n] \times [\omega_1, \omega_2]^T = [\eta_{mn}]$$

$$\omega_1 = \frac{\max\{\sigma_i | 1 \le i \le 3\} - \min\{\sigma_i | 1 \le i \le 3\}}{\max\{\sigma_i | 1 \le i \le 3\}} \times 100\%$$

$$\omega_2 = \frac{\max\{\sigma_i | 4 \le i \le 5\}s - \min\{\sigma_i | 4 \le i \le 5\}}{\max\{\sigma_i | 4 \le i \le 5\}} \times 100\%$$

where: $\omega_1, \omega_2$ is the weight coefficient.

## 4 Summary

Based on the analysis of drivers' psychological decision-making process under different influences and combined with Bayesian probability theory, this paper established a decision model of driver's driving behavior based on Bayesian probability theory. Considering the relative distance between the target vehicle and the leading vehicle, the relative distance between the target vehicle and the lateral object, the acceleration variation between adjacent vehicles, the relative speed between the target vehicle and the leading vehicle, the relative speed between the target vehicle and the lateral vehicle, the probability of driver's acceleration, deceleration, car following, lane changing, parking and other behaviors are studied, and the relationship between the driver's decision and the affected factors is determined.

# References

1. Zhang Q, Zhao J-X, Dong D-C (2008) Design of intelligent decision support system to traffic incident management. J Railway Sci Eng 5(3):83–88
2. Jin S, Wang D, Tao P, Li P (2010) Non lane based full velocity difference car following model. Physica 389(21):4654–4662
3. Xing Y, Gao Z, Qu Z, Hua H (2016) Study on vehicle delay based on the vehicle arriving distribution at entrance lanes of intersection. Transp Res Procedia 137:599–608
4. Wang X-Y, Yang X-Y (2008) Study on decision mechanism of driving behavior based on decision tree. J Syst Simul 20(2):415–419
5. Talaat H, Abdulhai B (2006) Modeling driver psychological deliberation during dynamic route selection processes. IEEE Intelligent Transportation Systems Conference, Toronto, Canada
6. Lee S, Son YJ, Jin J (2008) Decision field theory extensions for behavior modeling in dynamic environment using Bayesian belief network. J Inf Sci Int J 178(10):2297–2314

# Study on the Lateral Stability of B-Double Based on Clustering Analysis

**Hong-fei Liu, Qiang Xu, Hong-guo Xu, Cui-zhu Bao, Guo-jun Wang and Yi-hua Zhang**

**Abstract** A novel method is proposed to establish the stability criterion of B-double based on the clustering algorithm. The patterns recognizing in the lateral stability of B-double is studied. The vehicle model of multi-degree of freedom is established in the TruckSim. The off-line clustering center is obtained by K-means clustering. The TruckSim & Simulink co-simulation platform is built to identify the vehicle driving stability according to the online identification. The method is of data mining, which makes full use of the comparison of offline data and real-time data. The simulation results show that the method can accurately and real-time quantify the lateral driving stability of the B-double considering various factors, which can provide the criterion for intervention timing and degree of control system.

**Keywords** B-double · Stability identification · K-means clustering algorithm
Off-line clustering analysis · Online identification

## 1 Introduction

The vehicle stability criterion determines the intervention timing of the vehicle stability control system, which is the basis of vehicle stability control [1]. With the vigorous development of the automobile industry, improving the safety of vehicle driving and reducing the incidence of traffic accidents have become the key problem to be solved urgently. Achieving the goal by active safety control [2] has become the consensus both at home and abroad automobile industry. Chen [3] established a multi-body dynamics vehicle model for semitrailer trains, and the simulation tests

H. Liu · Q. Xu (✉) · H. Xu · C. Bao · G. Wang · Y. Zhang
College of Transportation, Jilin University, Changchun 130022, China
e-mail: 1219110352@qq.com

413

for rollover stability were performed. Mastinu et al. [4] proposed that bifurcation [5] analysis of a car model running on an even surface. The knowledge of the derived set of bifurcations seems important to fully understand the actual vehicle yaw motions occurring while running on an even surface and for conceiving robust control schemes for autonomous vehicles [6]. Yang Xiujian et al. [7] used the theory of nonlinear dynamics to study the equilibrium point bifurcation, phase trajectory, and Hopf bifurcation characteristics of semi-trailer trains under extreme operating conditions. Yu [1] designed a method to determine the stability region by introducing the yaw rate in the stable region based on the phase plane two-line method, and coordinated the control of mass center's side angle and the yaw rate.

Lateral stability of AHV at high-speed and rollover is highly dependent on the RWA ratio [8]. Sun et al. [9] proposed three major factors contributing to combination-trailer (CT) rollover which are: high-speed, sudden course deviation from high initial speed, and load shift. If the articulation angle between the leading and trailing units exceeds a critical limit, the driver is unable to control the motion of the vehicle by steering or braking.

Van de Molengraft-Luijten et al. [10] proposed the Hurwit Criterion to quickly find the stability critical value of the combined vehicle, characterizing vehicle stability by frequency domain analysis and rearforward amplification (RWA). Wu [11] investigates the application of the concept of Lyapunov exponents in the stability analysis of the nonlinear vehicle model in plane motion with two degrees of freedom for the first time. Based on the phase plane method, Luo et al. [12] designed a vehicle stability criterion based on the instability energy ratio.

All the above studies consider part of the vehicle stability parameters, and lack of trade-off relationship among vehicle driving stability parameters, which is not reliable. Therefore, this paper takes account of the most state parameter and its changing, based on the vehicle driving state data's mining analysis, and proposed a vehicle lateral stability criterion, that is, using K-means clustering on the B-double to classify the degree of risk. And is also provides scientific basis for the design of stability control strategy for B-double.

## 2    Construction of B-Double Model

The process [13] of using TruckSim to establish the model of B-double is as follows:

### 2.1    Select the Vehicle Type

From the main interface of TruckSim, select the B-double model. As shown in Fig. 1, the B-double consists of three-axis tractor, the first three-axle semi-trailer, and the second three-axle semi-trailer.

**Fig. 1** B-double model

## 2.2 Set the Vehicle Control Input

The simulation condition is the double lane change, set the vehicle speed, the other system can be default, the vehicle speed is 50–90 km/h, with growth of step 5.

## 2.3 Set the Vehicle Output Parameters

This paper considers the state parameters of each vehicle unit of the B-double, including longitudinal velocity, steering wheel angle, lateral velocity, lateral displacement, roll angle, hinge angle, yaw rate, roll rate, and lateral acceleration. The tire vertical load, the vehicle model outputs 32 parameters, the output parameters matrix is: dataOffline $= [U_1, U_2, U_3, SW, V_1, V_2, V_3, Y_1, Y_2, Y_3, \psi_1, \psi_2, \psi_3, \theta_1, \theta_2, \omega_1, \omega_2, \omega_3, \dot{\psi}_1, \dot{\psi}_2, \dot{\psi}_3, a_{y1}, a_{y2}, a_{y3}, F_{zL1}, F_{zL3}, F_{zL5}, F_{zL8}, F_{zR1}, F_{zR3}, F_{zR5}, F_{zR8}]$. Among them, the parameters of the subscript 1, 2, 3 on behalf of the tractor, the first semi-trailer, and the second semi-trailer.

## 3 Offline Clustering

The data of the TruckSim simulation is converted into Matlab and the indirect operation parameters are added, such as the slip angle of mass center and the load transfer rate. The correlation between the clustering variables is analyzed, some clustering parameters are eliminated. The clustering parameters and offline clustering centroids are obtained.

## 3.1  Correlation Analysis

The high correlation between clustering variables will affect the clustering results. Therefore, some clustering variables are removed by the correlation analysis before clustering. Here are some principles of parameters choosing: The state of the tractor is one of the most important information for the driver to judge whether the vehicle is safe or not. The same state parameters highly related of different vehicle units preferentially select the tractor state parameters. Delete the parameters which affect the correctness of the result. Some dynamic parameters stand for the driving stability of B-double, although there is a certain correlation among them, these parameters are still retained to comprehensively evaluate the safety level of the vehicle. Based on the above three principles and practical application, 13 representative clustering variables were selected. The simplified clustering parameter matrix is:

$$\text{dataOffline} = [U_1, SW, V_1, \psi_1, \psi_{2,}, \psi_3, \theta_1, \dot{\psi}_1, \dot{\psi}_2, \dot{\psi}_3, a_{y2}, \beta_1, \beta_3].$$

## 3.2  Offline Clustering Using K-Means

Clustering is a process of dividing data into different classes or clusters through *distance* or *similarity coefficient*, and making objects in the same cluster has a large similarity. Cluster analysis can be classified automatically from the sample data. The purpose of off-line clustering is to get off-line clustering centers and divide the vehicle driving stability into four grades. The meanings of the four hazard classes are shown in Table 1.

### 3.2.1  K-Means Offline Clustering Model

K-means clustering algorithm classifies the data points according to the calculated minimum distance of European distance [14]. The K-means clustering process is as follows:

(1) According to the need to determine the number of clustering $K$, where $K = 4$; (2) Initialize the cluster centers, in this paper, which is determined by equidistant points; (3) Set the maximum number of iterations J, in this article, $J = 1000$; (4) Set the offset of clustering center, in this article, $\Delta d = 0.0001$; (5) According to the Euclidean distance between each object and the cluster centers, each object is reallocated with

**Table 1**  The meanings of the four hazard classes

| Danger level | 1 | 2 | 3 | 4 |
|---|---|---|---|---|
| Meaning | Safe | Existing security threat | Typical potential danger | Dangerous |

the most similar clusters; (6) Update the cluster centers and recalculate the average of the objects in each cluster as a new clustering centroid; (7) Repeating execution (5) and (6), until each cluster is no longer changed, which is to satisfy execution (3) or (4).

Assuming that two n-dimensional data points are $A = (a_1, a_2,\ldots, a_n)$ and $B = (b_1, b_2,\ldots, b_n)$, the Euclidean distance between A and B points is: $\rho(A, B) = \sqrt{\sum_{i=1}^{n} (a_i - b_i)^2}, (i = 1, 2, \ldots, n)$.

With the increase of the iterations, the current clustering centers are *NewCenters*, and the last clustering centers are *enters*, the offset of clustering centers are: $\triangle d = \|NewCenters - Centers\|$.

### 3.2.2 Clustering Results Analysis

Conduct off-line clustering based on the data of B-double at the speed of 50, 55, 60, 65, 70, 75, 80, 85, and 90 km/h. The steering wheel angle of 50 km/h is shown in Fig. 2. Vehicle driving stability clustering results are shown in Fig. 3, each category represents a vehicle driving state.

According to the characteristics of the double lane change and the steering wheel angle of Fig. 2, the dangerous level of the (0, 3.05 s) straight-line running state corresponds to the state 3 in Fig. 3. The steering wheel is turning at 3.05 s, the vehicle starts to produce lateral displacement and swing, As the off-line data consist of the double lane change with increasing velocity, the stability of the subsequent steering condition is gradually reduced, which may lose stability eventually such as state 1 in Fig. 3. Figure 3 shows that the safest condition is 3, the most unstable condition is 1, and the sub-unstable condition is 4; In summary, the risk of vehicle conditions is of the order: $3 < 2 < 4 < 1$.

The degree of offline clustering can be reflected by the centroid offset with the changing curve of the iteration times, as shown in Fig. 4.



**Fig. 2** Steering wheel angle at the speed of 50 km/h
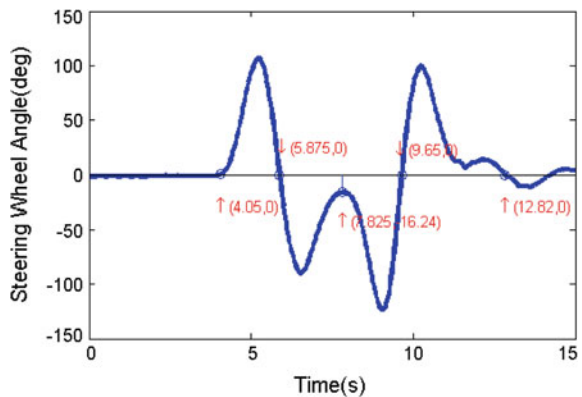
**Fig. 3** Off-line clustering
results
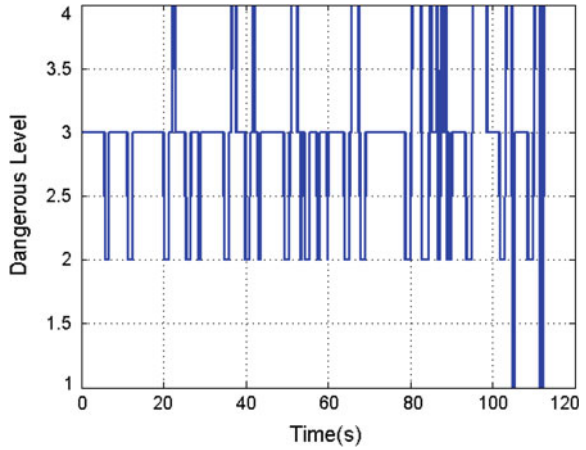


**Fig. 4** The centroid offset
with iterations
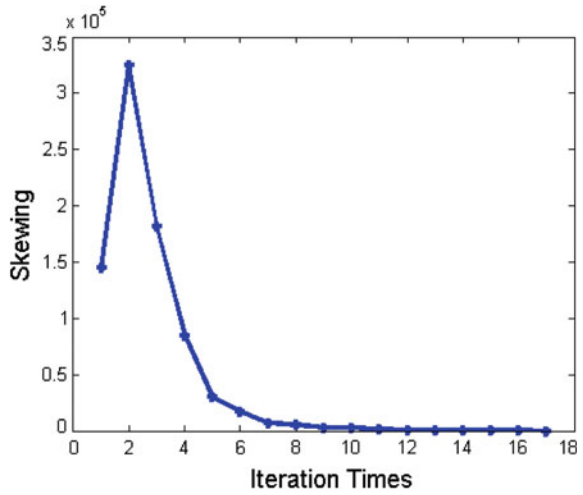


As can be seen from Fig. 4, the offset of the clustering center is mainly reduced as iteration times increases, and when iterating to step 17, the offset decreases to zero, the offline clustering is over.

After the adjustment of the clustering center, the sequence is 1, 2, 3, 4, whose dangerous level is gradually increased. The clustering centers are shown in Table 2.

**Table 2** Clustering centers

| Dangerous level | $U_1$/(km/h) | $SW$/deg | $V_{y1}$/(km/h) | $\psi_1$/deg | $\psi_2$/deg | $\psi_3$/deg | $\theta_1$/deg |
|---|---|---|---|---|---|---|---|
| 1 | 63.996 | 7.220 | 0.033 | −0.192 | −0.242 | −0.286 | −0.239 |
| 2 | 66.269 | −6.909 | 0.700 | 1.326 | 1.756 | 2.297 | 2.698 |
| 3 | 71.149 | −44.938 | −0.359 | −9.446 | −10.901 | −12.265 | −4.869 |
| 4 | 77.485 | −133.539 | −14.121 | −36.246 | −45.783 | −51.886 | −31.746 |

| Dangerous level | $\dot{\psi}_1$/(deg/s) | $\dot{\psi}_2$/(deg/s) | $\dot{\psi}_3$/(deg/s) | $a_{y2}$/(m/s²) | $\beta_1$/deg | $\beta_3$/deg |
|---|---|---|---|---|---|---|
| 1 | −0.078 | 0.012 | −0.202 | 0.001 | 0.000 | 0.001 |
| 2 | −0.096 | −0.144 | 1.539 | 0.109 | 0.011 | −0.016 |
| 3 | −8.056 | −9.079 | −11.605 | −0.159 | −0.007 | 0.045 |
| 4 | −60.762 | −55.991 | −57.475 | 0.135 | −0.183 | 0.286 |

# 4 Online Identification

## 4.1 Co-simulation of TruckSim-Simulink Platform

In order to judge the lateral stability of the vehicle in real time, the co-simulation of TruckSim-Simulink platform based on the offline clustering's centers is built. In this paper, the output of TruckSim is connected with the input of Simulink, and the vehicle driving state is identified. Figure 5 shows part of the co-simulation diagram.

The vehicle model is selected in TruckSim, the conditions and output parameters are set. Then the model of the vehicle is sent to Simulink. Lastly, the corresponding Simulink model is established according to the need, then the co-simulation of TruckSim-Simulink platform is set up. Online identification can determine the stability of the vehicle according to the Euclidean distance between these data and the clustering centers. The process is shown in Fig. 6.

## 4.2 Analysis of Online Clustering Results

The simulation for online clustering is based on double lane change at the speed of 62.5 km/h, steering angle input as shown in Fig. 7, Euclidean distance between simulated data points and clustering centers is shown in Fig. 8, the dangerous level is shown in Fig. 9.

It can be seen in Figs. 7, 8 and 9 that the (0, 3.05 s) of the double lane change is in a straight line and the Euclidean distance to each clustering center is stable, which belongs to the second hazard class. The steering wheel is beginning to turn at 3.05 s, the vehicle's real-time driving state and Euclidean distance are floating among the first, the second and the third hazard levels. Until 7.725 s, vehicles are gradually
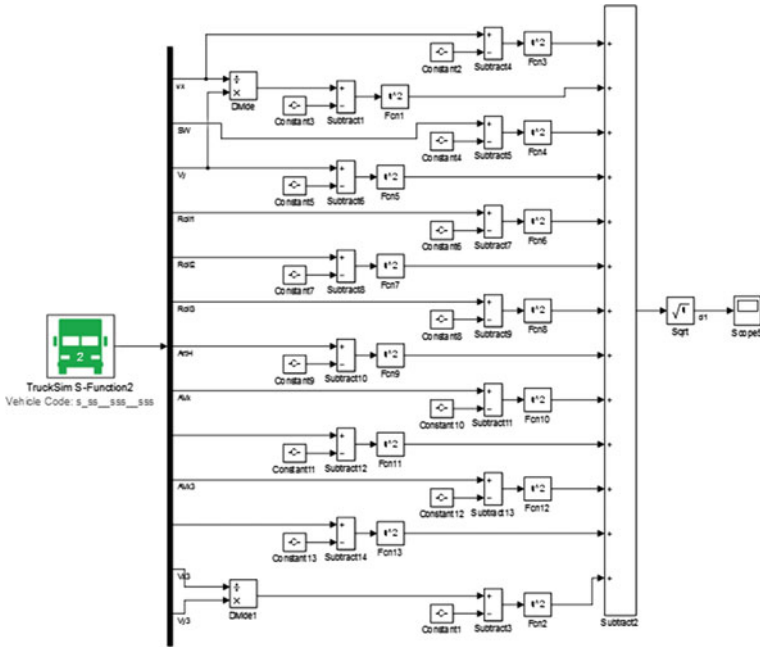
**Fig. 5** Part of co-simulation of TruckSim-Simulink platform diagram
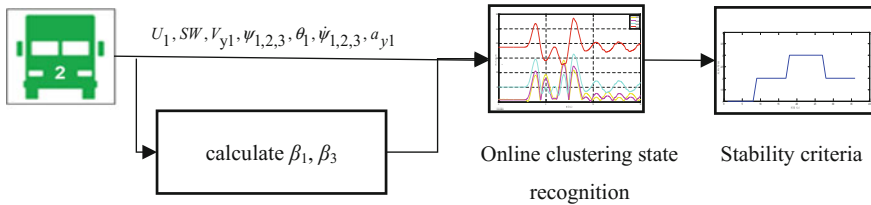


**Fig. 6** Online identification of vehicle driving stability diagram

becoming relatively stable within first and second hazard levels. And meanwhile the steering wheel is still rotating, it returns to 0 until 9.1 s. The above analysis shows that the double line change condition was mainly divided into 3 periods: (3.15, 4.62 s), (4.62, 7.725 s) and (7.725, 9.1 s). The first stage (3.15, 4.62 s) and the third stage (7.725, 9.1 s) have relative little effect on vehicle stability, and the second stage (4.62, 7.725 s) has a greater impact on vehicle stability.

Analyzing Figs. 8, 9 and 10, it shows that at the beginning of the straight-line driving phase, the side slip angle is zero. As steering wheel is turning at 3.125 s, the side slip angle is fluctuating. 4.62 s the side slip angle increases, the stability of the vehicle reached the second dangerous grade. At 4.75 s, the vehicle begins to produce a larger side slip angle and be accompanied by an increasing trend, indicating that the vehicle has occurred the more obvious side slip angle, driving stability is

**Fig. 7** Steering wheel angle at 62.5 km/h
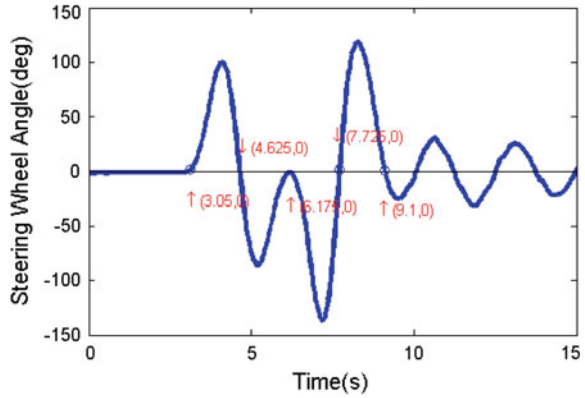


**Fig. 8** Online identification of Euclidean distance
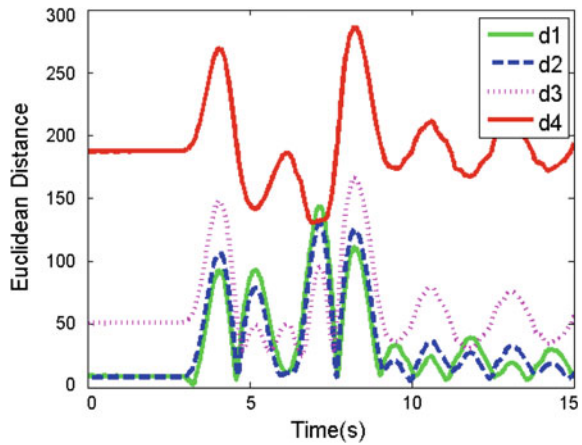


further reduced, then reduced to the third risk level. The more serious the degree of instability, the higher the risk level of the calculation result of the criterion, and further prove the validity of the stability criterion.

Double line change simulation of 50, 65 and 85 km/h is selected to verify the accuracy of the method from qualitative analysis and quantitative analysis. The change curve is shown in Fig. 11.

It can be seen from Fig. 11 that in the straight-line stage of the beginning, the stability of 50, 65, 85 km/h respectively belongs to the first, the second, the second hazard class. It can be obtained that with the increase of the vehicle speed, the lateral vibration of the B-double leads to the decrease of the linear stability of the vehicle [15].

For tracking of the specified path, the steering wheel is turning in advance with the increase of the speed, the vehicle is agile and high-risk level appears earlier, and when the vehicle speed is 85 km/h, the vehicle driving state will reach the most dangerous the fourth hazard level, followed by the early completion of the simulation

**Fig. 9** Online identification of vehicle hazard level
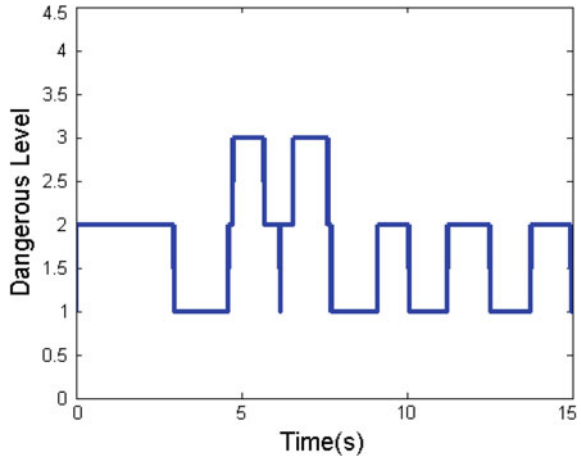


**Fig. 10** Side slip angle of tractor's mass center
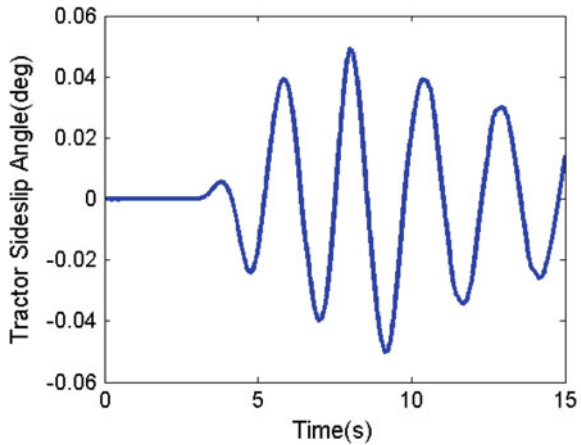


due to the vehicle instability, statistics of the proportion of the risk level shown in Table 3.

It can be seen from Table 3 that the proportion of the low-risk grade decreases with the increase of the vehicle speed, and the proportion of the high-hazard level gradually increases, which is consistent with the actual situation. And the correctness of the vehicle driving state determined by the clustering algorithm is explained.

In summary, the design of B-double in the lateral stability of the online identification system not only does it predicate the stability of vehicle lateral stability accurately according to the vehicle operating status data but also meets the real-time requirements of the system to achieve the initial aim of design.

**Fig. 11** Risk level change curve
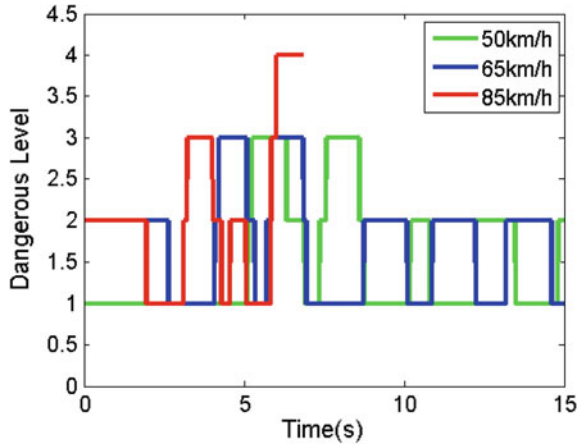


**Table 3** The proportion of dangerous levels under different speeds

| Dangerous level | 50 km/h (%) | 60 km/h (%) | 70 km/h (%) |
|---|---|---|---|
| 1 | 65.86 | 38.65 | 32.89 |
| 2 | 20.17 | 49.06 | 40.66 |
| 3 | 13.97 | 12.29 | 13.99 |
| 4 | 0 | 0 | 12.45 |

## 5  Summary and Conclusion

In this paper, a detailed study is made on the lateral handling stability judgment criterion of the B-double. The K-means clustering analysis method is used to classify the running state and obtain the off-line clustering centers according to the B-double's running data. Combining with the Euclidean distance of B-double's running data and clustering centers, the vehicle real-time stability judgment criterion is designed, and the co-simulation of TruckSim-Simulink platform is built to identify the B-double's stability online. The result shows that the criterion does divide the vehicle stability into four grades according to the vehicle driving state parameters, and the result of the classification is consistent with the actual vehicle risk condition. The judgment criterion provides the theoretical basis for the intervention timing and degree of the control system.

H. Liu et al.

# References

1. Zhuoping Yu, Bo L, Lu X et al (2015) Vehicle sideslip angle and yaw rate joint criterion for vehicle stability control. J Tongji Univ 43(12):1841–1849
2. Lu X (2015) Stability criterion for the vehicle under critical driving situation. J Mech Eng 51(10):103
3. Chen S (2014) Simulation analysis of rollover stability of semitrailer train. National University of Defense Technology
4. Mastinu G, Della Rossa F, Gobbi M et al (2017) Bifurcation analysis of a car model running on an even surface—a fundamental study for addressing autonomous vehicle dynamics. SAE Int J Veh Dyn Stab NVH 1(2):326–337, doi:https://doi.org/10.4271/2017-01-1589
5. Catino B, Santini S, Bernardo MD (2003) MCS adaptive control of vehicle dynamics: an application of bifurcation techniques to control system design. In: Decision and Control, 2003. Proceedings of IEEE conference on IEEE, 2003, 3:2252–2257
6. Sun T, Lee E, He Y (2016) Non-linear bifurcation stability analysis for articulated vehicles with active trailer differential braking systems. Differential Braking Systems 9(3)
7. Yang X (2012) Nonlinear dynamics and lateral stability of tractor semi-trailer vehicle. J Mech Eng 48(8):79
8. Prem H, Ramsay E, Pont J, McLean J, Woodrooffe J (2001) Comparison of modelling systems for performance-based assessments of heavy vehicles (performance based standards—NRTC/Austroads project A3 and A4), The National Road Transport Commission (NRTC), Working Paper
9. Sun T, He Y, Ren J (2013) Dynamics analysis of car-trailer systems with active trailer differential braking strategies. SAE Int J Passeng Cars—Mech Syst 7(1):73–85
10. van de Molengraft-Luijten MFJ, Besselink IJM, Verschuren RMAF et al (2012) Analysis of the lateral dynamic behavior of articulated commercial vehicles. Veh Syst Dyn 50(sup1):169–189
11. Wu C (2013) Stability analysis of a nonlinear vehicle model in plane motion using the concept of Lyapunov exponents. Veh Syst Dyn 51(6):906–924
12. Luo Y, Lai E (2014) A research on vehicle stability judgment based on energy method. Automot Eng 36(12):1534–1538
13. Mechanical Simulation Corporation (MSC). TruckSim 2016.1 Reference Manuals
14. Yang Y, Zhang Z (2006) Clustering method combining threshold algorithm with AntColony Algorithm. J Southwest Jiaotong University 41(6):719–722
15. Liu H, Xu H, Guan Z et al (2005) Study on shimmy of a semi-trailer combination vehicle driving on straight line. Automobile Technol 1:11–14

# The Research of Government Procurement Service System Design in Urban Public Transportation

Kun Yu, Zhaohui Zhong and Zhuo Wang

**Abstract**  Recent years, as with the cost increase of the fuel and social labor, the cost of urban public transportation enterprise is constantly rising. In addition to this, the expansion of the policy-oriented welfare to urban public transportation area by government, the decrease of enterprise income, leads to the sustainable development predicament of local urban city public transportation enterprise. Public transportation enterprise has highly relied on public transportation subsidies to maintain operation. Thus, the internal impetus driving of them is insufficient, the service level of which is lower than expected. Local government has carried out research on urban public transportation area procurement system. Although they have system design on operation cost programming, service quality evaluation, subsidies budget guarantee, the perspectiveness, systematicness, concertedness, fairness, operativeness and fineness of system needs to be improved. This thesis has considered the interaction and engagement of cost, ticket price, subsidies and service quality evaluation, designs public transportation area government procurement system comprehensively. It simulates the government procurement service system designing and policy releasing, improves the government offered public transportation service method, and fully mobilizes the initiative of operation cost control, service quality improvement, which finally enhances the fiscal subsidies efficiency. The total simulation is based on Qing Dao city.

**Keywords**  Government procurement system · System design · Urban public transportation · Subsidy method

K. Yu (✉)
China Academy of Transportation Sciences, No. 240 in Huixinli Street, Chaoyang 100029, Beijing, China
e-mail: 70713065@163.com

Z. Zhong
China Academy of Transportation Sciences, Chaoyang, China

Z. Wang
Dalian Institute of Science and Technology, Dalian, China

# 1 Introduction

As with the urban economic development, and the continuing growth of GDP, the fuel cost and manpower cost of the urban public transportation enterprise are constantly rising, Government has constantly offered benefits to public transportation. For example, senior people, soldiers, disabled people, are free of charge; General discount for students, IC card discount for citizens, and station transfer enjoys preferential discount. The constant expansion of urban public transportation area policy-oriented warfare and the continuing decrease of income of urban public transportation enterprise lead to the sustainable development predicament of local urban city public transportation enterprise. Public transportation enterprise has highly relied on public transportation subsidies to maintain operation. Thus, the internal impetus driving of them is insufficient, the service level of which is hard to improve.

Recent years, the State Council and National finance department has published "Instructions about procurement of service from government to social force", "Government procurement of service management stipulation" successively, in the latter, public transportation has been included into the fundamental service category of government procurement service instruction catalogue. On January 6 2016, Finance department and transportation department combined to publish "Instructions about propelling public transportation area government procurement service", to further figure out the specific requirements of urban public transportation area government procurement service. Local government has also researched on government procurement service system successively to solve the sustainable development of urban public transportation, enhance the efficiency of government subsidy, and improve the urban public transportation service level.

# 2 The Research of Local Government Procurement Service System in Urban Public Transportation

Central cities like Hangzhou, Guangzhou, and Shenzhen have incised in cost stipulation, developing reform on government provided public transportation service method in different degrees. They developed integrated design on public transportation area procurement service system, under full consideration of enterprises quantities, enterprise economic nature and current public transportation line operation modes, to publish proper cost management methods, subsidies system, and evaluation methods (Table 1).

Although relevant cities has practiced actively on propelling government procurement service system, according to "Government procurement of service management stipulation", and government procurement service real practice in London, and Singapore, the result has gap with government procurement system in terms of concept, method and goals. It also exists some problems in real practice, overall in the below serval perspectives. First, the imperfect of system and incomplete of policy results in

**Table 1** The design of local government procurement service system in urban public transportation

| ID | Name | Enterprise quantity | Enterprise economic nature | Line operation modes | The design of government procurement service system |
|---|---|---|---|---|---|
| 1 | Dalian | 5 | SE, PE | LINE | Published cost management method, subsidy method, service quality evaluation is researching |
| 2 | Kunming | 7 | SE, PE | LINE | Published quota subsidy method, cost management and new subsidy method is researching |
| 3 | Guangzhou | 13 | SE, PE, JC, FC | BIDDING | Published subsidy method |
| 4 | Hangzhou | 1 | SE | REGION | Published subsidy method and cost management |
| 5 | Ningbo | 6 | SE, PE | REGION | Region governments had published different subsidy methods |
| 6 | Chongqing | 1 | SE | REGION | Published special subsidy method |
| 7 | Nanchang | 1 | SE | EXCLUSIVE | Published cost management method |
| 8 | Zhuzhou | 1 | SE | EXCLUSIVE | Published subsidy method and cost management |
| 9 | Shenzhen | 3 | JC | FRANCHISE | Published subsidy method and cost management, etc. |
| 10 | Huzhou | 2 | PE | FRANCHISE | Published subsidy method, service quality evaluation |

**Enterprise economic nature**: SE—State-owned enterprise, PE—Private enterprise, JC—Joint-stock company, FC—Foreign company

**Line operation modes**: LINE—Public transportation enterprise operating in accordance with different lines, REGION—Public transportation enterprise operating in different regions, EXCLUSIVE—Only one public transportation enterprise exclusive operation, BIDDING—Public transportation enterprise operating lines by bidding management, FRANCHISE—Public transportation enterprise operating lines by franchise model

quantity and quality standards devoid of government procurement service. Second, the low correlation and delicacy of system have made them to insular. For example, the quality evaluation indicator has disjointed with operation cost evaluation, and the pricing cost is not unified with real cost. Third, the right and obligation of government and enterprise are vague. Fourth, most of the policy has not considered the reasonable repay which enterprise should gain in marketing trade relationship.

# 3  Urban Public Transportation Area Procurement Service System Design

## 3.1  System Design Frame

According to the fundamental concept and principle requirement of government procurement service by nation, and supported by big data, logistics network and other advanced technic application, based on the interaction and correlation between cost, ticket price, subsidies and evaluation, this thesis creates a set of correlation scheme and working system on operation service standard, operation service quality dynamic regulation, operation service quality evaluation, operation cost management stipulation, procurement service charge verification, and public transport ticket price adjustment, to constantly improve government public transportation service quality custody capability and the efficiency of subsidy, to ensure the sustainability of public transportation fundamental service, financial support, and enterprise development, which finally provides with satisfactory public transportation service and strong support to urban contracture and public transportation development (Fig. 1).



**Fig. 1**  The interaction between cost, ticket price, subsidies and evaluation
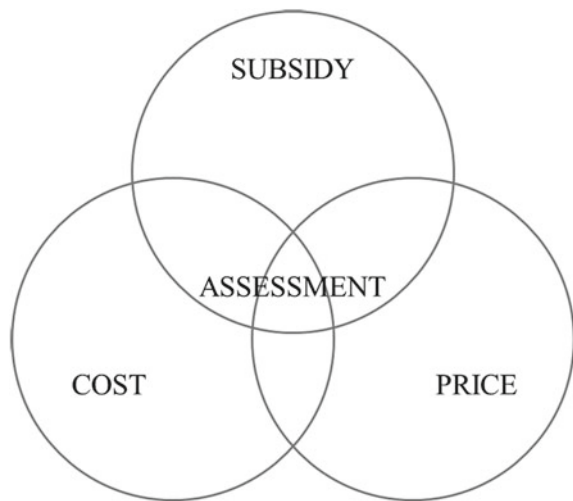
## 3.2 Main Research Contents

Base on the correlation between cost, ticket price, subsidies, and evaluation, this thesis researches a whole set of government procurement service system, which mainly includes, public transportation operation financial subsidies methods, cost management methods, service quality evaluation methods, and public transportation price management methods.

Public transportation operation financial subsidies methods: Based on the operation cost management methods, the operation cost, the actual income, and subsidy given to public transport enterprises should be assessed. According to the operation service quality evaluation methods, assess the completion of operation service plans agreed by public transportation enterprises, according to the assessment results to adjust the amount of subsidies, in the same, it should figure out the fund source and management process of subsidies clearly.

Public transportation operation cost management methods: It should be clearly included in the constitution of public transportation enterprise operation cost. For each item of operation cost budget and calculation standard, it should be regulated specifically. It also should suggest the main department and relevant working process.

Public transportation operation service quality evaluation methods: Based on the annual operation service plans as evaluation accordance, it evaluates on the service quality of public transportation enterprise. It shall regulate all items of evaluation method to confirm the effect of evaluation results to subsidies and path operation authority.

Public transportation price management methods: For urban public transportation price, it shall calculate based on labor cost, fuel cost, direct operation cost, social average salary, and citizen consuming index, to confirm the urban public transportation price index system and adjustment formula, to dynamically adjust the urban public transportation service price with the social cost and consuming ability.

## 3.3 Responsible Departments

The key of government procurement service system working is determined by the clear responsibilities of relevant government departments, strengthen the cooperative, active department coordination. This is the fundamental guarantee of the effective implementation of the system. The design of the government procurement service system design in urban public transportation is mainly related to the departments of finance, transportation and price.

Department of financial: Responsible for "Public transportation operation cost management methods", participate in "annual operation service plans", enhanced the amount of subsidy budget rigidity, strengthen the control of total subsidies, is conducive to maintaining fiscal sustainability.

Department of transportation: assessing the quality and quantity of public transportation enterprises operating service according to "annual operation service plans" and "public transportation operation service quality evaluation methods". It is an effective means to realize fine and standardized management.

Department of price: Responsible for "public transportation price management methods", participate in "public transportation operation cost management methods" with department of finance to achieve a reasonable calculation of operation cost, provide a scientific basis for the price adjustment of public transportation, and strengthen the persuasion of price adjustment.

## 4 Qingdao Government Procurement Service System in Urban Public Transportation

### 4.1 Overview of Qingdao Urban Transit

The public transit in central urban area of Qingdao is operated by three public transportation enterprises. There are 5122 busses in Qingdao in total in 2014, increasing by 3% comparing to year 2012. The financial subsidies provided by the city government is 1.538 billion yuan in 2014, increasing by 104% comparing to year 2012. In terms of passenger flow, the number is 0.836 billion in 2014, increasing by 3% comparing to year 2012. In conclusion, both the number of busses and financial subsidies has increased, while the passenger flow stays relatively the same, and the financial subsidies use efficiency is not high.

Since 2005, such policies were issued as "Assessment Approach for Public Transportation Operation Cost", "Review Approach for Policy-related Losses" in Qingdao, which clarified the range of financial subsidies for public transportation enterprises, and determined the review approach. Those policies helped government review the enterprises' losses and established a solid foundation for the public transit safeguard mechanism.

### 4.2 Issues in the Current Financial Subsidies System

First, the regulations are incomplete. The standards provided by the government are unclear and unspecific, which results in lack of reference when reviewing the funds use efficiency and service level. Second, both the operation cost management and financial subsidies are not accurate enough. The determination of labor cost, fuel cost, etc. are too simple to be fair enough. Third, the power and responsibility are not equal in two different levels of government. Currently, city government takes the full responsibility for all the public transit financial subsidies. Last, the subsidies are not provided in time. The implement strengths of financial subsidy system and regulation are not strong enough.

## 4.3 The Practices of Government Purchase of Services in Public Transit

According to the government purchase of services system and "Financial Affordability, Enterprise Sustainability, Public Affordability", targeting at the maximization of social and economic benefits for public facilities development supported by financial subsidies, learning from various practical experience of developing public transit both domestically and internationally, the research of "Assessment System of Financial Subsidies for Public Transit Cost" has been conducted, which emphasizes on supply methods for the optimization of public transit services and determines the regulation system consisting of the evaluations for the current public transit situation, algorithms for financial subsidies towards public transit operation, cost management methods, assessment methods for service level, operation service plans, etc.

## 5 Conclude

In this thesis, we considered the necessity of government procurement service system in urban public transportation, analyzed the existing problems in the current system, and researched a whole set design of government procurement service system. Based on the interaction and correlation between cost, ticket price, subsidies and evaluation, this thesis creates a set of correlation scheme and working system on operation service standard, operation service quality dynamic regulation, operation service quality evaluation, operation cost management stipulation, procurement service charge verification, and public transport ticket price adjustment, combined with the development of public transport and existing policy system in Qingdao, the research of "Assessment System of Financial Subsidies for Public Transit Cost" has been conducted, through publishing files and practice in Qingdao, which fully mobilizes the initiative of operation cost control, service quality improvement, improves the satisfaction of public transportation services continuously, increases the effectiveness of financial subsidies.

## References

1. State Council on the Guiding opinions of the Priority development of Urban Public Transport (2012) 64
2. General Office of the State Council Instructions about procurement of service from Government to Social force (2013) 96
3. Government procurement of service management stipulation (2014) 96

4.  Ministry of finance, Ministry of transport Guiding opinions on promoting government procurement of services in the field of transportation (2016) 34
5.  Provisions on the administration of urban bus and tram passenger transport (2017) 5
6.  Wang P et al (2010) A study on government purchasing public services from social organizations. Beijing University Press
7.  Zhao Y (2012) Analysis of the government purchasing social work service model. Soc Work

# Bicycle's Trajectory Prediction in Pedestrian-Bicycle Mixed Sections Based on Dynamic Bayesian Networks

**Hai-bo Wang, Xiao-yuan Wang, Ya-qi Liu, Dong Kong, Li-ping Liu and Chen Chen**

**Abstract**  Bicycle is the main factor that affects the traffic safety and the road capacity in pedestrian–bicycle sections of mixed traffic. It is important for implementing the bicycle safety warning and improving the active safety to predict bicycle trajectory in the mixed traffic environments under the condition of internet of things. The mutual influence of bicycle and its surrounding traffic participants in mixed pedestrian-bicycle sections was comprehensively analyzed and the phase of pedestrian-bicycle traffic was defined and reduced on the basis of phase field coupling theory. The experimental result shows that the model established in this paper has high accuracy and real-time performance, which provides the theoretical basis for the future research on the reduction of pedestrian-bicycle traffic conflicts and the construction of pedestrian-bicycle interactive security system.

**Keywords**  Phase field coupling · Pedestrian-bicycle mixed traffic · Trajectory prediction · Safety warning · Traffic phase

## 1 Introduction

The rapid development of automobile industry has caused car ownership to increase significantly. As a result, the motorway in many cities is constantly broadened, the slow traffic land for pedestrian and bicycle is squeezed gradually, and the conflict

H. Wang · X. Wang (✉) · Y. Liu · D. Kong · L. Liu · C. Chen
Institute of Intelligent Transportation, School of Transportation and Vehicle Engineering,
Shandong University of Technology, Zibo 255049, China
e-mail: wangxiaoyuan@sdut.edu.cn

X. Wang
State Key Laboratory of Automotive Safety and Energy, Tsinghua University,
Haidian Qu 100084, Beijing, China

H. Wang
College of Civil Aviation and Flight, Nanjing University of Aeronautics and Astronautics,
Nanjing 211106, China

between bicycle and pedestrian is becoming more and more serious. How to pre-dictably and dynamically predict the trajectory of bicycle in pedestrian-bicycle mixed environment is a core scientific issue which needs to be solved urgently.

Many scholars at home and abroad have conducted a significant amount of research on trajectory of moving object. A hybrid trajectory prediction method based on the location data was proposed by Jeung et al. [1], which was taken into account the motion patterns and motion functions of moving objects. The change of the geo-graphic coordinates of the trajectory is described by Mokhtar et al. [2] as a random process with several time parameters. Then, the temporal and spatial position of the moving object is checked in real time. The experimental results showing that it is reasonable to describe the uncertainty trajectory by uniform distribution. In order to solve the problem of the uncertainty trajectory of the moving object in the traffic net-work, Nodelman et al. [3] calculated the probability of the continuous position state change of the moving object by means of the time continuous Bayesian network, and finally the real-time prediction of the moving trajectory of the moving object was realized. Aiming at the problem of trajectory prediction of the moving objects in road network, on the basis of the massive trajectory information of the moving object, Markov adaptive trajectory prediction model, Gaussian nonlinear probability statis-tical model, and trajectory sequence prediction model of the continuous Bayesian network were established by Qiao et al. [4–6] for the trajectory prediction of mov-ing objects, respectively. Network-constrained moving objects dynamic trajectory R-Tree (NDTR-Tree) was proposed by Ding et al. [7]. The whole history trajectory of the moving object can be retrieved by using this index structure.

The recent studies on moving objects trajectory mainly focus on the trajectory pre-diction based on Euclidean space and constrained road network. There is no study on prediction of the trajectory aimed at the moving bicycle. And the study on prediction of bicycle trajectory in the pedestrian and bicycle mixed environment is also a blank. In view of this, trajectory of bicycle in pedestrian-bicycle mixed environment was studied in this paper. Pedestrian-bicycle mixed environment was divided and defined based on the phase field coupling theory. The trajectory prediction models of cyclists in different pedestrian-bicycle traffic phase were established with a large number of experimental data based on dynamic Bayesian network. The bicycle trajectory pre-diction model established in this paper not only has great significance for revealing the execution mechanism of bicycle in pedestrian-bicycle mixed environment but also can help to establish the pedestrian-bicycle traffic safety system.

## 2 Method

### 2.1 Definition of Pedestrian-Bicycle Traffic Phase

In this paper, the pedestrian-bicycle mixed section is divided into several virtual lanes according to traffic entity moving direction, as shown in Fig. 1. The interest-sensitive
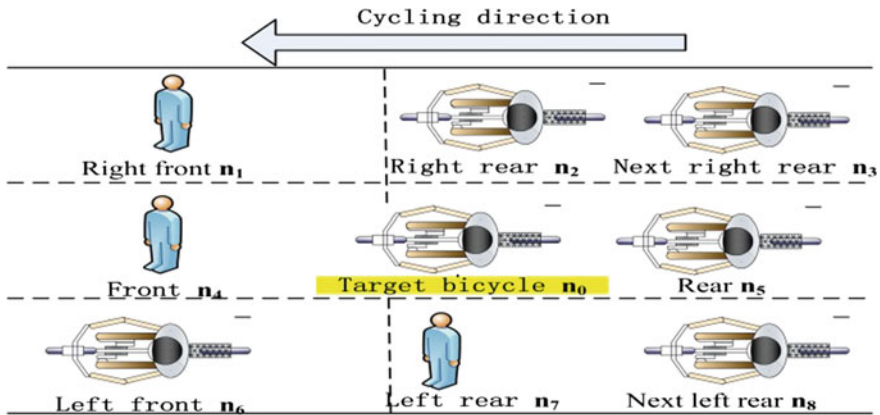
**Fig. 1** Diagram of traffic phase that the target bicycle and its cyclist located in the pedestrian-bicycle mixed sections

area of cyclist is divided into eight subareas including right front, right rear, next right rear, front, back, left front, left rear, and next left rear area with the location of front axle of target bicycle as the initial position.

## 2.2 Mathematical Expression of Pedestrian-Bicycle Traffic Phase

The form of fuzzy logic method is that carrying out approximate reasoning through using the linguistic variable. It is appropriate for describing the subjective judgment process of the cyclist movement [8]. The field intensity is calculated based on the fuzzy calculation method, and it described the attraction or repulsion interaction between the target bicycle and each traffic entity in the target cyclist's interest area. The effect size is used to describe field intensity in this paper, as shown in Table 1.

When the target bicycle is located in the middle area, as shown in Fig. 1, the pedestrian-bicycle traffic phase that the target bicycle and its cyclist $n_0$ can be

**Table 1** Effect size corresponding to different field strengths

| Field intensity | Strong repulsion field intensity $PE_1$ | Medium repulsion field intensity $PE_2$ | Weak repulsion field intensity $PE_3$ | Zero Z | Weak attraction field intensity $NE_1$ | Medium attraction field intensity $NE_2$ | Strong attraction field intensity $NE_3$ |
|---|---|---|---|---|---|---|---|
| Effect size | $[-1, -0.8)$ | $[-0.8, -0.4)$ | $[-0.4, 0)$ | 0 | $(0, 0.3]$ | $(0.3, 0.7]$ | $(0.7, 1]$ |
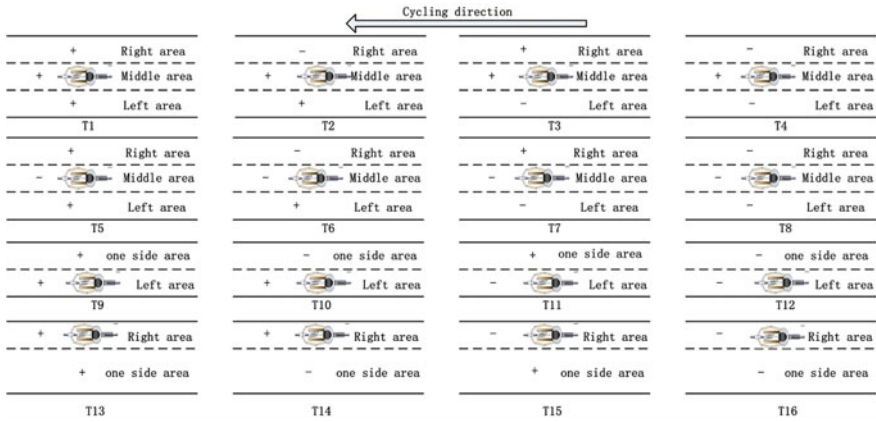
**Fig. 2** Simple pedestrian-bicycle traffic phase

expressed by $E_{n_0}^0 = $ [left front effect field, left rear effect field, next left rear effect field, front effect field strength, rear effect field, right front effect field, right rear effect field, and next right rear effect field] $= [E_{n_0}^{zq}, E_{n_0}^{zh}, E_{n_0}^{zch}, E_{n_0}^{q}, E_{n_0}^{h}, E_{n_0}^{yq}, E_{n_0}^{yh}, E_{n_0}^{ych}]$. When the target bicycle is located on the left or right area of pedestrian-bicycle mixed traffic sections, the derivation process of the pedestrian-bicycle traffic phase is similar with the situation that the target bicycle located in the middle area.

## 2.3 Simplification of Complex Pedestrian-Bicycle Traffic Phase

The intensity of repulsion and attraction field using fuzzy logic are denoted as "−" and "+" respectively. In summary, the complex pedestrian-bicycle traffic phase can be reduced to 16 types, as shown in Fig. 2.

## 2.4 Prediction Model of Bicycle Trajectory Based on Dynamic Bayesian Network

Developing static Bayesian network as time passing, the dynamic Bayesian network with $T$ time slices can be obtained [9, 10]. The dynamic Bayesian network inference can be expressed as follows:
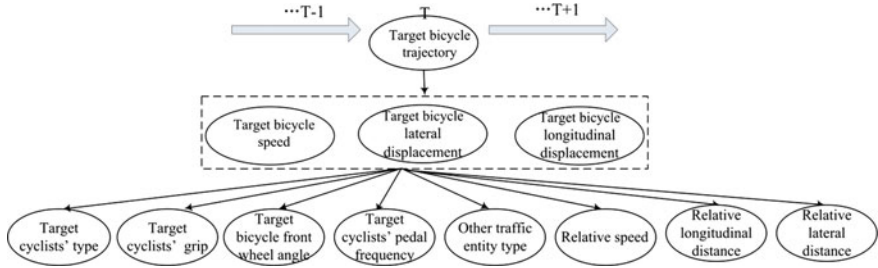
Fig. 3 Dynamic Bayesian network structure diagram
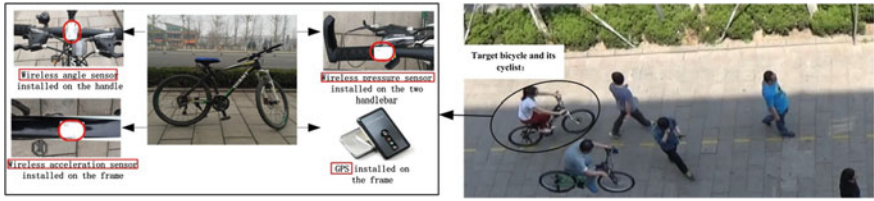


Fig. 4 Comprehensive information dynamic acquisition system of bicycle and its cyclist

$$
\left\{
\begin{aligned}
&P(x_{11}, x_{12}, \ldots, x_{1n}, \ldots, x_{T1}, \cdots, x_{Tn} | y_{110}, y_{120}, \ldots, y_{1m0}, \ldots, y_{T10}, \ldots, y_{Tm0}) = \\
&\sum_{y_{11} y_{12} \ldots y_{1m} \ldots y_{T1} \ldots y_{Tm}} \frac{\prod_{i,j} P(y_{ij}|\pi(Y_{ij})) \prod_{i,k} P(x_{ik}|\pi(X_{ik}))}{\sum_{x_{11} x_{12} \ldots x_{1n} \ldots x_{T1} \ldots x_{Tn}} \prod_{i,j} P(y_{ij}|\pi(Y_{ij})) \prod_{i,k} P(x_{ik}|\pi(X_{ik}))} \prod_{i,j} P(Y_{ij0} = y_{ij}) \quad (1) \\
&(i = 1, 2, \ldots, T; j = 1, 2, \ldots, m; k = 1, 2, \ldots, n)
\end{aligned}
\right.
$$

where $x_{ij}$ is a valued state of hidden variable $X_{ij}$. $y_{ij}$ is the value of observed variable of $Y_{ij}$. $\pi(Y_{ij})$ is the parent node set of $Y_{ij}$. $Y_{ij0}$ is the observed state of $Y_{ij}$, with the observed node $j$ in the time slice $i$.

### 2.4.1 Establishment of the Model

The dynamic Bayesian network model can be constructed by the causal relationship between the variables [9]. As shown in Fig. 3.

### 2.4.2 Data Acquisition and Processing

(1) Experimental installation

In the urban pedestrian-bicycle mixed sections, comprehensive information dynamic acquisition system of bicycle and its cyclist (as shown in Fig. 4) were used to collect and process the experimental data.

**Fig. 5** Experimental route

**Table 2** Test results of cyclist's psychological questionnaire

| Cyclist type | Conservative | Steady | Radical |
|---|---|---|---|
| Real scene test results (number of people) | 24 | 46 | 30 |

(2)  Experimental location and road conditions

The Huaguang road was elected as the experimental section, as shown in Fig. 5.

(3)  Experimental object

The results of the questionnaire test on 100 cyclists' psychological surveys are shown in Table 2.

This study was approved by the local institutional review board and written informed consent was obtained from all participant.

(4)  Data analysis

The experimental data is shown in Table 3.

## 3  Results

### 3.1  Model Calibration

The set of basic variable states in the dynamic Bayesian network model is shown in Table 4.

**Table 3** Experimental data

| Data | | Symbol | Data | | Symbol | Data | | Symbol |
|---|---|---|---|---|---|---|---|---|
| Vertical spacing between traffic entities and target bicycle RD (m) | Right front | $RD_1$ | Horizontal distance between traffic entities and target bicycle RS (m) | Right front | $RS_1$ | Relative speed between traffic entities and target bicycle RV (m) | Right front | $RV_1$ |
| | Right rear | $RD_2$ | | Right rear | $RS_2$ | | Right rear | $RV_2$ |
| | Next right rear | $RD_3$ | | Next right rear | $RS_3$ | | Next right rear | $RV_3$ |
| | Front | $RD_4$ | | Front | $RS_4$ | | Front | $RV_4$ |
| | Rear | $RD_5$ | | Rear | $RS_5$ | | Rear | $RV_5$ |
| | Left front | $RD_6$ | | Left front | $RS_6$ | | Left front | $RV_6$ |
| | Left rear | $RD_7$ | | Left rear | $RS_7$ | | Left rear | $RV_7$ |
| | Next left rear | $RD_8$ | | Next left rear | $RS_8$ | | Next left rear | $RV_8$ |
| Target bicycle front wheel steering angle (°) | | FA | Pedal frequency(circle/min) | | CP | Brake strength (N) | | CL |

**Table 4**  Set of variables

| Variable | State set |
|---|---|
| The type of target cyclist CT | Conservative type, steady type, radical type |
| Target bicycle front wheel angle FA | Large, medium, small |
| Target cyclists' grip CL | Large, medium, small |
| Target cyclist pedal frequency CP | Large, medium, small |
| The type traffic entity ET | Pedestrian, bicycle |
| Vertical spacing between traffic entities and target bicycle RD | Far, medium, near |
| The horizontal distance between traffic entities and target bicycle RS | Far, medium, near |
| The relative speed between traffic entities and target bicycle RV | Fast, medium, slow |

**Table 5**  State transition probability of dynamic Bayesian networks

| Trajectory (at time $t$) | $P(t + 1\text{time bicycle trajectory}|t\text{time bicycle trajectory})$ | |
|---|---|---|
| | Change | Constant |
| Change | 0.65 | 0.35 |
| Constant | 0.16 | 0.84 |

## 3.2  Model Solution

Different types of cyclists in different pedestrian-bicycle traffic phase have different effects on the transfer probability of the bicycle trajectory state. Therefore, the state transition probability table of the dynamic Bayesian network is given only in the case of radical cyclists in the pedestrian-bicycle traffic phase $T_1$. As shown in Table 5.

## 4  Discussion

### 4.1  Simulation Verification

Due to limited space, the simulation verification included only the lateral displacement of the different types of cyclists who operated the bicycle. The verification results are shown in Fig. 6.

Based on the above results, it is shown that the simulation results of the bicycle trajectory prediction model had good consistency with the actual situation in the pedestrian-bicycle mixed traffic environments, so the target trajectory can be predicted accurately in pedestrian-bicycle sections of mixed traffic.
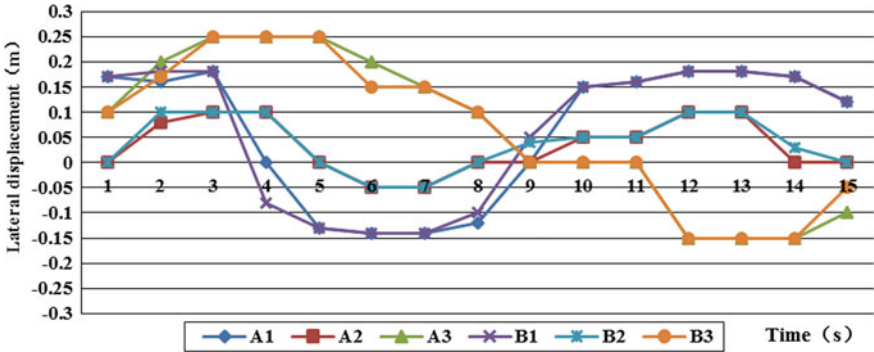
**Fig. 6** Comparison chart between simulation value and actual value of target cyclist's Lateral displacement. *Note* A1—Steady cyclists' actual value, A2—Conservative cyclists' actual value, A3—Radical cyclists' actual value, B1—Steady cyclists' simulation value, B2—Conservative cyclists' simulation value, B3—Radical cyclists' actual value

## 5 Conclusions

The real-time prediction of the bicycle trajectory is very important for revealing the execution mechanism of the bicycle accurately and enhancing the traffic safety in pedestrian-bicycle sections. In this paper, the complex pedestrian-bicycle mixed environment is defined based on the theory of phase field coupling (pedestrian-bicycle traffic phase). Furthermore, dynamic Bayesian network is used to predict bicycle trajectory of different types of cyclists in the pedestrian-bicycle traffic phase. The experimental results show that bicycle trajectory is predicted based on the dynamic Bayesian network in pedestrian-bicycle mixed environment can effectively avoid the conflict between bicycle and other traffic entities, and the execution mechanism of bicycles can be revealed more precisely, which provide a strong guarantee for studying the pedestrian-bicycle coordination, timely warning and improving active safety of pedestrian and bicycle.

# References

1. Jeung H, Liu Q, Shen HT, Zhou X A hybrid prediction model for moving objects. In: Proceedings of the 24th international conference on data engineering. IEEE Computer Society, Washington
2. Mokhtar H, Su J (2004) Universal trajectory queries for moving object databases. In: IEEE international conference on mobile data management, pp 133–144
3. Nodelman U, Shelton CR, Koller D (2003) Learning continuous time Bayesian networks. In: Proceedings of the 19th international conference on uncertainty in artificial intelligence, pp 451–458
4. Qiao S, Shen D, Wang X, Han N, Zhu W (2015) A self-adaptive parameter selection trajectory prediction approach via hidden Markov models. IEEE Trans Intell Transp Syst 16(1):284–296
5. Qiao S, Jin K, Han N, Tang C, Gesangduoji LA (2015) Trajectory prediction algorithm based on Gaussian mixture mode. J Softw 26(5):1048–1063
6. Qiao S, Tang C, Jin H, Long T, Dai S, Ku Y, Chau M (2010) PutMode: prediction of uncertain trajectories in moving objects databases. Appl Intell 33(3):370–386
7. Ding Z, Li X, Yu B (2009) Indexing the historical, current, and future locations of network-constrained moving objects. J Softw 12:3193–3204
8. Wang X, Zhang J, Ban X, Gao S (2013) Study on transformation mechanism of driver's propensity under two-lane conditions. Appl Mech Mater 411–414:1911–1918
9. Karami AH, Hasanzadeh M (2015) An adaptive genetic algorithm for robot motion planning in 2D complex environments. Comput Electr Eng 43(4):317–329
10. Rose C, Smaili C (2005) A dynamic Bayesian network for handling uncertainty in a decision support system adapted to the monitoring of patients treated by hemodialysis. In: Proceedings of the 17th IEEE international conference on tools with artificial intelligence

# Analysis and Optimization Research of Beijing's Quantity Control Policies on Motor Vehicles

**Yue-jun Liu, Tao Gu and Ling Zhou**

**Abstract**  In the process of urban motorization, due to scarce urban resources and limited environmental supporting capacity, most cities can only pursue intensive development instead of excessive development of sedan cars. As a result, major cities around the world have adopted various means to control the total quantity of motor vehicles so as to control the growth and use of motor vehicles, for the purpose of promoting the healthy development of urban motorization. This article has carefully analyzed implementation of Beijing's quantity control policies on motor vehicles, systematically summarized experience of foreign and domestic cities in formulating such control policies, and put forward a direction for the development of Beijing's quantity control policies on motor vehicles.

**Keywords**  Motor vehicles · Sedans · Quantity control · Economic means

The running and parking of motor vehicles require a large amount of land resources. Different cities may have worked out different ways to respond to motor vehicle development, owing to diversities in social and economic development as well as in national situation and geographic conditions. Typical Asian cities, represented by Beijing, Shanghai and Guangzhou in our country, basically have a large population and huge travel demand. However, small urban road area leads to small road capacities, and low transit trip ratios cause prominent contradictions between traffic demand and supply. Therefore, urban roads can only bear relatively low vehicle parc, and many cities have implemented restrictions on vehicle purchase.

Y. Liu (✉) · T. Gu · L. Zhou
Beijing Municipality Key Laboratory of Urban Traffic Operation Simulation and Decision Support, Beijing Transport Institute, Chaoyang 100073, Beijing, China
e-mail: liuyuejun002@126.com

# 1   Analysis of Beijing's Quantity Control Policies on Motor Vehicles

## 1.1   Background of Implementation

Since 2005, the three major problems named "high-speed growth, high-intensity use and high-density concentration" of sedan cars confronting Beijing have become increasingly prominent [1]. Especially in 2010, Beijing's vehicle parc had a net increase of 800,000, which caused severe traffic problems. Traffic congestion in morning and evening rush hours had become the norm and converted from node congestion to regional congestion. At such growth rate, if no effective measures were taken at that time, Beijing's vehicle parc might have exceeded 6 million by 2012, and TPI of Beijing's central city might have been over 9.5 with average traffic speed of road network within the 5th ring roads less than 15 km/h. For this reason, Beijing municipal government issued the *Opinions of Beijing Municipality on Further Promoting Scientific Development of Capital Transport and Mitigating Traffic Congestion* ("28 measures for reducing congestion") [2] on December 23, 2010, and quantity control policies on sedan parc have been enacted at the right time.

## 1.2   Development History of Policies

Since 2011, Beijing has fully implemented quantity control measures for sedans. In order to cope with problems and contradictions arising in the implementation of sedan quantity control policies and further control sedan quantity, Beijing has made adjustments to sedan quantity control policies between 2011 and 2017. In 2012, adjustments were made to determine that unused over index shall return to the lottery pool, stipulate distribution index, update validity period of new index application, and allow newly registered enterprises to participate in license plate lottery. In 2014, demonstration model using new energy configuration was added to encourage the development of new energy sedans, and meanwhile, stepwise odds of winning for personal lottery applicants was set. In 2016, further adjustments were made to rules for stepwise odds of winning, and new energy waiting rules were issued [3].

## 1.3   Results of Implementation

Since Beijing implemented control policies on sedans, the high-speed growth of sedans has been effectively curbed, winning valuable time for study and implementation of new transport policies as well as adjustments to and perfection of urban transport planning. The implementations of quantity control policies have effec-
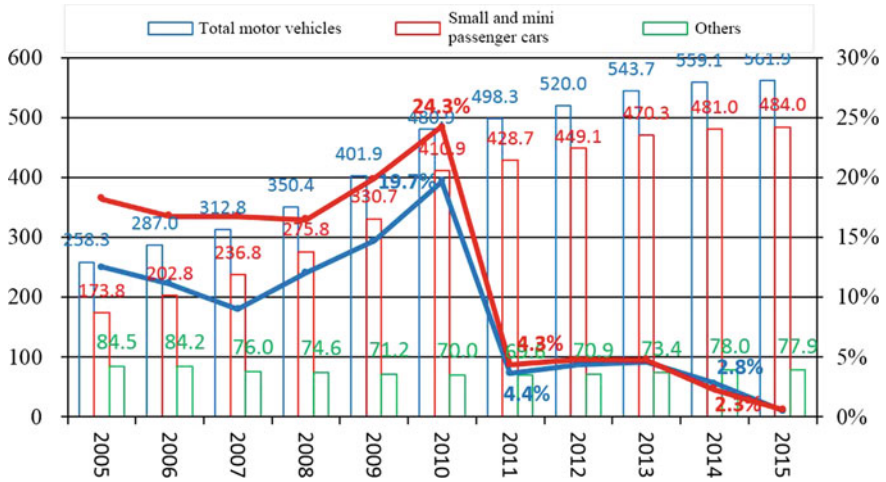
**Fig. 1** Growth of motor vehicles in Beijing in recent decade

tively restrained the rapid growth of motor vehicles. As a result, the growth of motor vehicles has significantly slowed down (Fig. 1).

As of the end of 2011, Beijing's vehicle parc has reached 4.983 million, with a net YOY increase of 3.6% (173,000 motor vehicles); Beijing's private car parc has reached 3.717 million, with a net YOY increase of 4.2% (151,000 private sedans), reaching a new low since 2000. Since new sedan control policies were carried out in 2014, the annual sedan growth has been further limited to within 150,000 vehicles, and the motor vehicle growth rate has been further reduced to 2.8%.

It can be seen from the growth of motor vehicles and small and mini passenger cars in recent decade that the rising trend of motor vehicles highly coincides with that of small and mini passenger cars, while the parc of other motor vehicles basically remain in balance, indicating that sedan control policies have effectively restrained growth rate of motor vehicles in Beijing through sedan control measures.

## 1.4 Pressure

The implementation of sedan quantity control policies in Beijing has effectively curbed the rapid growth of motor vehicles in the city, easing traffic congestion in Beijing's central city to some extent and achieving the desired results. Nonetheless, vehicle parc is still on the rise despite the control policies. The policies' impact of improving traffic will gradually weaken, and traffic congestion in the central city will become more serious. In addition, with constantly accumulated demand for car purchase, applicants who are in urgent need of buying cars but repeatedly fail to obtain the coding in the lottery will inevitably feel dissatisfied. They may even
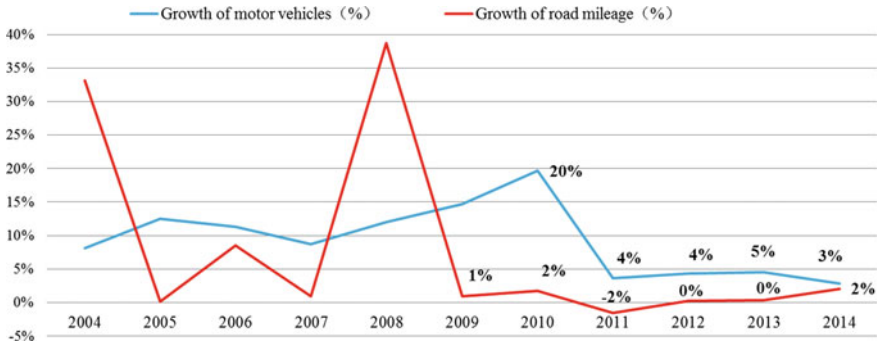
**Fig. 2** Comparison of growth rates of motor vehicles and road mileage in Beijing from 2004 to 2014

question the fairness and equity of control policies, impairing the understanding and support of the society towards the control policies. The pressure confronting government in implementing the control policies can be divided into pressure on traffic system, pressure on natural environment and pressure on society.

### 1.4.1 Pressure on Traffic System

The issue of high-speed growth of motor vehicles has not been solved in spite of the relatively slower growth rate. Although at present high-speed growth of motor vehicles has been curbed, the growth rate is still much larger than that of urban road mileage (<1%). Given the large base figure, if we assume Beijing has an annual growth of 240,000 motor vehicles, the city has to witness a rise of nearly 1 million vehicles for four years; with the deepening of control policies, the annual increment, currently restrained to 150,000 vehicles, is still much higher than the growth rate of urban road mileage; besides, given that new energy vehicles are not bound by purchase quota policy, the traffic system is still faced with increasing pressure (Fig. 2).

Issues of "high-intensity use and high-density concentration" are still not truly alleviated. Beijing's traffic is deeply trapped in the three "high" issues. Although high-speed growth is to some extent eased, the issues of "high-intensity use and high-density concentration" of sedan cars are not truly alleviated. In 2011, Beijing had a net increase of 174,000 motor vehicles, which were mainly distributed in the central city; even with the existing control policies, the quantity of motor vehicles in the central city will continue to rise in the future, meaning Beijing's traffic system will be confronted with severer situation. The vehicle parcs of Dongcheng District and Xicheng District are much higher than that of other districts and will continued to raise under the current control policies.

### 1.4.2 Pressure on Environment

The analysis of the source apportionment of PM2.5 conducted by Beijing Municipal Environmental Protection Bureau indicates that: The four major sources of PM2.5 in Beijing are motor vehicles, coal burning, industrial production and dust. Herein, regional transport and local discharge are respectively responsible for about 28–36% and 64–72% of total PM2.5 emission, and motor vehicles are responsible for 31.1% of PM2.5 discharged locally [4]. In spite of the implementation of quantity control over motor vehicles, the total vehicle quantity is still increasing, and the environmental pressure caused by motor vehicles is still a huge challenge.

### 1.4.3 Pressure of Society

The applicants repeatedly fail to win the change to buy cars and the odds of winning are getting lower and lower. As of June, 2016, the odds of winning for ordinary sedan index application in Beijing have hit a record low, being only 0.138%. In addition, according to statistics of Beijing Municipal Bureau for Transport Administration, Beijing has a monthly increase of 50,000 individuals holding driving licenses, far beyond the current monthly quota for sedans. The number of possible car buyers is rising, leading to greater pressure on license plate lottery.

It is hard to meet the rigid demand of special groups. As the number of applicants rises, the odds of winning continuously drop. The rigid demands of families that have just become wealthy, or have persons with disabilities, pregnant women or seriously ill patients while having no sedan at all cannot be satisfied, leading to complaints about the inhumane sedan control policies.

Successful applicants do not buy cars or sell or rent the index out. On the one hand, although some people with irrational demands have drawn the lucky number, they have no plan to buy cars, which leads to unused overdue index and even black market operation, further causing social contradictions and arousing attention of the society. On the other hand, a large number of people who are not anxious to buy cars apply to participate in the license plate lottery to have a try. Such behaviors have occupied public social resources and reduced the odds of winning of other applicants.

## 2 Analysis of Quantity Control Policies on Motor Vehicles in Other International and Domestic Cities

Currently, two major measures are taken to control the quantity of motor vehicles in and abroad. First is purchase restriction and second is use restriction. At present, cities in European and American countries, represented by London, tend to emphasize and adopt comprehensive measures in reducing car use. By contrast, cities in Asian

countries, represented by Beijing, Shanghai, Guangzhou, Tianjin and Tokyo, mainly adopt comprehensive measures of car purchase restriction and car use restriction [5].

## 2.1  Implementation of Quantity Control Policies on Motor Vehicles in Other Domestic Cities

### 2.1.1  Shanghai: Plate Bidding System

Since 1994, Shanghai has been the first to auction the new quota for passenger cars and put private car license plates up for nonpublic auction with reserve prices. After car buyers win the auction, they can go to vehicle administration office to apply for vehicle licenses and they have the right to use motor vehicles in Shanghai's central city (areas within the outer-ring roads). The system of open auction has played an important role in controlling growth rate of motor vehicles. Now the average price of license plates is up to RMB89,000 and remains an upward trend.

### 2.1.2  Guangzhou: License Plate Lottery + Plate Bidding System

Since August, 2012, Guangzhou has adopted a model of "paid auction + unpaid lottery" to distribute incremental quota for medium and small passenger cars. After a one-year trial period, "license plate restrictions" was officially issued with a validity period of five years. As per the restrictions, the stipulated incremental quota for medium and small passenger cars in Guangzhou is 10,000 vehicles per month, and will be distributed to "unpaid lottery" for new energy vehicles, "unpaid lottery" for ordinary vehicles and "paid auction" in a proportion of 1:5:4. To be more specific, 10% of incremental quota goes to "unpaid lottery" for new energy vehicles; 50% goes to "unpaid lottery" for ordinary vehicles; 40% goes to "paid auction".

### 2.1.3  Tianjin: License Plate Lottery

Since 0:00 on December 16, 2013, Tianjin municipal government has started management of the whole city's incremental quota for sedan cars, and its distribution model is similar to that of Guangzhou. The stipulated incremental quota for small passenger cars is 9,000 vehicles per month, and the quota will be distributed to "unpaid lottery" for new energy vehicles, "unpaid lottery" for ordinary vehicles and "paid auction" in a proportion of 1:5:4. To be more specific, 10% of incremental quota goes to "unpaid lottery" for new energy vehicles; 50% goes to "unpaid lottery" for ordinary vehicles; 40% goes to "paid auction".

## 2.2 Experience of Other International Cities in Quantity Control Policies on Motor Vehicles

In the process of urbanization and motorization, due to scarce urban resources and limited environmental supporting capacity, it is impossible for most cities to overdevelop sedan cars. Major cities around the world have adopted various means to control the total quantity of motor vehicles so as to curb the growth and use of motor vehicles, for the sake of healthy development of urbanization and motorization.

### 2.2.1 Strictly Control Growth Rate of Motor Vehicles in the Light of Capacities of Land and Roads in Urban Areas

(1)  Hong Kong

Hong Kong has a large population (7.1 million) with relatively little land (1104 $km^2$). Given the rigid restrictions of land resources, growth of motor vehicles has all along been under strict control. Since the transport strategy of vigorously developing rail transit and limiting the use of private cars was determined in 1970s, Hong Kong has taken a series of measures year by year, such as raising first registration tax and license tax for private cars, doubling charge of using subsea tunnel and working out stricter annual vehicle inspection and TDM policy. These measures have strictly controlled growth rate of motor vehicles, achieving an average annual growth rate of vehicle parc of only 2% [6].

(2)  Singapore

Singapore has a total land area of 710 $km^2$ and a population of 5.2 million. In order to alleviate traffic congestion and improve traffic operation efficiency, the government of Singapore has adopted the means of managing private traffic demand and taken a series of measures, such as motor vehicle quota system, additional registration fees, consumption tax, highway tax, road toll, and area licensing scheme to restrict the growth of vehicle parc. Once the growth rate of motor vehicles exceeds the support capacity of traffic, new traffic policies will be issued to further strengthen the control. Particularly, the government has implemented motor vehicle quota system to limit the number of marketable and registrable cars, keeping the annual growth of motor vehicles within 1.5%.

### 2.2.2 Control Demand by Economic Means and Control Space-Time Distribution of Motor Vehicles by Fine Means

When major cities around the world tackle the reckless growth of motor vehicles arising in the process of urbanization, except adopting strict administrative means when necessary, most of the time they would make use of such means like motor

vehicle purchase tax and parking permit to raise the threshold of owing sedan cars, and lift the cost of car use though area licensing scheme, such as congestion charge and low emission zone.

(1)   Congestion Charge

Stockholm started to put the policy of congestion charge into trial use in July, 2005. Congestion charge has greatly improved the accessibility of Stockholm's central city and dramatically reduced travel time. Particularly, the delay time for roads connecting the central city and the suburb has been shortened by one third in morning peak hours and by one second in nonpeak hours. The reduction in motor vehicle flow in the central city has obviously improved air quality and reduced $CO_2$ emission by 14%. What's more, public health, traffic safety and urban environment have had remarkable improvement as well.

(2)   Low Emission Zone

On February 4, 2008, in order to alleviate air pollution caused by traffic, London launched the plan of "low emission zone". In the case of any lorry that weighs over 12 tons with its emission failing to reach Euro III Emission Standard, the driver shall pay an emission charge of 200 lb, and violators will be fined 1000 lb. In the meantime, with the deepened influence of the policies, the objects and standards of restrictions of low emission zones will be constantly adjusted and updated. Since 2006, there have been over 10 countries and over 100 cities implementing the policy of "low emission zone" in Europe.

(3)   Parking Management

Parking management is a fine regional control means universally adopted by major cities around the world. To take Japan as an example, Japan issued the Parking Law in 1962, explicitly stating that the owners of sedan cars (excluding small passenger cars with displacement below 550 CC) must have night parking spaces when registering sedans; otherwise, they are not allowed to buy them. In case the owner of a motor vehicle changes address or change parking address of the motor vehicle, he or she must go to the public security organ for registration. There are two kinds of night parking permit: free and long-lease night parking permits. The parking space must be less than 2000 m away from the owner's unit or house. Meanwhile, the owner must post the mark of the parking permit on the rear windshield for the convenience of supervision. As the free curb parking was banned, the holding cost of car owners has sharply increased, which effectively controls vehicle growth in central city of major cities.

### 2.2.3   Encourage Small-Displacement Vehicles and New Energy Vehicles

Gradually increase the proportion of small-displacement vehicles in the process of quantity control, and at the same time, some cities will consider including the index

of low emission vehicles and new energy vehicles (such as zero-emission civilian all-electric sedans) in a separate quota system, so as to encourage low emission. Singapore has started to implement VQS since May, 1990 [7]. In the vehicle quota bidding system, the quotas for low emission cars and high emission cars shall be distributed in a proportion of 2:1. Each year, the quota for small emission sedan cars (below 1600 CC) makes up two-thirds of the total quota.

### 2.2.4 Change the Concept of Car Use and Improve Green Travel Facilities

Major cities around the world pay attention to changing the concept of car use and improving green travel facilities while implementing quantity control over motor vehicles. Copenhagen was a city dominated by sedan cars. Since 1960s and 1970s, local government has started to establish regional cycleway network. The city has all along had a tradition of using bicycles, making it a well-known "cycling city" [8]. Over 40% citizens choose to cycle to work and they persist in using bicycles even in bad weather such as rainy or snowy days. In 2006, the government of New York reconstructed the Times Square by turning the original motorway into a new public square. The reconstruction has increased business opportunities, improved pedestrian safety, beautified the open space and purified the air [9].

## 3   Conclusion and Suggestions

As a megacity, Beijing has to follow an intensive, sustainable development road in its process of urbanization, so it must take rational measures to control its motorization. Take into account the situation and pressure confronting Beijing's existing quantity control policies on motor vehicles, efforts shall be made in the following two aspects to further improve and optimize the quantity control policies on motor vehicles: On the one hand, Beijing shall stick to objective laws of metropolises to lower the growth rate of sedans step by step. On the other hand, Beijing shall start with guidance on demands, strive to improve relevant supporting measures, adopt price lever, and market mechanisms to reasonably lead irrational demand, so as to gradually reduce the force of administration. In this way, the quantity of motor vehicles will transition from high growth to low growth and eventually to zero growth; vehicle emission will transition from high emission to low emission and eventually to zero emission; the control measures for motor vehicles will transition from administrative means to fine economic means.

# References

1. Guo J, Liu Y, Yu L (2011) Traffic congestion in large metropolitan area in China. Urban Transport of China (02)
2. Opinions of the People's Government of Beijing Municipality on Further Promoting Scientific Development of Capital Transport and Mitigating Traffic Congestion: http://zhengwu.beijing.gov.cn/gzdt/gggs/t1145922.htm
3. Detailed Rules for the Implementation of the Interim Provisions on Quantity Control for Small Passenger Cars in Beijing (2013 Revision): http://www.bjhjyd.gov.cn/bszn/20131128/1385625116338_1.html
4. Beijing Municipality Officially Releasing Research Results of Source Apportionment of PM2.5: http://www.bjepb.gov.cn/bjepb/323265/340674/396253/index.html
5. Zhao Y, Su K, Zeng J (2013) Comparison of Beijing, Shanghai and Guangzhou's new control management policies on motor vehicles. Sci Technol Innov Herald (12)
6. Zhen X (2010) Experience and Inspiration from Singapore and Hong Kong's management of private cars. China Transp Rev (05)
7. Luo Z (2009) Singapore travel demand management: key strategies & characteristics. Urban Transp China (06)
8. Wang Y (2015) Study on development strategy for urban green transport development. Chang-an University
9. Lu X (2013) Enlightenment from transformation and green development of New York for Beijing. Urban Insight (01)

# Analysis of the Influence of Urban Road Traffic Flow Parameters on the Acoustic Environment

**Weidong Liu, Xingquan Guan, Yan Xing, Jinling Wang and Wei Cai**

**Abstract**  On the basis of measuring the traffic noise data of Shenyang urban sub road in Shenyang, this paper starts with the speed and traffic flow, analyzes the data by SPSS statistical analysis software, and uses linear fitting, statistical analysis and other methods. The two factors were analyzed, and the conclusions were drawn: First, the traffic noise and speed are approximately linear in a certain speed range, that is to say, the noise value increases with the increase of the speed of the vehicle. Second, the logarithmic positive correlation between traffic flow and traffic noise is that, with the increase of flow rate, the noise value at the initial stage increased significantly. Then when traffic reaches to a certain number, the increasing trend is not very obvious. And the road traffic noise model was established by using Cadna/A software, and the spatial distribution of road traffic noise was analyzed by the software.

**Keywords**  Traffic flow parameters · Traffic noise · Simulation · Cadna/A

**Foreword**

In the various sources of noise in city, traffic noise is the most serious. About 50–70% city noise comes from the traffic noise, which gives people a great deal of trouble in normal life and learning [1]. The data shows that all types of urban functional areas in the day compliance rate was higher than the nighton <2015 China Environmental Status Bulletin> [2]. The rate of monitoring point time average compliance in 308 countries carrying out that the average rate of daytime monitoring points was 92.4%,

W. Liu · X. Guan (✉) · Y. Xing · J. Wang
School of Transportation Engineering,
Shenyang Jianzhu University, Shenyang 110168, Liaoning, China
e-mail: 44667276@qq.com

W. Cai
Shanghai Jin Wei Electric Appliance Manufacturing Co., Ltd, Shanghai 201313, China

and the average rate of nighttime monitoring was 74.3%. It can be seen that the systematic study of the impact of traffic flow parameters on the acoustic environment provides the basis for the management of traffic noise pollution, which is of great significance to improve the urban environment and improve people's quality of life [3].

# 1 The Effect of Speed and Flow on Traffic Noise

## 1.1 Data Collection

Measurement of traffic noise is mainly the equivalent continuous A level, Leq (A). In order to prevent the impact of mutual noise between vehicles, a small traffic flow of the road is generally selected when measuring the vehicle noise, recording arrival at the test point speed and the maximum noise level of a single arrival of the vehicle. Referencing the measurement method of traffic noise in city about the standard GB/T14623-1993 <urban area of environmental noise measurement method>, sound level meter is located between the nonmotorized lane and the sidewalk, from the ground height of 1.2 m, weather conditions for the sunny little weather, wind about 2 or so.

Monitoring data collected a total of 100 groups of small vehicle speed—noise data, 50 groups of large cars—noise data. It is known that the maximum speed is 31 km/h and the maximum speed is 76 km/h; the minimum noise is 65.1 dB(A) and the maximum noise is 73.7 dB(A) [4]. Compared with the small car, large cars through the measuring point when the vehicle speed is low, the maximum speed of a large car 30 km/h, the maximum speed of 66 km/h from the lowest noise generated 74 dB(A), the maximum noise of 80.2 dB(A).

## 1.2 Analysis of the Influence of Vehicle Speed on Traffic Noise

The quantitative relationship between the speed and the noise of the small vehicle and the vehicle speed and the noise are obtained using SPSS software to analyze the data.

Figure 1 shows that the reference sound pressure level also has an increasing trend with the increase of the speed of the small car. The trend can be fitted with one element linear equation. After calculation and analysis, the model summary Table 1, Variance Table 2, Coefficient Table 3, residual Fig. 2 are exported.

Table 1 shows that the coefficient of determination is 0.664, which shows that the fitting effect of the regression equation is better. From Fig. 2, it can be seen that the residual values are less than 3, and it is not from the abnormal point. As seen
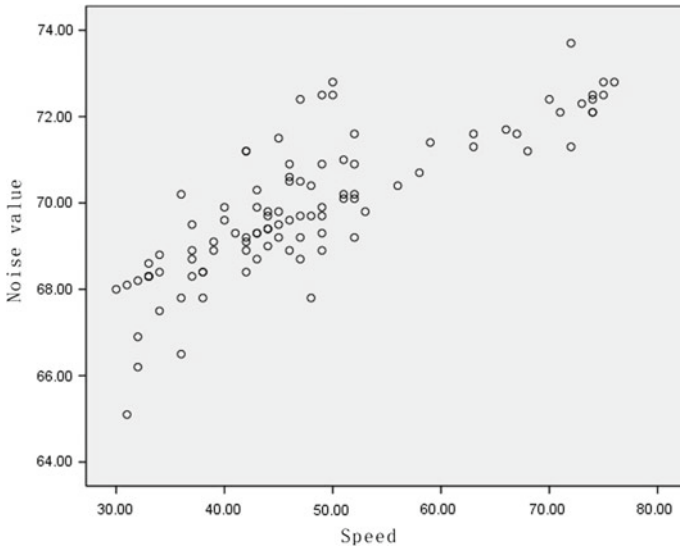
**Fig. 1** The small car reference sound pressure level and speed of the scatter diagram

**Table 1** Model summary[b]

| Model | R | R Square | Adjusted R Square | Std. Error of the Estimate | Durbin-Watson |
|---|---|---|---|---|---|
| 1 | 0.815[a] | 0.664 | 0.661 | 0.95391 | 1.975 |

[a]predictive variable: (constant), speed
[b]dependent variable: noise value

**Table 2** ANOVA

| Model | | Sum of Squares | df | Mean square | F | Sig. |
|---|---|---|---|---|---|---|
| 1 | Regression | 176.314 | 1 | 176.314 | 193.762 | 0.000[a] |
| | Residual | 89.175 | 98 | 0.910 | | |
| | Total | 265.490 | 99 | | | |

from Table 2, F test value is 193.672, significant sig $=0$, indicating a reference level of speed linear regression were highly significant. From Table 3 we can see that the constant term a is 64.736 and the speed coefficient B is 0.108. So the small car (level) reference radiation model as shown below is given by

$$L_0 = 64.736 + 0.108v \tag{1}$$

The method of the large car (level) reference radiation model is the same for the small car. The analysis results show that the fitting effect of the linear regression

**Table 3** Coeffficient[a]

| Model | | Unstandardized coefficients | | Standardized coefficients | t | Sig. |
|---|---|---|---|---|---|---|
| | | B | Std. error | Beta (β) | | |
| 1 | (Constant) | 64.736 | 0.383 | | 169.018 | 0.000 |
| | Speed | 0.108 | 0.008 | 0.815 | 13.920 | 0.000 |

[a]dependent variable: noise value
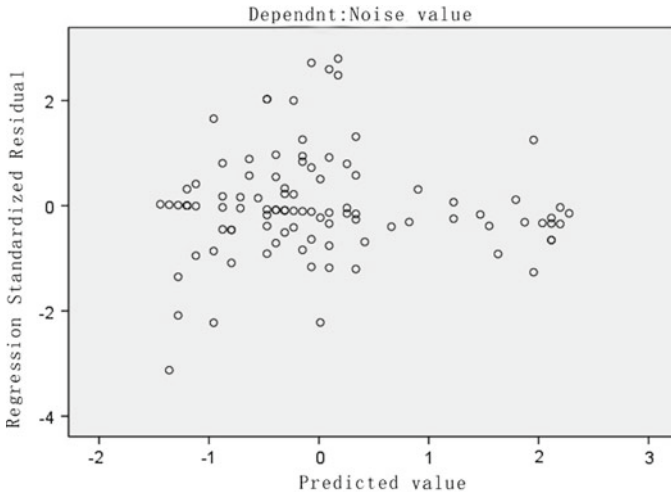


**Fig. 2** The small car model residual map reference level

equation is better. The large car (level) reference radiation model as shown below is given by

$$L_0 = 72.101 + 0.101v \tag{2}$$

From the above two models, we can know that the control speed is very good for reducing noise. But the result of the output noise is that the noise is too large to be made directly to the 4 a class [70 dB (a) at night of 55 dB (a) during the day], because in the field survey data, more than 80% of the large cars are basically a heavy truck. In order to solve this problem, it can be planted green or replaced with high-quality asphalt pavement to reduce the impact of noise on the residential.

**Fig. 3** Changes of vehicle flow within 16 h one day

Vehicle flow (V/20min)
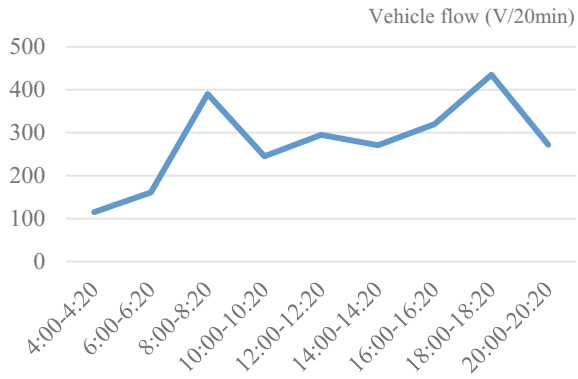
**Fig. 4** Changes of Leq(a) within 16 h one day

Leq(A)/dB
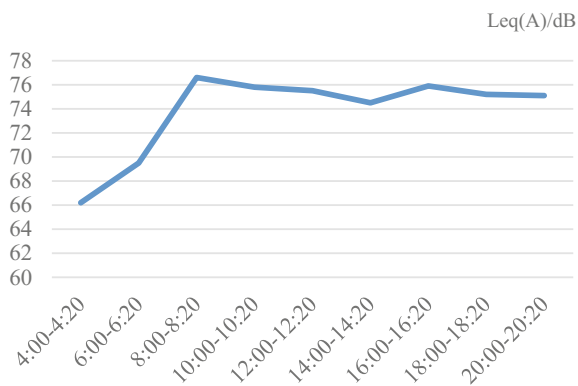
## 1.3 Analysis of the Influence of the Traffic Flow on the Traffic Noise in the Straight Line Segment

The traffic flow and traffic noise in this section of the road are plotted in Figs. 3 and 4. From the above analysis, it can be known that when the vehicle flow rate is higher than 161/20 min, the road traffic noise increases with the increase of the traffic flow but when the vehicle flow rate increases to a certain level, the traffic noise by the impact of the trend is not obvious and basically no change with the change of the car flow on straight road section of urban road. That is, the urban road traffic noise and traffic flow in a straight line is positive correlation. When the traffic flow is less than 161/20 min, the traffic noise increases with the increase of the traffic flow, and the trend is not obvious when the traffic flow rate exceeds 245/20 min and basically tend to be stable.

The superposition of the noise generated by the road vehicles is not a simple superposition of the level, but the superposition of energy. Therefore, it is not the more vehicles on the road as the traditional theory describes, the greater the noise generated. But with the increase of traffic, traffic noise at the initial stage of the

rapid increases, when the traffic reached a certain level, this growth trend is not very obvious. Namely, traffic noise and traffic flow are positive correlation.

## 2 Road Traffic Noise Simulation Based on Cadna/A Software

### 2.1 Establishment and Validation of Simulation Model

This paper selects the road for simulation modeling as the two-way carriageway, and the sensitive point is the second and third residential buildings on the right side of the road (the middle two buildings in the middle of the figure). In the Cadna/A software, a 6 lane road is set up with a length of 800 m and a width of 21 m. The established model is shown in Fig. 5.

Different traffic flow noise simulation results can be obtained by setting different traffic, vehicle speed, and heavy vehicle. Set the road traffic to 1200/h (which accounts for 15% of the proportion of the car), and the speed is 50 km/h. Select the calculation area and divide mesh setting the length of 0.3 m, width of 0.3 m, and receiving point height of 1.2 m. Then the results are shown in Fig. 6.

By comparing the predicted and measured values of the high-level noise, the predicted values and the measured values of the noise in each floor of the residential building are compared and analyzed, which are shown in Table 4.

Table 4 shows that the difference between the predicted value and the measured value is small. Therefore, the road traffic noise model established has high accuracy and can be used for road traffic noise simulation analysis.
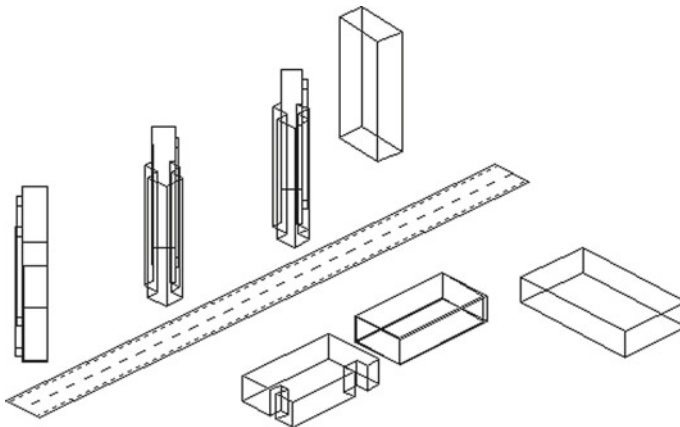


**Fig. 5** Established 3D model
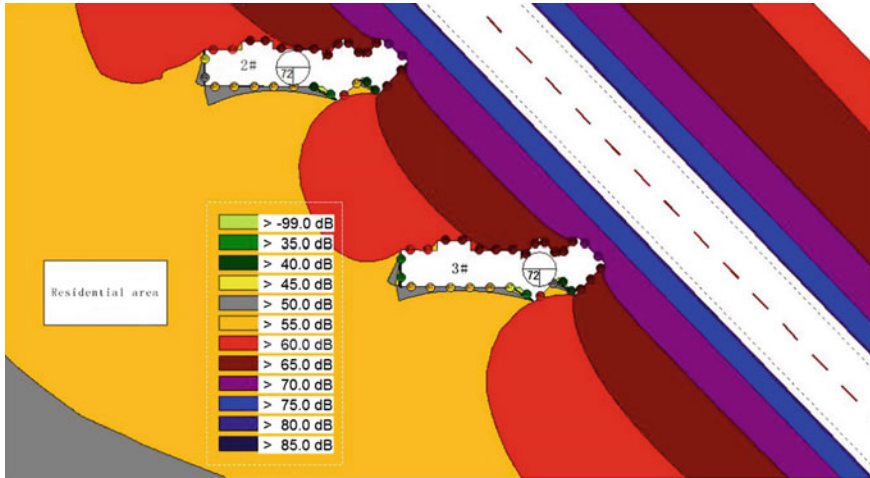
**Fig. 6** 1.2 m high-level noise distribution map

**Table 4** Predictive value and measured value of high-level noise

| The distance from the road shoulder (m) | Predicted noise value (dB) | Actual noise value (dB) |
|---|---|---|
| 2 | 82 | 81.6 |
| 4 | 78 | 77.5 |
| 6 | 76 | 76.6 |
| 8 | 75 | 75.3 |
| 10 | 74 | 73.8 |
| 12 | 73 | 71.2 |
| 14 | 72 | 70.9 |

## 2.2 Effect of Flow Rate and Vehicle Speed on Noise

On the establishment of the model, to maintain traffic, speed, car than the same. Select the calculation area and divide mesh setting the length of 0.3 m, width of 0.3 m, and receiving point height of 2.5 m. Then the results are shown in Fig. 7 after simulation analysis. And noise profile is shown in Fig. 8.

Figure 7 is the distribution of the sound field of the 2.5 m high level position in the presence of a residential building. The existence of residential buildings has broken the symmetry of the noise along both sides of the road, and the shape of the sound field is concave to the side of the house. In the distance from the road under the same conditions, noise sensitive point is located in a residential building behind a small value, indicating that the housing has a damping effect on the noise; the greater the vertical distance from the road, the noise value is small, the residents of 2.5 m high noise value of 69 db (A). Figure 8 is the distribution of sound field radiated by
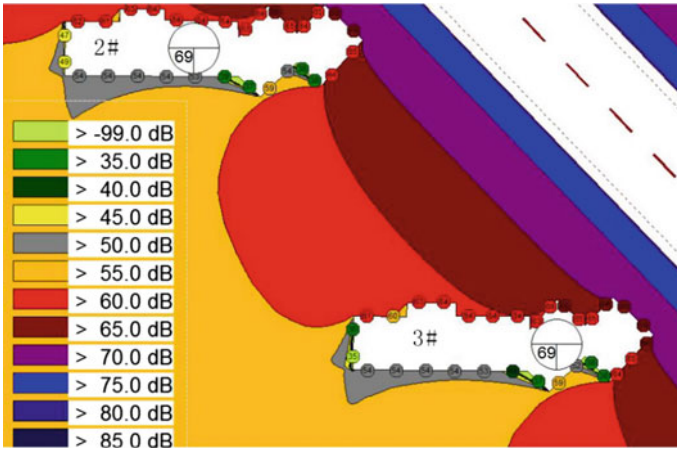
**Fig. 7** 2.5 m high-level noise distribution map
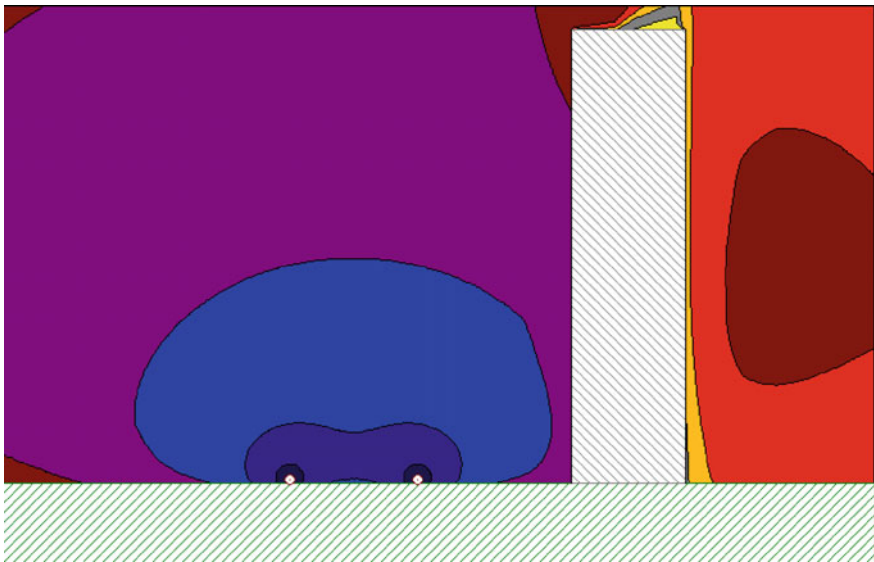


**Fig. 8** Noise profile

the road traffic flow in the vertical direction. As is shown that the existence of the residential building breaks the trend of the sound field in the vertical direction. The sound pressure level of the road decreases with the increase of the height, and the noise value of the 2–19 Floor is shown in Table 5 (The distance is 20.18 m).

**Table 5** The noise value of the 2–19 floor

| ID | Height/m | Day/dB (A) | Night/dB (A) | ID | Height/m | Day/dB (A) | Night/dB (A) |
|---|---|---|---|---|---|---|---|
| 2 floor | 4.2 | 75 | −0.4 | 11 floor | 31.2 | 72 | −3.4 |
| 3 floor | 7.2 | 75 | −0.4 | 12 floor | 34.2 | 71.6 | −3.8 |
| 4 floor | 10.2 | 74.7 | −0.6 | 13 floor | 37.2 | 71.2 | −4.1 |
| 5 floor | 13.2 | 74.4 | −1 | 14 floor | 40.2 | 70.9 | −4.5 |
| 6 floor | 16.2 | 74 | −1.4 | 15 floor | 43.2 | 70.6 | −4.8 |
| 7 floor | 19.2 | 73.5 | −1.8 | 16 floor | 46.2 | 70.2 | −5.1 |
| 8 floor | 22.2 | 73.1 | −2.2 | 17 floor | 49.2 | 69.9 | −5.5 |
| 9 floor | 25.2 | 72.7 | −2.6 | 18 floor | 52.2 | 69.6 | −5.8 |
| 10 floor | 28.2 | 72.3 | −3 | 19 floor | 55.2 | 69.3 | −6 |
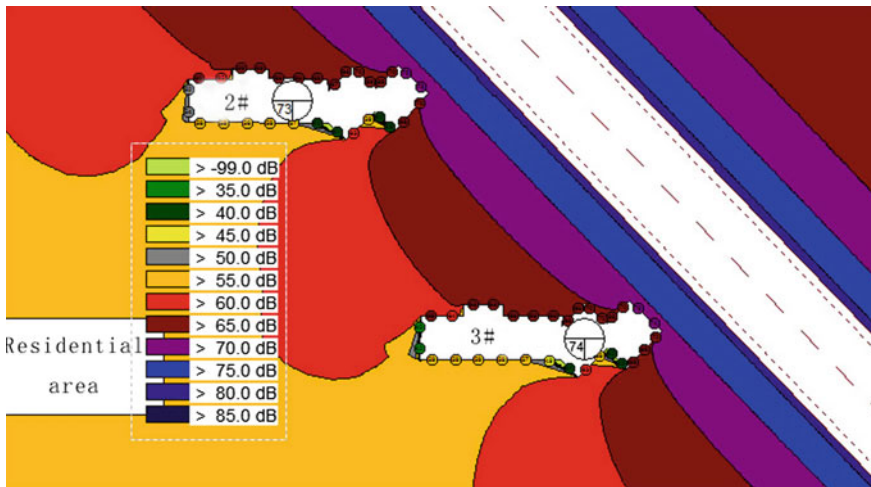


**Fig. 9** $q = 1500$ car/hour $v = 50$ km/h 2.5 m high-level noise level distribution map

For the established model, the model can be obtained with the same traffic flow characteristics and the noise simulation results can be obtained by changing the vehicle speed or the flow rate. As shown in Figs. 9 and 10, when the traffic flow is increased from 1000 pcu/h to 1500/h, the level of the horizontal noise level in the 2.5 m elevation is increased from 69 dB (A)–74 dB (A), and the noise level before the low level residential building is increased from 70 dB (A)–75 dB (A). The speed of car is reduced from 50 to 40 km/h, and the level of horizontal noise at 2.5 m in front of the residential building is reduced from 69 dB (A)–67 dB (A). The noise level before the low level residential building is reduced from 71dB (A)–68 dB (A).
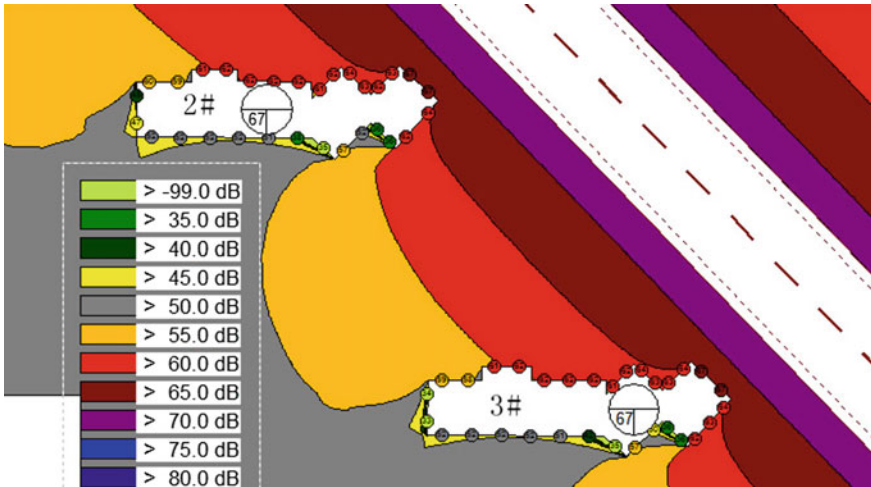
**Fig. 10** $q = 1000$ car/hour $v = 40$ km/h 2.5 m high-level noise level distribution map

## 3 Conclusion

Traffic noise plays an important role in the evaluation of urban environmental quality, which has become a major concern of the environmental protection department[5]. Based on the field data, this paper analyzes the effect of traffic flow and vehicle speed on the noise from the traffic flow parameters, which are the key factors influencing the traffic noise. The establishment of road traffic noise simulation model by the software obtains the distribution of different traffic flow characteristics under the condition of noise level in space. Then according to the noise distribution, we can determine whether the study area should be set up sound barrier and how to set up sound barrier.

## Reference

1. Li F, Li Q, Guan X (2009) The influence of highway traffic noise on the environment and its treatment measures. J Hunan Agric Univ 35(1):44–47
2. Feng X (2014) Research on the relationship between traffic flow factor and road traffic noise. Master's thesis, Northeast Forestry University, Harbin
3. Shi B, Hu X, Qiu R (2016) Influence factors and control strategies of urban traffic noise. J Putian Univ 23(5):105–108
4. Li L, Yuan X (2012) Discussion on highway traffic noise control measures. Sichuan Environ 31(5):140–142
5. Hu Y (2008) Study on the relationship between traffic noise and traffic flow state. J Transp Eng Inf 6(1):6–9

# Research on Evaluation Model of Danger Degree in Driving

**Keyou Guo, Yiwei Wang, Xiaoli Guo and Qichao Bao**

**Abstract** The existing safe driving model all evaluated the potential dangers in driving based on single-factor analysis results. This study proposed a multifactor driving danger evaluation model including three factors—lane, vehicle distance, and vehicle type. The abstract information of lane, vehicle type, and vehicle distance was first quantified as specific values; then, we conducted crossover analysis on the quantified parameter and established the linear model; finally, through multiple regression, the logical relationships between these three factors and danger coefficient were acquired. Meanwhile, the model parameters were analyzed based on the theory in statistics. Results demonstrate that the proposed danger evaluation model can reasonably describe the effects of these three factors on the safety in driving.

**Keywords** Safe driving · Evaluation model · Multiple regression · Lane detection · Vehicle distance detection · Vehicle type recognition

## 1 Introduction

Safe driving has always been a research hotspot in intelligent traffic. Using Otsu method, Xu Meihua performed lane detection based on the geometric characteristics of lanes on the road, Hough voting results, the correction among road images and the width of lane lines and then monitored lane departure in combination with the measured yaw angle values [1]. Chen Benzhi performed lane fitting with the use of hyperbolic model; based on the acquired lane information, the mapping relationship between world coordinate system and image coordinate system was established through camera parameters, and the lane departure warning in world coordinate system was converted to the warning in image coordinate system; finally, the departure decision was made using space-time warning system [2]. Peng Jun measured the

---

K. Guo (✉) · Y. Wang · X. Guo · Q. Bao
School of Material Science and Mechanical Engineering, Beijing Technology and Business University, Beijing 100048, China
e-mail: guoky@th.btbu.edu.cn

relative distance and the relative velocity, and thereby calculated the time to collision (TTC) with the barriers in front; then, they compared the calculated results with the decision-making threshold values calculated using equal-step method and made the safety warning [3]. Liu Zhiqiang first detected the lane markings based on edge distraction function (EDF), identified vehicles according to the textures underneath the vehicles and the symmetry characteristics, measured the distance on the basis of the geometrical mapping relation between image coordinate system and world coordinate system, and made the anti-collision warning in combination with the calculation of critical safe vehicle distance [4, 5]. Feng Zhong-Xiang and Guo Yingshi made the decisions based on the driving behaviors or personal driving experiences [6, 7].

In previous studies, safety warning was mainly made based on a single factor in driving, while the effects of the multiple-factor fusion on driving warning evaluation scheme were poorly investigated. This study proposed a multiparameter driving danger evaluation model for comprehensively analyzing the effects of lane, vehicle type and distance on the danger degree in driving.

## 2 Evaluation Parameters in the Model

### 2.1 Lane Detection

Figure 1 illustrates the procedures of lane detection. Firstly, using LDA [8] (Linear Discriminant Analysis) the optimal discriminant vector space between road and lane was calculated as below

$$\varphi = \begin{bmatrix} 0.540 & -0.841 & 0.024 \end{bmatrix}^{\mathrm{T}} \tag{1}$$
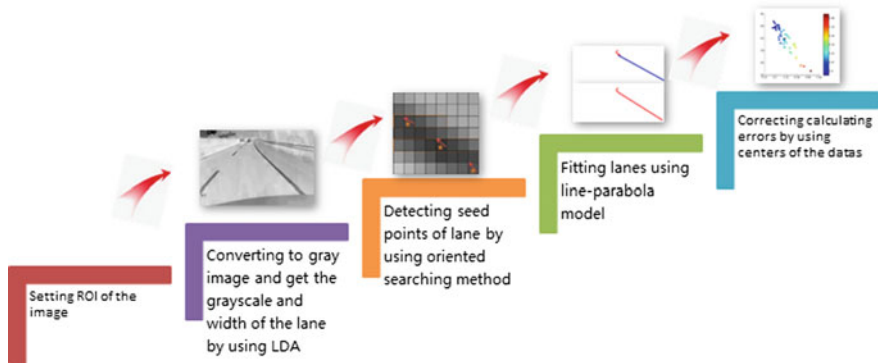


**Fig. 1** Flow chart of lane detection results (below)

**Fig. 2** Comparison between traditional gray processing results (above) and LDA processing (below)
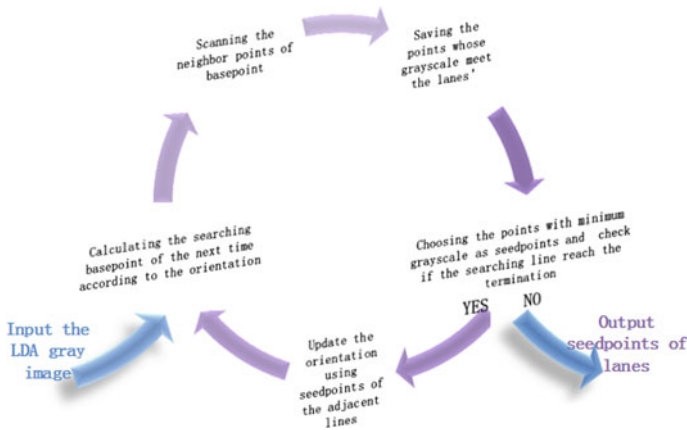


**Fig. 3** Flow chart of scanning algorithm

The region of interest (ROI) was projected to the optimal discriminant vector space for generating the gray images adapted to road images [9], as shown in Fig. 2.

We conducted gray-value sampling analysis on the images after LDA gray processing. After lane gray information and width were acquired, the seed points were detected by guided interlaced scanning algorithm [10]. Finally, the lanes were fitted by least square method according to line-parabola model (Figs. 3 and 4).

Lane detection results should be corrected by calculating the data center (DC). When the threshold deviated from the DC to a certain degree, the current results can be corrected by the detection results of the last frame. Figure 5 compares the detection results before and after optimization.
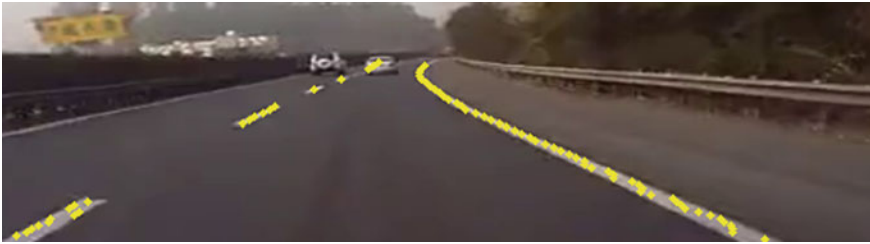
**Fig. 4** Scanning results of seed points
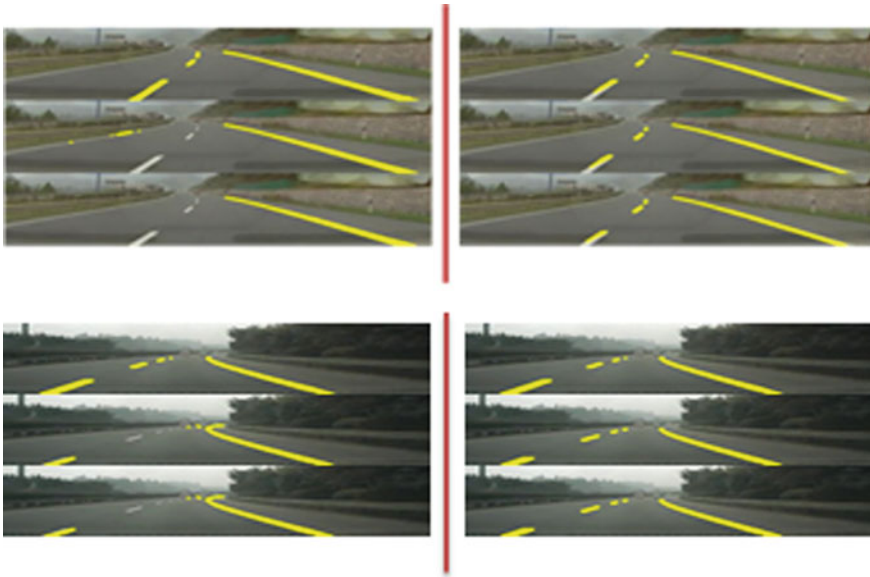


**Fig. 5** Comparison between the results before and after video sequence continuous optimization

## 2.2 Vehicle Distance Detection

The P4P [11] model was used for calculating the distance between the vehicle and the vehicle in front. Firstly, based on the principle of Zhang's camera calibration algorithm [12], the camera's intrinsic parameters can be solved using the combination of singular value decomposition [13] and PLS:

$$
M = \begin{bmatrix} f_x & 0 & c_x \\ 0 & f_y & c_y \\ 0 & 0 & 1 \end{bmatrix} = \begin{bmatrix} 953.66269 & 0 & 656.14355 \\ 0 & 956.86172 & 382.61027 \\ 0 & 0 & 1 \end{bmatrix} \quad (2)
$$

**Fig. 6** Vehicle license plate detection results

Next, the vehicle license plate image was located through color space conversion and Sobel comprehensive searching [14]. Based on the size, length-to-width ratio and the inclination angle of the minimum enclosing rectangle, several candidate vehicle license plate regions were selected, which were then classified by a support vector machine (SVM) classifier. The results are shown in Fig. 6.

After the camera's intrinsic parameters and vehicle's license plate information were determined, the model was reestablished using PNP theory in projective geometry. The length information was integrated into the model. Then, the rotation matrix R and translation matrix T between the world coordinate system where the vehicle's license plate was located and the world coordinate system where the camera was located were constructed. The translation matrix T was used for calculating the relative distance between the two vehicles. The establishment of model was detailedly described in Ref. [15]. The calculation results are shown in Fig. 7.

## 2.3 Vehicle Type Detection

The input images were preliminarily screened using LBP feature classifier trained by Adaboost algorithm [16], and then further use HOG classifier trained by SVM for identifying the preliminary selection results [17, 18]. In this study, 10,256 samples were used for the training of LBP feature classifier. For SVM training 1130 small vehicle samples, 1206 medium vehicle samples and 1282 oversize vehicle samples
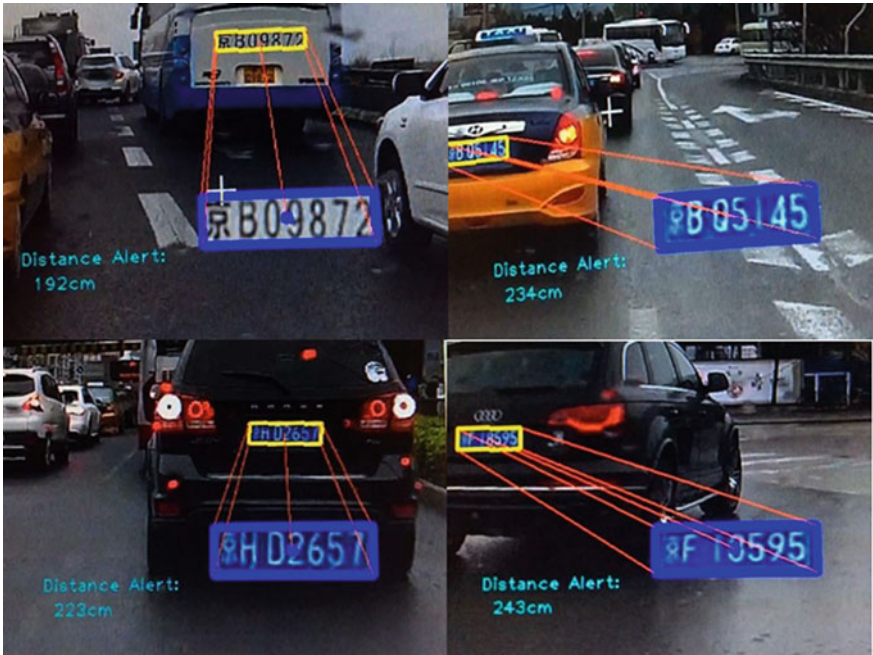
**Fig. 7** Calculation of the vehicle distance



**Fig. 8** Multi-classification identification results of vehicle types

were used. Additionally, 2549 negative samples were also included in the training process. Figure 8 shows the multi-classification results of vehicle types.

# 3 Establishment of the Evaluation Model of Driving Danger Degree

The dangers of driving lie in multiple driving factors. In this study, lane, vehicle type, and vehicle distance were taken into overall consideration for evaluating the driving danger. Furthermore, these indexes should be quantified in actual modeling. The qualification criterion is described below.

1. Lane module: during the driving process, the front vehicle and the following vehicles can run in a same lane or different lanes, which were quantified as 0 and 1, respectively.
2. Vehicle type module: According to actual conditions, this index can also be divided into four conditions, no vehicle in front, small vehicle in front, medium vehicle in front and oversize vehicle in front, which were quantified as 0, 1, 2, and 3, respectively.
3. Vehicle distance module: According to *Highway Traffic Management Regulations in People's Republic of China*, the following distance should be no less than 50 m when driving on a highway at a speed of below 70 km/h; No less than 100 m when driving on a highway at a speed of over 70 km/h. Therefore, the vehicle distance can be discussed according to the following three conditions: over 100 m, 50–100 m and smaller than 50 m, respectively, which were quantified as 0, 1 and 2, respectively.

## 3.1 Basic Principle in Evaluation Model Establishment

1. In case of no vehicle in front, the output of vehicle type detection module was 0, i.e., the danger coefficient equaled to 0.
2. When the distance from the vehicle in front exceeded or equaled to 100 m, the current vehicle distance can guarantee the safe driving of these two vehicles in a safe distance, i.e., the output of vehicle distance was 0 and the danger coefficient was 0.

When the vehicle in front and the object vehicle were not in a same lane, and meanwhile, the detected was small vehicle and the distance between two vehicles exceeded 50 m, these cases show the lowest danger level, with the corresponding danger coefficient of 1 (Tables 1 and 2).

3. Effects of the difference in vehicle type on danger coefficient

**Table 1** Danger coefficient in case of standard driving

| Danger coefficient | Lane | Vehicle type | Vehicle distance |
|---|---|---|---|
| 1 | 0 | 1 | 1 |

**Table 2** Relationship between vehicle type and danger coefficient

| Danger coefficient | Lane | Vehicle type | Vehicle distance |
|---|---|---|---|
| 1 | 0 | 1 | 1 |
| 2 | 0 | 2 | 1 |
| 3 | 0 | 3 | 1 |

**Table 3** Relationship between distance and danger coefficient

| Danger coefficient | Lane | Vehicle type | Vehicle distance |
|---|---|---|---|
| 2 | 0 | 1 | 2 |
| 4 | 0 | 2 | 2 |
| 6 | 0 | 3 | 2 |

**Table 4** Relationship between lane and danger coefficient

| Danger coefficient | Lane | Vehicle type | Vehicle distance |
|---|---|---|---|
| 2 | 1 | 1 | 1 |
| 4 | 1 | 2 | 1 |
| 6 | 1 | 3 | 1 |
| 4 | 1 | 1 | 2 |
| 8 | 1 | 2 | 2 |
| 12 | 1 | 3 | 2 |

Vehicle weight and volume can affect the safety in driving. Under the same other conditions, the passengers in heavier and larger vehicles can be well protected than those in lighter and smaller vehicles. Therefore, when the vehicle type was increased by a level, the danger coefficient of driving was doubled compared with the standard driving condition.

4. Effects of the difference in vehicle distance on danger coefficient

In this regard, whether the vehicle behind can successfully braked within the current distance can affect the safety in driving. The energy conversion in a vehicle's braking can be written as:

$$E_0 - f \cdot S = E_1 \tag{3}$$

where $E_0$ denotes the vehicle's initial kinetic energy, $E_1$ denotes the vehicle's remaining kinetic energy, and $f \cdot S$ denotes the energy produced by friction in braking process. After the braking, the vehicle's remaining kinetic energy decreased gradually with the decrease of the driving speed. As described in Eq. (3), the vehicle's remaining kinetic energy is linearly and inversely proportional to the traveling distance. Therefore, the risk was doubled as the vehicle distance was increased by a level (Tables 3 and 4).

5. Effects of lane condition on danger coefficient

The lane where the vehicle runs can also affect the safety in driving. Specifically, for the vehicles in different lanes, the common accidents are scratching; for the vehicle in a same lane, the common accidents are rear-end. In generally, collision is more dangerous than scratching, and thereby, the danger coefficient when the vehicles are in same lanes is greater than that when the vehicles in a same lane. In this study, the former was set as double of the latter.

## 3.2 Multiple Regression

After the effects of lane, vehicle type and distance on driving safety were comprehensively evaluated, we performed cross-over analysis on these three factors. Assuming that the combination of two or three factors overall affected the driving safety, finally the driving danger degree was defined as the sum of the danger degrees under the above four conditions:

$$\text{Danger} = A \cdot d_{\text{lane}} + B \cdot d_{\text{vehicle}} + C \cdot d_{\text{distance}} + D \cdot D_{\text{lv}} + E \cdot D_{\text{vd}} + F \cdot D_{\text{ld}} + G \cdot D_{\text{lvd}} + H \quad (4)$$

where

$$
\begin{aligned}
D_{\text{lv}} &= d_{\text{lane}} \cdot d_{\text{vehicle}} \\
D_{\text{vd}} &= d_{\text{vehicle}} \cdot d_{\text{distance}} \\
D_{\text{lv}} &= d_{\text{lane}} \cdot d_{\text{distance}} \\
D_{\text{lvd}} &= d_{\text{lane}} \cdot d_{\text{vehicle}} \cdot d_{\text{distance}}
\end{aligned}
$$

In addition, a constant term H was introduced for reducing the effects of random error. Finally, the driving danger degree was defined as the sum of the danger degrees under the above four conditions:

## 4  Results and Discussion

Using multiple regression [19, 20], the model was solved and the acquired coefficients are listed in Table 5.

Accordingly, the established model is written as:

Table 5  Parameters in multiple regression model

| Parameter | Coefficient | P-value |
|---|---|---|
| H (a constant) | (0.00) | 0.00 |
| E | 1.00 | 0.00 |
| G | 1.00 | 0.00 |
| Others | 0.00 | >0.1 |

$$\text{Danger} = D_{\text{vd}} + D_{\text{lvd}} \tag{5}$$

It can be concluded that, whether for lane, vehicle type or vehicle distance, the combined effects of two or three factors on driving should be considered, among which vehicle distance and type were main influential factors of danger. The effect of lane condition on danger degree should be established on the basis of vehicle type and distance.

## 5 Conclusions

This study merged the lane detection results into the evaluation model of driving danger and performed multiple regression to establish the model based on the reasonable quantification of lane detection results, vehicle type recognition results and vehicle distance results and the analysis of energy conversion in collision. Results show that the model can reasonably account for the effects of three factors (lane condition, vehicle type and vehicle distance) on the safety in driving.

## References

1. Xu M, Zhang K, Jiang Z (2013) Algorithm design and implementation for a real-time lane departure pre-warning system. J Traffic Transp Eng 16(3):149–158
2. Chen B (2013) Lane recognition and departure warning based on hyperbolic model. J Comput Appl 3:2562–2565
3. Peng J, Wang J, Wang N (2011) Intelligent vehicle collision warning algorithm based on machine vision. J Highw Transp Res Dev 28(S1):124–128
4. Liu Z, Wen H (2007) Monocular vision-based vehicle collision warning system. Comput Appl 27(8):2056–2058
5. Zhong Y, Yao J (2001) A formula of the critical safety distance between two moving vehicles. J Hunan Univ (Nat Sci Ed) 28(6):54–58
6. Feng Z, Yuan H, Liu J, Zhang WH, Liu H (2012) Influence of driver personal characteristics on vehicle velocity. J Traffic Transp Eng 12(6):89–96
7. Guo Y, Ma Y, Fu R, Meng N, Yuan W (2012) Influence of driving experience on gazing behavior characteristic for car driver. J Traffic Transp Eng 12(5):89–96
8. Jelsovka D, Hudec R, Breznan M (2011) Face recognition on FERET face database using LDA and CCA methods. Int Conf Telecommun Signal Process 2011:570–574
9. Yoo H, Yang U, Sohn K (2013) Gradient-enhancing conversion for illumination-robust lane detection. IEEE Trans Intell Transp Syst 14(3):1083–1094
10. Guo K, Wang Y, Guo X Lane classification algorithm combined LDA and LSD. Comput Eng Appl, 1–8
11. Du X, He Y, Chen L, Gao S (2016) Pose estimation of large non-cooperative spacecraft based on extended PnP model. 2016 IEEE international conference on robotics and biomimetics (ROBIO), Qingdao, 2016, pp 413–418
12. Chi D, Wang Y, Ning L, Yi J (2015) Experimental research of camera calibration based on ZHANG's method. J Chin Agric Mech 36(2):287–289, 337
13. Ma T, Yao R, Shao Y, Zhou R (2009) A SVD-based method to assess the uniqueness and accuracy of SPECT geometrical calibration. IEEE Trans Med Imaging 28(12):1929–1939

14. Israni S, Jain S (2016) Edge detection of license plate using Sobel operator. 2016 International conference on electrical, electronics, and optimization techniques (ICEEOT), Chennai, pp 3561–3563
15. Fengmei Sun, Weining Wang (2006) Pose determination from a single image of a single parallelogram. ACTA AUTOMATICA SINICA 32(5):746–752
16. Sun Q, Lu X, Chen L, Hu H (2014) An improved vehicle logo recognition method for road surveillance images. Seventh Int Symp Comput Intell Des Hangzhou 2014:373–376
17. Guzman S, Gomez A, Diez G, Fernandez DS (2015) Car detection methodology in outdoor environment based on histogram of oriented gradient (HOG) and support vector machine (SVM). 6th Latin-American conference on networked and electronic media (LACNEM 2015), Medellin, 2015, pp 1–4
18. Lee SH, Bang M, Jung KH, Yi K (2015) An efficient selection of HOG feature for SVM classification of vehicle. Int Symp Consum Electron (ISCE) Madrid 2015:1–2
19. Xie G, Wang Z, Hei X, Takahashi S, Nakamura H (2016) Data-based axle temperature prediction of high speed train by multiple regression analysis. 2016 12th international conference on computational intelligence and security (CIS), Wuxi, 2016, pp 349–353
20. Kitamura T, Tsujiuchi N, Koizumi T (2006) Hand motion estimation by EMG signals using linear multiple regression models. 2006 international conference of the IEEE engineering in medicine and biology society, New York, NY, 2006, pp 1339–1342
21. Liu Z, Ott J, Shen Y (2010) P-value distribution in case-control association studies. 2010 IEEE international conference on bioinformatics and biomedicine workshops (BIBMW), Hong, Kong, 2010, pp 306–308
22. Rögnvaldsson T, Norrman H, Byttner S, Järpe E (2014) Estimating p-values for deviation detection. 2014 IEEE eighth international conference on self-adaptive and self-organizing systems, London, 2014, pp 100–109

# Vision-IMU Based Obstacle Detection Method

Yi Xu, Song Gao, Shiwu Li, Derong Tan, Dong Guo, Yuqiong Wang and Qiang Chen

**Abstract** Obstacles' accurate classification is the first step in traditional obstacle detection methods, and the step causes the problem of high time and space complexity. In this paper, an obstacle detection method based on the principle of pinhole imaging is proposed to solve the problem. The monocular camera and inertial measurement unit are used as the basic sensing units in proposed method. The obstacle detection steps and indoor experiments are shown to expound the detection process of the Vision-IMU based obstacle detection method. The Vision-IMU based obstacle detection method and Adaboost cascade detection method are used to detect obstacles in indoor experiments, and the Producer's Accuracy, the User's Accuracy, the Overall Accuracy, and κ are used as evaluating indicators to compare test results, and the results show that the Vision-IMU based obstacle detection method has higher accuracy. The processing time of the Vision-IMU based obstacle detection method and Adaboost cascade detection method are compared, and it is shown that the Vision-IMU based obstacle detection method has faster processing speed.

**Keywords** Monocular vision · Inertial measurement unit · Obstacle detection
Pinhole imaging

Y. Xu · S. Gao (✉) · D. Tan · D. Guo · Y. Wang
School of Transportation and Vehicle Engineering, Shandong University of Technology,
Zibo 255000, China
e-mail: gaosongsdut@163.com

S. Li · Q. Chen
School of Transportation, Jilin University, Changchun 130022, China

S. Gao
Collaborative Innovation Center for New Energy Vehicle of Shandong Universities, Zibo 255000,
China

Q. Chen
School of Automotive and Transportation, Tianjin University of Technology and Education,
Tianjin 300222, China

# 1 Introduction

Monocular environmental perception method has been paid more attention to and has been studied deeply in the aspect of road obstacle detection because of meeting the human visual cognitive habit and low cost. Symmetry, edge, and shadow features are the prior knowledge used in road environment perception [1–3]. Histogram of Oriented Gradient (HOG), Gray Level Co-occurrence Matrix (GLCM), Scale Invariant Feature Transform (SIFT), and Haar-like features have been widely used in obstacle identification and tracking because of their high efficiency and simplicity [4–9]. Deformable Parts Model (DPM) has been widely used in the obstacle detection because of combining prior knowledge of the object to be identified and characteristics of HOG [10, 11]. With the development of artificial intelligence, machine learning algorithm has been gradually introduced into the monocular obstacle detection method to improve the accuracy. Pomerleau, Jochem et al. applied artificial neural network to the identification of traffic environment [12]. Xiao et al. used random forest method to obtain better results in structured road detection [13]. Sivaraman et al. proposed an active learning framework based on Haar features and adaptive boosting algorithm (Adaboost) [14] to detect vehicles in high way environment. Song et al. improved the robustness and real-time of vehicle detection through the integration of Adaboost and convolutional neural network (CNN) [15]. The continuous development of Generative Adversarial Networks (GAN), SegNet, and other new concepts of machine learning increase the potential for improving the accuracy of monocular obstacle detection [16, 17].

The methods of above monocular obstacle detection methods are based on accurate classification of obstacles, and obstacles must be recognized in 2D images before distance estimation and speed estimation [18–22]. However, if objects' height information in images can be calculated according to inverse perspective transformation, obstacles contained in objects will be detected, obstacle classification will be bypassed, time and space complexity of obstacle detection will be reduced, and the efficiency of monocular obstacle detection. It has been found that in the process of analyzing the pinhole imaging of stereo obstacles, there will be difference between the imaging of three-dimensional obstacles and the road plane if the camera moved, and the difference can be quantified by the distance difference between the imaging points. The Vision-IMU based obstacle detection method capturing images using a single camera and obtaining camera moving distance and camera pose using the IMU is proposed to detect obstacles in moving.
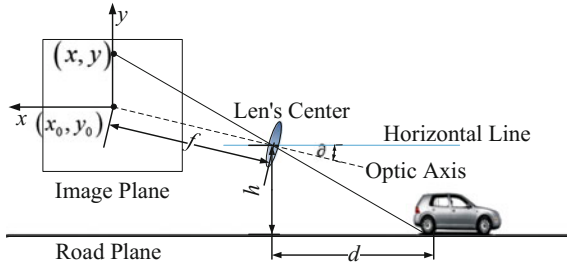
**Fig. 1** Schematic diagram of pinhole imaging

## 2 Principle of Vision-IMU Based Obstacle Detection Method

### 2.1 Principle of Still Obstacle Detection

Image acquisition is the process of mapping objects in 3D space to 2D image plane, and this process can be simplified as a pinhole imaging (see Fig. 1). The effective focal length of the camera is $f$, the installation height of the camera is $h$, and the pitch angle of the camera is $\partial$. The coordinate origin of the plane coordinate system $(x_0, y_0)$, that is, the intersection between the image plane and the camera optical axis, is usually set to $(0, 0)$. The intersection of the front obstacle and the road plane is $P$, and the coordinates of point P in the image plane coordinate system are $(x, y)$. The horizontal distance (d) between the point P and the camera can be obtained:

$$d = \frac{h}{\tan(\partial + \arctan[(y_0 - y)/f])} \tag{1}$$

The first imaging point of obstacle is $A$ (see Fig. 2), $y$ axis is moved from $y_1$ to $y_2$ in the image plane because of the camera's movement, and the imaging point of obstacle's top is $B$. Assuming that $A$ is the imaging point of $A'$ on the road plane, and $B$ is the imaging point of $B'$ on the road plane, then the horizontal distance from the camera to $A'$ is $d_1$, and the horizontal distance from the camera to $B'$ is $d_2$. $d_1$ and $d_2$ can be calculated by Eq. (1), and relationship is $d_1 = d_2 + \Delta d$. But the real relationship is $d_1 = d_2 + \Delta d + \Delta l$. Therefore, the target point is not on the road if $d_1 \neq d_2 + \Delta d$, and thus, still obstacles can be recognized by $\Delta l$ if c can be acquired using IMU.
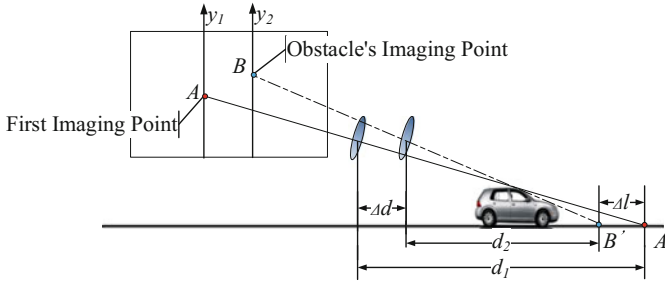
**Fig. 2** Schematic diagram of still obstacle imaging
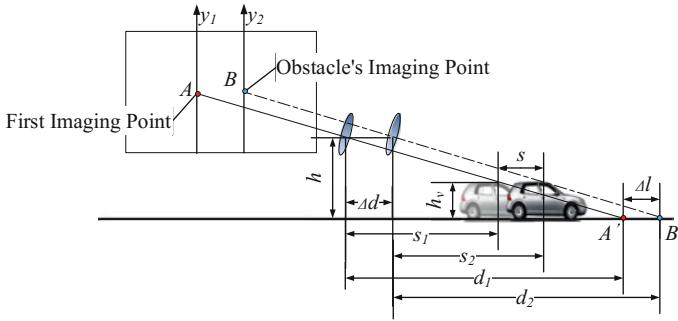


**Fig. 3** Schematic diagram of moving obstacle imaging

## 2.2 Principle of Moving Obstacle Detection

When the front obstacle moves along the horizontal direction (see Fig. 3), the distance from camera to obstacle's top point at the previous moment is $s_1$, the distance from camera to obstacle's top point at the following moment is $s_2$, the relationship between $d_1$, $d_2$, $s_1$ and $s_2$ is:

$$\begin{cases} d_2 = d_1 + \Delta l - \Delta d \\ s_2 = s_1 + s - \Delta d \end{cases} \tag{2}$$

The relationship between obstacle height $h_v$, $h$, $d_1$, $d_2$, $s_1$, and $s_2$ according to the characteristic of right triangle is

$$\begin{cases} \frac{h_v}{h} = \frac{d_1 - s_1}{d_1} \\ \frac{h_v}{h} = \frac{d_2 - s_2}{d_2} \end{cases} \tag{3}$$

$\Delta l$ can be calculated according to Eqs. (2) and (3) as $\Delta l = \frac{h \times s - h_v \times \Delta d}{h_v - h}$. Obstacles thus can be recognized under any circumstances that do not meet $h \times s = h_v \times \Delta d$.

Thus, it can be seen that the method of distinguish between the road surface and the obstacles ahead using monocular camera and IMU is feasible, and the process of differentiation only needs to track and calculate the position of feature points, therefore, the consumption of time and space can be reduced.

# 3 Implementation of Vision-IMU Based Obstacle Detection Method

## 3.1 Process of Vision-IMU Based Obstacle Detection Method

(1) Camera parameter updating based on IMU data

    (1) Calibration of camera initial parameters. Calibrate the monocular camera mounted on a stationary vehicle, get camera focal length $f$, mounting height $h$, pitch angle $\partial$, get $p$ (the pixel size of the photosensitive chip).

    (2) Continuous inertial data acquisition. At the beginning of $t = 0$, continuously acquire inertial data by IMU rigidly connected with monocular camera with frequency $F$.

    (3) Camera parameters updating. Calculate $\Delta d$ in period $\Delta t$ according to inertial data.

(2) Image processing and obstacle detection

    (1) Feature points extraction at $t$. Segment image at $t$, extract ROI, extract points on the upper edge of ROIs as feature points.

    (2) Horizontal distance calculation at $t$. Call camera parameters at $t$. Assuming feature points are located at the horizontal plane, calculate horizontal distance $d_1$ between feature points and the camera at $t$.

    (3) Feature points tracking. Acquire road image at $t$ ($t = t + \Delta t$), extract ROI and track the feature points at $t$ ($t = 0$).

    (4) Horizontal distance calculation and obstacle detection. Assuming feature points are at the horizontal plane, calculate horizontal distance $d_2$ between feature points and the camera at $t$ ($t = t + \Delta t$). Compare $\Delta l$ ($\Delta l = |d_1 - \Delta d - d_2|$) and $k$ ($k$ is a set threshold, $k > 0$). The feature point is at horizontal plane and the ROI is not the obstacle if $\Delta l \leq k$. The feature point is not at horizontal plane and the ROI is the obstacle if $\Delta l > k$ (Fig. 4).

## 3.2 Obstacle Detection Experiment

OV5640 camera unit and JY61p IMU are mounted on movable platform (see Fig. 5a). The obstacle is simulated by vehicle scaling model (see Fig. 5b). Traffic mark, road
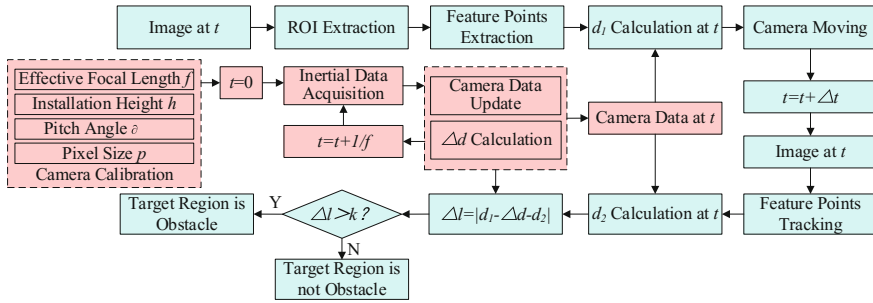
**Fig. 4** Vision-IMU based obstacle detection method flow chart
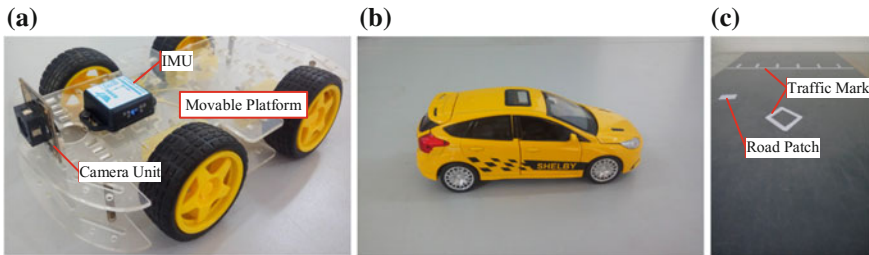


**Fig. 5** Indoor experiment equipments. **a** Movable platform, Camera unit and IMU. **b** Vehicle scaling model (obstacle). **c** Traffic mark and road patch

repair patches, and other visually significant non-obstacles are simulated by pieces of paper attached to the plane (see Fig. 5c). One of the indoor obstacle experiments are processed as follows.

Effective focal length of the camera $f = 6.779$ mm, installation height of the camera $h = 6.572$ cm, pitch angle of the camera $\partial = 0.132$ rad, pixel size of the photosensitive chip $p = 1.4 \, \mu$m.

The angular acceleration and acceleration data are acquired by the IMU with $F = 100$ Hz. The camera pose is solved using the four element method, and the pitch angle of the camera $\partial$ is updated. The horizontal distance $\Delta d = 4.00$ cm in period $\Delta t = 2s$ is calculated using acceleration data.

The image at $t = 0$ is processed by image edge detection and morphological closed operation. Connected regions that the number of pixels is over the threshold $c = 100$ are suspected obstacle regions (ROIs). ROIs' pixel number is $c_0 = \{c_{01}, c_{02}, \ldots, c_{0n}\}$. The midpoints of the highest points in the vertical direction of ROIs are feature points (see Fig. 6c).

Assuming feature points are located at the horizontal plane, camera parameters are called at $t$, and horizontal distance $d_1$ is calculated.

The road image at $t$ ($t = t + \Delta t$) is acquired. Edge detection and morphological closed operation are processed for ROI extraction. Connected regions around ROIs are searched, the connected regions which number of pixels is closer to $c_0$ are con-
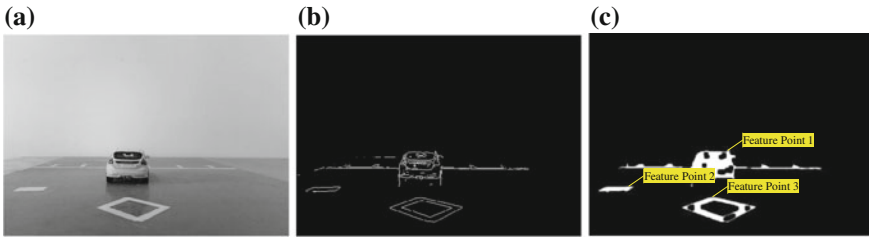
**Fig. 6** Feature points localization. **a** Image at $t = 0$. **b** Result of edge detection. **c** Morphological processing and feature points (the * are feature points)
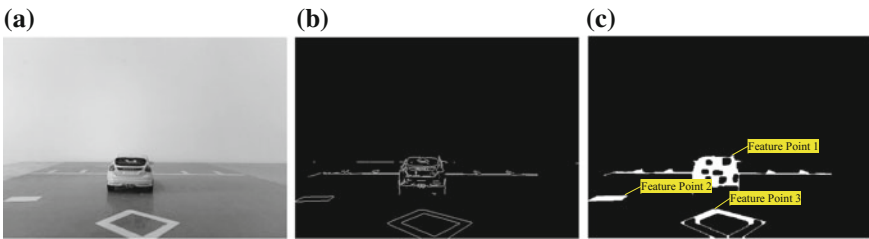


**Fig. 7** Feature points tracking. **a** Image at $t = t + \Delta t$. **b** Result of edge detection. **c** Morphological processing and feature points (the * are feature points)
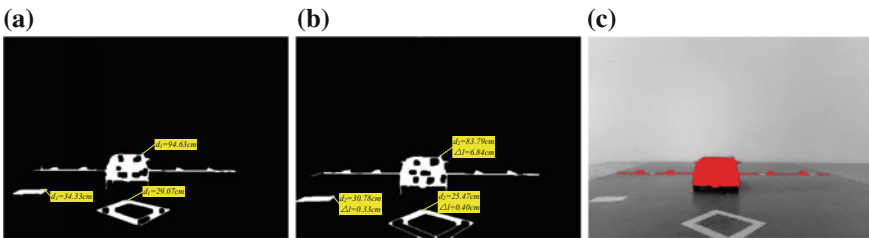


**Fig. 8** Obstacle detection. **a** Horizontal distance $d_1$. **b** Horizontal distance $d_2$ and $\Delta l$. **c** Detected obstacle (the red region is confirmed obstacle)

sidered as ROIs' image regions at $t = t + \Delta t$. Midpoints on the upper edge of ROIs are considered as feature points (see Fig. 7c).

Assuming feature points are at the horizontal plane, horizontal distance $d_2$ between feature points and the camera at $t$ ($t = t + \Delta t$) is calculated. $\Delta l$ and $k$ ($k = 2$ cm) are compared to confirm obstacles, and the confirmed ROIs are marked (see Fig. 8c).

**Table 1** Confusion matrix of detection result

| | | Actual | |
|---|---|---|---|
| | | Positive | Negative |
| Detected | Positive | $b_i$ | $a_i$ |
| | Negative | $c_i$ | $d_i$ |

# 4 Effect Analysis of Vision-IMU Based Obstacle Detection Method

Adaboost cascade detection method is a typical machine learning method, and it is widely used in obstacle because of its high accuracy and speed in target recognition [23–26]. A 20 levels Adaboost cascade detector using the HOG feature is built, and the maximum false detection rate for each level of the cascade detector is 0.2. The car_train image data set of Stanford University Krause is artificially labeled, and the labeled regions are taken as the positive samples. The Pasadena_Houses_2000 image data set of the computer vision research group of California Institute of Technology is selected to provide negative samples. Adaboost cascade detector is trained using positive and negative samples.

Indoor experiments are processed, and in the experiments, horizontal distances between camera and vehicle are 30, 40 and 50 cm, average speeds of movable platform are 2, 4 and 6 cm/s, average speeds of vehicle scaling model are 0, 2 and 4 cm/s. Data of indoor experiments are processed by Vision-IMU based obstacle detection method and trained Adaboost cascade detector to compare the detection accuracy and detection speed.

## 4.1 Analysis of Detection Accuracy

Producer's Accuracy (PA), User's Accuracy (UA), Overall Accuracy (OA), and κ are widely used in the field of remote sensing and pattern recognition because of high universality [27–29]. PA, UA, OA, and κ are thus used as the evaluation indexes.

The number of pixels that are detected as obstacles by detection method but actually are not obstacles is $a_i$. The number of pixels that are detected as obstacles and actually are obstacles is $b_i$. The number of pixels that are not detected as obstacles by detection method but actually are obstacles is $c_i$. The number of pixels that are not detected as obstacles by detection method and actually are not obstacles is $d_i$. Confusion matrix of detection results is shown in Table 1.

$a = \sum_{i=1}^{n} a_i$, $b = \sum_{i=1}^{n} b_i$, $c = \sum_{i=1}^{n} c_i$, $d = \sum_{i=1}^{n} d_i$, and PA can be calculated as:

$$PA = \frac{b}{b+c} \tag{4}$$

**Table 2** Confusion matrix of Vision-IMU method detected results

|  |  | Actual | |
|---|---|---|---|
|  |  | Positive | Negative |
| Detected | Positive | $1.917 \times 10^5$ | $1.457 \times 10^4$ |
|  | Negative | $3.132 \times 10^3$ | $8.085 \times 10^6$ |

**Table 3** Confusion matrix of Adaboost cascade method detected results

|  |  | Actual | |
|---|---|---|---|
|  |  | Positive | Positive |
| Detected | Positive | $1.694 \times 10^5$ | $3.975 \times 10^4$ |
|  | Negative | $2.543 \times 10^4$ | $8.060 \times 10^6$ |

**Table 4** Comparison of detection accuracy

|  | PA | UA | OA | κ |
|---|---|---|---|---|
| Vision-IMU method | 0.984 | 0.929 | 0.998 | 0.967 |
| Adaboost cascade method | 0.869 | 0.810 | 0.992 | 0.847 |

UA can be calculated as

$$UA = \frac{b}{a+b} \tag{5}$$

OA can be calculated as

$$OA = \frac{b+d}{a+b+c+d} \tag{6}$$

κ can be calculated as

$$\kappa = \frac{(a+b) \times (b+d) + (c+d) \times (b-a)}{(a+b) \times (a+d) + (b+c) \times (c+d)} \tag{7}$$

Confusion matrix of Vision-IMU method detected results is shown in Table 2. Confusion matrix of Adaboost cascade method detected results is shown in Table 3. Comparison of detection accuracy is shown in Table 4 and Fig. 9.

It can be seen in Table 4 and Fig. 9 that the accuracy indexes of Vision-IMU based obstacle detection method are higher than the accuracy indexes of Adaboost cascade detector in vehicle obstacle detection. The essence of Adaboost cascade detection method is Bias classification, its accuracy is affected by the quality and quantity of training samples, and the accuracy of Adaboost cascade detection method thus be reduced. In addition, an Adaboost cascade detector can only detect one class of

**Fig. 9** Histogram of detection accuracy



Legend: Vision-IMU Method; Adaboost Cascade Method
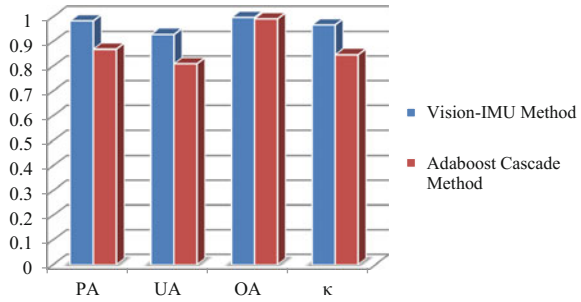
**Table 5** Average time of obstacle detection

| | Before moving/s | After moving/s | Total time/s |
|---|---|---|---|
| Vision-IMU method | 0.202 | 0.385 | 0.587 |
| Adaboost cascade method | – | – | 0.808 |

targets, if obstacles in experiments are not vehicles, Adaboost cascade detector will not detect obstacles effectively.

## 4.2 Analysis of Detection Speed

Data of images and camera poses before and after moving should be processed in the Vision-IMU based obstacle detection method, the time of processing image and camera pose data before and after moving is counted separately in the Vision-IMU based obstacle detection method to compare detection speeds of the Vision-IMU and Adaboost cascade obstacle methods. The average time of obstacle detection is shown in Table 5.

It can be seen in Table 5 that the speed of Vision-IMU based obstacle detection method is faster than the speed of Adaboost cascade obstacle detection method. Only one of camera parameters, the camera pitch angle, is used in Vision-IMU based obstacle detection method, and the processing scale of camera pose data thus is reduced. Midpoints on the upper edge of ROIs are considered as feature points, and time consumption for distance calculation thus is reduced.

## 5 Conclusion

The Vision-IMU based obstacle detection method based on the principle of pinhole imaging, monocular camera, and inertial measurement unit is proposed to bypass obstacle classification and to reduce time and space complexity for road environment perception. The theoretical feasibility of detection method combining monocular camera with inertial measurement unit is proved through deriving horizontal distances from camera to still obstacle and moving obstacle. The obstacle detection steps and indoor experiments are shown to expound the detection process of the Vision-IMU based obstacle detection method. The Vision-IMU based obstacle detection method and Adaboost cascade detection method are used to detect obstacles in indoor experiments, and the PA, the UA, the OA, and κ are used as evaluating indicators to compare test results, the results show that the Vision-IMU based obstacle detection method has higher accuracy, and the reason of high accuracy is analyzed. The processing time of the Vision-IMU based obstacle detection method and Adaboost cascade detection method are compared, the results show that the Vision-IMU based obstacle detection method has faster processing speed, and the reason of faster processing speed is analyzed.

In indoor experiments, the accuracy of displacement based on inertial data can be guaranteed mainly because the movable platform mounted with monocular camera and IMU is not moving continuously, and the effects of Vision-IMU based obstacle detection method thus are ideal. During real vehicle driving, data needs to be acquired and processed continuously, the error accumulation based on pure inertial measurement unit will be more significant, and detection accuracy of the Vision-IMU based obstacle detection method thus may be affected. Therefore, author will analyze the causes of data drift in inertial measurement system, will explore the error correction method in vehicle Vision-IMU based obstacle detection system, and will provide reference for vehicle obstacle detection system to improve accuracy and to reduce time and space complexity.

## References

1. Liu T, Zheng N, Zhao L, et al (2005) Learning based symmetric features selection for vehicle detection. In: Proceedings of intelligent vehicles symposium, IEEE. IEEE, pp 124–129
2. Tsai LW, Hsieh JW, Fan KC (2007) Vehicle detection using normalized color and edge map. IEEE Trans Image Process 16(3):850–864
3. Mori H, Charkari NM (1993) Shadow and rhythm as sign patterns of obstacle detection. In: IEEE international symposium on industrial electronics, 1993. Conference Proceedings,

ISIE'93-Budapest. IEEE, pp 271–277

4. Ravindran V, Viswanathan L, Rangaswamy S (2016) A novel approach to automatic road-accident detection using machine vision techniques. Int J Adv Comput Sci Appl 7(11):235–242

5. Yousef KMA, Al-Tabanjah M, Hudaib E et al (2015) SIFT based automatic number plate recognition. In: International conference on information and communication systems. IEEE, 36–39

6. Elkerdawi SM, Sayed R, Elhelw M (2014) Real-time vehicle detection and tracking using haar-like features and compressive tracking. ROBOT2013: First Iberian robotics conference. Springer, Berlin, pp 381–390

7. Elkerdawy S, Salaheldin A, Elhelw M (2015) Vision-based scale-adaptive vehicle detection and tracking for intelligent traffic monitoring. In: IEEE international conference on robotics and biomimetics. IEEE, pp 1044–1049

8. Miller N, Thomas MA, Eichel JA, et al (2015) A hidden Markov model for vehicle detection and counting. In: Computer and robot vision. IEEE, pp 269–276

9. Momin BF, Mujawar TM (2015) Vehicle detection and attribute based search of vehicles in video surveillance system. In: International conference on circuit, power and computing technologies. IEEE

10. Pepikj B, Stark M, Gehler P et al (2013) Occlusion patterns for object class detection. In: IEEE conference on computer vision and pattern recognition. IEEE, pp 3286–3293

11. Hu Q, Paisitkriangkrai S, Shen C et al (2015) Fast detection of multiple objects in traffic scenes with a common detection framework. IEEE Trans Intell Transp Syst 17(4):1002–1014

12. Pomerleau DA (1993) Knowledge-based training of artificial neural networks for autonomous robot driving. Robot learning. Springer, Berlin, pp 88–97

13. Xiao L, Dai B, Liu D et al (2016) Monocular road detection using structured random forest. Int J Adv Rob Syst 13(3):101

14. Sivaraman S, Trivedi MM (2010) A general active-learning framework for on-road vehicle recognition and tracking. IEEE Trans Intell Transp Syst 11(2):267–276

15. Song X, Rui T, Zha Z et al (2015) The AdaBoost algorithm for vehicle detection based on CNN features. In: The, international conference, pp 1–5

16. Goodfellow I, Pouget-Abadie J, Mirza M et al (2014) Generative adversarial nets. In: Advances in neural information processing systems, pp 2672–2680

17. Badrinarayanan V, Kendall A, Cipolla R (2017) SegNet: a deep convolutional encoder-decoder architecture for scene segmentation. IEEE Trans Pattern Anal Mach Intell 2017:1–14

18. Tang SJW, Ng KY, Khoo BH et al (2015) Real-time lane detection and rear-end collision warning system on a mobile computing platform. In: IEEE, computer software and applications conference. IEEE Computer Society, pp 563–568

19. Trivedi MM, Moeslund TB (2015) Trajectory analysis and prediction for improved pedestrian safety: integrated framework and evaluations. In: Intelligent Vehicles Symposium (IV), 2015 IEEE. IEEE, pp 330–335

20. Yao J, Ramalingam S, Taguchi Y et al (2015) Estimating drivable collision-free space from monocular video. In; 2015 IEEE Winter Conference on Applications of computer vision (WACV). IEEE, pp 420–427

21. Wang H, Yuan C, Cai Y (2015) Smart road vehicle sensing system based on monocular vision. Optik-Int J Light Electron Opt 126(4):386–390

22. Park KY, Hwang SY (2014) Robust range estimation with a monocular camera for vision-based forward collision warning system. Sci World J 2014

23. Viola P, Jones MJ (2001) Robust real-time object detection. Int J Comput Vision 57(2):87

24. Schapire RE (1990) The strength of weak learn ability. Mach Learn 5(2):28–33

25. Schapire RE (1999) A brief introduction to boosting. In: Sixteenth international joint conference on artificial intelligence. Morgan Kaufmann Publishers Inc., pp 1401–1406

26. Freund Y, Schapire RE (1999) A decision-theoretic generalization of on-line learning and an application to boosting. J Comput Syst Sci 55(1):119–139

27. Patel AK, Chatterjee S, Gorai AK (2017) Development of machine vision-based ore classification model using support vector machine (SVM) algorithm. Arab J Geosci 10(5):107

28. Perea-Moreno AJ, Aguilera-Ureña MJ, Meroño-De Larriva JE et al (2016) Assessment of the potential of UAV video image analysis for planning irrigation needs of golf courses. Water 8(12):584
29. Khehra BS, Pharwaha APS (2016) Classification of clustered microcalcifications using MLFFBP-ANN and SVM. Egypt Inform J 17(1):11–20

# Research on Coordinated Transportation of Passenger Transport and Logistics Between Cities

## —Taking Jiaozuo City as an Example

**Xianghong Li, Gaobo Zhao, ZhiQin Xue and Biao Liang**

**Abstract** The study is based on the phenomenon that there are obvious excessively supply of baggage luggage warehouse of passenger bus between the cities in off-peak hours and there are the demands for logistics express for explosive growth. The means of transporting objects and the needs of passenger objects were investigated by random extraction with questionnaire. The characteristics of passenger transport and logistics express were described by analyzing the questionnaire, then the passenger transport operational status between Jiaozuo city and other cities was extracted. The feasibility and key issues about coordinated transportation of passenger transport and logistics between cities were analyzed. Specific measures and suggestions about it were discussed. A new low-carbon logistics service mode is developing, combining to passenger transport between cities to remaining capacity and improving the operation efficiency of public transport system.

**Keywords** Passenger transport and logistics between cities · Coordinated transportation · Third-party platform construction

X. Li (✉) · G. Zhao · Z. Xue
School of Energy Science and Engineering, Henan Polytechnic University, Jiaozuo 454000, China
e-mail: lixianghong001@126.com

B. Liang
School of Electrical Engineering and Automation, Henan Polytechnic University, Jiaozuo 454000, China

# 1 Introduction

According to incomplete statistics, the luggage compartment of each bus has about 40% spare traffic volume (about 600–800 kg) and about 45% space (about 3–4 m$^3$) [1]. Therefore, the full use of excess capacity, combined with the convenience and speed of public transportation can not only simplify public transportation operation organization and reduce resource investment but also increase passenger transport companies' operating income, expand transportation method for logistics, and provide new opportunity for city logistics [2]. Under this background, this paper has carried out a research on coordinating intercity public passenger transportation and logistics [3].

Domestic and foreign research on coordinated transportation of passenger transport and logistics between cities is less. Cheng Hua used bar code technology to optimize the operation process, reduce the cost of passenger express delivery, and enhance the competitiveness of passenger transport [4]. Gao Peng combined the situation of the domestic and international small pieces of express development, summarized the existing problems and shortcomings in the development of China's small pieces of express, and put forward the development countermeasures [5]. Yang Zhongzhen used the survey data to build a behavior model to analyze customer's choice express way, and based on this model, analyzed customer's behavior and calculated the sensitivity of the customer to the density of passenger express outlets. Finally, he proposed recommendations about integrating passenger transport and bus terminal site resources, and provided marketing strategy to expand market share for passenger express enterprises [6]. In short, the domestic and international passenger and freight transport research was the initial stage, and coordinated the transportation of passenger transport and logistics between cities less.

Because the city public transport have the characteristic that the idle rate of bus passenger luggage compartment is higher in time and space, this paper carried out research on coordination bus freight to achieve the reuse of idle resources.

# 2 Data Sources

As far as Jiao Zuo is concerned, the survey shows that the average number of transporting objects per person per year is 3, and the population of JiaoZuo city is about 817 thousand, so only the number of the annual use of transport cargo through passenger car in Jiaozuo city is 2,451,000. The market for the delivery of cargo is considerable. This is most of the share of the courier company, and the use of other modes of transport is very seldom. This paper aims to enhance the scope of service by improving the quality of service in transporting cargo through passenger car.

**Table 1** The issue and recovery of the questionnaires

| Mode of questionnaire | Issue amount | Recovery amount | Rate of recovery | Effective questionnaires |
|---|---|---|---|---|
| Field release questionnaire | 500 | 500 | 100% | 482 |

## 2.1 The Selection of Investigation Radius

This paper consulted the express company of Yuan Tong and Yun Da's site distribution. The Jiaozuo passenger station was selected as the center point, and then we determined the radius of investigation, respectively by 1, 2, 5 km. Within this radius, questionnaire survey was conducted.

## 2.2 Questionnaire Design Attributes

The content of the questionnaire design was divided into three parts: the first part was used to collect respondent's individual information; the second part was used to collect respondent's transport cargo information; the third part was the core part, which was used to collect respondent's the information of transport cargo through passenger car. This section was mainly used to learn whether the respondents knew transport cargo through passenger car, whether they used this mode, as well as the frequency of using it. Through these information, we got the feedback information of its users. In particular, we carried out further investigation on these users, and then collected this mode's advantages, shortcomings and views about this kind of logistics mode. During this period, we learned the information of users' needs when they transported cargo. This information was used to anticipate the latter period of the APP features.

## 2.3 The Issue and Recovery of the Questionnaires

In order to fully understand the information of JiaoZuo city residents and Henan Polytechnic University's transporting cargo through passenger cars, the questionnaire was issued mainly in the way of field release.

As shown in Table 1, the questionnaire was carried out between December 2015 and January 2016. 500 questionnaires were issued, and 500 were recovered, so the recovery rate was 100%, among which 482 were effective questionnaires.

## 3   Analysis on the Research in Jiaozuo City

### 3.1   Analysis of the Characteristics of the Cargo Transportation Mode

#### 3.1.1   Transport Cargo Mode Distribution

In this survey, in order to statistic respondent's the mode of transport cargo, this question was designed: "which mode you often use to transport cargo", and the options were divided into: courier companies, postal, transport cargo through passenger car, railway passenger cargo, or other. People selected courier companies accounted for 88.79%, selected postal accounted for 14.42%, selected transport cargo through passenger cargo accounted for 11.44%, and selected railway passenger cargo accounted for 2.06%, as shown in Table 2:

#### 3.1.2   The Evaluation of Transporting Cargo Through Passenger Car and Goods Type

According to the survey results, the advantages of this mode as follows: choose "fast" accounted for 44.89%, "safety" accounted for 11.68%, "cheap" accounted for 17.52%, "convenient" accounted for 37.59%, "the courier cannot reach" accounted for 11.31%, "the other" accounted for 17.15%. This mode drawbacks are: choose "the price is too high" accounted for 34.62%, "the distance is too far and not easily" accounted for 24.52%, "check procedures did not express a clear" accounted for 37.98%, "don't have the security as express" accounted for 25.96%, "the other" accounted for 13.46%. As shown in Table 3:

Based on the advantages and disadvantages of passenger shipping, in order to better analyze the characteristics of this mode, this paper classified the express type of this mode: emergency cargo, important cargo, large cargo (such as box), small cargo (such as documents, letters), and so on. The results of choicing "Emergency cargo" accounted for 48.07%, "important cargo" accounted for 7.02%, "large objects (such as trolley)" accounted for 36.84%, "small cargo (such as documents, letters)" accounted for 22.11%.

**Table 2**  Distribution of transport cargo in the survey

| Mode | Percentage (%) |
| --- | --- |
| Courier companies | 88.79 |
| Postal | 14.42 |
| Transport cargo through passenger car | 11.44 |
| Railway consignment | 2.06 |
| Other | 2.06 |

**Table 3** The evaluation of transporting cargo through passenger car

| Advantages | Percentage (%) | Disadvantages | Percentage (%) |
|---|---|---|---|
| Fast | 44.89 | Charge too high | 34.62 |
| Safety | 11.68 | Too far, not convenient | 24.52 |
| Cheap | 17.52 | Check procedures not clear | 37.98 |
| Convenient | 37.59 | Not express security | 25.96 |
| Courier cannot reach | 11.31 | Other | 13.46 |
| Other | 17.15 | | |

# 4 Problems and Solutions

## 4.1 Problems Existing in Transporting Cargo Through Passenger Car

This mode could make full use of the remaining space of cargo of a passenger car, which can not only provide income for the passenger transport company but also can be convenient for the public. As a result, it should be fully developed, but in practice, most of the utilization rate was very low in this mode and passenger check-in service business was also very poor, causing a waste of resources. Through our questionnaire and the interview with the shipping agency for passenger car, some existed problems were discovered in this mode at present:check-in procedures not promising; expensive charge; using it not convenient; Poor Safety.

## 4.2 Solutions to the Problems

### 4.2.1 Establish a Third-Party Platform

This article put forward an improved operation mode for the problems above in order to make the passenger coach consignment more standardized and reasonable and let more customers choose this mode. A third-party platform will be established which combined the data of the mass demand for the express transport and the idle space resources in the coach to transport the express.

We integrated all coach timetables in the bus station and the real-time data of the present surplus space when designed the platform. Users only needed to update once, and the best time passenger coach consignment information can be accessible. It can follow the express company to possess reasonable distribution office, which will be facilitated the masses sending express nearby. Users can inquire the latest coach, fix in advance if there was surplus in the baggage compartment, and will

get serial number and using password after the online payment. Cargo will be sent to the nearby office leaning on the serial number and using password and to the corresponding coach timely based on the needs, which ensured customer's cargo arrived at the destination in the minimum time.

In this way, customers will only need to inquire and pay online and then send the cargo to the nearby office, which simplifies the consignment program greatly. Meanwhile the platform cuts down the cost of the express via increasing volume and solve the problem of high charge.

### 4.2.2 Perfect Consignment Procedure

In this information society, the procedure of passenger coach consignment resembles a black box as before. On the one hand, customers cannot grasp the real-time condition of their cargo after handing the express to the coach station; while on the other. Working in the coach station is correspondingly complex and error-prone as the station contacts the customer only over the phone. Therefore, this article will develop an APP utilizing data cloud technology to assist the customers and the station. This APP can collect available coach consignment space timely while customers can gain access to the needed coach information, such as coach departure time, arrival time, track positions constantly, fix in advance online and pay online, which made the passenger coach consignment more standardized and reasonable and allowed a safer using experience to the customers.

### 4.2.3 Add Sending-and-Receiving Site

In this rapid economic growth society, the living standards of the people is higher and their payment capacity is stronger, thus their service requirement increases. Express had provided the service of home delivery and pick-up for a long time. Passenger coach consignment should improve service quality according to the requirement of the service object. Coach station can add the service of home delivery and pick-up and enhance service quality to promote the economic benefit of the station. Coach station can set sending-and-receiving site in cities and develop city networking business if construction conditions were allowed. Passenger coach consignment can provide rapid and on-time consignment service for customers owing to the fact that the departure interval of the coach is short and departure time is regular.

### 4.2.4 Make Suitable Toll Standard

From the point of charge price, at present, the toll standard hanging in Jiaozuo coach station was the one that our nation issued in 1985 which was too obsolete to be adopted by the toll staff in the station. According to our investigation, the toll in Jiaozuo coach station was based on the experience of toll staff without unified

standards. We proposed that coach should improve toll standards referring to the toll standards of express company so as to increase service attraction.

### 4.2.5 Rev up Publicity

From the point of propaganda, suggestions came that stations can hang identification cards in the waiting room and stick advertisement in the coach, as station can attract large passenger flow to take the bus every day, to play a favorable propaganda effect.

## 5 The Third-Party Platform Construction Concept

This paper developed an APP called Passenger coach consignment for the problems above. The achievement of the system mainly applies Android which is supported by JAVA language development and background data processing. The main technology of the system includes JSOUP crawling web data, multithread concurrent task processing technique, asynchronous task processing, JDBC technique, using JSON data encapsulation and analysis and using HTTP protocol to complete the data transmission between server and Android (Fig. 1).

   The first step is to register a "Passenger coach consignment" account number so as to keep the information and record of the customer. The second is to log on cell phone side "Passenger coach consignment" APP via account number and password. The third is to select data, place of departure, and destination which needs to be inquired, it will present a page similar to coach timetable after that. Customer can know the departure time, surplus space and the number of people who have booked the luggage compartment at present. The fourth is to click reservation button and then fill in the general volume of the cargo and some matters needing attention. The last is to pay the fee which is counted by the system according to the information customer filling in and relevant state provisions. Customer can query to the ordered record in 'My Order' after ordering.
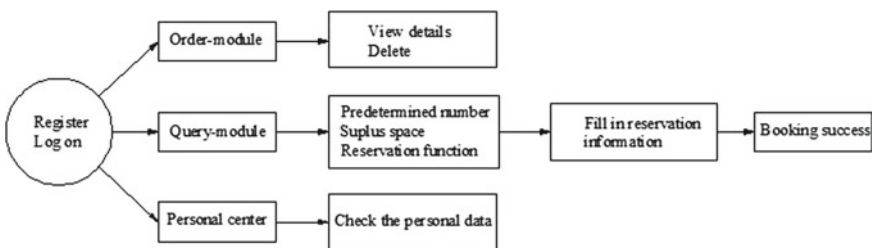


**Fig. 1** Express passenger flow chart

# 6   Summary and Outlook

1. The paper carried out research on coordination bus freight and achieved the reuse of idle resources, as the city public transport has the characteristics of bus passenger luggage compartment idle rate higher in time and space.
2. The main reasons for the low utilization rate of passenger coach consignment included the confused consignment procedure, high charge, poor convenience, and poor security. In order to solve the problems above, some useful resolutions and strategies were put forward and applied. At the same time, the concept of " Internet plus" was applied in passenger coach consignment management, so the third-party APP service platform, combined with the advantages and disadvantages of passenger transport, was developed, which favors improving service quality.

# References

1. Chen Z Chain's modern logistics industry development. Inner Mongolia University', pp 45–53
2. Liu Y (2013) The study on the modern logistics development in the context of low-carbon economy. China Bus Trade 11:50–58
3. Shan T (2011) The PRTB express delivery optimization research. Highw Transp Logistics 2011(12):50–18
4. Cheng H, Sun X (2012) Study on competitiveness in roadway parcel express transportation. Transp Technol 31(9):28–31
5. Gao P, Dong H, Zhang Z (2011) To learn fast small freight transport again. Highw Transp Logistics 2011(1):189–192
6. Yang Z, Zou W (2009) Competitiveness and marketing strategy of road passenger transport based express. J Transp Syst Inf Technol 9(5):11–16

# Study on the Influence of Vehicle Structural Parameters on Vehicle Handling Stability

**Xian-sheng Li, Da-wei Xing, Xue-lian Zheng, Yuan-yuan Ren, Xiang-yu Meng and Jie Sun**

**Abstract**  In order to explore the strategy that improves the vehicle handling stability, a 3-DOF vehicle model of angle step input was simulated based on MATLAB. The influence of vehicle structural parameters on vehicle handling stability based on high lateral acceleration was analyzed. Then, the influence of suspension sway bar on vehicle handling stability based on field vehicle test also was analyzed. The results show that, wheelbase, damping shock absorber and suspension roll angle stiffness are the important factors that influence the vehicle handling stability when the vehicle has a high lateral acceleration. With the increasing of vehicle velocity, the importance of stabilizer bar on vehicle handling stability enhance as well. Understeer and roll characteristic is improved by changing the diameter of the sway bar. Furthermore, the vehicle handling stability is improved and the security of vehicle driving is enhanced.

**Keywords**  Driving stability · Body roll angle · Stabilizer bar · Structural parameter · Matlab

## 1 Introduction

According to statistics, about 40% traffic accident associated with vehicle instability when the speed of vehicle traveling is between 80 and 100 km/h [1]. The main reason for the instability of the vehicle is the poor safety performance of the vehicle. It is

X. Li · D. Xing · X. Zheng (✉) · Y. Ren · X. Meng
School of Transportation, Jilin University, Changchun 130022, China
e-mail: zhengxuelian@jlu.edu.cn

D. Xing
Jilin Provincial Expressway Administration, Changchun 130022, China

J. Sun
TRW Asia Pacific Co Ltd, Changchun 130022, China

necessary to define the main structural parameters that affect the handling stability of the vehicle, which can provide a reference for the vehicle designing and improvement of vehicle handling stability.

At present, the test methods of vehicle driving stability are divided into two kinds: field vehicle test and simulation [2–5]. And the evaluation methods can be divided into subjection evaluation and objection evaluation [6, 7]. The field vehicle test method is the best basic method. But the cost is higher and the risk is bigger. The simulation method has been widely used in the simulation test of vehicle handling stability. Subjective evaluate the vehicle's stability based on felling of testing. Objective evaluation is to collecting the physical parameter that relates with vehicle stability. For example, yaw rate, lateral acceleration, roll angle.

Combining MATLAB simulation with filed vehicle test, the influence of vehicle structure parameters on vehicle driving stability was analyzed. Furthermore, the influence of front suspension stabilizer bar on vehicle handling stability was analyzed.

## 2   Vehicle Dynamics Model

### 2.1   Car Coordinate System

An absolute space coordinate system *X-Y-Z* was built. The longitudinal direction of the vehicle body is X-axis. The lateral direction of the vehicle body is Y-axis. The vertical direction of vehicle body is Z-axis. Under the condition of vehicle static, the coordinate system of vehicle's spring x-y-z was established. When the straight intersection of the gravity center of the vehicle and the vehicle roll axis mingled, the point as the start point of *x-y-z*. Similarly, taking the same point as the coordinate origin. That coordinate system is fixed to the lower part of the vehicle. As shown in Fig. 1.

**Fig. 1**   Coordinate system
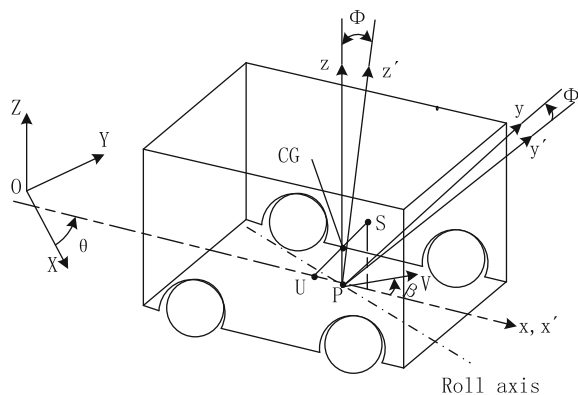
## 2.2  Construction of Vehicle Dynamics Model

Assuming that roll motion is around the X-axis and the yaw movement is around Z-axis. Meanwhile, assuming that the lower part of the vehicle has no roll movement and make the same yaw movement as the vehicle body, without considering the camber thrust that caused by wheel camber.

The vehicle motion equation was established by using three degrees of freedom: the yaw motion, the roll motion, and the lateral motion,

$$
\begin{aligned}
&mV(\tfrac{\mathrm{d}\beta}{\mathrm{d}t}+r)\cos(\beta)-m_S h_S \tfrac{\mathrm{d}^2\varphi}{\mathrm{d}t^2}=2F_f+2F_r\\
&I_z \tfrac{\mathrm{d}r}{\mathrm{d}t}-I_{xz}\tfrac{\mathrm{d}^2\varphi}{\mathrm{d}t^2}=2F_f l_f-2F_r l_r \qquad\qquad\qquad (1)\\
&I_x \tfrac{\mathrm{d}^2\varphi}{\mathrm{d}t^2}-I_{xz}\tfrac{\mathrm{d}r}{\mathrm{d}t}-m_S h_S V(\tfrac{\mathrm{d}\beta}{\mathrm{d}t}+r)\cos(\beta)=(-K_\varphi+m_S g h_S)\varphi-C_\varphi \tfrac{\mathrm{d}\varphi}{\mathrm{d}t}
\end{aligned}
$$

where

$m$      is the mass (kg).
$V$      is the velocity of the point P (m/s).
$\beta$      is the side slip angle of the point P (rad).
$r$      is the yaw rate (rad/s).
$m_s$     is the sprung weight (kg).
$h_s$     is the rolling moment arm (m).
$\varphi$      is the roll angle of the vehicle body (rad).
$F_f$     is the cornering force of the front wheel (N).
$F_r$     is the cornering force of the rear wheel (N).
$I_z$     is the moment of inertia around the Z-axis (kg m$^2$).
$I_{xz}$    is the product of inertia around the X-axis and Z-axis (kg m$^2$).
$l_f$     is the distance of vehicle center with vehicle front-axle (m).
$l_r$     is the distance of vehicle center with rear-axle vehicle (m).
$I_x$     is the moment of inertia around the X-axis (kg m$^2$).
$K_\varphi$     is the roll angle stiffness of the suspension (N m/rad).
$g$      is the gravitational acceleration (m/s$^2$).
$C_\varphi$     is the roll damping of the suspension (N m s/rad)

The cornering force of the tire is expressed by the magic tire formula that was proposed by Pacejka et al. [8].

## 3  The Influence of Vehicle Structural Parameters on Vehicle Handling Stability

The vehicle's driving safety and comfort will be improved by researching about the influence of that vehicle's structure parameters to vehicle' driving stability.

**Fig. 2** The roll angle total variance with different structural parameters
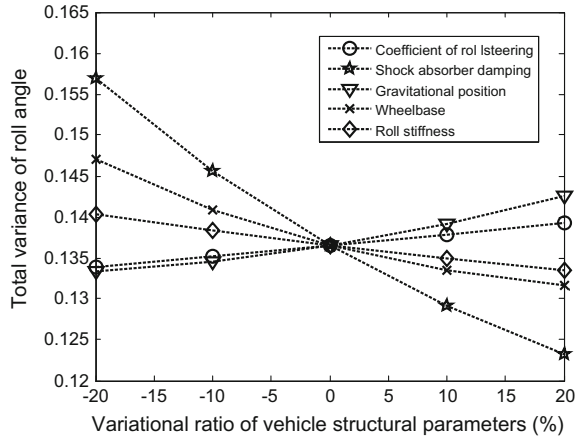


The evaluation indexes of the total variance were selected to analyze the vehicle's roll stability. The total variance of vehicle roll angle indicates the risk of rollover. And the smaller total variance, the lower risk of rollover.

The equation of total variance is

$$E = \int\limits_{0}^{\infty} (y(t)/y_0 - x(t)/x_0)^2 d_t \qquad (2)$$

where

$E$    is total variance,
$y(t)$ is output of system,
$x(t)$ is input of system,
$y_0$  is the steady-state value of $y(t)$,
$x_0$  is the steady-state value of $x(t)$ [9]

The results of MATLAB simulation of the body roll angle as shown in Fig. 2, under the condition that vehicle speed is 30 km/h and the steering wheel of front is step input with 4.7 rad degree angle.

As can be seen from Fig. 2,

- When the center of gravity moves forward by 20%, the total variance of roll angle decrease from 0.136 to 0.133. The total variance decline, the vehicle roll stability is improved.
- When the roll steering coefficient of front wheel decrease by 20%, the total variance of roll angle decrease from 0.136 to 0.134. The total variance decline, the vehicle roll stability is improved.
- When the roll angle stiffness of front suspension decrease by 20%, the total variance of roll angle increase from 0.136 to 0.141. The total variance improves, the vehicle roll stability is declined.

- When the wheelbase shortens to 20%, the total variance of roll angle increase from 0.136 to 0.147. The total variance improves, and the vehicle roll stability is declined.
- When the shock absorber damping decrease by 20%, the total variance of roll angle increase from 0.136 to 0.156. The total variance improves, and the vehicle roll stability is declined.

The above show that wheelbase, shock absorber damping, roll stiffness of the front suspension, center of gravity, and roll steering coefficient of front wheel are having an influence on the roll stability of vehicle when the vehicle is driven at high speed. Where, the center of gravity and the roll steering coefficient of the front wheel have little effect on vehicle roll stability.

Vehicle is a complex system. There is a certain relationship between the various components and have a mutual influence. For example, appropriately improving the damping of the shock absorber can increase the stability of the vehicle. When the rear wheelbase of the vehicle is changed, it will lead to the changing of the load distribution of the front-axle and rear-axle. Therefore, it is difficult and expensive to improve the safety of vehicle when changing the parameters of shock absorber damping, vehicle wheelbase, and so on.

The stabilizer bar is installed in the vehicle suspension system, which will change the value of roll angle stiffness of the suspension. It is convenient, inexpensive, and effective. So, the influence that stabilizer bar to the vehicle driving stability can be analyzed so that exploring the strategy that improves the vehicle handling stability.

## 4 The Influence of Stabilizer Bar on Vehicle Handling Stability

### 4.1 Roll Stiffness of the Stabilizer Bar

Generally, the stabilizer bar is installed in the front suspension and rear suspension or only in the front suspension. The diagram of stabilizer bar is shown in Fig. 3.

The relationship of the roll angular stiffness of front suspension and the angular stiffness of stabilizer bar is as follows:

$$K_f = K + C_{\varphi b} \tag{3}$$

where

$K$     is the roll angular stiffness of the front suspension,
$C_{\varphi b}$   is the angular stiffness of stabilizer bar.

The equation of angular stiffness of stabilizer bar is as follows: [10]
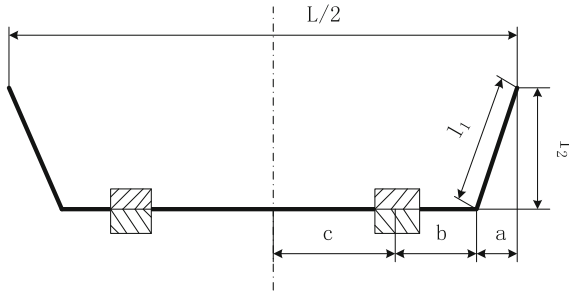
**Fig. 3** Sway bar
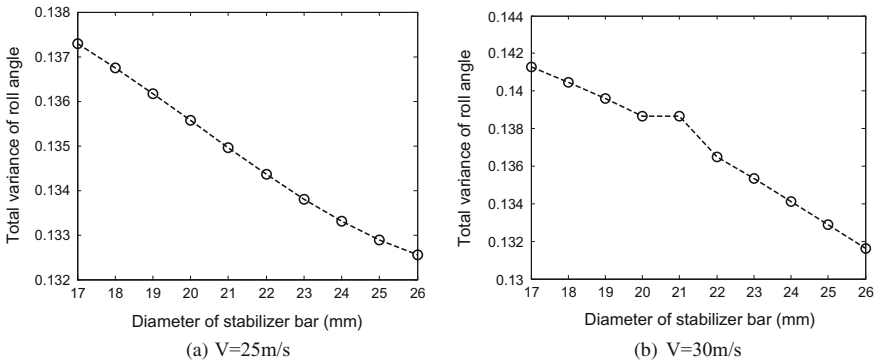


**Fig. 4** Relationship of stabilizer bar with roll angle total variance

$$C_{\varphi b} = \frac{3E_1 I L^2}{2[l_1^3 - a^3 + \frac{L}{2}(a+b)^2 + 4l_2^2(b+c)]} \qquad (4)$$

where

$E_1$   is the elastic modulus,
$I$    is the second moment of area,
$d$    is the diameter of the stabilizer bar. $E_1 = 2.06 \times 10^5$ MPa, $I = \pi d^4/64$, $mm^4$.

## 4.2   The Influence of Stabilizer Bar Diameter on Vehicle Driving Stability

(1)   Simulation results

The relationship of the total variance of roll angle and the diameter of stabilizer bar in high lateral acceleration is shown in Fig. 4.

**Table 1** Roll angle total variance with different diameter of the stabilizer bar

| Diameter of stabilizer bar (mm) | Total variance | |
|---|---|---|
| | $V = 25$ m/s | $V = 30$ m/s |
| $d = 17$ | 0.1373 | 0.1413 |
| $d = 18$ | 0.1367 | 0.1405 |
| $d = 19$ | 0.1362 | 0.1396 |
| $d = 20$ | 0.1356 | 0.1386 |
| $d = 21$ | 0.1350 | 0.1386 |
| $d = 22$ | 0.1344 | 0.1365 |
| $d = 23$ | 0.1338 | 0.1353 |
| $d = 24$ | 0.1333 | 0.1341 |
| $d = 25$ | 0.1329 | 0.1329 |
| $d = 26$ | 0.1326 | 0.1316 |

As can be seen from Fig. 4, the total variance of roll angle will decrease when the diameter of stabilizer bar of front suspension increases. So, the execution result of steering wheel instruction will be improved.

The total variance of roll angle in different velocities and diameter of stabilizer bar, are shown in Table 1.

As can be seen from Table 1, when the diameter of stabilizer bar of front suspension improves from 17 mm to 26 mm and the vehicle velocity is 25 m/s, the total variance of roll angle will decrease from 0.1373 to 0.1326. The total variance will decrease by 3.44%; when the vehicle velocity is 30 m/s, the total variance of roll angle will decrease from 0.1413 to 0.1316. The total variance will decrease by 6.9%. Therefore, the sensitivity of the stabilizer bar of front suspension on vehicle handling stability will be improved with the vehicle velocity improvement.

(2)  The results of field vehicle test

In an A-class vehicle design of the front suspension system, the stabilizer bar of the diameter of 21 and 23 mm was installed in the vehicle. Then, the steady static circular test and the high lateral acceleration steering test were implemented. The results of the test are shown in Tables 2 and 3.

As can be seen from Tables 2 and 3,

- In the case of stabilizer bar of 21 mm diameter, the understeer is 0.31 in the steady static circular test, or is 2.07 in the steering test of higher lateral acceleration. In the case of stabilizer bar of 23 mm diameter, the understeer is 0.36 in the steady static circular test, or is 2.24 in the high lateral acceleration steering test. When the diameter of stabilizer bar is 23 mm, the roll angle stiffness of front suspension will be effectively improved. The vehicle gets a better understeer.
- In the case of stabilizer bar of 21 mm diameter, the roll of vehicle body is 0.55 in the steady static circular test, or is 4.57 in the steering test of higher lateral acceleration. In the case of stabilizer bar of 23 mm diameter, the roll gradient of

**Table 2** Test results of stabilizer bar diameter is 21 mm

| Test content | Parameters | Results | | |
|---|---|---|---|---|
| | | Left turn | Right turn | Mean |
| Steady static circular test | Understeer(°/m/s2) | 0.32 | 0.30 | 0.31 |
| | Roll of vehicle body (°/g) | 0.54 | 0.55 | 0.55 |
| Steering test of higher lateral acceleration | Understeer (°/g) | 2.10 | 2.04 | 2.07 |
| | Roll gradient (°/g) | 4.52 | 4.62 | 4.57 |

**Table 3** Test results of stabilizer bar diameter is 23 mm

| Test content | Parameters | Results | | |
|---|---|---|---|---|
| | | Left turn | Right turn | Mean |
| Steady static circular test | Understeer(°/m/s2) | 0.35 | 0.37 | 0.36 |
| | Roll of vehicle body (°/m/s2) | 0.47 | 0.48 | 0.48 |
| Steering test of higher lateral acceleration | Understeer (°/g) | 2.26 | 2.21 | 2.24 |
| | Roll gradient (°/g) | 3.98 | 4.42 | 4.20 |

vehicle body is 0.48 in the steady static circular test, or is 4.20 in the high lateral acceleration steering test. When the diameter of stabilizer bar is 23 mm, the roll stiffness of front suspension will be effectively improved. The roll of vehicle body will be significantly reduced.

## 5 Conclusion

By the MATLAB simulation and test of the field vehicle, the structure parameters of the vehicle have an influence on the vehicle handling stability. The research shows:

(1) The wheelbase, shock absorber damping, and roll angle stiffness of front suspension have an important influence on the roll stability of the vehicle in the high lateral acceleration. The center of gravity and roll steering coefficient of front wheel have a little influence on the roll stability of vehicle in the high lateral acceleration.

(2) By changing the diameter of the stabilizer bar of the front suspension, the understeer of vehicle and characteristic of roll got better. And the influence strength

of the stabilizer bar of front suspension for the vehicle handling stability will enhance with the velocity improvement in the high lateral acceleration.

The research results can provide a theoretical basis for the design and improvement of vehicle handling stability, as well as to improve the simulation accuracy.

# References

1. Zhang Y (2007) Study on the development of vehicle stability control system based on active braking. Shanghai Jiao Tong University
2. Zhang H (2012) Research on bus handing stability analysis and control strategy. Jilin University
3. Yang M (2014) Research on rural road bus driving stability and driver's visual and physiological characteristics. Jilin University
4. Ahmadi R, Fajri P, Ferdowsi M (2013) Dynamic modeling and stability analysis of an experimental test bench for electric-drive vehicle emulation. In: Power and energy conference at Illinois. IEEE, pp 88–94
5. Yan ZM, Cai JJ, Qu SQ et al (2014) The analysis of amphibious vehicle handling stability based on ADAMS/car. Adv Mater Res 1006–1007(1006–1007):294–297
6. State key laboratory of automotive simulation and control, Jilin University (2008) Subjective evaluation report of vehicle chassis driving performance. Changchun: State key laboratory of automotive simulation and control, Jilin University
7. Hung BM, You SS, Kim HS (2016) Nonlinear vehicle stability analysis. In: The advanced engineering-theory and applications international conference
8. Pacejka HB, Sharp RS (1991) Shear force development by pneumatic tyres in steady state conditions: a review of modelling aspects. Veh Syst Dyn 20(3–4):121–175
9. Wen F, Sun Y (2007) Discussion on evaluation index of vehicle handling stability in open loop test system. 9th Nat Conf Ground Mach Syst
10. Liu W (2001) Automotive design. Tsinghua University Press

# Design of Wireless Monitoring and Pre-warning System of Brake Temperature for Truck Safety Operation

**Fengyuan Wang, Jian Zhong, Mingjie Zhang, Chaohui Yang and Lichao Yang**

**Abstract** In order to detect truck multi-brake temperature in real time, achieve hierarchical warning of high-temperature state, assist driver in completing brake behavior and ensure the safety of the truck brake, a wireless monitoring and pre-warning system of brake temperature for truck safety operation was developed. Based on MCU, milli-volt level voltage signal produced by detecting the brake temperature through PT1000 platinum thermal resistance temperature sensor was sent to LM2904 for signal amplification. Then, the amplified signal was converted to a digital signal by ADS1115 and sent to the receiver master chip and displayed through E31-TTL-50 wireless module. After comparing with the critical value, the system will carry out the hierarchical alarm. This system realized the detection and display of signal in real time and the remote monitoring. In the chapter, the design of the system in hardware and software was introduced. Furthermore, an experiment was conducted to ensure the effectiveness of the system.

## 1 Introduction

In the continuous downhill, turning or emergency stop and other conditions, the brakes need to carry out long-term high-intensity braking, the brake temperature will rise quickly, resulting in decreases of brake friction plate friction coefficient and the braking torque. This is the thermal recession of the brakes. The suitable working temperature brake of friction plate is during 100–350 °C, but many poor

F. Wang · J. Zhong (✉) · M. Zhang · L. Yang
School of Automotive and Transportation, Qingdao University of Technology, Qingdao 266520, China
e-mail: 17863964958@163.com

C. Yang
R&D Center, Qingte Group Ltd Co., Qingdao 266109, China

brake friction plates will fail at a temperature of 250 °C with a sharp decline of the friction coefficient. High brake temperature will directly lead to the rise of tire pressure and temperature, more seriously, may cause a puncture accident. A puncture accident often causes the driver to lose control of the vehicle and lead to a violent traffic accident.

In order to solve the hazard mentioned above during the truck driving, this paper designed a wireless monitoring and pre-warning system of brake temperature for truck safety operation. It adopts an integrated circuit board to control the multichannel temperature signal input, integration degree of the system is high. The system achieves flexible layout with the use of wireless transmission. The system monitors the multi-brake temperature in real time and carries out classification warning for high-temperature status. As a result, it provides a reliable early warning information for the decision-making of driver's braking behavior to avoid risks, improves the safety of the truck driving greatly [1–4].

## 2   System Structure and Working Principle

The three-wire PT1000 platinum thermal resistance temperature sensor mounted on the brake shoe real-time monitors the temperature of each truck brake and passes it to the signal conversion module and there is a corresponding function relationship between the rise of temperature and the increase of thermal resistance. The signal conversion module is composed of measuring bridge, signal amplifying circuit, and analog-to-digital conversion circuit. The measurement bridge converts resistance change of the sensor to voltage signal and eliminates the effect of the wire resistance. Amplified voltage signal was converted into digital signal by the analog–digital conversion circuit and then was sent into the master chip. Master chip achieves the control of data transceiver, completion of data conversion, switch between work and sleep mode, data storage, and other functions. The wireless transmitter module consists of a wireless transmitter chip, other circuit accessories, and an antenna, mounted on the truck frame. The hardware of wireless receiving module is the same as the transmitting modules, the function is receiving signal, and transmits the signal to the master chip of receiver. Display alarm module integrated wireless receiver module, the master chip of receiver, buzzer, and display screen to achieve digital display of multi-channel brake temperature and screen flash and buzzer alarm under 200 alarm degrees, 280 alarm degrees. When the receiver circuit board is power off, the transmitter master and the wireless module will enter the sleep mode. When the temperature of the system is below 150 °C, the wireless module is in the sleep mode; When the temperature of the system is above 150 °C, the wireless module is in the working mod. The system structure is shown in Fig. 1 [5–7].
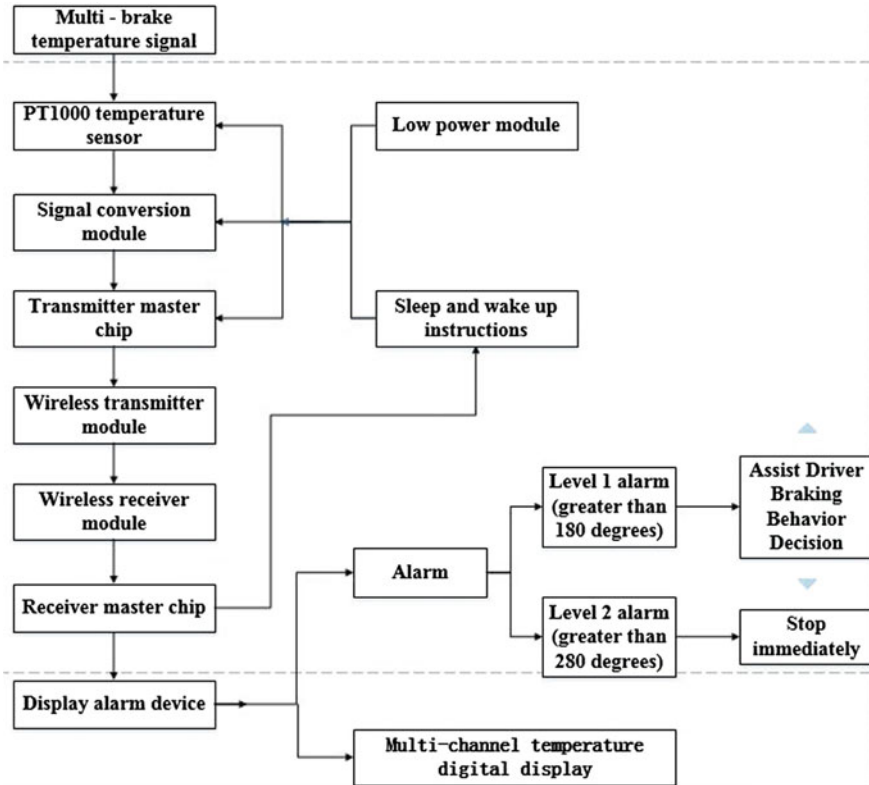
**Fig. 1** System structure diagram

## 3 System Hardware Design

### 3.1 STM32C8T6 Master Microcontroller

The system's main control MCU is 32-bit low-power microcontrollers STM32C8T6. Operating voltage is 2–3.6 V, operating frequency is 72 MHz, there are high-speed memory (64 K bytes flash memory and 20 KB bytes SRAM), 32 enhanced I/O ports and two APB bus peripherals in the MCU.
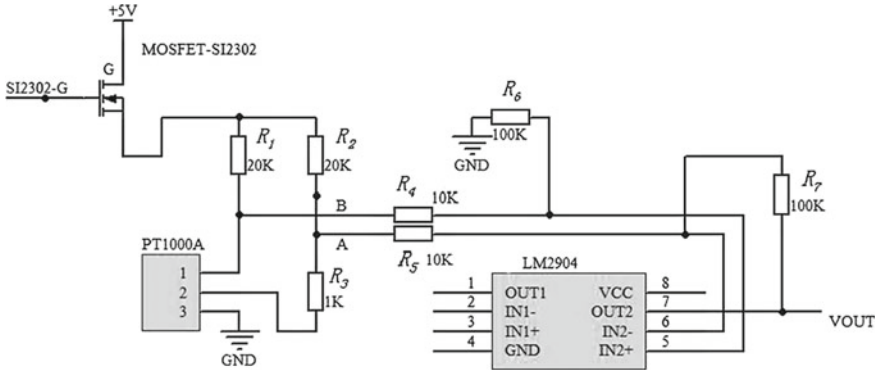
**Fig. 2** Signal processing circuit

## 3.2 Signal Processing Circuit

In the normal operation of the truck, the PT1000 platinum thermal resistance temperature sensors installed in the brake shoes monitors each brake temperature in real time.

The measurement bridge converts the sensor resistance to the corresponding voltage signal and eliminates the wire resistance error. Measurement bridge and LM2904 integrated amplifying circuit are shown in Fig. 2, the reference resistance is 1000 $\Omega$. When the temperature is greater than 0 °C, the sensor resistance is greater than the reference resistance, functional relationship between the potential difference $V_T$ and resistance $R_T$ is

$$R_1 = R_2 = 20\,K\Omega, V_0 = 5\,\text{V}, V_T = 5 \times 2 \times 10^4 \times \left[ \frac{R_T - 1000}{(2 \times 10^4 + 1000)(2 \times 10^4 + R_T)} \right] \quad (1)$$

Sending the sensor's highest temperature 450 °C into the formula, the resistance $R_{\text{MAX}} = 2642\,\Omega$ at this time, into the formula, the voltage value $V_{\text{MAX}} = 0.345$ V. Because the input limit voltage of the selected analog-to-digital conversion chip ADS1115 is 4.096 V, the voltage limit of the regulator tube IN4730 is 3.9 V, and the magnification of the amplifier circuit is determined to be 10 times. The system uses the differential amplifier circuit. The following part applies the principle of superposition for the output voltage of the amplifier circuit $u_0$.

According to the superposition principle, the total output voltage is

$$u_0 = u_0' + u_0'' = -\frac{R_7}{R_5}u_A + \left(1 + \frac{R_7}{R_5}\right)\left(\frac{R_6}{R_4 + R_6}\right)u_B \quad (2)$$

$$R_4 = R_5, R_6 = R_7, \quad \text{So,}\, u_0 = \frac{R_7}{R_5}(u_B - u_A) \quad (3)$$

$R_7 = 100\,K\Omega$, $R_5 = 10\,K\Omega$, amplifier magnification of amplified circuit is 10 times.

### 3.3 433 MHz Wireless Data Transceiver Module

The features of narrowband transmission are power density concentration, long transmission distance, strong anti-interference ability. The module has the software FEC forward error correction algorithm, its coding efficiency is high, error correction ability is strong. Referring to power consumption parameters, the wireless module's normal power is 50 MW, standby current is 1.7 µA. Under the strong shielding condition of the real vehicle experiment, the stable transmission distance of E31-TTL-50 is more than 30 m. In summary, the wireless module E31-TTL-50 met the requirements of transmission distance, anti-shielding, low power consumption, and low data loss, which was suitable for the system.

## 4 Software Design

### 4.1 Software Overall Design

The main flowchart of software was shown in Fig. 3. The receiver sends a wake-up signal to transmitter when the receiver is power on. After transmitter receives the wake-up signal, transmitter will be powered on and reset, collect and process the data to determine whether the data will be sent to the receiver, then enters the standby mode, waiting for the next wake-up. The receiver receives the data, after judgment and processing, the temperature will be displayed on the display and transmission frequency of wake-up signal will be set according to the level of the temperature [8, 9].

### 4.2 Temperature Signal Acquisition and Processing

Analog IIC communication is used in the communication between the ADS1115 and the microcontroller, collecting the 6-way temperature and the battery voltage in order. After the collected data is processed and put into the array, the next step will be carried out.

### 4.3 Main Control Program of Transmitter

After receiving the wake-up signal, the transmitter will reset. Set the system clock and peripheral module clock source with low power consumption, and then initialize the ports of I/O, serial port, RTC, SD memory, and wireless module to meet the requirement of system function. And then start the watchdog mode, the program
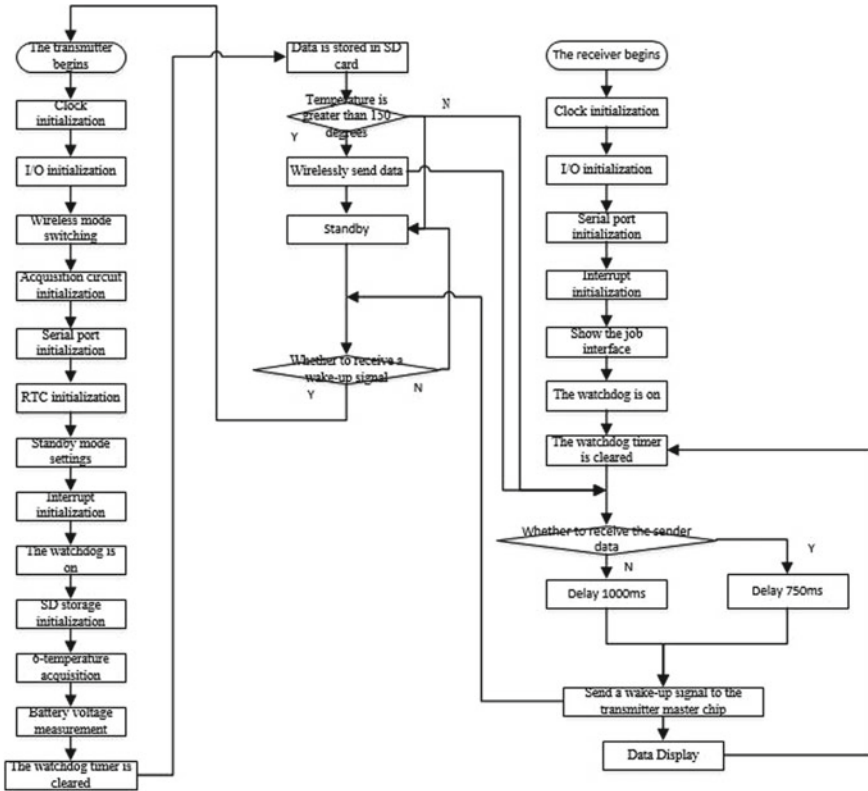
**Fig. 3** Software total flowchart

can be automatically reset when "run fly" happens. If there is any brake temperature greater than 150 °C or 2 min from the last transmission, open the wireless module, The collected data will be sent to the display and MCU enters the standby mode; if the 6-way temperature is all lower than 150 °C, wireless module does not send data, enter the standby mode directly, waiting for the next wake-up.

## 4.4 Main Control Program of Receiver

When the temperature is below 150 °C, the transmitter sends data every two minutes to the receiver to ensure the normal operation of the transmitter. When the temperature is less than 150 °C less than 220 °C, the transmitter sends the data to the receiver every second, there will be high temperature warning on the display and the buzzer will do voice prompts with 70 times/min in order to warn the driver brake temperature has exceeded the appropriate operating temperature, measurements like reducing the

braking frequency should be carried out immediately to guarantee the safety. When the temperature is greater than 220 °C, transmitter sends data to the receiver every 750 ms, and the screen shows a dangerous alarm and buzzer does voice prompts in order to warn the driver that the brake is at dangerous state. The driver has entered the dangerous state of the brake, and the driver should stop the truck immediately.

## *4.5 Data Transmission Through Wireless Module*

When the system needs to send data, M0 pin is set to a low level, the microcontroller sends the data to the wireless module through the serial port PA9, then wireless module sends data out. When the MCU of the transmitter is in sleep mode, the wireless module receives the wake-up signal from the receiver, send high level to the wake-up pin through the wireless serial port TX pin to achieve the function of long-distance wake-up. M1 pin of receiver wireless module is connected to ground, M0 pin is connected to 3.3 V, receiver wireless module is always in the wake-up mode in order to wake-up the transmitter.

## 5  The Effectiveness Test of System

In order to test the effectiveness of the system, we carried out the working test for the system in the brake torsion test stand to simulate the actual braking conditions. Room temperature was 15 °C, friction liner friction coefficient was 0.4, drilled M6 screw hole whose depth was 12.5 mm in the end of aluminum rod near the brake shoe, the PT1000 sensor (thread length is 20 mm, probe length is 25 mm)was screwed into the screw hole. The brake chamber pressure started at 0.6 MPa, became 0.8 MPa after 15 min and kept 0.8 MPa until the end of the experiment. Recorded infrared thermometer and the system display temperature readings synchronously, temperature difference curve of measurement system between the drum surface and after aluminum rod thermal conductivity can be obtained. The result was shown in Figs. 4 and 5.

The following conclusions can be obtained from the graphs in Figs. 4 and 5,

(1)  As can be seen from Fig. 4, the system temperature reading and brake drum temperature were positively correlated, the temperature difference was relatively constant, the system can achieve the purpose of measuring the brake temperature.

(2)  As can be seen from Fig. 5, the functional relationship between the temperature difference and the surface temperature of brake drum is obtained by fitting the polynomial function of 6 times:
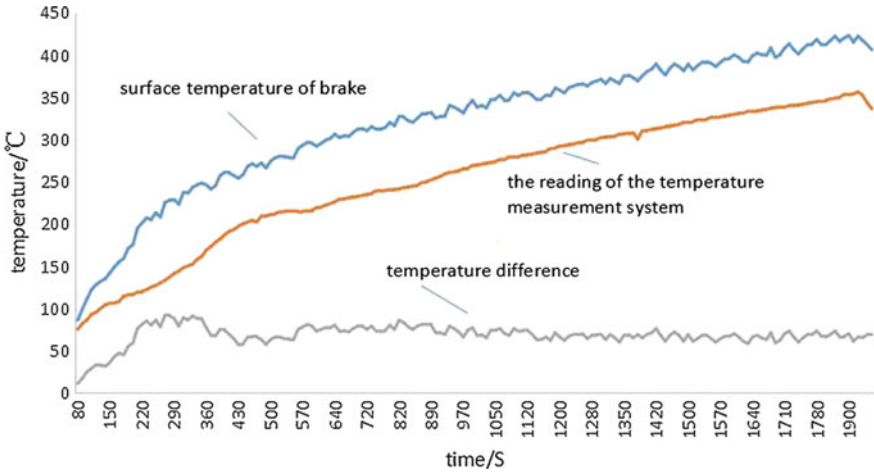
Fig. 4 Variation curve of temperature difference over time
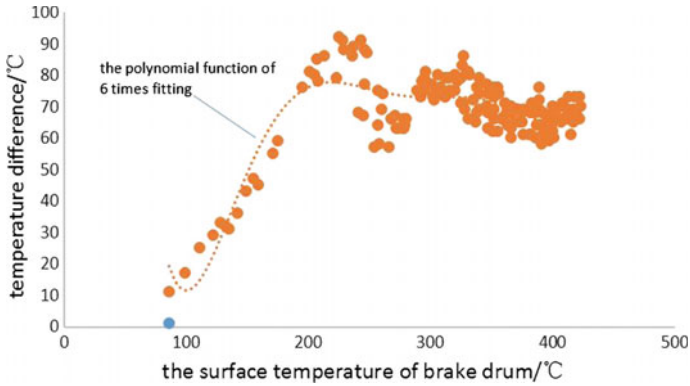


Fig. 5 Variation curve of temperature difference and brake drum surface temperature

$$y = 7 \times 10^{-12}x^6 - 10^{-8}x^5 + 7 \times 10^{-6}x^4$$
$$- 0.0023x^3 + 0.4043x^2 - 34.374x + 1124.9 \tag{4}$$

$y$ is the difference between the surface temperature of the brake drum and the reading of the temperature measurement system, and $x$ is the surface temperature of the brake drum.

## 6  Conclusion

The author designed a wireless monitoring and pre-warning system of brake temperature for truck safety operation to deal with risks such as the brake thermal recession and the high tire temperature during the truck operation. The signal processing circuit of high precision based on PT1000 thermal resistance sensor is designed by using the principle of bridge and integrated amplifier circuit, which greatly improves the accuracy of temperature measurement. Using the same integrated circuit board to control multichannel temperature signal input, the system was highly integrated, reducing the system cost-effectively. Using wireless data transmission, the system possessed more flexibility of installation and layout, eliminating the wiring costs. The system realized monitoring the brake temperature of the truck and the classification warning of the high-temperature state, which provided the reliable early warning information for the driver's decision in the braking behavior, improving the safety of the truck driving greatly.

## References

1. Wu YQ (2014) Simulation of temperature distribution in disk brake considering a real brake pad wear. Tribol Lett 56:205–213
2. Kwon MH (2016) Cooperative control for friction and regenerative braking systems considering dynamic characteristic and temperature condition. Int J Automot Technol 17(3):437–446
3. Verma P C (2016) Role of the friction layer in the high-temperature pin-on-disc study of a brake material. Wear 56–65
4. Guo J (2014) Truck brake temperature monitoring and early warning system research. Jilin University, Changchun
5. Pengfei Yang (2010) Drum brake temperature monitoring system design based on nRF2401. Sci Technol Herald 28(18):84–88
6. Sun Y, He J (2017) High precision multi-channel temperature measurement system based on LabVIEW. Instrum Tech Sens 1:96–100
7. Zhou P (2012) Design of the temperature detection system based on STC89C52 single-chip. Mod Electron Technol 35(22):10–13
8. Li Y, Yang S (2017) Study on monitoring method of temperature rise of dry air-core reactor based on distributed optical fiber temperature measurement. Instrum Tech Sens 2:43–50
9. Wang H (2016) Friction stir welding temperature monitoring platform development. Donghua University, Shanghai

# Impact of Travel Ability on Travel Choice of the Elderly Leisure Activities

**Ren Dong, Zhen-wei Li, Guang-hao Yu and Min He**

**Abstract** Travel choice of elderly leisure activities is often restricted by their own travel behavioral competence. On the basis of defining travel ability, factor analysis is used to extract the characteristic variable with the 663 questionnaire survey data. Discrete choice model is used to analyze the effect of travel ability on the choice of trip and departure time in elderly leisure activities. The result shows that: (1) bus and walk are the main ways of daily elderly leisure activities. (2) Up and down bus steps and maintaining balance within bus are the characteristic variables which can express precisely travel ability of the elderly. (3) Travel ability affects trip modes of seniors mainly and has an indirect effect on departure time. According to the differences in travel ability, improving urban leisure facilities planning and traffic system design has a direct effect on improving the accessibility of the elderly.

**Keywords** Urban traffic · Travel behavior · Travel ability analysis · Elderly Leisure · Disaggregate model

## 1 Introduce

The choice that elderly travel demand adapts to the current traffic facilities results in elderly travel behavior, while travel behavior capability has a direct effect on travel choice. The study on aging travel behavior is lack of analyzing travel choice competence resulted from weakened travel behavior capability from the perspective of different activities characters and spatial barriers, which cannot demonstrate

R. Dong · Z. Li · G. Yu · M. He (✉)
Faculty of Transportation Engineering, Kunming University of Science and Technology, Kunming 650500, China
e-mail: minhe@kmust.edu.cn

elderly "activity-travel" behavior mechanism clearly. So the analysis of travel choice based on travel behavior capability has a great contribution to improving urban traffic facilities (especially public transport), planning urban traffic and making policy for aging society.

The main purpose of the study on the behavior of aging population in the developed countries is to assess the safety of motor vehicle driving and to provide the mobility for the elderly who have not driven, so as to avoid the isolation of the elderly or "social death" [1]. Age is often used as a variable for comparison and analysis based on a resident trip survey in most of the relevant studies. Tacken [2] demonstrated that the elderly reduce their travel less as they get older based on the national travel survey data of Finland in 1979–1994. Rosenbloom [3] argued that the seniors over 75 years old have some difficulties or obstacles to take the bus because of physical dysfunction, which restricted the motorized travel and resulting in the decrease of outdoor travel frequency. Giuliano [4] identified that the elderly reduce their activity range as they get older with analysis of different age groups according to the data of "Nationwide Personal Transportation Survey" in 1995 US. Newbold [5] made a similar conclusion that the frequency of the older travel decreases when they get older with the analysis of the Canadian travel survey data from 1986, 1992 and 1998.

The income level and lifestyle of the aging population between China and foreign countries are different, and there is a big difference in travel demand. Mao, Zhang and Chen [6–8] argued that age and gender are the main influencing factors of urban elderly's travel behavior choice with the analysis of travel characteristics and influencing factors based on the city residents to travel survey data. Chai [9] demonstrated that travel behavior of the elderly differs by the characteristics of leisure, shopping and medical treatment three kinds of outdoor activities.

In summary, travel behavior of senior is analyzed with two trip-based and activity-based analysis methods. Both two methods consider that age is the main factor affected travel behavior, which leads elderly body dysfunction. However, Dong [10] analyzed the relationship among characteristic variables of the urban elderly leisure behavior, and presented that age has a restrictive effect on the elderly travel indirectly. Tang [11] analyzed epidemiological survey data of 2786 seniors over 55 years old in Beijing 1997, and argued that age is not the main impact of the elderly physical dysfunction, but mainly due to chronic diseases. Obviously, age is not sufficient to reflect physical dysfunction of the elderly truly. In the late 1960s, Lawton [12] proposed the Instrumental Activities of Daily Life (IADL) to assess the elderly self-care ability including driving and taking public transport.

In fact, the elderly are easily influenced by travel behavior capacity and change their outdoor activities travel behavior. The analysis of the relationship between travel behavior capacity and choice of the elderly leisure activities travel will provide a theoretical basis for the elderly travel behavior mechanism. Travel behavior capacity is proposed as a new direct influencing factor, and analysis of travel choice of the elderly outdoor leisure activities based on travel behavior capacity can improve the accuracy and precision on the study of the elderly travel behavior.

This article is organized as follows. First, the travel ability is proposed and the characteristics of travel ability are summarized. Second, the explanatory variables of travel ability are extracted with factor analysis based on elderly leisure survey data, followed by a description of a subset of these variables that were chosen for this study. Third, the effect of urban elderly travel ability, personal attributes, and leisure activities characters to travel choice is analyzed with the discrete choice model. Finally, conclusions on the effect of travel ability on the elderly travel behavior are presented.

## 2 Travel Ability

### 2.1 Concept and Characteristic

As a short description of travel behavior capability, travel ability expresses the physical function and manipulative skill required by the traveler when taking independently all or part of urban public transport modes and individual transport modes in daily outdoor activities. Travel ability has three basic characteristics: first, travel ability is closely related to activity characteristics and spatial behavior characteristics. Travel ability reflects the behavior capability to overcome trip obstacle independently in traveler's "activity-travel" and has a direct impact on travel choice of "activity-travel". Second, travel ability has different contents with different body functions. For non-elderly travelers, travel ability is expressed as manipulative skills (drive or ride). However, travel ability mainly express as body functions for elderly travelers. Finally, travel ability is a latent variable. Manipulative skills are easy to know by observation and inquiry. In comparison, it is difficult to measure body function directly and accurately.

### 2.2 Characteristic Variables

In order to make a reasonable analysis of characteristics variables qualitatively and quantitatively, it is necessary to consider characteristics of traveler's attributes, physical function, activity characteristics, spatial behavior characteristics. This paper draws on the WHO-IADL, a tool for measuring the daily activities of the World Health Organization, constructs a number of observation variables related to leisure "activity-travel" behavior and their structures, finally extract characteristic variables with factor extraction.

# 3 Extraction of Characteristics Variables

## 3.1 Theoretical Basis and Research Hypothesis

The Push–Pull theory explains well why people involved in leisure from two aspects of internal motivation and external incentives. Internal motivation reflects people's inner demand for participation in leisure, while the external incentive is outer attraction of leisure participation. Based on the socioeconomic characteristics, the elderly consider the applicable traffic services under the combined action of internal motivation and external incentives, finally realize the leisure activities in the specific places. This process derives the most suitable travel behavior for the elderly.

Based on the Push–Pull theory, this study assumes that a real leisure activity results from choosing leisure ranges and activities by the elderly under the influence of age, place of residence and accessibility to leisure motivation. This hypothesis argues that latent variables included individual attributes, leisure motives, and leisure location environmental awareness coupled with traffic service system through specific characteristics of leisure location and activities, finally determine and influence travel behavior.

## 3.2 Data Collection

### 3.2.1 Explanatory Variable

Explanatory variables (symbols, explanations, and assignments are given in Table 1) are proposed in this study. A latent variable of travel ability contains three kinds of the variable framework, namely, walking variable, bus, and bicycle, and the framework of bus covers the main part of bus trip process. The questionnaire has contained elderly self-drive problems in leisure activities but not included in Table 1 due to less sample size of elderly leisure activity by self-drive and few studies on impactor factors and their threshold of the driving ability decline for elderly seniors.

### 3.2.2 Description and Variables

The official survey was conducted from September 8–21, 2014. Survey location contains a number of city parks, community squares, green space, comprehensive farmers market, supermarket and other activity centers in 4 administrative regions of Kunming. Survey method was a random sampling method. A total of 690 questionnaires were issued, 663 valid questionnaires were retrieved and the questionnaires efficiency was 96.1%. Statistical distribution characteristics of the travel mode and the departure time are respectively shown in Figs. 1 and 2.

**Table 1** Explanation of variables

| Category | Explanatory variable | Remarks |
|---|---|---|
| Individual attributes | Gender, age, family structure, education, income | Independent variables |
| Leisure motivation | Exercise body, feeling relaxed and happy, emotional communication, hobbies and interests, entertainment, filling up time | |
| Leisure environment awareness | Natural scenery, fresh air, being clean and hygienic, resting facilities, athletic facilities, trip distance, transportation convenience | |
| Travel ability | Walking time, walking time with 5 kg weight, time for waiting bus by standing, up and down bus steps, maintaining balance in bus, the number of stops by standing in bus, riding time | |
| Location characteristics | Level, scale, environment | Dependent variables |
| Activity characteristic | Kinds of activities, partner, activities duration | |
| Travel behavior | Trip modes, departure time, trip distance, frequency | |

**Fig. 1** Travel way distribution of elderly leisure activity
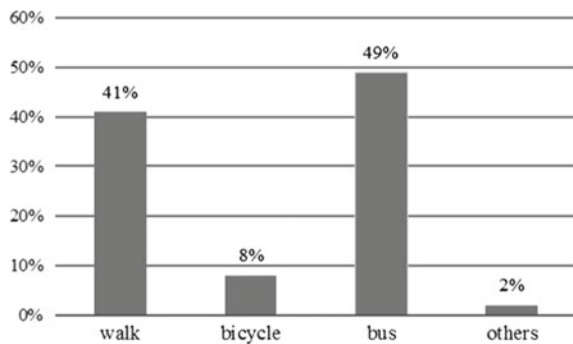


Statistical results show that the proportion of the bus is slightly higher than the walk, and two of them reach 90%. Departure time of the walk is concentrated in 7:15–8:15 am, and the bus' is an average delay of 1–2 h. Statistics of observed variables for travel ability are shown in Table 2.

**Fig. 2** Distribution of
departure time
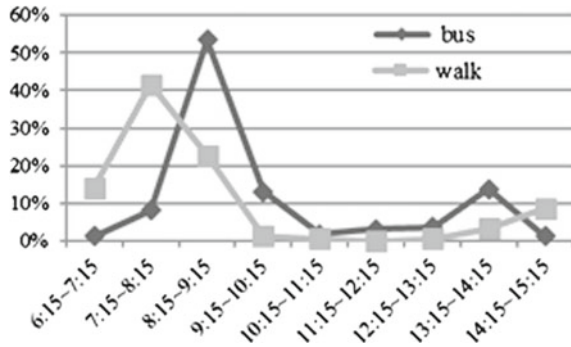


**Table 2** Statistical characteristics of observed variables of travel ability

| Category | Observation variables | Mean | Standard deviation | Variance |
|---|---|---|---|---|
| Walk | Walking time | 3.20 | 0.782 | 0.612 |
| | Waking time with 5 kg weight | 2.75 | 0.873 | 0.762 |
| Bus | Time for waiting bus by standing | 3.15 | 0.791 | 0.626 |
| | Up and down bus steps | 2.67 | 0.908 | 0.825 |
| | Maintaining balance in bus | 2.66 | 1.221 | 1.492 |
| | Number of stops by standing in bus | 3.03 | 0.935 | 0.874 |
| Bicycle | Riding time | 1.06 | 1.543 | 2.382 |

## 3.3 Extraction of Characteristic Variables

As can be seen, proportion of walk is relatively large, and walk is also a typical way to enjoy community-wide leisure activities (square fitness activities). Therefore, variable eigenvalues of the walk are statistically significant and suitable as control variables. The major obstacle of urban elderly leisure activities is to overcome the moving difficulty in a large space. Four variables of the bus are suitable as control variables based on characteristics.

In Table 2, measuring variables of walk and bus, respectively, have the common variance components that explain travel ability. However, as characteristic variables, they should confirm the principle of independence. In this paper, Kaiser–Meyer–Olkin (KMO) statistical test and Bartlett spherical test are used to test the measuring variables with SPSS.20 statistical analysis software. KMO statistic number is 0.919 (in practice, KMO > 0 is good). Bartlett spherical test value is 2358.412, and significant at 0.000 level, which indicates that the correlation matrix of measuring

variables does exist common factor and the suitability of factor analysis. A common factor is extracted from the measuring variables of travel ability, eigenvalues and contribution rate of variance are, respectively, 6.027 and 79.338%.

Based on factors loading of observed variables on a common factor. The loading of two variables maintaining balance in the bus (0.942) and up and down bus steps (0.933) are close to 1, which can be a good expression of travel ability, while the rest of loading of the variables are less than 0.900.

# 4 Analysis of the Influence of Travel Ability on Choice Travel

## 4.1 Influence of Travel Ability

### 4.1.1 Trip Choice Model

Based on the random utility theory [13], in order to satisfy demand of activity, the elderly choose the most utility program under the combined action of travel motivation and constraints factors, and the kinds of utility item vary according to the characteristics of the programs and attributes of the decision makers. Assume that the travel option of elderly n is set to $A_n$, the utility function of the $i$th program is chosen as:

$$U_{in} = V_{in} + \varepsilon_{in} \tag{1}$$

where:

$V_{in}$   fixed term in the utility function of elderly n chooses program $i$
$\varepsilon_{in}$   random term in the utility function of elderly n chooses program $i$

Assuming the random term of the utility function obeys the Gumbel distribution, the probability that the $n$-th elderly chooses the $i$-th program from the $j$ programs is as follow:

$$P_{in} = \frac{e^{U_{in}}}{\sum_{j \in A_n} e^{U_{jn}}} \tag{2}$$

### 4.1.2 Model Calibration and Inspection

The ways to participation of elderly leisure activity are divided into bus and walk, and departure time is divided into 6:15–8:15 am, 8:15–10:15 am and 13:15–15:15 pm. Choice model of travel mode and departure time were established with Nlogit 4.0 software and parameter calibration results are shown in Table 3. $\rho^2$ and $\bar{\rho}^2$ are usually

evaluate the proximity between the predicted values and the observed values in the model checking. When $\rho^2$ and $\bar{\rho}^2$ reach 0.2–0.4, it indicates that the accuracy of model is higher. The evaluation results in Table 3 show that travel choice model can well explain the choice behavior of the elderly leisure activities trip modes and departure time.

### 4.1.3   Influence Level

This paper uses *odds* to analyze influence level of main control variables on travel choice in the elderly leisure "activity-travel". The *odds* [14] is the ratio of the probability that the event will happen to the probability that the event will not happen. The *odds* calculation results are shown in Table 4.

Table 4 shows that, for the elderly with strong ability of up and down bus steps, probability of choosing bus is 1.848 times that of choosing non-bus. Probability of choosing non-bus is 0.570 times that of choosing bus for the elderly with strong ability of maintaining balance in bus. Travel ability of the senile elderly is relatively weaker, probability of taking bus is 0.655 times that of taking non-bus. Obviously, the elderly with strong travel ability intend to choose bus. However, travel ability has no direct impact on departure time.

## 4.2   Influence of Travel Choice

### 4.2.1   Travel Mode Choice

The elderly with strong travel ability can arrive in leisure place which has better environment by bus (1.604 times by non-bus), and participate in leisure activities which go on for a longer period by bus (1.257 times by non-bus). However, the elderly with walk travel ability have difficulty in arriving in long-distance and large leisure place due to difficulties of taking bus.

### 4.2.2   Influence of Departure Time

Table 4 shows that the two explanatory variables of travel ability have an indirect impact on departure time by trip modes, individual attributes, leisure location and leisure environment, and the most significant impact factor of which is trip modes. The elderly with strong travel ability tend to choose bus and set off in the forenoon (2.117 times in the early morning). The senile elderly have smaller activity range due to weak travel ability. So the senile elderly tend to short-distance trip (0.543 times long-distance trip) and leave in the early morning (2.098 times in the forenoon). At the same time, they prefer small scale of location (0.612 times the big scale of

**Table 3** Parameter calibration

| | Travel modes | | | | Departure time | | | | | |
| | Non-bus | | Bus | | [06:15–08:15] | | [08:15–10:15] | | [13:15–15:15] | |
| | Parameters | t-value | Parameters | t-value | Parameters | t-value | Parameters | t-value | Parameters | t-value |
|---|---|---|---|---|---|---|---|---|---|---|
| Age | – | – | −0.423*** | 3.773 | 0.741*** | 4.202 | – | – | – | – |
| Gender | – | – | – | – | 0.509 | 1.456 | – | – | – | – |
| Family structure | 0.215*** | 2.935 | – | – | – | – | 0.674*** | 3.026 | 0.674*** | 3.026 |
| Activities duration | – | 4.274 | 0.229** | 2.542 | – | – | 0.127 | 0.607 | 0.127 | 0.607 |
| Trip distance | −0.459*** | | – | | −0.610*** | −3.212 | – | – | – | – |
| Scale of location | −0.362*** | 5.867 | – | | −0.491** | −2.083 | – | – | – | – |
| Environment | – | | 0.473*** | 2.826 | – | | 0.504** | 2.374 | 0.504** | 2.374 |
| Up and down bus steps | – | | 0.614*** | 3.562 | −0.227 | −0.367 | −0.227 | −0.367 | – | – |
| Maintaining balance in bus | −0.562*** | 3.942 | – | | – | | – | | 0.793 | 1.269 |
| Departure time | – | | 0.331** | 2.376 | – | | – | | – | – |
| Trip modes | – | | – | | – | | 0.750*** | 3.397 | 0.750*** | 3.397 |
| Rho squared ($\rho^2$) | 0.253 | | | | 0.404 | | | | | |
| Adjusted rho squared ($\bar{\rho}^2$) | 0.227 | | | | 0.383 | | | | | |

***, **, * respectively shown significant at 1, 5, 10%

**Table 4**  Influence level

| Control variables | Response variables | | | | |
|---|---|---|---|---|---|
| | Trip modes | | Departure time | | |
| | Non-bus | Bus | [6:15–8:15] | [8:15–10:15] | [13:15–15:15] |
| Gender | – | 0.655 | 2.098 | – | – |
| Family structure | 1.239 | – | – | 1.962 | 1.962 |
| Leisure duration | – | 1.257 | – | – | – |
| Trip distance | 0.631 | – | 0.543 | – | – |
| Scale of location | 0.696 | – | 0.612 | – | – |
| Environment | – | 1.604 | – | 1.655 | 1.655 |
| Up and down bus steps | – | 1.848 | – | – | – |
| Maintaining balance in bus | 0.570 | – | – | – | – |
| Departure time | – | 1.392 | – | – | – |
| Trip modes | – | – | – | 2.117 | 2.117 |

location). The elderly tend to long-distance place by bus after 8:30 am (1.392 times before 8:30 am).

Family structure has an effect on departure time. The elderly lived with more generations set off after 8:15 (1.963 times in the early morning). Departure time for choosing a better environmental location is also later. It's because the elderly lived with more generations undertake more family responsibilities, which delay departure time. In order to arrive in a better place, the most elderly take the bus and set off during 8:15–10:15.

## 5  Conclusion

This paper puts forward and expounds the basic concept of travel ability, and analyzes the influence of travel ability on the travel choice of urban elderly leisure activities, finally gets the following conclusions: (1) bus and walk are the main ways of the urban elderly daily leisure activities in China. (2) The travel ability of the elderly is characterized by two explanatory variables of up and down bus steps and maintaining balance in bus. (3) Differences of travel ability have a direct effect on travel choice of the elderly leisure activities, which affect departure time.

This paper demonstrates that travel ability is a direct factor to travel behavior of the elderly study on travel choice of the elderly leisure activities with respect to travel

ability is absolutely needed. The research has great theoretical and practical significance for urban planning and transportation policy. The elderly with weak travel ability have difficult to arrive long-distance and better leisure place by bus, which results in restriction of leisure motivation and decline in quality of the elderly life. Planning the elderly community leisure facilities can improve quality of the elderly life within reach of walking based on travel ability. Providing transportation service pattern adapted to special leisure demand of the elderly, for example, corresponding subscription bus service based on travel ability, can improve individual mobility and accessibility of the elderly.

# References

1. Lawton J (1998) The dying process: patients' experiences of palliative care. Routledge, London
2. Tacken M (1998) Mobility of the elderly in time and space in the Netherlands: an analysis of the Dutch national travel survey. Transportation 25(4):379–393
3. Rosenbloom (2001) Sustainability and automobility among the elderly: an international assessment. Transportation 28:375–408
4. Giuliano G, Hu HH, Lee K (2003) Travel patterns of the elderly: the role of land use. Metrans Transportation Center
5. Newbold KB, Scott DM, Spinney JEL et al (2005) Travel behavior within Canada's older population: a cohort analysis. J Transp Geogr 13(4):340–351
6. Mao H, Ren F (2005) Research on characteristics, problem and improvement suggestions of traffic for Chinese old people. J Chongqing Jianzhu Univ 27(3):30–34
7. Zhang Z, Mao B, Liu M et al (2007) An analysis of travel patterns of the elders in Beijing. J Transp Sys Eng Inf Technol 7(6):11–20
8. Chen TS, Yue F, Yang L et al (2007) A study of factors influencing travel choice behavior of older Chinese. J Southwest Jiaotong Univ (Soc Sci) 8(5):17–21
9. Chai Y et al (2010) Activity space of urban elderly in China. Science Press, Beijing
10. Dong R, Han W, Li L et al (2015) Study on influencing factors of urban elderly travel behavior. J Kunming Univ Sci Technol (Nat Sci Ed) 04:38–45
11. Tang Z, Xiang M (2003) Physical function and its associated factors in elderly people in Beijing. Chin J Gerontol 23(1)
12. Lawton MP, Brody EM (1969) Assessment of older people: self-maintaining and instrumental activities of daily living. Gerontologist 9:179–186
13. Guan H (2004) Disaggregate model: a tool of traffic behavior analysis. China Communications Press, Beijing
14. Ben-Akiva ME, Lerman SR (1985) Discrete choice analysis: theory and application to travel demand. MIT press

# The Influence of Driving Experience on the Physiological Characteristics of the Driver Under Stress Scene

**Xian-sheng Li, Fan-song Meng, Yuan-yuan Ren, Xue-lian Zheng, Jing-hai Zhang and Jia-hui Yan**

**Abstract** To study the influence of driving experience on physiological characteristics of drivers under the stress scene, it carries out the principal component analysis method to select the appropriate physiological indexes to analyze of the physiological data of different driving experience drivers. By means of mathematical statistics, the physiological data of drivers were analyzed and compared, and the physiological characteristics of drivers with different driving experiences were obtained. It shows that drivers with fewer experiences showed great physiological load in various stress scenarios; and experienced drivers due to situational awareness have less physiological fluctuations in the baseline period and the recovery period; experienced drivers show the superiority under stress scenarios which the risk appears slowly, while the risk appears suddenly, the advantage of experienced drivers have lower superiority. The growth rate of skin electric rate and heart rate can reflect the influence of driver's experience on physiology.

**Keywords** Aerodynamic characteristics · Stealth characteristics · Numerical calculation · Polarization

As vehicle holdings increase, traffic conflict in the stress scenario is becoming more and more serious. So many researchers have studied various aspects of stress scenarios and drivers. Vedagiri established an evaluation system between the vehicle and pedestrian crosswalk conflict severity for stress scenarios [1]. Kadali studied the evaluation system of human protective measures under stress state [2]. Himes established an evaluation system of the state security of the early warning system

X. Li · F. Meng · Y. Ren (✉) · X. Zheng · J. Zhang
School of Transportation, Jilin University, Changchun 130022, China
e-mail: renyy@jlu.edu.cn

J. Yan
Mitsubishi Electric (China) Co., Ltd. Shanghai Branch, Shanghai 200336, China

529

under the intersection stress scenario [3]. Yang analyzed the driver's risk perception time under different stress scenarios [4]. All of the above research results are not related to the influence of driving experience on the physiological characteristics of drivers. However, by the end of 2015, 280 million car drivers of China, the number of drivers whose driving experiences are less than 1 year are about 36 million 130 thousand people, account for the total number of drivers 11% [5]. Therefore, it is necessary to study the influence of driving experience on driver's physiology.

# 1 Stress Scene Classification

In order to explore the influence of driving experience on driver's physiological characteristics under stress situation, in this paper, according to the differences of the traffic conflict participants in the stress scenario, the scene is divided into four types: vehicle to vehicle, vehicle to non-motorized vehicle, vehicle to pedestrian, and vehicle to traffic environment [6]. In this paper, we set up the following 4 kinds of scene:

(1) Scene 1 (i.e., people across): this scene belongs to the motor vehicle–pedestrian conflict, when driving is through the crosswalk, pedestrians from the side of the road suddenly walk out of a parked truck head transverse static.
(2) Scene 2 (i.e. motor vehicle approaching): this scene is a motor vehicle–motor vehicle conflict. In the process of driving a vehicle, the other vehicle approaches the driver of the vehicle.
(3) Scene 3 (i.e. non-motor vehicles): this scene is a motor vehicle–non-motor vehicle conflict. In front of the non-motorized vehicle in the left and right lane, and constantly changing speed, affecting the driver's normal driving.
(4) Scene 4 (i.e., weather changes): this scene is a motor vehicle—external environmental conflict. When the vehicle is traveling to the tunnel exit, the abrupt change of the weather affects the driver.

# 2 Driver Physiological Index Selection

Based on the analysis of the physiological characteristics of drivers at home and abroad [7–9], it was found that the indexes which were closely related to the driver and the most important indicators of the physiological characteristics were skin electricity, EMG, heart rate, LF, SDNN, and PNN50. The six indicators are widely recognized as an important characterization parameter to study the physiological characteristics of drivers. In this paper, the principal component analysis method is used to select a more scientific and comprehensive index to reflect the physiological characteristics of drivers from the above six indexes.

**Table 1** Result of principal component analysis

| Principal component | Eigenvalue | Variance contribution rate | Cumulative contribution rate |
|---|---|---|---|
| △EDA | 1.826 | 32.917 | 32.917 |
| △HR | 1.518 | 32.452 | 65.369 |
| LF | 1.036 | 28.149 | 93.518 |
| △EMG | 0.632 | 2.697 | 96.215 |
| SDNN | 0.517 | 1.923 | 98.138 |
| PNN 50% | 0.471 | 1.862 | 100.000 |

$$X = \begin{bmatrix}
3.92 & 0.6 & 0.33 & 0.32 & 3.1 & 0.32 \\
4.26 & 0.32 & 0.87 & 0.29 & 1.6 & 0.43 \\
3.36 & 0.75 & 0.59 & 0.27 & 3.9 & 0.31 \\
1.76 & 0.57 & 0.78 & 0.27 & 4.6 & 0.16 \\
3.15 & 0.68 & 0.37 & 0.36 & 5.8 & 0.13 \\
5.13 & 0.7 & 0.62 & 0.25 & 3.3 & 0.35 \\
4.26 & 0.83 & 0.42 & 0.18 & 5.2 & 0.25 \\
0.82 & 0.76 & 0.53 & 0.34 & 2.9 & 0.37 \\
2.15 & 0.32 & 0.87 & 0.46 & 1.3 & 0.29 \\
2.88 & 0.87 & 0.72 & 0.31 & 2.7 & 0.16 \\
3.76 & 1.23 & 0.83 & 0.32 & 3.7 & 0.42 \\
2.65 & 0.63 & 0.28 & 0.17 & 5.2 & 0.62 \\
3.26 & 0.53 & 0.53 & 0.27 & 3.3 & 0.57 \\
5.23 & 0.59 & 0.34 & 0.21 & 2.8 & 0.31 \\
2.35 & 0.86 & 0.72 & 0.13 & 4.6 & 0.38 \\
3.54 & 0.85 & 0.15 & 0.53 & 2.9 & 0.25 \\
4.79 & 0.62 & 0.56 & 0.36 & 3.8 & 0.29 \\
3.26 & 0.6 & 0.51 & 0.46 & 2.6 & 0.51 \\
5.21 & 0.33 & 0.23 & 0.18 & 5.1 & 0.26 \\
2.18 & 0.52 & 0.36 & 0.37 & 3.8 & 0.37
\end{bmatrix}$$

First of all, the above six indexes are selected as the original data of the principal component analysis, that is to say, there are 20 samples and the other 6 variables. The original data can be sorted into the original matrix $X$. Because of the significant difference in the number of levels in the original matrix $X$, it will affect the accuracy of the results. Therefore, it is necessary to standardize the original matrix before analysis. SPSS software is used to standardize the data in the original matrix, and then the principal components of the matrix are analyzed. Analysis of the principal components of the root, contribution rate, and cumulative contribution rate, as shown in Table 1.
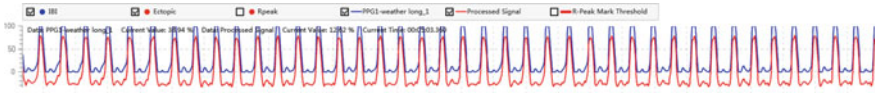
**Fig. 1** Raw signal and de-noise signal

**Table 2** Information of drivers

| No. | Age | Year | No. | Age | Year | No. | Age | Year |
|-----|-----|------|-----|-----|------|-----|-----|------|
| 1 | 24 | 1 | 7 | 47 | 13 | 13 | 45 | 20 |
| 2 | 36 | 8 | 8 | 38 | 13 | 14 | 42 | 21 |
| 3 | 26 | 8 | 9 | 39 | 17 | 15 | 48 | 22 |
| 4 | 40 | 9 | 10 | 36 | 17 | 16 | 45 | 25 |
| 5 | 35 | 9 | 11 | 46 | 19 | 17 | 45 | 26 |
| 6 | 36 | 10 | 12 | 37 | 19 | 18 | 50 | 31 |

Table 1 and Fig. 1 showed that the cumulative contribution rate of the first three principal components was up to 93.518%. Therefore, the growth rate of EDA and HR, as well as LF of heart rate contributes about 93.52% of information. The above three indexes were selected to analyze the influence of driving experience on the physiological characteristics of drivers.

## 3 Experimental Design and Data Preprocessing

### 3.1 Driver Selection

18 participants were selected to carry out the driving test. Information about the participants was listed in Table 2.

### 3.2 Test Scheme

A total of 36 experiments, each driver to travel for two laps, each lap in the course of the two laps were encountered in different stress scenarios, each driver met a total of 4 scenes of two. Before the start of the experiment, the subjects were familiar with the acceleration, braking and steering wheel performance of the simulation system. After being tested, the test began, and the driver's physiological data were collected.

### 3.3  Data Preprocessing

#### 3.3.1  Driving Electrical Signal Preprocessing

ECG signal is extremely weak, its amplitude is 0.8–1 μV, the spectrum is concentrated in the 0.05–100 Hz. The difference of the actual ECG signal size is different. The collected ECG signals are mixed with interference such as power frequency interference and baseline drift, and various noise bands overlap with each other. During the experiment, the ECG signal will be affected by different environment, so the collected ECG signal cannot be used directly, and it must be processed by filtering and noise reduction. The former (blue) and later (red) are shown in Fig. 1.

#### 3.3.2  Driver Electrical Signal Preprocessing

In addition to the characteristics of the weak signal, strong noise, and so on, it has the characteristics of easy to be affected by the equipment and the drift is serious, it is easy to be affected by the shock response, and it is difficult to separate the useful information. The traditional de-noising method in the short term low energy of the transient signal, through the filter not only smooth, SNR is not greatly improved, and the trigger signal is blurred, these trigger points contain important information of drivers based on physiological changes of physiological activities, on behalf of the corresponding. This paper adopts the continuous decomposition of the original signal deconvolution skin obtained with trigger signal data points, as shown in Figs. 2 and 3.

## 4  Analysis of the Influence Mechanism in Stress Scene

To study the stress scene more careful driving experience effect on the driver of this section will be divided into stress scene baseline, stress and recovery period of three
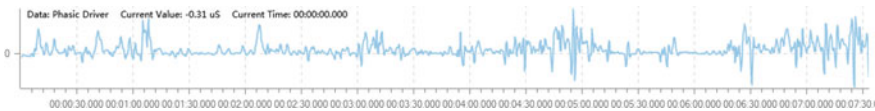


**Fig. 2**  Phasic driver
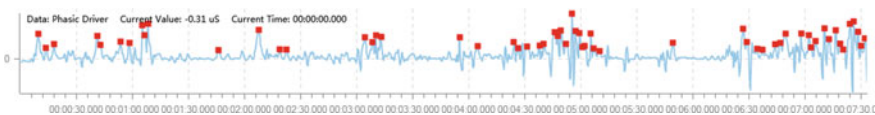


**Fig. 3**  Phasic driver with SCR onset
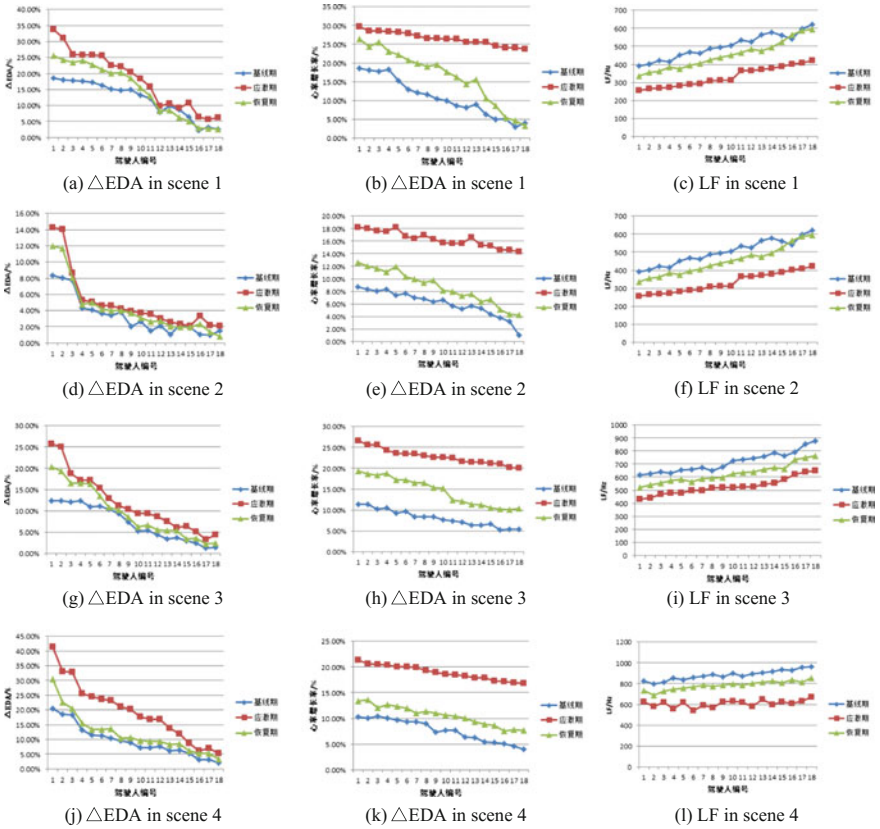
Fig. 4 Physiological characteristics of different stress scenarios

periods should analyze the impact of stress on physiological characteristics of scene driving experience driver.

In order to explore the influence of driving experience on the physiological characteristics of drivers under stress, the increment, heart rate and heart rate variability of 18 drivers under different stress scenarios were analyzed by LF. The analysis results are shown in Fig. 4. With the increase of driving experience, the growth rate and the rate of heart rate of drivers were all decreased, while the LF value showed an upward trend. The difference of stress scene under different driving experience driving growth rate of heart rate test, found that various types of stress scenarios, compared with the experienced driverless experienced driver showed higher workload.

At the same time, with the increase of the driving experience, three periods of transcutaneous electrical increment gradually approaching, the small differences analysis due to the driving experience, the driver will form a mental model, at the same time appears to predict the situation awareness of other road users will do next or what

the traffic situation may occur in what event. With the increase of the driving experience, baseline three physiological indexes of drivers and recovery period gradually approaching, the analysis is due to the driver has rich driving experience and situational awareness, so early in the physiological index fluctuation and in the later period of rapid recovery.

Compared with the experience of less experienced drivers, the drivers at risk appear more sudden stress scenarios such as scenario 1 and scenario 4, physiological indexes of the baseline recovery period and the physiological indexes and stress period compared to the more significant;In danger of relatively slow stress scenario as in scenario 2 and scenario 3, experienced driver performance more stable, analysis because of the risk of the slowly emerging allows the driver to have enough time for expectation and recognition of potential danger; On the other hand, the risk of slow, the driver can take full advantage of the risk of the expected clues, improve the response to potential hazards.

## 5  Conclusion

(1) Skilled driving people show a higher workload of various types of stress scenarios, with the increase of driving experience, driving experience accumulated by the situational awareness will make people driving at baseline and recovery range of physiological period decreased.

(2) Long driving is dangerous to the sudden stress in the scene, and the driver in driving the short baseline physiological recovery period and the physiological indexes and stress period is large, there is a large fluctuation. However, in the context of the slow stress, the experienced drivers have less flexibility and strong adaptability.

(3) In the aspect of skin electric growth rate and the growth rate of heart rate, the experienced drivers and drivers with less experience than the baseline period and recovery period relative to the range smaller stress period, the physiological reaction is more stable. However driving experience didn't have clearly differences compared to the index ,also the LF of heart rate variability is weaker than others.

# References

1. Vedagiri P, Kadali BR (2016) Evaluation of pedestrian-vehicle conflict severity at unprotected midblock crosswalks in India. Transp Res Rec 2581:48–56
2. Kadali BR, Vedagiri P (2016) Proactive pedestrian safety evaluation at unprotected mid-block crosswalk locations under mixed traffic conditions. Saf Sci 89:94–105
3. Himes S, Gross F, Eccles K et al (2016) Multistate safety evaluation of intersection conflict warning systems. Transp Res Rec 2583:8–16
4. Peng-fei YANG, Rui FU, Peng-cheng YU (2013) Time characteristics of drivers' stress perception in virtual urban road environment. J Chang'an Univ (Natural Science Edition) 33(2):73–78
5. Shen H, Zhou K (2016) In 2015 the rapid growth of motor vehicles and drivers of new car about 17810000 car ownership growth record of. Veh Saf (2):41–41
6. Chen Y, Pan L, Wei W (2011) Using kinetic energy to evaluate the severity of different types of traffic conflict at signalized intersections. ICCTP 2011
7. Pei Y, Zhou K, Zhang C (2011) Analysis of driver's psycho-physiological and eye movement characteristics under alcohol effect. J Harbin Inst Technol 13(5):80–86
8. Miriam CI, Eduardo LC, Mikel I (2014) Muscle conduction velocity, surface electromyography variables, and echo intensity during concentric and eccentric fatigue. Muscle d Nerve 49(3):389–397
9. Li X, Shin L, Zhou P et al (2014) Pear spectral analysis of surface electromyography (EMG) at matched contraction levels of the first dorsal in muscle in stroke survivors. CI Finical Veuro Physiology 125(5):988–994

# Research of Model on Connectivity of Road Network Considering Traffic Flow Status in China

**Ya-ping Zhang and Tao Qi**

**Abstract** Connectivity is an important index to evaluate the performance of road network, which plays an important role in urban transportation planning, design, and management. The current connectivity studies often focus on the physical structure of the road network, and lack of analysis of the status of traffic flow. In fact, traffic flow status affects the connectivity of road network, and different traffic flow status leads to different connectivity indices for a road network. Therefore, this paper will modify the traditional model on connectivity of road network considering traffic flow status. First, the paper will select speed as the main parameter to reflect the traffic flow status and build a satisfaction model on vehicle driver speed on the basis of survey; Second, the paper will analyze the connectivity of roads and intersections and propose a modified model on connectivity of road network considering traffic flow status on the basis of the traditional connectivity research, which improves the applicability of road network connectivity. Third, the paper will verify the validity of the modified model by examples. In the end, the paper will give the suggestions to improve the traffic performance of the road network through the traffic management according to the modified model.

**Keywords** Connectivity · Traffic flow status · Satisfaction · Speed

## 1 Introduction

There are many methods to evaluate the performance of road network, such as travel time, connectivity, and so on [1]. Connectivity is an important index to evaluate the performance of road network [2]. Connectivity is often evaluated the reliability of road network [3].Scholars have done a lot of researches on the connectivity of road network. The evaluation of road network connectivity began in 1980s [4], when

Y. Zhang (✉) · T. Qi
School of Transportation Science and Engineering, Harbin Institute of Technology, Harbin, Heilongjiang, China
e-mail: zxlt0905@163.com

scholars applied the concept of connectivity to the road network, forming the basis of road network connectivity theory [5]. At present, connectivity evaluation is used more in highway [6, 7] and less in urban road network. Generally, the connectivity index is used to evaluate the connectivity of urban road network, but it is too simple to overall evaluate the connectivity of road network. Zhou [8] has modified the connectivity index model, studied on the influence of traffic organization and the physical structure of the road network and analyzed carefully the influence of "right-in and right-out" and "one-way" traffic organization. The traditional connectivity researches suggest that roads and intersections are the basis of road network connectivity [9] and the physical structure of the road network are the main factor influencing the connectivity of road network [10]. The current evaluation model on connectivity of road network mainly focus on the Graph Theory [11], which ignores the impact of traffic flow status on connectivity of road network.

Scholars generally [12] distinguish the connectivity of the road according to its physical structure as connected or interrupted. The connectivity index of connected road is calibrated to 1 while the connectivity of interrupted road is calibrated to 0 [13]. However, traffic flow status affects the connectivity of the road, and different traffic flow status leads to different connectivity of the road. Therefore, it is not reasonable to mark the connectivity of the road with 1 or 0. This paper analyzes the traffic flow status of the road and select speed as the parameter to measure the size of road connectivity, combining the model on driver's satisfaction with speed, assign the connectivity of the road to a value of [0,1].

In this paper, the research on connectivity is mainly in three aspects: connectivity of roads, connectivity of intersections and connectivity of road network. The connectivity of a road is based on the positive and negative direction of the road; The connectivity of the intersection is related to the connectivity of the roads which is connected to the intersection and the value of the connectivity of the intersection is equal to the sum of the connected roads; The key of this paper is the connectivity of road network, which is related to the connectivity of roads and intersections in the road network.

## 2    Background

### 2.1    Traditional Model

Scholars often use connectivity index to describe the connectivity of road network. Connectivity index is used to describe the relationship between roads and intersections in the road network, the model is as follows:

$$J = \sum_{i=1}^{N} m_i/N = 2M/N \tag{1}$$

here

$J$   connectivity index;
$N$   the number of the intersections in the network;
$m_i$  the number of roads connected to No. $i$ intersection in the road network;
$M$   the number of roads in the road network.

According to Formula (1), the connectivity of road network depends entirely on the number of roads and intersections in the road network. Formula (1) is easy to calculate. Zhou Tao quantitatively analyzes the influence of traffic organization on the connectivity of urban road network and modifies Formula (1), the modified model as follows:

$$J = \sum_{i=1}^{n} (r_i/d_i^{in})/N \qquad (2)$$

Formula (2) takes into account the impact of traffic organization on connectivity of road network and the parameters are quantified by different traffic organization conditions.

## 2.2 Traditional Mode

Traditional model on the connectivity of road network only considers the physical structure of the road network and lack of analysis of traffic flow status and traffic organization. Formula (2) takes into account the impact of traffic organization on the connectivity of road network, but also lack of analysis of traffic flow status.

There is a general assumption in the current research on the connectivity of road network: the connectivity index of the connected road is calibrated to 1 while the connectivity of interrupted road is calibrated to 0. However, traffic flow status has an influence on the connectivity of road and road network. The connectivity index is calculated according to Formula (1) or (2) is not entirely reasonable. Therefore, in order to compensate for the shortcomings of existing research, this paper will analyze the influence of traffic flow status on the connectivity of road network, and modify the model on the connectivity of road network.

## 3 Analysis of Factors of Connectivity

### 3.1 The Physical Structure of the Road Network

The physical structure of road network mainly refers to the number of roads and intersections in the road network. The physical structure of the road network has

an important influence on the traffic performance of the whole road network. The intersection is where there is a conflict. The connectivity of road network will be worse as the intersections increase. At the same time, the physical structure of the road network will have an impact on traffic flow. The physical structure of road network mainly refers to the number of roads and intersections in the road network.

## 3.2 Traffic Flow Status

Traditional model on connectivity of road network is often built by describing the physical structure of the road network, lack of analysis of traffic flow status. However, different traffic flow status leads to the different connectivity of road network and traffic flow status has an influence on the connectivity of road network. It is an necessary to analyze the traffic flow status to evaluate the connectivity of road network. The traffic flow is made up of cars driving on the road which is consequent and stable. The traffic flow status of different roads is different and the connectivity of roads is different. Traffic flow parameters generally refer to *the average flow of the road, the average speed of the road and the average traffic density*. The average speed of the road can reflect the traffic performance of the road and the traffic status of the road. The higher the average speed of the road, the better the traffic performance. Therefore, in order to quantitatively describe the impact of traffic flow on the performance of road network, the average speed of the road is selected as the parameter reflecting the traffic flow status. By analyzing the relationship between traffic flow status and connectivity of roads, the paper will build the modified model on the connectivity of road network based on Formula (1).

## 4 Methodology

### 4.1 Connectivity of the Road

The influence of traffic flow status on connectivity of road network is reflected in the average speed of the road. Assume that the traffic on each section of the road network is continuous and the average speed of each section is generally stabilized. The average speed can reflect the connectivity of the road. In order to quantify the impact of speed on the connectivity of the road, this paper introduces the concept of driver's satisfaction model on speed. Scholars generally assign its connectivity index to 1 (or 0) according to the physical structure of the road, which is not reasonable. In this paper, the connectivity index of the road is assigned to a value in the interval [0, 1] according to satisfaction model on speed.

This survey chooses 200 vehicle drivers in Harbin as the respondents, and investigates the driver's travel satisfaction with speed. The main content of the survey

**Table 1** Investigation on driver's satisfaction with speed of road

| Speed (km/h) | Scores | Speed (km/h) | Scores |
| --- | --- | --- | --- |
| 10 | 18.2 | 40 | 77.6 |
| 15 | 22.8 | 45 | 85.6 |
| 20 | 29.8 | 50 | 93.6 |
| 25 | 38.2 | 55 | 100.0 |
| 30 | 51.1 | 60 | 100.0 |
| 35 | 65.2 | 65 | 100.0 |
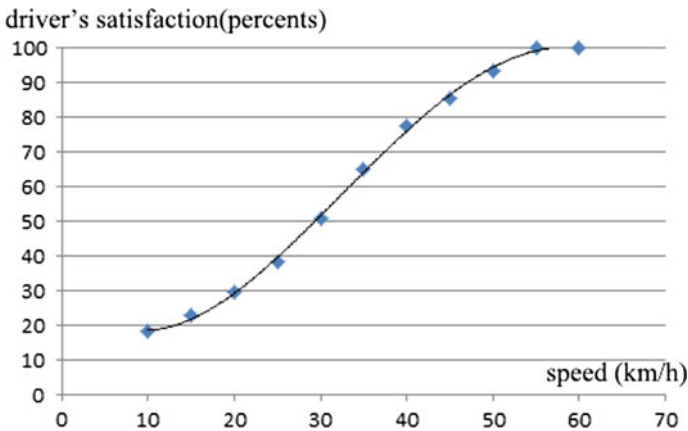


**Fig. 1** The fitted curve of satisfaction with driver's speed of road

is driver's satisfaction with different speed. Speed is divided into 10–65 km/h with 12 grades according to the actual road traffic survey. Satisfaction is reflected by the results of the vehicle driver's scores. The survey sets up five score grades: terrible (0–20), bad (20–40), acceptable (40–60分), good (60–80), very good (80–100), Questionnaires were aged between 18 and 65 years old, with a total of 182 valid questionnaires. The average score for each speed grade is shown in Table 1.

As shown in Table 1, when the speed varies between 10 and 50 km/h, the vehicle drivers' satisfaction is increasing. When the speed is higher than 55 km/h, the vehicle drivers' satisfaction on the road is the highest. Then, we use the software SPSS to fit the satisfaction and the speed of the road, Taking the speed as the independent variable, the travel satisfaction as the dependent variable, fitting out the speed and travel satisfaction curve, as shown in Fig. 1.

The formula for the fitting curve is calibrated as follows:

$$p = 0.0012v^3 + 0.122v^2 - 1.5895v + 22.879 \tag{3}$$

here:

$p$   drivers' satisfaction;
$v$   the average speed of the road.

This paper reassigns the connectivity index of the road according to formula (3), The connectivity of the road is calculated as follows:

$$a = p/100 \tag{4}$$

Here,

$a$   the connectivity of the road;
$p$   driver's satisfaction.

## 4.2   The Connectivity of the Road Network

The connectivity of the road network is related to the number of intersections within the road network and the connectivity of the intersections. The connectivity index of the intersection is the sum of the connectivity of roads connected with the intersection. The road has a positive and negative connectivity of two directions. In this paper, the average of the connectivity in both directions of the road is taken as the connectivity index of the road. It is necessary to analyze the connectivity of the intersection to calculate the connectivity index of the road network. The connectivity index of the intersection is the sum of the connectivity of the roads connected with the intersection.

As shown in Fig. 2, the numbers in the figure represent the speed on both sides of the road and the unit is km/h. It is known that the speed of both directions of the road and the satisfaction can be acquired according to Formula (3). According to the relationship between the vehicle driver's satisfaction and the connectivity of the road, the connectivity index of the road can be acquired. Therefore, the connectivity of the intersection is 2.62.

The connectivity of the road network is related to the number of intersections within the road network and the connectivity of the intersections. This paper builds a model on the connectivity index of the road network by constructing the relationship between road connectivity and road network connectivity. The Formula (5) is derived from the Formulas (3) and (4), which describes the relationship between the average speed of road and connectivity index of the road. Formula (6) describes the relationship between the connectivity index of the intersection and the connectivity index of the road. The Formula (8) is derived from the Formulas (5) and (7), which is the modified model on the connectivity of the road network.

The model on the connectivity of the road:

$$a_{ij} = p_{ij}/100 = 0.0012v_{ij}^3 + 0.122v_{ij}^2 - 1.5895v_{ij} + 22.879 \tag{5}$$

**Fig. 2** Speed distribution of
intersection
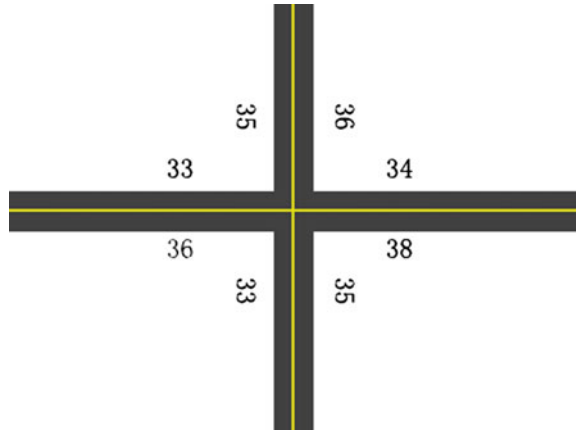


The model on the connectivity of the intersection:

$$c_i = \sum_{j=1}^{m} a_{ij} = \sum_{j=1}^{m} 0.0012v_{ij}^3 + 0.122v_{ij}^2 - 1.5895v_{ij} + 22.879 \qquad (6)$$

The model on the connectivity of the road network:

$$J = \sum_{i=1}^{N} c_i = \sum_{i=1}^{N}\sum_{j=1}^{m} a_{ij}/N \qquad (7)$$

$$J = \sum_{i=1}^{N}\sum_{j=1}^{m} 0.0012v_{ij}^3 + 0.122v_{ij}^2 - 1.5895v_{ij} + 22.879/N \qquad (8)$$

here:

$J$     the connectivity of the road network;
$N$     the number of the intersections in the road network;
$v_{ij}$    the average speed of the No. $i$ road connected with No. $j$ intersection;
$a_{ij}$    the connectivity of the No. $i$ road connected with No. $j$ intersection;
$c_i$     the connectivity of the No. $j$ intersection;
$m$     the number of roads connected with the intersection.

The modified model describes the relationship between the connectivity of road
network and the road traffic flow as the main parameters of the vehicle speed in each
road of the road network.

# 5 Examples

In this paper, two typical road networks in Dao-wai area and Dao-li area are selected as examples to verify the modified model on the connectivity index of road network. Figures 3 and 4 are the average vehicle speed distribution of two areas and the number in the pictures represents the code of intersection. The number at both sides of the road represents the speed of the direction and the unit is km/h.

According to Formula (6), the connectivity of each intersection can be acquired. Different intersections of the same network have different connectivity. Even if the physical structure of the same intersection, because of its traffic flow status is different, its connectivity is different. It is known that the connectivity of each intersection in the road network. According to Formula (8), the connectivity of two areas can be acquired. The results as shown in Table 2.

As shown in Table 2, the scores represent drivers satisfaction with Dao-wai area and Dao-li area which is based on the survey. It is obvious that Dao-li has a higher connectivity index than Dao-wai. According to the traditional model, Dao-li area's connectivity index is almost equal to Dao-wai's, which is not reasonable. According to the modified model, Dao-li's connectivity index is higher than Dao'wai's, which is reasonable. Therefore, the modified model on the connectivity of road network considering the traffic flow status has a better applicability than the traditional model.

This paper verifies the superiority of the modified model than the traditional model. The modified model considers the influence of traffic flow on the connectivity of road
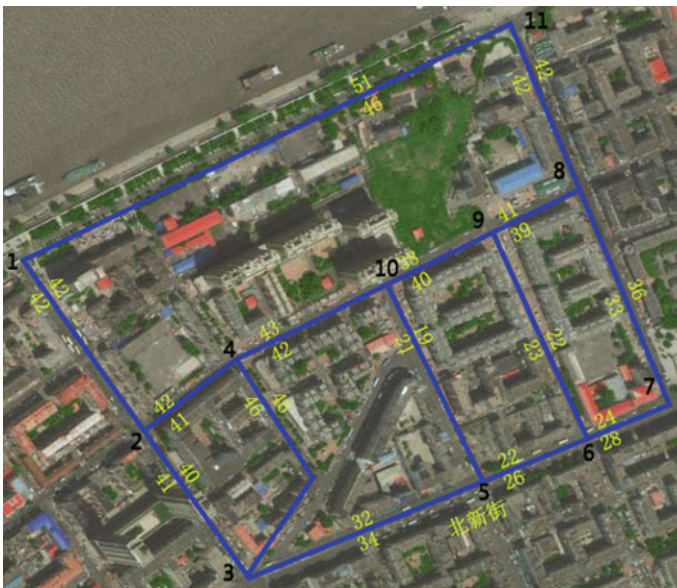


**Fig. 3** Speed distribution of Dao-wai area

**Fig. 4** Speed distribution of Dao-li area

**Table 2** The results of connectivity calculation

| Area | Traditional model results | Modified model results | Scores |
|---|---|---|---|
| Dao-wai | 3.82 | 2.67 | 76 |
| Dao-li | 3.83 | 2.97 | 82 |

network and the actual experience of the vehicle driver in the road network while the traditional model only considers the influence of physical structure of road network. The calculation results of modified model are closer to the actual situation of road network performance.

# 6 Conclusions

The paper points out the shortcomings of traditional research on connectivity of road network and carefully analyzes the influence of traffic flow on the connectivity of road network to build a modified model on connectivity of road network. The modified model not only considers the physical structure of the road network, but also considers the traffic flow status factors which were not considered before. According to the conclusion, the paper proposes the following suggestions:

(1) According to the model on driver satisfaction with speed, the traffic manager can evaluate the running status of the road and issue traffic information to induce drivers in the network.

(2) According to the average speed of the road and the modified model on connectivity index of the road network, the traffic manager can evaluate the running status of the road network and take the appropriate traffic management measures

# References

1. Mackie PJ, Jara-Diaz S, Fowkes AS (2001) The value of travel time savings in evaluation. Transp Res Part E 91–106
2. Wardman M (2004) Public transport values of time. Transp Policy 2–3
3. Nicholson A (2003) Assessing transport reliability: malevolence and user knowledge. In: The network reliability of transport: proceeding of the 1st international symposium on transportation network reliability (INSTR). Pergamon Press, Kyoto
4. Iida Y, Wakabayashi H (1989) An approximation method of terminal reliability of a road network using partial minimal path and cut set. In: Proceedings of the fifth WCTR, pp 367–380
5. Iida Y (1999) Basic concepts and future directions of road network reliability analysis. J Adv Transp 33(2):125–134
6. Lu J, Wang WW (2004) Urban road network planning factor system. J Traffic Transp Eng 04:62–67
7. Yin Y, Ieda H (2001) Assessing performance reliability of road network under non-recurrent congestion. Transp Res Rec 1771:148–155
8. Zhou T (2015) Analysis on the evaluation factors of urban road network connectivity. UTC J 01:60–65
9. Xiong Q (2015) Study on optimization model of highway traffic network layout considering different connectivity requirements between nodes. Appl Res Comput (11):3352–3355
10. Li F (2016) Complex network characteristics of urban road network. J Shandong Univ Technol 06:16–19+25
11. Cao WW, Zhang H (2016) Road automatic selection method considering structure and geometric characteristics. J Wuhan Univ Technol 1–4
12. Song HQ (2017) Evaluation of urban road importance based on complex network and automatic road network synthesis method. J Wuhan Univ Technol (01):8–12
13. Zhang PD (2016) The expression of urban road network based on topological intensity. J Wuhan Univ Technol (02):178–183+213

# Analysis of the Low-Carbon Efficiency of Chinese Transport Sectors from 2007 to 2015

**Fei Ma, Xiao-dan Li, Qi-peng Sun, Fei Liu and Wen-lin Wang**

**Abstract** To evaluate the carbon emission efficiency of transport sectors in China, the concept of low-carbon transport efficiency (*LCTE*) is proposed. On this basis, the *LCTE* in China's provinces and autonomous regions is calculated using the evaluation method of cross-data envelopment analysis (DEA) with the data during the period of 2007–2015. The result shows that the overall level of China's *LCTE* is mostly in the middle and lower level, meanwhile the difference of provincial and autonomous regions is great. This means there is a lot of room for China's low-carbon transport efficiency to improve. The average value of *LCTE* is 0.54, which shows a steady trend of development from 2007 to 2013. While there are large fluctuations from 2013 to 2015 in many provinces and autonomous regions, of which Ningxia and Liaoning are the largest, whose change are the decrease of 40.7% and the increase of 79.1%, respectively. This indicates that current situation of transport carbon emission in China is not optimistic, and the main reason is that the western region is relatively backward.

**Keywords** Low-carbon transport efficiency · Transport sectors · Cross-data envelopment analysis

## 1 Introduction

With the development of China's economy, energy consumption, and $CO_2$ emissions have risen sharply. Carbon emission efficiency continues to grow in all sectors. In energy utilization activities, due to highly dependent on the huge amount of fossil fuels, the transport industry has become the most important source of $CO_2$ emissions. Therefore, how to mitigate the carbon emissions of the transport industry has become an imminent problem to achieve China's sustainable development.

F. Ma (✉) · X. Li · Q. Sun · F. Liu · W. Wang
School of Economics and Management, Chang'an University, Xi'an 710064, China
e-mail: mafeixa@163.com

The research on low-carbon transportation mainly has the following aspects: by estimated the emissions of greenhouse gas (GHGs) from road and rail shaft infrastructure, Dimoula found that road construction had less impact on the environment than railways [1]. The effect of gender on carbon emissions explored by Waygood [2]. Figliozzi (2011) analyzed the $CO_2$ emissions for different levels of congestion and time-definitive customer demands. Results from these case studies indicated that the impacts of congestion or speed limits on commercial vehicle emissions were significant but difficult to predict [3]. Mascia [4] investigated the effectiveness of transport management tools in reducing transport congestion and associated emissions of $CO_2$, $NO_x$, and black carbon. The second is the measurement and calculation for low-carbon transport and prediction.

At present, there are related literature to explore the efficiency evaluation methods: Rezaee [5] used data envelopment analysis (DEA) and game theory to evaluate the efficiency of different bus lines. Zhao [6] researched the influence of a single node on the entire transport network performance by using micro-simulation model, and Chang [7] analyzed the environmental efficiency of China's transport industry by using SBM-DEA. Second, from the view of the efficiency, the various evaluation methods of DEA such as cross-DEA, super efficiency DEA, DEA-based SEM (structural equation model) were used. These documents and methods do not directly measure the efficiency of low-carbon transport, but laid the theoretical and methodological basis for the relative researches.

In summary, most of literature mainly focus on the low-carbon transport itself, while lack for the interpretation of low-carbon transport efficiency and related study. This paper argues that low-carbon transport efficiency (*LCTE*) is the ratio of output and input of low-carbon transport. According to the data of transport carbon emissions, transport GDP, energy consumption, infrastructure investment and practitioners in 31 provinces and autonomous regions of China from 2007 to 2015, the cross-DEA model is used to calculate the low-carbon transport efficiency of China.

The paper is organized as follows: we first provide the calculation model of cross-DEA as well as the study data in Sect. 2. In Sect. 3, the *LCTE* of 31 provinces and autonomous regions in China have been calculated. Finally, the conclusions are made in Sect. 4.

## 2   Models and Data

### 2.1   *The Efficiency Analysis Method*

Data envelopment analysis (DEA) is a kind of multi-input and multi-output efficiency evaluation method proposed in the United States in 1978 [8] (Banker et al. 1981), but the index weight of traditional DEA model is subjective and unrestricted. In 1986, Sexton proposed the efficiency evaluation method of crossed DEA, which mainly used the self-evaluation system to eliminate the shortcomings of the traditional DEA

method that relies on the self-evaluation system to sort the decision-making unit. This method can judge the most optimal decision-making units, which solve the problem that the weight coefficient is too extreme and unrealistic in the traditional DEA method, avoiding the tendency of the decision maker to determine the weight subjectively. Due to the optimal solution and the uniqueness of the weight in the DEA model, the DEA cross-evaluation value is uncertain [9, 3]. Therefore, we use the crossed DEA evaluation method to measure the efficiency of low-carbon transport. The crossed DEA model is as follows:

**Step 1**: The traditional DEA model is used to calculate the self-evaluation value $E_{ii}$ $(1 < i < n)$

Suppose there are *DMU*s,

$$\text{DMU}_i = \begin{bmatrix} x_i \\ y_i \end{bmatrix} \quad (1 \leq i \leq n) \tag{1}$$

where $x_i = (x_{1i}, x_{2i}, \ldots, x_{mi})^{\text{T}}$, $y_i = (y_{1i}, y_{2i}, \ldots, y_{si})^{\text{T}}$, $x_i$ and $y_i$ are the $m$ inputs and $s$ outputs of $\text{DMU}_i$ respectively.

$$X = (x_1, x_2, \ldots, x_n), \quad Y = (y_1, y_2, \ldots, y_n) \tag{2}$$

where $X, Y$ is the input index matrix and output index matrix, respectively.

Suppose $v = (v_1, v_2, \ldots, v_m)^{\text{T}}$, $u = (u_1, u_2, \ldots, u_s)^{\text{T}}$, $(u, v \geq 0)$ are the weight vector of input and output indicators, respectively.

The ratio of total output $O_i$ and the total input $I_i$ of $\text{DMU}_i$ is as follows:

$$E_{ii} = \frac{O_i}{I_i} = \frac{\sum_{l=1}^{s} u_l y_{li}}{\sum_{t=1}^{m} v_t x_{ti}} = \frac{y_i^{\text{T}} u}{x_i^{\text{T}} v} \tag{3}$$

where $E_{ii}$ is the efficiency evaluation index of $\text{DMU}_i$, which is calculated by the best weight, so it is also called the self-evaluation value of $\text{DMU}_i$.

$v = (v_1, v_2, \ldots, v_m)^{\text{T}}$, $u = (u_1, u_2, \ldots, u_s)^{\text{T}}$, $(u, v \geq 0)$ is the weight vector of input and output indicators.

If $E_{ii} = 1$, $\text{DMU}_i$ is effective; If $E_{ii} \leq 1$, $E_{ii}$ is not effective. But in reality, there will be more than one *DMU* can reach 1, only using $E_{ii}$ cannot distinguish which is the best in these decision-making units.

**Step 2**: Solve the following linear programming:

$$\begin{cases} \min \ y_k^{\text{T}} u \\ \text{s.t. } y_j^{\text{T}} u \leq x_j^{\text{T}} v (1 \leq j \leq \to n), \ y_i^{\text{T}} u = E_{ii} x_i^{\text{T}} v, \ x_k^{\text{T}} v = 1, \ u \geq 0, \ v \geq 0 \end{cases} \tag{4}$$

where $i \in \{1, 2, \ldots, n\}$, $k \in \{1, 2, \ldots, n\}$.

**Step 3**: Using the optimal solution $u_{ik}^*$ and $v_{ik}^*$ of the above linear programming to solve cross evaluation $E_{ik} = \frac{y_k^{\mathrm{T}} u_{ik}^*}{x_k^{\mathrm{T}} v_{ik}^*}$. The bigger value of the $E_{ik}$ is more favorable to DMU$_k$, but is more unfavorable to DMU$_i$.

**Step 4**: Establish a crossed evaluation matrix by all of the $E_{ik}$:

$$E = \begin{bmatrix} E_{11} & E_{12} & \dots & E_{1n} \\ E_{21} & E_{22} & \dots & E_{2n} \\ \dots & \dots & \dots & \dots \\ E_{n1} & E_{n2} & \dots & E_{nn} \end{bmatrix} \tag{5}$$

where $E$ is the cross-evaluation matrix, in which the diagonal elements are self-evaluation values and the nondiagonal elements are cross-evaluated values. Many scholars use the average $e = \frac{1}{n} \sum_{k=1}^{n} E_{ki}$ of the $i$th column as an indicator of evaluating the DMU$_i$. And $e_i$ can be regarded as the total evaluation of the DMU$_i$ for each decision unit.

## 2.2 Data Sources

According to the definition of low-carbon transport efficiency, the input indicators selected in this paper are transport energy consumption, investment in transport infrastructure and the number of practitioners in the transport industry. The output indicators are the transport GDP and carbon emissions. The data of energy consumption are derived from the Statistical Yearbook of China's 31 provinces and autonomous regions (2007–2015). The statistical yearbook of Zhejiang, Heilongjiang, Chongqing, and Tibet did not include these data, so the energy consumption of the transport sector of these provinces and autonomous regions are gotten by the average value of the energy consumption of transport industry with its neighboring provinces. The data of transport infrastructure investment and transport industry practitioners are from the official website of National Bureau of Statistics (2007–2015), of which the transport industry practitioners indicators are the sum of practitioners in railway, road, waterway and urban public transport. Due to the lack of urban public transport practitioners data in 2011–2015, the approximate values are calculated by exponential smoothing method. The carbon emissions from the transport sector are calculated by the method provided by the National Greenhouse Climate Inventory Guidelines designated and the Kyoto Protocol designed by IPCC (Intergovernmental Panel on Climate Change)

The specific formula is

$$E_t = \sum_i m_i \varepsilon_i \mu_i \tag{6}$$

where $E_t$ is the carbon emissions for the period $t$, $m$ is the $i$th primary energy consumption physical quantity (coal, oil, and natural gas), $\varepsilon_i$ is the conversion coefficient of standard coal for $i$th energy, $\mu_i$ is the carbon emission coefficient of $i$th energy.

## 3   Results and Analysis

Using MATLAB7.0 to measure the efficiency of low-carbon transport efficiency in China's provinces and autonomous regions during the period of 2007–2015, and sort the LCTE by the size of efficiency value (see Table 1).

As can be seen from Table 1, the *LCTE* is divided into four stages, in which the efficiency values are mostly in the middle and lower level and large of the differences between provinces and autonomous regions, the specific analysis is as follows:

The regions with high efficiency of low-carbon transport (efficiency mean greater than 0.73) are: Hebei, Jiangsu, Qinghai, Ningxia, Shandong, and other provinces. For example, according to the data of Hebei province in 2015, the low-carbon transport investment was 207.754 (billion RMB), the number of practitioners were 303.5 (thousand people), the energy consumption was 11.0785 (million tons), the carbon emission was 7.53,338 (million tons), and the transport GDP was 235.909 (billion RMB). The transport GDP is nearly 2 times to the average, while the carbon emissions are equal with the mean. The higher transport GDP and relatively low-carbon emissions are the significant reasons for the high efficiency of low-carbon transport in Hebei province from 2007 to 2015. The regions with a moderate level (efficiency value between 0.54 and 0.73) of low-carbon transport efficiency are Tianjin, Shanghai, Jiangxi, Henan, Guizhou, Fujian, Zhejiang, Guangdong, Anhui, Hainan, Qinghai, and other provinces, which mainly locate in the mid and east of China. In Tianjin, for example, Tianjin's low-carbon transport investment in 2015 was 75.719 (billion RMB), the number of practitioners were 127.9 (thousand people), and the low-carbon transport energy consumption was 5.5086 (million tons of standard coal), transport GDP was 72.909 (billion RMB) and the carbon emissions was 3.1679 (million tons). In contrast, the low-carbon transport investment of Beijing was 71.495(billion RMB), transport GDP was 98.387 (billion RMB), which was closed to Tianjin, while its number of practitioner were 667 (thousand people), energy consumption was 12.0823 (million tons), and carbon emission was 6.9485 (million tons). These input-type and reverse-type indicators are generally about 3 times to the corresponding indicators of Tianjin. In contrast, Tianjin's investment is smaller but the output is bigger, and the development of low-carbon transport is better while there is still room for improvement.

It still needs to take appropriate measures to improve the low-carbon transport efficiency. The regions with a low level of low-carbon transport efficiency (efficiency value of less than 0.54) are Tibet, Sichuan, Yunnan, Yunnan, Yunnan, Hubei, Guangxi, Xinjiang, Xinjiang, Shaanxi, Tibet, Sichuan, Yunnan, which mainly distributes in the east, central, and west of China, while it still mainly distributes in the central and west of China. The development of low-carbon transport in these areas

**Table 1** The *LCTE* in different provinces and autonomous regions of China in 2007–2015

| Interval | Province[a] | 2007 | 2008 | 2009 | 2010 | 2011 | 2012 | 2013 | 2014 | 2015 | Mean |
|---|---|---|---|---|---|---|---|---|---|---|---|
| 0.72–0.9 | 1 | 0.89 | 0.93 | 0.92 | 0.85 | 0.86 | 0.86 | 0.85 | 0.90 | 0.90 | 0.88 |
| | 2 | 0.71 | 0.76 | 0.79 | 0.9 | 0.89 | 0.87 | 0.86 | 0.67 | 0.79 | 0.80 |
| | 3 | 0.72 | 0.82 | 0.83 | 0.83 | 0.78 | 0.70 | 0.69 | 0.68 | 0.66 | 0.74 |
| | 4 | 0.64 | 0.79 | 0.80 | 0.79 | 0.79 | 0.78 | 0.81 | 0.48 | 0.75 | 0.74 |
| | 5 | 0.77 | 0.84 | 0.83 | 0.80 | 0.77 | 0.69 | 0.56 | 0.60 | 0.66 | 0.73 |
| 0.54–0.72 | 6 | 0.62 | 0.68 | 0.67 | 0.76 | 0.73 | 0.57 | 0.75 | 0.67 | 0.76 | 0.69 |
| | 7 | 0.51 | 0.46 | 0.42 | 0.65 | 0.69 | 0.71 | 0.69 | 0.92 | 0.67 | 0.64 |
| | 8 | 0.62 | 0.61 | 0.58 | 0.56 | 0.58 | 0.70 | 0.73 | 0.59 | 0.63 | 0.62 |
| | 9 | 0.71 | 0.60 | 0.69 | 0.57 | 0.54 | 0.56 | 0.66 | 0.62 | 0.64 | 0.62 |
| | 10 | 0.62 | 0.67 | 0.67 | 0.66 | 0.62 | 0.58 | 0.61 | 0.51 | 0.62 | 0.62 |
| | 11 | 0.51 | 0.62 | 0.60 | 0.56 | 0.60 | 0.56 | 0.69 | 0.58 | 0.64 | 0.60 |
| | 12 | 0.73 | 0.64 | 0.62 | 0.58 | 0.52 | 0.50 | 0.57 | 0.56 | 0.64 | 0.60 |
| | 13 | 0.56 | 0.55 | 0.56 | 0.64 | 0.58 | 0.52 | 0.63 | 0.53 | 0.58 | 0.57 |
| | 14 | 0.61 | 0.57 | 0.52 | 0.54 | 0.56 | 0.59 | 0.55 | 0.51 | 0.60 | 0.56 |
| | 15 | 0.59 | 0.58 | 0.61 | 0.66 | 0.62 | 0.54 | 0.54 | 0.41 | 0.45 | 0.56 |
| | 16 | 0.45 | 0.45 | 0.43 | 0.56 | 0.70 | 0.67 | 0.57 | 0.56 | 0.58 | 0.55 |
| | 17 | 0.77 | 0.71 | 0.41 | 0.47 | 0.44 | 0.45 | 0.5 | 0.47 | 0.62 | 0.54 |
| 0.36–0.54 | 18 | 0.56 | 0.52 | 0.47 | 0.50 | 0.47 | 0.52 | 0.60 | 0.47 | 0.59 | 0.52 |
| | 19 | 0.42 | 0.37 | 0.49 | 0.49 | 0.56 | 0.54 | 0.53 | 0.43 | 0.77 | 0.51 |
| | 20 | 0.53 | 0.63 | 0.64 | 0.54 | 0.52 | 0.51 | 0.40 | 0.27 | 0.31 | 0.48 |
| | 21 | 0.50 | 0.45 | 0.47 | 0.44 | 0.47 | 0.47 | 0.54 | 0.45 | 0.46 | 0.47 |
| | 22 | 0.49 | 0.40 | 0.37 | 0.38 | 0.47 | 0.51 | 0.56 | 0.54 | 0.50 | 0.47 |
| | 23 | 0.36 | 0.29 | 0.36 | 0.45 | 0.56 | 0.42 | 0.47 | 0.50 | 0.52 | 0.44 |

(continued)

**Table 1** (continued)

| Interval | Province[a] | 2007 | 2008 | 2009 | 2010 | 2011 | 2012 | 2013 | 2014 | 2015 | Mean |
|---|---|---|---|---|---|---|---|---|---|---|---|
| | 24 | 0.44 | 0.37 | 0.39 | 0.45 | 0.38 | 0.39 | 0.47 | 0.51 | 0.45 | 0.43 |
| | 25 | 0.37 | 0.36 | 0.41 | 0.46 | 0.42 | 0.39 | 0.46 | 0.38 | 0.43 | 0.41 |
| | 26 | 0.67 | 0.42 | 0.36 | 0.33 | 0.32 | 0.39 | 0.41 | 0.24 | 0.42 | 0.40 |
| | 27 | 0.35 | 0.34 | 0.37 | 0.39 | 0.42 | 0.39 | 0.45 | 0.40 | 0.46 | 0.40 |
| | 28 | 0.38 | 0.37 | 0.39 | 0.38 | 0.36 | 0.39 | 0.41 | 0.40 | 0.38 | 0.38 |
| 0.18–0.36 | 29 | 0.34 | 0.45 | 0.46 | 0.37 | 0.31 | 0.33 | 0.34 | 0.14 | 0.33 | 0.34 |
| | 30 | 0.48 | 0.38 | 0.29 | 0.28 | 0.24 | 0.22 | 0.27 | 0.31 | 0.36 | 0.32 |
| | 31 | 0.25 | 0.21 | 0.20 | 0.16 | 0.16 | 0.20 | 0.21 | 0.18 | 0.19 | 0.19 |

*Note* [a]Region number: 1. Hebei, 2. Jiangsu, 3. Qinghai, 4. Ningxia, 5. Shandong, 6. Tianjin, 7. Shanghai, 8. Jiangxi, 9. Henan, 10. Guizhou, 11. Neimenggu, 12. Fujian, 13. Zhejiang, 14. Guangdong, 15. Anhui, 16. Hainan, 17. Shanxi, 18. Hunan, 19. Liaoning, 20. Gansu, 21. Jilin, 22. Heilongjiang, 23. Beijing, 24. Chongqing, 25. Hubei, 26. Xinjiang, 27. Guangxi, 28. Shaanxi, 29. Xizang, 30. Sichuan, and 31. Yunnan
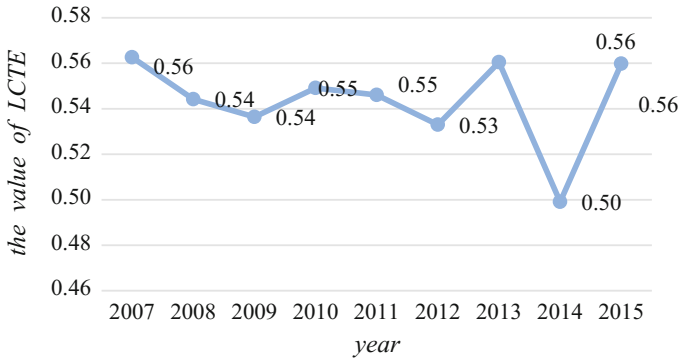
**Fig. 1** Evolution of China's *LCTE* in 2007–2015 years

is imminent. Yunnan, for example, its low-carbon transport investment was 181.517 (billion RMB), the number of practitioners was 154 (thousand people), energy consumption was 7.42865 (million tons), carbon emission was 4.2722 (million tons), transport GDP was 30.449 (Billion RMB). Yunnan's low-carbon transport infrastructure investment, practitioners and energy consumption indicators are at a lower level, and its transport GDP is only the one-third of the mean of all the provinces and autonomous regions, so its low-carbon transport efficiency is relatively low.

As shown in Fig. 1, China's low-carbon transport efficiency shows a steady trend of development from 2007 to 2013, while it has a significant fluctuation from 2013 to 2015, and the overall level is low (efficiency value is less than 0.54).

From 2007 to 2013, due to the slow increase in infrastructure investment year by year and the steady growth in transport GDP, the low-carbon transport efficiency fluctuated within 0.5%. The average low-carbon transport efficiency of China falls by 10.9% from 2013 to 2014, with 22 provinces declining during the period, and Ningxia (as shown in Fig. 2) declines the most from 0.81 to 0.48, with a decline rate at 40.7%. The sharp increase in infrastructure investment and the increase in transport carbon emission are important causes of the decline. The low-carbon transport efficiency of China increases by 12.14% from 2014 to 2015, with an increase of efficiency value in more than two-thirds of the provinces and autonomous regions, of which Liaoning (as shown in Fig. 2) is the most significant area, with an increase of 79.1%. The increase in low-carbon transport GDP and the decrease in practitioners are the key factors during this period.

## 4    Conclusions

The *LCTE* of China's provinces is divided into four stages, among which the efficiency values are mostly in the middle and lower level, provincial and autonomous regions vary greatly. In other words, there is a lot of room for China's low-carbon

**Fig. 2** The value of *LCTE* of Liaoning and Ningxia from 2007 to 2015 years
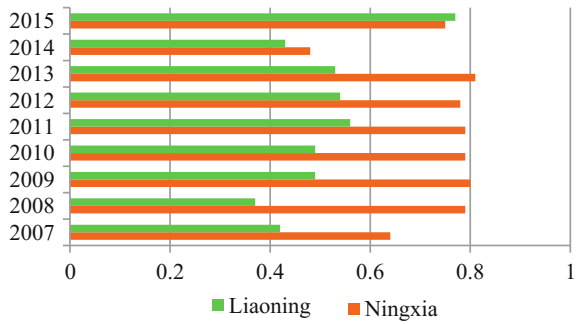
transport efficiency to develop, and the regional governments should take relevant measures to improve the overall level of China's low-carbon transport efficiency according to the actual situation. China's *LCTE* has a stable development in 2007–2013, while significant fluctuations occur in 2013–2015, and the overall level is low (the efficiency value is 0.56), indicating that current transport carbon emission situation of China is not optimistic. The main reason for this situation is that the western region is relatively backward, thus reducing the overall level of development. From the original data, we can see that the eastern and western inputs are nearly equal, but the western output is less than one-half of the eastern part.

This paper mainly focuses on the measurement of low-carbon transport efficiency but doesn't decompose the impact factors of low-carbon traffic efficiency, so we did not do sensitivity analysis. In future research, the impact of various factors on the contribution of low-carbon transport efficiency should be taken into account and to give more targeted responses.

# References

1. Dimoula V, Kehagia F, Tsakalidis A (2016) A holistic approach for estimating carbon emissions of road and rail transport systems. Aerosol Air Qual Res 16:61–68
2. Waygood EOD, Avineri E (2016) Communicating transportation carbon dioxide emissions information: does gender impact behavioral response? Transp Res Part D 48:187–202
3. Ferreira M, D'Orey PM (2012) On the impact of virtual traffic lights on carbon emissions mitigation. IEEE T Intelli Transp Syst 13(1):284–295
4. Mascia M, Hu S, Han K et al (2016) Impact of traffic management on black carbon emissions: a microsimulation study. Netw Spat Econ 17(1):269–291

5. Rezaee MJ, Izadbakhsh H, Yousefi S (2016) An improvement approach based on DEA-game theory for comparison of operational and spatial efficiencies in urban transportation systems. Transp Eng 20(4):1526–1531
6. Zhao Y, Triantis K, Murray-Tuite P, Edara P (2011) Performance measurement of a transportation network with a downtown space reservation system: A network-DEA approach. Transp Res Part E 47(6):1140–1159
7. Chang Y, Zhang N, Danao D, Zhang N (2013) Environmental efficiency analysis of transportation system in China: a non-radial DEA approach. Energ Policy 58(9):277–283
8. Charnes A, Cooper WW, Cooper (1984) Some models for estimating technical and scale ineffi- ciencies in data envelopment analysis. Manage Sci 30(9):1078–1092
9. Green RH, Doyle JR, Cook WD (1996) Preference voting and project ranking using DEA and cross-evaluation. Eur J Oper Res 90:461–472

# Establishment and Calibration of Traveled Speed Function for Traffic Network Based on Macroscopic Fundamental Diagram

**Deyong Guan, Lianhua An and Huijia Leng**

**Abstract** This paper proposes a three-dimensional generalization of macroscopic fundamental diagram (MFD), which relates average speed to average density and inhomogeneity of density. Considering temporal and spatial characteristics of traffic demand, the paper defines the total number of vehicle kilometers (TVK) instead of traffic flow to depict traffic efficiency of road network, and deduces macroscopic traffic relations of network-wide properties. Traveled speed function is established and calibrated by the statistical method and theoretical deduction. Function parameters are estimated by Levenberg–Marquardt algorithm. In diagrams, the change path on time series of traveled demand is shown as a single peak mostly and bimodal seldom with a single peak of density. Both vary consistently if in a good traffic state, otherwise, traffic jam will happen at bimodal points and time window before the traveled peak. Given a traffic network, the average speed is an exponential function of average density and spatial spread of density. A dataset of Qingdao city in Chinese is applied to calibrate parameters of traveled speed function and made an analysis of estimation error. It proves this method is reasonable.

**Keywords** Macroscopic fundamental diagram · Traveled speed function · Total number of vehicle kilometers · Traffic efficiency

## 1 Introduction

The study of traffic law is aimed at formulation of proper macroscopic variables which characterize the relationship between travel demand and road characteristics. The relationship of speed-density and flow-density has been basis of traffic flow theory. Greenshields et al. first proposed linear model [1], expressed flow as a function of density, and this was a fundamental diagram (FD) of a single street. Greenberg put forward a logarithmic model that the speed was a function of density, with two

D. Guan (✉) · L. An · H. Leng
Transportation College, Shandong University of Science and Technology, Qingdao 266590, China
e-mail: guandeyong@sdust.edu.cn

parameters: free speed and congestion density [2]. Some researchers proposed different exponential models with two or three parameters [3–5]. Network fundamental diagram was first studied by Godfrey [6], illustrating the relationship between average flow and average density on a traffic network. But the concept on macroscopic fundamental diagram of traffic network was first proposed by Daganzo [7]. It mainly described the relationship between average flow, average density and average speed from a network respect. Especially the diagram of average flow and density. Afterwards, many researchers aimed to explain the existence of MFDs, found that the data of Yokohama city fits quite well [8]. Owing to the spatial and time characteristic of density, the observation condition is also an important factor influencing the shape of MFD. Helbing proved that MFD curves influenced by aggregated density and spatial density distribution [9]. Mazloumian et al. proved that the aggregated flow is a function of aggregated density and its spatial variation [10]. Geroliminis and Sun demonstrated that the spatial distribution of density is a key factor to obtain a well-defined MFD, if there is no need for strict homogeneity of traffic states [11]. The calibration method of traffic function depends on the supposed function formula. The least square method (LSM) is aiming to minimize fitted errors to have a best fitted equations, and has been widely applied to calibrate the coefficients for regression models. Wang et al. used data from Georgia State Route 400 to calibrate the relationship between speed and density by LSM [12]. For the problem of nonlinear function with multivariate objective, Levenberg–Marquardt algorithm is widely used.

The distribution of density is a key factor influencing the relationship between speed and density on a network. This paper is organized as follows: Sect. 2 first defines traffic efficiency, that is a total number of vehicle kilometers (TVK), instead of traffic flow to describe traffic state. And give the macroscopic traffic relations of network-wide properties. Section 3 establishes traveled speed function of traffic network, then give the calibration method of function parameters based on big data. Section 4 uses a dataset of Qingdao city in Chinese to calibrate parameters of traveled speed function and analyze estimation errors. Section 5 makes a summary and discuss the further study.

## 2  Definition of Traffic Properties on Network Aspect

As a classic index, traffic flow cannot depict traffic capacity in a global view. It is difficult to define the direction of flow as a vector. In this paper, we define a new index to evaluate the operation state of traffic. Traffic network capacity is put as the maximum number of vehicle kilometers which network can output, where vehicles in road network have evenly distributed and optimal speed.

Total number of vehicle kilometers (TVK) based on traffic efficiency is taken as the evaluation index of network capacity, calculated as follows:

$$G_E = \sum_{i=1}^{m} N_i V_i \tag{1}$$

$m$ stands for the total number of vehicles on the traffic network, unit: pcu, $V_i$ represents the average space speed of total vehicles on the traffic network, unit: km/h.

If the average density $\bar{\rho}$ and total length $L$ of vehicle lanes on network are given, the total number of vehicle kilometers $G_E$ can be calculated as below:

$$G_E = \bar{\rho} \cdot L \cdot \bar{V}_s \tag{2}$$

The average density of the network composed by $n$ links are determined as the follows:

$$\bar{\rho} = \frac{\sum_{i=1}^{n} (\rho_i \cdot l_i \cdot n_i)}{\sum_{i=1}^{n} (l_i \cdot n_i)} \tag{3}$$

$\rho_i$ stands for the density of link $i$, $l_i$ stands for the length of link $i$, $n_i$ stands for the lanes of link $i$.

The average space speed of the network is calculated as follows:

$$\bar{V}_s = \frac{1}{\frac{1}{N} \sum_{i=1}^{N} \frac{1}{V_i}} = \frac{NL}{\sum_{i=1}^{N} t_i} \tag{4}$$

$L$ is total link length of the given traffic network, $t_i$ is the travel time of vehicle $i$, $V_i$ is the travel speed of vehicle $i$, $N$ is the total number of vehicles.

Owing to inhomogeneous distribution of density in the network, the traffic network capacity varies with the density variance of different links. The spatial spread of density is estimated by the square root of the weighted variance of densities in all links [13]:

$$\gamma = \sqrt{\frac{\sum_i l_i \cdot (\rho_i - \bar{\rho})^2}{\sum_i l_i}} \tag{5}$$

$\gamma$ is the standard deviation of density, also called the spatial spread of density, $l_i$ represents the length of the link $i$, $\rho_i$ represents the density of the link $i$, $\bar{\rho}$ represents average density of traffic network.

# 3  Establishment of Traveled Speed Function

## 3.1  Definition of Traveled Speed Function

The distribution of vehicles in the road network is characterized by network average density and standard deviation of density. Suppose density of traffic network $\rho$ as a discrete random variable, considering standard deviation of density, traveled speed function of the network is established as below:

$$\bar{V}_s(\bar{\rho}_s, \gamma) = \bar{V}_f \cdot \exp\left\{-\frac{1}{a}\left[\frac{\bar{\rho}_s(1+\gamma)}{\rho_m}\right]^b\right\} \tag{6}$$

$a$, $b$ is relative parameters, which can be obtained by observations. $\bar{V}_f$ is harmonic means of free speed of links. $\rho_m$ is the optimal density of traffic network.

Considering the relationship between average density and speed in traffic theory $\bar{V}_s(\rho_m, 0) = V_m$, we can deduce $a = -1/\ln(\frac{V_m}{\bar{V}_f})$ and $V_m = \bar{V}_f \cdot \exp(-\frac{1}{a})$.

Then traffic efficiency $G_E = G_E(\bar{\rho}_s, \gamma)$ is determined by average density and its standard deviation. The optimal traffic efficiency $G_{Em}$, optimal density $\rho_m$, and optimal speed $V_m$ can extract from traffic big data.

## 3.2  Calibration of Traveled Speed Function

The time sequence of travel demand appears "bimodal curve" or "four-peak curve". And it has a corresponding relationship with traffic density: If there is no traffic jam, they will have the same changing trend. If there is a traffic congestion, they will be inconsistent. Optimal value of traffic benefit appears before or after travel peak, and can be extracted from traffic big data. Levenberg–Marquardt algorithm is used to calibrate the function parameters. Specific solution algorithm can find in reference [14]. The relationship among traffic variables is shown in Fig. 1, taking the data of business district in Chinese city as an example.

The diagram in Fig. 1b reveals the parabolic trend on TVK-average density relationship, combined with time series of density and travel demand Fig. 1a, we find that average density and travel demand vary consistently in most time, while the road is in a good traffic state. But there is still some converse change in travel peak. The optimal value of traffic benefit appears at 7:55 and 17:50, and they have an approach value 923.42 pcu km/h. The diagram in Fig. 1c highlights a cubic trend on the average density-spatial spread of density relationship. It shows that the standard deviation of density varies with average density, and different values of density spread might correspond to the same value of average density. Considering real traffic state, it demonstrates that the same amount of vehicles in traffic network could be evenly distributed or more concentrated in some zones.

**(a)**



**(b)**



**(c)**
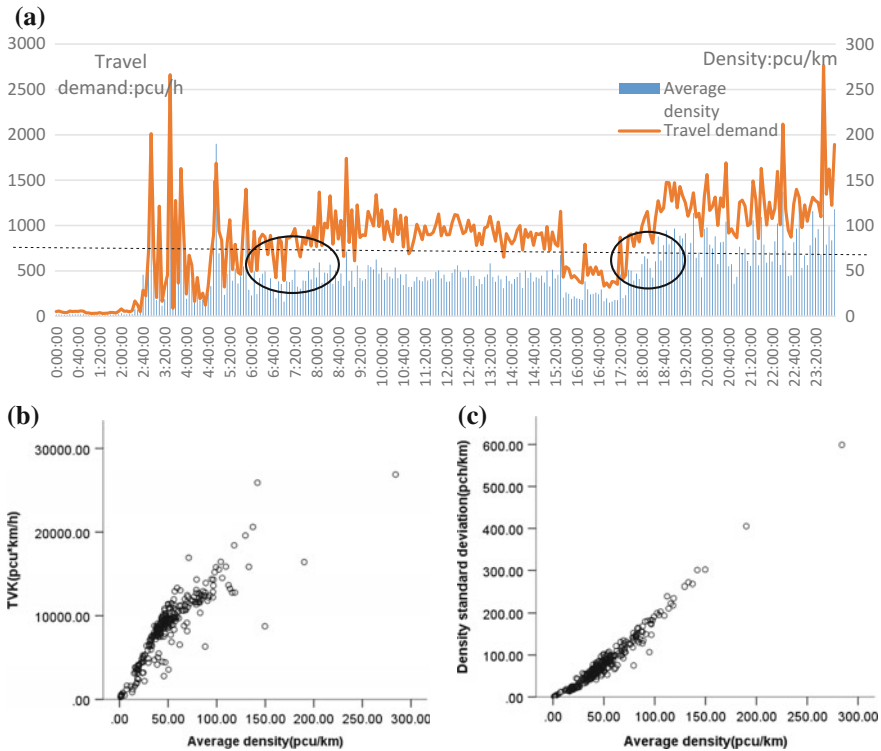


**Fig. 1** Time series of average density and travel demand (**a**), relationship of TVK and average density (**b**) and relationship of average density and standard deviation of density (**c**)

## 4  Case Study

The main characteristic of big data is realizing parallel transmission of real-time data. Through recorders of driving vehicles and GPS online information, vehicle location information on time and space are easily obtained. In the most city, fixed vehicle detectors cover artery roads, collector streets, and key branches, every minute detecting and uploading average speed, time occupancy, passed vehicles and other key attributes of traffic flow to Data Center. Then traffic efficiency, weighted average density, and average spatial speed can be calculated based on these data. The data from Taidong business district in Qingdao (a Chinese city), and the specific characteristics of Taidong business district are shown in Table 1. Time series of whole day collected every five minutes on February 20, 2017. Data resource: http://www.qdznjt.com/trafficIndex/realTimeIndex#.

The macroscopic fundamental diagram of traffic network variables (average density, average speed and standard deviation of density) is shown in Fig. 2.

**Table 1** Key characteristics of the data in Taidong business district

| Total length | 9.72 km |
|---|---|
| Number of main links | 9 |
| Statistic time | 00:00–25:55 |
| Aggregation time | 5 min |
| Area | 60.2872 ha |
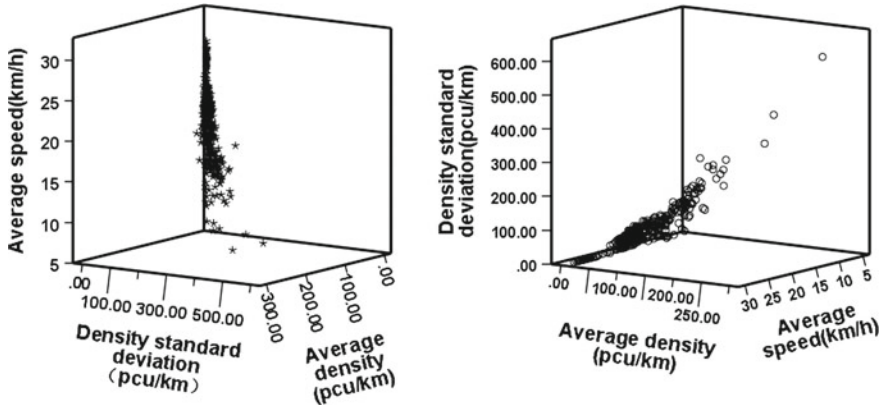


**Fig. 2** Three-dimensional MFD in Taidong business district: speed-density and its standard deviation (left), standard deviation of density-average speed and density (right)

Figure 2 is obtained from 24 h data a day. We can see that traffic congestion is not evenly distributed in space and time respective. The average speed declines rapidly with increasing average density and spatial spread of density, and they approach an exponential relation. It demonstrates that some parts of road network are more congested than others, and the density distribution is very uneven in most time of this day. As congestion spread wildly on the whole network, the distribution of density is decreased. There is more flat and broad distribution of density in time and space.

Given the initial parameters $a_0 = 1$, $b_0 = 0$, use Levenberg–Marquardt algorithm calibration the Eq. (6). The calibration result of function parameters is $a = 1.48$, $b = 0.069$. From time series of traffic variables like Fig. 1, we can obtain optimal traffic state: $G_E = 8358$ pcu km/h, $\rho_m = 28$ pcu km/h, $V_m = 30.71$ km/h. Network travel speed function is

$$\bar{V}_s(\bar{\rho}_s, \gamma) = 46.96 \cdot \exp\left\{-0.675677 \cdot \left[\frac{\bar{\rho}_s(1 + \gamma)}{28}\right]^{0.069}\right\}$$

The error analysis of calibration results are demonstrated in Fig. 3.

From Fig. 3 we can see that the observations of speed fluctuates fiercely at 2:20–6:30 am, due to the morning market in Taidong business district. At the same time, low speed reflects a terrible traffic condition in the early morning. It fits not
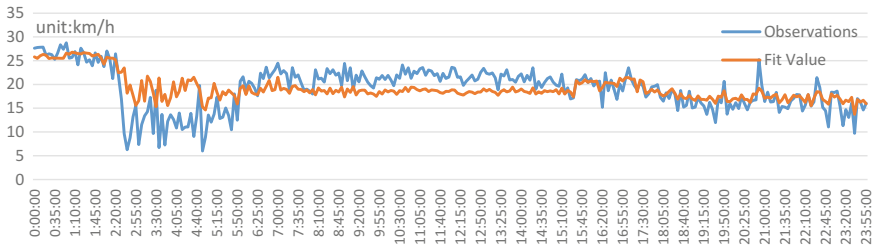
**Fig. 3** Comparison curve between fit value and observations

well in this period, but mostly fit value have the same trend as observations, and calibration errors fluctuate within an acceptable range, so the calibration result is reliable.

## 5 Conclusion

In this paper, we studied the relation between speed and density on a network, and give a three-dimensional projection of average speed, average density and spatial spread of density based on the macroscopic fundamental diagram. A three-dimensional function giving average speed as a function of average density and spatial spread of density was established, supposed as an exponential function estimated parameters by Levenberg–Marquardt algorithm. The total number of vehicle kilometers (TVK)was defined to depict traffic efficiency of the road network. The change trend of travel demand is shown as a single peak with a single peak of density if in good traffic condition, and presents a bimodal with a single peak of density if there is traffic congestion. The former appears more than the later in most city, this demonstrated that only the density cannot describe the traffic state well for the inhomogeneity of density, and the inhomogeneity should be discussed in temporal and spatial aspect. Optimal traffic state (with optimal density and maximum TVK) can be obtained from traffic big data directly. Data of Qingdao in Chinese is applied to prove the method reasonable. This study provides a method estimating traffic state and constructing their formula of traffic relations from a network perspective, then evaluation system on different cities can be established. Given the optimal state obtained from big data, the further study is an implementation of effective measures to keep traffic state at an optimal level.

# References

1. Greenshields BD, Bibbins JR, Channing WS, Miller HH (1935) A study of traffic capacity. Highway Res Board 14:448–477
2. Greenberg H (1959) An analysis of traffic flow. Oper Res 7(1):79–85
3. Newell GF (1961) Nonlinear effects in the dynamics of car following. Oper Res 9(2):209–229
4. Underwood RT (1961) Speed, volume, and density relationship: quality and theory of traffic flow. Yale Bureau of Highway Traffic, pp 141–188
5. Wang H, Li H, Chen QY, Ni D (2011) Logistic modeling of the equilibrium speed-density relationship. Transp Res Part A 45(6):554–566; Wang H, Ni D, Chen QY, Li J (2013) Stochastic modelling of the equilibrium speed-density relationship. J Adv Transp 47(1):126–150
6. Godfrey JW (1969) The mechanism of a road network. Traffic Eng Control 11(7):323–327
7. Daganzo CF (2007) Urban gridlock: macroscopic modeling and mitigation approaches. Transp Res Part B 41(1):49–62
8. Geroliminis N, Daganzo CF (2008) Existence of urban-scale macroscopic fundamental diagrams: some experimental findings. Transp Res Part B 42(9):759–770
9. Helbing D (2009) Derivation of a fundamental diagram for urban traffic flow. Eur Phys J B 70(2):229–241
10. Mazloumian A, Geroliminis N, Helbing D (2010) The spatial variability of vehicle densities as determinant of urban network capacity. Philos Trans Royal Soc A: Math Phys Eng Sci 368(1928):4627–4647
11. Geroliminis N, Sun J (2011) Properties of a well-defined macroscopic fundamental diagram for urban traffic. Transp Res Part B 45(3):605–617
12. Wang H, Li H, Chen QY, Ni D (2011) Logistic modeling of the equilibrium speed-density relationship. Transp Res Part A 45(6):554–566
13. Knoop VL, Hoogendoorn SP (2013) Empirics of a generalized macroscopic fundamental diagram for urban freeways. Transp Res Rec: J Transp Res Board 2391:133–141
14. Qiang ZHU, Shaokang LI, Zhen XU (2016) Study of solving nonlinear least squares under large residual based on Levenberg-Marquardt algorithm. China Measur Test 42(3):12–16 (In Chinese)

# Analysis and Prediction of Passenger Flow of High-Speed Night Train

**Bo Li, Xiang-chun Qi, Qiao Li and Xiao Yang**

**Abstract**  High-speed night train is a new personalized product of high-speed railway to meet the market demand in China. Based on the existing operation conditions of high-speed night train, by recapitulating its relevant advantages and comparing with characteristics of high-speed day train, conventional train, and civil flight products, it comes to a conclusion that the high-speed night train has certain competitiveness and has well expanded the high-speed railway service portfolio. By analyzing the passenger flow characteristics of high-speed night train according to the ticketing data, it is found that the passenger flow characteristics of Beijing–Guangzhou and Shanghai–Shenzhen high-speed night trains are similar, both have relatively stable passenger flows, and also have a certain share in the passenger transportation market. Through analysis on passenger flow composition of high-speed night train, it is found that the high-speed night train is a supplement to high-speed day trains, and the passenger flow basically consists of transfer passengers. At last, based on calculation of passenger transfer inclination, neural network method, time series method, curve estimation method, and multiple regression method are used to, respectively, predict the passenger flow of high-speed night train during the "13th Five-Year Plan". The result can provide certain data support to the reasonable operation of high-speed night train under network conditions.

**Keywords**  Railway transportation · Passenger flow prediction · High-speed night train · Passenger flow characteristics

In view of such a huge transportation market in China, there are growing demands for personalized and tailored high-speed railway service products, for which the high-speed night train is a new service product responding to the market demands taking advantage of the prosperous development of high-speed railways in China. Normally, the high-speed night train departs from 17:00 to 24:00 of the day and arrives at 5:00–9:00 of the next day, with a total journey time of 5–16 h [1], which is generally considered as reasonable for the passengers. It integrates the travel time with the night

B. Li (✉) · X. Qi · Q. Li · X. Yang
China Academy of Railway Science, 100081 Beijing, China
e-mail: boli@rails.cn

rest time, allowing continuous activities in the daytime. The transportation demand of passenger flow and service characteristics are the effective supports to the actual operation of high-speed night train. Therefore, the prediction and analysis of night passenger flow are of important research value and practical significance.

# 1 Existing Operation Conditions of High-Speed Night Train in China

High-speed night trains in China started operation on January 1, 2015, and its operation has experienced three phases.

(1) Phase one: From January 1, 2015 to March 15, 2015, 8 pairs of high-speed night trains were put into service from Beijing West to Guangzhou South/Shenzhen, and Hongqiao of Shanghai to Guangzhou South/Shenzhen North, and operation ceased for one day every week.

(2) Phase two: From March 15, 2015 to May 20, 2016, 12 pairs of high-speed night trains were put into service from Beijing West to Guangzhou South/Zhuhai, and Hongqiao of Shanghai to Guangzhou South/Shenzhen North, and operation ceased for three days every week (Tuesday, Wednesday, and Thursday).

(3) Phase three: From May 20, 2016 till now, 10.5 pairs of high-speed night trains are in service from Beijing West to Guangzhou South/Shenzhen North/Zhuhai, and Hongqiao of Shanghai to Guangzhou South/Shenzhen North, and Beijing West to Guiyang North, and operation ceased for 3 days every week (Tuesday, Wednesday and Thursday).

Above description indicates that the high-speed night trains running along Beijing–Guangzhou high-speed railway and Shanghai–Shenzhen high-speed railway are very typical in China.

# 2 Analysis of Characteristics of High-Speed Night Train Service

High-speed night trains are competitive when compared with those transportation services such as high-speed day trains, conventional trains, and civil flights. The attributes of high-speed night train service are reflected in the following aspects:

(1) Departure at about 20:00 and arrive at about 7:00 in the next morning, is suitable and conforms to people's daily routine;

(2) Travel at night satisfies the travel demand without sacrificing passengers' rest, greatly increasing passengers' utilization efficiency of travel time;

(3) It operates stably, provides conformable travel experience, convenient dining, toilet manners, and free movement during the trip;

(4) Its ticket price is relatively higher than conventional train ticket, but is still lower than that of civil flight;
(5) It provides obviously higher punctuality than conventional trains and civil flights;
(6) Higher safety.

Above all, main advantages of high-speed night trains include safety, timeliness, appropriate ticket price, suitable departure and arrival time, high quality of transportation service, etc. With respect to conventional railway passenger transportation, high-speed night train is faster, greatly shortening the travel time of passengers. As comparing to high-speed daytime trains, high-speed night train could expand the service portfolio of high-speed railway and provides more options for passengers. Comparing with civil flights, it significantly increases the passengers' utilization ratio of time and reduces the limits to trips due to weather conditions.

## 3 Analysis of Passenger Flow Characteristics of High-Speed Night Train

### 3.1 Analysis of Passenger Flow Proportion of High-Speed Night Train

As per the ticketing data of high-speed railway of 2012–2015, the passenger flows from Beijing West to Guangzhou South and from Beijing West to Shenzhen North have been sorted and analyzed, as shown in Tables 1 and 2. From 2012 to 2014, the high-speed night train was unavailable. Traffic volumes are for high-speed day trains; the passenger flow of 2015 is divided into two categories: high-speed day train and high-speed night train.

It is known from Table 2 that the number of passengers transported by high-speed night train of Beijing–Guangzhou section in 2015 takes up 39.4% of the total high-speed railway passenger flow. The number of passengers transported by high-speed night train of Beijing–Shenzhen section takes up 59.8% of the total high-speed railway passenger flow. It can be seen from Fig. 1 that the high-speed night train and the high-speed day train are supplementary to each other and share the passenger transportation tasks of the channel. The night train has more advantage over the day train.

**Table 1** Passenger flow of Beijing West–Guangzhou South/Shenzhen North high-speed railway of 2012–2014

| Section | Year 2012 | | | Year 2013 | | | Year 2014 | | |
|---|---|---|---|---|---|---|---|---|---|
| | Up | Down | Total | Up | Down | Total | Up | Down | Total |
| Beijing–Guangzhou | 4.0 | 5.8 | 9.8 | 334.4 | 370.9 | 705.3 | 331.2 | 364.8 | 696.0 |
| Beijing–Shenzhen | 0.6 | 1.0 | 1.7 | 78.7 | 83.2 | 161.9 | 97.3 | 140.6 | 237.9 |

*Unit* 10,000 persons

**Table 2** Passenger flow of Beijing West-Guangzhou South/Shenzhen North high-speed railway of 2015

| Section | Total high-speed railway passenger flow | | | High-speed night train | | | High-speed day train | | |
|---|---|---|---|---|---|---|---|---|---|
| | Up | Down | Total | Up | Downnn | Totalal | Up | Downnn | Totalal |
| Beijing–Guangzhou | 50.5 | 52.8 | 103.3 | 18.9 | 21.7 | 40.7 | 31.6 | 31.1 | 62.7 |
| Beijing–Shenzhen | 24.5 | 27.4 | 51.9 | 14.8 | 16.2 | 31.0 | 9.6 | 11.2 | 20.8 |

*Unit* 1000 persons

| | Guangzhou-Beijing | Beijing-Guangzhou | Sum | Shenzhen-Beijing | Beijing-Shenzhen | Sum |
|---|---|---|---|---|---|---|
| ■ Day Train | 62.5% | 58.8% | 60.6% | 39.4% | 40.9% | 40.2% |
| □ Night Train | 37.5% | 41.2% | 39.4% | 60.6% | 59.1% | 59.8% |
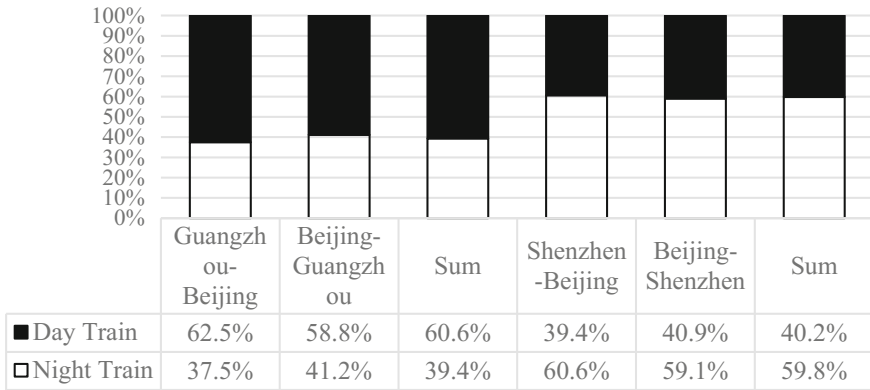
**Fig. 1** Proportional relation diagram of traffic volumes borne by high-speed night train and day train

**Fig. 2** Fluctuations of passenger flow at weekend
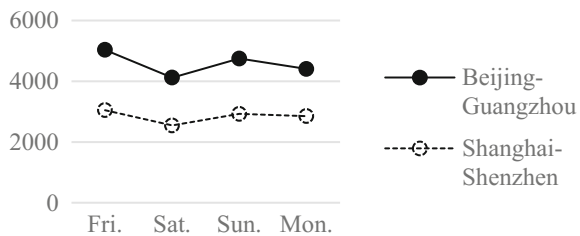


## 3.2 Analysis of Passenger Flow Fluctuation of High-Speed Night Train

The characteristics of passenger flow fluctuations (as shown in Fig. 2) of Beijing–Guangzhou and Shanghai–Shenzhen high-speed night trains are analyzed according to the ticketing data of Beijing–Guangzhou and Shanghai–Shenzhen high-speed railways in 2015.

(1) The fluctuation rule of passengers traveling at weekend nights is as shown in Fig. 2. As passenger flow of high-speed night train mainly consists of business, tour, and family visit flows, and the peak of business return and leisure travel occurs on Friday.

(2) Fluctuations of passenger flow on holidays. Fluctuations of passenger flow during national holidays are as shown in Fig. 3. Fluctuations of passenger flow during New Year holidays are as shown in Fig. 4 (high-speed night train was not in service on the day before the New Year's Day of 2015). By weighted averaging, the passenger flows during Tomb-Sweeping Day holidays, Dragon Boat Festival holidays, the holidays of Labors Day, and Mid-Autumn Festival holidays, the fluctuations of passenger flow during "three-day vacations"
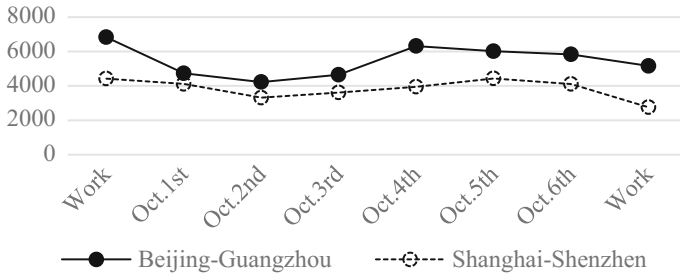
**Fig. 3** Fluctuations of passenger flow during national holidays



**Fig. 4** Fluctuations of passenger flow during New Year's Day holidays

**Fig. 5** Fluctuations of passenger flow during "Three-day Vacations"
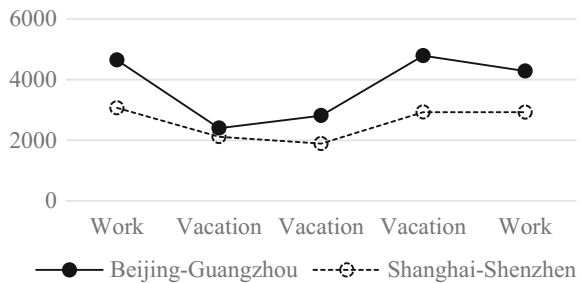


are shown in Fig. 5. The fluctuations of passenger flow during Spring Festival holidays are as shown in Fig. 6.

(3) The monthly fluctuations of passenger flow of Beijing–Guangzhou and Shanghai–Shenzhen night trains of 2015 are as shown in Fig. 7.

From the analysis above, it can be seen that the fluctuations of passenger flow of Beijing–Guangzhou and Shanghai–Shenzhen high-speed night trains have the following rules:

(1) The passenger flow of high-speed night train mainly consists of business, tour, and family visit flows;

(2) The passenger flows of Beijing–Guangzhou and Shanghai–Shenzhen high-speed night trains have certain fluctuation rules, and the fluctuation rules are similar;

**Fig. 6** Fluctuations of passenger flow during Spring Festival holidays



| | Jan | Feb | Mar | Apr | May | Jun | Jul | Aug | Sep | Oct | Nov | Dec |
|---|---|---|---|---|---|---|---|---|---|---|---|---|
| Beijing-Guangzhou | 4.4 | 8.2 | 8.2 | 11.9 | 15.1 | 13.1 | 16.6 | 18.1 | 15.0 | 12.5 | 11.2 | 10.2 |
| Shanghai-Shenzhen | 3.5 | 4.4 | 5.7 | 8.6 | 10.3 | 8.9 | 9.2 | 10.3 | 9.0 | 9.1 | 8.1 | 6.7 |
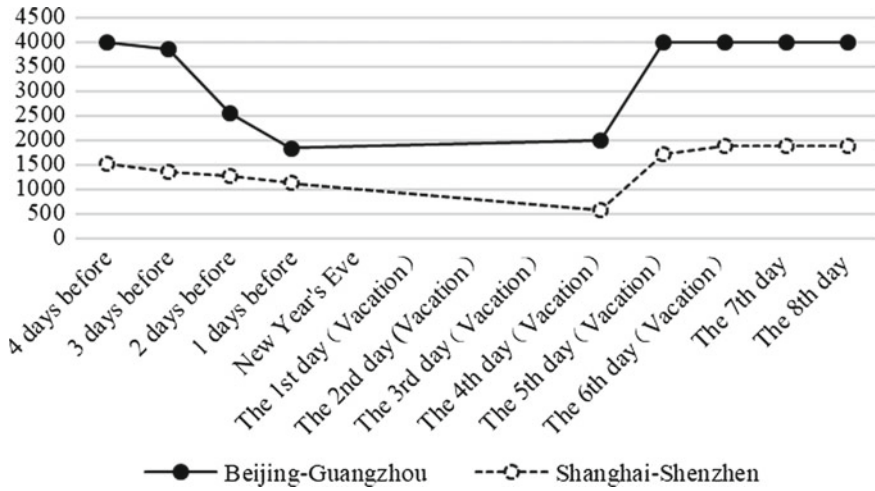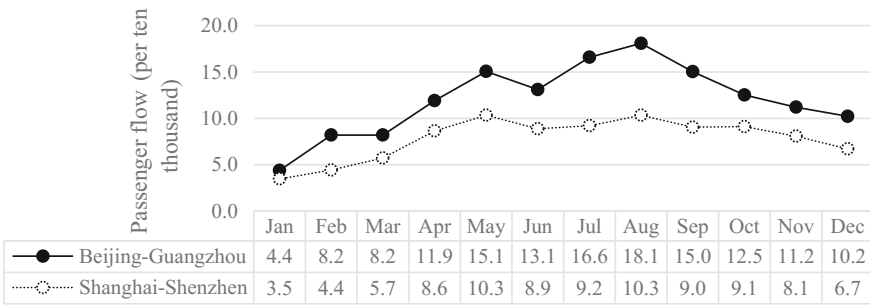
**Fig. 7** 2015 monthly fluctuations of passenger flow of Beijing–Guangzhou and Shanghai–Shenzhen high-speed night trains

(3) During weekend, "three-day vacations", and national holidays, passenger flow peaks basically emerge on the previous day and the last day of holiday;

(4) During Spring Festival holidays, night trains are not available from the New Year's Eve to the fourth day of the New Year, thus, the passenger flow fluctuations is represented as a "basin-shaped" change;

(5) In the whole year, the passenger flow peak is in August; it goes up stepwise before August and gradually reduces month by month after August.
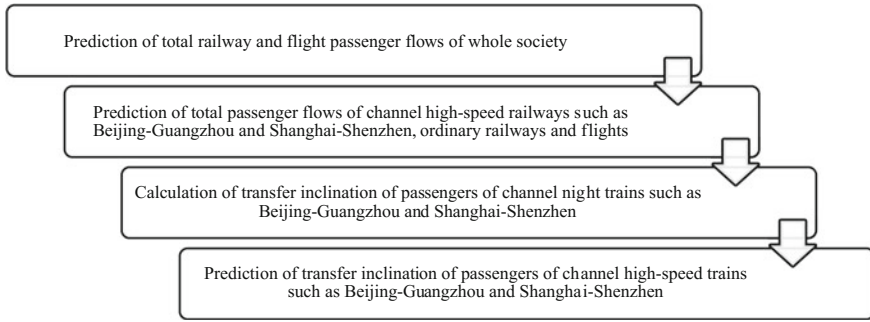
**Fig. 8** Prediction framework of high-speed railway passenger transportation demand

## 4 Prediction of Passenger Flow of High-Speed Night Train

The passenger flow of high-speed railway mainly comprises of three parts: tendency flow, transferred flow, and induced increase flow [2]. High-speed night train is defined as the supplementary service to high-speed day train. The passenger flow thereof basically consists of transfer flow. In addition, the statistics of passenger questionnaires show that the induced increase flow of high-speed night train is less than 1% of the volume. The high-speed night train was started in 2015, thus, the tendency passenger flow data is also insufficient because of the short operation period. Therefore, the prediction of passenger flow of high-speed night train only aims at the transfer passenger flow of high-speed trains and conventional trains of the whole line. The detailed prediction framework is as shown in Fig. 8.

(1) Prediction of Total Passenger Flow

In the seven prediction indicators, including GDP, population number, length of railways in service, quantity of railway passenger cars, household consumption expenditure, domestic airline transportation length, and quantity of civil transport airplanes, are respectively, used as the economic indicators that may affect the demands of railway passenger flow and flight passenger flow. The above-mentioned indicators during the "12th Five-Year Plan" obtained from statistics are as shown in Table 3.

To increase the accuracy and precision of prediction, four methods including neural network, time series, curve estimation, and multiple regress are used in combination with multi-angle qualitative analysis to, respectively, predict and figure out the total demand of nationwide railway and flight passenger transportation during the "13th Five-Year Plan"; the results of the prediction are as shown in Table 4.

(2) Prediction of Passenger Flow of High-speed Railway, Conventional Railway, and Flight of the Channel

Based on the prediction of annual flight and railway passenger flow, the passenger flow of each channel is calculated, respectively, according to its average share ratio from 2012 to 2015, so as to obtain the flight passenger flow, the high-speed railway

**Table 3** Summary of indicators required for prediction of passenger flow during the "12th Five-Year Plan"

| Year | 2011 | 2012 | 2013 | 2014 | 2015 |
|------|------|------|------|------|------|
| GDP (RMB 100 billion) | 484.1 | 534.1 | 588.0 | 635.9 | 676.7 |
| Permanent resident population (10,000 persons) | 134,735 | 135,404 | 136,072 | 136,782 | 137,462 |
| Average household consumption (RMB) | 13,133.6 | 14,698.9 | 16,190.2 | 17,806.4 | 19,308.0 |
| Length of railways in service (10,000 km) | 9.3 | 9.8 | 10.3 | 11.2 | 12.1 |
| Quantity of railway passenger cars (100 Nr.) | 528.4 | 557.6 | 568.4 | 589.0 | 650.0 |
| Domestic airline transportation length (10,000 km) | 199.6 | 199.5 | 260.3 | 287.0 | 292.3 |
| Quantity of civil transport airplanes (100 Nr.) | 17.6 | 19.4 | 21.5 | 23.7 | 26.5 |

**Table 4** Prediction results of flight and railway passenger transportation amount during the "13th Five-Year Plan"

| Year | Flight | | | | Railway | | | |
|------|--------|--|--|--|---------|--|--|--|
| | Neural network | Time series | Curve estimation | Multiple regression | Neural network | Time series | Curve estimation | Multiple regression |
| 2016 | 42,036.68 | 43,882.74 | 47,611.06 | 43,351.65 | 266,721.6 | 268,839.45 | 270,887.70 | 260,676.50 |
| 2017 | 43,099.31 | 47,019.14 | 51,988.47 | 47,372.95 | 275,723.2 | 286,021.89 | 292,594.90 | 277,975.50 |
| 2018 | 43,879.96 | 51,253.68 | 56,579.93 | 51,758.68 | 280,148.00 | 303,204.34 | 315,594.00 | 296,419.40 |
| 2019 | 44,388.94 | 54,151.37 | 61,385.44 | 56,431.25 | 282,171.90 | 320,386.78 | 339,885.00 | 315,595.50 |
| 2020 | 44,763.59 | 59,570.90 | 66,404.99 | 61,602.94 | 283,022.00 | 337,569.23 | 365,467.90 | 336,349.70 |

*Unit* 10,000 persons

passenger flow and the conventional railway passenger flow of each channel during the "13th Five-Year Plan".

(3) Calculation of Passenger Transfer Inclination

To precisely calculate the transfer intention of passengers to high-speed night train, many questionnaires and surveys are made in long-distance passengers in Harbin, Chengdu, Guangzhou, etc. The transfer rates of flight, high-speed railway and conventional railway passengers are obtained through statistics and analysis, and the results are as shown in Table 5.

(4) Prediction of Passenger Flow of High-speed Night Train

The predicted passenger flow of high-speed night train by channel can be obtained in combination with the results above. Different prediction methods may give different results, the fluctuation range of passenger flow prediction is given herein, and

**Table 5** Results of passenger transfer inclination survey

|  | Transfer rate of conventional railway passengers (%) | Transfer rate of high-speed railway passengers (%) | Transfer rate of flight passengers (%) |
|---|---|---|---|
| Transfer rate | 24.47 | 23.26 | 25.61 |

**Table 6** Results of passenger flow predictions of high-speed night trains of Beijing–Guangzhou and Shanghai–Shenzhen channels

| Year<br>Channel | 2016 | 2017 | 2018 | 2019 | 2020 |
|---|---|---|---|---|---|
| Beijing–Guangzhou | 4794.8–5236.3 | 4930.1–5697.8 | 5015.9–6183.3 | 5066.4–6692.8 | 5099.6–7226.3 |
| Shanghai–Shenzhen | 4532.5–5034.9 | 4654.2–5487.7 | 4736.7–5963.4 | 4787.8–6461.9 | 4823.3–6983.3 |

*Unit* 10,000 persons

detailed calculation results are as show in Table 6 (which shows only prediction results of some channels).

# 5 Conclusion

By analyzing the passenger flow changes in high-speed night trains of Beijing–Guangzhou line and Shanghai–Shenzhen line of 2015, characteristics of high-speed night train are summarized herein; and the passenger flows of high-speed night trains represented by Beijing–Guangzhou and Shanghai–Shenzhen channels during the "13th Five-Year Plan" are predicted with models, i.e., neural network.

The main research conclusion is as follows:

(1) The weekly passenger flow fluctuation rules of Beijing–Guangzhou railway and Shanghai–Shenzhen railway are similar.
(2) High-speed night train can expand the service portfolio of high-speed railway passenger transportation. Compared with civil flights, it increases effective time for passengers and mitigates their traveling fatigue. High-speed night train is more competitive than the other two kinds of transportation.
(3) In view of the advantages of high-speed night train and the results of ticketing data analysis, high-speed night train will attract some passengers from high-speed day train and conventional train. The transport market prospect is optimistic.
(4) In the seven prediction indicators, i.e., GDP, population number, length of railways in service, quantity of railway passenger cars, household consumption expenditure, domestic airline transportation length, and quantity of civil transport airplanes, are, respectively, used as the economic indicators that may affect the demands of railway passenger flow and flight passenger flow. Methods such as neural network method, time series method, curve estimation method, and

multiple regression method are used to predict the passenger flow of high-speed night train. The result of prediction can provide support to the reasonable operation of high-speed night train under network conditions.

# References

1. Wang C (2014) Schematic study on operation of night train on Beijing-Guangzhou High-speed Railway, Beijing Jiaotong University
2. Wang W (2016) Prediction and study of railway passenger flow under influence of high-speed railway. Railway Transp Econ 38(4):42–46
3. Aimin Wang (1995) Study on application of neural network to fuzzy comprehensive evaluation. Syst Eng Theor Pract 15(10):37–42

# Research on the Energy-Dissipating Properties of SMA Wires Used in Smart Automotive Safety Systems

**Xin Chen, Yi Liu, Chuanliang Shen, Zhipeng Wu, Xiaoyu Ma, Shengtong Qiu and Tairong Sun**

**Abstract** The energy dissipation properties of martensite NiTi SMA wires under two different loads, including a quasi-static tensile load and an impact load, are studied through our newly designed testing plants. Meanwhile, by changing the temperature of the SMA wires, the controllability of energy dissipation of the SMA wires is discussed in detail. The results indicate that martensite NiTi SMA wires show excellent energy dissipation capabilities under the loads. It is also found that the energy dissipation properties of the SMA wires can be improved by changing their temperature. The energy dissipation properties of martensite NiTi SMA wires demonstrate that NiTi SMAs have the possibility to be applied in smart automotive safety systems.

**Keywords** NiTi SMA wires · Static test · Impact test · Energy dissipation Temperature load

## 1 Introduction

Intelligent materials and structures refer to a new type of materials and structures that combine actuators, sensors and microprocessor control systems with parent materials [1]. In addition to the carrying capacity of the common materials, they can perceive and deal with internal and external information (such as stress, strain, heat, electromagnetic radiation, etc.) [1]. Shape memory alloy(SMA) is one of the most typical intelligent materials, which has been widely used in mechanical, medical, construction, and aerospace fields due to its excellent ductility, fatigue properties, corrosion resistance, and biocompatibility [2]. At present, with the development of wire-driven technology, a large number of shape memory alloy actuators have been

X. Chen · Y. Liu · C. Shen (✉) · Z. Wu · X. Ma · S. Qiu · T. Sun
State Key Laboratory of Automotive Simulation and Control, Jilin University,
Changchun 130025, China
e-mail: shencl@jlu.edu.cn

applied to the automotive domain to replace the traditional electromagnetic motors [3–5].

NiTi alloys have become one of the most widely researched and applied SMAs due to their excellent shape memory effect and superelastic effect [6], which are closely related to the martensitic transformation(the reverse transformation). In addition, NiTi SMA wires also demonstrate many other excellent mechanical properties, such as high damping characteristics, high ductility, variable stiffness, excellent fatigue properties and anti-corrosion [7, 8].

In fact, NiTi SMA's high energy dissipation and impact resistance properties can be exploited to design automotive energy dissipating and protection devices [9–11], which can effectively improve the vehicle safety and pedestrian protection effect. When the SMA wires are in the martensite phase, which has a lower stiffness, they can help protect pedestrians. And when the SMA wires are in the austenite phase, which has a higher stiffness, they can help protect the vehicle. Furthermore, in the case of low-speed collision, the SMA wires can be restored to its original shape by heating. Therefore, the intelligent control of the SMA-based energy dissipating devices can be realized through SMA's temperature sensitivity and resistance properties.

In this paper, the energy dissipation properties of martensite NiTi SMA wires under two different loads are studied through experiments in detail. The loads include a quasi-static tensile load and an impact load. In addition, the temperature of the SMA wires is controlled by a DC regulated power supply, and then the controllability of energy dissipation of the SMA wires is discussed in detail.

## 2 Testing Methodology

### 2.1 Materials

Equi-atomic-ratio martensite NiTi SMA wires with 0.5 mm diameter were used during the experiments. The phase transformation temperatures of martensite NiTi wires were tested through DSC (Differential Scanning Calorimeter) experiments with $A_s = 35$ °C and $A_f = 62$ °C.

### 2.2 Testing Plants

#### 2.2.1 Static Testing Plant

In order to test the energy dissipation properties of martensite NiTi SMA wires under static tensile load and different temperatures, a static tensile machine, a DC regulated power supply, and a temperature measuring instrument are employed in this paper as shown in Fig. 1.

## 2.2.2 Impact Testing Plant

As is shown in Fig. 2, a drop impact testing plant is built for the impact experiments. And Fig. 3 demonstrates the impact testing process.

During the experiments, the dropping weight falls from its initial position. When it collides with the supporting plate, an impact load is applied to the tested wire through the guide bar. The force and displacement of the tested wire are recorded by the force sensor and displacement sensor respectively. The tested wire is heated in the form of electricity supplied by the DC regulated power supply. The temperature measuring instrument is used to measure the temperature of the tested wire in real time.

**Fig. 1** Static testing plant
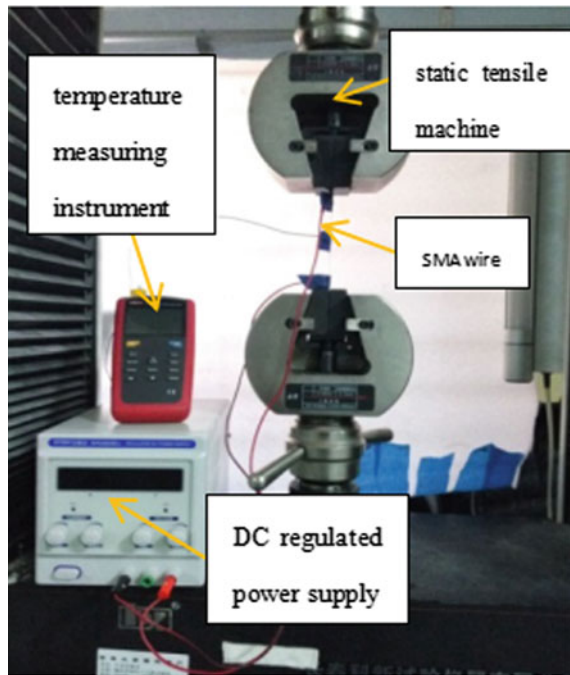
**Fig. 2** Impact testing plant
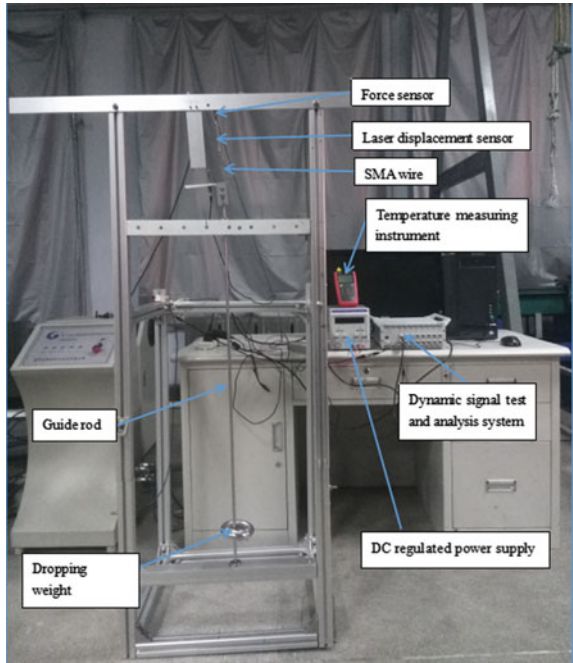


**Fig. 3** Impact testing process
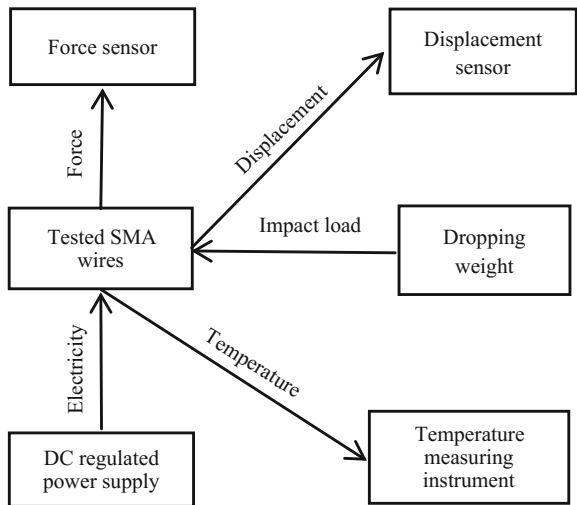
# 3    Results and Discussion

## 3.1    *Energy Dissipation Properties of NiTi SMA Wire Under Quasi-static Tensile Load*

In this section, the tensile speed is set to 1 mm/min. Stress–strain curves of the SMA wires are firstly obtained according to the force and displacement value measured by the sensors. The area of the stress–strain curves under different strain amplitudes can be obtained by integrating, which is equal to the energy absorption density, $W_d$, of the SMA wires. The energy absorption density under different strain amplitudes is shown in Table 1. Figure 4 presents the relationship between the energy absorption density and strain amplitude of the SMA wires, from which we can see that the relationship between the energy absorption density and strain amplitude is approximately linear. The energy absorption density increases from 1.7 to 9.4 MJ/m$^3$, which is a 452.9% raise, when the strain amplitude increases from 2 to 8%. Therefore, strain amplitude has an important effect on the energy absorption density of martensite NiTi SMA wire.

Similarly, the energy absorption density of the SMA wires at different temperatures can be obtained by integrating the stress–strain curves. From Table 2 and Fig. 5 show the relationship between the energy absorption density and the temperature

**Table 1**   Energy absorption density under different strain amplitudes

| Strain amplitude | 2% | 3% | 4% | 5% | 6% | 7% | 8% |
|---|---|---|---|---|---|---|---|
| $W_d$ (MJ/m$^3$) | 1.7 | 3.4 | 4.2 | 5.4 | 6.6 | 8.5 | 9.4 |

**Fig. 4**   Effect of strain amplitude on energy absorption density
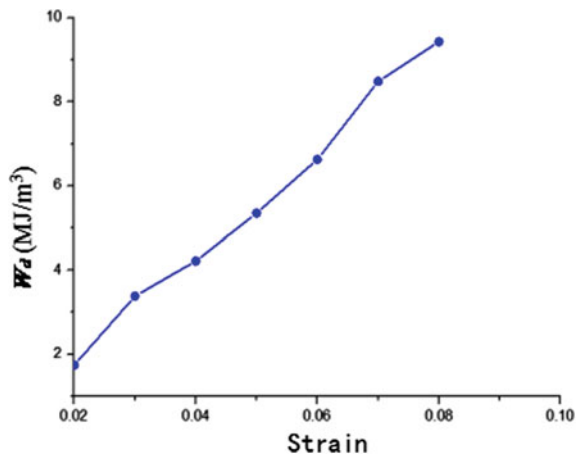
**Table 2** Energy absorption density at different temperatures

| Temperature (°C) | 20 | 50 | 80 |
|---|---|---|---|
| $W_d$ (MJ/m$^3$) | 7.63 | 10.39 | 12.93 |

**Fig. 5** Effect of temperature on energy absorption density
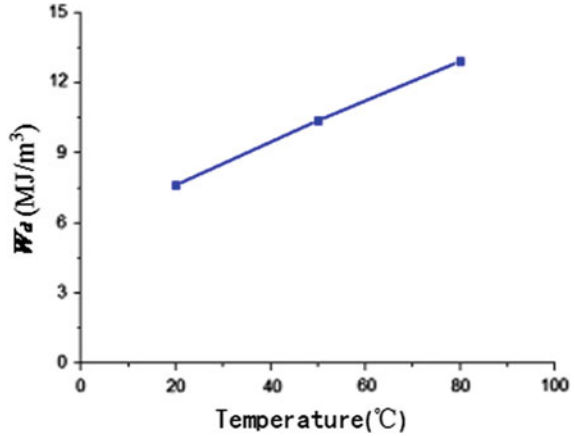


of the SMA wires, we can clearly see that the energy absorption density increases significantly as the temperature of the SMA wires increases from 20 to 80 °C.

## 3.2 Energy Dissipation Properties of NiTi SMA Wire Under Impact Load

The impact experiment of NiTi SMA wire is carried out by using the above impact testing device. The dropping weight is 0.25, 0.5, and 0.75 kg, respectively.

The energy absorption density is obtained by integrating the stress-strain curve, as is shown in Fig. 6, which presents the trend of energy absorption density changing with the increase of the impact load. It is apparent that the mass of the dropping weight has an important effect on the energy dissipation properties of SMA wire. When the mass is 0.25, 0.5, and 0.75 kg respectively, the corresponding energy absorption density is 5.6, 66.5, and 103.8 MJ/m$^3$.

From Fig. 7 we can see the intuitive influence of temperature on the energy absorption density of the SMA wires. The energy absorption density increases from 23.8 to 53.7 MJ/m$^3$ as the temperature increases from 35 to 65 °C. The experimental results show that temperature can effectively change the mechanical properties of SMA wire, especially the energy dissipation properties.

**Fig. 6** Effect of impact load on energy absorption density
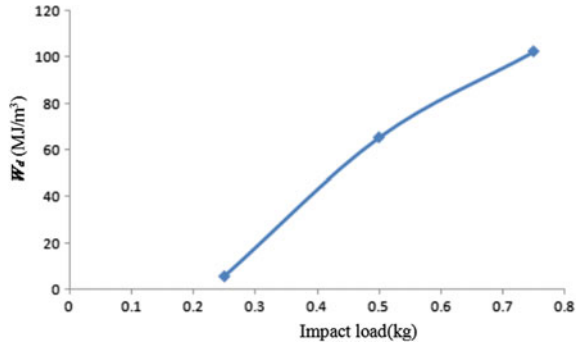


**Fig. 7** Effect of temperature on energy absorption density
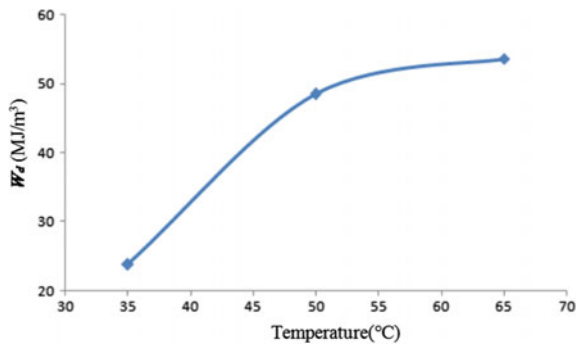


## 4 Conclusion

This paper studies the energy dissipation properties of martensite NiTi SMA wires under two different loads and their controllability of energy dissipation in a specific temperature range at length. The experimental results show that:

(1) When a quasi-static tensile load is applied to the NiTi SMA wires, their capabilities to absorb energy are apparently affected by their strain amplitudes and temperature. The energy absorption density increases from 1.7 to 9.4 MJ/m$^3$, which is a 452.9% raise, when the strain amplitude increases from 2 to 8%. As for the effect of temperature, the energy absorption density increases linearly with the increase of temperature.

(2) When the NiTi SMA wires are impacted by a dropping weight, the energy absorbed by the NiTi SMA wires increases as the mass of the dropping weight increases. When the mass increases from 0.25 to 0.75 kg, the corresponding energy absorption density increases about 18 times. Besides, the temperature is another important factor that affects the energy dissipation capabilities of the SMA wires. The energy absorption density increases from 24.2 to 54.4 MJ/m$^3$ as the temperature increases from 35 to 65 °C.

From the results, we can conclude that NiTi SMA wires can be exploited to design automotive energy dissipating and protection devices, and the devices' protection effect can be changed to adapt to different vehicle speeds by adjusting the wires' temperature.

# References

1. Xinmin Zhang (2013) The research process of smart materials. FRP/CM Z2:57–63
2. Pengfei Xue, Fei Zhang, Yan Li, Deyuan Zhang (2015) Progress in Ti-based shape memory alloys. Chin J Rare Metals 01:84–90
3. Butera F, Coda A, Vergani G (2007) Shape memory actuators for automotive applications. In: Nanotec IT newsletter. AIRI/nanotec IT, Roma, pp 12–6
4. Stoeckel D (1990) Shape memory actuators for automotive applications. Mater Des 11:302–307
5. Butera F (2008) Shape memory actuators for automotive applications. Adv Mater Processes 166:37
6. Jani JM, Leary M, Subic A, Gibson MA (2014) A review of shape memory alloy research, applications and opportunities. Mat Des 56:1078–1113
7. Jani JM, Leary M, Subic A et al (2014) A review of shape memory alloy research, applications and opportunities. Mater Des 56(4):1078–1113
8. Janke L, Czaderski C, Motavalli M et al (2005) Applications of shape memory alloys in civil engineering structures—overview, limits and new ideas. Mater Struct 38(5):578–592
9. Strittmatter J, Gümpel P, Zhigang H (2009) Long-time stability of shape memory actuators for pedestrian safety system. J Achiev Mater Manuf Eng 34:23–30
10. Gheorghita V, Gümpel P, Chiru A et al (2014) Future applications of Ni-Ti alloys in automotive safety systems. Int J Automot Technol 15(3):469–474
11. Strittmatter J, Clipa V, Gheorghita V et al (2014) Characterization of NiTi shape memory damping elements designed for automotive safety systems. Mater Eng Perform 23(7):2696–2703

# Research on Visual and Physiological Characteristics of Drivers Under Stress Scene


Check for updates

**Xian-sheng Li, Da-wei Xing, Yuan-yuan Ren, Fan-song Meng, Xue-lian Zheng and Jia-hui Yan**

**Abstract**  To research the visual and physiological characteristics of drivers under stress scene, the visual and physiological data of drivers under different stress scenarios were analyzed. By using the method of dynamic clustering, Pearson test, and mathematical analysis, the visual and physiological characteristics of the driver in the stress situation were studied. In the meanwhile, the characteristics of the driver's HRV were analyzed in time domain and frequency domain, which were selected as the analysis index. It shows that: the driver's visual distribution is more concentrated under the stress scene and drivers are more accustomed to obtain traffic information from near the front of the region which they regard as the main area, when objects in the scene moving, the driver will judge the moving range of the object to selected 1–2 related auxiliary area for information retrieval. The driver used to gaze the main area and scan the auxiliary area. In terms of the rate of increase in heart rate, different stress scenarios will have a significant impact on the driver's heart rate growth rate. In the HRV time domain characteristics, the driver to the two objectives of pedestrians and bicycles has a longer degree of tension, and the weather, the vehicle, the degree of tension of is intermittent. In the frequency domain characteristics of HRV, the driver's mental workload has increased when he encounters pedestrians and bicycles, the driver's mental workload has reduced when he encounters motor vehicles and external weather conditions.

X. Li · D. Xing · Y. Ren (✉) · F. Meng · X. Zheng
School of Transportation, Jilin University, Changchun 130022, China
e-mail: renyy@jlu.edu.cn

D. Xing
Jilin Provincial Expressway Administration, Changchun 130022, China

J. Yan
Mitsubishi Electric (China) Co., Ltd. Shanghai Branch, Shanghai 200336, China

585

# 1   Introduction

With the rapid increase of the number of cars in the world, the traffic safety problem becomes more and more serious, so traffic stress scene has become a hot point in the field of traffic safety. Many experts and scholars have carried out extensive and in-depth research on it, and have achieved fruitful research results in traffic index identification and safety evaluation [1–3]. However, the theory of road traffic design, which has been widely recognized for many years, has pointed out that the design of future road is based on the traffic demand and physiological response of road users [4]. Vedagiri et al. established the evaluation system of the severity of pedestrian and pedestrian stress scenarios on the crosswalk [5]. Noble et al. studied the effects of vehicle adaptive stop display system on driving behavior and safety in emergency situations [6]. It shows that, regardless of whether the driver is cautious or risky, the adaptive stop display system has a good protective effect on the driver's safety in emergency situations. Brookhuis et al. used electrocardiogram to study the driver's psychological pressure on the congested urban expressway and the highway without traffic barrier. It shows that women are more likely to have too much stress than men and are more likely to have an accident in an emergency [7]. Through the above studies, we found that there are fewer researches on the influence of stress scenes on the visual and physiological characteristics of drivers. Therefore, this paper intends to set up different types of traffic stress scenarios in the test scenario by driving simulator test. During the course of the experiment, the visual and physiological data of the driver were collected and collated. Through the analysis of test data, the effects of different stress scenarios on the visual and physiological characteristics of the driver have been determined. Furthermore, it provides some theoretical reference for the research and design of intelligent transportation, intelligent vehicle, and auxiliary driving equipment.

# 2   Test Scheme and Scene Partition

## 2.1   Test Objective

The test was designed to test the data of eye movement, visual, and physiological indexes under different stress scenarios in the driving process of the virtual environment of 8 degrees of freedom. The changes of eye movement and physiological data of the driver in response to the stress scenarios were analyzed, and the influence of stress scenes on driver's visual and physiological characteristics was studied.

## 2.2 Test Scheme

The driver selected for the study includes both professional and nonprofessional drivers, and 4 different stress scenarios were encountered for each driver driving a total of two laps. The average time for each driver was 25 min. Ergo LAB man—machine environment synchronization platform was used to collect the changes of EMG, EDA, and ECG parameters of drivers in real time; Collect the data of the driver in real time, and make statistical analysis. In the duration of the experiment, two cars following researchers were responsible for observing the driver's eye movement data and timely to improve the abnormal data and emergency situations.

## 2.3 Division of Stress Scene

According to the participants in different stress scenarios, stress scene is usually divided into 4 following types: motor vehicle—motor vehicle stress scene, motor vehicle—non-motor vehicle stress scene, vehicle—pedestrian stress scene, motor vehicles—environment stress scene. The specific situation of each scene was refined, and the following 4 kinds of stress scenes were set up in this experiment:

(1) Scene 1 (Vehicle approaching scene): This scene is a motor vehicle—motor vehicle stress scene, that is, in the course of the vehicle, there are other vehicles approaching the driver's vehicle from the left. (2) Scene 2 (There is a non motor vehicle in front of the scene): This scene is a motor vehicle–non-motor vehicle stress scene, that is, in front of a non-motor vehicle from the right side of the vehicle moved to the driver in front of the driver's normal driving. (3) Scene 3 (Pedestrian crossing scene): This scene belongs to the vehicle–pedestrian stress scene, that is, when the driver is about to cross the crosswalk, pedestrians suddenly cross from the front of obstacle. (4) Scene 4 (Weather change scene): This scene belongs to the vehicle–environment stress scene, that is, when the driver drives out of the tunnel, the weather is changing rapidly, it encountered a rainy day.

## 3 Test Data and Analysis Methods

## 3.1 Driver's EMG Signal Processing Method

In addition to the general biomedical signal with weak signal, strong noise, strong randomness, and other characteristics, but it also has some of its own characteristics: (1) it is easy to be affected by the equipment and its drift is more serious than the normal physiological signal; (2) the band is very low, transcutaneous electrical signals extracted by the surface of the body belongs to the ultra-low-frequency signal, its spectrum distribution in the range of 0.08–0.2 Hz, the periodic disturbance is not
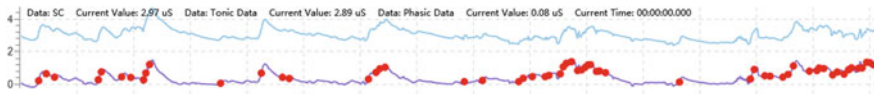
**Fig. 1** Raw data and gradually-changed signals
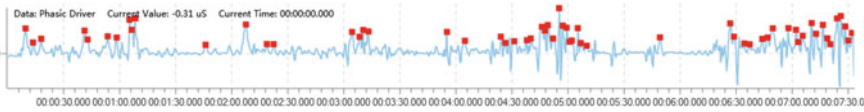


**Fig. 2** Phasic driver with SCR onset

obvious, vulnerable to shock response, and difficult to separate the useful information. When the traditional noise reduction method is used to deal with the transient signal with short time and low energy, the signal to noise ratio is not improved greatly, and the trigger point of the signal is blurred, The locations of these trigger points contain important information on the physiological research of drivers, and represent the corresponding changes of psychological activities. In this paper, the method of continuous deconvolution was used to decompose the three kinds of data, such as the gradual signal, the excitation signal, and the trigger point of the galvanic skin response. As shown in Figs. 1 and 2.

## 3.2 Analysis Method of Psychological Characteristic Index

### 3.2.1 Heart Rate Index Analysis Method

ECG is a random signal, even in the same environment, different individuals also have differences in physical conditions, which will result in different driving heart rate. Therefore, it is difficult to compare the value of heart rate to reflect the stress of the driver, so the heart rate is used to explore the psychological characteristics of the driver. The rate of heart rate increase is that the driver's heart rate increment is the difference between the heart rate of the driver and the state of calm, and the percentage of heart rate in calm state.

### 3.2.2 Heart Rate Variability Analysis

It refers to the difference of heart rate, which is one of the subtle changes in time and its regularity. The measurement of heart rate variability index is based on R–R interval measurement. The method can be divided into time domain method and frequency domain method.

Time Domain Characteristics of HRV

The sympathetic nerve and vagus nerve can be coordinated to maintain normal cardiac and normal heart rate changes. The imbalance of coordination between the two can lead to dysfunction of cardiovascular system, which can lead to severe arrhythmia. Therefore, the time domain characteristics of driver HRV can be used as an important index to reflect the autonomic nervous function and the regulation of cardiovascular function, and to reflect whether the heart activity is normal or not [8].

Drivers commonly used HRV time domain indicators are SDNN, RMSSD, SDNN index, and PNN50 (%), can be solved using the following formula [9, 10]:

(1) SDNN, Normal R–R interval index difference, and unit is ms.

$$SDNN = \sqrt{\frac{1}{N} \sum_{i=1}^{N} \left(RR_i - \overline{RR}\right)^2} \tag{1}$$

In the formula, $N$ is the total number of normal heartbeats; the first $I$ interval of RR; the mean value of the interval between $N$ beats. The greater the standard deviation, the higher the HRV, and vice versa. The normal value is more than "100 ms", if less than "50 ms" it is abnormal, which means that HRV obviously decreases.

(2) RMSSD, the mean square of the difference between the two adjacent R–R intervals, and unit is ms.

$$RMSSD = \sqrt{\frac{1}{N-1} \sum_{i=1}^{N-1} (RR_{i+1} - RR_i)^2} \tag{2}$$

$N$ is the total number of normal heartbeats and is the length of the adjacent two sinus cardiac cycles. RMSSD was used to estimate the composition of short distance HRV, the normal value was $27 \pm 12$.

(3) SDANN index: Mean value of the standard deviation of each minute interval in the whole record, and unit is ms.

$$SDANN\ index = \frac{\sum_{i=1}^{N} SD_i}{N} \tag{3}$$

Among them, $SD_i$ is the standard deviation of RR interval, which is calculated by first 5 min. Describe the size of the heart rate variability within 5 min to characterize the slowly changing components of HRV. SDNN index (SDNN index), is the standard deviation of each 5 min NN interval in the 24 h record, its normal value is 81 + 24 ms.

(4) PNN50, is the ratio of the R–R interval between the adjacent R–R interval was greater than 50 ms and the ratio of all the R–R intervals, and unit is %.

$$PNN50 = NN50/Total\,NN \times 100\% \tag{4}$$

In the formula, $N$ is the specified time the total number of hops; NN50 refers to the number of R–R intervals in which the difference between the adjacent R–R intervals is greater than 50 ms; Total NN is the number of all the R–R intervals. NN50 reflects the abrupt change of RR interval, which is more sensitive to vagus nerve activity, the normal demarcation point is 75%.

(5) Percentage of standard value: It refers to the difference between the standard value and the actual value and the standard value, which can be used to represent the close to the standard value, the smaller the percentage of the actual value and the standard value of the closer.

Frequency Domain Characteristics of HRV

Frequency domain analysis of driver HRV is power spectrum analysis, which is based on a certain period of time. It provides the basic information about the distribution of energy with frequency. Results show the power spectrum of human heart rate variability is generally 0–0.5 Hz.

The current study shows that there is a certain correlation between the 3 frequency bands of HRV, which is extremely low frequency, low frequency (low frequency, LF) and high frequency in the frequency domain analysis. The LF value of the individual's HRV index can well reflect the individual workload, and the LF decreases with the increase of individual workload. Therefore, in the follow-up analysis, LF was used to characterize the HRV under driver stress.

## 4   Analysis Index Selection

### 4.1   Driver Visual Index Selection

SPSS software is used to standardize the data in the original matrix, and then the principal components of the matrix are analyzed. Analysis the principal components of the root, contribution rate and cumulative contribution rate, as shown in Table 1.

The results of Table 1 show that the cumulative contribution of the first three principal components is up to a factor of 90.919%, which means that the first three principal components cover about 90.919% of all the information, and thus the first three principal components. That is, the duration of gaze reflects the time of extracting the target information, which represents the difficulty of extracting information; The percentage of fixation points can be used to get the target and the area of interest of the driver, which is helpful to study the driver's intention; The percentage of saccadic time can be used to obtain information about the area in which the driver is more accustomed to saccadic eye movements. Therefore, the above three indexes were

**Table 1**  Result of principal component analysis

| Principal component | Eigenvalue | Variance contribution | Accumulating contribution rate |
|---|---|---|---|
| Fixation duration | 1.918 | 31.963 | 31.963 |
| Percentage of fixation point | 1.369 | 22.814 | 54.778 |
| Percentage of glance time | 1.085 | 36.141 | 90.919 |
| Percentage of visits | 0.752 | 4.387 | 95.306 |
| Visit time | 0.511 | 2.076 | 97.382 |
| Sweep percentage | 0.365 | 2.618 | 100.000 |

selected to analyze the influence of the driver's visual characteristics under the stress scenario.

## 4.2  Selection of Drivers' Physiological Indexes

The study found that the main factors that can reflect the degree of stress and mood changes are heart rate, skin potential, EMG, and EEG. In the above indicators, EEG and transcutaneous electrical power can be used to characterize the nervous system, but the EEG is very complex and difficult to extract.

Heart rate index shows that the situation of heart and emotional stress As an important physiological index of blood circulation, heart rate is widely used in sports. HRV refers to the change of heart rate speed difference, it is the analysis of the continuous changes mainly reflecting the instantaneous heart rate.

## 5  Analysis the Influence of Stress Scene on Driver's Visual Characteristics

## 5.1  Division of Drivers' Gaze Area

### 5.1.1  Selection of Region Division Method

The division of the driver's gaze area is the premise and basis for the study of the driver's attention allocation and gaze transfer model. Reasonable and effective division of the driver's eye area can be used to refine the driver's attention area, and it is also helpful to improve the accuracy of eye movement analysis. At present, there are three main research methods in the area of driver's attention, the main advantages and disadvantages of them are shown in Table 2.

**Table 2** Traditional research methods in the area of fixation

| Method | Advantages | Disadvantages |
|---|---|---|
| Subjective division method | Simple, small workload | Strong subjectivity, low precision |
| Mechanical partition method | Covers a comprehensive, high accuracy | Stiff boundary and poor credibility |
| Video playback method | Small error, eliminate individual difference | Heavy workload, easy to miss |
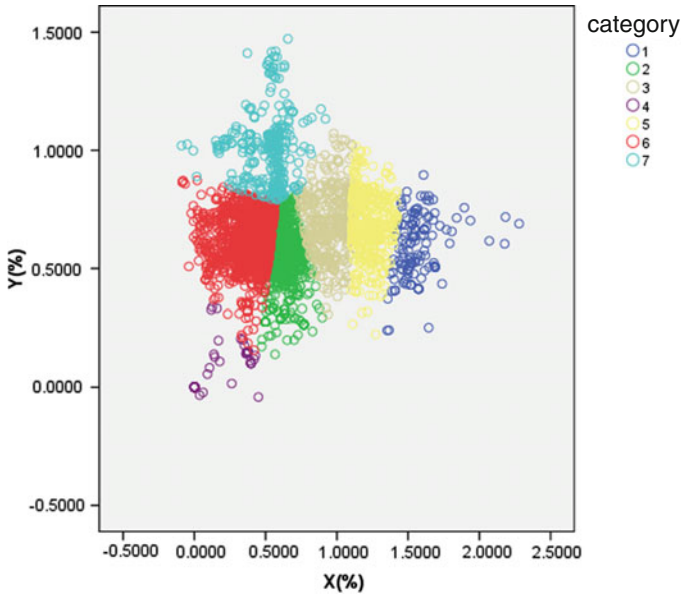


**Fig. 3** The fastclus results of driver's fixation point position

## 5.1.2 Clustering of Gaze Point Location

The driver's fixation point is taken as the clustering variable in the view plane, and the position of the fixation point is clustered. Using SPSS software K-mean clustering function to complete the dynamic clustering process, In the process of clustering, the number of classes is divided into 6 categories, 7 categories, 8 categories, 9 categories and 10 categories, and the comparison of the results is that the clustering results are divided into the following 7 categories. After each driver's point of view is divided into 7 categories, the figure is almost the same, and the law of the boundary is similar, and Fig. 3 shows the clustering results.

**Fig. 4** Driver's gaze region correspondence

### 5.1.3 The Results of Clustering and the Corresponding Region and Target

As it can be seen from Fig. 4, the driver's point of view is divided into 7 distinct areas after clustering, divided into the area of the District 1, District 2, District 3, District 4, District 5, District 6, and District 7. These 7 areas are the drivers' fixation area, and the target of the 7 regions can be determined by the playback of the video recording with the fixation point. The corresponding relationship between the clustering results and fixation region are shown in Table 3 and Fig. 3.

## 5.2 Analysis of Driver's Visual Characteristics in Scene 1

### 5.2.1 Analysis on the Characteristics of Driver's Fixation Duration

As it can be seen from Table 3, most of the time in which the driver has been set up in the test is used to keep an eye on the AOI 2 and the AOI 4 region, which are the middle region and the right side of the front. The average fixation time of these two regions was 4.30 and 1.19 s, respectively, accounting for about 68 and 26% of the total fixation time in each region, and the duration of these two regions accounted for about 94% of the total area duration of fixation. In case of the vehicle approaching the right and stop in the right lane finally, driver mainly pay attention to the area near the front and the area which the vehicle final stop, at the same time the driver is more concerned about the area which is near the front. At the same time, the driver will choose another relevant area as an auxiliary area to obtain the information.

**Table 3** Clustering results correspond to the fixation region

| No. | Area name | Include target | AOI |
|---|---|---|---|
| 1 | Right sidewalk area | Pedestrian and non motorized vehicles on the right side of the road | AOI 6 |
| 2 | Left front area | Current lane with left lane and left vehicle | AOI 3 |
| 3 | Near front area | In front of the vehicle, the vehicle is in front of the vehicle | AOI 2 |
| 4 | Dashboard area | Dashboard area | AOI 7 |
| 5 | Right front area | The right lane and the right side of the vehicle | AOI 4 |
| 6 | Opposite lane area | Left lane area and opposite lane | AOI 5 |
| 7 | Far ahead area | Vehicles and other targets in the distance ahead | AOI 1 |

### 5.2.2 Analysis on Distribution Characteristics of Driver's Fixation Point

It can be seen from Table 4 that the fixation points are mainly distributed in AOI 1, AOI 2, and AOI 4, which are the far, the near middle and the right side. In the middle and right side of the two areas of the highest proportion of the average number of points were 60 and 20%, respectively, accounting for about 80% of the whole area. It is shown that under this stress scenario, the driver is more concerned about the area near the front and the final vehicle. Therefore, the drivers who have experienced the stress scenario will have early warning of memory and psychological preparation for the future danger, at the same time the driver can obtain about 80% of the required information from the main and auxiliary areas.

### 5.2.3 Analysis on Percentage of Drivers' Glance Time

According to the analysis of Table 5, we can see that although the percentage of glance time is still in a high percentage, the percentage of glances in the left and right sides has been greatly improved. It can be concluded that the driver has a high degree of attention to the near front area, and the traffic information of the left and right sides is obtained by scanning. From the table, we can find that the proportion of the glance time on the right side is higher than that of the left side, so the driver can take the glance in the auxiliary area to ensure the timely acquisition of information. Even if the target vehicle is parked on the right side of the road, the driver is still

**Table 4** The duration of fixation of different fixation regions in scene 1

| No. | | AOI 1 | AOI 2 | AOI 3 | AOI 4 | No. | | AOI 1 | AOI 2 | AOI 3 | AOI 4 |
|---|---|---|---|---|---|---|---|---|---|---|---|
| 1 | Duration | 1.4 | 1.1 | 0 | 0.47 | 11 | Duration | 0.18 | 1.98 | 0 | 0.12 |
| 2 | Duration | 0.37 | 8.93 | 0.43 | 3.43 | 12 | Duration | 0 | 7.31 | 0 | 2.36 |
| 3 | Duration | 0 | 3.25 | 0 | 4.07 | 13 | Duration | 0 | 6.97 | 0 | 0 |
| 4 | Duration | 1.7 | 4.17 | 0 | 0.13 | 14 | Duration | 0 | 9.03 | 0.38 | 1.32 |
| 5 | Duration | 1.78 | 3.45 | 0 | 0.75 | 15 | Duration | 0.12 | 6.15 | 0.63 | 0.28 |
| 6 | Duration | 1.73 | 5.67 | 0 | 0.98 | 16 | Duration | 2.88 | 1.2 | 0 | 2.2 |
| 7 | Duration | 0.07 | 2.37 | 0 | 0.22 | 17 | Duration | 0 | 2.33 | 0 | 0 |
| 8 | Duration | 0 | 2.62 | 0 | 1.97 | 18 | Duration | 0.88 | 1.02 | 0 | 1.72 |
| 9 | Duration | 0.12 | 7.47 | 0 | 1.28 | 19 | Duration | 0.08 | 1.88 | 0 | 0.65 |
| 10 | Duration | 0 | 3.62 | 0 | 0.97 | 20 | Duration | 1.02 | 3.78 | 0 | 0.72 |

**Table 5** The percentage of the number of fixation points in different fixation areas in scene 1

| No. | | AOI 1 | AOI 2 | AOI 3 | AOI 4 | No. | | AOI 1 | AOI 2 | AOI 3 | AOI 4 |
|---|---|---|---|---|---|---|---|---|---|---|---|
| 1 | Percentage | 0.33 | 0.5 | 0 | 0.17 | 11 | Percentage | 0.08 | 0.75 | 0 | 0.08 |
| 2 | Percentage | 0.13 | 0.32 | 0.06 | 0.48 | 12 | Percentage | 0 | 0.1 | 0.5 | 0.2 |
| 3 | Percentage | 0 | 0.8 | 0 | 0.2 | 13 | Percentage | 0 | 1 | 0 | 0 |
| 4 | Percentage | 0.17 | 0.67 | 0 | 0.17 | 14 | Percentage | 0 | 0.41 | 0.18 | 0.41 |
| 5 | Percentage | 0.18 | 0.45 | 0 | 0.27 | 15 | Percentage | 0.14 | 0.43 | 0.29 | 0.14 |
| 6 | Percentage | 0.1 | 0.6 | 0 | 0.3 | 16 | Percentage | 0.3 | 0.6 | 0 | 0.1 |
| 7 | Percentage | 0.09 | 0.73 | 0 | 0.18 | 17 | Percentage | 0 | 1 | 0 | 0 |
| 8 | Percentage | 0 | 0.33 | 0 | 0.67 | 18 | Percentage | 0.25 | 0.5 | 0 | 0.25 |
| 9 | Percentage | 0.15 | 0.75 | 0 | 0.1 | 19 | Percentage | 0.2 | 0.6 | 0 | 0.2 |
| 10 | Percentage | 0 | 0.68 | 0 | 0.16 | 20 | Percentage | 0.2 | 0.7 | 0 | 0.1 |

constantly scanning to obtain information, to ensure that the target vehicle subsequent to the safety of the vehicle does not affect the behavior (Table 6).

## 6 Analysis the Influence of Stress Scenes on Physiological Characteristics of Drivers

Whether there is a significant influence on the physiological characteristics of the driver by the stress scene type, the data need to be further analyzed. Therefore, in this section, we will analyze the data in order to quantitatively analyze whether there is a significant relationship between the stress scene type and the driver's physiological characteristics.

**Table 6** The percentage of scanning time of different fixation regions in scene 1

| No. |  | AOI 1 | AOI 2 | AOI 3 | AOI 4 | No. |  | AOI 1 | AOI 2 | AOI 3 | AOI 4 |
|---|---|---|---|---|---|---|---|---|---|---|---|
| 1 | Percentage | 0.33 | 0.5 | 0 | 0.17 | 11 | Percentage | 0.08 | 0.75 | 0 | 0.08 |
| 2 | Percentage | 0.13 | 0.32 | 0.06 | 0.48 | 12 | Percentage | 0 | 0.1 | 0.5 | 0.2 |
| 3 | Percentage | 0 | 0.8 | 0 | 0.2 | 13 | Percentage | 0 | 1 | 0 | 0 |
| 4 | Percentage | 0.17 | 0.67 | 0 | 0.17 | 14 | Percentage | 0 | 0.41 | 0.18 | 0.41 |
| 5 | Percentage | 0.18 | 0.45 | 0 | 0.27 | 15 | Percentage | 0.14 | 0.43 | 0.29 | 0.14 |
| 6 | Percentage | 0.1 | 0.6 | 0 | 0.3 | 16 | Percentage | 0.3 | 0.6 | 0 | 0.1 |
| 7 | Percentage | 0.09 | 0.73 | 0 | 0.18 | 17 | Percentage | 0 | 1 | 0 | 0 |
| 8 | Percentage | 0 | 0.33 | 0 | 0.67 | 18 | Percentage | 0.25 | 0.5 | 0 | 0.25 |
| 9 | Percentage | 0.15 | 0.75 | 0 | 0.1 | 19 | Percentage | 0.2 | 0.6 | 0 | 0.2 |
| 10 | Percentage | 0 | 0.68 | 0 | 0.16 | 20 | Percentage | 0.2 | 0.7 | 0 | 0.1 |

**Table 7** EDA sample size for each type of conflict

| Scene | Scene 1 | Scene 2 | Scene 3 | Scene 4 |
|---|---|---|---|---|
| Number | 713 | 397 | 382 | 550 |

**Table 8** EDA Pearson test results for each type of conflict

|  |  | EDA | Type |
|---|---|---|---|
| EDA | Pearson relevance | 1 | 0.3008 |
|  | Significant (bilateral) |  | $9.543 \times 10^{-10}$ |
|  | N | 397 | 4 |
| Type | Pearson relevance | 0.3008 | 1 |
|  | Significant (bilateral) | $9.543 \times 10^{-10}$ |  |
|  | N | 397 | 4 |

## 6.1 The Analysis of the Influence of Stress Scene Type on the Driver's EDA

In order to make clear the influence of the stress scene type on the driver's skin electrical response, the correlation analysis was performed on the stress test data. Table 7 is the statistical results of the skin response data of the 7 stress scenarios.

The results were shown in Table 8. The P value of the data obtained by Pearson correlation analysis is $9.543 \times 10^{-10} < 0.05$, reject original hypothesis, that is the type of stress scene has a significant effect on the driver's galvanic skin response.

**Fig. 5** Comparison of
different types of conflict on
the impact of the EDA signal
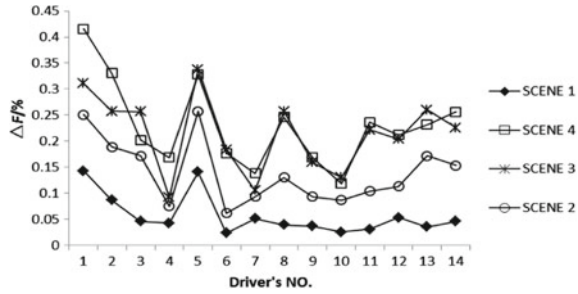


## 6.2  Analysis of the Influence of Stress Scene Type on Driver's EDA

### 6.2.1  Comparison of the Effects of Different Stress Scenarios on EDA

Analysis from Fig. 5 we can know, the four types of stress scenarios which are set in this paper, the significant degree of influence on the skin electrical signal from strong to weak was the cross stress scene and the weather stress scene, the front stress scene, the approximate stress scene.

The results showed that the mean values of skin electrical growth rate of the 4 kinds of stress scenarios were T:0.2306, H:0.2145, Q:0.1393, B:0.0572. Based on the analysis, the simulation to the driver of sudden changeable in the weather is less than the first two, which is due to the relatively low degree of risk caused by the change of weather; The emergence of pedestrians on the driver to stimulate the weakening of the reasons have been described above; In the stress scenario of non motor vehicles, the driver's action is not obvious because the driver took action when he was far away, The approximate stress scene is due to the reasons for setting the scene, if the driver is too slow, and the approaching vehicle will appear in advance, so the driver's degree of stimulation is relatively weak.

## 6.3  Analysis of Driver Heart Rate

In order to analyze the driver's heart rate growth rate under different stress scenarios, the data measured by the above method are drawn into the heart rate increase trend of all the subjects, as shown in Fig. 6.

Figure 6 shows that there is significant difference in the rate of increase in heart rate of the driver in the four scenes. Heart rate growth rate decreases in accordance with the scene 3, scene 2, scene 4, scene 1. The mean values of heart rate increase in the above four scenarios are 26.53, 22.82, 18.94, 16.19%, respectively. Thus, the driver is more alert to the appearance of the people and the change in the weather and the intensity of the vehicle approaching weakened. The driver's approach to other vehicles is less

**Fig. 6** Driver's heart rate
growth rate
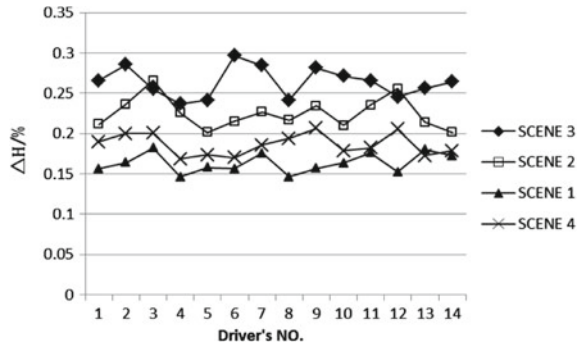


stressful than the weather. While atrocious weather was encountered by drivers as soon as they come out of the tunnel, a great effect on driver's psychological was generated.

## 6.4  Driver HRV Characteristic Analysis

### 6.4.1  Analysis of Drivers' HRV Time Domain Characteristics

The percentage of standard value of each index can be obtained, and the percentage decreases gradually. That is, the driver in accordance with the indicators of the heart of the scene 3, scene 2, scene 1, scene 4, the distance from the standard index is getting closer and closer. It can know from the analysis, the first two scenes in the target involves pedestrians and bicycles with less protection of the target. It can be inferred that the driver after the encounter of two kinds of passion should be the king of the psychological changes in the degree of tension, and has not been in the same degree of tension. Draw the box diagram of the driver's ECG data, four cases of the driver's ECG box diagram is as shown in Fig. 7.

Through the observation and analysis of Fig. 7, it is found that the distribution of psychological index of four drivers in the first two scenarios except SDANN index is more concentrated; the latter two are more dispersed and more volatile. Analysis of the reasons can be seen, drivers are more sensitive to the appearance of pedestrians and bicycles, and the duration of stress is longer.

## 7  Discussion

On the visual side, the driver will be concerned about the location of the target; The average percentage of drivers for the main areas of information acquisition is often as high as 60–70%. While the average percentage of fixation point is about

(a) Scene 1 ECG index box chart



(b) Scene 2 ECG index box chart



(c) Scene 3 ECG index box chart



(d) Scene 4 ECG index box chart
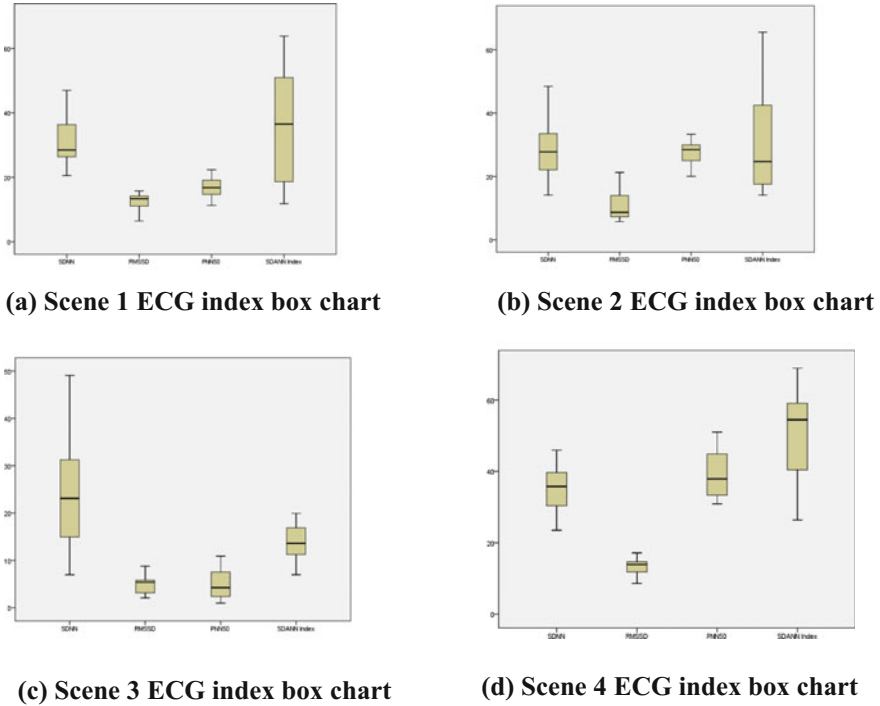
**Fig. 7** ECG index box chart of different scene

10–20%. The driver knows all the information from the main and auxiliary areas about 80–90%. Therefore, it is more effective to use the visual strategy of the main and auxiliary areas to drive safely. The eye movements of the main areas of the acquisition of information were mainly based on fixation, while the eye movements in the supplementary areas were mainly glances.

Physiologically, In the area of skin electricity, only the pedestrian or the external environment to participate in the type of stress scenarios affect the driver's skin electrical signal, In terms of the rate of heart rate increase, different stimulus targets have different effects on the heart rate of drivers. In the time domain characteristics of the HRV, the driver of pedestrians, bicycles, these two objects vigilance is high, and the degree of tension is longer than others. From this analysis, we can see that the driver's psychological load increases when the pedestrian and bicycle are not the same, while the driver in the face of motor vehicles and external weather conditions of the scene, the driver's tension is eased.

# References

Kadali BR, Vedagiri P (2016) Proactive pedestrian safety evaluation at unprotected mid-block crosswalk locations under mixed traffic conditions. Saf Sci 89:94–105

Himes S, Gross F, Eccles K et al (2016) Multistate safety evaluation of intersection conflict warning systems. Transp Res Rec 2583:8–16

Blom Henk AP, Bakker GJ (2015) Safety evaluation of ad-vanced self-separation under very high en route traffic demand. J Aerosp Inf Syst 12(6):413–427

(Su) Babu Markov (1983) Road conditions and traffic organization (trans: Qi Z). Chinese Architectural Industry Press, Beijing

Vedagiri P, Kadali BR (2016) Evaluation of pedestrian-vehicle conflict severity at unprotected midblock crosswalks in India. Transp Res Rec 2581:48–56

Noble AM, Dingus TA, Doerzaph ZR (2016) Influence of in-vehicle adaptive stop display on driving behavior and safety. IEEE Trans Intell Transp Syst 17(10):2767–2776

Brookhuis Karel A, De Waard D (1993) The use psychop-hysiology to assess driver status. Ergonomies 36(12):1099–1108

Wu J (2009) Study on the method of heart rate variability analysis. Beijing Jiaotong University, College of computer and information technology, Beijing

Xiaofang L, Ye Z (2011) Analysis method and application of heart rate variability. Foreign Med Sci Biomed Eng 24(1):4245

Cheng Y, Li G, Gao X (2014) Changes in attention allocation characteristics of drivers driving on exp-ressway. China Saf Sci J 24(10):71–76

# A Short-Term Traffic Flow Prediction Method Based on Long Short-Term Memory Network

**Yusheng Ci, Gaoqun Xiu and Lina Wu**

**Abstract**  In order to achieve the higher accuracy of the short-term traffic flow prediction, this paper proposed a prediction method based on the Long Short-Term Memory Network (LSTM) model. First, the original traffic flow data is processed by difference and scaling, so the trend is removed. And then the LSTM model is proposed to learn internal characteristic of the traffic flow and make the forecast. Comparing LSTM method with the traditional prediction model (back propagation neural network, BPNN), the experiment result shows that the proposed traffic flow prediction method has the better learnability for the short-term traffic flow and achieves higher accuracy for the prediction.

**Keywords**  Short-term traffic flow prediction · Deep learning · LSTM

## 1 Introduction

The goal of short-term traffic flow prediction is to provide such traffic flow information, so the traffic flow prediction is vital for traffic and it plays an indispensable role in ITS. Much research has been focused on the subject since 1980 [1, 2], but their performance is not particularly good [3]. In recent years, the deep learning has drawn a lot of academic interest for the traffic flow prediction [4–7]. In the past decades, the special model of deep learning, short-term memory neural network (LSTM) has attracted many attentions from worldwide researchers in term of the superior capability for the time series prediction. But there are not enough research of transportation to pay attention to the LSTM. Duan et al. [8], Zhao et al. [9], Fu et al. [10] explored

Y. Ci · G. Xiu (✉)

School of Transportation Science and Engineering, Harbin Institute of Technology, Harbin 150090, China
e-mail: xiu18846433869@163.com

L. Wu

College of Automobile and Traffic Engineering, Heilongjiang Institute of Technology, Harbin 150050, China

a the LSTM model for travel time and traffic flow prediction and have a good performance. In order to achieve the higher prediction accuracy, this paper proposed a short-term traffic prediction model based on LSTM neural network. Through memory blocks of the LSTM, the model could automatically reserve historical sequence information and capture the nonlinearity and long temporal dependency of the traffic flow series, thus it shows superior capability for the time series prediction. Comparing proposed model with the well-known models (single back propagation neural network), the results show that the LSTM model achieves the higher accuracy and generalizes well.

The rest of this paper is organized as follows. Section 1 introduces the principle and network structure of LSTM neural network. Section 2 describes how to process the initial traffic flow data and then proposes a model for the short-term traffic flow prediction based on LSTM. Section 3 presents the experiment design and results analysis. Section 4 concludes this paper.

## 2 Short-Term Traffic Flow Prediction Model Based on LSTM

### 2.1 LSTM

The Long Short-Term Memory network is a new deep learning network from the recurrent neural network (RNN), proposed in 1997 for language models and was well-known for ability to learn longtime information of the time series [11]. The LSTM network is common because it can process anything a conventional computer can compute as long as it was provided the proper weight matrix and enough network units. Especially, the LSTM network is suited to learn from experience to process, classify process and predict the time series which have the longtime lags of unknown size between important events. For the LSTM, remembering information for long periods of time is the default behavior, not something it struggles to learn. The key to the LSTM model is the memory units that allow the network to learn when to forget historical information and when to update the memory cell with new information. The memory block is a set of recurrently connected subnets. The internal structure of the memory cell is shown in Fig. 1.

The LSTM uses the memory cell to store and access information of the long periods of time, and the vanishing gradient problem will be mitigated. At time $t$, the memory unit records all historical information up to the current moment and it is controlled by three "gates": Input gate, Forget gate, Output gate. These doors are logical units that do not send their actions as input values to other neurons units, but rather to set weights at the edges of the other parts that are connected to the memory cell. This memory unit is a linear neuron with internal connections.

The forget gate controls what information needs to throw away from the cell state. It looks at $h_{t-1}$ and $x_t$, and outputs a number between 0 and 1 in the cell state $c_{t-1}$. 0
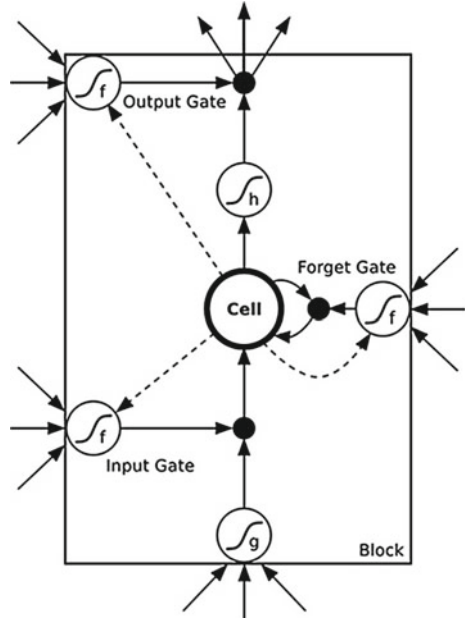
represents "completely threw this" and while a 0 represents "completely retain this".
The input gate controls how much new information is added to each memory cell.
The output gate controls how much information is output in every memory unit.

Suppose the input sequence of a certain section is $\mathbf{x} = (x_1, x_2 \ldots x_t)$, the vector
sequence of the memory cell in LSTM is $\mathbf{h} = (h_1, h_2, \ldots h_t)$, $\mathbf{y} = (y_1, y_2, \ldots y_n)$
is the output sequence. The formula for each part of the LSTM memory cell is as
follows:

Input gate:

$$i_t = \sigma(W_{xi} x_t + W_{hi} h_{t-1} + W_{ci} c_{t-1} + b_i) \tag{1}$$

Forget gate:

$$f_t = \sigma(W_{xf} x_t + W_{hf} h_{t-1} + W_{cf} c_{t-1} + b_f) \tag{2}$$

Output gate:

$$o_t = \sigma(W_{xo} x_t + W_{ho} h_{t-1} + W_{co} c_t + b_f) \tag{3}$$

Cell input:

$$\tilde{c}_t = g(W_{xc} x_t + W_{hc} h_{t-1} + b_c) \tag{4}$$

Cell output:

$$c_t = f_t c_{t-1} + i_t \tilde{c}_t \tag{5}$$

$$h_t = o_t h(c_t) \tag{6}$$

where $x_t$ is the input at time $t$, $h_t$ is the hidden layer output and $h_{t-1}$ is the its former output, $c_t$ is the memory cell output state and $c_{t-1}$ is its former state, $W_{xi}, W_{xf}, W_{xo}, W_{xc}$ are the weight matrices connecting $h_{t-1}$ to the three gates and cell input. $\sigma$ is the standard sigmoid function $\frac{1}{1+e^{-x}}$. The $i, f, o$ are, respectively, input gate, forget gate and the output gate, $c$ is the cell activation vectors, and all of which are the same size as hidden vector $\mathbf{h}$.

## 2.2 Traffic Prediction Model Based on LSTM

Here, traffic flow predicted model is define as predicting future traffic volume $y$, from the historical traffic volume. Suppose the input traffic flow sequence of a certain section is $\mathbf{x} = (x_1, x_2, x_3 \ldots x_n)$, the stationary sequence after difference process is $\tilde{\mathbf{x}} = (\tilde{x}_1, \tilde{x}_2, \tilde{x}_3 \ldots \tilde{x}_n)$, the vector sequence of the memory cell in LSTM is $\mathbf{h} = (h_1, h_2, h_3 \ldots h_n)$, the output predicted $y$ is the final predicted traffic flow sequence, $\tilde{y}$ is the predicted sequence before inverse difference.

$$h_t = m(W_{xh}\tilde{x}_t + W_{hh}h_{t-1} + b_h) \tag{7}$$

$$\tilde{y}_t = W_{hy}h_t + b_y \tag{8}$$

$$y = o(\tilde{y}_t) \tag{9}$$

where $m$ is the function of the hidden layer, $b$ term is the bias vectors (e.g. $b_h$ is the hidden bias vector), $o$ is the inverse difference function. It can be seen from the function that the predicted results at the current time is reflected by the previous time, which reflects the long temporal dependency of the traffic flow series. The structure of the traffic flow forecasting model based on LSTM is shown in Fig. 2.

To build the traffic flow prediction model based on LSTM, five key hyperparameters will be determined, the time steps, the dimension of the input layer, the number of the hidden layer, the number of hidden layer units (memory blocks in LSTM), the size of the output layer. The time steps are separate time steps of a given variable for a given observation. We will keep it simple and frame the problem as each time step in the original sequence is with one timestep and one feature. The size of the input layer is equal to the input historical sequence length. Training the LSTM model is time-consuming and quite complicate, so the number of hidden layer in the model is designed to 1 without deep structure. We choose 5 as the number of the hidden layer. The hidden units of the model are the memory cell mentioned above. The output layer of the model is 1 layer. To get well performance, the internal connection of the

**Fig. 2** The structure of traffic flow prediction based on LSTM
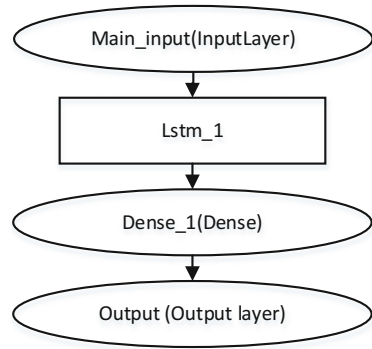


LSTM is full recurrent. The network requires a single neuron in the output layer with a linear activation to predict the traffic flow at the next time step. The output layer is the dense layer. The optimization of the dense layer is Nadam and the loss function is assigned as MSE. In the model, we'll choose the fixed method, fit the model once on all of the training data, then predict each new time step one at a time from the test data.

A deep learning library written in Python called Keras is applied in the implementation of the model, and this is capable of running on top of Theano.

## 3 Experiments

### 3.1 Data Description and Experiment Design

The experimental data is obtained from the Caltrans Performance Measurement Systems (PEMS), the traffic flow of the system is collected every 30 s from the 15,000 individual detectors on the California freeway. The sampling time interval of the original data is 5 min, in the paper, we aggregated into 1-h interval for prediction and we randomly selected one freeway in PeMS for prediction experiment. In this paper, we collected the traffic flow data on 225 days in 2011, the data of first 170 days (3.17–9.3) data is the training data, the data of later 40 days (9.3–10.13) is used as test data. Because LSTM can have a good performance to memorize long-continuous historical data, so the experiment will not delete the holiday data. We can see from Fig. 3 that the prediction result from the LSTM model and the actual data deviation is small, the prediction traffic flow and the real traffic flow can match very well. So we can draw the conclusion that the LSTM model has an excellent performance in the short-term traffic flow prediction.
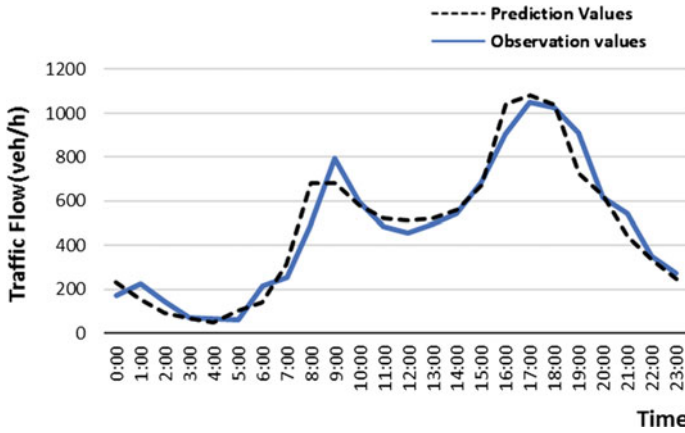
**Fig. 3** Comparison of real observation traffic flow and prediction traffic flow

## 3.2 *The Prediction Accuracy Comparison*

In this part, we observe the prediction effect of the method by comparing our approach with the traditional methods for traffic flow prediction. Over the past period of time, the neural network has been widely used in the traffic flow forecast and it has achieved relatively good results [12]. To compare the performance of the traffic flow prediction model, we use two criteria performance indexes: the root mean square error (RMSE) and the mean relative error (MAE) as the evaluation indexes. They are defined as follows:

$$\text{RMSE} = \sqrt{\frac{1}{n} \sum_{i=1}^{n} (y_t - x_t)^2} \tag{10}$$

$$\text{MAE} = \frac{1}{n} \sum_{i=1}^{n} |y_t - x_t| \tag{11}$$

where $y_t$ is the final predicted traffic flow, $x_t$ is the actual traffic flow at time $t$. In Table 1, we can find that the RMSE and MAE in LSTM model lower than the BP Neural Network, and then we can draw the conclusion that the LSTM model is more accurate than the BP Neural Network model for the short-term traffic flow prediction. To sum up, although the model structure is simple, the LSTM model can learn the characteristic of traffic flow which is not linear and have the longtime dependency, and it has a good performance for the short-term traffic flow prediction.

**Table 1** Prediction error

| The prediction model | Metrics | |
|---|---|---|
| | RMSE | MAE |
| LSTM | 94.07 | 63.28 |
| BPNN | 263.21 | 188.38 |

## 4 Conclusion

In this paper, to improve the prediction accuracy of the traffic flow, a short-term traffic flow prediction method based on LSTM model is proposed. The LSTM model is used to predict the traffic flow data by reserving historical sequence information and capturing internal characteristic of the traffic flow series. The experimental results show that the method has a good learnability for the big short-term traffic data and the prediction result is more accurate than the traditional prediction method. Therefore, the method is an effective method for short-term traffic flow prediction and it has practical significance for the development of ITS. But the model uses a single-step prediction method; the actual LSTM can be set to multi-step prediction in order to achieve greater volume and faster training. We should deep study in the future, build a deep LSTM network to achieve better prediction effect.

## References

1. Levin M, Tsao YD (1980) On forecasting freeway occupancies and volumes. Transp Res Rec 773
2. Williams BM, Hoel LA (2003) Modeling and forecasting vehicular traffic flow as a seasonal ARIMA process: theoretical basis and empirical results. J Transp Eng 129(6):664–672
3. Park D, Rilett LR, Han G (1999) Spectral basis neural networks for real-time travel time forecasting. J Transp Eng 125(125):515–523
4. Huang W, Song G, Hong H et al (2014) Deep architecture for traffic flow prediction: deep belief networks with multitask learning. IEEE Trans Intell Transp Syst 15(5):2191–2201
5. Kuremoto T, Kimura S, Kobayashi K et al (2014) Time series forecasting using a deep belief network with restricted Boltzmann machines. Neurocomputing 137:47–56
6. Wenhao H, Guojie S, Haikun H et al (2014) Deep architecture for traffic flow prediction: deep belief networks with multitask learning. IEEE Trans Intell Transp Syst 15(5):2191–2201
7. Fu R, Zhang Z, Li L (2017) Using LSTM and GRU neural network methods for traffic flow prediction. Chin Assoc Autom, IEEE
8. Duan Y, Lv Y, Wang FY (2016) Travel time prediction with LSTM neural network. IEEE Int Conf Intell Transp Syst, IEEE, 1–4 Nov 2016
9. Zhao Z, Chen W, Wu X et al (2017) LSTM network: a deep learning approach for short-term traffic forecast. IET Intel Transp Syst 11(2):68–75

10. LyuYisheng DuanYanjie, Wenwen Kang et al (2014) Traffic flow prediction with big data: a deep learning approach. IEEE Trans Intell Transp Syst 16(2):865–873
11. Hochreiter S, Schmidhuber J (1997) Long short-term memory. Neural Comput 9(8):1735–1780
12. Vlahogianni EI, Karlaftis MG, Golias JC (2005) Optimized and meta-optimized neural networks for short-term traffic flow prediction: a genetic approach. Transp Res Part C: Emerg Technol 13(3):211–234

# Influence Factors Analysis on Ride Comfort of Double Semitrailer Train

**Hao Zhang, Hong-wei Zhang and Wei Wang**

**Abstract** Simplify vibration model of double semitrailer train based on relevant ride comfort theory. Force analysis of every parts in system was carried out to consider the train ride comfort at the aspects of vertical and pitching vibration. Vibration differential equation was established in vehicle coordinate system based on Darren Bell principle. The power spectral density of road surface is chosen as the expression of road surface roughness, and the relation between spatial frequency spectrum density and time frequency spectrum density is defined, confirming the input spectrum for vehicle. Simulation speed is 70 km/h on B-class road. Seat, 30 cm at the end of the first cargo compartment, 30 cm at the end of the second cargo compartment were the three selected points to analyze ride comfort resulting from fifth wheel lead, suspension stiffness, suspension damping and tire stiffness. This research could provide technology support for improving ride comfort of double semitrailer train.

**Keywords** Double semitrailer · Ride comfort · Road roughness · Simulation analysis

Ride comfort of double semi-trailer train mainly refers to maintain the vibration and shock environment of double semi-trailer train on the occupant's comfort and cargo safety are within certain limits. The vibration mainly result from road, engine, power train and rotating parts, such as wheels. Vehicle vibration would not only cause passengers fatigued and freight damaged but also affect normal service life of vehicle because of components abrasion. In addition, bad ride comfort would also limit Vehicle power and economy. It is extremely important to ensure vehicle good vibration to provide a good environment to drivers' psychological and physiological

H. Zhang (✉) · H. Zhang · W. Wang
Research Institute of Highway Ministry of Transport, Beijing 100088, China
e-mail: kuyuwen@qq.com

H. Zhang · H. Zhang · W. Wang
Key Laboratory of Operation Safety Technology on Transport Vehicles Ministry of Transport, Beijing 100088, China

H. Zhang · H. Zhang · W. Wang
Jiangsu University of Technology, Changzhou City 213001, Jiangsu Province, China
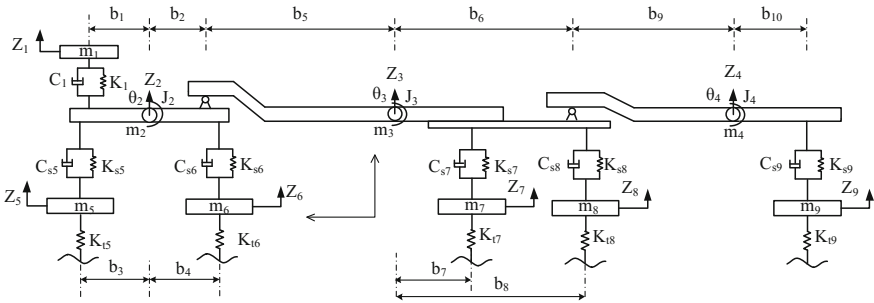
**Fig. 1** Simplified vibration analysis model of double semitrailer train

state. The comfort of the vibration environment could ensure that the passengers have a good condition to work after arriving. As a result, ride comfort is a significant indicator during vehicle driving. How to match tractor and semitrailer for an excellent ride comfort is the main content of this study.

# 1 Establishment of Vibration Model of Double Semitrailer Train

## 1.1 General Vibration Model of Double Semitrailer Train

In order to simplify model and easily to calculate, hypothesis for vibration model of double semitrailer train was made as follows. Vehicle is symmetrical and the left road excitation is same with the right. Vertical and longitudinal vibration are investigated, and horizontal vibration is ignored. Keep the vehicle running at a constant speed, and the tires are always in contact with the ground. Chassis and axles are regarded as rigid bodies. Ignore tire damping. Vibration model of double semitrailer train could described by dynamic model shown in Fig. 1 based on the hypothesis above. The degree of freedom of system are displacement and angle including $z_1$, $z_2$, $z_3$, $z_4$, $z_5$, $z_6$, $z_7$, $z_8$, $z_9$ and $\theta_2, \theta_3, \theta_4$. Parameters of dynamic model of double semitrailer train was shown in Tab. 1.

## 1.2 Deduction of Motion Equation of Double Semitrailer Train

Dynamic equation of vehicle could established based on Lagrange equation.

$$\frac{\mathrm{d}}{\mathrm{d}t}\left(\frac{\partial T}{\partial \dot{q}_i}\right) - \frac{\partial T}{\partial q_i} + \frac{\partial U}{\partial q_i} + \frac{\partial E}{\partial \dot{q}_i} = Q_i \tag{1}$$

In Fig. 1 $m1$ is total mass of seats and drivers, $m2$ is sprung mass of tractor, $m3$, $m4$ is sprung mass of semitrailer, $m5$, $m6$ is unsprung mass of tractor, $m7$, $m8$, $m9$ is unsprung mass of semitrailer, $J2$ is pitching moment of inertia of tractor, $J3$, $J4$ is pitching moment of inertia of trailer, k1 is seat stiffness, ks5, ks6 is suspension stiffness of tractor, ks7, ks8, ks9 is suspension stiffness of trailers, kt5, kt6 is tire stiffness of trailers, kt7, kt8, kt9 is tire stiffness of semitrailer, c1 is seat damping, cs5, cs6 is suspension damping of tractor, cs7, cs8, cs9 is suspension damping of semitrailer.

$T$, $U$ and $E$ refer to kinetic energy, potential energy and dissipation energy of vehicle system respectively. Generalized coordinate vector is $q = \{z_1, z_2, z_5, z_6, z_7, z_8, z_9, \theta_2, \theta_3, \theta_4\}^{\mathrm{T}}$.

Kinetic energy of vehicle system is

$$T = \sum_{i=1}^{9} \frac{1}{2} m_i \dot{z}_i^2 + \frac{1}{2} J_2 \dot{\theta}_2^2 + \frac{1}{2} J_3 \dot{\theta}_3^2 + \frac{1}{2} J_4 \dot{\theta}_4^2 \tag{2}$$

Potential energy of system is

$$\begin{aligned}
U = &\frac{1}{2}k_1[z_1 - (z_2 - b_1\theta_2)]^2 + \frac{1}{2}k_{s5}[(z_2 - b_3\theta_2) - z_5]^2 + \frac{1}{2}k_{s6}[(z_2 + b_4\theta_2) - z_6]^2 \\
&+ \frac{1}{2}k_{s7}[(z_3 + b_7\theta_3) - z_7]^2 + \frac{1}{2}k_{s8}[(z_3 + b_8\theta_3) - z_8]^2 + \frac{1}{2}k_{s9}[(z_4 + b_{10}\theta_4) - z_9]^2 \\
&+ \frac{1}{2}k_{t5}(z_5 - r_1)^2 + \frac{1}{2}k_{t6}(z_6 - r_2)^2 + \frac{1}{2}k_{t7}(z_7 - r_3)^2 + \frac{1}{2}k_{t8}(z_8 - r_4)^2 + \frac{1}{2}k_{t9}(z_9 - r_5)^2
\end{aligned} \tag{3}$$

Dissipation energy of system is

$$\begin{aligned}
E = &\frac{1}{2}c_1[\dot{z}_1 - (\dot{z}_2 - b_1\dot{\theta}_2)]^2 + \frac{1}{2}c_{s5}[(\dot{z}_2 - b_3\dot{\theta}_2) - \dot{z}_5]^2 + \frac{1}{2}c_{s6}[(\dot{z}_2 + b_4\dot{\theta}_2) - \dot{z}_6]^2 \\
&+ \frac{1}{2}c_{s7}[(\dot{z}_3 + b_7\dot{\theta}_3) - \dot{z}_7]^2 + \frac{1}{2}c_{s8}[(\dot{z}_3 + b_8\dot{\theta}_3) - \dot{z}_8]^2 + \frac{1}{2}c_{s9}[(\dot{z}_4 + b_{10}\dot{\theta}_4) - \dot{z}_9]^2
\end{aligned} \tag{4}$$

Independent coordinates, $z_3$ and $z_4$, could be expressed as

$$z_3 = z_2 + b_2\theta_2 + b_5\theta_3, \quad z_4 = z_2 + b_2\theta_2 + (b_5 + b_6)\theta_3 + b_9\theta_4 \tag{5}$$

Motion equation of system could be proposed according to Lagrange equation

$$M\ddot{z} + C\dot{z} + Kz = K_t r \tag{6}$$

## 2  Ride Comfort Simulation and Analysis of Double Semitrailer Train

### 2.1  Theoretical Calculation of Vehicle System

The system in this paper is a linear system with 5 dimensional inputs and 10 dimensional outputs. The Fourier transform between the input and output is

$$Z(j\omega) = H(j\omega)Q(j\omega) \tag{7}$$

$H(j\omega)$ is system frequency response function. After Fourier transform for (6), the following equation could be concluded:

$$-\omega^2 M Z(j\omega) + j\omega C Z(j\omega) + K Z(j\omega) = K_t Q(j\omega) \tag{8}$$

If

$$D = -\omega^2 M + j\omega C + K, \quad E = K_t \tag{9}$$

Then the frequency response function could be described as:

$$H = D^{-1}E \tag{10}$$

The input power spectrum matrix of system is

$$G_q = \begin{bmatrix} G_{11} & G_{12} & \cdots & G_{1m} \\ G_{21} & G_{22} & \cdots & G_{2m} \\ \vdots & \vdots & \ddots & \vdots \\ G_{m1} & G_{m2} & \cdots & G_{mm} \end{bmatrix} \tag{11}$$

The output (response) power spectrum matrix of system is

$$G_z = \begin{bmatrix} G_{z_1 z_1} & G_{z_1 z_2} & \cdots & G_{z_1 z_m} \\ G_{z_2 z_1} & G_{z_2 z_2} & \cdots & G_{z_2 z_m} \\ \vdots & \vdots & \ddots & \vdots \\ G_{z_m z_1} & G_{z_m z_2} & \cdots & G_{z_m z_m} \end{bmatrix} \tag{12}$$

For liner system, there is the following equation:

$$G_z = H G_q H^{\mathrm{H}} \tag{13}$$

**H** is frequency response function matrix, $\boldsymbol{H}^{\mathrm{H}}$ is conjugate transpose of Frequency response function matrix.

## 2.2 Road Excitation for Double Semitrailer Train

Road roughness normally described by road power spectral density, $G_q(n)$ fits the following equation:

$$G_q(n) = G_q(n_0)\left(\frac{n}{n_0}\right)^{-w} \tag{14}$$

where: $n$—spatial frequency, reciprocal of wavelength, refers to the number of wavelength in unit length, $\mathrm{m}^{-1}$; $n_0$—Reference frequency, $n_0 = 0.1$ $\mathrm{m}^{-1}$; $w$—Frequency index, rake ratio on double logarithmic coordinates, in classified road, $w = 2$; $G_q(n_0)$—the value of road spectrum in reference frequency, called pavement roughness coefficient, $\mathrm{m}^2/\mathrm{m}^{-1}$.

We know that $f = un$ and spectral density can be described as:

$$G_q(f) = \frac{1}{u}G_q(n) \tag{15}$$

when $w = 2$, the above equation could be deducted to:

$$G_q(f) = G_q(n_0)n_0^2 u/f^2 \tag{16}$$

The following equation could be established on the hypothesis that all wheels driving at the same road

$$G_{qij}(f) = \begin{cases} = G_q(f), & j = i \\ = G_{qji}^*(f) = G_q(f)e^{-j2\pi f L_{ij}/u}, & j \neq i \end{cases} \quad (i, j = 1, 2, \cdots 5) \tag{17}$$

where, $G_{qii}(f)$—Road spectrum for wheel $i$; $G_{qji}(f)$, $(i \neq j)$—Cross spectrum between wheel $i$ and wheel $j$, $G_{qji}^*(f)$ is conjugate of $G_{qji}(f)$; $L_{ij}$—distance between wheel $i$ and wheel $j$.

## 2.3 Test Method for Ride Comfort of Vehicle

Root Mean Square (RMS) value of weighted acceleration is calculated according to the vibration direction and the sensitivity of human body to vibration frequency through the following method. $\bar{a}_w$ is calculated according $G_a(f)$, the Self power

spectral density function for acceleration deriving from equal bandwidth frequency analysis. We firstly calculated 1/3 octave band RMS of acceleration:

$$\bar{a}_j = \left[ \int_{f_{uj}}^{f_{ij}} G_a(f)\,df \right]^{\frac{1}{2}} \tag{18}$$

where, $\bar{a}_j$—the $j$th ($j=1, 2, \ldots 23$) 1/3 octave band RMS of acceleration whose center frequency is $f_j$, m/s$^2$; $f_{ij}, f_{uj}$,—Upper and lower frequency of 1/3 octave band center frequency, Hz; $G_a(f)$—Self power spectrum density function for acceleration, m$^2$/s$^3$. Then we calculate $\bar{a}_w$:

$$\bar{a}_w = \left[ \sum_{j=1}^{23} (\omega_j \cdot \bar{a}_j)^2 \right]^{\frac{1}{2}} \tag{19}$$

where, $\bar{a}_w$—Single axial RMS of weighted acceleration, m/s$^2$; $\omega_j$—Weighting coefficient of $j$th 1/3 octave band, in this study, only vertical $\omega_k$.

## 3   Simulation Analysis for Influence Factors

Fifth wheel lead, suspension stiffness, suspension damping and tire stiffness are the main factors that was taken into consideration. All variables have 5 sets data, including original value and its $\pm 20\%$, $\pm 10\%$. The reference point, 30 cm at the end of the first cargo compartment and the second cargo compartment, was choose to analyze the influence of ride comfort on cargos. Simulation speed is 70 km/h and road condition is class-B.

### 3.1   Influence of Fifth Wheel Lead Changing on Ride Comfort of Train

Fifth wheel lead is changed by changing the value of $b_2$. Increased $b_2$ could reduce fifth wheel lead, otherwise, smaller $b_2$ would make longer fifth wheel lead. Longer fifth wheel lead would worsen ride comfort performance at seat and the first reference point, while it has little influence on the second reference point, as shown in Fig. 2.

(a) seat

(b) first cargo compartment



(c) second cargo compartment
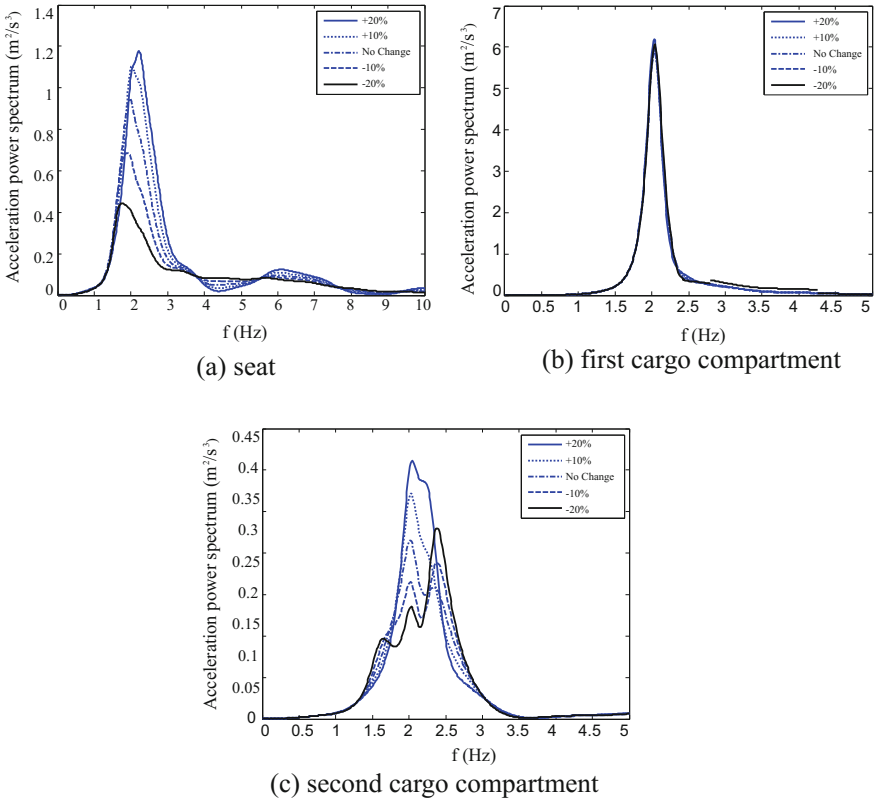
**Fig. 2** Acceleration power spectrum with different fifth wheel lead

## 3.2 Influence of Suspension Stiffness Changing on Ride Comfort of Train

Influence of suspension stiffness on ride comfort of train was concluded through increase or decrease suspension stiffness of tractor and trailer by 20 and 10%. The reference point, 30 cm at the end of the first cargo compartment and the second cargo compartment, was choose to analyze the influence of ride comfort on cargos. Front suspension stiffness of tractor have little influence on reference point, as shown in Fig. 3.

Reduce rear suspension stiffness of tractor have a positive influence on the ride comfort at seat position, but it worsen the ride comfort of reference point at cargo compartment, as shown in Fig. 4.

Suspension stiffness of trailer have a significant influence on ride comfort at seat and reference point. Smaller suspension stiffness of trailer could contribute a better ride comfort, as shown in Fig. 5.

(a) seat



(b) first cargo compartment



(c) second cargo compartment
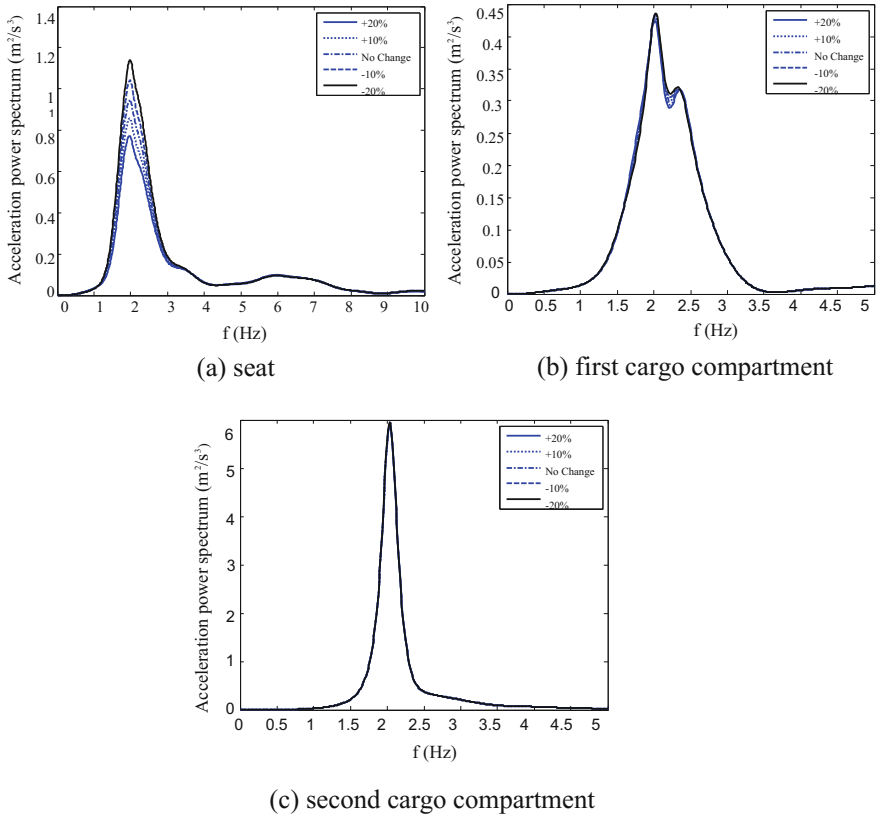
**Fig. 3** Acceleration power spectrum with different front suspension stiffness of tractor

## 3.3   Influence of Suspension Damping Changing on Ride Comfort of Train

Influence of suspension damping on ride comfort of train was concluded through increase or decrease suspension damping of tractor and trailer by 20 and 10%. The reference point, 30 cm at the end of the first cargo compartment and the second cargo compartment, was choose to analyze the influence of ride comfort on cargos.

Increasing front suspension stiffness of tractor could improve the seat ride comfort and it have little influence of ride comfort at reference point, as shown in Fig. 6.

Increase rear suspension stiffness of tractor could improve seat ride comfort while slightly reduce the ride comfort at first reference point. Rear suspension stiffness of tractor have little influence on the second reference point, as shown in Fig. 7.

(a) seat



(b) first cargo compartment



(c) second cargo compartment
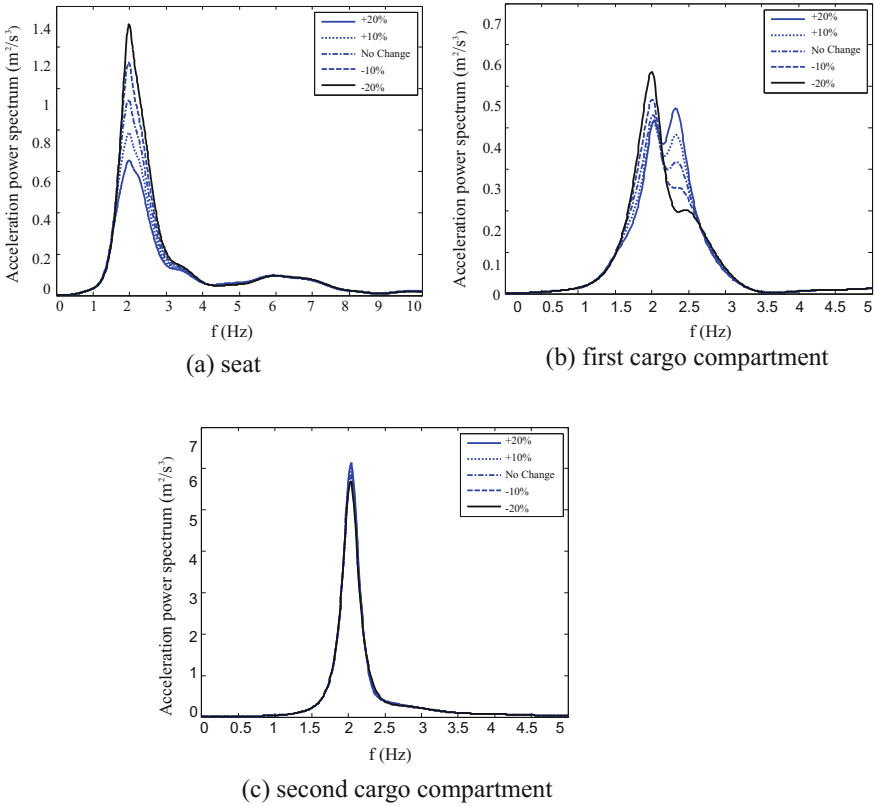
**Fig. 4** Acceleration power spectrum with different rear suspension stiffness of tractor

## 3.4 Influence of Tire Stiffness Changing on Ride Comfort of Train

Influence of tire stiffness on ride comfort of train was concluded through increase or decrease tire stiffness of tractor and trailer by 20 and 10%. The reference point, 30 cm at the end of the first cargo compartment and the second cargo compartment, was choose to analyze the influence of ride comfort on cargos.

Suspension damping of trailer have a strongly significant influence on ride comfort performance at seat and reference point. Increased damping of trailer could improve ride comfort at seat and reference point in cargo component, as shown in Fig. 8.

Reducing front tire stiffness of tractor could improve ride comfort at seat position ant it has little influence on ride comfort at reference point, as shown in Fig. 9.

(a) seat



(b) first cargo compartment



(c) second cargo compartment
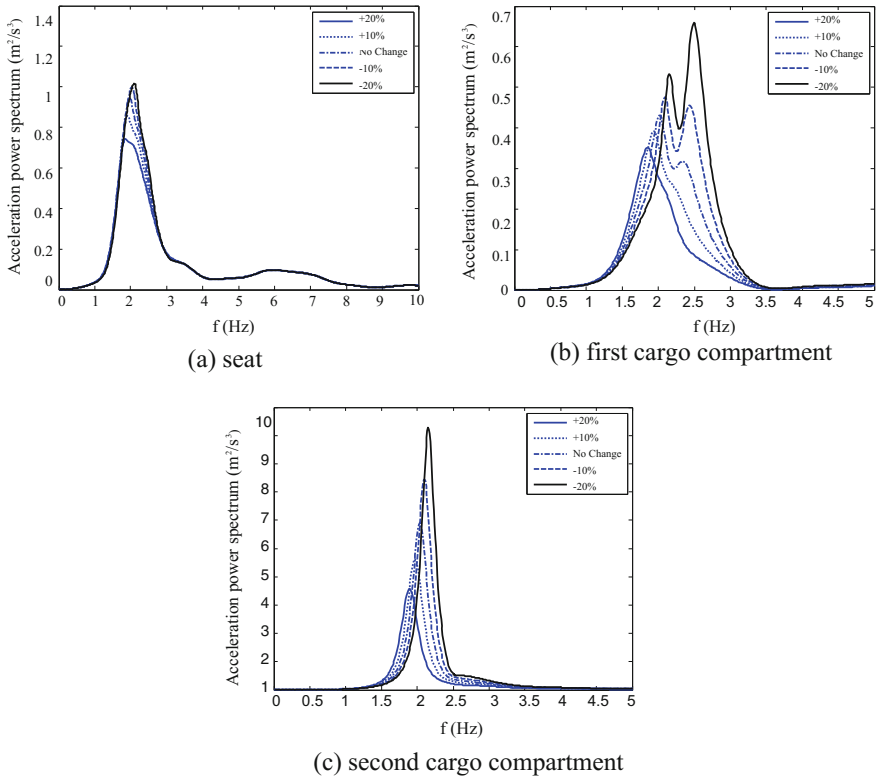
**Fig. 5** Acceleration power spectrum with different suspension stiffness of trailer

Rear tire stiffness of tractor have little influence on ride comfort, reduce trailer tire stiffness can improve ride comfort at seat and reference point at first cargo component at a cost of ride comfort reduction at second cargo component.

## 4  Conclusion

Ride comfort simulation model of double semitrailer was built in vehicle coordinate system based on Darren Bell principle. The power spectral density of road surface is chosen as the expression of road surface roughness, and the relation between spatial frequency spectrum density and time frequency spectrum density is defined, confirming the input spectrum for vehicle. Simulation speed is 70 km/h on B-class road. Seat, 30 cm at the end of the first cargo compartment, 30 cm at the end of the second

(a) seat

(b) first cargo compartment

(c) second cargo compartment
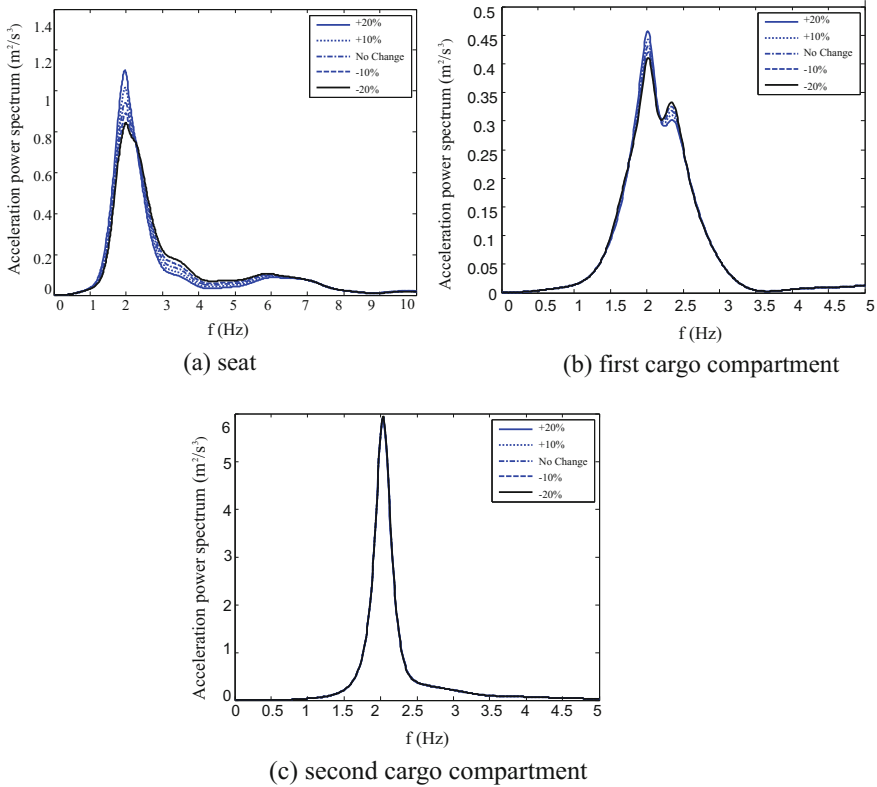
**Fig. 6** Acceleration power spectrum with different front suspension damping of tractor

cargo compartment were the three selected points to analyze ride comfort resulting from fifth wheel lead, suspension stiffness, suspension damping and tire stiffness. Analysis results show that increased front suspension damping and decreased front tire stiffness of tractor could improve the ride comfort at seat position, while those factors have little influence on reference point at cargo component. Decrease suspension stiffness and increase suspension damping of tractor have a positive influence on seat and reference points ride comfort. This research could provide technology support for improving ride comfort of double semitrailer train.

(a) seat
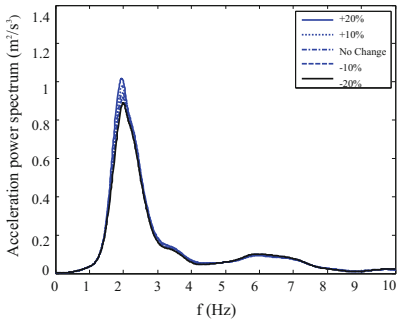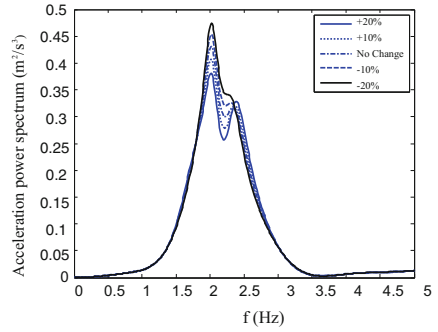


(b) first cargo compartment
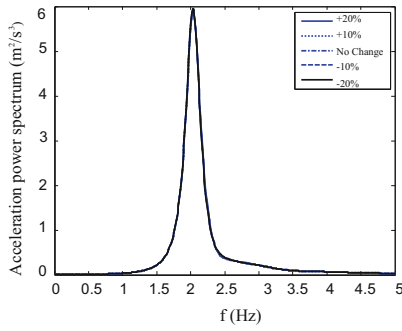


(c) second cargo compartment

**Fig. 7** Acceleration power spectrum with different rear suspension damping of tractor

(a) seat

(b) first cargo compartment

(c) second cargo compartment
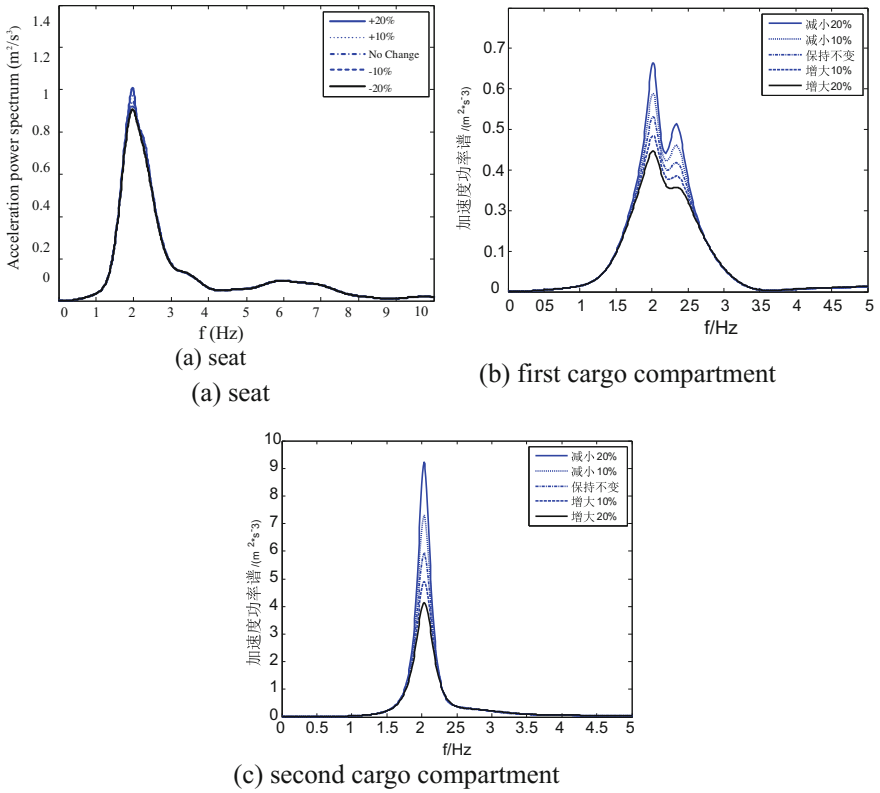
**Fig. 8**  Acceleration power spectrum with different suspension damping of trailer

(a) seat



(b) first cargo compartment



(c) second cargo compartment

**Fig. 9** Acceleration power spectrum with different front tire stiffness of tractor

# References

1. Guo Z (2009) Modern combination vehicles design and use. Beijing Institute of Technology Press, Beijing
2. Yu Z (2000) Vehicle theory, 3rd edn. Machinery Industry Press, Beijing
3. Xu Hong-guo (2009) Automotive theory. China Communications Press, Beijing
4. Abe M (2009) Vehicle handling dynamics. Elsevier Ltd
5. Liu X, Haibo Lv, Zhang H, Shan Y (2015) Effect of structure parameters and model processing method of tractor-semitrailer combination on the ride performance. J Chongqing Jiaotong Univ (Natural Science)
6. Chen T(2015) Simulation and experimental study on ride comfort of tractor semitrailer. School of mechanical engineering, Nanjing University of Science and Technology, Nanjing (Dec 2015)

# Automated Detection Algorithm for Traffic Incident in Urban Expressway Based on Lengthways Time Series

**Hong-wei Li, Su-lan Li, Hong-wei Zhu, Xing Zhao and Xiaoli Zhang**

**Abstract** The paper proposes an automatic traffic accident detection algorithm for the urban expressway. The algorithm is established on longitudinal time series theory based on catastrophe theory and statistics theory. The results: (1) the lengthways time series of traffic parameters data manifests a good stability than the transverse time series and it can detect accident when the losing data are more; (2) no matter what traffic flow stats are, the model can detect accident accurately. The model developed in the study can be directly used by traffic engineers and managers to detect traffic accident.

## 1 Introduction

As the arterial road in city traffic, urban expressway plays an important role in the entire urban transport system. For instance, urban expressway accounts for 5% of the total road area of the central area of Shanghai,but assume 20% of the total traffic flow [1]. Traffic accidents are major contributors to delay and have far-reaching consequences for safety, congestion, pollution, and the cost of travel [2]. Take Shanghai, for example, approximately 60 of traffic accidents occur in 1 day in Shanghai. Traffic congestion caused by traffic accident accounted for between 50 and 75% of total congestion in urban expressway [3, 4]. So accidents are one of the major causes of loss of time and increases in avoidable costs in transportation networks in China.

H. Li (✉) · X. Zhao · X. Zhang
College of Civil and Transportation Engineering, Hohai University, Nanjing 210098, China
e-mail: lihongwei-2008@163.com

S. Li
School of Transportation, Wuhan University of Technology, Wuhan 430063, China

H. Zhu
Wuhan Transportation Science Research Institute, Wuhan 430015, China

Timely and accurate incident detection is vital in reducing incident congestion, post-incident delay and the potential for additional incidents. Automated incident detection (AID) systems, which employ an incident detection algorithm to detect incidents from traffic data, aiming to improve the accuracy and efficiency of incident detection over a large road network.

## 2   Accidents Detection Technique

AID could be classified as loop detectors and grouped into five categories in terms of their theoretical foundation: (1) comparative algorithms; (2) statistical algorithms; (3) time series algorithms; (4) filtering/smoothing algorithms; and (5) artificial intelligence algorithms. The types of statistical incident detection algorithms are California algorithms [5], Bayesian algorithm [6], the autoregressive integrated moving average (ARIMA) model [7], DWT-LDA models [8, 9], and so on. The California algorithm has a high error rate; the Bayesian algorithm is complex; the ARIMA method is complex and has a high error rate; the DWT-LDA model has low detection rates.

This paper describes the development of proposes a comparative AID algorithm on longitudinal time series-based catastrophe theory, and statistics theory. Based on the proposed longitudinal time series of traffic parameters, automated detection algorithms for the traffic accident were designed with gain amplification principle.

## 3   Accidents Data

The data required for model development in this study were assembled from loop detectors held at urban expressway in one city in China. The length of urban expressway is 10 km, the design speed is 80 km/h, and the basic traffic capacity is 2100 pcu/h/lane. The distance between two entrances and exit ramps is 1 km approximately. There is no signal controlling along the urban expressway. For the main line of urban expressway under consideration, the detector station spacing ranged between 450 and 600 m, with an average spacing of about 500 m for the 12 detector stations. On ramps of urban expressway under consideration, the detector station average spacing is about 200 m for the 2 detector stations.

# 4  Algorithm Design

## 4.1  Time Series

According to the time axis, the time series of traffic parameters data was divided into two types, the transverse time series of traffic parameters data and the lengthways time series of traffic parameters data. The former referred to the data series of traffic parameters data ordered by the sequence of 24 h a day in a specific site; the latter referred to the data series of traffic parameters data ordered by the sequence of a week with a specific date at the same time and in the same site. These two-time series were shown in Fig. 1. In Fig. 1, the lengthways time series of traffic parameters data manifests a good stability which could be used to build the estimation method of traffic parameters in normal traffic status in order to get the estimated value of traffic parameters on each moment of every normal traffic status. The lengthways time series can overcome the disadvantage of the transverse time series. Therefore, this paper establishes AID algorithm using the historical data of the lengthways time series as the basis.

## 4.2  Catastrophe Theory

Catastrophe theory is a means for mathematically modeling the dynamic processes that underlie traffic accidents. The changing trends of traffic parameters when an incident occurs are shown in Fig. 2. From 15:05 to 15:50, traffic volume decrease sharply and speed also reduced. On the contrast, occupancy increase.

Based on the definition of abnormal traffic status, the long-term trend of traffic parameters data represented the normal status of traffic flow and its short-term processing alone represented the abnormal status of traffic flow. So long as the actual traffic status on certain moment was compared with the normal traffic status on the same moment, we could determine whether the traffic flow showed the short-term processing along, namely the abnormal status.



**Fig. 1** The two type time series of traffic volume
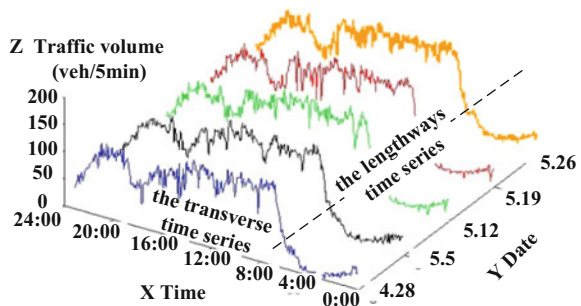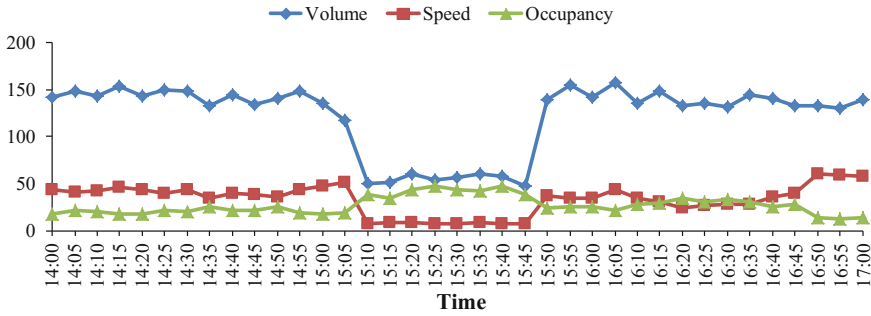
**Fig. 2** The trend of traffic parameters on the accidents

## 4.3 Expression of Normal Traffic Status

In normal traffic status, the lengthways time series of traffic parameters data had a good stability, which could be used to build the estimation method of traffic parameters in normal traffic status in order to get the estimated value of traffic parameters on each moment of every normal traffic status. Because of the good stability of the lengthways time series of traffic parameters data, we could estimate through the method of moving average, exponential smoothing, autoregressive integrated moving average, and other classical prediction methods. Considering the simplicity of calculation, this paper took the method of moving average as an example. The estimated values of traffic parameters in normal traffic status were

$$\hat{x}_{jk}^{p}(t) = \frac{1}{n} \sum_{i=j-n}^{j-1} x_{ik}^{p}(t) \qquad (1)$$

where $\hat{x}_{jk}^{p}(t)$—the estimated value of traffic parameter $x$ in normal traffic status at moment $t$ and site $p$ of day $k$ of week $j$; $x_{ik}^{p}(t)$—the historical data of traffic parameter $x$ in normal traffic status at moment $t$ and site $p$ of day $k$ of week $I$; $x$ could be traffic volume, place speed, time occupancy ratio, overall speed, etc., and $t$—the end moment of time interval for uploading data of detectors; $j$—week $j$ or the current week of the lengthways time series data; $p$—the site number of detector collecting traffic parameters data or the road section number of collecting travel time data; $k$—the specific dates in one week such as on Monday, Tuesday, Wednesday, etc., $n$—the time window scale of lengthways time series.

In order to adapt to the gradual change process of long-term trend of traffic data series and improve the accuracy of estimated values of traffic parameters in normal traffic status, it was necessary to update historical data continuously. Because it was difficult to obtain the historical data without traffic accidents throughout the day closer to the current in the actual application, this paper put forward the following updating method of historical data:

(1) Obtain the initial historical data series in accordance with the principle for selecting historical data.
(2) If the traffic flow was in normal traffic status at current moment, date and specific site, and will distance as far as the current date the historical data of the moment to delete, the historical data of the moment farthest to the current date would be deleted and the traffic flow parameters data at current moment would be included in the series; Otherwise, did not update historical data series.
(3) Repeat the second step until the updating of historical data of each moment at all sites on that very day within end of 24 h

## 4.4 Establishment Model

From the analysis of change law of traffic parameters data, we could conclude that when there was a traffic incident, the traffic flow operation status in the upstream of the incident would change abnormally with the decrease of traffic flow and speed as well as the increase of the occupancy ratio.

In order to show the difference between real-time traffic status and normal traffic flow status, the authors put forward the concept of traffic status variability index.

The studies on automated detection algorithms for traffic incidents showed that the more use of traffic parameters, better detection effect of incidents. Therefore, the traffic status variability index should contain all possible obtained traffic parameters with time and space comparability. Taking the data collected by induction coils as an example, the authors designed traffic status variability index according to the gain amplification principle as shown in Eq. (2).

$$I^p(t) = \frac{\frac{\hat{q}^p(t) \cdot \hat{v}^p(t)}{\hat{o}^p(t) + 0.001}}{\frac{q^p(t) \cdot v^p(t)}{o^p(t) + 0.001}} \qquad (2)$$

where $I^p(t)$—the traffic status variability index at moment $t$ and site $p$; $q^p(t)$—the measured traffic volume at moment $t$ and site $p$; $v^p(t)$—the measured traffic speed at moment $t$ and site $p$; $o^p(t)$—the measured occupancy ratio at moment $t$ and site $p$; $\hat{q}^p(t)$—the traffic volume of normal traffic status at moment $t$ and site $p$ based on the lengthways time series; $\hat{v}^p(t)$—the traffic speed of normal traffic status at moment $t$ and site $p$ based on the lengthways time series; $\hat{o}^p(t)$—the occupancy ratio of normal traffic status at moment $t$ and site $p$ based on the lengthways time series.

The traffic flow was in abnormal status, the traffic status variability index would change obviously as shown in Fig. 3. On the basis of the estimated values of traffic parameters in normal traffic status and real-time traffic parameters. We should calculate the traffic status variability index at the current moment, and compare the index with specific threshold value. After that we could judge whether the traffic flow at this site was in an abnormal status. Based on this, in order to reduce the false alarm rate, we should judge the abnormal traffic status through many times for confirmation.

**Fig. 3** The results of DR
and FAR on different
threshed
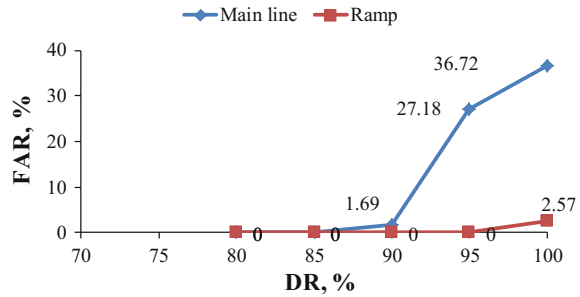


Finally, the discrimination algorithm was used to determine the location of traffic incidents. Based on the basic thoughts, the process of LST-AID algorithm was:

(1)  Acquire the historical data of lengthways times series of each traffic parameter, and estimate these parameters in the normal traffic status with specific methods as seen in 2.2;
(2)  Get the real-time measured data of traffic flow parameters, calculate the traffic status variability index at current moment, and determine whether the abnormal traffic status occurs;
(3)  In order to reduce false alarm rate, results of the detection of abnormal traffic status need to be confirmed many times with different methods in various situations;
(4)  Determine the location of traffic incidents with the specific discrimination equation as seen in Eq. (3).

$$u^p(t) = \begin{cases} 1 \cdots z^p(t) = 1 \cdot \text{and} \cdot z^{p-1}(t) = 0 \\ 0 \cdots \text{other} \end{cases} \tag{3}$$

where: $u^p(t)$—whether the traffic incidents in the downstream road section occurred at moment $t$ and site $p$, 1 represented yes and 0 no; $z^p(t)$—whether the data of detectors was in abnormal traffic status, 1 represented yes and 0 no.

## 4.5  Decision Thresholds

When the traffic status variability exceeded a certain threshold, we may think that the abnormal traffic status happened in that site and at that time under the condition of the design of a suitable method to express the normal traffic status and the traffic status variability measurement index.

At present, a majority of researchers choose DR-FAR curve for a decision threshold (DTs). Draw DR-FAR curve on different thresholds, chooses a reasonable threshold according to practice demand of the DR and FAR. Generally, it is difficult

to approach a threshold which makes DR and FAR achieves optimal. Therefore, improve DR under the premise of the certain FAR.

## 5 Data Analysis

### 5.1 Comparing Threshold

Frequency histogram and cumulative distribution curves for variability index at the mainline and ramps are compared in Fig. 4. As shown in Fig. 4, cumulative curves for variability index at the ramp line are to the left of the curves for variability index at the main line, indicating the fact that the main line is effective in detecting accidents. The results of DR and FAR on different threshed are shown in Fig. 3. The effect of the model using on the ramp is better than the main line.

### 5.2 Variability Index Trench

In this section, the variability index (I) trends on the accidents will be analyzed. Figure 4 is the variability index (I) trends which accidents occur on low volume state (0:30–1:15), sharply decreasing state (5:55–6:00), peak volume state (15:05–15:50), slow decreasing state (20:20–20:55).

The results can be obtained as follows,

(1)  When traffic flow was in abnormal status, the traffic status variability index would change obviously as shown in Fig. 4.
(2)  No matter what traffic flow stats, the model can detect accident accurately.
(3)  The value of the variability index is not influenced by traffic flow stats, but by the changing of the traffic parameters before and after accidents.
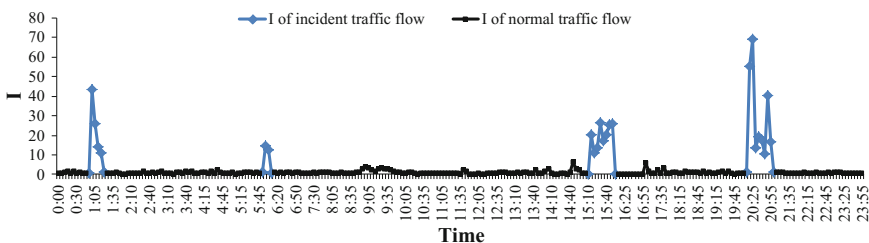


**Fig. 4**  Variability index trench on the accidents

# 6   Conclusion

Existing AID algorithms are established on the transverse time series. From the aspect of the transverse time series, the main problems existed in previous research are the fluctuations of the volume are largest. The result is higher false alarm rate, longer testing time, and lower robustness. Besides, it was difficult to detect traffic incidents when the loss data are more. From Fig. 1, the lengthways time series of traffic parameters data manifests a good stability which could be used to build the estimation method of traffic parameters in normal traffic status in order to get the estimated value of traffic parameters on each moment of every normal traffic status. The lengthways time series can overcome the disadvantage of the transverse time series. Therefore, this paper establishes AID algorithm using the historical data of the lengthways time series as the basis.

Based on the definition of abnormal traffic status, the long-term trend of traffic parameters data represented the normal status of traffic flow and its short-term processing along represented the abnormal status of traffic flow. So long as the actual traffic status on certain moment was compared with the normal traffic status on the same moment, we could determine whether the traffic flow showed the short-term processing along, namely the abnormal status.

From the analysis of change law of traffic parameters data, we could conclude that when there was a traffic incident, the traffic flow operation status in the upstream of the incident would change abnormally with the decrease of traffic flow and speed as well as the increase of the occupancy ratio. Propose a comparative AID algorithm on longitudinal time series-based catastrophe theory, and statistics theory.

The advantages can be found from variability index trench on the accidents. First, when traffic flow was in abnormal status, the traffic status variability index would change obviously. Second, no matter what traffic flow stats, the model can detect accident accurately. Third, the value of variability index is not influenced by traffic flow stats, but by the changing of the traffic parameters before and after accidents.

# References

1. Giuliano G (1989) Incident characteristics, frequency, and duration on a high volume urban freeway. Transportation research board, national research council. Transp Res Part A 23(5):387–396
2. Mahmassani, HS, Haas C, Zhou S, Peterman J (1998) "Evaluation of incident detection methodologies." Research Report 1795-1. Center for Transportation Research, University of Texas at Austin, Austin, TX
3. Ouyang P, Zhang X, Sun L (2008) Traffic incident duration prediction grounded on bayesian decision method based tree algorithm. J Tongji Univ (Natural Science) 36(3):319–324

4. Ma DF, Wang DH, Bie YM, Jin S (2016) Recognition of bottlenecks on urban roads using queue detector data. KSCE J Civ Eng 20(7):2955–2964
5. Payne HJ, Helfenbein ED, Knobel HC (1976) Development and testing of incident detection algorithms, vol 2: research methodology and results. Report No. FHWA-RD-76–20, Federal Highway Administration
6. Zhang K, Taylor MAP (2006) Towards universal freeway incident detection algorithms. Transp Res C 14:68–80
7. Ahmed MS, Cook AR (1977) Analysis of freeway traffic time-series data using Box-Jenkins techniques. Transp Res Rec 722:1–9
8. Jenkins techniques." Transportation Research Record, No. 722, TRB, National Research Council, 1–9
9. Teng H, Qi Y (2003) Application of wavelet technique to freeway incident detection. Transp Res Part C: Emerg Technol 11(3):289–308

# Application of Docker Container in Intelligent Traffic Cloud

**Hong Zhao and Ze-yu Han**

**Abstract** In intelligent traffic system based on traditional cloud computing technology, the virtual machine is used to provide application services. However, it has quite a few disadvantages, such as low resource utilization, high management complexity, and complicated migration processes because an entire operating system needs to be installed in the virtual machine. Docker, a lightweight operating system-level virtual technology, is introduced to construct the PaaS (Platform as a Service) layer that as the container cloud platform supports the applications of SaaS (Software as a Service) layer and provides application resiliency in application-centric mode through the unified service set. On the test cloud platform, the same applications are deployed in the virtual machine and the Docker, respectively, the utilization of CPU and memory, the Docker lived in is only 10–15% compared to the virtual machine, and the time to migrate a resource is only 8–10% compared to the virtual machine. Therefore, the Docker is more suitable to establish intelligent traffic cloud.

As is known to all of us, human social production, life, and economic development have been inseparable from the traffic. What's more, people have a strong dependence on traffic and put forward more demand as well with the rapid development of the economy and the progress of science and technology. The United States, Japan, and Europe as the pioneers began to use information technology to solve the problem in the 1990s. In the existing traffic system, it forms an advanced three-dimensional transport system based on information technology, which is intelligent traffic system [1].

Connections between vehicles, roads, and persons were enhanced by ITS (Intelligent Traffic System) through the use of information, communication, computer and other technologies on the more perfect transportation infrastructure. More importantly, ITS achieves the goal of improving the operational efficiency and reducing

H. Zhao (✉) · Z. Han
School of Computer and Communication, Lanzhou University of Technology, Lanzhou 730050, China
e-mail: 594286500@qq.com

**Fig. 1** China's ITS system
framework
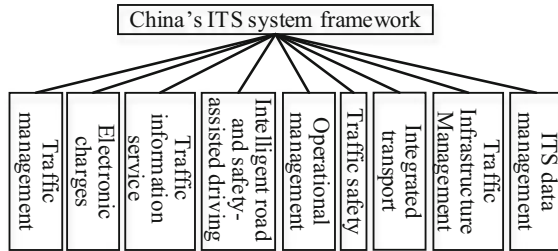


the accident and the pollution through enhancing the orderliness and control of the
operation of the traffic system to build an efficient, convenient, safe, environment-
friendly and comfortable integrated transport system [2]. In the mid-1990s, China's
ITS began to develop rapidly and "The framework of China's ITS" (second edition)
was completed in 2005, which has made substantial progress in standardization, sys-
tematization, practicality, and so on, and the current framework of ITS in China has
been determined [1], as shown in Fig. 1.

The advanced computer technology such as cloud computing and internet of
things is introduced in the construction of traffic management information system
with the development of information technology. So that the sharing of resources,
data integration, precise analysis, and intelligent control can be developed, which
formed an intelligent traffic cloud [3, 4]. But this type of traditional intelligent traffic
cloud has quite a few disadvantages.

Low resource utilization. Application services are supported by using a virtual
machine in traditional intelligent traffic cloud, which requires installing the operating
system before deploying the application services. However, lots of memory and CPU
resources will be consumed by the operating system that results in low performance.

High management and maintenance cost. Different deployment environment is
required by the difference of the application services. In most cases, the new appli-
cation's deployment environment needs to be reinstalled to deploy a new applica-
tion service each time, so the application service deployment environment and the
application itself cannot be packaged as a whole module for effectively reuse and
management.

Complex migration process. Operating system and application's deployment envi-
ronment must be reinstalled for the overall migration of the application service
when an application service needs to be migrated from one resource pool to another
resource pool.

The architecture of intelligent traffic cloud based on a virtual machine was pro-
posed by MEI Duo in his PhD thesis [3]. Storage services of traffic data are provided
by the IaaS layer that integrates all the traffic information resources together to form
a large traffic data repository. Parallel computing and large data analysis of the cluster
services and development platform of the traffic application service is provided by
the PaaS layer thought virtual machines to deploy, which takes up a lot of resources.
At the same time, the complexity of management is caused by massive data man-

agement and cluster management. All services for all subsystems, contained in an intelligent traffic system, are provided by the SaaS layer thought virtual machines to deploy, which is not only low resource utilization, difficult migration but also difficult to manage.

# 1 Introduction of Docker

Container technology is a way of sharing server resources [5]. What's more, the great flexibility for system administrators in the processes of building operating system instances on demand can be provided by container technology [6]. The majority of the current container is based on the Linux kernel [5]. The operating system needs to be added as a supportive environment in order to run the different environment of the app. So that the operating system layer is streamlined to further facilitate management and higher operational efficiencies. The Linux system is divided into two parts, one is the uniform kernel, and the other is the diverse release environment, such as CentOS, Ubuntu, Red Hat, and so on, which are the release environment that issues their own management execution procedures on the periphery of the same Linux kernel. At the same time, the container technology was born because of a streamlined solution that multiple release environments share the same kernel function is provided. In general, the same kernel was shared by the multiple release environments, and quarantined running space for the application is provided by the container, that is, each container contains an exclusive full user environment space and the operating environment of other containers do not be affected for changing within a container.

The Docker container as the basic unit for resource partitioning and scheduling used by Docker and the entire software runtime environment is encapsulated. It is a platform designed for developers and system administrators to build, publish, and run distributed application [6], and which is a cross-platform, portable and easy-to-use container solution. Developer's application and package dependencies of the application can be packaged into a portable container and is published into any popular Linux machine with the Docker engine. The sandbox technology is completely used by containers, which do not have any interface with each other and little performance overhead and easily running in machines and data centers. Most importantly, the application component level's "one package, run anywhere" is achieved without relying on any language, framework and operating system [7].

Consistent and standard application environment is ensured by Docker in the application's lifecycle. Environmental resource management is quite complex from the development environment to the application development to the application deployment migrations and from various operating system to various middleware to various applications, the process of deploying multiple application instances can be simplified by using Docker.

In Linux container, CGroup is used for resource allocation, the namespace is used for resource isolation, and runs a container only needs the operating system's release environment, shares the same host operating system kernel [8]. Compared to KVM

and other virtualization technology, Docker is more flexible and fast. Simultaneously, provisioning system of the virtual machine is in the minute level, and the container is in the second level.

Docker, based on the original Linux container, sets a series of standardized configuration methods to package application and dependent runtime environment. The concept of "one encapsulation, running everywhere" is really realized, which greatly improves the container cross-platform.

Fortunately, an image repository, organized and managed in a form similar to GitHub, is built by Docker official, which has accumulated thousands of images. Additionally, because of Docker's cross-platform compatibility, it is equivalent to provide users with an application store so that everyone can download the microservice components freely [9], which provides developers with great convenience, and Docker also supports private image repository.

## 2 Application of Docker Technology in Intelligent Traffic Cloud

### 2.1 The Basic System Framework of Intelligent Traffic Cloud Based on Docker Technology

Because of the lack of intelligent traffic cloud based on virtual machine, the architecture of intelligent traffic cloud based on Docker is designed according to ITS architecture in China, as shown in Fig. 2. IaaS (Infrastructure as a Service) layer is resource-centric to manage the entire data center resource that provides resources in a flexible manner. However, PaaS layer, designed a Docker cloud platform, enables itself to be application-centric in the data center to provide application resiliency to support the applications of SaaS layer. Therefore, various type of container pools are included in PaaS layer, such as the APP container pool (AC1 … ACn), the tool container pool (TC1 … TCn) and the data storage container pool (DC1 … DCn). What's more, Private Repository provides free image resource to support the platform and Docker Hub provides a wide base of the image to support the platform. When creating applications, all kinds of the image can be directly obtained from the container pool to complete the application of the various levels of packaging. While in the SaaS layer, the official images and private images are used to encapsulate various applications to provide a range of collection services to end users. The information collection system of the Convergence Layer, which is distributed throughout the country, is deployed locally through the Docker. The traffic information is collected for simple processing and sent to the cloud for further data processing and analysis, which provides big data analysis and supports for the intelligent transportation system.

The Docker image is hierarchical to the application's encapsulation [10]. The container is based on the Linux operating system in most cases, and a Docker software
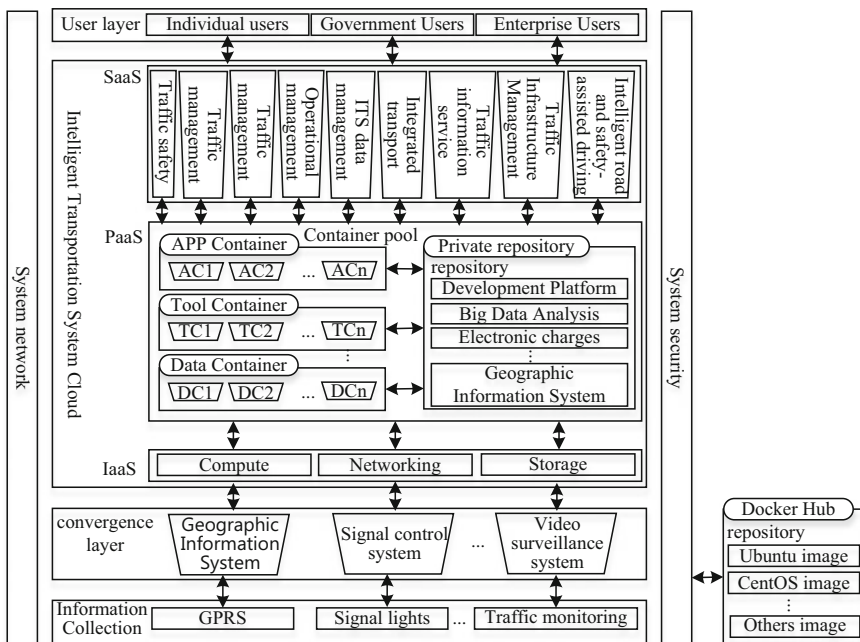
**Fig. 2** Architecture of intelligent traffic cloud based on Docker

is deployed in it [10]. The operating system does not need installed to run a variety of containers with Docker, only installed a variety of Applications. In addition, when application is packaged with Docker, the application itself and its dependent packages are packaged together so that the container application is portable and can be run in a different Linux environment without needing to re-install dependent environment. The SaaS layer and convergence layer's hierarchical structure of Docker application image is shown in Fig. 3. The bottom of the application container is the application of the basic environment for running. The Ubuntu distribution environment is shown in Fig. 3, which obtained from the Docker hub; above it, packaging the database container image (DC), The MySQL database is shown in Fig. 3, which provides database support for the Web application, and it can also be configured for external database; above it, packaging the application container image (APP), the Java-based web applications is shown in Fig. 3; and a tool container (TC), the Tomcat, as a lightweight WEB application server, is shown in Fig. 3, which provides support for running of Web applications. Through this hierarchical package, the application itself and its dependencies are packaged together to form a complete application image that uploads to the private image repository, which deployed on the SaaS layer to provide a unified service interface. In the Convergence Layer, the application will run up only need to install the Docker engine and download the application image through the network.

**Fig. 3** Image hierarchical structure of Docker application
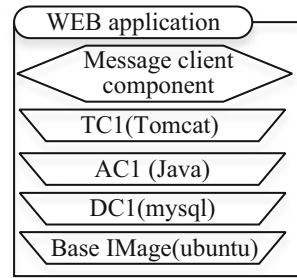


## 2.2 Docker Platform Experiment

The performance test is carried out on two nodes cloud computing platform, it uses two IBM x3650 M3 server computers, one as a controller node, and the other as a compute node. The operating system uses Ubuntu server 14.04. The specific configuration is as follow:

CPU: Intel(R) Xeon 5130 CPU @ 2.33 GHz
RAM: 8GiB DDR2 Synchronous 800 MHz
Disk: ST133DM002-1ER14C x4 (133 GB 7200 r/min)

OpenStack(Mitaka) cloud platform is used by the system as the experimental version, and multi-node deployment of devstack is adopted.

LINPACK is used as the mainstream testing tool for CPU performance testing. It plays an important role in fairly, completely and systematically evaluating a machine's floating-point performance. Running the runme_xeon64 test script to calculate the dense linear algebraic question from 1,000 to 45,000 levels, the number of tests per order is 4 times to 1 times decreasing, The test results of Native(Host OS), Docker and KVM (virtual machine) in CPU performance are given in Table 1. Relative to the physical, Docker has little loss of computing power, while the virtual has a very significant loss. For virtual machines, since a virtual hardware layer is added, applications running on the virtual machine are running on the hypervisor virtual CPU when performing numerical calculations, so about 50% of the computing power is lost.

Use IBM test tools to copy/scale/add/triad four tests on memory, the test result of Memory bandwidth performance is shown as Table 2, Docker and Native memory bandwidth performance is basically the same, but KVM and others slightly different. Because of the read and write memory address is continuous, high volume, the kernel will be optimized for this operation, and the number of virtual addresses to physical addresses is relatively small.

Form Table 3, a more obvious performance gap can be seen between the Docker and the KVM in Memory random access performance, the Docker is significantly better than the KVM, almost double.

**Table 1** CPU performance test

| Size | LDA | Align | Native(Gflops) | Docker(Gflops) | KVM(Gflops) |
|------|------|-------|----------------|----------------|-------------|
| 1000 | 1000 | 4 | 9.3437 | 9.0949 | 3.7868 |
| 2000 | 2000 | 4 | 27.1717 | 23.3068 | 11.0375 |
| 5000 | 5008 | 4 | 44.2333 | 39.2364 | 19.1695 |
| 10000 | 10003 | 4 | 44.0367 | 54.2655 | 24.2219 |
| 15000 | 15006 | 4 | 50.0541 | 48.3416 | 27.3552 |
| 18000 | 18008 | 4 | 56.7938 | 52.0565 | 21.4054 |
| 20000 | 20026 | 4 | 60.0415 | 68.2376 | 28.0256 |
| 22000 | 22048 | 4 | 61.4552 | 69.0096 | 29.0231 |
| 25000 | 25003 | 4 | 64.2644 | 64.5307 | 30.3508 |
| 26000 | 26004 | 4 | 62.4321 | 64.6455 | 30.3265 |
| 27000 | 27000 | 4 | 63.5444 | 63.7645 | 30.4153 |
| 30000 | 30007 | 1 | 64.4905 | 65.1906 | 30.4954 |
| 35000 | 35000 | 1 | 63.4128 | 63.1944 | 30.6245 |
| 40000 | 40000 | 1 | 64.1271 | 65.1352 | 30.6256 |
| 45000 | 45000 | 1 | 65.3508 | 65.3176 | 30.6345 |

**Table 2** Memory bandwidth performance test

| Function | Native(GB/s) | Docker(GB/s) | KVM(GB/s) |
|----------|--------------|--------------|-----------|
| Copy | 7.5374 | 7.4384 | 7.0751 |
| Scale | 7.6467 | 7.5441 | 7.1243 |
| Add | 9.1267 | 9.0176 | 8.1171 |
| Triad | 9.1163 | 9.0548 | 8.3338 |

**Table 3** Memory random access test

| Native(GUP/s) | Docker(GUP/s) | KVM(GUP/s) |
|---------------|---------------|------------|
| 0.124146598 | 0.131209286 | 0.192567652 |
| 0.127914879 | 0.137854575 | 0.192675471 |
| 0.128253397 | 0.144492456 | 0.204622258 |
| 0.125556543 | 0.133854656 | 0.196874828 |

On the OpenStack compute node, the same web application, based on MySQL + java + tomcat, is deployed through the virtual machine (single core, 1 GB memory, 8 GB hard disk) and Docker respectively. Its CPU usage as shown in Figs. 5 and 6, the node 4 Dockers deployed is much smaller than the node 4 virtual machines deployed in resource utilization, and the Docker lived in is only 10–15% compared to the virtual machine lived in.
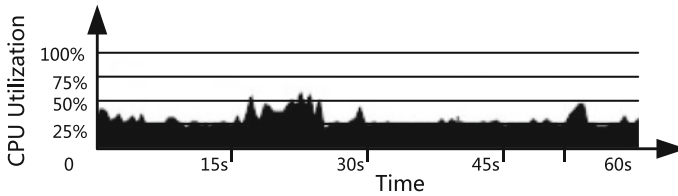
**Fig. 5** CPU utilization for compute node that deploy 4 virtual machines
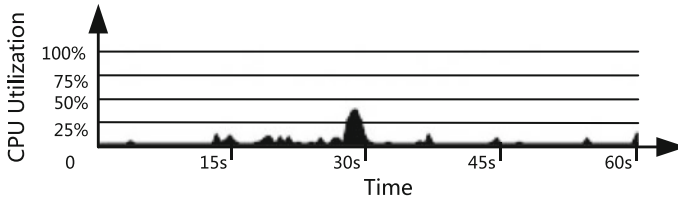


**Fig. 6** CPU utilization for compute node that deploy 4 Dockers

## 3 Conclusions

The intelligent traffic cloud is an open platform that should be integrated, advanced, secure, automated, easy-to-expand and serves all traffic participants and traffic management. Moreover, intelligent traffic cloud based on Docker technology not only can reduce the cost of the intelligent traffic cloud data center hardware and software, but also the intelligent transportation system can be innovated on the basis of information fusion. Most importantly, it serves the vast traffic participants with a more open attitude and can attract more developers. In this scheme, the different types of Development Platform Container, such as Windows and Linux and other development platforms, is used to carry out the development of traffic cloud services by different developers. And, government developers may have specific resource access rights, such as traffic lights control, electronic charges and other data, then they can apply for Development Platform Containers that are government application development and have resource access restrictions; Developers of different enterprises visit the traffic data is quite different, it can apply for Development Platform Container that is suited their industry and have resource access restrictions; Individual developers, they can also apply for Development Platform Container that has the corresponding data access restrictions. More enterprises and individual participate in traffic cloud construction in this way, and it is rather than the government's special investment.

# References

1. Na Zhao, Jiabin Yuan, Han Xu (2014) Survey on intelligent transportation system. Comput Sci 41(11):7–11
2. Ke Zhang, Tongyan Qi (2005) The latest achievements of Chinese national ITS architecture. J Transp Syst Eng Inf Technol 5(5):6–11
3. Mei D (2015) Research on model for traffic bottleneck guidance coordinated with traffic control based on cloud computing. Jilin University, 2015
4. Tang B (2015) Intelligent transportation system based on cloud computing. Nanjing University of Posts and Telecommunications, 2015
5. Docker Inc. What is Docker [EB/OL]. https://www.docker.com/what-docker, 2017,4,21
6. Boettiger C (2015) An introduction to Docker for reproducible research. ACM SIGOPS Operating Syst Rev 49(1):71–79
7. Zhejiang University Software Engineering Lab. Docker and Kubernetes under the Hood. Posts & Telecom Press, 2015
8. Bernstein D (2015) Containers and cloud: from LXC to Docker to Kubernetes. IEEE Cloud Comput 1(3):81–84
9. Boettiger C (2015) An introduction to Docker for reproducible research [J]. ACM SIGOPS Operating Syst Rev 49(1):71–79
10. Guan X, Wan X, Choi BY et al (2017) Application oriented dynamic resource allocation for data centers using docker containers. IEEE Commun Lett 21(3):504–507

# Research on the Evaluation Focus of Bus Drivers' Safety Capability

**Hua-cai Xian, Weichao Chen, Meng Zhang, Qun Zhou and Dong-mei Yang**

**Abstract** Bus drivers have been a great concern because of the particularity of their work. Based on the survey data of 973 drivers in Jinan Second Bus Company, this paper analyzes the driver's basic situation, personality factors, safe driving attitude, safe driving behavior, job satisfaction, and job burnout. And at the same time, this paper analyzes the differences in safety attitude, safety behavior, and personality characteristics of drivers with different safety types, and establishes the regression model with the driver safety type as the result variable, the safety behavior and the security attitude as the forecast variable. Through the prediction of the regression model, the driver is divided into different security types, so as to guide the safety-related work.

**Keywords** Driving behavior · Bus driver · Driving safety · Evaluation

## 1 Introduction

Urban public transport is one of the most effective ways to solve urban traffic problems. In recent years, the Chinese government has introduced a series of policies to encourage the development of public transport, so as to promote public transport priority. The proportion of bus passenger sharing rate in a variety of modes of transport remains a continuous improvement, and urban residents are increasingly inseparable from public transport. At the same time, public transport, as a city mode of transport adapted to sustainable development, must provide urban residents safe, fast, and

H. Xian (✉) · M. Zhang
Transportation and Logistics Engineering College, Shandong Jiaotong University, Jinan, Shandong 250023, China
e-mail: xianhc11@163.com

W. Chen · Q. Zhou
Jinan Second Bus Company, Jinan, Shandong 250023, China

D. Yang
Department of Dongfeng Commercial Vehicle Technical Center, Wuhan, China

comfortable travel conditions. Bus, as an important carrier of urban passenger transport, plays an increasingly important role in today's public transport. Although the bus shares some advantages such as its relatively slow speed, relatively short driving distance, it has so many potential dangers. What is worse, at the same time, because of the number of bus passengers, once in the event of traffic accidents, passengers would collide in the compartment, crowded, so they even prone to death tragedies [1, 2]. It not only does harm to the passengers but also cause a bad social impact. To this end, to take effective measures to prevent the occurrence of bus accidents becomes the first bus operation to consider in dealing with this issue.

At present, researches on driver safety assessment have been studied. In the year of 2016, Dr. Li Yang analyzed the safety evaluation index of the multi-attribute driving behavior of driver's basic information, visual perception, decision-making reaction and psychological bear ability, vehicle control and running status. He used TOPSISI to establish driving Behavioral Security Evaluation Model [3]. In 2015, Lisheng Jin used fuzzy network analysis method to study the driver's safety under the condition of multi-task driving, and established the driver's multi-task driving safety evaluation model [4, 5]. In 2013, Dr. Yang Pengfei studied the key technologies of safety assessment, such as safety awareness, potential hazard prediction ability, driving ability and stress responsibility, and then established the corresponding evaluation model [6]. In 2008, the scholars Versdnmr and Hurts based on the theory of planned behavior and studied the cause of the accident theory, and then concluded that the accident can directly result from the unsafe behavior. And in the end, they created the establishment of a model for the study of driver safety behavior [7]. In 2007, Zhang Yujing, a researcher at Beijing Jiao Tong University, studied the safety awareness of the driver of the taxi [8]. According to the four aspects, the safety awareness of the driver of the taxi was analyzed, and the scale of psychological measurement was used to develop the safety awareness measure table.

Based on the above analysis, there are many researches on the safety evaluation of driver's driving at home and abroad, but there are few studies on the driving safety of the driver of the bus. So this article aims to accurately evaluate the driving safety of the bus driver, which based on the questionnaire analysis. It aims to explore the influence factors and deep-seated reasons for affecting the ability of the bus drivers, and then extract the driver's driving safety tendency evaluation index to create the Establishment of Bus Driver Safety Evaluation Model. Based on the analysis results, it puts forward the suggestions of safety promotion to the driver, and then improves the safety capability of the bus driver, and provides theoretical and technical support for improving and promoting the safety management of road transportation.

# 2 Experimental Methods

## 2.1 Questionnaire Design

There are six parts of the questionnaire and the questionnaire contents are shown in Table 1.

**Table 1** The questionnaire design

| Number | Questionnaire | Content |
|---|---|---|
| 1 | The driver's basic situation questionnaire | Collect the demographic variable basic information of drivers: name, sex, age, driving experience, engaged in bus driver time, education, marital status, number of children, appraise the family economic conditions |
| 2 | Cartel 16PF personality questionnaire [9] | Collect the pilot personality traits of drivers: stability respectively is stability, persistence, anxiety, self-discipline, and tension, persistence, anxiety, autorhythmicity, tension |
| 3 | The driver's safety driving attitude questionnaire [10] | Collect the safe driving attitude data of drivers: including the score of Safe driving, Fatigue driving, drinking drive, The traffic rules, furious driving, life, and the total score of attitude towards safe driving |
| 4 | The driver's safety driving behavior questionnaire [11] | Collect the safe driving behavior data of drivers:including the score of Impulsive behavior, "Speeding and intentional misconduct", "mis-action", and the total score of driver safety |
| 5 | The driver's job satisfaction questionnaire | Collect the job satisfaction of drivers: including the score of Intrinsic satisfaction, External satisfaction, general satisfaction and the total score of job satisfaction |
| 6 | The driver's job burnout questionnaire [12] | Collect the job burnout of drivers:including the score of "Emotional exhaustion", dehumanization", "Personal accomplishment" and the total score of job burnout |

## 2.2 Survey Object

The author of this study regarded 973 bus drivers in Jinan Bus Company as the object of investigation. By consulting the two branches of the Ministry of Security data, the drivers participated in the investigation were classified as "had security incidents and violations", "had security complaints", "there have been no safety related issues" are these three categories. Although the drivers did not occur accident or had any illegal behavior, the passengers complained that there may be some security risks, which belongs to less safe type; And last one is the case of "no security-related issues", that is the drivers have been no security incidents and violations and there has not been a category of security complaints, which belongs to the more secure type. In this study, "security incidents and violations occurred" was named "1" category, "had a security complaint" was named "2" class, "no security-related issues" was named "3". The higher the number, the higher the level of security standards, and the "1" and "2" class are defined as the accident-prone class driver.

## 2.3 Analytical Methods

In this study, SPSS 19.0 was used to analyze the relationship between driver's safety and driving safety, and the basic information of the driver was described. The author regards the correlation analysis of the characteristics, the one-way ANOVA, the regression analysis of the driver's safety type as the result variable, and the safe driving behavior and the safe driving attitude as the predictive variable.

## 3 Bus Driver Driving Safety Assessment

## 3.1 Questionnaire Recovery

The author issued questionnaire a total number of 973, and they all recollected, so the recovery rate is 100%. Deleting those questionnaire whose data seriously missing, or the answer not serious and a high risk of lying (polygraph scores high) of the questionnaire about 180, the questionnaire efficiency is 81.2%. Among them, there are 104 women, accounting for 13.1%; 689 men, accounting for 86.9%. The average age of them is 34.0 years, the standard deviation is 6.7; the average driving age is 18 years, and the standard deviation of 122.5. The questionnaire is divided into two parts, of which 600 are used to establish the driver safety evaluation model, and the other 193 for the model validation. Two samples of the three categories of drivers were extracted according to the corresponding proportion to ensure the true validity of the sample.

**Table 2** Different safety types of security behavior and security attitude score

| Dimension | Frequency | Percentage | Cumulative Percent | Mean value of security behavior | Mean value of security attitude |
|---|---|---|---|---|---|
| Having security incident | 150 | 18.9 | 18.9 | $29.50 \pm 6.75$ | $90.78 \pm 14.44$ |
| Having safety complaints | 217 | 27.4 | 46.3 | $26.55 \pm 8.29$ | $100.24 \pm 17.65$ |
| Having no safety problems | 426 | 53.7 | 100.0 | $23.99 \pm 7.53$ | $105.59 \pm 22.43$ |

## *3.2 Driver Safety Assessment*

### 3.2.1 Description of the Security Type

Different safety types of security behavior and security attitude score are shown in Table 2.

### 3.2.2 Correlation Analysis

The correlation analysis is a statistical method to study the correlation between random variables. The results of this study are shown in Table 3. The numerical values represent the correlation coefficients of the two variables. The larger the absolute value of the correlation coefficient, the greater the correlation; the positive value represents the positive correlation between the two variables, that is, if there is a growth of the other variable, the other side of the variable also shows a growth trend; negative value represents a negative correlation between the two variables. When one variable grows, the other variable shows a downward trend. The "**" at the top right of the correlation coefficient represents a significant level at 0.01 level, and "*" represents a significant level at the 0.05 level, and no sign indicates that the statistical significance was not significant.

### 3.2.3 Analysis of Variance

The variance analysis is a significant test for the difference in the mean of two or more samples.

**Table 3** Correlation analysis of safety type and safety behavior, safety attitude and safety type, safety attitude, safety behavior and personality traits, job satisfaction, and job burnout

| Dimension | Safety type | Anxiety | Tonicity | Stability | Perseverance | Automaticity | Job satisfaction | Occupational burnout |
|---|---|---|---|---|---|---|---|---|
| Safety type | – | $-0.42^{**}$ | $-0.57^{**}$ | $0.46^{**}$ | $0.45^{**}$ | $0.45^{**}$ | $0.17^{**}$ | $-0.08^{*}$ |
| Safety behavior | $-0.48^{**}$ | $0.15^{**}$ | $0.27^{**}$ | $-0.27^{**}$ | $-0.29^{**}$ | $-0.22^{**}$ | $-0.18^{**}$ | $0.20^{**}$ |
| Safety attitude | $0.27^{**}$ | $-0.11^{**}$ | $-0.05$ | $0.11^{**}$ | $0.28^{**}$ | $0.12^{**}$ | $0.09^{**}$ | $0.05$ |

**Table 4** Analysis of the variance of security behavior and security attitude of different security types

|  | Having security incident | | Having safety complaints | | Having no safety problems | | F | P |
|---|---|---|---|---|---|---|---|---|
|  | M | SD | M | SD | M | SD |  |  |
| Security behavior | 29.50 | 6.75 | 26.55 | 8.30 | 20.74 | 5.58 | 120.22 | 0.00 |
| Security attitude | 90.78 | 14.44 | 100.24 | 17.65 | 105.60 | 22.43 | 31.24 | 0.00 |

**Table 5** Analysis of the variance of personality traits of different security types

|  | Having security incident | | Having safety complaints | | Having no safety problems | | F | P |
|---|---|---|---|---|---|---|---|---|
|  | M | SD | M | SD | M | SD |  |  |
| Anxiety | 5.05 | 1.41 | 3.71 | 1.19 | 3.16 | 1.65 | 91.63 | 0.00 |
| Tonicity | 5.31 | 1.18 | 3.96 | 1.25 | 2.8 | 1.53 | 191.03 | 0.00 |
| Stability | 2.08 | 0.95 | 3.61 | 1.41 | 4.37 | 1.86 | 113.55 | 0.00 |
| Perseverance | 2.09 | 1 | 4.12 | 0.91 | 4.65 | 2.24 | 117.51 | 0.00 |
| Automaticity | 2.02 | 1.08 | 3.87 | 1 | 4.4 | 2.08 | 111.12 | 0.00 |

## Analysis of Variance of Safety Type Impact on Safety Behavior and Security Attitude

Table 4 presents a significant difference in group safety behavior and security attitudes with different types of safety.

## Analysis of Variance of Personality Type of Safety Type

There are significant differences in the five personality traits of groups, showing different types of safety. Table 5 is the analysis of variance of personality traits of different security types.

## Analysis of Variance for Job Satisfaction and Occupational Burnout of Different Security Types

Table 6 presents that there are significant differences among different security types and the level of occupational burnout is edge-correlated.

**Table 6** Analysis of variance for job satisfaction and occupational burnout of different security types

|  | Having security incident | | Having safety complaints | | Having no safety problems | | F | P |
|---|---|---|---|---|---|---|---|---|
|  | M | SD | M | SD | M | SD |  |  |
| Job satisfaction | 76.23 | 17.08 | 72.22 | 16.81 | 84.25 | 27.15 | 21.46 | 0.00 |
| Occupational burnout | 47.08 | 14.85 | 46.48 | 15.11 | 44.26 | 15.71 | 2.61 | 0.07 |

**Table 7** Eigenvalues, variance contribution rates and cumulative contribution rates of principal components

| Component | Eigenvalue | Variance contribution rate (%) | Cumulative contribution rate (%) |
|---|---|---|---|
| F1 | 2.285 | 32.640 | 32.640 |
| F2 | 1.145 | 16.360 | 49.000 |
| F3 | 0.877 | 12.533 | 61.533 |
| F4 | 0.840 | 12.000 | 73.533 |
| F5 | 0.714 | 10.197 | 83.730 |
| F6 | 0.603 | 8.610 | 92.340 |
| F7 | 0.536 | 7.660 | 100.000 |

### 3.2.4 Bus Driver Safety Prediction

Through the above analysis, we select seven measures which include Tonicity $x_1$, Stability $x_2$, Security Behavior $x_3$, Perseverance $x_4$, Anxiety $x_5$, Automaticity $x_6$, and Security Attitude $x_7$ to build our Bus Driver Safety Prediction Model. The principal component analysis (PCA) is sensitive to the relative scaling of the original variables. So the method of PCA in SPSS11.0 is selected to build the Bus Driver Safety Prediction Model. The initial eigenvalues, variance contribution rates, and cumulative contribution rates are shown in Table 7.

As can be seen from Table 7, the cumulative contribution rate of the first five principal components amounts to 83.730%, covering 83.730% of all information and meeting the requirement of cumulative contribution rate more than 80%. So, five principal components are correctly chosen in the study. According to the variance contribution rate, the weights of seven measures are certain and we build the Bus Driver Safety Prediction Model is shown as the formula.

$$F = -0.18\chi_1 + 0.21\chi_2 - 0.21\chi_3 + 0.49\chi_4 - 0.29\chi_5 + 0.34\chi_6 + 0.63\chi_7$$

Clustering Analysis is selected to divide the safety level. The driving safety high level, average level, and low level are separately less than 51, among 51–66 and higher than 66.

### 3.2.5 Model Validation

In this paper, 193 samples were selected to validate the model validity. The results show that the model can effectively characterize the driving safety of the driver, and the accuracy is 89.2%, which can be used as an important basis for evaluating the safety of the driver.

## 4 Summary and Prospect

The regression equation can be used to assist in the evaluation and prediction of new drivers and to establish a training mechanism to reduce the likelihood of accidental drivers of accidents. The specific approach is the newly assigned reserve driver to test and the collected data for PCA analysis. According to the Clustering Analysis results, the data will be classified. In the formal induction, the drivers are asked to carry out targeted, differentiated, and focused on specialized training. As for the high level, average level, and low level of these three types of personnel, the companies should strengthen their training according to varying degrees, so as to strengthen their safety awareness and safety attitude of the training, and effectively buried the seeds of safety, laying a solid foundation for safe work in the next step.

In addition, the study both takes the horizontal comparison, and long-term follow-up survey, based on the classification of training. Through long-term, dynamic comparison of new drivers into the security incidents, and according to the occurrence of security complaints, we judge whether a training has played a practical effect or not, and then determine whether it has promotion value.

## References

1. Nevile M, Haddington P. "In-car distractions and their impact on driving activities". Report RSGR-2010-001, Departmentof Infrastructure and Transport, Road Safety Grant
2. Young KL, Mitsopoulos-Rubens E, Rudin-Brown CM, Lenn'e MG (2012) The effects of using a portable music player on simulated driving performance and task-sharing strategies. Appl Ergon 43(4):738–746
3. Li Y (2016) Study on driving behavior safety multiple attribute evaluation methods and its applications. A Dissertation, Submitted for the Degree of Doctor, Jilin University, p 23
4. Jin L, Xian H et al. (2014) Research on evaluation model for secondary task driving safety based on driver eye movements. Adv Mechan Eng 2014:1–8
5. Xian Huacai, Jin Lisheng (2015) The effects of using in-vehicle computer on driver eye movements and driving performance. Adv Mechan Eng 2015:1–8
6. Yang P (2013) Research on the evaluation focus of operation drivers' safety capability. A Dissertation, Submitted for the Degree of Doctor, Chang'an University, pp 3–10

7. Verschuur WL, Hurts K (2008) Modeling safe and unsafe driving behavior. Accid Anal Prev 11
8. Zhang Y (2007) The measurement and evaluation of taxi driver safety consciousnes. A Dissertation, Submitted for the Degree of master, Beijing Jiaotong University, p 21
9. Hosking SG, Young KL, Regan MA (2005) The effects of text messaging on young novice driver performance (Final Report) The National Roads and Motorists' Association Motoring Services, Melbourne, Australia
10. International Standards Organization (2002) Road vehicles measurement of driver visual behaviour with respect to transport information and control systems. Part 1. Definitions and Parameters, ISO Com-mittee Standard 15007-1. International Standard Organization, Geneva, Switzerland
11. Fuller HJA (2010) The virtual driver: integrating physical and cognitive human models to simulate driving with a secondary in-vehicle task. The University of Michigan, USA
12. Salmon Paul M, Lenné Michael G et al (2011) The effects of motion on in-vehicle touch screen system operation: a battle management system case study. Transp Res Part F 14:494–503

# The Shared Bike Trip Characteristics in Xuanwu District of Nanjing

**Wenzhu Zhou, Zhibin Li and Yang Chen**

**Abstract** In view of the newly emerged travel pattern of bike sharing, questionnaire survey, intention investigation, and statistical analysis are used to study the trip characteristics of shared bikes. The results showed that beceause bicycle charing is convenient, time saving and with unfixed borrow location, most people choose sharing bicycle as the travel mode instead of choosing public bicycles, private bicycles and walking.

## 1 Background

With the rapid development of social economy, the number of people who own private cars is on the rise. The popularization of the private cars caused many problems such as consumed a lot of resources and lead to the cities' climate and environment deterioration gradually. Therefore, how to improve the use of bicycles and reduce the energy consumption of motor vehicles have become an important topic for a very long time [1–4].

In 2016, the shared bicycle which is represented by MOBIKE, OFO, has come into being. As there is no pile, no fixed service site, it is convenient for people to set aside outdoor, and it helps truly realize the transfer demand in the last mile, bike-sharing has been rapidly developed in recent years. In China, first-tier cities such as Beijing, Shanghai, Guangzhou, and Nanjing have set up shared bicycles. It is estimated that by the end of 2016, the total number of users of bike-sharing market in China reached 18.8 million, and it is expected that the size of the shared bicycle market will continue to grow substantially in 2017 and reach 50 million by the end of the year [5–7].

W. Zhou (✉) · Y. Chen
School of Architecture, Southeast University, Nanjing, China
e-mail: zwz-1234567@163.com

Z. Li
School of Transportation, Southeast University, Nanjing, China

As bike-sharing is booming across cities in China, a critical and substantial interest issue is focusing on the trip characteristics of shared cycling. Furthermore, as a new mode of transportation, few studies have attempted to discern this traffic mode. The objective of this paper is to study the characteristics of bicycle sharing from a case study of Nanjing, China.

## 2 Study Area and Data

Nanjing is the central city of China's Yangtze River Delta region, and 6 million people live in central city. Nanjing locates in the China's Yangtze River Delta region with 6 million people in the urban areas. Xuanwu Disrict locates in the northeastern of the city and it covers 74.22 km$^2$ (as shown in Figs. 1 and 2). In the context of sustainable development of low-carbon transport, the Nanjing municipal government built the third generation of public bicycle system with 41,500 lock stars, and 1500 service sites. The system requires real-name card, allowing free use within 2 h. In Xuanwu District, there are 4842 public bicycles, 154 service sites with the density of 2/km$^2$, including 48 in transfer stations, 51 residential area, 46 in public facilities, and 9 in tourist attractions. At the end of 2016, private investment companies represented by Mobike and OFO developed a fourth-generation shared bicycle with no lock posts and shipped about 70,000 vehicles throughout Nanjing. The number of shared bikes in the city is more than the regular public bikes operated by the government. The shared bikes quickly received attention and popularity among travelers due to the freedom to stop and taking no restrictions from the pile.

The survey was completed by the students of the Southeast University City, Department of Urban Planning in the spring of 2017. They set up survey points in the subway station, residential area, office area, business center, and public bicycle piles, and randomly selected traveler who used bike sharing, public bikes, and other transport modes. 491 valid samples were collected, of which 157 choose to use shared bicycles, and there were 54 people who were not currently using shared bicycles but could intentionally ride and otherwise travel who do not intend to use shared bikes sum up to 230.

## 3 Travelers' Attributes and Travel Characteristics

As for user (including the intended people), the proportion of men (57.7%) is higher than women (42.3%), which is also consistent with the actual situation that men are stronger than women. From the situation of age distribution, the younger adults (26–40) are the main force of bike sharing, leasing up to nearly 44.6%. Among the young people (15–25) represented by middle and college students, the proportion of flexible travel and rental is also higher, which is 30.3%. While the middle-aged population (36–50) rental accounted for 22.4%, the 60+ age group have the lowest

**Fig. 1** Location of Xuanwu
District in Nanjing



number of rental bikes, about 2.7%, which may be related to the fact that older people do not pay for the Internet. Among those who do not use shared bicycles, middle-aged people and the elderly accounted for more than half of the total, up to 58%. Compared with those who do not own bikes or motor vehicles, people who have them are less likely to use or wish to use a shared bicycle. But there are still a small amount of people (of 15.8%) who have a bike will be turned to use a shared bike to connect the bus travel because of travel distance.

It is noteworthy that there are 23.3% of those who have a car will choose or willing to choose to share the bicycle connected subway travel, which shows the sharing of cycling + subway mode has certain advantages to transfer car travel, which is possibly due to no congestion, high time reliability, and easy access.

The purpose of the trip is as follows: the respondents answered two types of purpose of the commute travel and its return, and flexible travel and return trip two types of purpose. The statistics show that the shared bicycle has a more significant impact on the travel of the purpose of the trip. The flexibility (including the return) of the users (including the intention) is 62%, and the commuter (including the return) travel accounted for 38% of the total, which may be due to the elastic travel distance is short, travel mode is not fixed, and traveler awareness is strengthening. Travel time and distance: statistical analysis shows that 55% of the tenants use the length of
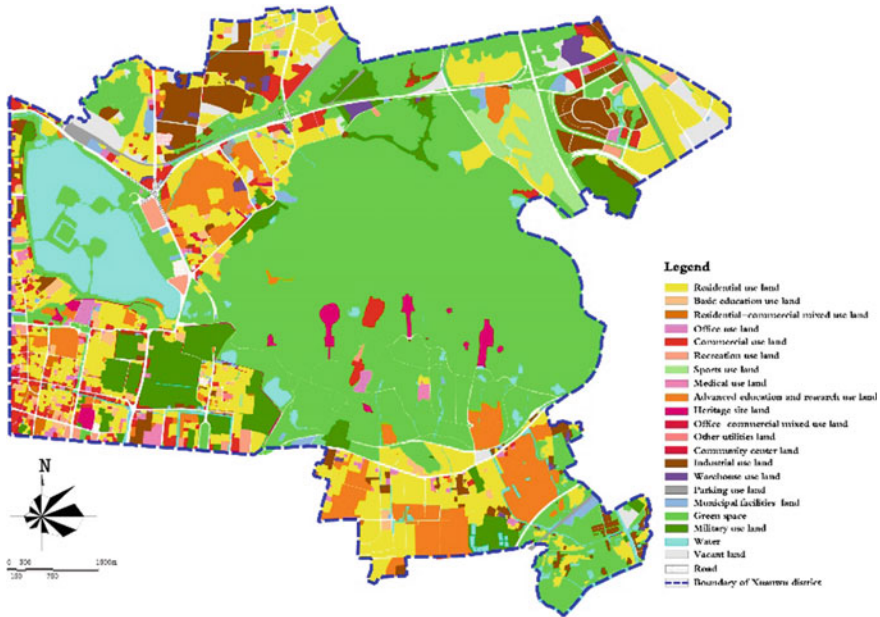
**Fig. 2** Current situation of land use

time within 10 min, and the use of time within 30 min use reached 93%, the average travel time of 18 min, which fits the function orientation that public bicycle on a short-distance travel.

The shared bicycles with the speed of 10 km/h are used to calculate riding distance (consider the intersection delay). Travel distance within 2 km accounted for 72%, within 3 km accounted for 86%, which is consistent with the public bike for short-distance travel characteristics. The relationship between the travel distance and the leasing amount is logarithmic normal distribution, and the leasing amount increases gradually with the increase of the distance. After the lease amount in the range of 0.6–1.2 km reaches the peak value, the distance decreases with the continuous growth of the distance (Figs. 3 and 4).

Travel costs: In order to ensure the safety of transactions, the traveler needs to pass the real-name certification and pay 99–300 in deposit. The costs are not the same, the cheapest is OFO, students spend 0.5 Yuan/h, and general 1 Yuan/h (Table 1).

## 4  Conclusion

This paper takes Xuanwu District, Nanjing as an example to analyze the main factors such as sharing the characteristics of cycling in the area. The main conclusions are as follows: from the age distribution, the young people (26–40) is the main force to
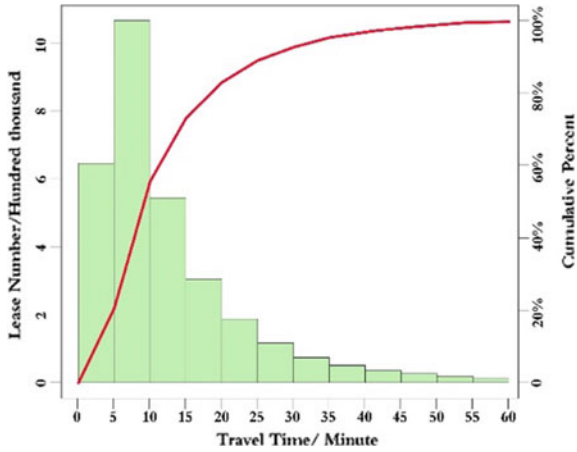
**Fig. 3** The distribution of travel time
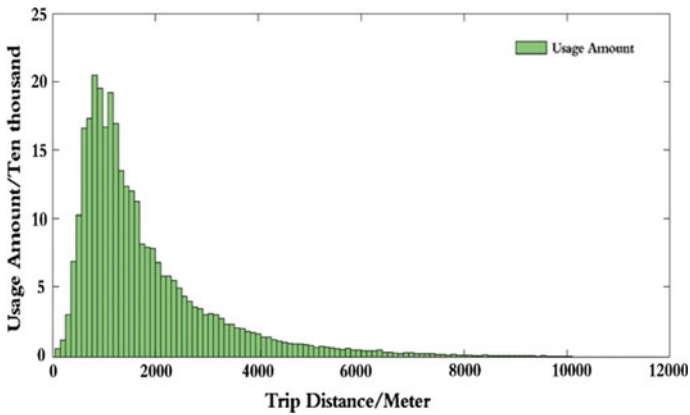


**Fig. 4** Travel distance histogram of travel mode

share bicycle rental; people who have bicycles or electric bicycles are less likely to use or willing to use shared bicycles than those who own cars. Among the people who own cars, about 23.3% will choose or willing to choose shared cycle of subway ride, which shows the shared bicycle + subway mode on the transfer of car travel has certain advantages. On the purpose of travel, the use of sharing bicycle is more flexible than the rigid trip, the transfer mode is slightly higher than the whole mode, and the travel time is mainly on the short time and 2 km distance within.

**Table 1** Travelers' attributes and travel characteristics

| Attribute | Mean | Variance | Whether to use or be willing to use a public bike | | | | |
|---|---|---|---|---|---|---|---|
| Gender | 0.53 | 0.39 | | Men | Women | | |
| | | | Use or wish to use (%) | 57.70 | 42.30 | | |
| | | | No use (%) | 52.80 | 47.20 | | |
| Age | 39.7 | 11.3 | | 15–25 | 26–40 | 41–60 | >60 |
| | | | Use or wish to use (%) | 30.30 | 44.60 | 22.40 | 2.70 |
| | | | No use (%) | 20.00 | 22.00 | 33.00 | 25.00 |
| Monthly income | 4872 | 1468 | | <2000 | 2000–5000 | 5000–10,000 | >10,000 |
| | | | Use or wish to use (%) | 25.40 | 40.60 | 17.80 | 16.20 |
| | | | No use (%) | 15.20 | 23.60 | 27.50 | 33.70 |
| Owning a bike or motor vehicle | 0.69 | 0.21 | | Yes | No | | |
| | | | Use or wish to use (%) | 15.80 | 63.60 | | |
| | | | No use (%) | 84.20 | 36.40 | | |
| Owning car | 0.27 | 0.56 | | Yes | No | | |
| | | | Use or wish to use (%) | 23.30 | 69.80 | | |
| | | | No use (%) | 76.70 | 30.20 | | |

# References

1. Fishman E, Washington S, Haworth N (2013) Bike share: a synthesis of the literature. Transp Rev 33(2):148–165
2. Maurer LK (2012) Feasibility study for a bicycle sharing program in Sacramento, California. In: Paper presented at the transportation research board 91st annual meeting, Washington DC
3. MOHURD (2012) Code for design of urban road engineering. Ministry of Housing and Urban-Rural Development, China
4. Rixey R (2013) Station-level forecasting of bikesharing ridership: station network effects in three US systems. Transp Res Rec J Transp Res Board (2387):46–55
5. Shaheen S, Zhang H, Martin E, Guzman S (2011) Hangzhou public bicycle: under- standing early adoption and behavioral response to bikesharing in Hangzhou. China 2247:34–41

6. Wang X, Lindsey G, Schoner JE, Harrison A (2016) Modeling bike share station activity: effects of nearby businesses and jobs on trips to and from stations. J Urb Plan Dev 142(1):04015001
7. Zhao J, Deng W, Song Y (2014) Ridership and effectiveness of bikesharing: the effects of urban features and system characteristics on daily use and turnover rate of public bikes in China. Transp Policy 35:253–264

# The Forecast of Total Induced Traffic Volume in the Building Project

## —Taking Changchun City Automobile Trade Logistics Park as an Example

**Liu Yang, Wang Jinling, Bian Shuai, Xing Yan, Bai Zhu and Zhang Siqi**

**Abstract** In this paper, we take the example of Changchun City automobile trade logistics park. Based on the design parameters of the project plan given by the design department, we forecast the occurrence quantity of daily peak hours of induced travel in the different functional areas of the building project, attractive quantity of working day morning peak hours, occurrence quantity of rest day evening peak hours, and attractive quantity of rest day evening peak hours, considering the construction area of different functional areas, per unit area residents travel rate, peak hours to increase the number of trips, and other factors. Through analysis and calculation, induced traffic demand can be obtained in the peak hours of building projects. The early peak in the $n$ years is 13,440 (person-time/h). The evening peak in the $n$ year is 13,357 (person-time/h). The early peak in the $n$+5 year is 15,380 (person-time/h). The evening peak in the $n$ +5 year is 15,472 (person-time/h). The traffic volume in the $n$ year early peak is 2766 (veh/h). The traffic volume in the $n$ year evening peak is 2853 (veh/h). The traffic volume in the $n$+5 year early peak is 3685 (veh/h). In this paper, the prediction of induced traffic volume of Changchun Kuancheng automobile trade logistics park can provide database for traffic planning and design. It also can effectively avoid the emergence of traffic congestion so as to meet the needs of road traffic in the coming years.

**Keywords** Induced traffic volume · Residents travel rate · Demand forecast
New project

Study on the induced traffic demand has already begun from the 1970s, but the development is relatively slow. With the increasingly serious traffic congestion in urban road network, the research on the traffic demand induced by building projects has attracted the attention of scholars both at home and abroad. As in 1955, the traffic demand of the Edens Expressway was studied by the Highway Department of Cook County [1]. In 1964, Frye [2] conducted a study on the Dan Ryan Highway.

L. Yang · W. Jinling · B. Shuai · X. Yan · B. Zhu · Z. Siqi (✉)
School of Transportation Engineering,
Shenyang Jianzhu University, Shenyang 110168, Liaoning, China
e-mail: 359063088@qq.com; 21027819@qq.com

In 1989, Pells [3] studied a series of new roads, and concluded that there was a significant impact on the traffic demand, which was induced by the road construction or expansion. In 2001, Noland [4] used statistical data from all 50 states in the United States to analyze the induced increase of each road type; In 2005, Yang et al. [5] put forward the economic forecast model of the traffic volume of the highway, and made a quantitative analysis of the traffic volume of the highway. In the above study, although the induced traffic volume prediction is added to traffic forecast, most are aimed at a single project and do not have universality. Based on the concept of induced traffic volume, the development process and classification of the induced traffic volume were studied by Min [6] in 2006. The application scope of various forecasting methods and the law of the development of the traffic volume in different regions are also analyzed and summarized. In 2011, Hu [7] utilized gravity model to predict the induced traffic volume on the basis of the generating mechanism of expressway traffic volume. The importance of traffic demand forecasting is also verified through an example. Su [8] in 2011, using instrumental variable method to analyze the data of the state highway, the elastic coefficient of per capita car kilometers relative to the highway mileage is obtained. The results of these studies can be applied in different building projects. The analysis and prediction of this paper are based on the gravity model to forecast the induced traffic volume.

## 1 Research Background

"Changchun City automobile trade logistics park" [hereinafter referred to as (Building Projects )] is the JinDazhou group company responsible for the development and construction. It is a large automobile trade zone, which includes 4S stores, large vehicle trading center, industrial machinery exhibition center, test drive site, automobile sales, logistics center, vehicle administrative office, car line, financial services center, the home of staff and workers, cultural entertainment and commercial center, and other related facilities. Building project covers an area of 543 thousand and 442 $m^2$, with a total construction area of 657 thousand and 580 $m^2$, and is expected to invest 1 billion 500 million yuan. The project is east from the North Road of Triumph, west to the boundary line of Luyuan District, north begins from Xing Wang Road, and south to the high-speed railway control line. There are XinGuangfu Road Market, Yurun Group, and Yihe Pharmacy, etc. The specific location of the project is shown in Fig. 1.

According to the overall plan of the building project, the project will be built to form the Northeast's largest automotive regional professional market. It can be expected that the project will be put into generate and attract a large number of traffic flow and the flow of people, increase the corresponding parking demand, and has some influence on the surrounding road network traffic. According to the "Technical standards for traffic impact assessment of building projects", when the new building area is more than 100 thousand $m^2$, the traffic impact evaluation analysis should be done. [Building Project] with a total construction area of 657 thousand and 580 $m^2$,

**Fig. 1** Schematic diagram
of the project location
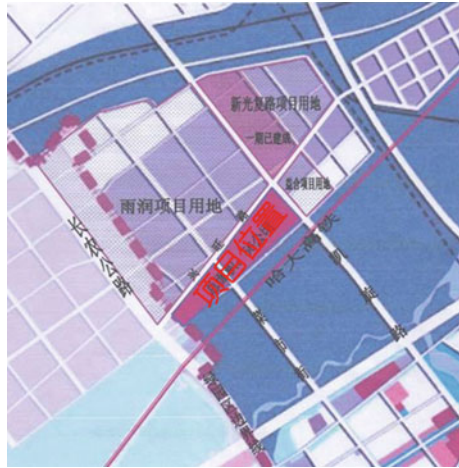


is more than the threshold of the traffic impact assessment. Therefore, in order to cooperate with the preparatory work of the project, according to the "large public construction traffic impact assessment system" and its accessories, it is a need to carry out the traffic impact analysis to ensure that the traffic impact on the surrounding area is within the allowable range. This paper mainly forecasts the [Building Project] induced traffic demand.

The building project covers an area of 543 thousand and 442 m$^2$, with a total construction area of 657 thousand and 580 m$^2$. Land is for commercial use. The main economic and technical indicators of the [Building Project] are shown in Table 1.

The completion date of this project is the first *n* years. Referring to "technical standards for building project traffic impact assessment" and "guidelines for the preparation of traffic impact analysis of Tongji University", the ratio of the construction scale of the project to the starting threshold is greater than 5. So, the normal use of the early years (*n* years) and the normal use of fifth years (*n* + 5) should be evaluated.

## 2 Induced Travel Forecasting Method

### 2.1 Residential Area-Induced Travel Forecast

The following formula is used to predict the induced travel volume in peak hours of the residential area:

Induced travel volume in peak hours = Residential construction area × Travel rate per unit area

where

# 4S store area

---

where
Dormitory construction area is 41,680 m$^2$ in the $n$ years; Travel rate per unit area in the working day morning peak is 5.5 people/100m$^2$; Travel rate per unit area in the rest day evening peak is 4.0 person/100m$^2$;
Dormitory construction area is 41,680 m$^2$ in the $n+5$ years; Travel rate per unit area in the working day morning peak is 6 people/100m$^2$; Travel rate per unit area in the rest day evening peak is 4.5 person/100m$^2$;

Calculation result:
Induced travel volume in the working day morning peak in the $n$ years is 2292.4;
Induced travel volume in the rest day evening peak in the $n$ years is 1667.2;
Induced travel volume in the working day morning peak in the $n + 5$ years is 2500.8;
Induced travel volume in the rest day evening peak in the $n+5$ years is 1875.6.

## 2.3   Sales Area-Induced Travel Forecast

The following formula is used to predict the induced travel volume in peak hours of sales area:
   Induced travel volume in peak hours=Sales construction area×Travel rate per unit area

where
Sales construction area is 364,550 m$^2$ in the $n$ years; Travel rate per unit area in the working day morning peak is 1.8 people/100 m$^2$; Travel rate per unit area in the rest day evening peak is 1.9 person/100 m$^2$;
Sales construction area is 364,550 m$^2$ in the $n + 5$ years; Travel rate per unit area in the working day morning peak is 2.1 people/100 m$^2$; Travel rate per unit area in the rest day evening peak is 2.3 person/100 m$^2$;

Calculation result:
Induced travel volume in the working day morning peak in the $n$ years is 6561.9;
Induced travel volume in the rest day evening peak in the $n$ years is 6926.45;
Induced travel volume in the working day morning peak in the $n+5$ years is 7655.55;
Induced travel volume in the rest day evening peak in the $n+5$ years is 6926.45.

## 2.4   Matching Area-Induced Travel Forecast

The following formula is used to predict the induced travel volume in peak hours of the matching area:
   Induced travel volume in peak hours=Matching construction area×Travel rate per unit area

where

Matching construction area is 88,900 m$^2$ in the $n$ years; Travel rate per unit area in the working day morning peak is 2.7 people/100 m$^2$; Travel rate per unit area in the rest day evening peak is 3.0 person/100 m$^2$;

Matching construction area is 88,900 m$^2$ in the $n+5$ years; Travel rate per unit area in the working day morning peak is 3.0 people/100 m$^2$; Travel rate per unit area in the rest day evening peak is 3.2 person/100 m$^2$;

Calculation result:

Induced travel volume in the working day morning peak in the $n$ years is 2400.3;

Induced travel volume in the rest day evening peak in the $n$ years is 2667;

Induced travel volume in the working day morning peak in the $n+5$ years is 2667;

Induced travel volume in the rest day evening peak in the $n+5$ years is 2844.8.

## 2.5   Service Area-Induced Travel Forecast

The following formula is used to predict the induced travel volume in peak hours of service area:

   Induced travel volume in peak hours=Service construction area×Travel rate per unit area

where

Service construction area is 56,600 m$^2$ in the $n$ years; Travel rate per unit area in the working day morning peak is 1.9 people/100 m$^2$; Travel rate per unit area in the rest day evening peak is 2.1 person/100 m$^2$;

Service construction area is 56,600 m$^2$ in the $n+5$ years; Travel rate per unit area in the working day morning peak is 2.2 people/100 m$^2$; Travel rate per unit area in the rest day evening peak is 2.4 person/100 m$^2$;

Calculation result:

Induced travel volume in the working day morning peak in the $n$ years is 1075.4;

Induced travel volume in the rest day evening peak in the $n$ years is 1188.6;

Induced travel volume in the working day morning peak in the $n+5$ years is 1245.2;

Induced travel volume in the rest day evening peak in the $n+5$ years is 1358.4.

## 3   Statistical Analysis of the Induced Travel Volume in Each Functional Area

Travel rates and induced travel volume for various functional areas during peak periods are shown in Table 2.

   Due to the different features of the various functional areas, the number of people in the functional areas and the proportion of attracting people are not the same. When calculating the actual traffic attraction, it is a need to multiply the respective

coefficients first, namely, "the number of people that induced traffic attracted=the number of people travel×attraction rate". Referring to "technical standards for building project traffic impact assessment" and "guidelines for the preparation of traffic impact analysis of Tongji University", the occurrence and the attraction rate of each function area are shown in Table 3.

From Tables 2 and 3, we can see: "the number of people that induced traffic attracted=the number of people travel×attraction rate", get induced traffic occurrence times and the number of people who have been attracted in the peak hours in the *n* year and in the *n*+5 year. As shown in Table 4.

## 4 Summary

This paper is based on the project planning and design parameters given by the design department. Considering the construction area of different functional areas, per unit area residents travel rate, induced travel volume in peak hours, and other factors,

**Table 2** Travel rates and induced travel volume for various functional areas during peak periods

| Domain | Rate of travel of the year *n* (person-time/100 m²) | | The number of the people in the year *n* | | Rate of travel of the year *n*+5 (person-time/100 m²) | | The number of the people in the year *n*+5 | |
|---|---|---|---|---|---|---|---|---|
| | The working day morning peak | The rest day evening peak | The working day morning peak | The rest day evening peak | The working day morning peak | The rest day evening peak | The working day morning peak | The rest day evening peak |
| Residence | 1.1 | 0.9 | 1109.3 | 907.65 | 1.3 | 1.0 | 1311.05 | 1008.5 |
| Dormitory | 5.5 | 4.0 | 2292.4 | 1667.2 | 6 | 4.5 | 2500.8 | 1875.6 |
| Sales area | 1.8 | 1.9 | 6561.9 | 6926.4 | 2.1 | 2.3 | 7655.55 | 8384.6 |
| Matching area | 2.7 | 3.0 | 2400.3 | 2667 | 3.0 | 3.2 | 2667 | 2844.8 |
| Service area | 1.9 | 2.1 | 1075.4 | 1188.6 | 2.2 | 2.4 | 1245.2 | 1358.4 |

**Table 3** Occurrence rate and attraction rate of each functional area in the peak hours

| Domain | Peak hour occurrence rate (early working day) | Peak hour attraction rate (early working day) | Peak hour occurrence rate (rest day–night) | Peak hour attraction rate (rest day–night) |
|---|---|---|---|---|
| Residence | 0.7 | 0.3 | 0.42 | 0.58 |
| Dormitory | 0.75 | 0.25 | 0.36 | 0.64 |
| Sales area | 0.29 | 0.71 | 0.4 | 0.6 |
| Matching area | 0.32 | 0.68 | 0.68 | 0.32 |
| Service area | 0.40 | 0.60 | 0.60 | 0.40 |

**Table 4** Induced traffic occurrence times and the number of attracted people in the peak hours in *n* year and in *n+5* year

| Domain | Working day of the year *n* (morning peak) | | Rest day of the yearn (evening peak) | | Working day of the year *n+5* (morning peak) | | Rest day of the year *n+5* (evening peak) | |
|---|---|---|---|---|---|---|---|---|
| | Occurrence times | The number of attracted people | Occurrence times | The number of attracted people | Occurrence times | The number of attracted people | Occurrence times | The number of attracted people |
| Residence | 777 | 333 | 381 | 526 | 918 | 393 | 424 | 585 |
| Dormitory | 1719 | 573 | 600 | 1067 | 1876 | 625 | 675 | 1200 |
| Sales area | 1903 | 4659 | 2771 | 4156 | 2220 | 5435 | 3354 | 5031 |
| Matching area | 768 | 1632 | 1814 | 853 | 853 | 1814 | 1934 | 910 |
| Service area | 430 | 645 | 713 | 475 | 498 | 747 | 815 | 543 |
| Total | 5597 | 7842 | 6279 | 7078 | 6365 | 9015 | 7202 | 8270 |

the occurrence and attractive quantity in the working day morning peak hour, and the occurrence and attractive quantity in the rest day evening peak hour of different functional areas of building projects were predicted. In the paper, the Changchun Kuancheng automobile trade logistics park was forecasted and analyzed, which could provide the basis data for traffic planning and design, and avoid the traffic jam.

# References

1. Cook County Highway Department (1995) Expressway influence on parallel routes: a study of Edens expressway traffic diversion and generation trends. Chicago
2. Frye F (1964) Redistribution of traffic on the Dan Ryan expressway corridor. CATS Research News (6), pp 6–16
3. Pells SR (1986) User response to new road capacity: a review of published evidence. ITS, The University of Leeds, Working paper 283. 1989
4. Noland RB (2001) Relationships between highway capacity and induced vehicle travel. Transp Res Part A 35(1):47–72
5. L Yang, X Zhang, AN Shi (2005) Study on the freeway induced traffic volume economic forecasting. J Chongqing Jiaotong Univ (Natural Science Edition) 24(6):123–125
6. Min C, Hangfei L, Chao Y (2006) Review of forecasting methods for induced traffic. Shanghai Highw 3:55–59
7. Hu W (2011) The analysis of error on highway traffic volume prediction. Xi'an, Chang'an University
8. Su Q (2011) Induced motor vehicle travel from improved fuel efficiency and road expansion. Energy Policy 39(11):7257–7264

# Analysis of Influencing Factors of Integrated Freight Transport Volume Based on Gray Markov Model

Ya-ping Zhang, Yue-e Gao, Yan-wen Xie and Shou-ming Qi

**Abstract** To get the quantitative analysis of the influencing factors of the freight traffic volume, the Gray correlation method is used to analyze and filter 3 factors, which have significant influence between the volume of total freight and volume of freight transport (5 kinds of transportation modes) with 14 influencing factors. And the forecasting accuracy of the Gray Markov forecasting model is used to screen the main influence factor on the volume of freight transport, which is based on the Gray relational analysis results. The calculation results show that the impact on volume of freight transport is mainly due to the economic factors, followed by the size of the transport, transport destination, and transportation modes between the internal competition and other types of factors.

**Keywords** Integrated freight transport · Gray relational analysis · Gray Markov model · Influencing factors

## 1 Introduction

The establishment of roads, railways, waterways, civil aviation, pipelines, and other modes of transport of the integrated transport system gives new opportunities of development for the transport industry. Scholars have studied the relationship between economy and freight, such as Zhou et al. constructed the Chinese transport service index (CTSI) [1]. But there is a problem, which is to determine the main influencing factor of the freight. Rang and Kang compared the Gray model and several artificial neural network (ANN) models for real-time flood forecasting [2]. Ke established a random simulation method to compare the forecasting performance

Y. Zhang · Y. Gao · Y. Xie (✉) · S. Qi
Transportation Planning and Management, School of Transportation Science and Engineering, Harbin Institute of Technology, Harbin 150090, China
e-mail: xieyanwen_xyw@163.com

Y. Gao
China Transportation Association, Beijing 100825, China

between Gray prediction models and other kinds of prediction models [3]. Ma et al. presented an unbiased Gray Markov chain method to forecast civil aviation volume of freight transport [4]. Song used fuzzy linear regression model to analyze the impact factors of urban volume of freight transport [5]. Gu and Lu studied the influence of the relevant variables on the change of railway passenger capacity and its degree of influence based on the principal component regression theory and the multiple linear regression model [6]. At the quantitative research aspect, Guo and Zhang used the Gray Markov model to improve the forecasting accuracy of railway freight and highway freight, respectively [7, 8].

Domestic and foreign scholars have researched the influencing factors of the volume of freight, but most of them are mainly having the qualitative research of single mode of transportation. Further studies are needed for quantitative analysis of the influencing factors of volume of freight transport. Therefore, this paper makes a quantitative analysis, which can provide the theoretical basis for the construction of the comprehensive freight index and provide the train of thought for analysis of factors in other fields.

## 2 Selection of Influencing Factors of Volume of Freight Transport

In recent years, our scholars gradually concerned about the area of volume of freight transport. However, the research on freight transport in our country mainly focuses on the improvement of method of freight forecasting, and there is little research about the influencing factors of freight transport. Therefore, this study will analyze the influencing factors of volume of freight transport.

### 2.1 Selecting Index of Influencing Factors

The freight demand of a country and region is affected by many factors. According to the literature, this paper considers the conditions, which the actual channel can provide, and bases on some principles. Screening out the following factors to study, total society GDP $X_1$, the added value of the primary industry $X_2$, the added value of the secondary industry $X_3$, the added value of the tertiary industry $X_4$, total population $X_5$, investment in fixed assets $X_6$, total retail sales of consumer goods $X_7$, total export–import volume $X_8$, total energy production $X_9$, railway mileage $X_{10,}$ road mileage $X_{11}$, pipeline oil (gas) mileage $X_{12}$, inland waterway mileage $X_{13}$, and regular flight mileage $X_{14}$.

# 3   Analysis of Gray Correlation

Considering the comprehensiveness of the factors influencing the research object, we need to select many different factors. The drawback of selecting more factors is that some factors are not correlated with the research object. However, the analysis of Gray correlation method is used to eliminate redundant factors and simplify the analysis steps, which makes the results more in line with the actual situation.

## *3.1   The Method of Calculating Gray Correlative Degree*

Let $x_0$ (k) be the $k$ number of $X_0$ (as the reference sequence); $x_i$ (k) is the k number of $X_i$ (for comparison sequence); then the Gray correlation degree of comparison sequence $X_i$ and reference sequence $X_0$ is:

$$\gamma(X_0, X_i) = \frac{1}{n} \sum_{k=1}^{n} r(x_0(k), x_i(k)) \tag{1}$$

among them, in general

$$r(x_0(k), x_i(k)) = \frac{\min_j \min_k |x_0(k) - x_j(k)| + \rho \max_j \max_k |x_0(k) - x_j(k)|}{|x_0(k) - x_j(k)| + \rho \max_j \max_k |x_0(k) - x_j(k)|} \tag{2}$$

## *3.2   Results and Analysis of Calculation of Gray Relational Degree*

(1)   Data preprocessing

The volume of freight transport data included volume of total freight, volume of road freight, volume of railway freight, volume of waterway freight, volume of civil aviation freight, and volume of pipeline freight, and influencing factors data included total society GDP $X_1$, the added value of the primary industry $X_2$, the added value of the secondary industry $X_3$, the added value of the tertiary industry $X_4$, total population $X_5$, investment in fixed assets $X_6$, total retail sales of consumer goods $X_7$, total export–import volume $X_8$, total energy production $X_9$, railway mileage $X_{10,}$ road mileage $X_{11}$, pipeline oil (gas) mileage $X_{12}$, inland waterway mileage $X_{13}$, and regular flight mileage $X_{14}$ data in the period from 2000 to 2014 are collected. To facilitate the calculation, and to eliminate the different effects of the magnitude of the data and the calculating main body, all data of freight samples are needed to be preprocessed. The general model of the component value should be between [0, 1],
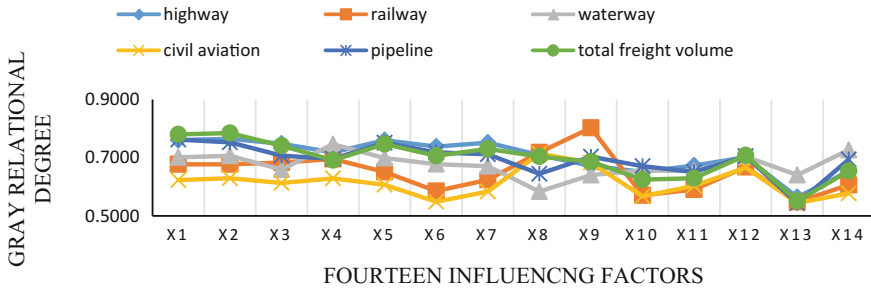
**Fig. 1** The different factors corresponding to the Gray relational degree

so before the calculation, the input sample data should be normalized. The specific treatment is as follows:

$$x_{\text{normal}} = \frac{x_i - x_{\text{min}}}{x_{\text{max}} - x_{\text{min}}} \tag{3}$$

(2)  Analysis of calculating results

based on data from 2000 to 2014, which is collected from Country Data of China and Statistical Yearbook of China, the Gray relational degree between the influencing factors and the volume of freight transport $X_0$ (volume of total freight and volume of five kinds of transportation modes) are calculated, respectively. The results of calculating the Gray relational degree $\gamma$ $(X_0, X_i)$ using Eqs. (1) and (2) are shown in Fig. 1. The results show that: (1) for the volume of total freight, volume of road freight, and volume of pipeline freight, total society GDP, the added value of the primary industry, and total population have the remarkable influence on volume of freight transport; (2) the railway is mainly responsible for a large number of energy transport and service transport, and has a great contribution to import and export goods; (3) water transport is mainly responsible for the transport of services and transport of industrial and construction industry, and may have a competitive relationship with the shipping; (4) civil aviation transport mainly bear transport of the import and export freight, large transport of energy transport of goods, and transport of industrial and construction goods.

## 4   Establishment of Gray Markov Forecasting Model

The aim of researching main influencing factors of freight traffic is to analyze the changing law of volume of freight transport by influencing factors, and then forecast the future demand. Predictions of predictive model can help decision-makers to make the right decisions and improve its quality. According to the literature review, the predictions of the accuracy of the Gray Markov model is more accurate than
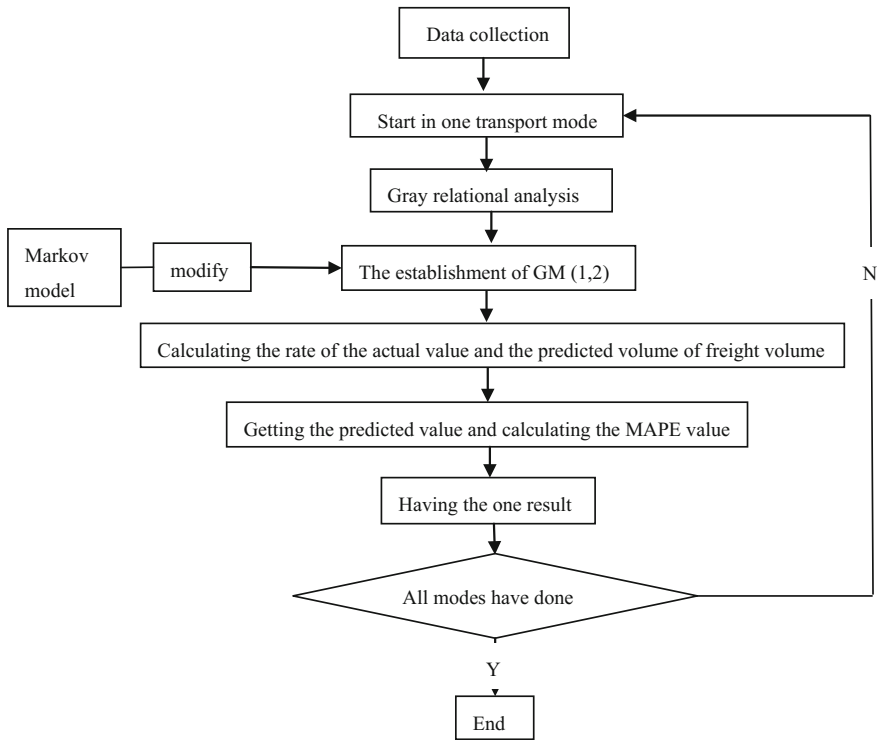
**Fig. 2** The flow chart of the establishment of Gray Markov forecast model of volume of freight transport

general Gray model, and it is feasible to establish GM (1, 2) model about different influencing factors and research object. The Markov model is used to modify the results. Predictions of the accuracy of the pros and cons can provide us with some reliable recommendations.

## 4.1 Gray Markov Forecast Model of Volume of Freight Transport

To achieve the aim better, we select the most suitable factors to analyze the volume of freight transport. In this study, we use the knowledge of Gray relational analysis, Gray prediction model, and Markov model to solve the problem. The steps are shown in Fig. 2. In addition, the MAPE [9] value is a measurement of predicted accuracy.

**Table 1** The results of calculation

| Types of data years | The volume of total freight $X_1$ | The added value of the primary industry $X_2$ | Gray prediction results $\tilde{X}_1^{(0)}(i)$ | $X_1^{(0)}(i)/\tilde{X}_1^{(0)}(i)$ | State $E_i$ | Gray Markov predicted results |
|---|---|---|---|---|---|---|
| 2000 | 0.0000 | 0.0000 | 0.0000 | 1.0000 | 3 | |
| 2001 | 0.0153 | 0.0187 | 0.0163 | 0.9404 | 2 | |
| 2002 | 0.0444 | 0.0392 | 0.0471 | 0.9423 | 2 | |
| 2003 | 0.0733 | 0.0687 | 0.0826 | 0.8878 | 1 | |
| 2004 | 0.1238 | 0.1143 | 0.1354 | 0.9144 | 1 | |
| 2005 | 0.1792 | 0.1593 | 0.1876 | 0.9553 | 2 | |
| 2006 | 0.2415 | 0.2198 | 0.2582 | 0.9354 | 2 | |
| 2007 | 0.3265 | 0.3148 | 0.3694 | 0.8838 | 1 | |
| 2008 | 0.4370 | 0.4076 | 0.4782 | 0.9138 | 1 | |
| 2009 | 0.5222 | 0.4571 | 0.5362 | 0.9738 | 3 | |
| 2010 | 0.6705 | 0.5721 | 0.6711 | 0.9991 | 3 | |
| 2011 | 0.8325 | 0.7067 | 0.8290 | 1.0042 | 3 | |
| 2012 | 0.9762 | 0.8064 | 0.9460 | 1.0320 | | 0.9171 |
| 2013 | 0.9765 | 0.9004 | 1.0562 | 0.9237 | | 1.0062 |
| 2014 | 1.000 | 1.0000 | 1.1732 | 0.8525 | | 1.1068 |

**Table 2** The range of division of the state value

| State | $E_1$ | $E_2$ | $E_3$ |
|---|---|---|---|
| Range | 0.8838–0.9141 | 0.9142–0.9646 | 0.9647–1.0042 |

## 4.2 Analysis of the Results

The data is substituted in the Gray Markov freight forecasting model, with the volume of total freight $X_1$ and the added value of the primary industry $X_2$ as an example, the GM (1, 2) model forecast value, the ratio of $X_1^{(0)}(i)/\tilde{X}_1^{(0)}(i)$, and the results of division of state are shown in Table 1. The division of state range is shown in Table 2.

It is in the state $E_3$ in 2011, thus, $P(0) = (0, 0, 1)$. The state of the results shows that the transfer matrix is $P = \begin{pmatrix} 0.500 & 0.250 & 0.250 \\ 0.500 & 0.500 & 0.000 \\ 0.000 & 0.333 & 0.667 \end{pmatrix}$, then $P^2 = \begin{pmatrix} 0.375 & 0.333 & 0.292 \\ 0.500 & 0.375 & 0.125 \\ 0.167 & 0.389 & 0.444 \end{pmatrix}$, $P^3 = \begin{pmatrix} 0.354 & 0.358 & 0.288 \\ 0.438 & 0.354 & 0.208 \\ 0.278 & 0.384 & 0.338 \end{pmatrix}$, so $P(1) = P(0)P = (0.000, 0.333, 0.667)$, $P(2) = P(0)P^2 = (0.167, 0.389, 0.444)$, and $P(3) = P(0)P^3 = (0.278, 0.384, 0.338)$.

The weighted calculation is performed with the value of the transition probability, and the predicted value is modified to obtain the results of forecasting values in 2012–2014 that is shown in Table 3. The same method of calculation is used to

**Table 3** The predictive results of Gray Markov model

| Years | The range of predicted value | The median of predicted value | Rate | Predictive value |
|---|---|---|---|---|
| 2012 | $E_1$: 0.8361–0.8647 | 0.8504 | 0 | 0.9171 |
|  | $E_2$: 0.8648–0.9125 | 0.8887 | 0.333 |  |
|  | $E_3$: 0.9126–0.9500 | 0.9313 | 0.667 |  |
| 2013 | $E_1$: 0.9335–0.9655 | 0.9495 | 0.167 | 1.0062 |
|  | $E_2$: 0.9656–1.0188 | 0.9922 | 0.389 |  |
|  | $E_3$: 0.0189–1.0606 | 1.0398 | 0.444 |  |
| 2014 | $E_1$: 1.0368–1.0723 | 1.0546 | 0.2778 | 1.1068 |
|  | $E_2$: 1.0724–1.1316 | 1.1020 | 0.3843 |  |
|  | $E_3$: 1.1317–1.1780 | 1.1549 | 0.3379 |  |

**Tab.4** The MAPE standard values of the predicted value of combining total volume of freight transport with the three factors

| The volume of total freight and the factor | MAPE (%) |
|---|---|
| The volume of total freight and the added value of the primary industry | 9.94 |
| The volume of total freight and the total society GDP | 6.62 |
| The volume of total freight and total population | 6.78 |

**Table 5** Gray relational degree ranking the first three factors,pros and cons of the predicted accuracy

| The dependent variable $X_0$ | Gray relational degree ranking the first three factors' pros and cons of predicted accuracy |
|---|---|
| Volume of total freight | total GDP > total population > the added value of the primary industry |
| Volume of road freight | the added value of the primary industry > total GDP > total population |
| Volume of railway freight | total energy production > total export–import volume > the added value of the tertiary industry |
| Volume of waterway freight | the added value of the primary industry > regular flight mileage > the added value of the tertiary industry |
| Volume of pipeline freight | total GDP > the added value of the primary industry > total population |
| Volume of civil aviation freight | total energy production > total export–import volume > the added value of the primary industry |

calculate the volume of total freight and the other two influencing factors. And the MAPE values of the three influencing factors are calculated to compare. The results are shown in Table 4.

The above calculation steps are repeated for volume of road freight, volume of railway freight, volume of waterway freight, volume of civil aviation freight, and volume of pipeline freight, and the results are shown in Table 5.

Comparing the results of this prediction with the results of Gray correlation, we can know that: (1) the influence factors of the volume of road freight, the volume of railway freight, and the volume of pipeline freight are the same, therefore, what factor ranks the first is the best factor to analyze the volume of freight transport of the kind of transportation way, namely, the added value of the primary industry, the total energy production, and total society GDP; (2) the volume of total freight, volume of waterway freight, and volume of civil aviation freight factors are different, respectively, this paper, respectively, chooses the total society GDP, regular flight mileage, and total export–import volume as the best choice by comprehensive balance.

In a word,the results can be drawn as follows: (1) the transport of forestry, animal husbandry, and fisheries (i.e., primary industries) is mainly by road transport; (2) Energy production (including raw coal, crude oil, and natural gas, etc.) is mainly by rail transport; (3) The number of pipeline freight is closely relative to the economy. The greater the total society GDP, the more the construction of the pipeline; flight routes mileage have a certain impact on the waterway freight, and the two ways may be competitive; (4) The import and export trade mainly depends on air transport; (5) The volume of total freight is mainly related to the total society GDP. The more developed the national economy, freight demand will be greater.

## 5    Conclusions and Discussion

The Gray relational degree and the Gray Markov model are used to filter the influencing factors and the influencing factors which can reflect the change in volume of freight transport are chosen. This method of combining the two methods to analyze quantitatively the influencing factors is a new method, and it is different from other documents, which is only on a way of transport freight research. This paper researches the volume of total freight and five modes of transport, so the results are more comprehensive. The conclusions are as follows: (1) the main influencing factors of the volume of total freight of society are the total society GDP, and the quantity of freight is closely related to the economic situation of society. (2) The main influencing factors of volume of road freight are the added value of primary industry. And the transportation of forestry, animal husbandry, and fishery is mainly by road route. (3) The main factors affecting the volume of railway freight are the total energy production, and energy resources mainly use large transport of rail transport. (4) The main influencing factors of volume of waterway freight are regular flight mileage, and the water transport and aviation have relatively strong competitive relationship. (5) The main influencing factors of civil aviation volume are total export–import volume, and the import and export trade mainly relies on air transport. (6) The main influencing factors of volume of pipeline freight are the total society GDP. The quantity of pipeline transportation is mainly related to the economic situation of society.

In summary, the analysis of the influencing factors of volume of freight transport is mainly about the economic factors, followed by the factors such as the size of the traffic, the transport location, and the internal competition within the different modes of transportation.

## References

1. Zhou J, Fu Z, Tian M (2015) Construction of China's transportation service index based on CTSI index. J Syst Eng Pract 35(4):965–972
2. Rang MS, Kang MG, Park SW et al (2006) Application of grey model and artificial neural networks to flood forecasting 1. Jawra J Am Water Resour Assoc 42(2):473–486
3. Ke Z (2013) Random simulation method for accuracy test of grey prediction model. Grey Syst 3(1):26–34
4. Ma J, Chen Z. Tse K (2013) Forecast of civil aviation volume of freight transport using unbiased grey-fuzzy-Markov chain method. In: International conference on information management, innovation management and industrial engineering, vol 3. pp 528–531
5. Song R (2015) Application of fuzzy linear regression model in predicting the volume of freight transport of city. J Inf Comput Sci 12(1):191–200
6. Gu S, Lu X (2015) Analysis of China railway passenger volume's influence factors based on principal component regression. In: International conference on logistics, informatics and service sciences, pp 1–5
7. Guo K, Ma Y, Wang T (2009) Prediction of volume of railway freight based on improved gray-markov chain method. J Lanzhou Jiao tong Univ 28(6):124–127
8. Zhang W, Cui S, Deng H (2011) Mark Markov forecasting model for highway freight transport volume. J Wuhan Univ Technol Transp Sci Eng 35(4):658–661
9. Wang Q, Wang X, Xia F (2009) Integration of grey model and multiple regression model to predict energy consumption. In: International conference on energy and environment technology. IEEE Computer Society, pp 194–197

# Simulation and Experimental Verification on the Influence on Tail-Lift to the Vehicle Frame

**Chengqiang Zong, Haiyan Ji, Hongwei Zhang, Huina Zhang and Xiansheng Li**

**Abstract** With the rapid development of logistics industry in China, the use of tail-lift has entered a high-speed developing period. However, as a new industry, the standard of the tail-lift installation is still lacking. This paper mainly focused on the influence of tail-lift installation on vehicle frame. We built the ADAMS model of tail-liftand finite element of vehicle frame, and analyzed the influence on tail-lift to the vehicle frame while tail-lift in full-loaded status or in traveling position. Finally, experimental verification test of vehicle is carried out. The results show that the simulation is almost consistent with the real vehicle test data, and the maximum stress value of vehicle frame is less than the yield limit of the material.

**Keywords** Tail-lift · Vehicle frame · Finite element analysis · Experimental verification of vehicle

Tail-lift on vehicle (hereinafter referred to as tail-lift) is a lifting device intended for installation on or in a wheeled vehicle and which is used for loading and/or unloading this vehicle, and usually is mounted on the rear end of a vehicle [1]. The workers can carry out the cargo loading and/or unloading by using of tail-lift whenever and/or wherever, especially convenient for large units and heavy units. The use of the tail-lift can greatly improve handling efficiency, save workers, improve the security of operating personnel, and reduce the damage rate of goods during loading and/or unloading [2]. With the continuous development of domestic logistics industry, increasing staff costs, and demand for higher handling efficiency, there are more demands for tail-lift [3, 4]. However, there are few vehicles equipped with tail-lift when delivery from vehicle manufacture factory, and there is lack of relevant standards for the installation of the tail-lift in China. The tail-lift installed after

C. Zong · H. Zhang · H. Zhang
Research Institute of Highway, the Ministry of Transport, PRC, Beijing 100088, China

H. Ji (✉) · X. Li
School of Transportation, Jilin University, Changchun 130012, China
e-mail: jihy15@mails.jiu.edu.cn

vehicles leave manufacturer is regarded as illegality in many provinces in China, and the security and standardization of the tail-lift installation need to be regulated. This paper mainly studied the influence to the safety of vehicle frame after the installed tail-lift according to practical situation.

# 1 Structural Characteristics of Tail-Lift

Tail-lift usually consists of platform, drive system (including oil cylinder, steel bearing, lifting arm, etc.), rear underrun protection device, electric control system (including fixed electric control box and wire controller), supporting elements, and oil source (including motor, pump, hydraulic control valve, pipeline, tank and so on). The typical tail-lift structure is shown in Fig. 1.

# 2 Model Construction

## 2.1 Model and Assembly of Tail-Lift

In this paper, we choose the most used tail-lift in domestic, and select the type of YT-QB15/150S tail-lift made by Cadrolift Hydraulic Company, in which maximum load is 1500 kg and platform vertical travel distance is 1500 mm, and the total mass of tail-lift is 570 kg when equipped with steel platform (including rated hydraulic oil).

The part model of the tail-lift was built first and then assembled in Solidworks. The model of supporting elements is shown in Fig. 2, and assembly model in Solidworks is shown in Fig. 3 (distance between two hanging plates can be adjusted according to the distance between the longitudinal beams of the vehicle frame).

**Fig. 1** Typical tail-lift structure
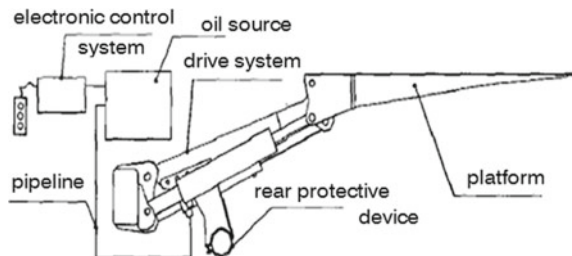
**Fig. 2** The model of
supporting elements



hanging plate
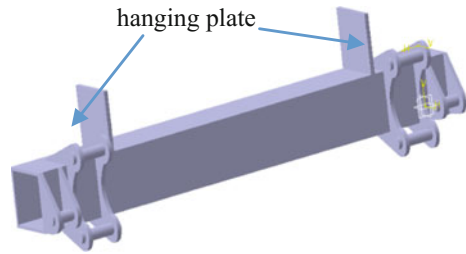
**Fig. 3** The assembly model
of tail-lift in exploded view
of SolidWorks
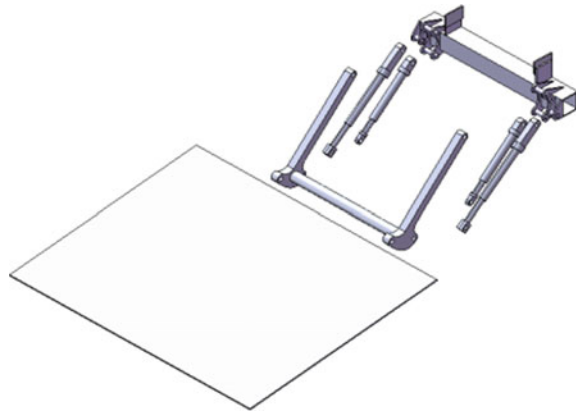


## 2.2 Establishment of Vehicle Frame Model

The selected vehicle is mostly used in the urban logistics distribution, which has been installed tail-lift when delivery from vehicle manufacture factory. Its type is vehicle is BJ5169XYK-A5 manufactured by BeiqiFoton Motor Co., Ltd., which is a wing-opening van, and complete vehicle kerb mass is 7200 kg (including the weight of YT-QB15/150S tail-lift), and dimensions is 9995 mm (length) × 2530 mm (width) × 3950 mm (height).

When building the model of vehicle frame, we ignore the parts (such as small holes) which will not affect finite element analysis by experience, and make vehicle frame's entity model [5].

After importing the entity model into the finite element analysis software, 4 node tetrahedral element (Tet) is used for model meshing when take the length of the whole beam and computational complexity into consideration. The mesh size is medium, and endowed with the material properties (16 manganese steel, elastic modulus is $2.1e^5$ MPa, poisson ratio is 0.3, yield limitation is 343 MPa), the vehicle frame model after meshing is shown in Fig. 4 [6].

**Fig. 4** Meshing model of
vehicle frame
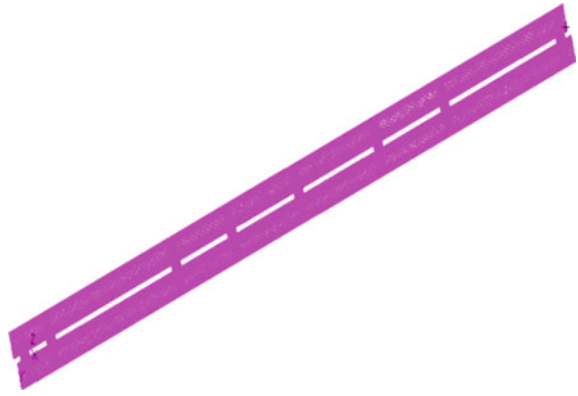


# 3   Stress Analysis and Simulation of Vehicle Frame

## 3.1   Force and Torque Analysis of Tail-Lift in Full-Loaded Status

The force of vehicle frame transferred from tail-lift is mainly exerted by the hanging plate, which is connected with the vehicle frame by bolts, therefore, we can get the force on hanging plate by simulation in ADAMS. The tail-lift is a typical cantilever mechanism, and the location of loading cargo centroid on platform will affect the actual maximum load, therefore, each tail-lift is equipped with a tail-lift loading curve, and the loading curve of YT-QB15/150S is shown in Fig. 5. The load is a cuboid with dimensions of 1200 × 2000 × 1000 (length × width × height) (mm × mm × mm), which has a single density, and total mass is 1500 kg, centroid is 600 mm away from platform inside edge during simulation. After loading this cuboid, the tail-lift reached its maximum load. We can get the force and monument acting on hanging plate when tail-lift load this cuboid. However, the total volume of hydraulic oil is about 15L, which occupies little proportion of tail-lift's weight, and we ignore circulating of hydraulic oil during simulation. The simulation of tail-lift in ADAMS is shown in Fig. 6.

We can get the force and torque changes acted on two side hanging plates when applying displacement on the one side hydraulic cylinder, as shown in Fig. 7 (negative means direction of force or torque is opposite to positive direction). It can be seen that sum of forces acted on two side hanging plates are mostly same with the sum of tail-lift and cuboid's weight, but the other side does not have torque due to one cylinder hydraulic driving mode, and torque is concentrated on the other side, and the maximum torque is 3.05e4 kN·mm. In fact, two-cylinder hydraulic driving mode is mostly used in tail-lift loading cargo, and the cargoes' distributed on tail-lift platform is usually unbalanced, so the maximum force or torque on one side hanging plate can be up to 60% of the one side driving simulation results.

**Fig. 5** Loading curve of YT-QB15/150S
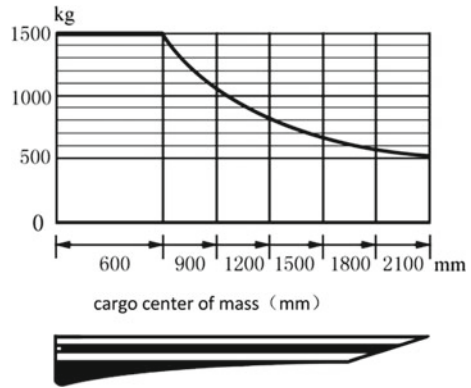


**Fig. 6** Full-loaded tail-lift in ADAMS
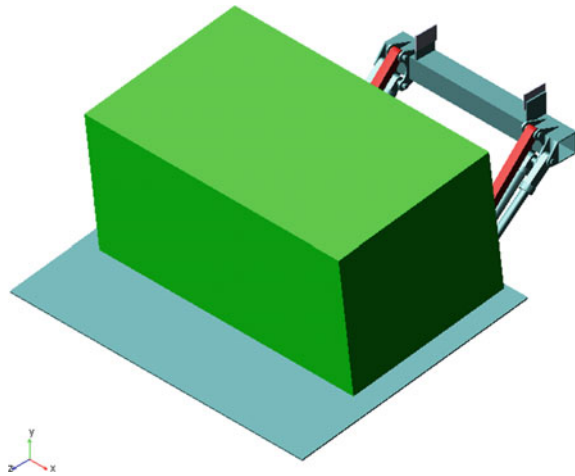


To ensure the safety of tail-lift's selection and installation, the maximum force and torque in different time are selected during simulation process. The safety factor is 1.2, force is $-10.8$ kN (acted on two side hanging plates separately), and torque is $1.83e^4$ kN·mm (acted on two side hanging plates separately).

## 3.2 Force and Torque Analysis of Tail-Lift in Traveling Position

The tail-lift will be packed up or folded in its traveling position when vehicle running on the road. When vehicle passing through the bumpy road, tail-lift will generate a greater impact on the vehicle's longitudinal beam, therefore, it is essential to analyze
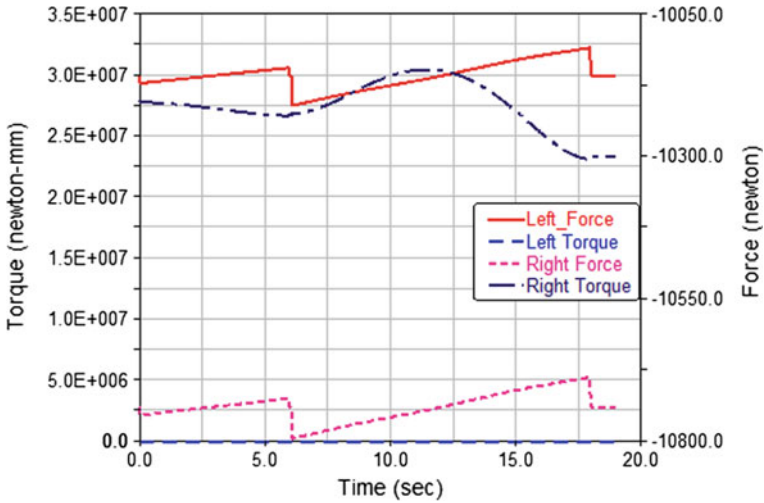
**Fig. 7** Force and torque on two side hanging plates

**Fig. 8** Tail-lift in traveling
position



the beam's force and torque according to road condition. Figure 8 shows the status
of packed up tail-lift.

The force and torque at hanging plate change variously during the retraction
process of YT-QB15/150S, as shown in Figs. 9 and 10. In the retraction process of
tail-lift, the torque is uniform firstly, and then the torque increases rapidly during the
middle of closing action. However, the force increases rapidly, and then decreased
slowly which do not keep pace with torque. It can be seen from figure that forces
on two side hanging plates are almost the same, but the torque has a great distance
which mainly results from one side driving simulation.
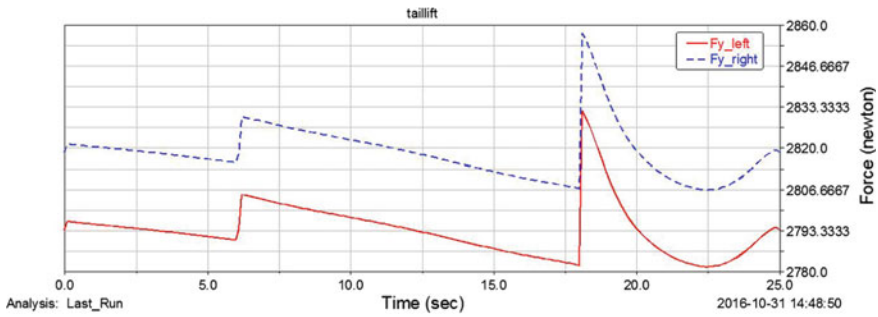
**Fig. 9** The force acted on hanging plate during tail-lift packed up to traveling position
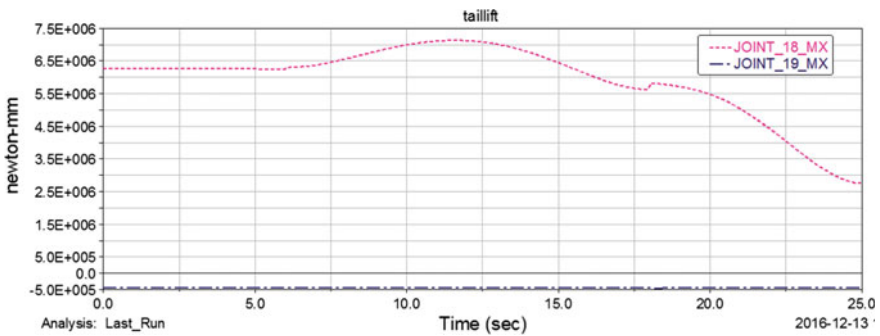


**Fig. 10** The torque acted on hanging plate during tail-lift packed up to traveling position

The force generated during tail-lift packed up to traveling position is less than the processing of full-loaded cargo loading as seen from simulation result. Therefore, we only need to simulate the force and torque full-loaded cargo loading when vehicle is in stationary state. When vehicle is running on bumpy road, the tail-lift will generate impact load to vehicle beam which is greater than the weight of itself. It is necessary to analyze the reliability of vehicle frame under this ultimate condition by simulation. The vertical acceleration of the vehicle while passing through cobblestone road is shown in Fig. 11, and the sample frequency is 100 Hz. Combing with the process of tail-lift packed up and vehicle in severe road conditions, the maximum force is −2.9 kN (acted on two side hanging plates separately), torque is 3.9e3 kN·mm (acted on two side hanging plates separately, 60% of one side hanging plate maximum value), and the vertical acceleration is 0.4 g.

**Fig. 11** Vertical
acceleration of vehicle
passing through a road
surface
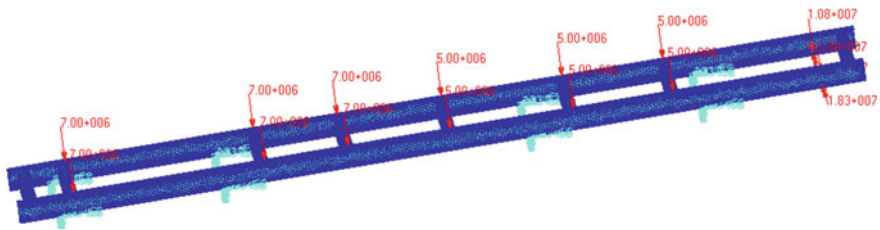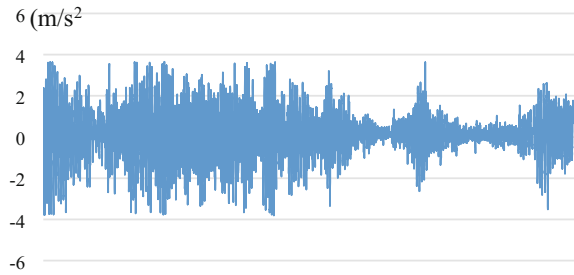




**Fig. 12** Vehicle kerb weight and constraints

## 3.3 Constraints and Loads on Vehicle Frame

The constraints of vehicle are generally located in the connecting part of vehicle frame
and axle, due to the engine, gear box, and other accessories installed in front part of
the vehicle frame, and it is heavier than back part of the vehicle frame when vehicle
is not loaded. The forepart shares 60% of vehicle kerb weight evenly which takes up
40% length of longitudinal beam, and the remaining 40% of vehicle kerb weight is
on the other part the vehicle frame [7–9]. The installation position of hanging plate
is 500 mm away from longitudinal beam's edge, loading area is 150 mm × 150 mm,
constraint and load are shown in Fig. 12. The value of force and torque is mentioned
in Chap. 3.

### 3.3.1 Analysis on the Stress of Vehicle Frame with Tail-Lift
in Full-Loaded Status

The force and torque in simulation are same as Sect. 3.1, the stress nephogram is
shown in Fig. 13. The most stress of vehicle frame is varied from 5 to 40 MPa, and
the maximum stress is 114 MPa, which is concentrated stress and located at the lower
surface's rear end of rear suspension, and less than the yield limit of manganese steel.
There is a great impact on the area of hanging plate corresponding to vehicle frame
while tail-lift in full-loaded status, hence, the maximum stress of vehicle frame is
located at the rear end of rear suspension, and local stress nephogram is shown in
Fig. 14.
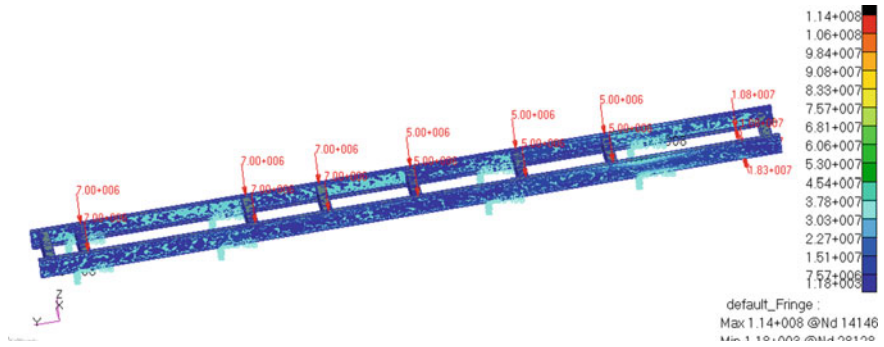
**Fig. 13** Stress nephogram of vehicle frame with tail-lift in full-loaded status
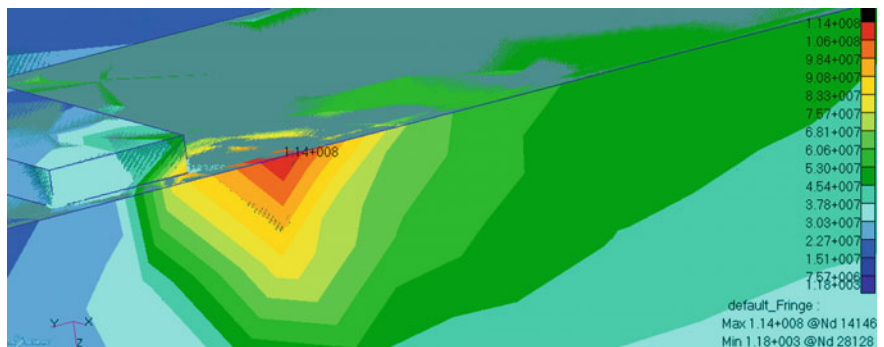


**Fig. 14** Local stress nephogram near rear suspension

### 3.3.2 Analysis on the Stress of Vehicle Frame with Tail-Lift in Traveling Position

The force and torque in simulation are same as mentioned in Sect. 3.2, and the stress nephogram is shown in Fig. 15. The simulation results show that the most stress of vehicle frame is varied from 5 to 30 MPa, and the maximum stress is 110 MPa which occurred in the almost same location with the analysis of vehicle frame with tail-lift in full-loaded status, and the stress generated by impulse load is less than full-loaded tail-lift.
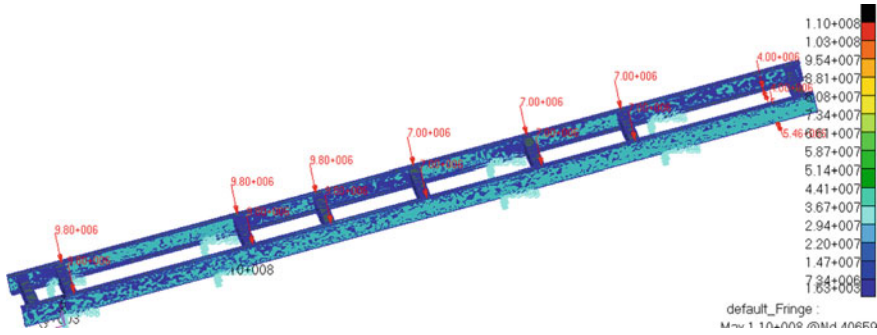
**Fig. 15** Stress nephogram of vehicle frame with tail-lift in traveling position

**Fig. 16** Sticking position of strain gage



left longitudinal beam right longitudinal beam
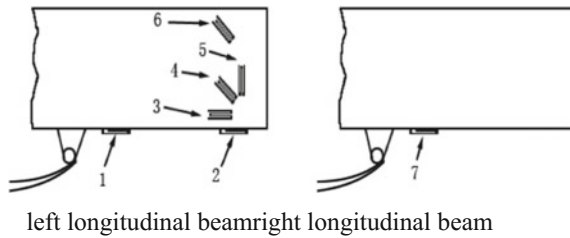
## 4 Experimental Verification

In order to verify the simulation results, we carried out the stress test of tail-lift in full-loaded status and in traveling position in the road traffic proving grounds, Ministry of Transport, the parameter of vehicle and tail-lift are same with simulation as mentioned in Chap. 3.

### 4.1 Test Scheme

The most common used stress testing method is strain gage testing, we placed strain gage and strain rosette on outer surfaces and lower surfaces of vehicle longitudinal beam which near to hanging plate of tail-lift, sticking position of the strain gage is shown in Fig. 16.

### 4.2 Stress Testing for Tail-Lift in Full-Loaded Status

The sand bucket is used as the mass block during test, and weight of bucket is about 25 kg. The tail-lift is adjusted to horizontality, and then the buckets are placed layer

**Fig. 17** Stress testing for tail-lift in full-loaded status



**Table 1** Maximum measured stress of different measuring points with tail-lift in full-loaded status

| Test point | 1 | 2 | 3 | 4 | 5 | 6 | 7 |
|---|---|---|---|---|---|---|---|
| Maximum stress(MPa) | −64.05 | −12.01 | −43.83 | −16.55 | 8.02 | 4.52 | −51.87 |

by layer symmetrically, and total mass of sand bucket is 1500 kg ± 25 kg which centroid is 600 mm away from platform inside edge. Loads on platform of tail-lift are shown in Fig. 17, and the maximum measured stress of different measuring points is shown in Table 1.

The maximum stress of vehicle frame in test data is 64.05 MPa, which is less than the yield limit of manganese steel. The test result has little difference with the simulation, and test point 1 and test point has the larger stress, which located at lower surfaces of vehicle longitudinal beam near to rear suspension.

### 4.3 Stress Testing for Vehicle with Tail-Lift in Traveling Position Passing Through Typical Pavements

Stress is measured while vehicle with tail-lift in traveling position passes through washboard roads, potholes roads, block roads, and cobblestone roads. The maximum stress is 119 MPa which occurred on block roads that is less than the yield limit of manganese steel. The strain's test result of one strain gage is shown in Fig. 18 while vehicle passing through cobblestone roads, which can be converted to stress by formula. Table shows maximum stress results of all test point while vehicle with tail-lift in traveling position passes through cobblestone roads (Table 2).
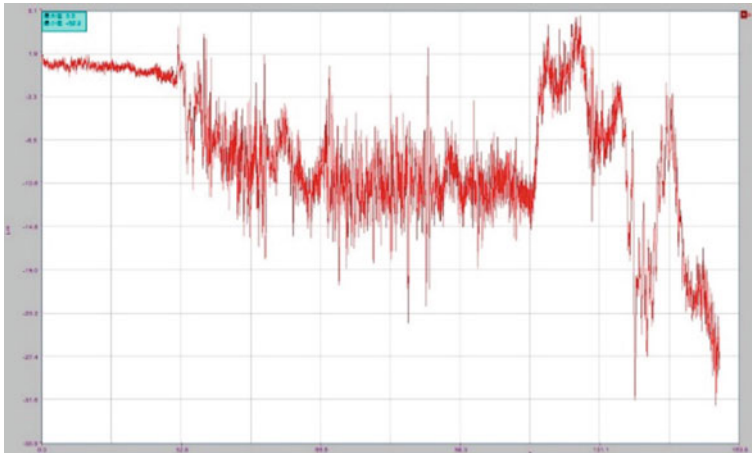
**Fig. 18** Strain of one test point

**Table 2** Maximum stress of test point while vehicle passes through cobblestone roads

| Test point | 1 | 2 | 3 | 4 | 5 | 6 | 7 |
|---|---|---|---|---|---|---|---|
| Maximum stress(MPa) | −20.31 | 7.14 | −10.04 | −9.60 | −4.81 | 14.22 | −12.05 |

## 5  Conclusion

The strength of vehicle frame is crucial to the safety of cargo transportation. We analyzed the influence of tail-lift installed on vehicle after it leaves the manufacturer. We carried out simulation and experimental verification, and drew several conclusions as follows:

(1) The YT-QB15/150S tail-lift is fitted with vehicle which type is BJ5169XYK-A5 whenever tail-lift is in full-loaded status or in traveling position, the maximum stress is located at lower surfaces of vehicle longitudinal beam near to rear suspension, and the impact generated by full-loaded cargo unloading is roughly the same with generated by tail-lift while vehicle passing through the bumpy road.

(2) The maximum load that tail-lift can bear will have greater impact on vehicle frame, if its lifting mass is too large, frequent loading and/or unloading of full-loaded goods may lead to vehicle frame's fatigue, and more seriously it will bring about some security risks on the vehicle structure.

# References

1. Shen X (2011) On the development of China's automobile tail manufacturing industry. Logistics Technology (Equipment Edition), (5)
2. Feng F (2012) Motion simulation and structural optimization of automotive hydraulic lifting tail plate. Jiangxi, Huadong Traffic University
3. Huang F, Yan Z, Chen X (2016) Analysis on the market demand of China's automobile tail board industry. Special Purpose Vehicle
4. Zong C, Zhang H, Zhang X, Zhang H (2016) Automotive lifting tail plate installation and use of technical requirements interpretation. Commercial car.2016.08
5. Baibin (2012) Dynamic and static analysis of all terrain vehicle structure based on WorkBench. J Shenyang Inst Eng
6. Chen Z, Wang W (2012) Finite element analysis of vehicle girder bridge. Mechanics 39(12):33–37
7. Su E (2003) Finite element modeling and analyzing of automobile drive axle housing. Jilin University, Changchun
8. Yu D, Wei J, Qiu Y, et al (2011) Finite element analysis structural strength on lifting axle housing of heavy-duty truck. J Dalian Jiaotong Univ 32(5):24–28
9. Xue S (2005) Finite element method. Beijing, China Building Materials Industry Press

# An Indicator-Based Method for Bus Routing Adjustment

Yi-ling Deng

**Abstract**  Increasing the ridership of bus transit through bus routing adjustment is one of the main tasks of transit agencies. A new method to characterize and classify bus routes according to their coverage, transfer and overlap level in meeting the needs of public transit planning is described. Geographic transit network and land use data are used to calculate seven indicators for each bus route: residential area coverage, non-residential area coverage, land use mix, transfer index to/from bus, overlap index with bus, transfer index to/from metro and overlap index with metro. Hierarchical clustering analysis is used to indicate where the largest potential scope exists for adjusting the bus transit system and hence can be used to guide transit planners. The method was applied in Nanjing, China aiming to identify improvable bus routes. Six bus route clusters were generated using hierarchical clustering. The profiles of each cluster are analysed and corresponding strategies for bus routing adjustment are proposed. ANOVA test shows there is a significant difference at the route-level ridership among these clusters, which verifies the reasonability of the method.

**Keywords**  Bus routing adjustment · Hierarchical clustering · Coverage
Transfer · Overlap

Y. Deng (✉)
College of Civil Engineering and Architecture, Zhejiang University of Technology,
Hangzhou 310014, China
e-mail: yiling@zjut.edu.cn

# 1 Introduction

Bus routing adjustment is an effective way to accommodate new travel patterns and attract new ridership, at the same time, may improve transit system efficiency, effectiveness or reach. While most transit operators undertake regular adjustments of frequency and service levels, bus routing adjustment or bus network restructuring is rare mainly due to the significant barriers to their re-development, e.g. user opposition to change and lack of clear-cut, practical and measurable design criteria for evaluating the 'goodness' of transit routes and comparing sets of routes [1].

China's cities are experiencing rapid growth, the spatial land use changes day by day as well as the travel patterns. There is also a growing reliance on urban rail transit to serve passengers in large China's cities. However, most bus networks are still based on historical development patterns and are rarely adjusted as cities grow and transportation systems change. The transit operators have been realized the apparent importance of accommodating new travel patterns and coordinating buses and urban rail transit. The introduction of urban rail transit in large cities also offers a great opportunity to take the actions. The remaining hindrance is a practical approach to evaluate existing bus networks and support bus routing adjustment.

To bridge the gap, this study evaluates the coverage, transfer and overlap levels—the three perspectives emanating from the broad spectrum of bus routes—using Geographic Information System (GIS) and then conducts hierarchical clustering analysis for all the bus routes based on these indicators. It should enable the transit planner to identify the different types of bus routes and to select improvable bus routes from the transit network. This information could also give them some strategies to optimize bus route.

Following the introductory section, section two reviews the previous research in this area. Section three introduces the design principles of the indicators of bus routes and provides the procedures of indicator calculation and clustering analysis. Section four presents the method application in the Nanjing, China. The paper ends with the conclusions and potential improvements.

# 2 Literature Review

Pratt and Evans suggested that bus routing adjustment or bus network restructuring is the strategy of reworking an existing bus network to rationalize or simplify routes, accommodate new travel patterns, reduce route circuitry, ease or eliminate transfers required for bus travel, or otherwise alter route configuration [1]. Although bus route adjustment is often based on experienced personnel, historical and political precedents than on a rational assessment of existing conditions of bus routes, as a commonly accepted view, quantitative approaches are needed to address the problem, especially for the complex bus networks in large cities. Quantitative approaches could be mathematical models or indicator-based methods. Most studies use mathematics

models to identify possible transit links and then aggregate to form routes according to some simulation or heuristic algorithms [2].

Comparing to mathematical models, indicator-based methods are much easier to use and have been used in many practical circumstances to help transit planners address the immense complexity of designing transit network. Some studies conduct zonal-based analysis to identify the existing or potential (after implementing planned facilities or services) service gap using factors that most effectively quantify the public transit service and needs [3–7]. Other studies focus on route-based analysis, especially for urban rail transit or bus rapid transit project. For example, Chatman et al. concluded that multiple indicators determine fixed-guideway transit project success and developed a spreadsheet tool to predict the impacts of proposed fixed-guideway projects [8]. The TCRP report 'elements needed to create high ridership transit systems' summarized various route- or system-level measures—including design measures such as coverage, span of service, frequency of service, travel time and performance measures such as productivity, crowding and reliability—and suggested benchmarks should depend on the nature of the agency's service network and environment [9]. The Utah Transit Authority calculated a Transit Preparedness Index (TPI) to identify those parts of its service area that have the characteristics to support a successful transit investment [10]. Consulting firms have developed proprietary indicator-based tools such as the Transit Competitiveness Index (TCI) to score different travel markets in terms of how well transit is likely to compete with the automobile [11]. Route-level indicator-based analysis is also used to evaluate bus operations and environmental effects. Jiménez et al. grouped bus routes into clusters using kinematic measured data [12] and macroscopic geographical and functional variables for bus routes which no kinematic measurements are available [13]. André and Villanova studied the bus network in Paris using two methods to evaluate and classify the lines from an environmental perspective [14].

The dramatic expansion of land use and introduction of railway transit change the regional travel patterns in China's large cities, which motivate transit agency to conduct bus routing adjustment. However, the evaluation of transit network is usually data intensive. Although some successful practices of evaluation of transit network have been proposed in overseas researches, new indicators-based method is still needed to conquer data problems and support the bus routing adjustment in China's large cities.

## 3 Methodology

### 3.1 Design the Indicators

It is envisioned that this indicator-based method will provide transit planners and decision-makers with a valuable tool for identifying improvable bus routes. Although the main purpose of bus routing adjustment is to increase ridership, the cost-

effectiveness of existing transit service and social equality among different types of residents (such as rural residents and urban residents) should also be taken into consideration. In most large China's cities, public transit already accounts a large share. Zhang et al. gathered the trip rate data of 24 China' large cities—the average population is 3.12 million. It shows the average public transit mode share is 24.75% [15]. BCL—a virtual research community calculated the 500 m transit coverage ratio in 281 China's cities (the ratio of urban land overlaid with 500 m bus stop buffers). Among the 86 large cities in which the population is greater than 5 million, the 500 m transit coverage ratio is 0.72 [16]. For these cities, where the transit markets have been well developed and the transit coverage ratios are relatively high, the bus routing adjustment should not only focus on coverage expansion. More importantly, it should improve the effectiveness of bus routes and overall performance of bus network.

The land use served by bus route is one of the most important determinate of route-level ridership. The presence of diverse land use served by bus route also contributes to higher revenue and better utilization of transit capacity as it creates more balanced and consistent passenger flow at all times of the day and all days of the week. The indicators should be able to capture those features of the service area.

Although bus routing adjusting may improve overall system effectiveness by removal of redundant services and the introduction of new or better-targeted services, it will impose a disruption on passengers. A concern in bus routing adjusting is whether alterations that force existing transit riders to change their familiar patterns run the risk of driving away patronage. It is also the reason why most transit agencies do not want to adjust bus routes, although they may realize some deficiencies of existing bus networks. An increasing amount of literature suggests an efficient public transport network should encourage interchange between bus routes and between buses and urban railway transit in an efficient and effective manner. The indicators should be able to capture the overlap and transfer levels.

Finally, bus route indicators in this method consist of the following two types: for service areas, there are residential area coverage, non-residential area coverage and land use mix; for transfer and overlap levels, there are include transfer index to/from bus, overlap index with bus, transfer index to/from metro and overlap index with metro.

### 3.1.1 The Service Area Indicators of Bus Routes

The geographic land use data are used to calculate the residential area coverage, the non-residential area coverage and the land use mix.

Following the rule-of-thumb, a 400 m (1/4 mile) buffer is defined as the catchment area of bus stop. Seven types of land uses entered the indicator calculation, and are as follows: residential, commercial, educational, industrial, office, government and transport. The service areas of each stop are calculated and summed to get the service areas of each route. Residential area coverage is the sum of residential building floor area served by the route; non-residential area coverage is the sum of commercial,

educational, industrial, office, government and transport building floor area served by the route.

The different land use mix levels contribute different on ridership and also need to be taken into consideration. The land use mix takes the following formula.

$$\text{land use mix}_i = 1 - \left(\frac{\text{RA}_i}{\text{RA}_i + \text{NRA}_i}\right)^2 - \left(\frac{\text{NRA}_i}{\text{RA}_i + \text{NRA}_i}\right)^2 \tag{1}$$

where

RA     residential area coverage;
NRA   non-residential area coverage;
$i$        the labels of bus routes.

### 3.1.2 The Transfer and Overlap Level Indicators of Bus Routes

The geographic data of bus stops and metro stops are used to calculate the transfer index to/from bus, overlap index with bus, transfer index to/from metro and overlap index with metro. These indicators are named to transfer bus index, overlap bus index, transfer metro index and overlap metro index for simplification consideration. For one bus route, if one of its stops is less than 200 m from one stop of another bus route, we define these routes have transfer potential and the transfer bus index scores 1. The final transfer bus index of this bus route is the sum of scores applied to the whole bus network. It is worth noting, if two routes have more than one stop less than 200 m, the transfer bus index only scores once. The transfer bus index can be formulated as:

$$\text{transfer bus index}_i = \sum_{j=1, j\neq i}^{n} \text{transfer bus score}_{ij} \tag{2}$$

$$\text{transfer bus score}_{ij} = \begin{cases} 1 \ (\text{exist at least one transfer stop}) \\ 0 \ (\text{otherwise}) \end{cases} \tag{3}$$

where

$n$     total number of bus routes;
$i, j$   the labels of bus routes.

For one bus route, if it has m stops that are less than 200 m from stops of another bus route, the overlap with other bus index scores $C_2^m$. The permutation formula means there are $C_2^m$ combinations of boarding and alighting stops can be serviced by the other bus route. For example, if there are three overlapped stops, trips between stop 1 and stop 2, between stop 2 and stop 3 and between stop 1 and stop 3 can use the other bus route. So the overlap effect is multiplicative if the bus route has more

overlapped stops. The final overlap bus index of this bus route is the sum of scores applied to the whole bus network. The overlap bus index can be formulated as

$$\text{overlap bus index}_i = \sum_{j=1, j \neq i}^{n} \text{transfer bus score}_{ij} \tag{4}$$

$$\text{overlap bus score}_{ij} = C_2^m \tag{5}$$

where

$n$    total number of bus routes;
$m$    number of overlapped stops between bus route $i$ and bus route $j$;
$i, j$    the labels of bus routes

The same formulas with some minor modifications can be applied to calculate the transfer metro index and overlap metro index. The function forms are as follows:

$$\text{transfer metro index}_i = \sum_{j=1}^{n} \text{transfer metro score}_{ij} \tag{6}$$

$$\text{transfer metro score}_{ij} = \begin{cases} 1 \ (\text{exist at least one transfer stop}) \\ 0 \ (\text{otherwise}) \end{cases} \tag{7}$$

where

$n$   total number of bus routes;
$i$   the labels of bus routes;
$j$   the labels of metro lines.

$$\text{overlap metro index}_i = \sum_{j=1}^{n} \text{transfer metro score}_{ij} \tag{8}$$

$$\text{overlap metro score}_{ij} = C_2^m \tag{9}$$

where

$n$   total number of bus routes;
$m$   number of overlapped stops between bus route $i$ and metro line $j$;
$i$   the labels of bus routes;
$j$   the labels of metro lines.

## 3.2 Clustering Analysis

There are three ways to do indicator-based analysis—benchmark analysis, composite score analysis and clustering analysis. The benchmark analysis establishes goals or

thresholds for all indicators. The bus routes that do not meet the designated goal or threshold level for that type of route or service entails making the adjustment. This approach has been suggested in the report [9]. Composite score analysis normalized and weighted the indicators according to the level of influence to get a composite score. The most well-known application of this approach is the Walk Score [17]. Since the proper threshold or weight cannot be simply determined in this study, clustering analysis is used to find the groups of bus routes which are disseminated with others.

Clustering analysis refers to a very broad set of techniques for finding clusters in a dataset. Two best-known clustering approaches are K-means clustering and hierarchical clustering. In K-means clustering, the observations are partitioned into a pre-specified number of clusters, while in hierarchical clustering, the number of clusters is not set in advance. Hierarchical clustering ends up with a tree-like visual representation of the observations, called dendrogram. For the consideration of flexibility, hierarchical clustering is performed in this study.

The seven indicators have different scales. Large-scale indicators such as land use coverage tend to have a much larger effect on the inter-bus route dissimilarities, and hence on the clustering ultimately obtained, than small-scale indicators such as land use mix. Therefore, the indicators are scaled to the distributions which have mean zero and standard deviation one to ensure all variables are equally important in hierarchical clustering.

Finally, a hierarchical clustering based on the dissimilarity measure of Euclidean distance was performed. As it is a standard algorithm to do clustering analysis, the mathematical details are not illustrated here. For further reference, see [18].

## 4 Application

### 4.1 Study Context

Nanjing is the capital of Jiangsu Province, China. It covers an area of 4723 km$^2$ and had a population of 8.16 million in 2016. Like other large China's cities, Nanjing is experiencing rapid urbanization and motorization. In the last decade, Nanjing's built-up area reached 653 km$^2$ in 2016 by an annual growth rate of 11.9%; private car ownership reached 866 thousand in 2016 by an annual growth rate of 25.3% [19].

The transit network of Nanjing consists of 410 fix-route bus routes and 7 metro lines in 2016. All urban bus routes and some rural bus routes are operated by six transit companies; other rural routes are contracted to a private person. The average bus route length is 16.1 km. The data from transit agency show the average transit transfer rate is 1.34, the average transit travel time is 49.0 min and daily transit ridership is 3.35 million.

**Table 1** Descriptive statistics of the raw indicators

| Indicator name | Min | Max | Mean | sd |
|---|---|---|---|---|
| Residential area coverage (m²) | 0 | 2.53e+7 | 7.39e+6 | 4.97e+6 |
| Non-residential area coverage (m²) | 1.05e+5 | 3.29e+7 | 8.42e+6 | 5.89e+6 |
| Land use mix | 0 | 0.50 | 0.45 | 0.09 |
| Transfer metro index | 0 | 2 | 0.77 | 0.70 |
| Overlap metro index | 0 | 94 | 4.27 | 10.62 |
| Transfer bus index | 0 | 120 | 45.60 | 29.61 |
| Overlap bus index | 0 | 3181 | 461.66 | 453.62 |

## 4.2 Method Application

The method is applied to the bus network in Nanjing. The descriptive statistics of raw scores of the seven indicators are shown in Table 1.

The magnitudes of these raw indicators vary a lot. After scaling these indicators, we used hierarchical clustering to get the dendrogram, shown in Fig. 1. Each leaf of the dendrogram represents one of the 410 bus routes. As moving up the tree, some leaves begin to fuse into branches. Cutting the dendrogram at a height of 6.5 results in six clusters. Cutting the dendrogram lower will obtain more clusters if more clusters are needed for analysis.

The mean of the scaled indicators by clusters are calculated and depicted in Fig. 2. The differences among six clusters are obvious. The features of clusters are analysed in order of cluster size as well as the potential adjustment strategies.

Cluster three has 179 bus routes (43.7% of the network). The three service area indicators are all above zero, indicating these bus routes serve dense and mixed urban area. These routes perform well on the overlap and transfer indicators. The overlap bus and overlap metro indicators are near zero, while the transfer bus and transfer metro indicators are both above zero. It means they offer a lot of transfer chances and have a small chance be replaced by other routes. These bus routes should be stable in the future.

Cluster four has 155 bus routes (37.8% of the network). The two coverage indicators are below zero while the land use mix are near zero, indicating these bus routes serve the rural area. The four overlap and transfer levels indicators are all below zero. The ridership of these bus routes is probably low, but they could also be stable in the future for the coverage and equality consideration. Some innovative operations should be considered for these bus routes such as demand responsive transit.
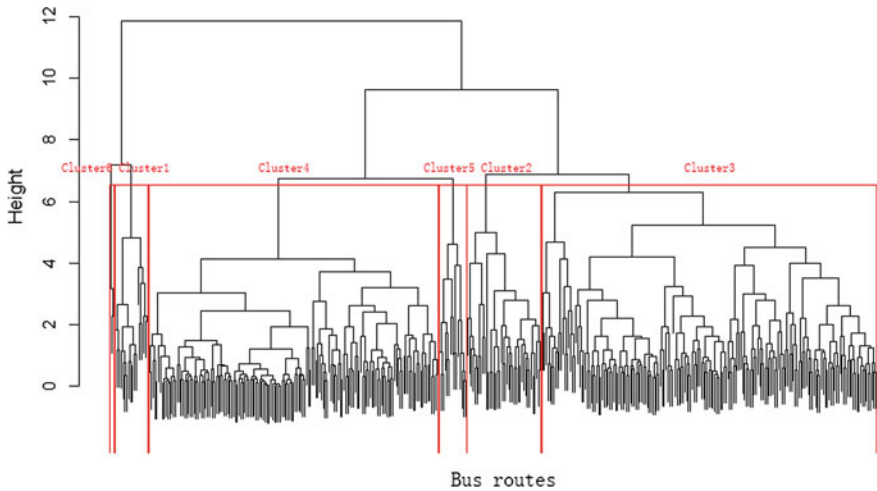
**Fig. 1** Dengrogram of 410 bus routes

Cluster two has 40 bus routes (9.8% of the network). These bus routes serve dense and mixed urban area and travel along bus corridors as they have the highest overlap bus index among all the clusters. It is not easy to judge whether the cluster should be stable or need to be adjusted. The detailed route-by-route review could be done for these bus routes to find such high-level overlap is reasonable or not.

Cluster one has 18 bus routes (4.4% of the network). These bus routes serve most dense and mixed urban area and travel along the metro corridors as they have high overlap metro index. As all other indicators perform well, the detailed route-by-route review may help to find their relationship with metro.

Cluster five has 15 bus routes (3.7% of the network). The features of these bus routes are similar to cluster four except for a much lower land use mix. Adjusting these bus routes to improve their connection to residential area may increase the ridership.

Cluster six has three bus routes (0.7% of the network). Cluster six is an extreme counterpart of cluster one except for the highest overlap metro index. These bus routes could be reviewed and adjusted to reduce the competitiveness and improve the coordination with metro lines.

Any time clustering is performed on a data set clusters will be found. But we need to know whether the clusters are meaningful and interpretable, that is, whether the results can represent true subgroups in the data, or whether they are simply a result of clustering the noise. The bus route-level ridership data for a typical weekday are used to test whether there is a significant difference of ridership among these clusters. As the bus routes are operated by six transit companies and some rural routes are contracted to a private person, ridership data of 375 bus routes (91% of all bus routes) are gathered. The boxplot of the ridership by clusters is shown in Fig. 3 to provide 0th (lower whisker), 25th (lower hinge), 50th (median), 75th
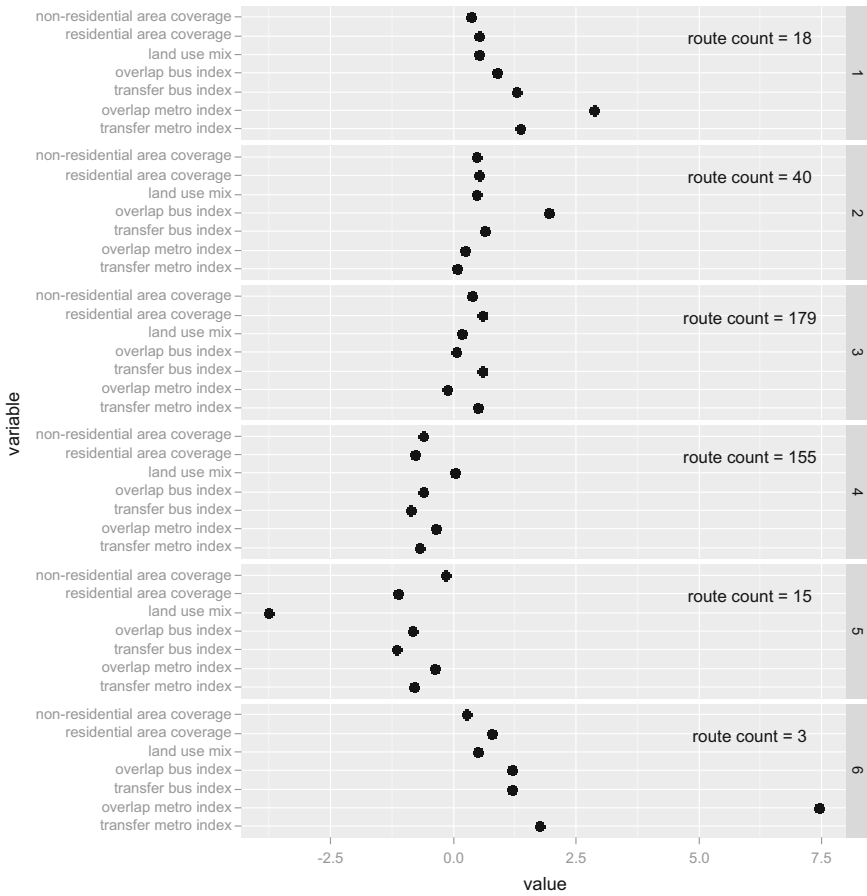
**Fig. 2** Mean of the scaled indicators by clusters

(upper hinge), 100th (upper whisker) percentiles and outliers of ridership records. The distributions of six clusters are quite different. ANOVA test also shows there is a significant difference of ridership among these clusters. The F value is 28.44 with 5 degrees of freedom, which mean the difference is significant at 0.001 level.
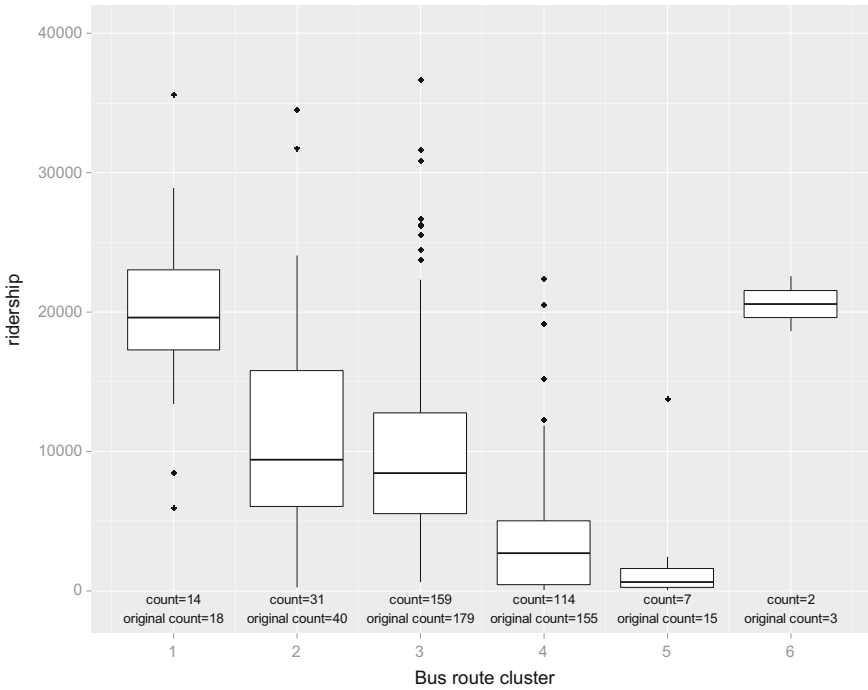
**Fig. 3** Boxplot of the ridership by clusters Note: 'Count' gives the number of bus routes with ridership record in the cluster, which is used to draw the boxplot. 'Original count' gives the original number of bus routes in the cluster

## 5   Conclusions

In the context of China's large cities, although transit infrastructure development has boomed in recent years and transit tends to have a significant mode share in most cities, evaluation of bus network and bus routing adjustment have rarely been done. This study proposed a method to identify improvable bus routes by clustering bus routes based on seven standardized indicators about the coverage, transfer and overlap levels of bus routes. This method only requires the geographic transit network and land use data. These data are available officially to local transit agencies and also can be crawled from the online map service. It can be applied on a yearly basis and easily transferred to other cities. Jiedao (the smallest geographic unit for population census) level population and employment data may improve the accuracy of the approach. If such detailed data are available to local transit agencies or consulting corporations undertaking the transit planning by chance, it might be a good choice to use population- and employment-based coverage indicators instead of the land use-based coverage indicators.

# References

1. Bus routing and coverage (2004) Transportation Research Board
2. Asadi Bagloee S, Ceder AA (2011) Transit-network design methodology for actual-size road networks. Transp Res Part B: Methodol 45(10):1787–1804
3. Currie G (2004) Gap analysis of public transport needs: measuring spatial distribution of public transport needs and identifying gaps in the quality of public transport provision. Transp Res Rec: J Transp Res Board 1895:137–146
4. Currie G (2010) Quantifying spatial gaps in public transport supply based on social needs. J Transp Geogr 18(1):31–41
5. Polzin SE, Pendyala RM, Navari S (2002) Development of time-of-day-based transit accessibility analysis tool. Transp Res Rec: J Transp Res Board 1799:35–41
6. Al Mamun S, Lownes NE (2011) Measuring service gaps: accessibility-based transit need index. Transp Res Rec: J Transp Res Board 2217:153–161
7. Minocha I, Sriraj PS, Metaxatos P et al (2008) Analysis of transit quality of service and employment accessibility for the greater Chicago, Illinois, region. Transp Res Rec: J Transp Res Board 2042:20–29
8. Making effective fixed-guideway transit investments: indicators of success (2014) Transportation Research Board
9. Elements needed to create high ridership transit systems (2005) Transportation Research Board
10. Weber county to salt lake city commuter rail project (2005) Utah Transit Authority
11. The transit competitive index web tool: development and applications. Cambridge Systematics and Transportation Analytics
12. Jiménez F, Román A, López JM (2013) Methodology for kinematic cycle characterization of vehicles with fixed routes in urban areas. Transp Res Part D: Transp Environ 22:14–22
13. Jiménez F, Serradilla F, Román A et al (2014) Bus line classification using neural networks. Transp Res Part D: Transp Environ 30:32–37
14. André M, Villanova A (2004) Characterisation of an urban bus network for environmental purposes. Sci Total Environ 334:85–99
15. Zhang H, Chen X, Li X (2011) Trip rate and travel time: a perspective in china city. Transportation Research Board 90th Annual Meeting. Washington, D.C.
16. Bus coverage of chinese cities [EB/OL]. http://www.beijingcitylab.com/ranking/, 6/20/2016
17. Walkscore [EB/OL]. http://www.walkscore.com/, 6/20/2016
18. Hastie T, Tibshirani R, Friedman J et al (2009) The elements of statistical learning, 2nd edn. Springer, Berlin
19. China City Statistical Yearbook (2016) China city statistical yearbook. China Statistics Press, Beijing, China

# Identifying the Impacted Area of Congestion Charging Based on Cumulative Prospect Theory

Qing-yu Luo, Xin-yu Guan, Wen-jing Wu and Hong-fei Jia

**Abstract** A precise quantitative framework needs to be developed to identify the impacted area of road network by congestion charging. In this paper, a framework is constructed, which includes modeling traffic network based on CPT as a foundation and proposing identifying method on the basis of defining traffic impact threshold. To study the road network performance under congestion charging, a route choice model with an improved reference point is set based on generalized travel cost and a stochastic user equilibrium model based on CPT is adopted. Two indicators, variation of total travel time and the degree of saturation increase, are chosen as determination parameters in identifying method. Finally, a case study shows that the impacted area can be identified quantitatively. This paper puts forward a new thought and quantitative method to analyze the impacted area of traffic management policies.

**Keywords** Congestion charging · Traffic impact · Reference point · Route choice · Impacted threshold

## 1 Introduction and Literature

Urban traffic network is so complex that any subtle change may bring about unpredictable effects, there are chances that the hasty implementation of traffic congestion charging policy may cause more serious traffic problems. Thus, it is essential to know what congestion charging (CC) will bring to the road network before implementation.

Previous researches focus on modeling [1–3] or simulating [4] traffic network performance under CC, using several evaluation indicators to measure the changes of traffic conditions, but none of them establish the correspondence between traffic conditions and the impacted area. Therefore, it cannot provide a direct reference for policymakers. Thus, a precise quantitative framework is needed. Otherwise, models for analyzing the traffic performance under CC have some drawbacks. Some are

Q. Luo (✉) · X. Guan · W. Wu · H. Jia
School of Transportation, Jilin University, Changchun 130022, China
e-mail: luoqy@jlu.edu.cn

based on EUT which is proved to be inconsistent with traveler's real decision-making behavior [5]. It is improved that CPT is more suitable for describing the decision-making progress in road network [6–8], but researches lacking the consideration of travel cost, travelers' attributes and travel attributes [3, 9], which are crucial for travelers in making route choice decision under CC.

According to the analysis above, one precise quantitative framework, which includes modeling the road network more accurately based on CPT and proposing identifying method which makes impacted area of CC quantitative is needed. In this paper, we are assuming that traffic demand is fixed under CC and traffic mode transfer is not been considered.

## 2   Model Traffic Network Based on CPT

### 2.1   Improved Route Choice Model Based on CPT

#### 2.1.1   Model Reference Point

The reference point is a vital "datum point" in the CPT, which reflects the "expectation" of one choice. When making route choice, people focus on the "gain" or "lost" which is relative to the reference point. Thus, it is essential to identify the influencing factors and model it. Previous researches take time into account when modeling it, but actually, travelers also value travel expenses especially under CC. Meanwhile, travelers' attributes and travel attributes are key factors in decision-making progress, which include travelers' income and travel purpose. In order to take both time and travel expenses into account, we define generalized travel cost, which is the sum of travel time cost and travel expenses. The formula is as follows in Eqs. (1, 2, 3):

$$F_a = R_a + S_a \tag{1}$$

$$C_a = \mu \zeta T_a + \eta F_a \tag{2}$$

$$\zeta = \frac{I}{30 \times 8 \times 60} \tag{3}$$

where $R_a, S_a, F_a, C_a$ is the fuel expense, CC rate, total travel expense and generalized travel cost of link $a$, respectively. $\mu, \eta$ is the weight of perceived travel time and cost, respectively, which is decided by income and trip purpose, $\zeta$ is travel time value, $I$ is travelers' income each month.

It has been proved that the travel time of routes obeys a normal distribution [9], assuming perceived travel time is equal to travel time, thus, means and variance of perceived travel time are as follows in Eqs. (4, 5):

$$T_r^w = \sum_a T_a \sigma_{a,r}^w \quad \forall w \in W, r \in R_w \tag{4}$$

$$T_r^w \sim N(t_r^w, (\sigma_r^w)^2) \quad t_r^w = \sum_a E(t_a)\delta_{a,r}^w \quad (\sigma_r^w)^2 = \sum_a (\sigma_a^w)^2 \delta_{a,r}^w \qquad (5)$$

where $T_r^w$ is the perceived travel time of route $r$ between OD pair $w$. $\delta_{a,r}^w$ is the relation between link $a$ and route $r$. $W$ is a set of OD pairs. $R_w$ is a set of route. When link $a$ is on route $r$, $\delta_{a,r}^w = 1$; otherwise, $\delta_{a,k}^w = 0$.

Regarding the fuel expense and CCR is constant. $\mu, \eta, \zeta$ is decided by travelers' attributes which is also constant in one trip. $C_r^w$ is expressed in Eq. (6), obeys a normal distribution as follows in Eq. (7):

$$C_r^w = \mu\zeta T_r^w + \eta F_r^w \quad \forall w \in W, r \in R_w \qquad (6)$$

$$C_r^w \sim N(c_r^w, (\sigma_{c,r}^w)^2) \quad c_r^w = \mu\zeta \sum_a E(t_a)\delta_{a,r}^w + \eta \sum_a F_a \quad (\sigma_r^w)^2 = \mu^2\zeta^2 \sum_a (\sigma_a^w)^2 \delta_{a,r}^w \qquad (7)$$

In former researches, travelers set safety margin to travel time [9], which can reflect differ attitude under risk. Thus, we adopt the time settings in modeling reference point and improve it with generalized travel cost. Thus, reference point model is as follows in Eq. (8):

$$C_{desired}^w = \frac{1}{p}\left[\mu\delta\left(\sum_{i=1}^{p} t_k^w + \phi^{-1}(\rho)\sum_{i=1}^{p} \sigma_{t,k}^w\right) + \eta\sum_{i=1}^{p} F_r^w\right] \qquad (8)$$

where $p$ is the number of paths under Dial's algorithm which reduce the invalid paths in route choice [11]. $\rho$ is the reliability demand of travel time. $\phi^{-1}$ is the inverse function of the normal distribution. The reference point takes both time and expense into consideration, the setting of $\mu, \eta$ reflects how travel purpose influence the route choice.

### 2.1.2 Define Value Function

Travelers estimate the value of each alternative route before making route choices. The value function proposed by Kahneman and Tversky [7] can well satisfy the decision-makers risk preference characteristic under route choice, which calculates the value function as in Eq. (9):

$$v(x) = \begin{cases} x^\varphi & x \geq 0 \\ -\lambda(-x)^\varphi & x < 0 \end{cases} \qquad (9)$$

where $x = C_{desired}^w - C_r^w$ is the changing amount of effectiveness. $\lambda, \varphi$ are parameters that reflect the risk attitude. In accordance with Kahneman and Tversky's experiments [7], $\lambda = 2.25$, $\varphi = 0.08$.

### 2.1.3 Define Weighting Probability Function

Travelers' subjective perception on route is not equal with the actual one. In CPT, the probability weight function can show the subjective cognition behavior of travelers to the objective probability, the function [7] is as follows in Eq. (10):

$$w\left(p_r^w\right) = \frac{p_r^{w^\gamma}}{p_r^{w^\gamma} + (1 - p_r^{w^\gamma})^{\frac{1}{\gamma}}} \tag{10}$$

When $C_{desired}^w > C_r^w$, $\gamma = 0.61$, when $C_{desired}^w \leq C_r^w$, $\gamma = 0.69$ [7]. $p_r^w$ is actual probability which can be obtained by the distribution function. As $C_r^w$ follows normal distribution function, thus, $x = C_{\text{desired}}^w - C_r^w$ has various possibilities. We list all the possibilities by numerical size are as follows:

$$x_k^w = \{x_{k,-m}^w < \cdots < x_{k,j}^w < \cdots < x_{k,0}^w < \cdots < x_{k,i}^w < x_{k,n}^w\} \quad x_{k,0}^w = 0 \tag{11}$$

where $x_{k,i}^w$ presents the possibility of gaining, $x_{k,j}^w$ presents the possibility of losing.

Thus, when $C_{\text{desired}}^w > C_r^w$, the weighting probability function can be expressed as follows in Eq. (12):

$$\pi^+\left(p_{k,i}^w\right) = w^+(p_{k,i}^w + \cdots + p_{k,n}^w) - w^+(p_{k,i+1}^w + \cdots + p_{k,n}^w) \tag{12}$$

When $C_{\text{desired}}^w \leq C_r^w$, the weighting probability function can be expressed as follows in Eq. (13):

$$\pi^-\left(p_{k,j}^w\right) = w^-(p_{k,-m}^w + \cdots + p_{k,j}^w) - w^+(p_{k,-m}^w + \cdots + p_{k,j-1}^w) \tag{13}$$

### 2.1.4 Define Travel Prospect Value

According to CPT, $PS_r^w$ is the prospect value of route $r$, it can be calculated as follows in Eq. (14):

$$PS_r^w = \sum_{i=0}^{n} \pi^+(p_{k,i}^w)V(x_i) + \sum_{i=-m}^{-1} \pi^-(p_{k,j}^w)V(x_j) \tag{14}$$

### 2.1.5 Route Choice Mechanism Based on CPT

In CPT, travelers will choose the route with maximum prospect value based on the judgment they give. Hence, the route choice model is described as the function in Eq. (15):

$$PS_r^w = \text{Max}\left[PS_1^w, PS_2^w, PS_3^w \ldots PS_n^w\right] \tag{15}$$

## 2.2 Stochastic User Equilibrium Model Based on CPT

Some researchers study on the network equilibrium based on CPT. Yang [9] use the cumulative prospect value (CPV) to establish a stochastic user equilibrium model, which can simulate the road network more accurate compared to the one which is based on utility vale. Aveneri [10] shows that setting of reference pint value influence a lot to the equilibrium based on CPT. In this paper, we improved reference point, thus, we adopt the model proposed by Yang and replace the $PS_r^w$ with the formula we set in Eqs. (1–15). The model is as follows in Eq. (16):

$$\min Z(f) = \frac{1}{\beta_p} \sum_o \sum_d \sum_r f_r^w \ln f_r^w - \sum_a \int_0^{x_a} PS_r^w(w)dw$$

$$\text{s.t.} \sum_r f_r^w = q_w \quad \forall o, d$$

$$f_r^w \geq 0 \quad \forall k, o, d$$

$$x_a = \sum_o \sum_d \sum_r f_r^w \delta_{a,k}^w \quad \forall a \in A \tag{16}$$

where $\beta_p$ reflects the travelers' understanding about the road network. $x_a$ is the volume of link $a$. $f_k^w$ is the volume of route $k$ between OD pair $w$. $o$, $d$ are sets of origin and destination of $w$, respectively. The model can be solved by method of successive average. By solving the model above, we can get traffic flow of routes and links under and without CC, which is the foundation of identifying the traffic impact area.

## 3 Traffic Impact Identification

### 3.1 Set Traffic Impact Threshold

In order to identify the impacted area, one criterion is essential to be designed which is used to judge whether the impact is within acceptable range. In this paper, we name the criterion as traffic impact threshold (TIT).

From the view of integrated aspect, the running efficiency may be higher or lower under CC. Thus, we select the variation of total travel time ($\triangle T_1$) as compare indicator and set the TIT value ($\triangle T_0$) with 0.

$$\triangle T_1 = T_h^0 - T_h^1 \tag{17}$$

where $T_h^0, T_h^1$ is the total travel time before and under CC, respectively, which can be got through stochastic user equilibrium model before and after CC, respectively.

From the view of locality aspect, the congestion transfer may occur or not under CC. Thus, we select the degree of saturation increase ($\triangle S'$) as compare indicator and set the TIT value ($\triangle S_i$) regarding 'construction project traffic impact assessment standard' and traffic survey we take. The value and evaluation criteria are listed in Table 1.

$$\triangle S' = \frac{S_1 - S_0}{S_0} \qquad (18)$$

where $S_1$ and $S_0$ is link section saturation under and before CC, respectively, which can be obtained by dividing link traffic flow to link capacity. Link traffic flow can be got through stochastic user equilibrium.

Referring Table 1, by comparing $\triangle S'$ calculated by Eq. (17) with $\triangle S_i$, a conclusion whether the link is significant influence can be obtained.

## 3.2 Identification Method

(1) When $\triangle T_1 < \triangle T_0$, which means CC lower the running efficiency, therefore, from the aspect of whole network, traffic impact is unacceptable, the impacted area includes the whole road network.

(2) When $\triangle T_1 > \triangle T_0$, which means CC higher the running efficiency, therefore, from the aspect of whole network, traffic impact is acceptable. Next, check

**Table 1** Evaluation criteria of road significant influence

| $i$ | Saturation | $\triangle S_i$ (%) | Significant influence range |
|---|---|---|---|
| 1 | [0.00, 0.40] | 50 | Degree of saturation increased by 50% and above |
| 2 | [0.40, 0.60] | 30 | Degree of saturation increased by 30% and above |
| 3 | [0.60, 0.75] | 25 | Degree of saturation increased by 25% and above |
| 4 | [0.75, 0.90] | 15 | Degree of saturation increased by 15% and above |
| 5 | [0.90,1.00] | 10 | Degree of saturation increased by 10% and above |
| 6 | [1.00, –] | 5 | Degree of saturation increased by 5% and above |

whether the links have been significant influence. Links which have been significant influence are impacted area under CC.

# 4 Case Study

## 4.1 Case Remarks

Assuming traffic demand is fixed, travelers are in a classic road network [11]. The network structure, link number, traffic demand and the capacity of each link are shown in Fig. 1. Due to space limitations, the length of each link in the road network is not listed. Travelers in network are classified into six types by income and trip purposes, including travelers' income interval ($IR$), the proportion of each kind of traveler ($P_i$), the representative income of each income interval ($I$), travel time value ($\zeta$), travel purpose ($P_z$), the proportion of each travel purpose ($P_m$), the attributes are listed in Table 2. For all travelers $\rho = 50\%$.
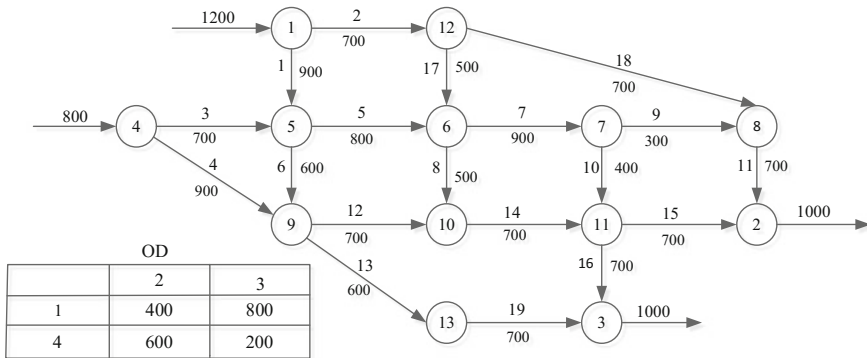


Fig. 1 Structure of network and traffic demand

Table 2 Traveler attributes in route choice

| $IR$ | $P_i$ | $I$ | $\zeta$ | $P_z$ | $\mu$ | $\eta$ | $P_m$ |
|---|---|---|---|---|---|---|---|
| Below 2000 | 0.3 | 1000 | 0.07 | W | 0.6 | 0.4 | 0.8 |
| | | | | N | 0.5 | 0.5 | 0.2 |
| 2000–6000 | 0.4 | 4000 | 0.28 | W | 0.7 | 0.3 | 0.8 |
| | | | | N | 0.6 | 0.4 | 0.2 |
| above 6000 | 0.3 | 8000 | 0.56 | W | 0.8 | 0.2 | 0.8 |
| | | | | N | 0.7 | 0.3 | 0.2 |
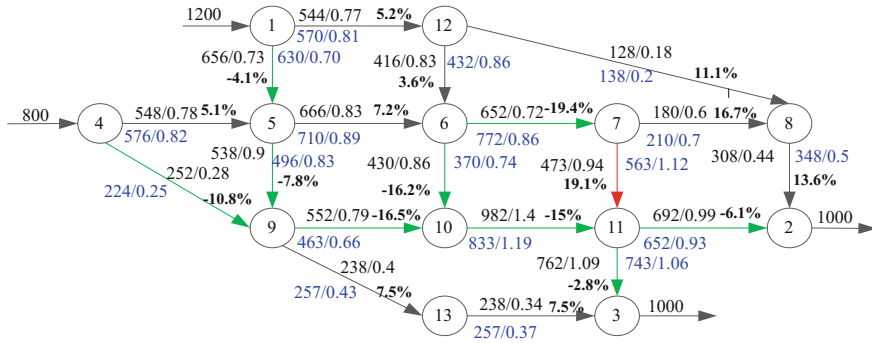
**Fig. 2** Traffic network with and without CC

## 4.2 Identifying the Impacted Area Under CC with 5RMB Rate

According to route choice model we proposed, travelers with different attributes have different prospect values. With the stochastic user equilibrium model based on CPT we adopted, the traffic volume of each route before CC can be obtained. Thus, each link volume and saturation is shown in Fig. 2 with black figure. The total travel time is 231 h. The saturation of link 14 is 1.4 which indicates the traffic flow is unstable and congestion appears. Therefore, charging link 14 with 5RMB rate. Parts of travelers change their travel routes after CC. With the same model proposed in Sect. 2, change charging rate of link 14 from 0 to 5, each link volume and saturation under CC can be obtained as shown in Fig. 2 with blue figure. The total travel time is 209 h. In Fig. 2, the black, green and red lines state links with acceptable bad influence, good influence and significant influence, respectively.

With the method we proposed in Sect. 3, the impacted area can be obtained as follows:

(1) When $T_h^0 = 231h$ and $T_h^1 = 209h$, $\triangle T_1 = 22h > \triangle T_0$, CC improves the road network efficiency.
(2) Calculating $\triangle S'$ of each link (shown in Fig. 2 with black bold) and referring Table 1, link 10 has been significant influence. Thus, the impacted area under 5RMB with given network is link 10.

When designing CC scheme, choosing where and how to charge is super important. In some schemes, road efficiency is improved but congestion transfer occurred, which does not meet the requirement. By setting the parameter values that correspond to the traveler, the impacted area under CC can be identified.

# 5　Conclusions

Congestion charging can mitigate traffic congestion problem to some extent, but the implementation without careful consideration may bring with severe problems on the contrary. The method we proposed makes it possible to identify the impacted area before implantation. We can get a conclusion from the previous work:

(1) A framework is designed for identifying the impacted area of CC, which includes modeling the network under CC and proposing identifying method. A case shows that the framework is feasible.
(2) We establish route choice model based on CPT with improved reference point, define traffic impact scope and set TIT, which makes it complete and practical for identification.
(3) Case testifies that CC cannot eliminate congestion efficiently if the CCR is not well designed.
(4) For future research, the effect of CC on traveling demand and mode transfer should be considered.

# References

1. Ge YE, Stewart K, Sun B et al (2016) Investigating undesired spatial and temporal boundary effects of congestion charging. Transportmetrica B 4(2):1–23
2. Guo W, Yao DY, Jian-Ming HU (2006) Study on network performance evaluation modeling under congestion pricing. J Highw Transp Res Dev 01:105–109
3. Xu H, Lou Y, Yin Y et al (2011) A prospect-based user equilibrium model with endogenous reference points and its application in congestion pricing. Transp Res Part B: Methodol 45(2):311–328
4. Sabounchi NS, Triantis KP, Sarangi S, Liu S (2014) A framework for evaluating the dynamic impacts of a congestion pricing policy for a transportation socioeconomic system. Transp Res Part A: Policy Pract 59(1):357–383
5. Avineri E, Prashker J (2004) Violations of expected utility theory in route-choice stated preferences: certainty effect and inflation of small probabilities. Transp Res Rec J Transp Res Board 1894(1):222–229
6. Avineri E, Prashker JN, Avineri E et al (2003) Sensitivity to uncertainty: the need for a paradigm shift. Ann Meet Transp Res Board 11(7):2406–2419
7. Tversky A, Kahneman D (1992) Advances in prospect theory: cumulative representation of uncertainty. J Risk Uncertainty 5(4):297–323
8. Jou RC, Chen KH (2013) An application of cumulative prospect theory to freeway drivers' route choice behaviours. Transp Res Part A: Policy Pract 49(C):123–131
9. Yang J, Jiang G (2014) Development of an enhanced route choice model based on cumulative prospect theory. Transp Res Part C: Emerg Technol 47:168–178
10. Avineri E (2006) The effect of reference point on stochastic network equilibrium. Transp Sci 40(4):409–420
11. Sang N, Dupuis C (1984) An efficient method for computing traffic equilibria in networks with asymmetric transportation costs. Transp Sci 18(2):185–202

# Drivers' Collision Avoidance Pattern Before Imminent Intersection Accidents

**Mengxia Hu, Wenhui Zhang, Penghui Li, Zhixiao Zheng and Yibing Li**

**Abstract** There is a tendency that drivers do not usually use optimal strategy in imminent intersection conflicts. Drivers usually swerve to the same direction as the obstacle, which sometimes results in accidents. In this paper, driving simulation experiments were conducted focusing on drivers' reaction—especially, the swerving behavior—in critical intersection situations. The influences of incursion side and obstacle velocity were examined during the experiments. The results proved the existence of drivers' same-direction-pattern (SDP) swerving maneuver, as the proportion of same-direction-swerving (SDS) was tremendously higher than what it should be in both left- and right incursion situations. The work serves as a foundation for further research on accident causation and Advanced Driver Assistant Systems (ADAS) development.

**Keywords** Collision avoidance · Swerving maneuver · Intersection conflict Same-direction-pattern

## 1 Introduction

Driving behavior study is always an important aspect of Advanced Driver Assistant Systems (ADAS) development [1]. Learning and modeling, the well-performed behavior as well as examining and preventing the failures could both benefit the automotive safety research. Driver's reaction under imminent conditions affects the outcome of conflicts. Drivers do not always choose optimal maneuver in critical situations, and some of those could result in crashes [2]. There were research somewhat related but not specific to seemingly irrational behaviors, but few discussion had

---

M. Hu · P. Li · Z. Zheng · Y. Li (✉)
State Key Laboratory of Automotive Safety & Energy, Tsinghua University, Beijing 100084, China
e-mail: liyb@mail.tsinghua.edu.cn; tarl@mail.tsinghua.edu.cn

W. Zhang
Traffic School, Northeast Forestry University, Harbin 150040, China

been made on such behaviors in critical situations, and the reason for this sub-optimal maneuver is still unclear.

One of the methods approaching to this issue is accident data analysis. By means of macroscopically statistical research and microscopically case study, investigators are able to obtain regularity, tendency, as well as relationship between reaction and outcome. Edwards and Malone [3] and Limpelt and Gamero [4] described the different drivers' behavior using 4000 and 3000 cases, respectively. Evidence observed through accident studies show that some drivers involved in accidents were attempting inappropriate behavior [5]. To be more accurate, the difference between incursion sides [6], the sequence of braking and swerving [7], etc., were analyzed. Such approaches render very important data, however, they are limited in that they can only describe the collision cases so they are unable to represent a whole map of general driver reaction.

Therefore, investigators conducted experiments to examine how drivers respond to hazards in conflicts rather than accidents. Although there are arguments about such experiments' ignorance of interaction effect [8], they were still useful in evaluating the influence of independent factors. Both field tests [9, 10] and driving simulation tests [8, 22–24] were carried out and discussions on controlled parameters' effect to drivers were made. In particular, Weber [25–27] found that drivers were more likely to turn left while encountering a right incursion. Kastner [11] raised similar questions by assuming these reactions to be innate behavior, indicating that drivers might not rely on rational controlling under certain conditions. However, several detailed but important issues remain to be examined. First, optimal maneuver, in general, has not yet been actually analyzed. There could be more than one maneuver feasible for avoiding, on the other hand, optimal maneuver could be different due to experimental design. As a result, it could be helpful for further examination if the optimal behavior could be generalized under the condition of different factors (e.g., velocities, positions, accelerations, swerving angles, etc.). Second, the swerving into danger [12] definition indicated the relatively higher collision rate—which is important—but it is an overall result and could probably ignore the possible interactive effect among behaviors. Besides, it should be noted that these behaviors were mostly observed under right incursion conditions in previous studies, which could not be explained at present.

Therefore in this study, driving simulation experiments were carried out aiming at verifying whether drivers' executed behaviors diverge from the theoretical ones. In particular, incursion side is included as a factor in the experiment. Compared to some other works' [13, 14] designing that the obstacle's movement was usually accelerating or decelerating, the obstacle was set to move at a constant speed. The influence of obstacle's velocity was also examined, in order to compare with the effect of different acceleration in the works mentioned above.

## 2  Methods

### 2.1  Apparatus

Driving simulation is one of the most commonly used methods on near-collision behavior research because of its security and ease of use on parametrization design. In this study, a six degree of freedom motion-based Driving Simulator (DS) in Tsinghua University was used for experiment, using five multi-synch projectors to create a 220° forward field-of-view and a 36° rear view. The reaction behavior was described by means of driving data recorded by DS at a rate of 60 Hz (Fig. 1).

### 2.2  Subjects

Seven females and 27 males between the ages of 21 and 48 participated in this study. Four of those (three females and one male) did not finish the experiment because of motion sickness, so all of their data was taken out in order to prevent the effect of unusual driving behavior caused by motion sickness. To be eligible, subjects had to have a valid driver's license and have not previously participated in similar emergency behavior studies. Besides, as this study was aiming at finding the typical reactions of drivers, there was a requirement of subjects' having at least 2 years and 20,000 km driving experience.
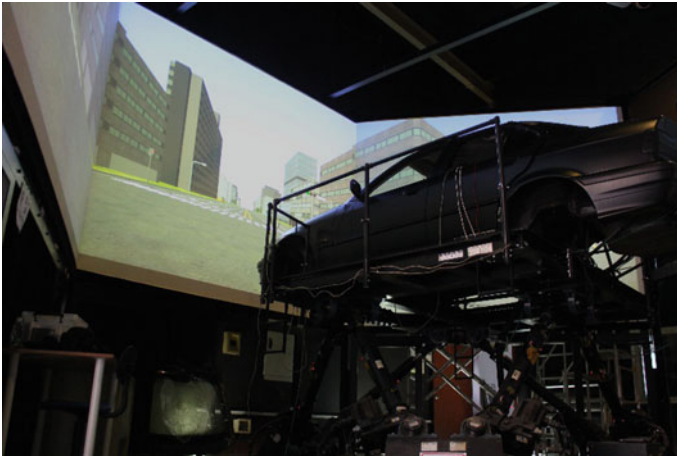


**Fig. 1**  Driving simulator and the urban scenario

## 2.3   Experimental Design and Measures

The study was performed as $2 \times 2$ within-subjects design with incursion side (left vs. right) and obstacle velocity (fast vs. slow) as factors.

To make sure that participants would not stop before reaching the intersections when a conflict was about to be executed, the traffic lights were set to be green for the drivers in each critical scenario. Although the obstacle was designed to be approaching at a uniform movement, it could probably be noticed before the trigger point if it was always moving. Therefore, the obstacle was originally stopped at an obstructed place. When the incident was triggered, then it moved out and passed through the intersection at a constant velocity. The original position of obstacle was set according to its designed speed and TTC. In this experiment, TTC for each scenario was set as 2.0 s, making the conflict relatively urgent. To provide adequate space for swerving, each road is designed to have five lanes in total, and the subject is asked to drive in the third lane. There were no other moving vehicles or bicycles affecting the drivers' decision-making on routing selection when the ego vehicle was approaching the critical scenario. The sequence effect of the factors was balanced in the experiments.

## 2.4   Procedure

Subjects were told that the purpose of the experiment was to estimate the performance of DS and data recording system, so they were informed to drive as if they were actually driving in the real world for the data comparison between the simulation and reality. In the beginning, subjects drove in a practice scenario for 5–10 min in which no data was collected. The practice scenario contained a rear-end conflict and a pedestrian crossing incident. Both of the conflicts were not as urgent as the real scenario, because they are just for making sure the participants could get used to swerving and braking reaction behavior. Afterward, the real scenario of the urban environment with a speed limit of 50 km/h began. Participants were instructed to drive through a total of 20 intersections, four of which were randomly selected as conflict scenarios while the others were for decoys. The experiment lasted about 30 min for each participant.

## 3   Results

## 3.1   Reaction Pattern

Drivers' reaction maneuver could be divided into lateral reaction, longitudinal reaction, and their combination. During the whole extent of experiments no drivers

**Fig. 2** Proportion of avoidance maneuvers in different situations
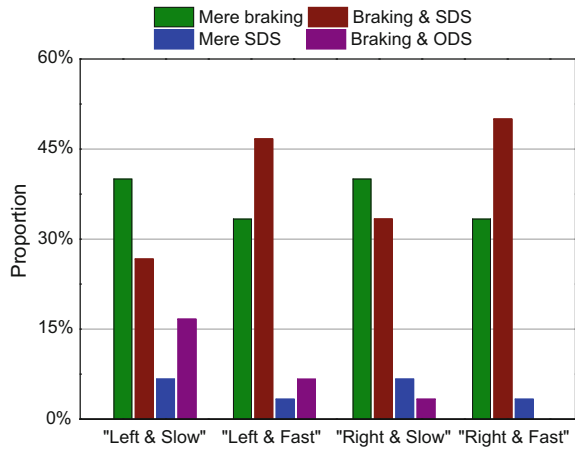
attempted accelerating, so braking is the only longitudinal behavior in this study. Figure 2 shows the proportion of each reaction adopted in the experiments. Overall, braking is the most applied reaction among all. Mere braking shared a large proportion of reaction, and most of the swerving reactions were also adopted along with braking. Neither incursion side nor obstacle velocity had a significant influence on drivers' choice of braking.

Obviously, SDS was extraordinarily more frequently adopted as drivers' swerving maneuver than ODS. If only the two swerving behaviors were taken into consideration, SDS shared 86.9% among all eligible situations. When evaluating the factors' influence on SDS, ODS, and no swerving behavior, a trend could be observed that more SDS occurred when the obstacle moved faster or approaching from the right side. Wilcoxon signed-rank tests showed a significant effect by both incursion side ($p = 0.014$) and obstacle velocity ($p = 0.033$), while Sign tests indicated the significant effect by only obstacle velocity ($p = 0.035$) but not incursion side ($p = 0.388$). Specifically, the difference caused by obstacle velocity mainly existed in left incursion situation (Wilcoxon signed rank test, $p = 0.033$; Sign test, $p = 0.070$).

There were 88.7% of SDS and 100% of ODS combined with braking, showing a strong relationship between drivers lateral and longitudinal maneuvers. Mere swerving, by contrast, only appeared in six cases. Besides, there were 13 cases in which the drivers did not react at all, which is a vital issue [10].

## 3.2  Collision Rate

There were plenty of collisions in the experiment. In summary 71.7% of the conflicts ended in crashes. The collision rates of each critical scenario are represented in Fig. 3. A trend could be noticed that more collisions occurred when the obstacle
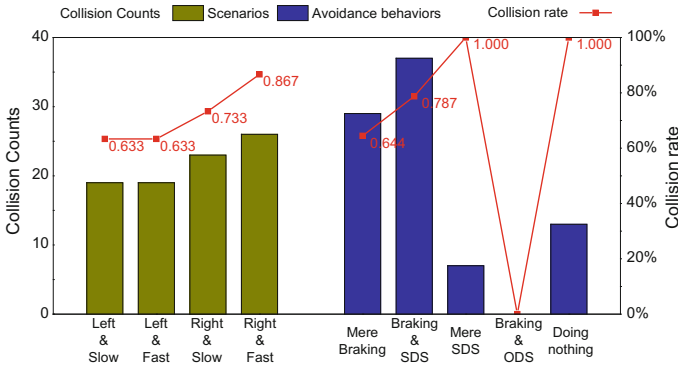
**Fig. 3** Collision rates related to scenarios and avoidance maneuver

came from the right side. The statistical results indicated the significant difference between incursion side ($\chi^2(1) = 4.10$, $p = 0.043$), but no significant difference could be found between the two obstacle velocity situations ($\chi^2(1) = 0.657$, $p = 0.418$).

Comparing to the difference caused by factors, the difference related to reaction behavior shown in Fig. 3 seemed to be much greater. One striking phenomenon is that SDS along with braking contributed great amount of collision counts (37 cases) as well as collision rate (78.7%) among the reacted cases, which were even more than braking alone (29 cases, 64.4%). That is, when braking was applied to be the longitudinal reaction, it could be even worse to swerve along with obstacle's moving direction than doing nothing on steering wheel. However, the difference is not statistically significant ($\chi^2(1) = 2.31$, $p = 0.128$). There were two situations leading to 100% collision rate in this study: mere SDS and doing nothing. However, those situations contained too few data (7 and 13 cases, respectively) for further analysis. ODS (ODS along with braking, to be specific) had perfect performance on evading, that none of the eight cases finally collided.

## 3.3  Reaction Time

As some drivers used braking as their first reaction while some others first used swerving, reaction time in this study was defined as the time between the trigger point and drivers' first reaction. Although there was a trend that drivers tended to react faster under left incursion than right incursion, the difference is not significant. Similarly, drivers seemed to make faster reaction when the obstacle moved faster, the difference is also not significant. It could be because of the limitation of data size, or the rough estimation of the reaction time (a more accurate calculation should be based on the use of eye tracker).

## 4   Discussion

Driving simulation experiments clearly demonstrated the same-direction-pattern (SDP) phenomenon: among all the swerving reactions, ODS's proportion was as low as 12.9%. Although there were differences among scenarios, this phenomenon did not change much. In the "Left and Slow" scenario in which the ODS appeared most, the proportion was yet no more than one-third. All the other scenarios provided an even lower proportion of ODS. Such result indicates the existence of an emergency swerving pattern: drivers tend to swerve to the same direction as the oncoming obstacle in critical intersection situations.

This SDP seems not to be a good choice. Usually, the best reaction for evading the obstacle is ODS along with braking—or mere braking if the driver insists not to make a lane change. SDS only works in fewer cases when along with no-braking or low-decelerating, but such longitudinal maneuver does not often occur suggested by both other studies [5, 9] and results in this study (only seven mere steering behavior occurred in the experiment). In other words, on the basis of the widespread use of braking, SDP is a bad phenomenon. One thing should be noticed that this does not mean the high probability of braking usage is always good. On one hand, sometimes accelerating could be better than braking if ego vehicle could arrive at the potential collision point much earlier than obstacle; on the other hand, drivers' preference of braking rather than swerving could also lead to evitable accidents which could have been avoided by swerving [2].

The outcome of SDP is the high rates of collision. During the driving simulation tests, 81.5% of SDS (including SDS with braking and mere SDS) resulted in a crash. This is the second highest collision rate among all, only less than doing nothing. In contrast, ODS seemed to work great in the experiment, resulting in no accident at all. It is reasonable because based on the experimental design, collisions could be possibly avoided by sharp braking reactions if the drivers could react fast enough. On the basis of this, ODS enlarges the effect of braking and helps the drivers to bypass the obstacles' tail more easily. One of the surprising results is that all of the seven mere SDS cases ended up in the crash, which seems to be different with the kinematic conclusion. One possible explanation is the reaction time. In fact, some of the drivers did not carry out a fast reaction even when they were not distracted, which could also be the reason for the overall higher collision rate in this study than some others [9, 13, 14]. As a result, the conflict could be too urgent to be easily avoided by only swerving.

In summary, the SDS is more likely to be a bad choice based on theoretical analysis, and usually results in more collisions in practice, but is highly adopted by drivers. This suggests the SDP to be a kind of instinctive reaction. As such pattern has not been thoroughly discovered before, more investigation on its causation is required.

# 5 Conclusion

This paper is aiming at investigating drivers' avoidance pattern in imminent intersection situations. Kinematic analysis was made to provide feasible and optimal strategies, and driving simulation experiments were carried out for collecting actual driving data. By comparing the theoretical and executed maneuver, the SDPs existence—which is responsible for higher collision rate—have been proved under both left and right incursion conditions. Several possible reasons for SDP was discussed, yet have not been determined and require further investigation. The extent of SDP could be lower when the obstacle approaches from left side and when its velocity is lower.

# References

1. Figueiredo L, Jesus I, Machado JAT, Ferreira JR, Martins (2001) Towards the development of intelligent transportation systems. In: Intelligent transportation systems proceedings, pp 1206–1211
2. Adams LD (1994) Review of the literature on obstacle avoidance maneuvers: Braking versus steering (Tech. Rep. No. UMTRI-94-19)," Ann Arbor: University of Michigan, Transportation Research Institute
3. Edwards ML, Malone S (1982) Driver crash avoidance behavior. Unpublished manuscript. National Highway Traffic Safety Administration. NHTSA Driver Performance Handbook
4. Limpert R, Garnero FE (1974) The accident avoidance potential of the motor vehicle: accident data, vehicle handling and safety standards. In: Proceedings of the third international congress on automotive safety, vol 11. Washington D.C., GPO, 61p
5. Malaterre B, Ferrandez F, Fleury D, Lechner D (1988) Decision making in emergency situations. Ergonomics 31(4), 643–655
6. Ferrandez F, Fleury D, Lepesant D (1984) Analysetypologique des manoeuvresd'urgence. Rapport ONSER
7. Hatterick GR, Bathurst JR (1976) Accident avoidance skill training and performance testing (Final Report No. DOT/HS 801852). Falls Church, VA: URSIMatrix Company
8. Hancock P, Ridder SD (2003) Behavioural accident avoidance science: understanding response in collision incipient conditions. Ergonomics 46(12):1111–1135
9. Sieber M, Färber B (2016) Driver perception and reaction in collision avoidance: implications for ADAS development and testing. In: 2016 IEEE intelligent vehicles symposium (IV) Gothenburg, Sweden, 19–22 June 2016
10. Xuedong Y, Rami H, Essam R (2008) Analyses of factors of crash avoidance maneuvers using the general estimates system. Traffic Inj Prev 9:2
11. Kramer F, Israel M (2014) "VirtuellerGreifreflex" — einKonfliktpotenzial und die Möglichkeiten der Kompensation in Personenkraftwagenmithilfemoderner Assistenzsysteme ["Virtual Grasp Reflex" — a potential for conflict and the possibilities of compensation in passenger cars with the aid of modern assistance systems]. VKU Verkehrsunfall Fahrzeugtechnik 52(11):390–399
12. Weber S (2013) GibtesStandardreaktionenimUnfallgeschehen? Internal presentation for AUDI AG, Ingolstadt, Germany, 25 Nov 2013

13. Weber S, Färber B (2015) Driver reactions in critical crossing situations. In: 2015 IEEE 18th international conference on intelligent transportation systems. Las Palmas
14. Weber S, Blum K, Ernstberger A, Färber B (2015) Standard reactions—driver reactions in critical driving situations. In: 6th international conference on applied human factors and ergonomics and the affiliated conferences, Las Vegas
15. Lechner D, Malaterre G (1991) Emergency maneuver experimentation using a driving simulator. In: Presented at Autotechnologies, 5th Conference and Exposition, Monte Carlo, Monaco. Report No. SAE 910016
16. Hankey JM, McGehee DV, Dingus TA, Mazzae EN, Garrott WR (1996) Initial driver avoidance behavior and reaction time to an unalerted intersection incursion. In: Proceedings of the Human Factors and Ergonomics Society 40th annual meeting. Human Factors and Ergonomics Society, Santa Monica, CA, pp 896–899
17. McGehee DV, Mazzae EN, Baldwin GHS, Grant P, Simmons CJ, Hankey J, Forkenbrock G (1999) Examination of drivers' collision avoidance behavior using conventional and antilock brake systems on the Iowa driving simulator (Final rep.). University of Iowa, Iowa City

# Satisfaction Evaluation Model of Intercity Bus Service with Different Educational Background Travelers: A Case Study in Guangzhou and Foshan

**Weiwei Qi, Jiajun Mei, Huiying Wen and Yaping Wu**

**Abstract**  Guangzhou and Foshan, the two cities belong to the core area of the Pearl River Delta, the border areas of two cities are about 200 km, so they are unique to natural conditions of the intercity traffic construction. This year, the traffic infrastructures between Guangzhou and Foshan are very fast. There are many ways to travel between the two cities, including the subway, city rail, city bus, and so on. The complex travel groups with different educational backgrounds between the two cities of Guangzhou and Foshan have concerned whether the intercity bus service is satisfactory, and the city manager and the public have also concerned about the topic. The satisfaction indexes of the intercity bus travel can give a good feedback to the intercity travel situation. So, the indexes of economic convenience, reliability, comfort, and accessibility are selected to build a comprehensive index system. Then, the satisfaction evaluation model of intercity bus service with different educational background travelers is established via the entropy weight method. The calculation results show as follows: There is a higher demand for travel time for the intercity travelers under the bachelor's degree. The college degree travelers pay more attention to the reliability and comfort of the intercity travel. The master's degree traveler's demand for intercity travel is more comfortable and reliable, but the demand for accessibility is relatively low. The travel demand for doctoral degree travelers is close to the master, and the demand for economic convenience and comfort is relatively high. Finally, the research results can provide a practical thought train for the evaluation method of the intercity public transport service level, and also provide the reference goal for the accurate service of the intercity transportation facilities.

**Keywords**  Satisfaction evaluation model · Intercity bus service
Entropy weight method · Educational background · Guangzhou and Foshan

W. Qi (✉) · J. Mei · H. Wen · Y. Wu
School of Civil Engineering and Transportation, South China University of Technology,
Guangzhou 510641, China
e-mail: qwwhit@163.com

# 1 Introduction

Customer satisfaction is a prominent aspect of customer-oriented transportation services. To increase the quality of service and customer satisfaction, it is important to measure how the service provided is perceived and to determine customers' expectations and demands [1]. According to research results, service quality of public transportation is related to a series of attributes. The methods can be classified as stated importance methods or derived importance methods [2]. These two approaches have been used to estimate the relative importance of each attribute in terms of the service quality perceived.

The bus routes were important area for the multi-level regression modeling, which is used to estimate the relationship between overall satisfaction and social deprivation. The results indicate routes serving low SES neighborhoods get lower levels of satisfaction [3]. And a better network system of public transport usually makes costumer feel satisfied. Further, the costumers' expectations on public transport are a relative factor for satisfaction [4]. In order to design appropriate strategies that can improve customer satisfaction with service quality of public transport, the considerable research has been conducted to find the strongest attributes on the overall assessment of public service quality [5, 6].

The data about costumers' satisfaction is usually obtained from questionnaire, and the content of questionnaires focuses on performance standards and operator incentives, and their effectiveness in influencing the quantity and quality [7]. The changes in bus boardings are mainly driven by changes in km supplied, and that there are significant differences between the contract regions operated by governmental and private operators [8]. The analytical method is very important to satisfaction evaluation of public transportation. There are two common methods based on a priori information, i.e., exploratory factor analysis (EFA) and confirmatory factor analysis (CFA). The EFA classified the parameters into three groups. Subsequently, the CFA was used to confirm the factor structure [9]. Besides, researchers have studied road safety issues for bus transport management by considering related factors. Concretely, the factors of bus transport management are: drivers (behavior, training, and skills), vehicles (maintenance and advanced devices), and roads (weather conditions and facility integrity) [10].

The mathematical models established in this study enabled the satisfaction evaluation of intercity bus service with different educational background travelers, and the indexes of economic convenience, reliability, comfort, and accessibility are selected to build a comprehensive index system.

## 2  Data Acquisition Scheme and Preliminary Analysis

In 2016, the investigation was conducted on travel satisfaction of intercity bus in Guangzhou and Foshan. The survey was conducted in the 11 intercity bus stations of Guangzhou and Foshan, including intercity bus hub, large station, ordinary station, subway station, and intercity rail station. The satisfaction survey collected 3673 valid questionnaires via intercept inquiry method, and response rate of the questionnaire was 91.83%. The travel satisfaction questionnaire for intercity bus includes three parts: (1) **Basic information**, including gender, age, occupation, educational background, and income. (2) **Travel information,** including weekly trip times, travel frequency, trip purpose, the reason to choose this transport, and travel time. (3) **Satisfaction information,** including economical efficiency, convenience, reliability, comfort, accessibility, overall satisfaction, travel expectations, and subjective value perception.

The distribution data of educational background is shown in Fig. 1. The proportion of high school, technical secondary school, and following degree is 36.73%. The proportion of junior college's degree is 31.32%. The proportion of bachelor's degree is 28.74%. The proportion of master's degree is 2.34%. The proportion of doctoral degree is 0.87%. Bachelor's degree and below accounted for 96.79% of respondents, and the proportion of the main educational background (bachelor's degree, junior college's degree, high school, and so on) is relatively large and uniform in this part, which is around 30%.

The preferred means of transport are shown in Fig. 2. The proportion of motorcycle is 0.67%. Proportion of subway is 65.26%. The proportion of urban rail is 3.79%. The proportion of intercity bus is 17.79%. The proportion of taxi is 0.84%. The proportion of private car is 9.02%. The proportion of unit buses is 1.65%. And others
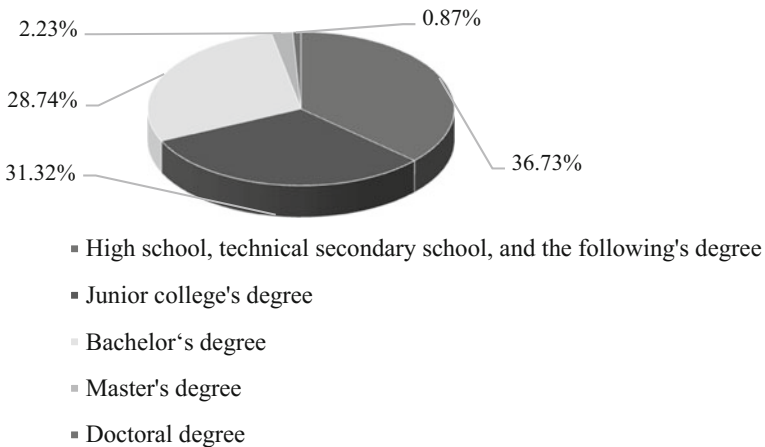


**Fig. 1**  Resident education proportion distribution of intercity traffic trip survey in Guangzhou and Foshan
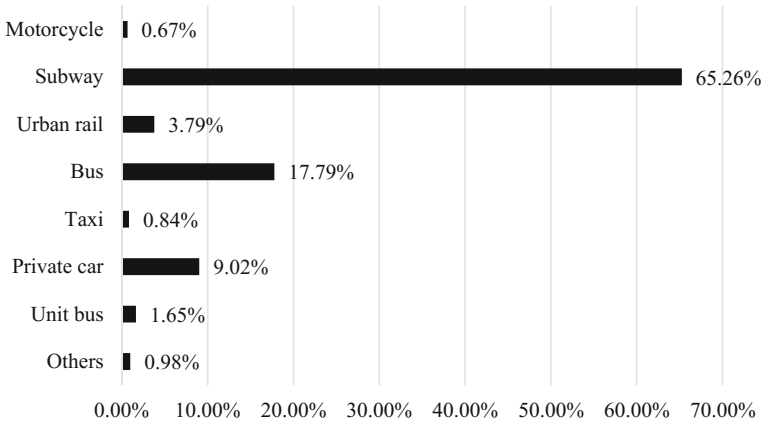
**Fig. 2** Resident trip distribution of intercity traffic trip survey in Guangzhou and Foshan

are 0.98%. So, the subway is the most popular mode, followed by bus, and then the private car. The result reflects the mode of public transportation between Guangzhou and Foshan can meet the needs for the vast majority of residents travel, and subway dominates in all the modes of transportation. The few respondents chose the taxi and motorcycles, the possible reason is riding comfort, safety coefficient, personal economic conditions, and so on.

## 3 Satisfactory Evaluation of Intercity Bus Trip Based on Entropy Weight Method

### 3.1 Construction for Evaluation Indexes System

In order to objectively evaluate and quantify the intercity travel satisfaction level of the residents in Guangzhou and Foshan, the satisfaction evaluation model is established via the entropy method. The model includes the index system, the index weights, and calculation for satisfaction index.

The satisfaction evaluation index system of intercity travel includes the target layer, criterion layer, and index layer, which is shown in Table 1. The target layer is intercity travel satisfaction value of Guangzhou and Foshan. The criterion layer involves economic convenience, reliability, comfort, and accessibility. The index layer includes round-trip cost, transfer times, travel time perception, the departure frequency, the departure time of first bus and last bus, riding comfort, carriage crowded degree, service staff attitude, bus route setting, and bus station settings.

**Table 1** Evaluation index system of intercity travel satisfaction in Guangzhou and Foshan

| Target layer | Criterion layer | Index layer |
|---|---|---|
| Satisfaction value of Guangzhou and Foshan intercity travel ($I$) | Economical and convenient efficiency ($I_1$) | Round-trip cost ($I_{11}$) |
| | | Transfer times ($I_{12}$) |
| | Reliability ($I_2$) | Travel time perception ($I_{21}$) |
| | | Departure frequency ($I_{22}$) |
| | | Departure time of first bus and last bus ($I_{23}$) |
| | Comfort ($I_3$) | Ride comfort ($I_{31}$) |
| | | Carriage crowded degree ($I_{32}$) |
| | | Service staff attitude ($I_{33}$) |
| | Accessibility ($I_4$) | Bus route setting ($I_{41}$) |
| | | Bus station settings ($I_{42}$) |

The satisfaction evaluation index system of intercity travel composed of so many indicators as a whole, and the index system reflects the satisfaction degree for intercity passenger in Guangzhou and Foshan.

## 3.2  Empowerment Step for Entropy Weight Method

In this paper, the entropy weight method is introduced to determine the weight for each index in the intercity travel satisfaction evaluation. The intercity travel satisfaction evaluation system of the target layer is set as $I$ in Guangzhou and Foshan. The indexes of the criterion layer are $I_1$, $I_2$, $I_3$, $I_4$, and the index layer is $I_{11}$, $I_{12}, \ldots I_{42}$. The $S_{pq}$ represents the evaluation score of weight for $I_{pq}$, and the $S_p$ represents the weighted evaluation score for $I_p$ ($p = 1, 2, 3, 4, q = 1, 2$ or $1, 2, 3$). At the same time, $n$ is the number of the intercity questioned passenger, which derives from the maximum and minimum normalized method of the processing result.

In the Guangzhou and Foshan, the entropy value of the index system for intercity travel satisfaction evaluation can be expressed as

$$E(I_{pq}) = -\frac{1}{\ln n} \sum_{r=1}^{n} P(y_{pqr}) \ln P(y_{pqr}) \tag{1}$$

$$P(y_{pqr}) = \frac{y_{pqr} + 1}{\sum_{r=1}^{n} (y_{pqr} + 1)} \tag{2}$$

Entropy of $I_{pq}$ is:

$$\omega_{pq} = \frac{1 - E(I_{pq})}{m - \sum_{p=1}^{4} \sum_{q=1}^{t} E(I_{pq})} \tag{3}$$

The $m$ is the number of index layer, $m = 10$; $t = 2$ or 3.

The entropy weight of each criterion layer is calculated by each entropy weight $\omega_{pq}$ of index layer:

$$\omega_p = \sum_{q=1}^{t} \omega_{pq} \tag{4}$$

At last, the target level is the weighted average of all indexes:

$$A = \sum_{p=1}^{4} \sum_{q=1}^{t} \omega_{pq} \times S_{pq} \tag{5}$$

## 4  Satisfaction Degree of Intercity Bus Service for Different Educational Background

In order to analyze the distribution differences with the intercity travel satisfaction degree in Guangzhou and Foshan, the satisfaction evaluation model has been established based on the different educational background. The data of intercity travel satisfaction, respectively, lists in Tables 2, 3, 4, 5, and 6, including the educational background of high school and the following's degree, junior college's degree, bachelor's degree, master's degree, and doctoral degree.

**Table 2** Travel satisfaction of the traveler with high school and the following's degree

| Criterion layer | $A_p$ | $\omega_p$ | Index layer | $S_{pq}$ | $\omega_{pq}$ |
|---|---|---|---|---|---|
| Economical and convenient efficiency | 0.5402 | 0.1550 | Round-trip cost | 3.644 | 0.0941 |
| | | | Transfer times | 3.240 | 0.0609 |
| Reliability | 1.1574 | 0.3823 | Travel time perception | 2.819 | 0.1291 |
| | | | Departure frequency | 2.993 | 0.1409 |
| | | | Departure time of first bus and last bus | 3.310 | 0.1123 |
| Comfort | 0.8154 | 0.2362 | Ride comfort | 3.790 | 0.0651 |
| | | | Carriage crowded degree | 3.072 | 0.1017 |
| | | | Service staff attitude | 3.693 | 0.0694 |
| Accessibility | 0.8810 | 0.2264 | Bus route setting | 3.553 | 0.0768 |
| | | | Bus station settings | 4.065 | 0.1496 |

According to the above results (in Tables 2, 3, 4, 5, and 6), the different degree of intercity travel satisfaction index could be calculated based on Formula (5). With the increase of education level, the satisfaction value of intercity travel shows a trend of gradual decline (in Table 7). In general, the travelers of higher degree have more demand for the quality intercity transportation services.

## 5 General Discussion

In the criterion layer (in Fig. 3), the intercity travelers with bachelor and following's degree pay more attention to travel time reliability. The intercity travelers with junior college's degree think highly of reliability and comfort. The demand of economic convenience and comfort are remarkably high to intercity travelers with master's degree and doctoral degree.

In the index layer (in Fig. 4), the travelers with junior college's degree or below degree focus on reliability-related indicators and station settings. The bachelor's degree travelers are more sensitive on the round-trip costs, travel time perception,

**Table 3** Travel satisfaction of the traveler with junior college's degree

| Criterion layer | $A_p$ | $\omega_p$ | Index layer | $S_{pq}$ | $\omega_{pq}$ |
|---|---|---|---|---|---|
| Economical and convenient efficiency | 0.4732 | 0.1419 | Round-trip cost | 3.387 | 0.0790 |
| | | | Transfer times | 3.269 | 0.0629 |
| Reliability | 1.0400 | 0.3650 | Travel time perception | 2.892 | 0.1231 |
| | | | Departure frequency | 2.531 | 0.1212 |
| | | | Departure time of first bus and last bus | 3.125 | 0.1207 |
| Comfort | 1.0340 | 0.3005 | Ride comfort | 3.801 | 0.0937 |
| | | | Carriage crowded degree | 2.822 | 0.1031 |
| | | | Service staff attitude | 3.731 | 0.1037 |
| Accessibility | 0.7654 | 0.1926 | Bus route setting | 3.688 | 0.0562 |
| | | | Bus station settings | 4.092 | 0.1364 |

**Table 4** Travel satisfaction of the traveler with bachelor's degree

| Criterion layer | $A_p$ | $\omega_p$ | Index layer | $S_{pq}$ | $\omega_{pq}$ |
|---|---|---|---|---|---|
| Economical and convenient efficiency | 0.5874 | 0.1761 | Round-trip cost | 3.362 | 0.1218 |
| | | | Transfer times | 3.276 | 0.0543 |
| Reliability | 1.0524 | 0.3588 | Travel time perception | 3.173 | 0.1355 |
| | | | Departure frequency | 2.328 | 0.1171 |
| | | | Departure time of first bus and last bus | 3.294 | 0.1062 |
| Comfort | 0.8001 | 0.2415 | Ride comfort | 3.813 | 0.0673 |
| | | | Carriage crowded degree | 2.734 | 0.0974 |
| | | | Service staff attitude | 3.609 | 0.0768 |
| Accessibility | 0.8077 | 0.2237 | Bus route setting | 3.439 | 0.0804 |
| | | | Bus station settings | 3.707 | 0.1433 |

**Table 5** Travel satisfaction of the traveler with master's degree

| Criterion layer | $A_p$ | $\omega_p$ | Index layer | $S_{pq}$ | $\omega_{pq}$ |
|---|---|---|---|---|---|
| Economical and convenient efficiency | 0.9855 | 0.2954 | Round-trip cost | 3.302 | 0.0753 |
| | | | Transfer times | 3.348 | 0.2201 |
| Reliability | 0.7909 | 0.2834 | Travel time perception | 2.823 | 0.0437 |
| | | | Departure frequency | 2.478 | 0.1398 |
| | | | Departure time of first bus and last bus | 3.214 | 0.0999 |
| Comfort | 0.9486 | 0.2946 | Ride comfort | 3.783 | 0.0828 |
| | | | Carriage crowded degree | 2.563 | 0.1195 |
| | | | Service staff attitude | 3.565 | 0.0923 |
| Accessibility | 0.4693 | 0.1267 | Bus route setting | 3.171 | 0.0354 |
| | | | Bus station settings | 3.911 | 0.0913 |

**Table 6** Travel satisfaction of the traveler with doctoral degree

| Criterion layer | $A_p$ | $\omega_p$ | Index layer | $S_{pq}$ | $\omega_{pq}$ |
|---|---|---|---|---|---|
| Economical and convenient efficiency | 1.1071 | 0.3229 | Round-trip cost | 3.542 | 0.1663 |
| | | | Transfer times | 3.308 | 0.1566 |
| Reliability | 0.6823 | 0.2524 | Travel time perception | 2.618 | 0.0992 |
| | | | Departure frequency | 2.464 | 0.0696 |
| | | | Departure time of first bus and last bus | 3.003 | 0.0836 |
| Comfort | 0.9686 | 0.3097 | Ride comfort | 3.770 | 0.0665 |
| | | | Carriage crowded degree | 2.464 | 0.1469 |
| | | | Service staff attitude | 3.696 | 0.0963 |
| Accessibility | 0.3828 | 0.1150 | Bus route setting | 3.615 | 0.0536 |
| | | | Bus station settings | 3.078 | 0.0614 |

**Table 7** Satisfaction value of intercity travelers with different educational background

| Degree | High school and the following's degree | Junior college's degree | Bachelor's degree | Master's degree | Doctoral degree |
|---|---|---|---|---|---|
| Satisfaction value | 3.39 | 3.31 | 3.25 | 3.19 | 3.14 |
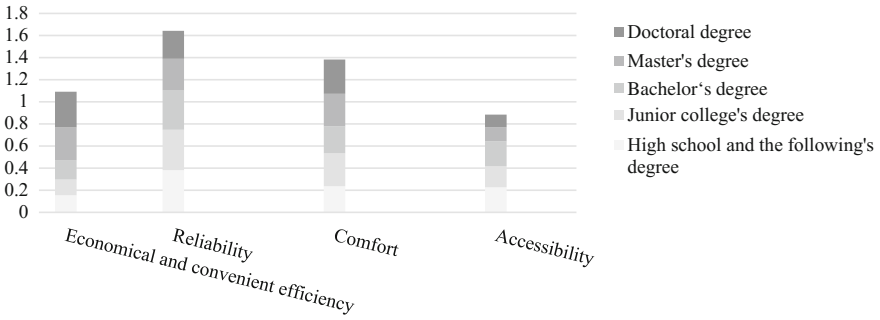
**Fig. 3** Comparison of criterion layer weights of intercity travelers with different educational background
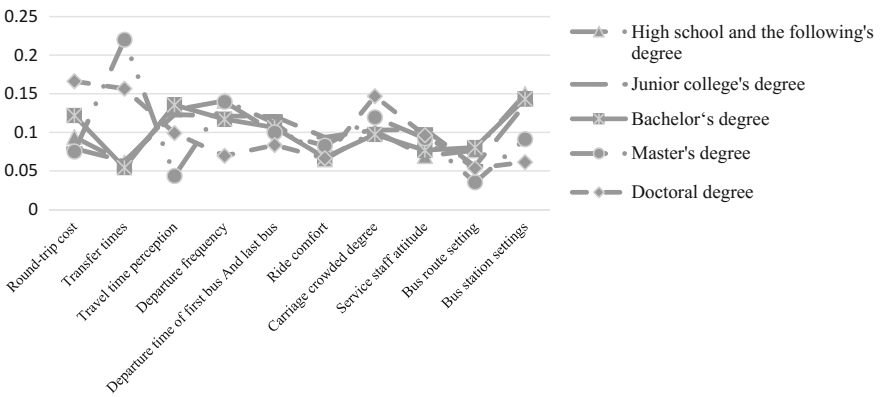


**Fig. 4** Comparison of indicator level weights of intercity travelers with different educational background

and station settings. The master's degree travelers require higher service on the number of transfers, departure frequency, and carriage crowded degree. The doctoral degree travelers are more concerned with round-trip costs, transfer times, and carriage crowding.

**Conflict of Interests**
The authors declare that there is no conflict of interests regarding the publication of this paper. The content of questionnaire has been confirmed by the Ethics Committee of SCUT.

# References

1. Alpu Ozlem (2015) A methodology for evaluating satisfaction with high-speed train services: a case study in Turkey. Transp Policy 44:151–157
2. De Ona J, De Ona R, Calvo FJ (2012) A classification tree approach to identify key factors of transit service quality. Expert Syst Appl 39(12):11164–11171
3. Grisé Emily, El-Geneidy Ahmed (2017) Evaluating the relationship between socially (dis)advantaged neighbourhoods and customer satisfaction of bus service in London, U.K. J Transp Geogr 58:166–175
4. Friman M, Fellesson M (2009) Service supply and customer satisfaction in public transportation: the quality paradox. J Public Transp 12(4):57–69
5. de Oña J, de Oña R, Eboli L, Mazzulla G (2015) Heterogeneity in perceptions of service quality among groups of railway passengers. Int J Sustain Transp 9(8):612–626
6. Eboli L, Mazzulla G (2015) Relationships between rail passengers' satisfaction and service quality: a framework for identifying key service factors. Public Transp 7(2):185–201
7. Wallis Ian P (2016) Demand and service impacts of competition for the market—Australian urban bus case studies. Res Transp Econ 59:330–342
8. Mulley Corinne, Ho Chinh (2013) Evaluating the impact of bus network planning changes in Sydney, Australia. Transp Policy 30:13–25
9. Sajjakaj J, Vatanavongs R (2016) Measurement modelling of the perceived service quality of a sightseeing bus service: an application of hierarchical confirmatory factor analysis. Transp Policy 45:240–252
10. Cafiso S, Di Graziano A, Pappalardo G (2013) Using the Delphi method to evaluate opinions of public transport managers on bus safety. Saf Sci 57(8):254–263

# Analysis of Public Transportation Performance Based on GPS Data: Case Study of Zhengzhou, China

**Yu-zhou Duan, Hang Jing, Yi-wen Wang and Kun Shi**

**Abstract**  To reduce traffic jam and pollution emissions, public transportation has been developing in recent years worldwide. There already have metro, bus rapid transit (BRT), and CBS (CBS) in Zhengzhou city. To grasp the transit performance deeply, vehicle running GPS data could be obtained in the Zhengzhou Traffic Information Center. Five different types of transit were compared from line distance, station distance, travel speed, and spot speed. Then, the traffic data of BRT and CBS were analyzed from different perspectives. Last proposed the corresponding recommendations for the Zhengzhou city.

## 1   Introduction

The increasing urban population has brought about traveling pressure, urban traffic becomes more and more congested. Although the authorities have adopted various measures to relieve traffic congestion, such as traffic restriction, license-plate lottery, and traffic congestion fee, the effect is limited. In the domestic large- and medium-sized cities, travel will still accompany by a traffic jam. Because of its high carrying capacity and low pollution emissions, public transport has become an effective way to ease traffic congestion in the existent situation, particularly after the proposed concept of Transit-Oriented Development (TOD).

Y. Duan · H. Jing (✉) · K. Shi
School of Civil Engineering and Architecture, Henan University of Technology, Zhengzhou 450001, China
e-mail: hautjh@126.com

Y. Wang
Zhengzhou Traffic Information Technology Co.LTD, Zhengzhou 450000, China

With the development of economy and science technology, there are many ways of public transit, such as metro rail transit (MRT), light rail transit (LRT), bus rapid transit (BRT), magnetic levitation, and so on. Compared with the conventional bus transit, the first three have a wide range of applications. In order to implement the policy of public transportation priority, Zhengzhou has been developing the urban public transit vigorously and is currently establishing a comprehensive integrated urban transportation system including metro, BRT and conventional buses. With the trend of intelligent transportation information, the Zhengzhou traffic information center (ZZTIC) is established, which is specially used to collect, monitor and release traffic information. Based on the data provided by ZZTIC, this chapter is mainly to analyze the operation of a conventional bus and BRT system and find out the crux of the currently running. Finally, some recommendations will be proposed for the rapid development of public transit in Zhengzhou.

## 2   Literature Review

There are plenty of researches on public transit. Through reviewing the literature on transit network planning problems and real-time control strategies for bus transport systems, Ibarra-Rojas et al. presented the trend from different views [1]. Almselati et al. tried to reduce traffic congestion and improve public transit, through examining passengers' willingness to pay (WTP) for and willingness to accept (WTA) using spike model [2]. Considering the information exchange between travelers and transit company, a novel approach utilizing automated customer feedback was proposed to improve the service quality [3]. By estimating the emissions savings from public bus services in two cities, Prabhu indicated that public bus services produce significant reductions in carbon emissions [4]. Collecting data on passengers and vehicles from smartphones to automatic transit vehicle location (AVL) data, high-resolution travel times and their relationships with the timetable were then derived [5].

With the rapid encroachments of the BRT construction, there are more and more studies of BRT. From Curitiba's main transit milestones and barriers in the BRT system, Lindau et al. proposed that it should develop improvements in the delivery of quality of service to transit users [6]. Deng et al. examined the performance and impacts of BRT in Beijing, which suggested that it is one of the key measures for promoting sustainable mobility [7]. The BRT system was shown to act as a significant role in reducing emissions, compared with those from a conventional diesel bus [8]. Through summarizing the development of BRT in nine cities of China, recommendations regarding China's BRT decision making, planning, systems designs, and operational management were provided [9].

# 3   Data Sources

The data were collected by ZZTIC, based on GPS and vehicle communication equipments. There has been an intelligent application system of urban public transportation, which can monitor and warn the public transit system, such as city bus, taxi, subway in real-time, then generate and store a large number of data. The data mainly includes the following four categories of information: basic information of line and station, vehicle running information, station speed and passenger flow information. Data format is shown as Table 1.

There are only two MRT lines in Zhengzhou, so comparisons were conducted between the BRT and CBS. In order to carry out a more detailed comparison, the CBS could be divided into four types: normal bus system, night bus system, peak bus system, and feeder bus system in the CBD. Therefore, five types of transit system were analyzed in this study, which starting with number, B, CBD, G, and Y, respectively. In this study, there are 208 normal lines, 40 BRT lines, 2 CBD lines, 3 peak lines and 22-night lines to be analyzed. The first and last time of the starting station and terminus of the normal bus and BRT system is 06:00–21:00. That of CBD, the night bus and peak bus is different, i.e., CBD 1—From east of convention and exhibition center is 6:30-22:30, G701—From Huayuan Road and Liuzhuang is 16:50–17:50 and 7:00–8:00, and from Business inner Ring and West Zhongyi Road is 17:25–18:25 and 7:35–8:35.

The data was download from the intelligent application platform system at the ZZTIC, and the time horizon is from June 20 to July 17, 2016. Through basic statistical and distribution estimation methods, we could get some results. The probability density distribution (PDF) model used in this study is shown as below.

$$\text{Log-normal distribution :} \quad f(x|\mu, \sigma) = \frac{1}{x\sigma\sqrt{2\pi}}e^{\frac{-(\ln x - \mu)^2}{2\sigma^2}} \tag{1}$$

$$\text{Normal distribution :} \ f(x|\mu, \sigma) = \frac{1}{\sigma\sqrt{2\pi}}e^{\frac{-(x-\mu)^2}{2\sigma^2}} \tag{2}$$

$$\text{T-location scale distribution :} \ f(x|\mu, \sigma, v)$$

$$= \frac{\Gamma\left(\frac{v+1}{2}\right)}{\sigma\sqrt{v\pi}\,\Gamma\left(\frac{v}{2}\right)}\left[\frac{v+\left(\frac{x-\mu}{\sigma}\right)^2}{v}\right]^{-\left(\frac{v+1}{2}\right)} \quad -\infty < x < \infty \tag{3}$$

$$\text{Logistic distribution :} \ f(x|\mu, \sigma) = \frac{\exp\left(\frac{x-\mu}{\sigma}\right)^2}{\sigma\left(1+\exp\left(\frac{x-\mu}{\sigma}\right)\right)^2} \tag{4}$$

where, $f(x)$—the probability density function (PDF) of x; $\mu$—Log Mean in Eq. (1); Mean in Eq. (2); Location parameter in Eq. (3); Mean in Eq. (4); $\sigma$—Log Standard deviation in Eq. (1); Standard deviation in Eq. (2); Scale parameter in Eq. (3); Scale parameter in Eq. (4); $v$—Shape parameter in Eq. (3); $\Gamma()$—the Gamma function in Eq. (3).

**Table 1** Data sample

| Line_no | Vehicle_no | Planned departure time | Departure time | Arrival time | Number of station (up) | Use or not | Storage time |
|---|---|---|---|---|---|---|---|
| 1 | 11147 | 7:50 | 7:35:20 | 10:03:20 | 12 | 1 | 10:03:20 |
| *Trip* | *Number of station (down)* | *Maximum station order (up)* | *Maximum station order (down)* | *Mileage* | *Empty mileage* | *Round* | |
| 0.6 | 0 | 14 | 0 | 14,659 | 0 | 2 | |
| *Line_no* | *Vehicle_no* | *Is_up_down* | *Station order* | *Station_name* | *On passenger number* | *Off passenger number* | *Time* |
| 1 | 11147 | up | 1 | Huashan Road | 5 | 3 | 20:12:37 |
| *Line_no* | *Is_up_down* | *Label_no* | *Distance* | *Station_ID* | *Station_name* | *LNG* | *LAT* |
| 1 | 0 | 1 | 184 | 37538 | Huashan Road | 113.5938 | 34.7506 |
| *Line_no* | *Is_up_down* | *Station_ID* | *Station_name* | *Speed* | *Time* | | |
| Y805 | 0 | 1709 | Shangdu Road and Dongzhou cun | 11.04 | 0:04:59 | | |

## 4  Analysis and Results

### 4.1  Analysis of the Basic Situation

Based on the bus line information, we could get some basic statistics at Table 2. From Table 2, the line distance of BRT is a small longer than the normal bus line. In addition, we find that there are too long and too short line in the Zhenghou city, which is adapted to special lines and areas. And the average line length and station distance are 12.8 km and 580 m, respectively.

In order to analyze the distribution of line length and station distance of the bus transit system in Zhengzhou city more comprehensive, we get the corresponding PDF using the kernel density estimation according to different types, the results are shown in Fig. 1. Noted that, the CBD lines and peak lines were not considered in the line distance distribution due to their small sample.

From Fig. 1, it can be found that the difference exists among different types of lines. Among them, line length distribution of night bus system is concentrative. And the PDF of BRT station distance is also concentrative. In contrast, the PDF of normal bus system is decontrolled. This is because the normal bus transit is still the dominant way to travel in a public transportation system, and there are lots of bus routes to meet the needs of passengers who travel in different places and different distances.

**Table 2**  The line station number and distance (distance: m)

| Type/item | | Station_no (up) | Distance_line (up) | Station_no (down) | Distance_line (down) | Average station distance (up) | Average station distance (down) |
|---|---|---|---|---|---|---|---|
| Normal | Max | 43 | 34,544 | 43 | 34,359 | 1919 | 1909 |
| | Min | 5 | 2695 | 5 | 3013 | 210 | 254 |
| | Average | 22.3 | 12,545 | 22.7 | 12,698 | 569 | 567 |
| BRT | Max | 52 | 40,515 | 52 | 40,983 | 978 | 954 |
| | Min | 9 | 7877 | 11 | 6705 | 403 | 418 |
| | Average | 23.9 | 14,825 | 23.8 | 14,515 | 617 | 603 |
| CBD | Max | – | – | 13 | 4711 | – | 367 |
| | Min | – | – | 11 | 3602 | – | 327 |
| | Average | – | – | 12 | 4187 | – | 347 |
| Night | Max | 27 | 15,950 | 29 | 16,609 | 1077 | 967 |
| | Min | 9 | 6570 | 9 | 8657 | 467 | 461 |
| | Average | 19.5 | 11,385 | 19.1 | 11,433 | 599 | 612 |
| Peak | Max | 17 | 14,931 | 17 | 14,816 | 999 | 928 |
| | Min | 10 | 9989 | 11 | 10,212 | 690 | 655 |
| | Average | 14 | 12,219 | 15 | 12,053 | 874 | 818 |
| Total | Max | 25 | 40,515 | 52 | 40,983 | 1919 | 1909 |
| | Min | 5 | 2695 | 5 | 3013 | 210 | 254 |
| | Average | 22.2 | 12,773 | 22.4 | 12,786 | 582 | 577 |

(a) PDF of the line distance



(b) PDF of the station distance
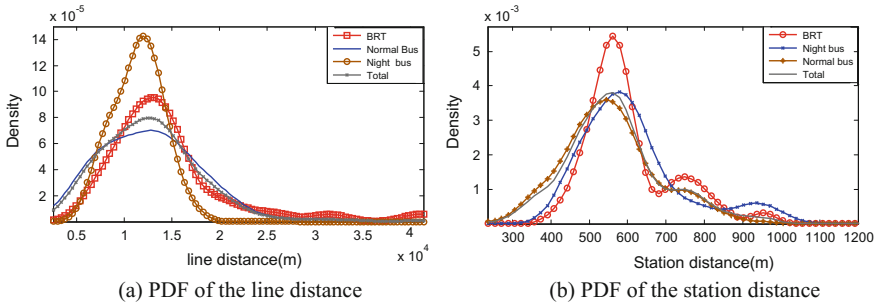
**Fig. 1** The PDF of the line and station distance

**Table 3** Raw data statistics

| Week | Round | Passenger mileage (km) | Empty mileage (km) | Empty rate (%) |
|---|---|---|---|---|
| Monday | 24,151 | 727,425.6 | 37,231.7 | 5.02 |
| Tuesday | 21,608 | 647,755.8 | 49,508.4 | 7.10 |
| Wednesday | 22,384 | 671,096.8 | 56,751.1 | 7.73 |
| Thursday | 21,401 | 641,326.9 | 48,096.7 | 6.98 |
| Friday | 18,422 | 552,376.3 | 50,940.5 | 9.12 |
| Saturday | 17,900 | 536,180.5 | 36,205.5 | 6.33 |
| Sunday | 12,375 | 371,643.8 | 28,952.3 | 13.57 |
| Mean value | 19,749 | 592,543.7 | 43,955.2 | 7.98 |

The data were collected for four weeks, as shown in Table 3. It can be found that travel activities on Monday are more frequent, while travel activity at the weekend is relatively small, corresponding empty rate is also higher.

## 4.2 Analysis of the Basic Situation

### 4.2.1 Travel Speed Distribution

Travel speed of bus vehicle within one line can directly reflect the operation performance, so the travel speeds of different types were compared next. From the Table 1, the departure time and arrival time are known, meanwhile, we know the operating mileage of every bus. Therefore, we can get travel time and the travel speed of every bus vehicle. Because there are some differences between the line facilities and the vehicle performance among different types of bus system, so we will discuss the distribution based on different forms. And the suitable distributions are used to fit them. The results are shown in Fig. 2.

(a) Normal bus system

(b) BRT system

(c) Night bus system

(d) Peak bus system
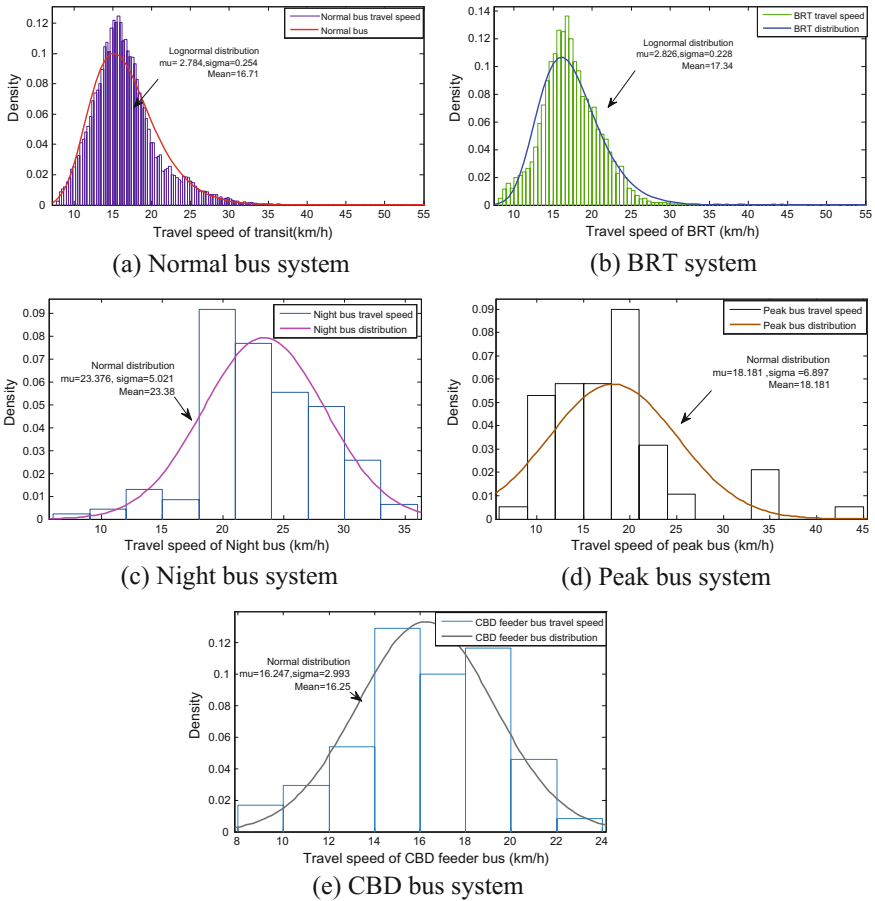
(e) CBD bus system

**Fig. 2** The PDF of travel speed of different type of bus system

From the Fig. 2, there is some difference among the bus lines. Fitting distribution of normal bus system and BRT is lognormal distribution, and the others fit in with the normal distribution. Based on the travel speed data, the travel speed of BRT is a small faster than the normal line but slower than the night line. The travel speed of night bus system is highest. Light condition of the night is not good as the daytime, however, the road conditions are much better because of the low traffic, so the running speed is high with lower delay. In addition, total travel speed is relatively low from the whole perspective.

(a) Normal bus system

(b) BRT system

(c) Night bus system

(d) Peak bus
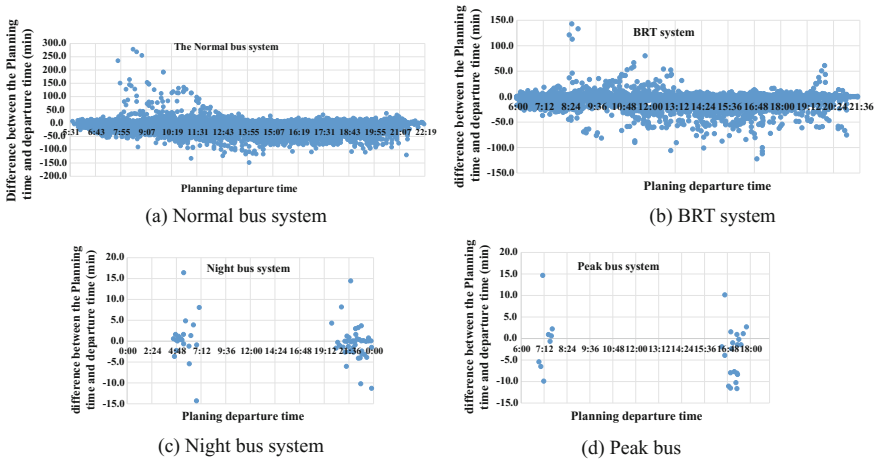
**Fig. 3** The time difference between the planning time and departure time

### 4.2.2 Travel Speed Distribution

Timetable is an important basis for public transportation enterprises. Under normal circumstances, the bus vehicle needs to be run in accordance with the timetable. Planning departure time is an important parameter in the timetable. Through comparing the planning and the actual departure time, we could estimate the traffic state. The difference between the two as the increase of the planning departure time is obtained, as shown in Fig. 3.

In order to show their differences more clearly, the PDF distributions of different bus systems were obtained, as shown in Fig. 4.

Combined with Figs. 3 and 4, there has been a departure delay for the normal bus system and BRT system in the morning peaks. And with different length, the night and peak bus system are lower than the other two, the night bus system especially. The reason is obvious. There are few buses and private cars in the urban road during the night time. In addition, there is an interesting phenomenon in Fig. 4. The bus incline to an earlier or a bit later departure time in contrast with the planning departure time, which will be verified in the future.

Next, the relationship between travel speed and the departure time is discussed. Because the effective time of night and peak bus system is a small part within one day, the normal bus and BRT system was selected to discuss. For a vehicle in a round, a departure time is corresponding to a travel speed. Take the data collection respectively. The results are shown in Fig. 5. Figure 5a shows the relationship in the normal bus system. The trend was varied with the departure time. And there are some peaks and thoughs in this figure. Figure 5b shows the varies of the BRT system, and there are two thoughs in the morning and evening peaks.

(a) Normal bus system

(b) BRT system

(c) Night bus system

(d) Peak bus system
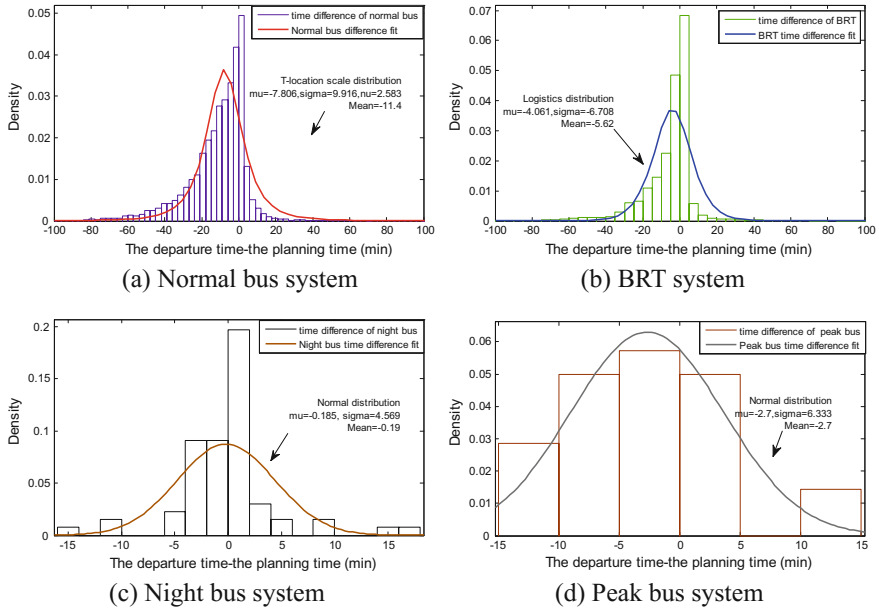
**Fig. 4** The PDF of time difference between the planning time and departure time
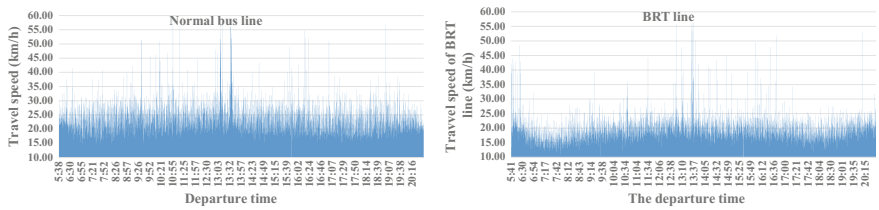


**Fig. 5** The relationship between the departure time and the travel speed of the line

To take one bus line, for example, the relationship was obtained, as showed in the Fig. 6. Take the two buses, one is 45 bus, and the other is B35, the two have the same trip to the starting station. Figure 6 verified the above conclusion, there are a though in the morning peak and evening peak, respectively. In other words, this could be a reference for passengers. For example, if we leave home at 7:30, we arrive at the destination at 8:30; and if we leave at 7:50, we may arrive at the close time. So, we could select our departure time reasonably as this.

(a) Normal bus system (No.45)                    (b) BRT system(B35)
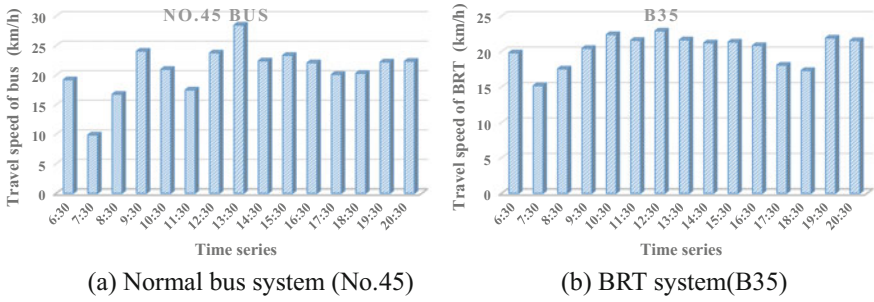
**Fig. 6** The travel speed of a bus line within one day
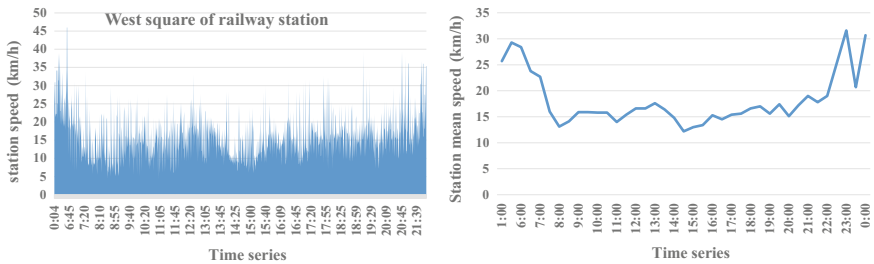


**Fig. 7** The speed around the railway station within one day

### 4.2.3 Station Speed Analysis

In addition, the station speed could be obtained by GPS. We can analyze the spot speed and estimate the traffic state of the area. For example, take the west square of railway station (ID 1118, 5530, 13439, 25904, 30525, 31528) as an example, around it there are 11 groups of bus (4, 57, 87, 99, 213, 217, 603, 981, B60, Y802, Y866). We can get the instantaneous velocity when passing the bus station, and estimate the traffic situation during a short period.

In addition, we could describe the map of traffic state based on the station speed. Combined with the trajectory data, we will analyze and estimate the operational performance of one vehicle, and provide the basic information to the traffic control system (Fig. 7).

## 5  Conclusion

Based on analysis of running data of public transport at Zhengzhou, this chapter focuses on the parameters values and their distribution of five different types of public transport, such as lines distance, station distance, travel speed, and instantaneous velocity. Through the analysis, it shows the differences between BRT and CBS in

the operation process. However, taking into account the most of the BRTs have a dedicated way and station in the current, so there is a certain gap between their operating results and expected value. In this chapter, a new attempt is made to analyze the operational situation of urban public traffic line from the whole. In the future, it will be combined with the micro-data of vehicles, and analyze them from the perspectives of a combination of macro and micro.

# References

1. Ibarra-Rojas OJ, Delgado F, Giesen R et al (2015) Planning, operation, and control of bus transport systems: a literature review. Transp Res Part B 77:38–75
2. Almselati ASI, Rahmat RABOK, Jaafar O et al (2015) Using spike model to reduce traffic congestion and improve public transportation in Malaysia. Transp Res Part D 38:59–66
3. Stelzer A, Englert F, Hörold S et al (2015) Improving service quality in public transportation systems using automated customer feedback. Transp Res Part E 89:259–271
4. Prabhu A, Pai M (2012) Buses as low-carbon mobility solutions for urban India. Transp Rec 2317(-1):15–23
5. Carrel A, Lau PSC, Mishalani RG et al (2015) Quantifying transit travel experiences from the users' perspective with high-resolution smartphone and vehicle location data: methodologies, validation, and example analyses. Transp Res Part C 58:224–239
6. Lindau LA, Hidalgo D, Facchini D (2010) Bus rapid transit in Curitiba, Brazil. Transp Res Rec 2193(-1):17–27
7. Deng T, Nelson JD (2013) Bus rapid transit implementation in Beijing: an evaluation of performance and impacts. Res Transp Econ 39(1):108–113
8. Zhang X, Liu Z, Hua W (2013) Lessons of bus rapid transit from nine cities in China. Transp Res Rec 2394(1):1–18
9. Chen X, Yu L, Song G et al (2012) Comparative study of emissions from bus rapid transit and CBSs: case study from Beijing. Transp Res Rec 2277(-1):11–20

# Identification Methods of Critical Combination of Vulnerable Links in Transportation Networks

**Lin Li, Jie Ma and Dawei Li**

**Abstract** This chapter presents two global optimization approaches for identifying the most critical combination of vulnerable links in a transportation network. The first approach is formulated with a bi-level framework. It can be applied to small-scale networks. The second proposed approach formulates this problem as a Mixed-integer Nonlinear Programming (MINLP). We revised the [MINLP] into a nicer form [RMINLP] to simplify the vulnerability problem into a discrete Network Design Problem (DNDP), so that it can be solved by many existing algorithms for DNDPs, and expand its scope of application. A numerical example of Sioux-Falls network is used to illustrate the two proposed approaches. The test results show that both approaches can provide a global optimization solution, while the second approach has a better property in computing efficiency.

**Keywords** Bi-level · Nonlinear programming · Discrete network design problem (DNDP) · Vulnerability analysis

## 1 Introduction

There is a great relationship between the performance of transportation infrastructure and the individuals' quality of life. However, it is well known that the transportation infrastructure is vulnerable to accidental damage. Thus, the vulnerability analysis (VA) of the transportation networks has become a hot issue in transportation research. One of the key technologies of VA for transportation networks is to identify the critical elements (e.g., sets of links or nodes) of a network, of which the failure would cause some extremely serious impacts on the entire system [1, 12]. By doing this, we can

L. Li
Branch of Intelligent Equipment and Information Engineering, ChangZhou Vocational Institute of Engineering, ChangZhou 213164, Jiangsu, China

J. Ma (✉) · D. Li
School of Transportation, Southeast University, Nanjing 210096, China
e-mail: majie9002@163.com

751

find the most vulnerable elements in the network and enhance them, so that the robustness of the overall network can be improved.

In this study, we focus on the identification of the critical combination of vulnerable links. However, the traditional approaches for identifying the critical link is to use a brute-force simulation-based approach [9]. Nevertheless, this kind of method consumes too much computing resources because of its brute-force simulation-based process. That is to say, this method is not very applicable for testing multiple-link failure in large-scale networks, because the calculating time may be exceedingly large.

This study makes efforts to narrow the research gap by proposing two approaches. We adopt an optimization approach which is formulated as a network design problem (NDP) that involves the decision on removal of links from the network. However, the road network design problem is generally non-convex. The non-convexity stems from both the traffic assignment equilibrium conditions and the travel time function. In this study, we formulate the problem as a mathematical program with equilibrium constraints (MPEC). In addition, we utilize the Bureau of Public Roads (BPR) function as the travel time function. Nevertheless, it is known that MPEC is inherently non-convex mainly because of its constraints. Thus, the global optimal solutions are generally difficult to be obtained [1]. To deal with this problem, we transform the MPEC into a single-level programming. There are many existing algorithms to solve the DNDPs [3, 4, 5, 7, 11]. However, the DNDPs is generally to minimize the total costs of the network, which means they try to minimize their convex objective functions, while the problems of VA is to maximize the convex objective functions. It makes these algorithms not available for VA. Wang et al. [10] proposed a method to linearize a model for the problem of VA. In this study, we simplify the problems of VA into DNDPs and make them available for being solved by the traditional algorithms for DNDPs.

Compared to existing literature (e.g., [1], the main contributions of this study are as follows:

(1) A Mixed-integer Nonlinear Programming is used to describe the vulnerability problems. With this method, we can identify the combination of vulnerable links rather than only one most vulnerable link;
(2) A global optimization solution can be obtained through the proposed method;
(3) Besides the combination of the vulnerable links, we can also obtain the ranking of different combinations.

While Wang et al. [10] considered the problem of VA as a MINLP and try to linearize it into a MILP then solve it with algorithms for MILP, in this study, we try to solve this problem in a different way that simplifying it into a DNDP and solving it with algorithms for DNDP. As a result, we boil down the problem of VA into a general DNDP and expand its scope of application.

The remainder of the chapter is outlined as follows. The next section presents the notation and network representation used in this chapter. The third section proposes the approaches for the vulnerability analysis problems. In the fourth section, a transportation network is used to demonstrate the applicability and efficiency of the proposed methods. The final section concludes the chapter and discusses future research issues.

## 2 Notation and Network Representation

The following notation is used in the formulation.

$A$      set of all links in the traffic network;

$c_r^w$      travel time on path $p$ between OD pair $w \in W$;

$f_r^w$      flow on path $p$ between OD pair $w \in W$;

$L$      a negative number whose absolute value is large enough;

$M$      a large enough positive number;

$N$      the number of links in the network;

$q_w$      the traffic demand between OD pair $w \in W$, which is given as a constant;

$R_w$      set of all paths between OD pair $w \in W$;

$t_a$      the travel time on link $a \in A$;

$\mathbf{v}$      a vector defined as network design decision, $\mathbf{v} = [v_a]$, $\forall a \in A$;

$v_a$      binary variable indicates whether a link is a vulnerable link: link $a$ is vulnerable if $v_a = 1$ or not if $v_a = 0$;

$V$      the number of vulnerable links in the traffic network;

$W$      set of all OD pairs in the traffic network;

$x_a$      the traffic flow of link $a$, $a \in A$;

$\delta_{a,r}^w$      the link-path incidence parameter, $\delta_{a,r}^w = 1$ if link $a$ belongs to path $r$ between OD pair $w$, or $\delta_{a,r}^w = 0$;

$\varepsilon$      a small enough positive number;

$\sigma_r^w$      binary variable indicates whether a path is used: path $r$ is used if $\sigma_r^w = 0$, and is not used if $\sigma_r^w = 1$.

## 3 Methodology

In this study, we use the typical Bureau of Public Road (BPR) function as our travel time function, since BPR function has some good properties. For example, BPR function is strictly increasing, which ensures the objective functions of many existing approaches for solving NDPs are strictly convex. The BPR function is as follows:

$$t_a = t_{a,0}[1 + \alpha_a(x_a/c_a)^{\beta_a}], \quad \forall a \in A \tag{1}$$

For finding the combination of vulnerable links, we propose a bi-level programming model as follows:

[UP: Upper-level Problem]:

$$\max_{\mathbf{v}} \sum_{a \in A} x_a t_a(x_a) \tag{2}$$

Subject to

$$\sum_{a\in A} v_a = N - V, \quad \forall a \in A \tag{3}$$

$$v_a \in \{0, \ 1\}, \quad \forall a \in A \tag{4}$$

[LP: Lower level Problem]:

$$\min \sum_{a\in A\backslash\overline{A}} \int_0^{x_a} t_a(x_a)\mathrm{d}x \tag{5}$$

Subject to

$$q_w = \sum_{r\in R_w} f_r^w, \quad \forall w \in W \tag{6}$$

$$x_a = \sum_{w\in W} \sum_{r\in R_w} f_r^w \delta_{a,r}^w, \quad \forall a \in A \tag{7}$$

$$f_r^w \geq 0, \quad \forall r \in R_w, \quad \forall w \in W \tag{8}$$

where the original objective function is

$$\min \sum_{a\in A\backslash\overline{A}} \int_0^{x_a} t_a(x_a)\mathrm{d}x + \sum_{a\in\overline{A}} v_a \int_0^{x_a} t_a(x_a)\mathrm{d}x$$

We can notice that $v_a \equiv 0$, $\forall a \in \overline{A}$, so the second term of it can be omitted. In this bi-level model, [LP] is a standardized process of solving the Traffic Assignment Problem (TAP) with the principle of User Equilibrium (UE). As a result, [LP] can provide the link flows $x_a$ when all the users reach the state of User Equilibrium in the network. In [UP], the decision variables of [UP] are the 0–1 variables $v_a$ rather than the variables of the lower level problem $x_a$. Thus, the objective function of [UP] is a function about the 0–1 variables. Both $x_a$ and $t_a$ in [UP] are determined parameters which are produced by [LP]. The real effect of [UP] is to find out the combination of $v_a$s which maximize the total costs of the whole network at UE state.

However, we should note that the commonly used full network scan approaches are to evaluate all possible combination of link closure using a form of traffic assignment. Although we have reduced the calculating time sharply through applying a bi-level model which deals with the 0–1 variables and TAP separately, this bi-level model is still an exhaustive process which enumerates all possible combination of the decision variables $v_a$. This property makes the model not so available to large-scale networks. For example, the calculating time of the case which has three closed links in Sioux-falls network with a personal computer may be longer than 10 h.

To reduce the calculating time, we propose another model which can be regarded as an enhanced approach and can be applied to larger scale networks. In this model, we change the BPR function $t_a$ as follows:

$$t_a = t_{a,0}[1 + \alpha_a(x_a/c_a)^{\beta_a}] + (1 - v_a)M, \quad \forall a \in A \tag{9}$$

The problem is formulated as a mixed-integer nonlinear programming as follows:

[MINLP]:

$$\max \sum_{a \in A \setminus \overline{A}} x_a t_{a,0}[1 + \alpha_a(x_a/c_a)^{\beta_a}] \tag{10}$$

Subject to

$$L \cdot \sigma_r^w + \varepsilon \le f_r^w \le M \cdot (1 - \sigma_r^w), \quad \forall r \in R_w, \quad \forall w \in W \tag{11}$$

$$L \cdot \sigma_r^w \le c_r^w - \pi^w \le M \cdot \sigma_r^w, \quad \forall r \in R_w, \quad \forall w \in W \tag{12}$$

$$c_r^w - \pi^w \ge 0, \quad \forall r \in R_w, \quad \forall w \in W \tag{13}$$

$$\sigma_r^w \in \{0, \ 1\}, \quad \forall r \in R_w, \quad \forall w \in W \tag{14}$$

Constraints (3), (4), (6)–(8)
where the original objective function is

$$\max \sum_{a \in A} x_a\{t_{a,0}[1 + \alpha_a(x_a/c_a)^{\beta_a}] + (1 - v_a)M\}$$

which can be written as

$$\max \sum_{a \in A \setminus \overline{A}} x_a t_{a,0}[1 + \alpha_a(x_a/c_a)^{\beta_a}] + \sum_{a \in A \setminus \overline{A}} x_a(1 - v_a)M$$
$$+ \sum_{a \in \overline{A}} x_a t_{a,0}[1 + \alpha_a(x_a/c_a)^{\beta_a}] + \sum_{a \in \overline{A}} x_a(1 - v_a)M$$

It can be noted that the last three terms of it are all equal to 0, so all of them can be omitted.

We should note that the objective function (10) is strictly increasing and strictly convex; constraints (11)–(14) depict the Wardrop's principle to describe route-choice behavior and the UE state.

One should note that different from the traditional NDPs, the model formulation of [MINLP] is to maximize the total network costs. Many existing solution algorithms for solving NDPs highly rely on the property that the objective function is convex and to be minimized. This is why many existing algorithms are not suitable for this

problem. To deal with this issue, we transform the objective function of [MINLP] into a much nicer form.

As can be seen in formulation (10), take the advantage of utilizing the BPR function as the link performance function, the objective function of [MINLP] is a polynomial which has some nice properties. Thus, we can replace the objective function with the following one:

[RMINLP: revised MINLP]:

$$\min \sum_{a \in A \setminus \overline{A}} n/x_a t_{a,0}[1 + \alpha_a(x_a/c_a)^{\beta_a}] \tag{15}$$

where n is a given number which is used to adjust the absolute value of the objective function and has no effects on the convexity and the monotonicity of the objective function. The constraints of [RMINLP] remain unchanged.

Then, we try to prove the equivalence and the convexity of [RMINLP]. As mentioned above, the objective function (10) is strictly increasing with respect to the link flow $x_a$. Due to the nice form of the BPR function $t_a$, the objective function (15), which is the inverse of the objective function (10), is strictly decreasing with respect to $x_a$. That is to say, while the objective function (15) reaches the minimum value, its inverse [the objective function (10)] will accordingly reach the maximum value. Therefore, the objective function (10) can be transformed into (15).

It is known that the four fundamental operations of polynomials are derivable. So, it is easy to know the values of the first-order and second-order derivatives of the objective function (15) as follows:

$$\frac{\partial}{\partial x_a} \sum_{a \in A \setminus \overline{A}} n/x_a t_{a,0}[1 + \alpha_a(x_a/c_a)^{\beta_a}] = \sum_{a \in A \setminus \overline{A}} -\frac{n\beta_a \alpha_a}{t_{a,0} c_a^{\beta}} \cdot \frac{x_a^{\beta-1}}{(1 + \frac{\alpha_a}{c^{\beta_a}} x_a^{\beta})^2} \propto -x_a^{-\beta-1} \tag{16}$$

$$\frac{\partial^2}{\partial x_a^2} \sum_{a \in A \setminus \overline{A}} n/x_a t_{a,0}[1 + \alpha_a(x_a/c_a)^{\beta_a}]$$

$$= \sum_{a \in A \setminus \overline{A}} \frac{n\beta_a \alpha_a}{t_{a,0} c^{\beta_a}} \cdot \frac{(\beta_a - 1)x_a^{\beta-2} \cdot (1 + \frac{\alpha_a}{c_a^{\beta}} x_a^{\beta})^2 - 2\frac{\alpha_a}{c_a^{\beta_a}}(1 + \frac{\alpha_a}{c_a^{\beta_a}} x_a^{\beta})x_a^{\beta-1}}{(1 + \frac{\alpha_a}{c^{\beta_a}} x_a^{\beta})^4} \propto x_a^{-\beta-2} \tag{17}$$

Formulas (16) and (17) are strictly below and above 0, which means the objective function (15) is strictly decreasing and strictly convex with respect to $x_a$. Thus, the convexity of the objective function (15) is proved.

Through the transforming proposed above, we change the objective function of [MINLP] to be minimized and the convexity of it remains unchanged. That is to say, by doing this, we transform this vulnerability problem into a discrete NDP (DNDP) which has the same form of the objective function (15). According to this property, we can apply many existing algorithms for solving discrete NDPs to deal

with the vulnerability problems. As a result, we simplify the problems of vulnerability analysis and expand its scope of application. For example, [MINLP] can only be solved through an approach of linearizing it into a mixed-integer linear problem [MILP] and solve it with algorithms for [MILP], however, [RMINLP] can be solved by many other approaches, such as the algorithms proposed by Ekström et al. [2], Liu et al. [4], Liu and Wang [3], Riemann et al. [7], and Wang et al. [11].

In the next section, we use two examples to illustrate the two methods proposed above.

## 4 Numerical Examples

In this section, to illustrate these two approaches more clearly, we use the well-known Sioux-Falls network as our numerical example. A personal computer with an
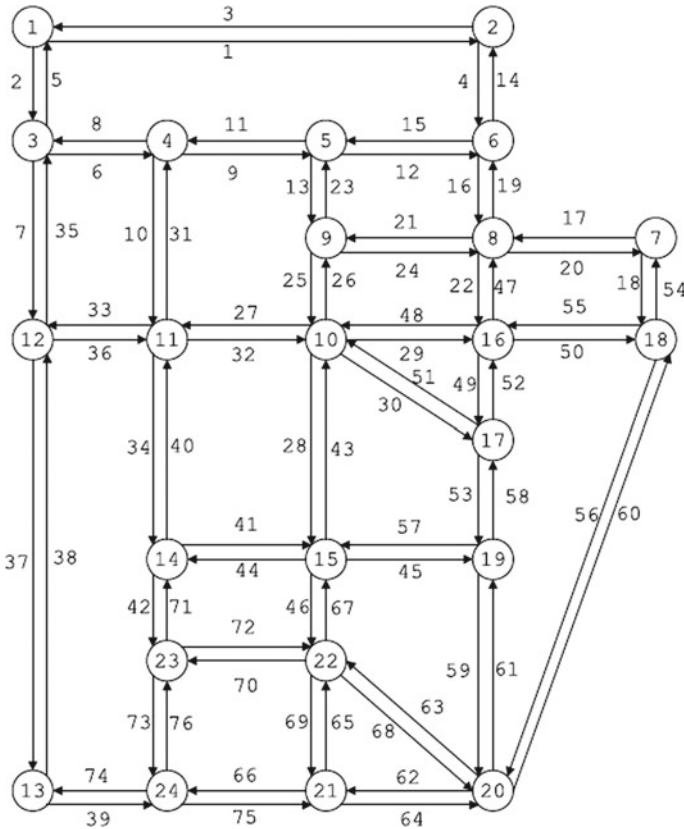


**Fig. 1** Sioux-Falls network with its OD pairs and capacities

**Table 1** Test results of the Sioux-Falls network with the bi-level model ($V=1$)

| $V=1$ | | | $V=2$ | | |
|---|---|---|---|---|---|
| Vulnerability order | Link number | Total cost | Vulnerability order | Link number | Total cost |
| 1 | 73 | 2.6E+07 | 1 | (43, 60) | 2.55E+09 |
| 2 | 69 | 2.2E+07 | 2 | (28, 56) | 2.54E+09 |
| 3 | 62 | 2.0E+07 | 3 | (7, 74) | 2.33E+09 |

Intel(R) Core(TM) i5 4210M @ 2.60 GHz Central Processing Unit (CPU), an 8 GB Random-Access Memory (RAM) and Windows 8.1 Enterprise operating system (64-bit) is used. The model was coded with MATLAB, calling CPLEX to solve the mathematical programming. The UE process is dealt with the Convex Combinations Method. Sioux-Falls Network has 24 nodes, 76 links, and 528 OD pairs. We regard this network as a large-scale network. The topology of it can be seen in Fig. 1.

First, we test the network with only one vulnerable link ($V=1$). When we take two vulnerable links into consideration, the calculating time increases sharply to nearly 16 h. Before our test, we need to exclude the following combinations of links, (20, 54), (17, 18), (38, 39), (37, 74), (1, 2), (3, 5), (5,14), (3, 4), (1, 14), and (2, 4), which may cause the OD pairs connection failure. The test results can be seen in Table 1.

Applying the original bi-level model to solve the vulnerability analysis problem may consume large computing resource and need a long calculating time. Subsequently, we test both of the above cases ($V=1, 2$) by solving [RMINLP].

Following the research of Liu et al. [4], in this study, we use an approximated global optimization solution method based on mixed-integer linearization approach to solve the problem. Besides, we should note that [RMINLP] is not only suitable for this approach, but other approaches for the DNDPs are also available. This property is one of the advantages of proposed [RMINLP]. Another advantage is that this approach can reduce a large part of the calculating time, while a global optimization solution is still produced. As a result, the test results of the Sioux-Falls network with the [RMINLP] model is the same as those with the bi-level model, but the calculating time is only 25 min for $V=1$ case and around 15 h for $V=2$ case.

# 5   Conclusion

In this study, we propose two approaches for identifying the most critical combination of vulnerable links in a transportation network. The first approach is a bi-level problem which can be applied to small-scale networks, because it is indeed a numerate approach. The second approach is a MINLP which can also provide a global optimization solution and is suitable for larger networks. Unlike the traditional NDP formulation which minimizes the total system travel costs with convex objective functions, the problem of finding critical vulnerable link(s) need to be formulated

as a maximization problem of convex objective functions. Therefore, many existing solution algorithms for solving traditional NDPs (e.g., [6, 8]) are not available for this kind of issues. To solve this problem, we proposed a RMINLP which reformulates the MINLP into a nicer form, a minimization of a convex objective function, so that it can be applicable for the traditional NDPs. As a result of doing this, we simplify the vulnerability problems into traditional NDPs and expand the scope of application of them. Both of the proposed methods can be used to determine the ranks of the combination of vulnerable links. The results of the numerical tests demonstrate that the set of most vulnerable links when multiple-link failure occurs is not simply the combination of the most vulnerable links for single-link case. In the numerical examples, we have tested the calculating time of both two approaches. The test results illustrate that the first approach may consume large computing resources when solving vulnerability problems in large-scale networks, while the second approach can be much more efficient when doing this. Both of the two approaches provide the same solution which is a global optimization one. However, the calculating time of both the two approaches increases sharply in terms of the increasing number of vulnerable links in the networks. To overcome this limitation of the proposed approaches, a more efficient solution method would be proposed in future studies.

With these proposed approaches, network managers can identifying critical links in road networks. By improving these critical links with limited construction costs to increase these links' capacity redundancy, we can improve the overall efficiency and robustness of the networks.

# References

1. Chen B, Lam WHK, Sumalee A, Li Q, Li Z (2012) Vulnerability analysis for large-scale and congested road networks with demand uncertainty. Transp Res Part A 46:501–516
2. Ekström J, Rydergren C, Sumalee A (2014) Solving a mixed integer linear program approximation of the toll design problem using constraint generation within a branch-and-cut algorithm. Transportmetrica A: Transport Science 10(9):791–819
3. Liu H, Wang DZW (2015) Global optimization method for network design problem with stochastic user equilibrium. Transp Res Part B: Methodol 72:20–39
4. Liu H, Wang DZW, Yue H (2015) Global optimization for transport network expansion and signal setting. Mathematical Problems in Engineering. Article ID 385713. https://doi.org/10.1155/2015/385713
5. Ma, J., Li, D., Cheng, L., Lou, X., Sun, C., & Tang, W. (2018). Link Restriction: Methods of Testing and Avoiding Braess Paradox in Networks Considering Traffic Demands. Journal of Transportation Engineering, Part A: Systems, 144(2): 04017076
6. Ma J, Cheng L, Li D (2018) Road maintenance optimization model based on dynamic programming in urban traffic network. J Adv Transp. In press

7. Riemann R, Wang DZW, Busch F (2015) Optimal location of wireless charging facilities for electric vehicles: flow-capturing location model with stochastic user equilibrium. Transp Res Part C: Emerg Technol 58:1–12
8. Szeto WY, Jiang Y, Wang DZW, Sumalee A (2015) A sustainable road network design problem with land use transportation interaction over time. Netw Spat Econ 15(3):791–822
9. Taylor MAP, Sekhar SVC, D'Este GM (2006) Application of accessibility based methods for vulnerability analysis of strategic road networks. Netw Spat Econ 6:267–291
10. Wang DZW et al (2016) Identification of critical combination of vulnerable links in transportation networks–a global optimisation approach. Transp A: Transp Sci 12(4):346–365
11. Wang DZW, Liu H, Szeto WY (2015) A novel discrete network design problem formulation and its global optimization solution algorithm. Transp Res Part E: Logistics Transp Rev 79:213–230
12. Zhu S, Levinson D, Liu HX, Harder K (2010) The traffic and behavioral effects of the I-35W Mississippi River bridge collapse. Transp Res Part A 44(10):771–784

# CO Emissions Estimation Model of Urban Tunnel Under One-Way Traffic Flow



**Bingkui Ji, Xueping Yao, Yuzhuo Men, Nianchuan Wang, Zhiqiang Li and Liwei Sun**

**Abstract** Due to strong regionally of the motor vehicle emission and relatively closeness of urban tunnel, motor vehicle exhaust pollution in the tunnel is very serious. Serious pollution cause serious harm to human body health. To estimate CO emissions of urban tunnel under one-way traffic flow, considering motor vehicle ownership, emissions standards, vehicle emissions, emission factors, and transportation operation factors, CO emission model of urban tunnel is proposed. Comprehensive emission factor of CO is computed by the method of mass balance. CO emission factor of different type vehicles is computed using the method multiple regression analysis. Real vehicle road test is designed to verify this CO emissions model of urban tunnel under one-way traffic flow.

**Keywords** Emissions · City tunnel · A motor vehicle · CO

According to the statistics of the main atmospheric pollutants emissions, about 84% carbon monoxide (CO) and 42% nitrogen oxides ($NO_x$) are from vehicle emissions in United States. About 76% carbon monoxide (CO) and 36% nitrogen oxides ($NOx$) are from vehicle emissions in Europe. According to domestic survey, about 80% carbon monoxide (CO) and 40% nitrogen oxide ($NO_x$) in Beijing are from vehicle emissions. About 61.8% carbon monoxide (CO) and 20.9% nitrogen oxide ($NO_x$) in Shanghai are from vehicle emissions. The over standard rate of $CO_2$ and CO are about 45 and 40% [1–3].

Vehicle exhaust has become one of the main pollution sources of harming urban resident's health. Therefore, effective control and reduce vehicle emissions are important means of improving urban air environment quality. The environmental air quality control strategy must be established based on accurate calculation for emissions and concentration of pollutants. At present, the study on motor vehicle exhaust emission

B. Ji · X. Yao (✉) · Y. Men · N. Wang · Z. Li · L. Sun
School of Mechanical and Electrical Engineering, Changchun Institute of Technology, Changchun 130012, China
e-mail: jd_yxp@ccit.edu.cn

B. Ji
e-mail: bingkui2008@163.com

of our country is mainly based on the individual motor vehicles. The prediction of regional vehicle emission concentration is rough, and targeted control measures are not put forward. This paper explores the prediction method of vehicle exhaust in city tunnel based on vehicle emission CO forecast [4, 5].

# 1 Road Test

## 1.1 Experimental Platform Construction

Road test experimental platform is built to collect emissions data, which include automatic smoke sampler-WJ-60B, exhaust gas analyzer-DELTA 1600-V, wind speed and direction sensor, and Camera equipment shown in Fig. 1.

## 1.2 Vehicle Road Test Condition

Select a city tunnel in Changchun as the test road, the tunnel is a double tube and four-lane dual carriageway, a single lane width is 3.5 m, height 4.5 m. The tunnel length is 1860 m. The speed limit is 60 km/h. Refer to the tunnel length standard of JTG D70-2004 [6], the tunnel is a long tunnel.

## 1.3 The Selection of Tested Emissions

The pollutants of vehicle emissions include CO, $CO_2$, $NO_x$, and PM2.5. CO is the main pollutant, which can represent the air quality of gasoline engine. If the CO



(a) DELTA 1600-V                    (b) WJ-60B                    (c) wind speed and direction sensor

**Fig. 1**  Test equipment

concentration is maintained at an acceptable level, other pollutants such as $NO_x$ and $CO_2$ can also be maintained at acceptable levels, so CO is selected as the estimate pollutants.

## 2 Estimation Model of CO Emission

The total amount of pollutants discharged in the urban tunnel depends on the type and quantity of vehicles, travel distance, road congestion state for a period of time. Considering the amount of vehicles, emission standards, vehicle emission types, emission factors, traffic operation, and so on, this paper proposes emission model of CO based on unit CO emission, travel distance, frequency, and time [7, 8]. According to vehicle engine power and China emission standard, the vehicles are divided into three categories: small, medium, and large cars based on measured results in this paper. According to traffic operation, estimate the CO emission from automobile pollutants through the average speed of road traffic.

$$Q_{\text{co}} = \sum_{i=1}^{n} k_i P_i D, \quad i = 1, \dots, n \tag{1}$$

where

$Q_{\text{co}}$—the total CO emissions of vehicles in the tunnel, mg ;
$k_i$—the emission factor of class I vehicle CO emission, mg/km ;
$P_i$—the number of class I vehicles passing through the tunnel;
$D$—the length of the tunnel, km.

Scientifically and accurately calibrating the parameters of emission model is an important basis for vehicle emission control and evaluation. $D_i$ is a known data, $P_i$ can be obtained by traffic survey, so the determination of vehicles emission factors is the key to estimate CO emission. The emission factor of single vehicle can be obtained by using the vehicle bench test. But establish an emission model needs more comprehensive emission factors of various vehicles. Mobile, MVEI, COPERT and other emission factor models can be used to estimate the comprehensive emission factors of vehicles, at the same time, the tunnel test, remote sensing technology and OBD technology also can be used to test the comprehensive emission factors. Many studies show that tunnel is suitable for testing the vehicle emission factor

# 3   CO Emission Factor Calculation

## 3.1   Mass Balance

In order to calculate CO emission factors of single vehicle, comprehensive emission factors of CO must be calculated first. The principle of mass balance is to regard the tunnel as an ideal cylinder [9–11], the diffidence that the product of CO concentration and ventilation volume of tunnel entrance subtract that of tunnel exit is the total mass of CO in vehicle pollutants as shown in Formula (2).

$$Q_{co} = (c_{out} \cdot S_{out} \cdot V_{out} \cdot T) - (c_{in} \cdot S_{in} \cdot V_{in} \cdot T) \tag{2}$$

where

$Q_{co}$ is the total emission mass of CO in vehicle pollutants in the tunnel (mg);
$c_{in}$, $c_{out}$ are the concentration of CO pollutants in tunnel entrance and exit (mg/m$^3$);
$S_{in}$, $S_{out}$ are the interfacial area of the tunnel entrance and exit (m$^2$);
$V_{in}$, $V_{out}$ are the tunnel entrance and exit wind speed (m/s);
$T$ is the time of vehicle running in tunnel (s).

At the same side of tunnel entrance and exit, two sampling points are installed which is 5 m away from the entrance and exit. The CO concentration is monitored continuously and automatically by using smoke sampler-WJ-60B and exhaust gas analyzer-DELTA 1600-V. Wind speed and direction of tunnel entrance and exit are recorded using wind speed and direction sensor. Vehicle types, quantity, and velocity are recorded using camera technology and image processing technology. The data are collected at 7:30–8:30 am, valid data are obtained after data processing as shown in Table 1.

Obtained calculation $Q_{co} = 30, 535$ mg

## 3.2   Calculation Method of Comprehensive Emission Factor

The total quality of CO in tunnel has been get by the mass balance method, CO comprehensive emission factors of all vehicles in the tunnel is calculated with the Formula (3).

**Table 1**   Valid data obtained from tunnel entrance and exit

|          | Wind speed (m/s) | Sectional area (m$^2$) | Time (s) | CO concentration (mg/m$^3$) |
|----------|------------------|------------------------|----------|-----------------------------|
| Imported | 4.82             | 55                     | 425      | 7.857                       |
| Exit     | 2.53             | 55                     | 425      | 15.485                      |

**Table 2** Total number and percentage of different vehicles

|  | Light-duty vehicle | Midsize car | Large vehicle | Total |
|---|---|---|---|---|
| Umber | 809 | 86 | 9 | 904 |
| Percentage (%) | 89.5 | 9.5 | 1 | 100 |

$$\bar{k} = \frac{Q_{co}}{N \times L} \tag{3}$$

where

$\bar{k}$ is the comprehensive emission factors of vehicle group in tunnel (mg/km);
$N$ is total number of vehicles passing through tunnels;
$L$ is the actual length between the two sampling points in the tunnel (km).

The total number and percentage of vehicles in the test samples are obtained according to the video statistics, as shown in Table 2.

The actual length of two sampling points between the entrance and exit of the tunnel is 1.85 km. According to the above data, the CO emission factor $\bar{k} = 18.26$ mg/km

The CO comprehensive emission factor reflects CO emission level of all vehicles through tunnel. It can basically represent CO emission factors under average vehicle speed, vehicle type combination, vehicle age distribution, and mileage distribution. If the vehicles through selected tunnel reflect the actual situation of vehicles and traffic in local area, the average emission factor calculated can represent the regional vehicle emission factors.

### 3.3 CO Emission Factors Calculation of Different Types of Vehicles

Because CO emission factor and vehicle composition are difference, and CO emission factor of various kinds of vehicles is also relatively stable, so the CO emission factors of various kinds of vehicles can be obtained using multiple regression analysis method. If the age and mileage data of all kinds of vehicles are known, the CO emission factors of every kind of vehicles with different age and mileage also can be calculated. According to the 12 samples collected by experiment, regression analysis is carried out on the CO emission factors of various kinds of vehicles by Formula (4).

$$\bar{k} = \sum_{i}^{3} k_i \cdot m_i + b \tag{4}$$

**Table 3** CO emission factors of different types of vehicles

|  | Light-duty vehicle | Midsize vehicle | Large vehicle |
|---|---|---|---|
| Emission factor | 13.25 | 17.14 | 22.81 |

where

$\bar{k}$ is comprehensive emission factor of CO in tunnel (mg/km);
$m_i$ is the percentage of $i$ kind of vehicles in tunnels (%);
$k_i$ is emission factors of the $i$ kind of vehicle (mg/km);
$b$ is a constant of a multiple regression equation.

The CO emission factors of light-duty vehicle, midsize vehicle, and large vehicle are obtained by Regression analysis as shown in Table 3.

Therefore, CO emissions estimation model of urban tunnel under one-way traffic flow is shown in Formula (4).

$$Q_{co} = 1.85(13.25P_1 + 17.14P_2 + 22.81P_3) \qquad (4)$$

$P_1$, $P_2$, and $P_3$ is the number of light-duty vehicle, midsize vehicle and large vehicle through the tunnel.

## 4    Conclusions

In this paper, the CO emission model of urban tunnel is proposed for estimating the CO emissions under one-way traffic flow of urban tunnels. In order to collect the data of CO concentration, the traffic data and the meteorological conditions in the tunnel, road test is carried out. The CO comprehensive emission factor is obtained by the mass balance method. Multiple regression analysis is used to calculate the CO emission factors of small cars, medium-sized vehicles, and large vehicles. Finally, the CO emission estimation model under one-way traffic flow of urban tunnels. is obtained.

# References

1. Cheng W, Liu Y, Gu Q, Li W, Guan C (2014) The forecasting methods of pollutant concentration caused by traffic exhaust gases in urban area a case history of forecast of $NO_2$ concentration produced by traffic in the major regions of SanYa city. Environ Eng 32:383–387
2. Pan S (2009) Research on vehicle exhaust emission concentrations & ventilation system of city-highway tunnel. Wuhan University of Technology, Wuhan
3. Wu X (2015) Research on vehicle emission in urban road network. Hunan University, Changsha
4. Wang X (2012) Study on prediction and control measures of motor vehicle pollutant emission. Chang'an University, Xi'an
5. Davis N, Lents J, Osses M et a1. Development and application of an international vehicle emissions model. Transportation Research Board 81st Annual Meeting, 2013–2016, Washington DC
6. Chongqing Communications Research and Design Institute (2004) JTG D70-2004 design specification of highway tunnel. China Communications Press, Beijing
7. Wang H (2015) Study on calculation and Co—Control effects of motor vehicle pollutant emission. Hefei University of Technology, Hefei
8. Yao L (2015) The quantitative analysis and microscopic prediction model of vehicle emissions. Southwest Jiaotong University, Chendu
9. Younglove T, Scora G, Barth M (2005) Designing on-road vehicle test programs for the development of effective vehicle emission models. Transp Res Rec 51–59
10. Yu K, Dong H, Li J, Hao W (2016) Research on prediction of vehicle exhaust based on measurement by PEMS. Comput Meas Control 24(9):58–61
11. Chan CK, Yao XH (2008) Air pollution in mega cities in China. Atmos Environ 42(1):41–42

# Identification for Truck Risk Status Based on Safety Stopping Distance

**Xue-ping Yao, Bing-kui Ji, Yu-zhuo Men and Fu-ming Hu**

**Abstract** Based on analysis of influencing factor for stopping distance, emergency stopping distance model was established in this paper, and the calculation method of the model parameters was put forward. Braking distance calculation model was simulated in MATLAB/Simulink and road brake test was carried out in different operating conditions. Through the analysis of simulation and test results, the feasibility of the model that calculates the stopping distance was verified, identification method of truck risk status was put forward based on calculating safety-driving distance and braking pressure data. This research provides a theoretical basis for early warning of truck risk status.

**Keywords** Truck · Risk identification · Stopping distance · Response time
Road test

The truck as long-distance transport vehicles, which had the characteristics of high quality, high center of mass and so on, and the longtime of driving will lead to vehicle braking performance decline; result in long braking distance for emergency braking. If the driving distance is not enough, rear-end accidents were more likely to happen and cause serious casualties. If the stopping distance in the current vehicle driving conditions can be real-time predicted, then safety-driving distance can be calculated indirectly, this provides early warning for safe driving to the driver, and prevent the happen of serious traffic accidents such as vehicle rear-collision effectively.

X. Yao · B. Ji (✉) · Y. Men · F. Hu
Department of Vehicle Service Engineering, School of Mechanical and Electrical Engineering,
Changchun Institute of Technology, Changchun 130012, China
e-mail: anmo179@163.com

# 1 Analysis for Influencing Factor of Stopping Distance

Driver factors, braking system parameters, vehicle state factors, and road environment factors are the main factors which affect vehicle stopping distance. Generally, drivers' reaction is emergency braking for the potential accident, therefore, the driver's response time is the main factor to decide whether he can avoid the accident [1, 2]; second, the braking system parameters affected braking force at the braking moment, brake pressure、wearing degree of brake shoes, and the rising temperature of brake shoes will influence on vehicle's braking efficiency [3, 4]. Third, at the driver's reaction stage of dangerous situation, vehicle was regarded as driving at constant speed that was initial speed of braking. The faster initial speed, the vehicle running distance is longer in the driver's reaction time. As well the heavier load, the vehicle stopping distance is longer, so the vehicle speed and load are main factors for vehicle state. Finally, vehicle braking efficiency depends on attachment coefficient between tire and road, the wheel will not be rolling but sliding on the road when brake force of ground maximizing. If the attachment coefficient is large, the brake force of ground will be larger, and the braking distance will be shorter [5], therefore, attachment coefficient was an influence on braking distance vastly is in vehicle emergency braking process.

# 2 Stopping Distance Model Building

## 2.1 Driver Reaction Time Model

Based on summarizing literature review [6, 7], the driver response speed in case of emergency was analyzed from the perspective of physiology. Average driver reaction time and variance at braking moment can be expressed by following formulas.

$$T_{\mathrm{mean}} = (0.7\mathrm{ex} + 1.25\mathrm{unex} + 1.5\mathrm{sur})(1 + 0.2\mathrm{age}) + 0.07\mathrm{gender} \tag{1}$$

$$S^2 = [0.4(1+0.2\mathrm{age})]^2 \tag{2}$$

ex (expected), unex (unexpected), sur (surprise) are expectation for 1 or 0, expressing three conditions of known, unknown and sudden.

– age: Old drivers (older than 65 years of age) is 1, young drivers t is 0,
– gender: Female is 1, male is 0.

The conclusion of the driver's reaction time at braking moment is different in different research. Newcomb body dynamics function was used to build driver's reaction time calculation model in empirical analysis of driver's reaction [8], this method was more suitable for the prediction of braking reaction time.

## 2.2　Dynamics Analysis of Vehicle Braking

Brake structure of test vehicle is leading and trailing shoe brake, actuating mechanism is mainly constituted by three parts, which are the brake chamber, the brake cam, and the brake shoe. In order to calculate braking force, dynamic mechanical analysis about those three parts in this paper, finally, improved calculation formula of braking torques was obtained which conforms to improvable theory of structure of the drum brake.

Test vehicle brake is nonequilibrium cam drum brake, and this type of cam which is fixed by the shaft have equal torque to the brake shoes, so only the torque of leading shoe was calculated and analyzed in this paper. For convenience, to calculate and analyze braking torque. Postulated conditions as drum brake and brake shoe are rigid absolutely, radius of brake lining surface is equal to the radius of brake drums and contact fully, deformation of friction lining obey Hooke's law were supposed in analyze. Brake structure and force analysis of vehicle brake were shown as Fig. 1.

Mechanical analysis equation is built as

$$
\begin{aligned}
F_{nl} &\times \sin\alpha \times (X_A - X_S) + F_{nl} \times \cos\alpha \times (Y_A + Y_S) + F_{\mu} \\
&\times (D_L \times \cos\delta - L \times \sin(\sigma - \delta)) - N \times L \times \cos(\sigma - \delta) = 0
\end{aligned} \tag{3}
$$

Brake force was expressed as

$$
F_{\mu} = \frac{A \times P \times R \times L_{AS} \times \eta}{r \times (1 + \cos\alpha \times \frac{m}{\cos\beta}) \times K \times D_L \times \cos\theta} \tag{4}
$$

where $L_{AS}$, $K$ are expressed as

$$
L_{AS} = \sin\alpha \times (X_A - X_S) + \cos\alpha \times (Y_A + Y_S) \tag{5}
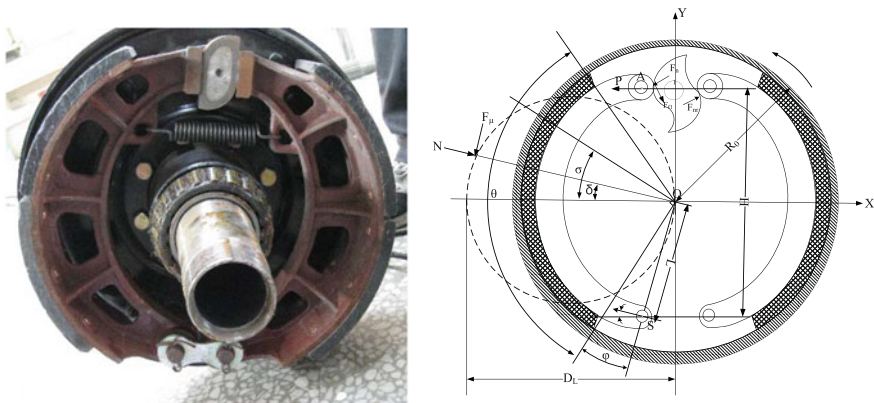$$



**Fig. 1** Brake structure and force analysis of vehicle brake

$$K = \frac{L}{R_0} \times \left[ \frac{\sin\theta \times (\mu \times \sin 2\sigma + \cos 2\sigma) + \theta}{4 \times \sin(\theta/2) \times \mu \times \cos\sigma} \right] - 1 \tag{6}$$

$X_A$, $Y_A$ are coordinates of point $A$. $X_S$, $Y_S$ are coordinates of point $S$, $L$ is the distance between support pin of the brake shoe to the center of brake drum. $R_0$ is radius of the brake drum. $\alpha$ is normal force's pressure angle of leading shoe to camshaft. $\delta$ is the angle between normal force and wrap angle bisector; $\sigma$ is the angle between maximum pressure line and wrap angle bisector; $\theta$ is wrap angle of friction lining; $\varphi$ is initial angle of the friction lining. $\mu$ is the friction coefficient between friction lining and brake drum, $\eta$ is mechanical efficiency of braking system, $m$ is a ratio of the trailing shoe impel force to the leading shoe impel force.

## 2.3   Braking Distance Model Construction

When the vehicle is braking, wheels movement mode include three states: the wheel is pure rolling approximately, there is relative motion in a certain degree between the tire and the wheel lock and sliding. Due to braking dynamics analysis is taken as the basis for the identification of vehicle safe driving distance, the maximum value in extreme conditions need to be considered in this paper, so two braking states, pure rolling and lock sliding were analyzed. When the brake force is greater than brake friction to make the wheel roll, the ground braking force is equal to the brake force $F_{xb} = F_{\mu}$. When the brake pedal force is large enough to make the ground braking force as constraint reaction of sliding friction and the value cannot exceed adhesive force, in this case, the ground braking force is equal to the adhesive force $F_{xb} = F_{\varphi}$. According to research literatures, the calculation formula of braking distance was expressed as

$$\begin{cases} s = \frac{1}{3.6}\left(\tau_2' + \frac{\tau_2''}{2}\right)v_0 + \frac{v_0^2}{25.92 \cdot \frac{F_\mu + F_W + F_i + F_f}{m}} & F_\mu < F_\varphi \\[4mm] s = \frac{1}{3.6}\left(\tau_2' + \frac{\tau_2''}{2}\right)v_0 + \frac{v_0^2}{25.92 \cdot \frac{F_\varphi + F_W + F_i + F_f}{m}} & F_\mu \geq F_\varphi \end{cases} \tag{7}$$

where $\tau_2$ is the action time of brakes, $F_\mu$ the braking force, $F_W$ is air resistance, $F_i$ is grade resistance, $F_f$ is rolling resistance, $F_\varphi$ is road adhesion, $m$ is the weight of the vehicle. According to the braking distance formula, braking distance is about braking force and the road adhesive force and adhesive force is influenced by road surface conditions, adhesive force is expressed under different road surface conditions as $F_\varphi = \varphi_b G$, in the formula, $\varphi_b$ is coefficient of road adhesion, $G$ is vehicle gravity.

## 3  Simulation

Based on the above calculation model of the stopping distance, braking distance simulation mode was build using the Simulink module of MATLAB. Brake line pressure data and load data were collected in vehicle brake test by sensors installed on the test vehicle. Structural parameters of the test vehicle and the driver's characteristic parameters were input into the simulation mode, the relationship between stopping distance and vehicle brake line pressure, vehicle load were analyzed. Finally compared with the results of simulation and road test, errors of stopping distance were calculated, and accuracy of the stopping distance model was verified in the paper.

Because of the braking distance is different while driving different type of vehicle under same condition, in order to ensure the consistency of experimental conditions, brake parameters of testing vehicle were used as the fixed parameters of simulation input. The parameters of test vehicle break system are as Table 1.

Bring braking system parameters into calculating formulas of braking force Eq. (4), braking force expressed as

$$F_\mu = 0.0171 \cdot P_f + 0.0114 P_r \tag{8}$$

$P_f$ is front braking line pressure, $P_r$ is rear braking line pressure.

Table 1  The test truck brake parameter

| Parameter of brake system | Value |
| --- | --- |
| $A_1$—The front brake chamber area (in$^2$) | 30 |
| $A_2$—The behind brake chamber area (in$^2$) | 20 |
| $R$—Adjusting arm radius (mm) | 110 |
| $r$—Cam basic radius (mm) | 20 |
| $R_0$—Drum brake radius (mm) | 210 |
| $L$—Brake drum circle into the distance of brake shoe support pin (mm) | 180 |
| $X$—Cam and brake shoe point to support pin distance in a horizontal direction (mm) | 12 |
| $Y$—Cam and brake shoe from point to support pin in the vertical direction (mm) | 330 |
| $\alpha$—The normal force pressure Angle led the hoof of the camshaft (deg) | 25 |
| $\beta$—From the foot pressure Angle of CAM method to force (deg) | 20 |
| $\theta$—Friction plate angle (deg) | 110 |
| $\eta$—The braking system efficiency | 0.75 |
| $u$—Friction coefficient | 0.35 |
| $m$—The actuation ratio | 3.5 |

The parameters of the driver reaction time model were consistent in road test and simulation, which brake type is predictable braking because of the driver have known the brake starting location, the speed of the vehicle and the position of braking, the brake type belongs to the predictable brake; The driver is 45 years old, male. Above conditions were brought into the driver reaction time calculation model, then driver reaction time was obtain as $\tau_1 = 0.7$ s, set the brake work time as $\tau_2 = 0.5$ s. Stopping distance model calibration test was carried out used test truck on real road and average wind resistance was obtained as

$$\bar{F}_w = \left| \frac{1}{v_0} \int_{v_0}^{0} \frac{C_D A v^2}{21.15} \, dv \right| = 0.039 \cdot v_0^2 \tag{9}$$

Average rolling resistance was expressed as

$$\bar{F}_f = \left| \frac{1}{v_0} \int_{v_0}^{0} G(a + b \cdot v) \, dv \right| = m \cdot (0.0125 + 0.00021 \cdot v_0) \tag{10}$$

Based on Eqs. (7)–(10) The stopping distance calculation formula was described as

$$\begin{cases} S = \frac{1}{3} v_0 + \frac{m \cdot v_0^2}{25.92 \cdot [0.0171 \cdot P_f + 0.0114 P_r + 0.039 \cdot v_0^2 + m \cdot (0.0125 + 0.00021 \cdot v_0)]}, & F_\mu < F_\varphi \\ S = \frac{1}{3} \cdot v_0 + \frac{m \cdot v_0^2}{25.92 [9.8 \cdot m \cdot \varphi_b + 0.039 \cdot v_0^2 + m \cdot (0.0125 + 0.00021 \cdot v_0)]}, & F_\mu \geq F_\varphi \end{cases} \tag{11}$$

Due to the driver adjust the operation intensity in braking test according to driving situation which is need to keep safe, the wheel is in the state of rolling rather than sliding when test vehicle was braking. Braking distance equation ($F_\mu < F$) was be used to build simulation model. Stopping distance-simulated program was described using MATLAB/Simulink as shown in Fig. 2.

The relationship between the vehicle stopping distance, braking line pressure, speed, and load were obtained in simulation and shown in Figs. 3 and 4. As can be seen from the diagram, when the vehicle is in a state of half load, braking distance was increasing with the initial brake speed, and decreasing with the brake pressure under the same speed. When initial brake speed is 60 km/h, stopping distance was increasing with the vehicle load, decreasing with the brake pressure under the same load.
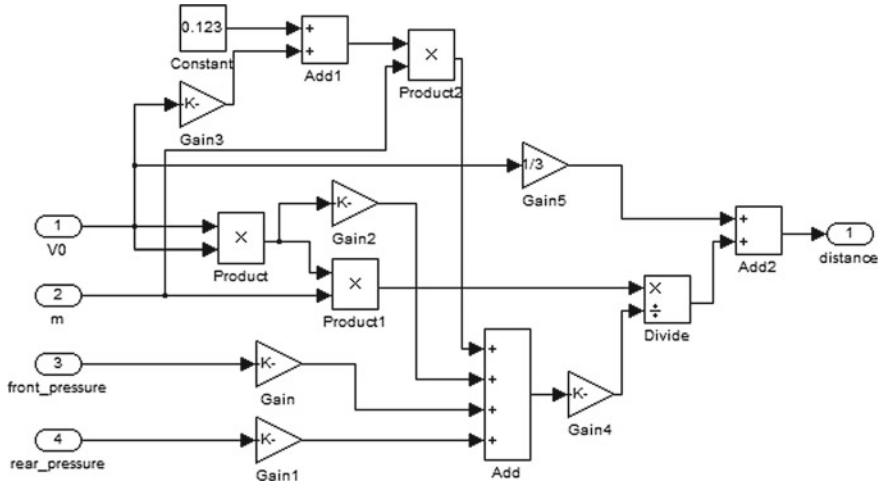
**Fig. 2**   Structure of simulated program for stopping distance

**Fig. 3**   Curved surface when truck is half load
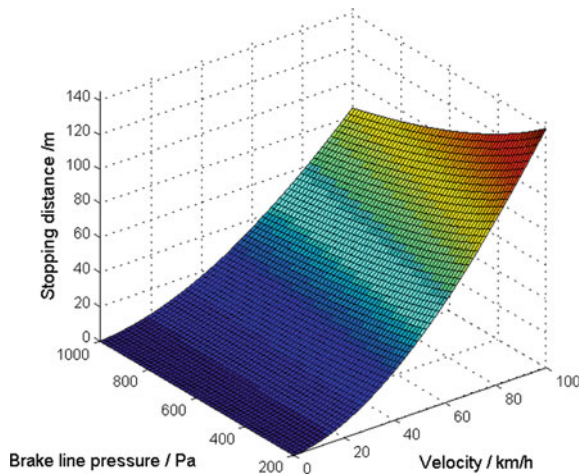


## 4   Risk Status Identification Based on Safety Distance

The conventional traffic environment is divided into two categories; the first category traffic environment is good traffic condition, wide vision, and free traffic environment. The second is bad weather and road conditions, slow traffic and narrow vision. In the first situation, when preceding vehicle was taken operation of emergency brake, the following vehicle brake immediately and keep safe distance with preceding vehicle until completely stop. In the second situation, preceding vehicle was blocked in situ (Bump into a fence and lug boss etc.), or goods fall from preceding vehicle, in that situation the safety distance is the driving distance from found obstacle to vehicle
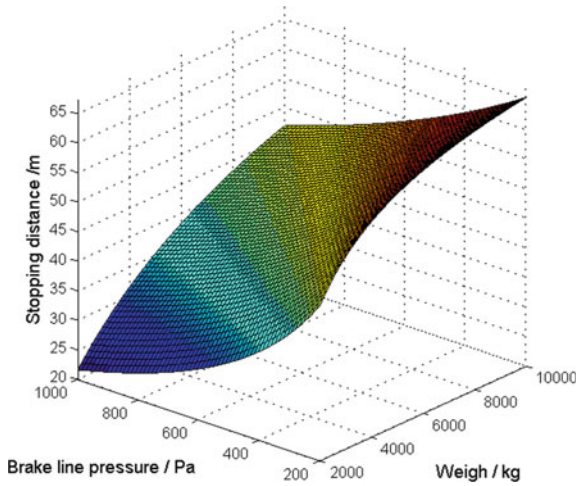
**Fig. 4** Curved surface when speed of truck is 60 km/h
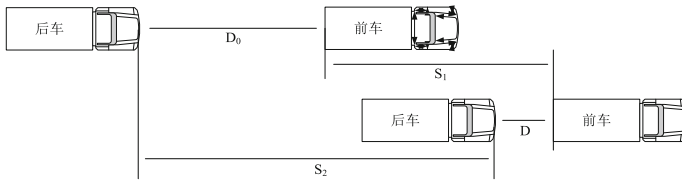


**Fig. 5** Following vehicle brake synchronously with preceding vehicle

**Fig. 6** Brake in extreme situation
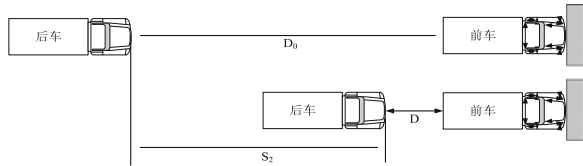


stopped, and there is still a distance to preceding vehicle(obstacles) when vehicle stopped. It is longer than the first situation, so the identification model of vehicle safe distance calculated in the second situation. As shown in Figs. 5 and 6.

Safe distance is determined by driving distance between two vehicles and braking distance, which is composed of four parts, stopping distance of preceding vehicle $S_P$, stopping distance of following vehicle $S_F$, distance between the two driving vehicles $D_0$, and distance between two vehicles when stopped. In the first situation, the condition to ensure traffic safety is $S_P + D_0 > S_F + D$. In second extreme situation, preceding vehicle was blocked in situ ($S_P = 0$), to ensure traffic safety, $D_0 > S_F + D$. Generally, the value of $D$ is 5 m. Safety distance was estimated conservatively according to the second situation as $D_0 \geq S_F + 5$. Summary above

the data of brake line pressure, load and speed can be collected by sensor, then applied to the prediction of the stopping distance [reference stopping distance model as Eq. (11)]. The risk status of driving truck was identified based on driving distance $D_{safe} \geq S_{stop} + 5$.

## 5    Conclusion

Influencing factor for stopping distance was analyzed in the paper. Calculation model of stopping distance was established on the base of the vehicle brake process analysis. The calculation method of model parameters was proposed through braking mechanical analysis; model parameters was obtained by calibration experiment using test truck. Braking distance calculation model was simulated in MATLAB/Simulink; Identification method of truck risk status was put forward based on calculating safety-driving distance and braking pressure data collection. This research provides a theoretical basis for early warning of truck risk status.

## References

1. Cho Y (2011) The simulation of ABS stopping distance. SAE
2. Tian X, Hu J (2012) Analysis of factors affecting pavement skid resistance. China Intelligent Transportation System Association, Beijing, pp 245–251
3. Michael DR, Song D, David LH, Thomas AK (2011) Light vehicle dry stopping distance—Vehicle speed correction, tire burnish, and surface friction correction. SAE International
4. Delaigue P, Eskandarian A (2004) A comprehensive vehicle braking model for predictions of stopping distances. J Autom Eng 218:1409–1417
5. Zhang T (2008) Study on the resin based friction material reinforce with ceramic whisker. Jinan Shandong University
6. Selig M, Ball A, Ash J, Schmidt K (2012) The influence of tyre contact patch and on the stopping distance of automotive vehicles. IOP Publishing Ltd.
7. Kloeppel E, Peters RD, James C, Fox JE, Alicandri E (1994) Comparison of older and younger driver the Human Factors and Ergonomics Society, 38th Annual Meeting of the Human Factors and Ergonomics Society, Part 2 (of 2), Nashville, Tennessee, USA, 24–28 October 1994
8. Olson PL, Cleveland DE, Fancher PS, Schneider LW, Sivak M (1982) Parameters affecting stopping sight distance. Interim Report, National Cooperative Highway Research Program (NCHRP) Project 15-8, University of Michigan Highway Safety Research Institute

# Simulation of Carbon Emission for Heavy-Duty Vehicle Queuing Systems

**Yao Yu, Jia-yu Zhai, Xue-gang Ban and Jin-xian Weng**

**Abstract**  Road traffic pollution has become one of the main sources of atmospheric pollution. Load of single heavy-duty vehicle often reaches tens of tons, and its exhaust pollution is also several times than small vehicles. Taking container truck as an example, which exhaust emission during the process of queuing will seriously aggravate regional air pollution in the port or terminal. Therefore, this paper uses the MOVES model to perform a simulation study for carbon emission in the process of the container truck queuing at the Shanghai port based on the in-depth analysis of the container terminal queuing system, taking into account the vehicle emission standards in China. Furthermore, the M/G/S/∞/∞/FCFS queuing model is utilized to analyze the trend and intrinsic relationship of the three types of truck carbon emissions, such as $CO_2$, $CO$, and THC under continuous speed variation. The research result can provide important decision-making support for low-carbon management.

**Keywords**  Low-carbon · Queue length theory · Carbon emission simulation
MOVES model

## 1   Introduction

With the rapid development of freight transportation, the proportion of heavy vehicles in highway logistics is increasing. Container transport and transshipment demand is huge in Shanghai port. To meet the demand, the exhaust emission of a large number of container trucks (hereinafter referred to as the truck) has produced serious environmental pollution in the exhaust port and the hinterland of area nearby. The

Y. Yu · J. Zhai (✉) · X. Ban · J. Weng
College of Transport and Communications, Shanghai Maritime University, Shanghai 201306,
China
e-mail: 1181791402@qq.com

X. Ban
Department of Civil and Environmental Engineering, University of Washington, 121G More Hall,
Seattle, WA 98195, USA

exhaust emission of single one is almost equivalent to the total emission of 30 light vehicles [1]. So the demand is very urgent, which is how to reduce the carbon emission of the truck in the port area and truly achieve the "resource saving and environment-friendly transportation development [2]".

Terminal gate is the key link of the truck when it is in and out, but also the traffic bottlenecks which cause the truck queue. Compared to the driving state, in the process of waiting at the gate, the truck will discharge more hydrocarbons (THC) and carbon oxides ($CO_x$).To solve the conflict between efficient port operation and truck emission pollution and achieve the goal of reducing the port total energy consumption and total carbon emission decline, it is urgent to control the carbon emissions of the truck queuing in the terminal gate. Therefore, definiting the internal evolution rule in the process of the truck queue and analyzing the truck carbon emission rule have become urgent problems to be solved at the container terminal.

## 2   Literature Review

The container terminal gate is the necessary operating channel that the external truck transfers containers to entry and exit yard. The existing studies mostly focus on the optimization problem areas aimed at improving the gate operation capacity and shortening waiting time of the truck. As some foreign scholars have proposed a reservation system to reduce the gate congestion [3–5], and proved that it can effectively reduce the number of truck queue; From the point of view of queuing theory, Guan et al. [6] used the M/Ek/c queuing model to calculate the average length of the truck queuing and constructed the optimization model. In addition, Zeng, Xu et al. [7, 8]. also established queuing network models, respectively, in order to estimate the time that the truck needs to wait in the gate. Liu et al. [9] have proposed M/G/S/∞/∞/FCFS queuing system model so that the gate process was optimized. However, the above studies were based on the minimization of the total time cost or the minimum cost of the total cost of the objective function to optimize, and not studied the smallest total carbon emissions from the perspective of low-carbon constraint.

Based on the analysis of emission reduction measures at home and abroad, Dong and Wang et al. [10, 11] have put forward the theoretical calculation formula of carbon emissions from container terminals, without quantifying method of the truck carbon emissions, and the proposed theoretical model is quite different from practice. And Lu et al. [12] gave a multi-objective optimization model by taking into account the two objectives of $CO_2$ emission and the truck multi-target scheduling, without considering the actual waiting and carbon emissions in low-speed process of the truck queuing at the gate. Based on the above research results, for the first time facing the key link of the terminal gate, this paper uses the MOVES simulation tools innovatively to simulate the truck carbon emissions during the queuing process, and in-depth analyzes the relationship between the different speed zones and the carbon emission under the actual queuing rules.

# 3 Analysis of the Dock Gate Operation Flow

The truck queue at the gate is divided into two parts, waiting to enter the gate and get out. According to the dock gate service rules (FCFS) and the process that the truck queuing in the terminal gate system is served, it can be classified as a typical multilevel queuing network.

According to the data of a container terminal in Shanghai and its scheduling rules, the gate has a total of 24 channels, that is, M/G/24/$\infty$/$\infty$/FCFS queuing system is satisfied. Based on the measured data (see Table 1), this paper constructs the queuing model of the gate truck of the dock. And based on the queuing model elements (input process, queuing rules, and service organization), the proposed queuing system makes the following assumptions:

- The truck is the "customer" in the gate operating system, the number of it is unlimited;
- That the truck arrives at the gate is independent and random events, also meet the independence of the time interval;
- The truck arrival obeys the FCFS rules, and the gate system is in real-time wait state;
- The dock gate (24) operations are independent of each other, the service capacity of each channel is the same, and each channel can only serve a truck at a time;
- The time interval of the truck arrival is independent of the service time that the truck is accepted in the channel;
- The gate system runs for a long time and can reach the steady state.

It can be seen from Table 1, the construction of the gate service system meets the multi-service desk waiting mechanism, and the vehicle queuing situation exists in the delivery and pick-up operation: Of which, the average length of the boxing operation is about 2.2 times the average team length in the suitcase; the average residence time and average waiting time in the delivery operation were higher than those in the case. The queuing of the vehicle arrived at the gate was longer than that of exiting gate;

**Table 1** Shanghai port gate system parameters table

| Type | Parameter | Value |
| --- | --- | --- |
| Delivery operation | Average queue length/veh | 166 |
| | Average waiting queue length/veh | 165 |
| | Average residence time/min | 27.73 |
| | Average waiting time/min | 29.55 |
| Suitcase operation | Average queue length/veh | 75 |
| | Average waiting queue length/veh | 74 |
| | Average residence time/min | 20.18 |
| | Average waiting time/min | 19.90 |

**Table 2** Carbon emission coefficient for different fuel types in China

| Fuel type | Low calorific value (KJ/Kg) | Unit calorific value Carbon content (Kg/KJ) | Carbon oxidation rate | Carbon conversion coefficient | Density (kg/L) | Carbon emission coefficient (kg/L) |
|---|---|---|---|---|---|---|
| Gasoline | 43,070 | 1.89000E−05 | 98 | 3 2/3 | 0.74 | 2.16 |
| Diesel | 42,652 | 2.02000E−05 | 98 | 3 2/3 | 0.86 | 2.66 |

due to the high rate of reloading of vehicles entering the port, the carbon pollution in the queuing phase is more serious. Therefore, it is an important basis for the effective formulation of strategies to control the carbon emission in the port area by analyzing the rate of carbon change in the process of queuing waiting in the gate.

## 4   MOVES Simulation Model Selection

Taking into account the vehicle operating conditions and the basic rate of emissions which are only for the United States native region in the MOVES and a greater difference in China from the United States in model division, road conditions and other aspects, so combined with "China Energy Statistics Year 2010" and "2006 IPCC Guidelines for National Greenhouse Gas Inventories" [13, 14], the correlation coefficient of diesel and gasoline is revised, respectively, as shown in Table 2.

## 5   Simulated Analysis

This paper uses Tables 1 and 2 as input parameters for the MOVES simulation environment; The simulation time is set to 1 h (9:00–10:00), the temperature is 25, 77 °C Fahrenheit, relative humidity of 72%. Arrival trucks are Combination Long-haul Truck and Combination Short-haul Truck, and fuel is gasoline, the corresponding standard average speed bin value ranges between 9.28 and 114.7 km/h. As this article is for the container terminal gate, so the selected truck vehicle speed range (9.28–60.28 km/h), the speed interval of 3. The following makes the simulation analysis for carbon, $CO_2$, CO, THC three kinds of carbon compounds and energy consumption, the results shown in Fig. 1.

As can be seen from the results in Fig. 1, the velocity has a great influence on the discharge of the vehicle. When the speed is less than or equal to 9.28 km/h, the vehicle energy consumption is large, the corresponding $CO_2$, CO and THC and other pollutants emissions are also in the highest position. But with the increase in speed, $CO_2$, CO, and THC and other pollutants emissions showed a monotonous decreasing trend, energy consumption is also a corresponding decline; Especially

(a) CO2 emission curve



(b) CO2 emission curve



(c) THC emission curve



(d) energy consumption curve
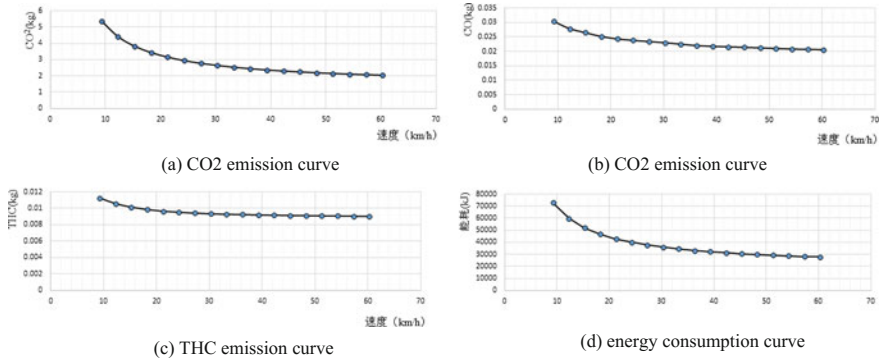
**Fig. 1** Changes of carbon emissions in single truck in 60 km/h or less
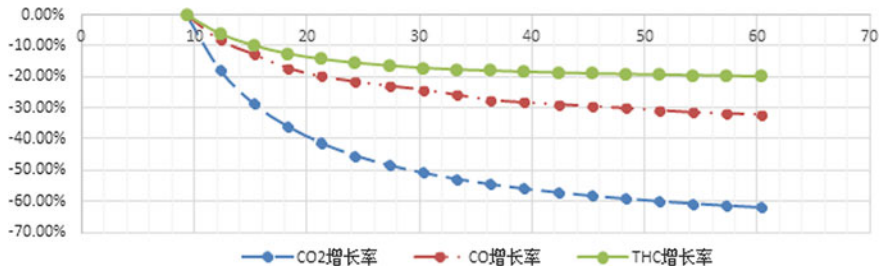


**Fig. 2** Carbon emission pollution growth rate curve

when the speed increases from 0 to 15.28 km/h, the carbon pollution emissions, and energy consumption decline gradient is obvious, when the speed is higher than 15.28 km/h, the carbon pollution emissions trend tends to be stable. The emission growth rate of each pollutant is shown in Fig. 2.

It can be seen from Fig. 2 that the growth rates of $CO_2$, CO and THC are $-61.93$, $-32.10$ and $-19.88\%$, respectively, with the increase of the average velocity. The overall analysis (speed less than or equal to 60 km/h) shows that in the low-speed range of vehicles, the total amount of carbon emissions is larger, but with the gradual increase in the average speed, the pollutant emission growth rate is significantly reduced, in this paper, the speed range is smaller, with the late rate of continuous increase, the pollutant emissions is not continuous decline, as shown in Fig. 3, with the increase of the average speed during the opening of the gate, the total amount of carbon pollution decreases first, and then increases, when the speed of the vehicle is higher than 60 km/h, it can be seen that there is a significant increase in carbon pollution, but the total fuel consumption is still maintained monotonically decreasing trend. Therefore, when the heavy load vehicle attributes under the premise of the speed is an important factor affecting its exhaust emissions.
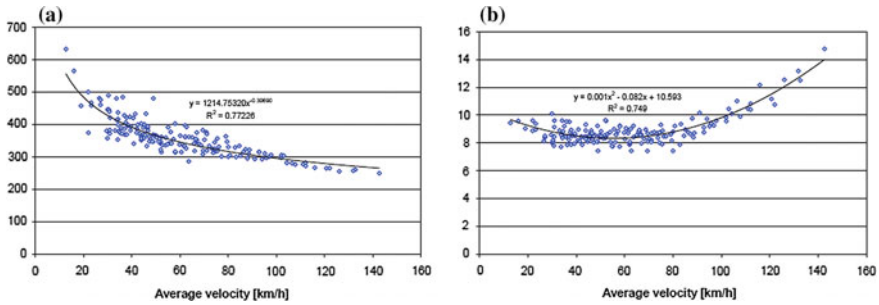
**Fig. 3** Fuel consumption (**a**) and carbon emissions (**b**) under the different speed range of truck

## 6   Conclusion

In this paper, the container heavy truck as an important element of the whole port transportation systems, whose carbon emissions changing is discussed while through the port/terminal gate. First, the actual situation of the heavy vehicle waiting at the gate is considered based on the queuing theory at Shanghai port gateway. Then, we analyzed the following key indexes including average queue length, average waiting queue length, average residence time, and average waiting time. Consequently, a new M/G/24/∞/∞/FCFS queuing system is proposed combined with MOVES simulation model. And the $CO_2$, CO, THC, and fuel energy consumption of heavy load vehicles were analyzed, respectively under queuing system were simulated and analyzed. And the trend of the above four indexes is obtained under different speed range. It obvious that the carbon emission pollution is monotonically decreasing when the average traveling speed of the vehicle is less than 60 km/h. And when the speed is higher than 60 km/h, the total amount of carbon emissions is reversed, showing an increasing trend. In the case of constant vehicle properties, speed is an important factor affecting its emissions.

## References

1. Bishop GA, Hottor-Raguindin R, Stedman DH et al (2015) On-road heavy-duty vehicle emissions monitoring system. Environ Sci Technol 49(3):1639–1645
2. Hudda N, Fruin S, Delfino RJ et al (2013) Efficient determination of vehicle emission factors by fuel use category using on-road measurements: downward trends on Los Angeles freight corridor I-710. Atmos Chem Phys 13(1):347–357
3. Morais P, Lord E (2006) Terminal appointment system study. Transport Canada Publication No. TP14570E. Transportation Development Center, Montreal, pp 134–140
4. Giuliano G, O'Brien T (2007) Reducing port-related truck emissions: the terminal gate appointment system at the ports of Los Angeles and Long Beach. Transp Res Part D: Transp Environ 12(7):460–473
5. Murty KG, Wan Y, Liu J et al (2005) Hong Kong International Terminals gain elastic capacity using a data-intensive decision-support system. Interfaces 35(1):61–75

6. Guan CQ, Liu RF (2009) Container terminal gate appointment system optimization. Marit Econ Logistics 11(4):378–398
7. Zeng QC, Zhang XJ, Chen WH et al (2013) Optimization model for truck appointment based on BCMP queuing network. J Syst Eng 28(5):592–599
8. Xu QL, Sun LJ, Hu XP et al (2014) Non-stationary arrive terminal set card booking optimization model. J Dalian Univ Technol 54(5):589–596
9. Liu CL, Ji MJ, Yu TL, Qiu J, Gao N (2011) The capacity of the container terminal operation system. Transp Syst Eng Inf 11(4):118–123
10. Dong G, Chen FY (2012) Typical port truck emission reduction measures at home and abroad and enlightenment to Shanghai. Shipping Econ Manage 2012(19):4–7
11. Wang WY, Zhang YC, Tang GL, Peng Y (2013) Calculation method of carbon emission in port container handling. Harb Eng Technol 50(4):6–10
12. Lu YQ, Yang B, Huang YF (2015) Both carbon emissions and efficiency of scheduling multi-objective optimization. Comput Simul 32(6):386–389
13. Department of Industrial Traffic Statistics, National Bureau of Statistics. China energy statistical yearbook. China Statistics Press, Beijing, 2005–2010
14. Hiraishi T, Krug T, Tanabe K et al (2014) 2013 supplement to the 2006 IPCC guidelines for national greenhouse gas inventories: Wetlands. IPCC, Switzerland

# Study on the Relationship Between Highway Freight Volume and Industrial Structure in China on VAR Model

**Kechao Sun and Chunguang Jing**

**Abstract** Transportation has played an important supporting role in the development of the national economy. Road transport is the pillar area of the transportation industry. Research on the Relationship between Highway Freight Volume (HFV) and Industrial Structure, it can provide theoretical support for the rational development of road freight advance strategy. This chapter analyzes the Relationship between (HFV) and the Primary Industry (PI), Secondary Industry (SI) and Tertiary Industry (TI), a smooth series of data were established by taking logarithms and eliminating singular data, using the Vector Autoregressive model (VAR) for analysis. This chapter also does the analysis of the cointegration test, Granger causality test, and impulse response functions, and get the relationship between HFV and PI, SI, and TI.

**Keywords** VAR model · Highway freight volume · Industrial structure · Granger causality test · Impulse response function

## 1 Introduction

Transportation has played an important supporting role in the development of the national economy. Road transport is the pillar area of the transportation industry. Research on the relationship between Highway Freight Volume (HFV) and Industrial Structure, it can provide theoretical support for the rational development of road freight advance strategy. This chapter analysis the relationship between (HFV) and the Primary Industry (PI), Secondary Industry (SI) and Tertiary Industry (TI), a smooth series of data were established by taking logarithms and eliminating singular data, using the Vector Autoregressive model (VAR) for analysis. This chapter also does the analysis of the cointegration test, Granger causality test, and impulse response functions, and get the relationship between HFV and PI, SI, and TI.

K. Sun (✉) · C. Jing
China Academy of Transportation Sciences, Beijing 100029, China
e-mail: sunkechao2004@163.com

## 2 Theories

### 2.1 The Construction of VAR Model

The traditional regression model is based on economic theory, analyzing the relationship between the economic variables of the time series, rather than the economic theory is the core idea in VAR model.

The general form of VAR is [1]:

$$Y_t = \alpha + \sum_{i=1}^{p} \beta_i Y_{t-i} + \varepsilon_t, \tag{1}$$

where $E(\varepsilon_t) = 0$, $E(\varepsilon_t, Y_{t-i}) = 0$, $i = 1, 2, \ldots, p$, $Y_t$ is the linear stochastic process with stationary variance of vector $(n \times 1)$, $\beta_i$ is Coefficient matrix $(n \times n)$, $Y_{t-i}$ is the $i$ order lag variable of vector $Y_t$, $\varepsilon_t$ is the error.

### 2.2 Determination of Unit Root Test and Determination of Optimal Time Delay

Since the establishment of the VAR equation is affected by the variable, it is necessary to test the stability of the variables first. The unit root test is the stability test of the sequence. ADF test and PP test are commonly used, this article uses ADF test, the model is as follows:

$$\Delta y_t = \gamma \quad y_{t-1} + \sum_{i=1}^{p} \beta_i \Delta y_{t-i} + \varepsilon_t, \tag{2}$$

where $t$ is the time trend formula, $\gamma$, $\beta$ is parameter, $\varepsilon$ is the error.

The original hypothesis of the test is H$_1$: $\gamma = 0$,the opposition is H$_0$: $\gamma < 0$. If the original data cannot reject the original hypothesis, then perform a first-order difference and the difference after the sequence of re-ADF test, the VAR model can be established based on the smooth sequence.

There are many test methods of determining the lag of the test, AIC and SIC guidelines are commonly used, the two values are as small as possible, LR test is usually used.

## 2.3 Cointegration Test

The cointegration test has the Engle2Granger method and the Johansen maximum likelihood method, the first method is suitable for covariance of two-variable models, the second is suitable for testing in multivariate VAR models.

In this chapter, the second method is introduced for the multivariate. The Johansen test is a method of testing the cointegration relationship between variables using a maximum likelihood estimate under a VAR system. The method is as follows:

Suppose $y_t$ is the vector sequence of $k \times 1$, then the VAR model of lag is as follows:

$$y_t = A_1 y_{t-1} + A_2 y_{t-2} + \cdots + A_p y_{t-p} + \varepsilon_t \tag{3}$$

The above equation is rewritten as a differential form:

$$\Delta y_t = \sum_{i=1}^{p-1} \Gamma_i \Delta y_{t-i} + \Pi y_{t-p} + \varepsilon_t \tag{4}$$

where, $\Gamma_i = \sum_{j=1}^{p-1} A_j - I$, $\Pi = \sum_{i=1}^{p} A - I$

In Formula (4), $\Pi$ represents all the long-term equilibrium information, $\Pi y_{t-p}$ is the error correction item.

## 2.4 Granger Causality Test

The basic idea of Granger's Causal Test is

If $Y$ is the cause of $X$, then $Y$ should precede $X$. For the stable variables $X$ and $Y$, the Granger test uses the following variable autoregressive equation:

$$Y_t = \alpha_t + \sum_{j=1}^{n} \beta_j X_{t-j} + \sum_{k=1}^{m} \gamma_k Y_{t-k} + \varepsilon_t \tag{5}$$

$$X_t = a_t' + \sum_{j=1}^{n} \beta_j' X_{t-j} + \sum_{k=1}^{m} \gamma_k' Y_{t-k} + \varepsilon_t' \tag{6}$$

Since the Granger test is affected by the number of lag items m and n of the variable, the stability of the sequence of variables and the cointegration relationship between the variables, it is necessary to determine the lag items m and n before performing the Granger test.

## 2.5   *Impulse Response Function*

Impulse response function is used to measure the influence of a standard deviation impact from random disturbance on the current and future values of endogenous variables, and can directly describe the dynamic interaction between variables and their effects. Each variable can be expressed as a linear combination of the current and lagged random impact terms, the impulse response function:

$$Y_t = \alpha + \sum_{i=0}^{\infty} A_i C C^{-1} \varepsilon_{t-i} \tag{7}$$

If $D_i = A_i C$, $U_{t-i} = C^{-1} \varepsilon_{t-i}$, then

$$Y_i = \alpha + \sum_{i=0}^{\infty} D_i U_{t-i} \tag{8}$$

## 3   Empirical Studies

## 3.1   *Inputs of the Model*

This chapter selected HFV (Highway Freight Volume), PI (Primary Industry), SI (Secondary Industry), TI (Tertiary Industry) in China Statistical Yearbook from 1990 to 2015, as showed in Fig. 1. In order to eliminate the singular data, the data for 2012 are replaced by the average of two adjacent data. Also, to eliminate the heteroscedasticity of the sequence and maintain its volatility, the logarithm of the four index data is taken, represent by lnHFV, lnPI, lnSI, and lnTI, as shown in Fig. 2. This article uses Eviews7.2 for data analysis and processing.

## 3.2   *Determination of Unit Root Test and Determination of Optimal Time Delay*

In order to avoid the occurrence of false return, according to the ADF test model, Using EViews7.2, The unit root test results of each variable are obtained, as shown in Fig. 1 (Table 1).

It can be seen from the Root Test Results with ADF t-Statistic, three variables are stationary, HFV is a second-order stable, conform to the prerequisite for cointegration test.
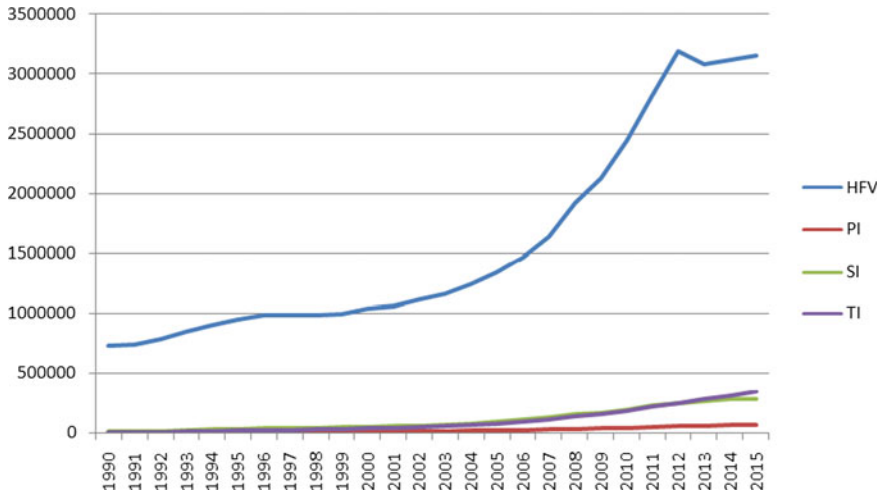
**Fig. 1** 1990–2015 HFV, PI, SI, and TI date charts
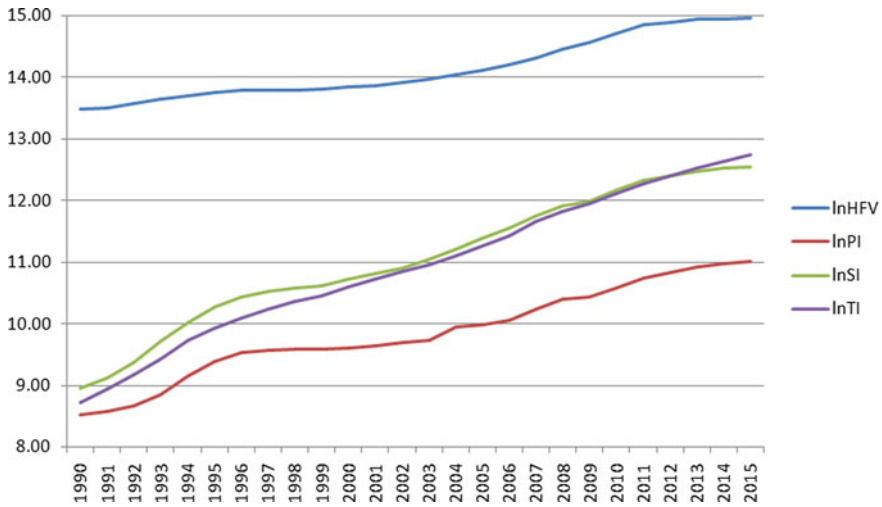


**Fig. 2** 1990–2015 HFV, PI, SI, and TI date charts after eliminating the singular data and taking logarithm

For the determination of the lagging order of the VAR model, the Eviews7.2 software is used to obtain the five evaluation indexes as shown in Tables 2, 3, 4, and 5. The five indexes are considered to be reasonable in the second order, that is, the VAR (2) model is established.

**Table 1** The root test results with ADF t-statistic

| Index | ADF test | 1% level | 5% level | Prob.[*] | Conclusion |
|---|---|---|---|---|---|
| lnHFV | −0.824808 | −3.737853 | −2.991878 | 0.7938 | Unstable |
| ΔlnHFV | −1.948096 | −3.737853 | −2.991878 | 0.3061 | Unstable |
| $\Delta^2$lnHFV | −5.719681 | −3.752946 | −2.998064 | 0.0001 | Steady |
| lnPI | −4.121206 | −4.440739 | −3.632896 | 0.0192 | Steady |
| lnSI | −4.272900 | −4.394309 | −3.612199 | 0.0130 | Steady |
| lnTI | −5.223180 | −4.440739 | −3.632896 | 0.0020 | Steady |

*Note* Δ denotes the first-order differential operator and $\Delta^2$ denotes the second-order difference operator

**Table 2** Endogenous variables: LNHFV

| Lag | LR | FPE | AIC | SC | HQ |
|---|---|---|---|---|---|
| 0 | NA | 0.226074 | 1.350921 | 1.400514 | 1.362603 |
| 1 | 92.69151 | 0.002405 | −3.192746 | −3.093560 | −3.169380 |
| 2 | 13.37741[a] | 0.001304[a] | −3.805911[a] | −3.657132[a] | −3.770863[a] |
| 3 | 0.460618 | 0.001396 | −3.740591 | −3.542220 | −3.693861 |

*Note* [a]indicates the lag order determined according to this criterion

**Table 3** Endogenous variables: LNPI

| Lag | LR | FPE | AIC | SC | HQ |
|---|---|---|---|---|---|
| 0 | NA | 0.347222 | 1.780022 | 1.829615 | 1.791705 |
| 1 | 78.71927 | 0.007429 | −2.065032 | −1.965847 | −2.041667 |
| 2 | 4.926412[a] | 0.006285[a] | −2.233408[a] | −2.084629[a] | −2.198360[a] |
| 3 | 0.589310 | 0.006677 | −2.175238 | −1.976867 | −2.128508 |

*Note* [a]indicates the lag order determined according to this criterion

**Table 4** Endogenous variables: LNSI

| Lag | LR | FPE | AIC | SC | HQ |
|---|---|---|---|---|---|
| 0 | NA | 0.714201 | 2.501223 | 2.550816 | 2.512906 |
| 1 | 101.3223 | 0.004935 | −2.473981 | −2.374795 | −2.450616 |
| 2 | 13.59912[a] | 0.002645[a] | −3.098815[a] | −2.950036[a] | −3.063767[a] |
| 3 | 1.184930 | 0.002719 | −3.073735 | −2.875364 | −3.027005 |

*Note* [a]indicates the lag order determined according to this criterion

**Table 5** Endogenous variables: LNTI

| Lag | LR | FPE | AIC | SC | HQ |
|---|---|---|---|---|---|
| 0 | NA | 0.935957 | 2.771629 | 2.821222 | 2.783312 |
| 1 | 123.1128 | 0.002176 | −3.293100 | −3.193914 | −3.269734 |
| 2 | 8.530900[a] | 0.001523[a] | −3.651185[a] | −3.502407[a] | −3.616137[a] |
| 3 | 0.344033 | 0.001640 | −3.579389 | −3.381018 | −3.532659 |

*Note* [a]indicates the lag order determined according to this criterion

**Table 6** Normalized cointegrating coefficients (standard error in parentheses)

| LNHFV | LNPI | LNSI | LNTI |
|---|---|---|---|
| 1.000000 | −2.455201 | 2.374705 | −1.041422 |
| | (0.18130) | (0.22028) | (0.14127) |

## 3.3 Cointegration Test and Granger Causality Test

On the basis of the established VAR (2) model, the covariance test is carried out according to the Johansen method in the Cointegration Test. The results are shown in Table 6.

The cointegration equation is

$$\ln \text{HFV} = -2.455201 \times \ln \text{PI} + 2.374705 \times \ln \text{SI} - 1.041422 \times \ln \text{TI}$$

It can be seen from the cointegration equation that there is a long-term equilibrium relationship between the national economy and transportation. Since the data are logarithmized, the coefficients before the variables are the elasticity of their output.

Granger causality tests are performed between the variables to determine the interaction between them. The order of the lag is second-order, the test results are shown in Table 7.

As can be seen from Table 4, at 5% of the significance level, a total of seven original assumptions were accepted, five original assumptions were rejected. LNTI and LNPI are two-way Granger causality relationship between LNTI and LNPI, LNTI and LNPI are two-way Granger causality relationship between LNTI and LNPI.

## 3.4 Create VAR Model

Using Eviews7.2, VAR (2) model is established for four variables such as LNHFV, LNPI, LNSI, and LNTI. The results of VAR model are shown in Table 8:

The results of the VAR model, the coefficient (R2) are used to measure the extent of the explanatory variables in the sample range using the VAR model. In the VAR model, the available coefficients are 0.997675, 0.998359, 0.998901, and 0.999559,

**Table 7** Pairwise Granger causality tests

| Null hypothesis | Obs | F-statistic | Prob. |
|---|---|---|---|
| LNPI does not Granger cause LNHFV | 24 | 0.71853 | 0.5002 |
| LNHFV does not Granger cause LNPI | | 3.90814 | 0.0379 |
| LNSI does not Granger cause LNHFV | 24 | 0.35385 | 0.7065 |
| LNHFV does not Granger cause LNSI | | 1.50542 | 0.2472 |
| LNTI does not Granger cause LNHFV | 24 | 1.16626 | 0.3329 |
| LNHFV does not Granger cause LNTI | | 1.17297 | 0.3309 |
| LNSI does not Granger cause LNPI | 24 | 12.9899 | 0.0003 |
| LNPI does not Granger cause LNSI | | 4.14482 | 0.0321 |
| LNTI does not Granger cause LNPI | 24 | 7.83851 | 0.0033 |
| LNPI does not Granger cause LNTI | | 4.04709 | 0.0343 |
| LNTI does not Granger cause LNSI | 24 | 5.05300 | 0.0174 |
| LNSI does not Granger cause LNTI | | 4.25737 | 0.0297 |

respectively, which means that the fitting effect is very good compared with the actual value. And from the VAR model, we can see the variables in the $t-2$ period and $t-1$ changes in the impact of the indicators, and also analyze the extent of the impact of the size of the numerical size.

## 3.5 Impulse Response Function

Impulse response function is used to evaluate the random disturbance of a standard deviation of the impact of other variables on the current and future value of the impact; it can be more intuitive to describe the dynamic interaction between variables. Figure 3 shows the influence of the impacts between LNHFV, LNPI, LNSI, and LNTI. The horizontal axis is equal to the number of retrospective periods, and the length per unit represents one period. The vertical axis represents the magnitude of the impact between the variables. The solid line represents the response function curve, and the two dashed lines represent the confidence interval boundary of the double standard deviation.

**Table 8** The results of VAR model

|  | LNHFV | LNPI | LNSI | LNTI |
|---|---|---|---|---|
| LNHFV(-1) | 1.432424 | −0.764710 | 0.187970 | −0.077691 |
| LNHFV(-2) | −0.367418 | 1.306540 | 0.106996 | 0.341252 |
| LNPI(-1) | −0.349346 | 0.089580 | −0.522980 | −0.590869 |
| LNPI(-2) | −0.145195 | −0.586453 | −0.320231 | 0.003724 |
| LNSI(-1) | −0.071438 | 1.374935 | 1.443540 | 0.660239 |
| LNSI(-2) | 0.434424 | −0.031521 | −0.052729 | −0.156353 |
| LNTI(-1) | 0.290990 | −0.795019 | −0.196900 | 0.776384 |
| LNTI(-2) | −0.342698 | 0.283706 | 0.199354 | 0.006413 |
| C | 0.536597 | −2.012711 | −0.065154 | −0.978781 |
| R-squared | 0.997675 | 0.998359 | 0.998901 | 0.999712 |
| Adj. R-squared | 0.996435 | 0.997483 | 0.998315 | 0.999559 |
| Sum sq. resids | 0.012279 | 0.016740 | 0.022595 | 0.007464 |
| S.E. equation | 0.028611 | 0.033406 | 0.038812 | 0.022308 |
| F-statistic | 804.6332 | 1140.382 | 1704.537 | 6515.932 |
| Log likelihood | 56.88092 | 53.16175 | 49.56243 | 62.85332 |
| Akaike AIC | −3.990077 | −3.680146 | −3.380203 | −4.487776 |
| Schwarz SC | −3.548307 | −3.238375 | −2.938433 | −4.046006 |
| Mean dependent | 14.18632 | 9.964247 | 11.21970 | 11.10374 |
| S.D. dependent | 0.479197 | 0.665874 | 0.945548 | 1.062150 |

## 4  Discussion

This chapter establishes the VAR model between LNHFV, LNPI, LNSI, and LNTI, and analysis of the cointegration test, Granger causality test and impulse response functions, the conclusion is as follows:

1. From the results of Cointegration Test, it can be seen that there is a long-term equilibrium relationship between HFV and PI, SI, TI, which shows that there is a close relationship between transportation and economy. Increase investment in transportation, and strive to improve the road freight for social and economic development is of great significance.
2. From the Granger causality test, it can be seen that there is a one-way Granger causality between LNHFV and LNPI. The road freight can promote the rapid development of the primary industry economy. PI, SI, and TI are two-way Granger causality among them, but also shows the coordinated development of China's three industries. HFV, SI, and TI have no Granger causality, it is recommended that the Government should pay attention to the development of road freight, pay attention to highway construction and road transport team economy to promote SI and TI.
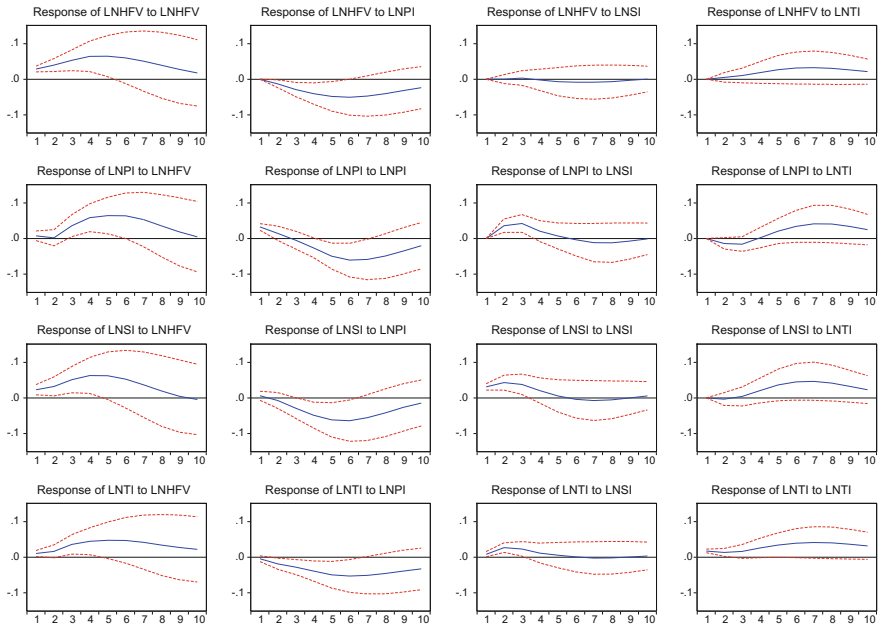
**Fig. 3** Impulse response diagram between LNHFV, LNPI, LNSI, and LNTI

3. From the VAR model, the degree of fitting is high, all above 0.9, indicating that the model is reasonable; the relationship between the variables in the model has been a clear reflection. From the economic point, the national economy and road freight should be mutually reinforcing.
4. From the impulse response function, it can be seen that the impact of HFV to TI promote the largest role, it is actually consistent with industry-based tertiary industry, it is recommended that China should pay more attention to HFV, which can be faster to promote the industrial structure to TI.

# References

1. Liu C, Sun K, Zhang Q (2011) Study on the relationship between traffic volume and economy development in Nanjing City based on VAR model. J Wuhan Univ Technol (Transp Sci Eng) 35(5):1058–1062
2. Lyu J, Fan W (2016) Example analysis on relationship between transport demand and GDP based on VAR model. Technol Econ Areas Commun 18(2):52–55
3. Peng C, Cheng F (2009) Transportation, income, holiday policies and domestic tourism income growth—based on VAR model. J Central S Univ For Technol (Soc Sci) 3(5):78–82

4. Ren R, Cheng L, Xie Z, Zong G (2012) Dynamic effect analysis on the relationship of transport infrastructure investment and economic development in China based on VAR model. Sci Technol Manage Res 32(4):85–89
5. Sun X, Chen X, Gao Y (2016) Correlation analysis of traffic performance index and bus performance index with econometric model. J Harbin Inst Technol 48(3):60–65

# Research on SVM-Based Highway Traffic Safety Evaluation Model

**Jian Cui, Haoyu Zhang, Jianyou Zhao and Yunjiao Zhang**

**Abstract**   To enhance the traffic safety level of highway, the paper proposes SVM-based highway traffic safety evaluation model. According to the screening principle and grading standard of evaluation index, and establishes road traffic safety evaluation index system including driver, vehicle, road, traffic management and supervision and determines weight of each index using AHP. Through matter element judgment method, the paper selects the learning sample of SVM evaluation model, constructs SVM-based highway traffic safety evaluation model, solves SVM evaluation model by using SVM multi-classification algorithm of partial binary tree, and optimizes parameters by using GA. Through collecting related data about traffic safety of Luoluan Highway in He'nan and combining the overall evaluation of such Highway using the model, the paper verifies the reliability of model.

**Keywords**   Highway · Traffic safety · SVM model · Safety evaluation

## 1   Introduction

In recent 30 years, highway construction developed rapidly in our country, it does a giant contribution to social and economic development, but it also produces negative effects such as traffic safety problem and environmental pollution. Road traffic accident is an emergent social accident with high occurrence frequency. It is produced under the joint effect of multiple factors and mainly related with driver, vehicle, road, traffic management, and supervision consequently [1] to solve the frequent occurrence problem of traffic accident, and it is necessary to construct SVM-based highway traffic safety evaluation model using driver, vehicle, road, traffic management, and supervision and carry out comprehensive evaluation by citing Luoluan Highway, which provided theoretical basis for the improvement strategy of highway traffic safety management.

J. Cui (✉) · H. Zhang · J. Zhao · Y. Zhang
School of Automobile, Chang'an University, Xi'an 710064, Shanxi, China
e-mail: 402250745@qq.com

## 2  SVM-Based Highway Traffic Safety Evaluation Model

SVM behaves many unique advantages in machine learning fields such as solving classification, regression, and density estimation. It is deemed as the optimal method against the classification and regression of small sample [2]. Therefore, the paper grades the implementation effect of road traffic safety method using SVM. The paper selects index from driver, vehicle, road, traffic management, and supervision, determines weights of 20 evaluation indexes using AHP, selects 40 learning samples using matter element judgment method, constructs SVM-based highway traffic safety model, and optimizes parameters of model.

### 2.1  Indicator Selection

The paper selects index according to the index selection principle and finally selects 20 indexes from driver, vehicle, road, traffic management, and supervision. According to expert scoring method and grading standard of related literature, the paper grades the index and finally defines the index as Grade I, Grade II, Grade III and Grade IV. Grade I means excellent, Grade II means good, Grade III means moderate, and Grade IV means poor [3]. At last, the paper constructs highway traffic safety evaluation index system including driver, vehicle, road, traffic management, and supervision, namely 7 indexes about illegal behavior of driver, 2 indexes about illegal behavior of vehicle, 5 indexes about illegal highway traffic design, 6 indexes about traffic management and supervision, and 20 indexes in total for the overall evaluation system, as shown in Table 1.

### 2.2  Selection of SVM Model Learning Sample

The paper determines the weight of each index using AHP and determines the learning sample of model using matter element judgment method.

#### 2.2.1  Index Weight Definition

In the implementation effect evaluation system of road traffic safety law, the relation among indexes is complicated, and the system includes multiple indexes and multiple attributes and AHP can solve the special problem of index system in research content. Thus, the section selects AHP to determine the weight of each index. We determine the weights of 20 evaluation index (see the following Table 2) according to the corresponding product of the calculated weight of Grade I index and weight of Grade II index.

**Table 1** Highway traffic safety evaluation index system

| Category | No. | Evaluation index | Unit | Evaluation rating | | | |
|---|---|---|---|---|---|---|---|
| | | | | I | II | III | IV |
| Illegal behavior rate of driver (P1) | P11 | Overspeed driving rate | % | 0–10 | 11–20 | 21–30 | 31–100 |
| | P12 | Illegal mobile phone use rate | % | 0–10 | 11–20 | 21–30 | 31–100 |
| | P13 | Safety belt use rate | % | 100–90 | 90–80 | 80–70 | 70–0 |
| | P14 | Illegal lane occupation rate | % | 0–10 | 11–20 | 21–30 | 31–100 |
| | P15 | Illegal lane changing rate | % | 0–10 | 11–20 | 21–30 | 31–100 |
| | P16 | Fatigue driving rate | % | 0–10 | 11–20 | 21–30 | 31–100 |
| | P17 | Drunk driving rate | % | 0–10 | 11–20 | 21–30 | 31–100 |
| Illegal index of vehicle (P2) | P21 | Oversize and overload vehicle rate | % | 0–10 | 11–20 | 21–30 | 31–100 |
| | P22 | Driving rate of fault vehicle | % | 0–10 | 11–20 | 21–30 | 31–100 |
| Illegal index of highway traffic design (P3) | P31 | Completeness rate of traffic management | % | 100–91 | 90–81 | 80–71 | 70–0 |
| | P32 | Completeness rate of safeguard facility | % | 100–91 | 90–81 | 80–71 | 70–0 |
| | P33 | Qualified rate of comprehensive road evaluation index | % | 100–91 | 90–81 | 80–71 | 70–0 |
| | P34 | Safe range of sight distance | m | 210–160 | 159–110 | 109–40 | 39–0 |
| | P35 | Irrationality rate of ramp setup | % | 0–10 | 11–20 | 21–30 | 31–100 |
| Illegal index of traffic management and supervision (P4) | P41 | Rights and interests protection rate of victim in traffic accident | % | 100–90 | 90–80 | 80–70 | 70–0 |
| | P42 | Electronic police law enforcement rate | % | 100–91 | 90–81 | 80–71 | 70–0 |

**Table 1**   (continued)

| Category | No. | Evaluation index | Unit | Evaluation rating | | | |
|---|---|---|---|---|---|---|---|
| | | | | I | II | III | IV |
| | P43 | Law revision cycle | year | 1 | 2 | 3 | 4–10 |
| | P44 | Annual time of business training | Each year | 10–8 | 7–5 | 4–3 | 2–1 |
| | P45 | Supervision rate of law enforcement | % | 100–76 | 75–51 | 50–26 | 25–0 |
| | P46 | Comprehensive law enforcement rate | % | 100–76 | 75–51 | 50–26 | 25–0 |

**Table 2**   Weights of various factors

| Index No. | P11 | P12 | P13 | P14 | P15 | P16 | P17 | P21 | P22 | P31 |
|---|---|---|---|---|---|---|---|---|---|---|
| Weight | 0.25 | 0.11 | 0.09 | 0.05 | 0.02 | 0.03 | 0.01 | 0.18 | 0.06 | 0.02 |
| Index No. | P32 | P33 | P34 | P35 | P41 | P42 | P43 | P44 | P45 | P46 |
| Weight | 0.05 | 0.07 | 0.02 | 0.03 | 0.02 | 0.02 | 0.02 | 0.01 | 0.01 | 0.02 |

The section determined the weights of 20 evaluation indexes by using AHP. The weights of P11–P46 are 0.25, 0.11, 0.09, 0.05, 0.02, 0.03, 0.01, 0.18, 0.06, 0.02, 0.05, 0.07, 0.02, 0.03, 0.02, 0.02, 0.02, 0.01, 0.01, and 0.02. The determination of weight of index lays foundation for determination of learning sample using matter element judgment method.

### 2.2.2   Selection of Learning Sample

The selection of learning sample is the premise of constructing SVM-based highway traffic safety evaluation model. The selection of learning sample affects the evaluation precision of highway traffic safety evaluation model.

The paper classifies the learning sample as training sample and testing sample. We carry out learning training with the training sample then verify the effectiveness of mode using the test sample. Only if SVM evaluation model passing effectiveness test can be applied to empirical research. The selection of training sample to generate several samples including 20 evaluation indexes through random function generation and grading standard in comprehensive evaluation system, and to realize the traffic safety evaluation of these samples through applying matter element judgment method, and matter element judgment program written in MATLAB language. Then, we select superior 40 samples from the evaluation result. These samples are acquired from investigation data. There are 10 samples for Grade I, II, III and IV,

respectively. We take these 40 samples as the training samples of SVM evaluation model, which provides data support for SVM evaluation model with good generalization ability. Similarly, we can verify the classification effect of SVM using 20 test samples screened in this way.

## 2.3 Analysis of SVM Model Theory and Parameter Optimization Algorithm

The paper classifies and evaluates the traffic safety effect of highway by using SVM theory.

### 2.3.1 Analysis of SVM Model Algorithm

The paper gets the training sample through random number generation and matter element judgment method. To verify the trained SVM evaluation classification effect, the paper tested the trained SVM with the test sample. Prior to training the training sample, we need to determine the used multi-classification algorithm and kernel function and related parameters of SVM.

(1) *Definition of Multi-Classification Algorithm*

Out of comprehensive consideration, the paper selects partial binary tree classification algorithm of hierarchy SVM multi-classification method as the multi-classification method of paper. The algorithm process is shown in Fig. 1.

After training the training sample as per the process shown in Fig. 1, input the test sample to the trained SVM for grade evaluation. The corresponding evaluation process of the test sample is shown in Fig. 2.

In Fig. 2, SVM1, SVM2, and SVM3 represented sub-classifier 1, 2, and 3 respectively. SVM1 = 1? expresses to judge whether the decision function of SVM1 sub-classifier is equal to 1 or not, the same for SVM2 = 1? And SVM3 = 1?.

(2) *Definition of SVM Optimal Parameter*

Prior to training SVM, we need to determine kernel function and related function of SVM. RBF kernel function $K(x, y) = \exp\left[-\frac{\|x-y\|^2}{2\sigma^2}\right]$ is one of the common functions of solving practical problem. The result of suing it was satisfying [4, 5]. The reason is that RBF function has separability and locality. The separability of kernel function is the ability of feature transformation obtained by the kernel function in separating these samples in the characteristic space on the premise of given training samples. Locality means the local nature that RBF kernel function has stronger interpolation ability, which could extract sample better [6]. Thus, we select RBF kernel function as the kernel function of SVM in the paper.
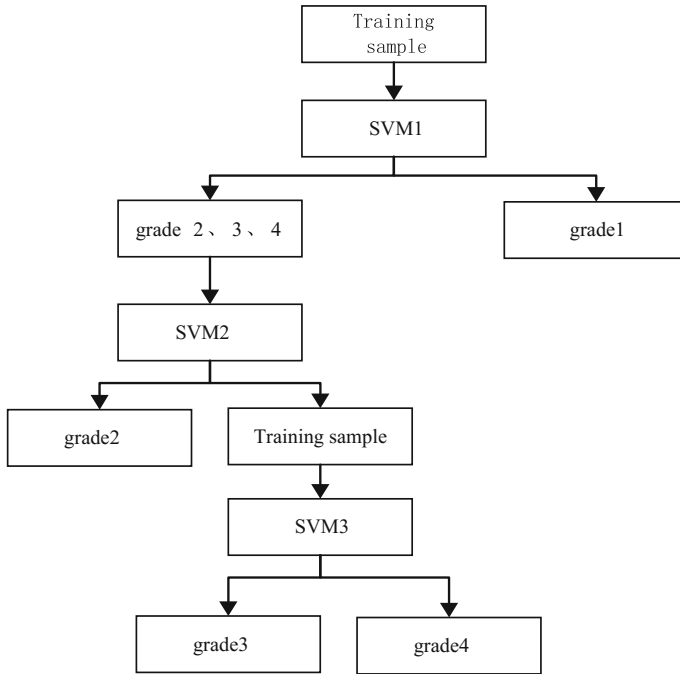
**Fig. 1** Partial binary tree

After determining RBF kernel function as the kernel function of SVM, we need to select parameter of kernel function further in an attempt to get good classification effect. The performance of SVM is mainly affected by the penalty parameter C and nuclear radius $\sigma$ [7]. Therefore, penalty parameter C and nuclear radius $\sigma$ will be SVM parameters determined in this paper. There are three nuclear radius $\sigma$ to be determined by the partial binary tree algorithm, recorded as $\sigma 1$, $\sigma 2$, and $\sigma 3$, which correspond to SVM1, SVM2, and SVM3. We determine optimal parameter by using GA.

Figure 3 displays the algorithm process and result that GA determines optimal parameter. We first carry out parameter initialization in the parameter optimization process of GA. Here, there are 30 initial populations and the maximal genetic algebra is 100. Similarly, the accuracy rate in the meaning of 5-CV is fitness function. After genetic manipulation such as selection, cross, and variation, we determine optimal solution.

After determining optimal parameter, we can conduct training and learning of SVM model and test the test sample so as to get the evaluation result of the test sample. Input the test sample to the trained SVM in Step 4, output corresponding decision function of SVM1, SVM2, and SVM3, and write the decision function value according to the testing process and output the evaluation grade.
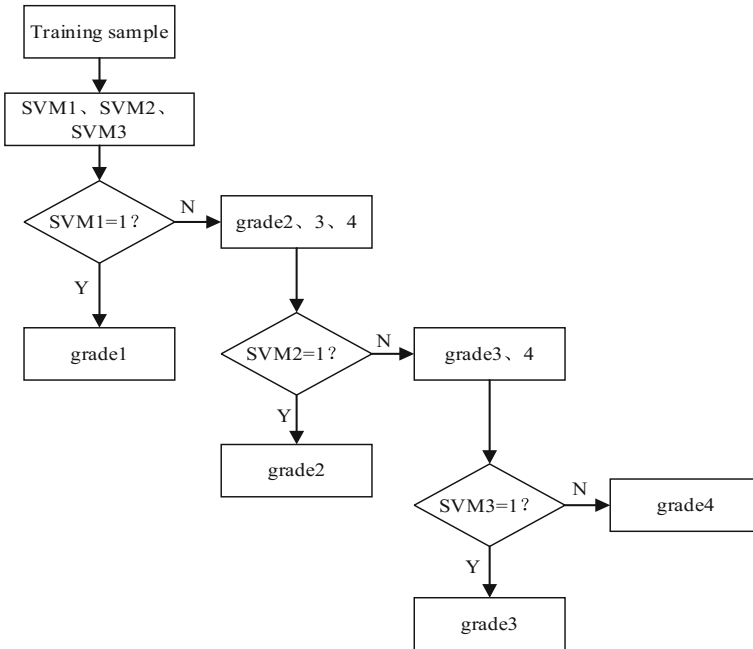
**Fig. 2** Evaluation process of partial binary tree

## 3 Instance Analyses

The paper collected related data of traffic safety along Luoluan Highway from 2012 to 2015 and applied SVM model to evaluate traffic safety.

Through traffic safety investigation of Luoluan Highway from 2012 to 2015 and combined with traffic safety evaluation index system of highway, the paper, after statistic analysis and computation, determines corresponding values of four types and 20 indexes in comprehensive evaluation index system. See Table 3.

Get the evaluation result by substituting traffic safety evaluation index of Luoluan Highway into SVM-based road traffic safety evaluation model for evaluation, inputting instance sample data of Luoluan Highway to the trained SVM and rerunning SVM for comprehensive evaluation of MATLAB program. The comparison diagrams between actual grade and forecasted grade of some evaluation samples are shown in Fig. 4. Hereinto, blue is the grade of actual test sample, red is the grade of forecasted test sample, and blue coincides with red. The operation result interface is shown in Fig. 5 and the evaluation result is shown in Table 4.

According to the evaluation result, it is known the result of the same matter element remains consistent and it conforms to the statistic result of such highway. The method is indicated to be practical and feasible.
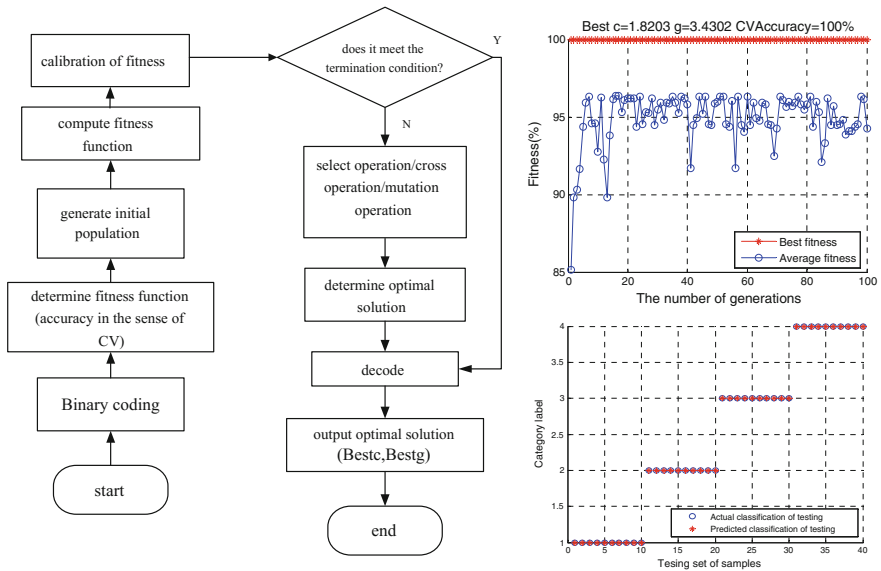
(a) Optimal parameter definition process using GA (b) Parameter optimization classification result of GA

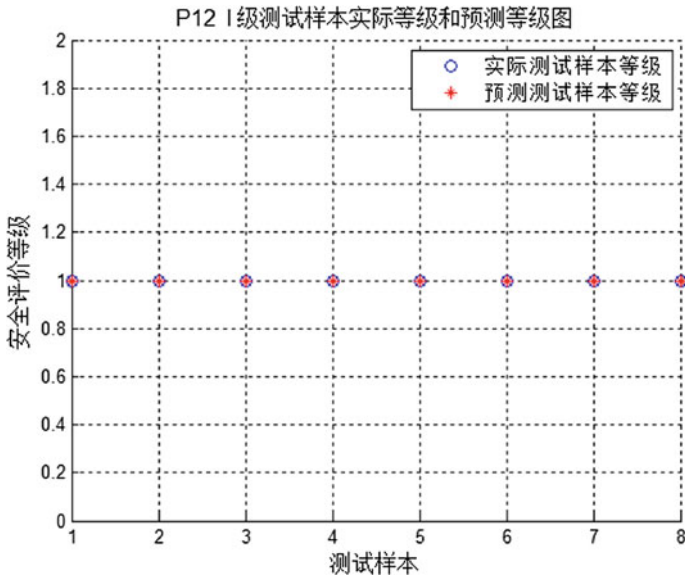**Fig. 3**  Parameter optimization using GA



**Fig. 4**  Comparison diagram between actual grade and forecasted grade of some

**Table 3**  Traffic safety evaluation index of Luoluan Highway

| Evaluation index | No. | Weight | In 2012 | In 2013 | In 2014 | In 2015 |
|---|---|---|---|---|---|---|
| Overspeed driving rate | P11 | 0.25 | 37.1% | 33.6% | 32.5% | 35.5% |
| Illegal mobile phone use rate | P12 | 0.11 | 10.3% | 17.6% | 21.9% | 23.7% |
| Safety belt use rate | P13 | 0.09 | 87.3% | 88.6% | 90.4% | 89.6% |
| Illegal lane occupation rate | P14 | 0.05 | 8.5% | 6.7% | 6.8% | 5.9% |
| Illegal lane changing rate | P15 | 0.02 | 18.7% | 16.9% | 14.3% | 11.2% |
| Fatigue driving rate | P16 | 0.03 | 23.2% | 21.6% | 20.8% | 18.3% |
| Drunk driving rate | P17 | 0.01 | 15.1% | 13.2% | 10.4% | 8.9% |
| Oversize and overload vehicle rate | P21 | 0.18 | 24.6% | 22.5% | 20.7% | 17.9% |
| Driving rate of fault vehicle | P22 | 0.06 | 12.3% | 11.5% | 10.1% | 11.1% |
| Completeness rate of traffic management | P31 | 0.02 | 80.8% | 83.5% | 84.6% | 88.9% |
| Completeness rate of safeguard facility | P32 | 0.05 | 78.9% | 80.2% | 84.6% | 88.7% |
| Qualified rate of comprehensive road evaluation index | P33 | 0.07 | 63.4% | 65.8% | 64.9% | 67.3% |
| Safe range of sight distance | P34 | 0.02 | 132 | 149 | 162 | 173 |
| Irrationality rate of ramp setup | P35 | 0.03 | 10.2% | 11.3% | 9.8% | 8.4% |
| Rights and interests protection rate of victim in traffic accident | P41 | 0.02 | 78.2% | 82.3% | 86.9% | 88.6% |
| Electronic police law enforcement rate | P42 | 0.02 | 32.6% | 38.5% | 40.3% | 43.1% |
| Law revision cycle | P43 | 0.02 | 0 | 0 | 0 | 0 |
| Annual time of business training | P44 | 0.01 | 6 | 6 | 7 | 8 |
| Supervision of law enforcement | P45 | 0.01 | 78% | 82% | 83% | 88% |
| Comprehensive law enforcement rate | P46 | 0.02 | 75% | 78% | 80% | 86% |

**Table 4**  Comprehensive evaluation of traffic safety of Laoluan Highway

| Evaluation method | In 2012 | In 2013 | In 2014 | In 2015 |
|---|---|---|---|---|
| SVM | III | III | II | II |
| Matter element | III | III | II | II |

In the process of evaluating optimal model of SVM, such evaluation indexes such as overspeed driving rate, fatigue driving rate, qualified rate of comprehensive road evaluation index, and time of law revision are in a poor grade, while illegal lane occupation rate, annual time of business training, and law enforcement supervision rate are in a superior grade. The impact of factors with poor grade is greater, which results in a poor grade. Through evaluating optimal model of SVM, not only does the paper conclude that Luoluan Highway traffic safety in recent two years is Grade
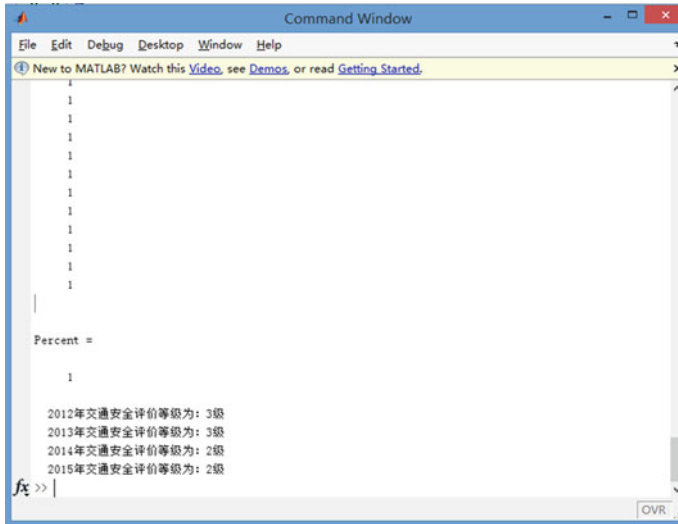
**Fig. 5** Traffic safety evaluation result interface of Luoluan Highway

II but also the grade of evaluating each index among attributes of each index rises constantly, which provides theoretical basis for the improvement strategy of the traffic safety management of such highway.

## 4 Conclusion

Starting from the viewpoint of system science and according to the screening principle and grading standard of evaluation index, the paper establishes evaluation index system of road traffic safety method including driver, vehicle, road, traffic management and supervision and applies AHP to define the weight of each index. Through the matter element judgment method, the paper determined the learning sample of SVM evaluation model and constructed SVM-based road traffic safety evaluation model. Moreover, the paper solves SVM evaluation model by using SVM multi-classification algorithm of partial binary tree and optimizes parameters by using GA. Through collecting related data about traffic safety of Luoluan Highway and applying SVM-based road traffic safety evaluation model, the paper makes overall evaluation of Luoluan Highway. The evaluation result is identical to the traffic safety statistics result of such highway, which verifies the reliability of the model. The paper provides support for improving traffic safety and management control strategy of highway and theoretical basis for enhancing traffic safety level of highway.

# References

1. Da-wei Z, Jin-peng H, Li-zhi S et al (2015) Analysis of types and causes of road traffic accidents. Auto Engineer 1:13–14
2. Qian-kun Z (2016) Primary and secondary school traffic safety evaluation based on SVM. Technol Econ Areas Commun 18(4):28–31
3. Qiang L, San-gen H, Hua-wei G et al (2017) Model building and research of urban road traffic safety evaluation system. J Guangxi Univ (Nat Sci Ed) (2)
4. Bai-chao F, Jian-yu W, Yu-ming B (2010) Binary tree SVM multi-class classification algorithm with feature selection. Comput Eng Des 31(12):2823–2825
5. Sheng-liang L, Zhi L (2007) Parameter selection in SVM with RBF kernel function. J Zhejiang Univ Technol 35(2):163–167
6. Zhi-hua S, Xiao-hou L (2010) Application of SVM based on RBF kernel function in capacity forecasting. Manager' J 6:394–395
7. Guo-sheng H, Lin Q, Guo-hong Z (2006) Survey of multi-classification algorithms based on support vector machine. Aerosp Electron Inf Eng Control 28(1):127–132

# Optimization of the Variable Area in Curbside Bus Stop

Jian-you Zhao and Tian Luo

**Abstract** Based on Markov chain, the paper establishes average queue length model of bus stop. By the model, the length of bus stop zones is determined. By VISSIM, the paper researches on a typical bus stop simulation and certificates Markov model in order to determine the feasibility and reasonableness of zone length. For the typical bus stop, paper studies the rehabilitation programs on the average queuing length, maximum queuing length and delays. Based statistical results, the paper determines a reasonable rehabilitation programs and gives an optimization design instances.

**Keywords** Public transport · Length of bus stop area · Markov chain
Queue length

## 1 Introduction

With the expansion of bus networks and the increase of passenger demand and passenger cars, the congestion of bus stops caused by platoon bus arrivals and insufficient spaces within the stops has formed new bottlenecks which deteriorate the already congested condition [1]. The bus stop area is too short, and buses have to wait outside for the station when they come to the station. Especially in case of a stop near to the intersection where a traffic light locates, the traffic capacity in the intersection and the bus station will be lowed. This will not only increase waiting time for passengers but also affect the capacity of community vehicles and buses [2]. On the other hand, the bus stop area is too long, in which the traffic capacity at the bus stops will be theoretically increased, and the actual traffic capacity at the bus stop does not increase with the expansion of the stop area due to disordered access and parking of the bus.

J. Zhao
School of Automobile, Chang'an University, Xi'an 710064, China

T. Luo (✉)
School of Automobile Engineering, Lanzhou Institute of Technology, Lanzhou 730050, China
e-mail: 458102446@qq.com

It reduces use efficiency of the bus stop, wastes the land, and increases the costs of stop [3].

The following two ideas are generally used to determine the length for bus stop area from upstream area to downstream area. The length has a direct impact on the capacity of the bus stop. Therefore, for a new stop to be constructed, the traffic capacity can be calculated or forecasted firstly, and based on which, the number of bus parking points required and the length of the station are determined [1]; for stops needing to be rebuild, the traffic capacity of the current bus stops should be calculated, then compare it with the actual numbers of buses to find whether the existing length of the bus stop can meet the demand [4]. The second one: To investigate the total length and the buffer space of the parking buses in a certain period of time by determining the law under which buses arrive at stops and its service time. The result should be employed as an important basis for determining the length of stop area.

## 2   Average Queue Length and Delay Model

Assumptions:

1.  The time of the bus arrives is a cyclical change at the peak period;
2.  The overtaking is not allowed in the bus stop;
3.  The arrival of the vehicle is subject to the Poisson distribution.

(1)  Estimation of the Queue Buses and the Probability of Every Events in a Peak Cycle

Event A1: At first, no bus at upstream area. There are $n$ ($n > 1$) buses at the end of that cycle. The probability of A2 is

$$P_{A1} = \int_0^\infty \left( \int_0^t f_{s_t} d_t \right)^{c-1} \left[ \frac{e^{-q} q^n}{n!} \right] d\, g(t), n \geq 1 \tag{1}$$

where $n$ represents the number of buses in berth; $f_{s_t}$ represents probability density function of the headways; $q$ represents serviced buses each cycle; $c$ represents the number of berths; and $g_{(t)}$ represents the probability density function of bus service time in berths.

Event A2: The waiting buses in upstream area are less than the number of berths. There are $n$ buses at the end of that cycle. Therefore, upstream area and all berths are occupied in the whole cycle [5]. The probability of A2 is

$$P_{A2} = \int_0^t \left( f_{s_t} d_t \right)^{c-m} \left[ \frac{e^{-q} q^n}{n!} \right] dg(t), 0 \leq m \leq c, n \geq 1 \tag{2}$$

where $m$ represents the waiting buses in upstream area.

Event A3: Waiting buses are more than c in upstream area, and some buses still are behind at the end of the cycle. Therefore, upstream area and all berths are occupied in the whole cycle. The probability of A3 is

$$P_{A3} = \int_0^t \left( f_{s_t} d_t \right)^c \frac{e^{-q} q^{n-m+c}}{(n-m+c)!} dg_{(t)}, m \geq c+1, n \geq m-c \tag{3}$$

Queue buses in different event A1, A2, and A3. $\overline{X_K}$, the queue lengths in the sequence.

$$\overline{X_K} = \begin{cases} n & m = 0, n > 1 \\ \frac{1}{2}n(n-1) & m \leq c, n = 0 \\ \frac{1}{2}(m+n-c-1)(c+n-m) & m \geq c+1, n \geq m-c \end{cases} \tag{4}$$

Waiting buses are more than c in upstream area, and some buses still be behind in bus stop.

According to assumption 2, waiting buses are not allowed to make any overtaking maneuvers, buses which are behind lead to blockage occurs in bus stop area. Meanwhile, the headway of vehicle is less than critical headway for high demand, and bus stop blockage is certain to occur. So, the probability of the blockage is generated by the following equation [6]:

$$P(B) = p(X_w > c) \cup p(h_i \geq \tau, i \leq c, h_a < \tau) \tag{5}$$

where $P(B)$—the probability of blockage occurs; $X_w$—the number of bus waiting in upstream area; $h_i$—headway between the $i$th bus and vehicles in bus-bay exit; $h_a$—headway of vehicles in adjacent lane of bus-bay exit; and $\tau$—the critical headway between bus and vehicles on the first berth.

(2) The Maximum Blockage Probability

The event that causes the blockage in stop consists of event A1, A2, and A3 to form a complete event group. Event B is the maximum threshold for blockage. Bayesian formula [7]:

$$P(A_k|B) = \frac{P(A_k B)}{P(B)} \tag{6}$$

(3) Average Queue Length and Zone Length

When the berth $C$ is constant, then $(\overline{L_b})$ depends on the four parameters of $m$, $n$, and $\overline{X_K}$. Thus, $P(A_k|B)$ is obtained by means of weighted. According to the full probability formula:
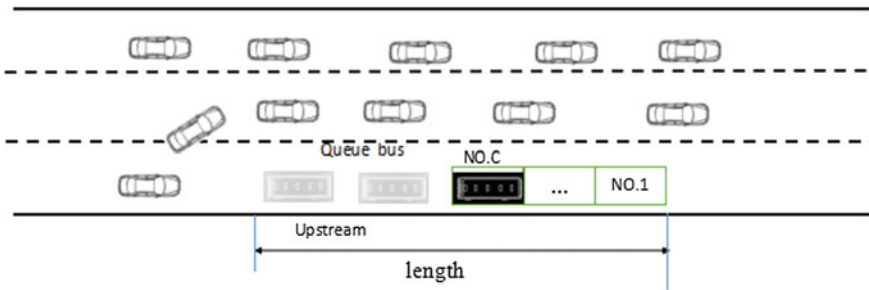
**Fig. 1** Area length and queuing length

$$\overline{L_b} = \sum_{k=1}^{n} P(A_k|B)\overline{X_k} \tag{7}$$

Bus stop zone length depends on average queue length, bus length, and the number of berth and safe distance in stop.

$$L = d_v \overline{L_b} + (c - 1)d_s \tag{8}$$

where $L$ represents bus stop zone length (m); $c$ presents the number of berth; $d_v$ represents bus length (m); and $d_s$ represents safe distance in stop (m).

For no overtaking and limited overtaking bus stop, the queuing time of the bus in the waiting zone depends on the service time of the NO.C, as shown in Fig. 1. When the berth NO.C is busy, the waiting time of the first car is recorded as $T_{qi}$:

$$T_{qi} = \begin{cases} \sum_{j=1}^{N} T_j & j = \left[\frac{i}{c}\right] + 1, \ i \neq Nc \\ \sum_{j=1}^{N-1} T_j & i = Nc \end{cases} \tag{9}$$

$$T_q = \frac{\overline{L_b}}{T} \tag{10}$$

where $N$—positive integer; $i$—the number of queueing buses in waiting zone; $T_j$—$j$th waiting time in waiting zone; $T_q$—average queueing time.

$$D_q = \sum_{i=1}^{n_b} \frac{T_{qi} - T_q}{n_b} \tag{11}$$

where $T_{qi}$—queueing time of the $i$th bus, s; $n_b$—buses. $D_q$—average queue delay(s).

## 3  Case

The actual survey shows that the peak hours have relatively large numbers of vehicles. Therefore, to guarantee accuracy of the data, the signal cycle of the investigation at the upstream intersection of the stop is 112 s. As a result, when investigating interval of the vehicle, 112 s is designed as a period to record the time when buses arrive at the stop. First record time when buses at the same line arrive at the morning peak hours (7: 40-8: 40) and the evening peak (18: 30-19: 30), then calculate the interval of buses at the same line, seeking the average of multiple data. The investigation of the A stop shows that the average arrival interval of buses of the 12 bus lines during the peak period as shown in Table 1.

When investigation was proceeding, road pavement and slope meets the design requirements [8]. Bus flow is 98 vph, traffic flow of adjacent lane is 895 vph, and effective ratio $= 0.7$ in traffic signal.

In the peak period, arrival time is in an unacceptable gap period. In this case, the vehicle arrived must pass through when an acceptable gap takes place after vehicles passing through the acceptable gap. At such period, the interaction between vehicles is relatively weak, so the road traffic flow can be described using Poisson distribution.

In previous studies, the relationship between blockage probability and the number of berths was study. With Increasing of berth, bus stop has done little to ease the congestion problem during peak hours [6]. Through the investigation of the actual situation, it is concluded that the existing length of the curbside bus stop should be 24 m. On the condition that the capacity, traffic flow, bus departure interval, bus station clear time, and other parameters do not change, the curbside bus stop should be changed into. Default vehicle speed in VISSIM software is distributed from 30 to 35 km/h, with the urban bus stop station speed of 13–23 km/h [9].

According to Eqs. (6) and (7), three berths should be designed at the stop. Based on the actual situation and VISSIM simulation, the following conclusions are made: the actual simulation result is that from the upstream queuing detector in the simulation period of 2400–4200 s, the average queue length is 66 m, and the maximum length is 97 m. Therefore, the vehicle will appear queuing in the stopping area; for the downstream queuing detector in the simulation period of 3000–4800 s, the average queue length is 48 m, and the maximum queue length is 53 m. In practice, two berths should be designed at the stop station. Therefore, the capacity of the stop is insufficient to meet the traffic demand during peak hours. Simulation results are shown in Fig. 2.

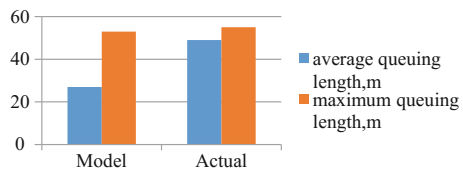**Fig. 2** Queuing length on upstream

**Table 1** Average arrival time in a Hush hour

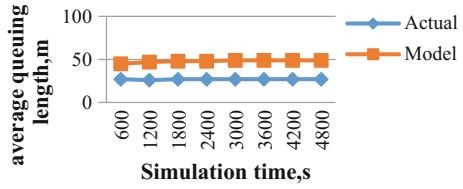| Bus lines | 1 | 2 | 3 | 4 | 5 | 6 | 7 | 8 | 9 | 10 | 11 | 12 |
|---|---|---|---|---|---|---|---|---|---|---|---|---|
| Average time (min/vel) | 4.24 | 7.66 | 11.2 | 8.25 | 5.5 | 6.67 | 10.3 | 7.7 | 6.48 | 12 | 9.3 | 6.5 |

**Fig. 3** Average queuing length



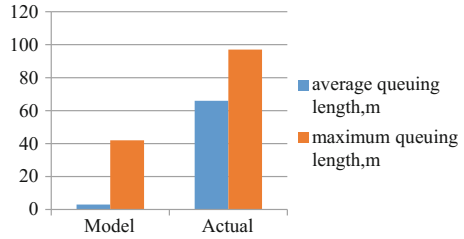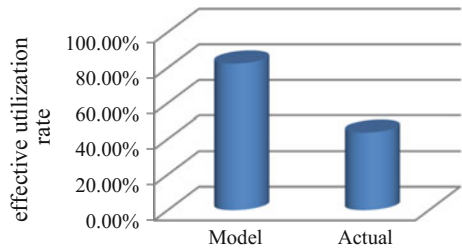**Fig. 4** Queuing length on downstream



**Fig. 5** Effective utilization rate of length



For the upstream queuing detector, the average queuing length is 27 m in the simulation period of 1800–4800 s, it is shown in Figs. 2 and 3.

In the data detected by the upstream queuing detector, the average queuing length and the maximum queuing length reflect the queuing and traffic capacity of the bus at the entrance to the bus stop.

For the downstream queuing detector, the average queue length is only 2 m in the simulation period of 1800–3600 s, meaning that buses bring a small load on the all berths.

As shown in Fig. 4, the average queuing length and the maximum queuing length in the data collected by the downstream queuing counter reflect the queuing and traffic capacity of the vehicle in the stopping area. The regional length model has an obvious advantage. Compared with the actual curbside bus stop, the average and the maximum queue length are small. The Fig. 5 shows the effective utilization rate of the length of the stop area in the model. And the maximum queue length of the downstream length has the highest effective availability of the length of the stop area with 29.7% increased.

With the increase in simulation time, the delay and average stopping time and the number of stops become more and more stable. According to the survey, the bus clearance time is usually 9–20 s, which is greater than the average stopping
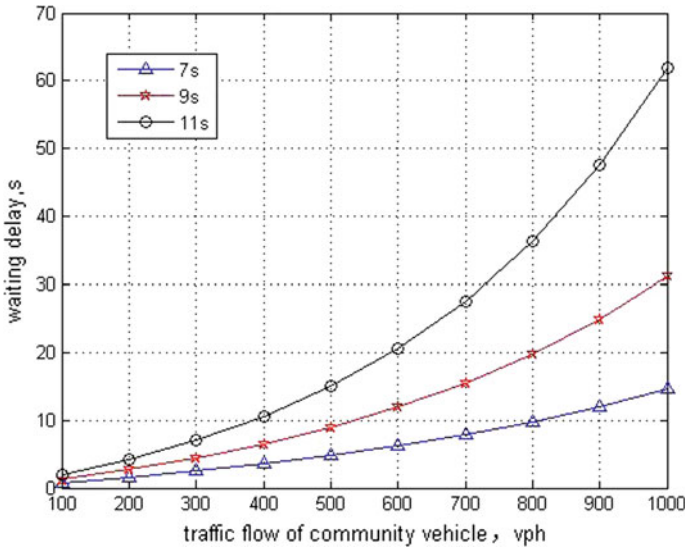
**Fig. 6** The Relationship between delay and demand

**Table 2** Delay parameters comparison in Vissim

| Parameters | Model | Actual |
|---|---|---|
| Bus delay, s | 17.4 | 45.1 |
| Average stop time, s | 6.1 | 30.1 |
| Stops | 0.26 | 1.11 |

time of the bus concluded by the simulation result of the model. The waiting delay increases as traffic flow increase, which varies from 100 to 1000 vph. As critical headway increases from 7 to 9 to 11 s, the waiting delay increases. As critical headway increases, the waiting delay increases as shown in Fig. 6[6].

According to the principle of the minimum delay, with the change of the simulation period, the total delay of bus based on Markov model regarding stop area is the smallest. If the length of current curbside bus stop expand to 43 m, then the bus has a lengthy delay. Therefore, in terms of shortening the delay period, the Markov model regarding stop area has great advantage.

Similarly, the 3600 s simulation draws a better stability in terms of bus delay, the average stopping times and the number of buses during the period of travel.

The simulation result based on the Markov model regarding stop area shows that during the period of 3600 s simulation, the length of the stop area has the shortest bus delay and the average stopping time, the least average stopping times, and the most numbers of vehicle passing through at the same time, as shown in Table 2.

# 4 Conclusion

It would be reasonable to convert the 24 m curbside bus stop into a 43 m curbside bus stop. As it expands the queue and causes the delay, increases land and grows load on the road. The optimal option is to expand the existing area to 43 m without modifying the current facilities but just specifying the area range. By indicating peak hours through the road signs to avoid access of social vehicles while no restriction in the general period. Therefore, the program is highly viable with lower costs for reconstruction and the maximum of land conservation.

# References

1. Fernandez R (2007) Passion 5.0—a model for microscopic simulation of multiple-berth bus stops. Traffic Eng Control 48(7):324–328
2. Basso LJ, Silva HE (2010) A microeconomic analysis of congestion management policies. In: 5th Kuhmo Nectar conference in transport economics Valencia, Spain
3. Tirachini A (2012) The economics and engineering of bus stops: spacing, design and congestion. The University of Sydney
4. Yun H (2011) Study on problems of the location and the number of berths of multiple routes bus stops. Southwest Jiaotong University, Chendu
5. Luo T, Zhao J (2015) Modeling bus bay blockage and influence of capacity on the adjacent lane. In: Cota international conference of transportation professionals, pp 1280–1291
6. Zhao J, Luo T, Zhang Y (2016) Modeling capacity and delay based on bus bay blockage and the influence of traffic flow. In: Cota international conference of transportation professionals, pp 2314–2325
7. Ross SM (2010) Introduction to probability models
8. Xiao H, Zhang X (2011) Setting form optimum determination for bus stop. Traffic Eng 9(18):45–50
9. Lv L (2006) Study on optimization design od bus stop. Southeast University, Nanjing

# A Study on the Generalized Cost Function of Regional Integrated Passenger Transport Based on Passenger Choice

**Yuee Gao, Yanli Ma, Luyang Fan and Lifei Han**

**Abstract** Understanding the characteristics of regional passenger travel mode selection can provide a theoretical basis for the traffic management to formulate relevant policies. In this paper, the characteristics of passenger travel mode selection are analyzed, and the micro and macro factors affecting the choice of travel modes are determined. Based on travel cost, time, safety, comfort, convenience, and other factors, the generalized cost function of passenger travel mode selection is constructed, and the function parameters are calibrated. The research results can provide theoretical support for the formulation of relevant policies.

## 1 Introduction

Conducting the research on generalized cost function of regional integrated passenger transport based on passenger choice is of great significance to the study which can determine the structure of the passenger transport in the regional integrated transport network.

In 1951, the American Planning Association used the time spent on travel demand as a basis to choose different modes of transportation, and proposed the concept of "equal timeline" [1]. Martin Molina et al. studied on the relationship between different zones and the trip time to the center. On the basis, they provide the structure of urban passenger transport [2]. Loudon Wingo constructs the economic model of the relationship between urban communication system and passenger transport structure [3, 4]. David Shaikh, Martin Fares, Roy Sampson, and three other American economists put forward that the spell progress between various passenger transport

Y. Gao · Y. Ma (✉) · L. Fan · L. Han
School of Transportation Science and Engineering, Harbin Institute of Technology, Harbin 150090, China
e-mail: mayanli@hit.edu.cn

systems in the traffic system is metabolism. The development of the whole system is because of its internal structure play a role [5]. Arnulf Grubler, the scholars of Austria constructed the transportation evolution model and put forward that the transportation mode has relationship with transportation structure [6].

Wang Zheng built the generalized Logit mode split forecasting model by analyzing the economic characteristics of the individual trip mode choice behavior and using the random utility theory [7]. Niu Xueqin et al. divided the factors that influence people's choice of transportation into two aspects: macro factors and micro factors. They also put forward a new method for traffic modal splitting through using the rule that people's choice of trip mode varied with the distance [8]. Liu Shuai and others used Probabilistic Neural Network theory to model traffic mode split [9]. He Guoguang and others constructed a Two-Level Game Model between transit trip and the private car driver, and determined the travel share [10]. Zhou Xuemei analyzed the characteristics of traffic mode of comprehensive transportation hub. She established the Nest Logit-based transportation mode choice model [11]. Deng Hunan discussed the construction of the urban transportation mode evaluation system under the condition of sustainable development, and established the multi-object evaluation model based the "distance" of the traffic mode point to the positive and negative ideal point [12].

Foreign scholars' researches about the traffic mode choice and traffic structure began relatively early, some relevant theories and methods are relatively advanced. Based on these results, some domestic scholars made a deep research on the urban residents' travel mode and improved some theoretical methods of foreign scholars. They found the characteristics and rules of short distance travel mode choice of urban residents. Despite the researches about regional integrated transportation system have great achievements, there are few researches on the choice of interregional passenger travel mode in long distance.

## 2 Analysis of Influencing Factors of Passenger Travel Mode Selection

The choice of the transportation mode is based on the needs of their own decisions, which needs to consider micro and macro factors affecting the choice of passenger travel mode.

### 2.1 The Micro Factors

Passengers in different countries or regions will vary in the choice of travel mode. Analysis of factors influencing the passenger travel mode choice mainly includes three aspects: the characteristics of passenger, trip characteristics, and characteristics of the passenger traffic mode.

**Table 1** The national income and passenger traffic volume from 2006 to 2015

| Year | Income of urban residents (yuan) | Income of rural residents (yuan) | Passenger turnover (million/km) | Passenger turnover ratio (%) | | | |
|------|------|------|------|------|------|------|------|
| | | | | Railway | Highway | Aviation | Waterage |
| 2006 | 6280.0 | 2253.4 | 12,261.1 | 37.0 | 54.3 | 7.9 | 0.8 |
| 2007 | 6859.6 | 2366.4 | 13,155.1 | 36.2 | 54.8 | 8.3 | 0.7 |
| 2008 | 7702.8 | 2475.6 | 14,125.6 | 35.2 | 55.3 | 9.0 | 0.6 |
| 2009 | 8472.2 | 2622.2 | 13,810.5 | 34.7 | 55.7 | 9.1 | 0.5 |
| 2010 | 9421.6 | 2936.4 | 16,309.1 | 35.0 | 53.6 | 10.9 | 0.4 |
| 2011 | 10,493.0 | 3254.9 | 17,466.7 | 34.7 | 53.2 | 11.7 | 0.4 |
| 2012 | 11,759.5 | 3587 | 19,197.2 | 34.5 | 52.8 | 12.3 | 0.4 |
| 2013 | 13,785.8 | 4140.4 | 21,592.6 | 33.4 | 53.3 | 12.9 | 0.4 |
| 2014 | 15,780.8 | 4760.62 | 23,196.7 | 33.5 | 53.8 | 12.4 | 0.3 |
| 2015 | 17,174.7 | 5153.17 | 24,834.9 | 31.7 | 54.4 | 13.6 | 0.3 |

*Note* Data from《2016 National Statistical Yearbook》

### 2.1.1 Passenger Characteristics

#### (1) Passenger's Income

In the choice of travel mode, there is a big difference between different income level of passenger travel. Usually, the lower income groups will be more sensitive to price factors, and the higher level of income groups on the service level of the high requirements. Table 1 shows the basic data of national income and passenger turnover. From Table 1, we can see the change of proportion of passenger turnover in various passenger transport modes and the people's income in the last 10 years in China.

From Table 1, we can see that the proportion of air passenger traffic is relatively small, but the trend has gradually increased. This change in the macro indirectly reflects the influence of the income level of passengers on the choice of travel mode.

#### (2) Passenger's Age

Different ages in passenger transportation options would have a certain tendency, such as the older population tend to choose the safety and comfort of the passenger is relatively high, and young people will value the effectiveness, and reduce travel time consumption as much as possible.

#### (3) Passenger's Occupation

The nature of occupation determines the passenger choice in long distance travel. The government and institutions staffs choose fast and comfortable way of transport modes; students or workers choose the cost is low. The influence of passenger occupation on the choice of passenger travel mode is shown in Fig. 1.

In Fig. 1, we can get the analysis of different occupation passenger's choice in high-speed railway, railway, and highway. The professional institutions, state-owned
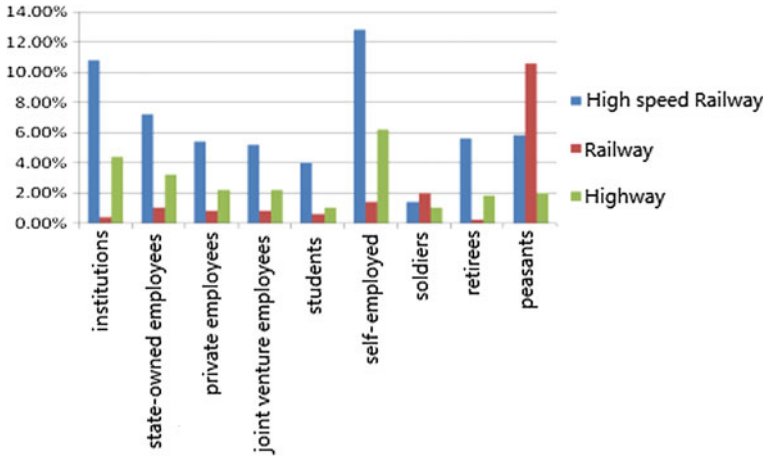
**Fig. 1** Distribution of different professional passenger's choice

employees, foreign enterprises and joint venture employees, self-employed, retirees, and other groups tend to choose a higher level of service; and the peasants and soldiers tend more to choose the ordinary railway passenger transport; highway passenger transport mode with a higher proportion of the self-employed.

### 2.1.2 Trip Characteristics

#### (1) Travel Purpose

The purpose of regional passenger travel generally includes business, business trip, visit relatives, recreational travel, and so on. In generally, business travel is more concerned with time, comfort and convenience, while visiting friends and traveling are more concerned with comfort. The destination distribution of passenger transport in China is shown in Fig. 2.

The proportion of travel for business is the first in all passenger transport modes. The main purpose of aviation is trade, business, and tourism.

#### (2) Travel Distance

The number of travel distance is the main factor that affects the choice of passenger travel mode. Research shows that the distance more suitable for railway passenger is 600 km, the distance of highway is superior to the railway travel is within 500 km, and the most suitable travel distance of aviation is over 800 km.

#### (3) Travel Time

Travel time is the total amount of time spent on the journey, including the time for the passenger to take a vehicle, the transfer time, the delay, and the waiting time.
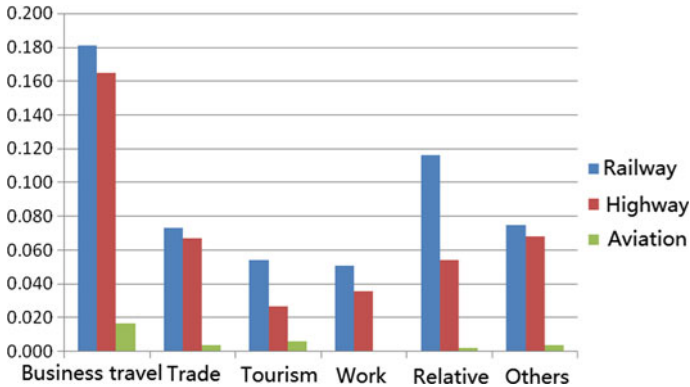
**Fig. 2** Distribution of passenger mode with different travel destination

### 2.1.3 Characteristics of Passenger Transport Mode

The characteristics of the passenger transport mode mainly refer to the characteristics of safe, comfortable, punctual, convenient, and economical in four kinds of passenger transportation: railway, highway, aviation, and water transportation.

(1) **Safety**

With the improvement of the speed of the various modes of transport, more and more attention has been paid to the issue of security, which affects the people's decision to choose the mode of passenger transport.

(2) **Comfort**

Gradually improved the living standards, the demand for passenger travel service level also has to be improved, and comfort requirements of passenger transport mode have changed greatly.

(3) **Punctuality**

People do not want to delay the extra time in the travel process, so the higher the punctuality of a type of passenger transport will have a great attraction for travelers.

(4) **Convenience**

The higher the convenience of the passenger travel mode, the more passengers will be attracted. And the passenger needs to pay more for the cost.

(5) **Economic**

The economic characteristics of various transport modes are the main factors to consider different income groups in selection of passenger mode. While passenger service production is combined with the economic characteristics of each passenger transport mode to attract different income groups.

## 2.2  Macro Factors

Including the social environment, economic development level, people's consumption level, traffic policy, and other external factors, these factors have an indirect impact on the choice of travel mode.

(1) **Social Environment**

The social environment mainly refers to the surrounding living environment, customs, and cultural environment to the visitors. These factors will ultimately affect the passenger's values and psychological quality. The choice of travel mode will be affected by these factors.

(2) **Level of Economic Development**

The level of economic development impact on the choice of passenger travel includes in two aspects. First, adequate passenger flow can increase financial revenue and ensure the construction of various transportation infrastructure. Secondly, with the development of economy, people's demand for the convenience and comfort of traveling will be higher and higher.

(3) **People's Consumption Level**

The choice of passenger travel mode is largely restricted by the level of consumption. With the continuous improvement of the living standard and consumption level, the demand for travel service level is higher.

(4) **Transport Policy**

The national policy is to make the transportation industry to coordinate the overall development. In a certain period of time, if one transportation's supply is adequate, it will be more attractive to people to choose.

In summary, the factors that can be used in the choice of travel mode can be expressed in Fig. 3.

## 3  Generalized Cost Function Considering Passenger Choice

Generalized cost includes not only the quantitative indicators such as time and money but also the qualitative indicators such as comfort, safety, and convenience, as shown in Fig. 4.

Trip cost is one of the most important factors in passenger travel, and the travel cost varies with the travel distance. The travel cost is calculated as Formula (1):
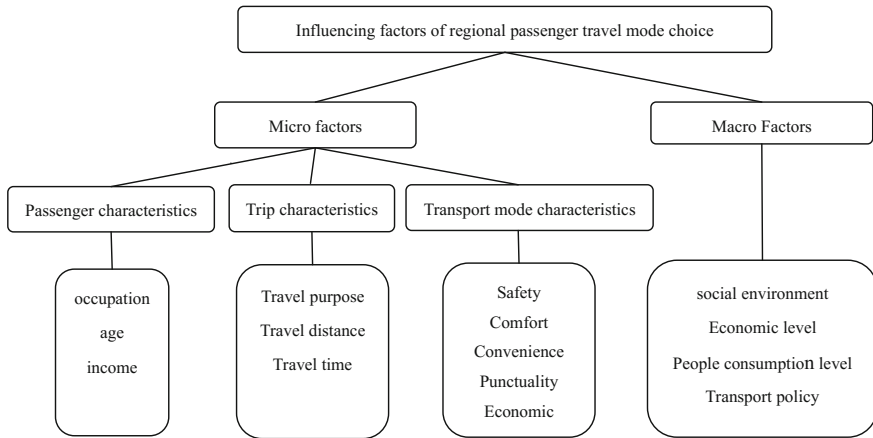
$$C_D = C_{SC} + C_{AC} + C_{TC}. \tag{1}$$

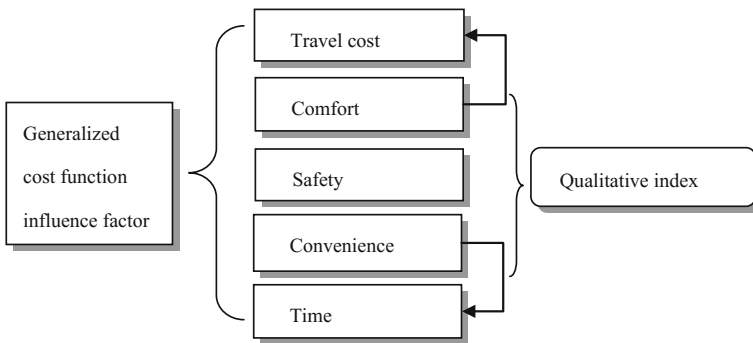**Fig. 3** Influence Factors of passenger travel mode choice



**Fig. 4** Influence Factors of passenger travel mode choice

Type $C_D$—direct costs incurred by passenger travel;
$C_{SC}$—short distance transportation fee;
$C_{AC}$—extra charge;
$C_{TC}$—fare.

Travel time refers to the time cost of the passengers from the origin to the destination, which is the direct cost of the time, but also the economic cost of indirect pay. The calculation of travel time $C_I$ as Formula (2):

$$C_I = C_{ST} + C_{WT} + C_{TT}. \tag{2}$$

Type $C_I$—travel time;
$C_{ST}$—short distance traffic time;
$C_{WT}$—station waiting time;
$C_{TT}$—normal travel time.

Travel safety $C_{TS}$ is an important factor affecting the choice of passenger transport mode. The railway is undoubtedly the most safe and stable mode and the lowest accident rate.

Travel comfort $C_{TC}$ also has a great impact on passenger travel choice. The stability of vehicle operation, and the convenience of passengers have a great impact on travel comfort.

The convenience of travel $C_{TE}$ mainly refers to the kind of subjective feeling, which is related to travel time.

Weight of influencing factors are $\lambda_0$ $\lambda_1$ $\lambda_2$ $\lambda_3$ $\lambda_4$. Generalized travel cost can be reduced as the Formula (3):

$$C = \lambda_0 C_D + \lambda_1 C_I + \lambda_2 C_{TC} + \lambda_3 C_{TS} + \lambda_4 C_{TE}. \tag{3}$$

Dimensionless processing should be performed in data processing.

## 4 Generalized Cost Function Calibration Considering Passenger Choice

Analytic hierarchy process (AHP) is a complex problem analysis. First, AHP establishes the hierarchical structure to describe the problem, and then judges the importance of all elements at each level. Second, AHP constructs a judgment matrix, and determines the weight of each level in the different elements combining judgment matrix. Eventually, the weight of all elements at each level can be identified.

AHP is used to calibrate the parameters ($\lambda_0$, $\lambda_1$, $\lambda_2$, $\lambda_3$, $\lambda_4$) of generalized cost. AHP is widely used to solve complex problems with multiple criteria and multiple objectives, which usually involves qualitative and quantitative problems.

### 4.1 Judgment Matrix

In the construction of the hierarchical structure, each variable in the next level compares the importance according to the investigation for one variable in last level. Then the construction of the judgment matrix Y forms as Table 2.

To determine the elements of the $y_{ij}$, the construction of judgment matrix is to be judged according to the following criteria: two factors are equally important, $y_{ij} = 1$; one factor is a bit important than another factor, $y_{ij} = 3$; one factor is obviously important than another factor, $y_{ij} = 5$; one factor is strongly important than another factor, $y_{ij} = 7$; one factor is extremely important than another factor, $y_{ij} = 9$; and the two factors are compared between these conditions, $y_{ij} = 2, 4, 6, 8$; $y_{ij} = 1/y_{ji}$. Two numerical are reciprocal. The judgment matrix $Y$ can be obtained according to the above comparison criteria. Matrix can calculate the relative importance vector $V_i$, as

**Table 2** Judgment matrix $Y$

| $X$ | $Y_1$ | $Y_2$ | … | $Y_n$ |
|---|---|---|---|---|
| $Y_1$ | $y_{11}$ | $y_{12}$ | … | $y_{1n}$ |
| $Y_2$ | $y_{21}$ | $y_{22}$ | … | $y_{2n}$ |
| ⋮ | ⋮ | ⋮ | ⋮ | ⋮ |
| $Y_n$ | $y_{n1}$ | $y_{n2}$ | … | $y_{nn}$ |

shown in the Formula (4). Then the weight of each index is obtained by normalizing the importance vector, the calculation as shown in Formula (5).

$$V_i = \left( \prod_{j=1}^{n} y_{ij} \right)^{\frac{1}{n}} \tag{4}$$

$$V_i^0 = \frac{V_i}{\sum_i V_i}. \tag{5}$$

## 4.2 Consistency Test

The consistency test needs the maximum eigenvalue($\lambda_{\max}$) and consistency index (C.I.) of judgment matrix and the values of the average random consistency index (R.I.) to calculate the consistency ratio. Then, we need to judge whether the matrix is consistent. It needs to redefine if it does not meet the need. Formula of the largest eigenvalue, consistency index, average random consistency index, and the consistency ratio is as follows:

$$\lambda_{\max} = \frac{1}{n} \sum_{i=1}^{n} \frac{\sum_{j=1}^{n} y_{ij} \cdot V_j}{V_j} \tag{6}$$

$$\text{C.I.} = \frac{\lambda_{\max} - n}{n - 1} \tag{7}$$

$$\text{C.R.} = \frac{\text{C.I.}}{\text{R.I.}}. \tag{8}$$

The average random consistency index is shown in Table 3.

**Table 3** Average random consistency index

| $n$ | 1 | 2 | 3 | 4 | 5 | 6 | 7 | 8 | 9 | 10 |
|---|---|---|---|---|---|---|---|---|---|---|
| *R.I.* | 0 | 0 | 0.58 | 0.90 | 1.12 | 1.24 | 1.32 | 1.41 | 1.45 | 1.49 |

**Table 4** Weight of influencing factors of traffic mode choice

| Passenger income level | Travel cost | Travel time | Comfort | Safety | Convenience | Consistency check |
|---|---|---|---|---|---|---|
| <1000 | 0.568 | 0.110 | 0.046 | 0.216 | 0.061 | 0.08 |
| 1000–3000 | 0.466 | 0.221 | 0.074 | 0.158 | 0.082 | 0.09 |
| 3000–5000 | 0.414 | 0.172 | 0.089 | 0.214 | 0.111 | 0.06 |
| 5000–8000 | 0.240 | 0.240 | 0.124 | 0.240 | 0.155 | 0.08 |
| >8000 | 0.059 | 0.270 | 0.155 | 0.217 | 0.299 | 0.08 |

Consistency test can be adopted if C.R.<0.1, the relative importance vector we get is the vector we need. Otherwise, it is necessary to determine the judgment matrix until it meets the requirements.

### 4.3 Weights of the Factors Affecting the Traffic Mode Choice

The research issued a total of 800 questionnaires returned in the passenger transportation centers, such as train station, airport, and highway. The questionnaire divided passengers into five levels by their income. According to the analysis of the survey data, the evaluation results about the influence factors of the passengers income level on traffic choice are shown in Table 4.

Making the income level of $P$, the generalized cost function can be obtained according to the results of the calibration from different groups:

$$P < 1000 \qquad C_1 = 0.568 C_D + 0.11 C_I + 0.046 C_{TC} + 0.216 C_{TS} + 0.061 C_{TE}$$
$$1000 < P < 3000 \quad C_2 = 0.466 C_D + 0.211 C_I + 0.074 C_{TC} + 0.158 C_{TS} + 0.082 C_{TE}$$
$$3000 < P < 5000 \quad C_3 = 0.414 C_D + 0.172 C_I + 0.089 C_{TC} + 0.214 C_{TS} + 0.111 C_{TE}$$
$$5000 < P < 8000 \quad C_4 = 0.240 C_D + 0.240 C_I + 0.124 C_{TC} + 0.240 C_{TS} + 0.155 C_{TE}$$
$$P > 8000 \qquad C_5 = 0.059 C_D + 0.270 C_I + 0.155 C_{TC} + 0.217 C_{TS} + 0.299 C_{TE}.$$

## 5 Conclusion

This paper analyzes the regional characteristics of passenger travel mode choice, and definite the micro and macro effects of passenger travel mode choice factors between regions. The micro level mainly includes three aspects: the characteristics of passengers, trip characteristics, and transport mode characteristics; macro aspects mainly include the social environment, the level of economic development, people's consumption level, and the transport policy. Travel mode choice generalized cost function is constructed by the factors: travel cost, time, safety, comfort, convenience and others, and the parameters of the functions are analyzed. The research results can provide theoretical support for the formulation of relevant policies.

# References

1. Xu Y (2006) Study on the evolution mechanism and optimization method of public transit system in large cities. Southeast University, Nanjing
2. Molina M, Hernandez J, Cuena J (1998) A structure of problem-solving methods for real-time decision support in traffic control. Int J Hum Comput Stud
3. Hag-Elsafi O, Alampalli S, Owens F (2001) Computer-aided implementation of a new procedure for design of end-plates and base-plates for traffic support structures. Eng Struct
4. van Wee B (2002) Land use and transport: research and policy challenges. J Transp Geogr
5. Zuoren Y, Zhang R (2003) Transport economics. China Communications Press, Beijing
6. Grubler A (1990) The rise and fall of infrastructures-dynamics of evolution and technological change in transport. Physica-Verlag, Heidelberg
7. Wang Z, Liu A (1999) Generalized LOGIT method for traffic classification prediction. J Tongji Univ 27(3):314–318
8. Niu X, Wang W, Yin Z (2004) Research on forecasting method of urban passenger transport mode. Highw Transp Technol 3(2):75–77
9. Zhou H, Yu X, Yang X (2010) Study on traffic mode choice model of comprehensive transportation hub. Traffic Inf Secur 28(156):64–66
10. He G, Ji Y, Liu F (2006) Traffic mode choice based on two-layer game. J Chang'an Univ 8(3):4–7
11. Liu S, Zhou T, Hu S (2008) Research on the traffic mode division model based on neural networ. Shanxi Archit 34(25):21–22
12. Deng X, Cheng L (2009) Urban traffic mode evaluation based on interval and multi objective. Transp Technol Econ 11(52):57–59

# Review and Implementation of Driving Fatigue Evaluation Methods Based on RR Interval

**Weiwei Guo, Chunling Xu, Jiyuan Tan and Yinghong Li**

**Abstract** The evaluation methods of driving fatigue have been the hot topics in the study of traffic. This paper studied the main existing driving fatigue evaluation methods based on RR intervals and verified the effectiveness of these methods by experiments. There were 15 drivers selected in the simulation driving experiment, and the pulse signal of them was collected and recorded during the test period. Average heart rate, time and frequency domain features of HRV, nonlinear features of HRV, and statistic of MSPC were chosen as the indexes to verify. The experimental results show that "$T^2$" of HRV time domain indexes, including MSPC, SDNN, RMSSD and total power, HRV frequency domain indexes like LF/HF, and the longer axis of Poincare scatter plot can distinguish the fatigue state and the waking state of drivers with a favorable effect.

**Keywords** Driver fatigue · RR intervals · Heart rate · Heart rate variability MSPC

## 1 Introduction

In a variety of incentives of a traffic accident, driving fatigue has become the second cause only to the drunk driving. Driving fatigue criterion has been a hot research topic in traffic safety field. The relevant scholars have done a lot of research about the methods to evaluate driving fatigue, one aspect of which is the method of calculating relevant indexes based on RR interval of a subject to evaluate whether the subject is in fatigue state. However, there was little paper to review the methods and verify the effectiveness of them. The purpose of this paper is to verify the validity of these methods to react driving fatigue.

W. Guo · C. Xu · J. Tan (✉) · Y. Li
Beijing Key Lab of Urban Intelligent Traffic Control Technology, North China University of Technology, Shijingshan 100144, Beijing, China
e-mail: tjyphilip@163.com

833

## 2 Reviewed Literature

Ross O. Phillips mentioned a "whole definition" in one of his papers, in which he stated that fatigue is a suboptimal psychophysiological condition caused by exertion [1]. Driving fatigue is a result of the combined action of several reasons. Long-time driving, insufficient sleep, changes of arousal level, boring driving situations, exhaust fumes, noise from the process of driving, and temperature rise in the car can cause driving fatigue [2]. Fatigue is a definition involving psychology, physiology, environment, and performance of the individual, and this decides what methods we should take to measure it. Subjective, physiological, and performance measures are all used to examine the development of fatigue [3], and RR interval is a common used physiological indexes.

### 2.1 Study of Heart Rate in Fatigue

Heart rate (HR) is the heartbeat of a person in one minute. An important reason for ECG to be a common indicator to monitor driving fatigue is the obvious difference of ECG in different states for the same person [4]. Dewar R. E. et al. found that the HR of subjects has declined from the start of the trip, as the driver adapts to driving, irrespective of task load [3]. P. Fadda et al. conducted a 4-h experiment of eight quay crane operators to study how the biological parameters change with the development of fatigue. The result indicated that HR, expressed by beat per minute (bpm), showed a significant decrease during the 4 h of the test [5]. Ashley Craig et al. carried out a driving simulation experiment to study the change of mental state of the driver during driving. Experimental results display that the HR of all the 35 selected drivers has a significant decrease after car driving [6].

### 2.2 Study of Heart Rate Variability in Fatigue

Heart rate variability refers to the variation of the difference between the successive heart rate cycles, which could be calculated from the heartbeat or pulse signal [7], but there are different theories about the characteristics of HRV in people's waking and fatigue states [8, 9]. It was pointed that HRV appears to be a better measure, with increase in variability being associated with lower arousal [3]. Patel and Lal [10] and Shinar [11] found that wakeful states presented higher LF/HF, an index of HRV, than drowsy states. Issey Takahashi et al. found that the root mean square of the difference between two adjacent RR intervals (RMSSD) increased as the development of fatigue increases, and so did the low-frequency power (LF) [12]. Furthermore, the HRV can estimate the activity of ANS (Autonomic Nervous System) from the signal obtained from surface ECG [13]. Drowsiness states are characterized

by a decrease in sympathetic activity and/or an increase of parasympathetic activity, while wakefulness states are opposite [14, 15]. However, there were some questions in the study. In the work of Noelia Rodriguez-Ibanez and his team, there were 10 professional drivers selected in a familiar driving task, and the ECG of them was acquired during the whole driving process. However, the results of SDNN, average RR internal, and LF/HF showed quite differences ($p < 0.05$) [16]. Another method of HRV analysis is Poincare plot, and it reflects the change rule of the D-value of adjacent RR intercals [17]. Kamen P. W. et al. pointed that Poincare plot was a visual presentation of parasympathetic activity. [18]. They also found that the "width" of the Poincare plot was significantly reduced during atropine administration, in other words, during awake state.

To summarize, there are three main kinds of analysis methods of HRV: the time domain analysis method, the frequency domain analysis method, and the nonlinear analysis method.

(A)  Time Domain Features

- AVNN (ms): The average value of RRI.
- SDNN (ms): standard deviation of RRI.

  – RMSSD (ms): The root mean square of difference of neighboring RRI.

- PNN50: The proportion of number of neighboring RRI whose difference is more than 50 ms.
- Total power: variance of RRI.

(B)  Frequency Domain Features

There were three frequency domain features calculated on the basis of PSD.

- LF: A part of HR PSD with lower frequency (0.04–0.15 Hz).
- HF: A part of HR PSD with higher frequency (0.15–0.4 Hz).
- LF/HF: The ratio of LF to HF.

(C)  Poincare Plot

Poincare plot is a "scatter plot", whose abscissa is the current RRI and the corresponding ordinate is the preceding RRI.

## 2.3  Statistics of MSPC in Fatigue

MSPC (Multivariate Statistical Process Control) is a widely used method for process state monitoring [19, 20]. Erika Abe et al. put forward a novel method combining HRV indexes with MSPC to predict driving accident caused by driver fatigue [21]. According to the results of their experiment, the $T^2$ statistic exceeded its control limit continuously before the accident caused by driver drowsiness, while that is

rarely exceeded in the awaking situation. However, the Q statistic was partially exceeded in both the accident and awaking dataset. There were also other papers that monitored HRV features by MSPC. Koichi Fujiwara et al. acquired RR interval data from epileptic patients and performed HRV analysis based on it [22]. Instead of monitoring each variable separately, MSPC analyzes the correlation among the variables by using PCA (principal component analysis) at first, then estimate the state according to two statistics Q and $T^2$.

## 3 Experiment and Data Analysis

### 3.1 Experimental Design

The driving simulation experiments were carried out in the driving simulator conducted by UC-WinRoad. The experiments were conducted 2 h after the lunch of drivers, which is the high incidence period of driving fatigue [23]. In the process of driving experiment, ErgoLab man–machine synchronization platform was used to gather drivers' pulse signals and send the information to the computer through wireless signal. Thus, the signal was collected and recorded in real time. At the same time, GoPro camera was used to collect and store the facial expressions of subjects. The facial and blink expressions were the contrast of drivers' mental state to evaluate the effectiveness of the various methods of fatigue recognition. Subjects should answer the questions related to his mental state after the experiment.

15 subjects were chosen in total in this paper. The average age of subjects is 24 and the average age of driving years is 1.5. All subjects are in good health and normal vision or corrected vision. All of the subjects in the experiment should not have any reviver drink like wine, coffee, etc. within 24 h before starting the experiment. There should be at least 7 h of sleep at the night before the experiment, and no rest before the experiment.

### 3.2 Data Analysis of Individual Participant

This section illustrates the calculation results of each index of one subject for example.

The pulse signal gathered by photoelectric volume pulse sensor is the pulse signal voltage value. First, smooth the voltage signal and the result is shown in Fig. 1.

Then, identify the peak of the waveform smoothed and calculate the original cardiac intervals, namely RRI. In order to facilitate the subsequent calculation, we used a spline method to resample the raw RRI data. The RRI data after process were at equal intervals as 1 s. Figure 2 showed the comparison of raw RRI and resampled RRI.
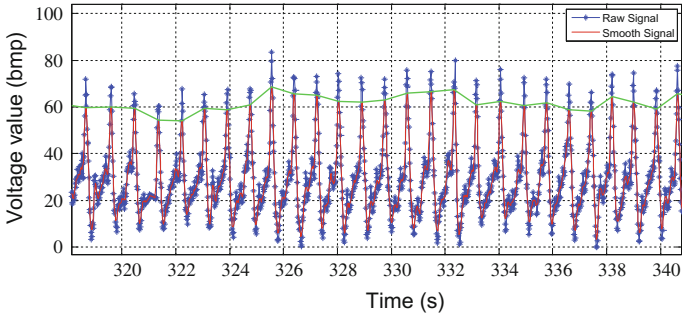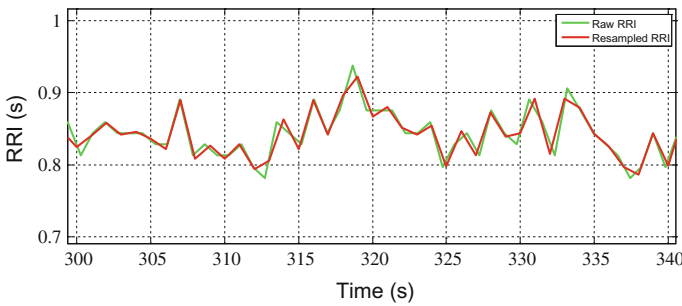
**Fig. 1** The processing of original signal



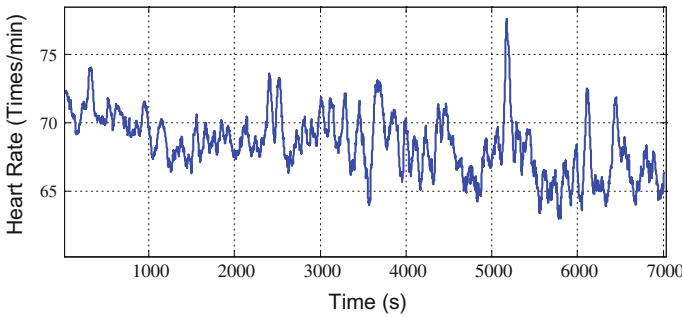**Fig. 2** The comparison of raw RRI and resampled RRI



**Fig. 3** Average of HR in whole test

- The Heart Rate

The HR of each subject was calculated per second on the basis of resampled RRI with a sliding window whose width was 1 min. The average heart rate of the subject above in the whole test processing is shown in Fig. 3.
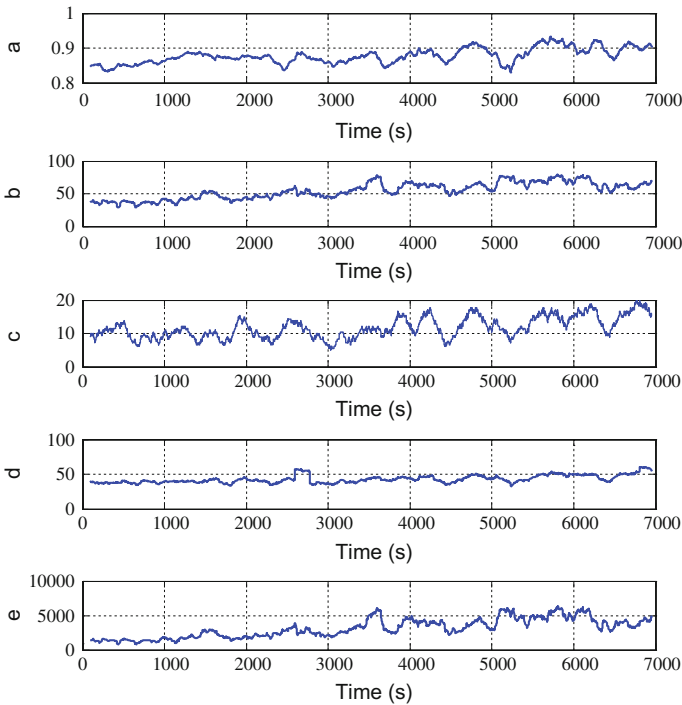
**Fig. 4** Time domain features of HRV

- Heart Rate Variability

It takes at least 3 min RRI data to calculate the more accurate results [1]. Therefore, a 3-min-width sliding window was used to obtain HRV features. The power spectrum density (PSD) of the resampled RRI was calculated by using an autoregressive (AR) model. Figures 4 and 5 show the time domain analysis indicators and frequency domain analysis indicators of heart rate variability of the subject above, respectively. Therein, "a" represents "AVRR (s)", "b" represents "SDNN (ms)", "c" represents "PNN50 (%)", "d" represents "RMMSD (ms)", and "e" represents "total power (ms2)".

- Nonlinear analysis of HRV

Figures 6 and 7 show the Poincare scatter plot of the subject above in 15 waking minutes and 15 fatigue min. Two periods mentioned above are both chosen according to the driver's subjective feeling and facial expressions.

- Indicators of MSPC (Multivariate Statistical Process Control)

In this paper, the eight features of one subject were the input to construct the PCA model for the participant himself. First, select 5 min wakeful data according to the video record of facial expression and subjective questionnaire survey to build the
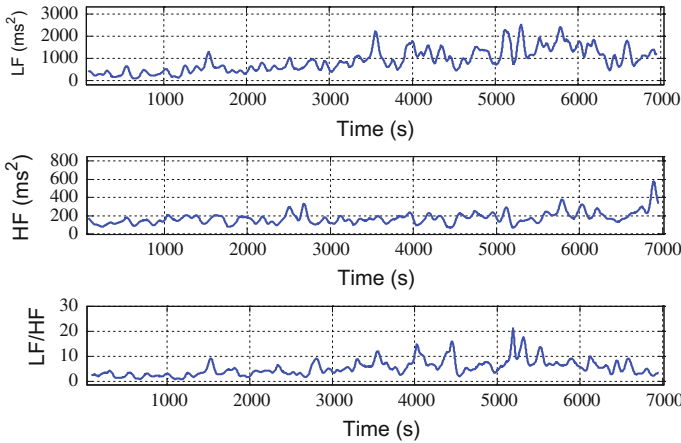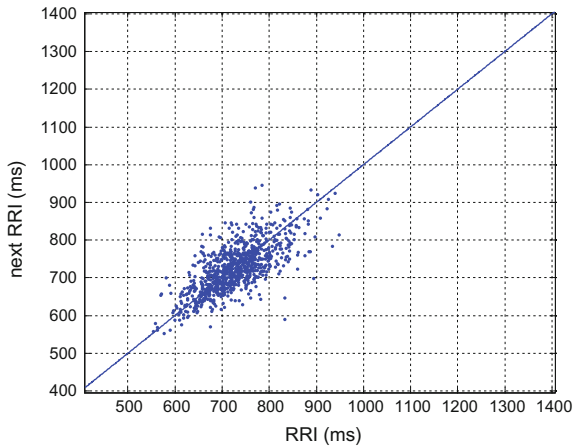
**Fig. 5** Frequency domain features of HRV

**Fig. 6** Poincare scatter plot of waking state



control limits for the subject. Adopt the principle components when the accumulating contribution rate is 80% so that the control limits calculated represented 80% confidence limits. Standardize the waking data using average and standard deviation. Then calculate the Q and $T^2$ statistics and judge whether the subject is in fatigue state. Compare the results with the video records and subjective questionnaire survey to verify the effectiveness of this method.

Figures 8 and 9 show the state discriminant index "$T^2$" and "Q" of MSPC of the subject mentioned above in the whole test processing.
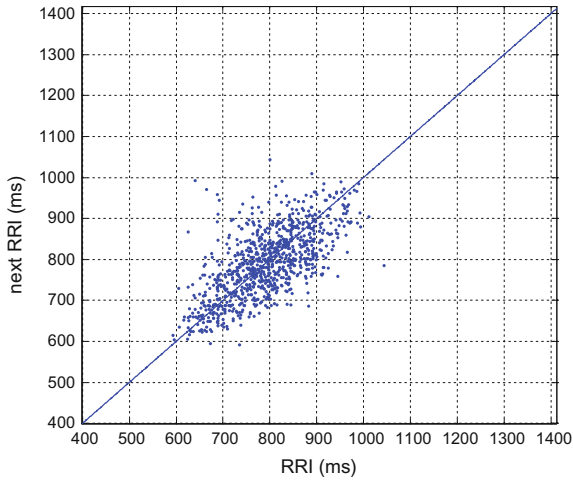
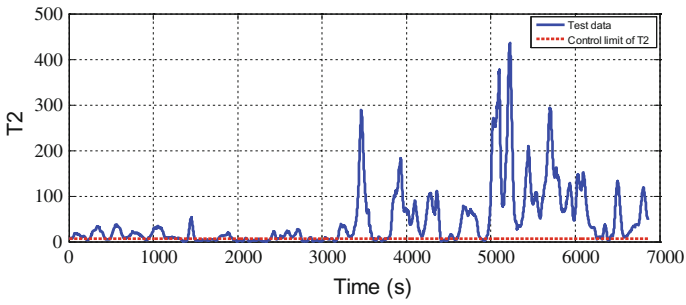**Fig. 7** Poincare scatter plot of tired state
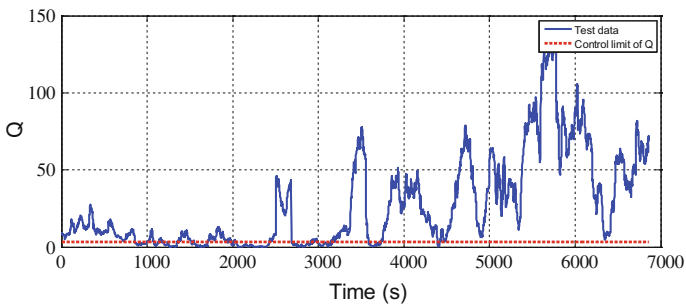


**Fig. 8** T$^2$ of MSPC



**Fig. 9** Q of MSPC

**Table 1** Comprehensive analysis of all the subjects

| Indexes | Number of increase in fatigue | Percentage (%) | Number of increase in awake | Percentage (%) |
|---|---|---|---|---|
| HR | 6 | 40 | 9 | 60 |
| AVNN (ms) | 9 | 60 | 6 | 40 |
| SDNN (ms) | 14 | 93.3 | 1 | 6.7 |
| RMSSD (ms) | 12 | 80 | 3 | 20 |
| PNN50 | 8 | 53.3 | 7 | 46.7 |
| total power | 14 | 93.3 | 1 | 6.7 |
| LF | 15 | 100 | 1 | 6.7 |
| HF | 13 | 86.7 | 2 | 13.3 |
| LF/HF | 15 | 100 | 1 | 6.7 |
| Minor axis of Poincare plot | 3 | 20 | 12 | 80 |
| Macro axis of Poincare plot | 13 | 86.7 | 2 | 13.3 |
| $T^2$ | 15 | 100 | 1 | 6.7 |
| Q | 13 | 86.7 | 10 | 66.7 |

## 3.3 Comprehensive Analysis of Multiple Subjects Data

13 indices of 15 subjects in total were analyzed and contrasted, the results of which are shown in Table 1.

Through the comparison of these indices of different subjects, it was shown that HR of all the subjects was in a state of fluctuation within a normal scale. The average heart rate in the fatigue state is lower than in the waking state in 60% of all the subjects. However, it was not a significant feature to determine that whether the present state is fatigue or not. For the frequency domain analysis indicators, the LF of all the subjects had a significant rise in the fatigue state, and one of them had a higher LF in the waking state. 86.7% of the subjects had a higher HF in the fatigue state than in the waking state, but the rising amplitude of it is smaller than that of LF. Thus, the ratio of these two indices LF/HF had an obvious rise in the fatigue state compared with the ratio in the waking state. The axial length of the Poincare scatter plot is not commonly used in the actual driving fatigue discriminant, though 86.7% of the subjects had a longer axis of Poincare scatter plot in the fatigue state than waking. For the two indices of MSPC, the effect of the index $T^2$ was superior to that of Q. All the subjects had a bigger $T^2$ in the fatigue state than waking and one of them had a bigger $T^2$ in waking state than fatigue also; but most of the subjects had a bigger Q in both states.

# 4   Conclusion and Expectation

Different driving fatigue evaluation methods based on RR interval had been verified in this paper. According to the results of experiments, the "$T^2$" of MSPC, SDNN, and RMSSD, total power of time domain indexes of HRV, LF/HF of the frequency domain indexes of HRV, and the longer axis of Poincare scatter plot have obvious difference in two different states of the drivers: waking and fatigue. In the future work, there should be more experiments and practices to confirm the topic here.

# References

1.  Phillips RO (2015) A review of definitions of fatigue—and a step towards a whole definition. Transp Res Part F Traffic Psychol Behav 29:48–56
2.  Ting PH, Hwang JR, Doong JL et al (2008) Driver fatigue and highway driving: a simulator study. Physiol Behav 94(3):448–453
3.  Dewar RE, Olson PL (2002) Human factors in traffic safety. Lawyers & Judges, Tucson, AZ
4.  Yang G, Lin Y, Bhattacharya P (2010) A driver fatigue recognition model based on information fusion and dynamic Bayesian network. Inf Sci 180(10):1942–1954
5.  Fadda P, Meloni M, Fancello G et al (2015) Multidisciplinary Study of biological parameters and fatigue evolution in quay crane operators. Procedia Manuf 3:3301–3308
6.  Lal SKL, Craig A (2002) Driver fatigue: electroencephalography and psychological assessment. Psychophysiology 39(3):313–321
7.  Malik M, Bigger JT, Camm AJ et al (1996) Heart rate variability. Standards of measurement, physiological interpretation, and clinical use. Eur Heart J 17(3):354–381
8.  Toscani L, Gangemi PF, Parigi A, Silipo R, Ragghianti P, Sirabella E, Morelli M, Bagnoli L, Vergassola R, Zaccara G (1996) Human heart rate variability and sleep stages. Ital J Neurol Sci 17:437–439
9.  Elsenbruch S, Harnish M, Orr WC (1999) Heart rate variability during waking and sleep in healthy males and females. Sleep 22:1067–1071
10. Patel M, Lal SKL, Rossiter P et al (2011) Applying neural network analysis on heart rate variability data to assess driver fatigue. Expert Syst Appl 38(6):7235–7242
11. Shinar Z, Akselrod S, Dagan Y, Baharav A (2006) Autonomic changes during wake-sleep transition: a heart rate variability based approach. Auton Neurosci 130:17–27
12. Takahashi I, Yokoyama K (2011) Development of a feedback stimulation for drowsy driver using heartbeat rhythms. 2011(4):4153–4158
13. Vicente J, Laguna P, Bartra A et al (2016) Drowsiness detection using heart rate variability. Med Biol Eng Compu 54(6):927–937
14. Baharav A, Kotagal S, Gibbons V, Rubin BK, Pratt G, Karin J, Akselrod S (1995) Fluctuations in autonomic nervous activity during sleep displayed by power spectrum analysis of heart rate variability. Neurology 45(6):1183–1187
15. Furman G, Baharav A, Cahan C, Akselrod S (2009) Early detection of falling asleep at the wheel: a heart rate variability approach. Comput Cardiol 35:1109–1112

16. Rodriguez-Ibañez N et al (2012) Changes in heart rate variability indexes due to drowsiness in professional drivers measured in a real environment. Comput Cardiol IEEE 39:913–916
17. Woo MA, Stevenson WG, Moser DK et al (1992) Patterns of beat-to-beat heart rate variability in advanced heart failure. Am Heart J 123(3):704–710
18. Kamen PW, Krum H, Tonkin AM (1996) Poincare plot of heart rate variability allows quantitative display of parasympathetic nervous activity in humans. Clin Sci 91(2):201–8
19. Kano M, Nagao K, Hasebe S, Hashimoto I, Ohno H, Strauss R, Bakshi BR (2002) Comparison of multivariate statistical process monitoring methods with applications to the eastman challenge problem. Comput Chem Eng 26(2):161–174
20. Nomikos P, MacGregor JF (1994) Control procedures for residuals associated with principal component analysis. AIChE J 40:1361–1375
21. Abe E, Fujiwara K, Hiraoka T et al (2014) Development of drowsy driving accident prediction by heart rate variability analysis. Asia-Pacific Signal and Information Processing Association, 2014 Summit and Conference. Siem Reap, Cambodia
22. Fujiwara K, Miyajima M, Yamakawa T et al (2016) Epileptic seizure prediction based on multivariate statistical process control of heart rate variability features. IEEE Trans Biomed Eng 63(6):1321–1332
23. Li PF, Wang DH, Liu DB et al (2011) Analysis on driving fatigue before and after lunch based on indices of physiology and psychology. J Changan Univ 31(4):81–86

# Risk Identification of In-Vehicle Information System Operation Based on Traffic Environment Complexity

**Yanli Ma, Luyang Fan and Gaofenga Gu**

**Abstract** In order to reduce driver distraction and its traffic safety problems caused by the operation of in-vehicle information systems, carried out IVIS (In-vehicle information system) operation risk identification based on different traffic environment conditions. In this chapter, on the basis of traffic environment complexity definition, designed the driving distraction experiments under different traffic conditions, the vehicle, road video scene, and driving conditions data were collected in the experiment in which forty participants interacted with an IVIS while driving. Combined with IVIS operation time and the traffic environment information, build operation risk identification model, determined the safety risks of different IVIS operations. The IVIS operation suggestions under different environment are presented. Results show that the model can accurately identify the safety risks of the IVIS operating under different environmental conditions. When traffic environment complexity is higher, some vehicle information system operations need to be warned or banned. Potential applications of this chapter include the strategy of driving behavior intervention and the evaluation of driver distraction.

**Keywords** IVIS · Driver distraction · Traffic environment · Safety risk identification · Intervention strategies

Y. Ma (✉) · L. Fan
School of Transportation Science and Engineering, Harbin Institute of Technology, Harbin 150090, China
e-mail: mayanli@hit.edu.cn

L. Fan
Chengdu Engineering Corporation Limited, Chengdu 610072, China

G. Gu
Guangzhou Transport Planning Research of Institute, Guangzhou 510000, China

# 1 Introduction

With the rapid development of information and electronic technology, vehicle navigation, and positioning and other new technology applied in the automobile industry rapidly. IVIS (In-vehicle information system) enriched in-car entertainment life and provide convenience for a driver, but at the same time also bring some hidden security danger. According to the national highway traffic safety administration, in the traffic accident caused by driver distraction, about 30% (1 million) traffic accident is caused by the in-car secondary task, and IVIS is an important factor caused an in-car distraction [16]. So it is of great significance to study the control strategies for IVIS, to reduce the number of traffic accidents caused by driver distraction, and promote the application of IVIS in the automotive industry [13].

Compared with the United States, Europe, Japan, and other countries, there is less study in the influence of IVIS on traffic safety in our country, and the theory of the negative influence on driver distraction caused by IVIS operation is not yet mature. Foreign scholars have carried out research on the influence of driver workload in different man–machine interface [10], IVIS equipment input form [11], use characteristics of different users [2, 6], ease use of in-vehicle information [14], etc. And give a safety design principle of vehicle information equipment [9]; optimize the IVIS equipment by simplifying the driver input operation, optimizing the form of the input device and the man–machine interface [15], etc. Provide advice on the limit of time required for operation of the vehicle equipment [3], the Society of Automotive Engineers (SAE) in the United States set a "SAE 15 SEC rule", points out that any static measurement completion time is longer than 15 s of task would threaten safe driving [12]. A number of studies have shown that navigation address input task to the driver's resource demand is higher; it is the most difficult in IVIS operation [5].

Some domestic scholars to study the effect of telephone distraction on driving performance [7], and management measures and recommendations about IVIS are less. There are many differences in IVIS, driving habits and traffic management laws at home and abroad. In different traffic conditions, driver workload is different, traffic security risks caused by operating in-vehicle equipment are also different [1].

Based on the above background, this chapter expects by the driving distraction experiments, on the basis of traffic environment complexity definition, build operation risk identification model. The model can accurately identify the safety risks of the IVIS operating under different environmental conditions, give the IVIS operation suggestions, and provide the basis for applications of in-vehicle equipment, driving behavior intervention and the evaluation of driver distraction.

## 2 Experiment

### 2.1 Participants

Selected 40 participants, who have driver license, took part in driving experiment, of which 27 males and 13 females, driving for 2–7 years. Each participant's driving range between 5000 and 10000 km, aged 22–36 years old. The participant's physical and mental conditions are healthy, without visual and auditory dysfunction. Meanwhile, not drinking or taking drugs.

### 2.2 Equipment

The experimental vehicle is a passenger car; the vehicle is equipped with remote front detection radar, the acceleration sensor, the traveling data recorder, the front detection camera, the yaw sensor, the steering wheel angle sensor, the brake sensor, and the steering signal.

Radar can detect the relative distance, relative velocity, and angle of the goals ahead of the road. Use Safe TRAC lane tracker to judge the transverse position and displacement of the vehicle. Use laser range finder to measure the real-time distance before and after the other target (including vehicles and pedestrians).

### 2.3 Experiment Site

Select a length of 5 km road in Nangang District of Harbin and the highway of Harbin to Liaoning Bayuquan as experiment site, city road for the main road, eight lanes, speed of 60 km/h, mainly for two-way six-lane highway section, the speed limit of 120 km/h. In order to reduce the influence of the weather and traffic conditions, the experiment time is not the peak time of good weather.

### 2.4 Procedure

In the process of driving, the driver can operate IVIS at a particular time. The operation type has the regulation on the car radio, the use of CD, vehicle navigation and MP3; record the change of the indicators in the process of driving. Specific experimental steps are as follows:

(1) Participants fill in the age, gender, driving age, mileage, and other basic information. Drivers were of good physical and mental health without visual and auditory disorders, drinking, and drugs. All participants gave their informed consent.

(2) Before the experiment, show the content of the experiment, explain the driving operation, and let drivers familiar with the experimental equipment.

(3) Required equipment installed in the front and rear car. The driving recorder is installed on the rear car, which is used to record the moving image in the driving process, and to measure the lateral deviation distance. Meanwhile, acceleration sensors are installed on the front and rear car to measure the accelerated speed.

(4) Decide the driver of the rear car; select the driver of the front car randomly. Require front drivers drive at nearly the speed of 50 km/h and the rear cars drive following under the condition of safe driving. The experimenter sits in the copilot's position.

(5) The starting position of the front and rear vehicles is 50 m, both after the front and rear cars are launched, open the vehicle recorder and camera. The front and rear car move forward at the same time according to the experimental instructions and open the acceleration sensor at the same time.

(6) Experimenter requires the driver to operate the IVIS and write down the driver's operation start and end time. The operation is divided into the adjustment of the car radio to a specific channel and fixed channel modulation. Similar three kinds of operations: car radio, car CD, and car navigation to see the route and no operation to drive. Experimenter records every operation start time, end time and equipment shut down time.

(7) Repeat step (5) and step (6), until each driver has operated differently difficult tasks three times.

(8) Collect and collate the experimental data and back up the experimental data.

## 2.5 Design

Driving main task load affected by road conditions, traffic volume, whether there is a pedestrian interference or traffic signals and other conditions. In different traffic conditions, the driving load is different, the risk of accident and conflict caused by operating in-vehicle equipment in different traffic conditions. According to the driver's subjective feeling of load, the traffic environment is divided into different roads, traffic, and signal control, and the traffic conditions are shown in Table 1.

Using field observation method, driving in different road traffic environment, testing time includes traffic flow peak and off-peak period, and recording the traffic environment of the vehicle passed by.

From the experimental results, we select 300 groups of IVIS operating segments, and the vehicle's external driving environment is more complex and the video data, including no traffic volume or traffic volume is small, as well as the condition of high traffic flow density, different road grade and the freedom degree of vehicle running

**Table 1** Traffic environment conditions of each level

| Traffic environment complexity | Traffic conditions | Saturation |
|---|---|---|
| 1 | Good road linear condition; Lane width ≥ 3.5 m; Complete sign and marking; With the central separation barrier; Smooth traffic; Fewer pedestrians; Complete traffic signal | [0, 0.4] |
| 2 | Good road linear condition; Complete sign and marking; Signs and markings are more complete; mainly for traffic signal control; traffic flow | (0.4, 0.6] |
| 3 | General road linear condition; Lane width ≤ 3.5 m; Without the central separation barrier; Traffic flow is not stable; car spacing is smaller | (0.6, 0.8] |
| 4 | Poor road linear condition; Poor visibility; Lane width ≤ 3.25 m; Without the central separation barrier; More Pedestrians and can free to cross the road; No traffic signal; Traffic jam; car spacing is smaller | (0.8, 1] |



**Fig. 1** Driving video record clips

(whether can choose travel speed freely), etc. Select video length is about 8 s, the purpose of choosing 8 s is to avoid a long time because of the complexity of the road traffic environment change, which can affect the complexity level evaluation of traffic environment. Driving video recording data is shown in Fig. 1.

# 3   Method

## 3.1   Independent Variables

The safety risk of IVIS operation is fuzzy. According to study about the effect of vehicle equipment operation time on driver distraction, it considered the operation is not safe when the operation time is more than 4 s [4, 8]. If the two kinds of operation time are 3.9 and 4.1 s, the difference between the two types of operation is small but the safety evaluation results are different, and not in conformity with the actual situation. In addition, the actual driving conditions of the vehicle, the traffic environment is always changing, and there is no clear boundary between good and poor traffic environment.

Fuzzy control is a nonlinear control theory, which is usually used to solve the complex relationship and it is difficult to establish an accurate mathematical model of the problem [17]. Through the fuzzy control algorithm to identify the security risks caused by IVIS distraction in different traffic environments, considering the road and traffic volume level, select the degree of saturation as the evaluation index of the traffic environment.

Vehicle equipment safety risk identification input is IVIS equipment operation time and traffic saturation. Determine the operating time and the road environment after fuzziness, and then the fuzzy control rules in the safety risk, IVIS equipment, and IVIS operation. After fuzzy inference and de-fuzziness, the output is the operational risk.

## 3.2   Variable Fuzzy

Use the membership function of a fuzzy subset to determine the membership degree of variables. Algorithm input is a total operation time and environmental rating, with 4S as the boundary point, the operation time is defined as short, medium, and long, and the fuzzy subsets are expressed as TS, TM, and TL. The domain language of the traffic environment is very worst, worse, medium, better, and very best. Fuzzy subsets are represented as VW, W, M, B, and VB. The domain language of the security risk of output is very small, small, medium, large, and very large. Fuzzy subsets are represented, respectively, as VS, S, M, L, and VL.

## 3.3   Determine Membership Degree Function

The operating time and traffic environment membership function as shown in type (1) and type (2). Fuzzy function images are shown in Figs. 2 and 3. Safety risk membership functions as shown in type (3), fuzzy function image is shown in Fig. 4.

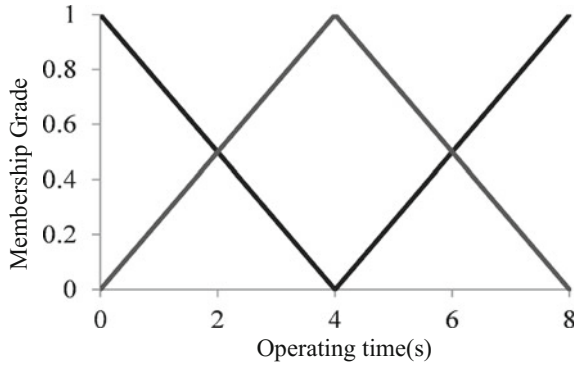**Fig. 2** Operating time membership function diagram



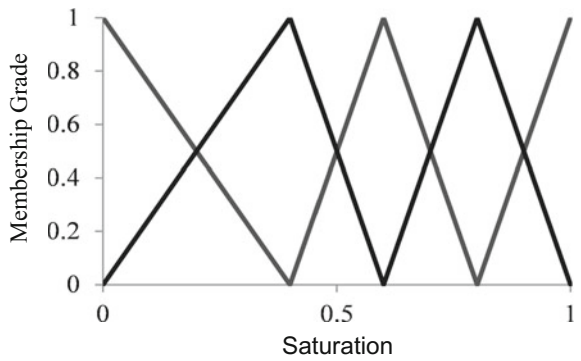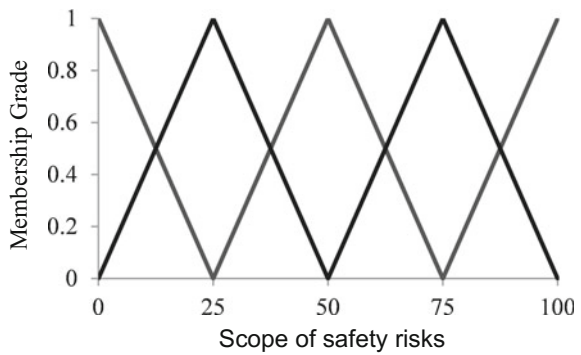**Fig. 3** Traffic environment membership functions



**Fig. 4** Safety risk membership functions



$$\mu_T = \begin{cases} \mu_{TS}(x) = (4-x)/4 & 0 \leq x \leq 4 \\ \mu_{TM}(x) = \begin{cases} x/4 & 0 \leq x \leq 4 \\ (8-x)/4 & 4 < x \leq 8 \end{cases} \\ \mu_{TL}(x) = (x-4)/4 & 4 < x \leq 8 \end{cases} \qquad (1)$$

**Table 2** Safety risk fuzzy identification rules

| Traffic environment operating time | VW | W | M | B | VB |
|---|---|---|---|---|---|
| TS | VS | S | M | L | L |
| TM | M | M | L | L | VL |
| TL | M | L | L | VL | VL |

$$\mu_H = \begin{cases} \mu_{VW}(y) = (0.4 - y)/0.4 & 0 \leq y \leq 0.4 \\[4pt] \mu_W(z) = \begin{cases} y/0.4 & 0 \leq y \leq 0.4 \\ (0.6 - y)/0.2 & 0.4 < y \leq 0.6 \end{cases} \\[8pt] \mu_M(z) = \begin{cases} (y - 0.4)/0.2 & 0.4 \leq y \leq 0.6 \\ (0.8 - y)/0.2 & 0.6 < y \leq 0.8 \end{cases} \\[8pt] \mu_B(z) = \begin{cases} (y - 0.6)/0.2 & 0.6 \leq y \leq 0.8 \\ (1 - y)/0.2 & 0.8 < y \leq 1.0 \end{cases} \\[8pt] \mu_{VB}(z) = (y - 0.8)/0.2 & 0.8 \leq y \leq 1.0 \end{cases} \tag{2}$$

$$\mu_R = \begin{cases} \mu_{VS}(z) = (25 - z)/25 & 0 \leq z \leq 25 \\[4pt] \mu_S(z) = \begin{cases} z/25 & 0 \leq z \leq 25 \\ (50 - z)/25 & 25 < z \leq 50 \end{cases} \\[8pt] \mu_M(z) = \begin{cases} (z - 25)/25 & 25 \leq z \leq 50 \\ (75 - z)/25 & 50 < z \leq 75 \end{cases} \\[8pt] \mu_L(z) = \begin{cases} (z - 50)/25 & 50 \leq z \leq 75 \\ (100 - z)/25 & 75 < z \leq 100 \end{cases} \\[8pt] \mu_{VL}(z) = (z - 75)/25 & 75 \leq z \leq 100 \end{cases} \tag{3}$$

## 3.4 Fuzzy Control Rules

According to the safety risk level of the driver operation on the vehicle equipment, the fuzzy control rules are set up as shown in Table 2.

## 3.5 Fuzzy Reasoning

Assume that the operating time is 3 s, the road saturation is 0.7, and then the membership degree is obtained as follows: $\mu_{TM}(3) = \frac{3}{4}$, $\mu_{TS}(3) = \frac{1}{4}$, $\mu_M(0.7) = \frac{1}{2}$, $\mu_B(0.7) = \frac{1}{2}$.

According to the membership degree and fuzzy rules, the four trigger rules are obtained.

$$Rule1 : \text{If } x \text{ is TS and } y \text{ is } M \text{ THEN } z \text{ is } M$$
$$Rule2 : \text{If } x \text{ is TS and } y \text{ is } B \text{ THEN } z \text{ is } L$$
$$Rule3 : \text{If } x \text{ is TM and } y \text{ is } M \text{ THEN } z \text{ is } L \;^{\cdot}$$
$$Rule4 : \text{If } x \text{ is TM and } y \text{ is } B \text{ THEN } z \text{ is } L$$

Within the same rule to take a small operation, each rule reasoning output as follows:

$$Rule1 : \min(1/4, \mu_M(Z))$$
$$Rule2 : \min(1/4, \mu_L(Z))$$
$$Rule3 : \min(1/2, \mu_L(Z)) \;^{\cdot}$$
$$Rule4 : \min(1/2, \mu_L(Z))$$

The risk estimate system the total output is the union of each output:

$$R(z) = \max\{\min(1/4, \mu_M(z)), \min(1/4, \mu_L(z)), \min(1/2, \mu_L(z)), \min(1/2, \mu_L(z))\}$$
$$= \max\{\min(1/4, \mu_M(z)), \min(1/4, \mu_L(z)), \min(1/2, \mu_L(z))\}. \tag{4}$$

## 3.6 De-fuzziness

Using the maximum average method, the maximum membership degree of the risk level come from type (4) is 1/2. Using the risk level of the membership function is calculated as follows:

$$z^* = \frac{z_1 + z_2}{2} = \frac{87.5 + 87.5}{2} = 87.5. \tag{5}$$

Risk level is 87.5, which can be considered the risk of operation on IVIS equipment is high at this time, not recommended for this operation. Similarly, according to the traffic environment complexity and operating time, judge the risk level of IVIS operation.

**Table 3** IVIS distraction intervention strategies under different traffic environments

| Operation type | Environmental classes | | | |
|---|---|---|---|---|
| | 一 | 二 | 三 | 四 |
| Radio | – | – | – | Warn |
| CD | – | – | Warn | Warn |
| MP3 | – | Warn | Warn | Ban |
| Navigation | – | Warn | Ban | Ban |

## 3.7 Suggestions on IVIS Distraction Control

Calculate the average time required for the operation of various types of IVIS equipment, and then the safety risk of the operation of IVIS equipment under different traffic conditions is obtained. For the high safety risk, it is not recommended to operate. For the operation with large difficulty under the complex environment should be banned. All kinds of equipment for early warning are shown in Table 3.

Simple and complex driving environment, the radio and CD operation will cause the driver distraction, reducing the average speed, the instantaneous velocity changes larger; subjective mental workload is high.

## 4 Summary and Conclusions

(1) Conducting the driving distraction experiments under different traffic conditions, obtain the front road video scene and driving vehicles data (such as speed, brake, front target, etc.) in normal condition on the road. Experimental methods and data can be used for related distracted driving research.
(2) On the basis of the definition of traffic environment complexity, assess the need for driving tasks, the safety risk identification model of IVIS operation is constructed. The model can accurately identify the safety risk of IVIS operation in different environments.
(3) Using the fuzzy control algorithm combined with the road traffic environment, analyzing the safety risk of IVIS operations under different environment complexity. IVIS operation suggestions under different environment are presented. When traffic environment complexity is higher, some IVIS operations need to be banned.
(4) The types of IVIS equipments are gradually diversified, and the IVIS operation time will be further increased. To reduce the operation time, operation interface in the car should be concentrated arrangement. Reduce the shift of the viewpoint and holding time of the driver in the different devices operations.

This study of IVIS distraction experiment was conducted in certain controlled conditions, the driver's driving behavior compared with natural driving condition still

has certain deviation. In order to reduce the influence of the experimental conditions on the drivers, suggested further study of the long-term natural driving experiment.

# References

1. Birrell SA, Young MS (2011) The impact of smart driving aids on driving performance and driver distraction. Transp Res Part F Traffic Psychol Behav 14(6):484–493
2. Brodsky W, Slor Z (2013) Background music as a risk factor for distraction among young-novice drivers. Accid Anal Prev 2013(59):382–393
3. Green P (1999) The 15-second rule for driver information systems. In: Proceedings of the ITS America ninth annual meeting
4. Gu GF (2014) Research on the impact of IVIS distraction on driving performance. Harbin Institute of Technology, Harbin
5. Hagiwara T, Sakakima R, Hashimoto T et al. (2013) Effect of distraction on driving performance using touch screen while driving on test track. In: Intelligent Vehicles Symposium (IV), 2013 IEEE, pp 1149–1154
6. Janke MK (1994) Age-related disabilities that may impair driving and their assessment. California State Department of Motor Vehicles, National Highway Safety Administration, Sacramento
7. Ma YL, Leng X, Qi L (2014) Study of characteristics of phone distraction on drivers and its influence on traffic safety operation. Appl Mech Mater 505–506:1093–1096 (Trans Tech Publications, Switzerland 2014)
8. Ma YL, Gu GF, Gao YE et al (2016) Driver distraction judging model under in-vehicle information system operation based on driving performance. China J Highw Transport 29(4):123–129
9. Mitsopoulos-Rubens E, Trotter MJ, Lenné MG (2011) Effects on driving performance of interacting with an in-vehicle music player: a comparison of three interface layout concepts for information presentation. Appl Ergonomics 42(4):583–591
10. Ranney TA, Baldwin GH, Smith LA et al (2013) Driver behavior during visual-manual secondary task performance: occlusion method versus simulated driving
11. Ranney TA, Harbluk JL, Noy YI (2005) Effects of voice technology on test track driving performance: Implications for driver distraction. Hum Factors: J Hum Factors Ergon Soc 47(2):439–454
12. Reed-Jones J, Trick LM, Matthews M (2010) Testing assumptions implicit in the use of the 15-second rule as an early predictor of whether an in-vehicle device produces unacceptable levels of distraction. Accid Anal Prev 2010(40):628–634
13. Regan M (2005) Driver distraction: reflection on the past, present and future. J Australas Coll Road Saf 12(2):22–33
14. Salvucci DD, Markley D, Zuber M et al (2007) iPod distraction: effects of portable music-player use on driver performance. In: Proceedings of the SIGCHI conference on Human factors in computing systems. ACM, pp 243–250
15. Weinberg G, Harsham B, Forlines C et al (2010) Contextual push-to-talk: shortening voice dialogs to improve driving performance. In: Proceedings of the 12th international conference on Human computer interaction with mobile devices and services. ACM, pp 113–122
16. Westat (2008) Driver distraction expert working group meeting summary and proceedings. National Highway Traffic Safety Administration
17. Wu GC, L Y, Yang XW (2008) Support vector machine classifier based on fuzzy partition and neighborhood pairs. Comput Appl 28(1):131–133

# Implementation of Congestion Charge Policy in China: Legal Analysis and Security Research

**Han-ru Li and Yuejun Liu**

**Abstract** The non-exclusiveness to certain extent of transport resources particularly represented by urban road resources tends to result in a market failure and bring about an excessive travel of sedan cars. If the subsequent huge external cost of congestion, safety, pollution and other areas is not directly paid by car users but jointly borne by the entire society, this will distort rational allocation of social resources and further stimulate to a big extent the pursue of sedan cars and waste of resources. As an important measure of the demand management policy, the congestion charge policy can effectively regulate the cost to use sedan cars and help government administration authorities correct the distorted resource allocation mode and establish a more efficient and fairer transport system. The implementation of the congestion charge, which is a typical economic measure regulating the use of sedan cars, and the refinement of related supporting measures will demand explicit legal support.

**Keywords** Congestion charge · Legal barrier · Legislative opinion and implementation security

As an economic measure to regulate the traffic demand, the congestion charge was first levied in Singapore as early as in 1975 [1]. Today, more than ten cities, including London, Stockholm and Singapore, carry out this policy, and London and Singapore are typical representatives of successful cases. In 2009, Guangzhou was the first city in China to suggest collecting the "traffic congestion charge" but encountered general opposition from citizens. Finally, the leader of the Bureau of Urban Utilities and Gardening of Guangzhou Municipality had to mitigate the strong opposition from citizens, saying that Guangzhou would temporarily not mull the "congestion charge" [2] Such problem exists not only in China but also in other countries. In 2007, the New York mayor suggested that New York should learn from London by collecting charges from vehicles entering the traffic congestion areas to mitigate the

H. Li (✉)
Highway Research Institute of Ministry of Communications, Beijing 100088, China
e-mail: hr.li@rioh.cn

Y. Liu
Beijing Transport Institute, Beijing 100073, China

traffic congestion in the city. However, the plan finally ended up with an abortion after the one-year discussion by the councilors of different districts of city [3]. This indicates that the traffic congestion charge is closely associated with the daily life of the public, so it will tend to trigger public debate and query and demand special legal support.

# 1 Analysis of Legal Barriers to the Congestion Charge Policy in Chinese Cities

## 1.1 Positioning of Congestion Charge Policy

Legal barriers to the implementation of the congestion charge policy now exist in China's current legal system. For one thing, the traffic congestion charge can be defined as either as an administrative or nonprofit charge or a governmental fund, pursuant to the Interim Measures Regarding the Administration of Administrative and Nonprofit Charge Standards and the Interim Measures Regarding the Administration of Government Funds. Nevertheless, the traffic congestion charge must be classified according to purpose and expenditure administration. The collection of the traffic congestion charge usually means collecting additional charges from users of roads in some areas during traffic congestion hours. Therefore, the charge is an economic measure to regulate the traffic demand in essence and aims to restrict the traffic flow density on urban roads during peak hours with the price mechanism, mitigate urban traffic congestion and improve the operating efficiency of the entire urban traffic system. Therefore, the traffic congestion charge should be identified as an administrative and nonprofit charge.

## 1.2 Laws Pertaining to Congestion Charge

At present, the congestion charge is not explicitly prescribed in national laws and administrative regulations as well as local regulations. For example, the People's Government of Beijing Municipality has recently proposed to research the collection scheme for urban congestion charge by issuing a series of normative documents, including *the Notice on Printing and Distributing the Beijing 2013–2017 Clean Air Action Plan* (Jing Zheng Fa [2013] No. 27) [4] and *the Notice on Printing and Distributing the Beijing 2013-2017 Action Plan for Control over Motor Vehicle Pollutant Emissions* (Jing Zheng Ban Fa [2013] No. 53) [5]. However, the aforesaid documents don't have the effectiveness level that empowers the collection of administrative charges, so they can't directly serve as the basis for the imposition of the congestion charge. Moreover, these documents also use such terms as "research and

formulate" and "research plan", which further indicates that there are no laws at the higher level justifying direct collection of the traffic congestion charge.

In 2002, the General Office of the State Council issued *the Notice on Relevant Issues Regarding the Remediation of Noncompliant Charges from Motor Vehicles and Treatment of Road Sites* [6], explicitly specifying that any region, authority and institution shall no longer set new administrative and nonprofit charge, governmental fundraising and governmental fund items involving motor vehicles, unless otherwise explicitly specified by laws, regulations and documents of the State Council.

*The Development Policy for Automotive Industry* [7] issued in 2004 prescribes that: "The state shall uniformly determine and announce items and standards for all administrative and nonprofit charges and governmental funds, and regulate all government charges pertaining to vehicle registration and use. Any region shall not set new administrative or nonprofit charge and governmental fund items or increase the amounts of these charges or funds pertaining to vehicle purchase, registration and use. When genuinely having the need to set new items or increase amounts, the region shall apply for approval through the procedure pursuant to laws, regulations and approval documents of the State Council."

## 1.3   Analysis of Legal Barriers to Congestion Policy

Under China's current legal system, the Notice on Relevant Issues Regarding the Remediation of Noncompliant Charges from Motor Vehicles and Treatment of Road Sites is an official document the State Council has issued to instruct the inferior governments in work, and in the legal sense, it is a policy document without the legal effect. As to the Development Policy for Automotive Industry of 2004, it was issued by the National Development and Reform Commission and approved by the State Council, and in the legal sense, it is a ministerial ordinance beyond the three legal levels (Table 1).

To conclude, the collection of the congestion charge lacks corresponding legal basis under the current legal system and conflicts with current legal documents. Therefore, under the current legal framework, the collection of the congestion charge should be supported by at least local regulations.

**Table 1** Three legal levels in China

| Legal level | Legislator | Legal effect |
|---|---|---|
| Law | The National People's Congress and its Standing Committee | High ⬇ Low |
| Administrative regulation | State Council | |
| Local regulation, autonomous regulation and separate regulation | Local People's Congress and its Standing Committee, or People's Congress in ethnic minority autonomy regions | |

## 2 Analysis of Foreign Legislation Regarding Congestion Charge

### 2.1 Analysis of London's Legislation Regarding Congestion Charge

London's policy of traffic congestion charge has enjoyed the protection from comprehensive laws and regulations formulated by the central government and the local government [8] including *the Greater London Authority Act 1999, the London Transport Act 2000 and the London Central District Congestion Charge Act 2004*.

#### 2.1.1 Greater London Authority Act 1999

*The Greater London Authority Act 1999*, formulated by the central government, mainly includes establishing the Greater London Authority, the London Mayor, the London Parliament and the Transport for London (TFL), granting the power on the TFL and the parliaments of different districts or the city to charge the possession or use of motor vehicles, organizing the TFL and conferring the London Authority and the local transport authority to charge the possession and use of motor vehicles.

#### 2.1.2 London Transport Act 2000

The London Transport Act 2000, formulated by the central government, mainly includes specifying the responsibilities of the TFL, organizing the TFL, conferring

the London Authority and local transport authorities to charge the possession and use of motor vehicles, establishing the legislation flow for charge policies and specifying relevant contents of charge policies.

The act sets forth the conditions precedent for relevant entities' establishment of the charge system, charge entities, legal approval flow, consultation flow about charge system, contents of charge policies, charge payers and exemption, penalty entities and setting and others (charge facilities and traffic signs). The key provisions mainly include: The congestion charge policy can be implemented only when the charge system can directly or indirectly support local transport planning; the local transport bureau shall implement the policy within respective jurisdiction; the charge entity can implement the charge system by issuing ordinances; the charge entity can revise or change the charge ordinance; and relevant government authority can establish provisions pertaining to the formulation and revision flow for the charge system, confirmation of objects exempted from charge, administration of incomes from the charge system and other aspects.

### 2.1.3  London Central District Congestion Charge Act 2004

In July 2000, the London Mayor published a document entitled Listen to the Voice of London to solicit comments on London Central District's plan to implement the congestion charge. The document was distributed to about 400 key stakeholders, such as the London Borough, members of the London Parliament, members of the European Parliament, commercial organizations, transport operators, motor vehicle institutions and disabled persons' institutions. In January 2001, the Mayor published the draft of the Transport Strategy. The document states the mayor's transport planning for London. The congestion charge policy made for the central district of London is an indispensable part of the strategy and one of the assisting measures and aims to help realize the mayor's objective to build a traffic system adapting to the 21st century in London. In July 2001, the Mayor published the Final Transport Strategy, and on July 23, the TFL issued the Charge Ordinance, which provides a legal foundation for the implementation of the charge system and elaborates major aspects of the system. The ordinance specifies that the congestion charge policy will be implemented as of 2003.

The London Central District Congestion Charge Act 2004 is an act that was formulated by the TFL on the basis of the Greater London Authority Act 1999 and the London Transport Act 2000 on September 30, 2004 and approved by the London Mayor for validation on November 1, 2004. It was amended for 16 times after the promulgation in 2004, and the final amendment was proposed by the TFL on August 1, 2014 and signed by the Mayor on December 9, 2014. The major content of the act is to specify various elements of the charge policy. For example, it establishes the provisions pertaining to the fine defined against the failure to pay the charge, locking of the vehicle and towing of the vehicle.

## *2.2 Analysis of Singapore's Legislation Regarding Congestion Charge*

### 2.2.1 Laws Regarding Congestion Charge Policy

The Road Traffic Act is the major act that the Singapore government has legislated to address the congestion charge policy [9]. The act specifies that road users must pay the charge and also stipulates that the minister of transport has the right to charge designated roads, and the road charges will be attributable to the uniform fund. The act specifies the charge policy in detail as follows:

(1) It specifies charged road, charge date, charge time period and charged vehicles.
(2) It specifies the way to collect the road charge, including the use of electronic equipment or other equipment to collect the charge and requiring vehicles install relevant equipment.
(3) If a user violates the charge policy, the court can require the user to pay the road use charge on top of the penalty against relevant illegal behavior, and the amount of the road use charge is determined by the person designated by the transport authority according to the date of violation and time period of violation.

### 2.2.2 Legal Provisions Regarding the Power of Relevant Policy Enforcement Officials

The act also specifies the power of enforcement officials in detail, including:

(1) The enforcement official shall have the right to require the car user prepare the vehicle for selective examination at any time according to the designated time and place;
(2) The enforcement official shall have the right to detain the vehicle that fails to correctly install relevant facility and write a ticket;
(3) The enforcement official shall have the right to notify the owner to take back a detained vehicle. Where the owner fails to take back the vehicle within 3 months as of the date of detention, the enforcement official can sell or dispose of the vehicle through open auction or in other appropriate manners one month after the announcement is published, and use relevant income from sale or disposal of the vehicle to pay the road use fee and expenses incurred during the implementation of this article. Where the vehicle owner fails to receive the surplus, if any, within 12 months, the surplus will be transferred to the uniform fund.

## 3 Research on Legal Security Regarding Traffic Congestion Charge in Chinese Cities

The smooth implementation of the congestion charge policy will involve security measures in different aspects. Legally, the city must consider the legislation involving congestion charge, carry forward security measures and exemption rules, and establish relevant standards relating to charge technology, security protection, penalty against violation and other areas.

### 3.1 Legislations Pertaining to Congestion Charge

For one thing, at the national law level, the 2014 Amendment Draft of *the Law of the People's Republic of China on the Prevention and Control of Atmospheric Pollution* stipulates that "the governments of provinces, autonomous regions and municipalities can specify types of restricted or limited vehicles as well as areas and times of emission control pursuant to the needs of atmospheric pollution prevention and vehicle emission pollution status in respective administrative zone, and publish the same to the society." After formal amendment, the law can serve as the legal basis for the collection of the congestion charge. For another, at the level of regional regulations, the Standing Committee of the Regional People's Congress can establish the provincial administrative regulation pertaining to congestion charge, and determine the legality, nature and relevant elements of the congestion charge.

#### 3.1.1 Legislation Procedure and Time

It takes about two years to complete the entire legislation procedure. For example, it takes the People's Congress of Beijing Municipality to establish local regulation, which contains four stages, including determination of the legislation plan, project initiation by the People's Government and the People's Congress, drafting of the draft regulation and solicitation of comments, and review of the draft regulation by the People's Government and the People's Congress, according to the Regulation of Beijing Municipality Regarding Establishment of Local Laws and Regulations, the Measures of the People's Government of Beijing Municipality Regarding Formulation of Regulations and Rules and other related provisions (Fig. 1).
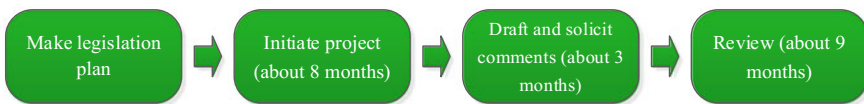


**Fig. 1** Time requirements for different stages of legislation regarding congestion charge

### 3.1.2 Consideration of Probability to Shorten the Time Through Special Legislation Procedure

Pursuant to prior legislation experience and practices of other provinces and munic-ipalities, if a legislation project involves people's life and security, attracts great attention from leaders and much concern from citizens, involves particularly impor-tant matters and requires urgent publishing, the legislation process can be expedited under the concern from leaders. For example, Beijing issued the Interim Provisions of Beijing Municipality Regarding the Regulation of Number of Small Passenger Vehi-cles, a government act, within one month, and Shanghai completed the legislation of the Measures of Shanghai Municipality Regarding the Investigation and Penalty against Illegal Passenger Transport Vehicles, a local regulation, within three months. However, the aforesaid regulations are both the legislations implemented prior to the issuance and implementation of the Legislation Law. The new Legislation Law stresses the dominant position of the People's Congress in the legislation process and specifies requirements in relation to legislation plan, solicitation of comments, legal review and other aspects. At present, the collection of the congestion charge has not been included in the legislation plan for 2015. Therefore, if the city wants to enlarge the legislation plan, streamline the legislation procedure and shorten the legislation time, it will have to obtain the written report from relevant leaders of the National People's Congress, the Municipal People's Congress, the CPC Committee of the city and the Municipal Government or the minutes of the high-level meeting. Moreover, the city will have to forge a consensus with the Municipal People's Government and the Municipal People's Congress.

### 3.1.3 Conditions Precedent for Initiation of Legislation Project Involving Congestion Charge

The legislation of congestion charge must clearly break down charge price, charge entity, charge object, time period of charge, charge area, charge mode, expense man-agement, purpose and other legislative elements, and demonstrate the necessity and feasibility of the project, and determine major contents of the legislation. All these are the conditions precedent for the initiation of the legislation project. The clearer and deeper the demonstration, the more possible to win the recognition from the CPC Committee, the People's Government and the People's Congress of the city. More-over, the city should seek extensive support from related authorities, representatives of the People's Congress and vast citizens to expedite the review process.

## 3.2 Carry Forward the Issuance of Security Measures for Congestion Charge and Research of Exemption Rules

It is a complex job to make and carry out the congestion charge policy. The ignorance of any link will trigger potential risk, directly affect the effect of the policy and even plunge the policy into a failure. The government must implement necessary security measures, achieve the expected expect of the policy and minimize the negative impact of the policy in order to mitigate various risks arising out of the implementation of the congestion charge, including commercial impact on charge areas, impact on residents' mobility in the areas, traffic congestion in adjacent areas due to bypass and chaotic parking.

## 3.3 Carry Forward the Work to Establish Relevant Standards for Charge Technologies

Establish technical standards for charge hardware. The entire congestion charge technology can be divided into the vehicle identification module, vehicle positioning module, charge module, inspection module, communication module and backstage service model. Every module must be based on corresponding hardware, which must conform to certain fundamental technical standards, product standards, process standards, inspection standards, safety standards, health standards and environmental standards during design, production and use.

Establishment of technical specifications. The government should suggest suitable technical specifications in time and do a good job to assure the early preparation, including design and production of hardware equipment for congestion charge.

## 3.4 Establish Security Prevention and Violation Penalty Standards

The government should establish security prevention standards to provide necessary security standards and provisions for participants, enforcement agencies and administration organs involved in the congestion charge policy and make the policy more feasible. At the same time, the government should establish the standard of penalty against violation, regulate behaviors of road users, assure the effect of implementation and mitigate traffic congestion in urban areas.

## 4   Conclusion and Suggestions

As an economic measure to mitigate the mobility issue during the urbanization process, the congestion charge policy will deliver a material impact on different interest groups and trigger extensive debates. Therefore, adequate legal authorization constitutes the condition precedent for implementation of the policy and carries a heavy weight to assure smooth implementation of the policy. Moreover, the government must reasonably specify the policy as to charge entity, charge object, time period of charge, charge area, charge mode, charge price, system design of charge technology, extensive installation, penalty against violation, power of enforcement officials and other aspects. At the same time, if the government decides to implement the congestion charge policy, the government must observe the principle of legality during implementation, pay attention to the principle of rationality and invite the public to take an active part to avoid possible social conflict after implementation.

## References

1. U.S. Department of Transportation Federal Highway Administration. Reducing congestion and funding transportation using road pricing in Europe and Singapore
2. Gao F (2012) Feasibility study on traffic congestion charge project of Guangzhou City—a reference to the implementation process of Stockholm's traffic congestion charge project. Mod Bus 19
3. Ming M, Yuan C, Guo X (2009) Impact assessment of implementation of congestion charge in central areas of metropolises. Technol Econ Areas of Commun 01
4. Notice of the People's Government of Beijing Municipality on Printing and Distributing the Beijing 2013–2017 Clean Air Action Plan (Jing Zheng Fa [2013] No. 27): http://zhengwu.beiji ng.gov.cn/gzdt/gggs/t1324560.htm
5. Notice of the General Office of the People's Government of Beijing Municipality on Printing and Distributing the Beijing 2013–2017 Action Plan for Control over Motor Vehicle Pollutant Emissions (Jing Zheng Ban Fa [2013] No. 53): http://zhengwu.beijing.gov.cn/gzdt/gggs/t1329 445.htm
6. Notice of the General Office of the State Council on Relevant Issues Regarding the Remediation of Noncompliant Charges from Motor Vehicles and Treatment of Road Sites (Guo Ban Fa [2002] No. 31): http://www.gov.cn/zhengce/content/2016-10/12/content_5117804.htm
7. Development Policy for Automotive Industry, Order 8 of the National Development and Reform Commission of the People's Republic of China: http://www.sdpc.gov.cn/zcfb/zcfbl/200506/t20 050614_7501.html
8. Transport for London (2003) Central London congestion charging impacts monitoring first annual report. Transport for London, London
9. Willoughby C (2001) Singapore's motorization policies 1960–2000. Transp Policy 8(2):125–139

# Prediction Modeling of Railway Short-Term Passenger Flow Based on Random Forest Regression

**Li-hui Li, Jian-sheng Zhu, Xing-hua Shan and Xia Zhang**

**Abstract** The predication of short-term passenger flow plays a very important role for improving service quality and revenue High-speed railway operation. To precisely predict the short-term passenger flow, impact factors need to be deeply analyzed and a reasonable predication model is required. This chapter analyzed the impact factors for short-term passenger flow and proposed a prediction model based on random forest regression. With the passenger flow data between Beijing and Shanghai from July to August in 2015, a predication model is trained and reached 91% accuracy for daily passenger flow. Finally, the importance of each impact factor has been analyzed, and this information can also help high-speed railway operation. It is shown that the prediction model based on random forest regression for predicting short-term passenger flow can help to improve the high-speed railway operation.

**Keywords** High-speed railway · Random forest regression
Prediction · Short-term flow

## 1 Introduction

The passenger flow is a very important factor in railway passenger transportation. The accurate prediction of passenger flow can help to improve operation efficiency and increase revenue. With accurate predication of passenger flow, the high-speed railway company can manage the tickets with a more scientific methodology. It can help to better fulfill the passenger's trip requirement and improve the revenue at the same time. Due to various complex factors like macroeconomic, geolocation, and weathers, the predication on short-term passenger is a complicated nonliner problem that cannot be described fully quantitatively.

L. Li (✉)
Postgraduate Department, China Academy of Railway Sciences, Beijing 100081, China
e-mail: lyhui820212@163.com

L. Li · J. Zhu · X. Shan · X. Zhang
Institute of Computing Technology, China Academy of Railway Sciences, Beijing 100081, China

Currently, to analyze the problem for short-term passenger flow, most of the research are based on causal relationship, time series, etc. Different models are chosen due to different data characteristics, or different predict purpose. Hao [1] chose using historical data to set up seasonal time series model SARIMA. Wang [2] did a research on urban rail transit network passenger flow in this way. Luo [3] did the research on Regression model for daily passenger volume of high-speed railway. As machine learning is widely used these days, researchers start using machine learning to do passenger flow predication. Liu [4] adopted PCA and BP neural network to predict the passenger flow. Li [5] used the radial basis function neural network to predict the passenger flow for specific date, and specific train trip. Xu [6] did research on short-term passenger flow forecasting for urban rail transit based on dynamic feedback neural network.

The random forest (RF) algorithm is a machine learning algorithm proposed by Leo Breiman and Cutler Adele in 2001. There are different researches adopting RF algorithm in agriculture and other industry [7–13]. However, there are very few literatures on using RF regression analysis in railway passenger flow predication.

This chapter takes the high-speed railway passenger flow between Beijing and Shanghai Hongqiao during July and August 2015 as the research object, and collects the impact factors like date, day of the week, the departure and arrival time, running time, and weather information as the input. We build a RF regression model to predict passenger flow, and the results show that the model is efficient to predict the short-term flow with a good accuracy. Then, this chapter compares the RF result with BP neural network result and indicates that RF regression can avoid overfitting issues.

## 2    Analysis on Impact Factors for Passenger Flow

There are many impact factors for high-speed railway passenger flow. Those factors are mainly divided into macro factors and micro factors. The macro factors include the geolocation, the economic, demographics, and other society factors. Besides those, National policies, holidays and main events are also considered as macro factors. Micro factors include transport facility, weather, traveler information, etc.

When analyzing the short-term passenger flow, the micro factors play more important roles as the macro factors usually do not change in short period.

Figure 1 shows the passenger flow between Beijing and Shanghai for Beijing–Shanghai high-speed railway in two weeks. The passenger flow cyclically changes per week, the passenger flow drops from Monday to Wednesday, and then starts increasing. Friday gets the biggest passenger flow, then Saturday drops, Sunday increases. Day of the week impacts a lot for passenger flow.

Based on the similar analysis of the impact factors, Fig. 2 listed the impact factors we are using to predict the short-term passenger flow. Those factors include train category, departure city, arrival city, departure time, running time, holidays, weather in departure city, weather in arrival city, and day of the week for the train. All those
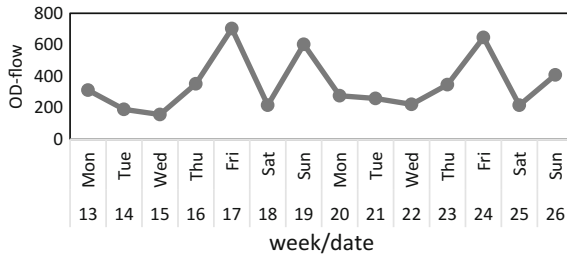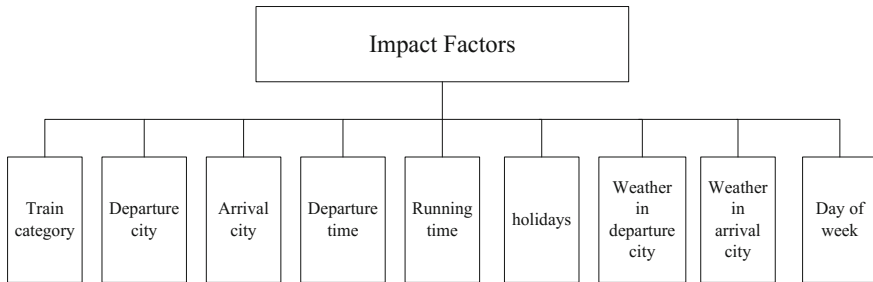
**Fig. 1** Week-cycle pattern



**Fig. 2** Impact factors

factors will be translated to train features, and the passenger flow volume will be used as observation based on given features.

## 3 Modeling of Passenger Flow Prediction

### 3.1 Random Forest Regression

This chapter takes the passenger flow data including features and volume, divides the data into training set and test set, then builds a predicting model based on Random Forest machine learning algorithm with the training set, and finally validates the model with the test set.

Random Forest (RF) is an ensemble learning method for classification, regression, and other tasks. This algorithm constructs a multitude of decision trees at training time. For regression, it outputs the mean prediction of the individual trees. Random decision forests can reduce the overfitting on training set comparing with single decision tree.

With the RF regression, this chapter model the passenger flow predication as the following:

1.  Define the training set as $Y_i \leftarrow X_i$, $Y_i$ denotes the volume of the passenger flow as the observation $X_i$ denotes the corresponding feature inputs.
2.  Then, define the regression model for a single decision tree regression as the following:

    (a) Based on the feature inputs $X$ and the observation, search the split variable and split value. The regression decision tree split the full space into M partitions $\{R_1, R_2, \ldots R_m\}$. And each partition be mapping to modeling $C_m$. The binary split defines partition as the following, j is the variable and s is the value for splitting.

    $$R_1(j, s) = \{X|X_j \leq s\} \tag{1}$$
    $$R_2(j, s) = \{X|X_j > s\} \tag{2}$$

    The target function to search the split variable and split value will be

    $$\min_{j,s}\left[\min_{c_1}\sum_{x_i \in R_1(j,s)}(y_i - c_1)^2 + \min_{c_2}\sum_{x_i \in R_2(j,s)}(y_i - c_2)^2\right] \tag{3}$$

    And then internal minimal value can be calculated with the following formula.

    $$\hat{c}_1 = \text{ave}[y_i|x_i \in R_1(j, s)] \tag{4}$$
    $$\hat{c}_2 = \text{ave}[y_i|x_i \in R_2(j, s)] \tag{5}$$

    (b) Second, control the tree structure. This includes two parts, find out when will the regression tree stop partition and how to prune the regression tree. In out modeling, we define when the splitting reaches the minimal nodes, it will stop partition. Finally, we define the cost-complexity criterion:

    $$C_a(T) = \sum_{m=1}^{|T|} N_m Q_m(T) + \alpha|T| \tag{6}$$

    The tuning parameter $\alpha$ behaves like the other regularization parameters we have seen, balancing stability (tree size) with goodness of fit. For any given $\alpha$, there is a tree $T\alpha$ which minimizes the above criterion.

The Random forest is composted with multiple regression trees. The random forest model is generated with the following steps.

1.  Draw $m$ bootstrap samples from the training set. Then grow $m$ regression decision tree, for those data not in sample set, will be regarded as OOB (out of bag) data, and used for validation.

2.  For each single regression decision tree, instead of choosing best split features from all the feature set, randomly sample $m$ features and choose the best one among the sampled ones.
3.  Every single regression decision tree will recursively split the nodes. The random forest can assign a global setting to control the node size of each regression decision tree.
4.  Follow Steps 1–3 to grow $k$ regression decision trees. The random forest calculates the RF result based on the decision tree output. Those OOB data is used for validating the RF model generated.

Comparing with other machine learning algorithm, RF regression needs less hyperparameters and can avoid overfitting issues.

## 3.2  Model Accuracy Validation

The model evaluation is an important part for modeling. The following indicators are used to evaluate the random forest model in this chapter.

Coefficient of determination ($R^2$) and root mean square error (RMSE) are used to evaluate the model. Coefficient of Determination is a number that indicates the proportion of the variance in the dependent variable that is predictable from the independent variable. RMSE is used to measure the differences between values predicted by the model and the values observed.

As Random forest accepts a series of features to train the model, measuring the importance of those features will help to understand the importance of different factors.

Gini exponent indicates the node purity. The bigger is the Gini exponent, means the lower is the node purity. To measure the importance of a feature, the mean of the Gini exponent can be regarded as the standard.

$$\text{gini}(T) = 1 - \sum_{j=1}^{n} p_j^2 \qquad (7)$$

In the formula, $p_j$ is the proportion of the $j$th sample data set on the current node.

## 4  Results and Analysis

To validate the short-term passenger flow prediction model, the summer passenger flow between Beijing and Shanghai for Jinghu high-speed railway has been chosen as the study object. The experiment data includes the passenger flow between July 3rd 2015 and August 27th, 2015. There are totally 4592 railway trips information.

**Table 1**  The normalized features sample

| From hour | From minute | Running time | From weather | To weather | Day of week | Volume of passengers |
|---|---|---|---|---|---|---|
| 0.307692308 | 0.836363636 | 0.702380952 | 0.464646465 | 0.474747475 | 0.833333333 | 0.210526316 |
| 0.307692308 | 0.836363636 | 0.702380952 | 0.464646465 | 0.828282828 | 0.333333333 | 0.224137931 |
| 0.384615385 | 0.090909091 | 0.738095238 | 0.464646465 | 0.828282828 | 0.333333333 | 0.185117967 |

Besides these, the weather data is also collected for Beijing and Shanghai during the analysis time. A random forest predictive modeling is built on those data.

## 4.1  Data Preparation

The railway trips metadata comes from the railway ticket database, includes the impact features analyzed before. The weather data are collected using the weather API from China National Weather Department.

Before using the features and observations, these data need to be cleaned and normalized. First, the feature departure date will be divided into Year, Month, Day, and the feature like departure time will be divided to depart hour and depart minute. After that all the features should be digitalized, like the weather, day of the week, will change to numeric type based on mapping dictionary. Finally, to equalize the impact of each input feature, data normalization need to be done. Each input feature will be normalized into range [0, 1].

The data looked as the following Table 1.

When all the features are normalized, the full data set will be split into two batches. One is used as training set, and the other is used as test set. In this chapter, the former 4 weeks' data in July is used as training set. And the later 4 weeks' data in August is used as test set.

## 4.2  Modeling and Validation

After all the data prepared, R studio and random forest package are used to simulate the modeling process. There are two key hyperparameters for the random forest regression model. The first one is how many features will be used for a single decision tree. 1/3 of the feature set will be the inputs for each decision tree input. The other hyperparameter is how many decision trees in the full random forest. A loop is used to find out the best decision tree count as Fig. 3 shown. After setting up those two hyperparameter, the RF regression models are trained with features and observations.

Then, evaluate this model with the test set with evaluation formula and accuracy formula. We get the coefficient is about 0.82 and RMSE is around 65, compared with the mean for each trip, the model fits good on the test data. Also, when referred to
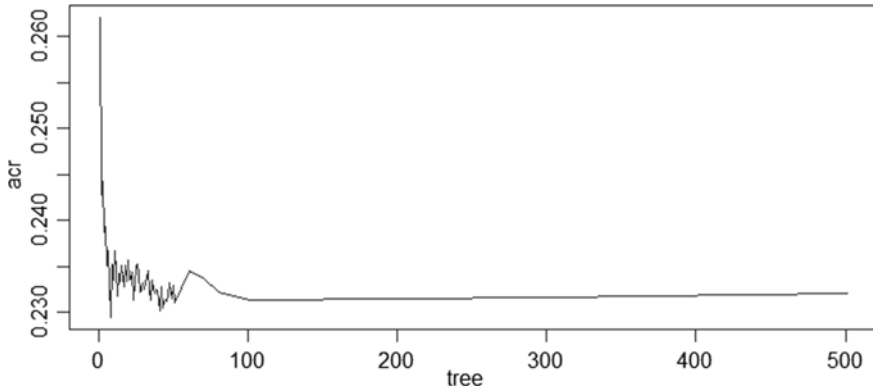
**Fig. 3** Decision tree Count

**Table 2** The evaluation values of the RF model

| | $R^2$ | RMSE | $Rs$ | $E_1$ | $E_2$ | $P$ | $\Delta$ |
|---|---|---|---|---|---|---|---|
| Single trip | 0.81791 | 65.1604 | 0.01598 | 0.04965 | 0.3597 | 0.6402 | 0.2119 |

the error rate, the error rate is about 0.2119. As for a single trip, there are also other occasional factors that will lead to volume change of passenger flow, the accuracy is good enough to help the operation company for tickets management optimization (Table 2).

If sum of all the trip volume of the passenger flow daily and get the daily passenger flow, the error rate can drop to 0.08937, and the accuracy is 91.21%. This is a significant improvement for short-term passenger flow prediction.

## 4.3 Factor Importance Analysis

Understanding which features contributes more to short-term passenger flow can help to efficiently improve the model and help the operators to better manage the tickets based on impact factors changes.

Based on Fig. 4, top impact factors include the running time, the departure time, the train trip capacity, the arrival time, day of the week, departure city weather, arrival city weather, and the train type. For both those two-difference importance measurement, the top impact features are very similar. The knowledge for the key impact factors can help to collect more detail data in the future and improve the predictive model. The high-speed railway operators can also leverage that knowledge when planning the train trip or optimize the revenue management.
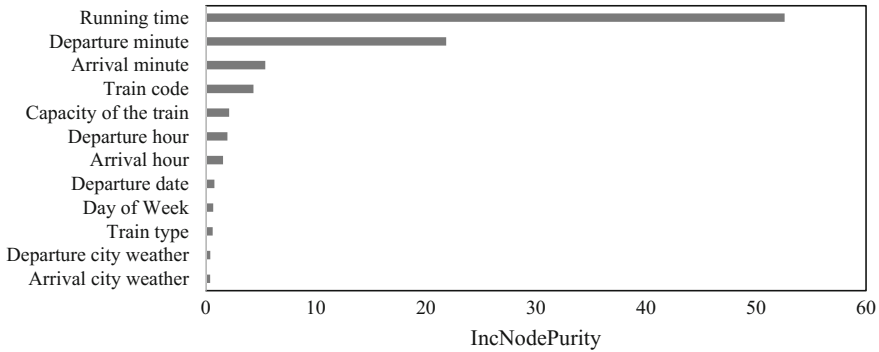
**Fig. 4** The Inc Node Purity of every feature

## 5 Conclusions

The prediction of short-term passenger flow helps to optimize the high-speed railway operation and improve the revenue. The chapter formulated a RF regression model, which is robust model, to predict the short-term passenger flow. The passenger flow data between Beijing and Shanghai from July to August in 2015 are adopted. The predicted results are shown that there is 91% accuracy for daily passenger flow. Comparing with classical BP network, the RF regression model can prevent overfitting issues during model fitting process, and fit different input features without changing the training process. It balances the features sets and decision tree quantities, and has good performance to get the result. Besides, the importance of impact factors is also obtained by this model, which can help the railway operators to take actions to adapt the impact factors and improve operation.

## References

1. Hao J, Cui Y, Han J (2015) Prediction of the railway passenger volume based on the SARIMA model. Math Pract Theory 45(18):95–104
2. Wang Y, Xu R (2010) Forecast of short-term metro passenger flow based on the periodically varying characteristics. Urban Mass Transit 1:46–49
3. Luo Y-J, Liu J, Sun X et al (2015) Regression model for daily passenger volume of high-speed railway line under capacity constraint. J Cent S Univ 22:3666–3676
4. Liu L (2016) Research of railway passenger volume forecast model based on PCA-BP neural network. Theory and Policy 38(6):43–47
5. Li X, Lv X, Liu J (2011) Forecast of railway short-term passenger flow based on RBF neural network. Railway Transport and Econ 33(6):86–89
6. Xu J, Wang D, Li C et al (2014) Short_term passenger flow forecasting for urban rail transit based on dynamic feedback neural network. Mod Trans Technol 11(5):43–46
7. Wang L, Ma C ,Zhou X et al (2015) Estimation of wheat leaf SPAD value using RF algorithmic model and remote sensing data. Trans Chin Soc Agric Mach 46(1):259–265

8. Zhao B, Tan Z, Deng K (2016) Calculation of the tangent of major influence angle based on random forest regression model. Met Mine 3:172–175
9. Sun X, Shu Q, Ou G et al (2015) Remote sensing estimation of the biomass of artificial simao pine forest based on random forest regression. For Resour Manage 1:71–76
10. Song K, Tan Z, Deng K et al (2016) Prediction of the horizontal factor based on random forest regression model. Met Mine 6:180–184
11. Liu R, Mao J, Li Y (2016) Facial landmarks location based on random forest regression. J Electro Meas Instrum 30(5):684–693
12. Hou Y, Yang K, Li K (2015) Network reconstruction with random forest regression and its application. Chin J Health Stat 32(4):558–561
13. Nan J (2016) The analysis of influencing factor about railway passenger forecast. Transport Dev Reform Top 38(2):35–40

# Application of Dimensionality-Reduction Algorithm in Interaction Action Recognition of Drivers

Qian Cheng, Xiao-bei Jiang and Wu-hong Wang

**Abstract** Human action recognition has many applications including design of human–machine system. Identifying the interaction between the driver and the vehicle information system is necessary to accurately identify the driver's intention and improve the stability of the vehicle. A machine learning-based framework for interaction action recognition of drivers was proposed in this chapter. Several dimensionality-reduction algorithms (PCA, Isomap, LLE, LE) for interaction action recognition are compared in this chapter. The test sequence is mapped into a low-dimensional space through these dimensionality-reduction algorithms, and traditional classifiers (naïve Gaussian, logistic regression, SVM, Kneighbors, DecisionTree) were trained in order to test the effect of dimensionality-reduction. Results show that "LLE+SVM" achieves the highest precision rate.

**Keywords** Dimensionality-reduction algorithms · Interaction action recognition

## 1 Introduction

In the last decade, human motion recognition has become a hot research direction of computer vision. The computer is supposed to be more intelligent to identify and understand people's daily movements. At present, action recognition is widely used in man–machine interaction, medical care, intelligent security, home intelligence, and other fields. In the field of traffic safety, understanding the interaction between the driver and the vehicle information systems has many benefits on identifying the driver's intention and improving the stability of the human–vehicle system.

Most of the research, which focus on human motion recognition, were based on video streaming. The RGB image contains a lot of information about the object while it produces high-dimensional data. Thus, the dimensionality-reduction algorithm has

Q. Cheng · X. Jiang (✉) · W. Wang
Department of Transportation Engineering, Beijing Institute of Technology, Zhongguancun South Street 5, Beijing 100081, People's Republic of China
e-mail: jiangxiaobei@bit.edu.cn

been an important part of the data preprocessing. Redundant and noise information were contained in the original high-dimensional space, causing errors and reducing accuracy in practical applications such as image recognition; We hope to reduce the error caused by redundant information and improve the recognition (or other applications) precision through dimensionality-reduction algorithm. Also, we want to find the intrinsic structural features of the internal data by these algorithms.

Many scholars use probabilistic models to build human dynamic models. The most classical method is the hidden Markov model (HMM) [1]. It builds the conversion probability and hidden state between the hidden states by learning the conditional probability between the observed values. Wang [2] uses the principal component analysis (PCA) to reduce the dimension of the training set. Conditional random field model (CRF) [3] were also used to establish the model of probability of motion. But all these probabilities assumes that all States of all motion have been known. If the selected human features are not so good, it is difficult to determine from the observation space. Thus, nonlinear dimensionality-reduction can be used to obtain the expression of compact motion in low-dimensional hidden space without this assumption. Several dimensionality-reduction algorithms (PCA, Isomap, LLE, LE) for interaction action recognition are compared in this chapter.

## 2 Method

### 2.1 Experimental Procedure

As shown in Fig. 1, about 6000 videos (each lasts 1 s, 25 frame/s) of three types of interaction motion (click, slide, rotate) were recorded. Then, features were obtained through grayscale picture.

Figure 2 shows the flowchart of the entire framework of interactive action recognition based on a variety of dimensionality-reduction algorithms. The framework was divided into two parts. In the training phase, we first extract the expression of human characteristics representing the human motion from the original training data, and then use the four-dimensionality-reduction methods to reduce the dimension of the



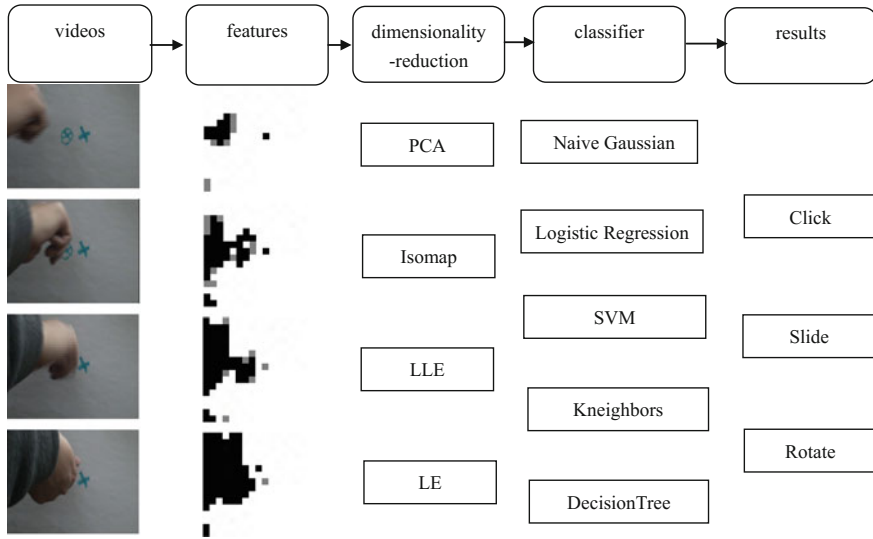**Fig. 1**  Three types of interaction motion (click, slide, rotate)

**Fig. 2** Procedure of experiment

training data representing each action, and get the motion model in low-dimensional space. In the recognition stage, we use the classical classifier (naive Gaussian, logistic regression, SVM, Kneighbors, DecisionTree) to map the action sequence data to the low-dimensional motion space query, and then match the test sequence and training data from the two angles of similarity and similarity, respectively. Two-third of the total number of samples were selected as training samples and the rest as test samples.

## 2.2 Dimensionality-Reduction Algorithms

### 2.2.1 PCA

Principal component analysis (PCA) is the most commonly used method for linear dimensionality-reduction. Its goal is to map the high-dimensional data to low-dimensional space through a linear projection while expecting the variance of the data in the projected dimensions achieve the largest. Then, less data can be used to keep the characteristics of original data.

### 2.2.2 Isomap

In the thought of isomap, embedding low-dimensional manifolds into high-dimensional space would cause misleading in calculating the straight distance in high-dimensional space. Using the property of homeomorphism between manifold on the local and Euclidean space, we find out the nearest neighbor points of every point based on Euclidean distance, then we can establish a nearest neighbor connection graph. As a result, the distance between two points is transformed into the shortest path problem between two points on the nearest neighbor connection graph.

### 2.2.3 LLE

Locally linear embedding (LLE) is a nonlinear dimensionality-reduction algorithm. LLE algorithm holds that every data point can be constructed by linear weighted combination of its nearest neighbors. It can make the data keep the original manifold structure after reducing the dimensionality.

### 2.2.4 LE

Laplacian Eigenmaps reconstruct the local structural features of data manifolds by constructing similarity relation diagram to reflect the inner manifold structure of the data. Its intuitive idea is the points that want to be related to each other (the points connected in the graph) are as close as possible in the space after the reduction of dimensions. Comparison of four-dimensionality-reduction methods were shown in Table 1.

## 3 Results and Discussion

Performance of the four-dimensionality-reduction algorithms were shown in Table 2. Different parameters for classifier are grouped in the training phase. The recognition

**Table 1** Comparison of four-dimensionality-reduction methods

|        | Linear | Supervised | Objective function |
|--------|--------|------------|--------------------|
| PCA    | Y      | N          | $\min \mathrm{tr}(W^T A W)$, s.t. $W^T W = I$ |
| Isomap | N      | N          | $\min \sum_i \sum_j \mathrm{dis}\,(x_{i,j}, x_{i,j+1})$ |
| LLE    | N      | N          | $\sum_n \left\| \vec{X}_i - \sum_j W_{ij} \vec{X}_j \right\|^2$ s.t. $\sum_j w_j = 1$ |
| LE     | N      | N          | $\min \mathrm{tr}\,(Y^T L Y^T)$, s.t. $Y^T \mathrm{D} Y^T = I$ |

**Table 2** Performance of the four-dimensionality-reduction methods

|  | Classifier | Parameters | Precision rate |
|---|---|---|---|
| PCA | Naive Gaussian | / | 72.5 |
|  | Logistic regression | alpha $=0.2$ | 81.6 |
|  | SVM | kernel $=$ 'linear', C $=1.0$ | 85.9 |
|  | Kneighbors | n_neighbors $=3$ | 77.4 |
|  | DecisionTree | criterion $=$ 'entropy' | 75.1 |
| Isomap | Naive Gaussian | / | 71.6 |
|  | Logistic regression | alpha $=0.15$ | 87.5 |
|  | SVM | kernel $=$ 'linear', C $=1.0$ | 88.6 |
|  | Kneighbors | n_neighbors $=3$ | 74.1 |
|  | DecisionTree | criterion $=$ 'entropy' | 77.8 |
| LLE | Naive Gaussian | / | 75.8 |
|  | logistic regression | alpha $=0.15$ | 90.4 |
|  | SVM | kernel $=$ 'linear', C $=1.0$ | 92.3 |
|  | Kneighbors | n_neighbors $=3$ | 80.4 |
|  | DecisionTree | criterion $=$ 'entropy' | 79.6 |
| LE | Naive Gaussian | / | 73.4 |
|  | Logistic regression | alpha $=0.2$ | 89.4 |
|  | SVM | kernel $=$ 'linear', C $=1.0$ | 89.5 |
|  | Kneighbors | n_neighbors $=3$ | 81.4 |
|  | DecisionTree | criterion $=$ 'entropy' | 78.1 |

rate in the set is roughly similar in the condition of common parameters in each classifier.

Results showed that "LLE+SVM" achieves the highest precision rate. Among all the classifiers, SVM classifier displayed the best classification performance in our dataset, while the Kneighbors performed the worst. Owing to LLE maintains the local characteristics of the sample during the dimensionality-reduction, it performed best among all dimensionality-reduction methods. For Decision Tree and naive Gaussian classifier, the four-dimensionality-reduction methods seemed to have no significant difference (Fig. 3).
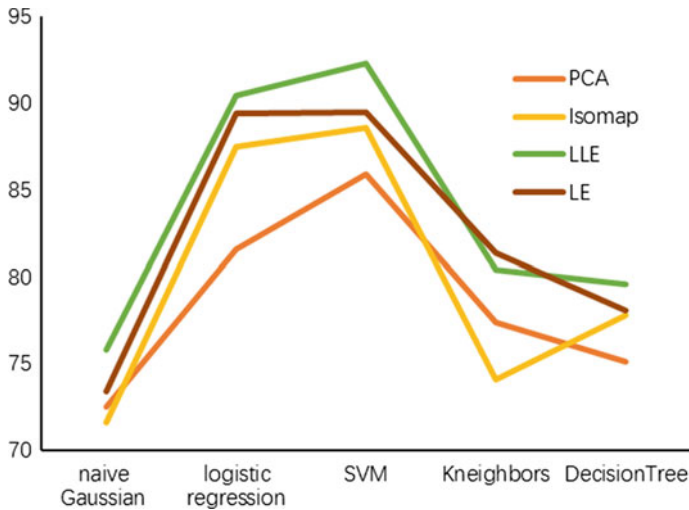
**Fig. 3** Performance of the four-dimensionality-reduction methods

## 4 Conclusions

This chapter presents an action recognition framework based on four different dimensionality-reduction algorithms. In the process of identification, different classifiers are used to classify operations. In the process of concrete implementation, the low-dimensional motion model of similar action is similar, which may result in false recognition of similar movement to a certain degree. In future work, hierarchical processing of the interaction action would be considered. The whole attitude would be divided into the fingers, palms, etc., and the dimension reduction method would be used to get the corresponding motion model of the various parts of the actions. The establishment of a layered model can enlarge the difference between the low-dimensional motion model of similar motion, thus improve the whole motion recognition rate.

## References

1. Yamato J, Ohya J, Ishii K (1992) Recognizing human action in time sequential images using hidden Markov model. In: Proceedings of IEEE computer society conference on computer vision and pattern recognition, Champaign, USA, pp 379–385

2. Wang KJ, Liu LL, Ben XY et al (2009) Gait recognition based on energy image and two dimensional principal component analysis. J Image Graph 14(12):2503–2509
3. Saul LK, Roweis ST (2003) Think globally, fit locally: unsupervised learning of low dimensional manifolds. J Mach Learn Res 4:119–155